EGS Exploration Methodology Project using the Dixie Valley Geothermal System, Nevada as a Calibration Site

Part I—Final Scientific Report Baseline Conceptual Model

2 January 2014*

DOE Award: DE-EE0002778

*Orginally submitted to the National Geothermal Data Repository as the EGS Exploration Methododlogy Project Baseline Conceptual Model

ALTAROCK
ENERGY INC

Table of Contents

List of Figures*

List of Tables*

List of Appendices

*Summarized captions are shown. Figure, table, and appendices are numbered consecutively from Section 1.

List of Plates

List of Acronyms

Acronym	Description
AltaRock	AltaRock Energy Inc.
ARRA	American Recovery and Reinvestment Act
asl	Above seal level
B&R	Basin and Range
BHT	Bottom hole temperature
BHTV	Borehole Televiewer
BLM	U.S. Bureau of Land Management
CBA	Complete Bouguer Anomaly
CNSB	Central Nevada Seismic Belt
COCORP	Consortium for Crustal Reflection Profiling
CSC	Coulomb Stress Change
DOE	U.S. Department of Energy
DVF	Dixie Valley Fault
DVFZ	Dixie Valley Fault Zone
DVGD	Dixie Valley Geothermal District
DVGS	Dixie Valley Geothermal System
DVGW	Dixie Valley Geothermal Wellfield
DVPF	Dixie Valley Producing Field
DVPP	Dixie Valley Power Partners
DVESA	Dixie Valley Extended Study Area
DVSA	Dixie Valley Study Area
EGS	Engineered Geothermal System
EM	Electromagnetic
GDB	ESRI ArcGIS geodatabase
GIS	Geographic Information System
HS	Hot Spring

List of Acronyms

Acronym	Description
HTGF	High Temperature Geothermal Fluids
Jg	Jurassic rocks
Jgnm	Jurassic rock, non-magnetic
MT	Magnetotelluric
NGDR	National Geothermal Daa Repository
NV	Nevada
NBMG	Nevada Bureau of Mines and Geology
PASSCAL	Program for Array Seismic Studies of the Continental Lithosphere
QFFDB	Quaternary Fault and Fold Database
Qp	Attenuation of the P-wave
Qs	Attenuation of the S-wave
QTbf	Quaternary-Tertiary basin fill
RF	Receiver Fault
rho	Seismic inferred density
SF	Source Fault
SF	Stillwater Fault
SFZ	Stillwater Fault Zone
S_{hmin}	Horizontal minimum stress direction
SME	Subject Matter Expert/Expertise/Experience
Terra-Gen	Terra-Gen Power, LLC
TGH	Temperature Gradient Hole
USGS	United States Geological Survey
Vp	P-wave velocity in km/sec
Vs	S-wave velocity in km/sec

1.Introduction

1.1 Goals and Objectives

The U.S. Department of Energy (DOE) has contracted with AltaRock Energy Inc. (AltaRock) to develop a calibrated Engineered Geothermal System (EGS) exploration methodology (Award No. DE-EE0002778). This activity is jointly funded by AltaRock. To achieve the project goal, the following five technical tasks (objectives), with a description of what was done, were completed:

- ***Task 1 –*** ***Collect and Assess Existing (baseline) Public Domain Geoscience Data***
  This task involves qualitatively assessing the geology, geophysics, geochemistry, hydrology, and well data in project area with particular emphasis on the existing Dixie Valley Geothermal Wellfield (DVGW).
- ***Task 2 –*** ***Design and Populate a Geographic Information System (GIS) Database***
  Development of a GIS-database ensures that the project data can be easily stored and managed for retrieval, visualization, and data integration.
- **Task 3 —** **Develop Baseline (existing data) Geothermal Conceptual Model, Evaluate Geostatistical Relationships, and Generate Baseline EGS Favorability (and Trust) Maps**
  This task integrates the geoscientific data assessed; re-interpret data as required; conduct geostatistical exploratory data analysis to discern relationships among key geoscience parameters; and generate favorability/trust maps for the calibration area to identify EGS drilling targets at a scale of 5km x 5km at depths from +1km above sea level (asl) to -4km asl.
- ***Task 4 –*** ***Collect New Field Data to Fill In Data Gaps and Improve Model Resolution (baseline and new data are combined to create an enhanced data set)***
  This task involves collecting new and interpreting the enhanced (1) gravity data to define the basin structure and subsurface faulting; (2) passive ambient seismic noise data to define the seismic parameters (Vp, Vs, rho, Qs, and Qp) and potentially identify areas of seismic anisotropy; (3) Magnetotelluric (MT) data to define subsurface resistivity, pathway for fluid flow, potential subsurface structure, MT structural as well as developing a conductive MT-based subsurface thermal map; and (4) soil CO_2 gas data for a focused investigation of zones of dilatation and compression. Additionally, develop 3-D conductive and convective thermal models.
- ***Task 5 –*** ***Repeat Task 3 for the Enhanced Data Set***
  This task integrates the new results into the baseline geoscientific data assessment; re-interprets data as required; conducts geostatistical exploratory data analysis on the enhanced data set; and revises the calibration area favorability/trust maps for the enhanced data.

1.2 Report Basis

To date, there is no accepted, invasive or non-invasive exploratory methodology for “greenfield” EGS sites proven to be both technically feasible and cost effective. Although drilling slimholes provides direct data on the primary resource favorability criteria (i.e., temperature, rock composition and stress regime), widespread use is cost prohibitive necessitating selective use. Developing a cost effective and reliable exploration methodology is, therefore, essential for the economic viability of EGS in regions beyond what has already been explored for hydrothermal resources. To determine whether an EGS exploration methodology can be calibrated using the Dixie Valley Geothermal System (DVGS, see Figures 1 and 2 and Section 1.3) as a laboratory test case, AltaRock has designed a project consisting of the five technical tasks presented in Section 1.1.

The Project Area consists of a 50km by 50km (31mi by 31mi) area roughly centered on the Dixie Valley Power Partners lease (DVPP, Figure 1). One of the key data sources for this study has been the extensive amount of information compiled and interpreted by Blackwell et al. (2005), the public domain in numerous DOE supported studies as well as non-DOE supported studies that have taken place over the past 40 to 50 years, and selected data released by Terra-Gen Power, LLC (Terra-Gen). This report does not attempt to re-interpret the bulk of the public domain data because we do not have access to the original data set. However, a re-interpretation of select data sets is presented where deemed appropriate. Original work by the authors is presented in the areas of gravity and magnetics, seismic, surface and subsurface structure, magneto-tellurics, cross-correlating these varied data sets, geostatistics, and in the development of the methodology.

Geothermal activity is present intermittently throughout Dixie Valley, over a distance of some 100km (62mi) in length (Figure 2). The overall study area for geological and geophysical regional setting purposes is a 50km^2 (19mi^2)square block that includes a sizable portion of Dixie Valley and the Stillwater Range. The “calibration” area covers a much smaller area, the Dixie Valley geothermal wellfield (DVGW), which includes the geothermal production wells, as well as dry wells drilled in and around the production area (see below). This reduction of the detailed study area has been necessary, as this is where the greatest concentration of data is available, but has also resulted in biases within the conclusions that need to be appreciated by the casual reader. It is also critical for all readers to appreciate and accept that the analysis presented herein is not constructed to be used as an exploration guide to the DVGS. While parts of the analysis presented can be used in exploration work in the DVGS, the reader is cautioned that supplementary analysis and integration is required to use the work herein as an exploration guide. Rather this project was designed, and this report is presented as a methodology to evaluate potential EGS areas.

As indicated above, the focus of this investigation is the DVGW (Figure 2) which includes the Dixie Valley geothermal production field currently generating over 60 MWs of electrical power (DVPP in Figure 1), and the dry and sub-commercial wells primarily located to the southwest and northeast of the producing field. The DVGW was chosen because it provides the most extensive public-domain geothermal database in the Basin and Range Province (B&R) including but not limited to the substantial body of geological, geochemical and geophysical data available for portions of the valley and 30 geothermal wells. This project had access to lithologic data for 22 of 30 wells, bottomhole temperature data (BHTs) for 26 wells, temperature-depth profiles for 10 wells, and 9 temperature gradient holes (TGHs). The availability of downhole data, especially geothermal well data, provides the basis for calibrating the exploration methodology.

This effort is designed to test the value of a select variety of exploration tools in the identification of locations favorable for EGS development using the Dixie Valley Geothermal System (DVGS) as an evaluation site . Anomalous high temperatures in the near-surface (upper 3km [9800ft]) within the B&R are produced by long-lived hydrothermal cells. The continuous upwelling flow of hot water, over long periods of time, conductively heats adjacent lower permeability rock. These areas of conductively heated lower permeability rock are prime targets for EGS development. The first task in the identification of these favorable EGS sites is to understand where and why traditional hydrothermal cells are located. This study has identified and described basic structural conditions that are necessary for a geothermal cell to develop. This knowledge now provides the basis for identifying favorable EGS targets, and for evaluating various exploration technologies for their abilities to assist in finding similar locations outside the study area.

This Final Scientific Report is presented in two parts. Part 1 covers the results of Tasks 1 to 3, the Baseline Conceptual Model, described above. Sections 2 through 6 of this report provide a compilation of the geology, structure, geophysics (gravity, magnetics, magneto-tellurics, seismic, and thermal), hydrogeology, geochemistry, and the DVGW setting. New and re-interpreted data are introduced for the sake of clarity, where appropriate. Section 7 discusses the Baseline EGS Conceptual Geothermal Model. Presented therein are the results of qualitative and quantitative cross-correlation of the various data sets and their potential significance. Section 8 describes the generation of the Baseline EGS favorability and associated trust maps.

Part II presents the results of Tasks 4 and 5, the Enhanced Conceptial Model, decribed bove. It contains Section 9 which discusses the new data collection performe din this project as well as the data synthesis by discipline. Section 10 presents the enhanced data implications and qualtitative correlations. Section 11 discusses the quantitative correlations. Section 12 discusses the rationale for not generatin enhanced favorability and trust maps. Section 13 provides the responses to nine questions posed in the proposal for this project. Section 14 provides the references used in this investigation. Note that the figures and tables are numbered sequentially through Parts I and II. Appendices in Part II are number sequentially and referred to as Part II-Appendix 1 through Part II-Appendix 11.

1.3 Background

The DVGW is an ideal region for this case study as it represents the largest and hottest B&R (deep circulation) hydrothermal system known and it has an extensive public domain database. The DVGW is part of a much larger DVGS which consists of a large number of potentially independent geothermal cells in Dixie Valley (Al Waibel, pers. comm., 2010) that lie along an active fault zone bounding the Stillwater Range in Dixie Valley, located in Churchill and Pershing Counties, Nevada (Figures 1 and 2). In addition to the geothermal systems along the east side of the Stillwater Range, others have been defined in the region, e.g., New York Canyon and Pirouette Mtn. (Figure 2), as well as a significant geothermal resource currently under development at Jersey Valley which lies just to the NE of the Project Area. Given the known and numerous potential geothermal systems present in this limited geographical region, the term Dixie Valley Geothermal District (DVGD) is used to reference all the geothermal systems present in the Dixie Valley region following the approach described by ITSI (2005), Waibel (1987), and well-established in the mining and oil/gas and mining industries.

The DVGW is considered for the purposes of this report as extending from the Dixie Comstock Mine and well 45-14 area to the southwest, to the Section 10 and Senator Fumarole Areas to well 76-28 to the northeast, and to well 62-21 to the southeast (Figure 1). It includes the area in and around the Dixie Valley Producing Field (DVPF) and Dixie Valley Power Partners lease (DVPP). The DVPP, lying south-southwest of the producing field, consists of at least four deep wells, one of which is the hottest geothermal well (285°C [545°F]) known in the B&R.

The DVGW has a complex structural setting and temperatures >>200°C [>>392°F] over a large area at relatively shallow depth (2-3km [6400-9600ft]). Additionally a large amount of subsurface information such as deep well data, surface geophysical surveys, and hydrologic and geochemical investigations from published literature, DOE sponsored projects, and other data provided by Terra-Gen Power exceeds the publically available information basis for any other geothermal areas in the B&R. Geothermal electrical production from the producing field (62 Mw_e) is significantly greater than that of any other geothermal system within the Great Basin.

The DVGS is considered a classic range-front fault system with production mainly from a complex structural setting involving brittle, permeable igneous units including a Jurassic mafic complex faulted against impermeable basement rocks. The producing field lies within a complex system of steep extensional faults which includes the well-known range-bounding fault and related subsurface structures, referred to in this report as the Dixie Valley Fault Zone (DVFZ), see Section 2.2.2. There is no young volcanism (<8Ma) within 50km (31mi) of Dixie Valley, thus there is no upper crustal magmatic source for the elevated heat flow. The majority of existing studies conclude that the heat source for geothermal fluids results from deep circulation within a highly extended terrain (Benoit, 1999; Blackwell et al., 2000; 2002; 2005; 2007). Other studies include deep circulation with some degree of magmatic influence evidenced by geophysical and geochemical data. The supporting evidence for this alternate interpretation includes helium enrichment showing a slight mantle component (Kennedy et al., 2005), magnetotelluric data imaging a potential deep feeder zone for geothermal fluids near the center of Dixie Valley (Wannamaker et al., 2007), and a small magmatic component for fluid-inclusion gases within veins from production wells (Lutz et al., 2002). While the majority of studies support the deep circulation model, these alternate hypothesis will also be discussed within the report.

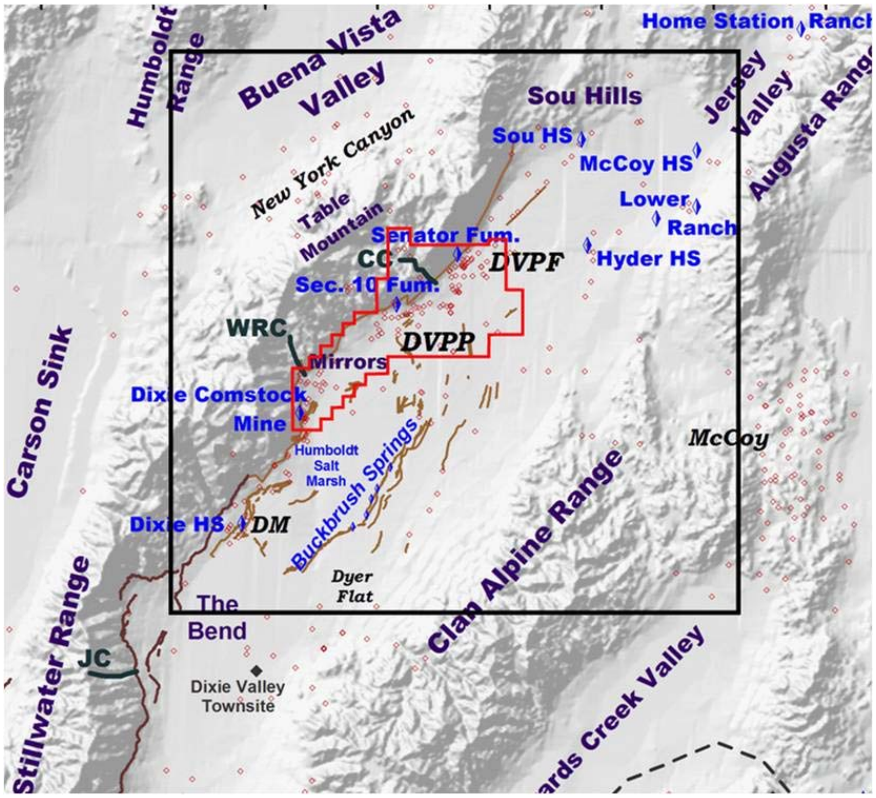

Figure 1. Dixie Valley Index Map. Areas of drilling are shown in black italic (DVPF – Dixie Valley Producing Field, DVPP – Dixie Valley Power Partners, DM – Dixie Meadows). Canyons (CC – Cottonwood Canyon, WRC – Whiterock Canyon) are identified. Geothermal electrical generation is from wells in the DVPF area. The EGS Exploration Methodology Project Area is shown as the black square. The Dixie Valley Geothermal Wellfield includes all the geothermal wells in the red outlined area; see text for a description. The figure and caption is after Blackwell et al. (2005).

1.3.1 Regional Setting

The DVGS lies within the northern part of the B&R and more specifically within the internally drained northern Great Basin (Figure 3). The highly extended terrains topography is dominated by north to northeast trending ranges bounded by normal faults and separated by basins filled with Cenozoic sediments and volcanic deposits. Despite relatively thin crust typical of continental rift basins, surface elevations are relatively high, indicating underlying anomalously low mantle densities. Additional salient regional features of the DVGS are that it:

- Lies within the Central Nevada Seismic Belt (CNSB), Figure 4A, which is a zone of focused contemporary seismicity with a NNE trend extending from the Walker Lane into central Nevada and has had the largest earthquakes (M_w>6-7) recorded in Nevada over the last century;
- Occurs in the Greater Lahontan Basin (includes the Carson Sink and Dixie Valley) and forms the lowest topographical valleys in western Nevada (Figure 4B);
- Lies in the area of highest heat flow in the Great Basin, the Battle Mountain heat flow high; and
- Coincides with a major lithospheric boundary separating thinner crust and lower surface elevation to the west from thicker crust and higher surface elevation to the east. The $^{87}Sr/^{86}Sr$ 0.706 line, an isotopic variation line relating to the composition and age of basement rocks, divides the Precambrian cratonal rocks to the east from Paleozoic to Mesozoic accreted terrains to the west and passes directly through Dixie Valley (Figure 3).

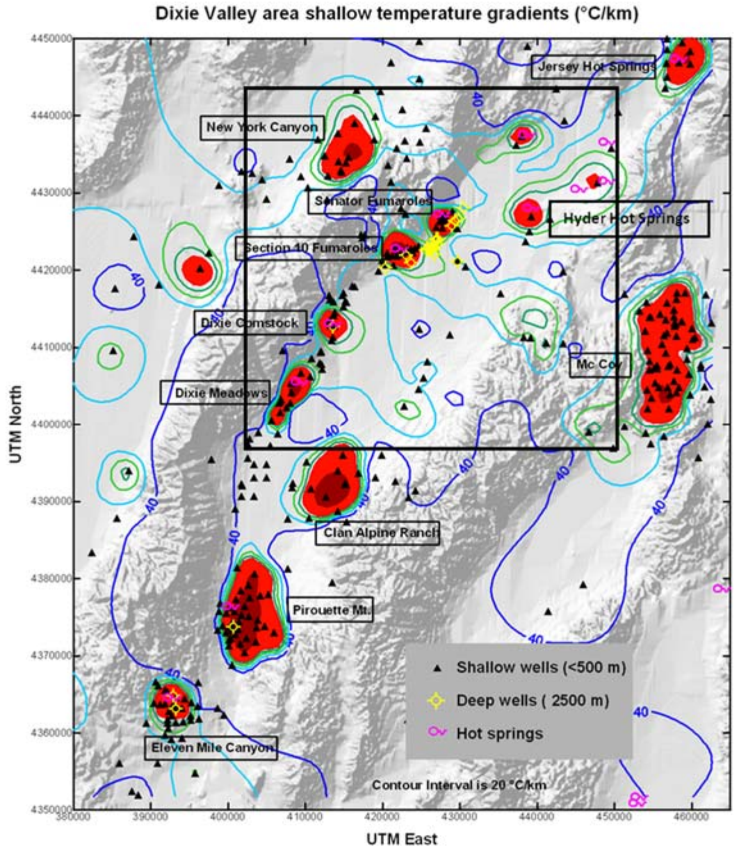

Figure 2. Shallow thermal anomalies and location of shallow thermal gradient holes and deep well locations in the Dixie Valley Geothermal District. Contour intervals are (20°C/km [1.5°F/100ft]). From 120 – 250 °C/km (8.75-18.5°F/100ft) the contours are a red fill and from 500°C/km (37°F/100ft) the contours are a dark red fill. Contours in the ranges are diagrammatic due to the lack of data. Well gradient locations are shown as black triangles for shallow wells (<500 meters [1640ft]) and as black circles for wells deeper than 500m. Black bounded box is the approximate boundary of the EGS Exploration Methodology Project Area. The figure and caption are after Blackwell et al. (2005).

1.4 AltaRock Project Team

The AltaRock team is comprised of a number of individuals with extensive expertise on the Dixie Valley Geothermal Resource in particular, as well as other geothermal systems in general. AltaRock Team members and their positions on the Team are:

- Dr. David Blackwell of Southern Methodist University, Thermal Task Leader;
- Dr. Philip Wannamaker of University of Utah, Earth Geosciences Institute, Magneto-tellurics Task Leader;
- Dr. B. M. Kennedy of Lawrence Berkeley National Laboratory, Geochemistry Task Leader;
- Dr. Trenton Cladouhos of AltaRock, Geology Task Leader;

- Dr. Ileana Tibuleac of University of Nevada Reno Seismological Laboratory, Seismic Task Leader;
- Dr. David von Seggren of University of Nevada Reno Seismological Laboratory;
- Dr. Robert Karlin of University of Nevada Reno, Gravity and Magnetics Task Leader;
- Dr. Ed Isaaks of Isaaks & Co., Geostatistics Task Leader;
- Dr. Hank Ibser of University of California Berkeley, Geostatistical Consultant;
- Mr. Matthew Clyne, GIS Task Leader;
- Mr. Owen Callahan, AltaRock geologist;
- Ms. Maisie Nichols, AltaRock geologist/geophysicist;
- Mr. Mike Swyer, AltaRock geologist/engineer/GIS analyst;
- Mr. Jon Sainsbury, AltaRock geologist;
- Mr. Al Waibel, Columbia Geoscience who contributed his geologic and geothermal expertise in the area and served on the Peer Review Committee;
- Ms. Susan Petty, AltaRock Energy who contributed her geothermal expertise in the area and served on the Peer Review Committee; and
- Mr. Joe Iovenitti of AltaRock, Principal Investigator.

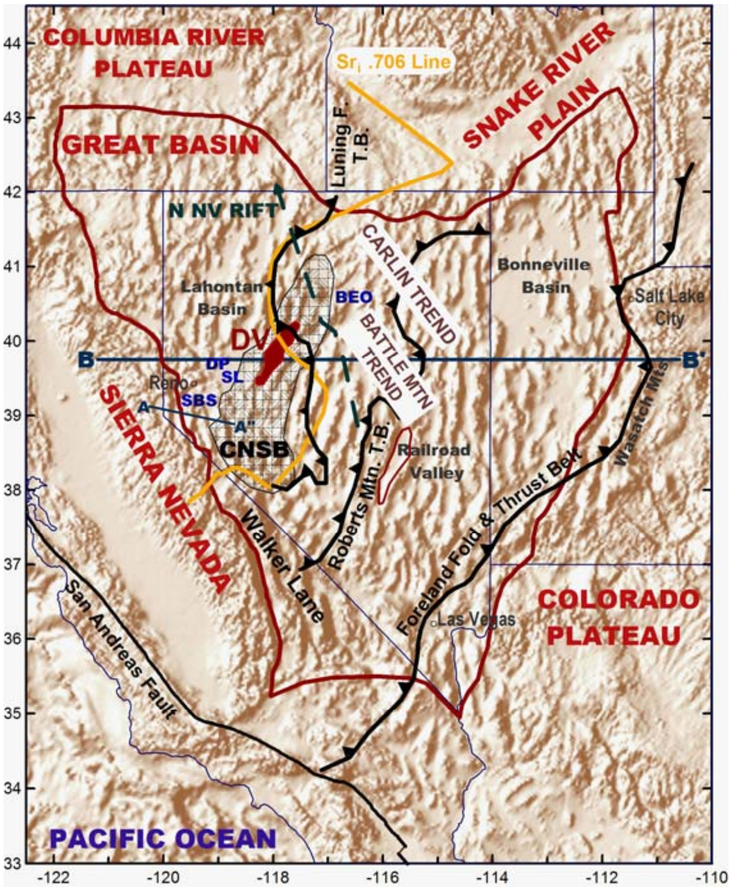

Figure 3. Regional map for Dixie Valley (DV). Major geothermal systems shown in blue text: BEO – Beowawe, DP – Desert Peak, SBS – Steamboat Springs, SL – Soda Lake & Stillwater. Faults and thrust belts shown with black, thrusts with triangles. Central Nevada Seismic Belt – CNSB shown with pattern. Northern Nevada Rift (Miocene) shown as dashed green line (Zoback et al., 1994). Strontium (Sr) 0.706 Line shown by solid yellow line (Tosdal et al., 2000). The figure and caption are from Blackwell et al. (2005).

1.5 National Geothermal Database

All the data and findings generated in this study will be submitted to the National Geothermal Database (NDGR). The Baseline Conceptual Geothermal Model data and findings (see Section 1.1, Tasks 1-3) were submitted to the NDGR in May 2013. This final report includes the Baseline Conceptual Model findings as well as the new data collected, enhanced data sysnthesis and interpretation, enhanced geostatistical analsysis, enhanced favorability and trust maps, as well as a discussion of a number of questions posed in the proposal for this project. The final report and its associated data will be submitted to the NDGR in XXXX.

2. Geology

Physiographically, the Project area is comprised of from the northwest Buena Vista Valley, the Stillwater Range (more specifically Table Mountain), the northern portion of greater Dixie Valley, the Clan Alpine and Augusta Ranges and a small portion of Edwards Creek Valley to the southeast, and the Sou Hills and portion of Jersey Valley to the north (Figure 1). The general geology of the DVGW in northern Dixie Valley is described below.

2.1 Stratigraphy

The rocks exposed in the Stillwater Range are intersected at depth by the wells within the geothermal field. The generalized geologic map (Figure 5) highlights the exposed bedrock within the ranges surrounding Dixie Valley. A detailed geologic map of the Humboldt Lopolith from Speed (1976), centered in northern Dixie Valley is presented in Appendix 1. A preliminary geologic map of the Stillwater Range from the Nevada Bureau of Mines and Geology (NBMG) is also provided in Appendix 1. The Stillwater Range consists of allochthonous thrust plates of Triassic and Jurassic oceanic sediments and Jurassic igneous rocks that were intruded by late Cretaceous to Tertiary granodiorite and overlain by mid-Cenozoic volcanic rocks. In Dixie Valley, the basement assemblage is overlain by late Cenozoic volcanics and basin-fill sediments, deposited during extensional events. It is noted that the discussion in this section is mostly from Waibel (1987). The generalized stratigraphy is summarized in Table 1.

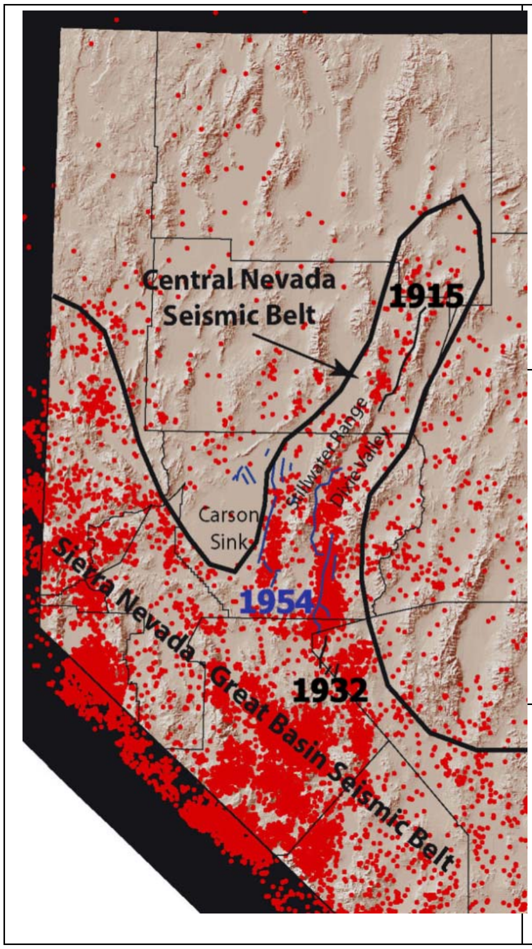

Figure 4A. Map of western Nevada, showing epicenters of recorded earthquakes M>4, surface ruptures of historic earthquakes, and the outline of the Central Nevada Seismic Belt. Red dots are earthquakes from 1850s to 1998 (from DePolo and DePolo, 1999). Surface ruptures of the 1915 Pleasant Valley earthquake (black lines). Surface ruptures of the 1954 Rainbow Mountain-Stillwater and Dixie Valley-Fairview Peak earthquake sequences (blue lines). Surface ruptures of the 1932 Cedar Mountain Earthquake (bottom black lines). The figure and caption are from Blackwell et al. (2005).

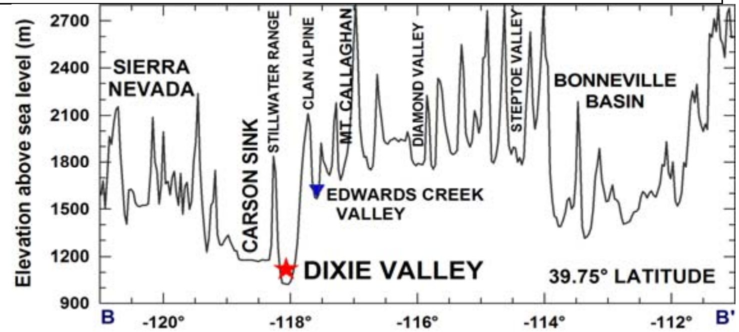

Figure 4B. East –West elevation cross section through the Basin and Range from the west side of the Sierra Nevada in California to the east side to the Wasatch Mountains in Utah. Dixie Valley (red star) is the lowest point on the cross section. The figure is from Blackwell et al. (2005) and the caption is after the report authors.

2.1.1 Basement Geology

Key features of the basement geology in the Project Area are presented from oldest to youngest. The notation for the major units as referenced in this report is also listed, e.g. (Tr) and described in Section 7. A minor unit, a Paleozoic-derived section is present near the Sou Hills in the NE corner of the Project Area and is not discussed.

Triassic marine sediments (Tr)

- Deposited in a passive margin on the western continental shelf and slope;
- Interweaved tectonically with Jurassic sedimentary and igneous rocks;
- Consists of mostly meta-sediments with some interbedded volcanics;
- May be more likely to deform plastically rather than fracture when subjected to high differential stress;
- Consists of:
  - Winnemucca (Fm): feldspathic metasandstone to arkose; and
  - Star Peak Group: slates, phyllites, and massive limestones which are the deepest layered rocks in northern Dixie Valley and have low permeability within faulted and sheared zones.

The majority of the Triassic meta-sediments exposed in the Project Area are derived from the Star Peak Group. While these meta-sediments are not expected have geothermal potential due to their low permeability and lack of fracturing, this formation possesses some possible localized EGS favorable characteristics within occasional zones of interbedded volcanics and intruding dioritic plutons. These intrusions are reported to contain open, but isolated faults and fractures and limited potential of hosting commercial geothermal hydrothermal production due to low permeability.

Jurassic shallow marine sedimentary rocks (Jbr)

- Boyer Ranch Formation (Jbr): mostly quartzite with some basal carbonate and minor conglomerates overlying, overridden and mechanically incorporated into the allochthonous oceanic crust;
- The quartz arenite portion is very well-indurated and fractured. It is associated with an injection zone within the northern producing field and the adjacent fumaroles, indicating that it is capable of hosting open fractures in permeable zones in association with fault planes. These characteristics and its connection with the hydrothermal system make the Boyer Ranch quartzites a suitable EGS target, while exposures are limited; and
- The Jbr is sufficiently exposed along the eastern edge of the Stillwater Range, adjacent to the producing zone including at the mouth of Cottonwood Canyon.

Jurassic mafic oceanic igneous rocks (Jz)

- Known as the Humboldt igneous complex, these rocks were originally interpreted as a locally intrusive “lopolith” by Speed (1967) but Waibel (1987) and others consider the unit to be an allochthonous fragment of oceanic crust with large blocks of ocean floor that have undergone low grade metamorphism containing spillite, keratophyre, trondhjemite-type rocks.
- Contains highly altered and fractured rocks within major fault zones;
- Tend to be very brittle and capable of maintaining good fracture permeability;
- Consists of a lower plutonic-derived section of mostly mafic crust overlain by a complex of mostly extrusive igneous rocks;
- Upper complex of igneous rocks (basalts, diorites, and gabbros) commonly occurs in thrust fault contact with the quartz arenite of the Boyer Ranch Fm (Lutz et al., 1997); and

- Overlying the plutonic rocks in the igneous complex (Lutz et al., 1997), and yielding an indicated K-Ar age of 150 ±3Ma (Page, 1965) are sericitized and veined hornblende diorite or anorthosite, and andesitic to basaltic extrusives.

Cretaceous granodiorite (Kgr)

- Found in some of the deep wells in the geothermal field;
- Likely correlates with plutonic rocks outcropping on the western and eastern sides of the Stillwater Range in New York Canyon and Job Canyon, respectively;
- Observed in the wellfield within the footwall block of a major piedmont fault (see Section 2.2.2) in fault contact with Jurassic rocks; and
- Shows some evidence of fracturing under high differential stress as seen in bottom of well 36-14 (see Section 6.3.2); however lack of permeability and significant production in this unit in the DVGW indicates that fractures in this rock type may be prone to sealing or the existing wells have not crossed a fault/fault zone where these rocks are fractured and these fractures are open. Thus, this unit is regarded as a strong EGS candidate.

Table 1. Generalized Dixie Valley and Stillwater Range Stratigraphy (compiled information from Waibel, 1987, 1999; Lutz et al., 1997; Denton et al., 1980).

Age	Lithology	Thickness
Pliocene to Recent	Basin-filling sediments composed of colluvial gravels, alluvial gravels, sands, and silts, eolian sands and silts, and lacustrine and playa silts and clays.	Up to 2,450m (8038ft)
Miocene 8-15 Ma	Basalt lava flows, agglutinates, scoria, and palagonite tuffs. Lava caps the range at elevations of up to 2500 meters and occurs in wells beneath 1830 to 2134 meters of basin-fill sediments.	90m (295ft) to > 580m (1902ft) in wells, up to 1000m (3280ft) in outcrops in Stillwater Range
	Lacustrine volcaniclastic sediments intercalated with carbonaceous siltstone; tuffaceous sediments	<152m (~500ft)
Oligocene	Silicic welded tuffs that crop out in the Clan Alpine and Stillwater Ranges, and are found below basin-fill sediments in wells.	1220m (~4000ft) in Clan Alpine Range, <300m (984ft) in Stillwater Range, <55m (180ft) in wells.
Cretaceous	Granodiorite, observed in deep wells in the geothermal field, and correlated with a pluton that outcrops on the west and east sides of the Stillwater Range.	N/A
Jurassic	Mafic complex – oceanic rocks: basalts, keratophyres, trondhjemites, albitites, plagiogranites, and gabbros.	Up to 760m (2493ft) in Stillwater Range
	Boyer Ranch Formation. Marine shelf and slope sediments - mostly quartzite, carbonates and minor conglomerate.	
Triassic	Winnemucca Formation: feldspathic metasandstone to arkose. Star Peak Group: marine sediments, carbonaceous shale, siltstone, silty carbonate rocks and massive, clean limestones.	≤3050 (10,004ft)
	Phyllite sequence, extensive black slates and shales.	>1000m? (3280ft?)

Cenozoic silicic volcanic units, associated intrusives, (Tv) and Miocene basalts (Tmb)

- Tilted and eroded silicic volcanic rocks overlie the Mesozoic basement rocks in the Stillwater and Clan Alpine Range (Figure 5) and are also found lying below valley-fill sediments in Dixie Valley;
- Show contemporaneous magmatism and extension with a close spatial and temporal relationship of eruption and tilting as evidenced by paleomagnetic data and K-Ar age dates (John, 1995);
- Contains Oligocene aged silicic volcanics (ash-flow tuffs and breccias) as well as interbedded volcaniclastics and occasional flows;
- Silicic volcanics exposed in the southern part of the Stillwater Range, south of the Dixie Meadows Hot Springs area and in White Rock Canyon (Figure 1), contains a tilted and eroded sequence of middle Cenozoic silicic ash flow tuffs, the associated caldera, and a subvolcanic granitic pluton (John, 1995). These silicic rocks comprise a large area of Tertiary volcanics (Tvl and Tvu in Figure 5) in the southern part of the range. This caldera may be the source of some or all of the silicic volcanic rocks present in the Clan Alpine Range and Pirouette Mountain area, at depth in Dixie Valley, and above the Mesozoic rocks in the Northern Stillwater Range
- Within Dixie Valley, the silicic sequence present in the wellfield below the basin-fill is overlain by Miocene lake deposits, which is in turn overlain by Miocene-aged basalt; and
- Capping the Stillwater Range, the Miocene Table Mountain basalt (Lutz et al., 1997) is a nearly flat-lying (dips up to 5°N) resistant series of basaltic to andesitic flows overlying intermittent volcaniclastics, lacustrine sediments and basement. The Miocene basalt represents the youngest volcanic unit in the area and is also found at depth within the Dixie Valley wellfield.

2.1.2 Basin Lithology (Q-Tbf)

The Dixie Valley basin-fill is composed of moderately-to-poorly lithified sediments derived from the surrounding mountain ranges. The basin-fill is at least 2500m (8200ft) thick based on wells that reach the underlying volcanic rocks. These underlying volcanic rocks include Oligocene rhyolitic pyroclastic deposits (ash flow tuffs and air-fall deposits) which correlate to welded silicic tuffs that crop-out in the Clan Alpine and Stillwater Ranges. Miocene (8-15Ma) basalt flows and lacustrine volcaniclastic deposits overlie the Oligocene section. The overlying poorly lithified sediments include coarse colluvium and alluvial fan deposits, sandy and silty eolian deposits, and lacustrine and playa deposits. Lacustrine and playa sediments include fine-grained clays and silts in the deepest parts of the basin, and sands to gravels in shoreline beaches and bars developed at and near lake margins. A summary of the basin-fill within the producing area of the DVGW is as follows:

- ~2000m (6560ft) thick in the non-productive DVPP area (Figure 1) area; ~2500m (8200ft) thick to the northeast in the productive DVPF;
- Unsorted conglomerate, alluvial gravels, sands and silts, and coarse colluvial deposits;
    - Increase in tuffaceous better sorted sediments toward the lower section;
    - Clay matrix: contains abundant expandable smectite with some geothermal alteration to non-expandable illite;
- Miocene Basalt (8-15Ma) underlies the basin-filling sediments and is bounded by major NE-trending valley-bounding faults:
    - Thickness in wells range from ~90m (300ft) to more than 580m (1900ft);
    - Overlies Miocene lacustrine sediments; and
- Oligocene silicic welded tuffs as thick as 300m (980ft) in the Stillwater Range and overlying lacustrine, carbonaceous sediments underlie the basalt and the intermittent lacustrine sediments.

2.2 Structure

2.2.1 Tectonic History

The B&R has undergone a dynamic tectonic history beginning with a passive continental margin setting during the early Paleozoic that followed late Precambrian rifting. Accretionary events expressed by a series of orogenies, due in part to changing configurations of offshore plate boundaries included the Devonian-Mississippian Antler orogeny, the Triassic Sonoma orogeny and the Jurassic to Cretaceous Nevada Orogenies (Dickinson, 2006). In the Stillwater Range, the Boyer fault and Fencemaker thrust, are evidence of the last in this series of crustal shortening events. The B&R underwent an additional prolonged period of compressional thickening expressed by the Sevier and Laramide orogenies during the Mesozoic and early Cenozoic as the province was located in a retro-arc position. Waibel (1987) has described the structural history as exposed in Dixie Valley and identified three main phases of deformation namely thrust faulting, early normal faulting, and current high angle normal faulting. The salient highlights of this work is outlined below.

Late Jurassic thrust faulting

- Triassic shelf-related marine sediments are overridden by Jurassic oceanic crustal rocks and quartzite;
- Horizontal cataclasite zones and small scale mélange-like features within localized shear zones are associated with the thrust faulting;
- Quartzite (Boyer Ranch Fm) associated with the Boyer Ranch Thrust lies over Upper Triassic slate and Lower Jurassic rocks. The structure, exposed in the Stillwater Range, is truncated by the range-front fault adjacent to the northern producing area and is possibly intersected by an injection well (38-32);
- Triassic to Jurassic marine siltstones, shales and volcaniclastic rocks are associated with the western originating Fencemaker Thrust overlying older rocks (Lutz et al., 1997). The low angle structure pinches out just north of the geothermal field and is likely encountered within the producing field (Lutz et al., 1997), see Figure 16A.

The Dixie Valley region appears to be structurally quiet from the Cretaceous through the Oligocene. In other words, no deformation is evident in the Project Area during these time periods.

Basin & Range crustal extension

- Series of early (pre-8 Ma) north-trending normal faults:
    - Exposed in the Stillwater and Clan Alpine Range as major north-trending structures;
    - Expressed as "early" narrow graben structures with north-striking trends continuing into Dixie Valley and buried beneath valley fill sediments based on geophysical data;
    - Show likely re-activation of some normal faults with a dextral strike-slip component under current stress regime;
    - Have been active before and after Oligocene silicic volcanism;
    - Shows evidence of rotation and listric faulting;
    - Contains N- to NNW-trending segments of the main range-bounding fault relating to early extension sealed under the current stress regime while NE-trending segments remain open (Lutz et al., 1997); and
    - Contain Miocene alteration, sericite (iilite) and wairakite veins, events associated with N-NNW faulting and the intrusion of andesitic dikes during the initial stages of BR extension in northern Dixie Valley (Lutz et al., 1998).
- Northeast trending, late Cenozoic high angle normal faults:

- Define the Stillwater Range and Dixie Valley physiographic features;
- Truncate the older north-trending structures preserved in the ranges;
- Uplift of the Stillwater Range occurred after eruption of the Miocene basalts;
- Contain younger carbonate alteration along NE striking segments of the Stillwater Fault normal to the present day extension direction (Lutz et al., 1997);
- Show WNW-ESE direction of extension superimposed on earlier E-W extension with the onset following late Miocene to early Pliocene basalt volcanism since about 8 Ma;
- Exhibits a likely strike-slip component along older N-striking faults; and
- Show localized zones of tension/compression due to combination of dip-slip (NNE faults) and strike-slip (N faults) movement.

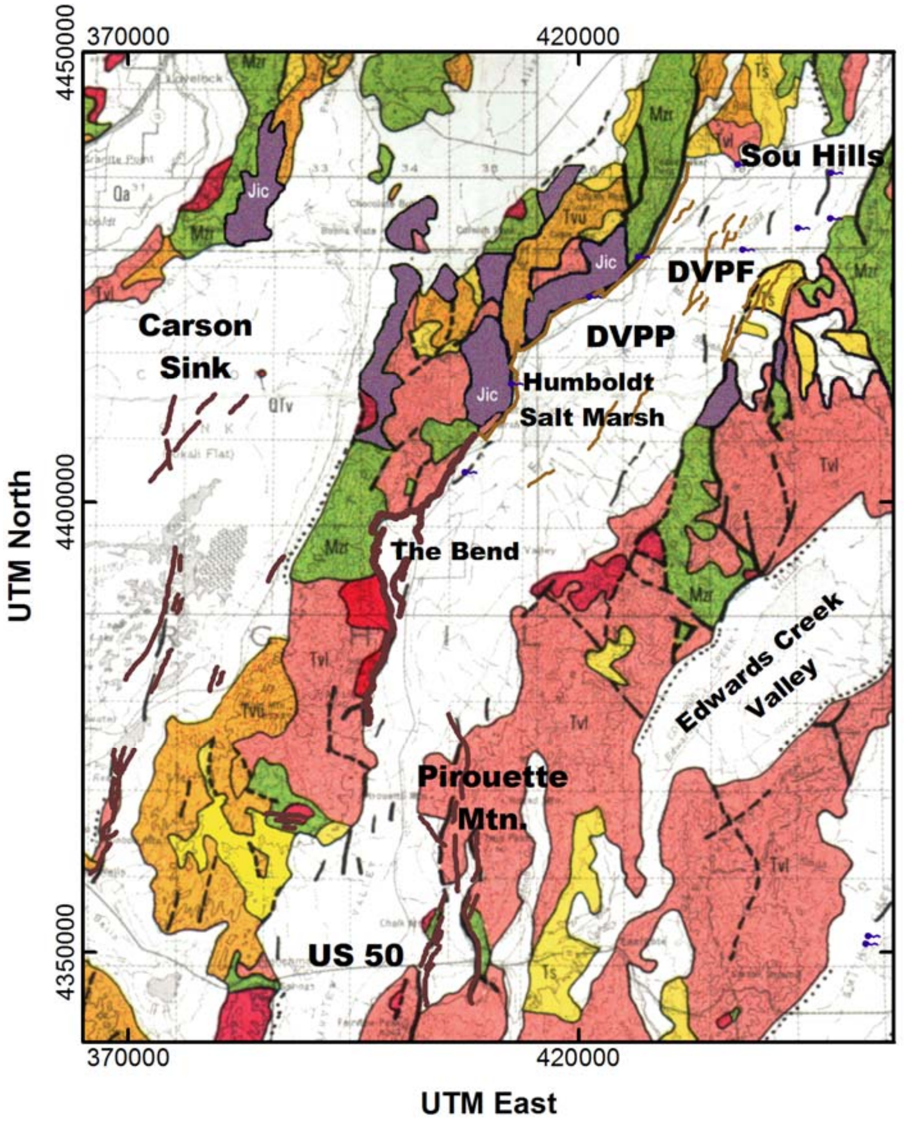

Figure 5. Bedrock Geology Map, modified from 1:1,000,000 Nevada Bureau of Mines and Geology map (Stewart and Carlson, 1977). Bright red denotes intrusive rocks; oranges are Cenozoic volcanics; yellow represents Cenozoic sediments, green represents Mesozoic sediments; purple represent the Jurassic section including the Humboldt igneous complex. Thick brown lines are 1954 fault breaks and thin light brown lines are other valley faults. The figure and caption are after Blackwell et al. (2005).

LEGEND

Mz sediments (Mzr)
Jz section/Humboldt igneous complex (Jic)
Intrusives (red)
Cz volcanics (Tvl;Tvu)
Faults (brown)

2.2.2 Structural Setting of the Dixie Valley Fault Zone

Early structural models for Dixie Valley (Okaya and Thompson, 1985; Benoit, 1999) identified a single, moderately east dipping (~54°) normal fault bounding the Stillwater Range on its eastern side, referred to as the Dixie Valley Fault (DVF). The single fault model was based on surface fault measurements, initial interpretation of the seismic data (e.g. profile SRC-3 in Section 3.5.1, Figure 17B), and the assumption that the producing wells located a few kilometers basinward were connected to the surface scarp of the range-front fault. Blackwell et al. (2005) proposed a steeply dipping, more complex structural setting consisting of a range-front fault and a piedmont fault based on wellfield data (see Sections 6.3.2 and 7) and gravity and magnetic data (see Section 3.1 through 3.5). This complex fault zone is referred to as the DVFZ; see discussion below. In the DVGW, the evidence favors two or more steeply dipping faults for the DVFZ; however, >20km (12mi) to the south, at Dixie Meadows, seismic-profiles have been interpreted by Abbott et al. (2001) to support the hypothesis that the range-front fault segment of the Dixie Valley Fault Zone (DVFZ) is a seismically active, low angle normal fault (Figure 6a). Because Dixie Meadows is in the southernmost portion of the project area, this apparent controversy is significant to this study.

The Dixie Meadows area is at the northern end of a NNE-striking DVFZ segment that produced the 1954 Fairview Peak-Dixie Valley seismic event (see Section 2.2.2). Based on two seismic lines in the area, Abbott et al. (2001) interpreted a 25-30°SE dip~ 10km (6mi) south of Dixie Meadows. Based on this interpretation, Kennedy-Bowdoin et al. (2004) also showed the range front fault with a ~35°SE dip at Dixie Meadows. Geophysical data suggests a more complex multi-fault setting at this location. Well 45-14, 10km to the north and the southernmost well in the DVGW, lies adjacent to a major north-striking structure within DVFZ that didn't rupture during the latest seismic event and encountered lithologies that require steeply dipping faults, as it lies within a structural block between a north-trending segment of the range front fault and the piedmont fault; see Section 5.3, 6.1.1 and 6.3.2 for a more detailed discussion.

There are two possible explanations for the interpreted change in dip from near vertical at 45-14 to low angle at Dixie Meadows and to the south:

1. The dip change over the 10km gap is accurate. The change in dip could have stopped the 1954 event rupture and may also be related to the change in fault strike from NE to N. This would also suggest that an accommodation zone between the intervening structures is present at Dixie Meadows as evidenced by numerous surface springs.
2. The seismically-inferred low angle fault could have been a mis-interpreted basalt reflector, a shallow dipping bedrock contract between the range front and piedmont fault, a buried landslide plane or a step-down zone of faulting that agrees with the general trend recognized along the DVFZ. Because our Project Area mostly coincides with the seismic gap (see Figure 6a) and not the 1954 earthquake segment, we do not need to decide between the two explanations here. However, a planned seismic survey in the area (under Task 4) may provide additional insight. The baseline conceptual model (Section 7) postulates a steeply dipping multi-fault model along the entire length of the DVFZ through the DVGW as required by the geologic, drilling, and geophysical evidence available within the Project Area.

The DVFZ is considered to be a series of step-down faults (complex system of subparallel steep dipping faults) including faults within the Stillwater Range, at the topographic break between the range and the valley (the range-front fault) and the piedmont faults east of the range front within Dixie Valley (Wallace and Whitney, 1984; Blackwell et al. 2005). Empirical evidence strongly suggests, and Blackwell et al. (2005) show that the DVFZ is complex fault zone, dominated, though not completely composed of, strands of steep normal faults. To the south of Hare Canyon (see Figure 1 and 6a, adjacent to Dixie Hot Springs [HS]) the 1954 fault scarps suggest much longer strands of normal faults than are observed to the north, from between Hare Canyon and the northern end of Dixie Valley. A generalized cross section within the DVPF (Figure 6b) shows a set of steeply dipping structures representing the DVFZ bounds the western edge of Dixie Valley. Within the range young, brittle, steeply east dipping normal faults cut the bedrock just west of the DVPF. Blackwell and others (Waibel, pers. comm., 2010) suggest these intra-range faults possess thermal significance due to the exposed hydrothermal alteration and zones of fumarole activity as the structures are considered to play an important role in the range structure. A complex system of steeply dipping normal faults has been mapped (see Figure 14) adjacent to the DVPF that show evidence of recent alteration (Plank, 1998). Mapping efforts and cross-sections from Gabe Plank (GBC Workshop, 2002) show only one possible active intra-range fault in this area, and considers the other faults in the range to be inactive splays of the main fault, which is common in extensional areas.

Besides the main, well exposed range-front fault bounding the western edge of Dixie Valley, a major steep piedmont fault and other discontinuous strands of normal faults occur a few kilometers basinward. The term piedmont fault, used by Blackwell and others to define the zone of faulting occurring parallel to the range-front within the pediment surface (alluvial slope derived from the range), applies to a blind fault/fault system that doesn't break the surface like the well-exposed range-front fault. Geophysical and drilling data (described in Sections 3.1, 3.2 and 6, respectively) provide evidence that this piedmont fault takes up the majority of the normal displacement along the structure and plays a crucial role in the producing field. The piedmont fault is buried by a thin cover of sediments and shows no surface expression. Within this report, the DVFZ refers to the 2-4km (1.2-2.5mi) wide zone of deformation bounding the northwest edge of Dixie Valley including the active intra-range faulting, the range-bounding fault, a major piedmont fault, and other associated faults and fracture zones.

Dixie Valley Fault

The Dixie Valley Fault (DVF), also referred to as the Stillwater Fault (SF), occurs along the western side of Dixie Valley and represents the main surface-bearing and range-bounding component of the DVFZ. The fault separates the bedrock of the Stillwater Range from the late Cenozoic sediments that fill the basin. Where exposed at the surface, the fault is steeply dipping to the east. The fault is one of the most active faults in the B&R with the most recent activity occurring as the Dixie Valley-Fairview Peak earthquake in 1954. The long-lived structure (intermittent for several million years) is marked by historic, Holocene, and/or Pleistocene fault scarps that cut and mostly vertically offset late Pleistocene and early Holocene alluvial fans and pediment surfaces. The trace of the fault extends from the southwest side of the Sou Hills at the north end of Dixie Valley (Figure 1) to the south end of the valley about 10km (6mi) north of highway US 50, a distance of about 80km (50mi). Other implications of the DVF are listed below.

- The DVF is the primary range-bounding, normal fault, between the Stillwater Range and Dixie Valley;
- The maximum total vertical displacement between the Stillwater Range and bedrock beneath Dixie Valley sediments in this target study area is approximately 3000m (9800ft), since Late Miocene, based on the top of the elevation of Late Miocene basalt flows observed in the Stillwater Range, and the depth these basalts were intersected in some of the deep wells in the producing field; and
- Deep pull-apart zones occur along the western edge of Dixie Valley and are associated with the most recent extensional regime (WNW-ESE). These pull-apart structures show the greatest vertical off-set, including the 3000m off-set in the Miocene basalts mentioned above. This amount of normal fault off-set is not a continuous characteristic of the DVFZ.

Seismicity

The DVF is part of a 250-km (154-mi) long system of faults in Nevada that have experienced historic surface rupturing earthquakes and that help to define the Central Nevada Seismic Belt - CNSB (Figure 3). The historical seismicity of Dixie Valley has been well-studied (see Section 3.5). Nearby earthquakes include the:

- 1915 Pleasant Valley earthquake to the north, which ruptured on a westward dipping fault system that extends into the northernmost Project Area;
- July 6 and August 23, 1954 Rainbow Mountain earthquakes to the southwest;
- December 16, 1954 Dixie Valley-Fairview Peak earthquakes to the south of Dixie Valley; and
- The Fairview Peak earthquake (Mw=7.0) was followed a few minutes later by the Dixie Valley earthquake (Mw =6.8) as the event propagated (south to north) into southern Dixie Valley. The northernmost ruptures terminated near Dixie Meadows.

Surface ruptures produced from these seismic events bound the western edge of Dixie Valley and include the 1954 break, 1915 ruptures within northern Dixie Valley and surface traces relating to a pre-historic “Bend Event” occurring during Holocene time (2.2 – 2.5 ka), Figure 6a.

Stillwater Seismic Gap (SSG)

The Dixie Valley geothermal system lies adjacent to a 45-km (28-mi) segment of the DVF, along which no evidence for recent surface-rupturing faulting has been found. This segment referred to as the Stillwater Seismic Gap, is between the 1915 Pleasant Valley and 1954 Dixie Valley earthquake rupture zones (Caskey and Wesnousky 2000). It was informally reported at the GBC Geothermal Workshop in 2002, that a vigorously spouting geyser briefly formed above the geothermal system during the 1954 seismic event. While this is based on unverified reports as the area was largely uninhabited at the time, this supports the opening of permeable pathways at depth within the Stillwater Gap during seismic events, regardless of if the rupturing produced a surface trace. Characteristics of the SSG include:

- No evidence of Holocene/historic surface ruptures has been found;
- Seismic creep may relieve stress and maintain fracture permeability or displacement is accommodated by a buried structure;
- Alternatively, faulting could have been confined to the range block where it would be more difficult to find and assign a date to; and
- The “Bend Event” (2.2-2.5 ka) likely propagated through this area, but is now eroded (Figure 6a).

2.2.3 Intra-basinal Faulting

Additionally, a number of intrabasin faults not directly associated with the DVFZ have also been recognized and assumed to play a role in accommodating extension within the valley. This includes the Buckbrush Springs fault system, a major surface-bearing system of intrabasinal faults, located basinward to Dixie Meadows on the eastern edge of the Humboldt Salt Marsh and south of the producing area (Figure 6a). The majority of the intrabasin faults are northeast striking, show mostly eroded surface expressions, are often associated with springs, cut alluvial sediments, and are interpreted as both east dipping and antithetic (west dipping) with a down to the west displacement direction. Major west dipping intrabasin faults bound the southeastern edge of the valley-fill sediments and underlying volcanics in Dixie Valley. Additionally geophysical evidence and surface scarps show that the major north-trending structures present in the Stillwater Range also continue into Dixie Valley. A more detailed discussion on these intrabasin faults within Dixie Valley is in the following Geophysics section, as they are mostly recognized by geophysical methods.

This structural section has focused on pre-existing work and interpretations that represent the general consensus of the structural setting in Dixie Valley. Models have been introduced that are no longer relevant in order to complete the discussion of the public domain data. While most work has previously referred to the major structure as the DVF or SF, herein the authors have introduced and described a complex set of steeply dipping structures consisting of two of more faults and referred to as the DVFZ. A re-interpretation of the structural data will be presented within Section 7 of this document that represents recent analysis from the AltaRock Team. Additionally, major observations are noted that describe the interaction and significance of the presently-active northeast trending structures with the earlier set of north-trending structures. These interpretations are the first attempt to characterize the relationship between the intersection of major fault trends that produce zones of compression and dilation in the DVFZ, and the relation to the occurrence of geothermal cells in Dixie Valley.

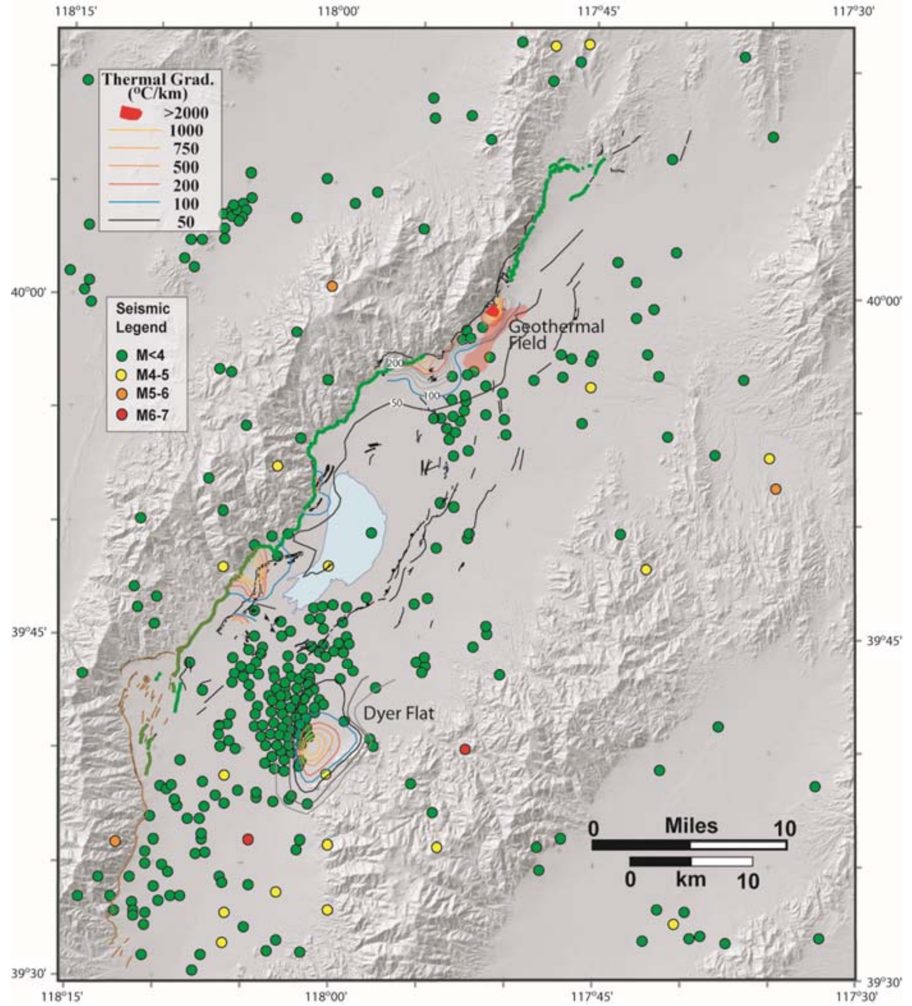

Figure 6A. Presented are the area seismicity, faults, earthquake epicenters, geothermal gradient, and range front fault scarp. Brown line represents northernmost surface ruptures of the 1954 Dixie Valley-Fairview Peak earthquake sequence; Green line represents the Bend Event (~2.5ka), which corresponds to the Stillwater Seismic Gap. Clusters of earthquake epicenters (dots) occur near the Dyer Flat thermal anomaly and south of the DVPF. Both are near where the intrabasin fault system joins the Dixie Valley fault system and an area of high geothermal gradients. The figure and caption are from Blackwell et al. (2005).

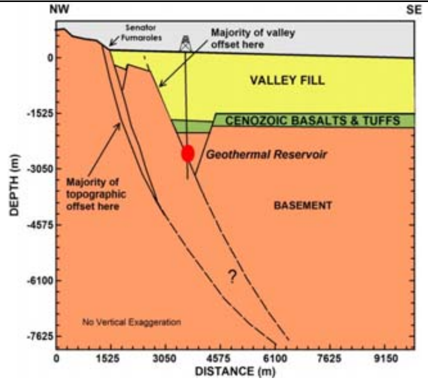

Figure 6B. Simplified cross section of Dixie Valley Producing Field showing valley fill sediments, Cenozoic volcanics deep in the section, basement and interpretation of fault structure (dashed lines). The figure and caption are from Blackwell et al. (2005).

2.2.4 Stress Modeling

Caskey et al. 2000 and Wesnousky et al. 2003 performed a detailed study on fault slip and the required stress conditions that would result from the 1915 Pleasant Valley ruptures and the 1954 ruptures and seismic activity on the Dixie Valley Fault (range-front fault segment), assuming that no slip occurred along the Stillwater Seismic Gap. The study assumes a single fault model with a 50° dip, although the majority of evidence presented herein agrees that extension is accommodated along several steeper dipping structures within the DVFZ. It is likely that slip occurred on piedmont faults within the Stillwater Gap segment of the DVFZ during the latest 1954 seismic event, which would significantly lower the expected accumulated stress in this area. The geothermal field is located within the central portion of the Stillwater Seismic Gap, where no surface rupturing has occurred from the last two major seismic events. Some main points from this analysis are described below and shown in Figure 7.

- The analysis determined an increased failure stress on faults and fractures associated with the geothermal reservoirs with contributions from both increased shear stress and decreased fault-normal stress;
- Large increases in failure stress are concentrated between the Holocene rupture endpoints of the DVF, i.e. range-bounding fault segment of the DVFZ;
- Fault-parallel fractures within the DVFZ are critically stressed for failure and hydraulically conductive within the geothermal field;
- The larger stress changes occur at the north and south ends of the seismic gap near the rupture endpoints (>5 bars); and
- The DVFZ and parallel fractures in the vicinity of the DVGF have experienced large positive stress changes (>10 bars) and are most strongly affected by tensile stress changes.

A re-interpreted Stress Modeling analysis that builds on this model and assumes slip did occur within the SSG can be found in Section 7.2.2.

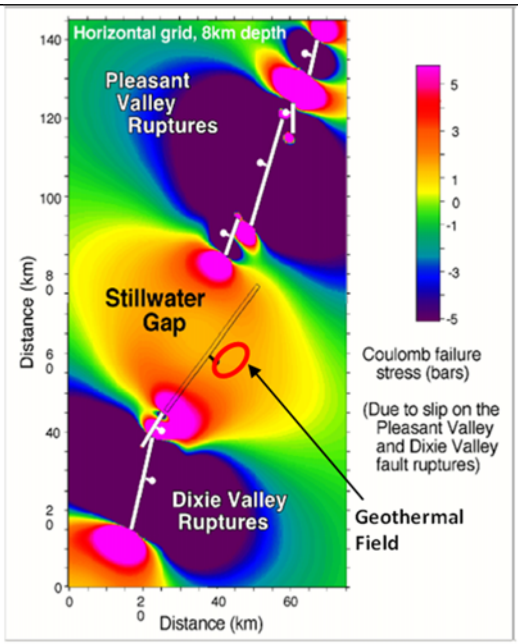

Figure 7. Coulomb failure stress changes in the Stillwater Gap associated with slip on the 1925 Pleasant Valley and 1954 Dixie Valley earthquakes ruptures (shown as white dislocations). Slip on the dislocations is constrained from detailed field studies of fault slip (Caskey et al., 1997; Wallace, 1984). Transparent dislocation represents the Stillwater Gap portion of the Dixie Valley fault. Calculations are shown on a horizontal grid at 8km (5mi) depth, for a friction coefficient of 0.75 and resolved on 038° 50SE oriented normal fault planes (same as Dixie Valley fault in the Stillwater Gap) along a -90° rake (dip slip direction of slip). The Dixie Valley geothermal field is shown. The figure and caption are from Caskey et al. 2000.

3. Geophysics

A variety of geophysical data collected in the Dixie Valley area and specifically within the wellfield were detailed in the Blackwell et al. 2005 comprehensive report. These surveys included Gravity, Magnetics, Magnetotellurics and Seismic, Thermal Modeling, and a variety of remote sensing techniques. The important aspects and results are presented in this section.

3.1 Gravity

Complete Bouguer gravity anomaly data was obtained from three public domain sources: (1) USGS Gravity Data of Nevada (Ponce, 1997); (2) UTEP PACES GEONET Gravity and magnetic data set repository - Gravity and magnetic data base of the United States http://irpsrvgis00.utep.edu/repositorywebsite/; and (3) gravity surveys compiled by David Blackwell at SMU (pers. comm., 2010). A complete Bouguer anomaly (CBA) map of the region (Figure 8); shows positive values within the ranges (bedrock) and negative values in the valleys (poorly consolidated sediments) arising from distinct density contrasts. Thus the regional gravity data defines the shape of the Dixie Valley basin and confirms that the basin is asymmetrical. There appears to be little evidence of a distinct regional trend.

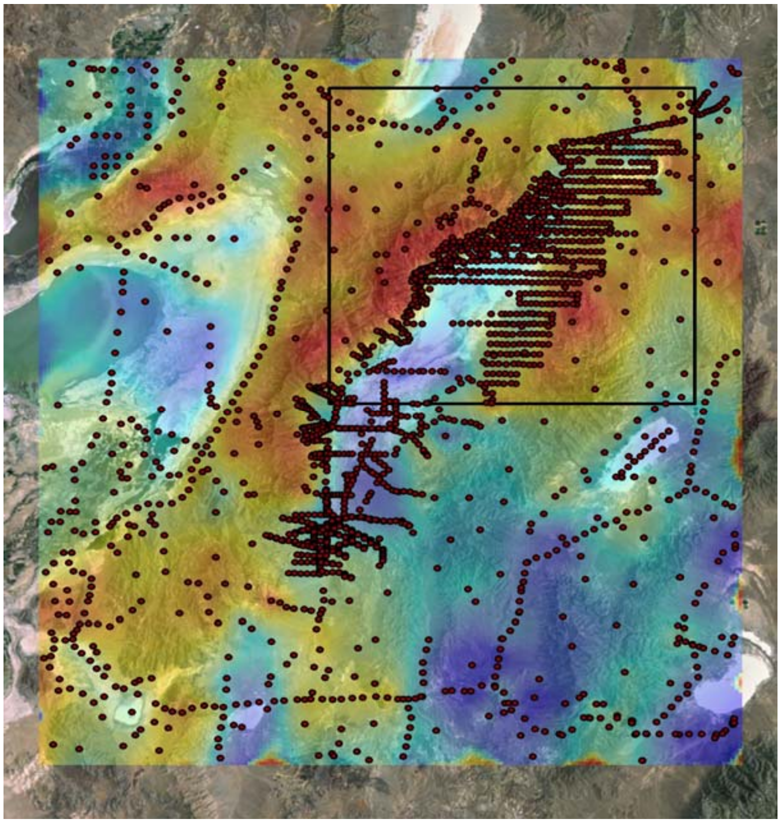

Figure 8. Complete Bouguer anomaly map of the region around Dixie Valley, NV. Highs (warm colors) correspond to the bedrock in the ranges, while lows (cool colors) represent loosely consolidated basin fill sediments. The color scale ranges from -129 to 0233 mgal. The Project Boundary is shown in black. The location of gravity stations are shown as red dots.

The horizontal gradient of the gravity field is particularly useful in locating contacts of greatest density contrast, with a high peak shown over sharp, vertical edges, which are presumably buried faults. A map detailing the maximum horizontal gradient shows the regions of gradient maximas (warm colors) occur along intrabasin faults as well as along the main range front fault (Figure 9A). The maximum horizontal gradient map is compared to the total magnetic anomaly map in Figure 9B.

A continuous gravity gradient occurs on the west side of the valley parallel and basinward to the range front fault and defines the main structural offset between the basement and valley fill. The location coincides with segments of the fault imaged by the aero-magnetic data (see section 3.2 and Figure 11) and strongly implies that the major piedmont faults within the valley accommodate most of the displacement between the range front and the valley bottom. The east side of the basin does not have a clearly defined gravity gradient maxima due to a number of potential factors including higher rates of subsidence, widely spaced displacement faults described as a zone of step-faulting (Wallace and Whitney, 1985; Blackwell et al. (2002; 2005), and the occurrence of large bodies of mafic rock beneath shallow basin-fill sediments that control much of the gravity signature. Salient features of the gravity data are:

- Emphasizes the asymmetry of the basin and confirms that the western side of Dixie Valley is fault controlled along a steeply dipping structure;
- Location of the maximum gravity slope is generally offset (1-3km [0.6-1.9mi]) into the valley from the range-valley contact and main range front fault;
- Major piedmont faults parallel to the trace of the range-front fault accommodates most of the displacement along the structure. These faults are where most of the geothermal producing wells are found; and
- While the principal fault trend is NE-SW, a gradient high in the south-central valley shows a more northerly trend, perhaps representing an earlier rifting episode when maximum stresses were oriented N-S (Figure 9A).

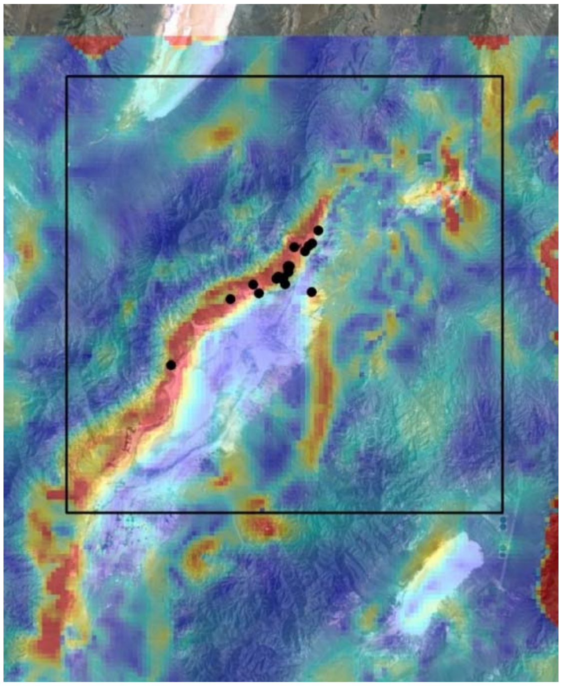

Figure 9A. CBA Total Horizontal Gradient of Dixie Valley. Well locations are shown by black dots, within the EGS ExplorMetodology Project Area area (black outline) superimposed. Warm colors represent areas of dense horizontal gradients.

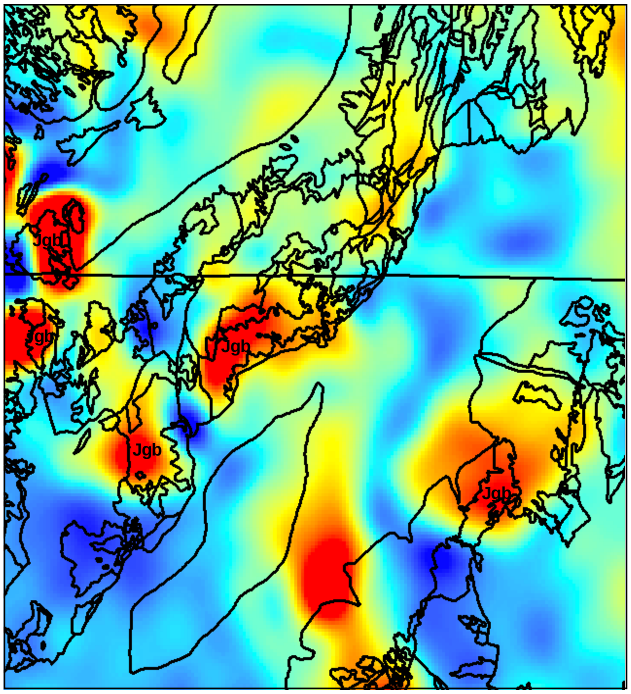

Figure 9B. Outline of geologic formations overlain on a total magnetic anomaly map of PACES data. Magnetic highs are primarily associated with exposed Jurassic igneous rocks (Jgb) in the Stillwater and Clan Alpine ranges.

3.2 Aero Magnetics

Aeromagnetic data were obtained from four sources: (1) The USGS magnetic database of North America (here referred to as the PACES) which was continued to a 300m (980ft) elevation (UTEP PACES GEONET http://irpsrvgis00.utep.edu/repositorywebsite/, 2011); (2) a USGS-sponsored helicopter survey of Dixie Valley (here referred to as HELIMAG) flown at 120m (390ft) (Graugh; 2002; http://pubs.usgs.gov/of/2002/ofr-02-0374/); and older aeromagnetic surveys flown by fixed wing aircraft at 1680 and 2290m (5500 and 7500ft) (Blackwell, pers. comm., 2010).

The total field anomaly map of the region shows discrete sub-circular magnetic highs (Figure 9B). The mafic Jurassic volcanics appear to be the only strongly magnetized units in the Dixie Valley area. In the Stillwater and Clan Alpine Ranges, the magnetic highs are almost exclusively associated with the Jurassic volcanic units, especially gabbros. The shape and intensity of the highs suggests that the volcanic units are positively magnetized which is consistent with their emplacement during the normally magnetized Jurassic Quiet Zone period. A number of magnetic highs are observed in Dixie Valley which presumably are associated with buried Jurassic igneous rocks. The distribution of Tertiary volcanics shows only a weak spatial correlation to the anomalies except in one case, while the widely distributed Tertiary rhyolites and limited Cretaceous granite exposures show no spatial association.

Graugh (2002 a,b), Smith et al. (2002), and Blackwell et al. (2007) analyzed the high resolution HELIMAG data within Dixie Valley to delineate intra-basin faults which may provide permeable conduits for geothermal fluids (Figure 10). The horizontal gradient method when applied to the data reveals steep magnetic gradients over near-vertical contacts (faults), shown on the horizontal gradient map as long narrow ridges (Figure 11A). Some of the shallow faults imaged in aero-magnetic data directly correlate to the surface traces of mapped faults (Figure 11B). The position and distribution of faults indicated by the magnetic data and mapped surface faults are consistent with a dominant northeast trending fault pattern (Figure 11C). The set of faults defined by magnetic anomalies at shallow depths must be very young, late Pleistocene or Holocene, and thus must be part of the presently active B&R system of extensional faulting. While the aero-magnetic data does locate a number of intra-basin faults, it does not extensively image a large piedmont fault on the west side of the valley as expected by the gravity and well data (Blackwell et al., 2005).

3.2.1 Intrabasin faults

Conclusions of the HELIMAG aeromagnetic data in relation to intra-basin faulting are:

- Northeast trending, steeply dipping and sub-parallel to the range-front fault;
- Show curved and branching shapes;
- Turn to a more easterly strike in northern Dixie Valley (including range-front) indicating a change in fault geometry at the northern end;
- Terminate south of the survey area as motion and displacement is transferred to nearby faults (to the west or east); and
- A north-trending structure occurs on the eastern bounding edge of Dixie Valley and projects near well 62-21 (Figure 9A). It likely intersects the main Dixie Valley western-bounding structure within the northern producing zone and coincides with known surface faults. The total field magnetic data indicates that the magnetic highs correspond to the Jurassic igneous suite.
- The Humboldt Salt Marsh is the deepest part of the valley (surface) down-dropped by faulting within the basin;
- Faults broaden and branch into a classic “horsetail” shape at the southern strands of the Humboldt Salt Marsh; and

- The Marsh lies at the southern end of a deep structural block bounded by fault systems that are projected to merge near the geothermal field at its most northern end.

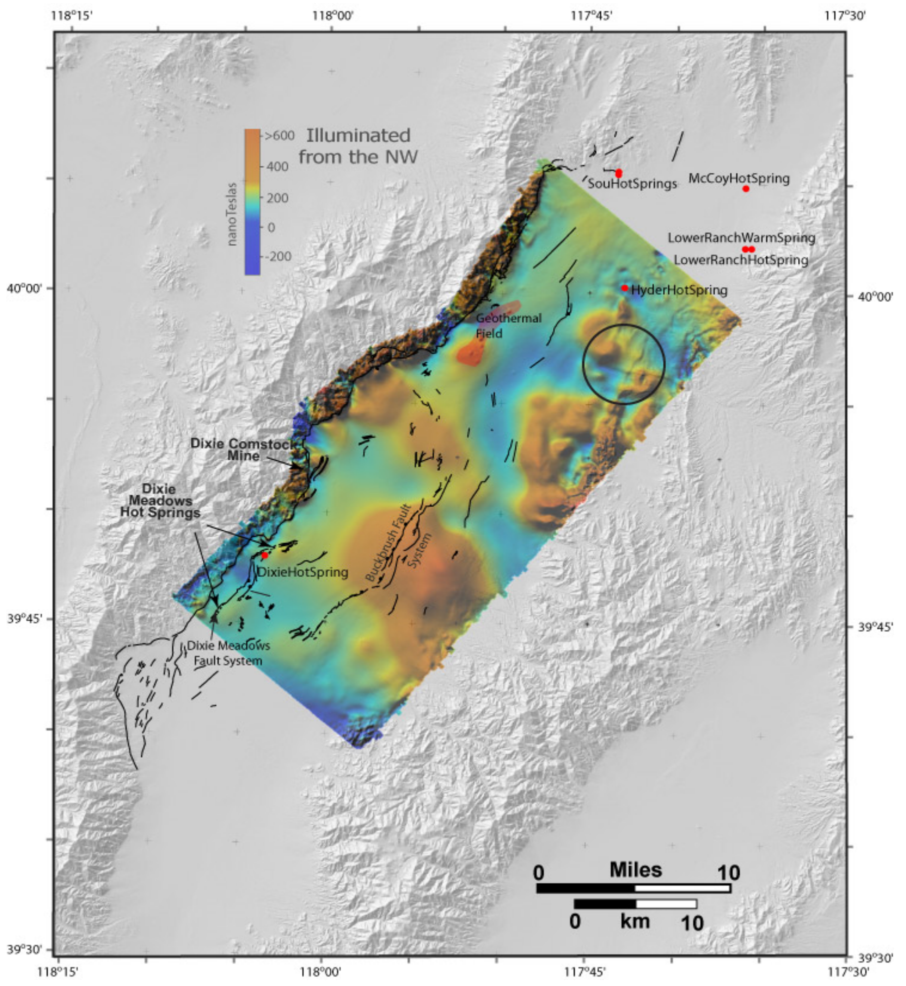

Figure 10. Reduced-to-Pole (RTP) low-level high-resolution aeromagnetic map and mapped faults superimposed on shaded relief topography. Note the strong NW-trending linear anomaly in the black circle and the Hyder Hot Springs "dimples" just N of the circle. The figure and caption are from Blackwell et al. (2005).

3.2.2 Magnetic Anomalies

Aero-magnetic mapping has the ability to image magnetic anomalies within the subsurface. Negative anomalies may result from the alteration of magnetic minerals along the walls of geothermal fluid channel pathways that transect mafic dominated sediments. Alternatively, they can also be linked to a high titanium (Ti) content in the mafic minerals making the mineral weakly magnetic and/or reversely magnetized rocks. Negative anomalies are present near Hyder HS in the northern valley and near Dixie Meadow HS (Figure 10). The smaller anomaly near Hyder HS suggests limited interaction of hot waters with magnetic wall rocks. The second area near Dixie Meadows lies within a higher geothermal gradient just southwest of the DVPF and suggests a higher degree and longer-lived geothermal system that has removed a large volume of magnetic minerals. The high-resolution aero-magnetic map (Figure 12) is focused within the DVPF and DVPP and salient features identified are:

- A large positive anomaly near the southern part of the geothermal field likely reflects strongly magnetic mafic rocks beneath the valley fill (occurring in the range directly to the west);
- A large negative anomaly (northern part of geothermal field) due to:
    - weakly magnetic sediments, reversely magnetized rocks; and/or

- destruction of magnetism by high temperature alteration of magnetic mineral.

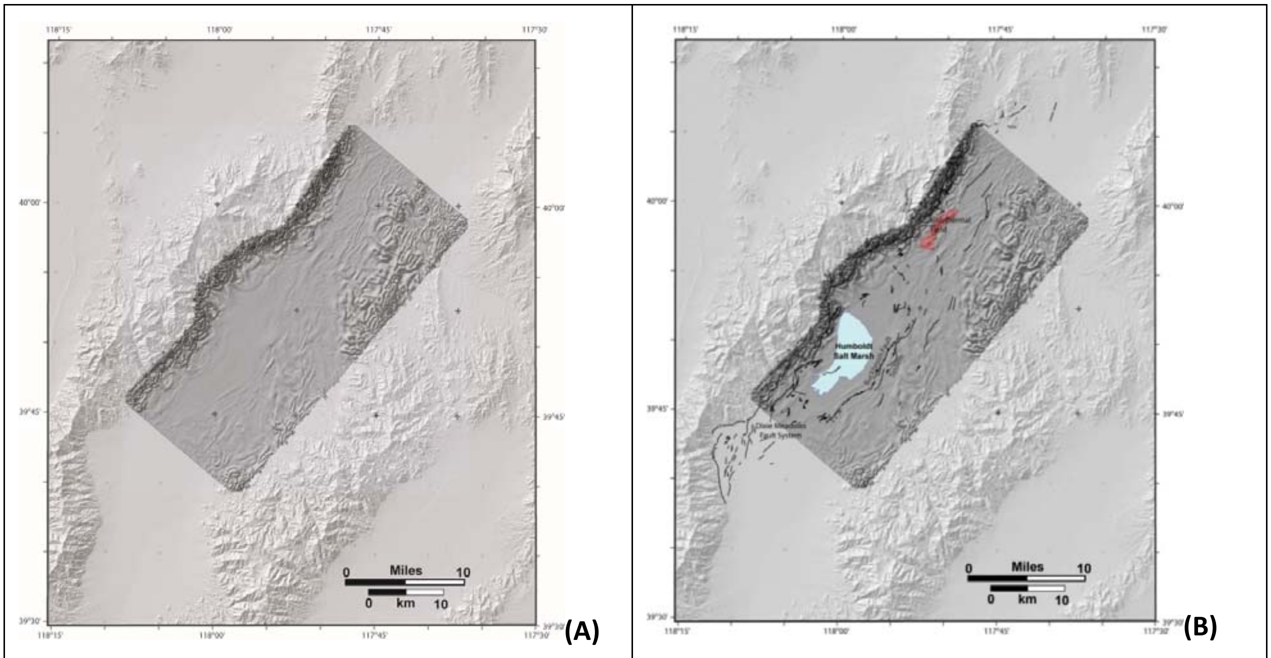

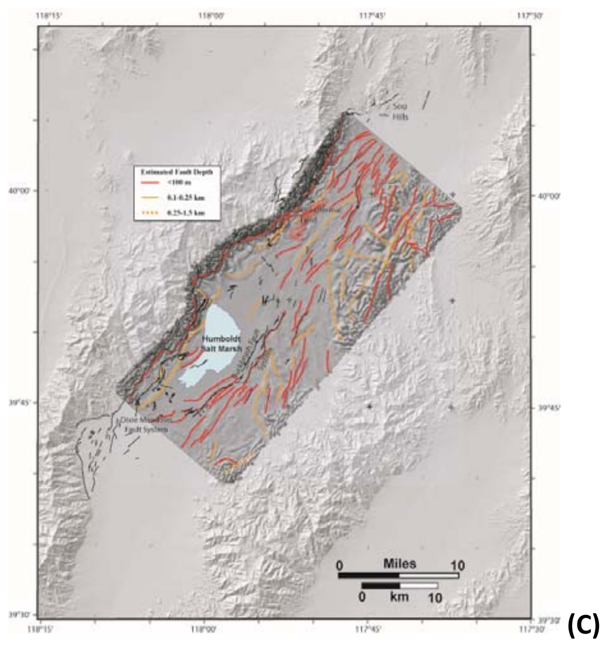

Figure 11. (A) High-resolution aeromagnetic survey and horizontal-gradient magnitude of pseudogravity map over shaded-relief lighted from NW; (B) horizontal gradient magnitude map with mapped faults superimposed; note that intrabasin faults with surface expression (black lines) correspond to several of the prominent linear aeromagnetic anomalies; (C) horizontal gradient magnitude of the high-resolution aeromagnetic survey showing the positions and distribution of faults indicated by the magnetic data, and faults mapped at the surface; black lines are faults mapped based on surface evidence (scarps, lineaments); red and orange colored lines are faults indicated by high-resolution aeromagnetic data. The figure and caption are after Blackwell et al. (2005) and modified after Grauch (2002).

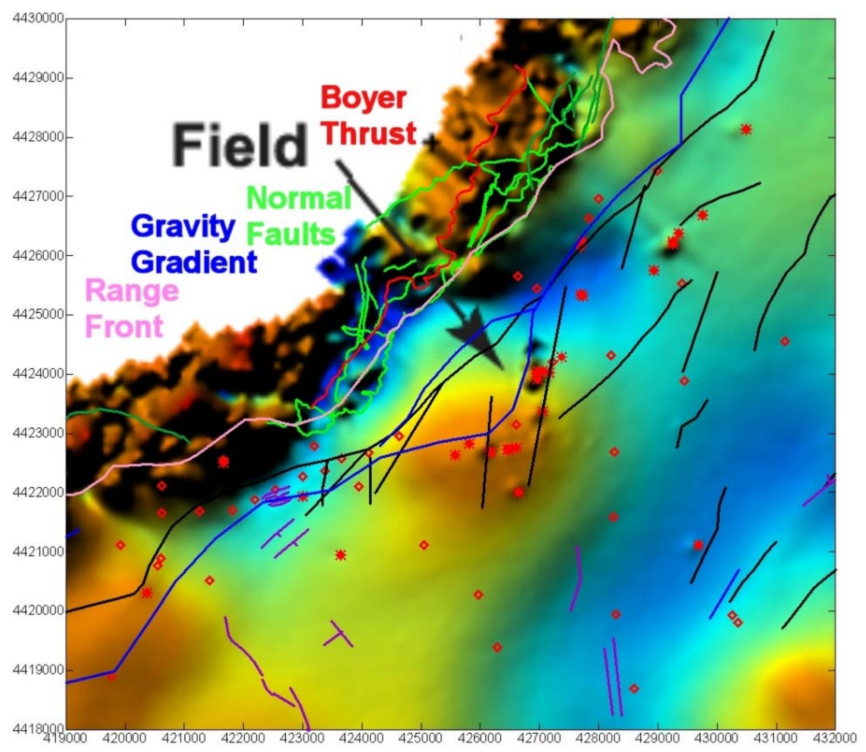

Figure 12. Detail of high resolution aeromagnetic map in the DVPP and DVPF areas (Figure 1) enlarged from Figure 10 and overlain with color-coded structures. Non-labeled features include: black lines are geophysical-inferred structures, purple lines are surface faults, red diamonds are temperature gradient holes (TGHs), and red stars are wells. The figure and caption are after Blackwell et al. (2005).

Dixie Valley Faulting

The combined horizontal gradients from both the gravity and magnetic data provide a detailed picture of the structure of Dixie Valley (Figure 13). The horizontal gravity gradient maximums show both north and north-east trends and coincide with surface faulting and the position of the horizontal gradients for the HELIMAG data. Smith and Blackwell (2001) have constructed a structure compilation map of Dixie Valley that shows the interpreted major structures indicated by the areas of dense gravity and magnetic horizontal gradients, seismic profiles and the surface geology (Figure 14). The faulting has been broken up into two dominant trends, north-east striking steep normal faulting reflecting the current stress regime superimposed over an earlier episode of north-south faulting. The importance of these two dominant fault trends and the significance of their associated intersections will be discussed in more detail in Section 7.2.1.

3.3 Gravity and Magnetics

The CBA gravity data and the HELIMAG aeromagnetic total field anomaly data representing the baseline gravity and magnetic data set were jointly modeled in along five lines labeled A-A’ to F-F’ in the geothermal area to create a 2½ D geophysical model consistent with the surface geology and well data (Figure 15A). The modeling was performed along pre-existing geologic cross-sections through the wellfield, with lines C-C’ through F-F’ lying perpendicular to the strike of the Stillwater Range and the Dixie Valley range-bounding fault and lines A-A’ and B-B’ parallel to the range. It was not possible to model the magnetics of the range-parallel line B-B’ because of 3-D effects due to the extensive Jurassic section exposed in the southeastern part of the range.

The modeling was performed by Dr. Bob Karlin, the Gravity and Magnetics Task Leader using a compilation of pre-existing data. Gravity modeling was done using the GM-Sys module of the Oasis Montaj program from Geosoft Inc. Measured gravity models of unknown shape were forward modeled by trial and error adjustment of density and polygon vertices. Once the fit was considered close, XZ positions were optimized using inverse methods. The objective was to minimize the RMS error between observed and computed values. A fit was considered acceptable if the misfit F was less than 1% (F=100*RMS error/profile gravity data range). As described in the GM-Sys manual, 2-D models may be visualized as a number of tabular prisms with their axes perpendicular to the profile; blocks and surfaces are presumed to extend to infinity in the strike direction. 2¾-D modeling, as implemented in GM-SYS, allows the prisms to be truncated at some distance in the plus and minus strike directions (± Y). It also allows the strike direction to be skewed relative to the profile azimuth.

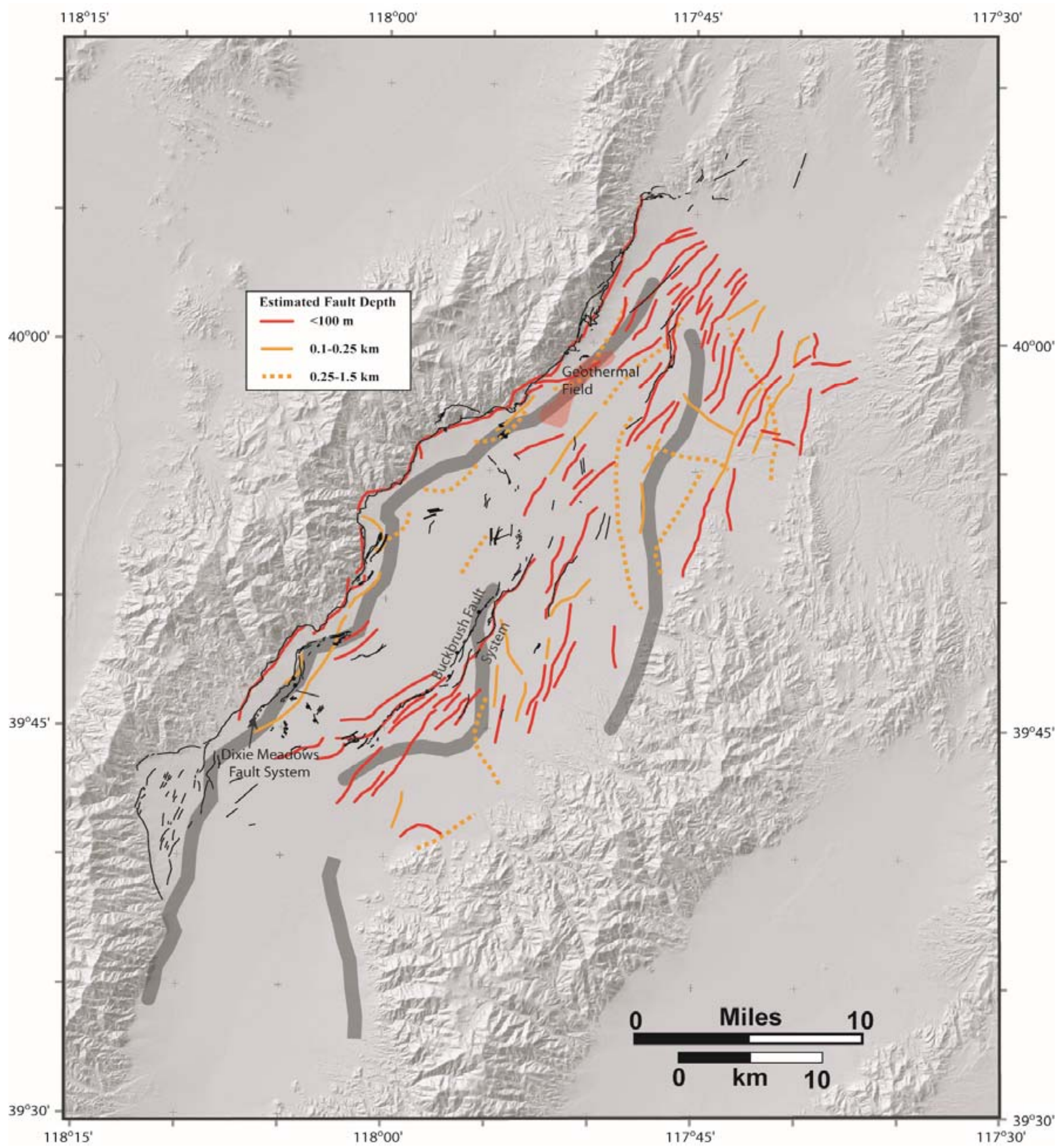

Figure 13. Horizontal gravity gradient maxima (wide gray lines) and faults from the surface geology (black lines) and from the horizontal gradient of the HELIMAG data (red lines) on a topographic background. Surface evidence of rampart faults & intrabasin faults occurs on or near gravity gradient maxima. The figure and caption are from Blackwell et al. (2005).

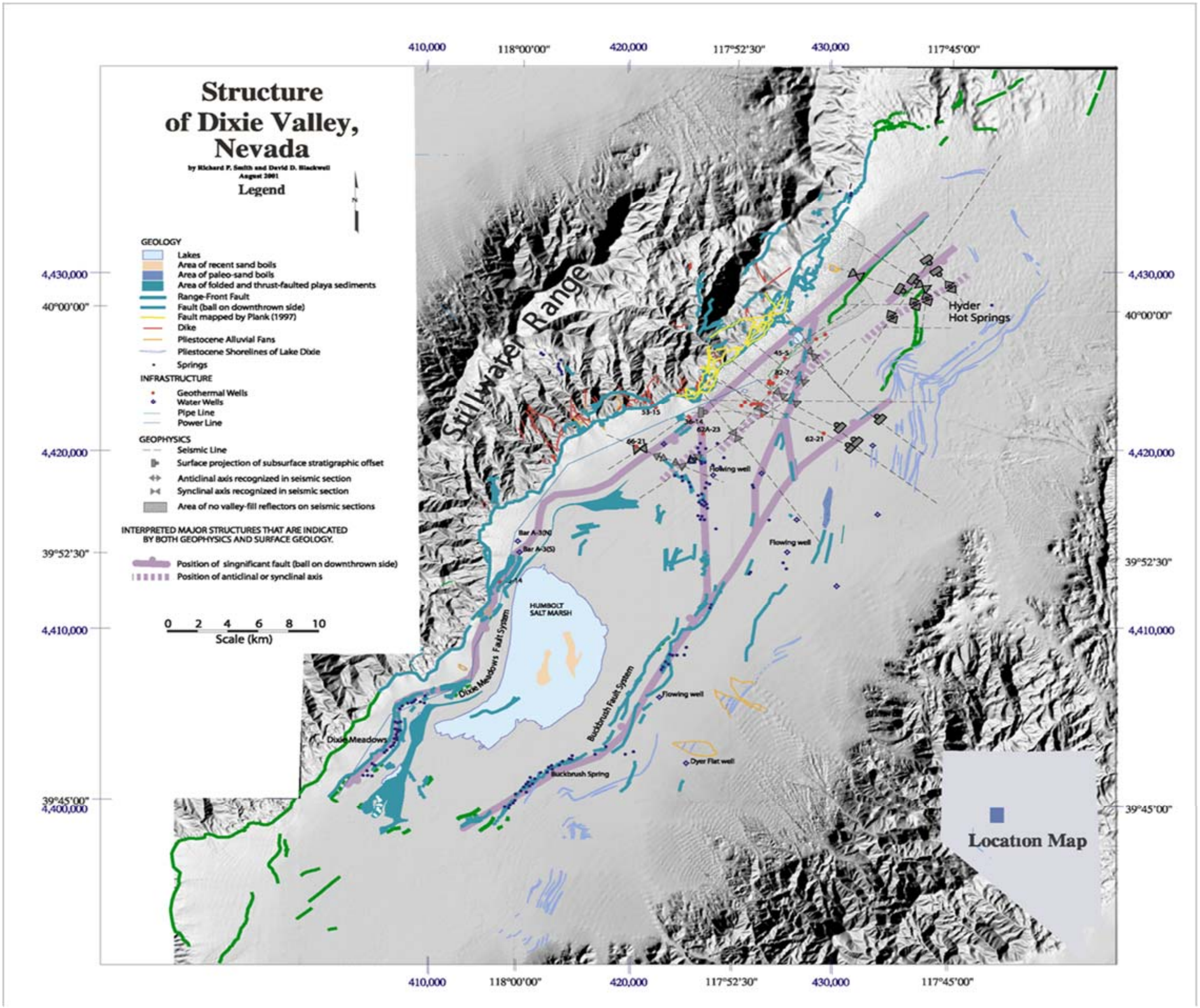

Figure 14. Structure of Dixie Valley (Smith and Blackwell 2001). Thick purple lines indicate the positions of interpreted major intrabasin faults based on geophysical data and surface geology. The figure and caption are from Blackwell et al. (2005).

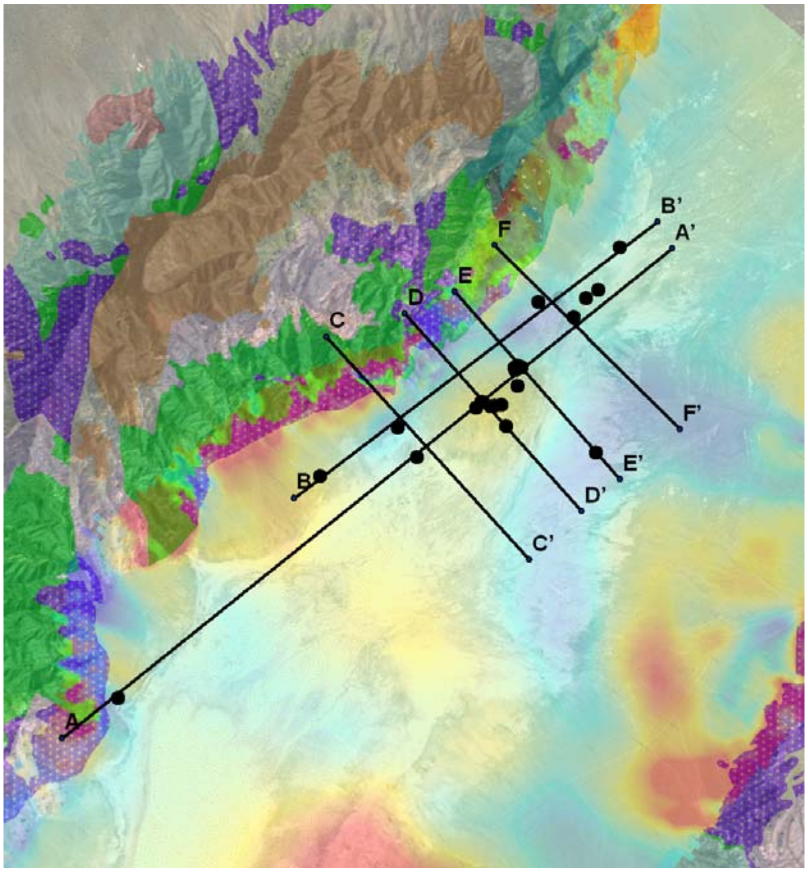

Figure 15A. Location of modeled lines A-A' through F-F' superimposed on the HELIMAG total magnetic field anomaly, the state geologic map and a satellite terrain map. Black dot are locations of geothermal wells. Purple to magenta colored hashed units are Jurassic gabbroic rocks (Jg), green colors area are Jurassic mafic volcanics (Jvb), tan colors are Cz silicic volcanics,brown colors are Cz basalts, and hashed pinkish-red is K-T granodiorite.

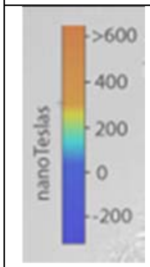

HELIMAG Scale
(Illuminated from the NW)

The methods used to calculate the gravity and magnetic model response are based on the methods of Talwani et al., 1959, and Talwani and Heirtzler, 1964, and make use of the algorithms described in Won and Bevis, 1987. Two-and-a-half dimensional calculations are based on Rasmussen and Pedersen, 1979. The GM-SYS inversion routine utilizes a Marqardt inversion algorithm to linearize and invert the calculations (Marqardt, 1963). Gravity and magnetics models are non-unique, i.e., several model families can be created to match the data. It is up to the interpreter to assess whether the model(s) are geologically reasonable.

The principles of successful modeling are to create the simplest models with the fewest number of densities, blocks and vertices. In the Dixie Valley area, a few constraints were available from well lithologies which defined basin depth. It is important to note that density contrasts, not absolute values are what control the gravity signature. Complete Bouguer gravity values were calculated with a background reduction density of 2.67 gm/cc. Models with basin fill densities ranging from 1.4 to 2.6 gm/cc were tested and only those with densities of 2.2 gm/cc or greater provided the requisite minimum basin thickness. The final basin fill density of 2.445 gm/cc was selected based on fitting the model to the observed basin fill depth in well 62-21 on line E-E'. Independent fits of lines D-D' and F'F' show basin fill depths are consistent with other wells in the area. In some of the lines, it was necessary to introduce a surficial (<100m [330ft]) low density layer of D ~1.5-1.8 gm/cc to account for very short wavelength gravity variations. This might represent the vadose zone or alternatively, lake and playa sediments.

Bedrock density values were determined by modeling the outcropping bedrock on the eastern flanks of the Stillwater Range. Geologic units in the Stillwater Range are varied and complex, ranging from gabbros to basalts to rhyolites to quartz arenites. The most dominant geologic units in the range in the study area are the Jurassic gabbros and Tertiary basalts. Line F-F’ is the only profile where the gabbros unambiguously are the only outcropping bedrock unit. The gravity signature of the Stillwater bedrock along line F-F’ was modeled using density values ranging from 2.6 to 3.0 gm/cc. A density of D=2.876 gm/cc. was found to provide the optimal fit to the slope of the CBA, and this value, which is typical of mafic volcanic rock was adopted for the rest of the lines. A slightly reduced density of 2.4 top 2.5 gm/cc proven necessary to model some near surface rocks in the Stillwater Range that are classified as rhyolites or mixed clay/limestone/arenites.

The effects of removing a slight NW/SE regional trend was tested on the gravity models (Figure 15B). The net effect was to slightly deepen the basins, but no significant changes were observed to the locations of the basin walls or the positions of postulated faulting.

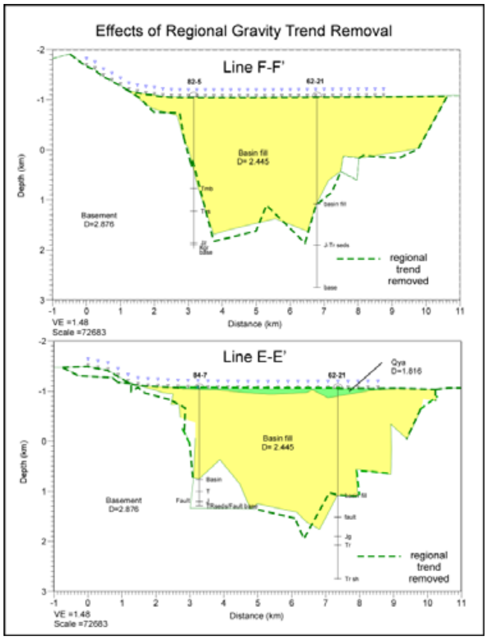

Figure 15B. Effects of removal of regional gravity trend (green-dashed lines) on lines F-F’ (top) and E-E’ (bottom).

Magnetization values were varied from M=0.001 to M=0.008 emu/cc. Values of M <0.003 and M>0.005 emu/cc did not yield acceptable fits. Values < 0.003 emu/cc required magnetized volumes in excess of 700m (2300ft) thick, which seems unrealistic. Models with magnetizations of M=0.003 to M= 0.005 emu/cc yielded acceptable fits. Increasing the magnetization above M=0.004 emu/cc somewhat decreases the volume of the magnetized bodies and to a lesser extent changes their relative positions. A series of modeling experiments were done to determine whether the Jurassic rocks were positively or negatively magnetized. Although some fits in the eastern part of the Dixie Valley basin allowed negatively magnetized units, the signature of the rocks in the Stillwater range required positively magnetized bodies. The prominent subsurface magnetic anomalies are positive highs implying buried normally magnetized bodies. Finally, the dominant magnetic field during most of the Jurassic was normal (i.e., positive), had very few reversals, and is known as the Jurassic Quiet Zone (Tivey et al. (2006)). Thus, for simplicity and consistency positively magnetized units were assumed in the modeling.

Ambient field directions of inclination = 64° and declination = 0 were used in the modeling. Field observations suggest that the units are extensively deformed and structurally complex and at times are steeply dipping to near vertical at the surface. The subsurface magnetizations are, of course, impossible to know. Changing the magnetic field directions could significantly alter the model fits, but for lack of knowledge we are left with little choice but to make the simplistic assumption that the Jurassic volcanics reflect modern values, implying that susceptibility rather than remanence controls the magnetization.

After a number of trials, a value of M=0.004 emu/cc was found to be optimal in modeling the magnetic signature of the Jurassic volcanics in all of the profiles. This is equivalent to using a susceptibility of .S=00079 cgs units using the ambient magnetic field of B= 51290.46 gammas found in the HELIMAG survey (Graugh et al., 2002) with an inclination of 64° and a declination of 0°. The final joint gravity/magnetics models with their data fits are shown for perpendicular lines C-C’ through F-F’ and A-A’ to B-B’ are shown in Figures 15C and 15D, respectively. The following observations can be made:

- The basin is 1.0 to 1.3km (0.6-0.8mi) thick and is wider in the vicinity of Line C-C’. Line A-A’ suggests that the basin may be divided into two subbasins going from south to north;
- The magnetic anomaly data can be successfully modeled with a single magnetic Jurassic mafic rock unit. The magnetic modeling and thus the fault locations and dip are very sensitive to the shape and location of the individual blocks as well as the interaction between blocks;
- The basin walls appear to be fault controlled and indicate a complex, steeply dipping to near vertical, multi-fault structural geometry for the DVFZ. The step-down fault zone indicates the majority of the normal-sensed displacement occurs on multiple piedmont faults. This interpretation replaces the original range-bounding, moderately dipping, single fault model; and
- All the wells (producing zone) occur within the block faulting zone and more specifically on the major piedmont structures.

3.4 Magnetotelluric (MT) Surveys

Electromagnetic (EM) and MT surveys within Dixie Valley have been used to image the structural resistivity as bedrock and unconsolidated sediments show sharp resistivity contrasts. In addition, increased fluid content due to fracturing as well as the development of conductive alteration minerals (clays) can show electrical resistivity contrasts. Thus, EM can also be used for finding blind geothermal systems, defining the extent of geothermal reservoirs and controlling structures, and locating/characterizing permeable fracture zones.

While these methods can be subject to limited resolution and other variables, a new generation MT-array system has been applied to three profiles over the Dixie Valley thermal area (Figure 16A). This study described in Wannamaker et al. (2007) is defined as state-of-the-art MT array measurements in contiguous bipole deployments across the Dixie Valley thermal area that have been integrated with regional MT transect data and other evidence. The purpose was to (1) resolve the complex structural setting; (2) delineate fault zones which have experience fluid flux as indicated by low resistivity; (3) infer ultimate heat and fluid sources for the thermal area; and (4) investigate the capability of well-sampled electrical data for resolving subsurface structure.

The northern profile (Figures 16A and 16B) and central profile (Figure 16D) show that shallow basement rocks extend for a considerable distance (1-2km [3280-6560ft]) SE from the topographic scarp of the Stillwater Range before plunging steeply down the main strand (major displacement along piedmont fault) of the DVFZ. The southern profile (Figure 16C) images a more steady dip likely suggesting a localized step-down zone. The findings reported in Wannamaker et al. (2003) supports a multi fault-step model, infers that an unknown amount of slide-block material may exist over the main DV range-front fault which complicates the structural framework, and images a low resistivity zone flanking the interpreted main offsetting fault that could be due to alteration from geothermal fluid outflow/upflow. A highly altered section of silicified alluvium near the surface encountered in well 38-32 likely supports this interpretation.

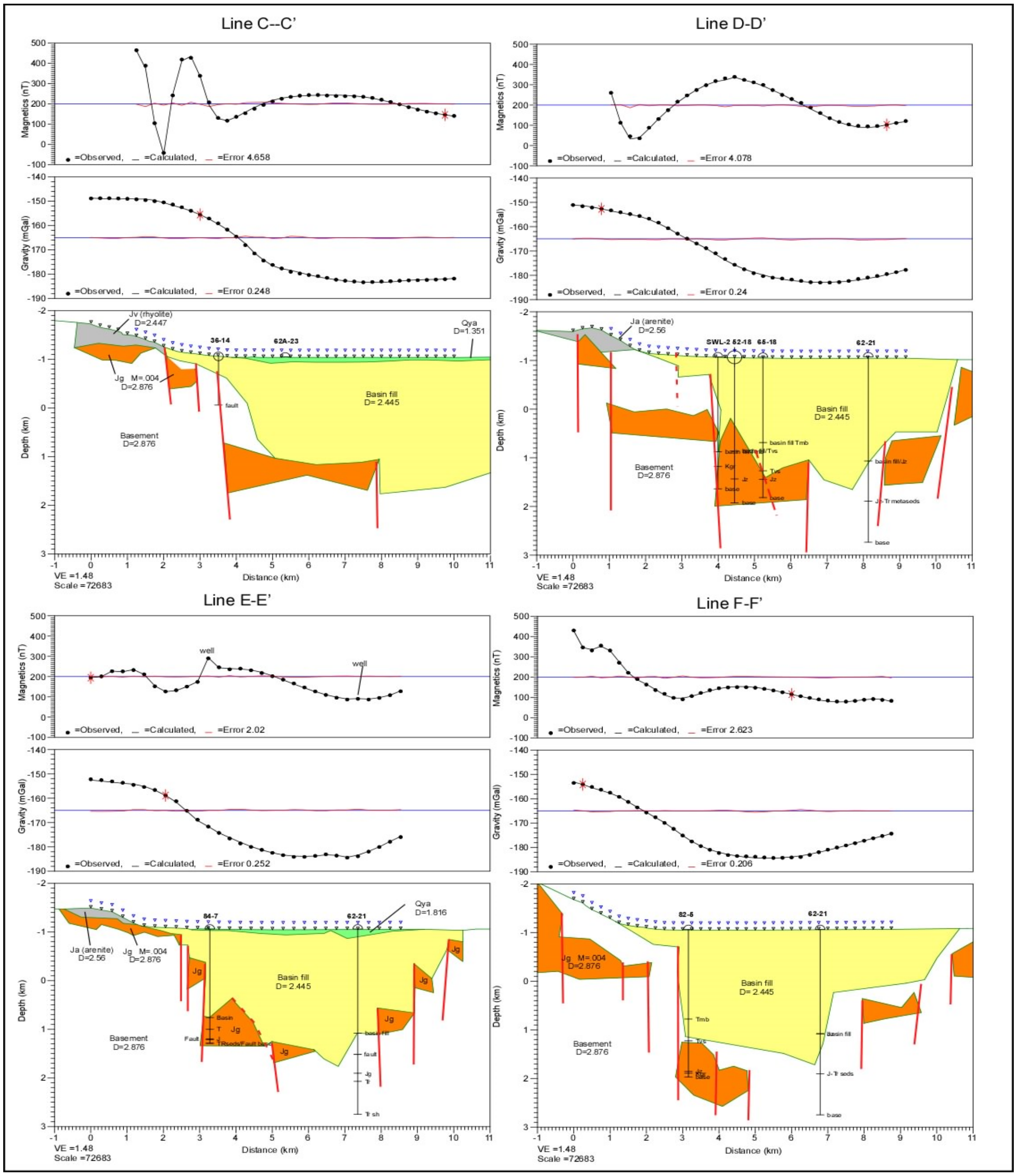

Figure 15C. Joint gravity and magnetic model of lines C-C' through F-F'. Fits of gravity and magnetic profiles are <1%. Postulated faults are shown in red. Surfaces are basin fill (yellow, D=2.445 gm/cc); Jurassic volcanics (orange, D=2.876 gm/cc, M=0.004 emu/cc); basement (white, D=2.876 gm/cc, M=0 emu/cc); lower density arenites or rhyolites (grey, D=~2.5 gm/cc, M=0 emu/cc).

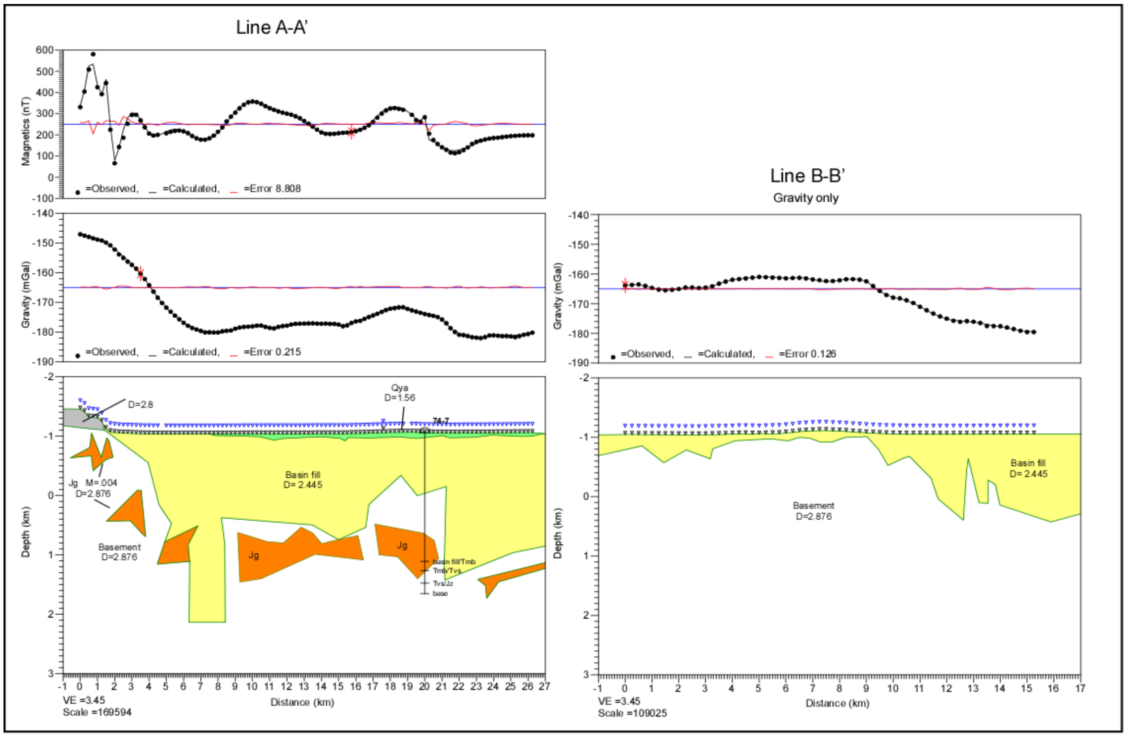

Figure 15D. Joint gravity and magnetic model of lines A-A' through B-B'.

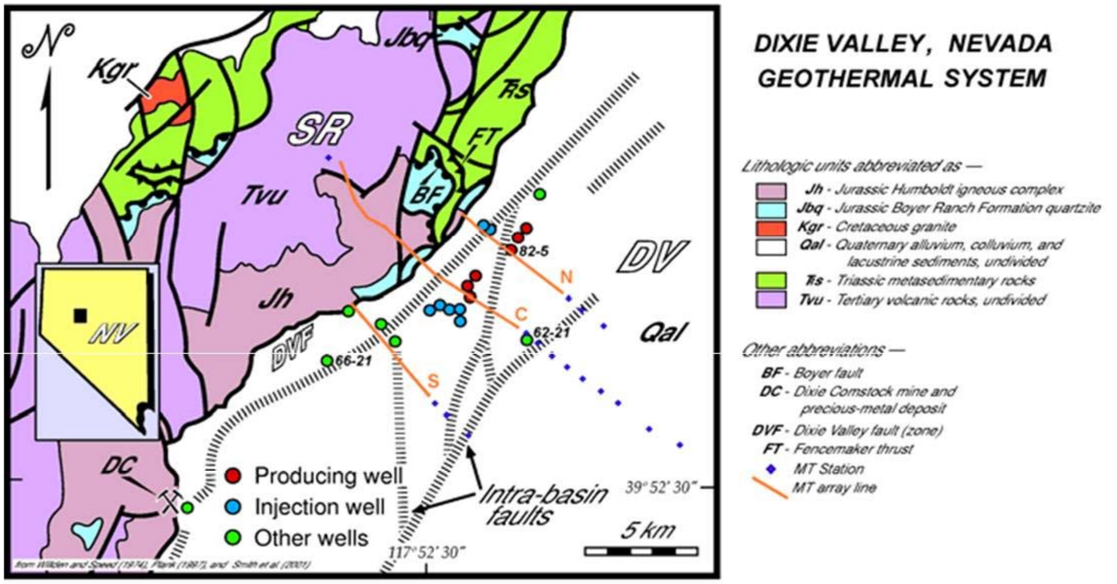

Figure 16A. Simplified geologic map of the Dixie Valley (DV)-Stillwater Range (SR) area surrounding the Dixie Valley thermal field. Orange-brown lines are the MT profiles lines (see text) Lines are labeled N (north), C (central), and S (southern). Blue diamonds are five-channel MT stations added to extend profiles across the valley. Original figure courtesy of Jeff Hulen. The figure and captions are after Wannamaker et al. (2007).

In a more recent analysis (Wannamaker et al., 2007) resolved the structural setting and supported a multi-fault steeply dipping structural model. The transition from low to high resistivity (~100 ohm-m) represents the basement interface within the resistivity models which is supported by drilling results. A large scale, very high resistivity domain is present below the approximate central portion of the Stillwater Range which could likely be attributed to the presence of Cretaceous aged intrusive bodies. In addition, all three inverted profiles show a low resistivity deep feeder zone for high temperatures fluids rising into central Dixie Valley (Figures 16B-D). This broad, subvertical conductor connecting from depth (greater than 10km [6.2mi], see Figure 16E) along the eastern base of DV has been interpreted as a presently inactive, large-scale faulting damage zone with fluidization and alteration (Wannamaker, pers. comm., 2010), and alternatively as a less significant alteration structure due to localized change in mineralogy (Waibel, pers. comm., 2010). It provides the possibility that the N-trending structures inferred by the geophysical data within the intrabasin are thermal-bearing structures (Figure 12) which merge with the NE trending active system of faults within the DVFZ in the vicinity of the geothermal field. This potential feeder zone is also imaged in the regional MT transect inversion (Wannamaker et al., 2006) that appears to connect to a pronounced low resistivity zone in the deep crust below the Humboldt Range (Figure 16E). This low resistivity zone has been interpreted as a region of magmatic underplating which would be a direct source for the active thermal fluids upwelling in Dixie Valley. If the resistivity models are correct, then it would imply some sort of magmatic input to the Dixie Valley geothermal system. However, one of the deepest wells in the DVGW, well 66-21, lies just to the east of this low resistivity zone and is relatively cold with respect to the producing wells and wells in the DVPP. A more detailed MT study will take place under Task 4 of the EGS Exploration Methodology Project. One objective will be to further resolve this low resistivity structure within central Dixie Valley.

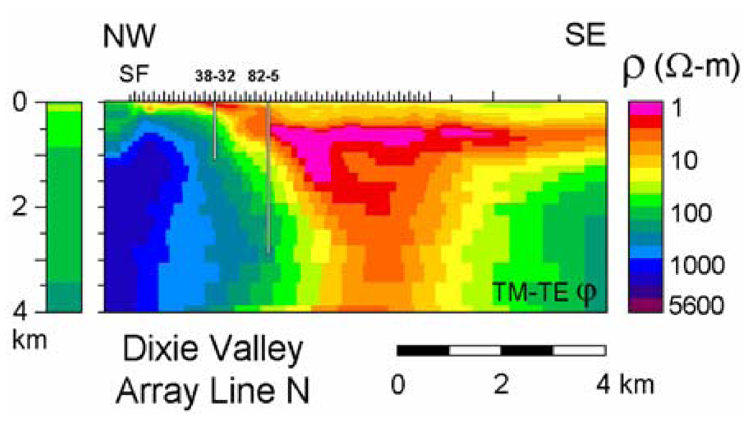

Figure 16B. Electrical resistivity section for the northern (N) profile across Senator fumaroles derived from 60 array MT sites taken with contiguous E-field bipoles, plus three stand-alone MT sites at the SE end. Tick marks are located at bipole centers. Bedrock-alluvium interface is interpreted to lie near the 70-100 ohm-m "contour".

3.5 Seismic

Dixie Valley is a structurally asymmetric basin bounded by a complex zone of faulting on the northwest and by step faulting to the southeast (Okaya and Thompson, 1985; Blackwell et al, 2005). The Dixie Valley Study Area (DVSA) extends from 39.7°N to 40.2°N and from 117.5°W to 118.2°W (Figure 1) and encompasses ~787mi^2 (2025km^2). To avoid boundary effects, we plan to estimate tomographic models over a much larger region than the project area in future planned work. As such, we have collected seismicity and ambient noise information within 200km (124mi) of DVSA. This extended study area, from 38.7°N to 41°N, and from 117°W to 119°W, is referred to as the Dixie Valley Extended Study Area (DVESA).

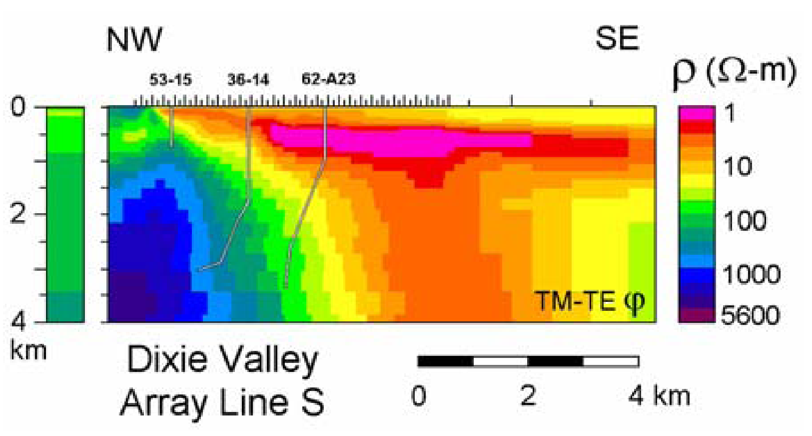

Figure 16C. Resistivity inversion section for the southern profile (S) across the Section 10-15 area for the dense MT array line S plus three stand-alone MT sites to the SE. The figure and caption are from Wannamaker et al. (2007).

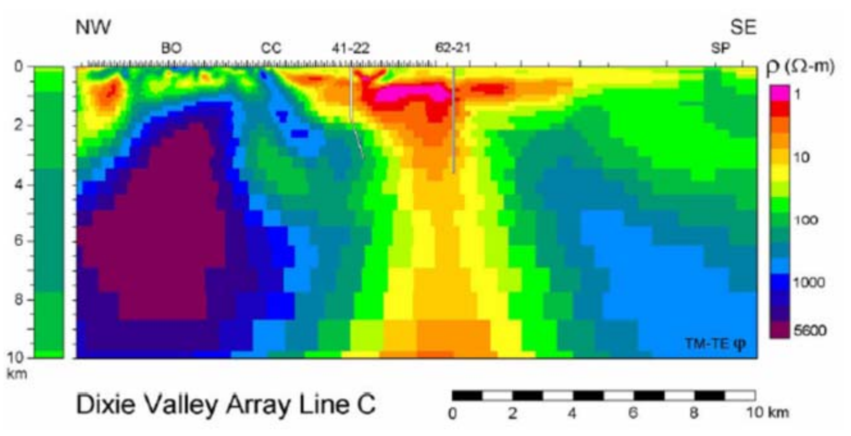

Figure 16D. Resistivity inversion section (C) across the Dixie Valley power producing field from 120 dense MT array measurements and 13 appended wideband MT soundings. The figure and caption are from Wannamaker et al., (2007).

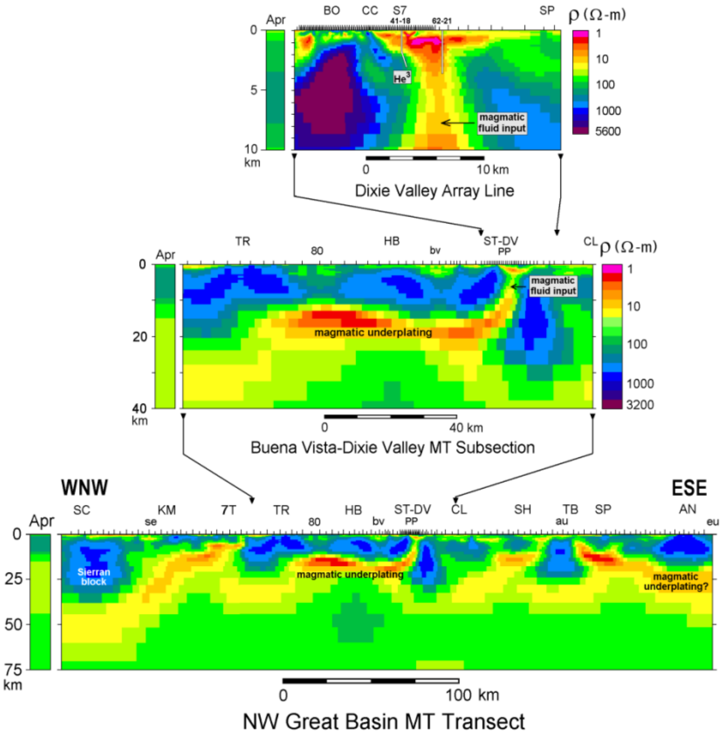

Figure 16E. MT structures of the central Great Basin show multi-scale magmatic-hydrothermal residence zones and pathways to the upper crust and geothermal systems. The figure and caption are after Wannamaker et al. (2006).

We expect our study will also address, directly or indirectly, several of the unresolved seismic issues in Dixie Valley. In this area, geophysical data interpretations in terms of fault parameters are controversial. For example, it is still debated whether the Dixie Valley earthquake in 1954 (M=6.8) was the first large, low-angle normal earthquake on land recorded historically. Seismic studies conducted by Abbott et al., 2001 at Dixie Hot Springs, inferred that the range front fault dips 25-30° to the southeast at this location (see Section 2.2.2 for additional discussion). Also, while most of the authors agree that the fault system penetrates deep into the crust, it is still debated whether there is a second order magmatic connection of the deep circulation system in Dixie Valley (McKenna and Blackwell, 2004; Wisian and Blackwell, 2004; Wannamaker et al., 2006). In addition, the nature of the seismic gap located on the Stillwater Range in northern Dixie Valley is yet to be resolved. The seismic gap (see Section 2.2.2 and 6.1.1 for additional discussion) lies between the 1954 Dixie Valley earthquake ruptures to the south and the 1915 Pleasant Valley ruptures to the north. The geothermal field is located between the endpoints of the 1954 and 1915 surface ruptures (Slemmons, 1956) within the seismic gap. The Stillwater seismic gap (Wallace and Whitney, 1984) falls within a major tilt domain boundary or transverse zone between the east-tilted Tobin range to the north and the west-tilted Stillwater Range. Fault slip rates in this area suggest that the gap may be simply a manifestation of the fact that major slip has not occurred in recent times.

3.5.1. Faults

Dixie Valley is the location of a complex fault system (Caskey et al., 1996). The Dixie Valley rupture zone does not fit a simple segmentation model. It is instead a complex interaction of separate fault zones (Bell, 1990). Due to the lack of systematic seismic studies, the depth and angle to which these fault zones penetrate the crust is still under debate. Several main faults have been distinguished, such as the Stillwater Fault (SF), a normal fault which bounds the Dixie Valley basin to the northwest and dips 52-54°, while the dip of this segment is debatable (see Section 2.2.2). This fault is estimated to be planar from the surface to a depth of at least 3km (9850ft). The SF is the producing reservoir for a 62 MW geothermal electric power plant originally built and operated by Oxbow Geothermal Corporation and currently owned and operated by Terra-Gen Power, LLC. There are well-documented lateral variations in productivity along the fault that are not fully understood. Work by Blackwell et al. (2005) and the current authors has shown that in the DVSA the Stillwater Range is bounded by a complex multi-fault system referred to as the DVFZ consisting of at a minimum a range-front fault and a piedmont fault; see Section 2.2.2. Based on the baseline data presented herein, the current Dixie Valley producing reservoir is located in the piedmont fault section of the DVFZ.

3.5.2 Previous Dixie Valley seismic experiments

Seismic Data Collection Experiments

1964. Studies of microearthquakes were carried out in the Fairview Peak Region, southwest of the DVSA, the earliest of which involved a network of five portable seismographs distributed in an area of about 2500km^2 (965mi^2) to the east of Fallon, Nevada (Oliver et al., 1966).

1965. A similar study of microearthquakes near Fairview Peak was carried out in 1965, using a small local network of four portable seismographs (Westphal and Lange, 1967). Three recording periods were covered in this study, totaling 129 days. The first was a period of low seismic activity during January and February, and the others followed the occurrence of magnitude 4.6 earthquakes in April and June. Results of the study deal primarily with the determination of focal coordinates for 244 events, based on a standard four-station location procedure, with the assumption of a uniform 5.0 km/sec P-wave velocity for the Fairview Peak area.

1965. The Lamont Geological Observatory and the University of Nevada undertook a cooperative microearthquake survey of selected areas in Nevada, using seismographs of high sensitivity (Oliver et al., 1966). The main purpose of this study was to compare short-term (i.e., daily) rates of occurrence of microearthquakes in seismically active areas with regional seismicity determined from the occurrence of large earthquakes over periods as long as several decades. Ten sites in western Nevada were monitored for periods from a few hours to several days, and the results of the study indicated that microearthquake activity was generally higher in areas of recent faulting, and lower in areas where large earthquakes had not occurred for 50 years or more.

1966. A small tripartite array (Stauder and Ryall, 1967) was established at the southern extremity of the surface faulting of the Fairview Peak earthquake of 1954. Over a period of six weeks an average 31 earthquakes per day were detected. Foci were found to concentrate between 10 and 15km (6.2 and 9.3mi) and to cluster toward the end of the surface faulting of the 1954 earthquake. The foci were also found to lie along two planar zones. The first was parallel to the fault plane solution (strike N 11° W, dip 62° E) of the 1954 Fairview Peak earthquake and terminated at the southern extremity of the surface fracture. The second began at this point and extended to the southwest, with loci distributed about a plane striking N 50° E and dipping 50° to the southeast. The latter zone apparently marked the southern terminus of the 1954 faulting.

1967. During the course of geothermal exploration in northern Dixie Valley, Thompson et al. (1967) reported that Southland Royalty Co. obtained 28km (17mi) of high-resolution seismic reflection data. The four seismic lines, recorded by Petroleum Geophysical Co. and processed by Western Geophysical Co., represented a detailed cross section of the northwestern side of northern Dixie Valley. Two of the four seismic lines were parallel to the Stillwater Range. The remaining two lines were oblique to nearly perpendicular to the range-front. Of these lines, SRC-3 was discussed by Okaya and Thompson in 1985. This seismic data is described by Blackwell et al. (2007) as difficult to interpret because "reflection data are only two dimensional and are thus of limited use in interpreting structures in Dixie Valley because of the three-dimensional velocity setting. There are many off-the-line reflection features in the data that complicate the interpretation, and even if the data were of modern vintage, the two dimensionality would still be a problem." The profiles have been reinterpreted by Optim LLC (Optim) in 1997 and reported in Anonymous (1998). A total of 34km (21mi) of 2-D seismic reflection data from the Dixie Valley geothermal field, were re-processed. The results revealed a completely different model for the geothermal field. This study used data recorded along nine seismic lines (Figure 17A, Appendix 2-Table 1.3), covering an area of approximately 160km^2 (62mi^2). A detailed discussion on seismic reflection line interpretation is provided below.

1984. Hague et al. (1987) reported on deep crustal profiles across the western B&R acquired by the Consortium for Crustal Reflection Profiling (COCORP). Uncorrelated field data were collected using a 96-channel off-end spread at 100m (328ft) group intervals, an 8-32Hz (2.0 octave bandwidth), 30s upsweep with an additional 20s listen time (50s record time).

1985. A reflection-spread "piggyback" data set was collected in Dixie Valley during the PASSCAL (Program for Array Seismic Studies of the Continental Lithosphere) northwestern Nevada seismic experiment. Catchings et al. (1986) reported that this experiment used explosive sources of up to 2700kg (5401lbs) recorded into receivers offset to 300km (186mi). The piggyback receiver array used five multichannel recording units to record 384 channels in two adjacent deployments. Middle crustal and very strong Moho (10s) reflections were identified.

2002. A crustal refraction profile was collected by Louie et al. (2004) from Battle Mountain, Nevada across western Nevada, the Reno area, Lake Tahoe, and the northern Sierra Nevada Mountains to Auburn, CA (Appendix 2-Table 3). Mine blasts and earthquakes were recorded by 199 Texan instruments extending across this 450km (280mi) long transect. Reftek RT-125 recorders were linked to 4.5Hz single geophones with an average inter-station distance of 4.5km (2.8mi).

3.5.3 Seismic Reflection Profiles

A closer look at seismic reflection profile interpretation in Dixie Valley in terms of fault structure: We are presenting herein more detailed results of an extensive suite of seismic reflection profiles in the Dixie Valley area, as interpreted by Blackwell et al. 2005. Problems with interpretations of these profiles are due to steeply dipping structures, variable lithologies, and degrees of lithification of the valley-fill sediments. As mentioned above, seismic data was collected in the late 1970s to early 1980s, with reprocessing performed in the 1990s. The profiles were concentrated within the DVPF and the DVPP (Figure 1) coinciding with the area of highest geothermal gradient (Figure 17a).

The seismic reflection interpretation most commonly cited (seismic line [SRC-3]) emphasized a 54° dip of the Stillwater Range bounding fault, with a broken up reflection pattern SE of the fault presumed to be due to scattering within a coarse alluvial fan along the down thrown edge of the hanging wall block (Figure 17b). Recent interpretation including analysis from thermal and drilling data revealed that, near the range front, the area is composed of massive bedrock on the footwall of a steeply dipping buried fault zone defined by the gravity gradient maximum (see Section 2.2.2 and Figure 11). In addition, seismic profiles reveal several intra-basin faults that show correlation to faults mapped on the surface. The seismic reflection profiles are generally in two predominant orientations, parallel to the dip "dip lines" or to the strike "strike lines" of the fault. The dip lines trend NE-SW (approximately perpendicular to the range-front and to the strike of major normal faults) while the strike lines trend NW-SE (parallel to the range front).

Strike Lines: The strike lines are supportive for imaging the depth to the basement (Figure 18), position and depth to basalt reflectors, and any cross-valley (NW-SE) structures including transfer zones between normal faults. Line 101 images a “flower” structure in correlation with the cross-valley transfer zones and shows the valley fill thickening to the north. SRC-1S images a basement high underlying the DVPP with accompanied “flower” structure. SRC-1N runs through the northern producing field and contains a lack of reflectors within the center due to the proximity of the piedmont fault. Line 5 running at an angle between the strike and dip lines (E-W) images several step faults towards the western line and shows the basalt thickens towards the valley depression. Interpreted line drawings of the majority of the seismic lines discussed are given in the seismic appendices in Blackwell et al. (2005).

Dip Lines: The majority of the seismic profiles cut roughly perpendicular to the DVFZ and the associated NNE to NE trending major structures. Specifically, 102, 9, 104, and 6 (Figure 17a) are shown with interpreted line drawings (Figure 19). Seismic lines SRC-3 & 102 run through the DVPF near the section 33 production wells and is regarded as the most well known and cited seismic reflection line in the B&R. It images the major range bounding fault as a more complex structure between wells 38-32 and 82-5. Within the eastern side of the valley, steeply NW dipping (antithetic) faults offset the basement and the overlying Miocene basalt reflector. Seismic lines 104 and 9 run just south of Cottonwood canyon between the producing field and the DVPP lease, and cuts through the Lamb Ranch injectors (section 18). The most important feature of this line is that it shows the structure of the deep, early, N-S oriented graben underlying the deepest part of the valley. The termination of valley reflectors coincides with the location of the maximum gravity gradient and images the main strand of the DVFZ just west of well SWL-3 (Figure 19). A steeply west dipping fault that bounds the eastern graben is supported by the seismic data and the structure is likely encountered by well 62-21, which lies near the center of Dixie Valley. This line also correlates with the geophysical data that the largest fault displacement along the seismic profile lies about 3km (2mi) basinward of the range-front fault. Seismic line 6 is the longest profile available extending from 1km (3280ft) east of Stillwater to 2km (6560ft) west of Clan Alpine and lying just north of lines 104 and 9. The line positions the main valley-bounding fault at the peak of gravity gradient (Figure 13A), and also locates several faults within the eastern valley (Figure 11).

In summary, the interpretation of seismic reflection lines from Blackwell et al. (2005) are:

- Piedmont faults are the main valley-bounding faults, are located by both the gravity and seismic data in the same location and often correlated with geologic mapping from air photos (e.g., fault scarps, small grabens);
- The deepest part of the valley underneath the producing field is an early N-S oriented graben that formed prior to the still active extensional phase expressed by NE-trending normal faults;
- A correlation exists between of the termination of the reflector points and the axis of the maximum gravity gradient; and
- In the central cross-section (Figure 19) the deep graben's shape appears to synclinal. The axis of this syncline within the basin-fill sediments is shown in Figure 14 and either supports sedimentation within a graben dominated structure, or could be a velocity pulldown feature due to lower velocity lacustrine dominated sediments in the lower section.

Limitations to the seismic reflection line data are:

- A simple model for basement and valley fill (density/velocity) was used, that doesn't include the Miocene and Oligocene volcanics (discussed in Section 2.1.1);
- Geophysical logs (sonic, gamma ray, etc.) often used in conjunction with seismic data are available for some of the wells, but the intervals and types vary; and
- Inability to clearly image (seismic) in the vicinity of the fault zone due to steeply dipping and complicated structures and shallow valley-fill above the basement wedge between the range-front and piedmont fault.

3.5.4 Seismic Events

A catalog of seismic events (earthquakes and quarry blasts) that occurred in DVESA from 2000 to 2010 and were located by the Nevada Seismological Laboratory was extracted from the UNR database (Appendix 3 and Figure 20). These events were recorded by seismic stations in and around Dixie Valley (Appendix 2-Table 1). Some of these seismic events were relocated and reinterpreted catalog of seismic events. Due to poor station coverage, however, location errors are on the order of 5 to 10km (3.1-6.2mi). The seismicity and the proposed array configuration proposed to be conducted in Task 4 indicate that there might be enough information for a Dixie Valley earthquake-based tomographic model.

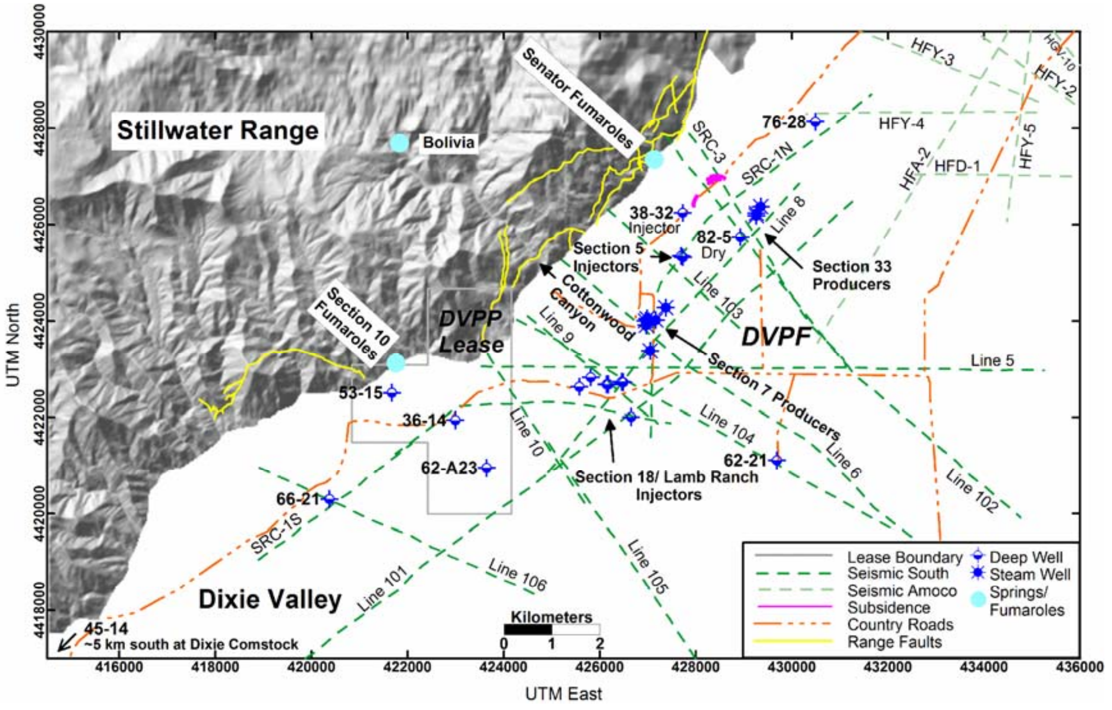

Figure 17A. Index map of Dixie Valley Power Partners (DVPP) and Dixie Valley Producing Field (DVPF) areas. Seismic profiles are labeled and shown as dashed green lines. The figure and caption are from Blackwell et al. (2005).

Historical seismicity in Dixie Valley (Blackwell et al., 2007) available from the United States Geological Survey (USGS) was added to the catalog and includes the July 6 (M_L 6.8) and August 23, 1954 (M_L 6.8) Rainbow Mountain earthquakes to the west of Dixie Valley, and the December 16, 1954 Dixie Valley (M_L 7.1)-Fairview Peak (M_L 7.2) earthquakes in and to the south of Dixie Valley.

2003 Seismic Sequence

A sequence of events (Appendix 2-Table 2; Figure 21) occurred in Dixie Valley in January 2003, about 26km (16mi) northeast of station DIX (Appendix 2-Table 1). The largest event and majority of the activity occurred from 6-13km (3.7-8.1mi). Using HYPODD (Waldhauser and Elsworth, 2000), the events were relocated (Figure 22a) in a cluster centered at 39.948°N, 117.863°W and depth 8.4km (5.2mi). The mechanism of the largest earthquake in this sequence is shown in Figure 22b. It shows normal faulting on dipping plane of approximately 45°SE assuming that all the events lie along a single structure. It is also possible that the swarms occurs along several faults as suggested in Figure 23. It is estimated that the other, smaller events, with similar waveforms (Figure 21), also had similar mechanism. Solving for the mechanism of these events is important to resolve the controversy on fault geometry in the DVSA.

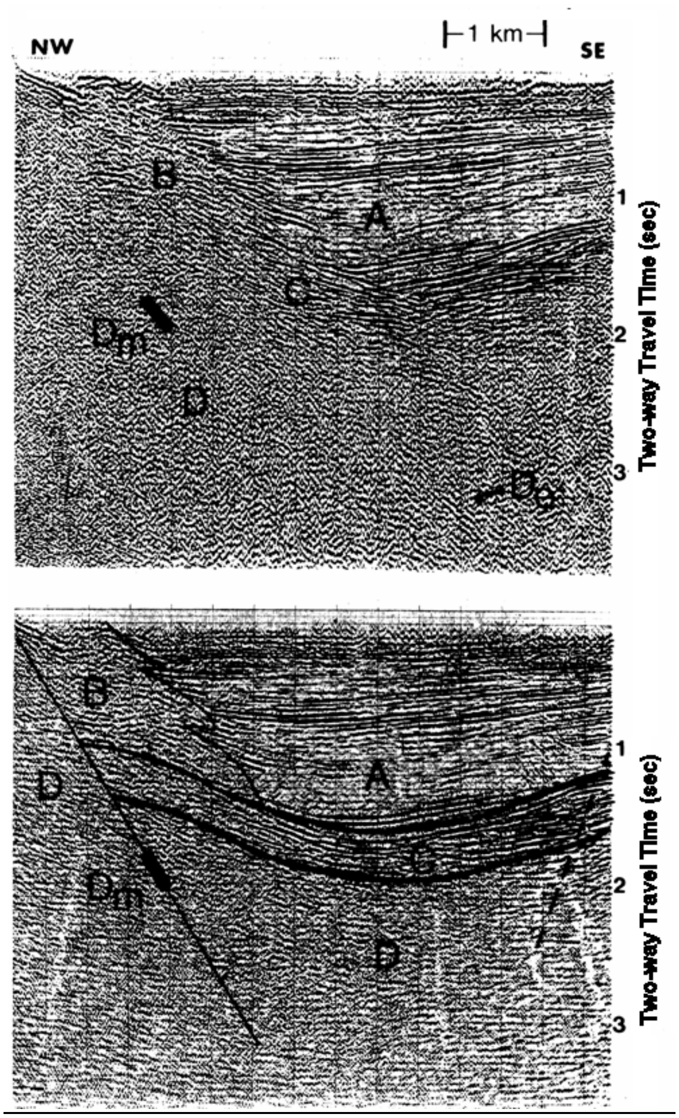

Figure 17B. Okaya and Thompson (1985) interpretation of reflection profile SRC-3. See Figure 17 for location of seismic profile. Interpretive Labels are as follows:

A=Valley Fill

B=Alluvial Fan - piedmont block

C=Basalt/volcanic

D=Basement

Dm=Supposed fault reflection

3.5.5 Databases Complied

We have acquired or compiled the following databases, including waveforms from the seismic experiments listed above:

- An Antelope (Datascope) database of earthquake and explosion waveforms available at UNR from 1984 to August 2010. These events occurred in an area from 38.7°N to 41°N and 117°W to 119°W. Four days of continuous waveforms from the 2003 earthquake sequence which occurred in Dixie Valley have been added to this database.
- Data from the 2002 Walker Lane experiment through the northern part of Dixie Valley was acquired from IRIS; and

A new database of ambient-noise extracted Green's functions, a key component of the initial velocity model estimation in DVESA 3.5.5.

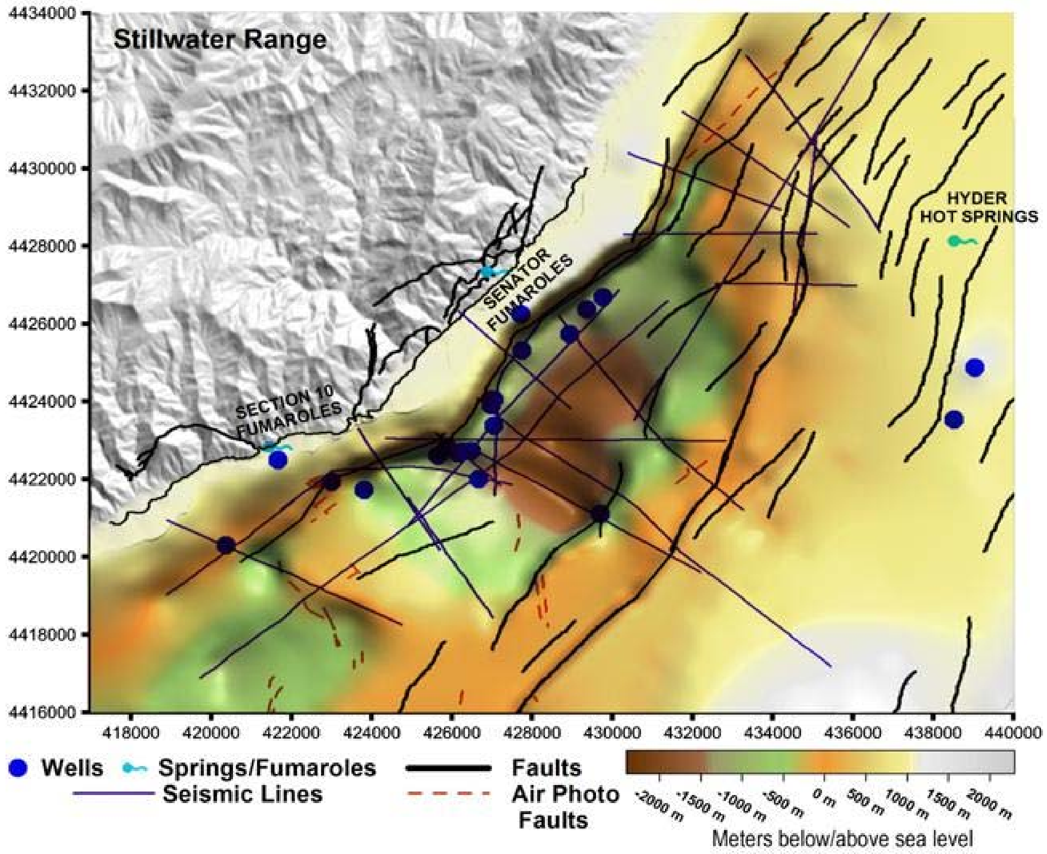

Figure 18. Dixie Valley basement configuration (valley fill removed) based on seismic and well data using fault lines to limit contours. Seismic profiles are shown in blue. Seismic-inferred faults are shown in black, while surface scarps are shown dotted in red. The figure is from Blackwell et al. (2005).

Seismic Velocity Models

We have acquired the following crustal seismic velocity models (Appendix 4-Tables 3 and 4) in and around Dixie Valley.

Global and regional models

- CRUST 5.1, a global crustal model with 240km (149mi) resolution (http://mahi.ucsd.edu/Gabi/rem.html, (Basin et al., 2000; Mooney et al., 1998);
- Model AK135, a global Earth model;
- CU_SDT1.0, a shear wave velocity model obtained from diffraction tomography over North America (Ritzwoller et al., 2002) which has 200km (124mi) resolution; and
- A shear wave velocity model for the Basin and Range by Priestley and Brune (1978).

Location-specific models

- The COCORP -derived model (Catchings, 1992) in a region shown in Figure 24;
- The UNR-estimated P and S-velocity model (Preston, 2010) from earthquakes (Figure 25);
- The re-processed seismic lines in Dixie Valley (Anonymous, 1998); and

- The Louie et al. (2004) Walker-Lane model.

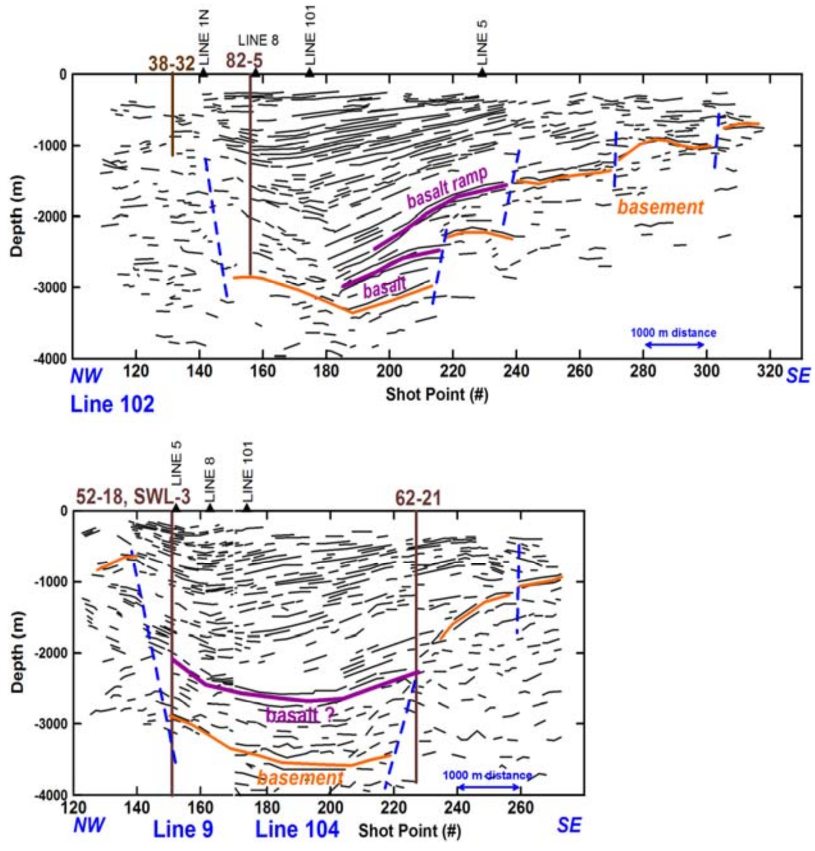

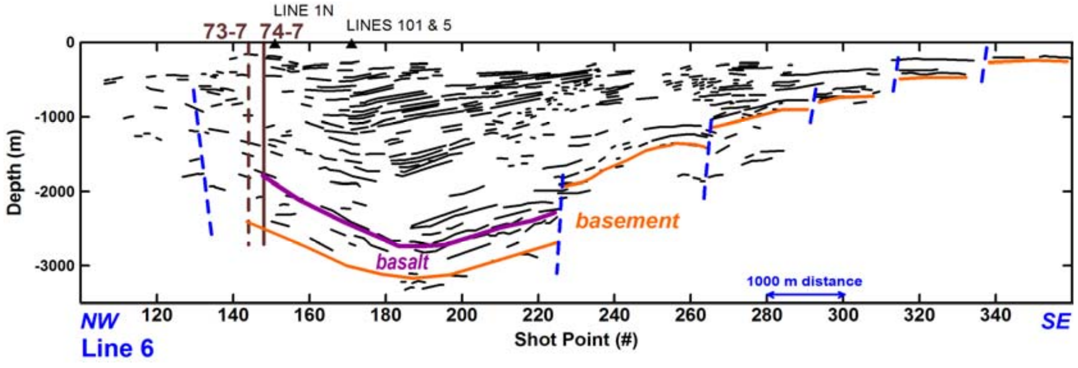

Figure 19. Interpreted line drawings of stacked sections for dip lines 102, 9, 104, and 6. Vertical brown lines are wells - solid are near the line and dashed are farther from line. The blue dashed lines represent approximate fault locations. Solid purple and orange lines are top of basalt and basement. The figure and caption are after Blackwell et al. (2005).

3.5.6 Integrated Seismic Model in Dixie Valley

The models in Appendix 4-Tables 3 and 4 were used to create an integrated model for the Project Area using algorithms written in Matlab. A set of depths of interest were chosen for all models. Each model is stored into a Matlab structure. The structure includes the model reference, the model area (which is a square oriented North-South, East-West), and the parameter model. The parameter model matrix consists of seven columns: depth, P-wave velocity in km/s, S-wave velocity in km/s, density (g/cm^3), P and S attenuation factors Qp and Qs and a "trust" factor, described below. "No information" is marked by the parameter value set to -99. The "trust" factor ranges from 0 to 1 and is, for example, set by the analyst up to 0.9 for reflection/refraction lines and is set to 0.01 for general (non-local) models. Using the "trust" parameter, seismic lines and local data are given higher weights than the general model

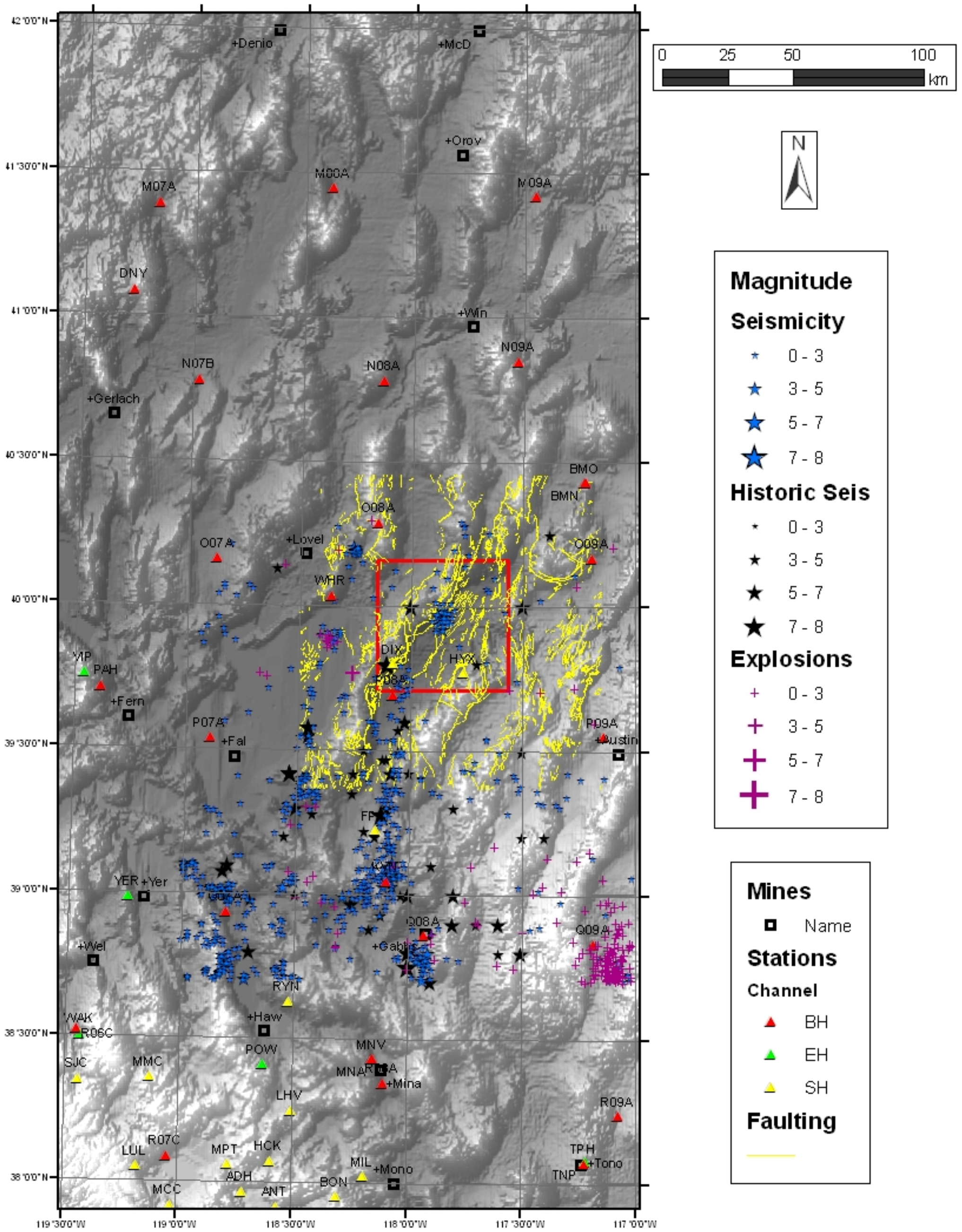

Figure 20. Natural and induced seismicity from 1900 to 2010 located by University of Nevada Reno (UNR) within 100km (62mi) of the Dixie Valley project area. The depth range is zero to 19km (~12mi). Earthquakes in the Dixie Valley area are listed by USGS (PDE- current catalog- 562 earthquakes, USHIS-historical catalog - 123 earthquakes) and UNR catalogs and explosions identified at UNR (298 events). Event locations are only approximate, see text for explanation. Faults are represented as yellow lines. The Project Area is shown as a red box.

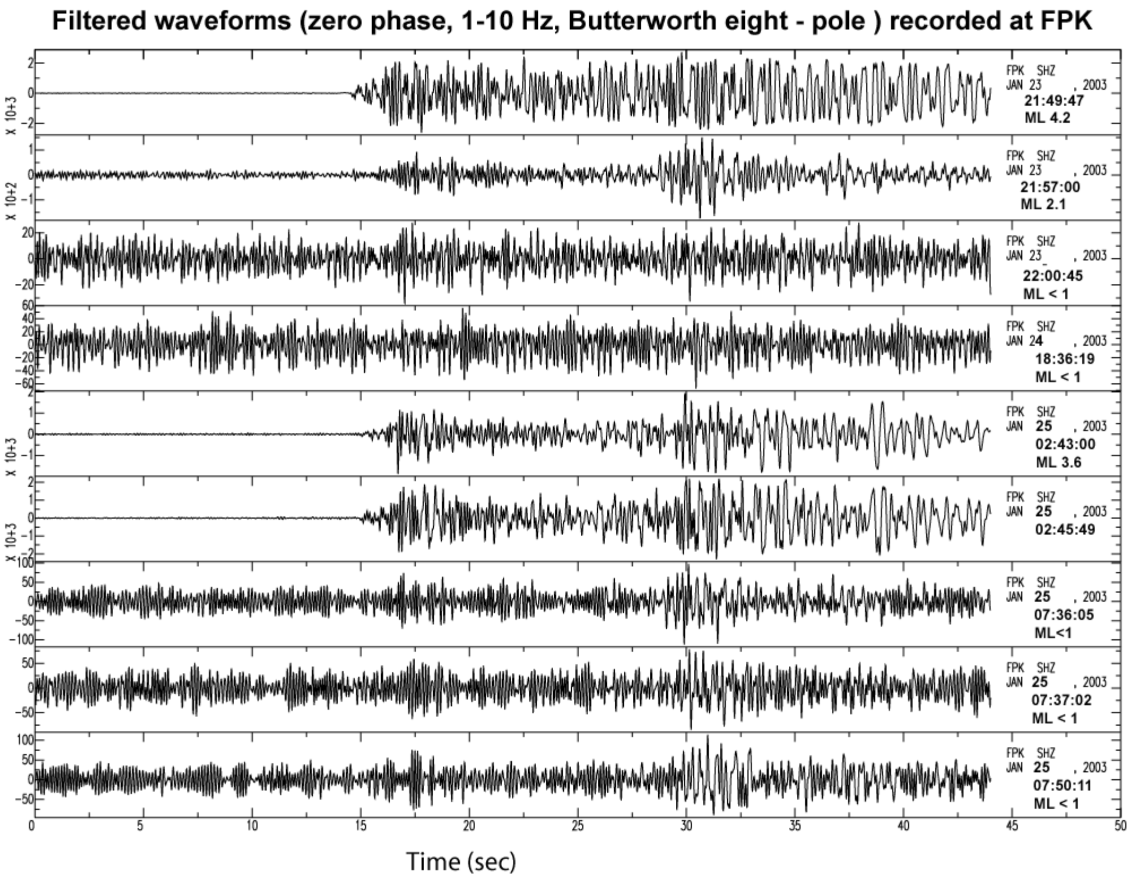

Figure 21. Waveforms recorded at station FPK from selected events in Appendix 2-Table 1.2.

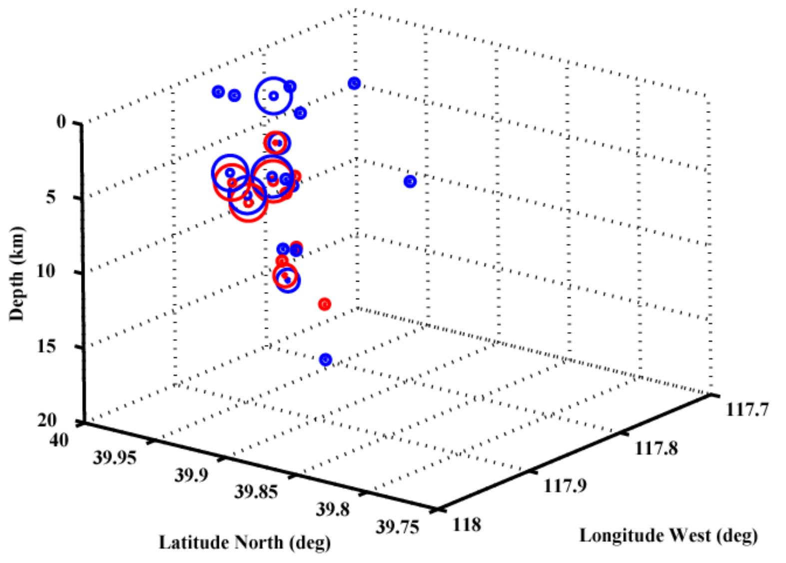

Figure 22A. Relocated events (red) and catalog events (blue) of the January 2003 sequence in Dixie Valley (Appendix 2-Table 2). All the events are represented by circles, proportional to magnitude. The largest earthquake was ML 4.2 and the smallest was ML< 2 (or less). The smallest earthquake magnitudes were not estimated because they were not recorded by enough stations.

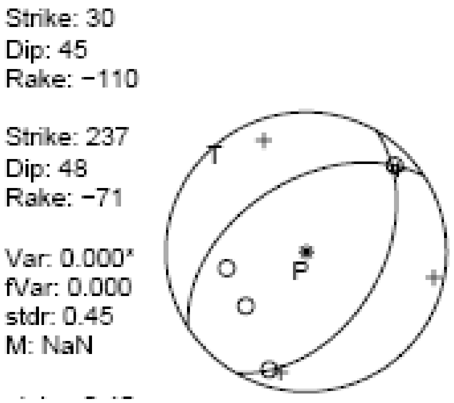

Figure 22B. Focal mechanism of the largest earthquake occurred at 39.95 N, 117.85W on January 23, 2003, 21:49:47, M$_L$ 4.2, depth 6.2km (3.9mi).

weights. A "slack" factor for each model represents a chosen extension of the model area. When, for example, the P-velocity model at a point characterized by latitude and longitude is requested by the user, the program finds all the models including the respective point and collects all the P-velocity values, together with their "trust" values. The resulting P-velocity at the respective point is a "trust" - parameter weighted mean, after the "-99" estimates are discarded. Sixty-four models are currently used for the integrated model, including all the information in the study area collected so far.

The P-velocity integrated model at 3km (9600ft) depth with the planned seismic deployment stations is shown in Figure 26.

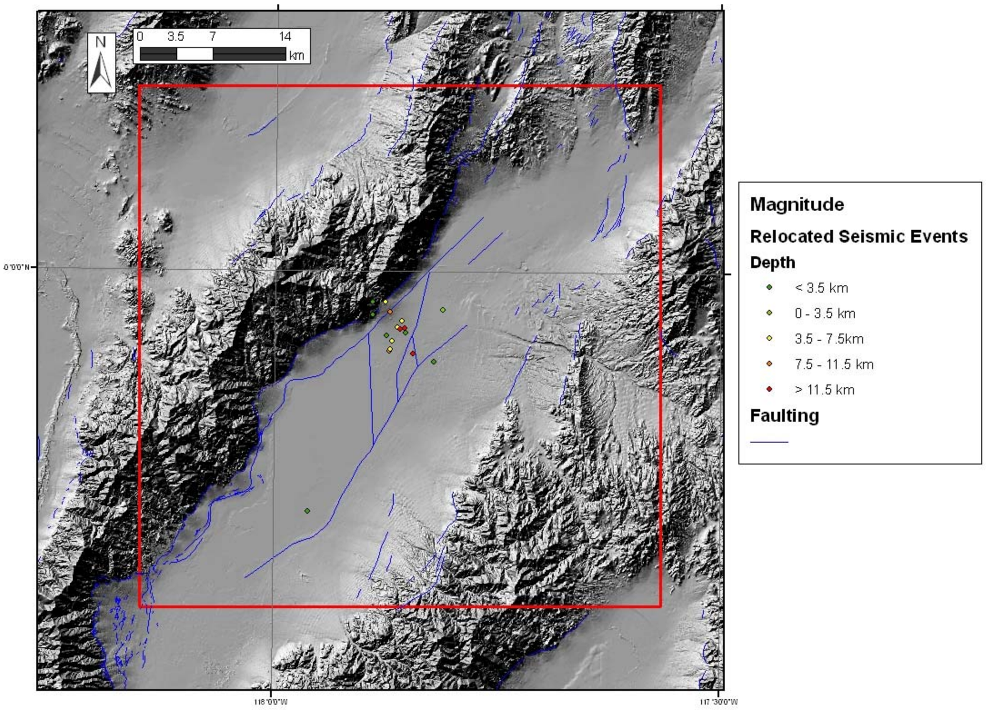

Figure 23. Plan view map of relocated events shown in Figure 22A.

3.5.7 New Seismic Noise Derived Velocity Model

We have extracted more than 2000 new Green's Functions (GF's), Figures 27 and 28 from cross-correlations of ambient noise at 61 stations within 200km (124mi) of Dixie Valley, with the objective to obtain higher resolution shear-wave velocity model than the current UNR model. To avoid model edge effects and due to the station distribution (Figure 20), Rayleigh group velocity maps need to be estimated in a larger area than the DVSA and this will be done in Task 4. Good correspondence of the GF extracted from ambient noise between Dixie Valley stations DIX ("SH"- analog short period sensor) and WHR ("BH" digital broadband sensor) with waveforms recorded at WHR (Appendix 2-Table 1) from an earthquake that occurred at 6km (3.7mi) depth 26km (16mi) northeast of the seismic station DIX is shown in Figure 28.

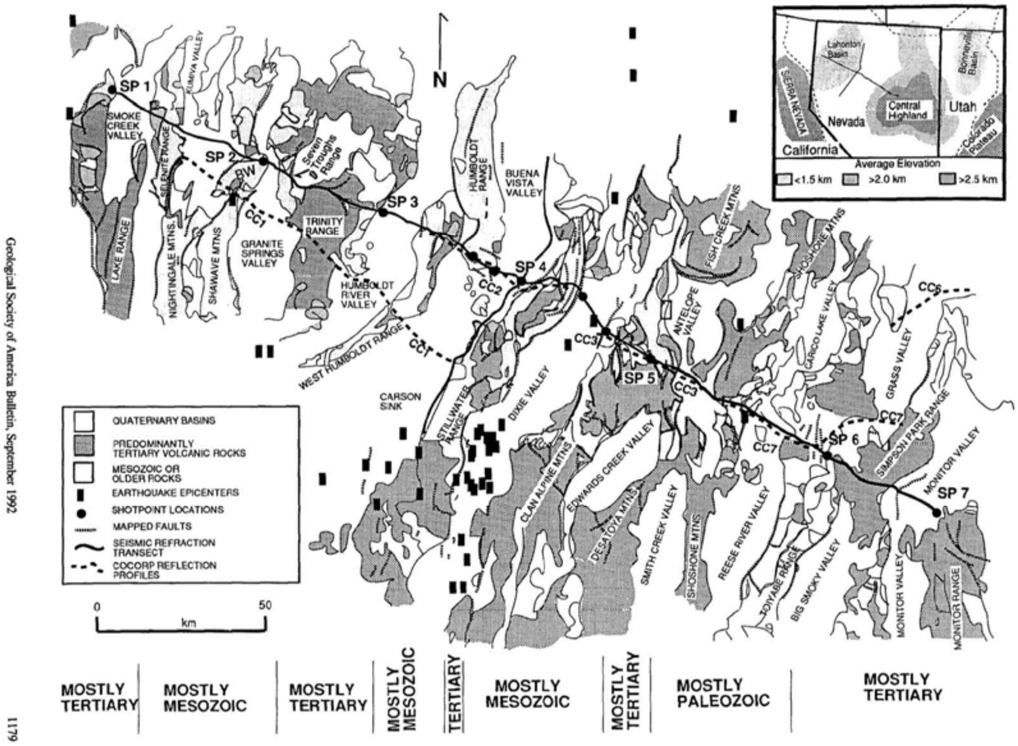

Figure 24. COCORP seismic profile (Appendix 2-Table 1.3) location from Catchings (1992).

3.5.8 Crust-mantle Boundary (Moho) Discontinuity Constraints

The depth of the crust-mantle boundary discontinuity (Mohorovicic or Moho) in DVESA is an important constraint on the tomographic model inversion.

Moho velocity and depth in Dixie Valley has been estimated by Catchings and Mooney (1991) as a 7.8km/s discontinuity at 30km (18.6mi) depth. In their studies in the northern part of Dixie Valley Louie et al. (2004), did not find a clear Moho signature. Northeast of Dixie Valley, at Battle Mountain, Nevada, the same authors observed anomalously thin crust over a limited region perhaps only 150km (93mi) wide, interpreted as a Moho depth of 19 to 23km (11.8-14.3mi). This area of thin crust is the part of a feature known as the "Humboldt Lineament" (or "Battle Mountain Heat Flow High") just west of Battle Mountain, which shows a high rate of extension normal to the trends of mapped faults in GPS analyses (Blewitt et al., 2002). The area of high extension rate is roughly 100km (62mi) in diameter. In Dixie Valley, Hauge et al. (1986) observed Moho reflections at 9-10s. Receiver functions (Appendix 2-Table 4) within 200km (124mi) from Dixie Valley are continuously estimated by the EarthScope Automated Receiver Survey (EARS), Crotwell and Owens (2005), however, the results in Dixie Valley have large errors.

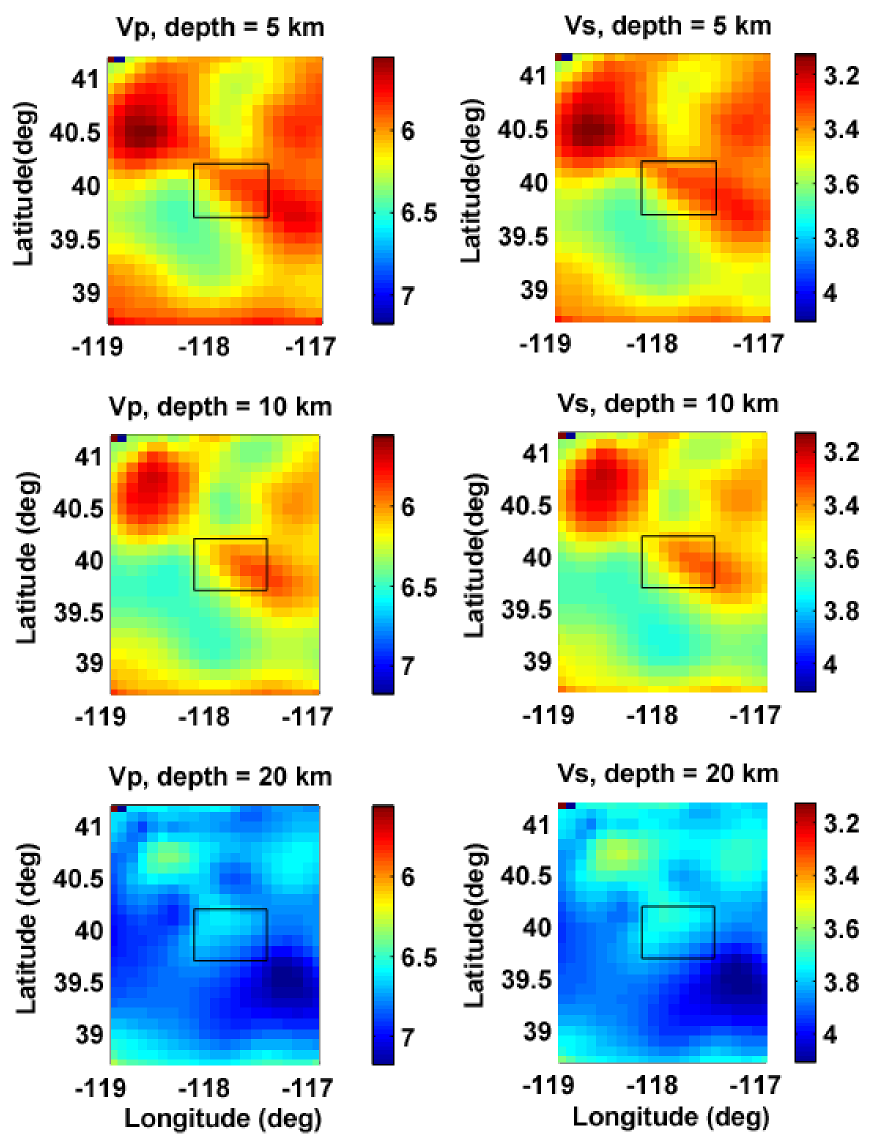

Figure 25. University of Nevada Reno (UNR) P - wave seismic velocity model in Dixie Valley from earthquake data (slices at 5, 10, 20km depth [3.1, 6.2, 12.3mi]) is shown in the left plots. UNR S-wave seismic velocity model in DV (same depth slices) is shown in the right plots. Note that the velocity is represented in 10x10km^2 (10x3.9mi^2) bins, however, the resolution of the western half of this model is~50km by 50km (19mi by 19mi) horizontally down to about 25km (9.7mi) depth for Vp and about 100km by 100km (62mi by 62mi) for Vs. The eastern half of the model has a worse resolution by about a factor of 2 compared to the western half (Leiph Preston, pers. comm.). The Project Area is shown as a black box.

3.5.9 Seismic Attenuation in Dixie Valley

Physicists can measure the ‘quality factor’ of materials, i.e., the efficiency of the material to pass energy at a particular frequency. The quality factor, Q, is defined as the ratio of stored to dissipated energy in material as seismic waves propagate through. Attenuation is defined as the reciprocal of Q and represents a measure of the absorption or loss of energy in the seismic waves as they pass through intervening material. Q-values range typically from 10 to 100 in laboratory measurements on sandstones and 100–1000 in igneous and metamorphic rocks (Johnston et al., 1979). These measurements are performed on small, simple samples and do not take into account large scale structures, fractures, and mixtures. Attenuation usually comes in two forms: intrinsic and scattering. Intrinsic attenuation relates to losses associated with heat and friction. Scattering attenuation is due to losses from waves reflected and refracted throughout the medium as they propagate from source to receiver. This implies that 3D Q-variations can be interpreted as being related to intrinsic physical properties of the rocks such as lithology, temperature, and porosity

Lees (2007) argues that attenuation is a relatively sensitive indicator of rock temperature in the upped 5km (3.1mi) of the crust. Seismic attenuation structure interpreted jointly with seismic velocity structure has the potential to strengthen the interpretation made on velocity structure alone. The attenuation image can also add independent information to the interpretation. For example, if a low velocity body beneath a caldera (such as at Medicine Lake volcano in northern California) is interpreted as a magma chamber, the interpretation is strengthened if the low velocity zone is also a high attenuation zone (Evans and Zucca, 1988). However, using P wave attenuation tomography Zucca and Evans, (1990), found that, beneath the Newberry volcano, low velocity and high attenuation were correlated in shallower layers, however, not correlated in deeper layers. According to Nakajima and Hasegawa (2003), consideration of attenuation, together with the Vp, Vs and Vp/Vs values may resolve fluid-related low -velocity zones consistent with highly conductive zones detected in MT surveys.

As a result of the Lg coda being composed of waves scattered in the upper crust, coda Q is a suitable expression of attenuation. The variations in Lg coda Q at 1Hz attenuation for the western US are shown in Figure 29 (Phillips and Stead, 2008) and are valid to a depth of around 3km (1.9mi). Low Q is correlated to volcanic areas (Cascades, Yellowstone, San Francisco field, and others surrounding the Colorado Plateau). The Lg Q values at 1Hz in the DVESA grid in Figure 29 are shown in Appendix 2-Table 5.

3.5.10 Seismic Velocity Variations as a Function of Rock Composition and Temperature

We have collected physical property relationships based on literature and relevant exploration analogs (Appendices 4, 5 and 6). Our investigations are summarized below.

Estimation of elastic rock parameters using seismic methods is inherently a remote method. Measurements are made on arriving wave travel time at the surface (P or S waves with velocity V_P or V_S) and on surface waves (Rayleigh) and used to infer properties deep within the earth. Variations of rock lithology or other physical parameters are estimated from the *P*- and *S*-wave velocity variations. This process leads to non-unique solutions because many rocks with differing physical states have similar seismic velocities and because inverting for subsurface properties from surface observations is poorly-constrained.

Seismic velocity depends on:

- Phase state (i.e., the presence or absence of partial melt);
- Composition (lithology, mineralogy and chemistry);
- Density;
- Temperature;
- Rock porosity; and
- Pressure.

.

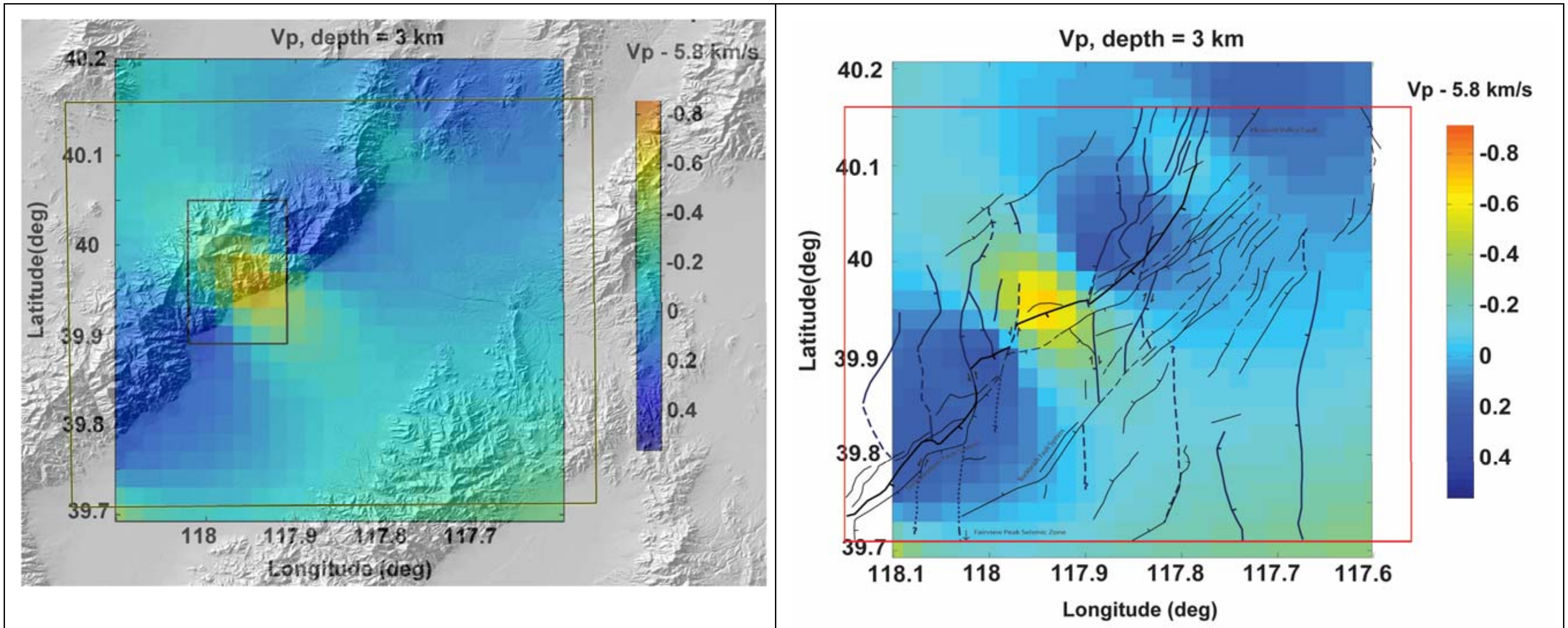

Figure 26. The P-wave velocity model at 3km depth was extracted using a 0.1 x 0.1 deg^2 grid and interpolated using the "Matlab 4 grid data" method. The model shows where the velocity differs from the average value (5.8km/s). The model on the left is superposed on a relief map, while the model on the right is superposed on a generalized structure map (see Section 7.2.1).

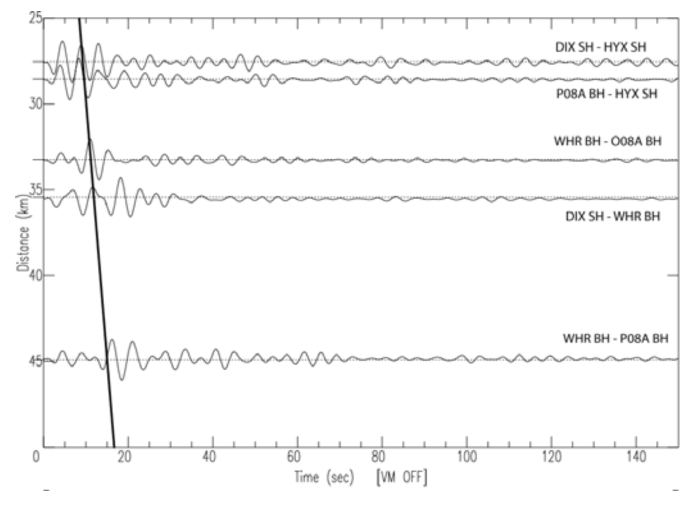

Figure 27. Newly extracted ambient noise results in Dixie Valley and vicinity using ambient noise crosscorrelations. Data was filtered with a 3 pole, zero phase ButteE in marworth filter from 0.15Hz to 0.3Hz (3 to 6 sec period). A 3km/s arrival time is represented by a black line in the plot. The Rayleigh component of the Green's Functions is clearly visible.

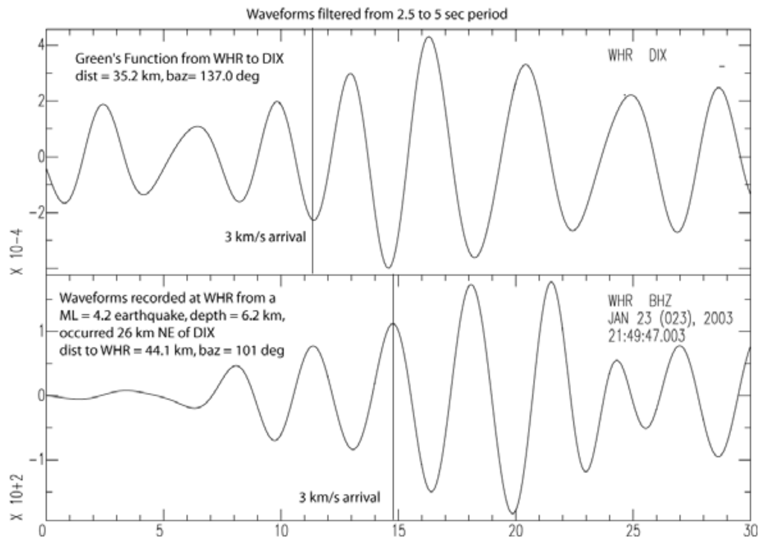

Figure 28. Shows a comparison of the GF extracted from ambient noise between stations DIX (SH - analog short period) and WHR (BH broadband) and waveforms recorded at WHR from an earthquake that occurred at a 6 km depth, 26km (16mi) northeast of DIX. Station DIX (Appendix 2-Table 1) is located in Dixie Valley. The plots show velocity in counts. The waveforms were filtered from 0.2 to 0.4Hz using a zero phase, six pole Butterworth filter.

For the majority of tomography studies, the seismic parameters under investigation include only four derived properties: velocity and attenuation of P- and S-waves, (Vp, Vs, Qp, Qs), and their respective ratios. These are the only properties that can be directly inverted for with seismic data. Reducing a myriad of geological and physical processes to four simple seismic observations is non-unique. Converting seismic field results to three-dimensional variations of rock states is tenuous, because a comprehensive data base of field based seismic properties related to rock physics laboratory studies is currently not available. Furthermore, most laboratory studies are performed in conditions significantly different from real earth situations and at frequencies substantially higher than typical seismic recordings (Kern, 1982).

Given these uncertainties, interpretation of tomographic images will be done using more geophysical information (i.e., geology, M, geochemistry, heat flow and gravity/magnetic investigations) than a simple velocity–density–temperature correlation. When coupled with experimental data on seismic properties of continental rocks at pertinent temperatures and pressures, the geological and geophysical data can be used to correlate measurements of seismic velocities with mineralogic composition at depth.

The utility of the seismic information as a thermal and rock property indicator is discussed in Appendix 4.

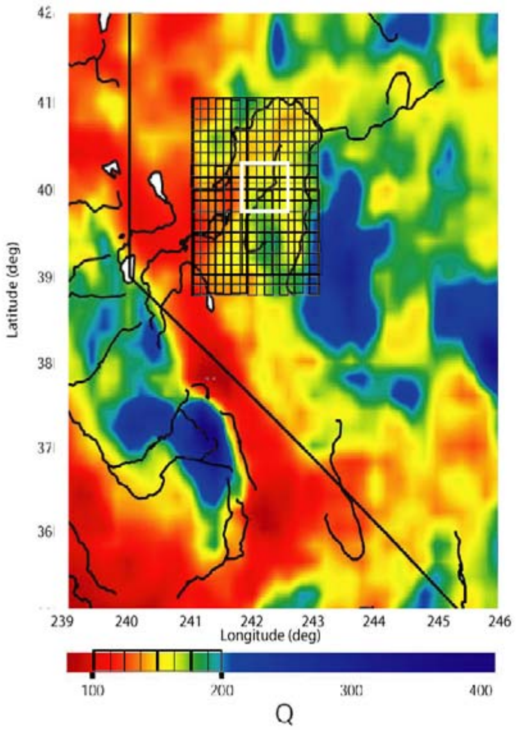

Figure 29. Lg coda Q @ 1 Hz for the western US as in Phillips and Stead, 2008 (Scott Phillips, pers. comm., 2010). The gridded area represents the DVESA. The Q values in the gridded area have been manually extracted and are shown in Appendix 2-Table 1.5. Project Area is shown in white.

3.6 Thermal

3.6.1 Background Conductive Heat Flow

A shallow temperature gradient map, shown in Figure 2 and also included as Figure 30, uses a number of constraints to assess the background heat flow in Dixie Valley. To analyze the conductive heat flow only, wells that were influenced by geothermal water circulation were not used. This includes most of the wells within the Senator fumaroles and the DVPP area. Additional constraints are:

- The total temperature dataset includes 25 TGHs within bedrock and 157 TGHs in the valley;
- While the temperature data used in this model includes only 13 holes within the ranges and 78 holes in the valley;
- Higher thermal conductivity of the bedrock in ranges compared to the valley fill;
- Gradient values at depths less than ~500m (1640ft) were used for contouring; and
- Temperature inputs from the range and valley were calculated separately due to topography and elevation.

3.6.2 Thermal Anomalies within Dixie Valley

There are around ten areas that have relatively dense thermal gradients within the Dixie Valley area (Figure 30). Four of these are located along the DVFZ and around six occur within the DVSA. The dense thermal gradient areas along the DVFZ include from north to south: (1) the Senator Fumaroles just northwest of DVPF; (2) the section 10 fumaroles within the DVPP; (3) the Dixie Comstock Mine; and (4) the Dixie Meadow anomalies. The anomalies occurring away from the DVFZ are located near Hyder HS (northeast of producing field) and near New York Canyon within Buena Vista Valley. Temperature-depth profiles of the Dixie Comstock Mine, Dixie Meadows, and Hyder Hot Springs are shown in Figure 31. These anomalies are described below. Two additional prominent anomalies in the Dixie Valley area include the McCoy and Clan Alpine Ranch anomalies, which lie primarily outside the Project Area, and are not directly discussed in this report.

Dixie Comstock Mine

- Stable isotope analyses of mineralized quartz breccia show that the ore fluid was 180°C (356°F), near-boiling meteoric water, possibly related to the present-day hydrothermal activity in Dixie Valley (Vikre, 1994).
- One deep well (45-14) has a maximum temperature of 196°C (385°F) at 2750m (9022ft) with an upper gradient of (52°C/km [3.9°F/100ft])within the upper 1200m (3900ft) of the hole and lower gradient of (12°C/km [0.9°F/100ft] with the section below 1200m;
- Curves in intermediate depth TGHs (SR-2, SR-2A) shows evidence of lateral flow at shallow depth; and
- “Hot” rock faces are observed within the mine and the area shows significant surface alteration.

Dixie Meadows

- Most TGHs have “normal” background gradients indicative of the area (58°C/km [4.3°F/100ft]);
- TGHs (8G1 and 8G2) have high initial gradients (600+°C/km [44.5°F/100ft]) that become isothermal by about 15m (50ft);
- Three anomalous temperature curves (8g1, 8g2, 8g3) indicate lateral flow of warm water (~75-125°C [167-257°F]) at very shallow depth;
- Extensive fluid flow at the hot springs and a weak fumarole at the range front ~1km (3280ft) west of the hot spring area imply lateral flow from the range front; and
- Hot springs are coincident with the sharp horizontal gravity gradient in this area suggesting possible vertical up-flow along the piedmont fault.

Hyder Hot Springs

- Located ENE of the producing field near the center of the valley (Figure 14);
- Occurs near a strong positive aeromagnetic anomaly related to a body of gabbroic rocks in the basement beneath the valley fill and at the intersection of two faults (Figure 10);
- Lies within an suggested accommodation zone between the east-dipping Dixie Valley Fault and the west-dipping Pleasant Valley structures (Drakos et al. 2011); and

- Intermediate depth TGHs (EDV-1, EDV-2, EDV-3) have gradients that change only at conductivity breaks from valley fill to basement indicating the background conditions for the valley in that area.

New York Canyon

- Thermal anomaly located west of the Stillwater Range in the Buena Vista Valley;
- May infer a large area of elevated heat flow beneath the Stillwater Range that could possibly connect to the thermal anomalies in Dixie Valley based on the suggested elevated thermal conditions under the Stillwater Range; and
- Occurs adjacent to a major north-trending structure and the range-bounding fault that bounds the western edge of the Stillwater Range, referred to as the Stillwater Fault.

3.6.3 Numerical Modeling

The general consensus of geothermal systems in the B&R assumes no magmatic component and that meteoric water enters the system via the ranges or valley-fill, heats up during deep circulation, and ascends along the permeable pathway, usually an active range-bounding fault. In the case of Dixie Valley, the geothermal system is unusually hot as temperatures in excess of 280°C (536°F) have been encountered at ~3km (9840 ft) depths.

Wisian and Blackwell (2004) and McKenna and Blackwell (2004) have numerically examined the conditions necessary for a reservoir temperature near 280°C (536°F) to be generated and sustained in the Dixie Valley geothermal system. Parameters used were the measured temperature along the producing fault and the predicted surface heat flow. Drilling indicates temperatures >190°C (374°F) at a 2.5 to 3.0km (8200-9800ft) depth along a strike length of at least 14km (8.6mi) along the west side of the valley (from the DVPF to Dixie Comstock Mine. Their analysis generated a steady state numerical model with upflow along a permeable range-bounding fault that dips 65°. The temperature and heat loss are dependent on the permeability of the basement. For lower permeabilities the modeling shows little convective heat transfer while high permeabilities imply that the system cools to a low regional temperature over time. The range of basement permeability considered is 10^{-15} m^2 to 10^{-16} m^2. It is noted that the model uses a single 65° dipping range-bounding fault to characterize the permeable upflow zone, while evidence presented in Section 2.2.2 show the structural setting is more complicated. For the purposes and scale of the model, this discrepancy should not greatly affect the modeling results.

Temperature Modeling Conclusions

- Temperatures in B&R geothermal systems are time dependent;
- Temperature is not a function of the fault permeability or fault depth as the modeling showed that a fault about 2km (6560ft) deeper than the standard model has similar behavior/temperature;
- Regional permeability deeper than 6km (3.7mi) was not required to generate the observed temperature distribution in the geothermal reservoir;
- A high temperature reservoir within an extensional geothermal system (>280°C [536°F]) is a function of oscillating high/low fault permeability maintained by seismicity along the range-bounding fault;
- Application of the model results to Dixie Valley indicate that the age of present thermal flow is within the range of 50,000 to 500,000 years. This indicates that the geothermal

system is younger than the Dixie Valley fault zone (implied periodicity) and this finding is also supported by spring deposit age-dates (see section 5.2.1); and

- Temperatures are high enough for sustained geothermal development (>150°C [302°F]) as long as the permeability channels remain open and the fault conducting the geothermal fluids doesn’t seal.

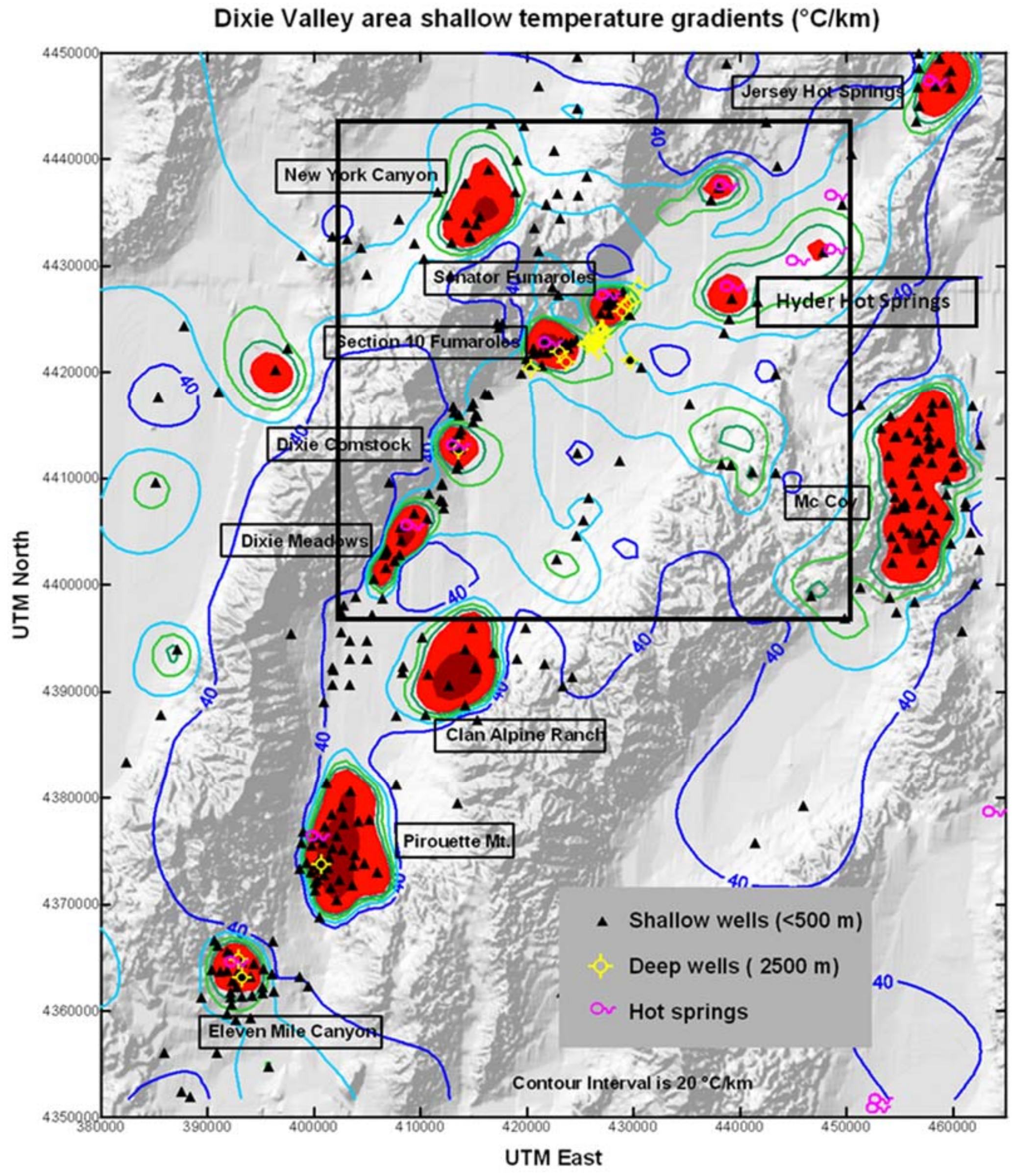

Figure 30. Thermal gradient and well locations in the Dixie Valley area. Contour intervals are (20°C/km [1.5°F/100ft]). From (120–250°C/km [8.75-18.5°F/100ft]) the contours are a red fill and from (500°C/km [37°F/100ft]) the contours are a dark red fill. Contours in the ranges are diagrammatic due to the lack of data. Well gradient locations are shown as black triangles for shallow wells (<~500meters [1640ft]) and as black circles for wells deeper than 500m (1640ft). Black bounded box is the approximate boundary of the EGS Exploration Methodology Study Area. The figure and caption are after Blackwell et al. (2005).

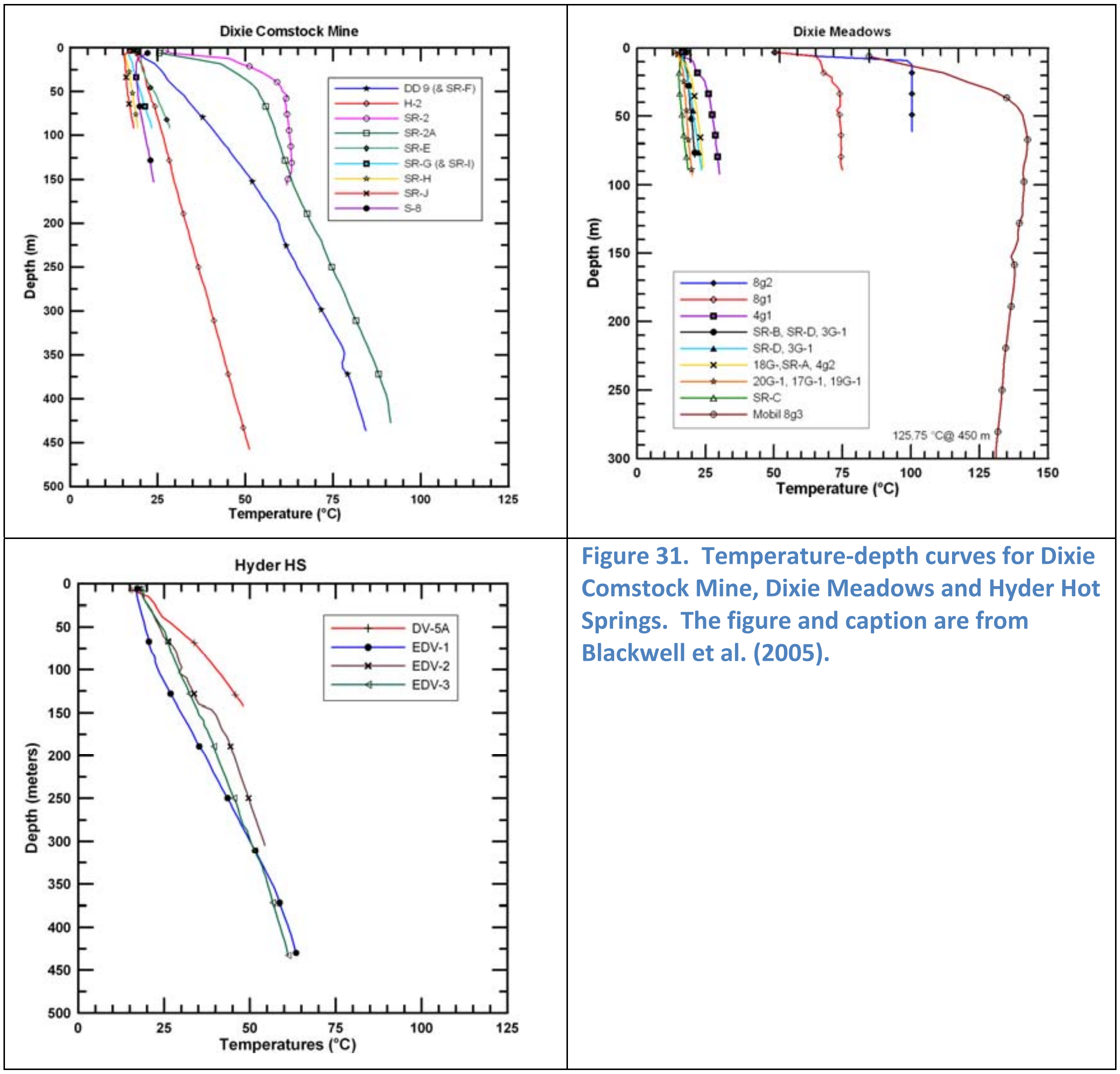

Figure 31. Temperature-depth curves for Dixie Comstock Mine, Dixie Meadows and Hyder Hot Springs. The figure and caption are from Blackwell et al. (2005).

4. Hydrology

4.1 Regional Setting

Dixie Valley is part of a larger drainage basin that includes Pleasant Valley and Jersey Valley to the north and Fairview Valley to the south, both of which flow (groundwater and surface water) into Dixie Valley. The Humboldt Salt Marsh is the lowest elevation in the basin and has no surface outlet. Evapotranspiration is the principal mechanism for shallow aquifer water and geothermal water to escape from this closed system, occurring at the Humboldt Salt Marsh and other playa settings within adjacent valleys.

During the Pleistocene, Lake Lahontan occupied the topographically enclosed valleys of the Western Great Basin including the Carson Desert and Carson Sink, immediately to the west of Dixie Valley (Figure 32A). Even during the highest stands of the lake, it was separated from the lower elevation Lake Dixie by a series of high passes. Lake Dixie was formed from local precipitation and glacial melt water and occupied the area within Dixie Valley (Figure 32B). The high stand of Lake Dixie was about 1097m (3566ft) above sea level, evident from preserved shorelines features on alluvial fans within the basin and bedrock on the range front. It covered an area of about 715km^2 (276mi^2) with a maximum water depth of about 70m (230ft) above the Humboldt Salt Marsh, and inundated a large portion of the length of the DVFZ. The high stand occurred at ~12-13 ka, coeval with the high stand of Lake Lahontan.

4.2 Groundwater

Shallow groundwater within Dixie Valley is recharged from precipitation in the drainage basin and surrounding ranges, and from adjacent valleys that provide surface and subsurface recharge to Dixie Valley. Groundwater is stored in both unconfined and confined (artesian) aquifers within the basin-fill sediments. Artesian aquifers in the Dixie town site area and in the area east of the Humboldt Salt Marsh are described as sandy to gravelly alluvial layers between fine-grained sediments (silts, clays). They occur at depths less than 70m (230ft) and are pressurized from infiltration in and near the Clan Alpine Range. Where these artesian aquifers intersect intrabasin faults, e.g., just east of the Humboldt Salt Marsh along the Buckbrush fault system, freshwater springs occur (Figure 33).

Another significant influence affecting groundwater in Dixie Valley is the outflow of geothermal fluids from the DVFZ into the basin-fill sediments. Salient features of the groundwater setting in Dixie Valley are:

- (197ft) in the southern valley;
- Contemporary precipitation is not sufficient for recharging valley aquifers and deeper geothermal systems;
- Recharge of shallow aquifers due to (1) precipitation on the mountains surrounding the basin, and (2) outflow of geothermal fluids from fault zones into basin-fill sediments;
- Considerable input of deep geothermal waters into the shallow aquifers (Nimz et al., 1999; Bruton et al., 2002); and
- Isotopic and geochemical data (Janik et al., 2002) suggest that a 10 to 25% addition of deep geothermal waters to the shallow aquifer waters is necessary to explain their isotopic and chemical composition.

- Depth to water table ranges from the surface at the Humboldt Salt March to over 60m 4.2.1 Buckbrush Fault System.

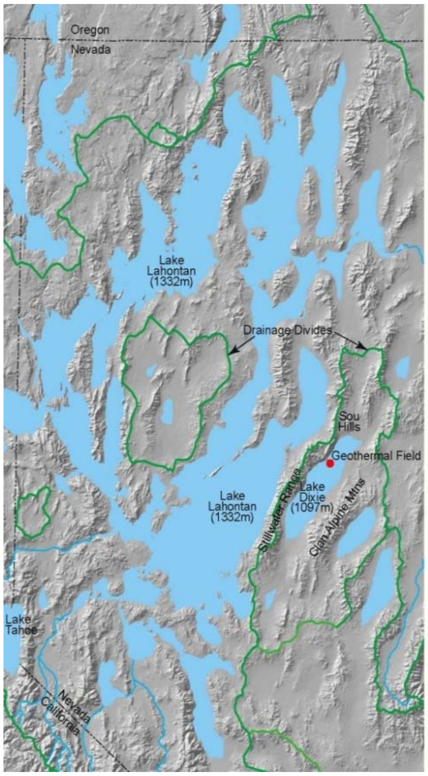

Figure 32A. Extent of the~13ka high stands of pluvial lakes Lahontan and Dixie. The figure is after Reheis (1999) and caption from Blackwell et al. (2005).

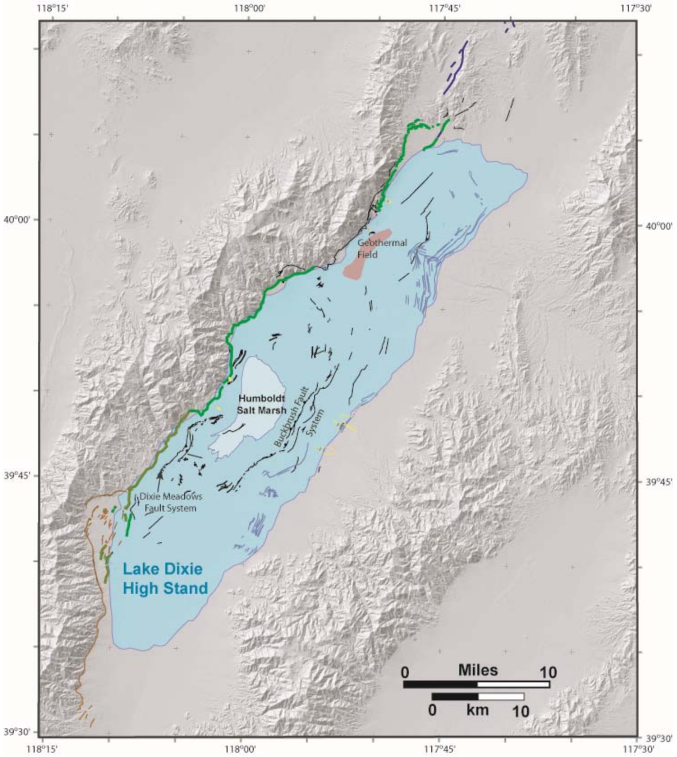

Figure 32B. Extent of the Lake Dixie high stand map~13 ka shorelines and intrabasin faults, and the contemporary extent of the remnant Humboldt Salt Marsh. Black lines = Dixie Valley Fault and faults in Stillwater Range; Brown lines = 1954 surface ruptures; Green lines = Bend Event (~2.5 ka) mapped intra-basin faults; Blue lines = preserved shoreline features; Yellow lines = preserved Pleistocene alluvial fans. Lake Dixie high stand from Caskey's DOE Workshop on Dixie Valley (2002). The figure and caption are from Blackwell et al. (2005).

Intrabasin springs occur along the Buckbrush fault system near the Humboldt Salt Marsh and along a northerly trend between the north end of the fault system and the southern part of the producing geothermal field (Figure 33). All the springs tap gravelly artesian layers containing shallow groundwater that are described in well logs within the area. Springs along the fault system are active presently while springs along the northern trend just to the north are considered recently active, but not active presently. It is suggested that the 1954 earthquake could have opened channels along the Buckbrush system and closed those just south of the geothermal system. Several of these shallow wells (TGHs) near the fault have warm water, as geochemical and isotopic data show that the artesian water in these wells and springs represents a mixture of cold meteoric water and warm water from geothermal activity derived from the Buckbrush fault zone.

4.3Geothermal Waters

The geothermal system is derived from recharge water that entered the fault zones and permeable sediments on the margins of the valley floor during the last glacial cycle. This requires long-term (thousands of years), and continuous flow-through of these deep seated waters. The majority of this flow enters the basin-fill sediments, with a small amount actually escaping to the surface in a few, scattered hot springs and fumaroles.

Geothermal gradients measured in wells throughout the valley define several places along the Dixie Valley fault where geothermal waters discharge into valley-fill sediments and flow basinward in the shallow subsurface. Outflow zones include Sou (Seven Devils) Hot Springs/Hyder Hot Springs in the northern valley, Senator Fumaroles (DVPF), Section 10 Fumaroles (DVPP), and Dixie Hot Springs (southern end of Humboldt Salt Marsh) which are shown in Figure 33. The location of these hot springs are controlled by the range bounding fault within the DVFZ and lie within the areas of high geothermal gradients within Dixie Valley (Figure 33). Additionally a local thermal gradient high east of Dixie Meadows referred to as the Clan Alpine Ranch anomaly (Figure 30) could also be considered an outflow zone of geothermal fluids derived from a dilatational zone occurring at a fault termination of a significant range-bounding fault on the eastern edge of Dixie Valley. This occurs within the southernmost boundary of the Project Area. Salient highlights of the origin of geothermal waters are:

- Isolated from present day meteoric recharge;
- Vertical local recharge from Lake Dixie with model dependent isotopic ages indicating waters are 12-20 ka;
- Recharged during the Pleistocene as the oldest recharge waters measured are ~14,000 years old based on model dependent ^{14}C ages; and
- Exact age of the system cannot be accurately assessed because the reservoir has been contaminated during nearly 20 years of production, steam separation and injection.

4.4 Hydrogeochemistry

The waters within the Dixie Valley basin compositionally overlap the waters from the Stillwater Range and the Clan Alpine/Augusta Ranges to the east. Stillwater Range derived waters typically have higher Mg and Cl, and lower Ca than waters from the Clan Alpine/Augusta Range most likely reflecting lithologic differences in the ranges. The overlap is expected as the valley sediments are derived of bedrock detritus from both of the surrounding ranges. Additionally the basin waters tend to have higher Na and K, which is typical of waters with the input of geothermal fluids, which indicate a third distinct source in their history.

While the sources for the Dixie Valley basin waters are largely constrained, the stable isotope geochemistry of the Dixie Valley related waters can be used to determine the possible recharge areas for the geothermal reservoir and associated hot spring systems. A plot of δD vs. $\delta^{18}O$ (Figure 34) of waters from the Stillwater Range, Clan Alpine Range, Dixie Valley Basin, and the production zone is used to determine spatial isotope distributions and relations among geographic areas (elevation). Waters from the pre-production reservoir do not isotopically resemble the waters from the surrounding ranges indicating that the ranges are not recharge sources for the reservoir. Additionally these cold waters from the ranges are isotopically enriched relative to cold waters in Dixie Valley basin which is unexpected as waters of high elevations usually show depleted isotopic compositions compared to those of lower elevation. According to Blackwell et al., (2005) and observations from Goff, Janik and others (1998; 2002), a reasonable explanation for this anomaly is that the basin waters are older and recharged when isotopic compositions of meteoric recharge were more depleted (Pleistocene recharge). Instead fluids from geothermal reservoir have similar δD values to Dixie Valley basin but are enriched in $\delta^{18}O$ by about 2.5 ‰, consistent with significant water-rock isotopic exchange. The authors imply that Dixie Valley was recharged at elevations higher than samples collected in the ranges or originated from an earlier time when precipitation was isotopically different.

5. Geochemistry

5.1 Introduction

Numerous geochemical studies have been undergone in Dixie Valley, with a more recent and comprehensive report compiled (Goff et al., 2002) that includes an extensive geochemical database based on samples collected and analyzed from 1996-1999. This report can be found as Appendix 7. General characteristics as summarized in Blackwell et al. (2005) can be found in Appendix 8 with the salient aspects described below. The geochemical studies conclude that groundwater samples from Dixie Valley are derived from either (1) younger meteoric waters from the surrounding ranges, (2) High Temperature Geothermal Fluids (HTGF) characteristic of the Dixie Valley producing reservoir, or (3) more commonly a mixture of the two.

The preliminary analysis of the geochemical data has further identified at least three primary fluid types within Dixie Valley that are geochemically distinct from the HTGF encountered in the geothermal wells. The distribution of these primary fluid types with respect to the regional Dixie Valley setting is shown in Figure 35A. The fluid types are characterized as (1) High Cl-low HCO_3,

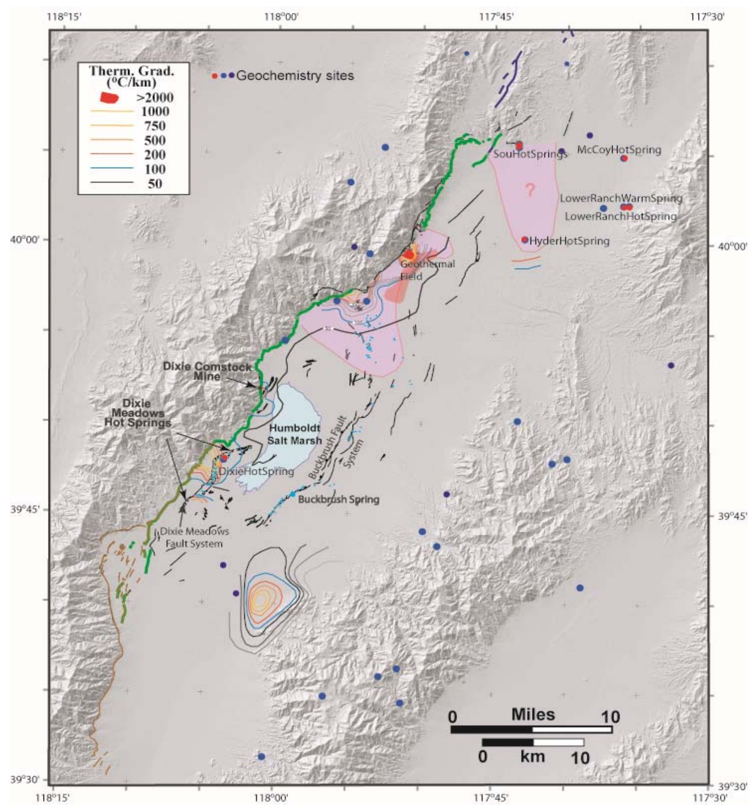

Figure 33. Map showing geothermal gradient, outflow zones, hot springs and range-front fault ages. Contours show geothermal gradient (°C/km) gray lines = 25°C/km (1.85°F/100ft) intervals. Pink shaded areas are outflow zones into groundwater table (Allis et al., 1999). Range-front faults are thick lines: Blue (to the north) = 1915 surface ruptures; brown (to the south) = 1954 surface ruptures; green = "The Bend Event"~2.5 ka surface ruptures. The Goff et al., 2002 geochemical sampling locations are: blue dots = springs and dark blue dots = wells. Shevenell and Garside, 2003 spring geochemical data = red dots. Smith et al., 2001 springs = small light blue dots. The figure and caption are from Blackwell et al. (2005).

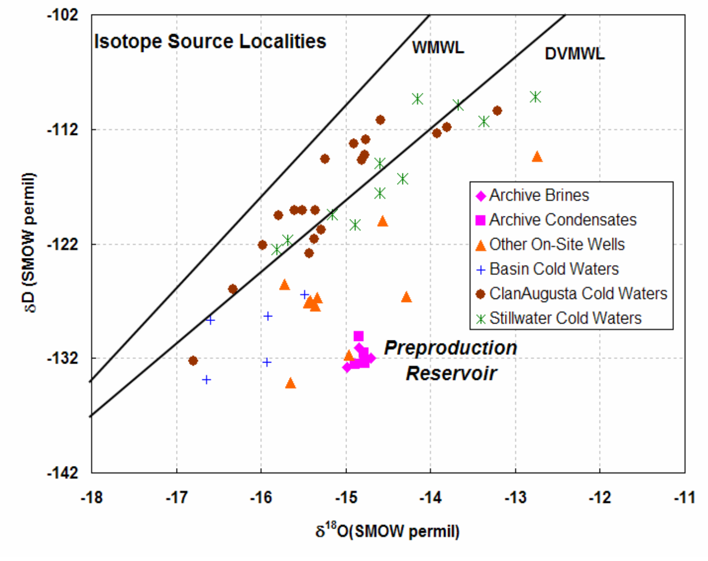

Figure 34. Deuterium versus oxygen-18 for Dixie Valley related waters from the Stillwater Range, Clan Alpine Range, Dixie Valley Basin, and the production zone. The data is from Goff et al. (2002). The figure and caption are from Blackwell et al. (2005).

(2) Low Cl-high HCO_3, and (3) Low Cl-low HCO_3. A further evaluation indicates significant fluid mixing and the presence of a fourth very dilute fluid component (B.M. Kennedy, pers. comm., 2010), Figure 35B. This component is classified as geochemically un-evolved near surface ground water. The evidence of mixing may explain inconsistencies in calculated chemical geothermometer temperatures, help deconvolve the impact of mixing, and enable more accurate calculations of water-rock equilibration temperatures.

Geochemical features of HTGF and mixed fluids are listed below:

Characteristics of High Temperature Geothermal Fluids (HTGF)

- reservoir pH between 6-9;
- Na-K-Cl waters;
- relatively high SiO_2, As, B, Br, and Li;
- dissolved CO_2 is another major component;
- relatively low concentrations of divalent cations (Ca, Mg, and Sr); and
- very low concentrations of trivalent cations (Al and Fe).

Characteristics of Mixed Fluids

- relatively high concentrations of SiO_2, Cl, Na, K;
- relatively high concentrations of four key trace elements, As, B, Br, and Li; and
- retains constant ratios such as B/Cl and Li/Cl.

5.2 Springs, fumaroles and shallow wells

Most of the thermal/mineral springs in the Dixie Valley region (Figure 35A)do not possess the high-temperature geochemical signatures described above and indicative of the geothermal reservoir. This implies that these waters either haven't equilibrated at high temperatures or are of mixed fluid composition consisting of high temperature fluids and cooler groundwaters. While mixed fluid generally retain constant ratios of conservative components (B/Cl and Li/Cl), the shallow well and spring waters display different ratios among themselves and when compared to the DVPF production fluids. Additionally shallow well and spring waters have very low arsenic to chloride ratios further suggesting that they are not related to production fluids. The lack of trends between the different fluids implies that each of somewhat isolated geothermal systems has a different geochemical history. Thus, each thermal system is geochemically unique and has evolved along a distinctive path that is influenced by the sources of water, interactions with local wall rocks, and relationship to crustal heat sources.

The As/Cl relationships of pre-production fluids (referred to as archive brines), production brines, thermal/mineral springs and thermal/mineral wells are shown in Figure 36. While the pre-production and production fluids define a similar trend, the thermal/mineral well and spring waters of the Dixie Valley region define no such trend. These waters do not lie on the mixing trend of the production fluids and also do not lie on a similar trend among themselves. This further indicates that all fluids originated from separate geothermal cells and that the geothermal fluids from springs and shallow wells are not part of the same system as the current electrical generation producing system at the DVPF.

5.2.1 Hot Springs and Fumaroles

Hot springs and fumaroles are located along the DVFZ and associated intrabasin faults where geothermal fluids rise along permeable segments of the fault and either discharge into the basin-fill sediments or more uncommonly at the surface. The following is an overview of the major hot springs and fumaroles within and around the Project Area (for locations see Figure 33). Provided below is a summary of the characteristics of the various hot springs in Dixie Valley.

Dixie Meadows

- max T=84°C (183°F)
- Group of at least 20 springs and seeps near the southern half of Humboldt Salt Marsh;
- Emerges from a hydrothermal plume rising along the DVFZ (range front or buried piedmont fault;
- Total discharge of as much as 200 liters/min (52gpm); and
- Relatively high silica and chloride.

Hyder HS

- T= 77°C (171°F) and 40 l/min (11gpm);
- Located near the middle of Dixie Valley about 4km (2.5mi) east of the DVPF;
- Two or more seeps and springs discharge from a soft travertine deposit (hill);
- Controlled by the intersection of buried faults or possibly explained by an accommodation zone between two adverse structures (Drakos et al. 2011);
- Mixed fluids including a parent fluid similar to the 62-21 well waters, but mixed with shallow aquifer water; and
- Spring system lies at the northernmost end of a positive aeromagnetic anomaly associated with a buried basement block of the Jurassic mafic complex.

Jersey HS

- T= 59°C (138°F) and 200 l/min (53gpm); and
- Issues from a modified pool with no obvious structural control except a localized step-over.

Lower Ranch HS

- max T = 41°C (106°F);
- Five HS and seeps from a major faulted travertine deposit in eastern Dixie Valley; and
- Water does not resemble Dixie production fluids.

Section 10 (unnamed) fumaroles

- max T = 98°C (208°F);
- NW of DVPP lease, no associated hot springs, steam vents only;
- Fumarole activity occurs directly along the range-front fault within a localized alteration zone;
- Also referred to as the Frying Pan fumaroles (Al Waibel, pers. comm., 2011);
- Sinter deposits with intergrown travertine, sulfur and other sublimates; and
- Fossil hot springs related to previous seismic activity on the DVFZ.

Senator fumaroles

- max T = 98°C (208°F);
- Only surface thermal manifestation of the subsurface, high temperature thermal anomaly;
- Present fumarole activity occurs on the northeast edge of an altered "mound" structure around 500m (1640ft) valleyward from the main range-front contact;
- No fossil hot springs or sinter deposits, forms a cluster of springs extending 600m (1970ft) along the DVFZ;
- The increased activity observed at the present time is mostly production related and due to draw-down of the geothermal reservoir (B.M. Kennedy, pers. comm., 2011); and
- Rocks within the main fumarole cluster are highly fractured and faulted Jurassic quartzite (Boyer Ranch) and overlying alluvial fan deposits.

The Dixie Valley region contains many hot spring deposits and alteration zones related to present and past hydrothermal activity and some of these deposits have been age-dated (Table 2).

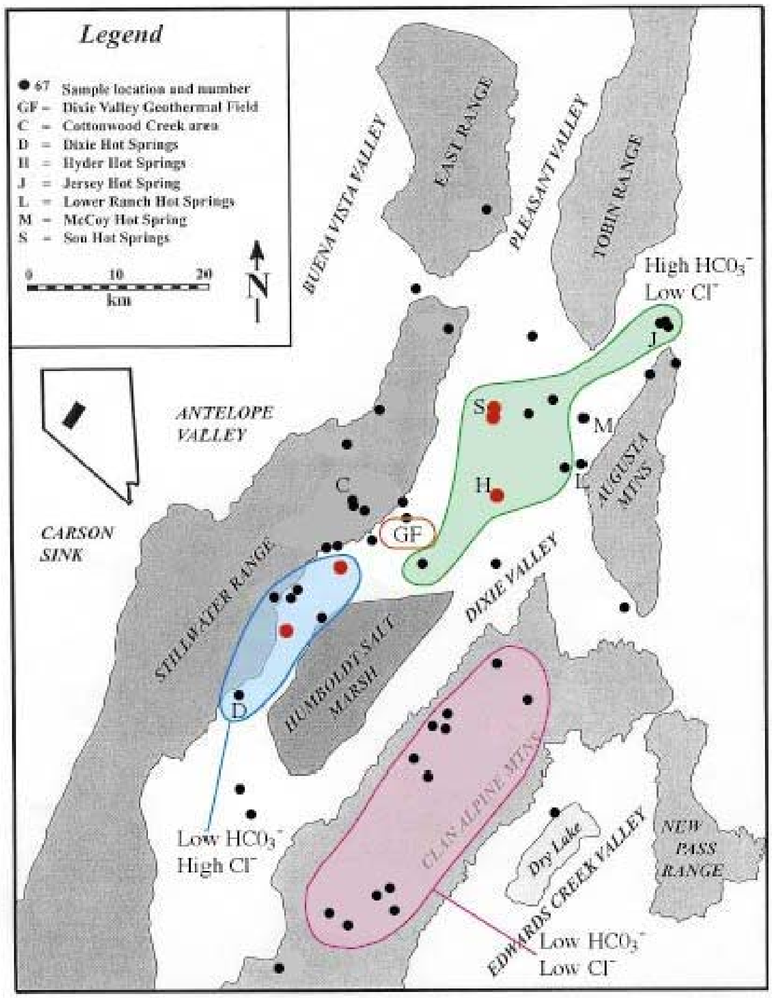

Figure 35A. Distribution of Dixie Valley fluid types with sample locations. The abridged data set is from Goff et al. (2002) and presented in Appendix 7.

5.3 Deep Wells

The following section details the salient elements of wells containing thermal waters but no associated near-surface thermal features .

5.3.1 Bolivan Artesian Well

This well is located well within the Stillwater Range at an elevation of around 1500m (4900 ft) within Cottonwood Canyon just upstream of an abandoned mining community (location shown on Figure 17a). It was originally drilled as a thermal gradient hole within highly altered Jurassic gabbro and limestone and is indicative of a localized geothermal anomaly in this area of the Stillwater Range (S. Johnson to D. Blackwell, pers. comm., 1997). The flow and geochemical characteristics of this well has been reported by Goff et al. 2002 as:

- Artesian well (40 l/min [11gpm]of 29°C [84°F] water);
- No free gas observed discharging from the well water; and
- Low Si, As, B, Br, Li; but 290ppm Cl indicating the waters don't resemble DVPF fluids.

- Currently, a small amount of fluid (1-2 l/min, 0.3-0.5 gpm) has been observed discharging from a near surface pipe (T. Cladouhos, pers. comm., 2010).

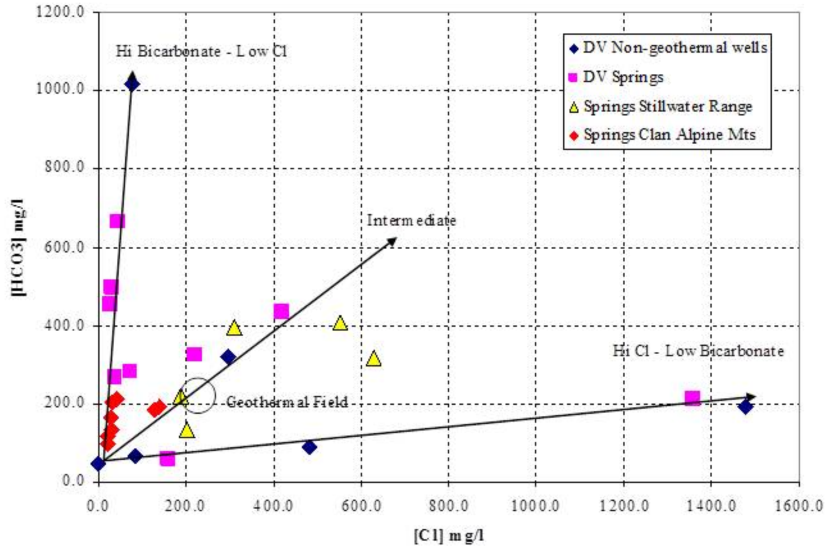

Figure 35B. Variations in Dixie Valley fluid compositions indicative of at least three and perhaps four independent end-member fluids and evidence for mixing of these end-member fluids with a dilute groundwater. The abridged data set is from Goff et al. (2002).

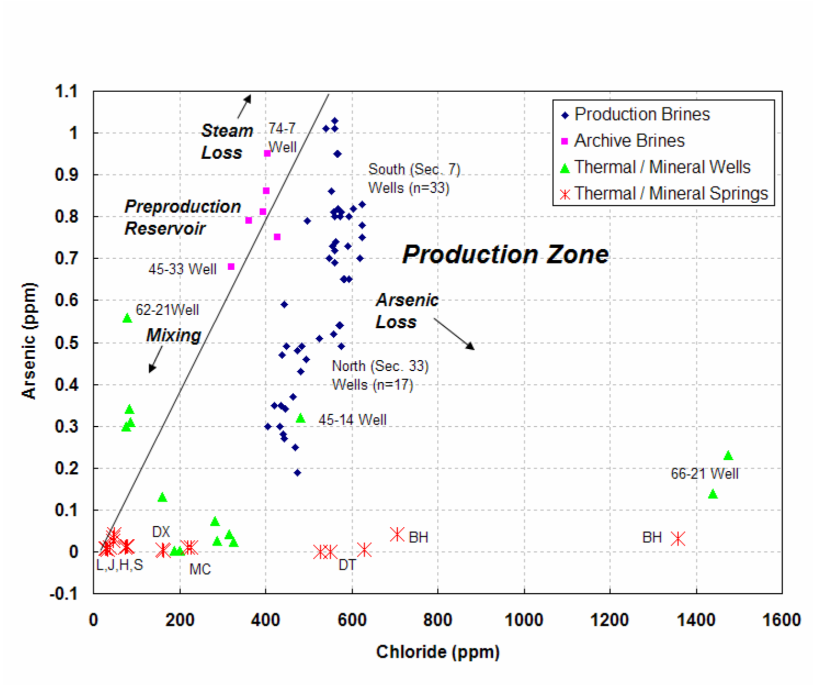

Figure 36. Plot of arsenic versus chloride for thermal and nonthermal waters of Dixie Valley region, Nevada. Thermal/Mineral Spring Labels: DX= Dixie Hot Spring, MC = McCoy Hot Spring, DT = Dead Travertine Spring, BH = Big Horn Spring, H = Hyder Hot Spring, S = Sou Hot Spring, J = Jersey Hot Spring, L = Lower Ranch Hot Spring. The archived brine samples (provided by Oxbow Geothermal Co.) provided baseline information on the pre-production geochemistry of the geothermal field. The data is from Goff et al. (2002) and the figure and caption are from Blackwell et al. (2005).

5.3.2 Dixie Federal Well 45-14

This well is located about 1km (3200ft) SE of the abandoned Dixie Comstock gold mine and is about 12km (7.4mi) SW of the DVPF (see Figure 40a). The well was drilled in 1979 within a fault block bounded by a north-trending segment of the range-front fault and the surface expression of the main piedmont fault within the DVFZ. Temperature surveys show a maximum temperature of 196°C (385°F) at a total depth of 2750m (9022ft). Chemical characteristics of the produced fluid are:

- High concentrations of SiO_2, As, B, Br, and Li;
- Low concentrations of Ca and Mg with a Cl content of 481ppm;
- Most similar in general composition to deep reservoir waters (Figure 26);
- Chloride variation plots indicate the fluid is not derived from the 245°C (473°F) reservoir;
- Very weak (8-15 l/min, 2–4 gpm) artesian flow (Dick Benoit of Magma Power Company to Joe Iovenitti of AltaRock, pers. comm., 2011); and
- Fluid entries at 1940m (6365ft) and 2510m (8235ft); rate of flow= 1.1 l/s or 14 gpm (Williams and Sass, 1997).

5.3.3 Dixie Comstock Mine

- The mine is located within the DVFZ, adjacent to a north-trending segment, just west of 45-14 (see Figure 40a);
- Typical stockwork epithermal ore deposit with "hot" rock faces reported in mine; and
- Possibly related to present hydrothermal activity in Dixie Valley.

5.3.4 Dixie Federal Well 66-21

The well is located in the valley just south of DVPP; and only 2km (6560ft) SW of the section 10 fumaroles (see Figure 40a). The well was also drilled in 1979 with a maximum recorded temperature of 215°C (419°F) at 2740m (8990ft).

- Weak artesian flow (Dick Benoit of Magma Power Company to Joe Iovenitti of AltaRock, pers. comm., 2011);
- Relatively moderate to high contents of (SiO_2, As, B, Br, and Li);
- Not part of the producing reservoir but has the general characteristics of HTGF;
- The Cl-concentration is 3x (1460ppm) that in the DVPF and represents the most saline groundwater in DV; and
- Water entry near the bottom has equilibrated at about 210°C (410°F).

5.3.5 Dixie Federal Well 62-21

This well occurs near the middle of DV about ~10km (6mi) east of 66-21 and ~4km (2.5mi) SE of DVPF. It is the deepest well drilled in DV at 3810m (12,500ft) and has a recorded maximum BHT of 184° (363°F). The intention was to target a major west-dipping intrabasin fault, that appeared to connect to Hyder HS (D. Blackwell, pers. comm., 2012).

- Contains moderate amounts of SiO_2, Br, and Li, and high amounts of As and B;
- Low concentrations of Ca and Mg with a Cl content of only 80 ppm;
- Fluid entry occurs at 2900m (9500ft) at the contact of gabbro and underlying Triassic slate;
- Open head: flows 140 l/min (37gpm) of water at about 76°C (169°F);
- Waters don't resemble Dixie production fluids (low Cl);
- Chemically and isotopically similar to Hyder HS; and

- Characteristics of moderate temperature geothermal fluids.

Table 2. Summary of Ages of Dixie Valley Spring Deposits (from Blackwell et al., 2005).

Site	Type	Material	Method	Date (ka)	Reference
Dead Travertine	Vein	Calcite	U/Th Disequilibrium	182 ± 4	Goff et al. (2002)
	Vein	Calcite	Protactinuim-231	161 ± 15	Goff et al. (2002)
	Travertine	Calcite	U/Th Isochron	100 ± 5	Dixon et al. (2003)
Lower Ranch	Travertine + Sinter	Quartz	U/Th Disequilibrium	54 ± 4	Goff et al. (2002)
	Travertine + Sinter	Quartz	Protactinuim-231	39 ± 2	Goff et al. (2002)
The Mirrors	Fault Gouge	Quartz	U/Th Disequilibrium	287 ± 16?	Unpublished, from Lutz et al.
Dixie Comstock Mine	Sinter Clast	Pollen/ Organics	^{14}C AMS	10.72 ± 0.07	Lutz et al. (2003)
Section 11 Altered Zone Terrace	"Zebra" Travertine	Unknown	^{14}C AMS	5. 04 ± 0.06	Lutz et al. (2003)
	Black Travertine	Calcite	U/Th Isochron	3.75 ± 0.33	Dixon et al. (2003)
Section 10 Sinters	Four Sinter Layers	Quartz, Opal, Calcite	U/Th Isochron	4.1 ± 0.1	Dixon et al. (2003)
Section 11 Sinter	Sinter	Organics	^{14}C AMS	2.18 ± 0.06	Lutz et al. (2003)
Section 15 Sinters	Sinter	Organics	^{14}C AMS	2.47 ± 0.05	Lutz et al. (2003)
	Sinter	Organics	^{14}C AMS	2.52 ± 0.05	Lutz et al. (2003)
	Sinter	Quartz, Opal, Calcite	U/Th Isochron	3.6 ± 0.1	Dixon et al. (2003)

5.4 Geothermal and Production Fluids

The DVPF production fluids show all the same characteristics as HTGF and are assumed to derive from deep circulation along the DVFZ. The pre-production fluids define a trend of similar As/Cl ratios, indicating that all the production fluids are interrelated (Figure 36). Within this figure, increased As and Cl would indicate steam loss (without loss of arsenic), while a decrease indicates mixing of reservoir fluids with more dilute groundwaters.

The cation and anion chemistry within the geothermal system indicates that a major NE-SW trend is apparent with an increase in Cl concentration and decrease in downhole flowing enthalpy of the pre-production fluids. This trend takes place in the DVPF and extends from section 33 (northwestern most producers, lowest Cl and highest enthalpy) to section 7 (central producers) to section 18 (southeastern most injectors, highest Cl and lowest enthalpy). Figure 40a shows the location of these sections representing the main production and injection zones within the producing field . The trend, when coupled with Na and K contents of the pre-production fluids, implies the presence of at least three fluids with distinctly different thermal and chemical histories. Non-condensable gas data also support the mixing of multiple fluids.

5.5 Helium Isotopic Data

The helium ($^3He/^4He$) isotope ratio provides very strong evidence for the presence of mantle derived fluids in geothermal systems, and therefore may be an indication of a potential heat source and the potential role mantle melting plays in the formation of a crustal geothermal system. Helium associated with crustal fluids with no mantle influence is characterized by low $^3He/^4He$ ratio (~0.02 Ra where Ra is the $^3He/^4He$ ratio in air). Helium associated with mantle fluids is enriched in ^3He, e.g., mid-ocean ridge basalts, and have $^3He/^4He$ ratios of ~8-9 Ra. Extensional geothermal systems in the B&R that have moderately elevated $^3He/^4He$ ratios (≤0.8 Ra), with no known mid to upper crustal magmatic activity, indicate a mantle component and suggest the occurrence of deep permeable pathways that cut through the upper and lower crust delivering mantle helium to the crustal hydrologic system. Helium sample sites in the B&R (Figure 37), show that Dixie Valley has moderately elevated helium ratios when compared to the surrounding B&R, and is described as a low level "He spike" not related to current magmatism (Kennedy and van Soest, 2007). It has been mentioned by Kennedy and others that the long history of seismicity along the DVFZ has possibly prevented the fault from permanently sealing, and thus keeping the pathways open.

The helium associated with fluids from the productive geothermal reservoir has an isotopic composition of 0.70 - 0.76 Ra and represents the highest ratios measured in the valley. The helium component in the Dixie Valley geothermal field fluids indicates that ~7.5% of the total helium in the system is derived from the mantle. Since there is no recent volcanics or other potential sources, the mantle derived helium is assumed to originate from upflow along the DVFZ. The helium composition from springs and wells that are not in direction communication with the fault zone are a mixture of this deep fluid with younger less helium enriched groundwater. The exception to this simple mixing trend are the fumarole sites (Senator and section 10) and Dixie Meadow HS which are not affected by shallow ground water and are directly connected to the deep geothermal system (Figure 37).

Spring geochemistry coupled with the local geology also indicates that the helium signature is not related to magmatic activity, and reflects localized zones characterized by deep permeable pathways and high vertical fluid flow rates. Kennedy and van Soest (2006) suggest two mechanisms for the modest enrichment of mantle Helium in the geothermal system (1) fluid circulation through an aged and non-active magma chamber (perhaps the source chamber for local Miocene basalts; and (2) fluid transport along the range-front fault from deep mantle sources. The data supports the latter mechanism and concludes that the most viable source for the ^3He is fluid transport up through faults, that are in direct communication with the mantle.

Fluids from springs, wells and fumaroles throughout Dixie Valley including from the DVPF were analyzed for noble gas abundances and isotopic compositions (Kennedy et al., 1996; 2002; 2005) and shown in Figure 38. The highest helium ratios occurred in the DVPF and at the Dixie Meadows, Section 10 fumaroles, and in a fluid sampled from 36-14. The noble gas data provides support for (1) fluid mixing; (2) gas loss related to boiling and phase separation; and (3) provides evidence that all of the springs, fumaroles, and non-geothermal wells sampled for noble gas analyses contain a noble gas component that is indistinguishable from the noble gases in the production fluids from the DVGS (Figure 38).

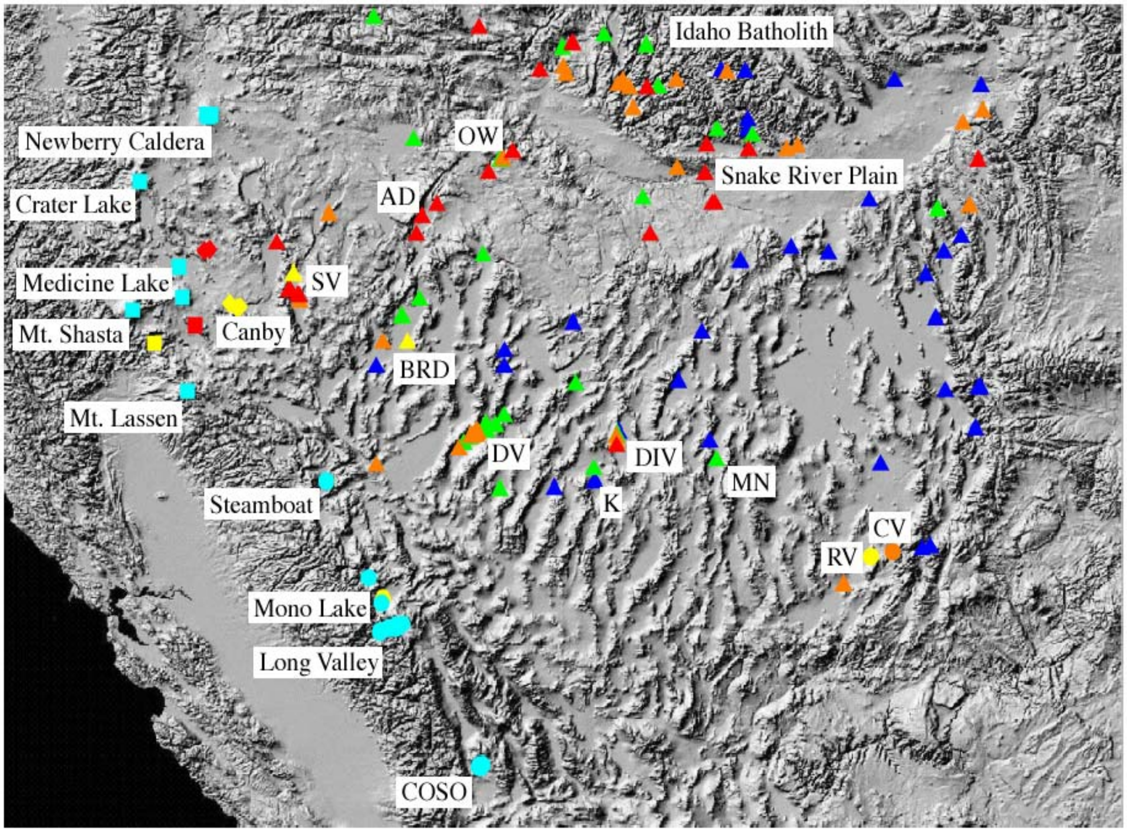

Figure 37. Shaded relief sample location map of the B&R and surrounding areas. The different symbols give an indication of the heat source: circle and squares, magmatic; triangles, extensional; and diamonds, not sure. The magnitude of the 3He/4He ratio at each locality is coded by color as follows: blue ≤ 0.3 Ra; 0.3 Ra > green ≤ 0.6 Ra; 0.6 Ra > orange ≤ 1.0 Ra; 1.0 Ra > red ≤ 2.0 Ra; 2.0 > yellow ≤ 3.0 Ra; cyan > 3.0 Ra. Certain features are labeled: SV: Surprise Valley; BRD: Black Rock Desert; AD: Alvord Desert; DV: Dixie Valley; OW: Owyhee River Canyon; DIV: Diamond Valley; K: Klobe hot spring: so far the lowest observed 3He/4He ratio in the B&R at 0.014 Ra; MN: Monte Neva hot spring; RV: Roosevelt hot spring and geothermal energy plant; CF: Cove Fort geothermal energy plant. The figure and caption after Kennedy and van Soest. (2007).

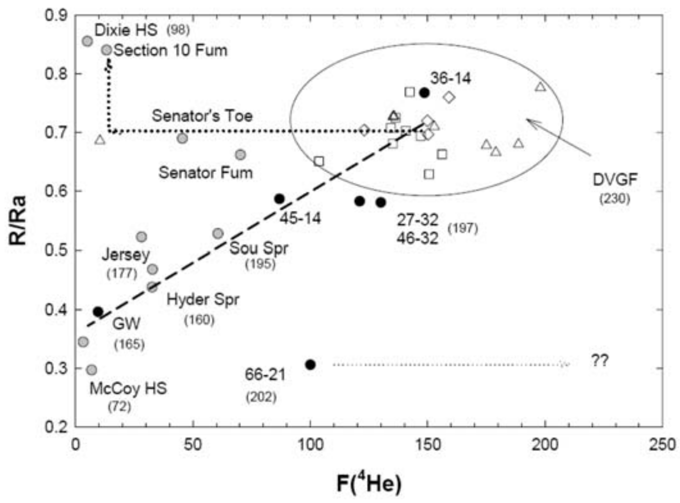

Figure 38. Non-atmospheric noble gases (radiogenic and mantle derived helium) in selected Dixie Valley springs, fumaroles, non-geothermal wells (circles) and geothermal wells (squares, diamonds and triangles). The figure and caption are from Kennedy and van Soest (2006).

5.6 Fluid-inclusion Gas Chemistry

Lutz et al. (2002) analyzed the composition of fluid-inclusion gases from (1) hydrothermally altered samples from outcrops along the eastern Stillwater Range, and (2) scale and vein samples from geothermal wells. The following section summarizes the work performed.

The purpose of the study was to establish the chemistry of the fluids trapped during alteration and mineral deposition and use such relationships to evaluate the origins of the inclusion fluids. The analysis indicated that fluids of different origins were involved in the formation of alteration minerals during the evolution of the Dixie Valley geothermal system, with a mixing between shallow meteoric, evolved meteoric (crustal), and magmatic end members. Geothermal vein samples from the wells are interpreted as mixtures of shallow meteoric and evolved meteoric (crustal) fluids. Fluid-inclusion gases from epidote-bearing fault gouge appear to have a strong crustal signature (low CO_2/CH_4 ratios), while hematite-bearing vein assemblages are purely meteoric in origin. Analyses with high N_2/Ar ratios indicate a magmatic origin for some fluid inclusion gases which agrees with the slight mantle-derived helium signature. There is also a small magmatic component to the gases in quartz-calcite veins from production wells, which was unexpected as the geothermal system was thought to be related to deep-circulation non-magmatic processes. The source of this magmatic component is unclear as no shallow magmatic bodies exist in the vicinity of Dixie Valley. The magmatic gases could originate from:

- An isolated, aged magma chamber supplying magmatic gases from U and Th decay (Kennedy et al., 1996);
- Miocene basalt which could be the source of the magmatic gas in the geothermal veins (Lutz et al., 2002); and/or
- Directly from the mantle through a deep-seated range front fault (Blackwell et al., 2005; Kennedy et al., 2005).

5.7 Injection Studies

The geothermal field's main production and injection zones are overviewed in Section 6.2. Geothermal Reservoir and shown previously in Figure 17A and as well as Figure 40A. Presented here is a discussion of the geochemistry injection investigations as summarized from Blackwell et al. 2005.

Since the onset of production in mid-1988,~300 x 10^9kg (6.6 x 10^{11}lbs) of flashed brine, condensed steam, and shallow groundwater has been injected into the Dixie Valley reservoir. The fluids were injected into three general zones (1) the shallow range-front fault near section 5 (depths near 1800m [5900ft]); (2) the piedmont fault in section 18 (depths of 2700 to 300m [8860-9840ft]); and (3) the Miocene basalt aquifer overlying the southern part of reservoir in section 18 (2170 to 2230m [7120-7320ft]).The brine is distinguished from the production fluid as it is enriched in Cl, ^{18}O and D, and depleted in non-condensable gases. Chloride trends and tracer testing show a high degree of connectivity between the injection and production wells. This assumes there is only one indigenous geothermal fluid entering the reservoir or individual wells within the DVPF.

5.7.1 Tracer Test – Reservoir Connectivity

Tracer testing performed within the geothermal system revealed a high degree of reservoir connectivity between all the injection wells (section 18 and 5) and the section 7 production wells (Rose et al. 2002). For the location on injection and production zones, see Section 5, Figure 17a and 40A. In previous studies including Rose et al. 2002, no tracers from section 5 or 18 injectors has ever been observed in the northern-most section 33 production wells. While section 32 injector wells show a degree of connectivity with the northern wells within section 33, a major flow barrier was thought to exist between the Section 5 wells and southern wells within section 33 (Figure 39). However findings from Lutz et al. (2003) and an analysis by Reed (2007) show that all of the section 33 wells (27-33, 28-33, 37-33) and the section 7 producers received the tracer from injection well 25-5 and thus there is no barrier to fluid flow in the geothermal reservoir. According to this more recent study, augmentation fluid injection may have re-established fluid pathways and reversed indications of the proposed barrier described above.

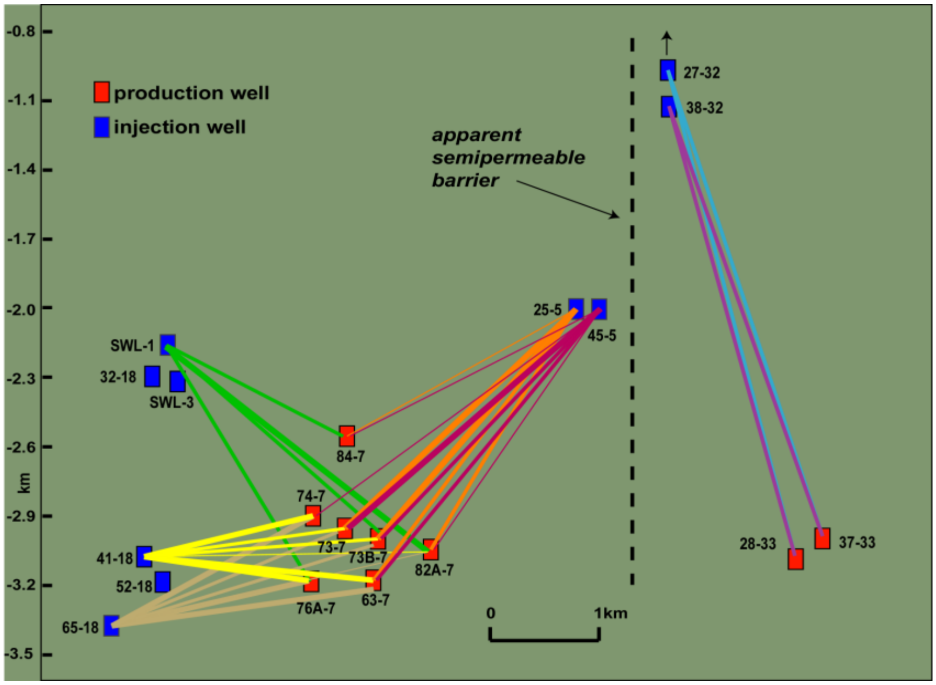

Figure 39. NE/SW Cross Section showing tracer flow patterns of the producing field based on tracer and connectivity test. The figure and caption are from Rose et al. (2002).

6. Dixie Valley Geothermal Wellfield

This section represents the available wellfield assessment acquired from the public literature, Blackwell et al. 2005, and selected proprietary data provided by Terra-Gen Corporation.

The DVGW encompasses the area (1) in and around the producing and injecting portions of the geothermal field, and (2) dry and sub-commercial wells to the northeast and southwest of the producing area, and lies primarily within the DVFZ (Figure 40a). The producing portion of the wellfield (DVPF, Figure 1) also lies adjacent to the Stillwater Seismic Gap (see Section 2.2.2). The DVGW for the purposes of this report incorporates all the geothermal wells[1] drilled in the Project Area and extends from 45-14 to the southwest, to 76-28 to the northwest, and to 62-21 to the east in central Dixie Valley (Figure 40A). The wellfield is bounded by the range-front fault to the west, as no geothermal wells have been drilled within the Stillwater Range. The DVGW contains the highest measured geothermal gradients (see Figure 33), surface expressions of hydrothermal circulation including Senator and section 10 Fumaroles, and numerous intrabasinal faults. As reported by Blackwell et al. (2005) the producing area lies at a complex structural intersection of intra-range normal faulting, the main range-bounding fault and two piedmont faults, a Landsat lineament, an InSAR lineament (Foxall and Vasco, 2003), and the gravity gradient maxima along the western margin of the basin (Figure 40B).

6.1 Structure

The structural model for the DVGW proposed by Okaya and Thompson (1985) and Benoit (1999) (discussed in Section 2.2.2) was a single range-bounding fault dipping at ~54° toward the basin. This model was based on the assumption that the faults encountered in the producing wells could be projected to the topographic break between the valley and range. A variety of geophysical data has been collected (Blackwell et al., 2005) supporting an alternative hypothesis that the contact between the range and valley blocks occurs along 2 or more, steeply dipping faults – rather than a single moderately dipping fault. This evidence includes reprocessed seismic lines (Figure 17a and 18), aeromagnetic and gravity data (Figure 12), geologic mapping, well data including temperature profiles (see Section 6.3), and interpretations from MT profiles (Figure 16A-16C). The baseline conceptual model assumes a steeply dipping multi-fault model along the entire length of the DVFZ through the study area as is required by the geologic, drilling, and geophysical evidence available (see Section 7.2 for a detailed discussion). Salient structural setting features within the producing field are that:

- Fractures feeding the geothermal system are steep (70° to 90°) within the upper 3.5km (11,200ft) of the crust;
- The DVFZ is complex and distributed laterally over several kilometers extending from within the range to deep in the basin fill;
- The source of heat is the flow of fluids within dilated zones along two steeply dipping faults, specifically the range-front fault and a major sub-parallel piedmont fault segment. For example 36-14, a sub-commercial well, records the highest temperature (~285°C [545°F]) and is inclined almost directly beneath the exposed range-front fault and encountered fractures with limited production in the last 30m (100ft) of the deviated wellbore. The majority of producing wells penetrate the steeply dipping, hydrothermal-bearing piedmont fault structure;

---

[1] TGHs are not considered in this report.

- The dip separation between the basement rocks exposed in the range and the basement below the valley is distributed between at least two faults: the range-front fault and the piedmont fault. The range-front fault creates the surface topographic break; a major piedmont fault takes up much of the displacement between the range and valley bottom; and
- Antithetic faults form mini-grabens on the hanging wall block of the major faults and are important features of the geothermal reservoir.

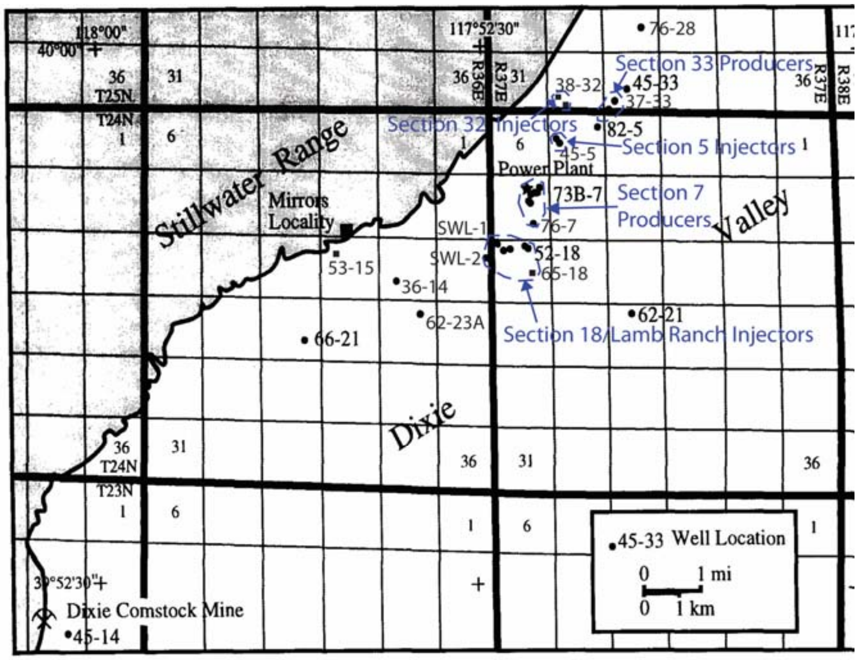

Figure 40A. Map showing the location of wells within the Dixie Valley Geothermal Wellfield (DVGW). The main production and injections zones are labeled by section number and outlined in blue. The Section 18 and Section 5 injectors are connected with the main production zone in Section 7, while Section 32 injectors are connected with the northernmost Section 33 producers. The figure and caption are after Lutz et al. 1998.

6.1.1 Stress Analysis

Borehole imaging and hydraulic fracturing experiments have been carried out in a number of Dixie Valley wells including 45-14 and 66-21 to the south, and production wells 37-33, 62-21, 73B-7 and 74-7 in the DVGW (Barton et al., 1997; 1998, and Hickman et al., 1997; 1998). Based on (compressional) breakouts and tensile fractures in the boreholes, the orientation of the least horizontal principal stress in the productive wells was determined to be 135°+/- 8° (NW-SE). The dip of the permeable fractures in the productive wells is about 60° to the SE, thus the authors further conclude that the producing wells intersect fractures that are optimally oriented for normal slip in the current stress field, and that shear slip maintains the permeability along primary and secondary fault planes. Sub-commercial to dry (nonproducing) wells such as that south of the DVPF have permeable fractures of more varied orientations. Well bore breakouts in wells 45-14 and 66-21 (Hickman et al., 1998) indicate greater horizontal maximum stress values in the vicinity of those wells than for either of the producing wells studied or well 62-21. They suggest that the higher ratio of maximum horizontal stress to vertical stress decreases the shear stress which drives fault slip, and thus even optimally oriented fractures are not critically stressed for frictional failure. In general, the zone of permeability in the subsurface is not limited to a single fault plane, rather, the geothermal system produces from primary and secondary features in intermittent areas along the DVFZ which appear to be dilatational due to the local relationship between the main fault and the stress field (see Section 7.3).

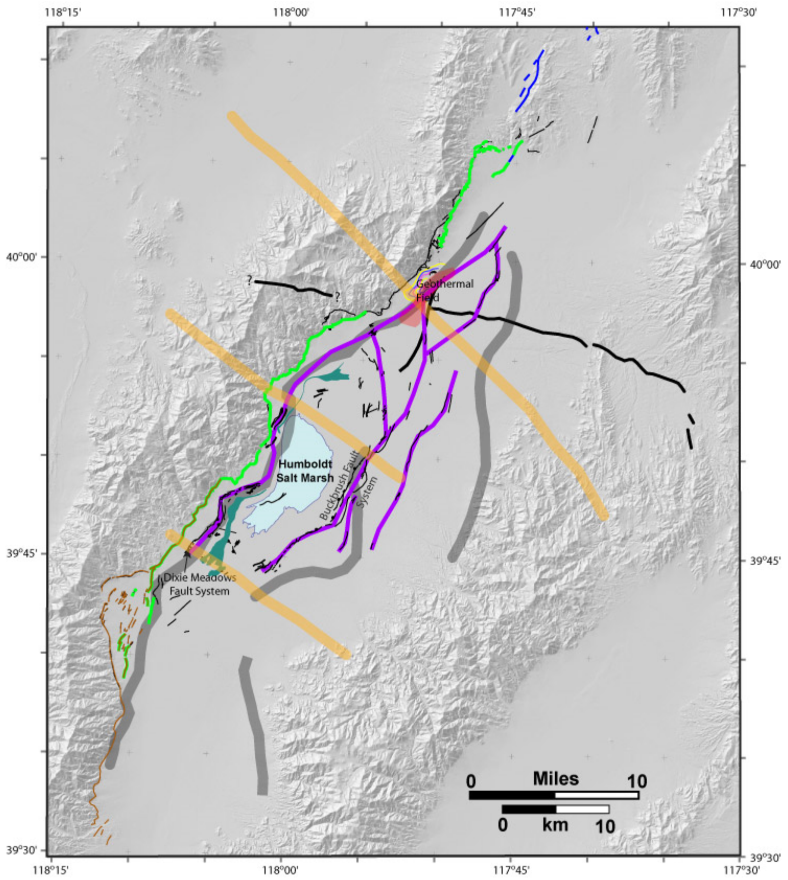

Figure 40B. Map showing NW-trending lineaments identified from Landsat images (yellow) crossing Dixie Valley. Also shown are mapped faults from Smith et al., 2001 (black lines), interpreted major fault zones (purple), the salt marsh thrust belt (dark green), positions of gravity gradient maxima (broad gray lines), lineaments identified in InSAR images by Foxall and Vasco, 2003 (bold black lines), and subsidence fringes identified in InSAR images (colored contours near the geothermal field). For the range-front fault, blue = 1915 surface ruptures; brown = 1954 surface ruptures; green = The Bend Event (~2.5ka) surface ruptures. Note that portions of the Bend Event and the 1954 surface ruptures overlap adjacent to Dixie Meadows. The figure and caption are from Blackwell et al. (2005).

This section summarizes studies that used the borehole televiewer (BHTV) to determine stress and permeability within the reservoir (Hickman et al., 1998; 2000). BHTV images analysis in well 82-5 focused on the fault zone at a depth of ~2071-2724m (6800-8940ft) to determine the nature, distribution and hydraulic properties of fractures within the DVGW and their relation to the local stress field. The orientation and magnitude of the horizontal minimum stress (S_{hmin}) is important for determining if fractures are optimally oriented and critically stressed in the current stress field. This is calculated using (1) tensile cracks forming perpendicular to the azimuth of S_{hmin}, (2) borehole breakouts (compressive rock failures) which form parallel to S_{hmin} , and (3) hydraulic fractures which will propagate in a plane perpendicular to the maximum principle stress (parallel to the strike of the fault zone). A necessary condition for high reservoir permeability is that the DVFZ be critically stressed for frictional (shear) failure in the current stress field. Tensional stresses along optimally oriented fractures result in shear slip along the fractures planes that force open the fractures due to irregular grooves and asperities along the slip surfaces. This develops permeability within the fault zone, which is maintained as tectonic forces re-stress the fractures to critical levels that results in another slip event (extensional failure) along the fracture planes. This intermittent seismicity is responsible for preventing the open fractures from becoming sealed by geothermal fluids over time.

Wells used in these studies are summarized below and reported to encounter the Stillwater Fault Zone (SFZ) at depths of 2 to 3km (6600-9800ft). The term SFZ is synonymous in this context with the DVFZ and more specifically refers to the both the range-front and piedmont fault portion of the DVFZ within its northernmost segment adjacent to the Stillwater Seismic Gap. Wells 73B-7, 82A-7, 74-7, 82-5 and 37-33 penetrate the piedmont fault, the highly permeable (producing) segment of the DVFZ, which is referred to as the SFZ within the Hickman et al.'s studies. Wells 66-21, 82-5 and 45-14 failed to encounter enough permeability within the adjacent fault/fracture zones.

Well 82-5 (dry well)

Well 82-5, located near the Section 5 injectors (Figure 40a and 41), and only 600m (2000ft) southwest of the most permeable production wells within the DVGW has been reported to pass through the main range front fault at 2833m (9300ft). According to the baseline conceptual model, (see Section 7) this well actually penetrates the steeply dipping piedmont fault. For reference purposes herein, where the SFZ is mentioned relative to this well, it refers to the piedmont fault segment of the DVFZ. Despite the favorable location, the well encountered low permeability in the fault zone and was dry. The authors here suggest that this well was deviated within a compressional zone where a N-S trending structure with a suggested right lateral component intersects the NE-trending piedmont fault (see Figure 14 and Section 7.2). The adjacent permeable section 33 producers lie within the corresponding dilated quadrant at this structural intersection. The following points detail the stress conditions based on the aforementioned fracture analysis (Hickman et al., (2000).

- Sealed fractures starting at ~2740m (8990ft) were encountered within the fault zone;
- S_{hmin} (observed just above the SFZ, i.e., the main piedmont fault within the DVFZ) :
  - Above 2660m (8730ft): N23°E ± 12° (parallel to the strike of the SFZ);
  - Below 2660m (8730ft): S66°E ± 13° (perpendicular to the strike of the SFZ);
- A nearly 90° rotation in the azimuth of the least horizontal principle stress (S_{hmin}) at ~2.7km (8800ft) depth is hypothesized to have been the results of a moderate-sized earthquake on a fault subparallel to the SFZ;
- Stress direction below ~2.7 km in 82-5, a dry well, agrees with stress directions observed in 73B-7 and 74-7 (producing wells), and 25-5 (injection well);
- Based on the orientation of S_{hmin} measured from borehole breakouts, the natural fractures within 50m (164ft) of the SFZ, are optimally oriented for normal slip; and
- Low productivity within this optimally oriented fracture zone is due to localized increases in the magnitude of S_{hmin} (reduction in shear stress) related to lithology with the presence of weak talc ($\mu<0.25$) within the main shear zone of the SFZ. This reduces the differential stress in the adjacent country rock and shields potential permeable fractures from high tectonic shear stresses.

The following wells were discussed in the Hickman et al. (1998, 2000), see Figure 41. Where only the calculated horizontal minimum stress is mentioned no other data was available. Note that if the horizontal minimum stress is perpendicular to the DVFZ and parallel to the ESE extensional axis, then the fractures are optimally oriented for normal faulting. Whether they are opened is a function of local lithology, stress magnitudes, alteration mineralogy and the degree of sealing.

Well 66-21: S_{hmin} = N20°W +-20° (dry well)

- Orientation of (S_{hmin}) is optimal for normal faulting on the piedmont fault segment of the DVFZ ; and
- Magnitude of S_{hmin} is too high to result in incipient frictional failure.

Well 45-14: S_{hmin}= N41°W +-12° (dry well)

- Magnitude of S_{hmin} is low enough for frictional failure (on optimal orientations);
- Fractures are not optimally oriented for normal faulting; and
- The range front fault segment of the DVFZ is locally rotated ~40° from the optimal orientation for failure.

Well 73B-7: S_{hmin} = N57W +- 10° (Production well)

Well 25-5: S_{hmin} = S64°E +-14° (Injection well)

Well 74-7: S_{hmin} = S55°E +-15° (Production well)

- Humboldt igneous group contains all the producing fractures; and
- The Stillwater Fault, i.e. range-front fault segment of the DVFZ, at this location reportedly dips S45°E at ~53°, which is the optimal orientation for normal faulting in current stress field. This shallow dip likely assumes that the Stillwater Fault (range-front fault) projects to the vicinity of section 7 producers, where actually the section 7 wells lies along a more steeply dipping piedmont fault.

6.2 Geothermal Reservoir

The basic setting of the producing geothermal reservoir lies within an open fracture network developed where crystalline portions of the Jurassic igneous complex within the hanging wall of the DVFZ are juxtaposed against Cretaceous granodiorite in the footwall (Lutz et al., 1997), as seen in the lithology logs of the Section 7 production wells (Appendix 9). Lutz et al. (1997) reports that production originates from two high temperature subhorizontal aquifers, mostly the Jurassic igneous rocks/quartzite at around 2500-3000m (8200-9800ft), and also from the Miocene basalt at around 2000-2500m (6600-8200ft). The authors of this report believe that the current geothermal production is originating from the piedmont fault segment of the DVFZ. Brittle rocks including the Jurassic diorites and gabbros (lower section of the Humboldt igneous complex) and the Boyer Ranch quartzite (within the narrow zone of faulting) are the best reservoir rocks in the producing field due to their fractured nature and high permeability. Productive zones within some wells (e.g. 76A-7 and 38-32) may lie within a re-activated thrust (ex. Boyer thrust) tectonically bounding the Jurassic igneous complex from the underlying Triassic marine sediments. It has been mentioned that a piedmont fault representing a major strand of the DVFZ is the major producing structure in the geothermal system. Thus, it is thought that the geothermal reservoir lies within the fault zone, intersecting structures and associated faults and fractures in the hanging wall block of this piedmont fault. The bounding conditions for the reservoir as defined by Lutz et al. (1997) are outlined below:

- **North:** leading edge of the Fencemaker allochthon that carries the Jurassic igneous complex;
- **South**: White Rock Canyon (Figure 1) that separates NNW-oriented fault segments from NE orientations;
- **East-West**: restricted to the narrow band of fracturing within the DVFZ;
- **Upper**: lithologic contact between Jurassic igneous rocks and younger sedimentary rocks; and
- **Lower**: Mesozoic (Boyer or Fencemaker) thrust at the base of the Jurassic section.

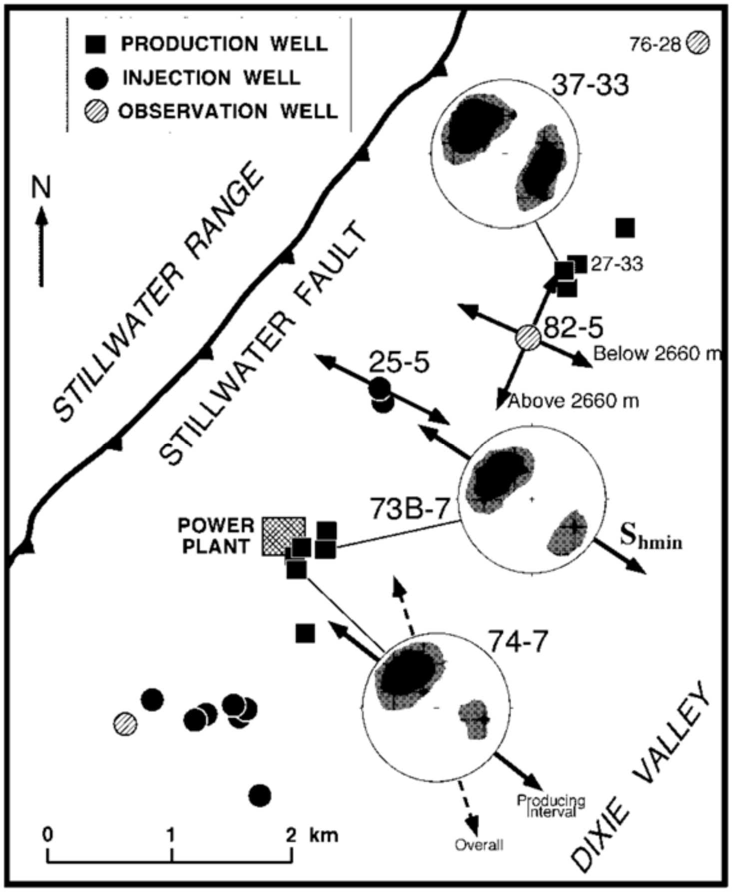

Figure 41. Map of the Dixie Valley Geothermal Field showing the orientation of S_{hmin} as outward-directed arrows. Also shown are lower hemisphere stereographic projections of poles to permeable fractures in selected productions wells, contoured using the Kamb method, demonstrating that these fractures and the overall Stillwater fault zone are well oriented for normal faulting in the current stress field (see Barton et al., 1998; Hickman et al., 1998). The figure and caption are from Hickman et al. 2000.

The Project Area lithology data per well is presented in Appendix 10. The temperature data for the DVGW is presented in Appendix 11. The wells in the producing field are shown in Figure 42 and a summary discussion of these wells by Reed (2007) is presented below.

- Wells SWL-1, SWL-3, and 52-18 inject fluid into a sub-horizontal, lower temperature 220°C (428°F) aquifer in Miocene basalts east of the range-front fault along the piedmont structure at depths between 2192m and 2248m (7200ft and 7373ft).
- Wells 25-5 and 45-5 inject fluid into shallow, lower temperature 205°C (401°F) zones associated with the Miocene basalt and/or Jurassic volcanics within the DVFZ (piedmont segment) at depths between 1776 and 1876m (3860 and 6155ft) according to Benoit (1992). It is reported in the 45-5 well log (Appendix 9), that a mylontized fault zone, assumed to be the piedmont fault segment of the DVFZ was encountered at a depth 1814-1881m (5951-6171ft).
- More recent wells 27-32 and 38-32 have only been used for injection of cold steam condensate and augmentation water into a shallow (180m [590ft] deep) fault zone which was originally an outflow plume from the reservoir.
- Section 33 wells (37-33, 28-33, 27-33) are assumed to produce from fractures in the encountered Jurassic igneous rocks and Boyer Ranch quartzites along the piedmont structure (see summarized well logs in Appendix 9).

The geothermal reservoir has been described above by Lutz et al. (1997) as occurring within specific fractured formations. Reed (2007) emphasizes the structure and relating fracturing in describing the geothermal reservoir as a set of sub-parallel fractures with narrow apertures (volumes up to 3.5 x 10^7 m^3 [1.2 x 10^9 ft^3]), long mean residence times (up to 1197 days) and large surface areas (for high heat transfer) developed in the fault zone and adjacent damage zone that provide permeability. The permeable zones provide conduits for fluid rising from depth and fluid flowing from injection to production wells. Antithetic sets of fractures provide permeable pathways for fluid injected into the Tertiary basalt zones to reach the main fractures.

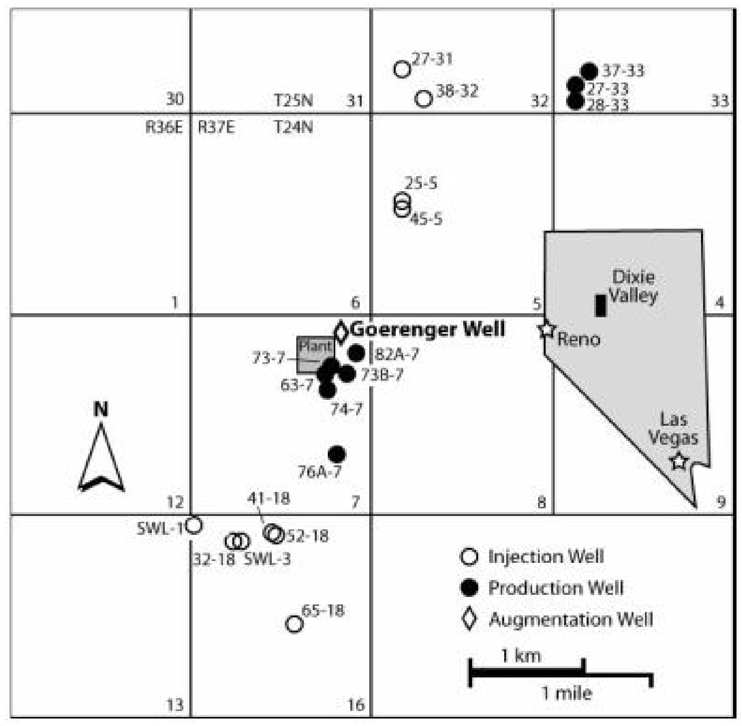

Figure 42. Map of the geothermal producing field showing Section 18/Lamb Ranch injectors and Section 5 injectors in conjunction with the main Section 7 producers. Section 32 injectors are connected with the Section 33 producers within the northern producing field. The Goerenger well is a shallow augmentation water well associated with the power plant. The figure is from and the caption is after Reed (2007).

6.3 Thermal Data

Due to the high thermal gradient, surface features including springs and fumaroles, the close proximity to the DVFZ, and high temperatures encountered at depth, the DVPP and the DVPF are the most explored and studied areas of Dixie Valley. While the setting of the subsurface within Dixie Valley is generally constrained based on geophysical work, the producing field has the most detailed subsurface information due to a number of temperature gradient holes (TGHs) and deep wells. Temperature-depth profiles for shallow wells (TGHs) within the DVPF and the DVPP are shown in Figure 43. Of the approximately 223 wells/TGHs drilled, 96 have available temperature-depth data as part of the SMU Western Geothermal Database (WGD): http://smu.edu/geothermal.

6.3.1 Shallow thermal regime

The highest gradients in shallow TGHs occur near the exposed range front fault, with the maxima near the Senator fumaroles (DVPF) and the section 10 fumaroles (DVPP) near well 53-15 (Figure 44). The occurrence of high gradients near 36-14 and 62-A23 bulge out into the valley for several kilometers and occur near the projected location where the Buckbrush fault system merges with the DVFZ (see Figure 30). The shallow thermal contours clearly show two plumes of thermal water leakage from the range front fault into the valley fill at depths less than around 100m (328ft), with the plumes appearing to originate at the two fumarole areas along the range/valley contact. While both the range front and piedmont fault are considered the major thermal bearing structures, the piedmont fault does not appear to contribute hot fluid to the shallow thermal regime. Its effect is likely masked by the shallow outflow of fluids from the range front fault as geothermal fluids derived from the piedmont structure are known to occur at deeper levels. The TGH temperature-depth profiles within the geothermal field around the Senator Fumaroles indicate significant lateral flow of warm water at shallow depths of around 25 and 100m (82 and 328ft) and at depths around 20 and 70m (65 and 230ft) within the DVPP (Figure 44). The southern plume coincides with a negative aeromagnetic anomaly between two positive anomalies (see Figure 10), also indicating probable leakage of geothermal water into the shallow valley fill with no surface manifestation directly associated with it.

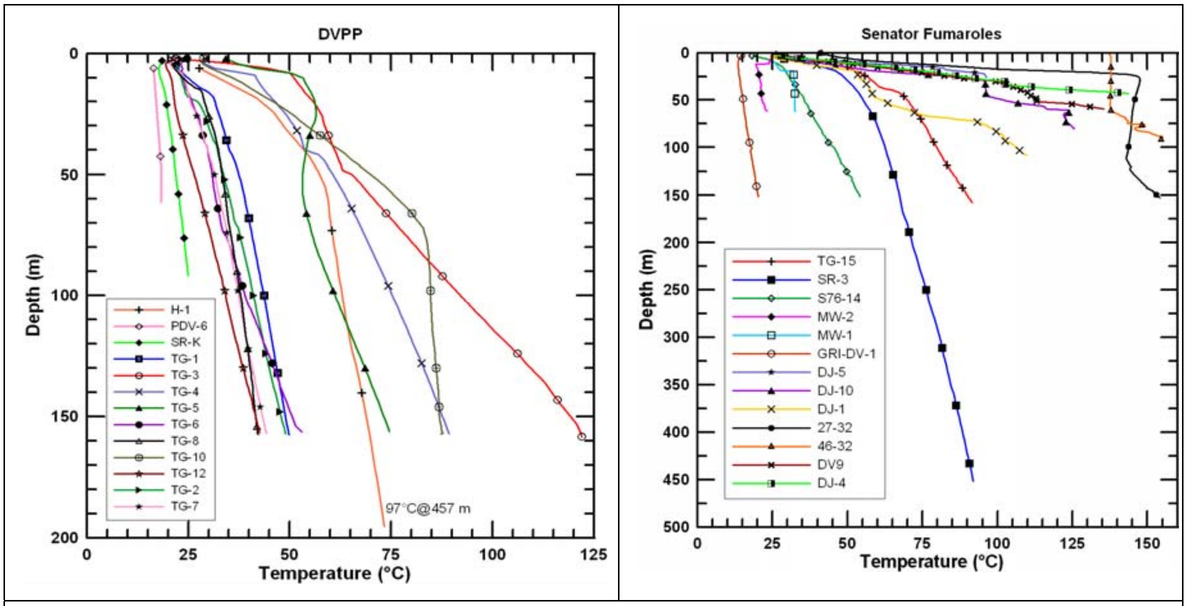

Figure 43. Temperature-depth curves for thermal gradient wells in the DVPP (right) and the Senator Fumaroles area (left). The figure and caption are from Blackwell et al. (2005).

6.3.2 Deep thermal regime

Data from deep wells within the DVPF show temperatures vary from 225°C to 245°C (437°F to 473°F) at depths of about 2500m (8200ft). The temperature in 36-14 (DVPP) produced from fractures near the bottom of the well and is by far the highest bottomhole temperature observed (~285°C [545°F]) in an B&R extensional geothermal system. Geologic and thermal data from wells support a steeply dipping fault zone consisting of at least two major structures as evident by the drilling of wells 62-23 (two legs) and 36-14 within the DVPP. Both legs (62-23 and 62-A23) were impermeable but the 62-A23 leg recorded a BHT of 267°C (512°F) at 3592m (11,785ft), which was hotter than the production wells in the DVPF to the north. A generalized cross-section (Figure 45A) shows that temperatures never became isothermal or decreased with depth in 62-A23, and that the piedmont fault, believed to be the main high-temperature geothermal upwelling zone was not crossed in either well 62-A23 (at depth) or 36-14, which crossed the fault at a very shallow depth. Furthermore, drilling of 36-14 unexpectantly intersected basement rocks (presumably the Jurassic mafic section) at only 1km (3300 ft) depth with no fault encountered. The well was then deviated towards the range-front fault of the DVFZ and continued to show increasing temperatures with depth.

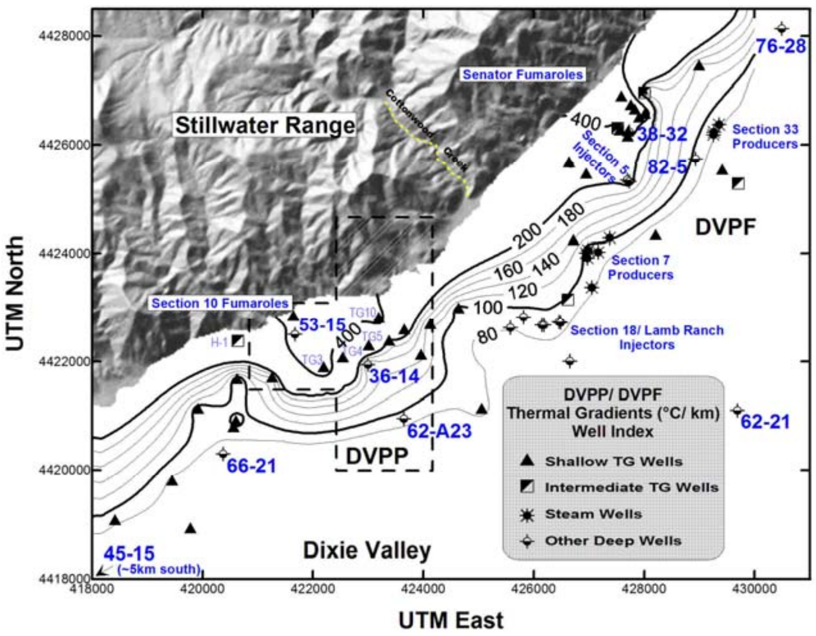

Figure 44. Deep wells and thermal gradient contours for the valley along the range front between the DVPP Lease (Section 10 fumaroles) and DVPF (Senator fumaroles) areas The figure and caption are from Blackwell et al. (2005).

The thermal and lithologic data, in particular the data from wells 45-14 and 36-14, indicate that the range-bounding fault must have a fairly steep dip (>70° E) at the north-trending segment near 45-14, and a near vertical dip along a northeast-trending segment adjacent to the DVPP, assuming the fault was not crossed within 36-14. Additionally the thermal data indicates a major geothermal fluid bearing structure (piedmont fault) is present between the wells 36-14 and 62-A23 (Figure 45A). The structure must also be steeply dipping and coincides with the inferred location of the maximum gravity gradient (see Figures 11 and 13). A cross section through the northern producing field (Figure 45B) also shows two major steeply dipping structures comprising the DVFZ based on the thermal data described above.

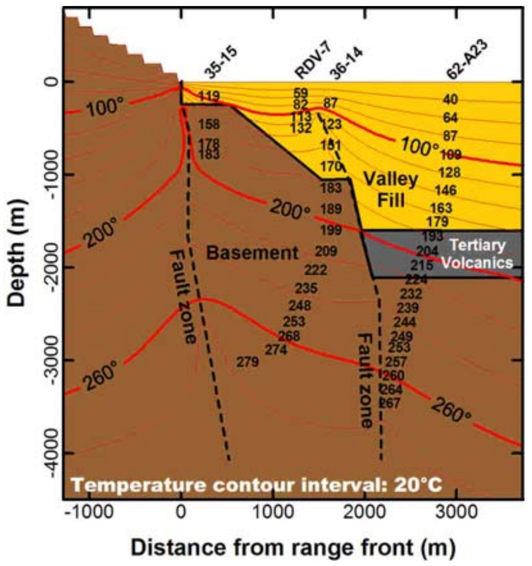

Figure 45A. Thermal model for the DVPP area based on temperature matching in the deep wells. The figure and caption are from Blackwell et al. (2005).

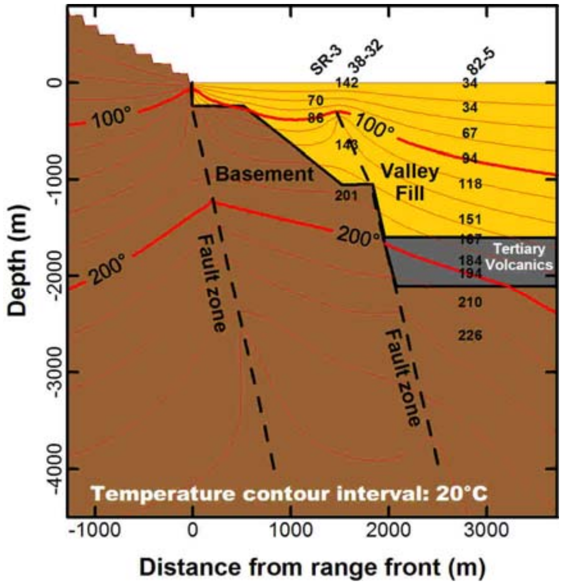

Figure 45B. Thermal model for the DVPF in section 32/33 based on temperature matching in the deep wells. The figure and caption are from Blackwell et al. (2005).

6.4 Summary of Geothermal Wells

Table 3 summarizes well data from Blackwell et al. (2005). This table is incomplete and doesn’t have information on the entire well database for the Project Area. Additional well information from other sources including both the public domain and private sector can be found in Appendix 9. This appendix contains: (1) Sunoco well lithology summary based on Sunoco mud logs and acquired with the permission from Terra-Gen Corporation (Terra-Gen), and (2) lithology summary based on the Nevada Bureau of Mines and Geology (NBMG) online geothermal database (see below). It is important to note that some of the wells included in both sources (Sunoco and NBMG) are not consistent, and the NBMG database is considered the less accurate source. Appendix 10 presents the general lithology from the wells that divides the geology into six stratigraphic units. Appendix 11 summarizes the temperature data that has been acquired mainly from the SMU geothermal database (see below) and data provided by Terra-Gen and includes mostly BHT measurements. Additional temperature data was extracted from the temperature-depth profiles shown in Figure 46, derived from Blackwell et al. (2005). The complete temperature data for the remaining wells was not available to this investigation. Links for the geothermal databases available online are provided below.

Southern Methodist University (SMU) geothermal database: http://smu.edu/geothermal
Nevada Bureau of Mines and Geology (NBMG) geothermal database:
http://www.nbmg.unr.edu/geothermal/mapfiles/nvgeowel.txt

6.4.1 Geothermal Wells within the DVPF

The well distribution within the DVPF can be found in Figure 42 which outlines the main production and injection zones. The production wells are clustered in two locations, section 7 in the center of the field and section 33 to the north. Injection wells include the section 18 wells and the section 5 wells between the two producing zones. Section 32 injectors in the northern producing field are in connection with the section 33 producers. Complete temperature-depth profiles for wells within and outside of the producing field are shown in Figure 46. Lithology and additional temperature data that has been acquired can be found in Appendices 9-11.

Well 38-32

This injection well was drilled in December 2000 between the range front and the producing wellfield (adjacent to Senator Fumaroles) and west of section 33 producers (see Figure 42). The well was thought to penetrate an extensive basin-fill section, however the well encountered a shallow zone of highly altered alluvium and intersected bedrock consisting of the Boyer Ranch quartzite at only ~400m (1312ft). The lithology of the well is included in Table 3, while a general cross-section within the vicinity of the well is shown in Figure 45B. Additionally a brecciated fault zone encountered at ~1000m (3300ft) complicates the structural framework. If this fault zone connects with range-bounding fault then a shallower fault dip is required within this area. This unexpected lithology has been interpreted by Johnson and Hulen, 2002 as a stranded “gravity slide” block between the Dixie Valley range-bounding fault and a shallowly buried fault to the east, of which the majority of the structural offset between the valley and the range occur on the latter fault (Figure 47). This cross-section depicts the “stranded block” which was buried by recent alluvium relies on the assumption that Cenozoic volcanics found within the brecciated zone are not derived from the Jurassic volcanic sequences. The major displacement on the piedmont fault east of the well is explained as either a relay ramp or a major splay from a steeply dipping master structure that curves to a more shallow dip near the surface (Johnson and Hulen, 2002).

Authors herein infer that this could also be explained by (1) a steeply dipping subsidiary structure within the DVFZ that lies between the range front and piedmont fault, or (2) a more northerly-trending cross or transfer fault that projects from the range to the vicinity of 38-32 to a change in strike along the piedmont fault (D. Blackwell, pers. comm., 2011). The wellfield is mostly distributed basinward, as this structure is not encountered by any wells other than 38-32. Additionally northeast of this area, geophysical evidence show that piedmont fault is distributed along at least three sub-parallel and merging segments, that could extend to the SW in the vicinity of Section 32. It is also noted that the Boyer Thrust is exposed a few kilometers to the west in the Stillwater Range and likely projects to the vicinity of this well, although the younger volcanics clasts within the fault zone suggest a younger structure.

Table 3. Well data outside of the producing field (from Blackwell et al., 2005)

Well	Location	Depth	Temperature	Lithology	Notes
45-14	Dixie Comstock Mine Southern-most well	2750m 9022ft	196°C (385°F)	0-335m (0-1100ft): unconsolidated fill 335-792m (1100-2600ft): silicic Cz volcanics 792-2774m (2600-9100ft): Tr metasediments	Most similar in comp. to deep reservoir waters, limited flow
66-21	South of DVPP	2988m 9800ft	215°C (419°F) @2470m	0-1250m (0-4101ft): basin-fill deposits 1250-1585m (4101-5200ft): Cz volcanics 1585-2455m (5200-8054ft): granodiorite 2455-2989m (8054-9806ft): metasediment Ophiolitic bottom	Most saline groundwater in DV HTGF water entry at 1463m (4800ft) (cased) and bottom
62-21	Middle of DV East of DVPP	3810m 12,500ft	184°C (363°F) @3318m	Lithology found in Appendix 9	Fluid entry@2900m (9512ft) (contact of gabbro and underlying Tr slate
82-5 (dry)	DVPF	~2750m 9022ft	226°C (439°F)	Lithology found in Appendix 9	Tight, does not flow Low permeability
38-32	DVPF	~1100m 3610ft	201°C (394°F)	0-150m (0-492ft): Basin-fill sediments 150-777m (492-2549ft): Boyer Ranch quartzite 777-1006m (2549-3300ft): Jz mafic igneous 1006-1113m (3300-3652ft): Brecciated FZ 1113-1168m (3652-3832ft): Tr phyllites	Intersected a stranded block between range front and piedmont fault Drilled in '00 Used as main injection well in Section 32
53-15	DVPP	1200m 3937ft	150°C (302°F)	Lithology unknown	500m (1640ft) from range-front
62-23 62-23A	DVPP DVPP	2900m 9514ft 3492m 11,457ft	250°C (482°F) 267°C (513°F)	Lithology unknown	Drilled in '92-92 Both legs tight Drilled within piedmont structure
36-14	DVPP	3050m 10,007ft	285°C (545°F)	Intersected basement at only ~1km (3280ft) Lithology unknown	Nearly vertically below topographic edge of Stillwater Range, limited flow from fractures in bottom of well

Well 25-5

This is an injection well into Miocene basalt at 1820, 1850 and 1870m (5970, 6070, 6135ft); sediment-basalt contact is at 1580m (5185ft) (Mallan and Wilt 2000).

Well 37-33

According to Hulen et al., (1999), this well:

- Yielded a small quantity of oil at the wellhead 170°C (338°F);

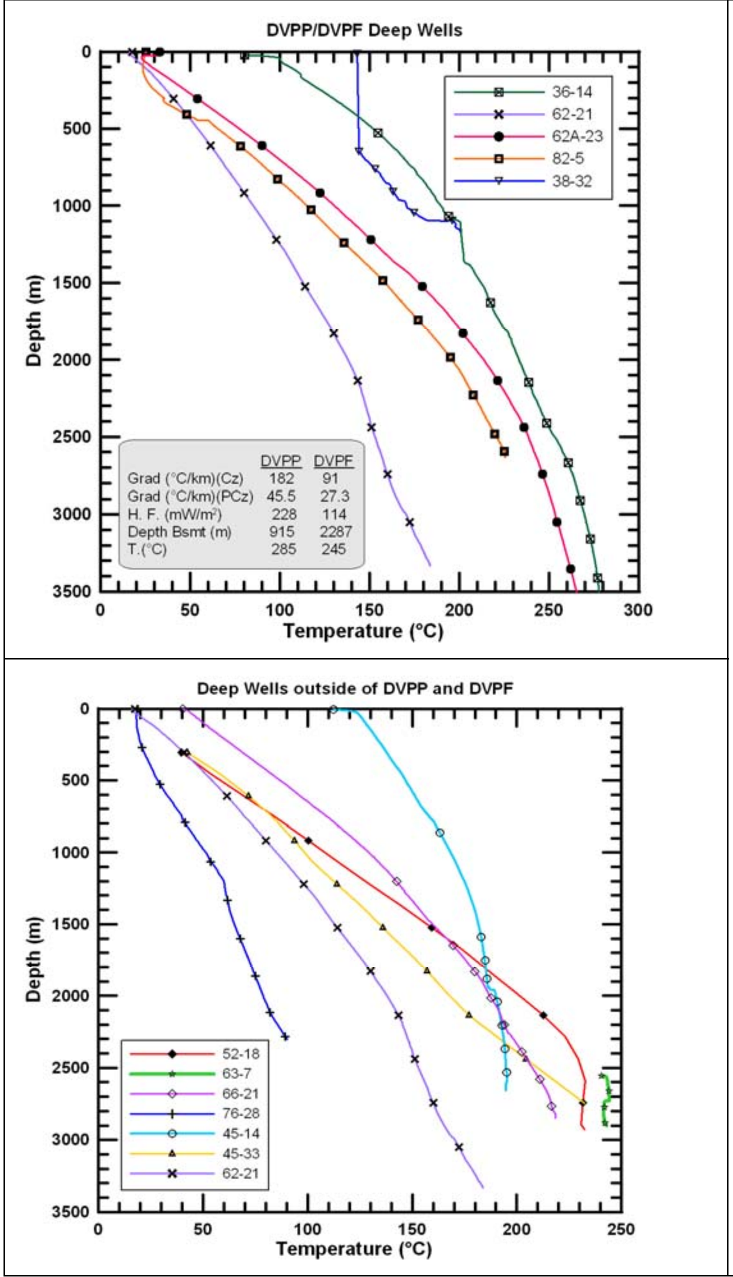

Figure 46. Temperature-depth curves for wells within the Dixie Valley Geothermal Wellfield. All profiles are equilibrium static profiles except 36-14, 66-21, and 45-14. The 36-14 profile below 2600m was derived from a Horner Plot build-up at various depths and these temperatures are considered equilibrium bottomhole temperatures. The wells 66-21 and 45-14 are weakly artesian and only the bottomhole temperature is considered static. Figure is taken from Blackwell et al. (2005). Caption derived from oral and written communication with D. Blackwell.

- Has the source of oil inferred to originate from the Oligocene-Miocene lacustrine sediments (Tma), which occur depositinally below the Miocene basalts;
- Is cased to a depth of 2604m (8543ft) with open hole section to a depth of 2816m (9240ft);
- Has thermal-fluid production from the piedmont fault within the DVFZ in the open hole section;
- Encountered the following lithology at the depths indicated: Tmb (1759-2158m[ft]); Tma (2158-2524m[]); Jhg (2524-2646m[ft]); Jbr (2646-2718m[ft]); Kgr (2718-2758m[ft]);
- Encountered the piedmont fault at 2718m (8917ft) between quartzite in the hanging wall and Cretaceous granodiorite in the footwall block.

Well 45-33

According to Lutz et al. (1998), this well has the following lithology at the depths indicated:

  - Lithology(m): Ts (0-2737m[0-8980ft]); Jhg (2737-2926m[8989-9600ft]); Jbr (2926-3124m[9600-10,250ft]); and

- The abbreviated lithology notations correspond to the following stratigraphic units: Ts: Tertiary basin-filling sediments; Tmb: Miocene basalts; Tma: Miocene lacustrine sediments; Tv: Oligocene silicic volcanics; Jhg: Jurassic Humboldt igneous group; Jbr: Jurassic Boyer Ranch quartzite; Kgr: Cretaceous granodiorite. The stratigraphic units are discussed in the next section in the Baseline Conceptual Model.

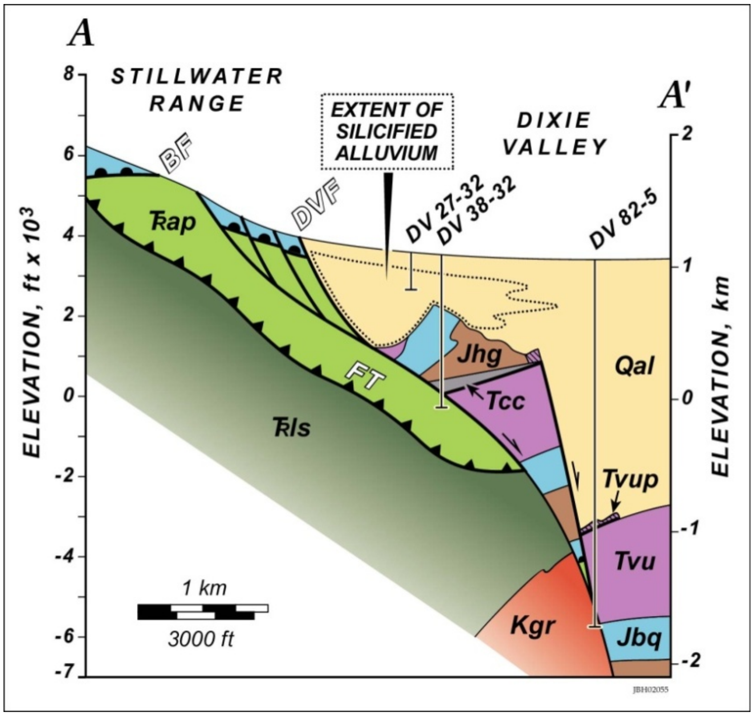

Figure 47. Cross-section of the Stillwater Range/Dixie Valley contact immediately south of the Section 33 producing wells. BF - Boyer Fault, DVF - Dixie Valley Fault, FT - Fenchmaker Thrust, Wells: DV27-32, DV38-32, DV82-5, Jbq - Jurassic quartzite, Jhg - Humboldt Igneous complex, Kgr - Cretaceous granite, Qal - Quaternary alluvium, Tcc - Slickensided cataclasite, TRapTriassic argillites and phillites, TRls - Triassic carbonaceous limestone, Tvu - Tertiary volcanic, undivided, Tvup - deformed Tcc. The figure and caption are from Johnson and Hulen (2002).

7. Baseline Conceptual Geothermal Model

7.1 Introduction and Background

7.1.1 Public Domain Highlights

The following Section 7.1.1 overviews important observations from the Baseline Model and reflects the salient highlights reported by Blackwell et al. (2005) with some additional commentary by the authors of this report.

The DVFZ has been determined to be a complex zone of faults (1-2km [3300-6600ft]wide), with multiple strands showing steep dips (75-85° or greater to a depth of at least 3km [1.9mi]) in the range and valley, in addition to the main range-bounding fault. A steeply dipping system of multiple fault strands is required by the gravity, temperature, drilling, surface mapping, and aeromagnetic survey results. Thus the structural offset is distributed across multiple zones rather than a single range-front fault plane as the extensional strain in Dixie Valley is not only accommodated by the range-front fault, but also by a multitude of other range and valley structures. The production wells within the DVPF and DVPP areas are located 2-3km (1.2 -1.9mi) into the valley and produce from blind valley (piedmont) segments of the piedmont fault segment of the DVFZ. The section 7 producers and section 18 injectors (Figure 40A) lie along the piedmont structure, which accommodates the majority of vertical displacement along the fault zone. As identified in this investigation, the producing geothermal system lies within intermittent dilatational zones along the DVFZ where fractures are optimally oriented and critically stressed for normal faulting and are open. Other important observations of the structural setting are listed below.

- The Dixie Valley setting shows the importance of buried relay ramps that lie basinward of exposed range-faults for future exploration.
- The “Stillwater Gap” could likely experience low level movement “creep” that maintains the fracture permeability along the fault.

Main points from the hydrology and geochemistry assessment are:

- Fluid loss in the geothermal system is due to leakage from the range front fault, piedmont faults, and interconnected intrabasin faults that all outflow directly into the valley-fill within several gravely interbedded artesian layers.
- Spring chemistry indicates a mixture of cold meteoric water derived from precipitation in the basin and surrounding ranges and deeply circulating geothermal water derived from the DVFZ.
- Shallow groundwater is derived from regional recharge from precipitation with 15-25% input of geothermal brines from depth.
- Geochemistry and isotope analysis show that the geothermal fluids are Pleistocene in age that have remained isolated from meteoric recharge. The isotopic ages for Dixie Valley geothermal waters are 12-20ka.
- The geothermal system has been intermittently to continuously active for approximately 100,000 years.
- Helium isotope data indicate small amounts of mantle derived fluid that infer a through-going fracture network that provides fast pathways from upper mantle to lower crust

and agrees with a deep-seated range-front fault model and deep meteoric water circulation interacting with the mantle-lower crust derived fluids.

- The helium data also suggest that the entire DVFZ extending south of the EGS study area may be a geothermal target.

Highlights from the thermal regime are:

- A 20+km strike length of the fault zone is presently the locus for fluid(s) circulating at temperatures over 200°C (up to 285°C) at 2 - 3km depth.
- Two distinct thermal fluid bearing structures (faults) include the exposed range front fault at shallow levels and a buried piedmont fault at deeper levels which is connected to the producing geothermal reservoir. However, the very high measured temperature in 36-14 which is in close proximity to the range-front fault indicates that hotter geothermal fluid is upwelling from depth along that structure.
- The explored known portion of the existing geothermal resource system (see definition in Section 7.2.1) can be defined as consisting of at least three separate geothermal cells/systems. The two main areas (5km [3.1mi] apart and 2km [1.2mi] wide) are showing temperatures (225 to 245°C [437 to 473°F) at depths of 2500m (8200ft) and over 265°C (509°F) below 3000m (9800ft). These areas lie adjacent to Senator and section 10 fumaroles, respectively. A third geothermal cell is evident to the south within the DVPP area.
- The geothermal cell/system thermal regime is locally in equilibrium in the 1-3km (3300-9800ft) depth range.

7.1.2 Introduction

The Baseline Conceptual Geothermal Model is based on work (1) presented in the previous compendium of baseline (i.e., existing) data, Sections 1-6, that represents primarily the literature assessment (by the current authors) of the DVGS, (2) limited private sector data, and (3) interpretations by this current project team. Complete cross-sections (sections) through the DVGW (see Section 7.3) can be found in Plates 1 & 2 with noted major assumptions within the sections found in Appendix 12. For locations of cross-section lines see Figure 48B.

At the conclusion of this discussion, we present a summary description of the assessment in terms of the hydrothermal geothermal system and the EGS. Both are presented because they are two aspects of a single geothermal process. Hydrothermal cells in the B&R convectively transport heat from deeper within the crust to the surface. The thermal energy, carried by the upwelling geothermal fluid, conductively heats the host rock in the vicinity of the fracture and fault hosted geothermal cell. Over time this thermal conductive process has the potential of heating a substantial body of rock, expanding progressively outward and away from the convective geothermal cell with time and flow rate. The thermal energy contained within this conductively heated rock is the EGS portion of the geothermal system of interest here.

7.1.3 Calibration of EGS Methodology

The DVGS was chosen for the development of a calibrated EGS exploration methodology because it best characterized geothermal systems in the B&R with a considerable amount of geoscience data and known well results in the public domain. The calibration has been achieved by (1) qualitatively integrating geophysical, geological, and geochemical data sets; (2) cross-correlating the geoscience data with known geothermal well results; and (3) quantitatively assessing the select geoscience parameters and correlations through geostatistics. This approach was coupled with subject matter expertise (SME) throughout the process.

To obtain high-resolution geophysical data, we defined a Project Area that is 50km x 50km (31mi x 31mi) approximately centered on the DVGW (Figure 48). The DVGW which includes the DVPF area that is currently producing at over 60 MW of electrical generation and the DVPP area to the southwest has 30 deep wells. Well data available to this project consisted of lithology for 22 wells, thermal data consisting of BHT measurements for 26 wells, and temperature-depth profiles for 10 wells. Additionally, temperature-depth profiles were available for nine TGHs. Since the DVGW contains the wells, most of the subsurface data, and numerous geophysical surveys (see Section 3), it was designated as the Wellfield Calibration Area. This area is defined as extending from the Dixie Comstock Mine and well 45-14 at southwest end to the Section 10 and Senator fumarole areas (the DVPP and DVPF respectively), to well 76-28 to the northeast, and to well 62-21 to the southeast (Figure 48).

7.2 Geologic and Structural Interpretations

7.2.1 Re-Interpreted Structural Analysis

The distribution of geothermal cells/anomalies (see discussion below) in Dixie Valley has been reported by previous investigators to be mostly controlled by the northeast-trending structures of the DVFZ (see Figures 30 and 33). The significance of the inherited, older set of north-trending structures that are present bounding structural blocks within the Stillwater Range and deep fault-controlled basins in Dixie Valley has largely been ignored, with the exception of (Waibel, 1987; Smith and Blackwell, 2001; Waibel, 2011; Iovenitti et al., 2011a, 2011b). Where these two structural trends intersect within the DVFZ, the localized stress field is altered, and zones of compression and dilatation are developed. If the dominant B&R normal fault trend (NNE-trending and steeply-dipping) was sufficient alone to transmit hydrothermal fluids from depths, then geothermal systems would be potentially found along the entire strike length of these faults, while this is clearly not the case as they are mostly found along isolated structurally controlled regions. Terminology for describing geothermal for the purpose of this report are (1) a geothermal cell is defined as a small localized conduit for geothermal fluids at a given structural setting, (2) a system is significantly larger than a geothermal cell but not sufficiently developed to be a geothermal resource, and (3) a geothermal resource represents a geothermal anomaly of sufficient size and mass that it can be produced.

Faulds et al. (2011) has described four examples of favorable structural settings for geothermal systems, specifically applicable to the B&R. These include (1) step-over or relay ramp between two overlapping normal fault segments with multiple minor faults providing hard linkage between two major faults, (2) terminations of major normal faults whereby faults break up into multiple splays or horsetail, (3) overlapping, oppositely dipping normal fault systems (accommodation zones) that generate multiple fault intersections in the subsurface, and (4) dilatational fault intersection between oblique-slip normal faults. In the case of the Dixie Valley geothermal setting, the structural mechanism appears to fall within the fourth example mentioned by Faulds involving the interaction of oblique-slip normal fault segments, and on a more broader scale, the third case. Evidence presented in this section suggests that the Dixie Valley geothermal system is strongly controlled by dilatational fault intersections.

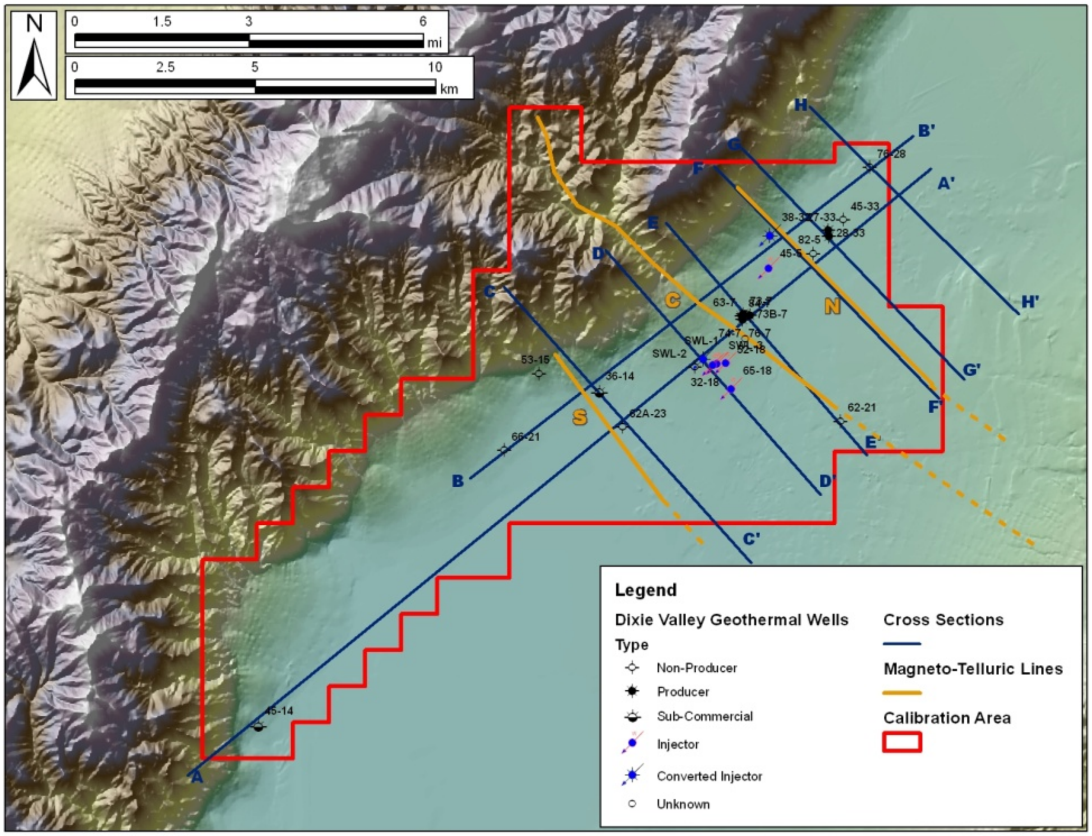

Figure 48. The Dixie Valley Geothermal Wellfield and Calibration Area. The Dixie Valley Producing Field (DVPF in Figure 1) is currently generating over 60MWs of electrical power. The Dixie Valley Power Partners area (DVPP in Figure 1) lies to the southwest of the DVPF and consists of three dry holes (66-21, 53-15, 62-23A) and one sub-commercial well (36-14). Location of cross-section lines is shown in blue. MT arrays are shown in orange.

Analysis of the overall structural setting of the Project Area reveals that the intersection of the pre-8 Ma N-trending B&R structures (Waibel, 1987) with the current NE-trending post-8 Ma B&R structures are coincident with the location of many of the shallow thermal anomalies and the current geothermal electrical production field (Figures 49A-C; Waibel, 2011; Iovenitti et al., 2011a; 2011b). In some cases, the older N-trending structures appear to offset NE-oriented structures within the DVFZ suggesting re-activation within the current stress regime. Thus, these structural intersections play an important role in the development of dilatation zones that host geothermal cells/systems/resource in the Project Area.

In the current stress regime with a least principle stress oriented NW-SE (S_{hmin} = N45°W [Hickman et al., 1998; 2000], see Section 6.1.1), the N to NNE-trending steeply dipping structures would be expected to exhibit some re-activation in a dextral strike-slip sense when evaluated with respect to a strike-slip faulting regime. In theory, where the greatest principle stress is oriented N45°E, roughly parallel to the strike of the Dixie Valley fault, a conjugate set of strike-slip faults is expected to occur at an orientation of 30° off of the greatest principle stress. Thus, when applied to Dixie Valley an inherited structure oriented approximately N15°E would be expected to exhibit dextral (right-lateral) strike-slip motion, while a cross-structure oriented ~N75°E is expected to exhibit a sinistral (left-lateral) strike-slip motion. It is important to note that while Dixie Valley is located in the northern B&R province that undergoes mostly pure extension along a roughly WNW-ESE axis, it is in close proximity to the north-trending, trans-tensional structural zone known as the Walker Lane Belt. Thus, it is thought that some of the dextral shear accommodated along this trans-tensional zone is transferred into the adjacent terraines. This is reported by Caskey et al. (1996), as right-lateral offset (right-oblique slip) evident along the east-dipping Fairview fault and related ruptures, abruptly transitioned to pure normal slip along ruptures exposed to the north along the southernmost Dixie Valley Fault ruptures.

Accordingly, Smith and Blackwell (2001) have identified the continuation of two major NS-trending structures present in the Stillwater Range to extend within the basin and through the producing field (Figure 49A). They show that the axis of a syncline within the middle section of valley-fill sediments, believed to occur syn-extensional as a hanging-wall block response to normal faulting, is offset in an apparent dextral (right-lateral) motion by the N-trending structures (see Figure 14). A major assumption in this structural interpretation is that the generally N-trending faults show relatively recent strike-slip motion as they offset segments of the range-front and piedmont fault within the DVFZ. Alternatively to the slip direction inferred along the two structures, the range-front fault and piedmont fault appear to be offset in a sinistral sense along a NNW to N-trending structure in the area near 45-14, southwest of the producing field (Figure 49B). This provides additional evidence for the re-activation of these older structures, following the formation of the DVFZ, and occurring within the time frame of the current stress regime. The reason for this opposite sense of motion has not been fully investigated. Four potential reasons to account for this sinistral slip could be the (1) configuration of the fault relating to dip direction, (2) transition zone between pure normal slip on the range-front fault segment of the DVFZ and oblique-slip along Fairview Peak and other southern Dixie Valley faults, (3) a complex interaction relating to an regionally observed dextral sensed shearing of the southern portion of the Stillwater Range, and (4) some combination of the above.

Specifically in reference to the third argument, a regional dextral sensed shearing adjacent to the trend of the southern Stillwater Range has been observed in mapping relationships as

(1) northerly-trending faults appear to be offset to the NE and show a pronounced right-step within the range and (2) intervening structural blocks are tilted and rotated. This apparent NE-trending dextral shear that influences the structure in the range could explain why faults occurring on the SE edge of this structural block show sinistral offsets. A largely coherent yet slightly tilted structural block that encompasses the Table Mountain basalts exists in the central Stillwater Range bounded by major north-trending faults. This block seems to play a role in dividing the structure of the Stillwater Range and separates the apparently sheared structural block to the southwest with the highly dissected northeastern Stillwater Range block which lies north of the producing field. While this relationship has been noted as a possible explanation for the change in structure, it is outside the scope of the project and has not been investigated further.

To illustrate the structural setting of the EGS Project Area, all known faults from a variety of datasets were integrated into a detailed structure map (Figure 49A). The data sets used to derive this structure map include mapping results from Page (1965) and Speed (1976), structures identified by Smith and Blackwell (2001), geophysical inferred structures including gravity/magnetic horizontal gradients (Blackwell et al., 2005), faults recognized by the state of

Nevada, and from the USGS Quaternary Fault and Fold Database (QFFDB). Thus the structure map shown in Figure 49A represents the compilation and interpreted relationship of all known faults and inferred structures in the Project Area.

Figure 49B presents a detailed geologic map of the project area derived from published geologic maps including Page (1965), Speed (1976), Stewart and Carlson (1978) and other State of Nevada Geologic Maps. This map represents a more precise analysis of the occurrence of known faulting delineated from faults inferred from geophysical methods, as well as other available structural data. The map clearly shows the Stillwater Range is sub-divided into discrete structural blocks bounding by N-trending structures. The structures are all assumed to be steeply dipping with dip directions derived from stratigraphic relationships, surface measurements, and geophysics.

Figure 49C depicts the major recognized structures with respect to the wellfield and location of shallow thermal anomalies as well as the expected areas of dilatation and compression occurring at these structural intersections. Thermal anomalies occurring at these intersections include from south to north, Dixie Meadows, Dixie Comstock Mine, unnamed, Section 10 Fumaroles within the DVPP, Senator Fumaroles within the DVPF, and New York Canyon on the western edge of the Stillwater Range. Other shallow anomalies within northern Dixie Valley including Hyder and Sou HS seem to be influenced by some other structural control not directly associated with the DVFZ. Drakos et al. (2011) attribute the occurrence of these hot springs to a structural accommodation zone between Pleasant Valley and Dixie Valley faults (Faulds et al., (2011) third example, see above).

Zones of Compression and Dilatation

The structural zones at the major fault intersections are divided into compressional and dilatational based on the expected movement within discrete structural blocks in their respective quadrants (Figure 49C). The model assumes the NE-trending normal faults exhibit pure normal slip, with slip vectors perpendicular from fault strike. For the NS-trending faults, the major assumption is the faults exhibit strike-slip motion under the current stress regime. The compressional and dilatational zones generalized the expected stress conditions due to the combination of slip on a NE-trending fault and the expected strike-slip component on a NS-trending fault. Where both vectors agree (in same directions) a zone of dilatation is inferred.

Where the vectors do not agree, a zone of compression is inferred, as movement on the strike-slip fault supersedes. Also a bend in a normal fault, apparent as the piedmont fault takes a significant left-step bend in the producing field, would also infer a dilated zone at the change in strike. It is noted that a convex bend relative to the hanging wall of fault would produce dilation in the hanging wall block. This structurally complexity and the apparent dilated nature could likely be explained as a smaller scale but prominent NNE-oriented fault that extends from within the range, to the western side of 38-32 and appears to offset the piedmont fault as it projects directly into the major change in strike (D. Blackwell, pers. comm., 2011; see Figures 49B and 49C). This is in concert with that portion of the DVFZ being dilated.

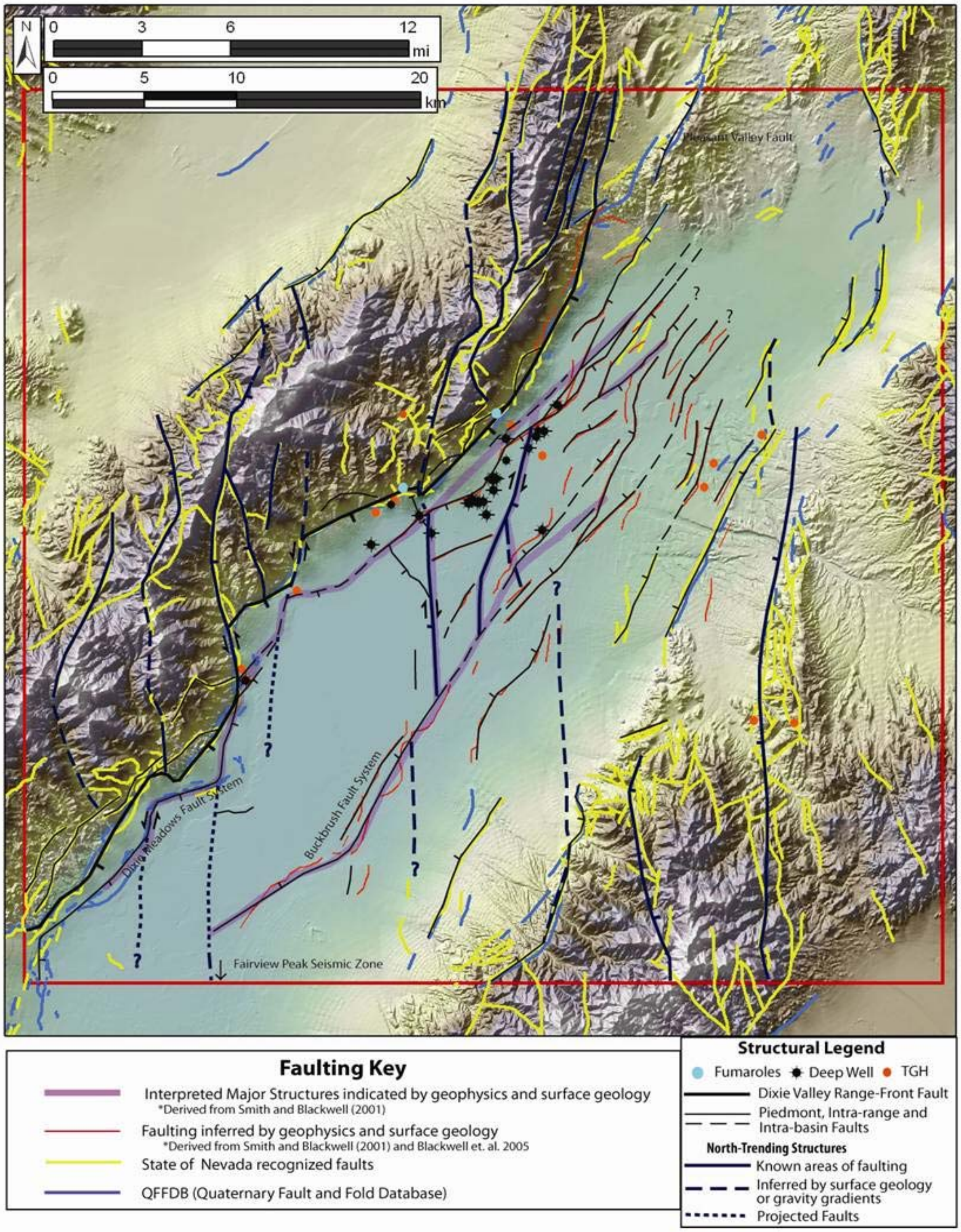

Figure 49A. Structure compilation map of the Dixie Valley EGS study area showing the correlation between interpreted structures and all recognized faulting in the area. Faults (in purple and red) indicated by both surface evidence and geophysics were derived from Smith and Blackwell (2001) and Blackwell et al. (2005). Faults shown in yellow are recognized by the State of Nevada, and faults shown in blue are from the USGS Quaternary Fault and Fold Database (QFFDB). Faults in black and dark blue represent the location of major structures based on all available data-sets. Dip directions were derived from stratigraphic relationships, surface measurements, and geophysics. See Figure 49B for well ID.

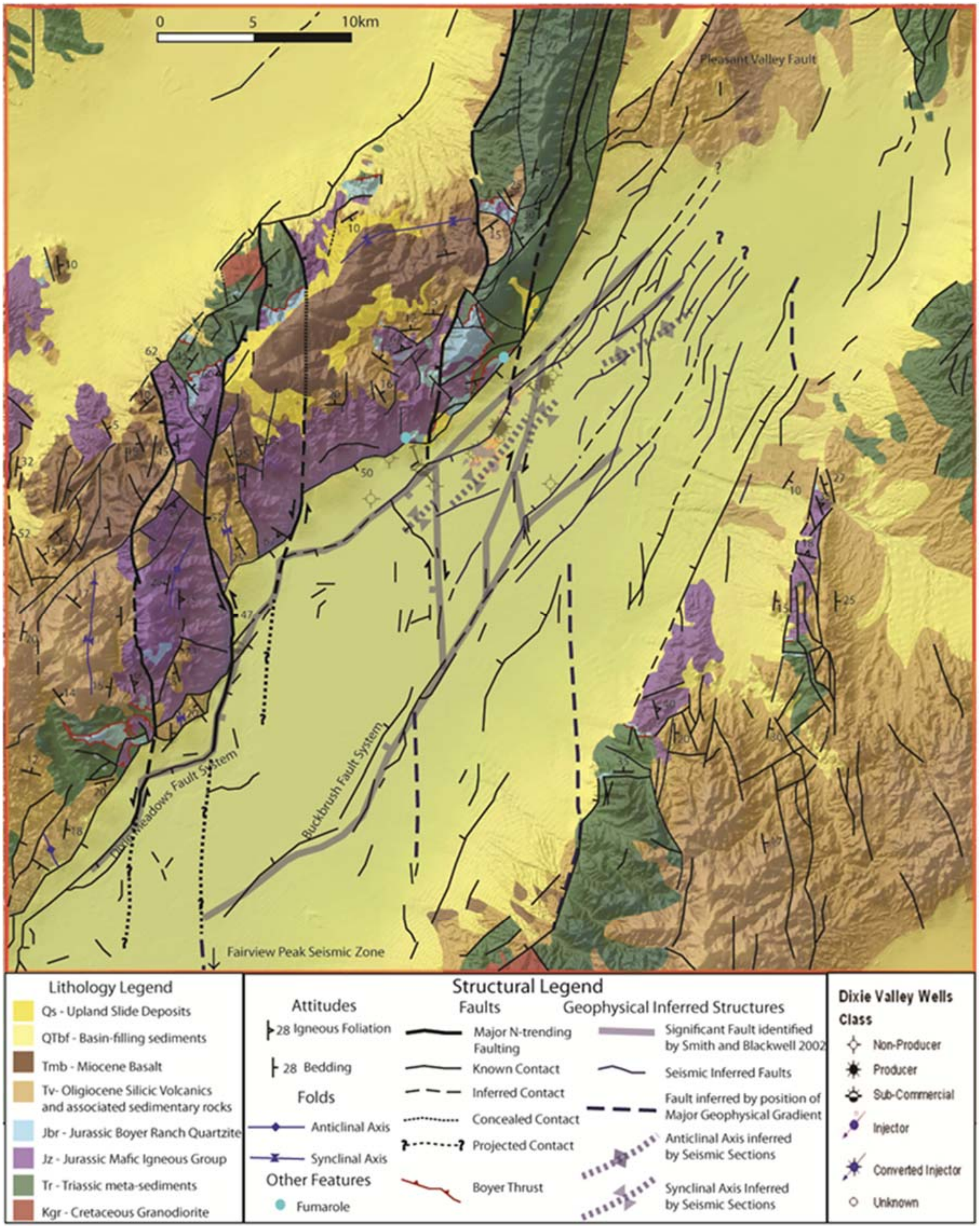

Figure 49B. Project Area Geologic Map showing lithology, structural data, recognized faults, and major structures recognized by geophysics. Major N-trending structures are emphasized and shown to divide the Stillwater Range into discrete structural blocks. Lithology and structural data was derived from previous published mapping results including Page (1965), Speed (1976), Stewart and Carlson (1978), and other State of Nevada Geologic Maps.

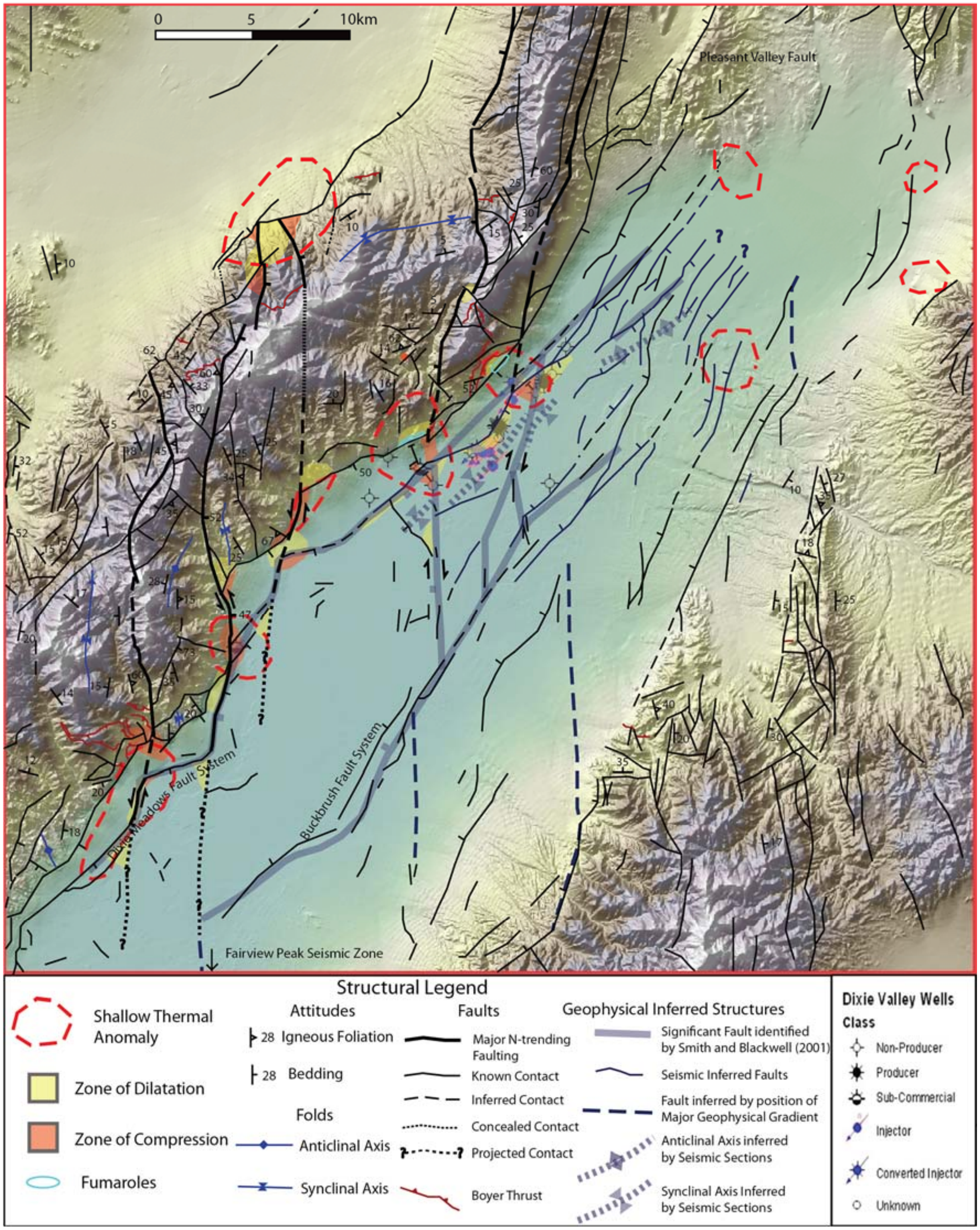

Figure 49C. Correlation between shallow thermal anomalies (dashed red lines) and identified structural intersections of N to NE-trending faults (dark blue lines) in northern Dixie Valley, Nevada. Light blue dots indicate the Section 10 (southwest of the producing field) and Senator fumarole areas (Figure 48a). Well symbols are shown in the associated Well Class Key. Expected zones of compression (red-orange shaded areas) and dilation (yellow shaded areas) occurring at the intersections of discrete structural blocks are inferred based on the interaction between the strike-slip and normal-slip component and other considerations. These localized structural zones were only defined where a thermal anomaly was present within the DVFZ and at New York Canyon, on the northwestern side of Table Mountain.

The extent of these zones shown in Figure 49C is purely arbitrary. For the purpose of this report we choose to define these zones as extending for about 1 km away from the fault intersection. In cases where fumaroles exist at the surface, these zones of dilation are extended to include such features. One scaling problem with the model is that the identified structural zones are very small compared to the size of the surface thermal anomalies and any thermal anomaly is likely to encompass both compressional and dilatational zones. This may be attributed in part to an upflow zone creating a thermal hydrologic mound in the shallow near-surface unconsolidated sediments. The geometry of the fault intersections at depth was not considered herein as the N-trending faults are assumed to be steeply dipping and near vertical at the surface. The interpreted stress quadrants (zones of compression and dilatation) were applied to the major fault intersections that correlated with a shallow thermal anomaly within the DVFZ. One exception to this is the New York Canyon anomaly which exists on the western edge of the Stillwater Range and is not in the area defined as the DVFZ. The thermal anomalies in northeastern Dixie Valley were not included in this analysis due to a lack of subsurface data.

It is at these structural intersections and within the associated dilated zones that geothermal fluids are present. Evidence for this postulation is:

1. the major thermal anomalies associated with the DVGW, adjacent to Section 10 and Senator Fumaroles occur at these structural intersections and consist of at least three separate geothermal cells developed within the associated dilated zones (evidence developed in this investigation and in Waibel [2011]);
2. the location of the two major fumaroles occurring within expected areas of dilation;
3. the Dixie Comstock and Dixie Meadows anomalies occur at a major fault intersection coinciding with a sharp bend in the range-front;
4. the New York Canyon thermal anomaly is associated with this type of structural intersection on the northwest side of the Stillwater Range;
5. the highly permeable Section 33 producing wells lie within a dilated zone;
6. well 82-5, a hot, dry well within the producing field has its bottomhole location within an intervening zone of compression between the section 33 and section 7 production wells (also see below for an potentially alternative/complimentary explanation);
7. the very hot and low permeability wells of the DVPP, 36-14[2] and 62-23A respectively, lies within a compressional zone, as does 45-14; and
8. well 36-14, deviated towards the Stillwater Range and the range-front fault segment of the DVFZ, encountered a fluid-bearing fracture zone within the last hundred feet of the wellbore, which correlates with the location of the range-front fault at depth and with an expected dilated zone near Section 10 (unnamed) fumaroles.

These structural intersections appear to explain the intermittent distribution of the shallow thermal anomalies that have developed within the Dixie Valley Geothermal District in the DGGW and at New York Canyon.

Additionally, the structural analysis and associated zones of compression and dilatation are also supported by the well and helium isotopic data (R/Ra), Figure 49D. The majority of productive wells lie within the expected zones of dilatation, with the exception of 45-33, which is thought to be non-productive based on mechanical problems in the well. The northernmost producing

---

[2] However, 36-14 was approaching the range-front segment of the DVFZ and a dilatational zone which occurs on the Stillwater Range side of the fault.

wells, 27-33, 28-33, and 37-33, all lie within a dilatational zone, while an adjacent dry hole, 82-5, lies with a zone of compression separating the aforementioned wells from the main production area to the southwest. Hickman et al. (2000) also reported that 82-5 is completed in a narrowly defined shear zone with abundant talc alteration and low shear stress at the depth where the well was expected to encounter the producing fault zone.

All the productive wells in the DVGW have relatively high R/Ra values indicating a magmatic gas component and deep source (Figure 49D). While 36-14 lies within a zone of compression, the high helium R/Ra value (0.77) could be explained as the well was inclined towards the range-front and is thought to nearly intersect the associated dilated zone. Fluids sampled outside of the DVFZ, e.g. 62-21, Hyder and Sou HS, have relatively lower helium R/Ra values. The two fumarole sites occurring at the range-front lie within zones of dilatation and have high reported helium R/Ra values , while it has been noted that the larger fumarole helium ratios are thought to result from air contamination (B.M. Kennedy, pers. comm., 2011).

One major factor affecting the productive nature of a well not previously discussed is the lithology overprint as some formations are not suitable to contain open fractures suitable for geothermal production. For example, non-producing wells 62-21, 62-23A and 66-21 were all completed in the Triassic shales/slates. Rock type at elevated temperature plays a significant role in whether a well is a producer or non-producer in a hydrothermal system and whether a well can host an EGS reservoir. Brittle rocks containing open-fractures are an ideal hydrothermal reservoir. When closed fractures are present in brittle rocks, the rock can be fractured through EGS. Non-brittle rocks would not be appropriate for either a hydrothermal system or EGS. Several examples of wells completed in poor reservoir rock exist within the DVGW. The non-producers 45-14 and 66-21 have bottomhole temperatures of 196°C (385°F)and 215°C (419°F), respectively, but were completed in Triassic shales/slates, not a suitable reservoir rock (D. Benoit, pers. comm., 2011) because it does not hold a fracture, in at least the areas drilled by these wells. 62-23A, had a very high reported bottom hole temperature of 279°C (534°F), but the Triassic section the well was completed in had very low permeability.

7.2.2 Re-Interpreted Stress Modeling

The baseline Dixie Valley stress modeling (Wesnousky et al., 2003), described in Section 2.2.4, was updated using Coulomb 3.1 Stress Modeling software. The purpose was to better characterize the expected fault-induced stress and strain conditions in Dixie Valley based on the conditions required by the Baseline Conceptual Geothermal Model. The background, methodology, and results of the modeling are described in detail in Appendix 13; see also http://earthquake.usgs.gov/research/modeling/coulomb/.

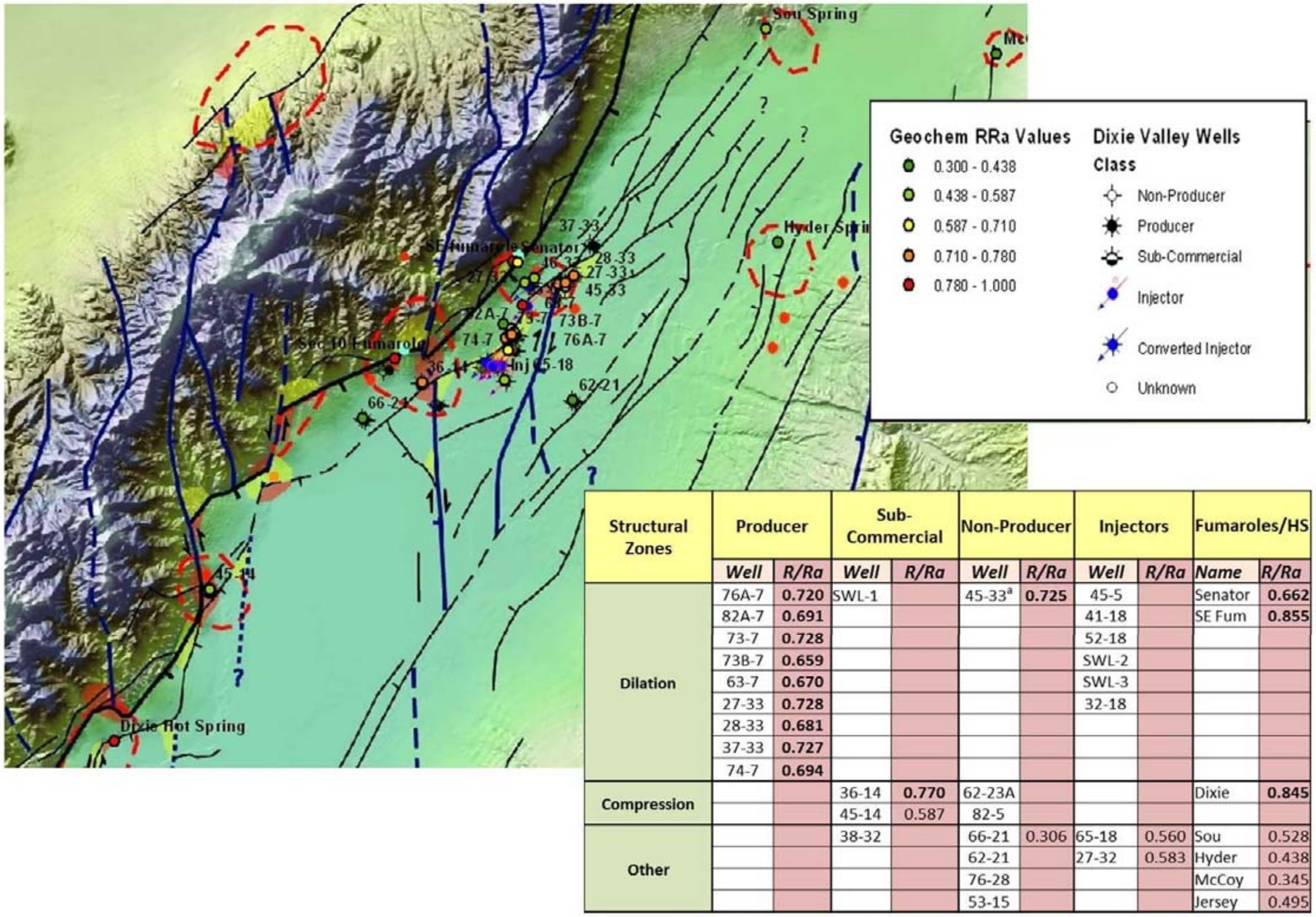

Structural Zones	Producer		Sub-Commercial		Non-Producer		Injectors		Fumaroles/HS	
	Well	***R/Ra***	***Well***	***R/Ra***	***Well***	***R/Ra***	***Well***	***R/Ra***	***Name***	***R/Ra***
Dilation	76A-7	**0.720**	SWL-1		45-33[a]	**0.725**	45-5		Senator	**0.662**
	82A-7	**0.691**					41-18		SE Fum	**0.855**
	73-7	**0.728**					52-18			
	73B-7	**0.659**					SWL-2			
	63-7	**0.670**					SWL-3			
	27-33	**0.728**					32-18			
	28-33	**0.681**								
	37-33	**0.727**								
	74-7	**0.694**								
Compression			36-14	**0.770**	62-23A				Dixie	**0.845**
			45-14	0.587	82-5					
Other			38-32		66-21	0.306	65-18	0.560	Sou	0.528
					62-21		27-32	0.583	Hyder	0.438
					76-28				McCoy	0.345
					53-15				Jersey	0.495

[a]Well data available to AltaRock is limited. It is unknown why this well is a non-producer.

Figure 49D. Correlation of Shallow Thermal Anomalies, expected zones of compression and dilatation at structural intersections, and well type within the Dixie Valley Geothermal Wellfield. Wells are color-coded based on their respective helium data (R/Ra). The table (bottom-right) shows the relationship between R/Ra ratios measured from wells and fumaroles and well type with respect to the well location and the occurrence of structural zones.

Valley-bounding normal faults have produced several large earthquakes over the past ~3000 years, including the 2-2.5ka “Gap” Earthquake along the Stillwater Seismic Gap (SSG) segment of the DVFZ range-front segment, the 1915 Pleasant Valley Earthquake along the Pleasant Valley Fault (PVF), and 1954 Dixie Valley Earthquake along the southern section of the DVFZ. The updated stress model takes these three events into account while the input parameters differ from the Wesnousky et al. (2003) model in assuming that slip has occurred along SSG and that the structures are steeper dipping (70°).

The Coulomb 3.1 model can calculate the expected strain and Coulomb Stress Change (CSC) on a receiver fault (RF) due to slip constraints on a source fault (SF) to determine whether failure along the RF is promoted or inhibited (Lin and Stein, 2004; Toda et al., 2005). A positive CSC infers failure is promoted, while a negative CSC infers that failure is inhibited. The strain is divided into a positive dilatation component, infering the fault is unclamped, while a negative compressional component infers the fault is clamped. This Coulomb model assumes a RF (with a specified strike, dip and rake) exists within each gridded cell used in this modeling (500m by 500m) and plots the CSC and strain at that location.

Several scenarios involving RFs were examined. The approach began with a "test-run" (referred to as the first scenario) that reproduced the Wesnousky et al. (2003) model results as a test to the model constraints. A second scenario assumed that slip occurs along a more complicated and multi-fault system, taking into account postulations from Blackwell et al. (2005) that the whole SSG did rupture in the "Gap" event. For Scenario 2, the range-front segment of the DVFZ (southern portion that experienced surface rupturing in 1954) is represented as 1 fault segment, the SSG as 3 segments, and unlike Scenario 1, we also include the PVF as 1 segment. These 5 segments respectively comprise the source faults and have differing orientations, slip rates and slip directions detailed in Appendix 13.

According to stress orientations and magnitudes reported by Hickman et al. (1998, 2000), the dominant population of permeable fractures within the fault zone near the DVGF is subparallel to the main fault, striking roughly NE and dipping 40-75 degrees SE, with a conjugate set striking roughly the same direction but dipping NW. Field observations suggest that roughly N-S oriented normal faults are also present (T. Cladouhos, pers. comm., 2010) and their role within the DVGF is described in Section 7.2.1. To be consistent with these observations, we explore three different types of RFs:

a. synthetic normal fault subparallel to SGS dipping 70^{o}E shown in Figure 50;
b. antithetic normal fault subparallel to SGS dipping 70^{o}W; and
c. normal fault oriented roughly N-S dipping 70^{o}W.

Assuming that the whole SGS fault segment ruptured 2-2.5 ka (in addition to the 1954 range-front fault segment of the DVFZ and 1915 PVF ruptures), the results presented in Appendix 13 show that the region near the DVGW lies within a zone of positive CSC and dilatation, suggesting that slip resulting from these Holocene ruptures promotes normal faulting on all three types of RFs. Stress data from selected wells within the DVGW supports these conclusions (see Section 6.1.1 and Table 4).

Table 4. Information from deep wells penetrating the fault zone at 2-3km depth. Red and blue indicate critically stressed and not critically stressed well sites (Hickman et al., 1998; 2000). See text for a description of Scenario 2.

Well	**Sh_{min}**	**Sh_{min}/Sv**	**Productive**	**Interpretation**	**Scenario 2**
73B-7	N57W±10	0.45-0.62 @ 0.4-2.5 km	Y	SFZ optimally oriented and Shmin low (**critically stressed**)	Consistent with well data
74-7	N52W	not reported	Y	SFZ optimally oriented and Shmin low (**critically stressed**)	Consistent with well data
66-21	N20W±20	0.55-0.64 @ 1.9–2.2 km	N	SFZ optimally oriented BUT Shmin high (**not critically stressed**)	Consistent with well data
45-14	N41W±12	0.55-0.64 @ 1.9–2.2 km	N	Shmin low BUT SFZ not optimally oriented (**not critically stressed**)	Consistent with well data

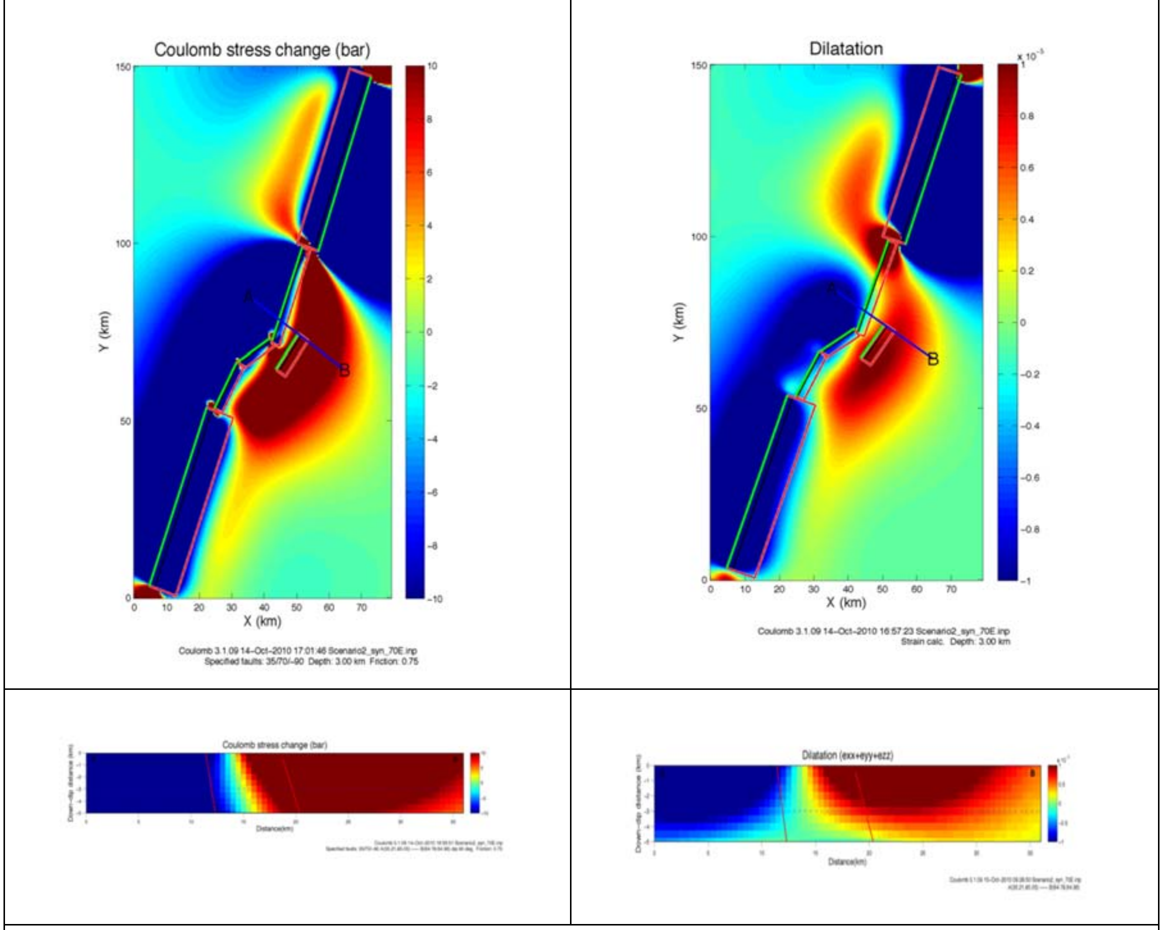

Figure 50. The expected CSC and strain (dilatation) along a synthetic normal fault (piedmont fault) striking subparallel to the DVF and dipping 70°E due to slip on differing segments on the DVF and PVF. The RF shown in the figure is representative as a hypothetical RF exists with each cell. The results from the other RFs can be found in Appendix 13.

7.3 Qualitative Geoscience Correlations

7.3.1 Summary Description of Geoscience Data Sets

The most complete 3-dimensional database for the geology, geophysics and geothermal setting of the geothermal system in Dixie Valley is located in the DVGW. It is recognized that this particular location cannot be used as a point-by-point template for geothermal cells (including the EGS target areas) throughout Dixie Valley. However it is the only area where a calibrated exploration methodology can be developed as a result of having subsurface data.

A series of cross-sections both perpendicular and parallel to the DVFZ (Plates 1 and 2) have been constructed to develop a baseline conceptual model of the geothermal system (both the hydrothermal and EGS), and provide a framework for the EGS favorability maps (see Section 8). The sections, based mostly on data from Blackwell et al. (2005), available well logs, and other public domain sources cited above, adhere to the steeply dipping multi-fault model for the DVFZ. They utilize the surface geology in the adjacent Stillwater Range, lithologic and thermal data from individual wells, and various geophysical surveys that infer the location of intra-basinal structures including gravity, magnetics, and seismic reflection profiles. The location of the eight cross-section lines (A-A’ to H-H’) with respect to the wellfield is shown in Figure 48 and Plate 1 & 2 . The sections were constructed to apply a series of 2-D sections to facilitate in the visualization of a 3-D model. The majority of the transects (C-H) were chosen perpendicular to the major structures, with the respective section locations chosen to cover the known productive (hydrothermal) and non-productive (potentially EGS) areas, all wells that had data available, and to transect major structures in the wellfield. See Appendix 12 for figures showing the various cross-sections and major assumptions used in their development.

Geology

The stratigraphy of the DVGS has been divided into six major and one minor stratigraphic units (Appendices 10 and 12) based on rock mechanical properties and the stratigraphic divisions used within idealized published and unpublished thermal models by Dave Blackwell (Blackwell et al. 2000; 2005). The units[1] include from youngest to oldest:

- Quaternary-Tertiary basin-filling sediments and lowermost tuffaceous sediments (QTbf);
- Miocene basalts (Tmb);
- Oligocene silicic volcanics including uppermost Miocene lacustrine sediments, volcaniclastics, and lowermost silicic tuffs (Tv);
- Cretaceous to late Tertiary granodiorite (Kgr);
- Jurassic mafic rocks (Jz[3]) known as the Humboldt igneous group or lopolith, and also interpreted as an ophiolite complex consists of an upper volcanic sequence and lower gabbro-dominated section; and
- Jurassic and Triassic meta-sediments (Tr) which also include the thrust bounded Jurassic Boyer Ranch quartzite (Jbr) which, where identified has been broken out separately because it is a favorable EGS target lithology.

The distribution of these stratigraphic units with respect to the surface geology exposed in the Stillwater, Clan Alpine, and other related ranges within the Project Area is shown in Figure 51.

---

[1] Note that in this report the term stratigraphic unit, lithology and geologic formation are used interchangeably since each of the seven major formational units identified in the DVGW have specific lithologies.

[3] In the gravity-magnetic modeling, the Jz stratigraphic unit is referred to as Jg and Jv; see Section 3.3 and 7.3.1 for an explanation.

The geologic sections in Plates 1 and 2 are based on the following general parameters, observations, and assumptions (see Appendix 12 for a more detailed discussion):

- Steeply dipping (75-90°) faults;
- DVFZ consists of the main range-bounding and intra-range faults, a major piedmont fault recognized by geophysical data, and the associated antithetic faults and associated fracturing away from the faults;
- Thickness of the defined stratigraphic units is primarily controlled by their occurrence in available well data, conceptual sections (Figure 31), and observations made from the surface geology exposed in the Stillwater Range;
- Early B&R N-S oriented normal faults which are likely re-activated as strike-slip faults under the current stress regime have mostly unknown dip directions and are drawn vertical without any normal-sensed offset; and
- Depth of the basin-fill sediments and the configuration of the basement profile (see Figure 18) are derived from Blackwell et al. 2005 that uses seismic interpretations, geophysical inferred bounding faults, and drilling results.

Thermal

The thermal sections use available well temperature data in the DVGW and thermal models through the wellfield (Figure 31, 45A and 45B) to construct a model of the temperature distribution at depth. While we can assume that the main thermal-bearing structures are the range-front and piedmont fault within the DVFZ, the well data and geologic model demonstrate that this is the case as a direct correlation is found between elevated temperature distribution and the major faults within the DVFZ (Plates 1 and 2). The elevated temperatures associated with these faults dip relatively steeply to the east towards the center of the valley, as the only temperature constraint at depth is found in 62-21, which lies in the valley on the SE-side of the DVGW. The “fall-off” in temperature to the west, under the Stillwater Range, is conjecture due to the lack of well data in that region.

While there is no direct evidence that the range front fault is directly connected to the producing hydrothermal system, it is believed to be a conduit for geothermal fluids from depth as evidenced by the (1) reported geothermal fluids in fractures from the last 30m (100ft) of 36-14, (2) fumaroles (~98°C [208°F]) at the surface trace, (3) recent seismic activity, (4) shallow outflow of geothermal fluids into basin-fill sediments (Figure 44), (5) comparable helium R/Ra values to the known producing field (see table imbedded in Figure 49D), and (6) very high temperatures (~285°C [545°F]) encountered at total depth in 36-14 (Blackwell et al., 2005).

The superpositioning of the wellfield temperature data on the MT and geology data provide the basis for constructing a model of the geothermal resource supporting the existing power plant and inferring EGS targets. Within this segment of Dixie Valley relating to the producing zone, discrete segments of the range-bounding and piedmont faults are transmitting hydrothermal fluids to shallower depths. Current production is derived from the piedmont section of the DVFZ. The main geothermal reservoir is thought to lie within dilatational zones along the piedmont fault where Miocene basalt and other Jurassic rocks capable of maintaining open fractures are truncated against impermeable granodiorite in the footwall block.

Magnetotellurics

Wannamaker et al. (2007) presented resistivity models along three MT arrays (N, C, and S) through the DVGW (see Section 3.4). The N and S arrays extend to a depth of 4km (2.5mi), while the C array is integrated with a regional MT transect (Wannamaker et al. 2006) and extends to a depth of 10km (6mi). The Dixie Valley MT arrays resolve the structural setting and support a multi-fault and steeply dipping model for the DVFZ. The transition from low to high resistivity (~100 ohm-m) represents the basement interface within the resistivity models which is supported by drilling results, as the arrays also show a high level of correlation with geologic sections. A discussion on the significant correlations found between the various geologic and geophysical datasets is provided discussed in Section 7.3.2.

Geochemical Data

Geochemical data within the DVGW was extracted from Goff et al. (2002) (see Appendix 7) from selected wells, TGHs, springs and fumaroles. The depth of the producing fluids sampled from the wells was estimated by our geochemistry SME, Dr. B. M. (Mack) Kennedy, Geochemistry Task Leader (see Section 1.4). The SME provided six potential geothermal indicators namely Silica (Si), Chloride (Cl), BiCarbonate, and helium F[^{4}He] measured in ppm as well as the BiCarbonate-Cl ratio, and helium R/Ra values. There are some difficulties in using and applying the geochemical data to the qualitative analysis, as the data is limited to isolated sampling points (point data) and it is not clear how to extrapolate the data.

Gravity-Magnetics

A lithology model based on the gravity and magnetics has been constructed along four sections that lie perpendicular to the DVFZ (C-F) and along the two sections lying parallel to the DVFZ (A and B), see Section 3.3. The complete Bouguer anomaly (CBA) gravity data (Ponce, 1997; Blackwell, pers. comm. to B. Karlin, 2010) and the HELIMAG aeromagnetic total field anomaly data (Grauch, 2002; Blackwell, pers. comm. to B. Karlin, 2010) were jointly modeled to create a 2 ½ D geophysical model consistent with the surface geology and selected well data (62-21) to infer the depth to basement.

The model divides the subsurface into four inferred stratigraphic units based on assigned density values that directly relate to recognized geologic units including (1) Jurassic volcanics and arenite exposed at the surface (Jv, Ja), (2) basin-filling sediments (Tbf), (3) a distinct magnetized Jurassic intrusive unit (Jg) and (4) basement inferring either Triassic meta-sediments or Cretaceous granodiorite. A near-surface low density unit within the valley was required to offset modeling effects and does not correspond to a specific mentioned unit, but could likely correlate with a near-surface clay-rich/evaporite layer. A complete description of the Gravity and Magnetics Joint-Modeling can be found in Section 3.3 with results shown in Figures 15A-D. The gravity and magnetic inferred lithology models are generally consistent with the geologic sections and identifies the presence of multiple faults in the DVFZ, a zone of step-faulting bounding the SE edge of Dixie Valley, and the occurrence of both a magnetized Jurassic unit (Jg) and non-magnetized Jurassic unit (Jznm) as postulated through comparison of the geologic and gravity/magnetic sections. While the geologic sections show Jurassic mafic rocks (also referred to as the Humboldt Lopolith) extending below the majority of Dixie Valley within the identified thrust sheet, the magnetic signature from these rocks isn't continuous across the area. The missing Jurassic rocks in the gravity-magnetic sections are most likely demagnetized and/or altered as a result of hydrothermal fluids in the DVFZ and correlate with the identified deep low resistivity zone along the MT sections, see discussion above.

Seismic Data

A variety of seismic data derived from the reflection profile data (Anonymous, 1998) and associated well data was re-analyzed at the University of Reno (UNR) by our seismic SME, Dr.

Ileana Tibuleac (see Section 1.4). The following parameters were provided that are considered potentially useful for EGS (1) P-wave velocity (Vp); (2) S-wave velocity (Vs); (3) density (rho); and (4) attenuation of the P and S-waves (Qp, Qs). Within the baseline seismic data, the resolution was greatest for the parameter Vp (~500 m) and in the vicinity of the reflection profiles. Resolution for the other parameters was too high (maximum of >10 km) to be used in the Baseline Conceptual Model.

A general qualitative correlation was found between temperature and Vp within a specified velocity range within the wellfield, although it has been noted by some team members that the correlations found could be reflecting a function of depth. Vp has been postulated to have a direct relationship to temperature (I. Tibuleac, pers. comm., 2010; Biasi et al., 1999), while the modeled velocity changes at depth is also due to other factors including heterogeneity of the rock, structures present, fracture density, fluids present, alteration, increased vertical stress due to the weight of the overlying rock, etc. A correlation between lithology and Vp was not found using the limited baseline data. These relationships are explored quantitatively through geostatistics in Section 7.4.

Seismic Reflection Profiles

Interpreted seismic reflection profiles extracted from Blackwell et al. (2005) were used to partially constrain the geologic sections, especially where there is a lack of well data. The profiles were mostly used to locate the depth of the basin-fill sediments but could not be used to accurately locate the major structures within the DVFZ due to the complicated structure and its steeply dipping nature. Sections A and B that extend parallel to the DVFZ utilize corresponding segments of the profiles SRC-1N and SRC-1S as well as line 101. Seismic profiles SRC-3, Line 102, Line 9 and portions of Line 104 are used for the sections perpendicular to the DVFZ, sections C-H, respectively. The seismic profiles show a very high level of correlation with the geologic sections as expected because the profiles were used to constrain the depth to basement where well data is absent. The correlation between the profiles and the other corresponding geoscience data can be found in Plates 1 and 2, respectively. The depth of the basin-fill sediments in the gravity/magnetic inferred lithology sections along section C-F also correlate well with the seismic reflection interpretations.

Stress Data Sets

Stress has been proven to be a difficult parameter model and assess. A coulomb stress model described in Section 7.2.2 used the available slip constraints and orientations on the major fault ruptures to model the expected stress change and strain on a given fault orientation and dip within the 500m by 500m cell resolution. The modeling procedure and results can be found within Appendix 13 and show that areas of dilation correlate with producing wells. Results from borehole stress studies agree with the Coulomb Stress model. Other stress parameters considered was the localized dilation and compression zones resulting at structural intersections and the calculated parameter vertical stress, used in the exploratory geostatistics (see Section 7.4).

7.3.2 Wellfield Correlation of Geoscience Data Sets

In an attempt to correlate the various data sets in Dixie Valley, cross-sectional data occurring within the DVGW has been directly compared to modeled geophysical data in the area. The generalized geologic and associated thermal sections (see Section 2.1.1 for a detailed stratigraphic discussion, 7.3.1 for a summary stratigraphic discussion, and Plates 1, 2 and Appendix 12 for the geologic sections) provide a basis for a correlation analysis that compare the sections with MT 2D models and 2 ½ D gravity/magnetic models. Other datasets included in the qualitative correlation analysis are associated interpreted seismic reflection profiles, and geophysical modeling of Vp in the vicinity of the wellfield (Plates 1 and 2). This qualitative correlation analysis is complemented by a quantitative statistical analysis discussed in Section 7.4.

Geologic Sections

The majority of the data occurred along sections lying perpendicular to the DVFZ (striking around N45°W) in the vicinity of the wellfield. These sections (C-H), can be directly compared with four seismic reflection profiles, three MT arrays (N, C, S), and combined gravity and magnetics modeled along lines C-F that infer the expected stratigraphy and structure at depth (Plate 1). The two sections with a northeast strike lying parallel to the DVFZ, sections A and B, compare the geology and thermal sections, segments of available seismic reflection profiles, and the combined gravity/magnetic inferred stratigraphy models along the respective lines (Plate 2). A detailed discussion on the geologic and thermal sections discussed in Section 7.3.1 can be found in Appendix 12, which lists the various assumptions and inferences used to construct the sections.

The geologic sections were found to correlate well with the MT profiles and the combined gravity/magnetic sections. General observations among these sections are (1) the MT profiles show a high level of correlation with the interpreted structure as shown in the geological sections, (2) a vertical-trending low resistivity zone seen in the three MT profiles within the valley most likely reflects a major alteration zone correlating with a set of north-trending structures, (3) the gravity/magnetic profiles reflect the interpreted generalized geology, and show the magnetic signature of the Jurassic mafic rocks doesn’t extend through this major north-trending intra-valley structure and is locally not present within the DVFZ, (4) the areas of elevated temperature (geothermal cells/system/resource) occur at the intersection of these earlier north-trending structures and northeast trending segments of the piedmont fault (Figure 49C).

The following details the correlations found between the different geoscience data sets on a cross-sectional basis. Four sections are included in this summary (C-C', D-D', E-E' and F-F') due to their variety of geophysical data to compare with the geologic sections (Plate 1). For individual cell[4] references, refer to Plate 1 as a grid with 500 meter spacing was overlain on the cross-section data for gridding and reference purposes. The horizontal scale is numbered with cell 1 starting at the NW end of the sections, while the vertical scale is lettered from A-L, starting with A that represents the cell from 2.0km to 1.5km asl. A table highlighting all significant correlations between the various data-sets is included as Appendix 14.

Cross-Section C-C’

Select geoscience data for section C-C' is shown in detail in Figure 52. This figure exemplifies the qualitative correlation and cross-correlations found between the geology, thermal, MT, and gravity/magnetic lithologic model. The section transects through the hot, low-permeability wells within the DVPP (Figure 48), south of the producing field. Elevated temperatures are found

---

[4] All available geoscience data has been gridded in 500m x 500m size blocks for quantitative analysis and EGS Favorability Mapping.

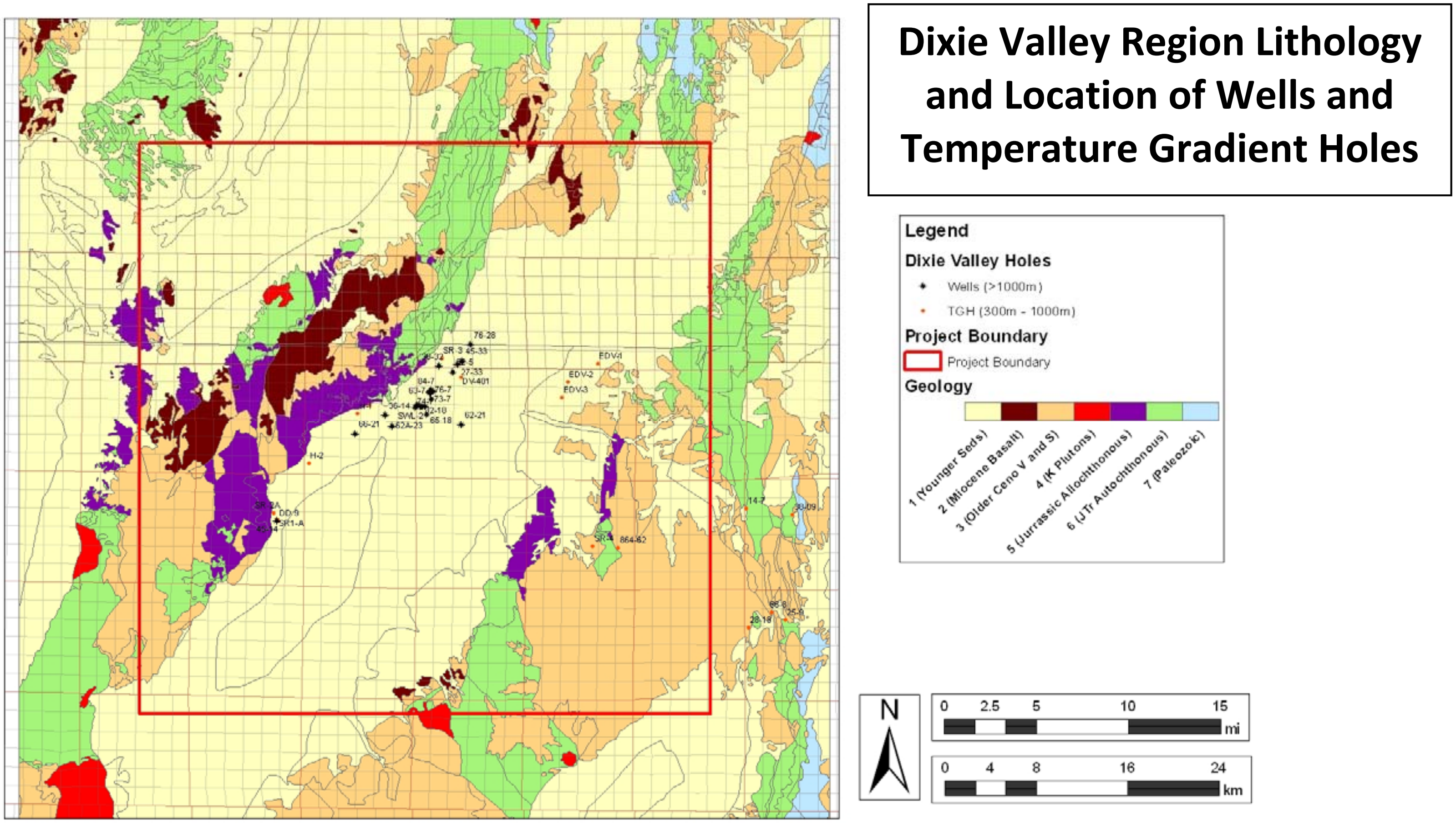

Figure 51. Dixie Valley generalized geologic map showing the six major surface stratigraphic units. Also shown are the Project Area (in red) and wellfield. Note that a minor Paleozoic unit (light blue) only occurs in the northeastern corner of the Project Area.

along both major faults within the DVFZ, expectedly due to convective fluid flow from depth. The main striking correlation is found along this section is between the geologic and resistivity model (top section in Figure 52). The resistivity distribution reflects the steeply dipping, multi-fault model for the DVFZ as the range-front and piedmont faults projected at depth tightly bound bodies of significantly higher resistivity within their respective footwall blocks. Modeled resistivity above around 500 ohm-m correlate with the interpreted location of the Cretaceous granodiorite (Kgr), a suitable rock type for EGS. A near surface zone of lower resistivity within the Stillwater Range projects where there is range-front fumarolic activity present at the surface (Section 10 fumaroles) and infers hydrothermal alteration at shallow depth. Additionally, a major NS-trending structure coincides with a vertical-trending low resistivity zone in the valley and with the termination of the magnetized Jurassic rocks (Jg). The Jg magnetic signature is also non-continuous though a portion of the DVFZ adjacent to the geophysical trace of the piedmont fault, and inferring hydrothermal alteration. The gravity- magnetic model shows multiple faults comprising the DVFZ (see cells 2-4) which is likely the case, although the structures (colored red) are placed in the model to bound discontinuous segments of the Jg unit.

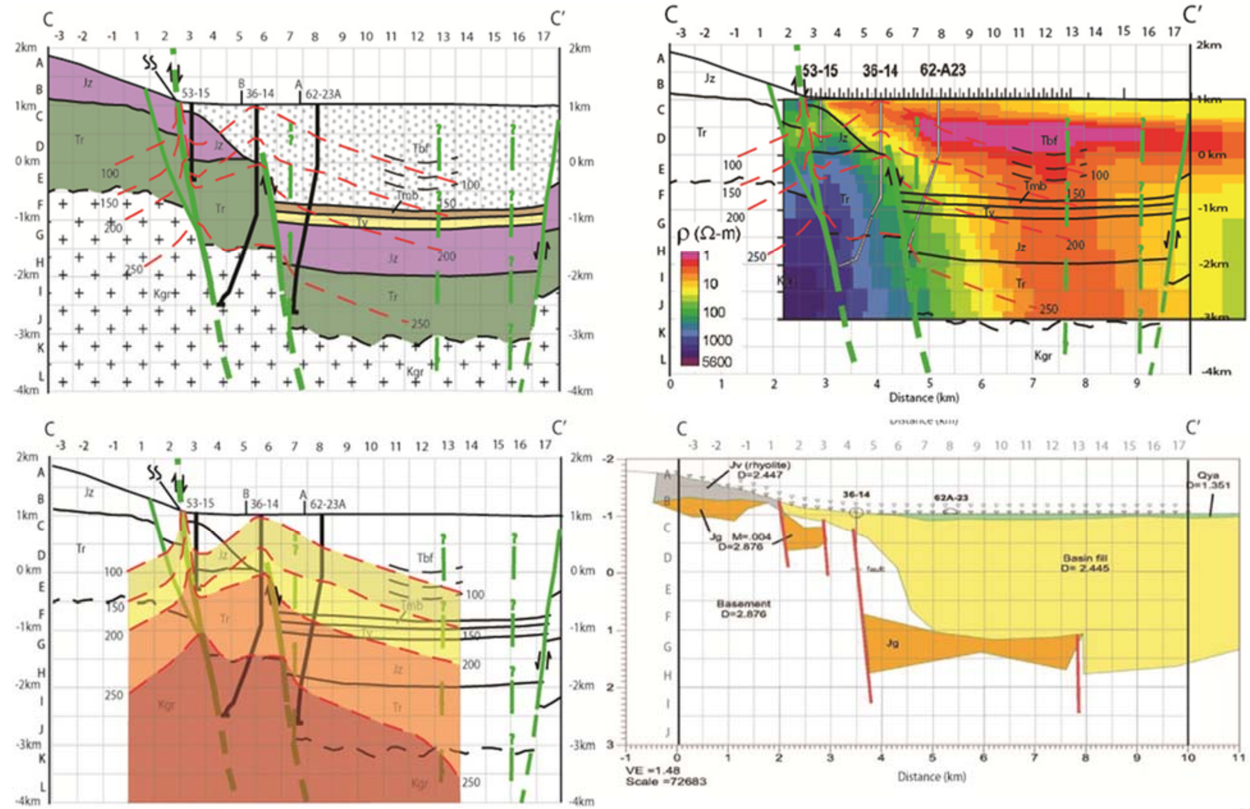

Figure 52. Correlation of the Geology, MT, Thermal, and Gravity-Magnetic Lithologic Model along Section C-C', see Figure 40 for location of C-C'.

Cross-Section D-D'

This section transects through the main injection zone (Lamb Ranch/Section 18, see Section 6.2) for the producing field. Significant correlations and lack thereof are listed below:

- The piedmont fault occurs in the same location in the geologic models, seismic reflection profile (Line 9/104), and within the gravity-magnetic model.
- Correlation between the volcanics (Tmb and Tv) is poor between the geologic inference and seismic reflection profile as the interpreted reflectors representing the basalt and basement horizons are thicker than the expression in the geologic sections.
- Gravity-Magnetic section intra-range structure correlates with a known surface fault in the Stillwater Range.
- Termination of Jg and bounding structure coincides with major NS-trending structure.
- Occurrence of magnetic rocks (Jg) in the vicinity of the main injection zone is much thicker than the known Jurassic rocks encountered in the wells.

Cross-Section E-E'

This "key" section has the most variety of geoscience data and extends through the Section 7 production wells adjacent to the power plant (Figure 53). The area of very high resistivity (above 1000 ohm-m) beneath the Stillwater Range along Array C has been attributed to the presence of relatively unaltered bodies of Cretaceous granodiorite at depth. Interestingly, the body lies a few kilometers NW of the range-front fault in contrast to the relationship found in Array S and appears to be bounded by a major intra-range steeply dipping fault that coincides with a recognized surface fault. This fault is shown as a moderately dipping (~65°) lower resistivity zone (~100 ohm-m) occurring around 1-2km (3300-6600ft) range-ward of the projection of the current range-front fault and infers significant hydrothermal alteration and/or thermal fluid bearing structures along this intra-range structure. Other correlations found along Section E-E' are:

- The extended region of relatively low resistivity northwest of the range-front fault along Array C coincides with a region of extensive parallel to subparallel faulting to the range-front fault (Figure 14 and 49A). Fault structures (steeply dipping resistivity zones) suggested in the resistivity profile in this region appear to correlate with the area of extensive surface faulting.
- Interestingly, a relatively higher resistivity block along the range-front fault segment of the DVFZ that extends into the main production zone near the Section 7 wells appears to correlate with the geothermal reservoir.
- The seismic reflection profile (Line 6) and the gravity-magnetic model infer multiple west-dipping faults bound the SE edge of Dixie Valley.
- The magnetic Jurassic rocks (Jg) occurring with the zone of step-faulting on the SE end of the section coincide with the geologic interpretation and surface mapping.
- A N-trending structure tightly bounds the higher resistivity present below the geothermal reservoir (see gridded cells G11-L11).
- The vertically-trending low resistivity zone in the valley correlates with the absence of magnetic Jurassic mafic rocks (Jg), referred to as a sub-unit Jznm (non-magnetic Jurassic rocks).

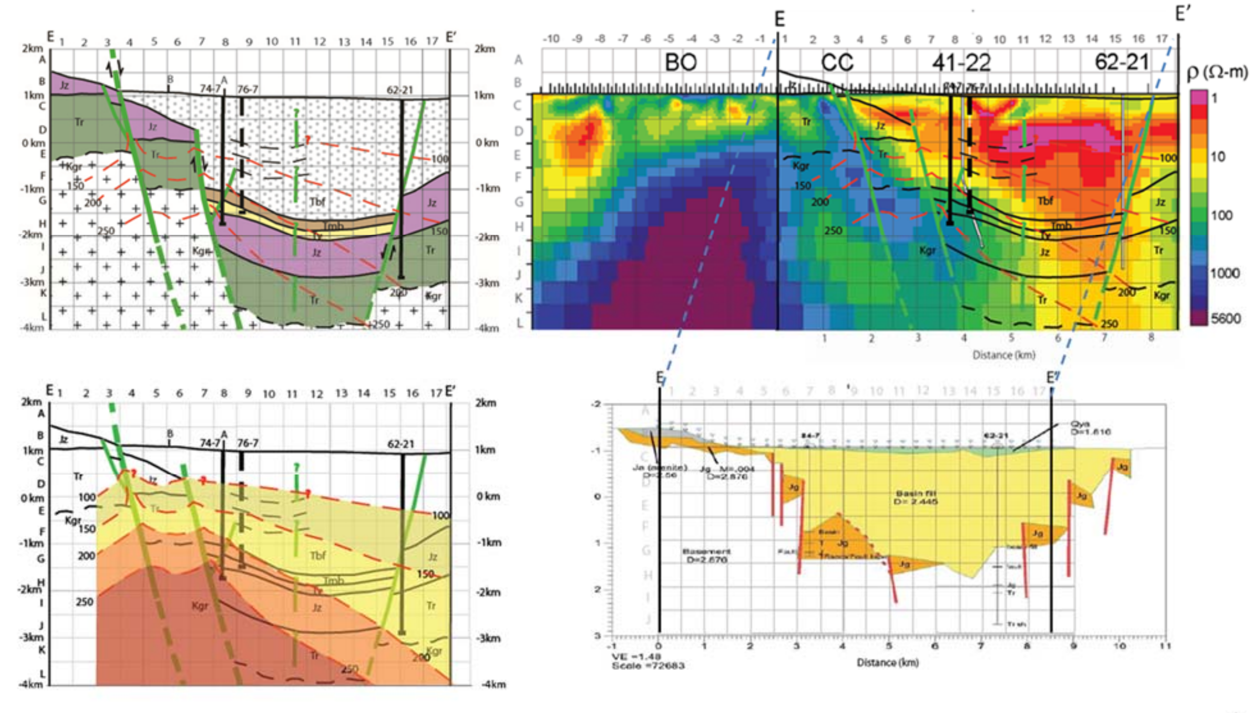

Figure 53. Correlation of the Geology, MT, Thermal, and Gravity-Magnetic Lithologic Model along Section E-E', see Figure 40 for location of E-E'.

Cross-Section F-F'

The section F-F' correlates with Seismic Line 102, MT array N, injection well 38-32, and the area between production zones with the Section 7 wells to the south and the permeable Section 33 wells to the north. Some correlations found not identified in the previous sections are:

- The magnetic Jurassic rocks (Jg) are discontinuous and do not occur in the area of the low resistivity, vertically-trending MT structure and within the DVFZ. The missing Jg is referred to as Jznm, see Section 8.6.1.
- Along Array N, a prominent fault occurring within the zone of step-faulting that bounds the eastern edge of Dixie Valley coincides with a sharp resistivity break.
- Range-front fumarolic activity present at the surface along Array N (Senator Fumaroles) show a correlation with a near surface zone of lower resistivity within the Stillwater Range.

Summary of Cross-Sectional Correlations

Overall, a high-level of correlation between the various geoscience data-set is found along the four sections (C-F) perpendicular to the DVFZ and transecting through the producing field. The highest temperatures found along Section C and F coincides with the intersection of NS trending structures with the NE trending structures of the DVFZ. Major structural discontinuities within the Stillwater Range that bound segments of the magnetized Jurassic section (Jg) correlate with both an area of dense intra-range faulting and shallow lower resistivity structures shown the MT data, particularly along Array C. The distinction between magnetic and non-magnetic Jurassic rocks (Jg and Jznm) between the geologic and gravity-magnetic sections correlates with the vertically-trending low resistivity zone in the valley and the DVFZ, as non-magnetic rocks occur within the two structures. The authors herein suggest that hydrothermal alteration within the DVFZ and an intra-valley structure identified by the MT data has demagnetized the Jurassic mafic rocks. A summary of the correlations found with the Gravity-Magnetic and Resistivity (MT) models are found below.

Correlation with Gravity-Magnetic Models

The gravity/magnetic inferred geology show an excellent correlation with the geologic and MT sections constructed independently along the same section lines (Plates 1 and 2). All three data sets evidence multiple and complex faulting in the DVFZ as interpreted structures bounding the distinct magnetized Jurassic mafic rocks (Jg) are steeply dipping to near vertical. The gravity-magnetic sections (C-F) all show another small piedmont fault splay in the DVFZ between the range-front and previously mentioned piedmont fault. The occurrence of the magnetic Jurassic units (Jg) was a very sensitive parameter in the gravity/magnetic modeling and the resulting modeled sections show a good correlation with the expected Jurassic unit in the geologic sections. The discontinuous nature of these mafic rocks along the gravity/magnetic sections is attributed to demagnetization of these rocks most likely resulting from hydrothermal alteration in the area of the DVFZ and altered/conductive rock in the region of the low resistivity zone identified by Wannamaker et al. (2006; 2007) in the valley (see discussion above).

- The basement depth and occurrence of basin-fill sediments (Tbf) within the Gravity-Magnetic sections correlates with the geologic sections and the seismic profiles;
- The Gravity/Magnetic models show more structures than are shown in the geologic sections:
  - Imply the structures are steeply dipping (85-90°)
  - Show multiple piedmont faults in the DVFZ
  - Imply a zone of step-faulting bounds the southeastern edge of Dixie Valley; and
- Major intra-valley structures bounding the magnetized Jurassic rocks along the modeled sections occur in approximately the same position as the N-trending structures within Dixie Valley identified by Smith and Blackwell (2001).

Correlation with Magneto-Telluric (MT) Resistivity Data

Plate 1 presents the three MT profiles reported by Wannamaker et al. (2006; 2007) with the associated geologic and thermal sections (generated in this study) superimposed (see also Section 3.4 and Figures 16B-16D). Arrays S and C, and their correlated geoscience cross-sections are shown in Figures 52 and 53, respectively. A high level of correlation is found between the MT profiles and the associated geology sections and associated structure. A vertical-trending low resistivity zone extends to a depth of at least 10 km along Array C and also occurs beneath the valley along all three arrays. This feature correlates with (1) the occurrence of N-trending structures (faults) along Arrays S and C, while no such direct correlation can be found along Array N and (2) missing magnetized Jurassic rocks (Jznm) in the gravity/magnetic models (Plates 1 and 2, Figure 15B and discussion above). This low resistivity feature is not considered an active thermal feature but rather interpreted as a major ancestral alteration zone as temperatures reported from 62-21 are low with respect to the producing geothermal system (maximum of 184°C [363°F]) upwelling along the DVFZ. Other correlations found are:

- A lateral body of very low resistivity (1-5 ohm-m) occurring in the shallow subsurface at a depth of ~500m (1600ft) occurs within all three MT arrays. This may correspond to a conductive layer within the basin-fill sediments, an aquifer showing the lateral flow of geothermal fluids mixing with groundwater, or a depth to the water table. Coincidently, a low resistivity zone of alteration extending at depth occurs below this near surface feature; and
- High resistivity below the Stillwater Range (>2000 ohm-m) may infer the presence of apparently unaltered granodioritic plutonic bodies.

Further delineation of geoscience relationships with the modeled resistivity data and expansion of these identified relationships within the DVGW is expected to be achieved after the more detailed MT survey under Task 4 is completed and interpreted. Additional questions to be addressed are (1) the potential causes for the dramatic changes in MT resistivity at depth, and (2) the apparent correlation between dipping resistivity structures and inferred fault structures. Table 5 presents the interpreted MT resistivity data relative to the geology and expressed in the sections.

Table 5. Correlation of the geology and MT data shown in Plate 1.

Unit	Class	Value (ohm-m)
Valley-fill sediments	Low Resistivity	<<100
Clay-rich/altered alluvium	Moderately conductive	<3-5
Basement/highly altered alluvium	Moderately High Resistivity	100
Jz and Tv sections	High Resistivity	100-500
Intrusive plutons (Kgr)	Very High Resistivity	>1000
Altered geothermal fluid zones	Low Resistivity	5-50

7.4 Quantitative Geoscience Correlations: Geostatistics

A variety of exploratory geostatistical techniques were applied to select geoscience parameters to (1) quantify the qualitative geoscience relationships described in Section 7.3, (2) test relationships independent of the qualitative geoscience correlations, and (3) explore if statistically quantified parameters can be used in the generation of the baseline EGS Favorability Maps (Section 8). Described below is the quantitative geostatistical analysis methodology.

7.4.1 Database, Parameters Description, and Gridding

The following steps were taken to prepare the data for geostatistical analysis (also see Section 8.2):

1. constructing a geostatistical database to store and manage the data;
2. identifying which geoscience parameters were appropriate to perform statistical analysis including but not limited to considering the resolution of the data; and
3. gridding the data within the Calibration Area[5] to place it in a form that each data set could be compared.

Constructing the Geostatistical Database

The overall project had a number of challenges with respect to data management and manipulation. Its scope was such that a large amount of data was going to be acquired, produced, and interpreted from a number of different sources. The project required a method for storing, managing, and updating these various data sets at almost its onset. Basically, all data used for the geostatistical analysis was stored and managed using *Microsoft EXCEL*. The data was (1) transferred into the GIS database for storage, use for EGS Favorability Mapping, and determining qualitative relationships and (2) provided to the Geostatistics Task Leader who then imported the data into a statistical program (e.g., *JMP Pro* by *SAS; RStudio*) for analysis. Appendix 15-Tables 15-1 through 15-11 present the data used for the geostatistical analysis.

Description of Parameters

A list of all the data parameters as well as a description of all characteristics of the geoscience parameters used in the geostatistical analysis is presented in Appendix 15. A description of the various tables follows:

---

[5] The Calibration Area was chosen as the DVGW because it is the only region within the Project Area that has wells with known properties (e.g., temperature) that will allow calibration of the data generated.

- Appendix 15-Table 15-1 presents a summary description of the various data available to this investigation;
- Appendix 15-Table 15-2 presents the type of geoscience parameters considered for the geostatistical analysis including but not limited to the individual parameter resolution;
- Appendix 14-Table 15-3 describes the assumptions in the construction of the geologic and temperature sections; and
- Apprendix 15-Tables 15-4, 15-5, 15-6, 15-7, 15-8, 15-9, 15-10 and 15-11 describe the lithology, well, seismic, gravity/magnetics modeling, MT parameters, temperature, Coulomb Stress Change modeling, and geochemical parameters, respectively.

Note that geochemical data was not used in the geostatistical analysis because of its limited geographic distribution and it was considered a point source nature.

Geostatistical exploratory data methods were applied to a variety of preliminary geoscience parameters (Appendix 15-Table 15-2). Task Leaders (see Section 1.4) provided potential parameters (numerical, a discrete numerical value and categorical, a descriptor for a parameter, e.g., lithology) derived from their respective field and/or models. The purpose was to create a baseline data-set that has been used to develop the Baseline Conceptual Geothermal Model and to quanitify any statistical relationships between the various parameters. These quantified relationships could then potentially cooroborate using the parameters to predict rock type, temperature or stress conditions, and/or provide additional sub-parameters that could be used in the generation of the EGS Favorability Maps. These sub-parameters would be used in conjunction with the major three parameters determined crucial to infer conditions suitable for EGS. The parameters are analyzed both qualitatively and quantitatively using geostatistics.

Typically geostatistical analysis is conducted on measured parameters. However, the data types available to this investigation are either measured, modeled/calculated, assigned or inferred (Appendix 15-Table 15-2) based on SME and have varying resolution. This is ***not an ideal case for geostatistical analysis***. A fundamental assumption applied here is that while the exploration data set is statistically not ideal, and some parameters are more reliable than others, the data can be used to determine statistical significance. The validity of this assumption rests on the notion that whatever uncertainty exists in the different parameters can be thought of as a measurement error, and is at least from a practical standpoint, unbiased. Causal relationships for any statistical relationship identified herein have not been investigated.

The main geologic parameter is a categorical data-set, rock type. It divides the stratigraphy into seven units (Appendix 15-Table 15-1). There are four assigned parameters relative to rock type that include density, rock strength, internal friction, and EGS favorability that were inferred by the geology and stress Task Leader (Appendix 15-Table 15-4). Interestingly, these assigned numerical parameters allow lithology to be indirectly analyzed as numerical data. Other geologic parameters include vertical stress and fracture intensity, which are calculated (modeled) values. Additionally two stress-related parameters derived from a Coulomb 3.1 Stress Model are Coulomb Stress Change (CSC) and strain (Appendix 15-Table 15-10).

Parameters derived from geophysical models include a categorical data set, namely lithology inferred by the joint gravity and magnetic model (Appendix 15-Table 15-7). Temperature is considered the most important parameter for EGS and was derived from measured data in wells and temperature models along key sections indicated in Plates 1 and 2 (Appendix 15-Table 15-9). The MT parameter is modeled resistivity at depth along arrays extending through the wellfield (Appendix 15-Table 15-8). Seismic parameters from a combined UNR generated model of baseline data include P-wave velocity (Vp), S-wave velocity (Vs), density (rho), and attenuation of the P and S-waves (Qp, Qs) as indicated in Appendix -Table-15-6. Vp was considered the only seismic parameter with an adequate resolution to be used in the baseline analysis. The only other directly measured parameter, geochemistry from wells, production fluids, temperature gradient holes, fumaroles and springs, was not used in the statistical analysis due to limited data points and the data being essentially point source. These data represent the available baseline geostatistical data set.

Gridding

The proposed plan for this project was to grid the entire EGS Project Area (50km^2 [31mi^2). However, as the project proceeded we realized that the only area that can be calibrated was the DVGW because it was the only region where well (subsurface) data, in particular temperature, was available. As such, we focused principally on this region, referred to as both the DVGW and Calibration Area (see Section 7.1.2 and Figure 48).

The Calibration Area was gridded (divided) into 500m by 500m cells to transfer the data into a consistent grid size for geostatistical analysis. A resolution of 500m (1640ft) was decided by the team to be an adequate resolution for the variety of data as a starting point. The first step was a qualitative analysis as selected cross-sectional data (lithology, temperature, MT and gravity-magnetic inferred lithology) was gridded along a pre-determined cross-section line. Section E-E' was gridded first, as a preliminary test, due to the variety of geoscience data located along the line and the proximity to the section 7 production wells. Once a qualitative correlation between the data-sets was established along section E-E', all other applicable data (e.g., seismic, MT, geochemistry, gravity and magnetics, etc.) was gridded along all six cross-section lines (A-F). The sections were divided into a 2-D grid of 500m by 500m cells from an elevation of 2km to -4km asl (6600ft to -13000ft asl). The valley floor of Dixie Valley is approximately +1km asl (3300ft), thus, a depth of -4km asl is at a depth of 5km (16,400ft).The reason the grid 's upper limit is 2km instead of at 1km equal to the valley floor is to incorporate the geologic data within the Stillwater Range. For example, the upper row of gridded sections, is bounded at 2km above and 1.5km (4900ft) below, and while most of the cells occur above the surface as air, a portion of the Stillwater Range occurs above 1.5km asl elevation and thus has a corresponding value (lithology, etc.) for a respective cell. Plates 1 and 2, and Appendix 12 presents the sectional grids as shown within the digitized sections and an example of the gridding can be found in Figure 52.

7.4.2 Exploratory Data Analysis

Only data gridded along sections C-C', D-D', E-E' and F-F' was used in the geostatistical analysis because they had the most varied and complete geoscience data and well control. Data was also gridded at 500m depth intervals with respect to wells to directly compare measured data (lithology logs, temp-depth profiles, etc.) with modeled geophysical data occurring within the intersection of the wellbore. Thus, two data sets have been used in the statistical analyses (1**) Section Data**, which includes all parameters gridded along cross-sections C-C', D-D', E-E', F-F' and the combined sections; and (2) **Well Data**, consisting of all directly measured data (temperature, lithology, faults, etc.) and all modeled data with respect to well location. These data sets can be found in the following Appendices 16a and 16b, respectively. To analyze the data, we conducted the following geostatistical analyses:

1. Correlation Analysis
    a. global linear correlations between selected geoscience parameters along the section lines and the combined section data;
    b. multivariate linear correlations by lithology per section and combined sections;
    c. domain analysis by geographic/geologic sub-element along the sections (i.e., Stillwater Range, DVFZ, and valley); and

   d. Correlation Analysis using the Well data that explores the relationship between temperature and Vp (discussed below).
2. Residual and Multiple Regression analysis
3. Classification and Regression Tree (CART) analysis
   a. Section Data; and
   b. Well Data.

The results of the Correlation Analysis elements 1a through 1c are equivocal and are discussed in detailed in Appendix 17. This may be part due to the paucity of data available, equivocal results in the methods used, or the fact that geostatistical analysis of exploration data is inherently problematical. The "paucity of data" hypothesis will be evaluated in the assessment of the enhanced data set (see Tasks 4 and 5 description in Section 1.1). One correlation analysis that was found very interesting as well as significant to the project was the relationship between measured temperature in wells and modeled Vp data. This relationship is described and assessed below.

Exploring the Temperature-Vp Relationship using well data

One of the objectives of the proposed development of a calibrated exploration methodology has been to determine if seismic data could be used to predict rock type and/or temperature at depth. The baseline (existing data) assessment of the available seismic data with respect to Vp; Vs, S-wave velocity; rho, density of the rocks; Qp, attenuation of the P-wave; and Qs, attenuation of the S-wave, (described in Section 3.5) revealed that the baseline data resolution is not sufficient for any seismic parameter other than Vp. Presented below is an analysis of the measured temperature – modeled Vp-depth relationship. The first step was to create a correlation plot comparing measured temperature in a well versus the modeled Vp in the area around the well. Each data point represents a gridded 500m by 500m cell that contained both a temperature and Vp value and is coded by well ID and formation type in the grid to determine if the relationship was dictated by well location, lithology, or depth sampled.

1. A linear fit was applied to all data with a resulting poor r-square value **(r^2) = 0.51**, see Figure 54.
2. The best-fit line was determined to be skewed by shallow data (low Vp values) or values occurring at the approximate surface (1km asl [3300ft]). These values had a low resolution with respect to the baseline seismic model. Removing the surface slice Vp data found that a 2-degree fit to the remaining data had a slightly higher correlation; **r^2 = 0.54**, see Figure 55.
3. Outlier data points corresponded to certain wells where the associated modeled Vp data had a very low confidence (trust) value (See Appendix 15, Table 15-6). Removing outlier wells (i.e., low seismic trust for Vp: 45-14, 53-15, 76-28, and 66-21) found a polynomial 2-degree fit to the data and a resulting **r^2 = 0.73**, see Figure 56. Thus, by considering the seismic trust factor identified by Dr. Ileana Tibuleac, Project Seismic Team Leader (see section 1.4)and removing the seismic data for the surface layer, a much better correlation was detected. The regression equation that represents the relationship between temperature and Vp is shown in Figure 56.
4. The data was also analyzed with respect to lithology to determine if another factor is influencing the Vp-Temperature relationship (Figure 56). Two trends can be observed from the plot relating to lithology. The data could be divided into a shallow domain within the basin-fill (QTbf) and a deep domain (depths of -1.0km asl and deeper) within the basement rocks. In general the QTbf increases in Vp with depth merging with the Vp of the basement rocks. This occurs around a Vp of 4.54 km/sec (10,200 mph).

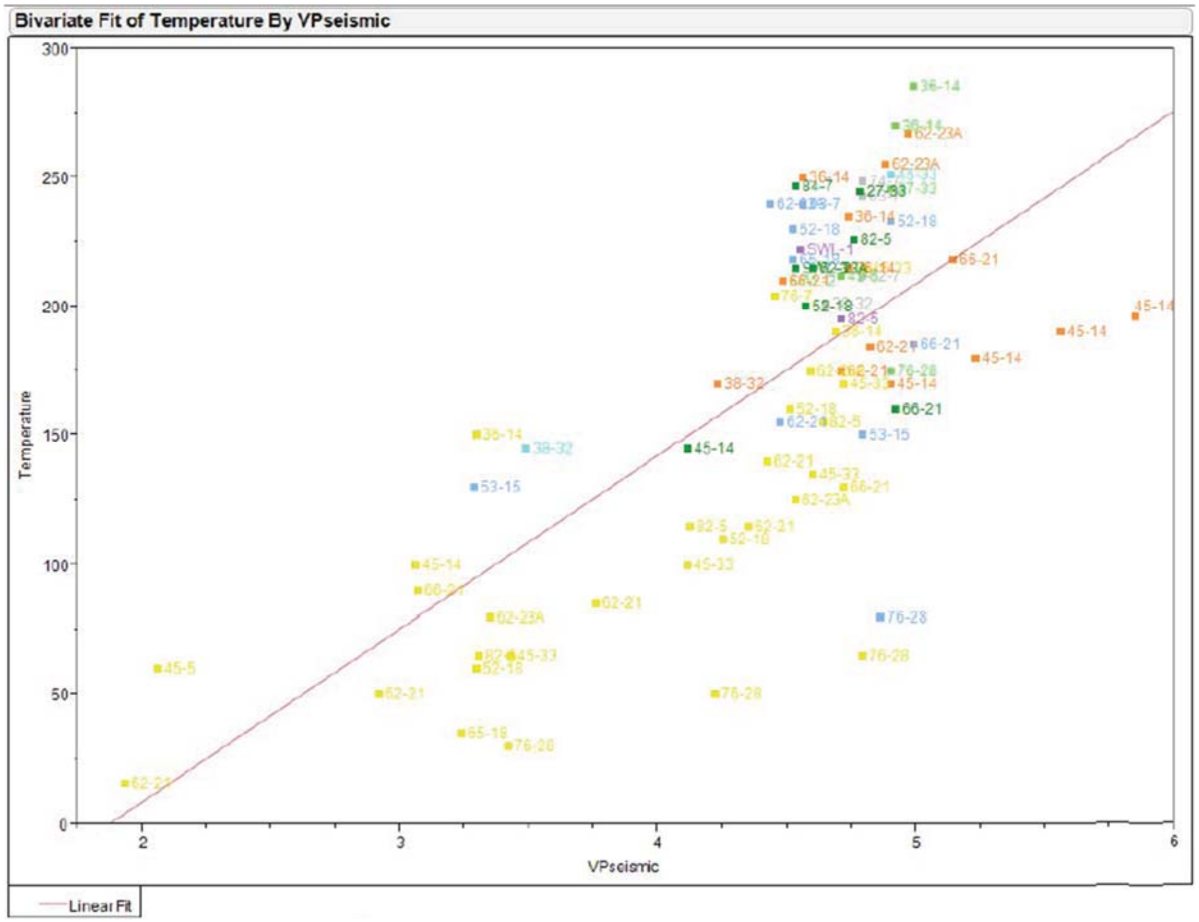

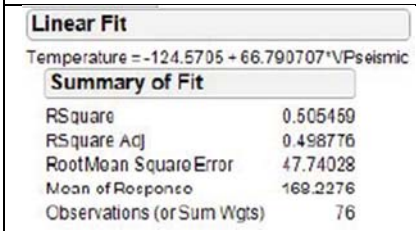
Linear Fit

Temperature = -124.5705 + 66.790707*VPseismic

Summary of Fit

RSquare	0.505459
RSquare Adj	0.498776
RootMean Square Error	47.74028
Mean of Response	169.2276
Observations (or Sum Wgts)	76

Figure 54. Correlation plot of Vp vs. Temperature for all well data. A linear fit to the data evidences a poor R-square value of 0.51 (correlation coefficient = 0.7141). The data is labeled by well name and color coded by lithology as follows: QTbf (yellow), Tmb (purple), Tv (dark green), Jz (blue), Tr (orange), Kgr (light green) and Jbr (turquoise). Terms reporting the summary of fit using linear regression are summarized with respect to Figures 54-56. *RSquare (R^2)*- estimates the proportion of variation in the response that can be attributed to the model rather than to random error. *RSquare Adjusted*- adjusts R^2 to make it more comparable between models with different numbers of parameters. *RootMean Square Error (RMSE)*- Estimates the standard deviation of the random error. *Mean of response*- overall mean of the response variables. *Observations*- records the number of observations in the model. For more information see: http://www.jmp.com/support/help/Regression_Reports.shtml#139075

Residual and Multiple Regression Analyses

In virtually all the correlation analyses described in Appendix 17, a consistent relationship has been evidenced between vertical stress, temperature, and Vp. We recognized that all three of these parameters generally increase with depth and potentially that may be the reason for the observed strong correlation. For example, since vertical stress is a calculated value relying on depth and the density of rocks overlying a respective cell, this parameter can be viewed as strong indirect inference to depth. Thus, a correlation of increasing temperature with increasing vertical stress could likely be an insignificant correlation. To evaluate this hypothesis, a residual analysis to remove the effect of depth was conducted and is described below. Additionally, a detailed analysis that explores the relationship between the correlated parameters, temperature and P-wave velocity, and the effect that other variables such as density, depth, etc. may have on this relationship is described in Section 7.4.2.

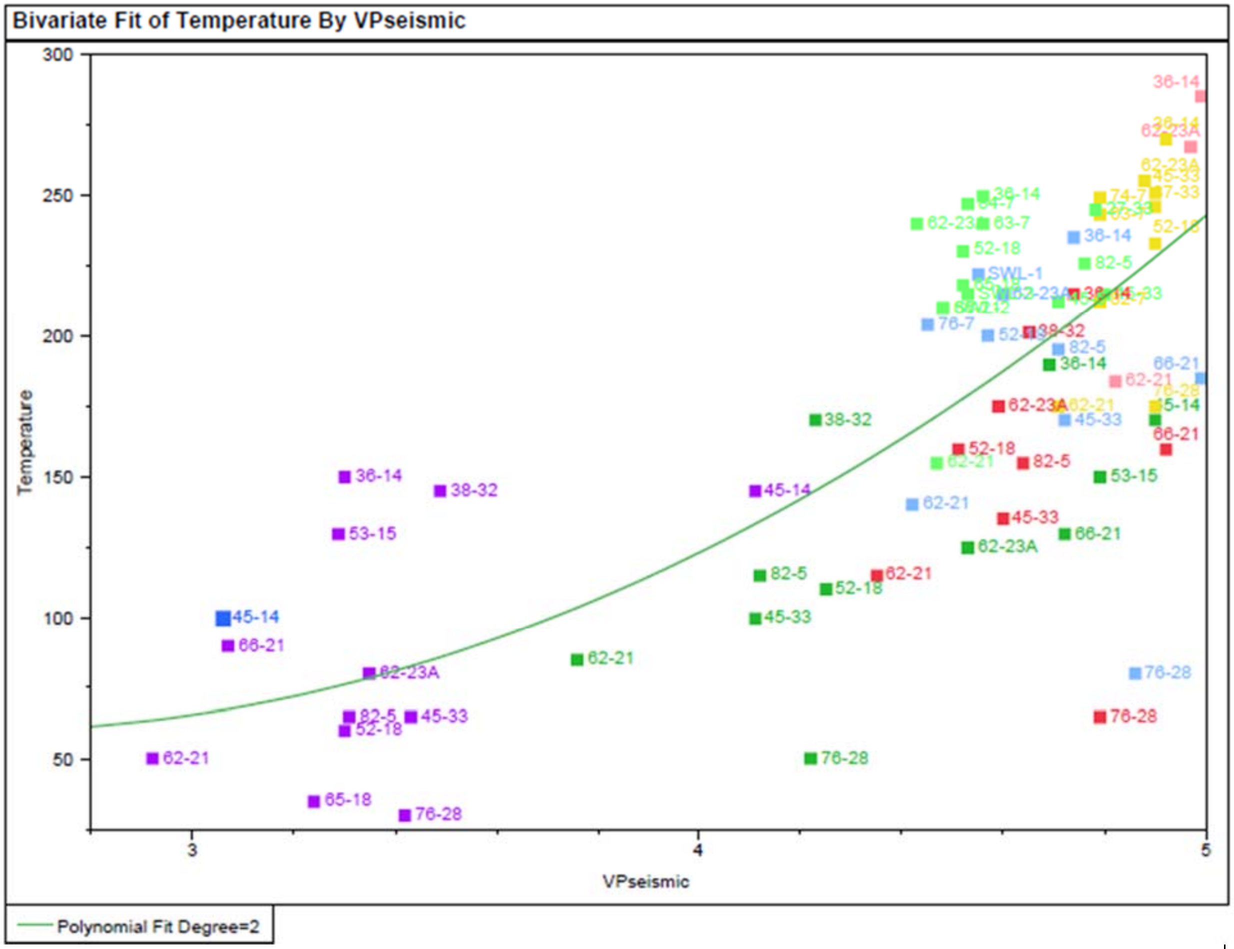

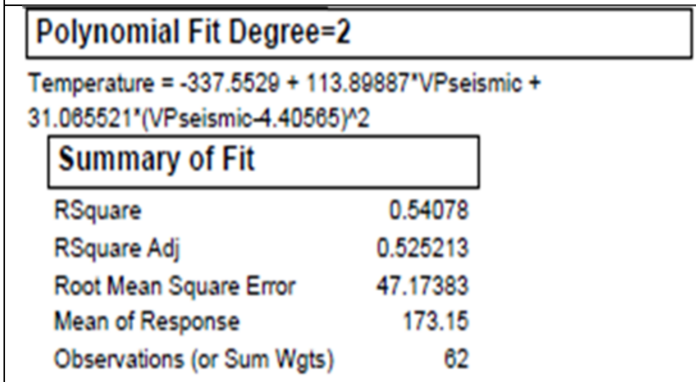

```
Polynomial Fit Degree=2
Temperature = -337.5529 + 113.89887*VPseismic +
31.065521*(VPseismic-4.40565)^2
Summary of Fit
RSquare                          0.54078
RSquare Adj                     0.525213
Root Mean Square Error          47.17383
Mean of Response                  173.15
Observations (or Sum Wgts)            62
```

Figure 55. Correlation plot of Vp vs. Temperature using all well data except for data occurring at the surface (elevation of 1km). The data is labeled by well name and color coded by depth as follows: 1.0km (blue), 0.5km (purple), 0.0km(dark green),-0.5km (red), -1.0km (light green)-1.5km (light blue), -2.0km (beige), -2.5km (pink). Polynomial Fit has a R-squared value of 0.54.

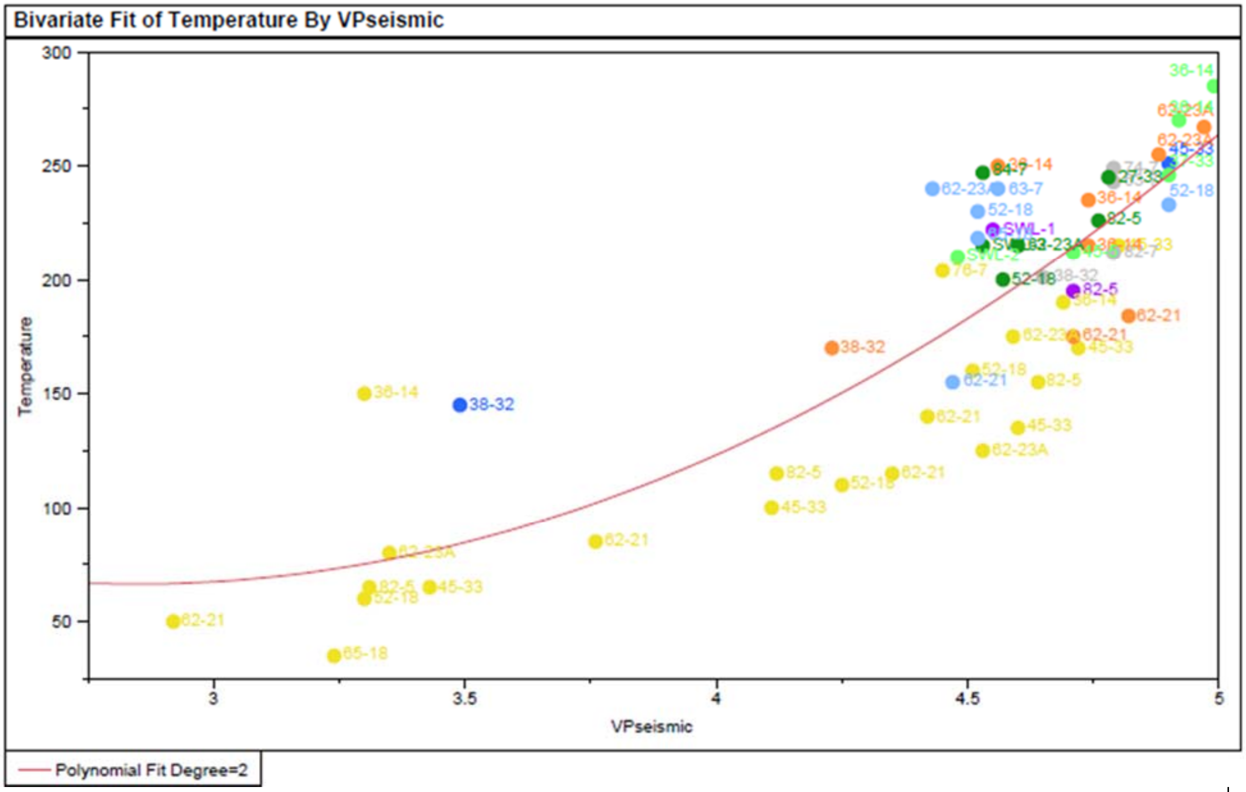

Polynomial Fit Degree=2

Temperature = -419.0699 + 133.71017*VPseismic + 42.561834*(VPseismic-4.416)^2

Summary of Fit

RSquare	0.724255
RSquare Adj	0.713649
Root Mean Square Error	34.33639
Mean of Response	182.8236
Observations (or Sum Wgts)	55

Figure 56. Correlation plot of Vp vs. Temperature using well data that excludes data from the surface (1km elevation) and outlier wells (53-15, 66-21, 45-14 and 76-28) with a low seismic trust value. The polynomial fit has a R-square value of 0.73. The data is labeled by well name and color coded by lithology as follows: QTbf (yellow), Tmb (purple), Tv (dark green), Jz (light blue), Tr (orange), Kgr (light green) and Jbr (dark blue).

Sectional Data

Figure 57 presents the global linear correlations for elevation (depth) and the selected geoscience parameters (fracIntens, vertStress, CSC, dilatation, temperature, Vp, Vs, and resistivity [MT]) for the combined sections (i.e., all cross-sectional data, see discussion above). Presented in this figure are both the correlation coefficients as well as the associated scatterplot matrices. The data suggests that linear and non-linear relationships exist between elevation and vertical stress, temperature, and Vp. *Note, however, that this is a two component analysis, e.g., temperature and depth, Vp and depth, etc.* The other parameters appear to have little to no relationship with elevation.

These identified relationships were further investigated analyzing the bivariate fit of temperature, vertical stress, and Vp by elevation, Figure 58, respectively. These three relationships show r^2-values of **0.90** (correlation coefficients of 0.9487), **0.89** (0.9434), **0.89** (0.9434), indicating, as expected, a strong relationship of the selected geoscience parameters with depth (i.e., elevation). The residuals of this bivariate fit were calculated and shown in the lower portion Figure 58. Next, the linear correlation of the key variables (temperature, CSC, dilatation, and resistivity [MT]) versus the residuals of vertical stress and Vp was performed (Figure 59A). No correlation coefficient greater than 0.7400 is observed, considered the cut-off value for being stastically significant (E. Issaks, pers. comm., 2011). Interestingly, the MT parameter was determined to be slightly correlated with the residuals of vertical stress**.** This finding is supported by a multiple regression of temperature vs. the residuals conducted to examine the relationship between temperature and temperature predicted by the residuals of vertical stress, Vp, and Vs (Figure 59B). The r^2-value for this regression analysis is **0.19** indicating that temperature cannot be predicted by the residuals. Thus, the overall two component residual analysis indicates that depth (or elevation) is the only link between (1) temperature and vertStress, and (2) temperarure and Vp. However, multiple regression analyses of temperature vs. key geoscience parameters was also performed. Figure 59C shows the result of using elevation, vertical stress, dilatation, Vp, and resistivity (MT) in predicting temperature, as well as the interaction among these parameters. The r^2-value for this multi-variable system is **0.94**. The predictor profiler in this figure illustrates the complex interaction of the geoscience parameters elevation, vertical stress, dilatation, Vp, Vs, and resistivity (MT). This multi-variable analysis clearly indicates that (1) the combination of a variety of geoscience parameters (described above) can be used to predict temperature and (2) there is a complex interaction between the geoscience parameters in this prediction. In summary, the residual analysis and the multiple regression (multi-variable) analysis had contrasting results.

Well Data

Multiple regression analyses were also applied using the well data set to determine if depth and temperature can be predicted from the seismic data (Vp) and other geoscience parameters. The analysis indicates that depth can be predicted from a combination of Vp and MT with a **r^2-value = 0.76**, see Figure 60A for all well data, and temperature can be predicted from lithology, Vp and resistivity (MT) with a **r^2-value = 0.85** using all well data excluding wells which have a low Vp trust factor (Figure 60B).

Precision of the Multiple Regression Results

Two statistical methods were used to evaluate the precision of the multiple regression findings, bootstrap, and cross-validation.

Bootstrap Method

The bootstrap technique involves taking a sample of equal size to the original dataset, with replacement, from the actual data (i.e.[6] from the empirical distribution). This sampling procedure is then repeated many times (10,000 in this analysis) and for each sample the original regression analysis was done, producing a new r^2 value for each sample. The empirical distribution of these 10,000 r^2-values enables calculation of a bootstrap confidence interval with endpoints at the 2.5 and 97.5 percentiles. 95% of the simulated r^2-values were between these two endpoints. The r^2-value measures the proportion of the variance of the predicted variable that can be explained by variables in the model.

One way the bootstrap method was used here was to compare different weighting schemes for the regression model based on the trust values assigned to each of the values of each variable. Large trust values correspond to values believed to be more accurate, so all the schemes considered weighted the high trust values more heavily. The three weighting schemes considered were:

---

[6] The confidence interval gives a range that is likely to contain a value that is being estimated. Traditionally, a confidence interval is determined analytically based on the theoretical distribution of the estimator. Out of every hundred 95% confidence intervals, about 95 should contain the true value being estimated. In order to avoid distributional assumptions (usually normality), a bootstrap procedure is used since it is based just on the empirical distribution observed in the data.

1. product of trust values for all variables in model.
2. sum of trust values for all variables in model
3. discard all data which has a below median trust value for any variable.

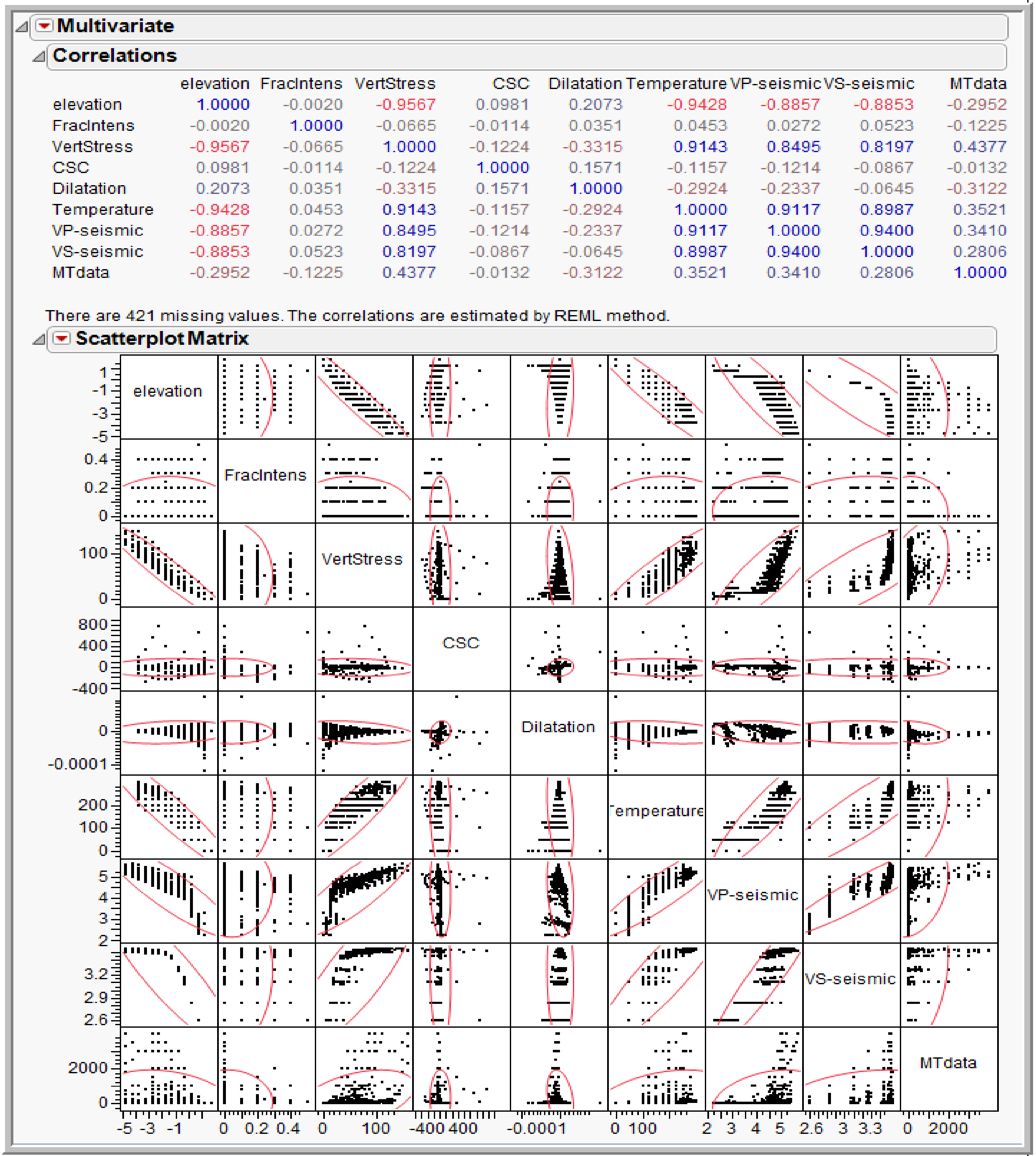

Multivariate

Correlations

	elevation	FracIntens	VertStress	CSC	Dilatation	Temperature	VP-seismic	VS-seismic	MTdata
elevation	1.0000	-0.0020	-0.9567	0.0981	0.2073	-0.9428	-0.8857	-0.8853	-0.2952
FracIntens	-0.0020	1.0000	-0.0665	-0.0114	0.0351	0.0453	0.0272	0.0523	-0.1225
VertStress	-0.9567	-0.0665	1.0000	-0.1224	-0.3315	0.9143	0.8495	0.8197	0.4377
CSC	0.0981	-0.0114	-0.1224	1.0000	0.1571	-0.1157	-0.1214	-0.0867	-0.0132
Dilatation	0.2073	0.0351	-0.3315	0.1571	1.0000	-0.2924	-0.2337	-0.0645	-0.3122
Temperature	-0.9428	0.0453	0.9143	-0.1157	-0.2924	1.0000	0.9117	0.8987	0.3521
VP-seismic	-0.8857	0.0272	0.8495	-0.1214	-0.2337	0.9117	1.0000	0.9400	0.3410
VS-seismic	-0.8853	0.0523	0.8197	-0.0867	-0.0645	0.8987	0.9400	1.0000	0.2806
MTdata	-0.2952	-0.1225	0.4377	-0.0132	-0.3122	0.3521	0.3410	0.2806	1.0000

There are 421 missing values. The correlations are estimated by REML method.

Scatterplot Matrix

Figure 57. Linear Correlations of Key Variables vs. Elevation (Depth) with calculated correlation coefficients above.

For weighing scheme (1) and (2) above, the weighting procedure essentially treats the weights as the inverse of the variance for each observation. For example, if the trust values for temperature, dilatation, vertical stress, Vp, Vs, and MT were each 4 for a particular data point, then scheme (1) would weight this observation as 4^6 (or 4096) times more important than an observation with trust values of 1 for all those variables. Weighting scheme (2) would weight it 4*6 (or 24) times. In weighing scheme (3), the median of each trust variable was found and any points strictly less than this value for any of the variables was simply thrown out. None of these weighting schemes performed better than regression analysis without any weights (see discussion above), and all the r^2-values were fairly close together. This is an indication that the data with lower trust values follow the same pattern as the high trust data. In addition to comparing the different weighting schemes and finding confidence intervals for the r^2-values, the values computed from the bootstrap method were used to consider whether elevation should be included in the model. Since elevation would not be relevant in eventual choice of a promising site, it is included in the model simply because it is related to temperature and thus perhaps should be controlled for. However, since vertical stress and other variables are highly correlated with elevation, inclusion of elevation is perhaps redundant. Leaving out elevation makes little difference in the r^2-value, supporting the idea that this parameter is redundant.

The 95% confidence intervals for each of these weighting schemes with and without elevation are shown in Tables 6A and 6B and a summary discussion follows. The first line in each table corresponds to the model described in Figure 59C. Investigations conducted are unclear why the r^2-values for this case presented in Tables 6A and 6B (0.86 and 0.83, respectively) differ from that indicated in Figure 59C, a r^2-value of **0.94**. Regardless, the outcome conveyed by a r^2-value of 0.94 or 0.86 is essentially the same: the model is able to explain quite a bit of the variability in temperature using these variables.

Table 6A. Results of the weighting analysis confidence interval determination using elevation in the parameters considered; see text for an explantion.

Weighting	Lower Bound	R squared est.	Upper Bound
None	0.84	0.86	0.88
Product of Trusts	0.83	0.86	0.88
Sum of Trusts	0.84	0.86	0.88
Discard Low Trust	0.78	0.83	0.88

Table 6B. Results of the weighting analysis confidence interval determination ignoring elevation in the parameters considered; see text for an explantion.

Weighting	Lower Bound	R squared est	Upper Bound
None	0.81	0.83	0.86
Product of Trusts	0.80	0.84	0.86
Sum of Trusts	0.81	0.83	0.86
Discard Low Trust	0.73	0.80	0.86

Cross Validation

The technique of cross validation was used to assess how well the model would make predictions for data not in the model. This technique involves leaving out part of the dataset when fitting the regression model, then using the left out data to test the utility of the model in predicting temperature for data not used to fit the model. More technically, the dataset was divided into 10 parts, and the regression model was then fit 10 times, each time with one of the 10 parts left out. Then the r^2-value was computed as 1-(variance of prediction errors)/(variance of temperature values). Since every point in the data set was left out for one of these 10 regressions, each point has a prediction error and this r^2-value is actually based on the same number of points. In general the r^2-value should be slightly smaller since the model wasn't influenced by the points for which the prediction errors were calculated. The cross validation was performed to verify that the model was successfully representing an actual relationship between the variables and not just a spurious relationship.

In addition, cross validation is useful in variable selection, particularly to avoid over-fitting, including variables which marginally increase r^2-values but whose relationship with the dependent variable does not appear to be anything more than random. The r^2-values computed based on the omitted data from the cross validation resampling were very similar to the original values, about 0.83, indicating that the model has validity in making predictions for data not used to fit the model. Furthermore, leaving out Vs and MT do not appreciably reduce the r^2-values, so those variables do not appear to add sufficient predictive ability to warrant their inclusion in the model. For the refined model based on predicting temperature using only vertical stress, dilatation, and Vp, the bootstrap 95% confidence interval for r^2 is 0.81 to 0.85, with a center (actual estimated r^2) of **0.83**. This is essentially the same model as the first line in Table 6A but with Vs and MT left out of the model.

The correlation analysis, performed by Dr. Ibser, Project Geostatistical Task Leader (see Section 1.4), that explored the relationships between the geoscience parameters was also utilized to analyze the favorability-trust maps presented in Section 8. The sensitivity of the favorability values to different weights (equal weighting compared to SME weights) was analyzed. We also considered using hierarchical modeling to assess the variability in the favorability maps in this Baslien Conceptual Model. An intrinsic part of the hierarchical model is the quantification of the variability in the measurement and modeling of variables used in subsequent analysis. However, for several of the variables (e,g, MT resisitivity), not much could be done that was not subjective. For other variables (e.g., gravity-magnetics), the variability could only be reasonably estimated by repeating the modeling process under different assumptions, and the modeling process itself is quite time intensive. As such, the hierarchical model was determined to be beyond the scope of the current project, especially given that the result would simply give another way to assess the variability in the favorability map without actually improving the results themselves.

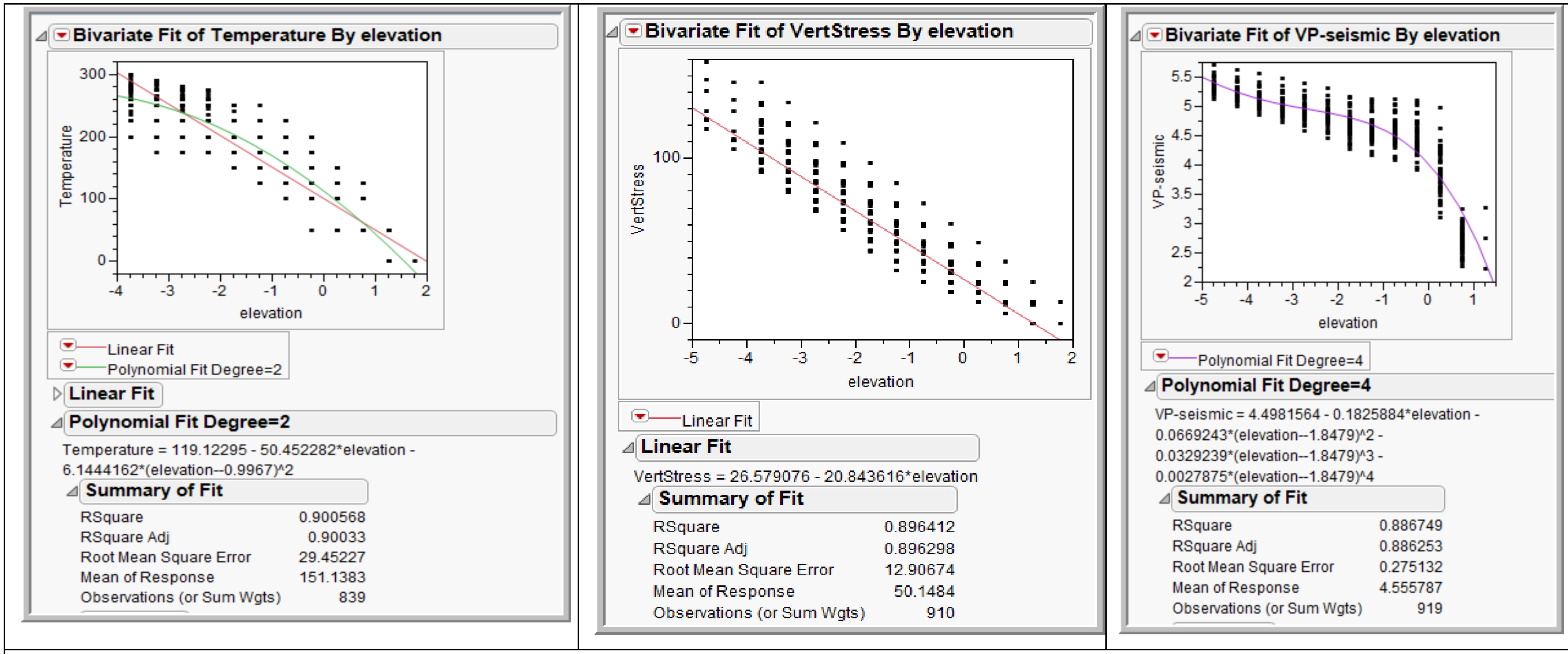

Bivariate Fit of Temperature By elevation

Linear Fit

Polynomial Fit Degree=2

Temperature = 119.12295 - 50.452282*elevation - 6.1444162*(elevation--0.9967)^2

Summary of Fit

```
RSquare                        0.900568
RSquare Adj                     0.90033
Root Mean Square Error         29.45227
Mean of Response               151.1383
Observations (or Sum Wgts)          839
```

Bivariate Fit of VertStress By elevation

Linear Fit

VertStress = 26.579076 - 20.843616*elevation

Summary of Fit

```
RSquare                        0.896412
RSquare Adj                    0.896298
Root Mean Square Error         12.90674
Mean of Response                50.1484
Observations (or Sum Wgts)          910
```

Bivariate Fit of VP-seismic By elevation

Polynomial Fit Degree=4

VP-seismic = 4.4981564 - 0.1825884*elevation - 0.0669243*(elevation--1.8479)^2 - 0.0329239*(elevation--1.8479)^3 - 0.0027875*(elevation--1.8479)^4

Summary of Fit

```
RSquare                        0.886749
RSquare Adj                    0.886253
Root Mean Square Error         0.275132
Mean of Response               4.555787
Observations (or Sum Wgts)          919
```

Figure 58. Bivariate Fit of Temperature, Vertical Stress and Vp-seismic by elevation with calculated residuals below.

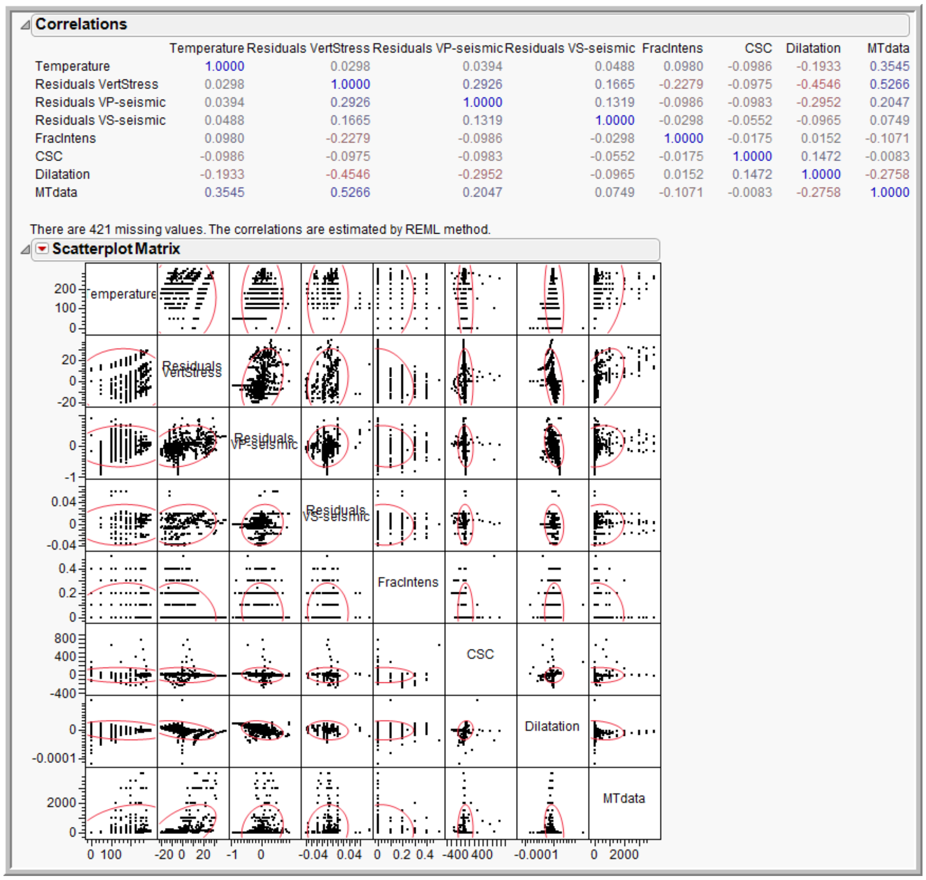

Correlations

	Temperature	Residuals VertStress	Residuals VP-seismic	Residuals VS-seismic	FracIntens	CSC	Dilatation	MTdata
Temperature	1.0000	0.0298	0.0394	0.0488	0.0980	-0.0986	-0.1933	0.3545
Residuals VertStress	0.0298	1.0000	0.2926	0.1665	-0.2279	-0.0975	-0.4546	0.5266
Residuals VP-seismic	0.0394	0.2926	1.0000	0.1319	-0.0986	-0.0983	-0.2952	0.2047
Residuals VS-seismic	0.0488	0.1665	0.1319	1.0000	-0.0298	-0.0552	-0.0965	0.0749
FracIntens	0.0980	-0.2279	-0.0986	-0.0298	1.0000	-0.0175	0.0152	-0.1071
CSC	-0.0986	-0.0975	-0.0983	-0.0552	-0.0175	1.0000	0.1472	-0.0083
Dilatation	-0.1933	-0.4546	-0.2952	-0.0965	0.0152	0.1472	1.0000	-0.2758
MTdata	0.3545	0.5266	0.2047	0.0749	-0.1071	-0.0083	-0.2758	1.0000

There are 421 missing values. The correlations are estimated by REML method.

(A)

Figure 59A. (top) Linear Correlations of key variables vs. the residuals of Vertical Stress and Vp.

Figure 59B. (bottom left) Multiple Regression of Temperature vs. Residuals. A very poor relationship is found between temperature and residuals.

Figure 59C. (bottom right) Multiple Regression of Temperature vs. Key Variables.

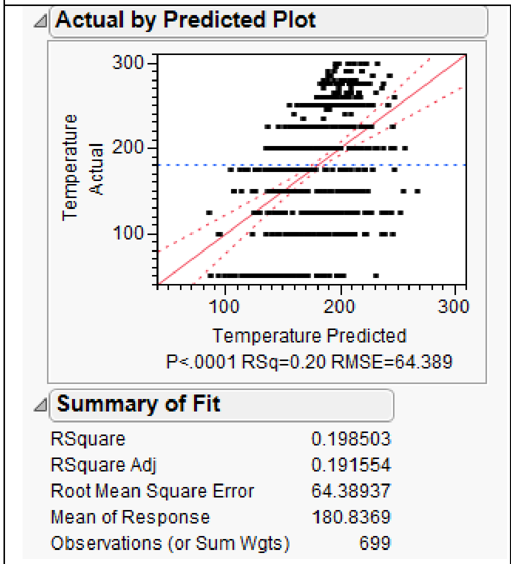

P<.0001 RSq=0.20 RMSE=64.389

Summary of Fit

RSquare	0.198503
RSquare Adj	0.191554
Root Mean Square Error	64.38937
Mean of Response	180.8369
Observations (or Sum Wgts)	699

(B)

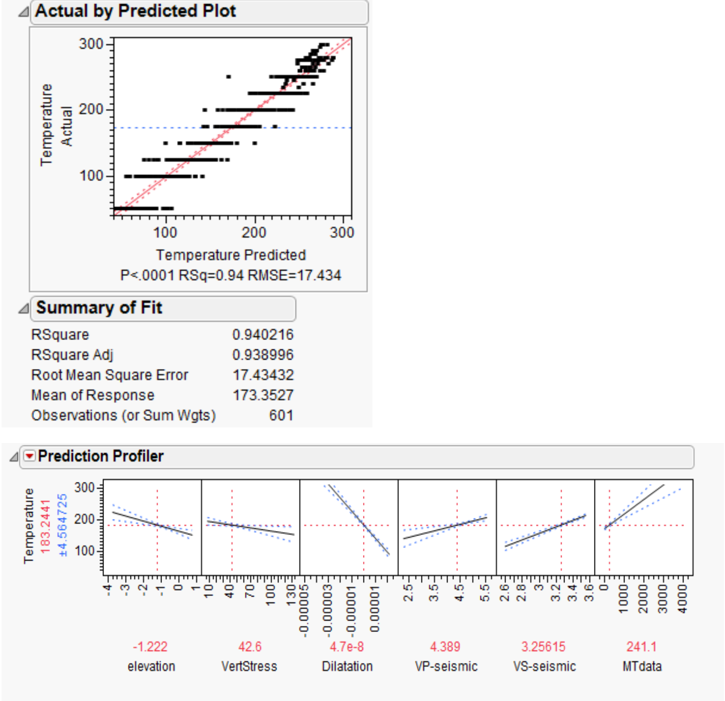

P<.0001 RSq=0.94 RMSE=17.434

Summary of Fit

RSquare	0.940216
RSquare Adj	0.938996
Root Mean Square Error	17.43432
Mean of Response	173.3527
Observations (or Sum Wgts)	601

(C)

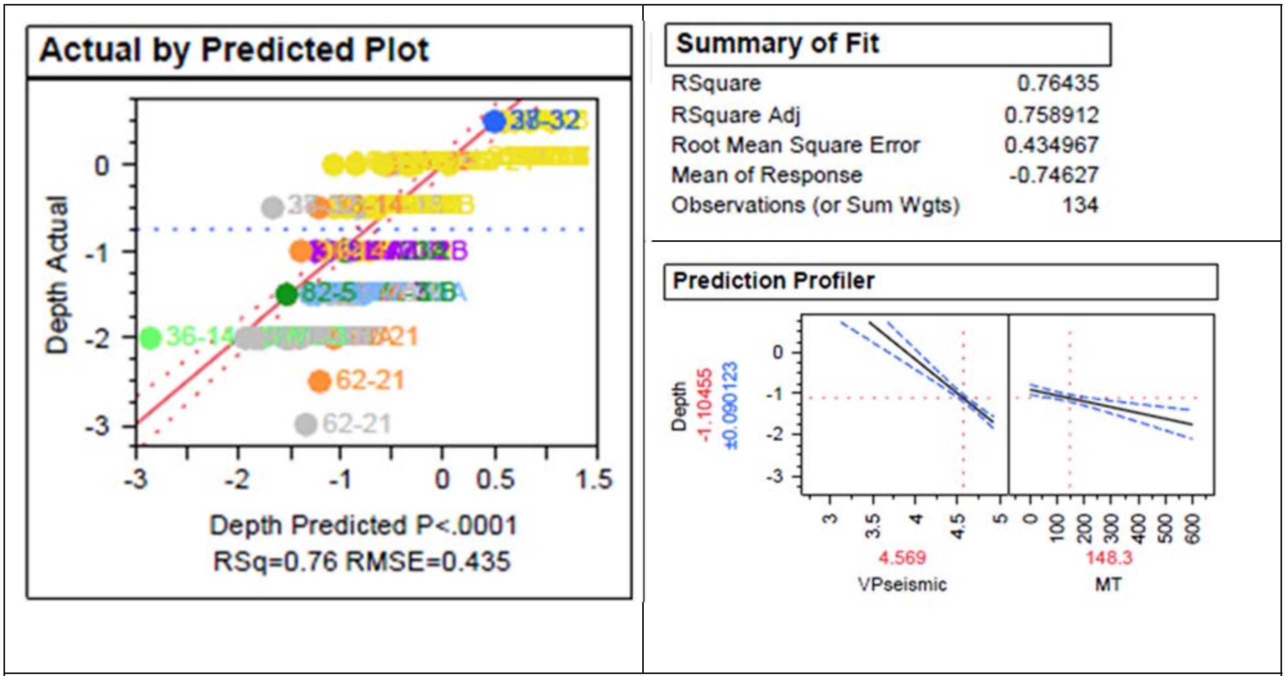

Figure 60A. Regression Analysis for predicting depth vs. depth predicted from Resistivity (MT) and Vp using all the well data excluding wells with a low Vp trust factor. The R-square value is 0.76. This three-component analysis suggests that the interaction of Vp and Resistivity (MT) can predict depth.

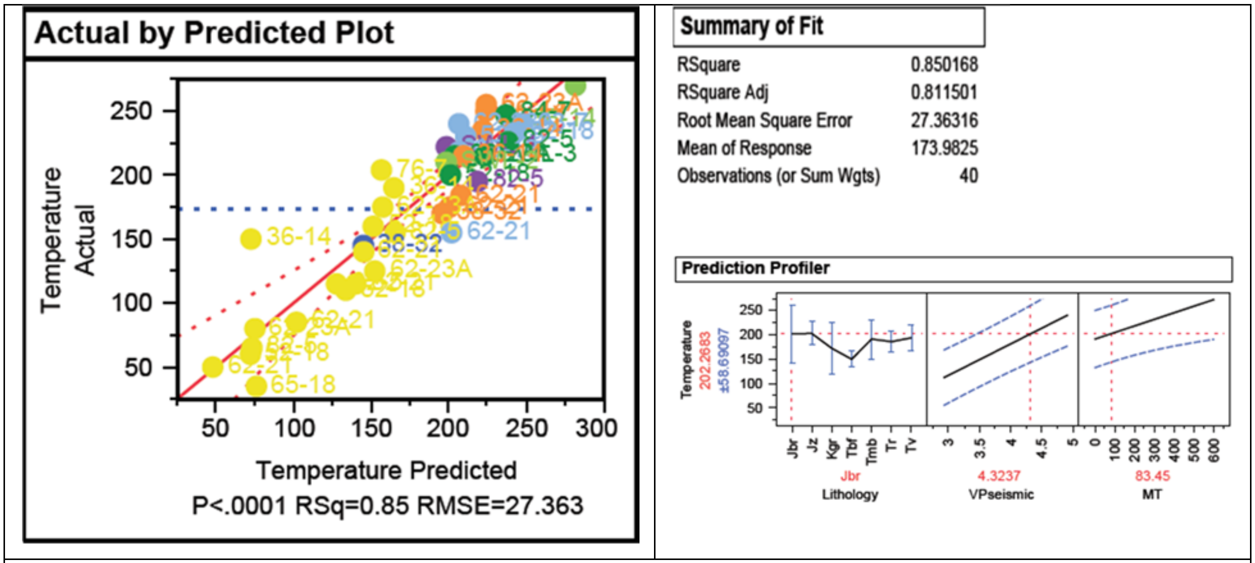

Figure 60B. Regression Analysis for predicting Temperature vs. Temperature Prediction using Lithology, Vp, and MT for all well data excluding wells with a low Vp trust factor. The R-square value is 0.85.

Vp-Temperature Relationship: Effect of Density and Depth

The observed Vp and temperature relationship described in Section 7.4.2 was found in the following analyses:

1. linear correlations along the cross-sectional data (Appendix 17);

2. multi-variate correlations with respect to lithology along the cross-sectional data (Appendix 17);
3. a direct correlation between the two variables using well data (Figures 54-56);
4. multiple-regression analyses using both the cross-section and well data (Section 7.4.2);
5. CART, see Section 7.4.2; and
6. a geologic analysis, described herein and Appendix 18.

This relationship was explored further to determine if other factors (depth, density, etc.) were influencing or responsible for the empirically derived relationship including an analysis of the relationship with respect to depth, lithology or geologic formation, and well type. Selected results from this assesment can be found in Appendix 18.

Geologic Analysis

The majority of the Dixie Valley wells lie within the convective heated portion on the DVFZ, while one deep well, 62-21 lies within the valley to the southeast, and is more indicative of the overall conductive regime. The previous analyses have used all the well data, indiscriminate of well location, with the exception of removing the selected wells that possessed low seismic trust values. The following analysis views the Vp data with respect to the two different domains to determine if increases in temperature and Vp with depth can be explained. By comparing Vp data within similar lithologies and at comparable depths within wells affected by the convective system to a purely conductive well, 62-21, one can analyze the Vp data independent of the influence from lithologic density or depth to determine if Vp values are different within the two domains. If Vp values are higher within the convective wells within the same lithology type at the same depth, and the temperature is significantly higher, it is inferred that the Vp values are affected by the convective geothermal system. Note that Vp should decrease with fracturing and fluid content. These factors are not considered in this analysis.The Lithology-Temperature-Vp-Depth relationship was analyzed and performed in two-parts using well data (1) per well compared to 62-21, a known conductive well, and (2) per lithologic formation. 62-21 was chosen as a "control" well as it was relatively cold compared to wells in the DVFZ, and intersected a varied group of lithologies. Figure 61A consists of a series of representative plots that show the Lithology-Temperature-Vp-Depth relationship for different wells, including the comparison to a purely conductive well, 62-21. Wells 66-21, 45-14, 53-15, and 76-28 were not included in this analysis, as these locations have low seismic trust values rendering the Vp data unreliable. The remaining wells with available data compared with 62-21 can be found in Appendix 18. The vast majority of wells show elevated temperatures and Vp values at comparable depths and lithologies when compared to 62-21 (Figure 61A and Appendix 18). The only exception is 62-23A, where at a depth of 2.5km (8200ft), Vp is slightly lower than 62-21 within the same lithology, even though the reported temperature is much higher.

Interestingly, a slight Vp decrease is found at depths of 2.5km for a number of wells (Figure 61A). This unexpected result occurred in the following wells: 36-14, 62-23A, 52-18, 65-18, SWL-1, SWL-2, and SWL-3 which consists of the DVPP area and the area of active injection within section 18. This could be a model interpolation effect, or could likely represent a decrease in Vp within the reservoir due to fluid content and/or fracturing. This also suggests that since Vp does not increase uniformly with depth, it further supports the observed empirical Vp-T relationship is not based solely on a function of depth.

Effect of Lithology and Depth

We recognized that both temperature and Vp are a function of depth and as such, continued evaluating this relationship both geologically and geostatistically.

The Vp data was plotted with respect to depth per the major lithologic formations identified in the geothermal wellfield and coded for temperature to determine (1) if the varied lithology, specifically the associated density (inferred by depth in this case), was a significant factor in the observed relationship, and (2) the variation in temperature per a given depth and lithology. Data occurring at the surface and outlier wells with low seismic trust (53-15, 45-14, 66-21, and 76-28) were removed from the data set to be consistent with the previous analysis. A general relationship between Vp and temperature was observed within the basin-filling sediments (QTbf) at any given depth and over the depth range considered (Figure 61B), while the remaining formations had too few data points to produce meaningful results. For plots pertaining to all the major formations, see Appendix 18.

Within the QTbf, the effect of depth on the inferred Vp-temperature relationship was examined (Figure 62). A strong relationship was found only at a depth of 1km (0km asl), with a r^2-value of 0.76. The remaining depths show no relationship, although this is based on limited data.

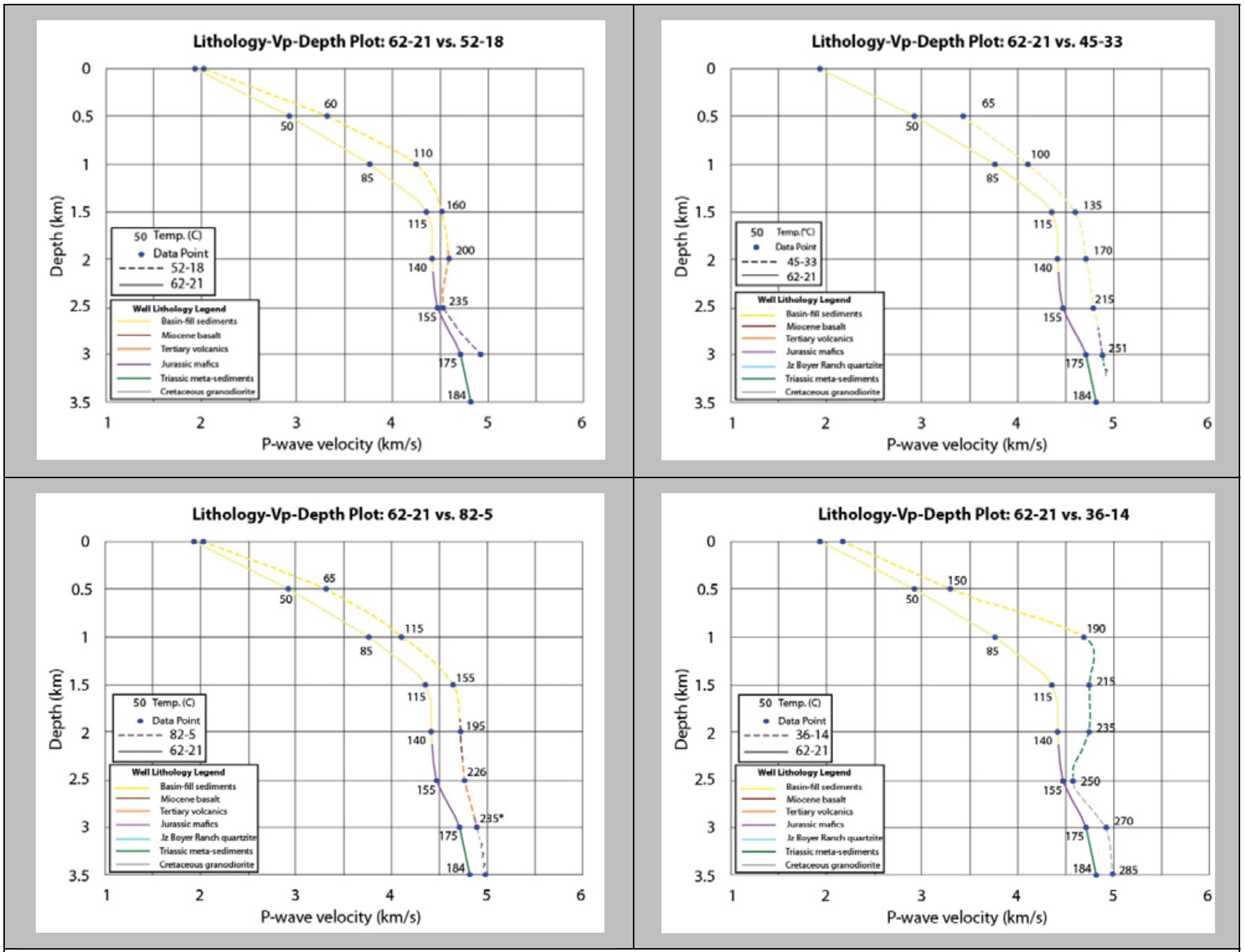

Figure 61A. Lithology-Vp-Temperature(°C)-Depth relationship . Wells are directly compared to 62-21: 52-18 (top left), 45-33 (top right), 82-5 (bottom left) and 36-14 (bottom right). All wells show elevated Vp values over similar lithologies (basin-fill vs. basement) and depths.

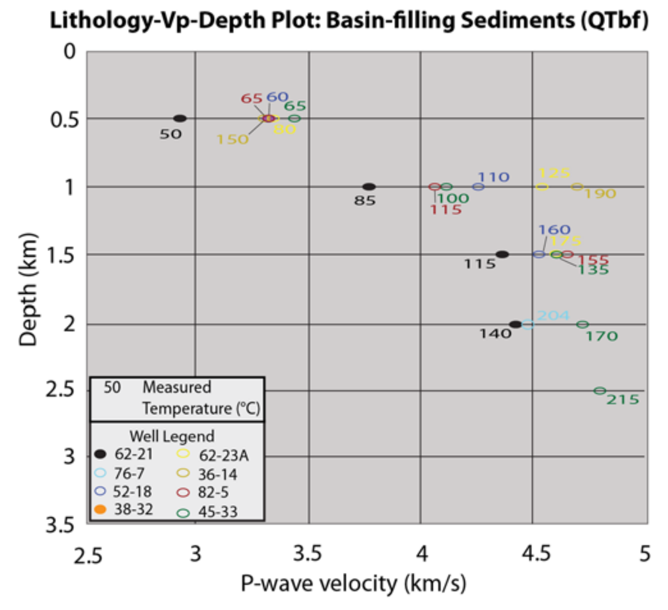

Figure 61B. Vp-Depth Relationship observed within the basin-filling sediments (QTbf). Wells with low seismic trust (53-15, 66-21, 76-28 and 45-14) and data occurring at the surface are not used in this analysis. Temperature are shown on the plot with the color-coded according to well name.

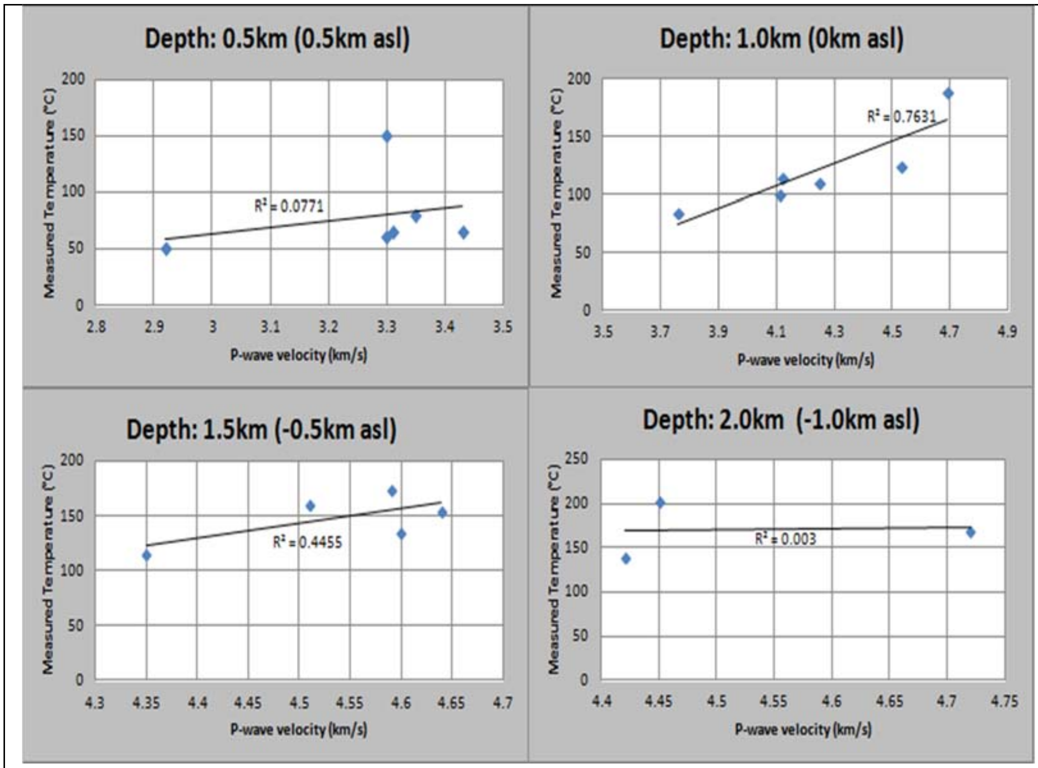

Figure 62. Vp-Temperature relationship observed within the basin-filling sediments (QTbf) at the respective depths.

The relationship between Vp and temperature seems to be mostly within the basin fill (QTbf) values. When those points are plotted separately, we see an r^2-value (for a quadratic fit) of **0.72** (Figure 63). The variables temperature, Vp, and depth are all strongly correlated. Since is not dependent on location, it is desirable to examine the relationship between temperature and Vp that is independent of depth. To do this, we have taken the residuals from a linear fit of temperature on depth. These residuals are the difference between the actual temperature and the predicted temperature, so what is left gives an estimate of the amount that a cell is hot or cold compared to cells at the same depth. Any relationship that remains between these residuals and Vp is thus independent of depth.

When comparing the residuals of temperature to Vp, in place of the actual temperatures, a negligible r^2-value of 0.09 is found, and the relationship disappears (Figure 63). Thus, the effect of depth cannot be separated from the Vp and temperture parameters. These two figures exemplify the more general phenomenon that the relationship between temperature and Vp is highly confounded with depth. Attempting to establish causality is beyond the scope of this study, but a plausible story might be that high levels of vertical stress (for example, at great depth) may cause both temperature and Vp to rise. A story such as this is consistent with both plots and does not contradict lab results showing that at constant pressure, temperature and Vp tend to be negatively correlated. Further investigation of this empirical relationship is required using the enhanced data set and in other geothermal fields to determine its viability as a non-invasive tool for approximating subsurface temperature distribution.

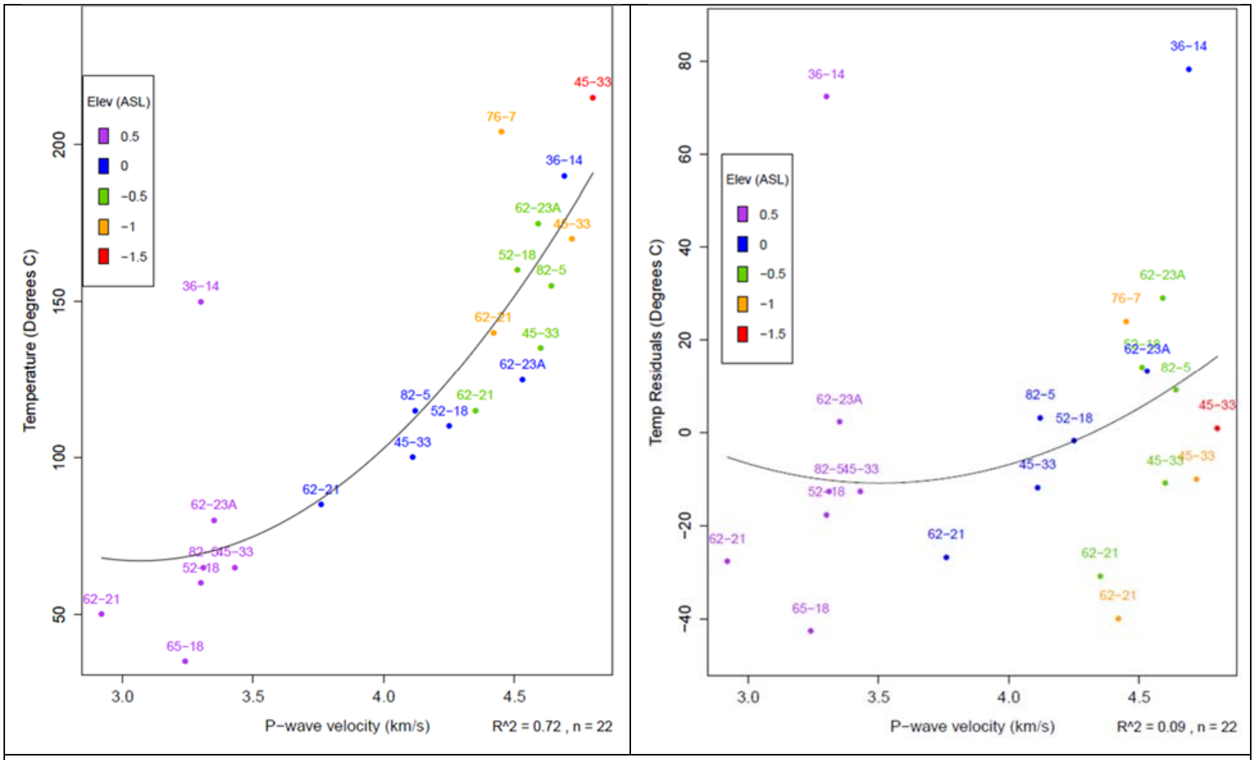

Figure 63. Relationship between Temperature and Vp within the basin-filling sediments (left) with a R-square value of 0.72. Relationship between Temperature residuals and Vp within the basin-filling sediments (right) with an R-square value of 0.09. Data is color-coded for depth in elevation above sea level.

Other analyses not included in this report that assess the Vp-Temperature relationship with respect to depth and geologic formation can be found in Appendix 18. Selected analyses and associated plots include:

1. Measured Temperature vs. Depth coded for lithology type;
2. Measured Temperature vs. Depth coded for P-wave velocity;
3. P-wave velocity vs. Depth coded for temperature;
4. P-wave velocity-Depth-Lithology plots for all wells with respect to 62-21

5. P-wave velocity-Depth-Lithology plots for major geologic formations.

Summary Assessment of the Vp-Temperature Relationship

A number of potential issues, inconsistencies and discrepencies, have arisen during the assessment of this relationship. First, there is a limited amount of measured temperature data, although this database is more extensive than typical exploration data sets. The preliminary baseline Vp data is generally of poor quality and was extracted by our Seismic Task Leader, Dr. Ileana Tibuleac, from OPTIM reflection lines and associated block velocity models coupled with low resolution regional seismic models and very general crustal-scale models. The analysis of the more "raw" baseline seismic data, specifically the variance of green functions, was not available. Secondly, a number of assumptions were made including the (1) overall analysis is based on gross averages of the lithology, temperature, and Vp data for a data cell on the order of 500m by 500m, (2) relationship was established by comparing modeled data (Vp) to measured data (temperature), (3) some of the wells in Dixie Valley occur within the same cell (500m by 500m) and thus a number of temperature measurements at a given depth, all of which have the same assigned Vp value, and (4) effect of fracturing and fluid content on the Vp relationship cannot be quantified.

The issue of depth confounding in the relationship has been validated by the various residual analyses. Interestingly the multiple regression analyses inferred that using a suite of parameters including Vp could accurately predict temperature. This concept is further explored below using CART. However, it is noted that the majority of geoscience parameters have an inherit depth influence. While the discussed Vp-temperature relationship is observed using the empirical baseline data, the effect of depth cannot be removed from the parameters used to establish an unique relationship. This relationship will be further assessed using the enhanced data set (baseline + new) that utilizes, expectedly, higher quality data collected from the passive seismic survey in 2011-12 (under Task 4).

Classification and Regression Tree Analysis (CART)

Introduction

One objective of the various exploratory geostatistical analyses is to define which parameters make good predictors, specifically for predicting conditions favorable for EGS. The aspects to be predicted using CART and referred to as response variables are (1) temperature; (2) lithology type using both the Section and Well Data, as well as predicting both; (3) productive ydrothermal cells; and (4) expected EGS favorable cells using the well data. Since the data is in both a numerical and categorical form, the principal geostatistical tool used in this evaluation is a CART analysis. While all potential parameters are considered as explanatory variables, a direct interest is made towards the predictive power of measurable geophysical parameters such as Vp, MT and gravity-magnetic inferred lithology (Grav_Mag).

Explanation of CART

CART is a statistical technique that can be used to determine the statistical relationship between a defined predicted or response variable and multiple undefined predictor or explanatory variables. As summarized from Lawrence and Wright (2001) who describe CART as a popular form of statistical analysis that operates by recursively splitting the data until ending points, or terminal nodes, are achieved using preset criteria by analyzing all explanatory variables and determining which binary divisions of a single explanatory variable best reduces deviance in the response variable. For each portion of the data that results from this split, the process is repeated, and continues until homogeneous terminal nodes are reached in a hierarchical tree.

Decision trees used in CART are designed to predict an item’s value for some variable based on other information available about the item. Classification trees predict what category an item falls into whereas regression trees predict the numerical value of a variable. For example, if you wanted to predict gender based on weight, you could use a classification tree with a single split where people above a certain weight would be predicted to be male and people below that weight would be predicted to be female. The predictions would have some errors, and the weight to split at would be chosen to minimize the number of errors. If you also have information on height, that probably would do even better at prediction, so you might choose an initial split based on a height value, with tall people predicted to be men and short people predicted to be women. Then subsequent splits might be made based on weight so that amongst the tall people, perhaps the heavy tall people are even more likely to be male than the lighter tall people, and a similiar split could be made for the short people. The split points are chosen to minimize the number of misclassifications. For more than two categories this is equivalent to choosing the split points so that a random item has the smallest possible chance of being misclassified. Thus if we have *i* categories, each with probability p*i*, we minimize the sum of *pi*(1-*pi*), summed over the *i* categories in each of the “leaves” at the end of the splits, or “branches.” Notice that if the categories are all perfectly classified, *pi* will be 1 for exactly one value of *i* and then (1-*pi*) will be 0 for that category.

A regression tree predicts the value of a numerical variable such as predicting height from weight. The process of splitting is done in such a way as to minimize the squared errors of the predictions when the predictions are the averages within the subgroups. So if we predict weight from height, we might first split into tall and short, and the predicted weights would be the average of the tall people and the average of the short people. Subsequent splits could be made based on weight in order to subdividethe population further into relatively homogenous groups based on weight. If the splitting is allowed to continue, the tree will grow until each person is on a leaf and the predicted weights are perfect. This splitting will have the undesirable effect of fitting noise, essentially making non-intuitive predictions. For example, if one person 66 inches tall weighs 180 pounds and someone 68 inches tall weighs 170 pounds, the full tree will predict these accurately, but that is counter to the more realistic general rule that taller people should be predicted to be heavier. Because of this pruning methods such as cross validation are used to reduce the tree in a way that presents an accurate idea of how the predictions should be done for data not including in the building of the tree. Amongst the advantages of CART are that it results in easily understandable prediction rules and it is free of underlying assumptions about the data and error structure. Drawbacks include that it is restricted by these binary splits and since the optimization is done from the top down it may not result in the globally optimal tree.

CART Methodology

The CART analyses described in this section were performed using the statistical program JMP Pro 9.0 by SAS which identifies CART as a partition analysis. The input data used two different data sets (1) all the combined sections (cross-sectional) data described above (Appendix 16a), and (2) the well data (see Appendix 16b). The parameters of interest are formatted in a pre-determined *EXCEL* sheet that lists the explanatory variable name in the column heading, while the rows correspond to specific cells or locations at specific depths that have multiple parameters. Each row must have a defined value for the various variables or the program cannot correlate other data to this value. The workbook is then transferred as a *.csv* file into the statistical program, where the CARTanalysis is conducted on the data by defining a response variable (parameter to be predicted) and one or more explanatory variables (parameters used for the prediction). The analysis then divides the explanatory variables into specific groups based on the means and standard deviation of the data. A r^2-value (from 0 to 1) is reported at each subsequent split that quantifies the accuracy of the prediction at that stage in the analysis. For selected cases, the split history and regression trees are shown in the geostatistical data figures presented in Appendix 19. The advantages of this technique are (1) the first variable that the program chooses to split on, infers that this variable is the most highly correlated to the predictor (Ed Isaaks, pers. comm., 2011) or alternatively that this variable has a large variability and is the most efficient for the analysis to subdivide, (2) users can turn response explanatory variables on/off to determine which ones make the best predictors, (3) split history can be pruned back to stop the analysis at a suitable r^2-value, and (4) the methodology works with both numerical (continuous) and categorical variables.

e initial CART analyses conducted on section and well data with respect to predicting temperature, lithology, and productive ive wells. The response variables are listed under the first column, followed by the type of data used. The eight possible ave an X, if they were considered in the analysis, and a bolded X if they were used in the analysis. The r^2-value listed quantifies 19 presents the individual CART figures for selected analyses.

Data Type	**Selected Geoscience Parameters Considered (X) and Used (X) in the Data Splitting Process**								**r^2 - value**	**Summary**
	T[a]	*Vp*	*Resist. (MT)*	*CSC*	*Dilat-ation*	*Fault Presence*	*Vert Stress*[f]	*Lith-ology*[bc]		
section	---	**X**	---	---	**X**	---	**X**	**X**	**0.91**	
	---	**X**	**X**	**---**	---	---	---	**X**	**0.8**	
	X	**X**	**X**	**X**	**X**	---	X	---	**0.82**	
	X	**X**	**X**	**X**	**X**	---	---	**---**	**0.54**	Removing VertStress dropped R^2 value by 34%
well	X	**X**	**X**	**X**	X	X	**X**	**X**	**0.66**	
	X	**X**	**X**	**X**	**X**	X	**X**	---	**0.52**	R^2-value dropped 21% when Lithology was removed and Dilatation was considered
	---	**X**	**X**	---	---	X	---	**X**	**0.62**	Vp, MT and Lithology accounts for 94% of the 0.66 r^2-value above
	X	**X**	**X**	---	---	X	---	**X**	**0.54**	
	---	**X**	---	---	---	---	---	---	**0.62**	
	---	**X**	---	---	---	---	---	---	**0.75**	R^2-valued increased by ~21%
	---	**X**	**X**	---	---	---	---	**X**	**0.75**	Adding Resistivity (MT) and Lithology does not change R^2-value relative to using Vp alone
	---	**X**	**X**	---	---	---	---	---	**0.78**	Highest R^2 value using Vp and Resistivity (MT)

ensity is a parameter that is directly related to the various lithology identified in this investigation; [c]Gravity-magnetic data was found to be highly such is not shown as a separate parameter; [d]Fracture Intensity was also considered in some of these analysis but not used; [e]Uses all data except (i.e., 66-21, 45-14, 76-28, and 53-15); [f]Vertical Stress

Sectional Data

CART analyses were performed with respect to all parameters gridded from the cross-sectional data (C-C', D-D', E-E' and F-F'), which is mostly modeled data. The parameters were gridded within 500m^2 cells from the valley surface (+1km asl) in 500m depth intervals to depths below the production zone (-4km asl). The sectional data set can be found in Appendix 16a. The analyses use CART to predict the Temperature or Lithology using (1) all parameters (explanatory variables) and (2) selected parameters based on the r^2-value.

Predicting Temperature

- Temperature vs. all parameters; **r^2 = 0.91** shown in Appendix 19-Figure 1. The data split on the following parameters: Vp, vertical stress, and then dilatation. While a high r^2-value infers that all the parameters can accurately predict temperature, it is noted that vertical stress is not a suitable parameter for predicting temperature.
- Temperature vs. Vp, lithology and MT; **r^2 = 0.80** shown in Appendix 19-Figure 6. This shows that temperature can just as accurately be predicted from the cross-sectional data using only the following three parameters: Vp, lithology and MT.

Predicting Temperature from Vp

Using the cross-section data, temperature could be predicted from (1) Vp with a r^2-value of **0.359**, (2) Vp and resistivity derived from the MT data with a r^2-value of **0.775**, and (2) Vp, MT and Lithology with a r^2-value of **0.800**.

Predicting Lithology

- Lithology vs. all parameters; **r^2 = 0.82** shown in Appendix 19-Figure 3. The first two splits in the data occurred on vertical stress. Previous analyses have determined that this calculated value has a likely dependence on depth and should not be used to predict lithology (see previous Section 7.4.2).
- Lithology vs. all parameters excluding vertical stress; **r^2 = 0.54** shown in Appendix 19-Figure 2. Once this parameter is removed, the prediction capability drops significantly.
- Lithology vs. Vp, MT and temperature; **r^2 = 0.53** shown in Appendix 19-Figure 4. The small drop in the r^2 value infers that Vp, MT and temperature are best predictor variables for lithology, when other high predictive power parameters are not considered (vertical stress, dilatation, etc.).
- Lithology vs. Vp; **r^2 = 0.23**. Vp cannot be used to predict lithology. The SME has noted that a better seismic parameter for predicting lithology is rho (density). Once the new seismic data is collected under Task 4, this parameter should have high enough resolution to be used as a predictor for lithology shown in Appendix 19-Figure 5.

Well Data

The Well Data includes all measured and reported well data (lithology, temperature, faults, geochemistry, etc.), calculated values (LithDensity, LithStrength, vertical stress, etc.), and modeled data (Vp, MT, Stress Data: CSC and dilatation, etc.) with respect to well location (Appendix 16b). For this data set, parameters were gridded within 500m^2 cells at 500m depth intervals from +1km asl to -3km asl. CART analyses can be used in this case to explore the predictive power of a variety of modeled parameters where the response variable (temperature or lithology type) existing as measured data is known with a great degree of certainty. This in a sense validates the correlations found using the section data. A second advantage of using the well data, is that since not all of the wells are producing wells, a CART analysis can potentially determine what is unique about the other parameters that infers whether a corresponding cell is productive or non-productive (hot/cold and dry).

Predicting Temperature using Vp

The CART predictions that determined if temperature can be predicted by Vp and other parameters using well data is summarized in Table 8. The results of this analysis are tabulated below and shown in Appendix 19-Figures 7-10. Temperature could be predicted from (1) Vp with a r^2-value of **0.621**, after only three divisions of the data (see the first row in Table 8). When the wells with low seismic trust were removed from the analysis, temperature could be predicted from Vp with a increased r^2-value of **0.75** (Table 8, row 2). This is similar to the results from the correlation plot shown in Figure 56, that show the strength of the relationship increases, when the low quality Vp data is removed. The CART analysis supports the observed empirical relationship between Vp and temperature and infers that the combination of the parameters Vp and MT cannot predict temperature better than Vp alone. This result is not consistent with the multiple regression analysis described above. In summary, Vp can be used to predict temperature using a subset of the well data. This relationship is explored further below.

Table 8. CART analyses predicting temperature using well data and P-wave velocity (Vp)

Data Used	R-square value	Appendix 19 Figure
All well data	0.62	7
Edited well data[7]	0.75	8
Edited well data + Resistivity (MT)	0.77	9
Edited well data, Resistivity (MT), Lithology	0.75	10

Predicting Productive Wells

Cells that are considered part of the hydrothermal system were defined and analyzed versus multiple geoscience parameters to determine which variables were suitable for predicting a productive well. Cells are in reference to the pre-determined 500m^2 assigned spacing used for gridding purposes and dividing up the wells in the Calibration area into different depth slices. In general the hydrothermal system includes the injecting or producing portions of the wells, usually the lowermost cells. For purposes of this analysis, productive wells are referred to as hydrothermal. Selected results are presented in Table 9. A complete table showing the wells used in the analysis, associated cells (depths in this case) that are considered productive, and cells that have a known lithology value is found as Table 10. In addition to predicting hydrothermal cells, a subsidary CART analysis was performed to predict EGS favorable cells. Using the well data, cells that were expected to be favorable for EGS and were not exclusively part of the hydrothermal system were identified. In some cases these two domains, hydrothermal and EGS, overlap due the 500m spacing resolution.The CART method was then used (1) to test if EGS favorable cells could be predicted, (2) compare the results to the prediction for hydrothermal cells, and (3) determine which response variable combination could predict EGS cells including combinations without the vertical stress parameter. See Table 10 for identified EGS favorable cells.

Appendix 19-Figure 11 (Fig. 19-11) presents the CART analysis for the prediction of productive vs. non-productive cells using all the available well data and the following select geoscience parameters: lithology, temperature, Vp, vertical stress, resistivity (MT), CSC, dilatation, and presence of a fault. In this analysis, the data was split using lithology, Vp, resistivity (MT), CSC, and vertical stress, with a r^2-value of **0.66**.

---

[7] Removed wells with a low Vp trust factor

A preliminary parametric sensitivity analysis was conducted to determine the effect of removing selected parameters (explanatory variables) from the analysis shown in Fig. 19-11 and Table 9. Appendix 19-Figure 12 presents the CART analysis for the prediction of productive (hydrothermal) wells using the same suite of select geoscience parameters indicated in Table 9 except lithology. In this case, the r^2-value decreases to **0.52** indicating that lithology is a critical parameter in differentiating productive from non-productive cells, as expected. Appendix 19-Figure 13 (Fig. 19-13) presents the same type of CART analysis but using only the selected geoscience parameters of Vp, resistivity (MT), fault presence, and lithology with a reported r^2-value of **0.62**. Appendix 19-Figure 14 provides the results of the addition of temperature to the parameters used in Fig. 19-11. Interestingly, the resulting r^2-value is **0.58**, lower than that in Fig. 19-13 but slightly higher than that in Fig. 19-11. This implies that temperature is not most critical parameter in predicting productive vs. non-productive cells, and that lithology, Vp and MT are the best combination of predictors for this case.

The analysis determined that the best explanatory variables for determining productivity are the combination of Lithology, Vp, and Resistivity (MT), with a r^2 value of **0.66**. The first split of the data occurred within the Lithology parameter, as the majority of the productive cells occurred in expected lithologies (Jz, Jbr, and Tmb), while the non-productive cells occurred in lithologies not part of the geothermal reservoir (Tr, Kgr and Tbf).

Table 9. CART parametric sensitivity analysis on selected geoscience parameters predictive of productive hydrothermal wells from the database for both non-productive and productive wells. Figures are referenced from Appendix 19.

CART Analysis Figure	**Selected Geoscience Parameters Considered** (X) **and Used (X) in the Splitting**								**r^2-value**
	Temp	*Vp*	*Resistivity (MT)*	*CSC*	*Dilatation*	*Presence of a Fault*	*Vertical Stress*	*Lithology*	
11	X	**X**	**X**	**X**	X	X	**X**	**X**	0.66
12	X	**X**	**X**	**X**	**X**	X	**X**		0.52
13	X	**X**	**X**			X		**X**	0.62
14		**X**	**X**			X		**X**	0.54

CART Sensitivity Analysis

The CART analyses described above explored differing combinations of multiple explanatory variables to find the highest r^2-values in predicting one of the four key response variables: temperature, lithology type, productive hydorthermal cells, and expected EGS favorable cells. The analyses determined which parameters are the best predictors. An extensive sensitivity analysis was performed using *JMP Pro 9.0* and the publically avaliable *RStudio* application to determine the prediction capabilities of the various geoscience parameters and the relationships and interactions between them. The analysis performs every possible parameter combination using seven key variables in a systematic format. Temperature and lithology type was predicted using both section and well data, while predicting the occurrence of productive hydrothermal and EGS favorable cells was determined using well data only. The individual CART analyses were evaluated mostly based on their associated r^2-value, but also due to the number of splits, explanatory variables used, explanatory variable first split on, shape of the r^2-curve and corresponding K-fold cross-validation curve. This analysis will determine (1) the best combination of explanatory variables to predict temperature, lithology type and productive hydrothermal/EGS favorable cells, (2) the influence of adding and removing variables, (3) the effect or removing depth (i.e. vertical stress) from the analysis and (4) relationships between key predictor variables.

Table 10. Identification of productive hydrothermal cells for Dixie Valley Wells and formations encountered at the selected depths indicated. Cells highlighted light orange are considered productive(zones of injection/production). Non-shaded cells are considered non-productive, while dark gray shaded cells lie below the wellbore. Lithologies that are bolded and in red represent the expected EGS Favorable cells, some of which overlap with the permeable (hydrothermal) defined cells.

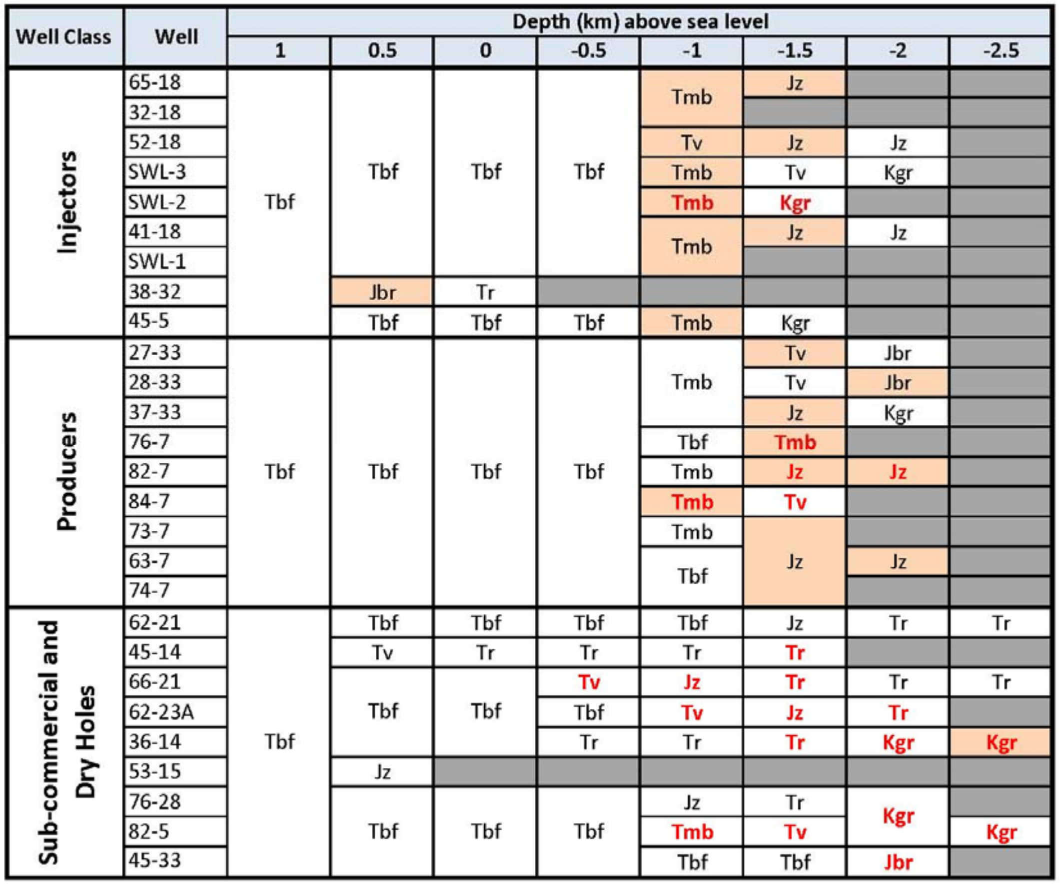

Well Class	Well	Depth (km) above sea level							
		1	0.5	0	-0.5	-1	-1.5	-2	-2.5
Injectors	65-18	Tbf	Tbf	Tbf	Tbf	Tmb	Jz	▨	▨
	32-18						▨	▨	▨
	52-18					Tv	Jz	Jz	▨
	SWL-3					Tmb	Tv	Kgr	▨
	SWL-2					**Tmb**	**Kgr**	▨	▨
	41-18					Tmb	Jz	Jz	▨
	SWL-1						▨	▨	▨
	38-32		Jbr	Tr	▨	▨	▨	▨	▨
	45-5		Tbf	Tbf	Tbf	Tmb	Kgr	▨	▨
Producers	27-33	Tbf	Tbf	Tbf	Tbf	Tmb	Tv	Jbr	▨
	28-33						Tv	Jbr	▨
	37-33						Jz	Kgr	▨
	76-7					Tbf	**Tmb**	▨	▨
	82-7					Tmb	**Jz**	**Jz**	▨
	84-7					**Tmb**	**Tv**	▨	▨
	73-7					Tmb	Jz	▨	▨
	63-7					Tbf		Jz	▨
	74-7							▨	▨
Sub-commercial and Dry Holes	62-21	Tbf	Tbf	Tbf	Tbf	Tbf	Jz	Tr	Tr
	45-14		Tv	Tr	Tr	Tr	**Tr**	▨	▨
	66-21		Tbf	Tbf	**Tv**	**Jz**	**Tr**	Tr	Tr
	62-23A				Tbf	**Tv**	**Jz**	**Tr**	▨
	36-14				Tr	Tr	**Tr**	**Kgr**	**Kgr**
	53-15		Jz	▨	▨	▨	▨	▨	▨
	76-28		Tbf	Tbf	Tbf	Jz	Tr	**Kgr**	▨
	82-5					**Tmb**	**Tv**		**Kgr**
	45-33					Tbf	Tbf	**Jbr**	▨

Reported lithology at depth indicated as identified by Blackwell et. al 2005; Lutz et. al 1998, 2002; Reed et. al 2009; Hulen et. al 1999; Plank (1999) and propritary data provided by Terra-Gen Power.

Lithology Explanation

Tbf: basin-filling sediments
Tmb: Miocene basalt
Tv: Oligocene silicic volcanics
Jz: Jurassic mafic rocks
Jbr: Boyer Ranch quartzite
Tr: Triassic meta-sediments
Kgr: Cretaceous granodiorite

☐ Non-Productive
🟧 Productive
▨ Cell lies below well

Parameter Overview

Within the preceding geostatistical analyses, the various geoscience parameters have been analyzed and eight key variables that show correlations have been recognized (see Section 7.4.1. and Appendix 15). These variables were chosen as the explanatory variables in the CART Sensitivity Analysis and are as follows: (1) **P-wave velocity** (Vp), (2) **Resistivity** derived from Magnetotellurics (MT), (3) **Coulomb Stress Change** (CSC), (4) **Dilatation**, (5) **Vertical Stress** (VertStress), (6) **Gravity-Magnetic inferred Lithology** (Grav_Mag), (7) **Lithology** derived from the geologic assessment and (8) **Temperature.**

Methodology

JMP Pro 9.0 is a user friendly statistical program that allows the user to upload excel files containing the various data with respect to cell location, and then run a *partition analysis* using the data. The user chooses his *Input Variable* (Predictor or response variable), and then chooses the *Explanatory Variable/s* from 1-7 variables. The approach shows the effect of systematically removing one variable at a time starting with considering all variables (7) and finishing with only one variable considered. Prior to starting the analysis the user should check the tabs labeled *Split History, K-fold validation and Column Contributors*. Split History shows how the r^2-values changes vs. the number of splits. The k-fold validation option checks the validity of the r^2-value by performing the same splits subsequently on a smaller subset of the data. If the two lines are intersecting or similar then the r^2-value has a higher level of confidence. The column contributor's option allows the user to see which parameters were used in the analysis. Once analysis is set-up, the analysis begins by repeatedly *splitting* the data (manually) until the r^2-value has reached a plateau and does no longer increase with each subsequent split. The r^2-value reported by the CART analysis must also match or be close to the k-fold validation curve. The user has the option of *pruning* back the tree to terminate the analysis at the desired node. Generally the less splits of the data, the more reliable the corresponding r^2-value.

The analyses were organized into a series of tables for each unique prediction that shows the effect of removing one variable all the way to removing six out of seven possible variables. Each table shows the variables used, variables considered, variable used for the first split, corresponding r^2-value, and number of splits for each possibility. The following lists the appendices that detail the three CART Sensitivity Analyses:

- Appendix 20a. Predicting Temperature using Section and Well Data;
- Appendix 20b. Predicting Lithology Type using Section and Well Data;
- Appendix 20c. Predicting Productive (hydrothermal) vs. Non-Productive Cells using Well Data; and
- Appendix 20d. Predicting expected EGS favorable cells using well data.

In the case of predicting EGS Favorable cells, the analysis was perfomed using *RStudio* a publically available user interface for performing various statistics (www.rstudio.com). Using the well data set, cells (depth intervals with respect to wells) considered favorable for EGS were designated as the response variable, while eight explanatory variables were chosen. The explanatory variables used were the same as for the previous three analyses, with the exception that the Gravity-Magnetic inferred Lithology parameter was replaced with whether a faults was present or absent. The analysis explored every combination from eight variables considered to only one considered, with the results organized by the number of variables used, and reported from highest to lowest with respect to r^2-value . Results are summarized in Appendix 20d, while selected results are highlighted in Table 11.

Results

The first variable that the analysis determined to split on was almost exclusively vertical stress, which has a strong dependence to depth. When this variable was removed, the analyses tended to choose Vp as the first split or next best choice, and the r^2-values dropped significantly. While vertical stress was considered a significant predictive parameter using CART and other geostaistical methods, a review of the results show that when vertical stress is removed from the CART analysis, similar r^2-values can be replicated with a different set of parameters (Table 11). For example, when predicting temperature using section data, a r^2-value of **0.871** is calculated using all available parameters including vertical stress, while a r^2-value of **0.885** can be achieved using only Vp, Lithology and Dilation. This case is true for all five predictions, with the exception of the predicting Lithology using Section Data which yields a r^2-value of **0.631** using all parameters, and only a **0.453** using Vp, MT, CSC, dilatation and lithology. While this implies that the combination of other parameters can replicate the predictive power of vertical stress, it is important to note that the low value in the range of r^2-values reported in Table 11, occurs when vertical stress is removed from the analysis. The results are summarized below.

Predicting Lithology using Section Data

- Highest r^2-values are in the 0.60 to 0.66 range.
- Temperature and CSC are the least used variables.
- Vertical stress was chosen as the first split the majority of the cases. The only other variables used as the first split was Vp, dilatation, and Grav_Mag, and in that order of occurrence. The majority of the cases these secondary variables were used as the first split when vertical stress was removed from the analysis.
- The analysis tended to follow a pattern of using only the variables vertical stress and dilatation together for a r^2-value of 0.653 after 7 splits, when the variable Vp and Grav_Mag were removed.
- Using Vp, Resistivity and Grav_Mag yielded an r^2-value of 0.406 after 5 splits.

Predicting Temperature using Section Data

- Highest r^2-values are in the 0.85 to 0.90 range.
- Vertical stress was the dominant first split, followed by Vp, then resistivity (MT), and lastly Grav_Mag. When none of these variables were considered, dilatation was used as the first spilt.
- Vertical stress and MT yielded a r^2-value of 0.876 after 4 splits, while vertical stress and dilatation yielded a r^2-value of 0.892 after 4 splits.
- Vp and MT alone can predict temperature with a r^2-value of 0.775 after 6 splits.
- CSC was rarely used in the analysis, and only when the variable dilatation was removed.
- The fact that vertical stress, when it is the only variable considered, can predict temperature with an r^2-value of 0.874 after 3 splits, suggests that depth is the controlling factor. Vp alone had a r^2-value of 0.359 after 5 splits, while resistivity alone had a r^2-value of 0.502 after 4 splits.
- Vertical stress, Grav_Mag, and lithology show a complex interaction between the variables and tend to group together.

Predicting Lithology using Well Data

- Highest r^2-values are in the 0.60 to 0.62 range.
- When vertical stress was considered, it was used as the first split 100% of the time. The variable used as the first split when vertical stress was removed was Vp, then Grav_Mag. If all three of these variables were removed, the analysis first split on dilatation.

- The three most commonly used variable were vertical stress, dilatation and Vp. The most common result was the analysis using these three variable regardless of the variable considered, with a r^2-value of 0.611 after 6 splits.
- Using vertical stress, Grav_Mag and Vp resulted in highest r^2-value of 0.621 after 7 splits.

Table 11. Classification and Regression Tree (CART) Sensitivity Analysis results using cross-section and well data. The first row for each response variable corresponds to r^2-value ranges with vertical stress considered, while the following rows, highlighted in green, show the r^2-values when vertical stress is removed from the analysis. In most cases with the exception of predicting Lithology using Section Data, a similar r^2 result can be achieved when vertical stress is removed from analysis. The explanatory variables used in the analyses include (1) temperature, (2) p-wave velocity (Vp), (3) resistivity from MT, (4) coulomb stress change (CSC) and (5) dilatational strain (dilatation) both from Coulomb Stress modeling, (6) vertical stress, (7) lithologic formations derived from the geologic assessment and (8) separately from the gravity-magnetic modeling.

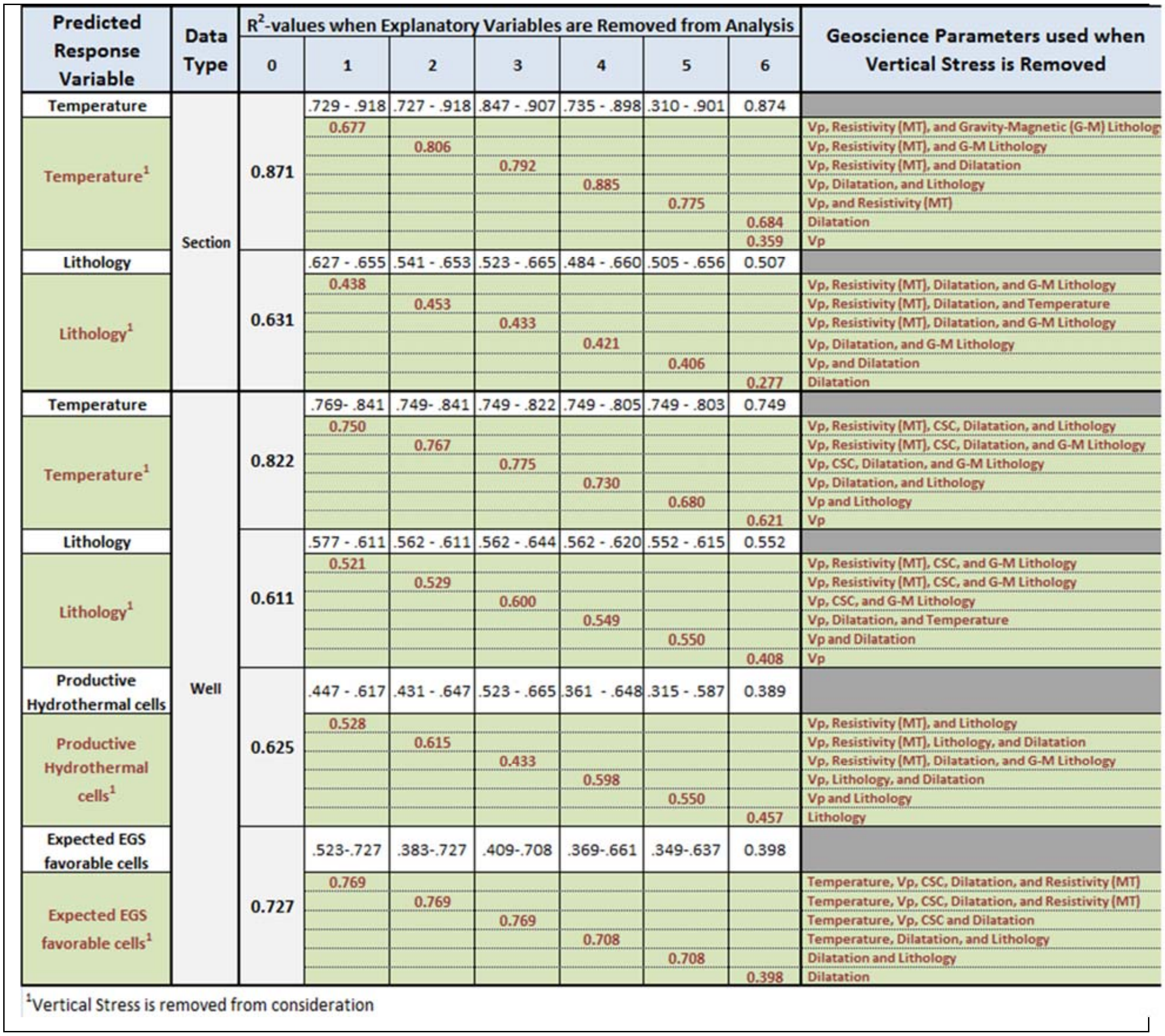

Predicted Response Variable	Data Type	R^2-values when Explanatory Variables are Removed from Analysis							Geoscience Parameters used when Vertical Stress is Removed
		0	1	2	3	4	5	6	
Temperature	Section	0.871	.729 - .918	.727 - .918	.847 - .907	.735 - .898	.310 - .901	0.874	
Temperature[1]			0.677						Vp, Resistivity (MT), and Gravity-Magnetic (G-M) Litholog
				0.806					Vp, Resistivity (MT), and G-M Lithology
					0.792				Vp, Resistivity (MT), and Dilatation
						0.885			Vp, Dilatation, and Lithology
							0.775		Vp, and Resistivity (MT)
								0.684	Dilatation
								0.359	Vp
Lithology		0.631	.627 - .655	.541 - .653	.523 - .665	.484 - .660	.505 - .656	0.507	
Lithology[1]			0.438						Vp, Resistivity (MT), Dilatation, and G-M Lithology
				0.453					Vp, Resistivity (MT), Dilatation, and Temperature
					0.433				Vp, Resistivity (MT), Dilatation, and G-M Lithology
						0.421			Vp, Dilatation, and G-M Lithology
							0.406		Vp, and Dilatation
								0.277	Dilatation
Temperature	Well	0.822	.769- .841	.749- .841	.749 - .822	.749 - .805	.749 - .803	0.749	
Temperature[1]			0.750						Vp, Resistivity (MT), CSC, Dilatation, and Lithology
				0.767					Vp, Resistivity (MT), CSC, Dilatation, and G-M Lithology
					0.775				Vp, CSC, Dilatation, and G-M Lithology
						0.730			Vp, Dilatation, and Lithology
							0.680		Vp and Lithology
								0.621	Vp
Lithology		0.611	.577 - .611	.562 - .611	.562 - .644	.562 - .620	.552 - .615	0.552	
Lithology[1]			0.521						Vp, Resistivity (MT), CSC, and G-M Lithology
				0.529					Vp, Resistivity (MT), CSC, and G-M Lithology
					0.600				Vp, CSC, and G-M Lithology
						0.549			Vp, Dilatation, and Temperature
							0.550		Vp and Dilatation
								0.408	Vp
Productive Hydrothermal cells		0.625	.447 - .617	.431 - .647	.523 - .665	.361 - .648	.315 - .587	0.389	
Productive Hydrothermal cells[1]			0.528						Vp, Resistivity (MT), and Lithology
				0.615					Vp, Resistivity (MT), Lithology, and Dilatation
					0.433				Vp, Resistivity (MT), Dilatation, and G-M Lithology
						0.598			Vp, Lithology, and Dilatation
							0.550		Vp and Lithology
								0.457	Lithology
Expected EGS favorable cells		0.727	.523-.727	.383-.727	.409-.708	.369-.661	.349-.637	0.398	
Expected EGS favorable cells[1]			0.769						Temperature, Vp, CSC, Dilatation, and Resistivity (MT)
				0.769					Temperature, Vp, CSC, Dilatation, and Resistivity (MT)
					0.769				Temperature, Vp, CSC and Dilatation
						0.708			Temperature, Dilatation, and Lithology
							0.708		Dilatation and Lithology
								0.398	Dilatation

[1] Vertical Stress is removed from consideration

Predicting Temperature using Well Data

- Highest r^2-values are in the 0.80 to 0.83 range.

- Using vertical stress only yielded a r^2-value of 0.749 after only 3 splits. This was one of the most common results, even when other variables were considered.
- Vertical stress is the most common first split. When removed the data splits on Vp, then lithology, then Grav_Mag when the subsequent variables are removed. When all of these are removed the analysis is forced to split on MT.
- Vp and MT alone can predict temperature with an r^2-value of 0.625 after only 3 splits.
- Vertical Stress, dilatation, and MT alone can predict temperature with an r^2-value of 0.83 after 6 splits.

Predicting Productive vs. Non-Productive Cells using Well Data

- The first split is lithology 100% of the time, when this variable is considered. When lithology is removed from the analysis, the first split is usually on Grav_Mag as expected, however the choice for the second split is much more random then the previous analyses.
- Considering and using all seven variables, the analysis first split on lithology with an r^2-value of 0.625 after 6 splits.
- Highest r^2-value are in the 0.63 to 0.67 range.
- Vertical stress and dilatation used alone have a r^2-value of 0.513 after 6 splits.
- Temperature was only used as a secondary variable, and CSC and temperature were the least common variables used.

Predicting EGS Favorable Cells using Well Data

- Cells determined to possess characteristic favorable for EGS were assigned separately from cells identified as productive (hydrothermal).
- Dilatation was the most considered an significant parameter and was used in the CART data divisions for analyses which produced the highest r^2-values. Temperature and lithology type were considered important secondary parameters.
- The parameters temperature, Vp, CSC, MT (resisitivity), and dilatation; temperature, Vp, CSC, dilatation and the presence of a fault could predict EGS favorable cells with an r^2-value of 0.769, while dilatation and lithology used alone yielded a 0.708 r^2-value.
- Vertical Stress was not a critical parameter and the majority of the analyses yielded higher r^2-values when the parameter was not used in the analysis.

Implications

Using the data gridded along the wellfield cross-sections (Section Data) yielded slightly higher r^2-values than using the data gridded in respect to well location (Well Data). This is interesting as it suggests that more accurate predictions can be made with a larger quantity of modeled data, rather than a smaller set of data containing relatively more hard data. Modeled values such as vertical stress and dilatation seemed to make the best predictors and have a unique relationship between them. While vertical stress was used as the first split for most of the predictions, similar predictions quantified by high r^2-values could be made without this parameter. Lithology was the first split used for determining whether a cell was productive or non-productive, while temperature was the first split for predicting favorable EGS cells. This implies that the rock type is the most important factor in determining whether a cell is productive or non-productive, not temperature and adversely temperature is the most important factor for predicting favorable EGS cells. Resistivity (MT) was used almost exclusively as a secondary parameter and when combined with Vp could predict temperature with high r^2-values. The significance or lack-of therof will be determined when similar statistical analyses are applied to the enhanced data set under Task 5 of this Project (see Section 1.1). Some important observations are (1) each analysis is unique as r^2-values for identical trials can vary by as much as 5%, (2) vertical stress seems to be a modeled parameter suitable for CART yet highly dependent on depth and is not required to consider in future analyses, and (3) CART provided a good complementary geostatistical analysis to validate findings obtained from other methods (bi-variate correlations, residuals, multiple regression, etc.).

Summary of Exploratory Geostatistics and Geologic Significance

It must be noted that this analysis should be considered a preliminary view of the exploration geostatistics of a geothermal system. Further work within this system, to be conducted using the enhanced data set (baseline + new) and in other geothermal systems should be conducted to determine (1) whether the correlations (and predictions) defined herein are universal in nature, and (2) the causal relationships within any particular correlation. The following lists the salient highlights of the geostatistical analyses:

Correlation Analysis

- The parameters temperature and vertical stress are correlated with p-wave velocity (Vp); All other correlations found are not consistent in the analyses conducted.
- Correlations between parameters cannot be analyzed soley on the correlation coefficient -value, but must take into account the data spread and range, effect of depth with modeled parameters, and significance based on SME and geologic inference.
- Temperature can be fairly accurately predicted from Vp using the well data set, especially when considering the variability and confidence (trust factor) of the baseline data. When the poor resolution areas were removed from the data set (surface data and wells with a low seismic trust), the r^2-value for the polynomial fit that quantifies the relationship has a value of 0.73.

Multiple Regression and Residual Analysis

While, the overall multiple regression and two component residual analysis indicates that depth (or elevation) is the only link between (1) temperature and vertical stress, and (2) temperature and Vp, a multicomponent analysis suggests that (1) the combination of a variety of geoscience parameters (a r^2-value of 0.94 was found using elevation, vertical stress, dilatation, Vp, and resistivity (MT) to predict temperature) can be used to predict temperature and (2) there is a complex interaction between the geoscience parameters in this prediction.

Classification and Regression Tree Analysis

Applying CART to both the Section and Well Data, the relationships among the geoscience parameters were investigated to determine if temperature, lithology, productive hydrothermal cells and expected EGS favorable cells can be predicted using the geoscience data and in part based on a combination of parameters that also showed high correlations within the previous analyses. The multi-step analysis showed that the geoscience data could predict the identifed variables, considered the significant parameters for inferring favorable EGS conditions, both with and without the vertical stress parameter (Table 11). The exception to this result was when predicting lithology type using the section data. An important observation is that temperature could be predicted using the combination of three key measurable geoscience parameters, gravity-magnetic inferred lithology (Grav-Mag), MT and Vp. For example, temperature can be predicted using the section data with an r^2-value of **0.91** using Vp, MT and lithology, while the productive nature (hydrothermal portion) of a well can be predicted with a r^2-value of **0.63** using Lithology, Vp and MT. Additionally, Vp was the critical parameter for predicting temperature and rock type when vertical stress was not considered. It is noted that difficulties remain for assesing the reliability of the CART results, when a number of the geoscience parameters have a embedded depth influence (vertical stress, Vp, temperature, and rock type).

The CART geostatistics have validated the qualitative correlations by the following points (1) the geologic and gravity-magnetic lithology model have a high degree of correspondence; (2) the resistivity parameter (MT) is one of the sensitive secondary parameters used to predict temperature and lithology; (3) Vp, while the parameter showed no qualitative correlation with the other geoscience data sets is a very important parameter for predicting lithology, temperature (see discussion below), the productive nature of a well, and expected favorable EGS area. It is important to note the combination of parameters had much higher r^2 values quantifying their prediction power than the parameters by themselves.

Assesment of the Vp-Temperature Relationship

While an empirical relationship is observed between measured temperature from wells and modeled P-wave velocity, depth was a confounding parameter. The relationship was assessed using both cross-sectional and well data, through (1) standard correlation analyses, (2) correlations factoring in the trust factor of the baseline seismic model, (3) multiple regression, (4) residuals to remove the effect of depth, (5) CART analyses to determine the effect of other parameters, (6) correlation with geologic formations, and (7) correlation to conductive vs. convective domains. While the relationship certainly exists throughout some analyses, others do not support the correlation. We will evaluate this confounding relationshio further using the forthcoming higher resolution seismic model using the enhanced data.

7.5 Summary

7.5.1 Hydrothermal System

The structural interface between the Stillwater Range and Dixie Valley is complex fault zone, reflecting the interaction between the current WNW-ESE extension axis of normal faulting with an earlier generation of N-trending B&R faulting. The intersection of these structures, in the current stress regime, produces zones of compression and dilatation along the fault zone. These dilatational zones are coincident with the occurrence of shallow thermal anomalies expressed along the DVFZ and at New York Canyon on the west side of the Stillwater Range. Additionally, the subsurface well data available to this project shows an excellent correltion betwwen productive wells and the inferred dilatation zones. While, the recognized thermal anomalies expressed at the surface occur at or near the range-front fault, additional geophysical evidence (i.e., MT data) suggest that portions of the intra-range setting are also hydrothermal, or were active in the past. Unfortunately, there is no well data in the range to validate this observation.

In reference to the strucutal mechanism, the data presented herein suggests that while the overall Dixie Valley geothermal system does lie in a regional accommodation zone between the west-dipping Pleasant Valley and east-dipping Dixie Valley , and occurs adjacent to a seismic gap with no recent surface breaks and inferred concentrated stress, localized dilatation on high-angle faults appears to be the dominant control for the location of geothermal cells along the DVFZ. The occurrence of the geothermal cells coincide with zones of dilatation along the fault zone and seem to be controlled by the intersection of major north-trending structures with the more northeast-trending fault zone.

The only area within Dixie Valley that has been studied extensively is the DVGW with established production and injection wells supplying the power plant now owned and operated by Terra-Gen and several dry to sub-commercial wells. Within this small segment of Dixie Valley, we observe the DVFZ comprised of the range-bounding fault and the valley-bounding piedmont fault, which are considered the major thermal fluid-bearing structures within the fault zone. These two structures are not believed to possess extensive lateral permeability along their entire length, but rather are thought to consist of intermittent zones of dilatiaton and compression depending on the orientation of faults and fractures with respect to the current stress regime. Fractures occurring within zones of dilatation along the DVFZ, assessed as steeply dipping fracture sets both parallel and anti-thetic to the main east-dipping NE-trending fault trend (see Section 6.1.1), are optimally oriented for extensional failure and should create a localized, naturally-occurring open network of permeability capable of geothermal fluid production.

The main production areas supplying the power plant are to the north in section 33, and to the south in sections 7 and 18 (Figure 30; Section 6). While there is shallow interconnectivity between these two areas, there is no evidence of production-depth interconnectivity. The shallow interconnectivity is currently used to facilitate the injection well array in both areas. All production (Section 7 and 33) is being derived from dilated segements within the fractured hanging wall block of the piedmont fault. Well 36-14, located approximately two miles to the west of the sections 7 and 18 production area, bottomed near the range-front segment of the DVFZ, had non-commercial geothermal production with a significantly higher temperature than that of the wells supporting the power plant, with no evidence of deep connectivity to the production wells based on the limited data available to this project. It should be noted that the significant downhole permeability and downhole productivity in 36-14 was found only in the last 30m (100ft) of the well trajectory. The well data show that within a distance of 10km there are three separate geothermal cells. There is thermal evidence that the piedmont fault extends into, or plays a role in the geothermal system encountered in the DVPP area around well 62-23A (see section 6.3.2). While geophysical data extends this piedmont structure throughout the entire length of the DVGW (Figures 13 and 14), we know that there is no single normal fault template that can describe the locations of geothermal cells in Dixie Valley. Instead, the occurence of geothermal cells is dependent on the more north-trending faulting intersecting the current northeast-trending faults, altering the localized stress conditions and creating zones of dilatation.

The thermal fluid producing components of the hydrothermal geothermal resource at Dixie Valley are dependent on the:

- fault and fracture orientation;
- irregularity of fracture surfaces that create asperities and force open the fractures following shear slip;
- degree of open fracture permeability at depth;
- magnitude of localized stresses with respect to the current stress-regime;
- lithology of rocks and sediments in and adjacent to the fault zone; and
- degree of sealing within the thermal fluid-bearing faults and fractures.

The major domains of the hydrothermal system are considered to be:

- intermittent dilatational zones along the piedmont fault including associated fractures and antithetic faults;
- fractured permeable zones within the Miocene basalt that truncates the piedmont fault within these zones of dilation;
- Limited permeability within the intervening structural block between the steeply dipping range-front and piedmont faults, extenuated by cross-faulting which connect the two structures; and
- intermittent dilatational zones along the range-front fault including associated fractures.

7.5.2 Engineered Geothermal System

The commercially exploitable EGS portions of Dixie Valley geothermal resources are dependent on the conductively heated rock juxtaposed to active geothermal cells/systems. Important parameters include temperature, stress-regime and the lithologic characteristics within the fault zone and surrounding rocks at depths of much less than 5km (16,400ft). Temperatures >200°C (392°F) are known to occur along a large region in and adjacent to the DVFZ at depths of ~2-3km (6560-9840ft). Coarse crystalline and metamorphic rocks such as the Cretaceous granodiorite, Boyer Ranch quartzite, and Jurassic low grade metamorphic and igneous rocks possess the favorable rock mechanical properties for EGS stimulation. Prime areas of interest include hot, brittle and relatively unfractured rock adjacent to the current production field and the hot area with limited fractures between the Dixie Comstock geothermal cell and the Hare and Mississippi Canyons geothermal cell(s)/systems(s). The potential EGS geothermal resource in Dixie Valley can be defined within the following three domains:

- the intervening structural block between the steeply dipping range-front and piedmont fault where there is low to no naturally-occurring permeability;
- zones of compression along the range-front and piedmont faults where natural induced stresses are keeping the fractures closed;
- sealed zones of dilation along the range-front and piedmont faults; and
- the footwall block of the range-front fault, and beneath, at least, the eastern portion of the Stillwater Range.

Optimal EGS targets are subsurface regions that are hot, have low permeability , are not proximal to a fault zone, and are comprised of brittle rocks that are under the correct stress conditions to produce open fractures. An example of a potentially favorable EGS target region is the DVPP area (Figure 1) where there exists very hot, non-producing wells 36-14, 62-23A, and 66-21 located a few kilometers south of the producing area. These are all low permeable wells within suitable rock types, with the exception of 62-23A which likely intersected brittle rocks (Jz), but bottomed out in the Triassic meta-sediment section, considered not capable of holding fractures. This favorable region includes the area around the Section 10 fumaroles away from the range-front fault, which is very hot at near surface conditions, and contains a substanstial block of intrusive rock, part of the Jurassic igneous complex, in the subsurface. The area lying between the Dixie Comstock geothermal area and the Hare Canyon geothermal area, a zone in which well 45-14 is located, also shows a high potential for EGS development, although the non-optimal EGS rock type at depth could be an important negative factor. The high measured S_{hmin} within 45-14, could likely be overcome though EGS stimulation. Countering the poor lithology, there appears to be a large region that is EGS favorable with respect to temperature. Somewhere in the 45-14 area there must be convective fluid flow from depth indicating permeable open structures that can be accessed through EGS techniques. Additionally, the area surrounding the permeable portions of Dixie Meadows, just to the south, also shows some EGS potential.

Our knowledge of the temperature distribution is limited to deep geothermal exploration and production wells, deep and shallow temperature gradient wells, assesment of controlling structures, and leakage of geothermal fluids and related chemical reactions on the ground surface within Dixie Valley. We can expand our thermal mapping by the identified Vp-temperature relationship, inferences from MT, possible geothermometry inferences, etc. No potential EGS targets are identified under the Stillwater Range or adjacent to the intra-range faults at this time due to the lack of any EGS indicator data at depth. We speculate that the range itself holds EGS potential due to (1) the drilling of 36-14, (2) the mining exploration hole referred to as the Bolivia well that encountered warm water, (3) zones of alteration found in the intra-range faults, (4) occurence of active fumaroles at the range-front boundary and (5) conductive modeling that show the range is an area of high heat flow.

8. Basline EGS Favorability and Trust Mapping

8.1 Introduction

A variety of exploratory geostatistical techniques were applied to select geoscience parameters to (1) quantify the qualitative geoscience relationships described in Section 7.3, (2) test relationships independent of the qualitative geoscience correlation discussed above; and (3) explore if parameters can be statistically quantified to be used in the formulation of the baseline EGS Favorability Map. The first two points are discussed in Section 7.4. This section describes:

1. the GIS database created for the EGS Exploration Methodology project;
2. parameters derived from the various geoscience data-sets;
3. the method of gridding the data within the Project Area and Wellfield Calibration Area;
4. exploratory geostatistical approaches and how the statistics factor into the EGS Favorability Map;
5. the generation of the favorability and trust maps; and
6. the findings of the favorability and trust maps.

8.2 GIS Database

As described in Section 7.4.1, the project produced a number of data management and data visualization challenges. The project required that a large amount of varied data be acquired, produced, and interpreted from a number of different sources. As such, an efficient and effective method for storing, managing, and updating these various data sets early in project development was needed.

The first step in addressing these issues was polling individual task leaders (Section 1.4) for an understanding of the format and quantity of data that would be provided before deciding the optimal data container to use. This also provided an opportunity to assure that the task leaders providing the data and the initial geostatistics task leader, Dr. Edward Isaaks and later in the project , Dr. Fletcher Ibser, were aware of each other's requirements. This process was accomplished by a series of individual telephone conference calls to the task leaders that culminated in a conference call to share the findings and initial conclusions.

We use an *ESRI ArcGIS* geodatabase (GDB) for the project. It provides a simple data container compatible for *ESRI* file types ("*.shp*", "*.lyr*"), many tabular data types ("*.csv*", "*.txt*"), and *Microsoft Access* data files ("*.mdb*"). The GDB format is a relational database that combines the inheritance of object-oriented databases with the ability to assign relationships to the data, and ties tabular data, also known as attribute data, to spatial data (physical location). This allows data management in a traditional database format, while allowing for the additional functionality provided by the spatiality of the data such as interpolating data between points. *ArcGIS* is an even better fit when considering that one of the objectives of the project is to produce an EGS favorability map. For example, *ArcGIS* provides tools that greatly simplify the process of weighing the various data sets to produce favorability values. This does require, however that all data have the same resolution, a requirement that creates a significant data management hurdle that is addressed below.

To describe the complexity of the data set resolution issue, it is important to first discuss the difference between vector and raster data sets. Vector data is represented by points, lines, or polygons. It is discrete data at a discrete location. Vector data is generally used to represent things like roads, well locations, and lease ownership. Raster data is represented by pixels or grids. It is data that is generally interpolated or measured across an area. Raster data is generally used to represent things like elevation, smooth contours, and interpolated data. Each data type has its own advantages and disadvantages (Figure 64).

Different data sets use different data types. We use gravity/magnetic data as an example to illustrate the difference between vector and raster data. Gravity/magnetic data are generally collected at discrete points where the sensor makes a measurement. The data that is collected is vector data, i.e., discrete measurements at discrete locations. This data is then often modeled across a broader area between the measurement stations. The data produced by the model is raster data, i.e., gridded or pixilated across a surface.

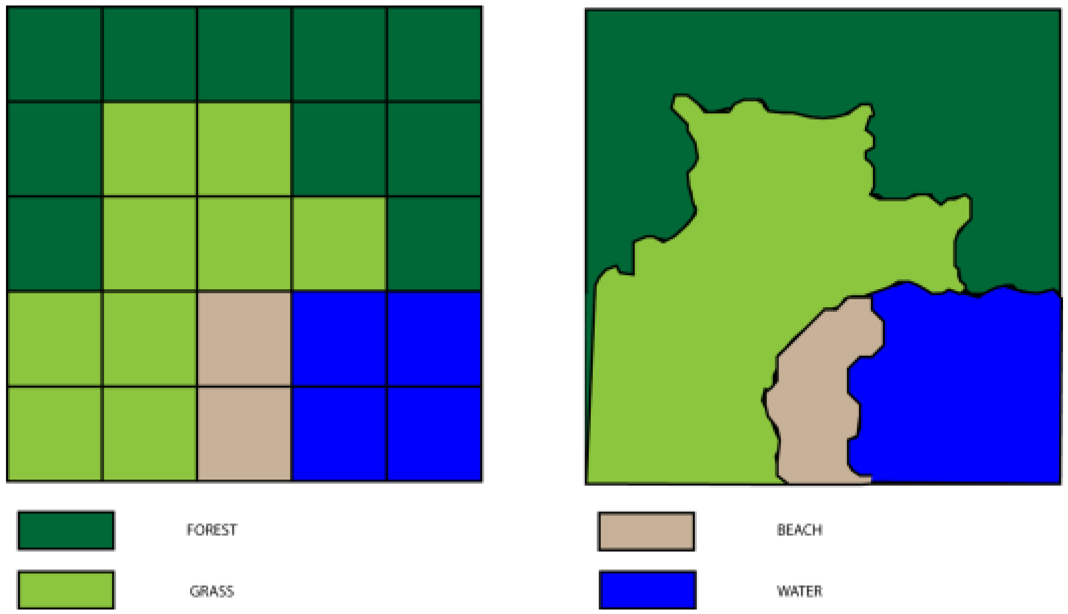

Figure 64. Idealization of vector (right figure) to raster (left figure) format conversion. For the EGS Exploration Methodology project it was necessary to convert the data from a vector format into a raster format to allow a common data resolution.

The “discretization” or “gridding” of the vector data and modifying existing raster data to achieve identical resolution across all the data sets was necessary before *ArcGIS* could process the models used to create a favorability map. This process required that a common raster or grid be created and that the discrete points are moved into the grids as accurately as possible. This process is either achieved by utilizing existing data models to output at the necessary resolution, or by hand, placing a grid over the vector data and assigning the values which occupy the majority of each grid block.

This method produces data at the same resolution and as such, it can be directly compared as “apples to apples.” In other words, the data values for one data set in each grid square can be compared directly to values in another data set for the same grid square. This is critical for not only creating a favorability map, but also providing a data format for performing statistical analysis. The downside of this process is a loss in data fidelity, e.g., edges that were clearly defined in the vector data set can become difficult to detect in the raster data. In generating the raster data, a data point in one grid square that does not comprise the majority of the grid is not considered in the analysis. For this reason, the original data sets in vector format are preserved.

8.3 Description of Parameters

Exploratory data methods (geostatistics) were applied to a variety of selected geoscience parameters. Task Leaders provided potential parameters (numerical and categorical) derived from their respective field and/or models. The purpose was to (1) create a baseline data set for the Baseline Conceptual Geothermal Model, (2) provide parameters that could be used to predict rock type, temperature, or stress conditions, and/or (3) provide additional sub-parameters that could be used in the formulation of the EGS Favorability Map. These sub-parameters would be used in conjunction with the major three parameters determined critical to determining the conditions suitable for EGS. The parameters are analyzed qualitatively and quantitatively using geostatistics. The data types are directly measured, modeled/calculated, or inferred/assigned based on SME and have varying resolution depending on the model.

A discussion of all the data parameters is given in Appendix 15 and also discussed in Section 7.4.1. Data under analysis for the baseline model include lithology type and associated lithologic parameters (including density, strength, internal friction, fracture intensity), vertical stress, combined gravity-magnetic inferred lithology, temperature, resistivity derived from MT, Vp derived from the baseline seismic model, Coulomb stress change and strain from a stress model, presense of a fault, and geochemical indicators from production fluids and springs. These data represent the available baseline data set, and while they were used for exploratory statistical analyses, not all of the parameters mentioned were used in the formulation of EGS favorability maps. Other parameters not incorporated in the statistical analysis but discussed among the Project Team include but are not limited to temperature gradients, geothermometry, seismic directionality, and compression and dilated zones based on the structure analysis.

As discussed earlier, there are three parameters of interest for the purpose of producing favorability maps: temperature, lithology, and stress. A discussion amongst the team resulted in the decision to include four sub-parameters in describing stress: compression/dilation zones, fault orientation, existence of mapped faults in a cell, and *Coulomb* stress modeling data. These are the parameters of focus for the favorability mapping process, though all collected data that could be represented spatially made it through the following process into *GIS* software.

8.4 Gridding

Data for the project was gridded into 500m^2 or 500m^3 cells with respect to the following domains:

1. Along the cross-sections C-C', D-D', E-E' and F-F' for use in the statistical analysis and refered to as Section Data (Section 7.4.2)
2. With respect to wells for use in the statistical analysis and referred to as Well Data (Section 7.4.2)
3. Along the cross-sections A-A', B-B', C-C', D-D', E-E', F-F', G-G', and H-H' and applied to coresponding cells in the Calibration Area with interpolation and extrapolation techniques used on applicable data sets
4. Within the Calibration Area, consisting of 500m^2 cells, and used for the generation of the EGS Favorability Maps.

The cross sectional data was gridded (see Section 7.4.1) to (1) introduce the process of data gridding to the task leaders and (2) provide a initial data set in the Calibration Area that could be interpreted statistically. Since the cross sections were defined spatially, it was possible to produce data across these sections for all data sets. The process of producing these raster data sets was relatively straightforward.

To create the favorability map, the data sets were gridded in a plan view format, within pre-defined cells dividing the Calibration Area, and from the top-down along 12 horizontal slices extending from +1km asl to -4km asl (3300ft asl to -13,000ft asl). Since the grids have a finite location in space, the data in the cross sections can be directly assigned to a similar grid in a top down alignment. The data was then interpolated between cross sections and extrapolated when feasible. In situations where data accuracy or coverage was lacking, it was necessary to leave grid values empty to maintain output data integrity. At this point, the relationships between the data sets required additional definition prior to producing the EGS favorability map. This process is explained in the following sections, with a special focus on the statistical analysis.

Data gridded along the horizontal slices comprising the Calibration Area includes lithology, gravity-magnetic inferred lithology, temperature, geochemical indicators, presence of a structure, fault/fracture orientation data inferring favorable/non-favorable stress conditions, zones of compression and dilation, MT resistivity data, and Vp. This data-set will be used to formulate the Baseline EGS Favorability Map within the DVGW.

8.5 Data Conversion

The majority of gridding work was performed in *Microsoft Excel*. This program was used because data (1) can easily be exported to *GIS* software, (2) can be edited in a tabular format or as an overhead plan view “map”, and (3) can be automated for repetitive tasks using *Visual Basic* macros. Data was applied to *EXCEL* templates of the gridded cross-sections and plan view maps by either the Task Leader or SME, or AltaRock personnel.

The first step in the process of the data conversion was to generate a workbook with eleven worksheets, made to represent the depth slices every 0.5km from +1km asl to -4km asl. Figure 65A shows the *EXCEL* template of the Calibration Area, with each cell representing a 500m by 500m grid-block. Figure 65B presents one of the thermal worksheets as an example. The top layer was selected at 1km asl because data values existed across the majority of the Calibration Area at that elevation and approximates the surface of Dixie Valley. Data already produced and gridded for the vertical cross-sections was then transferred into these horizontal sections. This was accomplished by picking the values from the cross-section data that lined up most accurately with the cells in plan view. The process was automated by a script and repeated for all data sets. In this way, a significant amount of data was filled into the plan view format without SMEs having to produce new data sets.

The second step in the process was to add “hard” (measured) data values. The wells with existing data were located in the plan view grid and values were filled into cells at each depth where data was available(Figure 65A). This was done for every well and data set for the available hard data. Most of these values are from well logs and include temperature, lithology, and some geochemistry information.

Data was then filled in between some data sets by interpolating between the existing hard and modeled data values. This was done for numerical data sets such as temperature and MT data using an automated interpolation function that was limited to a 1km (3300ft) radius around an existing data value. For categorical data sets, lithology and gravity-magnetic inferred lithology, a manual interpolation was applied between the cross-sections and hard data points (wells). The interpolation method used is described by the following equation:

$$V_t = \frac{V_1 + V_2 + V_3 + \ldots + V_n}{n}$$

where V_t is the total value and V_n represents the surrounding cells (up to 8 maximum).

In most cases existing models included values to -4km asl or were extended to that depth by the SMEs. For non-numerical data sets or ranges where no data existed at depth, inferences were made. For example, temperature data was inferred to -4km asl by downward continuation of the thermal gradient measured in a well.

Once all depth slices were populated for every data set, the data was converted from plan view to x, y coordinates for export to *GIS* software. The UTM coordinates for the center of the cells in the Calibration Area (see Sections 7.1.3 and 7.4.1) were calculated by starting at the SW corner of the Calibration Area which coincides with the WGS 1984 UTM Zone 11 projection at 412000 Northings and 4412000 Eastings and adding 250 in each direction. From there, each cell's center can be identified by adding 500 for each cell north or east. Z values were determined from the depth slices and are relative to sea level.

The third and final step in the process was to import the point data into *ArcGIS* and convert the points to raster values. Raster values are very similar to the *EXCEL* plan view cells in the gridding process. Each raster cell has a location and a value. The values present in the raster cells are the same as the values in the *EXCEL* cells, but *GIS* software enables the data to be utilized in a more robust manner, such as performing spatial analyses or overlay functions. Figure 66 illustrates the process of converting from plan view, to tabular data, and then raster data in *GIS*.

8.6 Integrated Geoscience Sections for EGS Favorability

Data generation for the three key EGS parameters of interest (lithology, temperature, and stress) is described in this section.

8.6.1 Lithology

The lithology[8] parameter incorporates the known lithologic units from the geologic sections (Section 7.3.1) with inferences from the gravity-magnetic inferred lithology (Section 7.3.1) and MT resistivity data (Section 7.3.1) to create an integrated lithology parameter. The gravity-magnetic inferred lithology sections B-B' through F-F' and MT array C were evaluated with their corresponding geology sections (see Plate 1, and Appendix 12). The gravity-magnetic inferred lithology incorporated the occurrence of a magnetized Jurassic unit (Jg) and allowed the Jurassic section (Jz) to be distinguished into magnetic and non-magnetic rocks (Jznm), see discussion in Section 7.3.1, which have differing EGS implications. Where there was no well or surface data to supersede, the geologic sections were modified to (1) incorporate the presence of Jznm within the aforementioned geophysical sections, (2) alter the depth to basement and overlying low density basin-fill using the gravity-magnetic sections,(3) alter the overall thickness of the Jurassic section using the gravity-magnetic sections, and (4) incorporate the very high resistivity bodies beneath the Stillwater Range as granodiorite. A major assumption in the lithology definition is that the very high resistivity below the Stillwater Range infers the presence of dry, unfractured granodiorite at depth.

---

[8] Note that in this report the term lithology and geologic formation are used interchangeably since each of the seven major formational units identified in the DVGW have specific lithologies.

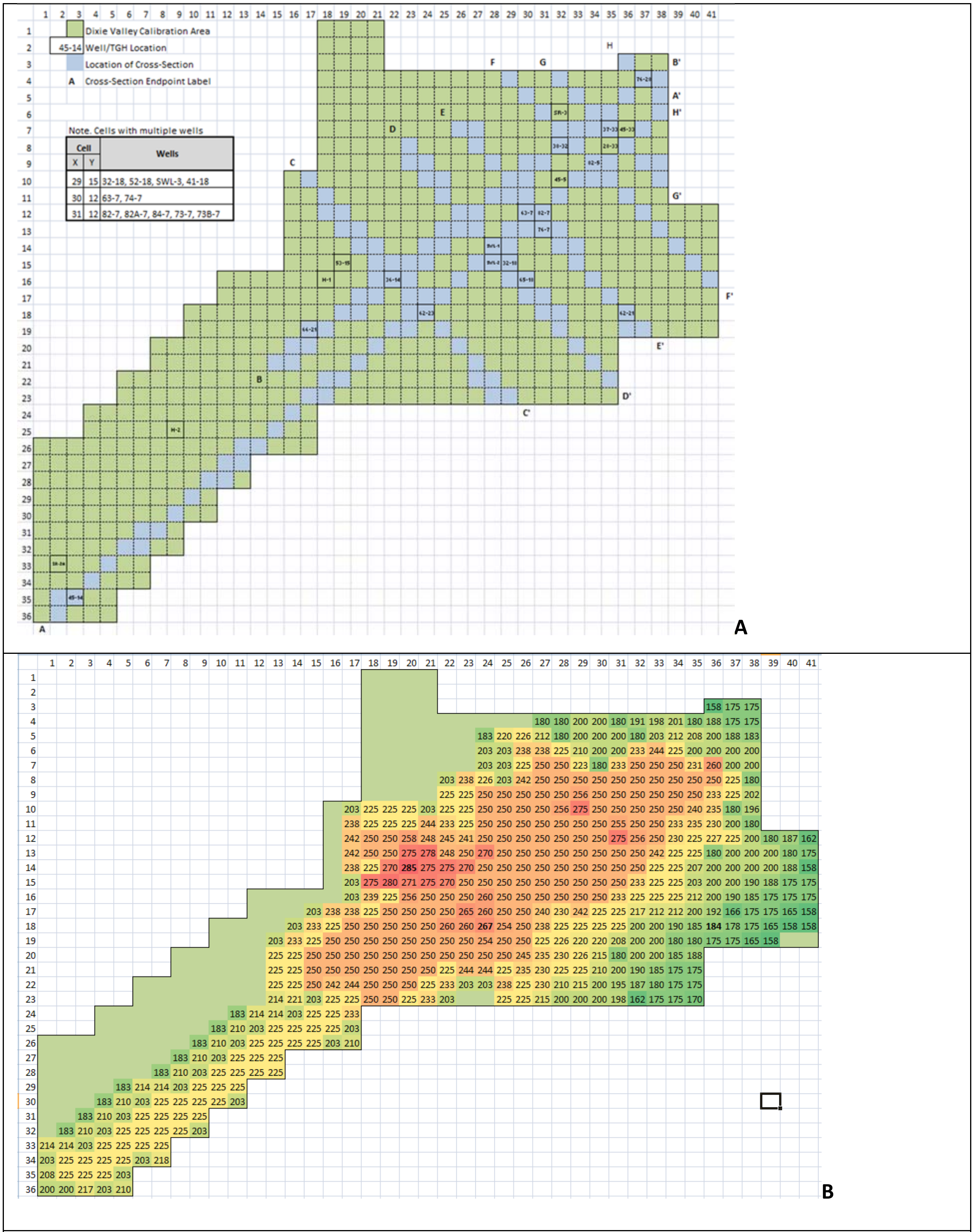

Note. Cells with multiple wells

Cell		Wells
X	Y	
29	15	32-18, 52-18, SWL-3, 41-18
30	12	63-7, 74-7
31	12	82-7, 82A-7, 84-7, 73-7, 73B-7

	1	2	3	4	5	6	7	8	9	10	11	12	13	14	15	16	17	18	19	20	21	22	23	24	25	26	27	28	29	30	31	32	33	34	35	36	37	38	39	40	41
1																																									
2																																									
3																																				158	175	175			
4																											180	180	200	200	180	191	198	201	180	188	175	175			
5																								183	220	226	212	180	200	200	200	180	203	212	208	200	188	183			
6																								203	203	238	238	225	210	200	200	233	244	225	200	200	200	200			
7																								203	203	225	250	250	223	180	233	250	250	250	231	260	200	200			
8																						203	238	226	203	242	250	250	250	250	250	250	250	250	250	250	225	180			
9																						225	225	250	250	250	250	250	256	250	250	250	250	250	250	233	225	202			
10																	203	225	225	225	203	225	225	250	250	250	250	256	275	250	250	250	250	250	240	235	180	196			
11																	238	225	225	225	244	233	225	250	250	250	250	250	250	250	255	250	250	233	235	230	200	180			
12																	242	250	250	258	248	245	241	250	250	250	250	250	250	250	275	256	250	230	225	227	225	200	180	187	162
13																	242	250	250	275	278	248	250	270	250	250	250	250	250	250	250	250	242	225	225	180	200	200	200	180	175
14																	238	225	270	**285**	275	275	270	250	250	250	250	250	250	250	250	250	225	225	207	200	200	200	200	188	158
15																	203	275	280	271	275	270	250	250	250	250	250	250	250	250	250	233	225	225	203	200	200	190	188	175	175
16																	203	239	225	256	250	250	250	260	250	250	250	250	250	250	233	225	225	225	212	200	190	185	175	175	175
17															203	238	238	225	250	250	250	250	265	260	250	250	240	230	242	225	225	217	212	212	200	192	166	175	175	165	158
18														203	233	225	250	250	250	250	250	260	260	**267**	254	250	238	225	225	225	225	200	200	190	185	**184**	178	175	165	158	158
19													203	233	225	250	250	250	250	250	250	250	250	254	250	250	225	226	220	220	208	200	200	180	180	175	175	165	158		
20													225	225	250	250	250	250	250	250	250	250	250	250	250	245	235	230	226	215	180	200	200	185	188						
21													225	225	250	250	250	250	250	250	250	225	244	244	225	235	230	225	225	210	200	190	185	175	175						
22													225	225	250	242	244	250	250	250	225	233	203	203	238	225	230	210	215	200	195	187	180	175	175						
23													214	221	203	225	225	250	250	225	233	203			225	225	215	200	200	200	198	162	175	175	170						
24											183	214	214	203	225	225	233																								
25										183	210	203	225	225	225	225	203																								
26									183	210	203	225	225	225	225	203	210																								
27								183	210	203	225	225	225																												
28							183	210	203	225	225	225	225																												
29					183	214	214	203	225	225	225																														
30				183	210	203	225	225	225	225	203																														
31			183	210	203	225	225	225	225																																
32		183	210	203	225	225	225	225	203																																
33	214	214	203	225	225	225	225																																		
34	203	225	225	225	225	203	218																																		
35	208	225	225	225	203																																				
36	200	200	217	203	210																																				

Figure 65. A. *EXCEL* template for the Calibration Area, with 500m^2 cells designated as either derived from a cross-section (light blue) or a well (outlined and labeled). B. *EXCEL* spreadsheet representing plan view slice of the thermal model at 2.5km below sea level. Bolded values represent measured data in wells.

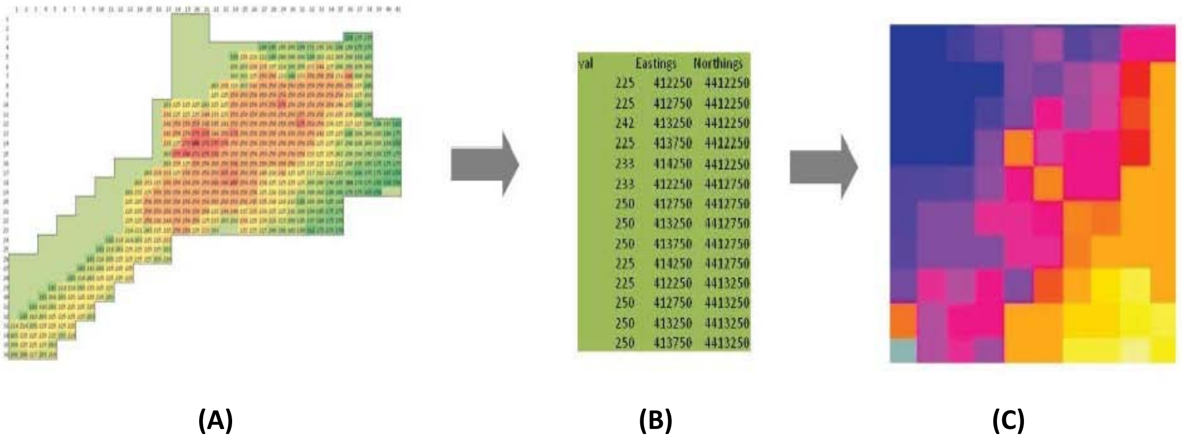

val	Eastings	Northings
225	412250	4412250
225	412750	4412250
242	413250	4412250
225	413750	4412250
233	414250	4412250
233	412250	4412750
250	412750	4412750
250	413250	4412750
250	413750	4412750
225	414250	4412750
225	412250	4413250
250	412750	4413250
250	413250	4413250
250	413750	4413250

Figure 66. (A) Data starts as plan view data in Excel; (B) is converted to tabular x, y coordinates; and (C) imported into GIS and converted to raster format.

8.6.2 Temperature

Temperature data has been derived from thermal sections presented in Plates 1 and 2 and is based on well data, shallow temperature gradients, and the conceptual convective model for the geothermal system active in the Calibration Area (Blackwell et al., (2005).

8.6.3 Stress Parameter

This parameter incorporates (1) fault/fracture orientation data, (2) Coulomb Stress Change/Dilatation from stress modeling results, (3) whether a structure is present or absent, (4) interpreted stress at structural intersections, occurrence of dilated zone (DZ), zone of compression (CZ) or neither.

Fault/Fracture Orientation

The *GIS* database was updated with the structures identified in Figure 49A. Faults with a strike of N30°E-N60°E were considered to infer favorable stress conditions as a fault oriented roughly N45°E ±15° would have a proper orientation to exhibit normal slip within the current stress regime. Another assumption was that gridded cells that have a specified fault orientation could be used to infer stress conditions in the surrounding cells or within 500 meters. All other orientations that did not fall in the N30°E-N60°E range were considered unfavorable, while gridded cells with no specified fault are considered unknown and weighted with a neutral rating. Fault dip direction was poorly constrained in areas and only considered where applicable.

Coulomb Stress Modeling

Using *Coulomb 3.1* stress modeling (see Section 7.2.2 and Appendix 13), a value of the expected CSC (-10 to +10 bars) and dilatation (-1 to +1 strain) can be calculated along a particular fault/fracture plane (for example, NE strike, 65° SE dip) within each given cell based on certain model constraints such as strike, dip, rake and maximum displacements along associated segments of the various range-front faults.

Fault Present/Absent

Whether a fault is present or absent in a given gridded cell within the Calibration Area has a viability inference on EGS Favorability and so has been incorporated into the integrated stress parameter. All faults gridded in the Calibration Area were derived from : State of Nevada, QFFDB, inferred structures from Blackwell and Smith (2002), inferred structures from the structure analysis in this investigation and geophysical gradients (see Section 7.2.1 and Figures 49A and 49B), structures inferred by gravity-magnetic modeling, and structures inferred by MT arrays. The presence of a fault within a given gridded cell is considered unfavorable for EGS due to induced seismicity concerns and potential loss of circulation zones, while the absent of a fault is considered more favorable for an EGS target. This point was a subject of debate among the team as the presence of a fault in a cell, increases the probability of that cell containing a dense fracture network, which would potentially make it more favorable for EGS when ignoring induced seismicity.

Compression and Dilated Zones

The intersections of major N-trending faults with the NE-trending structures within the DVFZ occur in several notable locations in the Calibration Area (Figure 48C). A localized stress change occurs at these intersections due to the fault orientation relative to the greatest principle stress and the apparent active strike-slip component along N-trending structures. The expected zones of compression and dilation that occur at these structural intersections show a high level of correlation with shallow thermal anomalies, well productivity, occurrence of fumaroles and geochemical data (including helium R/Ra ratios). Thus, this parameter has also been factored into the integrated stress rating. Dilated zones infer optimal stress conditions for EGS as faults/fractures are optimally oriented for normal slip in current stress regime and relatively lower S_{hmin} magnitudes exist, while zones of compression would infer slightly less favorable stress conditions, not optimally oriented and higher S_{hmin} values. One complication with incorporating this sub-parameter is a dilated zone would be expected to have geothermal fluids present at depth (hydrothermal) within open fracture networks which may not be favorable for EGS.

8.7 Favorability Mapping Process

The favorability and trust (described in Section 8.8) maps were produced using *ESRI's ArcGIS 10.0* software. *ArcGIS* software has many functions built in for analyzing data in different ways. A weighted overlay function was run on the data sets, incorporating slices of different data sets at the same depth. The use of this weighted overlay function requires the conversion of the data values to favorability values. A favorability value defines the favorability of EGS being present at a scale of one through nine. This scale was selected because it provides a neutral value (five) to describe data values which are not necessarily favorable or unfavorable and four variations of positive and negative favorability (slightly, moderately, very, and extremely).

Weights were also assigned to data sets. The reason for this is that certain data sets have a higher overall impact on favorability. For example, one can reasonably infer that temperature is a more powerful overall indicator of EGS favorability than the presence of faulting in a cell. The higher a data set's weight, the more its favorability values affect the final favorability of a cell. This allows for data sets to have a variable impact on the output, based on their importance to overall EGS favorability.

The weighted overlay function takes values from different data sets and creates a weighted average sum that is the output value for every cell. The input values of each data set must first be converted to a numerical value on a set scale. For example, favorability maps were produced by assigning favorability values on a scale of one through nine, with higher values indicating higher favorability, for each value in each data set, multiplying those values by each data set's weight (normalized to 1), then adding the sums of the weighted values in each cell. The following equation describes this process:

$$F_v = (d_0 * w_0) + (d_1 * w_1) + (d_2 * w_2) + \cdots + (d_n * w_n)$$

where F_v is the favorability value for a cell, d_0 through d_n is the favorability value of a cell's geoscience parameter data, and w_o through w_n is the weight for a particular data set (Tables 12 and 13).

A preliminary set of favorability values and weights used to create the initial favorability maps is described in Table 12. These favorability values/weights and maps were created to validate the methodology and data integrity. For example, if any glaring errors or obvious gaps in data were present, the input data would need to be scrutinized. No such errors or omissions were found in the draft maps, confirming the methodology with the output in line with expectations.

Before the final favorability maps were produced, a set of favorability values and weights needed to be created. To determine these values, an inquiry was circulated to the SMEs requesting that each SME express their opinion with respect to favorability and weight values, and the final version of these values was based on an unweighted average of all SME input received (Table 13). A method to determine favorability values quanitatively was discussed among the team, but not used to avoid a number of required assumptions.

8.8 Trust Maps

Upon review of the output of the preliminary favorability maps, a strong trend towards increased EGS favorability at depth was apparent. While this trend is a correct interpretation of the data used as input; the determination was made that it did not reflect our complete understanding (including our known uncertainties) of the region. While it is logical that more favorable lithological, stress, and thermal conditions exist at depth, our understanding of these regions is constrained by the quality and quantity of the data available. As a result it became apparent that a second set of maps, produced in a similar fashion as the favorability maps but describing the quality of the data used for input would assist in more complete understanding and assesment of the favorability maps.

Table 12. Preliminary weights and values used to test the generation of the favorability maps (see Section 8.7).

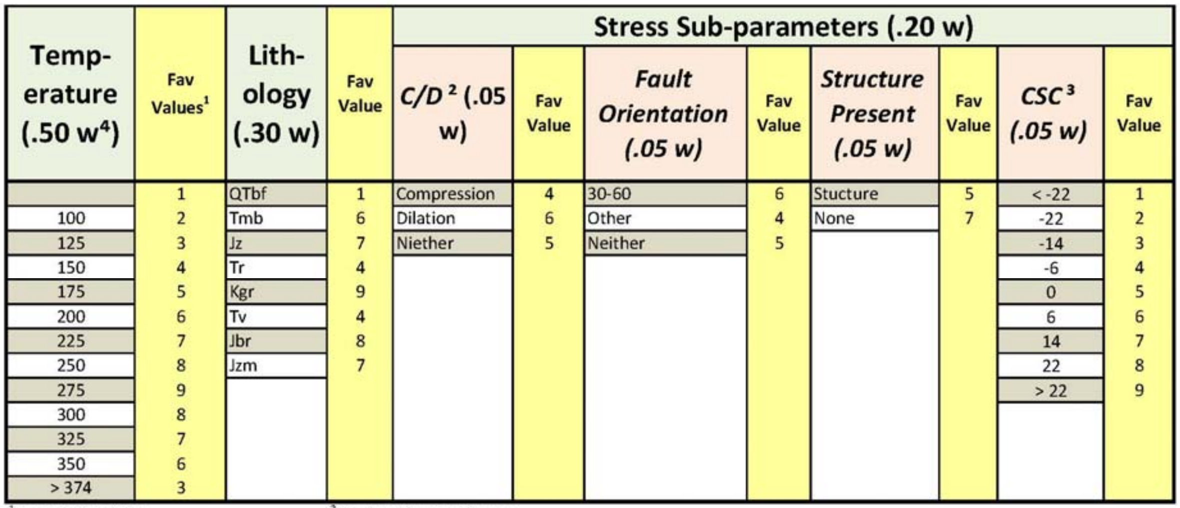

Temp-erature (.50 w[4])	Fav Values[1]	Lith-ology (.30 w)	Fav Value	Stress Sub-parameters (.20 w)							
				C/D [2] (.05 w)	Fav Value	*Fault Orientation (.05 w)*	Fav Value	*Structure Present (.05 w)*	Fav Value	*CSC [3] (.05 w)*	Fav Value
	1	QTbf	1	Compression	4	30-60	6	Stucture	5	< -22	1
100	2	Tmb	6	Dilation	6	Other	4	None	7	-22	2
125	3	Jz	7	Niether	5	Neither	5			-14	3
150	4	Tr	4							-6	4
175	5	Kgr	9							0	5
200	6	Tv	4							6	6
225	7	Jbr	8							14	7
250	8	Jzm	7							22	8
275	9									> 22	9
300	8										
325	7										
350	6										
> 374	3										

[1] Favorability Value
[2] Compression/Dilation
[3] Coulomb Stress Change
[4] Favorability weights

Each data value was scrutinized based on the method used to produce the data. While some data sets have a significant number of hard values, others are entirely modeled. A valuation of the data based on what we've described herein as a "trust factor" was then performed. The "trust factor" reflects the reliability of the data used to determine the favorability value on a cell by cell basis. As such, each cell of each data set was assigned a trust factor, either quantitatively or qualitatively. This trust factor was based on a scale of one through five, higher values indicating higher trust in the data, and is outlined in the following table (Table 14).

Hard data (5) is data which has been directly noted (e.g., geologic formation) or measured (e.g., temperature) in the field. Strongly modeled or interpolated data (4) is data which has been modeled or interpolated from a hard data point and is within one cell (500m) of that point. Weakly modeled or interpolated data (3) is data which has been modeled or interpolated, but is >500m from a hard data point and as such, is considered to be loosely constrained. Inferred data (2) refers to data which lacks hard value constraint, but can be inferred through other methodologies, such as thermal gradients for temperature data. Areas of no data (1) occur when no hard data are present to constrain values and no appropriate methodology exists to infer values.

The process of assigning these values to the existing data sets was primarily done manually in *EXCEL*. Hard data points, interpolated/modeled data points, and inferred data points had already been defined in the process of creating the original data sets. Each cell was assigned a trust value based on which of these methods was responsible for the data used and distance to the nearest hard data point. Six new data sets (temperature, lithology, stress factors) were created in this effort to describe the reliability of the original data sets. In some cases a trust factor could not be assigned to the modeled data directly due to a unquantified resolution or multiple inversions used in the modeling. In these cases, a value of 2.5 was used to assign a nuetral value to the data (e.g. Coulomb stress model).

Table 13. Final favorability and weight values using averaged values and weights based on Subject Matter Expert input.

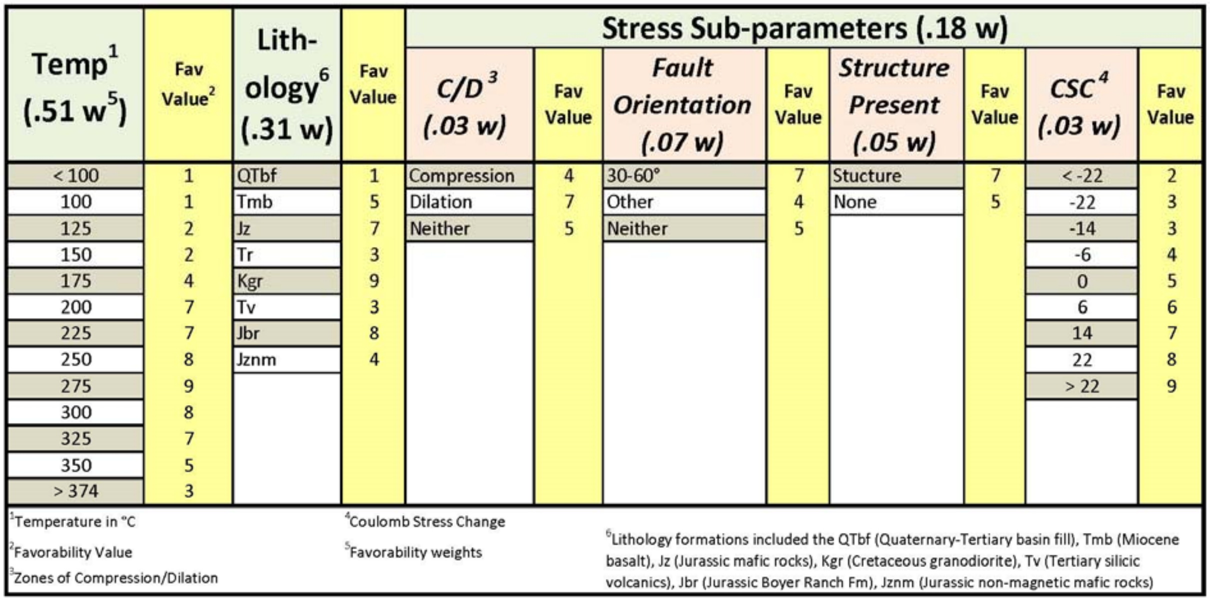

Temp[1] (.51 w[5])	Fav Value[2]	Lith-ology[6] (.31 w)	Fav Value	**Stress Sub-parameters (.18 w)**							
				C/D[3] (.03 w)	Fav Value	*Fault Orientation (.07 w)*	Fav Value	*Structure Present (.05 w)*	Fav Value	*CSC[4] (.03 w)*	Fav Value
< 100	1	QTbf	1	Compression	4	30-60°	7	Stucture	7	< -22	2
100	1	Tmb	5	Dilation	7	Other	4	None	5	-22	3
125	2	Jz	7	Neither	5	Neither	5			-14	3
150	2	Tr	3							-6	4
175	4	Kgr	9							0	5
200	7	Tv	3							6	6
225	7	Jbr	8							14	7
250	8	Jznm	4							22	8
275	9									> 22	9
300	8										
325	7										
350	5										
> 374	3										

[1] Temperature in °C

[2] Favorability Value

[3] Zones of Compression/Dilation

[4] Coulomb Stress Change

[5] Favorability weights

[6] Lithology formations included the QTbf (Quaternary-Tertiary basin fill), Tmb (Miocene basalt), Jz (Jurassic mafic rocks), Kgr (Cretaceous granodiorite), Tv (Tertiary silicic volcanics), Jbr (Jurassic Boyer Ranch Fm), Jznm (Jurassic non-magnetic mafic rocks)

Table 14. Scale used to assign trust values to existing data sets

Trust Value	Description
5	Hard data (measured, e.g., well)
4	Strong interpolation / model
3	Weak interpolation / model
2	Inferred
1	No data

The same weighted overlay function to define the favorability value was then performed on the trust data sets. The scale was modified for the maps to one through five to accommodate the scale of the trust factors. The same weights were used as in the favorability maps to preserve the respective impact of the data sets. Favorability and trust map pairs from +1km asl to -4km asl in 0.5km increments are presented as Figures 67 through 77 for average SME favorability values and weights. The favorability scale included in the figure is from 1-9 with 1 being represented by a dark blue and labeled *Very Unfavorable*, and a 9 being represented by magenta and labeled *Extremely Favorable*. The trust values scale shown is from 2-5, with 2 referring to little/no data (dark grey) and 5 referring to hard data (white).

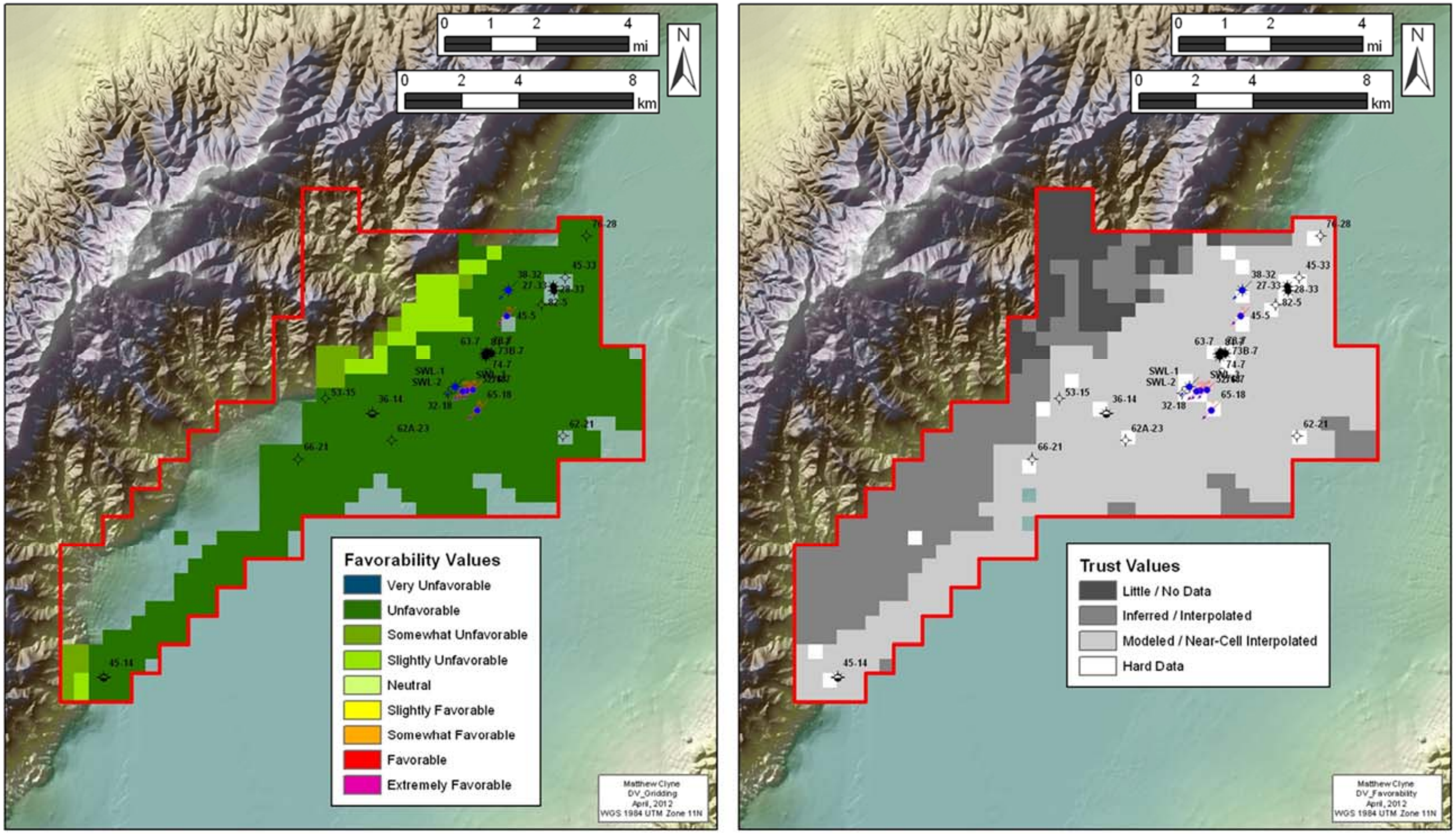

EGS Favorability-Trust Maps: Averaged Data and Weighting
Depth: 1.0km Above Sea Level

Figure 67. EGS Favorability map (left) and associated trust map (right) at 1.0km asl, the elevation of valley floor using average values based on Subject Matter Expertise input and weighting factors for temperature, lithology, and stress of 0.51, 0.31, and 0.18, respectively.

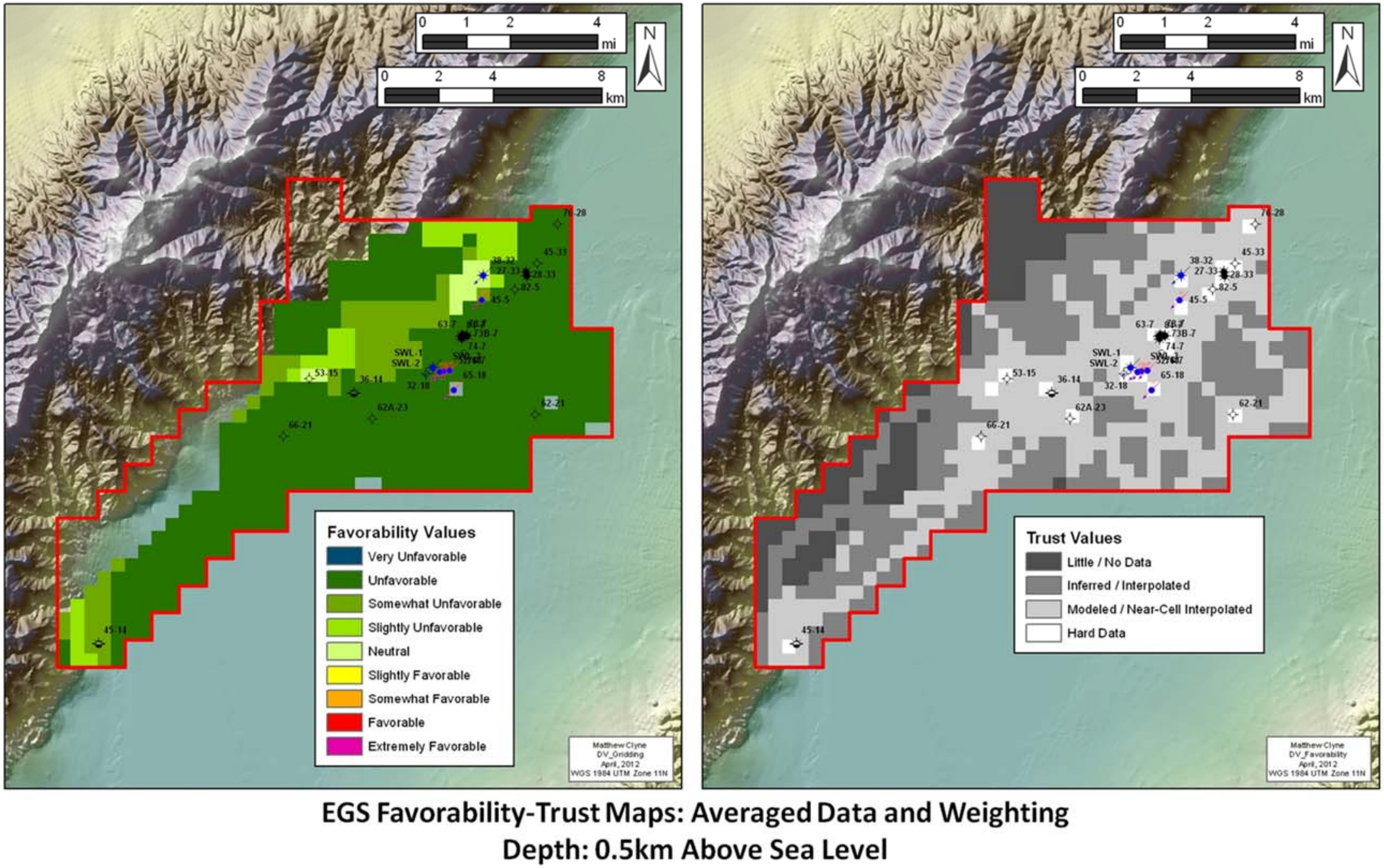

Figure 68. EGS Favorability map (left) and associated trust map (right) at 0.5km asl using average values based on Subject Matter Expertise input and weighting factors for temperature, lithology, and stress of 0.51, 0.31, and 0.18, respectively.

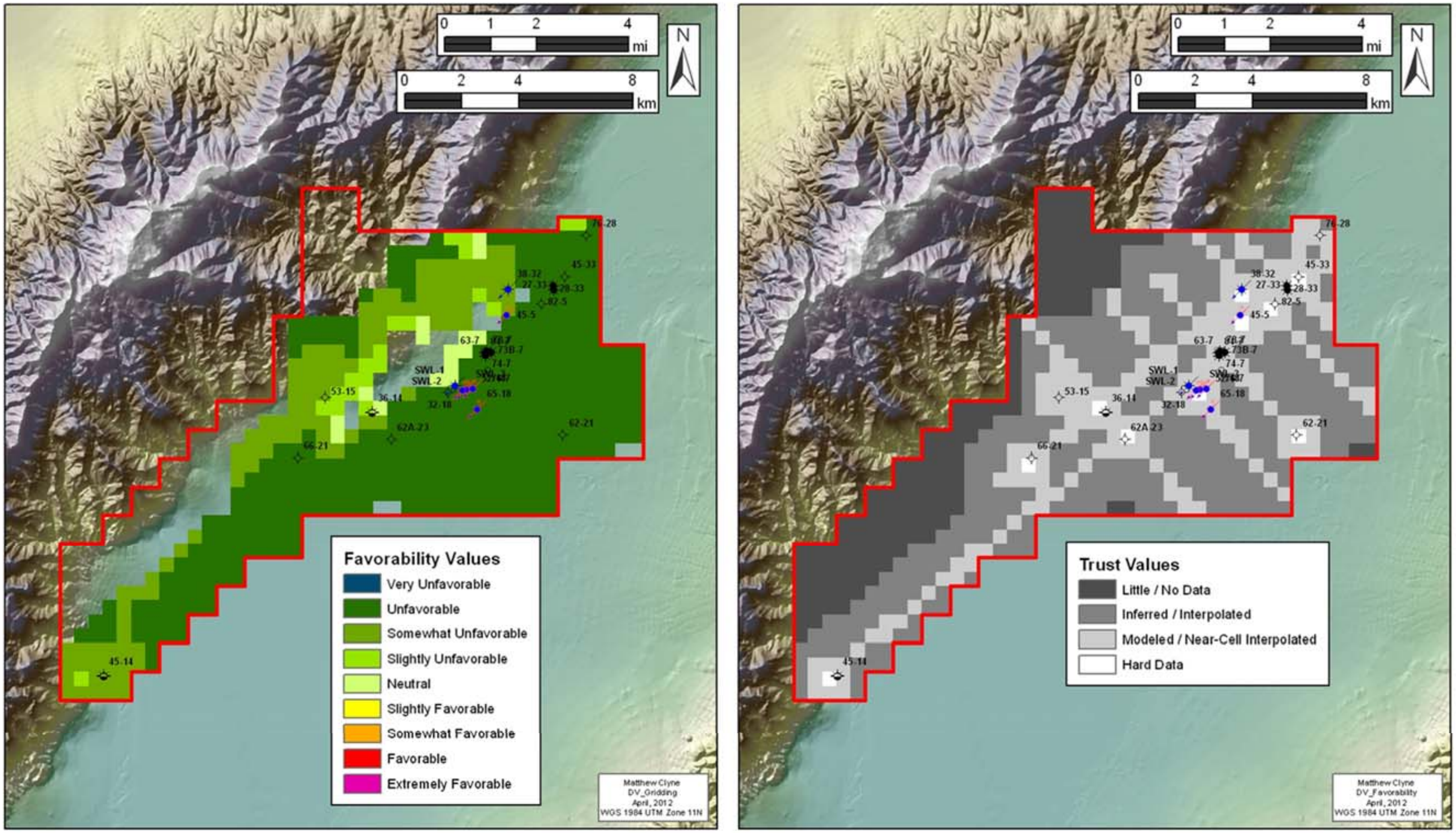

EGS Favorability-Trust Maps: Averaged Data and Weighting
Depth: 0.0km At Sea Level

Figure 69. EGS Favorability map (left) and associated trust map (right) at sea level (0km asl) using average values based on Subject Matter Expertise input and weighting factors for temperature, lithology, and stress of 0.51, 0.31, and 0.18, respectively.

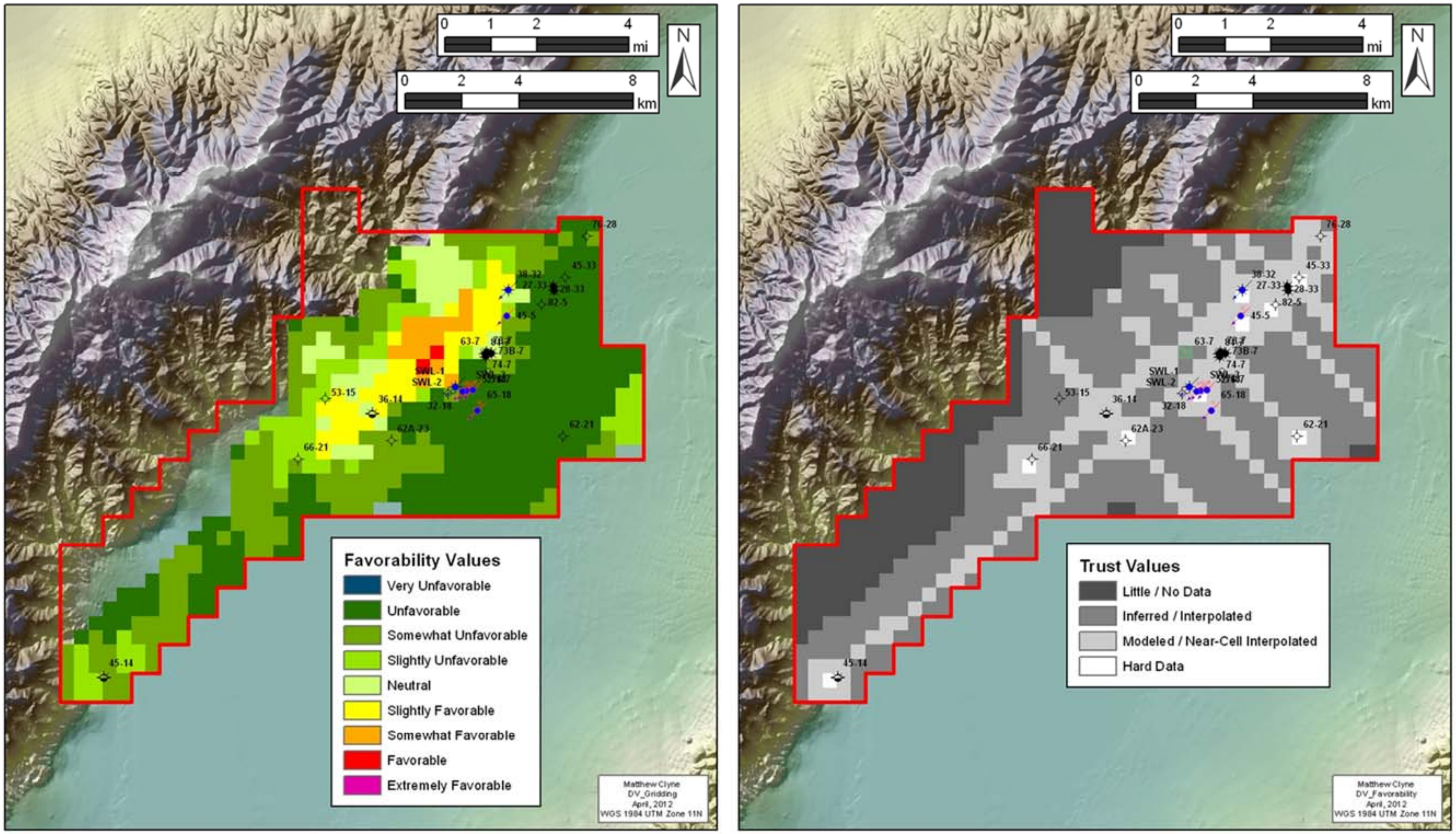

EGS Favorability-Trust Maps: Averaged Data and Weighting
Depth: 0.5km Below Sea Level

Figure 70. EGS Favorability map (left) and associated trust map (right) at -0.5km asl using average values based on Subject Matter Expertise input and weighting factors for temperature, lithology, and stress of 0.51, 0.31, and 0.18, respectively.

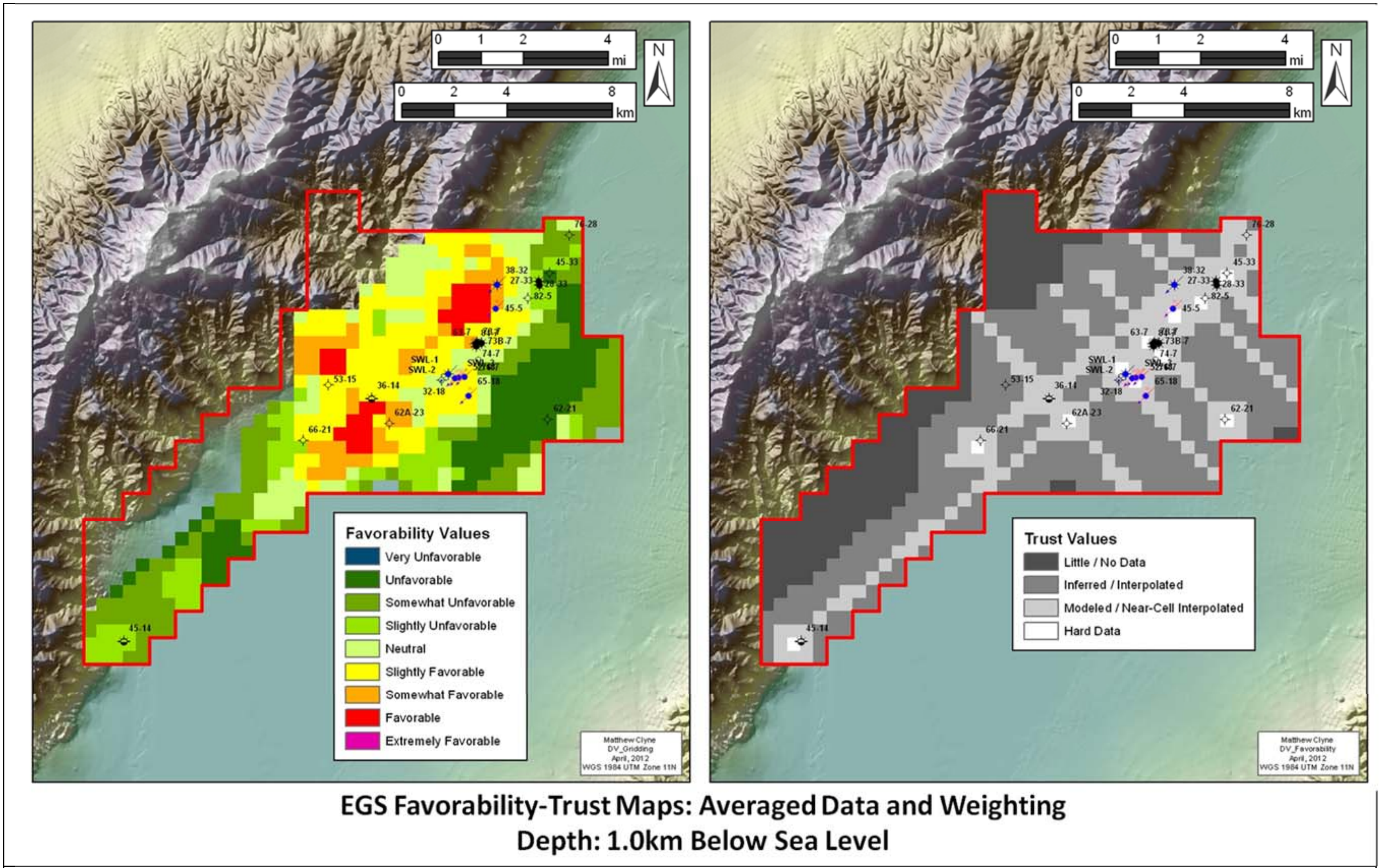

Figure 71. EGS Favorability map (left) and associated trust map (right) at -1.0km asl using average values based on Subject Matter Expertise input and weighting factors for temperature, lithology, and stress of 0.51, 0.31, and 0.18, respectively.

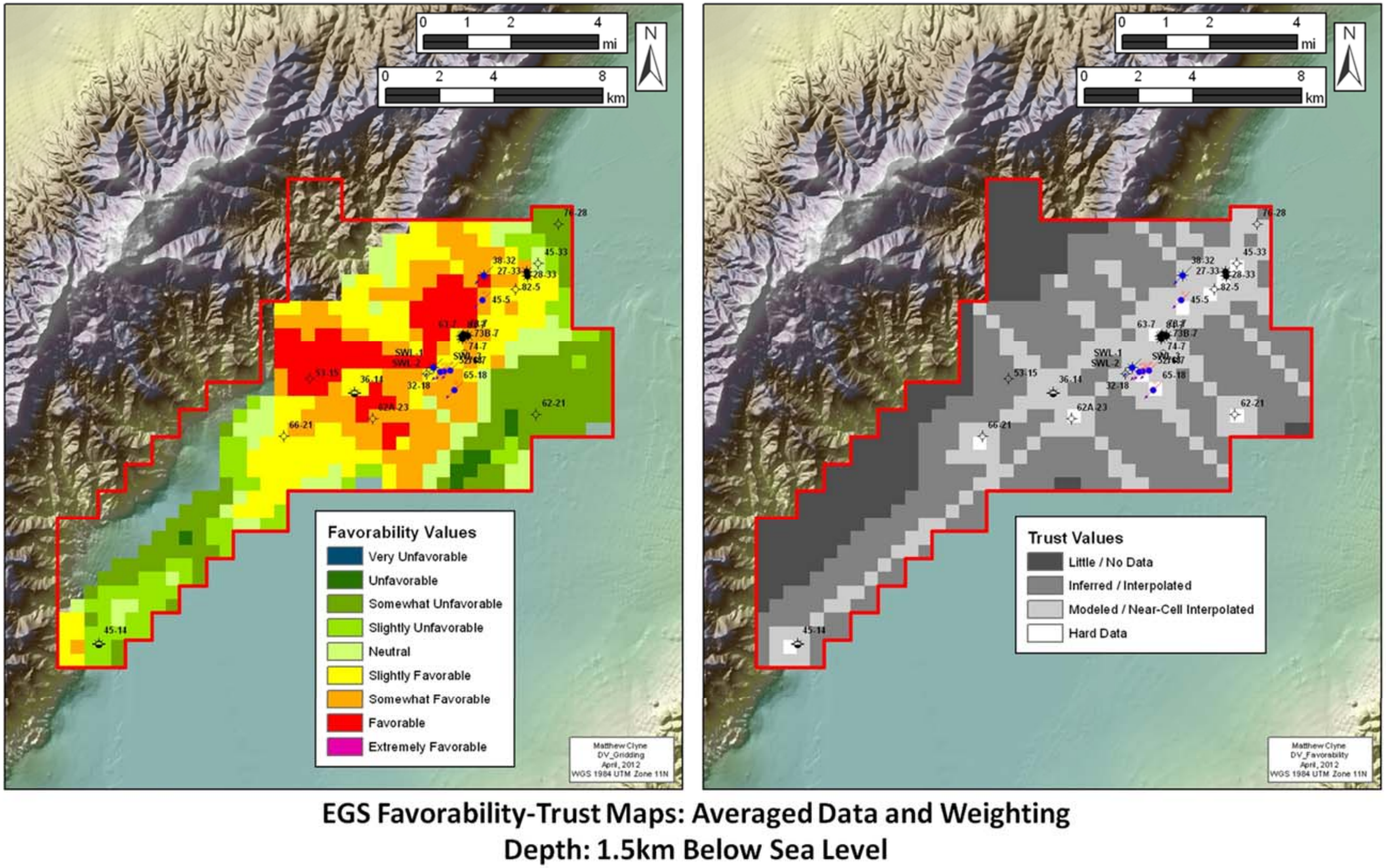

Figure 72. EGS Favorability map (left) and associated trust map (right) at -1.5km asl using average values based on Subject Matter Expertise input and weighting factors for temperature, lithology, and stress of 0.51, 0.31, and 0.18, respectively.

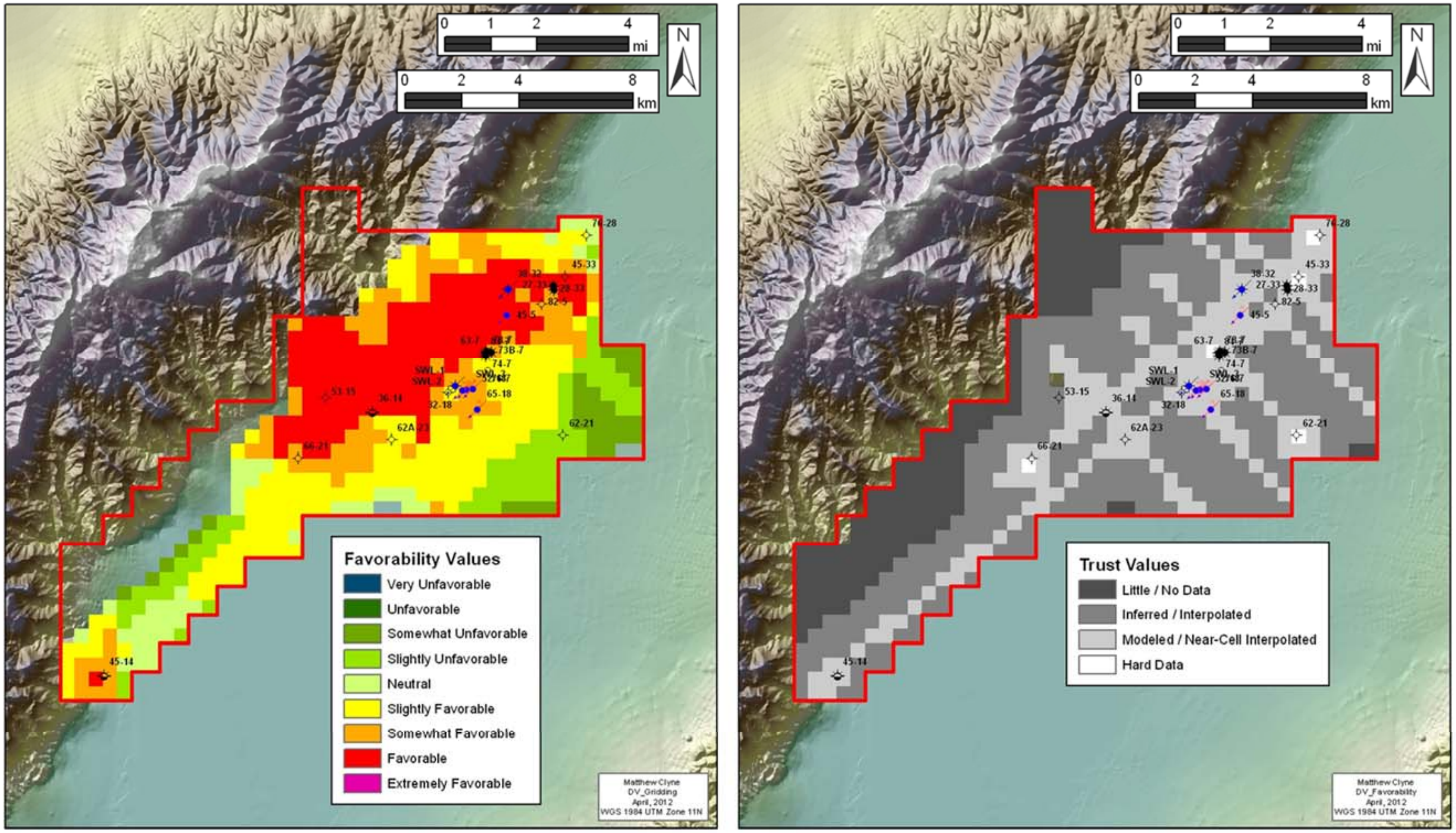

EGS Favorability-Trust Maps: Averaged Data and Weighting
Depth: 2.0km Below Sea Level

Figure 73. EGS Favorability map (left) and associated trust map (right) at -2.0km asl using average values based on Subject Matter Expertise input and weighting factors for temperature, lithology, and stress of 0.51, 0.31, and 0.18, respectively.

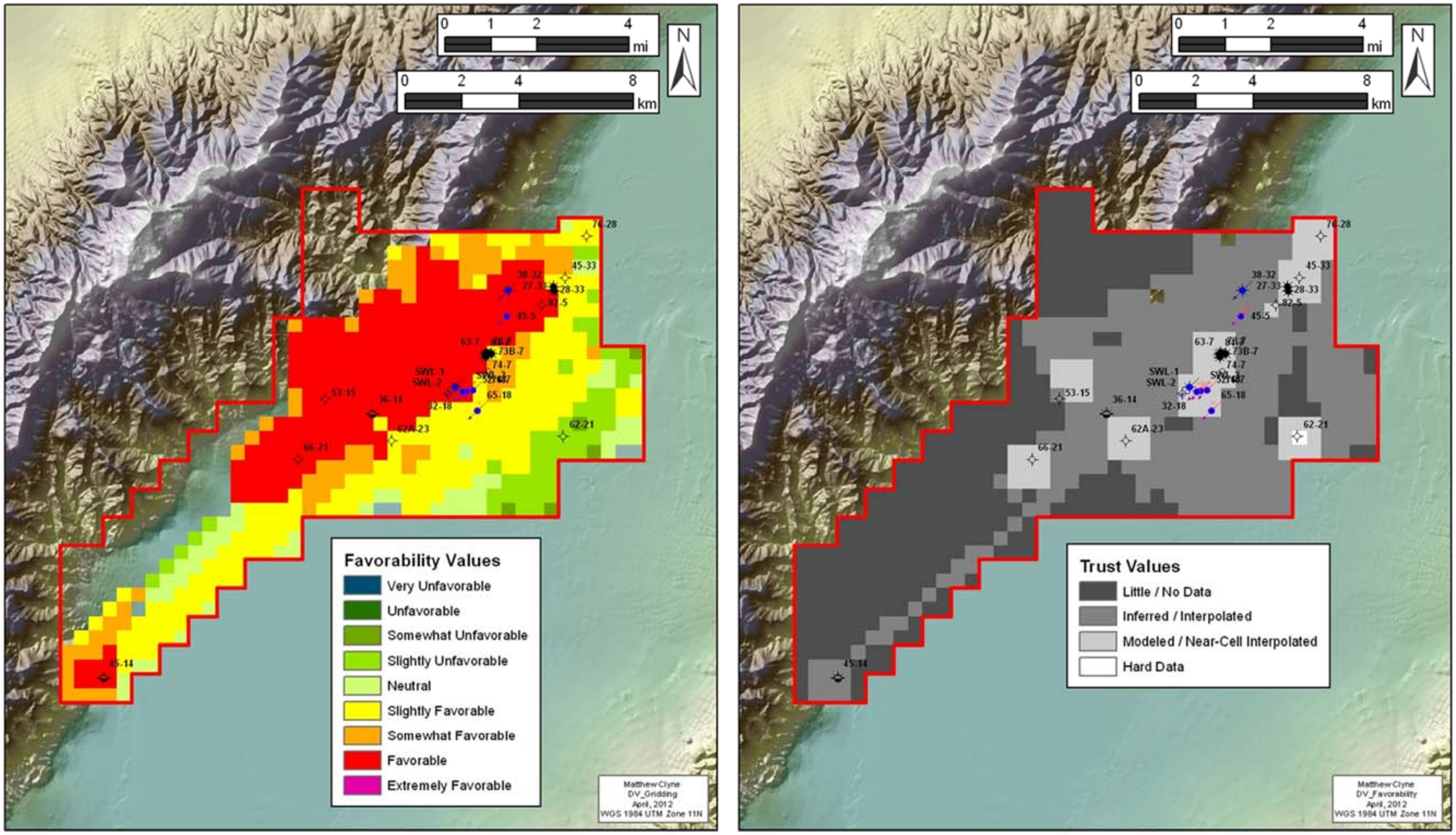

EGS Favorability-Trust Maps: Averaged Data and Weighting
Depth: 2.5km Below Sea Level

Figure 74. EGS Favorability map (left) and associated trust map (right) at -2.5km asl using average values based on Subject Matter Expertise input and weighting factors for temperature, lithology, and stress of 0.51, 0.31, and 0.18, respectively.

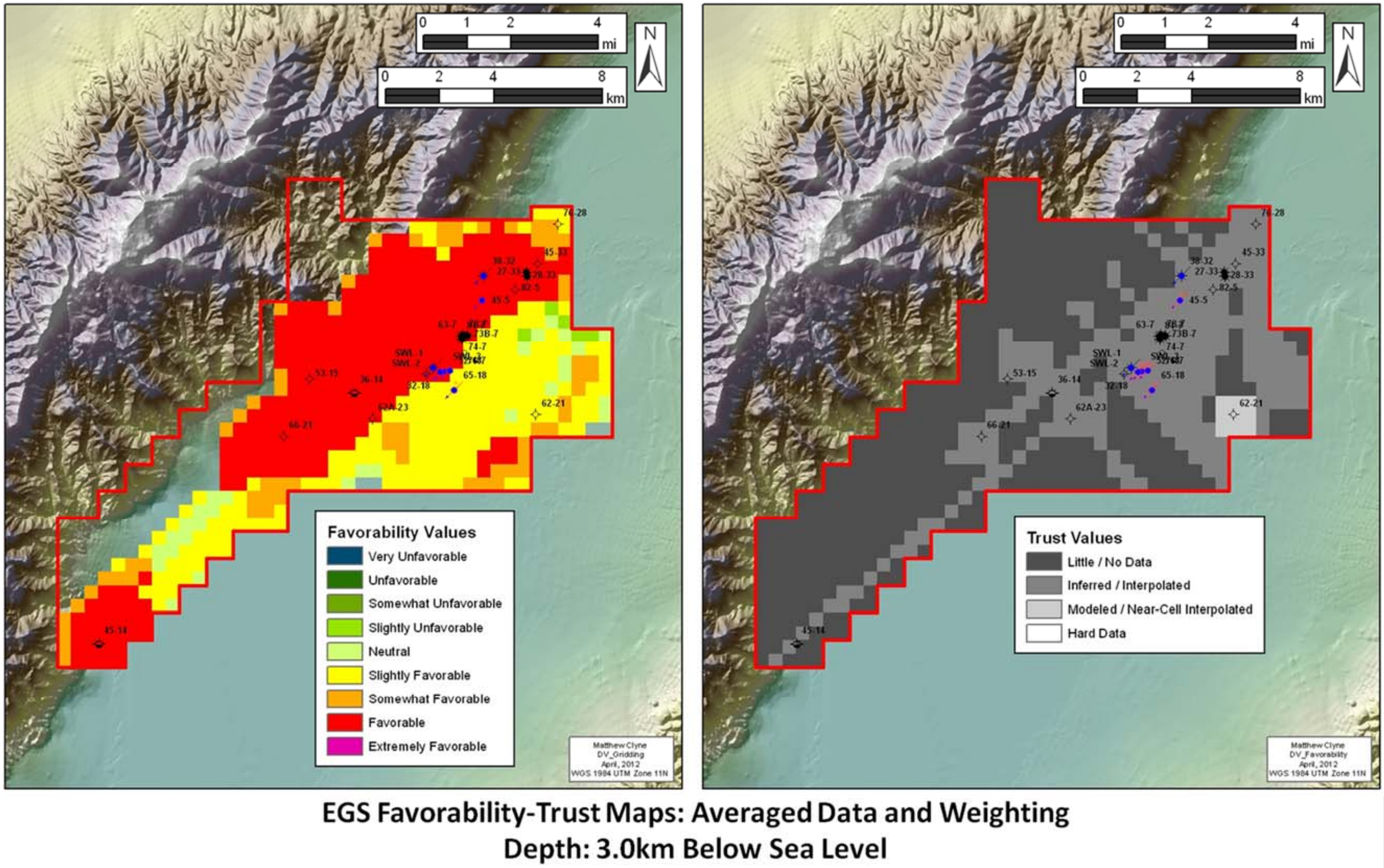

Figure 75. EGS Favorability map (left) and associated trust map (right) at -3.0km asl using average values based on Subject Matter Expertise input and weighting factors for temperature, lithology, and stress of 0.51, 0.31, and 0.18, respectively.

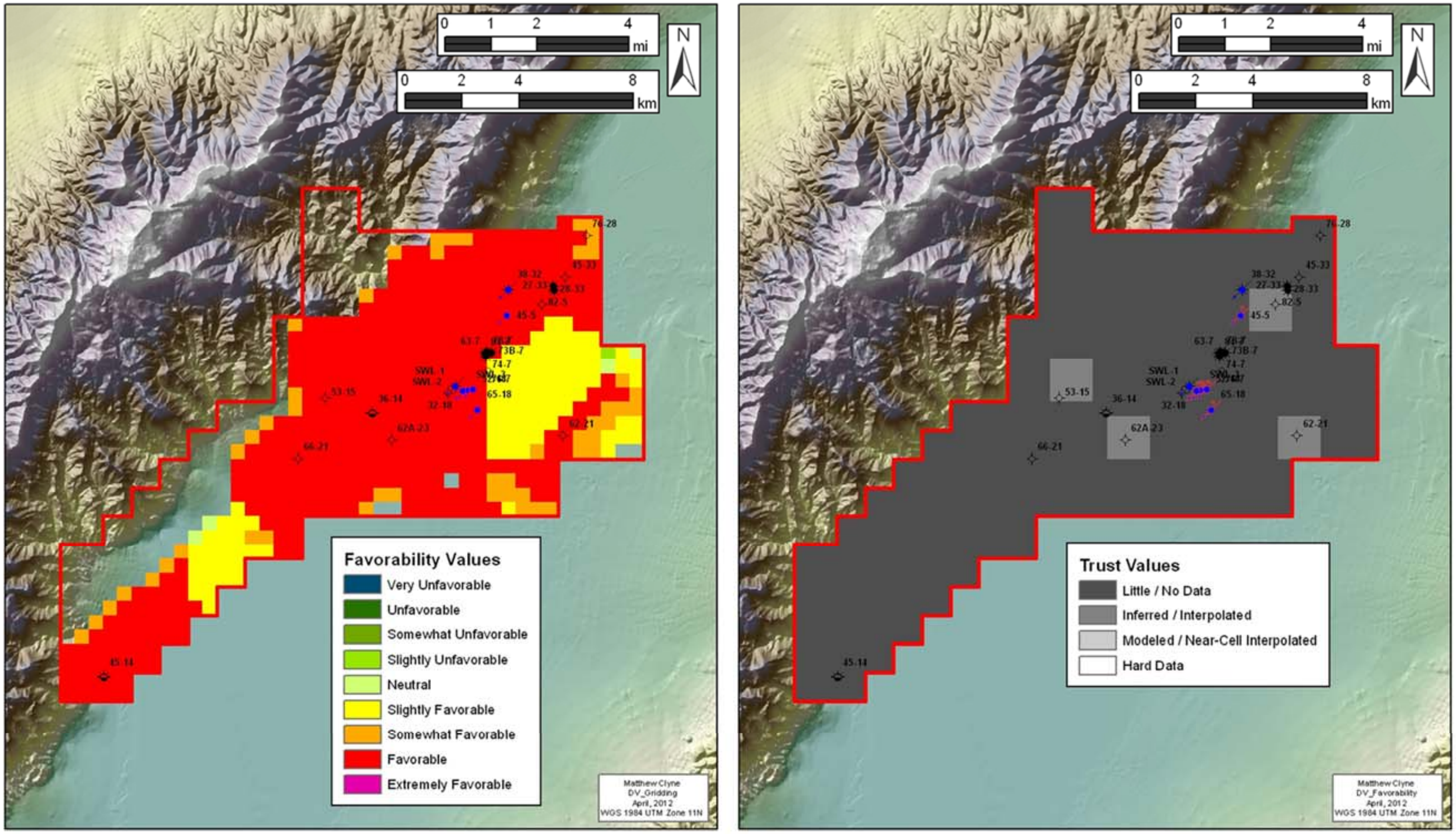

EGS Favorability-Trust Maps: Averaged Data and Weighting
Depth: 3.5km Below Sea Level

Figure 76. EGS Favorability map (left) and associated trust map (right) at -3.5km asl using average values based on Subject Matter Expertise input and weighting factors for temperature, lithology, and stress of 0.51, 0.31, and 0.18, respectively.

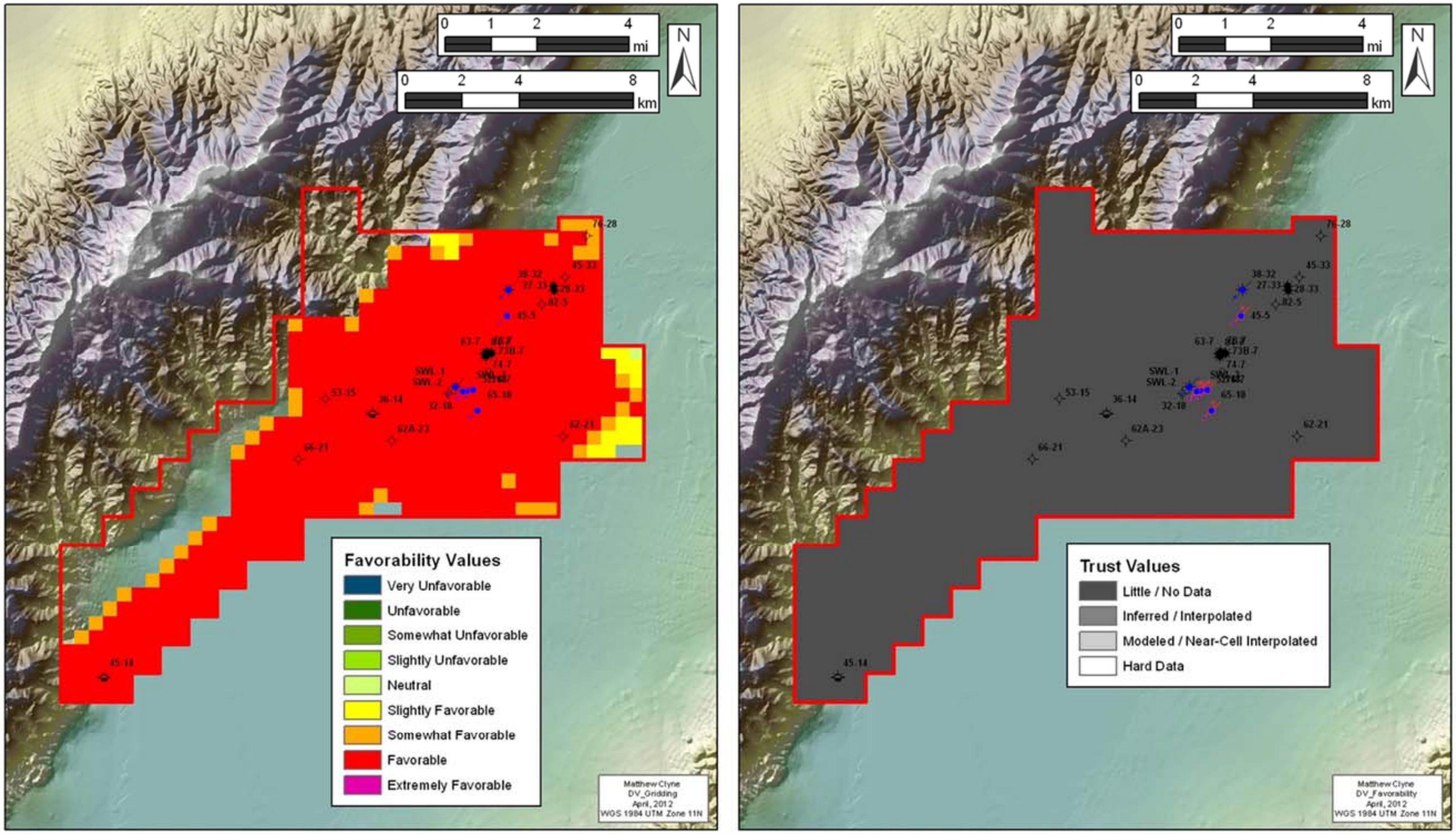

EGS Favorability-Trust Maps: Averaged Data and Weighting
Depth: 4.0km Below Sea Level

Figure 77. EGS Favorability map (left) and associated trust map (right) at -4.0km asl using average values based on Subject Matter Expertise input and weighting factors for temperature, lithology, and stress of 0.51, 0.31, and 0.18, respectively.

8.9 Results Calibration / Verification

The weights and favorability values used to create the favorability maps represent only one set of potential values. Using the opinions of the SME to infer the range of EGS favorability for the various data sets was considered the most accurate qualitative approach. More statistical or quantitative approaches to generate a unique set of favorability maps were explored (e.g., Dempster-Scafer Theory, Weights of Evidence, Hierarchical Modeling). The fact that the specific values of the various data sets that define potential EGS systems are obscure presents a problem for validation. Still, other possible methods exist which could provide insight on how to calibrate or verify our results.

Parametric analysis was used to examine relationships between the different variables. While the significant effort made to quantify the relationships between the various datasets, described in the geostatistics section (Section 7.4), it is possible to apply a similar approach using favorability maps. By altering the favorability values and weights in an organized manner, producing a large number of different favorability realizations, and comparing the output of these models with each other, it is possible to gain a better understanding of the relationships between the data sets. This process is time intensive and a methodology for implementing such an approach was beyond the scope of this project. However, such an approach is meritorious.

For practical considerations using the baseline data, we only examined the variation on potential favorability map outcome using the following two data sets:

1. Averaged Favorability Values and Average Weights derived from the SMEs, see Figures 67-77); and
2. Averaged Favorability Values derived from the SMEs with Equal Weights, see Appendix 21.

8.9.1 Averaged Favorability Values and Average Weights derived from the SMEs

The set of favorability and trust map pairs based on an average favorability value and average weights derived from the SMEs are shown in Figures 67-77. The favorability values for the respective data sets and the weighting of each data set were averaged from a poll of team SME. These values are given in Table 12.

While the favorability values increase with depth due the increased temperature and the presence of basement rocks (granodiorite), the paired trust maps show that the data from the lower depth intervals (-3.5 and -4.0 asl) are of very poor quality. Thus, even though the depth intervals are considered favorable, one must take into consideration the level of confidence in the data, i.e., the Trust Maps. The upper three maps (Figure 67-69) are generally unfavorable (1-5) as temperatures have not been reached levels suitable for EGS conditions. At -0.5km asl (Figure 70), a NE-trending area coincident with the DVFZ begins to show higher favorability values. This is due to elevated temperature along the fault zone due to convective processes, the presence of the Jurassic mafic rocks (a good EGS candidate rock type), and stress conditions that favor normal slip under the current stress regime (NE-aligned structures). At 1.0km and -1.5 km asl (Figure 71 and 72) three distinct areas are favorable including within the DVPP area, the vicinity of the bottomhole location of 36-14 at the Stillwater Range contact, and the block between the range-front fault and the piedmont fault to the northwest of the producing area. At the depth intervals -2.0km and -2.5km (Figures 73 and 74) the entire area DVFZ is considered favorable due to the elevated temperature and adequate stress conditions, while the lithology input is mixed.

Overall, the maps show that the area within the DVFZ is favorable for EGS, while the area within the valley in the vicinity of 62-21 is somewhat less favorable. This agrees with the large amount of evidence that supports the notion that the geothermal systems present in Dixie Valley are dependent on convective processes within the DVFZ. The area considered favorable does not extend southwest of 66-

21 (Figure 75), as there is limited data between this well and the 45-14. The gap of favorability between the DVPP and 45-14 to the SW could likely be due to a lack of data to determine favorability and decreased temperature estimates based on the limited surrounding data points. This area was a point of focus for the new data collection outlined in Task 4 of the project to enhance geophysical data resolution.

8.9.2 Averaged Favorability Values derived from the SMEs with Equal Weights

While the favorability values for the respective data sets did not change, an equal weighting scheme considering the three critical EGS parameters as well, i.e., temperature (0.32), lithology (0.32) and stress (0.34), was used to determine the variability between this approach and the one described above (Appendix 21). One important note is with the decrease for the temperature weighting (0.51 to 0.32) the maps are more reliant on the lithology and structure, and less so on the known elevated temperatures along the DVFZ. At the shallow depth of 1km below the valley surface (Appendix 21-Figure 4), the area west of the producers already shows *Somewhat Favorable Value* (rating of 7) relative to the previous realizations which was *Unfavorable and* described in Section 8.9.1. At -1.0km asl, the three distinct favorable areas identified by the Average Weighting Realizations are less pronounced and mostly have slightly lower favorability ratings of 7 (orange).

At -2.0km asl, the favorable area (rating of 8 shown in red) is much more confined to the piedmont and more dependent on the structure than the temperature. At -2.5km and -3.0km asl, the area of high favorability occurs within the structural block between the range-front and piedmont fault. Interestingly, the NE-oriented fault that intersects 62-21 in the valley, shows a *Somewhat Favorable* rating, even though there is no elevated temperature along this structure. The lowermost depth intervals show more varied favorability than the averaged realizations (Figures 74 and 75), yet are still confined to known structures.

It should be noted that since the SMEs value temperature highly and temperature increases with depth everywhere, the equal weights analysis tends to score shallow areas as being more favorable and deep areas as not as favorable. Consequently, the SMEs believe the equal weight analysis presented in this subsection does not accurately assess the EGS exploration requirements.

APPENDIX 1

GEOLOGIC MAPS

Table of Contents

List of Figures

Geologic Map

of the

Humboldt Lopolith

and surrounding terrane,

Nevada

R. C. Speed

Quaternary		Qs	upland slide deposits
		Qal	alluvium and lake deposits
		QTb	basalt
Tertiary		Tvs	rhyolitic rocks and associated sedimentary rocks
		Ta	andesite
Cret.		Kg	granodiorite
Jurassic, middle	Humboldt lopolith	gbx	polymict breccia of lopolith rocks age uncertain
		Jgk	keratophyre fine-grained igneous albitic rocks; locally quartz keratophyre
		Jgx	mixed albitic rocks mixed keratophyre, albitized metasedimentary rocks, albitized gabbro
		Jgd	diorite and quartz diorite feldspathic (An_{0-40}) rocks transitional between gabbro and keratophyre
		Jg1 Jg2 Jg3	hornblende gabbro and anorthosite: Jg1: generally unfoliated variable grain size and color index Jg2: moderately foliated locally well-layered Jg3: strongly foliated
		Jgp	hornblende picrite
		Jgm	microgabbro locally microdiorite
		Jgs	scapolitite
		Jvm	volcanic rocks, chiefly massive: lava, breccia, dikes
		Jvs	volcanic rocks, chiefly stratified: volcanic sedimentary rocks and lava
Jurassic, lower	Fencemaker allochthon	Jl	Lovelock Formation
		Jb	Boyer Ranch Formation
		Jm	Muttlebury Formation
		Jal	limestone of Grimes Canyon
Triassic, upper	Fencemaker allochthon, pelite sequence	JTRs	pelite, limestone and sandstone
		TRs	pelite and sandstone
		JTRm	Mud Springs Canyon Formation
		TRh	Hoyt Canyon Formation
		TRb	Bernice Formation
Triassic, lower and middle	carbonate sequence	TRu	post-Star Peak strata
		TRsp	Star Peak Group
		TRr	Koipato Group

Wildhorse thrust

Boyer thrust

Fencemaker thrust: dashes indicate inferred trace

attitude of homoclinal bedding extending ≥ 200 m.

attitude of igneous foliation

contact

thrust fault: teeth on upper plate
BT Boyer thrust
FT Fencemaker thrust
WT Wildhorse thrust

high-angle fault

depth to basement (pre-Tertiary rocks) below topographic surface; units in feet

Published by The Geological Society of America, Inc.
3300 Penrose Place
Boulder, Colorado 80301

PRELIMINARY GEOLOGIC MAP OF A PART OF THE STILLWATER RANGE, CHURCHILL COUNTY, NEVADA

By Ben M. Page

INTRODUCTION

That part of the Stillwater Range which lies in Churchill County is largely composed of Upper Triassic strata and a remarkable succession of post-Triassic volcanic and intrusive rocks. It contains important thrust faults, one of which may have resulted from gabbroic intrusion. There are many later normal faults, and recent movements on some of them have caused earthquakes.

Background information is available concerning the adjacent Mount Tobin 30' quadrangle (Muller, Ferguson, and Roberts, 1951), and the Buffalo Mountain 15' quadrangle (Wallace and others, 1959). Both quadrangles lie north of the area of this report. The geology of the Sand Springs Range to the south is described in a report for the Atomic Energy Commission by the University of Nevada (1962).

Most of the writer's field work was carried out in the summers of 1956-1958 and 1961, but some was done at other intervals. The Stanford University class in Field Geology made detailed geologic maps in the Sand Springs district in 1946, 1947, and 1951. The writer is indebted to the students and instructors, and to Prof. R. R. Compton in particular. Chapman Young (1963) studied an area extending north from White Cloud Canyon and this work has been very helpful. Important identifications of fossils from the Stillwater Range have been made by Prof. S. W. Muller and by Mr. N. J. Silberling. In recent years, Mr. R. C. Speed studied a gabbroic complex and related thrust faulting in the northern part of the Stillwater Range as well as the ranges to the west and east. He has been an invaluable source of ideas, encouragement and helpful criticism, and has kindly read this manuscript.

The writer wishes to thank the Geological Society of America and the Shell Companies Foundation for generous financial support.

ROCK UNITS

SEDIMENTARY ROCKS OF PALEOZOIC OR MESOZOIC AGE

Quartzites (qtz on map) of unknown stratigraphic position are found near Cox Canyon and north of IXL Canyon. The quartzite at Cox Canyon is almost wholly quartz sand with local interstitial calcite, it is free of shale intercalations, and it is several hundred feet thick. In these respects it resembles the Jurassic(?) quartzite of Cottonwood Canyon (see below), but it differs in being slightly coarser, less uniform in grain size, and in containing more smoky, rounded grains.

Various limestones (ls) and metasedimentary rocks (ms) occur in klippen and in small remnants engulfed in the gabbroic complex of the northern part of the map area.

TRIASSIC ROCKS

Metasedimentary rocks (T̄Rms)

Metasedimentary rocks adjacent to U. S. Highway 50 east of Sand Springs may represent more than one system. Included are: black chiastolite- and chloritoid-bearing phyllite; graphitic schist; metamorphosed silty, calcareous sediments; limestone, marble, and calc-silicate rocks; schistose sandy siltstone and graywacke; "stretched-pebble" conglomerate; quartz-muscovite schist; and schistose tuffaceous(?) material. The only fossils found in these rocks were collected in a single locality 1.2 miles west-northwest of the Summit King mine. They were identified as Myophoria sp. and Alectryonia(?) by S. W. Muller (oral communication, 1946), who suggests a probable Late Triassic age. The rock types of the vicinity contrast markedly with the Upper Triassic slates to the north, implying local depositional differences or tectonic transport.

Upper Triassic slate and phyllite (T̄Rsl)

Slate derived from marine muds is the most prevalent rock in the central part of the mapped area. Most is gray-black, weathering to pale gray, greenish gray, or light tan. The slaty cleavage is approximately parallel with the bedding except in the axial parts of folds where it is parallel with the axial planes. Recrystallization is generally only incipient, but in the vicinity of granitic bodies the rock contains chiastolite porphyroblasts .02 to 2 inches long. In a few areas phyllite prevails over slate.

Some of the slate sequence includes abundant fine-grained feldspathic quartzite interbeds 1 to 35 inches thick. These beds display a fascinating variety of sole marks, including flute casts, fillings of organic trails, and assorted convexities of unknown origin. Some quartzite beds show small-scale crossbedding, and the upper surfaces of many are covered with crescentic undulations that are thought to be linguloid ripple marks. All of these features are useful in determining tops and bottoms of folded strata. Generally the quartzite beds are thin and widely spaced, but just south of Shanghai Canyon, in lower Hare Canyon, and in a few other localities, there are rock sequences 50 to 300 feet thick in which quartzite predominates over intercalated slate.

Parts of the slate succession are interrupted at intervals by gray-weathering limestone beds 1 to 60 inches thick. More rarely, limestone occurs in prominent units 1 to 50 feet thick. Many of the carbonate rocks are calcarenites, and some contain limestone conglomerate and bioclastic material. Certain thin, lenticular carbonate beds are ferruginous and weather orange-brown.

The lower part of the section, just above the Cox Canyon thrust zone, differs from the bulk of the overlying slate, although it is not distinguished on the map. It is mainly lavender-weathering silty shale that locally contains black flinty streaks and nodules. Many thin black to gray limestone beds occur in this unit.

The stratigraphic thickness of the slate, phyllite, and interbedded rocks cannot be measured because of complex deformation, but it is estimated to be 5,000 to 10,000 feet, of which less than 10 percent is quartzite and limestone. The lavender silty shale member at the bottom of the exposed section is about 500 feet thick.

The slate and associated rocks, including the lavender silty shale, are Late Triassic in age, probably representing part of the Karnian and all of the Norian stages. This is indicated by poorly preserved fossils identified by S. W. Muller and N. J. Silberling, as summarized in the table below. It is concluded that parts of the slate sequence are chronologically equivalent to much of the Grass Valley, Dun Glen, Winnemucca, and Raspberry Formations of the Mount Tobin and Winnemucca quadrangles to the north (Muller, Ferguson, and Roberts 1951; Ferguson, Muller, and Roberts 1951; Silberling and Roberts, 1962).

FOSSILS FROM SLATE AND INTERCALATED STRATA (T̄Rsl), STILLWATER RANGE, CHURCHILL COUNTY, NEVADA 1/

	Fossil	Probable Stratigraphic Position	Area of occurrence*					
			1	2	3	4	5	6
Hydrozoan:	Heterastridium sp.	U. Triassic; u. Norian		x				
Coral:	Isastrea sp.	U. Triassic		x			x?	
Pelecypods:	Halobia sp.	U. Triassic; Karnain or Norian	x	x	x?	x?		x?
	Monotis sp. (locally, M. subcircularis Gabb)	U. Triassic; Norian		x		x		
	Plicatula?	U. Triassic?		x				
Ammonites:	Arcestes sp.	M. or U. Triassic	x	x				
	Juvavites?	U. Triassic		x				
	Choristoceras?	U. Triassic; u. Norian	x					
	Paratibetites?	U. Triassic; Norian		x				
	indet. trachyceratid	M. or U. Triassic			x		x	
	Malayites?	U. Triassic; top of lower Norian		x				
Belemnite:	Asteroconites sp.	U. Triassic; Norian		x				

*Area
1. Lavender silty shale 0.5 to 1 mile south of Cox Canyon.
2. Main slate terrain, Cox Canyon to White Cloud Canyon.
3. Slate area surrounding Hare Canyon.
4. Slate area near Fortieth Parallel, W. side of range.
5. Slate area near Fortieth Parallel, E. side of range.
6. Slate area between Mountain Well Rd. and Eleven Mile Canyon.

Note: Question mark after genus means identification is not certain. If identification is erroneous, the indicated stratigraphic position (middle column) may not apply.
Question mark after "x" in righthand columns means the indicated generic identification is not certain in that particular area because of poor fossil preservation.

1/ (Specimens collected by B. M. Page, and identified by S. W. Muller and/or N. J. Silberling, mainly 1956-1964).

The Upper Triassic sedimentary rocks of the region to the north of the mapped area are believed to have been deposited as part of a delta in a shelf sea, of which the shoreline lay to the east and southeast (Silberling and Roberts, 1962, p. 37; Silberling, oral communication, 1963). In the Stillwater Range, the features of the Upper Triassic slate and interbeds of quartzite seem to fit this hypothesis.

Undifferentiated limestones (T̄Rls)

A large sheet of black to gray Upper Triassic limestone forms much of the upper plate of the La Plata thrust between Mountain Well Road and Eleven Mile Canyon. Surprisingly few fossils are present, but three localities yielded the following, kindly identified by N. J. Silberling: Halobia sp., Monotis sp., Placites sp., and Metasibirites sp. All denote a Late Triassic age, and the strata containing Placites are referred to the middle or upper part of the Norian stage. Therefore the limestone is the same general age as part of the Upper Triassic slate sequence upon which it rests tectonically, implying significant lateral transport of rocks deposited in a different environment from that of the slate.

Other limestones labeled " T̄Rls" on map are known to be Triassic, and may possibly belong to the formation just described. Perhaps some of the limestone klippen of unknown age, labeled "ls" are similarly related.

JURASSIC ROCKS

Lower Jurassic limestone and shale (Js)

An unnamed formation in the Hughes Canyon (which extends from the adjacent Buffalo Mountain quadrangle into the northernmost part of the mapped area), is characterized by tan-weathering, platy, silty limestone and calcareous shale. It also includes a few relatively pure limestone beds. N. J. Silberling identified psiloceratacid ammonites from the silty limestone, and considers these to represent the Hettangian or Sinemurian stages of the Lower Jurassic. He found Upper Triassic fossils (Monotis Subcircularis, Halorites sp., Placites sp., and Rhabdoceras sp.) in rocks a few tens of feet distant. It is likely that the lowermost part of the silty limestone formation is Upper Triassic, but the bulk of it is certainly Lower Jurassic. The relationship of this formation to the Upper Triassic slate is doubtful. The contact may be a thrust fault, but the writer is inclined to think it is depositional. If the contact is depositional, the Hughes Canyon section is overturned, as the Jurassic beds dip toward the Triassic terrain and Monotis locally occurs above the Jurassic strata.

Jurassic rocks like those of Hughes Canyon are found in a small area in White Cloud Canyon, but are omitted from the map. Similar rocks are seen at the mouth of Fondaway Canyon. A more important occurrence 1 to 2 miles north of White Cloud Canyon has been carefully studied by Young (1963), who believes that the Jurassic section he examined is in depositional contact with the Upper Triassic slate. He found the following ammonites, which were identified by S. W. Muller: Waehneroceras sp. (indicative of Hettangian stage), Euphyllites sp. (Hettangian), Caloceras(?) sp. (Hettangian), Arietitidae (Sinemurian - L. Pliensbachian), Phylloceras sp. (Sinemurian - Valanginian), Dactylioceratidae(?) (L. Pliensbachian - Toarcian), Hildoceratidae(?) (U. Pliensbachian - Toarcian), and Harpoceratinae(?) (U. Pliensbachian - Toarcian). The Lower Jurassic Hettangian and Sinemurian stages are definitely represented, the Pliensbachian may be present, and the Toarcian is strongly indicated. Young points out that the maximum stratigraphic thickness is only 200 to 500 feet, and this, coupled with the phosphatic nodules observed in some beds, suggests slow deposition during a long time span. J. Corvalan (1962) found 1600 feet of Lower Jurassic strata in the Westgate area 40 miles to the south.

Jurassic(?) metavolcanic rocks (Jmv)

Between La Plata Canyon and Mountain Well Road is a sequence of altered and locally schistose rocks of which at least half are volcanic and the remainder sedimentary. The following are included: fine-grained slaty andesitic tuffs, schistose andesitic tuff-breccias, breccias, thin andesite flows, graphitic slate, quartzite, calcareous sandstone, and thin conglomerate lenses. The volcanic members retain few, if any, original minerals but show indicative relict textures. The presumed andesitic composition is not certain. Although the sedimentary members are better preserved, they are unfossiliferous. The formation is probably marine, at least in part, and it is more than 5,000 feet thick.

The metavolcanic rocks appear to rest unconformably upon allochthonous Upper Triassic limestone (T̄Rls). A "basal" breccia 25 to 100 feet thick, lies upon, and occupies fissures in, the limestone. However, the clasts of the breccia are obscure, white, altered material of probable volcanic origin rather than detritus from the underlying formation. The contact might possibly be a thrust fault; if it is not, the metavolcanics are post-Upper Triassic, but are older than the Late Jurassic orogeny which resulted in metamorphism and deformation. The Lower Jurassic silty limestone described in the preceding section is missing, as are Lower Jurassic rocks similar to those of the Westgate area (Corvalan, 1962) and the Pershing district (Wallace and others, 1959). Perhaps Lower Jurassic sediments were removed by erosion prior to the deposition of the metavolcanics. More probably, however the metavolcanics were carried in with the underlying limestone as a part of the La Plata thrust sheet, and may therefore represent a distant stratigraphic section.

Rocks somewhat similar to those just described occur 15 miles to the north near lower Cox Canyon, and are believed to belong to the same formation despite a great difference in structural relations. The northern metavolcanics structurally underlie, rather than overlie, the Upper Triassic rocks.

Jurassic(?) quartzite (Jqc)

A distinctive allochthonous quartzite occurs in remnants of the Boyer thrust sheet at the mouth of Cottonwood Canyon and elsewhere. It varies from black to white and from thin-bedded to massive, but in other respects it is remarkably uniform. The sand is well sorted, fine to very fine grained, and is mainly angular to subrounded. Quartz predominates to the exclusion of all other clastic components except rare specks of tourmaline and zircon. Interstitial carbonate, chalcedonic silica, and chlorite are locally present, and some of the rock is calcareous sandstone rather than quartzite. The formation is at least 500 feet thick and is not interrupted by shale intercalations. The age is not definitely known because fossils are lacking, but R. C. Speed (personal communication, 1964) recently found Jurassic basalt apparently resting concordantly on the quartzite 3 to 4 miles north of Dixie Meadows. This suggests, but does not prove, a Jurassic age for the quartzite.

Jurassic basalt (Jba)

North of the latitude of Dixie Meadows, Jurassic basalts occupy large areas. They occur as flows (locally amygdaloidal), lithic lapilli tuffs, tuff breccias, and breccias. These rocks are generally altered, and commonly contain chlorite and epidote which impart a greenish color. They have previously been regarded as andesites, but R. C. Speed (oral communication, 1964) finds that the composition is basaltic. He reports that the flows contain labradorite phenocrysts or microphenocrysts, some contain clinopyroxene, and a few have talc pseudomorphs after olivine. The groundmass of the flow rocks includes lineate plagioclase laths and alteration products of pre-existing clinopyroxene and glass. Speed notes that many of the flow rocks are petrographically identical with rocks of similar occurrence in the west Humboldt Range, where an analyzed specimen showed 52.92 percent SiO_2 (by weight) and normative plagioclase of composition An_{52}.

The rocks just described are found in the area of the Upper Jurassic gabbroic and dioritic complex and are not recognized with certainty beyond that area. They are more prevalent near the center of the complex than near the margins, and are intruded by some facies of the complex. It is likely that the intrusive and extrusive rocks are genetically related and almost contemporaneous.

Gabbroic and dioritic rocks (Jdg)

The northern quarter of the mapped area is dominated by the Jurassic basalts and by gabbroic and dioritic intrusives. The intrusives have been examined by R. C. Speed, who has made a detailed study of correlative rocks in the West Humboldt Range (Speed, 1962a, 1962b, and 1963). The rocks form a gabbroic suite consisting of hornblende gabbro, diorite, picrite, anorthosite, dolerite, keratophyre, and gabbroic pegmatite. The earliest parts of the suite are locally strongly differentiated and layered, and occur mainly along the margins of the intrusion. Speed considers the complex to be a tabular mass emplaced at shallow depth, probably less than 2500 feet. In places it may have erupted to form the associated basalts. Speed obtained a potassium-argon age determination from primary biotite in a gabbro specimen from the West Humboldt Range. The indicated age is 150± 3 million years; accordingly, the complex is probably Late Jurassic.

Commonly the gabbroic and dioritic rocks have been profoundly altered. For example, some of the rock is albitized and bleached white, and some is dolomitized, lacking original minerals and texture, and weathering yellow-brown.

CENOZOIC OR MESOZOIC ROCKS

A number of nonmarine rock units, chiefly volcanic, overlie Upper Triassic or Lower Jurassic formations and underlie Miocene(?) volcanics. They contain no fossils, and their age(s) may be either Late Jurassic, Cretaceous, or early Tertiary.

Landslide breccia (T-Jbr)

An interesting but limited lithified breccia near the south fork of Cox Canyon is more than 500 feet thick and is almost unstratified. It consists of blocks and fragments of three or four lithologic types. The basal part contains abundant Triassic slate fragments as well as fragments of Jurassic(?) metavolcanic rocks. The latter predominate in most of the mass, but a few horizons are chiefly composed of quartzite blocks, and others of limestone blocks. Most of the features suggest a landslide origin. The accumulation is overlain by devitrified welded tuff, and is intruded by porphyritic basaltic andesite and by white aphanitic felsite.

Latite flows, tuffs, and breccias (T-Jl)

Latite which weathers lavender or pale blue-gray is prevalent in the vicinity of Job Peak and southward to upper Eleven Mile Canyon. The only megascopic minerals are minute, sparse K-feldspar phenocrysts. These are scattered in a groundmass of microscopic feldspar laths that are sodic plagioclase in part. The groundmass is sprinkled with extremely fine brown specks. There are rare, tiny chlorite pseudomorphs after hypersthene(?), but no other vestiges of mafic silicates.

Some of the latite shows fine flow layering, limited horizons are spherulitic, and others are amygdaloidal. Columnar jointing is occasionally discernible. Some tuffs (including thin, stratified rhyolite crystal tuffs) and latite breccias accompany the flows. The total thickness is 2,000 to 6,000 feet.

The latite is intruded by Oligocene or Lower Miocene granite in the vicinity of Coyote Canyon, and is darkened and microscopically recrystallized.

Devitrified welded tuff (T-Jwt)

Remarkable welded tuffs resembling prophyries occur between Mountain Well Road and Cox Canyon. They compose Job Peak and much of the southern half of the mapped area. These rocks are not to be confused with younger welded tuffs included under "Tv" on the map. They are dull colored, weathering gray to brown, and are so completely compacted and uniform that joint systems and topography are not influenced by original structures. The welded tuffs are hard, dense, and crowded with euhedral feldspar crystals, and there is no megascopic indication of pyroclastic origin except the common presence of scattered angular lithic fragments such as Triassic slate, lavender latite, and various volcanic rocks. However, thin sections show fine "fluidal" banding and wispy relict structures faintly suggesting flattened shards and collapsed bits of pumice. All the former glass has given place to a microcrystalline, mosaic-like texture that has almost effaced the original features.

A number of different rock units are included here under "devitrified welded tuff". In all of them, the larger mineral grains are megascopic (0.5 to 2 mm.) and numerous, and include euhedral crystals and angular fragments of plagioclase (commonly andesine), orthoclase, perthite, and quartz. Quartz is very scanty to very abundant and the rock compositions probably range from latite through dacite to silica-rich rhyolite. No original mafic minerals are present, but chlorite pseudomorphs after biotite are common.

The devitrified welded tuff rests unconformably upon Upper Triassic slate, Upper Triassic limestone, and Jurassic(?) metavolcanic rocks; and its basal part locally contains fragments or boulders of the underlying formations. Near Coyote Canyon and elsewhere, it rests upon latite (T-Jl), and in places members 100 to 200 feet thick consist of latite blocks and fragments in a rhyolitic matrix. The total thickness of devitrified welded tuff is commonly greater than 2,000 feet, and may possibly attain 10,000 feet.

Some of the devitrified welded tuff outcrops show a faint planar structure expressed by short greenish streaks and platy lithic inclusions. Oddly, this structure generally dips 45° to 90°, whereas the base of the formation, where exposed, is less steeply inclined. The tuff was deposited on an uneven surface, and may have had an initial dip that was increased by downhill slumping while the mass was hot and soft. The dips were further increased by subsequent tectonic folding.

The devitrified welded tuff, unlike the younger volcanics (Tv), has been intruded by white felsite dikes and by Oligocene or early Miocene granodiorite and granite. The granitic rocks and the welded tuff may be genetically related; that is, after magma erupted to form the welded tuff, additional magma from the same source may have intruded the volcanic products. If this hypothesis is correct, the devitrified welded tuff is Oligocene or early Miocene.

Undifferentiated rhyolitic volcanic and intrusive rocks (T-Jvi)

An area northwest of Job Peak is underlain by a poorly exposed assemblage of extrusive and intrusive rhyolites. This assemblage probably includes some units that are designated elsewhere as "T-Jwt", "T-Jf", and "Tv", but it also includes various unfamiliar rocks. Because of complexity and inadequate exposures, it was not feasible to map the units separately.

Porphyritic basaltic andesite (T-Jpa)

The devitrified welded tuff and older formations are intruded by greenish gray porphyritic basaltic andesite. This rock has prominent plagioclase phenocrysts (calcic andesine to labrodorite) in a groundmass of felted plagioclase, -- apparently oligoclase to andesine. Chlorite, epidote, and calcite have formed pseudomorphs after pyroxene and biotite.

Extrusive basalts and andesites (T-Jba)

A number of rock units, perhaps of different ages, are grouped under "T-Jba". Volcanic flows and breccias 2 to 4 miles south of Cox Canyon have a mineral composition similar to that of the intrusive rocks described in the preceding section, and are probably extrusive equivalents. They appear to be 8,000 feet thick. These rocks are fractured, chloritized, and epidotized at the expense of original features, but two or three stratified tuff members 20 to 30 feet thick suggest an extrusive origin.

Altered basaltic andesite containing orthopyroxene, forms flows, breccias, and tuffs that rest unconformably upon Upper Triassic slate 2 to 5 miles north of Alameda Canyon. The basal material locally contains blocks, rounded pebbles, and cobbles of volcanic rocks, slate, granodiorite, and micrognaite.

Certain peaks between Fondaway and White Cloud Canyons are composed of andesitic breccia, tuff-breccia, and tuff. There are members of dense (welded ?) andesitic tuff with streaky planar structure and columnar jointing. The andesitic rocks, up to 1900 feet thick, postdate the Early Jurassic sedimentary rocks and predate Miocene(?) volcanics (Tv).

Basalt that is older than the Miocene(?) volcanics occurs on both sides of U. S. Highway 50 near the Summit King mine. It is locally strongly altered and bleached. Much of the basalt is distinctive because of its numerous thin, broad, scale-like labradorite phenocrysts. The groundmass consists of andesine or labradorite laths. Some varieties of the basalt show vestiges of small pyroxene crystals, and some contain pseudomorphs, probably after olivine. The basalt covers a thrust fault affecting Upper Triassic rocks, and is believed to be intruded by Late Cretaceous granodiorite, so its age is probably Jurassic or Early Cretaceous. Silicified wood from beneath the basalt was identified as Cupressanoxylon sp., by Virginia M. Page (oral communication, 1964).

Felsic porphyries and aphanitic intrusive rocks (T-Jf)

White felsite with no megascopic grains occurs as prominent dikes and irregular intrusive bodies. One such body south of Cox Canyon is 1 1/2 miles long and 1 mile wide, but despite its size, has extremely fine texture. Many aphanitic-porphyritic dikes and sills of various ages are also included under "T-Jf". A striking swarm of east-west felsic dikes cuts the devitrified welded tuff in a large area around Eleven Mile Canyon. Some felsic dikes are spatially and petrologically related to granitic plutons. Some are younger than the plutons but older than, or contemporaneous with, the Miocene and Pliocene volcanic rocks (Tv). Many of the younger dikes have phenocrysts of quartz and fresh feldspar in an aphanitic groundmass sprinkled with fresh biotite.

GRANITIC PLUTONS

A mass of Late Cretaceous granodiorite and porphyritic granite (Kg) dominates the Sand Springs Range and extends into the southernmost part of the mapped area. It is locally somewhat foliated, but otherwise does not differ greatly from the Tertiary granitic rocks farther north. According to a recent report (Nevada Bureau of Mines, 1962, p. 17), biotite from the granite and granodiorite gave potassium-argon ages of 79.6 (± 2.0) and 76.0 (± 2.0) million years, respectively. These rocks intrude Upper Triassic(?) metasediments about 1 mile south of U. S. Highway 50.

Granodiorite and quartz monzonite (both marked "Tg") near the center of the mapped area invade latite and devitrified welded tuff of probable Cretaceous or early Tertiary age. Biotite from a sample obtained in IXL Canyon gave a potassium-argon age of 28 ± 2.0 million years (R. C. Speed, oral communication, 1964). Evidently the rock is Oligocene or Early Miocene, depending upon the varying usage of these terms. The "dated" granodiorite is intruded by a younger coarse granite 1.5 miles south of Mud Spring. In fact, the terrain labeled "Tg" encompasses several successive intrusions, but they are not shown separately.

The granitic plutons labeled "TKg" near La Plata, Alameda, and White Cloud canyons are of unknown age.

Intrusion of the granitic mass in the area south of U. S. Highway 50 accentuated and coarsened the fabric of the invaded foliated rocks, and induced the growth of porphyroblasts (chiefly chiastolite and chloritoid). It produced marble and skarn in some adjacent limestones. The granitic mass near IXL Canyon had similar effects. A small intrusion 1 mile north of U. S. Highway 50 transformed limestone to a plagioclase-hornblende rock. Most of the other granitic plutons produced aureoles of black hornfels or chiastolite-bearing phyllite and minor amounts of quartzite and marble. Some plutons gave rise to white felsite dikes which cut the Triassic and Jurassic rocks.

Only the upper parts of the granitic bodies are exposed, judging from internal features and metamorphic environment. The pluton of the Sand Springs Range is somewhat more deeply exposed than the others.

ROCKS YOUNGER THAN THE GRANITIC PLUTONS

Miocene(?) volcanic rocks (Tv)

Extensive post-granitic volcanic rocks include silicic tuffs, welded tuffs, tuff-breccias, breccias, and flows. Some associated andesite is included. Although alteration is locally intense, many parts of the silicic suite retain fresh biotite and glass, unlike the earlier volcanics. Some units are white or brightly colored, few dikes cut the rocks, and in places the attitudes of the various members may be deduced from topographic expression. These characteristics are lacking in the Pre-Miocene volcanics. The total thickness is 1,800 feet in some eroded sections and might attain 3,000 to 4,000 feet in restored sections.

Some younger (Pliocene ?) white rhyolitic tuffs have been included with the foregoing rocks on the map.

Pliocene(?) basalt (Tb)

Near Mountain Well Road and La Plata Canyon, about 75 feet of basalt locally lies beneath the Pliocene sedimentary rocks and the youngest rhyolitic tuffs. The rock is sprinkled with square feldspar phenocrysts and fine crystals of augite and olivine. Some of the basalt is columnar.

Pliocene(?) non-marine sedimentary rocks and tuffs (Ts)

Dissected pediments and low hills commonly show exposures of poorly consolidated gravels, sands, clays, fissile white siliceous shales, and light colored tuffs. The sediments are fluvial and lacustrine, and locally interfinger with subaerial crystal and vitric ash. Near Eleven Mile Canyon the sequence is 650 feet thick, and near Mountain Well Road it is perhaps 1,500 feet thick. Fossils obtained to date do not have a restricted range. Silicified wood of Quercus(?) cf. chrysolepis, Salix sp., and Sequoia(?) sp. was identified by Virginia M. Page (written communication, 1959). Impressions of grass and willow leaves and a fragment of a small fish skeleton were found in siliceous shales. A thin lacustrine limestone yielded Ostracoda that B. E. B. (Cameron tentatively identifies as "Pseudoeucypris Pagei" Swain. The last-named species is reported from the Green River Formation (Eocene) near Sunnyside, Utah. However, the sediments described here are younger than the Oligocene or Miocene granitic intrusives. They seem roughly comparable to beds which are elsewhere called "Truckee" and "Esmeralda".

Plio-Pleistocene basalt and basaltic andesite (Qba)

The Stillwater Range is partly capped by olivine basalt in flows from 20 to 100 feet thick, aggregating 1,600 feet in some places. Locally the flows rest upon bright red scoriaceous material or gray ash. Northwest of Mountain Well 1,000 feet of breccias and flows of porphyritic pyroxene andesite lie upon folded and eroded Pliocene sedimentary rocks.

STRUCTURE

The structural features are shown in cross sections A-A' B-B', and C-C'. The various thrust faults, which are rather inconspicuous on the geologic map, may be found by referring to the INDEX MAP OF THRUST FAULTS, located to the upper left of the geologic map.

MESOZOIC FOLDS AND THRUST FAULTS

Folds in Upper Triassic slate

The slate between Cox Canyon and Fondaway Canyon is intricately folded in places. Intervening parts are nearly homoclinal, but about half the homoclinal sections are overturned. Although there are many exceptions, most beds that dip steeply south or southwest are overturned (cross sections). This indicated differential movement of the upper part of the body of slate toward the north or northeast with respect to the deeper part of the mass. The configuration of drag folds supports this interpretation. Many contorted beds are disrupted by low-angle displacements where folding gave way to minor thrust faulting. Folds in the Upper Triassic slate are transected by, and are therefore earlier than, the Boyer thrust of Late Jurassic age.

Cox Canyon thrust zone

Where the structural base of the slate body is exposed just south of Cox Canyon, the lavender shale member rests discordantly upon quartzite of unknown age. As much as 10 feet of brecciated shale occurs at the contact, and sheared shale overlying the breccia contains tectonic augen or lenses of limestone. Although the contact with the quartzite is locally very steep, on the whole it appears to be a thrust fault.

The quartzite south of Cox Canyon forms a tectonic, wedge-shaped mass which has been overridden by the slate and which in turn has overridden Jurassic(?) metavolcanics. Moreover, the metavolcanics have been thrust over a limestone of unknown age. Therefore the several rock units south of Cox Canyon appear to be tectonic slices in an imbricate thrust zone, as shown in Cross Section B-B'.

The extent of the Cox Canyon thrust zone is unknown, but it may underlie the entire slate terrain of the Stillwater Range (Page, 1959). The amount of "tectonic transport" is also unknown, and the direction and sense of relative movement are uncertain. The writer tentatively believes that the major folds in the slate formed at the time of thrusting; if this is so, the slate mass and the imbricated wedges moved north and northeast with reference to the underlying rocks. The time of thrusting was probably Middle or Late Jurassic, but may have been Cretaceous. In any case, it antedated various intrusions, including the Tertiary pluton of IXL Canyon, inasmuch as the intrusive rocks have invaded and obliterated the east extension of the thrust zone.

Boyer thrust

In the northern third of the map, there are several exposures of a remarkable thrust fault structurally higher than the Cox Canyon thrust zone. It is easily seen north of Cottonwood Canyon near Boyer Ranch Here and in other typical localities, distinctive fine-grained quartzite of unknown age has been thrust over Upper Triassic slate. Locally the quartzite has overridden Lower Jurassic rocks. There is a striking association between quartzite and intrusive diorite and gabbroic rocks in the upper plate, whereas the intrusive rocks are lacking (except for narrow dikes) in the slate beneath the thrust. The dioritic and gabbroic rocks clearly accompanied the quartzite at the time of transport, and R. C. Speed believes (as does the writer) that the igneous rocks were partly molten during this episode; in fact, the intrusion may have propelled the quartzite thrust sheet (Speed and Page, 1964).

The upper plate of the Boyer thrust is part of a sheet of gabbroic rocks and intruded metasediments extending from the West Humboldt Range to the Clan Alpine Range and occupying an area of 500 square miles. The parts exposed near White Cloud Canyon and near Dixie Meadows probably moved south with respect to the underlying rocks. The latter are little disturbed in most places, but in some localities seem to show a reversal of the earlier northward overturning. However, this interpretation is only tentative.

R. C. Speed (Speed and Page, 1964) has determined that one of the gabbroic intrusive bodies is Late Jurassic. If the intrusive complex is syntectonic, the thrusting is also of that age.

La Plata thrust

In the vicinity of Eleven Mile Canyon and La Plata Canyon, a sheet of allochthonous Upper Triassic limestone rests discordantly upon Upper Triassic slate. The tectonic base of the sheet is undulating and generally gently dipping. Both the limestone and the slate are strongly folded near the contact, and the latter is bordered by 1/2 to 15 feet of breccia. Jurassic(?) metavolcanics exposed near the head of La Plata Canyon, which apparently overlie the limestone unconformably, are probably a part of the thrust sheet rather than a later deposit, but are not seen in contact with the footwall rocks. Both the allochthonous limestone and the footwall slate are intruded by quartz monzonite, which (in view of the later dikes that transect it) may be Late Cretaceous rather than Tertiary. In this case, the La Plata thrust would probably be Late Jurassic or Early Cretaceous. The direction of transport is thought to be north or north-northeast, based on small folds near the thrust surface, but the evidence is inconclusive.

Sand Spring thrust

Several conspicuous limestone klippen occur in an east-west array just south of U. S. Highway 50. They may be remnants of the La Plata thrust, or they may belong to a different sheet. The limestone is gray, slightly recrystallized, barren of fossils, and of unknown stratigraphic horizon. It is distinctly bedded and is folded into a simple east-trending syncline. It rests in thrust-fault contact upon Upper Triassic(?) phyllite and schist which dip steeply but are almost undisturbed by the thrusting. No indication of the direction of thrusting has been found. The thrust fault is partly covered by later basalt flows which appear to be intruded by granodiorite of Late Cretaceous age; hence the thrusting was probably Late Jurassic or Early Cretaceous.

CENOZOIC STRUCTURES

Cenozoic folds

The early volcanic rocks such as the devitrified welded tuff, (T-Jmt), were folded along north-south axes prior to the emplacement of Oligocene or Early Miocene plutons. Volcanic rocks (Tv) later than the plutons were also folded along north-south axes, but only mildly. Some of the rhyolitic and dacitic units labeled "Tv" show unsystematic dips suggesting that gravitative slumping, sliding, and tilting has occurred. The Pliocene sediments are moderately folded along north-south axes, and slumping has accentuated some of the dips. The Pliocene-Pleistocene basalts are generally tilted rather than folded, and rarely dip more than 12°. A very gentle, open syncline modified by block faulting extends north-northeastward into the basalt terrain from the vicinity of Sand Springs.

Cenozoic normal faults

Much of the Stillwater Range is a horst sliced into narrow north-south trending blocks by normal faults. Some tilting has accompanied the block faulting; this is apparent in the Pliocene-Pleistocene basalts. The normal faulting involved an east-west extension of the crust, and probably it was induced by a reduction of confining pressure in that direction. Indeed, it looks as though the range sloughed off narrow subsidiary blocks during and after its uplift above the adjacent basins, mainly in response to gravity. Probably many normal faults also underlie the alluvium alongside the mountains.

Some normal faults in the interior of the range extend to the flanks and continue as marginal faults bounding the range. This condition may be seen at two widely separated places on the east side, at Coyote Canyon and at a point 9 miles southwest of Cottonwood Canyon.

Fault movements in the present century

Some of the normal faults in the vicinity are active, and have been responsible for earthquakes. In 1903, a fault displacement in the Louderback Mountains, adjacent to Dixie Valley on the southeast, broke the ground surface and caused the Wonder earthquake (Slemmons and others, 1959). In 1915, marginal faults along the flanks of the Tobin Range, China Mountain, and Sou Hills (all north of Dixie Valley) underwent sudden displacements responsible for the severe Pleasant Valley earthquake (Jones, 1915; Page, 1935). At this time, an internal north-south fault high in the Stillwater Range was reactivated, forming a fresh scarp 1 to 3 feet high. This fault is 5 to 7 miles north of the area shown on the accompanying map.

In July and August of 1954, faulting occurred along the east base of Rainbow Mountain, just west of the southern Stillwater Range. This created the Fallon-Stillwater earthquakes, of magnitude 6.8 on the Richter scale (Byerly, 1956; see also other reports on following pages of this volume). The fault displacements reached the ground surface.

On December 16, 1954, the Dixie Valley-Fairview Peak earthquakes (Tocher, 1957; see also other reports on following pages of this volume) originated from displacements on a number of separate faults in a zone extending from Dixie Meadows to a point 60 miles south of the east foot of Slate Mountain (see fold-out map in Slemmons, 1957). The two most important displacements occurred along the east base of Fairview Peak (southeast of the area mapped in this report) and along the east base of the Stillwater Range. The Fairview Peak fault movement produced an earthquake of magnitude 7.1 (Romney, 1957, p. 305). About 4 minutes and 20 seconds later, movement along the juncture of the Stillwater Range and Dixie Valley produced a second earthquake of magnitude 6.8. Romney's (1957, p. 306) analysis of seismic data placed the focus of the second earthquake at lat. 39.8° N., long. 118.1°W., depth approximately 40 km. This location falls under the eastern part of the range near the mouth of Hare Canyon. Probably the actual focus was on the marginal fault which bounds the range, somewhat east of the surface trace of the fault, inasmuch as the latter dips 45 to 75° E. The depth of focus may have been a good deal less than 40 km.

The fault movements of December 16, 1954 displaced the surface of the ground, as described by Slemmons (1957), leaving steep scarps that are marked by hachures on the accompanying map. The scarps are 1 inch to 12 feet high, but commonly surmount miniature graben, and therefore tend to exceed the net vertical displacement. Neglecting the miniature graben, the net vertical displacement is about 7 feet maximum. No significant strike slip occurred at the surface, although right lateral slip was observed in other parts of the region, especially along the east base of Fairview Peak south of U. S. Highway 50. Most of the 1954 faulting within the map area occurred at the immediate foot of the Stillwater Range. However, some displacements took place on the alluvial slopes at distances of 1 to 3 miles from the base of the mountains, where low late Pleistocene scarps were increased in height by a small increment, usually less than 3 feet. Everywhere along the foot of the mountain the west side of the faults rose relative to the east side. Displacements far out in the alluvium are mainly in the same sense, but are locally contrary. Most of the scarps shown on the map probably mark the traces of normal faults which dip in the direction of the relatively downthrown block.

Geodetic measurements of ground movements are summarized by Whitten (1957). Relative to points about 40 miles to the east and to the west, the Stillwater Range seems to have remained almost stationary, but Dixie Valley may have dropped as much as 7 feet (e.g., near IXL Canyon). Two triangulation stations on the east side of Dixie Valley, near Horse Creek and Wonder, moved southeast 3.4 feet and 3.7 feet respectively, relative to Job Peak. This probably represents elastic rebound subsequent to long-term regional movements of comparable magnitude. Whitten (1957, p. 323) notes that the disparity between the azimuth of crustal movement and the strike of the faults indicates a component of east-west extension, which would be consistent with displacement on north-south normal faults.

The recent faulting is a continuation of Quaternary vertical adjustments in response to gravity, caused by reduction of pressure in the east-west direction. Superimposed on these adjustments is a northwest-southeast right lateral component, most clearly evidenced south of Dixie Valley. This type of horizontal movement characterizes strain in coastal California, and now appears to affect the earth's crust inland at least as far as the region discussed here.

Crustal characteristics and block faulting in west-central Nevada, including the Stillwater Range, are discussed by Thompson (1959), with emphasis upon gravity data. The same author (1960) suggests that the east-west distension of the crust and the consequent normal faulting may result from a phase change near the boundary between crust and mantle.

MINERAL DEPOSITS

Copper

The Coppereid camp (now abandoned) in White Cloud Canyon, produced minor amounts of copper in the last century, and briefly supported a small smelter about 1893 (Lincoln, 1923, p. 13). Copper sulfide and secondary minerals occur in contact-metamorphosed limestone with erratically developed skarn and local masses of specularite and pyrite (Ransome, 1909, p. 59-61; Vanderburg, 1940, p. 52-53). A few carloads of copper ore were mined from deposits in diorite in Copper Kettle Canyon (Lincoln, 1923, p. 2). Copper is recorded from the nickel deposits of Cottonwood Canyon and in small showings between Cottonwood Canyon and White Rock Canyon 8 miles to the southwest. These showings, which are chiefly chalcopyrite and oxidation products in Jurassic basalt, are described by Carpenter (1911) and Vanderburg (1940, p. 47). Reportedly, they yielded a few wagon-loads of ore in 1861. Recurrent attention is accorded the "Bradshaw property" in altered Jurassic basalt in White Rock Canyon 10 miles north of Dixie Meadows. Copper minerals are found in limestone and lime-silicate rocks in the Sand Springs district 1 mile north of U. S. Highway 50, and in mine workings just west of the Summit King gold mine.

Fluorspar

Several hundred tons of fluorspar have been mined from small veins in limestone interbedded with slate near Cox Canyon (Horton, 1961, p. 9). The deposits border a mineralized normal fault 1 mile northeast of the mouth of the canyon. Other occurrences are reported from contact zones of granitic plutons. Fluorite is mentioned as a minor gangue mineral near the copper deposits of White Cloud Canyon, and occurs in a prospect in limestone near quartz monzonite in La Plata Canyon.

Gold

One of the few successful gold mines in the area was the Summit King, on U. S. Highway 50, where gold and silver were recovered from a vein of lamellar quartz. The vein strikes east-west, transecting Upper Triassic(?) schist and highly altered post-Triassic basalt. This mine was among the 10 largest producers of gold and silver in the State in 1948-49.

Small veins in Triassic slate and interbedded quartzite formerly attracted much unsuccessful prospecting in the Shady Run district encompassing Fondaway, Shady Run, Shanghai, and Mill canyons (Lincoln, 1923, p. 9; Vanderburg, 1940, p. 43). A small amount of gold and silver was produced from quartz and calcite veins in limestone in IXL Canyon, and prospects have been opened on the other side of the range in the watershed of Cox Canyon (Vanderburg, 1940, p. 32-35).

The Dixie Comstock mine at the east foot of the Stillwater Range near Humboldt Salt Marsh yielded a small amount of gold and silver from a vein in the marginal fault zone, but hot water was encountered (Vanderburg, 1940, p. 48) and the mine was closed. Gold is said to accompany albitic dikes in altered diorite in Corral Canyon (Ferguson, 1939, p. 18-19).

Iron

High grade magnetite ore has been successfully mined from deposits of small to moderate size in the Buena Vista Hills (Reeves, and Kral, 1955), and has been found in less accessible deposits in the Stillwater Range between lat. 39°50' and 40°02'N. In nearly all cases, the ore is in altered Jurassic basaltic or gabbroic rocks and is genetically related to the latter.

Nickel

Nickel and cobalt were mined in Cottonwood Canyon for 8 years in the 1880's, and briefly thereafter. Annabergite, $Ni_3As_2O_8H_2O$, and various other nickeliferous minerals occur with iron oxide in small stringers. Some of the stringers are in highly altered "aplite" (albitized rock?) near a fault close to the contact between extrusive Jurassic basalt and intrusive diorite. Other stringers are in highly altered basalt near the diorite contact. (Ferguson, 1939. See also Ransome, 1909, p. 55-58).

Quicksilver

Traces of cinnabar occur in the tungsten ore of Fondaway Canyon (see below), and have been reported elsewhere in the district. There has been little or no successful exploitation of quicksilver, however.

Silver

Silver was briefly mined near the main forks of La Plata Canyon in the early 1860's, and a small town and stamp mill were established. La Plata was the county seat from 1864 to 1868. Reportedly the main deposit was a quartz vein in granite, but other veins in the district are in limestone or slate near intrusives. There is no evidence of substantial production (Vanderburg, 1940, p. 38-39).

The most important silver output has come from the Summit King mine, described under "Gold". This mine ranked among Nevada's three largest producers in the period 1948-1951.

Minor amounts of silver accompany whatever gold is present in the various unproductive prospects of the region.

Titanium

Certain late-stage albitic members of the Upper Jurassic gabbroic and dioritic complex are highly titaniferous, and have been examined for possible titanium ore. One of the best known localities is Corral Canyon, about 5 miles southwest of Cottonwood Canyon. It is reported that anatase, TiO_2, is contained in white, altered, albitic dikes which transect diorite (Hand, 1955; Beal, 1963, p. 8-9). Similar deposits are reported between Corral Canyon and Cottonwood Canyon along the east flank of the range (Beal, 1963, p. 11). No titanium production has been realized so far.

Tungsten

In the 1950's, a small amount of high grade scheelite ore was mined from a narrow vein alongside a dike in the allochthonous limestone of lower Fondaway Canyon. No skarn is present. Other scheelite showings of high grade but small size occur in skarn adjacent to granodiorite 1 mile south of U. S. Highway 50 in the Sand Springs district. Scheelite occurs 1 mile north of the same highway in somewhat different deposits in limestone. Mineralized skarn is conspicuous at the north margin of the Tertiary quartz monzonite in the vicinity of IXL Canyon, but no appreciable amount of tungsten has been found there as yet.

REFERENCES

Beal, L. H., 1963, Investigation of titanium occurrences in Nevada: Nevada Bur. Mines Rept. 3.

Byerly, Perry, 1956. The Fallon-Stillwater earthquakes of July 6, 1954 and August 23, 1954 Historic introduction: Seismol. Soc. America Bull., v. 46, p. 1-40.

Carpenter, A. H., 1911, Boyer copper deposits, Nevada: Mining and Scientific Press, v. 103, p. 804-805.

Corvalan, J. I., 1962, Early Mesozoic biostratigraphy of the Westgate area, Churchill County, Nevada: unpublished Ph.D. thesis Stanford Univ.

Ferguson, H. G., 1939, Nickel deposits in Cottonwood Canyon, Churchill County, Nevada: Nevada Univ. Bull., v. 33, no. 5, Geol. and Min. Ser. no. 32.

Ferguson, H. G., Muller, S. W., and Roberts, R. J., 1951, Geology of the Winnemucca quadrangle, Nevada: U. S. Geol. Survey, Geol. Quad. Map GQ-11.

Horton, R. C., 1961, An inventory of fluorspar occurrences in Nevada: Nevada Bur. Mines Rept. 1.

Hand, David, 1955, Geology of the Corral Canyon area, Churchill County, Nevada: unpublished M.A. thesis, Univ. of Nevada.

Jones, J. C., 1915, The Pleasant Valley earthquake of October 2, 1915: Seismol. Soc. America Bull., v. 5, p. 190-205.

Lincoln, F. C., 1923, Mining districts and mineral resources of Nevada: Nevada Newsletter Pub. Co., Reno, Nev.

Muller, S. W., Ferguson, H. G., and Roberts, R. J., 1951, Geology of the Mount Tobin quadrangle, Nevada: U. S. Geol. Survey, Geol. Quad. Map GQ-7.

University of Nevada, 1962, Geological, geophysical, and hydrological investigations of the Sand Springs Range, Fairview Valley, and Fourmile Flat, Churchill County, Nevada: Report to Atomic Energy Commission for Shoal Project, Vela Uniform Program, 127 p.

Page, B. M., 1935, Basin-Range faulting of 1915 in Pleasant Valley, Nevada: Jour. Geology, v. 43, p. 690-707.

Page, B. M., 1959, Tectonic record of the Stillwater Range, western Nevada (abs.): Geol. Soc. America Bull., v. 70, p. 1739.

Ransome, F. L., 1909, Notes on some mining districts in Humboldt County, Nevada: U. S. Geol. Survey Bull. 414.

Reeves, R. G., and Kral, V. E., 1955. Iron ore deposits of Nevada. Part A, Geology and iron ore deposits of the Buena Vista Hills, Churchill and Pershing Counties, Nevada: Nevada Bur. Mines Bull. 53, 37 p.

Romney, Carl, 1957, Seismic waves from the Dixie Valley - Fairview Peak earthquakes: Seismol. Soc. America Bull., v. 47, p. 301-319.

Silberling, N. J., and Roberts, R. J., 1962, Pre-Tertiary stratigraphy and structure of northwestern Nevada: Geol. Soc. America Spec. Paper 72, 58 p.

Slemmons, D. B., 1957, Geological effects of the Dixie Valley - Fairview Peak, Nevada, earthquakes of December 16, 1954: Seismol. Soc. America Bull., v. 47, p. 353-375.

Slemmons, D. B., Steinbrugge, K. V. Tocher, Don, Oakeshott, G. B., and Gianella, V. P., 1959, Wonder, Nevada, earthquake of 1903: Seismol. Soc. America Bull., v. 49, p. 251-265.

Speed, R. C., 1962a, Humboldt gabbroic complex (abs.): Geol. Soc. America Spec. Paper 73.

______, 1962b, Scapolitized gabbroic complex, West Humboldt Range, Nevada: unpublished Ph.D. thesis, Stanford Univ.

Speed, R. C., 1963, Layered picrite-anorthosite gabbro sheet, West Humboldt Range, Nevada: Mineralog. Soc. America Spec. Paper 1, p. 69-77.

Speed, R. C., and Page, B. M., 1964, Association of gabbroic complex and Mesozoic thrusts, west central Nevada [abs.]: Geol. Soc. America Spec. Paper 82, p. 278-279.

Thompson, G. A., 1959, Gravity measurements between Hazen and Austin, Nevada: A study of Basin-Range structure: Jour. Geophys. Research, v. 64, p. 217-229.

Thompson, G. A., 1960, Problem of Late Cenozoic structure of the Basin Ranges: Internat. Geol. Cong., 21st, Copenhagen 1960, pt. 18, p. 62-68.

Tocher, Don, 1957, The Dixie Valley - Fairview Peak earthquakes of December 16, 1954: Introduction: Seismol. Soc. America Bull., v. 47, p. 299-300.

Vanderburg, W. O., 1940, Reconnaissance of mining districts in Churchhill County, Nevada: U. S. Bur. Mines Inf. Circ. 7093.

Wallace, R. E., Silberling, N. J., Irwin, W. P., and Tatlock, D. B., 1959, Preliminary geologic map of the Buffalo Mountain quadrangle, Nevada: U. S. Geol. Survey Mineral Inv. Field Studies Map MF-220.

Whitten, C. A., 1957, Geodetic measurements in the Dixie Valley area: Seismol. Soc. America Bull., v. 47, p. 321-325.

Young, Chapman, 1963, The geology north of White Cloud Canyon, Stillwater Range, Nevada: unpublished M.S. thesis, Stanford, Univ.

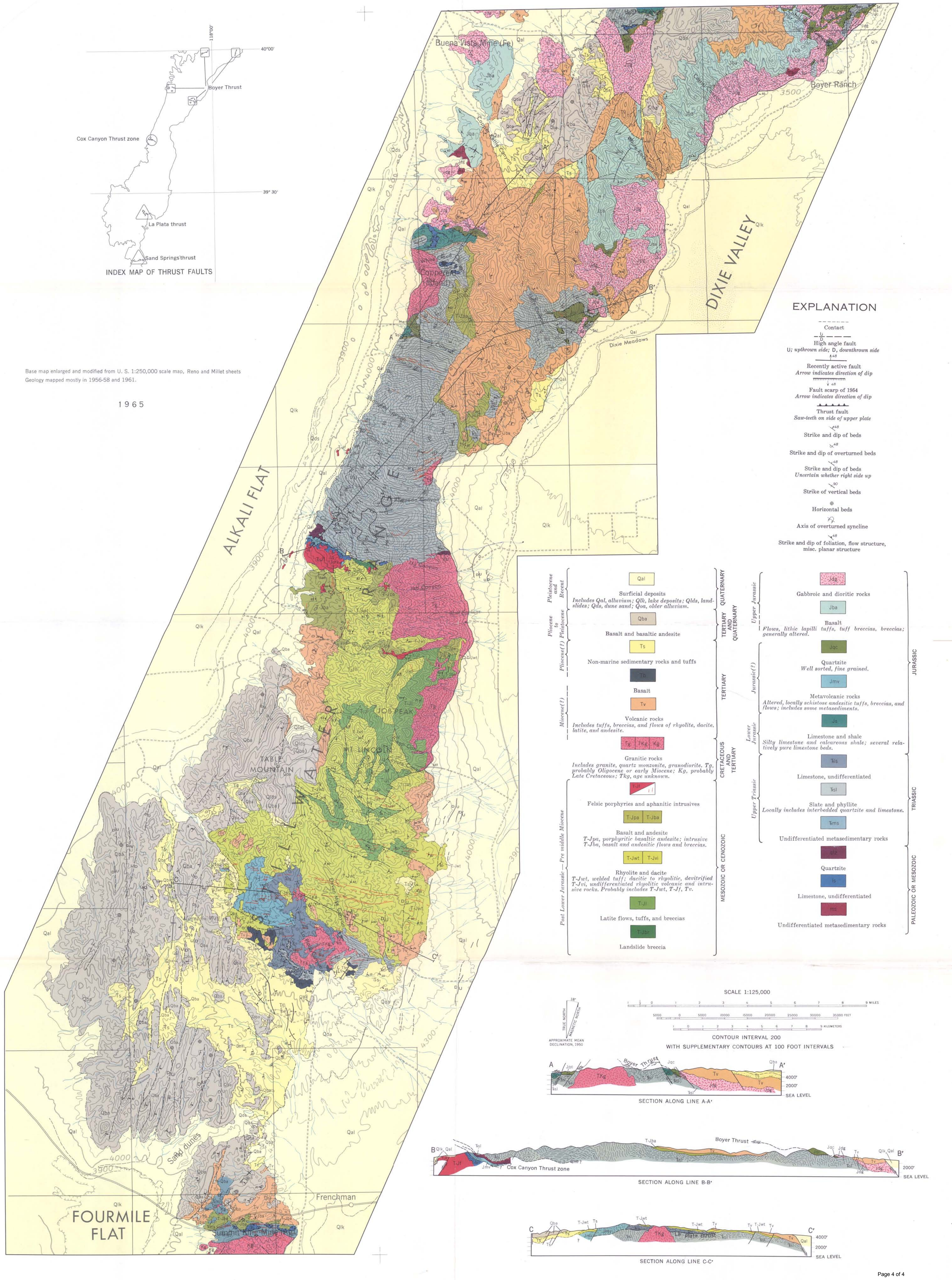

APPENDIX 2

DIXIE VALLEY SEISMIC DATA

Table of Contents

List of Tables

Table 1. The following stations (within 200 km of the study area) are used for seismic event and ambient - noise tomographic analyses in Dixie Valley. Three stations, shown with red letters, are in DVSA; see text for explanation of DVSA.

Station	Channel	Lat (deg)	Long (deg)	Elevation (m)
ADH	SH	37.9682	-118.7163	2.0430
ANT	SH	37.9177	-118.5650	2.0400
BMN	BH	40.4315	-117.2228	1.4800
BMO	BH	40.4315	-117.2218	1.5940
BON	SH	37.9551	-118.3027	2.5820
DIX	**SH**	**39.8021**	**-118.0830**	**1.1430**
DNY	BH	41.0861	-119.2789	2.0135
FPK	SH	39.2250	-118.1516	2.4940
HCK	SH	38.0754	-118.5932	1.8900
HYX	**SH**	**39.7727**	**-117.7642**	**1.6610**
KVN	BH	39.0484	-118.1012	1.8290
LHV	SH	38.2513	-118.5049	2.3530
LUL	SH	38.0522	-119.1813	2.2430
MCC	SH	37.9194	-119.0253	2.2550
MIL	SH	38.0247	-118.1868	2.0300
MMC	SH	38.3607	-119.1293	2.5480
MNA	BH	38.4341	-118.1555	1.5040
MNV	BH	38.4328	-118.1531	1.5240
MPT	SH	38.0633	-118.7804	2.1780
PAH	BH	39.7106	-119.3854	1.5200
POW	EH	38.4094	-118.6328	1.8900
RYN	SH	38.6281	-118.5238	1.6510
SJC	SH	38.3491	-119.4400	2.2460
TNP	EH	38.0820	-117.2191	1.9390
TPH	BH	38.0750	-117.2230	1.8840
VIP	EH	39.7555	-119.4615	2.4990
WAK	EH	38.5043	-119.4382	1.8900
WHR	BH	40.0362	-118.3621	1.4940
YER	EH	38.9852	-119.2406	1.8570
M07A	BH	41.3884	-119.1711	1.4000
M08A	BH	41.4483	-118.3792	1.2884
M09A	BH	41.4230	-117.4497	1.3558
N07B	BH	40.7797	-118.9711	1.3020
N08A	BH	40.7811	-118.1337	1.4929
N09A	BH	40.8520	-117.5244	1.6173
O07A	BH	40.1614	-118.8772	1.2030
O08A	BH	40.2903	-118.1550	2.1376
O09A	BH	40.1697	-117.1899	1.4917
P07A	BH	39.5399	-118.8893	1.2186
P08A	**BH**	**39.6946**	**-118.0800**	**1.0402**
P09A	BH	39.5516	-117.1395	1.7377
Q07A	BH	38.9383	-118.8078	1.2759
Q08A	BH	38.8606	-117.9316	1.4115
Q09A	BH	38.8340	-117.1816	1.7035
R06C	BH	38.5226	-119.4509	1.6980
R07C	BH	38.0890	-119.0469	1.9960
R08A	BH	38.3489	-118.1064	1.4198
R09A	BH	38.2397	-117.0718	1.7590

Table 2. Earthquakes in Dixie Valley located by the USGS and re-located at the Nevada Seismological Laboratory using HYPODD (Waldhauser and Elsworth, 2000). Relocation of events is important for DVSA fault description; see text for explanation of DVSA.

	USGS locations				**HYPODD - relocated events**		
	Longitude (deg)	*Latitude (deg)*	*Depth (km)*	*M_L*	*Longitude (deg)*	*Latitude (deg)*	*Depth (km)*
1	-117.8553	39.9591	6.250	4.2	-117.857096	39.957166	6.481
2	-117.8587	39.9515	3.740	2.1	-117.862712	39.951746	3.628
3	-117.8713	39.9322	10.170	---	-117.871672	39.931694	9.948
4	-117.8697	39.9353	5.950	---	-117.870272	39.933256	5.249
5	-117.8529	39.9534	11.040	---	-117.859098	39.950073	11.601
6	-117.8720	39.9385	5.520	---	-117.869027	39.940409	6.592
7	-117.8582	39.9468	12.850	2.3	-117.854150	39.951355	12.736
8	-117.8764	39.9753	5.830	3.6	-117.875659	39.974251	6.489
9	-117.8709	39.9668	7.270	3.8	-117.871419	39.965568	7.735
10	-117.8751	39.9446	0.000	3.6	-117.8751	39.9446	0.000
11	-117.8531	39.9472	0.000	---	-117.8531	39.9472	0.000
12	-117.8908	39.9736	0.000	---	-117.8908	39.9736	0.000
13	-117.8903	39.9626	0.000	---	-117.8903	39.9626	0.000
14	-117.8213	39.9223	0.000	---	-117.8213	39.9223	0.000
15	-117.8117	39.9670	3.290	---	-117.8117	39.9670	3.290
16	-117.8500	39.9258	17.890	---	-117.845443	39.928935	14.367
17	-117.9614	39.7926	0.000	---	-117.9614	39.7926	0.000

Table 3. Seismic velocity models available in Dixie Valley. The depth column contains depth (km) with layer minimum and maximum depth range. The "Area" column contains latmin, latmax, lonmin, lonmax for every model, where available, or only (lat, lon) when the model is available in one location. Corner values are relative to the Project Area outline (see Figure 1 in main body of baseline report). Negative depth shows elevation. The seismic models on the reflection lines in Dixie Valley (Anonymous, 1998) are described relative to the line end (for example, the model at 2 km from NW means that the reference point is the northwest-most line point). Some sources are from seismic models described in the main body of this report, see Section 3.5.

Depth (km)		Area Corner Values (latitude,longitude)	Vp (km/s)	Vs (km/s)	Density (g/cm^3)	Qp	Qs	Poisson ratio	Source
min	max								
-1.5	0	40.2, -117.6	4.0						Catchings, 1992 (sp4c[1])
0	2		4.5						
2	11		6.0						
11	13		6.15						
13	20		6.3						
20	26		6.6						
26	29.5		7.4						
29.5	36		8.0						
-1	0	40.2, -117.4	2.5						Catchings, 1992 (sp4d[1])
0	1		4						
1	4		4.5						
4	11		6.0						
11	13		6.15						
13	19		6.3						
19	24		6.6						
24	29.5		7.4						
29.5	36		8						
-1.5	0	40.3, -117.0	4.0						Catchings, 1992 (SP5[1])
0	1		4.0						
1	6		5.7						
6	14		6.0						
14	15		6.15						
15	21		6.3						
21	25		6.6						
25	29		7.4						
29	36		8.0						
-1.0	1	40.2, -117.9	2.5						Catchings, 1992 (SP4[1])
1	2		4.0						
2	8		4.5						
8	11		6.0						
11	12		6.15						
12	20		6.3						
20	24		6.6						
24	29		7.4						
29	36		8						
0	3	General Model	1.65	1	2	163	80		AK135
3	13		5.8	3.2	2.6	1478	600		
13	21		6.8	3.9	2.92	1368	600		
21	46		8.0355	4.48	3.64	950	394		
46	53		8.0379	4.4856	3.5801	872	417		
0	2.5	All-Basin and Range	3.5	2.1					Priestley and Brune (1978)
2.5	20		6.05	3.57	3.02				
20	35		6.66	3.85	3.1				
35	65		7.785	4.5	3.3				

Table 3. Seismic velocity models available in Dixie Valley. The depth column contains depth (km) with layer minimum and maximum depth range. The "Area" column contains latmin, latmax, lonmin, lonmax for every model, where available, or only (lat, lon) when the model is available in one location. Corner values are relative to the Project Area outline (see Figure 1 in main body of baseline report). Negative depth shows elevation. The seismic models on the reflection lines in Dixie Valley (Anonymous, 1998) are described relative to the line end (for example, the model at 2 km from NW means that the reference point is the northwest-most line point). Some sources are from seismic models described in the main body of this report, see Section 3.5.

Depth (km)		**Area Corner Values (latitude,longitude)**	**Vp (km/s)**	**Vs (km/s)**	**Density (g/cm^3)**	**Qp**	**Qs**	**Poisson ratio**	**Source**
min	max								
0	2.5	Battle Mtn	3.5	2.1					Priestley and Brune (1978)
2.5	18		6.05	3.7					
18	32		6.7	3.9					
0	0.5	39, -117; 40, -119	2.3	1.2	2.1				CRUST5.1
0.5	12		6.1	3.5	2.75				
12	23.5		6.3	3.6	2.8				
23.5	35		6.6	3.6	2.9				
35	50		8	3.6	3.3				
0	0.11	39.5, -119.5 40.5, -118.5		1.08					*CU_SDT1.0*
0.11	10.68			3.2146					
10.68	23.46			3.59					
23.46	29.63			3.6171					
29.63	35			4.4					
0	0.29	39.5, -118.5 40.5, -117.5		1.197					*CU_SDT1.0*
0.29	10.27			3.3913					
10.27	21.04			3.3917					
21.04	26.94			3.3975					
26.94	27.82			4.4053					
27.82	28.71			4.4046					
28.71	29.61			4.4036					
29.61	30.50			4.4021					
30.5	36			4.3901					
0	0.5	39, -118.25	3.3						Stauder and Ryal (1967)
0.5	2	39.25, -118	4.7						
-1.2	0.23	39.63, -118.183 39.63, -118.175	1.4		2.2				Abbott et al., (2001)
0.23	0.4		2.5		2.3				
0.4	0.43		2.75		2.67				
0.45	2		3.35		2.67				
-1.2	0.2	39.63, -118.175 39.63, -118.165	1.4		2.2				Abbott et al., (2001)
0.2	0.4		1.9		2.3				
0.4	0.5		2.1		2.3				
0.5	0.6		2.3		2.67				
0.6	2		3.4		2.67				
-1.2	0.2	39.63, -118.165 39.63, -118.157	2.1		2.2				Abbott et al., (2001)
0.2	0.33		2.5		2.3				
0.33	0.5		2.8		2.3				
0.5	0.6		3		2.3				
0.6	2		3.4		2.67				

Table 3. Seismic velocity models available in Dixie Valley. The depth column contains depth (km) with layer minimum and maximum depth range. The "Area" column contains latmin, latmax, lonmin, lonmax for every model, where available, or only (lat, lon) when the model is available in one location. Corner values are relative to the Project Area outline (see Figure 1 in main body of baseline report). Negative depth shows elevation. The seismic models on the reflection lines in Dixie Valley (Anonymous, 1998) are described relative to the line end (for example, the model at 2 km from NW means that the reference point is the northwest-most line point). Some sources are from seismic models described in the main body of this report, see Section 3.5.

Depth (km)		**Area Corner Values (latitude,longitude)**	**Vp (km/s)**	**Vs (km/s)**	**Density (g/cm^3)**	**Qp**	**Qs**	**Poisson ratio**	**Source**
min	max								
-1.2	0.2	39.63, -118.139 39.63, -188.139			2.2				Abbott et al., (2001)
0.2	1				2.3				
1	1.9				2.5				
1.9	3				2.67				
-1.2	0.2	39.63, -118.129 39.63, -118.129			2.2				Abbott et al., (2001)
0.2	1				2.3				
1	2.4				2.5				
2.4	3				2.67				
-1.2	0.2	39.63, -118.093 39.63, -118.093			2.2				Abbott et al., (2001)
0.2	1				2.3				
1	2.7				2.5				
2.7	3				2.67				
0	11.2	150km from Goldstrike 37.458908 -117.82103	6						Louie et al., (2004)
11.2	21.3		6.5						
21.3	30		7						
0	0.08	0-0.7 km from SW 39.9547, -117.8403 39.9609, -117.8402	1.5						SRCIN - A (Anonymous, 1998)
0.08	0.28		2.5						
0.28	0.7		3.5						
0.7	1.9		3.9						
1.9	2		4.2						
2	3		4.7						
0	0.36	0.7-1.2 km from SW 39.9609, -117.8402 39.9654, -117.8401	1.5						SRCIN - A (Anonymous, 1998)
0.36	0.7		2.5						
0.7	0.9		3.5						
0.9	1.2		3.9						
1.2	1.4		4.5						
1.4	3		5.1						
0	0.16	1.2 - 3 km from SW 39.9654, -117.8401, 39.9816, -117.8401	1.5						SRCIN - A (Anonymous, 1998)
0.16	1.2		2.7						
1.2	1.32		3.5						
1.32	1.45		4.2						
1.45	3		5.1						
0	0.125	0-6.2 km	1.5						SRCIN - B (Anonymous, 1998)
0.125	0.9		2.8						
0.9	1		3.5						
1	1.3		4.2						
1.3	3		5.1						

Table 3. Seismic velocity models available in Dixie Valley. The depth column contains depth (km) with layer minimum and maximum depth range. The "Area" column contains latmin, latmax, lonmin, lonmax for every model, where available, or only (lat, lon) when the model is available in one location. Corner values are relative to the Project Area outline (see Figure 1 in main body of baseline report). Negative depth shows elevation. The seismic models on the reflection lines in Dixie Valley (Anonymous, 1998) are described relative to the line end (for example, the model at 2 km from NW means that the reference point is the northwest-most line point). Some sources are from seismic models described in the main body of this report, see Section 3.5.

Depth (km)		Area Corner Values (latitude,longitude)	Vp (km/s)	Vs (km/s)	Density (g/cm^3)	Qp	Qs	Poisson ratio	Source
min	max								
0	0.125	0 -4.4 km from SW 39.9306, -117.9381 39.9425 -117.8885	1.5						(Anonymous, 1998) SRCIS-A
0.125	0.2		2.5						
0.2	0.7		2.8						
0.7	0.8		3.5						
0.8	0.9		4.2						
0.9	3		5.1						
0	0.125	4.4 - 5.7 km from SW 39.9425 -117.8885 39.9445, -117.8798	1.5						(Anonymous, 1998) SRCIS-A
0.125	0.2		2.7						
0.2	0.7		2.8						
0.7	0.8		3.5						
0.8	0.9		4.2						
0.9	3		5.1						
0	0.125	0-3.7 km from SW	1.5						(Anonymous, 1998) SRCIS-B
0.125	0.5		2.8						
0.5	0.9		3.4						
0.9	1		4.2						
1	3		5.1						
0	0.125	3.7-4.49 km from SW	1.5						(Anonymous, 1998) SRCIS-B
0.125	1		2.8						
1	3		4.2						
0	0.25	0-0.5 km from NW 39.9981, -117.8347 39.9941, -117.8319	1.7						SRC3 NW-SE
0.25	0.3		2.9						
0.3	0.6		3.5						
0.6	1		4.1						
1	1.7		4.6						
1.7	2.4		4.8						
2.4	3		4.9						
0	0.2	0.5-1 km from NW 39.9941, -117.8319 39.9901, -117.8291	1.9						SRC3 NW-SE
0.2	0.4		3						
0.4	1		3.4						
1	1.1		4.6						
1.1	2.1		4.9						
2.1	3		5						
0	0.2	1-2 km from NW 39.9901, -117.8291, 39.9821, -117.8235	1.5						SRC3 NW-SE
0.2	0.4		1.7						
0.4	1		2.9						
1	1.2		3.4						
1.2	2		4.7						
2	3		4.9						

Table 3. Seismic velocity models available in Dixie Valley. The depth column contains depth (km) with layer minimum and maximum depth range. The "Area" column contains latmin, latmax, lonmin, lonmax for every model, where available, or only (lat, lon) when the model is available in one location. Corner values are relative to the Project Area outline (see Figure 1 in main body of baseline report). Negative depth shows elevation. The seismic models on the reflection lines in Dixie Valley (Anonymous, 1998) are described relative to the line end (for example, the model at 2 km from NW means that the reference point is the northwest-most line point). Some sources are from seismic models described in the main body of this report, see Section 3.5.

Depth (km)		Area Corner Values (latitude,longitude)	Vp (km/s)	Vs (km/s)	Density (g/cm^3)	Qp	Qs	Poisson ratio	Source
min	max								
0	0.200	2-6 km from NW 39.9821, -117.8235 39.9511, -117.8017	1.54						SRC3 NW-SE
0.2	1		1.9						
1	1.25		3.2						
1.25	2.7		3.6						
2.7	3		4.2						
0	0.7	0 - 6 km from NE 39.9861, -117.7951 39.9461, -117.8446	2.2						(Anonymous, 1998) Line 101
0.7	0.75		3.2						
0.75	0.9		4.1						
0.9	1.3		4.7						
1.3	1.7		4.8						
1.7	3		5						
0	0.6	6-7.5 km from NE 39.9461, -117.8446 39.9371, -117.8557	2.2						(Anonymous, 1998) Line 101
0.6	0.7		3.2						
0.7	0.8		4.1						
0.8	1.2		4.8						
1.23	3		5						
0	0.7	7.5-13 km from NE 39.9371, -117.8557 39.9011, -117.9002	2.2						(Anonymous, 1998) Line 101
0.7	0.75		3						
0.75	0.85		4.1						
0.85	1		4.7						
1	1.5		4.8						
1.5	3		5.1						
0	0.3	13-15.3 km from NE 39.9011, -117.9002, 39.8861, -117.9188	1.6						(Anonymous, 1998) Line 101
0.3	0.7		2.2						
0.7	0.75		3.1						
0.75	1		4						
1	1.5		4.3						
1.5	2		4.7						
2	2.5		4.8						
2.5	3		5.1						
0	0.35	0-3 km from NW 39.9852, -117.8534 39.9662, -117.8283	2.1						(Anonymous, 1998) Line 103
0.35	0.4		3.1						
0.4	0.45		3.6						
0.45	0.5		4.2						
0.5	3		5						
0	0.35	3-3.2 km from NW 39.9662, -117.8283 39.9642 -117.8257	2.1						(Anonymous, 1998) Line 103
0.35	0.44		3.1						
0.44	0.5		3.6						
0.5	3		4.2						

Table 3. Seismic velocity models available in Dixie Valley. The depth column contains depth (km) with layer minimum and maximum depth range. The "Area" column contains latmin, latmax, lonmin, lonmax for every model, where available, or only (lat, lon) when the model is available in one location. Corner values are relative to the Project Area outline (see Figure 1 in main body of baseline report). Negative depth shows elevation. The seismic models on the reflection lines in Dixie Valley (Anonymous, 1998) are described relative to the line end (for example, the model at 2 km from NW means that the reference point is the northwest-most line point). Some sources are from seismic models described in the main body of this report, see Section 3.5.

Depth (km)		Area Corner Values (latitude,longitude)	Vp (km/s)	Vs (km/s)	Density (g/cm^3)	Qp	Qs	Poisson ratio	Source
min	max								
0	0.9	3.2 - 4 km from NW 39.9642 -117.8257 39.9602 -117.8204	2.1						(Anonymous, 1998) Line 103
0.8	2.2		3.1						
2.2	3		3.6						
0	0.125	0-0.5 km from NW 39.9445, -117.8644 39.9405 -117.8618	1.5						(Anonymous, 1998) Line 105
0.125	0.250		1.8						
0.250	0.75		2.5						
0	0.25	0.5 - 1 km from NW 39.9405 -117.8618 39.9365 -117.8592	1.8						(Anonymous, 1998) Line 105
0.25	0.5		2.5						
0.5	0.75		3.1						
0	0.17	1 - 1.5 km from NW 39.9365 -117.8592 39.9325 -117.8566	1.9						(Anonymous, 1998) Line 105
0.17	0.31		3.1						
0.31	0.4		3.4						
0.4	0.6		4.1						
0.6	0.7		4.8						
0.7	0.75		4.9						
0	0.125	1.5-2 km from NW 39.9325 -117.8566 39.9285 -117.8540	1.9						(Anonymous, 1998) Line 105
0.125	0.31		1.5						
0.31	0.4		2.7						
0.45	0.5		3.1						
0.5	0.55		3.4						
0.55	0.6		4.1						
0.6	0.65		4.4						
0.65	0.75		4.9						
0	0.25	2-2.5 km from NW 39.9285 -117.8540 39.9245 -117.8514	1.8						(Anonymous, 1998) Line 105
0.25	0.5		3.1						
0.5	0.6		3.2						
0.6	0.65		4.1						
0.65	0.75		4.4						
0	0.25	2.5 3 km from NW 39.9245 -117.8514 39.9205 -117.8488	1.8						(Anonymous, 1998) Line 105
0.25	0.6		2.5						
0.6	0.65		3.4						
0.65	0.75		4.1						
0	0.125	3-3.5 km from NW 39.9205 -117.8488 39.9175 -117.8468	1.5						(Anonymous, 1998) Line 105
0.125	0.75		2.4						
0	0.25	3.5 -4 km from NW 39.9175 -117.8468 39.9167, -117.8457	1.9						(Anonymous, 1998) Line 105
0.25	0.75		2.4						

Table 3. Seismic velocity models available in Dixie Valley. The depth column contains depth (km) with layer minimum and maximum depth range. The "Area" column contains latmin, latmax, lonmin, lonmax for every model, where available, or only (lat, lon) when the model is available in one location. Corner values are relative to the Project Area outline (see Figure 1 in main body of baseline report). Negative depth shows elevation. The seismic models on the reflection lines in Dixie Valley (Anonymous, 1998) are described relative to the line end (for example, the model at 2 km from NW means that the reference point is the northwest-most line point). Some sources are from seismic models described in the main body of this report, see Section 3.5.

Depth (km)		**Area Corner Values (latitude,longitude)**	**Vp (km/s)**	**Vs (km/s)**	**Density (g/cm^3)**	**Qp**	**Qs**	**Poisson ratio**	**Source**
min	max								
0	0.4	0-1.5 km from SW 39.953, -117.8798 39.9532 -117.8591	2.9						(Anonymous, 1998) Line 5
0.4	0.6		3.0						
0.6	0.8		3.6						
0.8	1		4.3						
1	3		4.7						
0	0.5	1.5 km from SW- 3 km from SW 39.9532 -117.8591 39.9533 -117.8454	2.1						(Anonymous, 1998) Line 5
0.5	0.7		3.1						
0.7	0.8		3.4						
0.8	0.9		4.2						
0.9	1.1		4.7						
1.1	3		5.1						
0	0.4	3-4 km from SW 39.9533 -117.8454 39.9534 -117.8316	1.9						(Anonymous, 1998) Line 5
0.4	0.8		2.1						
0.8	1		3.1						
1	1.16		3.4						
1.16	1.27		4.2						
1.27	3		4.7						
0	0.45	4-6 km from SW 39.9534 -117.8316 39.9535 -117.8109	1.8						(Anonymous, 1998) Line 5
0.45	0.9		1.9						
0.9	1		2.1						
1	1.1		3.1						
1.1	1.2		3.4						
1.2	1.3		4.2						
1.3	3		4.7						
0	0.25	6-7 km from SW 39.9535 -117.8109 39.9536 -117.7971	1.6						(Anonymous, 1998) Line 5
0.25	0.5		1.9						
0.5	0.8		2.4						
0.8	1		3.1						
1	1.3		3.4						
1.3	3		5.1						
0	0.25	7-8.5 km from SW 39.9536 -117.7971 39.9537 -117.7765	1.6						(Anonymous, 1998) Line 5
0.25	0.70		1.9						
0.7	1		2.5						
1	1.3		3.1						
1.3	1.4		3.4						
1.4	3		5.1						
0.25	0.5	8.5-9.2 km from SW 39.9537 -117.7765 39.9538 -117.7696	1.9						(Anonymous, 1998) Line 5
0.5	0.8		2.4						
0.8	1		3.1						
1	1.3		3.4						
1.3	3		5.1						

Table 3. Seismic velocity models available in Dixie Valley. The depth column contains depth (km) with layer minimum and maximum depth range. The "Area" column contains latmin, latmax, lonmin, lonmax for every model, where available, or only (lat, lon) when the model is available in one location. Corner values are relative to the Project Area outline (see Figure 1 in main body of baseline report). Negative depth shows elevation. The seismic models on the reflection lines in Dixie Valley (Anonymous, 1998) are described relative to the line end (for example, the model at 2 km from NW means that the reference point is the northwest-most line point). Some sources are from seismic models described in the main body of this report, see Section 3.5.

Depth (km)		Area Corner Values (latitude,longitude)	Vp (km/s)	Vs (km/s)	Density (g/cm^3)	Qp	Qs	Poisson ratio	Source
min	max								
0	0.1	9.2 -11 km from SW 39.9538 -117.7696 39.9539 -117.7489	1.6						(Anonymous, 1998) Line 5
0.1	0.4		1.9						
0.4	0.7		2.4						
0.7	0.9		3.1						
0.9	1.1		3.4						
1.1	1.2		4.3						
1.2	3		5.1						
0	0.3	11-11.5 km from SW 39.9539 -117.7489 39.9540 -117.7420	2.4						(Anonymous, 1998) Line 5
0.3	0.5		3.1						
0.5	1		3.4						
1	1.33		4.3						
1.33	3		4.8						
0	0.2	0-1.6 km from NW 39.9648 -117.8699 39.9548 -117.8552	2.1						(Anonymous, 1998) Line 9
0.2	0.4		3						
0.4	0.5		3.6						
0.5	0.6		4.2						
0.6	0.7		4.7						
0.7	3		5						
0	0.2	1.6-2.7 km from NW 39.9548 -117.8552 39.9488 -117.8464	1.6						(Anonymous, 1998) Line 9
0.2	0.4		2.2						
0.4	0.5		3.0						
0.5	2.6		3.6						
2.6	3		4.15						
0	0.2	2.7 -2.9 km from NW 39.9488 -117.8464 39.9468 -117.8435	1.8						(Anonymous, 1998) Line 9
0.2	0.4		2.2						
0.4	0.6		2.8						
0.6	2.7		3.1						
2.7	3		4.15						
0	0.5	2.9 - 3.5 km from NW 39.9468 -117.8435 39.9438 -117.8391	1.9						(Anonymous, 1998) Line 9
0.5	1		2.6						
1	2.7		3.1						
2.7	3		4.15						
0	0.5	3.5 - 6 km from NW 39.9438 -117.8391 39.9288 -117.8171	1.6						(Anonymous, 1998) Line 9
0.5	1		2.6						
1	2.7		3.1						
2.7	3		4.15						
0	0.5	0-0.7 km from NW 39.9583 -117.8776 39.9523 -117.8728	2.1						(Anonymous, 1998) Line 10
0.5	0.6		3.1						
0.6	0.7		3.4						
0.7	0.8		4.1						
0.8	3		5						

Table 3. Seismic velocity models available in Dixie Valley. The depth column contains depth (km) with layer minimum and maximum depth range. The "Area" column contains latmin, latmax, lonmin, lonmax for every model, where available, or only (lat, lon) when the model is available in one location. Corner values are relative to the Project Area outline (see Figure 1 in main body of baseline report). Negative depth shows elevation. The seismic models on the reflection lines in Dixie Valley (Anonymous, 1998) are described relative to the line end (for example, the model at 2 km from NW means that the reference point is the northwest-most line point). Some sources are from seismic models described in the main body of this report, see Section 3.5.

Depth (km)		Area Corner Values (latitude,longitude)	Vp (km/s)	Vs (km/s)	Density (g/cm^3)	Qp	Qs	Poisson ratio	Source
min	max								
0	0.15	0.7 - 1.2 km from NW 39.9523 -117.8728 39.9483 -117.8696	1.6						(Anonymous, 1998) Line 10
0.15	0.6		2						
0.6	0.7		3						
0.7	0.75		3.4						
0.75	0.8		4.1						
0.8	3		5						
0	0.1	1.2 - 2.8 km from NW 39.9483 -117.8696 39.9363 -117.8599	1.6						(Anonymous, 1998) Line 10
0.1	0.8		2						
0.8	1.1		3						
1.1	2.7		3.4						
2.7	3		4.1						
0	0.1	2.8 - 4 km from NW 39.9363 -117.8599 39.9273 -117.8526	1.6						(Anonymous, 1998) Line 10
0.1	0.6		2						
0.6	1.1		3.2						
1.1	2.7		3.4						
2.7	3		4.1						

[1] Represents a station location from Catchings (1992); see Figure 15 in the main body of this report.

Table 4. From the EarthScope Automated Receiver Survey (EARS) http://ears.iris.washington.edu/Data/Summary/. The estimated thickness is from the general crustal model CRUST2.0. Red values are most likely subject to error, due to few events, or high waveform complexity (equivalent to large parameter errors) for the available events. Note that P08A (Dixie Valley) is one of these stations. See the link above for more information on table terms.

Network	**Station**	**Latitude**	**Longitude**	**Elevation** (m)	**Estimated Thickness** (km)	**StdDev** (km)	**Estimated Vp/Vs** (km/s)	**StdDev** (km/s)	**Assumed Vp** (km/s)	**Vs** (km/s)	**Poisson's_Ratio**	**# Earthquakes**	**Complexity**
US	BMN	40.43N	117.22 W	1500	29	6.3	1.80	0.02	6.276	3.487	0.28	4	0.55
TA	P08A	39.69N	118.08 W	1.0	29	11	2.10	0.16	6.279	2.99	0.35	3	0.73
TA	P09A	39.55N	117.14 W	1.7	30	1.5	1.84	0.04	6.276	3.411	0.29	63	0.50
TA	P07A	39.54N	118.89 W	1.2	28	7.4	2.10	0.03	6.279	2.99	0.35	19	0.67
TA	N07B	40.78N	118.97 W	1.3	27	1.6	1.88	0.04	6.276	3.338	0.30	69	0.55
TA	O07A	40.16N	118.88 W	1.2	32	0.2	1.67	0.02	6.276	3.758	0.22	75	0.45
TA	N08A	40.78N	118.13 W	1.5	31	0.2	1.84	0.02	6.276	3.411	0.29	68	0.30
TA	O06A	40.17N	119.83 W	1.2	33	0.6	1.81	0.02	6.276	3.467	0.28	66	0.57
TA	N09A	40.85N	117.52 W	1.6	33	0.3	1.74	0.02	6.276	3.607	0.25	74	0.43
TA	Q07A	38.94N	118.81 W	1.3	35	9.2	1.66	0.15	6.279	3.783	0.22	6	0.66
TA	Q09A	38.83N	117.18 W	1.7	36	6.3	1.91	0.10	6.276	3.286	0.31	48	0.70
TA	Q08A	38.86N	117.93 W	1.4	42	0.5	1.61	0.02	6.276	3.898	0.19	64	0.66
TA	N07A	40.77N	118.97 W	1.3	66	11	1.74	0.11	6.276	3.607	0.25	2	0.82
TA	O09A	40.17N	117.19 W	1.5	25	0.2	2.08	0.02	6.276	3.017	0.35	53	0.63
TA	O08A	40.29N	118.15 W	2.1	32	0.3	1.65	0.02	6.276	3.804	0.21	42	0.25

Table 5. Approximate Q values extracted from Phillips and Stead (2008). Lat+0.125°, Long+0.125°

Latitude (deg)	Longitude (deg)	Q_{Lg} (@1 Hz)
38.75	-119.0000	125
	-118.8750	125
	-118.7500	125
	-118.6250	125
	-118.5000	137
	-118.3750	137
	-118.2500	137
	-118.1250	137
	-118.0000	137
	-117.8750	150
	-117.7500	162
	-117.6250	175
	-117.5000	162
	-117.3750	175
	-117.2500	175
	-117.1250	187
	-117.0000	250
38.875	-119.0000	125
	-118.8750	125
	-118.7500	125
	-118.6250	137
	-118.5000	137
	-118.3750	137
	-118.2500	137
	-118.1250	137
	-118.0000	137
	-117.8750	150
	-117.7500	162
	-117.6250	175
	-117.5000	175
	-117.3750	175
	-117.2500	175
	-117.1250	187
	-117.0000	250
39.0	-119.0000	125
	-118.8750	125
	-118.7500	125
	-118.6250	125
	-118.5000	137
	-118.3750	137
	-118.2500	137
	-118.1250	137
	-118.0000	137
	-117.8750	162
	-117.7500	175
	-117.6250	175
	-117.5000	175
	-117.3750	175
	-117.2500	175
	-117.1250	187
	-117.0000	250

Table 5. Approximate Q values extracted from Phillips and Stead (2008). Lat+0.125°, Long+0.125°

Latitude (deg)	Longitude (deg)	Q_{Lg} (@1 Hz)
39.125	-119.0000	125
	-118.8750	125
	-118.7500	125
	-118.6250	125
	-118.5000	137
	-118.3750	150
	-118.2500	150
	-118.1250	162
	-118.0000	162
	-117.8750	175
	-117.7500	175
	-117.6250	175
	-117.5000	162
	-117.3750	162
	-117.2500	162
	-117.1250	175
	-117.0000	250
39.25	-119.0000	125
	-118.8750	125
	-118.7500	125
	-118.6250	125
	-118.5000	137
	-118.3750	137
	-118.2500	137
	-118.1250	150
	-118.0000	162
	-117.8750	175
	-117.7500	175
	-117.6250	175
	-117.5000	162
	-117.3750	150
	-117.2500	150
	-117.1250	162
	-117.0000	250
39.375	-119.0000	125
	-118.8750	125
	-118.7500	125
	-118.6250	125
	-118.5000	137
	-118.3750	137
	-118.2500	137
	-118.1250	150
	-118.0000	162
	-117.8750	175
	-117.7500	175
	-117.6250	175
	-117.5000	162
	-117.3750	150
	-117.2500	150
	-117.1250	162
	-117.0000	250

Table 5. Approximate Q values extracted from Phillips and Stead (2008). Lat+0.125°, Long+0.125°

Latitude (deg)	Longitude (deg)	Q_{Lg} (@1 Hz)
39.5	-119.0000	125
	-118.8750	125
	-118.7500	125
	-118.6250	125
	-118.5000	138
	-118.3750	145
	-118.2500	145
	-118.1250	150
	-118.0000	162
	-117.8750	175
	-117.7500	175
	-117.6250	175
	-117.5000	162
	-117.3750	150
	-117.2500	150
	-117.1250	162
	-117.0000	250
39.625	-119.0000	125
	-118.8750	125
	-118.7500	125
	-118.6250	138
	-118.5000	138
	-118.3750	138
	-118.2500	150
	-118.1250	162
	-118.0000	175
	-117.8750	175
	-117.7500	175
	-117.6250	175
	-117.5000	162
	-117.3750	150
	-117.2500	150
	-117.1250	162
	-117.0000	250
39.750	-119.0000	125
	-118.8750	125
	-118.7500	125
	-118.6250	125
	-118.5000	125
	-118.3750	138
	-118.2500	150
	-118.1250	162
	-118.0000	175
	-117.8750	175
	-117.7500	175
	-117.6250	175
	-117.5000	162
	-117.3750	150
	-117.2500	162
	-117.1250	162
	-117.0000	187

Table 5. Approximate Q values extracted from Phillips and Stead (2008). Lat+0.125°, Long+0.125°

Latitude (deg)	Longitude (deg)	Q_{Lg} (@1 Hz)
39.875	-119.0000	125
	-118.8750	125
	-118.7500	125
	-118.6250	125
	-118.5000	125
	-118.3750	125
	-118.2500	125
	-118.1250	150
	-118.0000	162
	-117.8750	175
	-117.7500	175
	-117.6250	162
	-117.5000	162
	-117.3750	150
	-117.2500	162
	-117.1250	175
	-117.0000	187
40.0	-119.0000	125
	-118.8750	138
	-118.7500	125
	-118.6250	125
	-118.5000	125
	-118.3750	125
	-118.2500	125
	-118.1250	138
	-118.0000	175
	-117.8750	175
	-117.7500	175
	-117.6250	162
	-117.5000	150
	-117.3750	150
	-117.2500	162
	-117.1250	175
	-117.0000	175
40.125	-119.0000	125
	-118.8750	125
	-118.7500	138
	-118.6250	138
	-118.5000	138
	-118.3750	125
	-118.2500	125
	-118.1250	125
	-118.0000	138
	-117.8750	150
	-117.7500	162
	-117.6250	162
	-117.5000	150
	-117.3750	150
	-117.2500	150
	-117.1250	162
	-117.0000	162
	-119.0000	175

Table 5. Approximate Q values extracted from Phillips and Stead (2008). Lat+0.125°, Long+0.125°

Latitude (deg)	Longitude (deg)	Q_{Lg} (@1 Hz)
40.250	-119.0000	125
	-118.8750	125
	-118.7500	138
	-118.6250	138
	-118.5000	138
	-118.3750	138
	-118.2500	138
	-118.1250	138
	-118.0000	138
	-117.8750	150
	-117.7500	162
	-117.6250	150
	-117.5000	150
	-117.3750	150
	-117.2500	162
	-117.1250	162
	-117.0000	175

APPENDIX 3

SEISMIC EVENT CATALOG FOR THE GREATER DIXIE VALLEY PROJECT AREA - 38.7°N TO 40.3°N AND 117°W TO 119°W FOR THE PERIOD 1872-2010

Table of Contents

List of Tables

---

[1] identified by UNR analysts as explosions within 38.7°N - 40.3° N and 119°W -117°W

Table 1. Seismic Event Catalog (1872-1999)

Area: 38.7°N to 40.3°N, 117°W to 119°W
Time period: 1872-1999
Sources:
The United States Geological Survey (USGS) / Preliminary Determination of Epicenters (PDE);
The USGS USHIS-historical catalog;
The Nevada Seismological Laboratory (NSL)/University of Nevada, Reno (UNR) catalog;

The columns represent, in order:
1) CATALOG (**Catalog**);
2) YYYY (**Year**)
3) MM (**M**)
4) DD (**D**)
5) ORIG_TIME (HHMMSS) (**Time**)
6) LATITUDE(DEG)(**Lat**)
7) LONGITUDE(DEG)(**Long**)
8) DEPTH(km) (**Depth**)
9) MAGNITUDE (**Mag**)
10) MAGNITUDE _TYPE_AND_SOURCE (**Source**)
"XX" represents unknown values

Catalog	**Year**	**M**	**D**	**Time**	**Lat**	**Long**	**Mag**	**Source**
USHIS	1872	03	23	214100	40.00	-117.50	5.5	FASJG
USHIS	1873	11	05	170000	40.00	-118.00	5.5	FASJG
USHIS	1903	XX	XX	XXXXXX	39.50	-118.10	XX	XXXX
USHIS	1917	04	11	185955	40.00	-118.00	5.1	MLSJG
USHIS	1932	12	21	061005	38.75	-118.00	7.2	MSGR
USHIS	1932	12	22	074930	38.75	-118.00	4.5	UKJON
USHIS	1932	12	22	103415	38.75	-118.00	4.9	MLSJG
USHIS	1932	12	23	2006	38.75	-118.00	4.5	UKJON
USHIS	1932	12	24	124049	38.80	-118.00	5.0	MLSJG
USHIS	1932	12	25	035445	38.80	-118.00	5.5	MLSJG
USHIS	1932	12	25	183635	38.80	-118.00	4.5	MLSJG
USHIS	1932	12	26	0503	38.75	-118.00	5.3	MLSJG
USHIS	1932	12	28	030755	38.80	-118.00	4.6	MLSJG
USHIS	1932	12	29	062028	38.80	-118.00	5.2	MLSJG
USHIS	1932	12	29	063803	38.80	-118.00	5.0	MLSJG
USHIS	1932	12	29	064508	38.80	-118.00	5.0	MLSJG
USHIS	1932	12	30	041752	38.80	-118.00	4.6	MLSJG
USHIS	1932	12	30	160310	38.80	-118.00	4.6	MLSJG
USHIS	1933	01	02	154408	38.80	-118.00	4.5	MLSJG
USHIS	1933	01	02	170644	38.80	-118.00	4.7	MLSJG
USHIS	1933	01	04	010115	38.80	-118.00	5.1	MLSJG
USHIS	1933	01	05	065020	38.75	-118.00	5.7	MSGR

Catalog	Year	M	D	Time	Lat	Long	Mag	Source
USHIS	1933	01	06	130556	39.00	-117.80	5.1	MLSJG
USHIS	1933	01	06	1333	39.00	-118.00	4.5	MLSJG
USHIS	1933	01	11	172938	38.90	-117.80	5.2	MLSJG
USHIS	1933	01	17	010208	38.80	-118.00	4.8	MLSJG
USHIS	1933	02	13	220845	38.70	-117.90	5.5	MLSJG
USHIS	1933	03	12	204420	38.80	-117.60	5.0	MLSJG
USHIS	1933	04	30	161650	39.80	-118.10	4.5	MLSJG
USHIS	1933	06	11	083431	38.80	-117.50	5.2	MLSJG
USHIS	1933	07	17	205714	39.20	-118.15	4.6	MLSJG
USHIS	1933	10	27	105854	38.90	-117.60	5.5	MLSJG
USHIS	1936	01	14	052911	39.50	-117.50	4.6	MLSJG
USHIS	1936	03	26	224340	39.10	-117.90	4.5	MLSJG
USHIS	1936	07	02	1629	39.20	-117.50	5.0	FAWOO
USHIS	1936	09	21	0731	40.25	-117.38	4.5	MLPAS
USHIS	1950	10	23	081246	39.50	-117.50	4.5	MLBRK
USHIS	1952	11	18	040408	39.80	-117.70	4.6	MLBRK
USHIS	1954	07	06	111320	39.42	-118.53	6.8	MLBRK
USHIS	1954	07	06	111804	39.42	-118.53	5.5	MLBRK
USHIS	1954	07	06	112655	39.42	-118.53	4.8	MLBRK
USHIS	1954	07	06	1141	39.42	-118.53	4.5	MLBRK
USHIS	1954	07	06	1149	39.42	-118.53	5.7	MLBRK
USHIS	1954	07	06	125359	39.42	-118.53	4.5	MLBRK
USHIS	1954	07	06	131511	39.42	-118.53	5.2	MLBRK
USHIS	1954	07	06	133601	39.42	-118.53	4.5	MLBRK
USHIS	1954	07	06	145515	39.42	-118.53	4.5	MLBRK
USHIS	1954	07	06	220741	39.30	-118.50	6.0	MLBRK
USHIS	1954	07	07	061108	39.42	-118.53	4.6	MLBRK
USHIS	1954	07	08	021355	39.42	-118.53	4.8	MLBRK
USHIS	1954	07	08	040819	39.42	-118.53	4.5	MLBRK
USHIS	1954	07	08	125510	39.42	-118.53	4.7	MLBRK
USHIS	1954	07	08	193157	39.42	-118.53	5.3	MLBRK
USHIS	1954	07	09	085003	39.42	-118.53	4.9	MLBRK
USHIS	1954	07	10	012220	39.42	-118.53	4.6	MLBRK
USHIS	1954	07	11	0704	39.42	-118.53	4.6	MLBRK
USHIS	1954	07	11	095812	39.42	-118.53	4.6	MLBRK
USHIS	1954	07	12	101706	39.42	-118.53	4.5	MLBRK
USHIS	1954	07	12	160525	39.42	-118.53	4.6	MLBRK
USHIS	1954	07	30	020010	39.42	-118.53	5.1	MLBRK
USHIS	1954	07	31	172414	39.42	-118.53	4.5	MLBRK
USHIS	1954	08	02	101853	39.42	-118.53	5.4	MLBRK
USHIS	1954	08	03	212454	39.42	-118.53	4.7	MLBRK
USHIS	1954	08	05	050308	39.42	-118.53	4.7	MLBRK
USHIS	1954	08	24	055132	39.58	-118.45	6.8	MLBRK

Catalog	Year	M	D	Time	Lat	Long	Depth	Mag	Source
USHIS	1954	08	24	055746	39.58	-118.45		5.2	MLBRK
USHIS	1954	08	25	021713	39.58	-118.45		4.8	MLBRK
USHIS	1954	08	25	222110	39.58	-118.45		4.7	MLBRK
USHIS	1954	08	26	125615	39.58	-118.45		4.6	MLBRK
USHIS	1954	08	29	034106	39.58	-118.45		4.7	MLBRK
USHIS	1954	08	29	035805	39.58	-118.45		4.8	MLBRK
USHIS	1954	08	31	222032	39.58	-118.45		5.8	MLBRK
USHIS	1954	09	01	051846	39.58	-118.45		5.5	MLBRK
USHIS	1954	09	09	092105	39.58	-118.45		4.9	MLBRK
USHIS	1954	12	16	110711	39.28	-118.12	15	7.2	MLBRK
USHIS	1954	12	16	111134	39.80	-118.10	40	7.1	MLBRK
USHIS	1954	12	16	115036	39.28	-118.12		5.0	MLBRK
USHIS	1954	12	16	115730	39.28	-118.12		5.0	MLBRK
USHIS	1954	12	16	131503	39.28	-118.12		5.0	MLBRK
USHIS	1954	12	16	141657	39.28	-118.12		5.8	MLBRK
USHIS	1954	12	16	142410	39.28	-118.12		5.3	MLBRK
USHIS	1954	12	16	150942	39.28	-118.12		5.1	MLBRK
USHIS	1954	12	16	214843	39.28	-118.12		4.5	MLBRK
USHIS	1954	12	17	101526	39.28	-118.12		4.5	MLBRK
USHIS	1954	12	17	103329	39.28	-118.12		4.7	MLBRK
USHIS	1954	12	17	202706	39.28	-118.12		5.0	MLBRK
USHIS	1954	12	18	014536	39.28	-118.12		4.7	MLBRK
USHIS	1954	12	20	173647	39.28	-118.12		5.0	MLBRK
USHIS	1955	01	01	121354	39.00	-118.00		5.1	MLBRK
USHIS	1955	01	05	082040	39.00	-118.00		XX	XXXXX
USHIS	1955	01	09	091050	39.00	-118.00		5.0	MLBRK
USHIS	1955	01	11	102140	39.00	-118.00		4.7	MLBRK
USHIS	1955	01	19	021010	39.35	-118.25		4.6	MLBRK
USHIS	1955	01	25	232646	39.00	-118.00		4.7	MLBRK
USHIS	1955	02	11	161232	39.47	-118.10		4.7	MLBRK
USHIS	1955	02	19	235007	39.30	-117.80		4.8	MLBRK
USHIS	1955	03	08	200517	39.20	-118.55		4.5	MLBRK
USHIS	1955	03	11	142316	39.30	-118.10		4.5	MLBRK
USHIS	1955	03	13	084104	39.57	-118.05		4.6	MLBRK
USHIS	1955	03	14	182347	39.42	-118.25		4.7	MLBRK
USHIS	1955	05	08	103831	38.93	-118.12		4.5	MLBRK
USHIS	1955	05	30	212826	39.42	-118.00		4.5	MLBRK
USHIS	1955	06	08	122211	38.88	-118.17		4.5	MLBRK
USHIS	1955	06	19	1920	38.97	-118.25		5.2	MLBRK
USHIS	1955	06	19	192516	39.00	-118.50		5.0	MLBRK
USHIS	1955	09	29	054051	39.22	-118.20		4.5	MLBRK
USHIS	1955	11	02	061517	39.50	-118.05		4.6	MLBRK
USHIS	1955	11	21	202533	39.42	-118.08		5.5	MLBRK

Catalog	Year	M	D	Time	Lat	Long	Depth	Mag	Source
USHIS	1955	12	22	120507	38.98	-118.70		4.8	MLBRK
USHIS	1955	12	22	120654	38.98	-118.70		4.6	MLBRK
USHIS	1955	12	31	135104	39.00	-118.03		4.5	MLBRK
USHIS	1956	03	08	072620	39.03	-118.07		4.6	MLBRK
USHIS	1956	07	26	095317	39.55	-118.45		5.1	MLBRK
USHIS	1957	10	17	101409	39.28	-118.43		4.6	MLBRK
USHIS	1959	03	23	071020	39.60	-118.02		6.3	MLBRK
USHIS	1959	05	21	175140	39.47	-118.12		4.8	MLBRK
USHIS	1959	06	23	1435	39.08	-118.82		6.1	MLBRK
USHIS	1959	06	23	150434	39.10	-118.80		5.5	MLBRK
USHIS	1961	07	04	110911	40.13	-118.60		5.0	MLBRK
USHIS	1961	08	04	165609.10	39.20	-117.40	12	4.5	MLBRK
USHIS	1962	07	20	090210	39.50	-118.20	33	4.7	MLBRK
USHIS	1964	03	22	163055.20	38.80	-118.70	16	5.5	MLBRK
USHIS	1965	04	13	131422.10	38.90	-117.70	33	4.6	MLBRK
USHIS	1968	05	29	114107.10	39.07	-118.05	3	4.9	MLBRK
PDE	1975	07	13	011630.60	39.55	-117.68	5	4.0	MLBRK
PDE	1975	07	13	013654	39.56	-117.64	5	4.2	MLBRK
PDE	1976	04	02	125635.50	39.57	-117.67	5	4.1	MLBRK
PDE	1976	06	14	195710.90	39.01	-118.18	5	XX	XXXXX
PDE	1976	09	26	224437.20	39.37	-118.11	5	3.0	MLGS
PDE	1977	02	09	072404.60	39.21	-118.02	5	XX	XXXXX
PDE	1977	02	09	072408.30	39.20	-118.04	5	3.7	MLBRK
PDE	1978	01	13	033936	39.42	-117.57	5	4.1	MLBRK
PDE	1978	01	24	224525.80	39.07	-118.07	5	3.0	MLGS
PDE	1978	02	14	043522.50	39.62	-117.13	5	4.8	MLBRK
PDE	1978	02	15	092531	39.56	-118.44	10	3.7	MLBRK
PDE	1978	03	05	224617.20	38.94	-117.99	5	4.6	MLBRK
PDE	1978	09	05	222850.30	38.98	-118.16	5	3.6	MLBRK
PDE	1980	09	21	044946.40	38.87	-118.80	5	3.1	MLPAS
PDE	1981	12	01	161850	38.62	-118.19	11	4.5	MLBRK
PDE	1981	12	07	074751.60	38.67	-118.22	6	4.1	MLBRK
PDE	1981	12	13	01XXXX	38.67	-118.24	5	3.7	MLBRK
PDE	1981	12	19	205652.90	38.63	-118.21	17	4.4	MLBRK
PDE	1982	01	28	224844.64	38.62	-118.21	5	3.8	MLBRK
PDE	1982	01	28	225043.62	38.62	-118.09	5	4.3	MLBRK
PDE	1982	01	28	225903.56	38.61	-118.18	5	3.7	MLBRK
PDE	1983	07	21	234052.65	39.07	-118.18	5	3.3	MLGS
PDE	1984	02	16	111457.53	39.93	-117.76	8	5.2	MLBRK
PDE	1984	02	19	102241.29	39.98	-117.82	10	4.0	MLGS
PDE	1987	03	16	165105.92	39.65	-118.23	5	3.5	MLGS
PDE	1987	03	25	154839.15	40.14	-117.69	5	4.2	MLBRK
PDE	1987	03	25	160132.21	40.14	-117.69	5	4.2	MLBRK

Catalog	Year	M	D	Time	Lat	Long	Depth	Mag	Source
PDE	1987	03	25	161102.06	40.12	-117.74	10	3.8	MLBRK72
PDE	1988	07	01	020003.94	39.47	-118.47	0	3.3	MDREN40
PDE	1988	09	20	001609.66	38.96	-118.18	0	3.5	MDREN61
PDE	1988	09	23	154855.62	38.96	-118.17	0	3.5	MDREN62
PDE	1988	10	27	031632.91	39.03	-117.99	0	3.5	MDREN52
PDE	1988	12	04	123358.19	39.32	-118.16	0	3.0	MDREN24
PDE	1988	12	30	174136.95	39.09	-118.10	9	3.0	MDREN46
PDE	1989	02	15	053135.86	39.30	-117.34	5	3.6	MDREN
PDE	1989	02	18	140245.03	39.23	-117.33	10	3.3	MDREN65
PDE	1989	02	22	092859.01	39.26	-117.40	4	2.9	MDREN58
PDE	1989	02	22	094944.61	39.23	-117.34	0	3.5	MDREN64
PDE	1989	05	28	103344.55	39.52	-117.83	5	2.5	MLBRK14
PDE	1989	09	25	121503.59	39.58	-119.11	5	2.7	MLBRK95
PDE	1991	02	07	161655.74	39.49	-119.13	5	2.9	MDGM96
PDE	1992	02	28	124202.24	39.63	-118.28	5	3.0	MLGS27
PDE	1992	07	20	172221.07	39.30	-119.13	5	3.0	MLGS99
PDE	1992	07	20	173440.65	39.45	-119.09	5	2.8	MLGS93
PDE	1992	07	20	173605.38	39.44	-119.12	5	3.5	MLGS
PDE	1992	07	20	190657.11	39.33	-119.10	5	3.8	MLGS
PDE	1992	07	20	191547.61	39.43	-119.07	5	2.9	MLGS92
PDE	1992	07	20	200931.52	39.31	-119.11	5	4.3	MLBRK97
PDE	1992	07	21	115820.31	39.45	-119.06	5	2.9	MLGS91
PDE	1992	07	21	130142.52	39.44	-119.09	5	2.8	MLGS
PDE	1992	09	06	093548.68	39.35	-117.95	5	3.1	MLGS17
PDE	1993	03	01	123625.85	39.44	-118.54	5	2.8	MLGS46
PDE	1993	03	05	125413.71	39.22	-118.50	5	2.7	MLGS52
PDE	1993	05	17	084502.67	39.59	-118.06	5	4.0	MLBRK
PDE	1994	06	17	222610.11	38.93	-118.01	5	3.2	MLGS63
PDE	1995	03	04	171554.77	39.55	-118.11	5	3.5	MLGS10
PDE	1995	05	08	181945.33	38.68	-118.43	8	3.8	MLBRK98
PDE	1995	06	20	074101.28	38.80	-118.70	0	2.9	MLGS98
PDE	1995	07	27	004745.54	38.84	-118.10	5	3.1	MLGS73
PDE	1995	08	02	142707.25	38.84	-118.06	5	3.1	MLGS73
PDE	1995	09	22	144721.29	38.74	-118.58	19	4.8	MLBRK97
PDE	1996	02	29	124319.20	39.92	-117.90	5	3.5	MLGS47
PDE	1996	03	31	141250.56	38.82	-117.93	5	3.3	MLGS75
PDE	1996	08	06	062932.42	38.79	-118.71	5	3.5	MLGS99
PDE	1997	06	28	141251.67	39.73	-118.07	5	3.5	MLGS25
PDE	1997	06	30	223527.05	39.68	-118.07	5	3.5	MLGS20
PDE	1998	01	08	134138.38	39.55	-117.49	5	3.7	MLGS44
PDE	1998	09	04	145222	38.79	-117.97	15	3.4	MLGS78
PDE	1998	09	21	194556.47	39.65	-118.15	10	3.3	MLGS21
PDE	1998	12	12	062512	39.70	-118.01	14	3.5	MLGS22

Catalog	Year	M	D	Time	Lat	Long	Depth	Mag	Source
PDE	1999	03	18	040139	39.69	-118.03	11	3.0	MDREN21
PDE	1999	03	18	040537	39.69	-118.03	10	3.1	MDREN21
PDE	1999	03	18	151239	39.69	-118.03	11	3.3	MDREN21
PDE	1999	04	19	123658	39.70	-117.97	14	4.1	MLGS22
PDE	1999	06	02	095847.63	39.64	-117.82	5	3.0	MLGS22
PDE	1999	09	28	004724	39.68	-118.03	10	2.9	MDREN20
PDE	1999	10	20	004611	39.23	-117.34	11	3.2	MLGS64
PDE	1999	12	12	181238	39.69	-118.29	11	4.5	MLBRK

Table 2. Seismic Event Catalog (2000-2010)

Time period: 1999-2010

The columns represent, in order:

1) CATALOG (**Catalog**);
2) YYYY (**Year**)
3) MM (**M**)
4) DD (**D**)
5) ORIG_TIME (HHMMSS.XX) (**Time**)
6) LATITUDE(DEG)(**Lat**)
7) LONGITUDE(DEG)(**Long**)
8) DEPTH (km) (**Depth**)
9) LOCAL MAGNITUDE (**Mag**)- the empty spaces show that no magnitude could be estimated for the respective event

Catalog	Year	M	D	Time	Lat	Long	Depth	Mag
UNR	2000	01	01	1044 27.5530	39.7167	-118.0177	11.6110	2.00
UNR	2000	01	01	1736 51.4580	39.6806	-118.0520	8.8500	2.00
UNR	2000	01	02	1951 51.0520	39.3085	-118.6075	0.0000	1.96
UNR	2000	01	04	1245 10.5180	39.6235	-118.0595	13.5358	2.23
UNR	2000	01	10	1711 6.7560	39.3384	-118.1235	2.5493	2.23
UNR	2000	01	18	903 37.8840	39.0470	-118.1429	5.0130	1.89
UNR	2000	01	22	1417 3.4220	39.6629	-118.3231	0.0000	2.60
UNR	2000	01	28	339 46.0880	39.4372	-118.4509	14.9309	2.38
UNR	2000	01	28	357 42.2860	39.5538	-118.9515	7.9711	3.22
UNR	2000	01	28	1024 56.6810	39.6343	-118.9555	19.6384	1.52
UNR	2000	01	28	1311 51.3390	39.5371	-118.9863	8.1492	1.78
UNR	2000	01	28	2057 4.8800	39.5434	-118.9612	15.8336	2.47
UNR	2000	01	28	2154 2.5680	39.5344	-118.9931	8.6174	1.82
UNR	2000	01	31	2248 57.6040	39.5880	-118.9840	6.9878	1.64
UNR	2000	02	03	1256 50.2490	39.4958	-118.4429	0.0000	1.87
UNR	2000	02	09	2113 13.7110	39.5584	-118.9717	10.6792	2.23
UNR	2000	02	09	2113 54.5340	39.5515	-118.9560	7.8826	2.99
UNR	2000	02	10	1257 57.1700	39.0633	-118.1042	12.3907	1.94
UNR	2000	02	26	2129 14.3110	39.5687	-118.1654	7.5497	0.59
UNR	2000	04	09	1644 20.0940	39.8078	-118.5016	1.4338	1.96
UNR	2000	04	09	2051 23.7900	39.8130	-118.5068	0.0000	2.07
UNR	2000	04	13	2117 42.6330	39.5719	-118.3804	0.0000	2.61
UNR	2000	04	15	437 15.4150	39.5867	-118.0596	1.9972	1.92
UNR	2000	04	20	2240 32.2890	39.0210	-118.4290	10.0000	2.51
UNR	2000	04	26	802 8.5580	39.0829	-117.0902	0.0000	2.60
UNR	2000	04	29	910 30.9930	39.0804	-118.9286	9.9967	1.26
UNR	2000	05	15	2343 30.1200	39.3236	-118.2763	0.0000	2.76
UNR	2000	05	25	1746 25.0600	39.0237	-118.2682	10.0000	2.11
UNR	2000	05	25	2349 41.5390	39.7434	-118.5804	5.0000	2.85

Catalog	Year	M	D	Time	Lat	Long	Depth	Mag
UNR	2000	06	03	411 29.9480	39.1916	-118.0442	14.3619	1.75
UNR	2000	06	10	428 52.6580	39.6995	-118.0410	3.1368	2.69
UNR	2000	07	03	1111 10.9780	39.3248	-118.9254	8.3283	1.60
UNR	2000	07	03	2008 50.3000	39.3014	-117.5708	0.0000	2.14
UNR	2000	07	05	2333 0.1090	39.0323	-117.6248	10.0000	2.10
UNR	2000	07	06	602 16.9640	39.2120	-117.0474	10.0000	2.33
UNR	2000	07	09	129 44.7150	39.8345	-118.4843	11.5678	2.22
UNR	2000	07	13	1859 18.5650	39.0721	-118.3661	5.0000	1.49
UNR	2000	07	23	246 6.5560	39.6731	-118.4304	10.5312	1.55
UNR	2000	08	05	508 31.2160	39.1951	-117.4946	0.1909	2.88
UNR	2000	08	05	1235 37.5910	39.2058	-117.4472	0.0000	2.18
UNR	2000	08	10	1245 23.3460	39.4542	-118.1011	6.3787	1.98
UNR	2000	08	27	2326 49.0510	39.8239	-118.2575	0.0000	2.60
UNR	2000	08	29	2109 1.1280	39.1069	-118.1462	6.2963	2.92
UNR	2000	08	31	451 33.0830	39.3758	-118.4771	11.2602	1.44
UNR	2000	09	05	2110 10.1250	39.5905	-118.3014	4.7055	2.09
UNR	2000	09	16	912 30.9140	39.0281	-118.2223	7.0327	1.45
UNR	2000	09	17	1430 39.8530	39.7003	-118.0245	11.2667	1.89
UNR	2000	09	25	2115 50.2100	39.0127	-118.7845	7.4400	1.20
UNR	2000	10	21	846 49.4390	39.3512	-118.0882	14.6726	1.83
UNR	2000	10	29	1451 16.6340	39.8921	-118.3169	3.9785	1.93
UNR	2000	11	08	943 57.4220	39.0007	-118.0935	12.7052	1.76
UNR	2000	11	17	1906 10.2980	39.0006	-118.1110	7.4202	2.66
UNR	2000	11	18	1841 50.6690	39.7605	-118.0585	7.9685	3.82
UNR	2000	11	22	202 20.3440	39.0210	-118.4015	12.0419	2.75
UNR	2000	11	29	510 16.9420	39.3881	-117.9675	10.0000	2.33
UNR	2000	11	29	638 42.4680	39.8335	-117.5092	10.0000	2.90
UNR	2000	12	03	404 34.4540	39.3291	-117.3136	3.9420	2.10
UNR	2000	12	07	651 11.3790	39.0909	-118.0659	0.0000	1.98
UNR	2000	12	07	2013 16.8340	39.0142	-118.1286	7.7190	2.37
UNR	2000	12	07	2014 29.3700	39.0261	-118.1542	6.2684	1.54
UNR	2000	12	13	1922 29.6960	39.6543	-118.4528	0.0000	2.22
UNR	2000	12	21	2132 50.0520	39.9734	-117.8459	17.6751	1.09
UNR	2000	12	25	321 35.2810	39.0024	-117.8323	7.6639	2.10
UNR	2000	12	29	1505 16.5250	39.6908	-118.1063	2.7383	1.91
UNR	2001	01	09	1134 35.1870	39.1753	-118.1068	6.8512	2.16
UNR	2001	01	12	802 16.7560	39.2387	-118.1296	0.9434	1.98
UNR	2001	01	12	1716 18.0330	39.0311	-118.0717	10.6536	2.08
UNR	2001	01	17	540 15.5390	39.2183	-118.0928	7.4623	1.98
UNR	2001	01	18	1813 29.2550	39.8986	-118.8300	15.1003	1.97
UNR	2001	01	19	1449 22.7050	39.9173	-118.8348	4.7909	2.23
UNR	2001	02	07	601 26.5660	39.5378	-118.0743	9.6065	1.79

Catalog	Year	M	D	Time	Lat	Long	Depth	Mag
UNR	2001	02	13	2156 44.9460	39.6805	-118.0399	9.8172	2.24
UNR	2001	02	22	352 44.1090	39.4334	-117.7503	12.8373	2.31
UNR	2001	02	22	1458 15.0900	39.0502	-118.9794	16.8013	1.48
UNR	2001	03	12	1346 37.0060	39.0160	-118.2271	2.4373	1.42
UNR	2001	03	17	428 6.4320	39.5321	-118.0744	12.3469	2.01
UNR	2001	03	31	741 3.7730	39.6798	-118.3110	1.3456	2.25
UNR	2001	04	02	5 42.2770	39.2826	-117.5631	0.7271	2.13
UNR	2001	04	06	2305 3.8610	39.9596	-117.8610	2.6010	2.04
UNR	2001	04	25	422 16.6920	39.3578	-118.4174	5.3060	2.30
UNR	2001	05	10	919 10.9840	39.8801	-118.7859	0.0000	1.59
UNR	2001	06	01	33 23.2930	39.4228	-118.2029	0.4989	1.31
UNR	2001	06	13	113 23.0320	39.4370	-118.0700	11.0122	1.82
UNR	2001	06	15	1207 35.6620	39.6397	-118.4470	0.0000	1.66
UNR	2001	06	27	2024 31.3270	39.9875	-117.8478	0.0000	2.55
UNR	2001	08	01	800 47.0930	39.0222	-118.0754	4.8776	1.70
UNR	2001	08	08	2016 58.9130	39.0866	-118.0840	6.5509	1.97
UNR	2001	09	04	742 27.9130	39.0520	-118.1276	11.4787	2.10
UNR	2001	09	06	1008 5.6970	39.0392	-118.1225	1.9571	1.53
UNR	2001	09	07	346 29.4670	39.0719	-118.1128	9.3224	1.75
UNR	2001	09	13	2046 51.1470	39.2350	-118.0485	9.2545	2.17
UNR	2001	09	19	417 11.0300	39.2524	-118.1113	7.4550	2.34
UNR	2001	09	25	453 45.6750	39.0650	-118.0204	7.8875	1.95
UNR	2001	11	14	751 6.3090	39.0439	-118.2365	4.5820	1.64
UNR	2001	11	30	1438 15.5430	39.4931	-118.0366	7.6574	3.21
PDE	2001	12	19	081712.59	39.03	-118.11	8	3.1 MLREN
UNR	2002	01	01	343 28.5650	39.7145	-118.4429	9.1363	1.97
UNR	2002	01	01	2254 34.7520	39.0889	-118.2159	0.0000	2.02
UNR	2002	01	07	1513 34.3090	39.6523	-118.4746	3.4455	1.98
UNR	2002	1	10	1709 8.9090	39.1138	-118.0704	7.0110	3.31
UNR	2002	1	19	1956 9.0720	39.1119	-118.0260	3.7457	1.76
UNR	2002	1	26	752 52.2220	39.6270	-118.7208	15.2138	1.69
UNR	2002	1	31	1258 29.2110	39.0559	-118.1543	5.1785	2.73
UNR	2002	02	07	700 43.6820	39.6878	-118.2857	12.2270	2.34
UNR	2002	02	12	420 35.6270	39.0885	-118.0620	8.6757	2.11
UNR	2002	03	09	2136 7.0880	39.0619	-118.0944	9.3252	2.47
UNR	2002	03	12	1153 0.5040	39.7960	-118.0467	0.0000	2.06
UNR	2002	03	13	1006 8.6960	39.2988	-118.5265	15.1770	2.23
UNR	2002	03	23	945 43.9360	39.2807	-118.5429	14.1970	1.38
UNR	2002	03	23	945 44.3760	39.3064	-118.5607	0.0000	1.27
UNR	2002	04	04	0 17.1340	39.0544	-118.9555	14.0824	1.83
UNR	2002	04	24	1328 13.4580	39.7473	-117.9951	11.7396	1.82
UNR	2002	05	27	415 23.4320	39.0729	-118.0390	10.1784	1.06

Catalog	Year	M	D	Time	Lat	Long	Depth	Mag
UNR	2002	06	10	6 47.2620	39.0850	-118.0556	9.7778	2.55
UNR	2002	06	30	2253 7.7130	39.6289	-118.2914	7.8466	1.71
UNR	2002	07	02	1642 12.5490	39.9385	-117.8846	0.9050	1.90
UNR	2002	08	06	1709 9.6030	39.0941	-118.0863	9.3450	1.68
UNR	2002	08	06	1752 35.0920	39.0888	-118.9889	10.2355	1.85
UNR	2002	08	22	2037 51.5930	39.8984	-118.3180	7.0549	1.81
UNR	2002	08	22	2038 32.5440	39.8725	-118.3523	3.3615	1.80
UNR	2002	08	22	2039 30.8310	39.8704	-118.3499	4.3429	1.85
UNR	2002	08	22	2040 32.3770	39.8784	-118.3414	6.8684	1.76
UNR	2002	08	23	1312 17.0040	39.4111	-118.2109	8.8038	1.93
UNR	2002	08	29	1344 58.1820	39.0000	-118.7540	0.0000	1.30
UNR	2002	08	30	203 43.4920	39.0013	-118.8022	10.9466	2.01
UNR	2002	08	30	2308 8.3620	39.3622	-117.4293	6.4712	1.21
UNR	2002	09	02	912 50.2860	39.9704	-117.8549	17.8463	0.48
UNR	2002	09	03	844 18.4330	39.0506	-118.1942	3.1703	1.13
UNR	2002	09	03	2126 31.7650	39.4057	-118.4752	12.5193	3.05
UNR	2002	09	03	2132 33.9930	39.4048	-118.4471	16.9092	1.77
UNR	2002	09	03	2134 7.3770	39.4042	-118.4538	13.8131	2.34
PDE	2002	09	03	212631.77	39.41	-118.47	12	3.0 MLREN
UNR	2002	09	07	221 36.8010	39.0237	-118.8683	4.9167	1.70
UNR	2002	09	09	2316 16.8190	39.0338	-118.0775	7.8860	2.35
UNR	2002	09	23	1154 33.5110	39.0598	-117.0112	0.5867	2.60
PDE	2002	10	21	223057.41	39.53	-119.15	10	3.7 MLBRK
UNR	2002	10	30	926 32.8200	39.3890	-118.4858	12.1545	1.69
UNR	2002	11	01	1120 33.3610	39.0626	-118.0705	5.7034	1.44
UNR	2002	11	27	1231 25.6120	39.9020	-118.9363	8.9077	1.60
UNR	2002	12	08	1830 3.0390	39.0721	-118.0788	9.0215	1.52
UNR	2002	12	15	230 20.4460	39.0466	-118.5086	10.3324	3.89
PDE	2002	12	15	023020.45	39.05	-118.51	10	3.9 MLREN
UNR	2002	12	23	637 35.1620	39.0472	-118.5126	12.3593	2.56
UNR	2003	01	07	941 32.9050	39.0406	-118.5226	0.0000	2.45
PDE	2003	01	10	005322.65	38.82	-117.98	6	2.8 MDNC
PDE	2003	01	23	214946.76	39.96	-117.86	6	4.2 MLREN
UNR	2003	01	23	2157 0.3430	39.9515	-117.8587	3.7353	2.13
UNR	2003	01	24	2021 50.6960	39.9406	-117.8591	12.9837	2.21
PDE	2003	01	25	024300.32	39.97	-117.88	5	3.6 MLREN
PDE	2003	01	25	024549.36	39.97	-117.87	7	3.8 MLREN
UNR	2003	01	25	736 5.7410	39.9507	-117.9033	9.9457	2.03
UNR	2003	01	25	750 11.3120	39.9645	-117.8143	3.6058	2.13
UNR	2003	02	02	1408 35.3610	39.9348	-117.8568	12.8016	0.65
UNR	2003	02	06	841 59.8670	39.1508	-118.0833	7.5195	2.58
UNR	2003	02	06	1545 22.7880	39.4060	-118.4778	11.5232	1.91

Catalog	Year	M	D	Time	Lat	Long	Depth	Mag
UNR	2003	02	11	601 36.6640	39.0694	-118.1233	3.9450	1.31
UNR	2003	02	21	2307 58.0080	39.3974	-118.3881	0.0000	1.72
UNR	2003	02	25	2316 46.2660	39.9658	-117.8555	6.0357	2.28
UNR	2003	02	26	2207 12.7740	39.4277	-118.0686	11.1106	2.47
UNR	2003	02	28	334 25.9160	39.0925	-118.1099	10.5366	2.02
UNR	2003	04	5	1250 18.4450	39.4225	-118.0512	14.4167	2.08
UNR	2003	04	16	720 49.5400	39.0602	-118.0388	7.4480	2.27
PDE	2003	05	12	185539.37	39.08	-118.15	13	3.4 MLREN
UNR	2003	05	13	1236 46.0460	39.3325	-118.1358	7.9781	1.42
PDE	2003	05	14	051124.46	39.02	-118.21	10	2.9 MLREN
UNR	2003	05	14	513 42.5380	39.0193	-118.2055	10.6530	2.16
UNR	2003	05	15	153 55.6440	39.0603	-118.0636	8.2869	1.36
UNR	2003	05	15	1401 55.8820	39.5404	-117.6580	4.1172	2.13
UNR	2003	05	18	820 16.9730	39.5393	-117.6556	4.0077	2.39
UNR	2003	05	20	1716 2.2620	39.9827	-117.5774	5.7729	1.12
UNR	2003	05	28	1133 6.1670	39.1278	-117.1827	0.0000	2.11
UNR	2003	06	01	803 1.6610	39.0676	-118.0377	8.4953	2.07
UNR	2003	06	14	2211 4.0170	39.6452	-118.0387	0.0000	1.45
UNR	2003	06	30	1000 49.3340	39.3324	-117.7308	9.4485	1.78
UNR	2003	07	1	956 37.1730	39.4999	-118.1811	0.0000	1.80
UNR	2003	07	14	1222 3.8480	39.0471	-118.5383	9.5317	2.45
UNR	2003	07	21	17 29.7360	39.5507	-118.4515	11.8484	2.10
UNR	2003	07	22	1946 18.6500	39.8057	-117.6611	0.0000	2.27
UNR	2003	08	04	1937 12.8070	39.0662	-118.5091	5.2092	1.45
UNR	2003	08	17	1223 57.5190	39.3792	-118.4864	12.9014	2.33
UNR	2003	08	18	834 16.3730	39.2119	-118.0919	0.0000	1.68
PDE	2003	08	18	100700.38	39.97	-117.84	6	2.7 MLREN
PDE	2003	08	21	173337.25	39.59	-118.16	10	2.9 MLREN
UNR	2003	08	24	2012 51.1740	39.7812	-118.0077	8.7231	0.00
UNR	2003	08	24	2013 12.4170	39.7398	-118.0503	10.5445	0.02
UNR	2003	08	25	1113 20.8080	39.0361	-118.1888	13.4542	2.12
UNR	2003	08	28	1250 26.1600	39.4230	-117.2932	7.1758	1.65
UNR	2003	08	30	1750 28.6220	39.0767	-118.9927	10.2492	1.46
UNR	2003	09	05	2307 18.4660	39.0457	-118.9349	6.0281	1.90
PDE	2003	09	10	123747.96	39.37	-118.06	13	3.6 MLREN
UNR	2003	09	10	1900 39.7230	39.3549	-118.0570	11.0678	1.54
UNR	2003	09	12	541 7.7620	39.0156	-118.1858	7.0395	2.09
UNR	2003	09	15	328 29.3010	39.0114	-118.0731	10.7471	0.82
UNR	2003	10	18	751 8.0900	39.0032	-118.4593	12.9573	1.76
UNR	2003	10	19	1412 44.7170	39.1124	-118.0842	0.0000	1.63
UNR	2003	10	25	1253 30.9880	39.4930	-117.6005	9.0307	2.56
UNR	2003	10	26	1313 13.2240	39.0981	-118.0528	8.9601	2.24

Catalog	Year	M	D	Time	Lat	Long	Depth	Mag
UNR	2003	10	28	945 20.0250	39.4867	-118.0705	9.7083	2.65
UNR	2003	11	2	1423 4.2970	39.0366	-118.1085	4.2629	1.63
UNR	2003	11	12	1235 46.7370	39.1880	-118.2061	3.8641	2.03
UNR	2003	11	22	708 11.5800	39.2554	-118.1290	10.7254	2.32
UNR	2003	11	26	1415 16.8590	39.6158	-118.0911	6.8540	2.60
UNR	2003	12	02	1445 21.6790	39.0104	-118.8489	8.5029	2.19
UNR	2003	12	02	1521 17.3260	39.0136	-118.8509	9.0533	1.95
UNR	2003	12	02	2236 32.3050	39.0009	-118.8573	7.5990	0.92
UNR	2003	12	11	940 28.3170	39.1370	-118.1874	5.9790	2.10
PDE	2003	12	18	045120.08	38.98	-117.32	2	2.9 MLREN
PDE	2004	01	19	002333.56	39.34	-118.45	12	2.9 MLREN
UNR	2004	01	21	1557 37.8580	39.9263	-118.9126	0.0000	1.80
UNR	2004	01	25	717 48.4940	39.0451	-117.9882	0.0000	1.22
UNR	2004	02	09	2013 25.0450	39.0123	-118.8466	8.2469	2.11
UNR	2004	02	09	2248 48.0440	39.0173	-118.1727	11.8047	1.70
UNR	2004	03	03	311 45.9470	39.5788	-118.4290	12.5736	1.73
UNR	2004	03	17	634 40.0900	39.9807	-117.8304	0.2601	2.02
UNR	2004	03	21	1354 5.9830	39.0403	-118.1760	10.3832	1.65
UNR	2004	03	26	904 35.0990	39.5343	-118.1374	9.0624	2.11
UNR	2004	04	08	1551 56.2350	39.3350	-118.4809	14.1675	2.23
PDE	2004	05	12	073348	39.08	-119.00	7	3.0 MLREN
UNR	2004	05	18	2307 3.3640	39.2124	-117.3689	13.3102	2.45
UNR	2004	05	23	1651 2.9220	39.6704	-118.3067	6.3654	1.78
UNR	2004	05	27	1336 3.9040	39.5012	-118.4510	15.0782	2.32
UNR	2004	05	27	1551 7.5500	39.6280	-118.3959	0.0000	1.99
UNR	2004	05	28	556 4.3220	39.3648	-118.0975	11.4324	0.69
PDE	2004	06	10	041639.90	39.98	-117.85	6	3.4 MLREN
UNR	2004	06	18	753 47.6560	39.4029	-118.4633	13.1104	1.50
PDE	2004	06	19	161000.10	39.47	-119.15	12	2.9 MLREN
UNR	2004	06	24	1445 47.3190	39.0132	-117.4245	0.0000	1.94
UNR	2004	06	30	1126 28.3670	39.0153	-118.7973	10.9555	1.09
UNR	2004	06	30	1131 25.5600	39.0167	-118.7853	6.5655	1.02
UNR	2004	07	02	1341 59.6940	39.3054	-118.0593	9.9837	2.33
UNR	2004	07	05	906 34.7740	39.4157	-117.5334	13.4570	1.84
UNR	2004	07	10	1716 7.5950	39.1721	-118.0675	10.4267	1.95
UNR	2004	07	11	1940 19.0770	39.1730	-118.0820	5.2147	2.46
UNR	2004	07	21	249 57.4330	39.0492	-118.2272	12.0222	2.01
PDE	2004	07	29	105251.45	38.77	-117.91	12	3.1 MLREN
UNR	2004	07	31	18 21.6830	39.0418	-118.0882	10.8572	1.84
UNR	2004	08	01	755 33.6750	39.2045	-118.7695	0.0000	1.44
UNR	2004	08	10	1215 59.2490	39.2688	-118.0911	6.9291	2.73
UNR	2004	08	15	1640 12.7420	39.1627	-118.0691	10.2365	1.91

Catalog	Year	M	D	Time	Lat	Long	Depth	Mag
PDE	2004	08	27	080739.86	39.20	-118.05	8	2.9 MLREN
UNR	2004	09	02	1235 19.6820	39.6756	-118.0559	6.7476	2.30
UNR	2004	09	12	759 31.2330	39.1451	-118.0673	12.7385	2.04
UNR	2004	09	23	542 7.7200	39.3043	-118.1001	10.9392	2.61
UNR	2004	09	30	1749 27.9490	39.0556	-118.1055	10.9829	1.94
UNR	2004	10	05	1252 12.6980	39.5344	-118.1021	9.4798	1.85
UNR	2004	10	12	2059 41.5270	39.7136	-118.6315	12.9428	1.61
UNR	2004	10	16	1750 16.4910	39.3952	-118.6184	8.6022	1.97
UNR	2004	10	24	1443 6.4510	39.7163	-118.0489	11.0699	2.03
UNR	2004	10	29	2247 27.9170	39.0131	-118.8513	10.4179	1.45
UNR	2004	10	29	2257 42.4350	39.0153	-118.8409	7.7183	1.79
UNR	2004	10	29	2310 19.0340	39.0187	-118.8327	5.8057	1.58
UNR	2004	10	30	48 17.5050	39.0140	-118.8363	7.6975	2.97
UNR	2004	11	25	501 46.1230	39.0190	-118.8031	4.2558	1.86
UNR	2004	11	26	326 18.9250	39.3205	-118.0799	6.9934	2.17
UNR	2005	01	17	118 XX	39.1936	-118.0892	5.8076	2.63
UNR	2005	01	17	753 56.6510	39.3464	-117.8671	10.1153	1.79
UNR	2005	01	30	1709 54.0370	39.0941	-118.9887	3.9948	1.50
UNR	2005	02	18	851 0.2360	39.4003	-117.2352	3.3097	2.20
UNR	2005	02	22	142 34.3390	39.1045	-118.9888	3.0637	1.70
UNR	2005	03	24	552 59.3870	39.0413	-118.2013	6.9902	1.93
UNR	2005	03	29	1700 49.0900	39.6246	-118.0846	8.0318	1.59
UNR	2005	04	26	151 20.0960	39.0347	-118.7926	13.0958	1.40
PDE	2005	04	28	102743.26	39.10	-118.99	2	2.8 MLREN
UNR	2005	04	28	1030 54.5330	39.1046	-118.9904	0.0000	1.95
UNR	2005	04	28	1036 47.3780	39.1054	-118.9912	0.0000	1.73
PDE	2005	04	28	202715.18	39.10	-119.00	5	3.2 MLREN
UNR	2005	04	28	2133 42.7050	39.1055	-118.9968	2.0077	2.08
UNR	2005	04	29	453 51.6260	39.1026	-118.9980	4.7820	1.75
UNR	2005	04	29	1528 53.7720	39.1019	-118.9884	1.8272	1.47
UNR	2005	04	29	1529 33.2910	39.1007	-118.9875	3.0406	1.66
UNR	2005	05	01	145 40.2270	39.6840	-118.4383	10.1054	2.58
UNR	2005	05	03	1009 40.5590	39.1041	-118.9911	4.2576	2.00
UNR	2005	05	15	1916 47.6950	39.9396	-117.8338	1.0489	2.69
UNR	2005	05	17	316 27.2590	39.4856	-118.0513	0.0000	2.50
UNR	2005	05	20	2130 55.3570	39.0950	-118.1083	8.1533	2.49
UNR	2005	06	06	1031 20.6320	39.0861	-118.9964	4.5834	1.94
UNR	2005	06	09	709 34.3190	39.5052	-118.5002	9.0139	1.61
UNR	2005	06	13	2046 9.5050	39.2475	-118.0633	0.0000	2.28
UNR	2005	06	29	1014 47.8780	39.0738	-118.9986	9.6965	1.29
UNR	2005	07	02	1415 32.1850	39.2271	-117.9981	0.4045	2.63
UNR	2005	07	13	643 23.6490	39.3097	-118.7483	0.0000	1.21

Catalog	Year	M	D	Time	Lat	Long	Depth	Mag
UNR	2005	07	24	1059 36.8550	39.0491	-118.0790	0.0000	1.54
UNR	2005	07	29	1223 5.9960	39.1613	-118.1299	0.6407	2.37
UNR	2005	07	31	2305 5.4180	39.2031	-117.3831	15.0000	2.93
UNR	2005	08	01	1355 18.2950	39.1707	-118.0912	6.2461	2.14
UNR	2005	08	04	1006 38.6910	39.0963	-118.0167	8.6344	2.29
UNR	2005	08	05	847 56.9780	39.0290	-118.1091	6.9224	1.27
UNR	2005	09	07	1147 15.6080	39.0706	-118.0882	4.3153	1.45
UNR	2005	09	14	805 20.5600	39.0933	-118.0511	7.3861	1.84
UNR	2005	09	17	1748 15.5400	39.0928	-118.9962	6.8679	0.72
UNR	2005	09	27	336 24.9780	39.7457	-117.9958	4.3202	1.52
UNR	2005	09	28	1045 34.0280	39.5585	-118.1588	11.4461	1.75
UNR	2005	10	16	2011 53.4060	39.3315	-118.1206	10.1838	1.65
UNR	2005	10	20	1659 5.9250	39.3318	-118.1029	8.6068	1.75
UNR	2005	10	22	1113 33.7040	39.3595	-117.8976	7.6047	2.21
UNR	2005	10	30	1843 23.2320	39.9891	-117.8021	0.0000	2.02
UNR	2005	10	30	1905 26.4010	39.3588	-117.8947	0.0000	1.89
UNR	2005	11	14	2108 11.2500	39.4106	-118.7624	9.2351	1.53
UNR	2005	11	15	959 34.9120	39.0838	-118.9946	5.8278	0.82
UNR	2005	11	16	245 52.6850	39.5362	-118.4433	10.5482	1.52
UNR	2005	11	22	1136 34.3040	39.3379	-118.4662	12.7168	1.50
UNR	2005	11	22	1642 37.8680	39.3605	-118.4893	6.2925	1.41
UNR	2005	11	23	326 9.1640	39.3553	-118.4788	13.0450	2.21
UNR	2005	11	24	340 38.8400	39.3479	-118.4839	11.7533	1.67
UNR	2005	11	26	1244 56.9660	39.4028	-117.9499	10.0512	1.21
UNR	2005	11	26	1259 40.5500	39.4067	-117.9450	10.1374	1.87
PDE	2005	11	29	044541	39.08	-119.01	6	3.6 MLREN
UNR	2005	12	21	834 40.1550	39.0782	-118.9425	14.4184	1.69
UNR	2005	12	23	109 46.4340	39.4057	-117.9507	9.8382	1.73
UNR	2005	12	24	1836 25.4670	39.3501	-118.4770	13.6673	1.56
UNR	2005	12	25	411 56.2500	39.3526	-118.4869	14.5931	1.74
UNR	2005	12	28	655 54.6790	39.3622	-118.4937	10.0775	2.12
UNR	2005	12	30	1445 31.6820	39.0017	-118.1858	11.4833	1.82
UNR	2005	12	31	1404 26.7420	39.0016	-118.1816	11.0141	1.78
UNR	2006	01	18	408 53.3110	39.2591	-118.5517	0.0000	1.78
UNR	2006	01	24	1705 19.3780	39.3164	-117.4062	0.7409	2.31
UNR	2006	01	25	530 26.0240	39.3213	-117.4276	9.4654	1.85
UNR	2006	01	31	216 31.7440	39.0759	-118.1040	9.3524	2.49
UNR	2006	03	03	607 33.3880	39.0822	-118.2188	0.1087	1.88
UNR	2006	03	23	1452 21.5510	39.4119	-118.4571	11.5765	2.32
PDE	2006	04	05	120316.88	39.08	-119.01	4	3.4 MLREN
UNR	2006	04	06	2332 24.8880	39.9106	-118.3161	8.0830	2.25
UNR	2006	04	07	1331 18.1710	39.9170	-117.8570	0.4342	1.97

Catalog	Year	M	D	Time	Lat	Long	Depth	Mag
UNR	2006	07	14	552 56.4810	39.8902	-118.3564	4.0648	1.44
PDE	2006	07	24	210608.18	39.07	-118.06	6	3.5 MLREN
UNR	2006	08	16	623 23.0690	39.0631	-118.1342	0.0000	1.18
UNR	2006	08	18	1609 38.0510	39.3993	-117.6084	6.1963	1.88
UNR	2006	08	29	434 7.8800	39.7579	-118.0303	3.6440	2.00
UNR	2006	09	02	723 15.8440	39.0028	-118.7200	8.4498	1.34
UNR	2006	09	05	1021 12.3880	39.0716	-118.0695	10.9237	2.48
PDE	2006	09	24	124252.09	38.80	-117.91	11	3.3 MLREN
UNR	2006	10	02	1302 2.9320	39.2970	-118.0724	10.1675	2.06
UNR	2006	10	04	1329 2.3920	39.1127	-118.0779	12.7072	2.58
UNR	2006	10	06	907 39.8640	39.0962	-118.6342	14.4094	1.26
UNR	2006	11	17	2155 1.2600	39.7130	-118.0180	10.4068	1.80
UNR	2006	12	29	447 42.7620	39.0630	-118.0748	8.5437	2.37
PDE	2006	11	08	080310.93	40.21	-118.26	10	3.7 MLREN
PDE	2006	11	08	081346.68	40.19	-118.25	10	3.2 MLREN
UNR	2007	01	16	1137 46.5450	39.3684	-118.1048	8.6890	1.54
PDE	2007	01	16	151739.20	39.35	-118.10	10	2.8 MLREN
UNR	2007	01	17	1123 1.7990	39.3551	-118.1061	12.3968	2.00
UNR	2007	02	04	1610 47.0090	39.0217	-118.9191	6.7631	1.31
UNR	2007	02	04	2028 41.2030	39.2424	-118.8351	12.8629	2.16
UNR	2007	03	01	26 34.7640	39.0163	-118.8892	9.9570	1.40
UNR	2007	03	01	28 32.5330	39.0246	-118.8838	10.9602	1.31
UNR	2007	03	01	29 15.7300	39.0215	-118.8676	7.7429	1.00
UNR	2007	03	01	428 8.5950	39.0189	-118.8802	9.8275	1.50
UNR	2007	03	01	1706 13.1500	39.6921	-118.2969	8.7221	2.62
UNR	2007	03	15	210 9.8160	39.5971	-118.8257	12.3117	1.40
UNR	2007	03	17	2208 5.9110	39.0213	-118.8838	9.0374	1.38
UNR	2007	04	27	941 27.8400	39.0632	-118.1049	7.4360	1.33
UNR	2007	05	08	213 21.5750	39.3374	-118.4022	18.0694	2.10
UNR	2007	07	09	2349 30.4020	39.0952	-118.0662	9.1815	1.71
UNR	2007	07	10	426 17.6540	39.0175	-118.6285	72.1578	0.91
UNR	2007	07	16	530 31.5140	39.3612	-118.4076	10.4164	1.22
PDE	2007	07	30	091029.66	39.35	-118.40	16	2.6 MLREN
UNR	2007	08	07	638 15.1490	39.3950	-118.4604	18.4581	1.30
UNR	2007	08	14	1737 20.5980	39.3236	-118.4203	13.6504	1.23
UNR	2007	08	17	1712 51.9050	39.8703	-118.9240	12.2470	1.04
UNR	2007	08	22	1701 17.1000	39.3482	-118.4241	11.3482	1.40
UNR	2007	08	25	139 29.5850	39.5446	-118.4911	14.9058	1.24
UNR	2007	08	30	759 31.7950	39.5205	-118.4511	15.8526	2.24
UNR	2007	09	10	2029 28.0140	39.0311	-118.1976	7.7617	1.66
PDE	2007	09	25	060617.84	39.03	-118.55	12	3.3 MLREN
UNR	2007	10	02	1539 47.2440	39.1697	-118.0860	10.7900	1.18

Catalog	Year	M	D	Time	Lat	Long	Depth	Mag
UNR	2007	10	03	328 50.5810	39.4110	-118.3160	14.7567	1.62
UNR	2007	10	03	713 22.3140	39.0044	-118.5730	14.7501	1.02
UNR	2007	10	20	2134 31.8330	39.2948	-118.4394	7.1820	1.54
UNR	2007	11	10	948 55.0750	39.2399	-118.4835	15.0561	1.71
UNR	2007	11	14	2240 7.1960	39.2912	-118.8699	11.8942	1.35
UNR	2007	11	14	2315 15.1210	39.2746	-118.8422	14.5609	1.24
UNR	2007	11	15	145 36.2760	39.2904	-118.8621	5.5569	1.42
UNR	2008	01	06	180932.4550	39.7027	-118.4485	19.6984	1.71
UNR	2008	01	09	032418.9320	39.4607	-117.7106	15.2279	1.54
UNR	2008	01	12	110101.8080	39.9645	-117.8653	2.6773	1.54
UNR	2008	01	23	93101.6380	39.6982	-118.4303	18.6475	1.89
UNR	2008	02	04	105524.2800	39.0660	-118.0833	6.8026	1.54
UNR	2008	02	10	182614.0010	39.0223	-118.1981	11.2321	1.00
UNR	2008	02	25	183145.8300	39.1067	-118.0633	10.3249	2.35
UNR	2008	02	26	192810.2880	39.6071	-117.9296	10.3494	0.44
UNR	2008	02	27	070257.2840	39.6047	-118.1834	13.3841	1.33
UNR	2008	02	27	122040.8870	39.6048	-118.1714	14.6051	1.75
UNR	2008	02	28	052738.4470	39.0526	-118.0744	10.1106	2.18
UNR	2008	02	28	170408.4440	39.5525	-118.4795	12.2988	2.34
UNR	2008	02	29	000525.9510	39.3031	-117.9599	0.0000	1.96
UNR	2008	03	02	214209.3700	39.3888	-118.4773	13.0721	1.85
UNR	2008	03	04	164340.6270	39.0025	-118.1276	7.8950	1.51
UNR	2008	03	15	122251.8950	39.1313	-118.7650	18.2034	1.80
UNR	2008	03	15	182754.9190	39.5924	-118.1441	14.8079	1.72
UNR	2008	03	27	002317.4070	39.7933	-117.0634	0.0000	1.92
UNR	2008	03	28	014754.6050	39.2777	-118.1039	6.2336	1.82
UNR	2008	04	1	114250.8430	39.5083	-118.4325	13.4572	1.84
UNR	2008	04	13	081339.9420	39.2073	-118.8955	13.8213	1.79
UNR	2008	04	14	1706 34.4520	39.9846	-118.4564	0.0000	2.52
UNR	2008	04	24	1900 19.6500	39.8611	-117.1740	16.0000	1.81
UNR	2008	04	25	656 45.7230	39.7231	-118.0585	8.2115	1.42
UNR	2008	04	25	1641 46.0270	39.3807	-117.3102	12.0000	2.40
UNR	2008	04	26	922 59.6930	39.3029	-117.8561	0.0000	2.09
UNR	2008	05	07	1129 16.6400	39.8641	-117.6971	0.0000	2.59
UNR	2008	05	07	1748 30.2840	39.6441	-118.0896	0.0000	2.26
UNR	2008	05	07	2131 23.2590	39.3395	-117.1549	0.0000	2.66
UNR	2008	05	07	2151 52.0720	39.0809	-118.7105	0.0000	2.09
UNR	2008	05	08	1142 1.0840	39.9441	-117.6443	0.0000	1.92
UNR	2008	05	08	2129 53.1040	39.0424	-118.0121	16.0000	2.07
UNR	2008	05	11	1547 1.3730	39.3198	-117.2071	8.0000	2.36
UNR	2008	05	18	728 0.8950	39.0220	-117.8053	16.0000	2.05
UNR	2008	05	18	845 35.4810	39.1398	-118.9181	0.0000	2.78

Catalog	Year	M	D	Time	Lat	Long	Depth	Mag
UNR	2008	05	27	1117 47.8080	39.3478	-118.0899	3.7909	2.60
UNR	2008	06	26	1739 19.5770	39.8749	-118.3528	0.0000	2.78
UNR	2008	07	07	1654 39.2750	39.1044	-118.9570	6.5727	0.87
UNR	2008	07	09	1845 57.8470	39.1306	-118.1074	11.5259	2.04
UNR	2008	07	11	1013 25.3590	39.1013	-118.9440	6.2041	2.07
UNR	2008	07	12	19 29.8350	39.1029	-118.9456	6.6169	2.58
UNR	2008	07	12	26 20.7660	39.1018	-118.9618	7.7530	1.46
UNR	2008	07	12	55 39.0810	39.0985	-118.9601	7.1848	1.25
UNR	2008	07	12	130 7.3840	39.0981	-118.9399	9.3056	1.38
UNR	2008	07	12	415 10.9780	39.1074	-118.9501	5.8128	2.07
UNR	2008	07	12	437 2.9160	39.1038	-118.9593	8.0845	1.19
UNR	2008	07	12	828 49.8060	39.0964	-118.9706	10.1142	1.31
UNR	2008	07	13	1856 53.0040	39.3174	-118.1100	10.7927	2.85
UNR	2008	07	22	1045 5.0660	39.0993	-118.0915	12.7358	1.49
UNR	2008	07	25	1608 3.0430	39.2180	-118.0990	8.2046	2.54
UNR	2008	08	06	1938 53.5220	39.5811	-117.2819	0.0000	2.48
UNR	2008	08	20	1254 21.2490	39.9553	-117.8596	1.8037	2.85
UNR	2008	08	25	1912 4.2650	39.4181	-118.4552	11.0271	2.43
UNR	2008	09	7	814 41.5840	39.3390	-118.5127	8.0050	2.73
UNR	2008	09	8	1401 23.8700	39.3690	-118.4460	16.8981	2.11
UNR	2008	09	10	347 57.3390	39.0534	-118.1441	12.2560	2.49
UNR	2008	09	12	431 50.0290	39.0241	-118.8279	11.7383	1.46
PDE	2008	11	05	233225.28	39.06	-118.91	9	2.9 MLREN
UNR	2008	11	06	303 39.3400	39.0478	-118.0958	6.9416	1.37
UNR	2008	11	12	600 58.0810	39.5921	-118.1537	13.3916	1.40
UNR	2008	12	09	258 55.4350	39.6866	-118.4552	3.5838	1.62
UNR	2008	12	21	1348 30.5740	39.3137	-118.5444	3.8597	1.66
UNR	2008	12	28	1236 51.6570	39.1716	-118.1101	8.2780	1.71
UNR	2009	01	05	193919.9170	39.4078	-118.0501	0.6299	1.92
UNR	2009	01	12	093151.0640	39.7406	-117.5251	0.0000	1.47
UNR	2009	01	12	183506.4000	39.8480	-118.3403	0.0000	2.69
UNR	2009	01	12	191435.7300	39.7826	-118.5362	0.0000	1.53
UNR	2009	01	28	095800.3150	39.2966	-118.8969	14.2110	1.31
UNR	2009	01	31	082229.0240	39.9242	-117.8555	0.0000	3.20
UNR	2009	02	05	084718.5680	39.9429	-117.8203	0.1178	1.75
UNR	2009	02	12	214404.3530	39.1629	-118.0900	4.8110	2.50
UNR	2009	02	21	154519.2130	39.2912	-118.5605	16.8728	0.93
UNR	2009	03	05	081616.3430	39.0677	-117.6206	0.0000	1.47
UNR	2009	03	11	155701.5210	39.3767	-117.5035	4.7702	2.24
UNR	2009	04	02	112009.5510	39.0609	-118.5041	10.8140	2.52
UNR	2009	04	13	224317.3390	39.0973	-118.0856	13.5298	2.81
UNR	2009	04	30	125919.4340	39.1630	-118.2109	4.9133	2.28
PDE	2009	05	10	001411.05	39.16	-118.06	0	3.2 MLREN

Catalog	Year	M	D	Time	Lat	Long	Depth	Mag
UNR	2009	05	10	04416.8580	39.1715	-118.0834	4.0250	2.10
UNR	2009	05	15	094446.4210	39.3826	-118.1101	5.1216	1.80
PDE	2009	05	20	024130.59	38.88	-118.35	8	3.0 MLREN
PDE	2009	06	19	152601.67	39.30	-117.33	0	2.5 MLREN
UNR	2009	06	24	1404 20.7860	39.3151	-117.3452	0.0000	2.19
UNR	2009	06	24	2213 36.5590	39.3405	-117.3004	1.1147	2.19
UNR	2009	07	20	1904 57.6640	39.3917	-118.1775	12.6154	2.62
UNR	2009	07	22	055255.2120	39.4228	-118.0764	4.5027	2.36
UNR	2009	07	25	130822.6810	39.1818	-118.1752	0.3926	1.90
PDE	2009	08	24	143449.38	38.84	-117.96	4	2.5 MLREN
UNR	2009	08	28	131041.6800	39.3381	-118.0824	6.0924	1.48
UNR	2009	09	07	163729.0610	39.3665	-118.0743	13.9615	1.88
UNR	2009	10	03	0253 47.9300	39.5257	-118.4550	11.4279	2.79
PDE	2009	10	03	165622.05	39.97	-117.85	5	2.7 MLREN
UNR	2009	10	05	2158 42.3840	39.4066	-117.1333	9.7077	2.59
UNR	2009	10	06	20 28.2420	39.9523	-117.8538	9.3412	1.76
UNR	2009	10	07	554 28.8530	39.9635	-117.8525	3.3423	2.06
UNR	2009	10	10	2022 4.4520	39.9646	-117.8526	6.3342	1.99
PDE	2009	11	07	040946.56	38.66	-117.65	8	2.5 MLREN
UNR	2009	11	25	095602.7	39.0102	-118.2599	14.7134	1.31
UNR	2009	12	07	020240.4	39.9832	-117.8599	10.2671	1.54
UNR	2009	12	12	054950.0	39.9506	-117.8353	0.0000	1.69
UNR	2009	12	18	054718.4	39.2119	-118.5939	0.0791	1.62
UNR	2009	12	26	234101.4	39.0802	-118.0709	7.5461	1.56
UNR	2009	12	29	2243 47.9	39.1562	-118.2352	9.3191	1.59
UNR	2010	01	03	190844.7	39.1302	-118.1171	5.5992	1.91
PDE	2010	01	22	025229.29	39.01	-118.82	10	3.2 MLREN
UNR	2010	01	22	072640.6	39.0065	-118.8117	0.0000	1.53
UNR	2010	01	22	125409.5	39.3101	-118.5509	3.0513	2.04
UNR	2010	01	22	173246.9	39.0163	-118.8167	8.1949	1.35
PDE	2010	04	29	151653.4	39.06	-118.46	10	2.5 MLREN
PDE	2010	07	22	014625.6	39.01	-118.80	6	3.0 MLREN
PDE	2010	07	30	111346	38.62	-118.21	8	4.2 MLREN

Table 3. Seismic Events (298) located at NSL/UNR identified by UNR analysts as explosions within 38.7°N - 40.3° N and 119°W -117°W

The columns represent, in order:

1) MM/DD/YYYY (**Date**);
2) JJJ Julian Day (**Julian**)
3) ORIG_TIME (HHMMSS.XXX) (**Time**)
6) LATITUDE(DEG)(**Lat**)
7) LONGITUDE(DEG)(**Long**)
8) DEPTH (km) (**Depth**)
9) LOCAL MAGNITUDE (**Mag**)- the empty spaces show that no magnitude could be estimated for the respective event

Date	Julian	Time	Lat	Long	Depth	Mag
02/06/2001	(037)	20:16:50.917	38.7375	-117.0710	0.0000	2.23
03/20/2001	(079)	0:04:47.842	38.8031	-117.2240	0.0000	2.12
04/26/2001	(116)	19:08:02.388	38.7268	-117.1260	0.0000	1.99
05/04/2001	(124)	19:07:43.183	38.9694	-118.3787	0.0000	1.48
05/07/2001	(127)	19:11:57.483	38.9688	-117.0487	0.0000	2.12
05/29/2001	(149)	19:18:03.930	38.8826	-117.1118	0.0000	2.02
06/07/2001	(158)	19:14:37.117	39.1514	-117.1941	0.0000	2.32
06/11/2001	(162)	23:05:41.079	38.7439	-117.1686	0.0000	1.93
06/12/2001	(163)	19:07:54.117	38.8262	-117.1142	0.0000	
06/25/2001	(176)	19:13:02.588	38.7154	-117.0738	0.0000	1.81
08/14/2001	(226)	19:06:39.509	38.7592	-117.6044	0.0000	1.74
09/17/2001	(260)	19:11:32.996	38.7755	-117.0467	0.0000	2.15
12/13/2001	(347)	13:47:12.822	38.8188	-118.3134	0.0000	
01/02/2002	(002)	20:09:34.240	38.8885	-117.0619	0.0000	
01/28/2002	(028)	20:06:58.657	38.8729	-117.4889	0.0000	2.07
02/04/2002	(035)	23:44:25.687	38.8659	-118.3059	0.0000	1.59
02/22/2002	(053)	20:16:46.334	39.1224	-117.2497	0.0000	2.41
03/26/2002	(085)	19:43:40.935	38.9607	-118.3221	0.0000	1.38
06/13/2002	(164)	22:00:06.933	38.7275	-117.1417	0.0000	1.83
07/20/2002	(201)	18:27:06.440	39.8804	-118.3659	0.0000	1.66
08/27/2002	(239)	19:15:09.500	39.7196	-117.2639	0.0000	2.61
08/30/2002	(242)	19:02:04.891	38.7434	-117.1373	0.0000	1.84
09/10/2002	(253)	19:06:39.863	38.7448	-117.0665	0.0000	1.90
09/20/2002	(263)	1:48:20.483	39.9004	-118.3654	0.0000	1.81
11/18/2002	(322)	20:10:45.222	38.8290	-117.0095	0.0000	2.43
12/10/2002	(344)	20:12:28.835	38.7637	-117.2547	0.0000	2.35
12/19/2002	(353)	20:06:09.033	38.7002	-117.2144	0.0000	
01/17/2003	(017)	20:11:37.071	38.8291	-117.1557	0.0000	2.17
01/19/2003	(019)	1:42:59.091	38.8658	-117.8912	0.0000	2.59
01/21/2003	(021)	20:14:52.105	38.7497	-117.1773	0.0000	2.39
01/29/2003	(029)	20:14:54.422	39.5949	-117.1752	0.0000	2.55

Date	Julian	Time	Lat	Long	Depth	Mag
02/14/2003	(045)	20:13:00.079	38.8185	-117.1921	0.0000	1.91
02/22/2003	(053)	2:45:22.464	38.7760	-117.8789	0.0000	2.06
02/27/2003	(058)	20:09:47.478	38.9519	-117.2133	0.0000	2.22
03/05/2003	(064)	0:01:06.376	38.8623	-117.1265	0.0000	2.04
03/27/2003	(086)	22:56:47.863	40.2961	-118.1779	0.0000	2.01
04/22/2003	(112)	18:59:11.788	38.9010	-117.6861	0.0000	2.21
04/30/2003	(120)	19:07:33.038	38.8746	-117.0679	0.0000	2.11
07/09/2003	(190)	19:15:09.893	38.7509	-117.0182	0.0000	
09/18/2003	(261)	19:07:27.932	38.7054	-117.1228	0.0000	2.15
01/29/2004	(029)	21:49:27.356	38.8204	-118.3168	0.0000	2.08
01/30/2004	(030)	20:08:22.393	38.8555	-117.0783	0.0000	
03/16/2004	(076)	0:20:42.042	39.0622	-118.4186	0.0000	2.58
04/04/2004	(095)	21:28:39.348	39.1009	-118.0607	0.0000	1.75
06/20/2004	(172)	22:41:08.788	39.7115	-117.5524	0.0000	2.43
07/12/2004	(194)	17:42:27.671	39.8759	-118.3257	0.0000	1.63
07/14/2004	(196)	0:42:58.962	39.8630	-118.3581	0.0000	1.65
07/15/2004	(197)	23:53:41.519	39.8932	-118.3558	0.0000	1.53
07/29/2004	(211)	14:18:42.381	38.7416	-118.0023	0.0000	1.33
08/19/2004	(232)	4:14:27.653	39.7548	-118.6370	0.0000	1.52
09/05/2004	(249)	6:35:33.223	39.0431	-118.4444	0.0000	1.35
09/16/2004	(260)	4:04:05.668	39.8749	-118.3716	0.0000	1.86
11/18/2004	(323)	20:08:46.444	38.7349	-117.0811	0.0000	1.93
04/26/2005	(116)	2:58:12.374	39.8829	-118.3763	0.0000	1.65
04/28/2005	(118)	19:47:47.641	40.1443	-118.5618	0.0000	2.83
05/26/2005	(146)	19:08:56.523	38.7127	-117.1224	0.0000	2.00
08/09/2005	(221)	2:39:31.685	39.1676	-117.6181	0.0000	1.92
09/15/2005	(258)	2:44:24.741	39.7673	-118.6676	0.0000	1.54
10/06/2005	(279)	19:03:48.618	38.7309	-117.1685	0.0000	2.82
06/16/2006	(167)	19:14:03.958	38.7589	-117.0763	0.0000	1.85
07/12/2006	(193)	5:13:38.438	39.8880	-118.3698	0.0000	2.46
09/14/2006	(257)	16:08:30.356	39.0048	-117.4430	0.0000	1.93
10/12/2006	(285)	19:24:45.536	38.7801	-117.0473	0.0000	1.73
10/16/2006	(289)	20:01:55.381	38.7288	-117.1805	0.0000	1.91
1/31/2007	(031)	23:25:26.602	38.7006	-117.0484	0.0000	1.61
03/02/2007	(061)	23:07:50.202	38.7190	-117.0464	0.0000	1.58
03/07/2007	(066)	0:19:13.383	38.7068	-117.0125	0.0000	
03/15/2007	(074)	19:24:57.831	38.7228	-117.0487	0.0000	1.75
03/22/2007	(081)	19:09:47.137	38.7836	-117.0526	0.0000	
03/23/2007	(082)	19:11:53.458	38.8062	-117.0920	0.0000	2.29
04/04/2007	(094)	19:28:19.285	38.7058	-117.1078	0.0000	1.65
04/12/2007	(102)	19:21:25.054	38.7348	-117.0690	0.0000	2.16
04/16/2007	(106)	19:18:19.304	38.7461	-117.1244	0.0000	0.43
05/01/2007	(121)	16:59:56.131	40.1933	-118.3246	0.0000	1.85

Date	Julian	Time	Lat	Long	Depth	Mag
05/01/2007	(121)	23:09:15.706	38.9795	-117.1132	0.0000	1.72
05/11/2007	(131)	2:14:04.267	38.7093	-117.0622	0.0000	1.14
05/15/2007	(135)	19:02:29.419	39.8794	-118.3754	0.0000	1.45
05/16/2007	(136)	19:11:41.444	38.7104	-117.1126	0.0000	1.68
05/24/2007	(144)	0:30:14.037	38.7351	-117.0459	0.0928	1.50
05/25/2007	(145)	19:08:11.721	38.7294	-117.0805	0.0000	
06/15/2007	(166)	19:19:12.344	38.7140	-117.1146	0.0000	1.51
06/18/2007	(169)	19:33:34.295	38.7426	-117.0817	0.0000	1.69
06/20/2007	(171)	23:55:54.240	38.8092	-117.1002	0.0000	1.57
06/21/2007	(172)	19:22:58.048	38.7206	-117.0918	0.0000	1.77
06/28/2007	(179)	22:56:13.052	38.7277	-117.0830	0.0000	1.55
07/16/2007	(197)	19:19:24.512	38.7231	-117.1140	0.0000	1.80
07/27/2007	(208)	19:14:03.929	38.8246	-117.0695	0.0000	1.65
07/30/2007	(211)	19:16:28.766	38.7440	-117.0641	0.0000	1.68
08/02/2007	(214)	19:17:45.599	39.0312	-117.4053	0.0000	1.65
08/03/2007	(215)	19:10:42.355	38.7455	-117.0840	0.0000	1.50
08/06/2007	(218)	21:00:01.533	38.8189	-117.0863	0.0000	1.58
08/08/2007	(220)	22:38:38.796	38.7268	-117.1205	0.0000	2.07
08/09/2007	(221)	15:36:37.195	39.0554	-117.1388	0.0000	1.34
08/13/2007	(225)	19:07:42.808	38.9042	-117.0203	0.0000	
08/22/2007	(234)	4:13:52.129	39.3034	-118.4572	0.0000	1.20
08/29/2007	(241)	22:36:15.748	38.7861	-117.2402	0.0000	1.58
01/09/2008	(009)	0:00:38.857	38.7015	-117.0798	0.0000	
02/28/2008	(059)	20:00:35.187	38.7157	-117.1751	0.0000	
03/27/2008	(087)	19:21:10.563	38.7515	-117.0539	0.0000	
06/02/2008	(154)	17:31:58.791	38.8379	-118.0013	5.8884	2.17
06/02/2008	(154)	19:13:17.271	38.7794	-117.1084	0.0000	
06/06/2008	(158)	15:58:30.038	38.7382	-117.1366	0.0000	
06/06/2008	(158)	19:07:41.375	38.9087	-117.3378	0.0000	2.42
06/30/2008	(182)	19:17:31.272	38.8001	-117.0929	0.0000	2.24
07/03/2008	(185)	23:08:11.222	38.8107	-117.1153	0.0000	
07/07/2008	(189)	19:09:57.133	38.7414	-117.0965	0.0000	
07/09/2008	(191)	19:11:03.805	38.7099	-117.0857	0.0000	
08/06/2008	(219)	22:16:22.064	38.7809	-117.1486	0.0000	
08/11/2008	(224)	22:58:48.550	38.8681	-117.0734	0.0000	
08/14/2008	(227)	19:13:19.659	38.7807	-117.1277	0.0000	
08/20/2008	(233)	4:34:46.174	39.8552	-118.3700	0.6468	1.74
08/20/2008	(233)	19:20:28.532	38.7064	-117.0666	0.0000	
09/10/2008	(254)	19:25:20.316	38.7255	-117.1033	0.0000	
09/11/2008	(255)	19:21:31.493	38.7739	-117.1625	0.0000	
09/22/2008	(266)	19:48:57.252	39.1283	-117.3822	0.0000	
12/21/2008	(356)	22:05:19.929	38.8288	-117.1691	0.0000	
12/29/2008	(364)	20:13:41.239	38.7958	-117.1185	0.0000	

Date	Julian	Time	Lat	Long	Depth	Mag
01/06/2009	(006)	22:19:34.361	39.7688	-118.2612	0.0000	3.02
01/09/2009	(009)	13:19:09.461	39.8997	-118.4060	1.2185	1.58
01/15/2009	(015)	2:44:33.772	40.2050	-117.0940	0.0000	2.25
01/15/2009	(015)	20:04:35.647	38.7197	-117.0134	0.0000	
01/19/2009	(019)	20:10:05.839	38.7107	-117.1082	0.0000	1.94
01/28/2009	(028)	20:26:32.113	38.8043	-117.1054	0.0000	2.14
02/03/2009	(034)	20:25:56.371	38.7635	-117.1105	0.0000	2.12
02/04/2009	(035)	20:07:42.175	38.7664	-117.1095	0.0000	1.92
02/12/2009	(043)	0:21:10.948	38.7456	-117.0905	0.0000	2.10
02/22/2009	(053)	14:34:57.775	38.9750	-117.7470	0.0000	2.43
03/05/2009	(064)	8:16:16.657	39.0995	-117.7219	0.0000	
03/16/2009	(075)	19:09:07.247	38.7205	-117.0809	0.0000	1.76
03/17/2009	(076)	23:24:38.894	38.7625	-117.1187	0.0000	2.20
03/19/2009	(078)	19:09:38.880	38.7783	-117.0557	0.0000	
04/09/2009	(099)	19:06:08.794	38.8339	-117.0171	0.0000	1.69
04/22/2009	(112)	19:05:49.511	38.7443	-117.1175	0.0000	1.75
04/23/2009	(113)	19:03:30.451	38.7735	-117.1029	0.0000	2.11
04/28/2009	(118)	18:59:59.720	38.7900	-117.1247	0.0000	1.94
05/22/2009	(142)	19:51:50.948	38.7283	-117.0609	0.0000	
05/27/2009	(147)	22:54:25.068	38.7302	-117.0795	0.0000	1.97
06/02/2009	(153)	19:10:03.022	38.7879	-117.1033	0.0000	1.68
06/05/2009	(156)	19:15:20.815	38.7678	-117.0987	0.0000	1.99
06/11/2009	(162)	19:21:52.860	38.7263	-117.0933	0.0000	1.79
06/11/2009	(162)	23:09:46.086	38.7259	-117.1132	0.0000	1.59
06/16/2009	(167)	19:48:59.695	38.7557	-117.0879	0.0000	1.92
06/19/2009	(170)	19:23:25.325	38.7334	-117.0782	0.0000	2.10
06/25/2009	(176)	19:05:11.986	38.7889	-117.1177	0.0000	2.10
06/26/2009	(177)	19:15:14.251	38.7752	-117.1213	0.0000	1.85
07/15/2009	(196)	19:12:35.772	38.9063	-117.0780	0.0000	2.04
07/16/2009	(197)	19:00:28.183	38.7943	-117.0803	0.0000	1.64
07/27/2009	(208)	19:10:15.742	38.9640	-117.0831	0.0000	
07/29/2009	(210)	19:18:33.693	38.9699	-117.1471	0.0000	2.06
07/29/2009	(210)	20:03:39.885	38.7961	-117.1056	0.0000	2.31
07/30/2009	(211)	19:18:31.035	38.7707	-117.0919	0.0000	2.03
08/20/2009	(232)	19:13:00.907	38.9694	-117.1223	0.0000	1.82
08/25/2009	(237)	19:20:28.562	38.7932	-117.1649	0.0000	2.18
09/30/2009	(273)	23:02:28.329	38.7263	-117.0707	0.0000	
10/13/2009	(286)	22:08:12.371	38.9905	-118.4939	0.0000	
10/21/2009	(294)	19:20:38.239	38.7835	-117.1764	0.0000	
11/02/2009	(306)	20:10:55.241	38.8246	-117.0152	0.0000	
11/05/2009	(309)	23:58:23.614	39.0153	-117.3207	0.0000	
11/19/2009	(323)	22:42:28.550	38.9475	-117.1006	0.0000	
12/16/2009	(350)	20:30:38.141	38.8963	-117.0545	0.0000	

Date	Julian	Time	Lat	Long	Depth	Mag
01/07/2010	(007)	20:44:43.680	38.7591	-117.1252	0.0000	
01/13/2010	(013)	2:17:21.685	38.9089	-117.6975	0.0000	
01/21/2010	(021)	23:13:33.342	38.7074	-117.2277	0.0000	
01/25/2010	(025)	23:11:18.080	40.0735	-117.2543	0.0000	2.52
01/29/2010	(029)	12:26:28.170	39.7045	-117.4156	0.0000	
02/09/2010	(040)	20:23:01.303	38.7953	-117.0423	0.0000	1.89
02/12/2010	(043)	0:08:52.608	38.8878	-117.0666	0.0000	
02/18/2010	(049)	20:17:38.432	38.7021	-117.1877	0.0000	
02/26/2010	(057)	0:25:27.790	38.7163	-117.1721	0.0000	
03/10/2010	(069)	0:06:21.083	38.8162	-117.0475	0.0000	2.06
03/10/2010	(069)	23:28:25.395	39.3050	-118.4111	0.0000	
03/21/2010	(080)	19:41:16.693	38.8363	-117.0858	0.0000	1.90
04/13/2010	(103)	19:26:02.584	38.7638	-117.1586	0.0000	
04/30/2010	(120)	21:19:06.798	39.0787	-118.5301	0.0000	
05/04/2010	(124)	8:11:40.451	38.8349	-117.8969	0.0000	
05/05/2010	(125)	19:19:46.255	38.7453	-117.5317	0.0000	
06/03/2010	(154)	19:12:03.398	38.8180	-117.0221	0.0000	
06/10/2010	(161)	19:09:09.286	38.7787	-117.0611	0.0000	1.68
06/17/2010	(168)	19:20:36.012	38.8650	-117.0482	0.0000	
06/17/2010	(168)	19:21:19.722	38.8415	-117.2690	0.0000	
06/23/2010	(174)	19:21:40.442	38.7603	-117.1254	0.0000	
07/05/2010	(186)	22:10:35.482	39.2424	-118.5235	0.0000	
07/08/2010	(189)	19:21:04.721	38.8057	-117.1874	0.0000	

APPENDIX 4

SEISMIC INDICATORS OF THERMAL AND ROCK PROPERTIES

Table of Contents

1. Vp, Vs values

Although Lees (2007) argues that seismic velocity is a relatively insensitive estimator of temperature variations in rocks, seismic inversion for three-dimensional variations of velocity and attenuation are often used to delineate magma bodies in the crust and upper mantle. Laboratory measurements (Jaya et al., 2010) show that P-wave velocities decrease with increasing temperature in a systematic way (for P-velocity from 1-4 km/s and temperature from 0-300°C), implying that fluid characteristics, with modifications that allow for the presence of bubbles and microfracturing, account for much of the seismic velocity changes.

Lees (2007) summarizes (Table A4-1) tomographic inversions for P-wave and S-wave velocity/attenuation for large calderas, rift zones and smaller scale subduction zone volcanoes. The results vary considerably from place to place, most anomalies are found to be in the range of ±10% seismic velocity perturbation, a range often controlled by the method of smoothing or regularization imposed during inversion. At many volcanoes high velocity anomalies are observed in the shallow regions below magmatic active areas where conduits, dykes or sills are expected to be present. At other locations low velocity perturbations are seen and interpreted as magma accumulation. Most seismic tomography at volcanic regions involves exploring seismic velocity variations and, in some cases, seismic attenuation. Low velocity anomalies below volcanoes were seen at oceanic spreading centers in the east Pacific, Long Valley, Yellowstone, and volcanoes including Rabaul, Krafla, St. Helens, Mt. Rainier, Newberry, Medicine Lake, Unzen, Nikko- Shirane, Fuji, Klyuchevskoy, Campi Flegrei, and Pinatubo. These were interpreted as evidence for melt accumulation in various forms of dykes, sills or magma chambers. While a few examples showed evidence of shallow low velocity associated with active conduits, most low velocity anomalies attributed to melt accumulation lie deeper in the crust, in the range of 8–15 km depth. Lees suggests that, while it is not practiced yet, the combination of inverting for all four seismic parameters (Vp, Vs, Qp and Qs) simultaneously may offer a possible way to constrain resulting images and improve resolution.

Unruh et al. (2001) demonstrated that seismic imaging can provide valuable information about the structure of a conventional geothermal field hosted in crystalline (i.e., ‘’transparent”) rocks. Shallow seismic velocity structure estimated from inversion of P-wave first arrival times in the producing areas of the Coso field was relatively lower compared to the non-producing areas. This was explained by localized brittle faulting and hydrothermal alteration. In their study of the central Taupo Volcanic Zone, New Zealand, using local earthquake tomography, Sherburn et al. (2003), could not identify the shallow crustal (down to 6 km depth) basement rocks, however, they observed low Vp anomalies coincident with the location of caldera collapse structures, which they interpret as being associated with low-density volcaniclastic sediments.

Velocities tend to be sensitive to the pore fluid content. Usually the P-wave velocity is most sensitive and the S-wave velocity is less sensitive. Velocities almost always increase with effective pressure. For reservoir rocks they often tend toward a flat, high pressure asymptote. The pressure dependence results from the closing of cracks, flaws, and grain boundaries, which elastically stiffens the rock mineral frame. The only way to know the pressure dependence of velocities for a particular rock is to measure it in a laboratory. The amount of velocity change with pressure is a measure of the number of cracks; the pressure range needed to reach the high pressure asymptote is a measure of crack shape (e.g. aspect ratio).

While it is generally accepted that seismic velocity depends on the crack density and porosity, it is still not obvious how to translate seismic velocity data into a measure of permeability. Since the permeability is extremely sensitive to the crack width, the permeability of a rock containing fractures of several widths is controlled by a few largest fractures. Thus, a rock with a low density of wide, connected, open cracks and high seismic velocity would still have a high permeability. Seismic velocity and reflectivity are related via porosity to effective stress (Peacock et al., 1997).

A collection of parameters which influence seismic velocity from different regions in the world can be found in Appendix 4a and Appendix 4b.

2. Vp/Vs ratios

In general, Vp and Vs velocities decrease slowly with increasing temperature (Kern, 1982), until they approach the melting point where properties change rapidly. Increases in Vp/Vs ratio are related to increases of temperature, fracture, and especially partial melt (Sanders et al. 1995). Laboratory measurements and theoretical estimates (Mavko, 1980) of seismic wave propagation in the presence of melts show that physical properties vary considerably. Perturbations of seismic velocity due to 10% melt vary only by 10–40% for P-waves and can be 20–100% for S-waves (Iyer and Dawson, 1993). Vp/Vs ratio decreases can be associated with the presence of gas or supercritical fluids.

Fluid saturation generally induces higher P-wave velocity and saturated, unconsolidated sediments typically have high Vp /Vs ratios (Nicholson and Simpson, 1985). Saturation conditions and possibly porosity can thus occasionally be inferred from the comparison of Vp and Vs data (Lees and Wu, 2000). Vp is expected to increase when saturation increases while Vs remains nearly the same, driving Vp/Vs higher (Ito et al., 1979). However, partial melt may decrease Vp and fluid saturated zones will have a net low Vp, low Vs and thus, high Vp/Vs (Walck, 1988).

Vp/Vs ratios are sensitive to phase changes in geothermal systems. Water and steam filled pore spaces affect both P and S wave transmission differently. The ratio of P-wave velocity to the S-wave velocity (Vp/Vs) and Poisson's ratio (σ) are known to be directly related to the rock properties such as compressibility. O'Connell and Budiansky (1982) have shown that a rock's moduli are affected by the degree of water saturation. The velocity ratio (Vp/Vs) increases with pressure increases from vapor saturated (low pore-pressure) conditions to liquid saturated (high pore pressure) conditions (Ito et al., 1979). It is also known that S-waves are more intensely affected by anisotropy than P-waves and that Vp/Vs ratios are expected to vary with azimuth. This is important in delineating geological structures with contrasting physical properties within the reservoir. Such structures are normally important barriers or conduits for fluid flow in the reservoir. Many researchers have investigated how fluid-filled pores in matrix rocks affect seismic wave velocity, and have concluded that the velocity of the matrix rock containing fluids exhibits lower values than that without fluids (e.g. O'Connell and Budiansky, 1974; Mavko, 1980; Schmeling, 1985; Takei, 2002). On the other hand, it has been known that variation in Vp/Vs of matrix rock including fluids depends not only on the kind of fluids but also on the shape of the pores (e.g. Schmeling, 1985; Takei, 2002), which leads to complicated conclusions in interpretations of the causes of seismic velocity anomalies. However, it is certain that melt-filled inclusions result in high Vp/Vs (e.g. Takei, 2002). Nakajima et al. (2001a) discussed the causes of variations in Vp, Vs and Vp/Vs observed in the crust and upper mantle beneath NE Japan, and concluded that low Vp, low Vs and low Vp/Vs in the upper crust are caused by inclusions of H_2O within pores of a relatively large aspect ratio and that low Vp, low Vs and high Vp/Vs in the lower crust and uppermost mantle are caused by melt inclusions.

Vp/Vs variations depending on temperature variations are still ambiguous (e.g. Christensen, 1996) and are difficult to evaluate correctly. For example, the experimental results of Fielitz (1971) imply that Vp/Vs values of rock samples vary with temperature, while Kern and Richter (1981) measured Poisson's ratio of various rocks and concluded that it does not change much with temperature; the average change in Poisson's ratio for rock samples was ~1%, within experimental error.

Studies of Vp/Vs ratios have been done in several geothermal fields (McEvilly et al., 1978; Majer and McEvilly, 1979, Foulger et al., 1997, Julian, et al., 1996, 1998). These studies show that water dominated systems such as East Mesa, USA and Cerro Prieto, Mexico have high ratios of 1.55-1.68. These fields were also found to have low reservoir draw down during exploitation. Batini et al. (2010), applying tomography methods at the Larderello geothermal area, found a sharp low velocity zone in the center of the geothermal area, characterized by 15-20% diminished P wave velocity, and associated with a deep low-density body inferred by gravity studies. They have interpreted their results as evidence for an intrusive, still partially molten body that might be the heat source of the area. Steam dominated fields such as The Geysers and Coso Hot Springs, USA have lower ratios, and high reservoir draw down. Low V_P/V_S anomalies at The Geysers are found to correlate reasonably well with regions in the reservoir known or thought to be vapor dominated, consistent with the fluid compressibility mechanism. However, detailed examination of three dimensional inversions of compressional and shear velocities at The Geysers do not seem to support a simple interpretation based solely on variations in fluid compressibility.

There is a negative correlation between V_S and V_P/V_S, along with a notable lack of correlation between V_P and V_P/V_S. These observations (Boitnoit and Kirkpatrick, 1997**)** are at odds with simple interpretations based on poroelasticity, and suggest that the velocity anomalies reflect processes or phenomena not typically included in interpretations of field seismic data. These authors suggest that shear weakening) may influence the properties of field-scale features, or dry reservoir (low pore fluid compressibility) correlates with regions of low pore pressure (depleted reservoir), or the effects of variability in preferred orientation of fractures may also play a role in producing field scale *VP*/*VS* anomalies. Simiyu (1999) interpreted low Poisson ratio and low Vp/Vs values as be due to high temperature and steam/gas saturation in geothermal fields located in the Kenya rift south west of the Lake Naivasha. A low Vs and low Vp/Vs region relating to the old magma body of volcanoes around of the Otake-Hatchobaru geothermal area in central Kyushu, Japan was located at the depth deeper than 5 km by Yoshikawa and Sudo (2004).

3. Poisson's ratio

Poisson's ratio can be a useful indicator of lithology, pore fluid pressure and compressibility. On average, the Poisson's ratio is 0.25 (representing a "Poisson solid" where Lame's constant equals the shear modulus) for Earth's crust and upper mantle (Holbrook et al., 1988). Furthermore, there is a strong dependence of Poisson's ratio on the overall volume of cracks and their aspect ratios (Koch, 1992). Poisson's ratio can be computed from Vp/Vs and vice versa.

4. Vp*Vs

This parameter has been used to delineate porosity in sedimentary rocks (Iverson et al., 1989). It has been observed that lower *Vp*Vs* indicates an increase of porosity whereas *Vp/Vs*, constant for a specific lithology, does not change with porosity (Pickett, 1963; Tatham, 1982). In geothermal settings, porosity distributions may be more critical for understanding the physics of the field than lithologic variations (Lees and Wu, 2000).

5. Dispersion

Dispersion is the property of acoustic waves of different wavelength to propagate with different velocity. Fluid mobility determines pore-pressure distribution as a fully saturated rock is deformed slightly when a seismic wave passes. Thus, seismic properties are influenced not only by the kind of pore fluid but also by the fluid's ability to move within the rock (Batzle et al., 2006). According to Batzle et al. (2006), with sufficient information, waveform dispersion could be used as a fluid indicator or as a remote measurement of permeability. Dispersion is a complex function of heterogeneity, pore-fluid properties, and mobility.

6. Crustal Phase Properties and Correlation with Heat Flow, Temperature and Rock Composition

6.1 Pn, Sn velocity

In India, Sharma et al (1991) found an inverse relationship among Pn velocity and surface heat flow. Low Pn velocity is associated with elevated temperatures in the upper-most mantle. In the Basin and Range province, Chung (1977) showed that the pronounced low-velocity, low-Q zone and anomalous travel-time delays of both P and S waves are consistent with the combined effects of high temperature, chemical composition, phase changes, and partial melting. The observed low Pn velocity was consistent with high temperature, chemical composition, and the presence of a partially molten layer within the upper mantle, however, the observed teleseismic delay times resulted principally from the thickness of the low velocity zone. Thermal anomalies proposed to have sources in the crust in some areas are consistent with gravity and shear-wave anomalies and support studies in those areas, that suggest high crustal radiogenic concentrations in relatively less dense, granitic crustal rocks (Reiter, 2008).

6.2 Shear wave splitting (SWS, acoustic birefringence)

A single shear-wave propagating through anisotropic rock is split into two orthogonally polarized shear waves, one faster than the other. SWS is higher at low pressure and decreases with the pressure increase. Laboratory seismic measurements performed by Christensen (1978) have shown that crustal rocks can be strongly anisotropic for shear waves. More recent petrophysical investigations indicate that there is a close relationship between the intrinsic anisotropy (generated by preferred crystal orientations), the birefringence, and the rock structure (foliation and lineation). This relationship may yield information on the crustal structure from shear-wave splitting studies (Barruol and Kern, 1996). Thus, both petrophysical and seismological developments are pointing the way towards use of SWS as a tool to investigate crustal nature and structure.

Malin and Shlev, 1999, developed a method for mapping subsurface fracture density using the time differences of split shear waves from microearthquakes. In regions where a consistent direction of fracturing exists, shear waves from different source and receiver locations are systematically split into fast and slow components. The greater the fracture density, the greater the time differences between the fast and slow components for a given path length. Also, the greater the path length in the fractured rock, the greater the time difference. With a large number of spatially distributed sources and receivers, tomographic back projection of the time differences can be used to map the distribution of fracture density and orientation of the fractures.

To detect the geometry and density of fracture systems at the Coso geothermal field Vlahovic et al. (2002) applied shear-wave splitting to microearthquakes recorded by a permanent, 16-station, downhole, 3-component seismic array running at 480 samples/s. The analysis of shear-wave splitting (seismic birefringence) provided parameters directly related to the strike of the subsurface fractures and their density (number of cracks per unit volume), and, consequently, it is an important technique to outline zones of high permeability. Major fracture directions and orientations were consistent with the known strike of local sets of faults and fractures in local wells and at the surface, as well as with previous analyses of seismic anisotropy in the region.

6.3 Seismic noise

Clearly defined areas of seismic noise at 1.8 km depth have been found by Georgsson et al. (2000), to be associated with the active fracture zone at the eastern flank of the Bakkahlaup field, Iceland, and may partially reflect boiling within the reservoir or partial cracking due to cooling of rocks.

6.4 Seismic attenuation in the crust

Laboratory measurements (Jaya et al, 2010) on two Icelandic geothermal rock samples at simulated in-situ reservoir conditions show that at low temperatures seismic attenuation decreases with temperature due to the rapid decrease in the fluid viscosity. On the other hand, at higher temperatures the attenuation increases because of the generation of bubbles and thermal microfractures.

Laboratory experiments done at high temperature and seismic frequencies (e.g., Kampfmann and Berckhemer, 1985) show that Q_S and Q_P may drop by a factor of 5–10 as temperature increases close to solidus. Heterogeneities within the crust are randomly distributed and occur on a wide range of scales (Frankel and Clayton, 1986; Wu and Aki, 1988; Wu and Flattd, 1990). In the Earth's interior such variations occur at scales down to the grain size of rocks (Holliger et al., 1994). These heterogeneities are due to spatial variations in composition, porosity and fracturing, and changing conditions in pore pressure, temperature and stress. Wavelength-scale heterogeneity can produce significant seismic scattering and attenuation, and may be of importance in imaging the Earth's interior (Gibson and Levander, 1988; Holliger et al., 1994; Levander et al., 1994).

7. Density and Seismic Velocity

Birch (1961) gave a fundamental empirical relation between density ρ and seismic velocity Vp:

$$\rho = A(M)+BV_p$$

with the constants A and B, of which A is depending on the mean atomic weight M.

Introducing the seismic parameter $F=v_p^2-4/3\ v_s^2$ Birch's relation was modified by Anderson (1967) who proposed the density/velocity relation of:

$$\rho = AMF^n$$

with the constants A and n. Confining the density/velocity relations to rocks of constant Poisson's ratio and mean atomic weight Knopoff (1967) found a simple density definition of:

$$\rho = Av_p^{2/3}$$

Systematics in the relation between density and seismic velocity on the basis of mineralogical constitution are outlined in detail by Shankland (1977) and Buntebarth (1982).

Table A4-1. (from Lees, 2007)

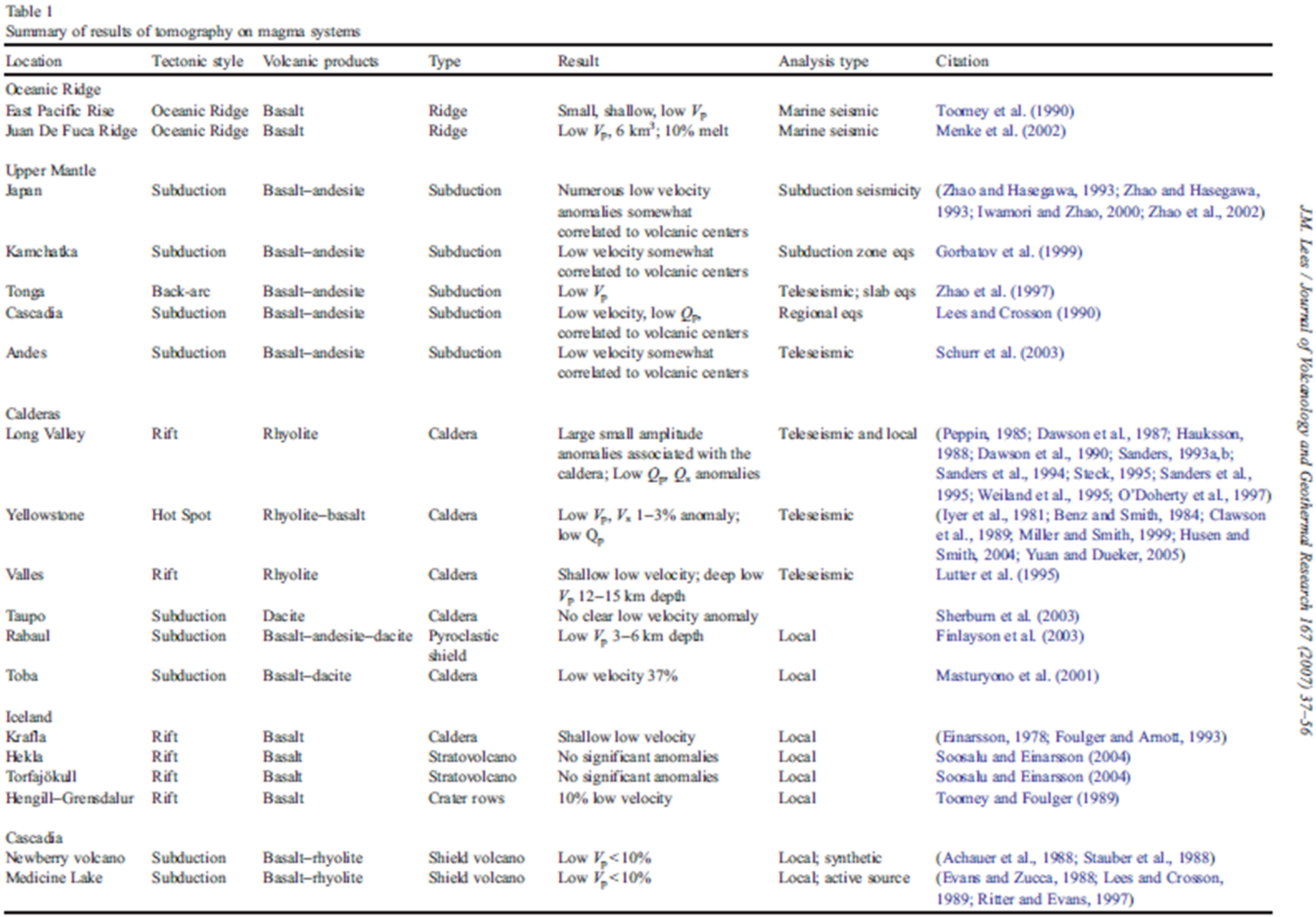

Table 1
Summary of results of tomography on magma systems

Location	Tectonic style	Volcanic products	Type	Result	Analysis type	Citation
Oceanic Ridge						
East Pacific Rise	Oceanic Ridge	Basalt	Ridge	Small, shallow, low V_p	Marine seismic	Toomey et al. (1990)
Juan De Fuca Ridge	Oceanic Ridge	Basalt	Ridge	Low V_p, 6 km^3; 10% melt	Marine seismic	Menke et al. (2002)
Upper Mantle						
Japan	Subduction	Basalt–andesite	Subduction	Numerous low velocity anomalies somewhat correlated to volcanic centers	Subduction seismicity	(Zhao and Hasegawa, 1993; Zhao and Hasegawa, 1993; Iwamori and Zhao, 2000; Zhao et al., 2002)
Kamchatka	Subduction	Basalt–andesite	Subduction	Low velocity somewhat correlated to volcanic centers	Subduction zone eqs	Gorbatov et al. (1999)
Tonga	Back-arc	Basalt–andesite	Subduction	Low V_p	Teleseismic; slab eqs	Zhao et al. (1997)
Cascadia	Subduction	Basalt–andesite	Subduction	Low velocity, low Q_p, correlated to volcanic centers	Regional eqs	Lees and Crosson (1990)
Andes	Subduction	Basalt–andesite	Subduction	Low velocity somewhat correlated to volcanic centers	Teleseismic	Schurr et al. (2003)
Calderas						
Long Valley	Rift	Rhyolite	Caldera	Large small amplitude anomalies associated with the caldera; Low Q_p, Q_s anomalies	Teleseismic and local	(Peppin, 1985; Dawson et al., 1987; Hauksson, 1988; Dawson et al., 1990; Sanders, 1993a,b; Sanders et al., 1994; Steck, 1995; Sanders et al., 1995; Weiland et al., 1995; O'Doherty et al., 1997)
Yellowstone	Hot Spot	Rhyolite–basalt	Caldera	Low V_p, V_s 1–3% anomaly; low Q_p	Teleseismic	(Iyer et al., 1981; Benz and Smith, 1984; Clawson et al., 1989; Miller and Smith, 1999; Husen and Smith, 2004; Yuan and Dueker, 2005)
Valles	Rift	Rhyolite	Caldera	Shallow low velocity; deep low V_p 12–15 km depth	Teleseismic	Lutter et al. (1995)
Taupo	Subduction	Dacite	Caldera	No clear low velocity anomaly		Sherburn et al. (2003)
Rabaul	Subduction	Basalt–andesite–dacite	Pyroclastic shield	Low V_p 3–6 km depth	Local	Finlayson et al. (2003)
Toba	Subduction	Basalt–dacite	Caldera	Low velocity 37%	Local	Masturyono et al. (2001)
Iceland						
Krafla	Rift	Basalt	Caldera	Shallow low velocity	Local	(Einarsson, 1978; Foulger and Arnott, 1993)
Hekla	Rift	Basalt	Stratovolcano	No significant anomalies	Local	Soosalu and Einarsson (2004)
Torfajökull	Rift	Basalt	Stratovolcano	No significant anomalies	Local	Soosalu and Einarsson (2004)
Hengill–Grensdalur	Rift	Basalt	Crater rows	10% low velocity	Local	Toomey and Foulger (1989)
Cascadia						
Newberry volcano	Subduction	Basalt–rhyolite	Shield volcano	Low V_p < 10%	Local; synthetic	(Achauer et al., 1988; Stauber et al., 1988)
Medicine Lake	Subduction	Basalt–rhyolite	Shield volcano	Low V_p < 10%	Local; active source	(Evans and Zucca, 1988; Lees and Crosson, 1989; Ritter and Evans, 1997)

J.M. Lees / Journal of Volcanology and Geothermal Research 167 (2007) 37–56

Table 1 (*continued*)

Location	Tectonic style	Volcanic products	Type	Result	Analysis type	Citation
Cascadia						
Mt. St. Helens	Subduction	Andesite–dacite and occasional rhyolite	Stratovolcano	High V_p 20% top of stopoing zone; Low V_p conduit and deep Low V_p	Local earthquake	Lees (1992)
Mt. Rainier	Subduction	Granodiorite–andesite	Stratovolcano	Low V_p 8–15 km	Local–regional eqs	(Lees and Crosson, 1990; Moran et al., 1999)
Alaska						
Redoubt	Subduction	Basalt–dacite	Stratovolcano	10% perturbations; no clear magma body	Local eqs	Benz et al. (1996)
Japan						
Unzen	Rift	Basaltic	Complex volcano	Low V_p	Local–regional eqs	Ohmi and Lees (1995)
Onikobe	Subduction	Basalt–dacite	Volcanic chain	Low V_p, V_s, high V_p/V_s	Local eqs	Nakajima and Hasegawa (2003)
Kirishima	Subduction	Basalt–dacite	Shield volcano	High and low velocity; low Q	Local–regional eqs	Yamamoto and Ida (1994)
Nikko-Shirane	Subduction	Basalt–dacite	Shield volcano	30% low V_p 5–15 km depth	Local eqs	Horiuchi et al. (1997)
Mt. Fuji	Subduction	Basalt–dacite	Stratovolcano	Low V_p below summit	Local–regional eqs	Nakamichi (2005)
Kamchatka						
Klyuchevskoy	Subduction	Basalt–dacite	Stratovolcano	Low V_p 25–40 km depth	Local–regional eqs	(Anosov et al., 1978; Ozerov, 2000)
Hawaii						
Halemaumau	Hot Spot	Basalt	Shield	Low V_p 6 km deep	Local eqs	Rowan and Clayton (1993)
Kilauea	Hot Spot	Basalt	Shield volcano	Low V_p, High V_p in shallow conduit	Local eqs	(Thurber, 1984; Rowan and Clayton, 1993; Okubo et al., 1997; Haslinger et al., 2001)
Italy						
Vesuvius	Subduction	Basal–dacite	Somma volcano	No shallow anomaly; Low V_p at 8 km depth	Local eqs	(De Natale et al., 1998; Zollo et al., 1998)
Campi Flegrei	Subduction	Basalt–dacite	Caldera	Low velocity 3–4 km; gas accumulation?	Local eqs	1988; Aster et al., 1992
Mt. Etna	Subduction	Basalt–dacite	Stratovolcanoes	High velocity	Local eqs	(Cardaci et al., 1993; Villasenor et al., 1998; Laigle and Hirn, 1999; Chiarabba et al., 2000; Aloisi et al., 2002)
Indonesia						
Pinatubo	Subduction	Basalt–dacite	Stratovolcano	Low V_p 6–11 km depth; 15% anomaly	Local eqs	Mori et al. (1996)
S. America						
Nevado del Ruiz	Subduction	Basalt–dacite	Stratovolcano	Low V_p and V_s	Local eqs	Londoño and Sudo (2003)
Tungurahua	Subduction	Andesitic	Stratovolcano	High V_p in upper 4–5 km	Local eqs	Molina et al. (2005)
Canary Islands						
Gran Canaria	Hot spot	Basaltic	Fissure vents	No low velocity	Local eqs	Krastel and Schmincke (2002)

APPENDIX 5

PARAMETERS WITH INFLUENCE ON SEISMIC VELOCITY

Table of Contents

1. Source - Christensen (1968)

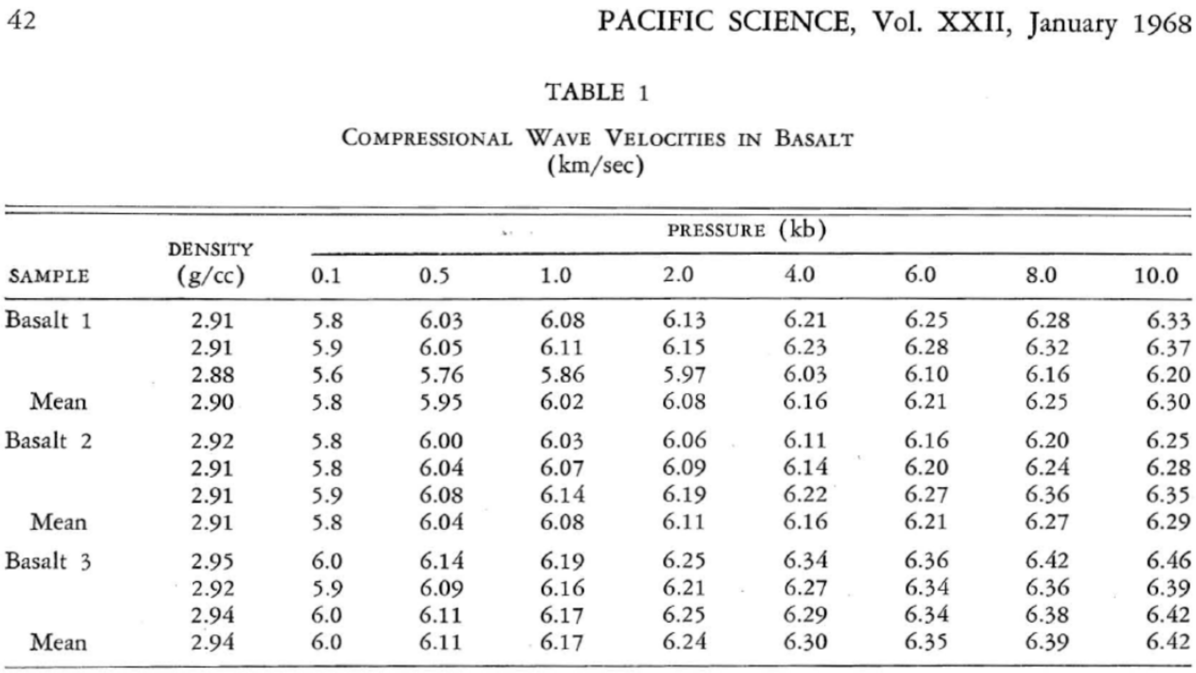

42 PACIFIC SCIENCE, Vol. XXII, January 1968

TABLE 1

COMPRESSIONAL WAVE VELOCITIES IN BASALT
(km/sec)

		PRESSURE (kb)							
SAMPLE	DENSITY (g/cc)	0.1	0.5	1.0	2.0	4.0	6.0	8.0	10.0
Basalt 1	2.91	5.8	6.03	6.08	6.13	6.21	6.25	6.28	6.33
	2.91	5.9	6.05	6.11	6.15	6.23	6.28	6.32	6.37
	2.88	5.6	5.76	5.86	5.97	6.03	6.10	6.16	6.20
Mean	2.90	5.8	5.95	6.02	6.08	6.16	6.21	6.25	6.30
Basalt 2	2.92	5.8	6.00	6.03	6.06	6.11	6.16	6.20	6.25
	2.91	5.8	6.04	6.07	6.09	6.14	6.20	6.24	6.28
	2.91	5.9	6.08	6.14	6.19	6.22	6.27	6.36	6.35
Mean	2.91	5.8	6.04	6.08	6.11	6.16	6.21	6.27	6.29
Basalt 3	2.95	6.0	6.14	6.19	6.25	6.34	6.36	6.42	6.46
	2.92	5.9	6.09	6.16	6.21	6.27	6.34	6.36	6.39
	2.94	6.0	6.11	6.17	6.25	6.29	6.34	6.38	6.42
Mean	2.94	6.0	6.11	6.17	6.24	6.30	6.35	6.39	6.42

2. Source – Kern (1982)

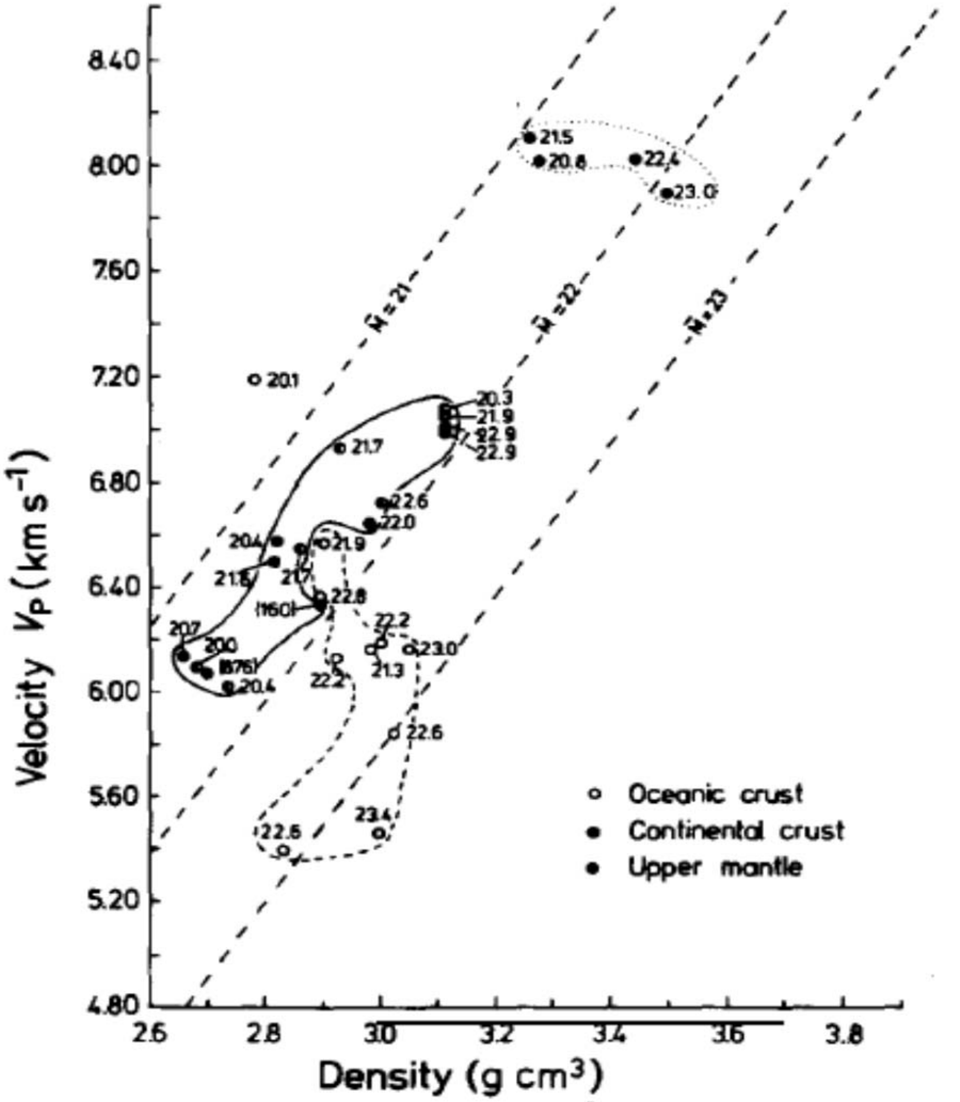

Fig. 2. Compressional-wave velocities v. density at 6 kbar confining pressure. The numbers attached to the symbols are mean atomic weights as calculated from the chemical analyses. Dashed lines represent lines of constant mean atomic weight, according to Birch (1961).

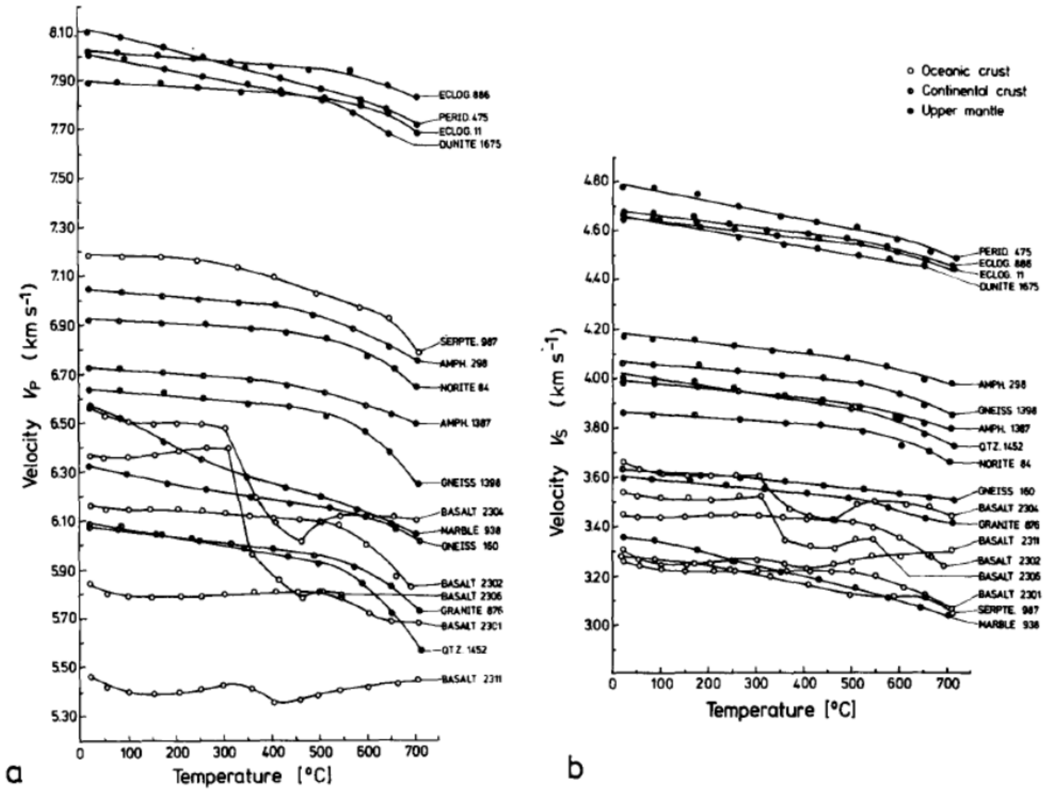

Fig. 5. Velocities of (a) compressional waves and (b) shear waves as a function of temperature at 6 kbar confining pressure for a series of selected rocks. V_P is the mean of the velocities measured in three orthogonal directions of the sample cubes. V_S is the velocity in one direction.

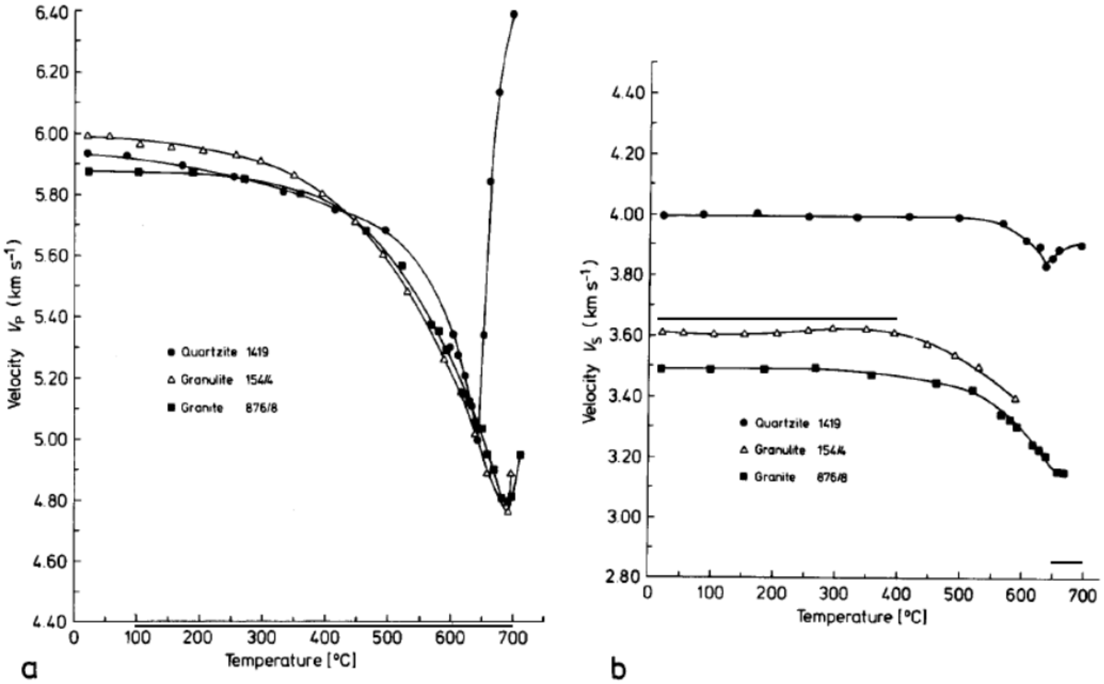

Fig. 7. Compressional-wave velocities (a) and shear wave velocities (b) as a function of temperature at 2 kbar confining pressure in quartzite, granite and granulite. The velocity curves are characterized by a kink which is associated with the $\alpha-\beta$ transition of quartz (from Kern, 1979).

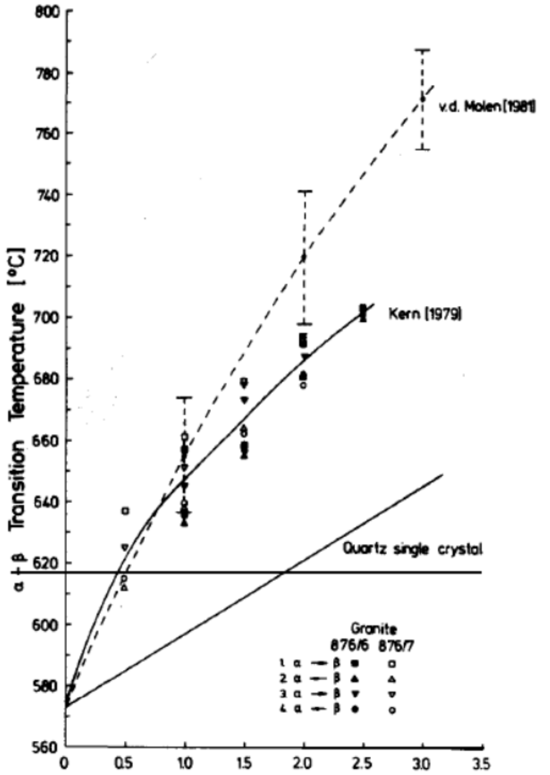

Fig. 8. The quartz $\alpha-\beta$ transition temperature in granite as a function of confining pressure, as obtained by V_P measurements. The dashed line presents results obtained by thermal expansion measurements on Delegate aplite (after van der Molen, 1981). The pressure dependence of $T_{\alpha-\beta}$ for quartz single crystals is also indicated.

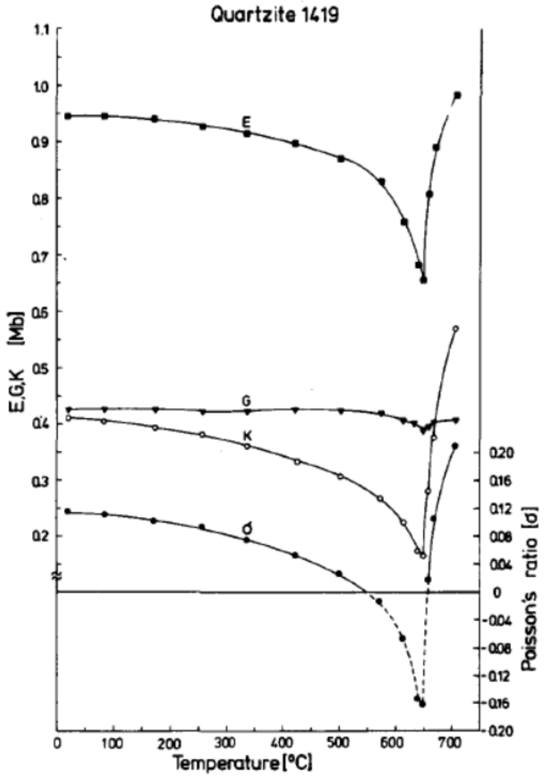

Fig. 9. Values of bulk modulus K, the shear modulus G, Young's modulus E, and the Poisson's ratio σ as a function of temperature at 2 kbar confining pressure for quartzite, calculated from the velocities according to the formulas for isotropic bodies (from Kern, 1979).

At the critical temperature V_P and V_S decrease irreversibly and further thermal cycling has no significant effect. This indicates that the irreversible dehydration breakdown reaction of zeolites contributes the major part for the decrease of wave velocities and not the fluid phase itself. To get more information about the causes for the velocity

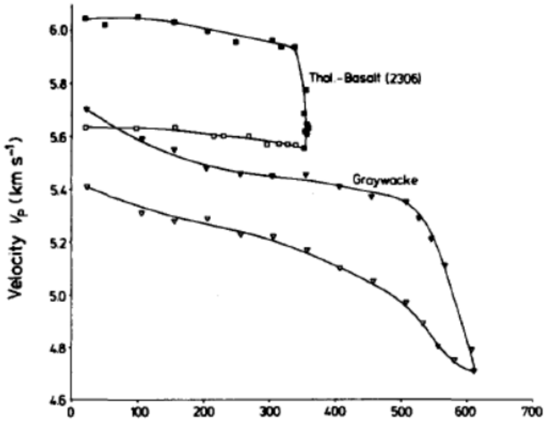

Fig. 10. Velocities of compressional waves for a jacketed sample of tholeiitic basalt (No. 2306) as a function of temperature at 6 kbar confining pressure (Kern and Richter, 1979) and for metagraywacke at 5 kbar confining pressure (Burkhardt et al., 1982). The solid symbols represent measurements on the way to higher temperature, the open symbols represent measurements on the way back to room temperature.

3. Source - Kern et al., (2001)

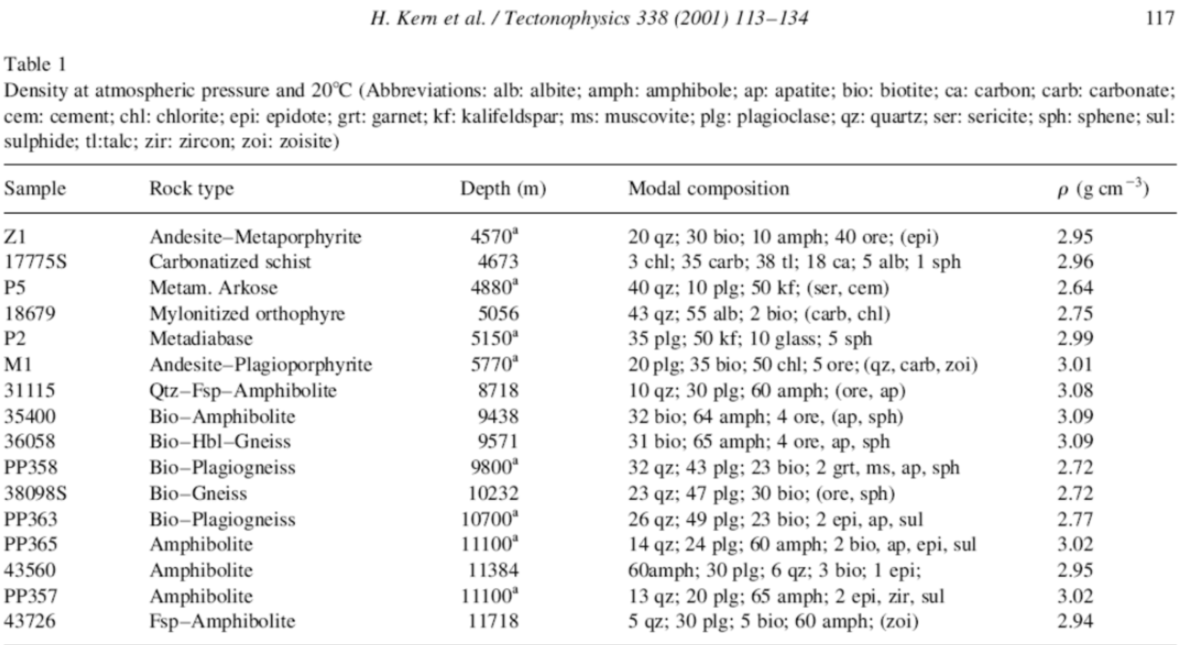

H. Kern et al. / Tectonophysics 338 (2001) 113–134 117

Table 1

Density at atmospheric pressure and 20°C (Abbreviations: alb: albite; amph: amphibole; ap: apatite; bio: biotite; ca: carbon; carb: carbonate; cem: cement; chl: chlorite; epi: epidote; grt: garnet; kf: kalifeldspar; ms: muscovite; plg: plagioclase; qz: quartz; ser: sericite; sph: sphene; sul: sulphide; tl:talc; zir: zircon; zoi: zoisite)

Sample	Rock type	Depth (m)	Modal composition	ρ (g cm^{-3})
Z1	Andesite–Metaporphyrite	4570[a]	20 qz; 30 bio; 10 amph; 40 ore; (epi)	2.95
17775S	Carbonatized schist	4673	3 chl; 35 carb; 38 tl; 18 ca; 5 alb; 1 sph	2.96
P5	Metam. Arkose	4880[a]	40 qz; 10 plg; 50 kf; (ser, cem)	2.64
18679	Mylonitized orthophyre	5056	43 qz; 55 alb; 2 bio; (carb, chl)	2.75
P2	Metadiabase	5150[a]	35 plg; 50 kf; 10 glass; 5 sph	2.99
M1	Andesite–Plagioporphyrite	5770[a]	20 plg; 35 bio; 50 chl; 5 ore; (qz, carb, zoi)	3.01
31115	Qtz–Fsp–Amphibolite	8718	10 qz; 30 plg; 60 amph; (ore, ap)	3.08
35400	Bio–Amphibolite	9438	32 bio; 64 amph; 4 ore, (ap, sph)	3.09
36058	Bio–Hbl–Gneiss	9571	31 bio; 65 amph; 4 ore, ap, sph	3.09
PP358	Bio–Plagiogneiss	9800[a]	32 qz; 43 plg; 23 bio; 2 grt, ms, ap, sph	2.72
38098S	Bio–Gneiss	10232	23 qz; 47 plg; 30 bio; (ore, sph)	2.72
PP363	Bio–Plagiogneiss	10700[a]	26 qz; 49 plg; 23 bio; 2 epi, ap, sul	2.77
PP365	Amphibolite	11100[a]	14 qz; 24 plg; 60 amph; 2 bio, ap, epi, sul	3.02
43560	Amphibolite	11384	60amph; 30 plg; 6 qz; 3 bio; 1 epi;	2.95
PP357	Amphibolite	11100[a]	13 qz; 20 plg; 65 amph; 2 epi, zir, sul	3.02
43726	Fsp–Amphibolite	11718	5 qz; 30 plg; 5 bio; 60 amph; (zoi)	2.94

[a] Correlation depth

Table 4
Compressional wave velocities (km s^{-1}) and velocity anisotropies (%) at various confining pressures (20°C) and temperatures (600 MPa)

Sample	Propagation direction	Pressure, MPa (20°C)						Temperature, °C (600 MPa)			
		25	50	100	200	400	600	100	200	400	600
Z1	*X*	6.39	6.47	6.53	6.61	6.68	6.73	6.72	6.69	6.61	6.55
	Y	6.35	6.41	6.47	6.54	6.62	6.66	6.65	6.62	6.54	6.48
	Z	6.39	6.44	6.51	6.59	6.67	6.71	6.69	6.67	6.60	6.54
	Mean	6.38	6.44	6.51	6.58	6.66	6.70	6.69	6.66	6.59	6.52
	Anis	0.67	0.95	0.95	1.05	1.04	1.04	1.09	1.01	1.05	1.04
17775S	*X*	5.30	5.64	5.86	6.02	6.14	6.20	6.17	6.12	6.10	6.08
	Y	4.93	5.32	5.57	5.74	5.88	5.97	5.93	5.86	5.83	5.78
	Z	4.06	4.62	5.01	5.26	5.44	5.58	5.56	5.51	5.47	5.41
	Mean	4.76	5.19	5.48	5.67	5.82	5.92	5.89	5.83	5.80	5.76
	Anis	26.07	19.55	15.47	13.43	12.03	10.46	10.33	10.52	10.81	11.62
P 5	*X*	6.55	6.56	6.58	6.62	6.66	6.69	6.67	6.62	6.51	6.32
	Y	6.46	6.48	6.51	6.53	6.60	6.64	6.61	6.57	6.45	6.24
	Z	6.70	6.71	6.76	6.81	6.85	6.88	6.86	6.82	6.73	6.55
	Mean	6.57	6.59	6.62	6.65	6.70	6.74	6.71	6.67	6.56	6.37
	Anis	3.62	3.51	3.75	4.12	3.79	3.62	3.68	3.85	4.36	4.87
18679S	*X*	5.29	5.66	5.93	6.18	6.29	6.32	6.31	6.27	6.20	6.11
	Y	5.28	5.69	6.01	6.23	6.31	6.33	6.30	6.27	6.20	6.07
	Z	4.56	5.14	5.73	6.17	6.34	6.40	6.36	6.33	6.25	6.12
	Mean	5.05	5.50	5.89	6.19	6.31	6.35	6.32	6.29	6.22	6.10
	Anis	14.46	10.15	4.75	1.00	0.89	1.20	0.96	1.02	0.87	0.77
P 2	*X*/c >	5.86	5.94	6.00	6.05	6.10	6.14	6.12	6.09	5.99	5.85
	Y	5.63	5.72	5.80	5.88	5.94	5.99	5.97	5.94	5.84	5.68
	Z	5.24	5.42	5.60	5.73	5.82	5.86	5.85	5.82	5.74	5.58
	Mean	5.58	5.69	5.80	5.88	5.95	5.99	5.98	5.95	5.86	5.71
	Anis	11.25	9.21	6.90	5.42	4.79	4.54	4.57	4.54	4.35	4.70
M1	*X*	6.60	6.65	6.69	6.73	6.78	6.82	6.79	6.73	6.61	6.40
	Y	6.55	6.60	6.65	6.70	6.75	6.79	6.76	6.70	6.58	6.36
	Z	6.56	6.60	6.66	6.73	6.79	6.83	6.79	6.73	6.62	6.39
	Mean	6.57	6.62	6.66	6.72	6.78	6.81	6.78	6.72	6.60	6.38
	Anis	0.67	0.76	0.57	0.48	0.53	0.54	0.44	0.49	0.61	0.56
31115	*X*	5.79	6.36	6.82	7.09	7.18	7.21	7.21	7.18	7.11	7.07
	Y	5.29	5.88	6.43	6.77	6.86	6.90	6.89	6.86	6.77	6.69
	Z	4.07	4.79	5.61	6.19	6.43	6.49	6.47	6.44	6.35	6.26
	Mean	5.05	5.68	6.29	6.68	6.82	6.86	6.86	6.83	6.75	6.67
	Anis	33.99	27.65	19.30	13.47	11.05	10.58	10.74	10.97	11.28	12.13
35400	*X*	4.64	5.10	5.43	5.69	5.87	5.99	5.96	5.91	5.82	5.76
	Y	5.42	5.82	6.21	6.56	6.77	6.86	6.84	6.82	6.78	6.78
	Z	5.49	6.07	6.67	7.16	7.42	7.50	7.49	7.49	7.50	7.52
	Mean	5.18	5.66	6.10	6.47	6.69	6.78	6.77	6.74	6.70	6.69
	Anis	16.38	17.17	20.42	22.84	23.08	22.26	22.63	23.33	25.08	26.33
36058	*X*	6.53	7.03	7.31	7.45	7.52	7.56	7.53	7.50	7.54	7.59
	Y	5.57	6.18	6.54	6.75	6.85	6.90	6.86	6.80	6.80	6.81
	Z	4.13	4.77	5.28	5.66	5.91	6.03	5.97	5.92	5.87	5.81
	Mean	5.41	6.00	6.37	6.62	6.76	6.83	6.79	6.74	6.74	6.74
	Anis	44.33	37.70	31.88	26.94	23.86	22.45	22.90	23.34	24.77	26.43

Table 4 (*continued*)

Sample	Propagation direction	Pressure, MPa (20°C)						Temperature, °C (600 MPa)			
		25	50	100	200	400	600	100	200	400	600
38098S	*X*	4.31	5.07	5.71	6.30	6.63	6.72	6.70	6.67	6.66	6.69
	Y	4.92	5.32	5.80	6.19	6.41	6.48	6.44	6.40	6.35	6.33
	Z	3.50	4.32	5.03	5.46	5.69	5.79	5.74	5.70	5.63	5.53
	Mean	4.24	4.90	5.51	5.98	6.24	6.33	6.29	6.26	6.21	6.18
	Anis	33.41	20.42	13.98	14.03	15.12	14.66	15.11	15.58	16.60	18.72
43560	*X*	5.29	5.96	6.48	6.83	6.96	7.00	6.99	6.96	6.92	6.86
	Y	5.11	5.69	6.29	6.69	6.84	6.88	6.85	6.84	6.80	6.69
	Z	3.86	4.98	5.85	6.56	6.83	6.88	6.87	6.86	6.82	6.74
	Mean	4.76	5.54	6.21	6.69	6.87	6.92	6.90	6.89	6.85	6.76
	Anis	30.13	17.72	10.12	4.02	1.88	1.71	2.03	1.71	1.81	2.57
43726	*X*	5.02	5.57	6.10	6.53	6.75	6.82	6.81	6.77	6.70	6.62
	Y	5.42	5.92	6.35	6.68	6.90	6.96	6.96	6.93	6.85	6.78
	Z	4.21	4.74	5.45	6.31	6.88	7.00	7.00	6.98	6.93	6.86
	Mean	4.88	5.41	5.97	6.51	6.84	6.93	6.92	6.90	6.83	6.75
	Anis	24.60	21.74	15.00	5.64	2.12	2.61	2.86	3.05	3.31	3.49
P 358	*X*	6.18	6.39	6.48	6.55	6.57	6.59	n.d.	n.d.	n.d.	n.d.
	Y	5.67	5.89	6.02	6.09	6.14	6.16	n.d.	n.d.	n.d.	n.d.
	Z	5.07	5.47	5.72	5.89	5.98	6.03	n.d.	n.d.	n.d.	n.d.
	Mean	5.64	5.92	6.07	6.18	6.23	6.26	n.d.	n.d.	n.d.	n.d.
	Anis	19.74	15.45	12.40	10.67	9.49	8.96	n.d.	n.d.	n.d.	n.d.
PP 363	*X*	6.14	6.35	6.42	6.50	6.56	6.58	6.55	6.54	6.50	6.43
	Y	5.88	6.09	6.22	6.28	6.32	6.36	6.32	6.28	6.23	6.12
	Z	5.15	5.40	5.58	5.70	5.79	5.85	5.81	5.79	5.69	5.58
	Mean	5.72	5.95	6.07	6.16	6.22	6.26	6.23	6.20	6.14	6.04
	Anis	17.17	16.04	13.80	13.07	12.41	11.58	11.82	12.13	13.19	13.92
PP 357	*X*	7.07	7.19	7.19	7.25	7.30	7.31	7.29	7.27	7.24	7.20
	Y	6.24	6.61	6.78	6.85	6.89	6.91	6.87	6.84	6.80	6.69
	Z	5.45	5.93	6.22	6.39	6.49	6.52	6.51	6.49	6.42	6.31
	Mean	6.25	6.58	6.73	6.83	6.89	6.91	6.89	6.86	6.82	6.74
	Anis	25.80	19.15	14.49	12.58	11.71	11.40	11.38	11.38	11.98	13.23
PP 365	*X*	6.84	6.94	7.00	7.02	7.05	7.08	7.05	7.03	6.97	6.88
	Y	6.96	7.06	7.10	7.13	7.14	7.14	7.12	7.10	7.06	6.95
	Z	5.89	6.06	6.15	6.23	6.28	6.33	6.30	6.27	6.19	6.07
	Mean	6.56	6.69	6.75	6.79	6.82	6.85	6.82	6.80	6.74	6.63
	Anis	16.33	14.99	14.04	13.22	12.49	11.81	12.06	12.24	12.78	13.27

Table 5
Shear wave velocities and maximum shear wave splitting values (km s^{-1}) at various pressures (20°C) and temperatures (600 MPa)

Sample	Propagation direction	Pressure, MPa (20°C)						Temperature, °C (600 MPa)			
		25	50	100	200	400	600	100	200	400	600
Z1	*X*	3.70	3.75	3.81	3.84	3.86	3.87	3.87	3.85	3.80	3.75
	Y	3.74	3.79	3.81	3.83	3.84	3.85	3.85	3.84	3.79	3.74
	Z	3.71	3.75	3.79	3.83	3.85	3.86	3.86	3.85	3.80	3.75
	Mean	3.71	3.76	3.81	3.83	3.85	3.86	3.86	3.85	3.79	3.75
	ΔV_S//Fol.	0.02	0.02	0.02	0.02	0.02	0.02	0.02	0.02	0.02	0.02
17775S	*X*	3.15	3.33	3.44	3.52	3.58	3.61	3.58	3.54	3.53	3.50
	Y	2.97	3.18	3.30	3.39	3.46	3.50	3.47	3.43	3.41	3.37
	Z	2.77	2.93	3.03	3.13	3.19	3.23	3.20	3.16	3.15	3.12
	Mean	2.96	3.14	3.26	3.35	3.41	3.45	3.42	3.38	3.36	3.33
	ΔV_S//Fol.	0.06	0.05	0.02	0.02	0.01	0.00	0.00	0.01	0.01	0.01
P 5	*X*	3.54	3.63	3.66	3.70	3.72	3.72	3.73	3.73	3.69	3.67
	Y	3.53	3.60	3.65	3.69	3.71	3.71	3.72	3.71	3.68	3.64
	Z	3.38	3.49	3.59	3.67	3.70	3.71	3.72	3.72	3.69	3.63
	Mean	3.48	3.57	3.63	3.68	3.71	3.71	3.72	3.72	3.69	3.64
	ΔV_S//Fol.	0.05	0.00	0.01	0.01	0.02	0.01	0.01	0.02	0.00	0.02
18679S	*X*	3.07	3.30	3.46	3.58	3.63	3.64	3.62	3.60	3.58	3.53
	Y	3.01	3.23	3.44	3.56	3.61	3.62	3.60	3.58	3.55	3.50
	Z	2.98	3.16	3.37	3.52	3.57	3.59	3.57	3.55	3.53	3.47
	Mean	3.02	3.23	3.42	3.55	3.60	3.61	3.60	3.58	3.55	3.50
	ΔV_S//Fol.	0.18	0.15	0.07	0.08	0.11	0.11	0.11	0.11	0.12	0.10
P 2	*X*	3.71	3.75	3.78	3.79	3.79	3.80	3.79	3.75	3.66	3.53
	Y	3.68	3.73	3.75	3.75	3.76	3.77	3.75	3.71	3.63	3.49
	Z	3.71	3.74	3.77	3.79	3.81	3.81	3.80	3.77	3.69	3.55
	Mean	3.70	3.74	3.77	3.78	3.78	3.79	3.78	3.75	3.66	3.52
	ΔV_S//Fol.	0.06	0.16	0.11	0.08	0.07	0.07	0.08	0.08	0.09	0.10
M1	*X*	3.62	3.67	3.71	3.73	3.74	3.74	3.72	3.68	3.59	3.45
	Y	3.64	3.70	3.72	3.72	3.72	3.73	3.71	3.67	3.58	3.44
	Z	3.60	3.64	3.68	3.70	3.72	3.73	3.71	3.67	3.59	3.44
	Mean	3.62	3.67	3.70	3.71	3.73	3.74	3.71	3.67	3.59	3.44
	ΔV_S//Fol.	0.01	0.01	0.02	0.01	0.01	0.01	0.01	0.01	0.01	0.01
31115	*X*	3.07	3.43	3.74	3.96	4.04	4.05	4.06	4.04	3.97	3.94
	Y	2.98	3.34	3.69	3.92	4.00	4.01	4.02	4.00	3.94	3.89
	Z	2.78	3.13	3.50	3.76	3.86	3.88	3.88	3.86	3.82	3.76
	Mean	2.94	3.30	3.64	3.88	3.96	3.98	3.99	3.97	3.91	3.86
	ΔV_S//Fol.	0.59	0.48	0.34	0.32	0.35	0.35	0.36	0.36	0.35	0.35
35400	*X*	2.69	2.83	3.00	3.16	3.26	3.31	3.28	3.23	3.15	3.14
	Y	2.95	3.17	3.40	3.60	3.70	3.74	3.72	3.69	3.62	3.59
	Z	2.69	2.96	3.28	3.55	3.71	3.76	3.74	3.71	3.65	3.62
	Mean	2.78	2.99	3.23	3.43	3.56	3.60	3.58	3.54	3.47	3.45
	ΔV_S//Fol.	0.89	0.95	1.05	1.08	1.05	1.03	1.05	1.08	1.08	1.07
36058	*X*	3.08	3.39	3.56	3.69	3.76	3.74	3.76	3.71	3.69	3.65
	Y	3.00	3.30	3.50	3.64	3.72	3.75	3.72	3.68	3.66	3.62
	Z	2.59	2.84	3.02	3.14	3.22	3.25	3.21	3.15	3.11	3.06
	Mean	2.89	3.17	3.36	3.49	3.57	3.58	3.56	3.51	3.49	3.44
	ΔV_S//Fol.	0.88	0.93	0.96	1.02	1.04	1.02	1.04	1.08	1.14	1.10

Table 5 (*continued*)

Sample	Propagation direction	Pressure, MPa (20°C)						Temperature, °C (600 MPa)			
		25	50	100	200	400	600	100	200	400	600
38098S	*X*	2.38	2.77	3.08	3.31	3.48	3.55	3.53	3.51	3.48	3.44
	Y	2.49	2.84	3.14	3.36	3.52	3.58	3.56	3.55	3.53	3.48
	Z	2.32	2.61	2.87	2.98	3.14	3.19	3.15	3.12	3.08	3.01
	Mean	2.40	2.74	3.03	3.22	3.38	3.44	3.41	3.39	3.36	3.31
	ΔV_S//Fol.	0.42	0.43	0.46	0.51	0.58	0.60	0.61	0.64	0.69	0.69
43560	*X*	2.96	3.82	3.91	3.96	4.00	4.02	4.01	3.98	3.91	3.87
	Y	2.76	3.85	3.90	3.95	3.99	4.00	3.99	3.96	3.90	3.84
	Z	2.63	3.75	3.80	3.84	3.88	3.89	3.88	3.85	3.79	3.75
	Mean	2.78	3.81	3.87	3.92	3.95	3.97	3.96	3.93	3.87	3.82
	ΔV_S//Fol.	0.38	0.27	0.07	0.01	0.00	0.01	0.02	0.02	0.02	0.03
43726	*X*	2.97	3.25	3.54	3.82	4.01	4.04	4.05	4.03	3.98	3.95
	Y	2.93	3.18	3.48	3.81	4.01	4.04	4.05	4.04	4.00	3.97
	Z	2.92	3.22	3.58	3.92	4.13	4.17	4.18	4.17	4.12	4.08
	Mean	2.94	3.22	3.53	3.85	4.05	4.08	4.09	4.08	4.03	4.00
	ΔV_S//Fol.	0.38	0.31	0.08	0.11	0.10	0.09	0.09	0.09	0.07	0.07
PP 358	*X*	3.36	3.50	3.59	3.63	3.64	3.64	n.d.	n.d.	n.d.	n.d.
	Y	3.23	3.42	3.53	3.58	3.60	3.61	n.d.	n.d.	n.d.	n.d.
	Z	3.16	3.32	3.41	3.49	3.52	3.53	n.d.	n.d.	n.d.	n.d.
	Mean	3.25	3.41	3.51	3.57	3.59	3.60	n.d.	n.d.	n.d.	n.d.
	ΔV_S//Fol.	0.20	0.17	0.15	0.17	0.18	0.17	n.d.	n.d.	n.d.	n.d.
PP 363	*X*	3.36	3.54	3.58	3.59	3.60	3.60	3.57	3.56	3.54	3.49
	Y	3.28	3.46	3.50	3.52	3.55	3.58	3.54	3.63	3.61	3.58
	Z	3.07	3.15	3.21	3.25	3.29	3.31	3.27	3.25	3.23	3.16
	Mean	3.24	3.38	3.43	3.46	3.48	3.50	3.46	3.48	3.46	3.41
	ΔV_S//Fol.	0.57	0.55	0.54	0.56	0.52	0.48	0.51	0.77	0.85	0.91
PP 357	*X*	3.76	3.88	3.94	4.02	4.03	4.03	4.02	4.00	3.98	3.93
	Y	3.63	3.78	3.91	3.99	4.01	4.01	4.00	3.98	3.96	3.92
	Z	3.58	3.73	3.83	3.89	3.92	3.92	3.91	3.90	3.89	3.82
	Mean	3.65	3.80	3.89	3.97	3.99	3.99	3.98	3.96	3.94	3.89
	ΔV_S//Fol.	0.30	0.24	0.23	0.27	0.27	0.27	0.27	0.28	0.29	0.28
PP 365	*X*	3.82	3.92	3.98	4.00	3.99	3.99	3.97	3.94	3.89	3.82
	Y	3.79	3.89	3.96	3.97	3.97	3.97	3.95	3.93	3.89	3.81
	Z	3.60	3.66	3.69	3.71	3.73	3.74	3.71	3.69	3.66	3.56
	Mean	3.74	3.83	3.88	3.89	3.90	3.90	3.88	3.85	3.81	3.73
	ΔV_S//Fol.	0.39	0.42	0.51	0.51	0.51	0.49	0.49	0.50	0.51	0.50

4. Source: Burke and Fountain (1990)

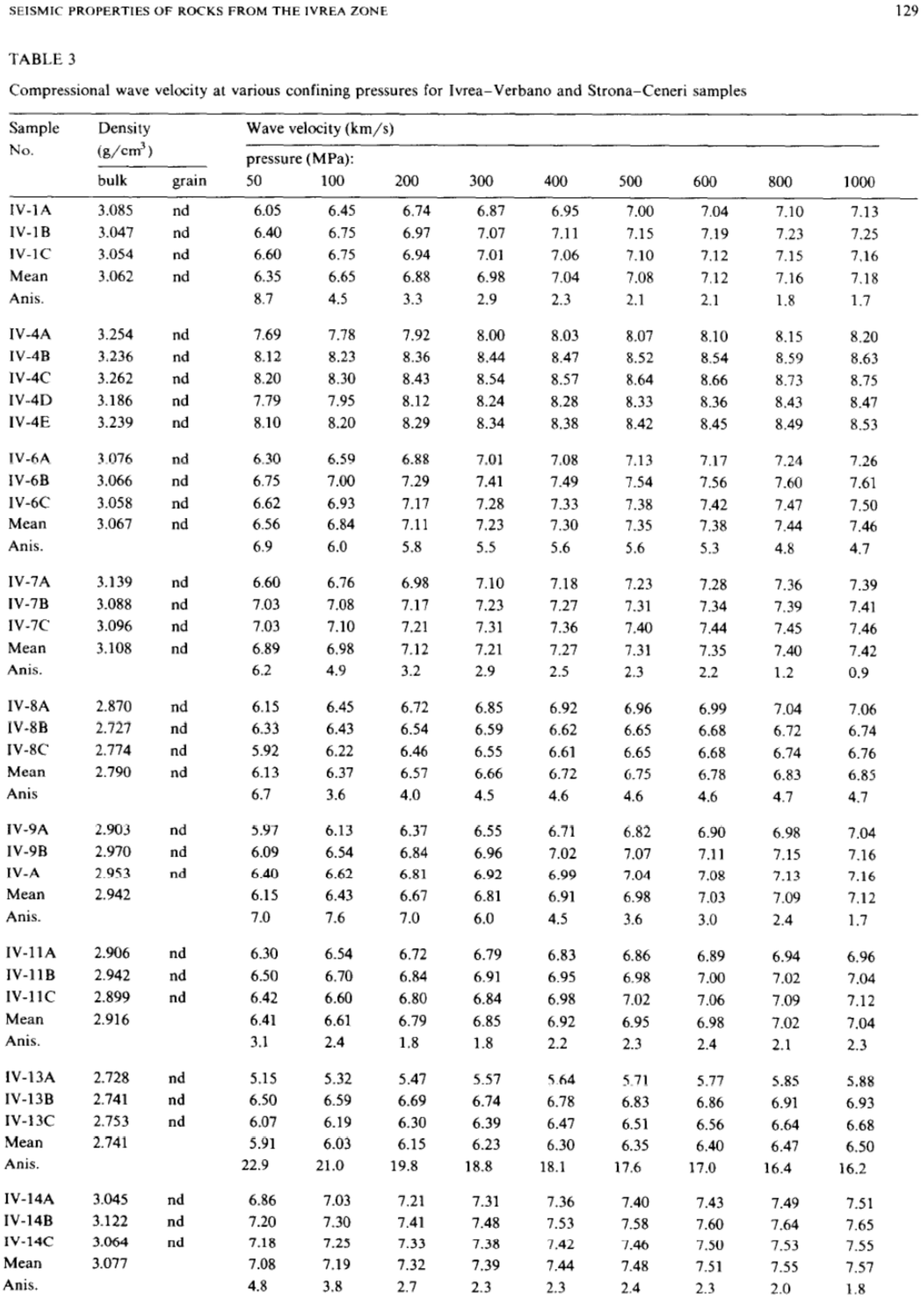

TABLE 3

Compressional wave velocity at various confining pressures for Ivrea–Verbano and Strona–Ceneri samples

Sample No.	Density (g/cm^3)		Wave velocity (km/s) pressure (MPa):								
	bulk	grain	50	100	200	300	400	500	600	800	1000
IV-1A	3.085	nd	6.05	6.45	6.74	6.87	6.95	7.00	7.04	7.10	7.13
IV-1B	3.047	nd	6.40	6.75	6.97	7.07	7.11	7.15	7.19	7.23	7.25
IV-1C	3.054	nd	6.60	6.75	6.94	7.01	7.06	7.10	7.12	7.15	7.16
Mean	3.062	nd	6.35	6.65	6.88	6.98	7.04	7.08	7.12	7.16	7.18
Anis.			8.7	4.5	3.3	2.9	2.3	2.1	2.1	1.8	1.7
IV-4A	3.254	nd	7.69	7.78	7.92	8.00	8.03	8.07	8.10	8.15	8.20
IV-4B	3.236	nd	8.12	8.23	8.36	8.44	8.47	8.52	8.54	8.59	8.63
IV-4C	3.262	nd	8.20	8.30	8.43	8.54	8.57	8.64	8.66	8.73	8.75
IV-4D	3.186	nd	7.79	7.95	8.12	8.24	8.28	8.33	8.36	8.43	8.47
IV-4E	3.239	nd	8.10	8.20	8.29	8.34	8.38	8.42	8.45	8.49	8.53
IV-6A	3.076	nd	6.30	6.59	6.88	7.01	7.08	7.13	7.17	7.24	7.26
IV-6B	3.066	nd	6.75	7.00	7.29	7.41	7.49	7.54	7.56	7.60	7.61
IV-6C	3.058	nd	6.62	6.93	7.17	7.28	7.33	7.38	7.42	7.47	7.50
Mean	3.067	nd	6.56	6.84	7.11	7.23	7.30	7.35	7.38	7.44	7.46
Anis.			6.9	6.0	5.8	5.5	5.6	5.6	5.3	4.8	4.7
IV-7A	3.139	nd	6.60	6.76	6.98	7.10	7.18	7.23	7.28	7.36	7.39
IV-7B	3.088	nd	7.03	7.08	7.17	7.23	7.27	7.31	7.34	7.39	7.41
IV-7C	3.096	nd	7.03	7.10	7.21	7.31	7.36	7.40	7.44	7.45	7.46
Mean	3.108	nd	6.89	6.98	7.12	7.21	7.27	7.31	7.35	7.40	7.42
Anis.			6.2	4.9	3.2	2.9	2.5	2.3	2.2	1.2	0.9
IV-8A	2.870	nd	6.15	6.45	6.72	6.85	6.92	6.96	6.99	7.04	7.06
IV-8B	2.727	nd	6.33	6.43	6.54	6.59	6.62	6.65	6.68	6.72	6.74
IV-8C	2.774	nd	5.92	6.22	6.46	6.55	6.61	6.65	6.68	6.74	6.76
Mean	2.790	nd	6.13	6.37	6.57	6.66	6.72	6.75	6.78	6.83	6.85
Anis			6.7	3.6	4.0	4.5	4.6	4.6	4.6	4.7	4.7
IV-9A	2.903	nd	5.97	6.13	6.37	6.55	6.71	6.82	6.90	6.98	7.04
IV-9B	2.970	nd	6.09	6.54	6.84	6.96	7.02	7.07	7.11	7.15	7.16
IV-A	2.953	nd	6.40	6.62	6.81	6.92	6.99	7.04	7.08	7.13	7.16
Mean	2.942		6.15	6.43	6.67	6.81	6.91	6.98	7.03	7.09	7.12
Anis.			7.0	7.6	7.0	6.0	4.5	3.6	3.0	2.4	1.7
IV-11A	2.906	nd	6.30	6.54	6.72	6.79	6.83	6.86	6.89	6.94	6.96
IV-11B	2.942	nd	6.50	6.70	6.84	6.91	6.95	6.98	7.00	7.02	7.04
IV-11C	2.899	nd	6.42	6.60	6.80	6.84	6.98	7.02	7.06	7.09	7.12
Mean	2.916		6.41	6.61	6.79	6.85	6.92	6.95	6.98	7.02	7.04
Anis.			3.1	2.4	1.8	1.8	2.2	2.3	2.4	2.1	2.3
IV-13A	2.728	nd	5.15	5.32	5.47	5.57	5.64	5.71	5.77	5.85	5.88
IV-13B	2.741	nd	6.50	6.59	6.69	6.74	6.78	6.83	6.86	6.91	6.93
IV-13C	2.753	nd	6.07	6.19	6.30	6.39	6.47	6.51	6.56	6.64	6.68
Mean	2.741		5.91	6.03	6.15	6.23	6.30	6.35	6.40	6.47	6.50
Anis.			22.9	21.0	19.8	18.8	18.1	17.6	17.0	16.4	16.2
IV-14A	3.045	nd	6.86	7.03	7.21	7.31	7.36	7.40	7.43	7.49	7.51
IV-14B	3.122	nd	7.20	7.30	7.41	7.48	7.53	7.58	7.60	7.64	7.65
IV-14C	3.064	nd	7.18	7.25	7.33	7.38	7.42	7.46	7.50	7.53	7.55
Mean	3.077		7.08	7.19	7.32	7.39	7.44	7.48	7.51	7.55	7.57
Anis.			4.8	3.8	2.7	2.3	2.3	2.4	2.3	2.0	1.8

.

TABLE 3 (continued)

Sample No.	Density (g/cm^3)		Wave velocity pressure (MPa):								
	bulk	grain	50	100	200	300	400	500	600	800	1000
IV-15A	3.077	nd	6.83	6.93	7.04	7.11	7.16	7.20	7.24	7.27	7.28
IV-15B	3.082	nd	7.22	7.32	7.44	7.51	7.53	7.56	7.58	7.62	7.65
IV-15C	3.081	nd	7.05	7.20	7.35	7.46	7.50	7.52	7.54	7.56	7.57
Mean	3.080		7.03	7.15	7.28	7.36	7.40	7.43	7.45	7.48	7.50
Anis			5.5	5.5	5.5	5.4	5.0	4.8	4.6	4.7	4.9
IV-16A	3.060	nd	5.76	6.20	6.64	6.81	6.89	6.95	7.00	7.05	7.06
IV-16B	3.076	nd	nd	6.08	6.89	7.00	7.12	7.20	7.27	7.35	7.37
IV-16C	3.050	nd	nd	6.22	6.87	7.14	7.28	7.37	7.43	7.49	7.51
Mean	3.062			6.17	6.80	6.98	7.10	7.17	7.23	7.30	7.31
Anis.				2.3	3.7	4.7	5.5	5.9	5.9	6.0	6.2
IV-17A	2.906	nd	6.95	7.05	7.16	7.22	7.26	7.29	7.32	7.36	7.38
IV-17B	2.905	nd	6.93	7.07	7.18	7.23	7.27	7.30	7.32	7.36	7.38
IV-17C	2.920	nd	6.47	6.75	6.98	7.09	7.15	7.20	7.24	7.28	7.29
Mean	2.910		6.78	6.96	7.11	7.18	7.23	7.26	7.29	7.33	7.35
Anis.			7.1	4.6	2.8	1.9	1.7	1.4	1.1	1.1	1.2
IV-19A	3.241	nd	7.03	7.30	7.55	7.68	7.75	7.80	7.84	7.89	7.91
IV-19B	3.250	nd	6.85	7.18	7.39	7.50	7.58	7.64	7.67	7.73	7.77
IV-19C	3.208	nd	6.75	7.10	7.36	7.49	7.57	7.63	7.67	7.73	7.74
Mean	3.233		6.88	7.19	7.43	7.56	7.63	7.69	7.73	7.78	7.81
Anis.			4.1	2.8	2.6	2.5	2.4	2.2	2.2	2.1	2.2
IV-20A	3.049	nd	nd	6.90	7.20	7.33	7.42	7.48	7.52	7.57	7.58
IV-20B	3.025	nd	6.25	6.74	7.18	7.31	7.39	7.44	7.48	7.53	7.55
IV-20°C	3.067	nd	6.25	6.80	7.19	7.34	7.42	7.47	7.51	7.57	7.59
Mean	3.047			6.81	7.19	7.33	7.41	7.46	7.50	7.56	7.57
Anis.				2.3	0.3	0.4	0.4	0.5	0.5	0.5	0.5
IV-21A	2.727	nd	4.94	5.24	5.53	5.64	5.73	5.80	5.86	5.95	5.99
IV-21B	2.725	nd	5.78	6.01	6.22	6.32	6.39	6.45	6.52	6.55	6.59
IV-21C	2.722	nd	5.76	5.97	6.16	6.28	6.35	6.41	6.45	6.49	6.50
Mean	2.725		5.49	5.74	5.97	6.08	6.16	6.22	6.28	6.33	6.36
Anis.			15.3	13.4	11.6	11.2	10.7	10.5	10.5	9.5	9.4
IV-22A	2.751	nd	5.70	5.86	6.00	6.07	6.12	6.16	6.19	6.21	6.24
IV-22B	2.753	nd	6.45	6.53	6.64	6.72	6.79	6.83	6.86	6.91	6.93
IV-22C	2.753	nd	6.10	6.27	6.37	6.43	6.48	6.50	6.53	6.59	6.65
Mean	2.752		6.08	6.22	6.34	6.41	6.46	6.50	6.53	6.57	6.61
Anis.			12.3	10.8	10.1	10.1	10.4	10.3	10.3	10.6	10.4
IV-23A	2.953	nd	6.26	6.37	6.49	6.55	6.60	6.64	6.68	6.75	6.77
IV-23B	2.945	nd	6.52	6.60	6.73	6.81	6.86	6.91	6.95	7.02	7.05
IV-23C	2.964	nd	6.68	6.84	7.00	7.09	7.16	7.20	7.23	7.27	7.31
Mean	2.954		6.49	6.60	6.74	6.82	6.87	6.92	6.95	7.01	7.04
Anis.			6.5	7.1	7.6	7.9	8.1	8.1	7.9	7.4	7.7
IV-24A	2.977	nd	6.10	6.36	6.56	6.68	6.76	6.80	6.84	6.91	6.95
IV-24B	2.972	nd	6.77	7.11	7.53	7.70	7.80	7.86	7.91	7.97	8.00
IV-24C	3.043	nd	6.78	7.05	7.41	7.64	7.83	7.98	8.06	8.16	8.22
Mean	2.997		6.55	6.84	7.17	7.34	7.46	7.55	7.60	7.68	7.72
Anis.			10.4	11.0	13.5	13.9	14.3	15.6	16.0	16.3	16.4

TABLE 3 (continued)

Sample No.	Density (g/cm³)		Wave velocity pressure (MPa):								
	bulk	grain	50	100	200	300	400	500	600	800	1000
IV-25A	3.055	nd	6.57	6.87	7.13	7.24	7.31	7.38	7.44	7.50	7.52
IV-25B	3.132	nd	6.65	6.91	7.19	7.35	7.39	7.42	7.45	7.52	7.57
IV-25C	3.067	nd	6.28	6.67	6.95	7.13	7.20	7.25	7.30	7.37	7.38
Mean	3.085		6.50	6.82	7.09	7.24	7.30	7.35	7.40	7.46	7.49
Anis.			5.7	3.5	3.4	3.0	2.6	2.3	2.0	2.0	2.5
IV-26A	3.298	3.298	7.44	7.48	7.53	7.57	7.60	7.63	7.65		
IV-26B	3.234	3.235	7.29	7.38	7.45	7.49	7.53	7.55	7.57		
IV-26C	3.321	3.231	7.60	7.65	7.72	7.76	7.80	7.85	7.87		
IV-26D	3.297	3.297	7.58	7.64	7.70	7.74	7.77	7.81	7.83		
IV-27A	2.883	2.928	6.55	6.69	6.80	6.85	6.87	6.90	6.93		
IV-27B	2.908	2.960	6.35	6.54	6.67	6.72	6.76	6.79	6.81		
IV-27C	2.879	2.934	6.34	6.56	6.66	6.71	6.75	6.78	6.80		
Mean	2.890	2.941	6.41	6.60	6.71	6.76	6.79	6.82	6.85		
Anis.			3.3	2.3	2.1	2.1	1.8	1.8	1.9		
IV-28A	2.908	2.986	6.31	6.48	6.58	6.61	6.64	6.67	6.70		
IV-28B	3.060	3.108	6.20	6.52	6.74	6.82	6.87	6.90	6.92		
IV-28C	3.009	3.081	6.21	6.52	6.71	6.77	6.81	6.85	6.86		
Mean	2.992	3.058	6.24	6.51	6.68	6.73	6.77	6.81	6.83		
Anis.			1.8	0.6	2.4	3.1	3.4	3.4	3.2		
IV-29A	2.950	3.073	5.85	6.19	6.44	6.55	6.62	6.65	6.67		
IV-29B	2.926	2.990	6.23	6.50	6.72	6.85	6.90	6.94	6.96		
IV-29C	2.971	3.065	6.19	6.43	6.63	6.73	6.79	6.83	6.86		
Mean	2.949	3.046	6.09	6.37	6.60	6.71	6.77	6.81	6.83		
Anis.			6.2	4.9	4.2	4.5	4.1	4.3	4.3		
IV-30A	2.897	2.906	5.78	5.95	6.16	6.27	6.31	6.35	6.39		
IV-30B	2.865	2.921	6.31	6.42	6.53	6.58	6.62	6.64	6.66		
IV-30C	2.855	2.891	6.29	6.52	6.67	6.72	6.74	6.76	6.79		
Mean	2.872	2.906	6.13	6.30	6.45	6.52	6.56	6.58	6.61		
Anis.			8.7	9.1	7.9	6.9	6.6	6.2	6.0		
IV-31A	2.895	2.986	5.45	5.67	5.87	6.00	6.09	6.14	6.18		
IV-31B	2.937	2.995	6.25	6.43	6.62	6.73	6.80	6.84	6.87		
IV-31C	2.867	2.941	6.26	6.39	6.52	6.60	6.67	6.71	6.73		
Mean	2.900	2.974	5.99	6.16	6.34	6.44	6.52	6.56	6.59		
Anis.			13.5	12.3	11.8	11.3	10.9	10.7	10.5		
IV-32A	2.735	2.828	5.17	5.80	6.12	6.25	6.31	6.35	6.36		
IV-32B	2.743	2.828	5.78	6.29	6.55	6.67	6.72	6.74	6.75		
IV-32C	2.737	2.831	nd	6.30	6.53	6.59	6.63	6.64	6.65		
Mean	2.738	2.829	nd	6.13	6.40	6.50	6.55	6.58	6.59		
Anis.				8.2	6.7	6.5	6.3	5.9	5.9		
IV-33A	2.615	2.703	5.14	5.55	5.84	6.00	6.09	6.15	6.20		
IV-33B	2.618	2.689	5.28	5.70	5.96	6.11	6.18	6.22	6.25		
IV-33C	2.628	2.709	5.48	5.80	6.06	6.16	6.22	6.26	6.30		
Mean	2.620	2.700	5.30	5.68	5.95	6.09	6.16	6.21	6.25		
Anis.			6.4	4.4	3.7	2.6	2.1	1.8	1.6		

TABLE 3 (continued)

Sample No.	Density (g/cm^3)		Wave velocity pressure (MPa):								
	bulk	grain	50	100	200	300	400	500	600	800	1000
IV-35A	2.731	2.785	5.64	6.82	6.92	5.95	5.99	6.02	6.04		
IV-35B	2.742	2.821	6.42	6.56	6.64	6.67	6.70	6.73	6.75		
IV-35C	2.737	2.794	5.91	6.04	6.12	6.15	6.19	6.23	6.25		
Mean	2.737	2.800	5.99	6.47	6.56	6.26	6.29	6.33	6.35		
Anis.			13.0	12.0	12.2	11.5	11.3	11.2	11.2		
IV-37A	2.671	2.744	5.09	5.51	5.77	5.87	5.92	5.96	5.98		
IV-37B	2.673	2.747	5.75	6.00	6.23	6.31	6.35	6.37	6.39		
IV-37C	2.692	2.749	5.30	5.70	5.99	6.09	6.15	6.18	6.20		
Mean	2.679	2.747	5.38	5.74	6.00	6.09	6.14	6.17	6.19		
Anis.			12.3	8.5	7.7	7.2	7.0	6.6	6.6		
IV-38A	2.724	2.789	4.95	5.31	5.55	5.67	5.74	5.79	5.81		
IV-38B	2.740	2.805	5.50	5.93	6.23	6.38	6.46	6.50	6.52		
IV-38C	2.719	2.801	5.63	5.96	6.24	6.36	6.42	6.46	6.49		
Mean	2.728	2.798	5.36	5.73	6.01	6.14	6.21	6.25	6.27		
Anis.			12.7	11.3	11.5	11.6	11.6	11.4	11.3		
IV-39A	2.744	2.839	5.10	5.37	5.69	5.89	5.97	6.03	6.07		
IV-39B	2.760	2.838	5.20	5.65	5.99	6.20	6.32	6.39	6.43		
IV-39C	2.795	2.840	5.74	6.00	6.28	6.40	6.46	6.51	6.54		
Mean	2.766	2.839	5.35	5.67	5.99	6.16	6.25	6.31	6.35		
Anis.			12.0	11.1	9.9	8.3	7.8	7.6	7.4		
IV-40A	3.320		8.04	8.19	8.30	8.32	8.35	8.38	8.41		
IV-40B	3.309		7.73	7.99	8.10	8.15	8.19	8.21	8.23		
IV-40D	3.309		8.14	8.22	8.44	8.50	8.52	8.54	8.56		
IV-41A	2.651	2.726	5.35	5.75	5.93	6.00	6.04	6.07	6.09		
IV-41B	2.652	2.732	5.40	5.90	6.24	6.33	6.38	6.42	6.44		
IV-41C	2.652	2.728	5.20	5.90	6.14	6.25	6.30	6.33	6.35		
Mean	2.652	2.729	5.32	5.85	6.10	6.19	6.24	6.27	6.29		
Anis.			3.8	2.6	5.1	5.3	5.4	5.6	5.6		
IV-42A	2.633	2.667	5.05	5.61	5.98	6.11	6.19	6.24	6.26		
IV-42B	2.642	2.689	5.19	5.65	6.00	6.13	6.18	6.22	6.25		
IV-42C	2.559	2.613	5.41	5.81	6.12	6.22	6.27	6.31	6.34		
MEAN	2.611	2.656	5.22	5.69	6.03	6.15	6.21	6.26	6.28		
Anis.			6.9	3.5	2.3	1.8	1.4	1.4	1.4		
IV-43A	2.688	2.758	5.11	5.35	5.59	5.70	5.77	5.81	5.85		
IV-43B	2.730	2.765	5.74	5.91	5.98	6.02	6.05	6.07	6.10		
IV-43C	2.717	2.767	5.34	5.66	5.93	6.06	6.12	6.17	6.21		
Mean	2.712	2.763	5.40	5.64	5.83	5.93	5.98	6.02	6.05		
Anis.			11.7	9.9	6.7	6.1	5.9	6.0	5.9		
IV-44A	2.589	2.634	6.25	6.35	6.41	6.44	6.48	6.50	6.52		
IV-44B	2.604	2.636	5.81	6.05	6.20	6.28	6.33	6.36	6.37		
IV-44C	2.600	2.650	5.80	6.02	6.15	6.23	6.27	6.30	6.34		
Mean	2.598	2.640	5.95	6.14	6.25	6.32	6.36	6.39	6.41		
Anis.			7.6	5.4	4.2	3.3	3.3	3.1	2.8		

TABLE 3 (continued)

Sample No.	Density (g/cm^3)		Wave velocity pressure (MPa):								
	bulk	grain	50	100	200	300	400	500	600	800	1000
IV-45A	2.934	2.981	5.65	6.08	6.46	6.61	6.68	6.71	6.74		
IV-45B	3.004	3.071	5.86	6.28	6.70	6.87	6.97	7.03	7.06		
IV-45C	2.916	2.992	5.88	6.27	6.68	6.85	6.94	7.00	7.04		
Mean	2.951	3.015	5.80	6.21	6.61	6.78	6.86	6.91	6.95		
Anis.			4.0	3.2	3.6	3.8	4.2	4.6	4.6		
IV-46A	3.254	3.342	7.87	7.93	7.96	7.98	8.00	8.03	8.05		
IV-46B	3.278	3.354	8.15	8.19	8.22	8.24	8.26	8.28	8.30		
IV-46C	3.295	3.366	7.73	7.78	7.84	7.86	7.89	7.93	7.95		
Mean	3.276	3.354	7.92	7.97	8.01	8.03	8.05	8.08	8.10		
Anis.			5.3	5.1	4.7	4.7	4.6	4.3	4.3		
IV-47A	2.771	2.840	5.73	6.02	6.30	6.41	6.47	6.51	6.53		
IV-47B	2.772	2.851	5.88	6.14	6.35	6.44	6.49	6.52	6.53		
IV-47C	2.781	2.855	5.88	6.17	6.38	6.46	6.51	6.55	6.57		
Mean	2.775	2.849	5.83	6.11	6.34	6.44	6.49	6.53	6.54		
Anis.			2.6	2.5	1.3	0.8	0.6	0.6	0.6		
IV-48A	3.231	3.272	6.67	6.80	6.92	6.95	6.99	7.02	7.04		
IV-48B	3.298	3.368	6.83	6.93	7.02	7.06	7.09	7.12	7.14		
IV-48C	3.266	3.325	6.85	6.98	7.09	7.13	7.15	7.17	7.19		
Mean	3.265	3.322	6.78	6.90	7.01	7.05	7.08	7.10	7.12		
Anis.			2.7	2.6	2.4	2.6	2.3	2.1	2.1		
IV-49A	3.027	3.085	6.25	6.85	7.14	7.25	7.29	7.33	7.35		
IV-49B	2.989	3.064	6.25	6.82	7.01	7.08	7.12	7.15	7.17		
IV-49C	2.989	3.045	6.28	6.82	7.05	7.13	7.17	7.19	7.21		
Mean	3.002	3.065	6.26	6.83	7.07	7.15	7.19	7.22	7.24		
Anis.			0.5	0.4	1.8	2.4	2.4	2.5	2.5		
IV-50A	3.028	3.106	5.95	6.24	6.41	6.48	6.51	6.54	6.56		
IV-50B	3.031	3.084	6.79	6.93	7.05	7.13	7.14	7.16	7.17		
IV-50C	3.049	3.124	6.46	6.69	6.90	6.99	7.05	7.08	7.11		
Mean	3.036	3.105	6.40	6.62	6.79	6.87	6.90	6.93	6.95		
Anis.			13.1	10.4	9.4	9.5	9.1	9.0	8.8		
IV-51A	2.993	3.013	5.77	6.01	6.22	6.32	6.39	6.44	6.47		
IV-51B	2.938	3.010	5.75	6.10	6.42	6.57	6.64	6.66	6.68		
IV-51C	2.790	2.871	5.67	5.96	6.19	6.30	6.35	6.40	6.43		
Mean	2.907	2.965	5.73	6.02	6.28	6.40	6.46	6.50	6.53		
Anis.			1.7	2.3	3.7	4.2	4.5	4.0	3.8		
IV-52A	2.654	2.700	5.78	5.97	6.12	6.18	6.23	6.27	6.30		
IV-52B	2.716	2.737	6.09	6.30	6.47	6.54	6.59	6.63	6.65		
IV-52C	2.679	2.716	6.32	6.44	6.55	6.62	6.67	6.69	6.71		
Mean	2.683	2.718	6.06	6.24	6.38	6.45	6.50	6.53	6.55		
Anis.			8.9	7.5	6.7	6.8	6.8	6.4	6.3		
IV-53A	2.656	2.692	5.21	5.53	5.72	5.80	5.84	5.87	5.89		
IV-53B	2.685	2.728	5.98	6.12	6.25	6.32	6.38	6.42	6.45		
IV-53C	2.673	2.694	5.82	5.97	6.11	6.17	6.21	6.25	6.28		
Mean	2.671	2.705	5.67	5.87	6.03	6.10	6.14	6.18	6.21		
Anis.			13.6	10.0	8.8	8.5	8.8	8.9	9.0		

TABLE 3 (continued)

Sample No.	Density (g/cm^3)		Wave velocity pressure (MPa):								
	bulk	grain	50	100	200	300	400	500	600	800	1000
IV-54A	2.632	2.661	5.62	5.78	5.92	6.01	6.07	6.10	6.12		
IV-54B	2.648	2.664	6.03	6.06	6.10	6.14	6.18	6.20	6.23		
IV-54C	2.641	2.659	5.82	5.89	5.95	5.99	6.02	6.04	6.06		
Mean	2.640	2.661	5.82	5.91	5.99	6.05	6.09	6.11	6.14		
Anis.			7.0	4.7	3.0	3.6	2.9	2.5	2.5		
IV-55A	2.646	2.693	5.20	5.47	5.69	5.82	5.89	5.94	5.97		
IV-55B	2.656	2.698	5.29	5.62	5.88	6.01	6.09	6.14	6.18		
IV-55C	2.640	2.694	5.25	5.60	5.84	5.97	6.05	6.10	6.14		
Mean	2.647	2.695	5.25	5.56	5.80	5.93	6.01	6.06	6.10		
Anis.			1.7	2.7	3.3	3.2	3.3	3.3	3.4		

5. Source: Brocher (2008)

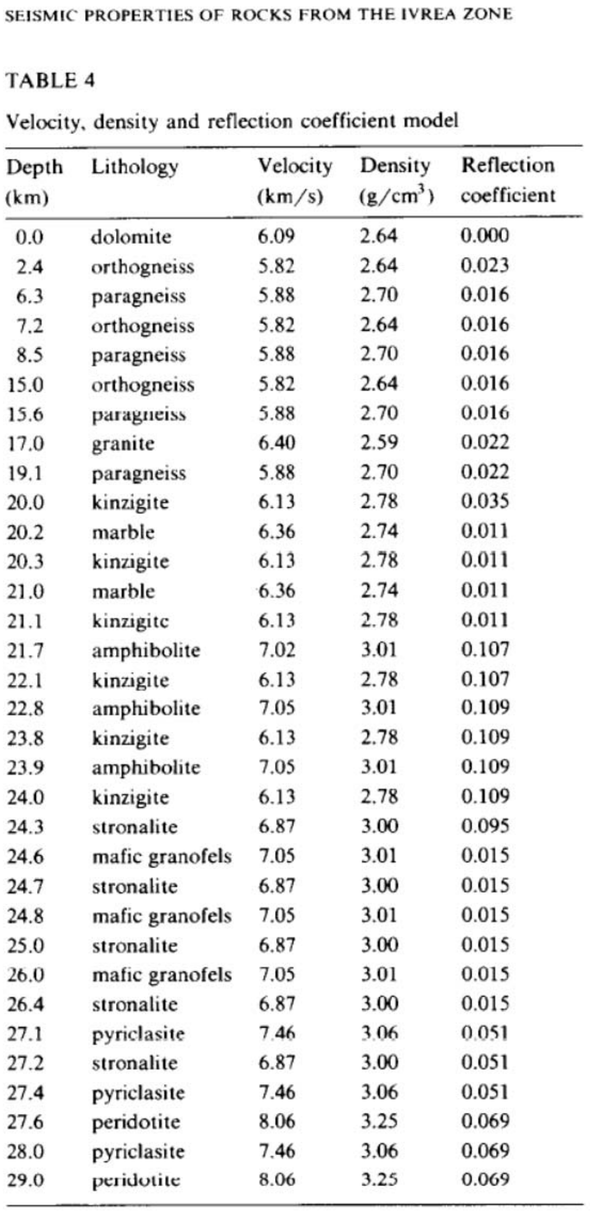

SEISMIC PROPERTIES OF ROCKS FROM THE IVREA ZONE

TABLE 4

Velocity, density and reflection coefficient model

Depth (km)	Lithology	Velocity (km/s)	Density (g/cm^3)	Reflection coefficient
0.0	dolomite	6.09	2.64	0.000
2.4	orthogneiss	5.82	2.64	0.023
6.3	paragneiss	5.88	2.70	0.016
7.2	orthogneiss	5.82	2.64	0.016
8.5	paragneiss	5.88	2.70	0.016
15.0	orthogneiss	5.82	2.64	0.016
15.6	paragneiss	5.88	2.70	0.016
17.0	granite	6.40	2.59	0.022
19.1	paragneiss	5.88	2.70	0.022
20.0	kinzigite	6.13	2.78	0.035
20.2	marble	6.36	2.74	0.011
20.3	kinzigite	6.13	2.78	0.011
21.0	marble	6.36	2.74	0.011
21.1	kinzigite	6.13	2.78	0.011
21.7	amphibolite	7.02	3.01	0.107
22.1	kinzigite	6.13	2.78	0.107
22.8	amphibolite	7.05	3.01	0.109
23.8	kinzigite	6.13	2.78	0.109
23.9	amphibolite	7.05	3.01	0.109
24.0	kinzigite	6.13	2.78	0.109
24.3	stronalite	6.87	3.00	0.095
24.6	mafic granofels	7.05	3.01	0.015
24.7	stronalite	6.87	3.00	0.015
24.8	mafic granofels	7.05	3.01	0.015
25.0	stronalite	6.87	3.00	0.015
26.0	mafic granofels	7.05	3.01	0.015
26.4	stronalite	6.87	3.00	0.015
27.1	pyriclasite	7.46	3.06	0.051
27.2	stronalite	6.87	3.00	0.051
27.4	pyriclasite	7.46	3.06	0.051
27.6	peridotite	8.06	3.25	0.069
28.0	pyriclasite	7.46	3.06	0.069
29.0	peridotite	8.06	3.25	0.069

" Initial tests of the model indicate that the Vp model generally compares favorably to regional seismic tomography models, but locally, the velocities assigned to a couple of units were in error: the Vp used for sedimentary rocks filling the La Honda Basin was too low, as was the Vp used for the Great Valley Sequence. Although they do not adversely affect the waveform fits, forward forward modeling suggests that the Vp and Vs model may be about 5% too fast on average (D. Dreger, personal comm., 2007; Rodgers et al., 2008). Because the velocity errors are largely restricted to the Franciscan Complex, within which the great majority of the modeled raypaths are located, they suggest that the relations proposed for the Franciscan Complex overpredict Vp by about 5%."

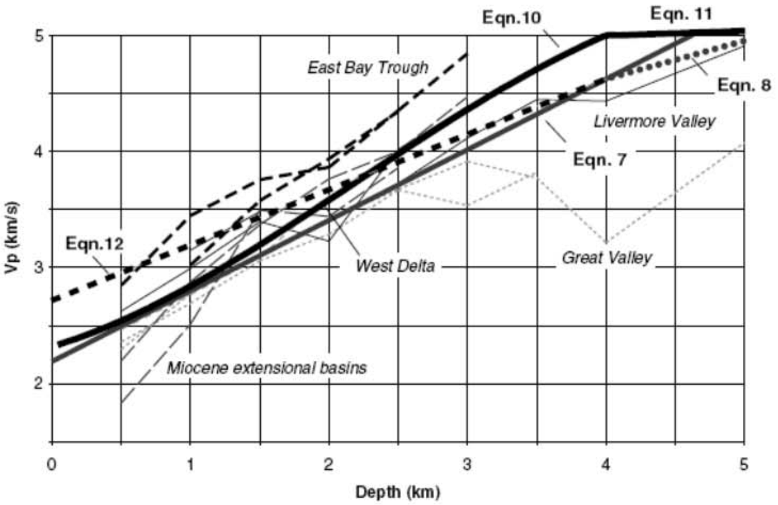

Figure 5. Average velocities within sedimentary basins in the greater San Francisco Bay Area, calculated by averaging the velocities predicted by linear regression of the sonic well logs at 0.5-km intervals (Brocher, 2005c). Averages calculated from the regressions of the upper and lower parts of the logs are shown with identical pattern to emphasize that they yield similar results. Heavy solid line shows the linear regression made directly to a subset of these well log data.

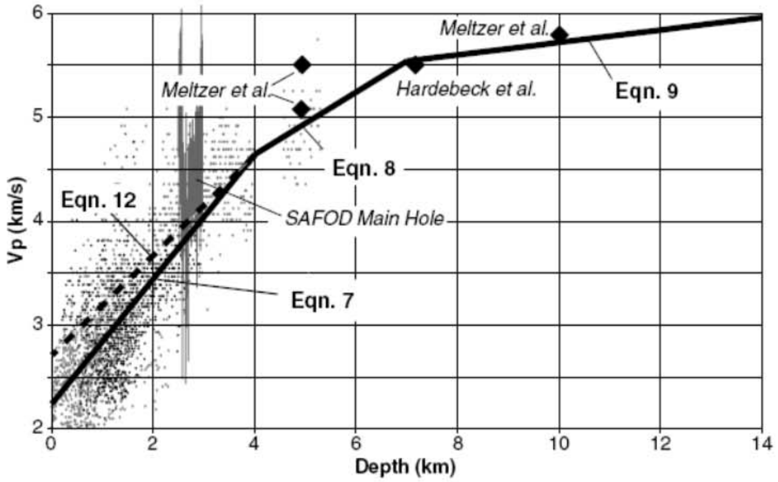

Figure 6. Linear regression (equation 6) of sonic velocity logs from 50 boreholes including 26 in the Great Valley and Sacramento delta, 15 in the Livermore Valley, and 9 in the East Bay trough (from Brocher, 2005c). Gray lines show sonic log from the SAFOD main hole, phase 2 sampling sedimentary rocks (Hickman *et al.*, 2005). Equations (8) and (9) are fit to seismic refraction/tomography velocities reported by Meltzer *et al.* (1987) and Hardebeck *et al.* (2007). Gray dots show sonic log values for Cenozoic sedimentary rocks; black dots show sonic log values for Great Valley sequence rocks (both from Brocher (2005c)).

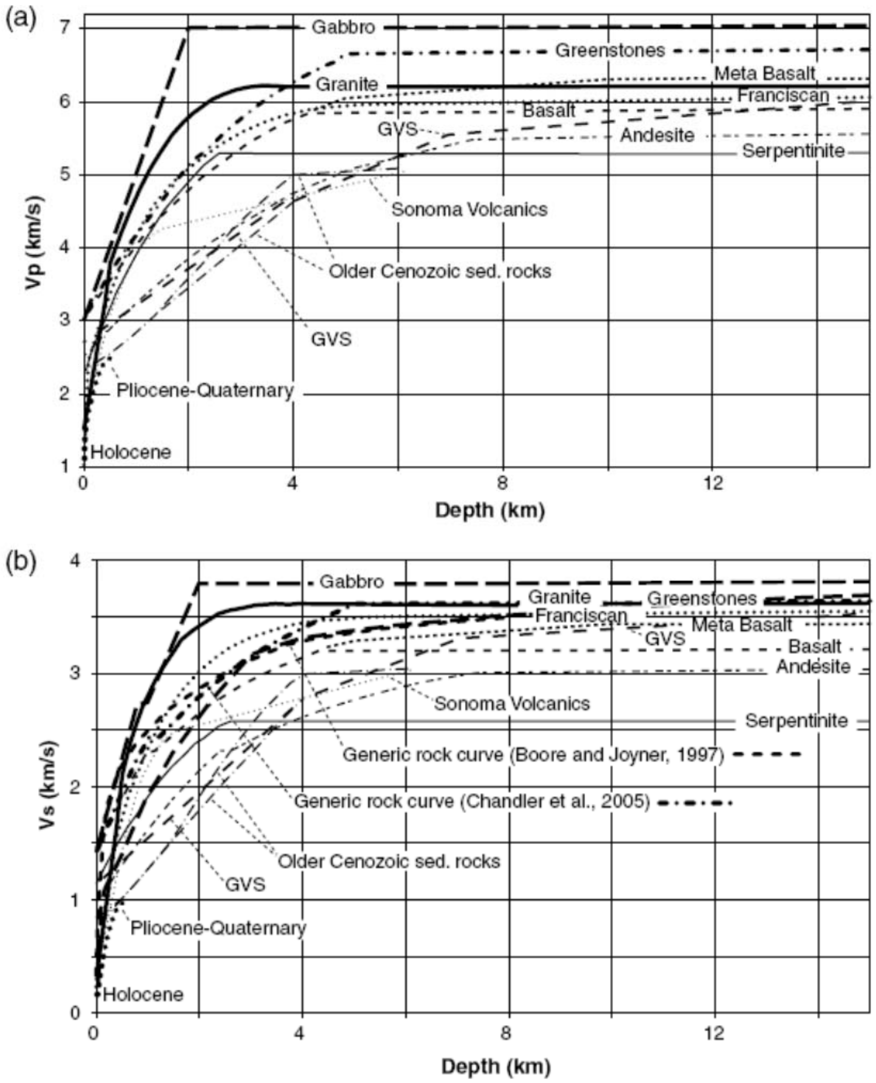

Figure 10. (a) Summary of the Vp versus depth relations for several rock types. (b) Summary of the Vs versus depth for the same rock types. Note that at higher velocities, the relative order of the curves differ from those in Figure 10a due to variations in the conversion from Vp to Vs with rock type (Table 3). Generic Vs versus depth curves proposed by Boore and Joyner (1997) and Chandler *et al.* (2005) are shown for comparison.

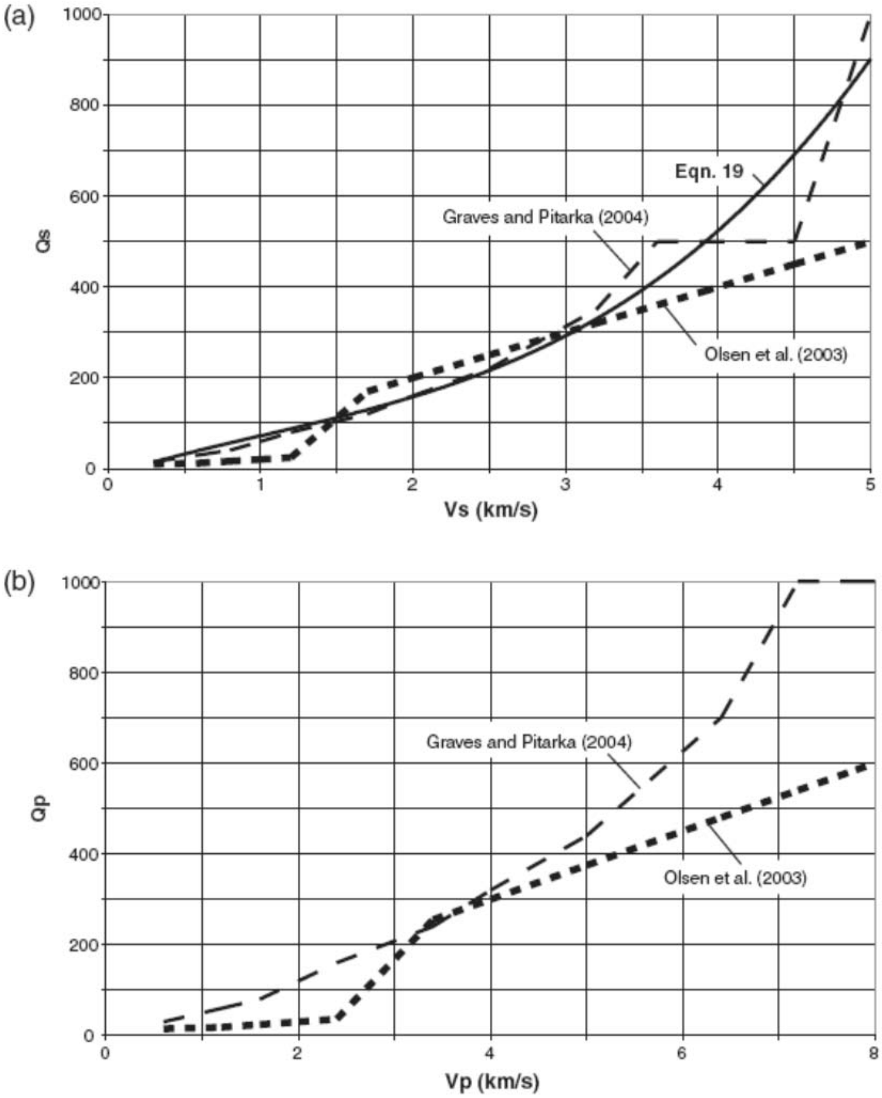

Figure 9. Comparison of attenuation versus velocity relations published by Olsen *et al.* (2003) and Graves and Pitarka (2004) for (a) Qs and Vs and (b) Qp and Vp.

Table 4

Summary of Vs and Vp versus Depth Relationships

Relation	Depth Range	Rock Type
$Vp = 0.7 + 42.968z - 575.8z^2 + 2931.6z^3 - 3977.6z^4$	($z < 0.04$ km)	Plio-Quaternary deposits
$Vs = 0.215 + 10.932z - 138.1z^2$	($z < 0.04$ km)	Plio-Quaternary deposits
$Vp = 1.5 + 3.735z - 3.543z^2$	(0.04–0.5 km)	Plio-Quaternary deposits
$Vp = 0.7 + 31.4z$	($z < 0.05$ km)	Tertiary sed. rocks
$Vs = 0.2149 + 18.3z - 138.1z^2$	($z < 0.04$ km)	Tertiary sed. rocks
$Vp = 2.24 + 0.6z$	(0–4 km)	Tertiary sed. rocks
$Vp = 4.64 + 0.3(z - 4)$	(4–7 km)	Tertiary sed. rocks
$Vp = 5.54 + 0.06(z - 7)$	(> 7 km)	Tertiary sed. rocks
$Vp = 2.314 + 0.35z + 0.2z^2 - 0.03z^3$	(0.04–0.5 km)	Miocene basin fill
$Vp = 4.99 + 0.04(z - 4)$	(4–7 km)	Miocene basin fill
$Vp = 2.75 + 0.4725z$	(0.05–4 km)	Great Valley sequence
$Vp = 0.7 + 36z$	($z < 0.05$ km)	Franciscan Complex
$Vp = 2.5 + 1.963z - 0.424z^2 + 0.043z^3 - 0.002z^4 + 0.0000335z^5$	(0.05–9 km)	Franciscan Complex
$Vp = 6.0 + 0.01(z - 9)$	($z > 9$ km)	Franciscan Complex
$Vp = 1.5 + 4.41z$	($z < 0.05$ km)	Granitic rocks
$Vp = 2.5 + 2.9299z - 0.824z^2 + 0.1019z^3 - 0.0061z^4 + 0.0002z^5$	(0.05–4 km)	Granitic rocks
$Vp = 6.20 + 0.002(z - 4)$	($z > 4$ km)	Granitic rocks
$Qs = -16 + 104.13Vs - 25.225Vs^2 + 8.2184Vs^3$		($Vs > 0.3$ km/sec)
$Qs = 13$ for $Vs < 0.3$ km/sec		
$Qp = 2Qs$		

Vp and Vs in km/sec; depth, z, in kilometers.

6. Source: Krishna (1988)

834 V. G. KRISHNA

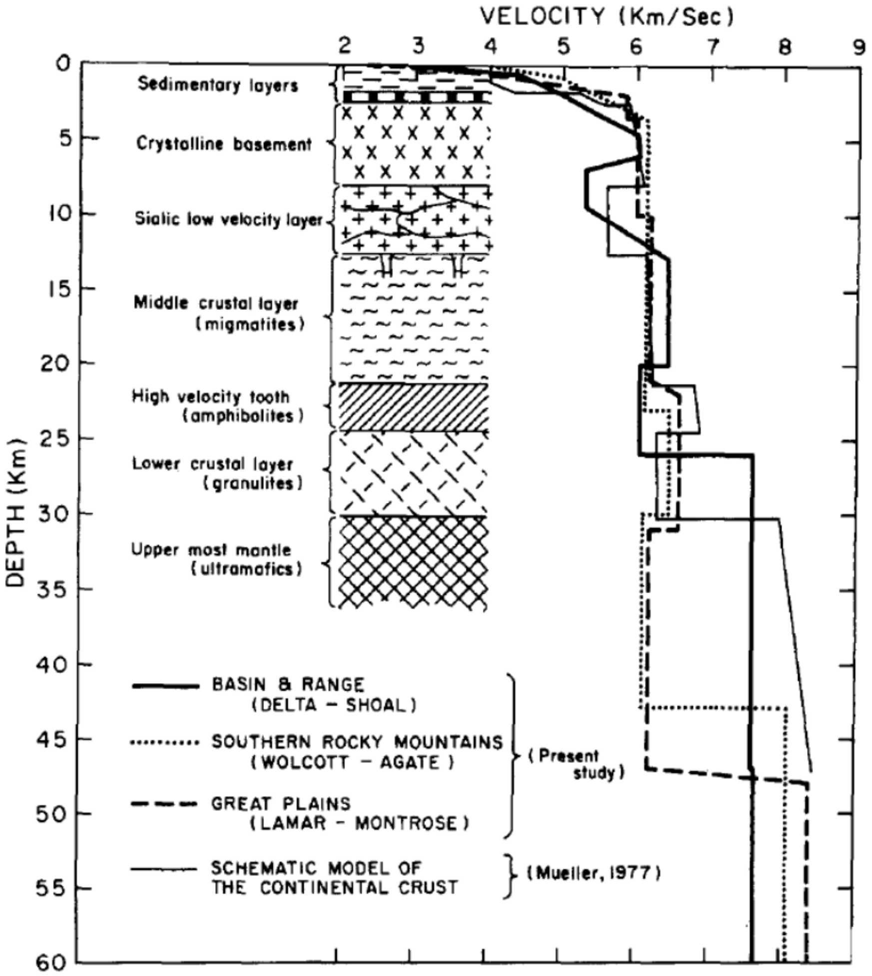

FIG. 15. Crustal *P* velocity-depth models for the Basin and Range, Southern Rocky Mountains and the Great Plains provinces in the Western United States obtained in the present study, along with the schematic model (shown for comparison) of the continental crust proposed by Mueller (1977).

7. Source – Mavko (2008)

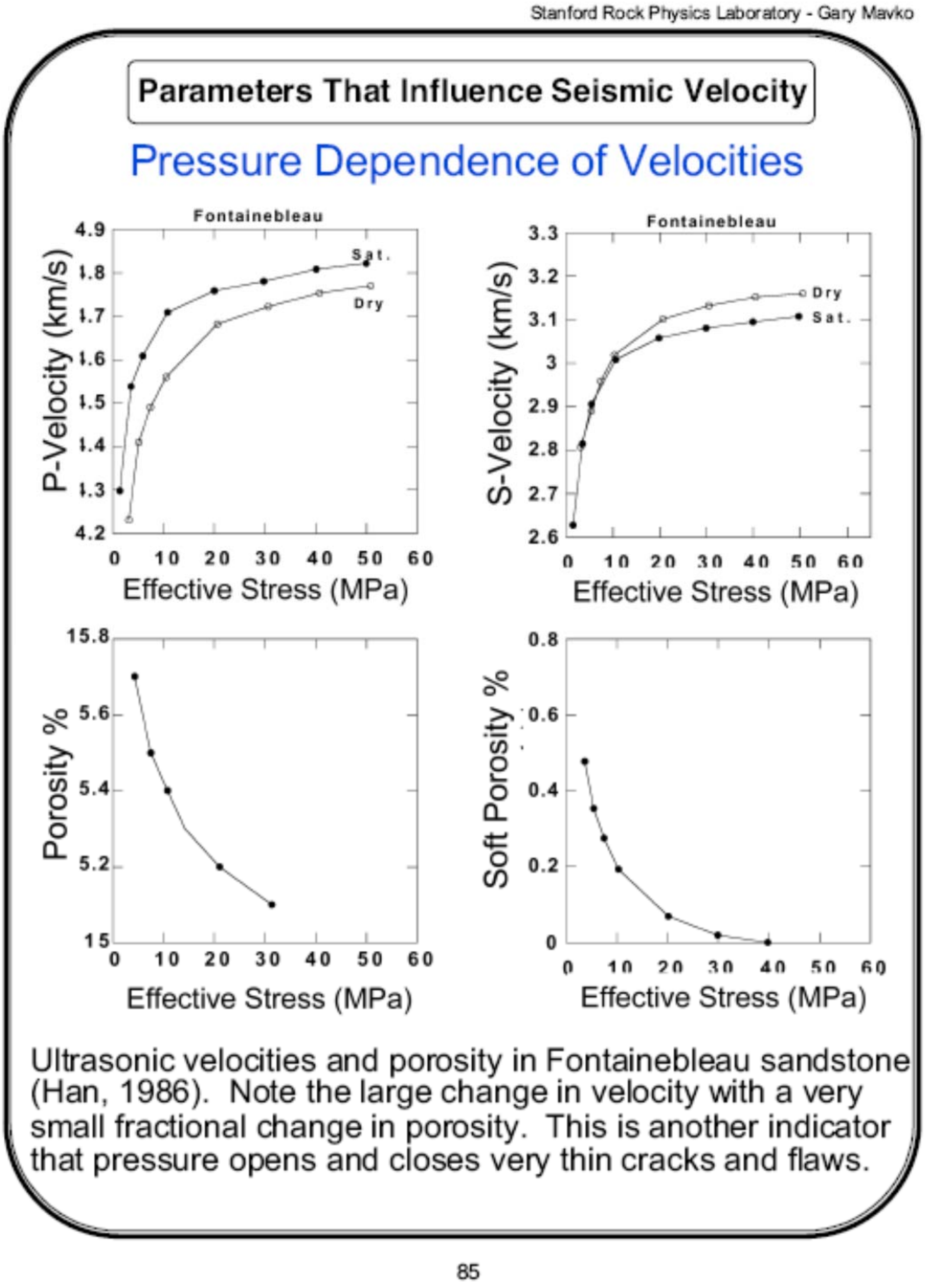

Stanford Rock Physics Laboratory - Gary Mavko

Parameters That Influence Seismic Velocity

Pressure Dependence of Velocities

Ultrasonic velocities and porosity in Fontainebleau sandstone (Han, 1986). Note the large change in velocity with a very small fractional change in porosity. This is another indicator that pressure opens and closes very thin cracks and flaws.

85

Parameters That Influence Seismic Velocity

Seismic Velocity and Overpressure

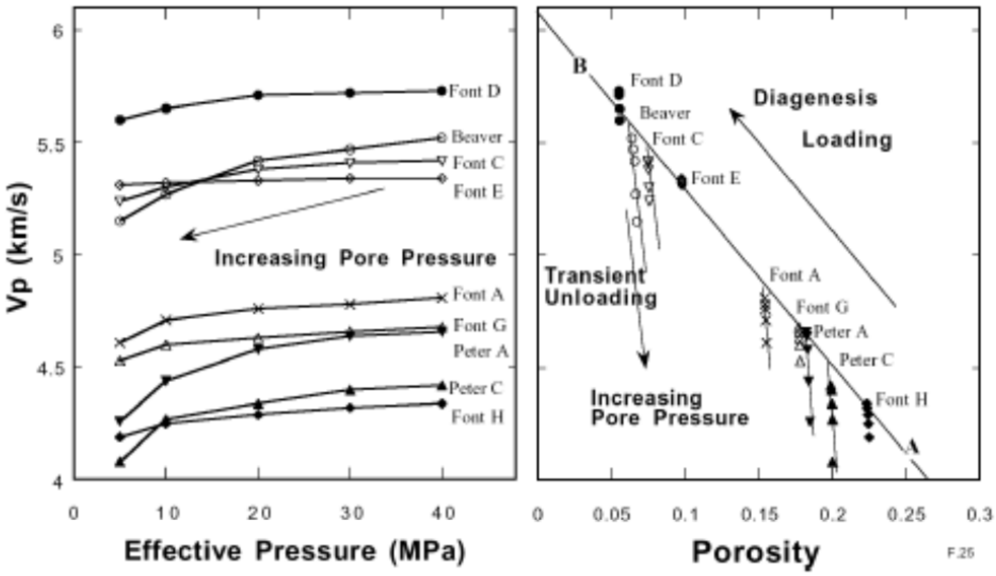

Curves on the left show the typical increase of velocity with effective pressure. For each sample the velocity change is associated with the opening and closing of cracks and flaws. These are typical when rapid changes in effective pressure occur, such as during production.

Curves on the right show the same data projected on the velocity- porosity plane. Younger, high porosity sediments tend to fall on the lower right. Diagenesis and cementation tend to move samples to the upper left (lower porosity, higher velocity). One effect of over- pressure is to inhibit diagenesis, preserving porosity and slowing progress from lower right to upper left. This is called "loading" type overpressure. Rapid, late stage development of overpressure can open cracks and grain boundaries, resembling the curves on the left. This is sometimes called "transient" or "unloading" overpressure. In both cases, high pressure leads to lower velocities, but along different trends.

Parameters That Influence Seismic Velocity

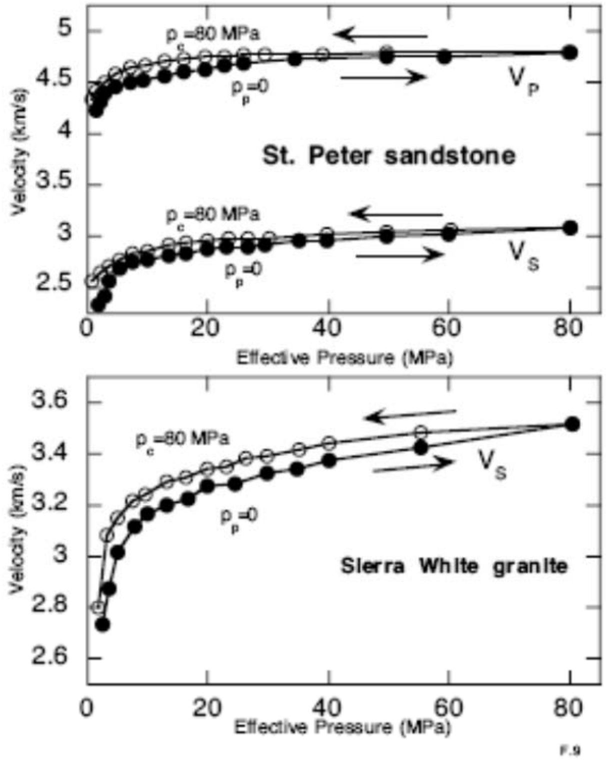

Experiments that illustrate the effective pressure law. In the first part of the experiment, effective pressure is increased by increasing confining pressure from 0 to 80 MPa, while keeping pore pressure zero (solid dots). Then, effective pressure is decreased by keeping confining pressure fixed at 80 MPa, but pumping up the pore pressure from 0 to nearly 80 MPa (open circles). (Jones,1983.)

The curves trace approximately (but not exactly) the same trend. There is some hysteresis, probably associated with frictional adjustment of crack faces and grain boundaries. For most purposes, the hysteresis is small compared to more serious difficulties measuring velocities, so we assume that the effective pressure law can be applied. This is a tremendous convenience, since most laboratory measurements are made with pore pressure equal 0.

Parameters That Influence Seismic Velocity

Pierre shale (ultrasonic), from Tosaya, 1982.

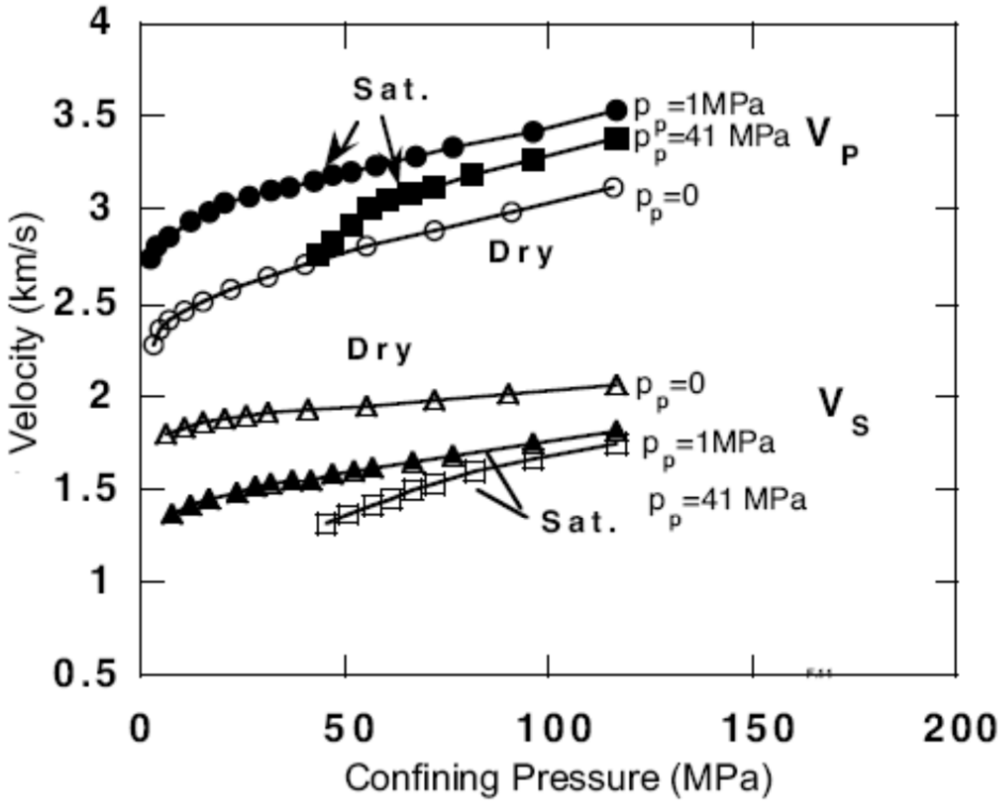

For shales, we also often see an increase of velocity with effective pressure. The rapid increase of velocity at low pressures is somewhat elastic, analogous to the closing of cracks and grain boundaries that we expect in sandstones.

The high pressure asymptotic behavior shows a continued increase in velocity rather than a flat limit. This is probably due to permanent plastic deformation of the shale.

Parameters That Influence Seismic Velocity

Alkanes

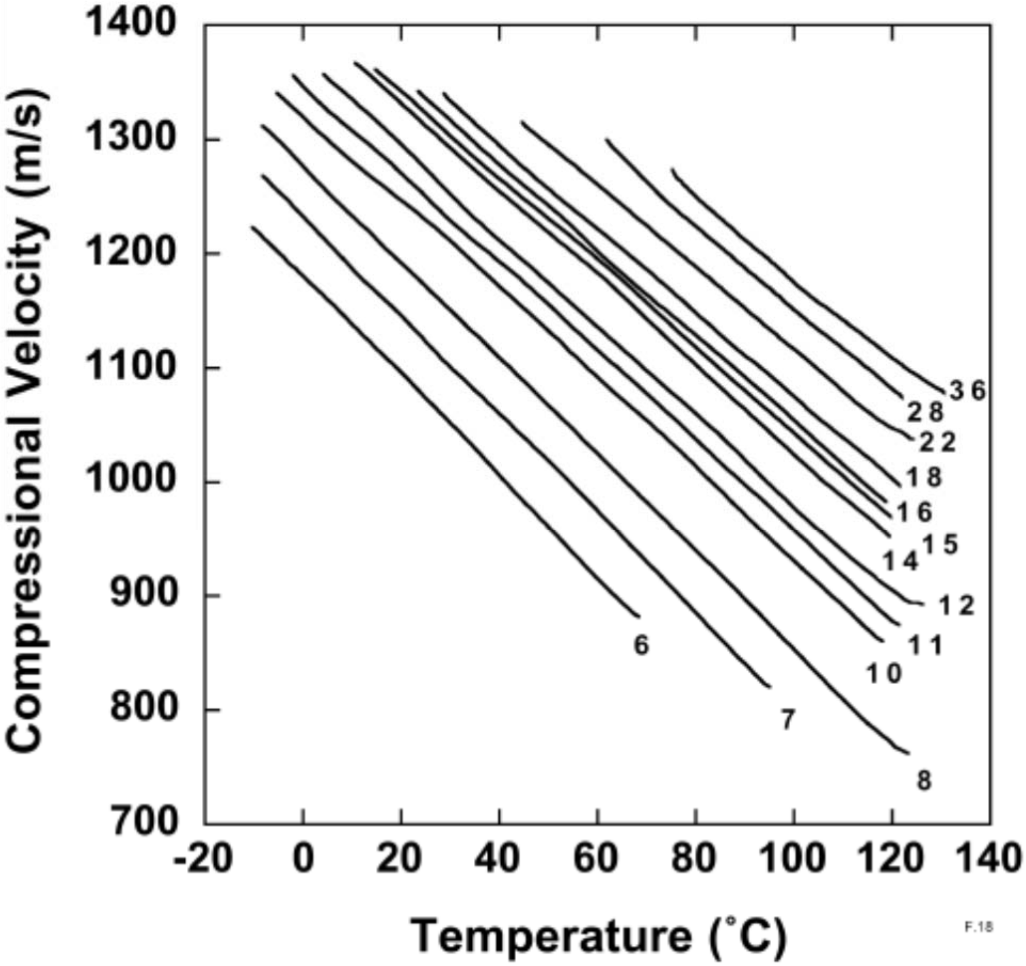

Compressional velocities in the n-Alkanes vs. temperature. A drastic decrease of velocity with temperature! The numbers in the figure represent carbon numbers. From Wang, 1988, Ph.D. dissertation, Stanford University.

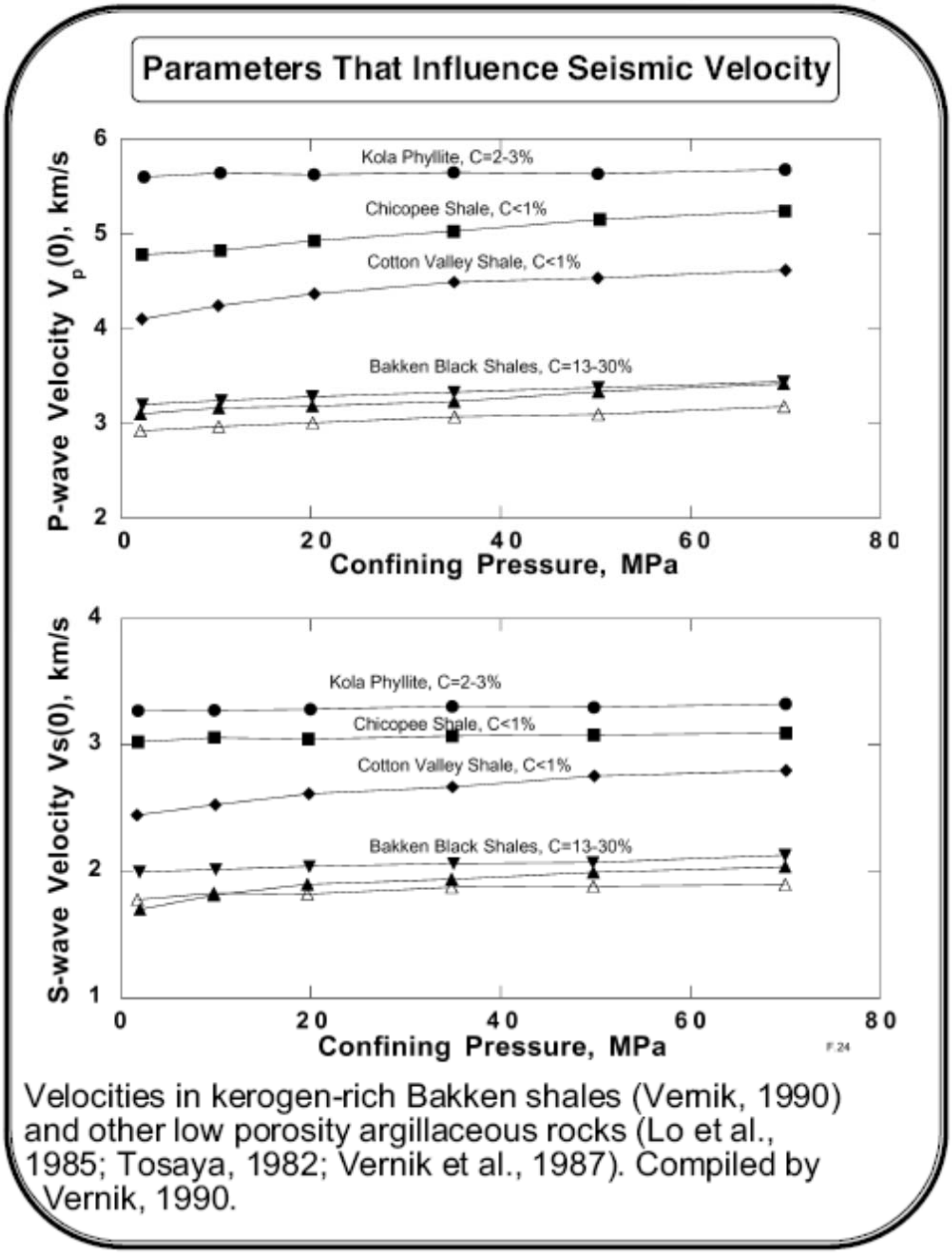

Parameters That Influence Seismic Velocity

Velocities in kerogen-rich Bakken shales (Vemik, 1990) and other low porosity argillaceous rocks (Lo et al., 1985; Tosaya, 1982; Vernik et al., 1987). Compiled by Vernik, 1990.

8. References

Brocher, T., 2008, Compressional and Shear-Wave Velocity versus Depth Relations for Common Rock Types in Northern California. Bulletin of the Seismological Society of America, vol. 98, no. 2, April, p. 950–968. doi: 10.1785/0120060403

Burke, M.M. and Fountain, D.M., 1990, Seismic properties of rocks from an exposure of extended continental crust-new laboratory measurements from the Ivrea Zone. Tectonophysics, vol. 182, p. 119-146. Elsevier Science Publishers B.V., Amsterdam.

Christensen, N.I.,1968, Compressional wave velocities in basic rocks. Pacific Science, Vol. XXII, January.

Kern, H., Popp, T., Gorbatsevich, F., Zharikov, A., Lobanov, K.V., and Smirnov, Y.P., 2001, Pressure and temperature dependence of Vp and Vs in rocks from the superdeep well and from surface analogues at Kola and the nature of velocity anisotrophy. Tectonophysics, vol. 338, p. 113-134.

Kern, H., 1982, Elastic-wave velocity in crustal and mantle rocks at high pressure and temperature: the role of the high—low quartz transition and of dehydration reactions. Physics of the Earth and Planetary Interiors, vol. 29, p. 12-23.

Krishna, April 1988, Crustal velocity models in the western United States from travel times and amplitudes of seismic refraction data, Bulletin of the Seismological Society of America, Vol. 78, No. 2, pp. 816-837.

Mavko, G., 2008, Parameters that influence Seismic Velocity, Stanford Rock Physics Laboratory, Presentation, Stanford University, California.

APPENDIX 6

SELECT SEISMIC VELOCITY AND ROCK PROPERTIES

Depth (km)	Vp (km/s)	Vs (km/s)	Vp/Vs	Density (g/cm^3)	Pres-sure (Mpa)	Temp-erature (°C)	Lithology	Rock Porosity	Atten-uation	Location	Source	Reference
0.0 - 0.2	1.6			1.6			Unconsolidated sediments			Bakkahlaup field, Öxarfjördur region, NE-Iceland	seismic and gravity	Georgsson et al. (2000)
0.05 - 0.5	2.3 - 3						Sediments					
0.4-1	3.4 - 3.6			2		200						
0.6-1.4	4.4 -4.7			2.7			Unaltered/young basalts and/or sediments					
1-2.7	5.2 - 5.5			2.7			Basaltic lavas					
1.8-3	5.5			2.8			Altered basaltic lavas					
0-1	2.2 - 2.8	1.2-1.7								Solfatara, W12, Campi Flegrei caldera, Italy	seismic	Vanorio et al. (2010)
1.1-2	2.8 -3.4	1.7-2										
2.2-3	3.4 - 4.3	2-2.2										
3.1-4	4.3 - 4	2.2-3.4										
4.1-5	4 - 5.5	3.4-4.2										
5.1-6	6.5 - 6.4	4.2-3.9										
			1.44 / 1.36		5	350	tuffite	0.2/0.5		Campi Flegrei caldera, Italy	modeled data	Vanorio et al. (2010)
			1.45 / 1.37		10			0.2/0.5				
			1.46 / 1.38		15			0.2/0.5				
			1.47 / 1.39		20			0.2/0.5				
			1.48 / 1.395		25			0.2/0.5				
			1.49 / 1.42		30	350	tuffite	0.2/0.5		Campi Flegrei caldera, Italy	modeled data	Vanorio et al. (2010)
			1.495 / 1.44		35			0.2/0.5				
			1.52 / 1.465		40			0.2/0.5				
	0-1	3.3	1.64							Otake-Hatchobaru Geothermal Area at Kuju, Japan, a volcano in Central Kyushu	seismic tomo-graphy	Yoshikawa and Sudo (2004)
	1-3.5	3.43	1.64									
	3.5-5	4.14	1.64									
	5.1-8	5.56	1.64									

Depth (km)	**Vp** (km/s)	**Vs** (km/s)	**Vp/Vs**	**Density** (g/cm^3)	**Pres-sure** (Mpa)	**Temp-erature** (°C)	**Lithology**	**Rock Porosity**	**Atten-uation**	**Location**	**Source**	**Reference**
		6.02		2.5-3.5	100	20	granite, precambrian			Scandinavia	synthetic data	Rybach and Bunterbath (1984)
		5.97			100		gneiss					
		6.88			100		Amphibolite, Gabbro					
		8			100		Ultrabasic rock					
0.75 - 1.25	5.1								50	Siljan Ring survey, in the Baltic Shield	stochastic modeling of a variety of seismic data	Line et al. (1998)
0.7 - 1.5	5.6								125			
1 - 2.5	5.8								200			
1.5 - 2.5	5.9								500			
2.25 - 4	6								625			
4 - 5.25	6.3								700			
0 - 0.5	4.5	2.43								Coso Geothermal Area, Inyo County, California	seismic tomo-graphy	Lees and Wu (2000)
0.5 - 1	4.48	2.59										
1 - 1.5	4.86	2.96										
1.5 - 2	4.8	2.95										
2 - 2.5	5.25	3.14										
2.5 - 3	5.212	3.16										
3.5 - 4	5.51	3.27										
4 -5.5	5.59	3.42										
no depth info	4						Tertiary volcanic rocks			Dixie Valley, Nevada	reflection profiles	Catchings (1992)
no depth info	5.7-6.15						Upper crustal crystaline rocks in the felsic range					
1.0-10.0	6						granitic					
10.0-15.0	6.15				3 kBar		mylonites					
15-22	6.3				6-8Kbar	500-700	diorite					
22-25	6.6				8-10Kbar	700-1200	largely mafic (gabbro)					
25-39	7.4						Mafic/ultramafics					
29-36	8						Peridotite (Moho)					

Depth (km)	Vp (km/s)	Vs (km/s)	Vp/Vs	Density (g/cm^3)	Pres-sure (Mpa)	Temp-erature (°C)	Lithology	Rock Porosity	Atten-uation	Location	Source	Reference
0-2	4.7						hard rock			Dixie Valley, Nevada	seismic	Stauder and Ryal (1967)
0-2	3.3						alluvial fan			Dixie Valley, Nevada	seismic	Catchings (1992)
2.0-10.0	4-5.7						tertiary rocks					
no depth info	2.6-3.6						heavy oil-saturated Uwalde Carbonate			laboratory	labora-tory	Bazle et al. (2006)
no depth info	3-3.5						Foxhills Sandstone					
0-0.1				2.2			Modern basin fill			Dixie Valley, Nevada	gravity	Abbott et al. (2001)
0.1-1				2.3			middle Miocene (13-15 Ma) capping basalt					
1-2.4				2.5			late Oligocene-early Miocene volcanic tuffs, flows, and sediments					
2.4-3.2				2.67								

APPENDIX 7

DIXIE VALLEY GEOCHEMICAL DATA (GOFF ET AL., 2002)

LA-13972-MS
Approved for public release;
distribution is unlimited.

Geochemical Data on Waters, Gases, Scales, and Rocks from the Dixie Valley Region, Nevada (1996–1999)

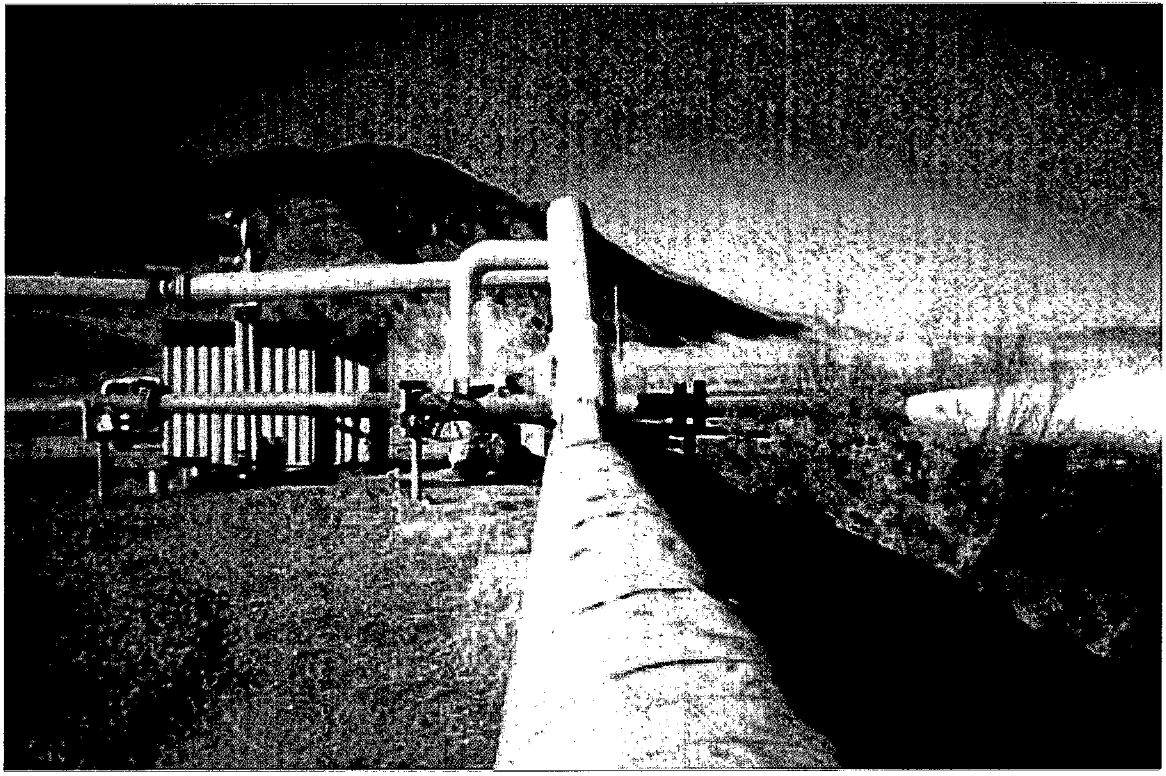

Los Alamos
NATIONAL LABORATORY

Dixie Valley
SMU GEOTHERMAL LAB
OSTI-12

DISCLAIMER

Cover Photo: Photo looking NNE of 37–33 production well and flow lines from the northern production zone, Dixie Valley geothermal field, Nevada. Geothermal brine and steam are being vented into a holding pond on the right side of photo. The Stillwater Range towers above Dixie Valley in the left background. The break in the slope between the range and the valley marks the approximate position of the Stillwater fault zone (photo by F. Goff).

Los Alamos National Laboratory, an affirmative action/equal opportunity employer, is operated by the University of California for the United States Department of Energy under contract W-7405-ENG-36.

This report was prepared as an account of work sponsored by an agency of the United States Government. Neither the Regents of the University of California, the United States Government nor any agency thereof, nor any of their employees make any warranty, express or implied, or assume any legal liability or responsibility for the accuracy, completeness, or usefulness of any information, apparatus, product, or process disclosed, or represent that its use would not infringe privately owned rights. Reference herein to any specific commercial product, process, or service by trade name, trademark, manufacturer, or otherwise does not necessarily constitute or imply its endorsement, recommendation, or favoring by the Regents of the University of California, the United States Government, or any agency thereof. The views and opinions of authors expressed herein do not necessarily state or reflect those of the Regents of the University of California, the United States Government, or any agency thereof. Los Alamos National Laboratory strongly supports academic freedom and a researcher's right to publish; as an institution, however, the Laboratory does not endorse the viewpoint of a publication or guarantee its technical correctness.

LA-13972-MS
Issued: August 2002

Geochemical Data on Waters, Gases, Scales, and Rocks from the Dixie Valley Region, Nevada (1996–1999)

Fraser Goff
Deborah Bergfeld
Cathy J. Janik*
Dale Counce
Mike Murrell

* U.S. Geological Survey, MS 910, 345 Middlefield Road, Menlo Park, CA 94025
cjanik@usgs.gov

Los Alamos
NATIONAL LABORATORY

Contents

Figures

Tables

Geochemical Data on Waters, Gases, Scales, and Rocks from the Dixie Valley Region, Nevada (1996-1999)

by

Fraser Goff, Deborah Bergfeld, Cathy J. Janik,
Dale Counce, Mark Huebner, and Mike Murrell

ABSTRACT

This report tabulates an extensive geochemical database on waters, gases, scales, rocks, and hot-spring deposits from the Dixie Valley region, Nevada. The samples from which the data were obtained were collected and analyzed during 1996 to 1999. These data provide useful information for ongoing and future investigations on geothermal energy, volcanism, ore deposits, environmental issues, and groundwater quality in this region.

INTRODUCTION

The Dixie Valley geothermal system is located roughly 160 km northeast of Fallon in west central Nevada and supports a 62-MWe double-flash power plant that became operational in 1988. Located in the Basin and Range tectonic province, Dixie Valley trends north-northeast and is 120 km long by about 20 km wide. It is bounded by the Stillwater Range on the west and by the Clan Alpine Range to the east (Waibel 1987; Honjas et al. 1997; Lutz et al. 1997). Geothermal fluids are produced from the subsurface extension of the normal Stillwater fault zone and associated fractured rocks at depths of 3,050 to 2,800 m. The fault zone architecture is considered to be complex (Caine et al. 1996). The Dixie Valley geothermal system displays fault and fracture permeability typical of the Basin and Range. Convective heat flow in the geothermal system exceeds 300 mW/m^2, and conductive temperature gradients range from 100°C to >200°C/km (Williams et al. 1997).

Producing geologic formations penetrated by geothermal wells are exposed in the Stillwater Range west of the power plant. These rocks consist of Triassic to Jurassic marine quartzite, siltstone, shale, and volcaniclastic rocks overlain by the Humboldt Lopolith (Speed 1976), a complex of oceanic crustal rocks that includes gabbro, diorite, and basalt (Waibel 1987; Lutz 1997). The Triassic to Jurassic units have been imbricated into four similar stratigraphic packages by three thrust faults and were later intruded by Cretaceous granodiorite. Uplift and erosion exposed these older rocks by the mid-Tertiary during which an extensive complex of Oligocene ignimbrites was emplaced throughout the region. The Miocene Table Mountain Basalt rests on earlier rocks in the subsurface of Dixie Valley and in the bordering ranges. Within Dixie Valley, the basalt is found at 1,280 m below sea level and is overlain by a variety of late Tertiary basin-fill deposits. The mouths of all major canyons are now filled by alluvial fans, and the axis of Dixie Valley is occupied by alluvium, playa deposits, and the Humboldt Salt Marsh.

Extensive alteration from previous hydrothermal activity and present geothermal fluids affects most geologic units, particularly along range front faults. A series of active and dead hot springs and fumaroles is sporadically distributed along the Stillwater fault from a zone a few kilometers north of the Dixie Valley power plant (Senator fumarole group) to a point about 20k southwest of the power plant (Dixie hot springs). Additional hot and mineral fluids discharge as springs or occur as shallow aquifers throughout the Dixie Valley region.

The authors have been engaged in a series of geothermal investigations in the Dixie Valley region since October 1996 (Bruton et al. 1997; Goff et al. 1998; Kennedy et al. 1999; Nimz et al. 1999; Goff and Janik 2000; Bergfeld 2001; Bergfeld et al. 1998, 2001; Stamates 2001). During these investigations, large quantities of unpublished chemical and isotopic data on waters, gases, rocks, and hot spring deposits have accumulated. Because this data may be useful to other research groups and interested regional stakeholders, we are releasing this information into the public domain. This report contains the locations, field measurements, and analytical results of these accumulated data. No attempt is made herein to interpret the scientific meaning of these data.

PROJECTS SUMMARY

The following geothermal collaborations were responsible for production of the data included in this report:

1. A study of rock-water interaction, corrosion, and scaling of production/injection horizons, production wells, and injection wells with C. Bruton, Lawrence Livermore National Laboratory (LLNL) and J. Moore (Energy and Geoscience Institute).
2. A study of temporal and spatial stable isotope variations in production fluids of the Dixie Valley geothermal reservoir with C. J. Janik, U.S. Geological Survey (USGS).
3. A study of recharge sources and fluid ages with respect to the Dixie Valley region and the Dixie Valley geothermal system with G. Nimz (LLNL) and C. J. Janik (USGS).
4. A study of the distribution and flux of anomalous CO_2 and elevated steam discharge at the "dead zone" on the north edge of the Dixie Valley geothermal system with D. Bergfeld, Los Alamos National Laboratory (LANL) and C. J. Janik (USGS). This project was one of those contained in Bergfeld's Ph.D. thesis.
5. An evaluation of gold, mercury, and other trace metals contents in Dixie Valley production fluids and scales with S. Johnson, Oxbow Geothermal Company.
6. An investigation of the geology and age of selected travertine and sinter deposits within and along the flanks of Dixie Valley with M. Murrell (LANL) and C. J. Janik (USGS).
7. An investigation examining the tritium relations of Dixie Valley geothermal and regional fluids with M. Stamates and L. Shevenell (University of Nevada- Reno). This project made up a portion of Stamates' M.S. thesis.

LOCATIONS AND FIELD PARAMETERS

Latitude, longitude, and elevation of the sampling sites appear in Table 1, and the sites are keyed to map numbers on the regional and detailed maps of Figures 1 and 2. Table 1 also provides the name of the 1:100,000 topographic quadrangle and the lithology of each sampling site. Field parameters for the sampling sites appear in Table 2. All field and analytical data are keyed to sample numbers that are listed as initial entries in most of the tables. Temperatures were measured with thermocouples and digital thermometers, or occasionally, from gauges on geothermal wells. Pressures were obtained from gauges on geothermal wells, from a portable digital pressure gauge that was piped into our sampling equipment, or from power plant data. Steam fractions (y) were provided to us by the operator of the geothermal field. The field pH of produced fluids, injection fluids, and power plant fluids was usually measured with a pH electrode. The field pH of background waters was measured with pH-sensitive papers. Field alkalinity and conductivity of produced fluids, injection fluids, and power plant fluids were determined by pH titration and with a portable conductivity meter, respectively. The field Eh was obtained with a field portable electrode. Flow rates of wells, power plant fluids, and injection lines were provided to us by the operator of the geothermal field. Flow rates of background fluids were generally measured with a bucket or beaker and a stopwatch.

SAMPLING METHODS

Water Samples: Field procedures for sampling waters have been described in detail by Trujillo et al. (1987), Werner et al. (1997), and Goff and McMurtry (2000). Generally, four basic samples are collected at each water collection site: (1) a 125-ml plastic bottle of filtered (0.45 mm), unacidified water for anions, (2) a 125-ml plastic bottle of filtered (0.45 mm) water, acidified to pH ≤2 with spectrographically pure, concentrated HNO_3 for cations, silica, and trace metals, (3) a 30-ml glass bottle of raw water for deuterium and oxygen-18 isotope measurements, and (4) a 500-ml glass or plastic bottle of raw water for tritium measurements. Sampling for trace metals analysis followed a clean-hands protocol in order to avoid the introduction of contaminants. Samples were collected in precleaned, acid-washed (nitric acid) bottles and preserved with trace-metal grade reagents.

Aluminum and Silica Samples of Production, Injection, and Other Waters: Special samples were collected for total and ionized aluminum to allow for thermodynamic modeling of mineral phases in equilibrium or nonequilibrium with the production and injection well fluids (Bruton et al. 1997; Gallup 1998). The filtered, acidified sample described above was used for total aluminum analyses. Ionized aluminum was extracted from 500 ml of filtered sample using an oxine-MIBK method modified from Barnes (1975). Both 0.2- and 0.45-μ filters were used on the samples before extraction proceeded. Final extracts were stored in silica-glass vials in coolers and refrigerators before analysis. In early 1999 C. Bruton (LLNL) indicated that the analyzed values for ionized aluminum determined previously were probably too low, due possibly to coagulation of colloid particles and loss of aluminum during filtering. Thus, 1999 samples were determined on unfiltered oxine-MIBK extracts.

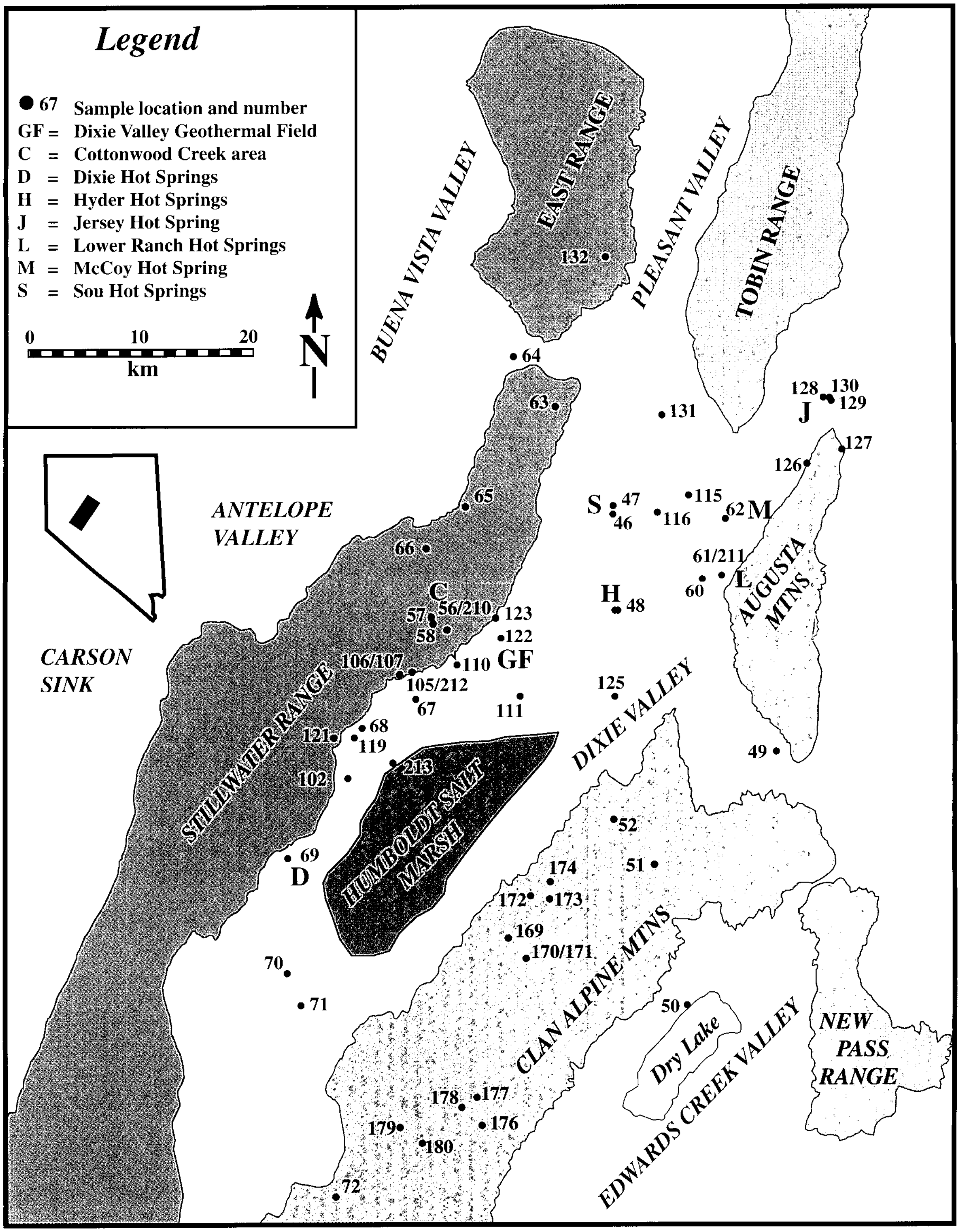

Figure 1. Regional map of the Dixie Valley region, Nevada, showing the locations of samples (Table 1).

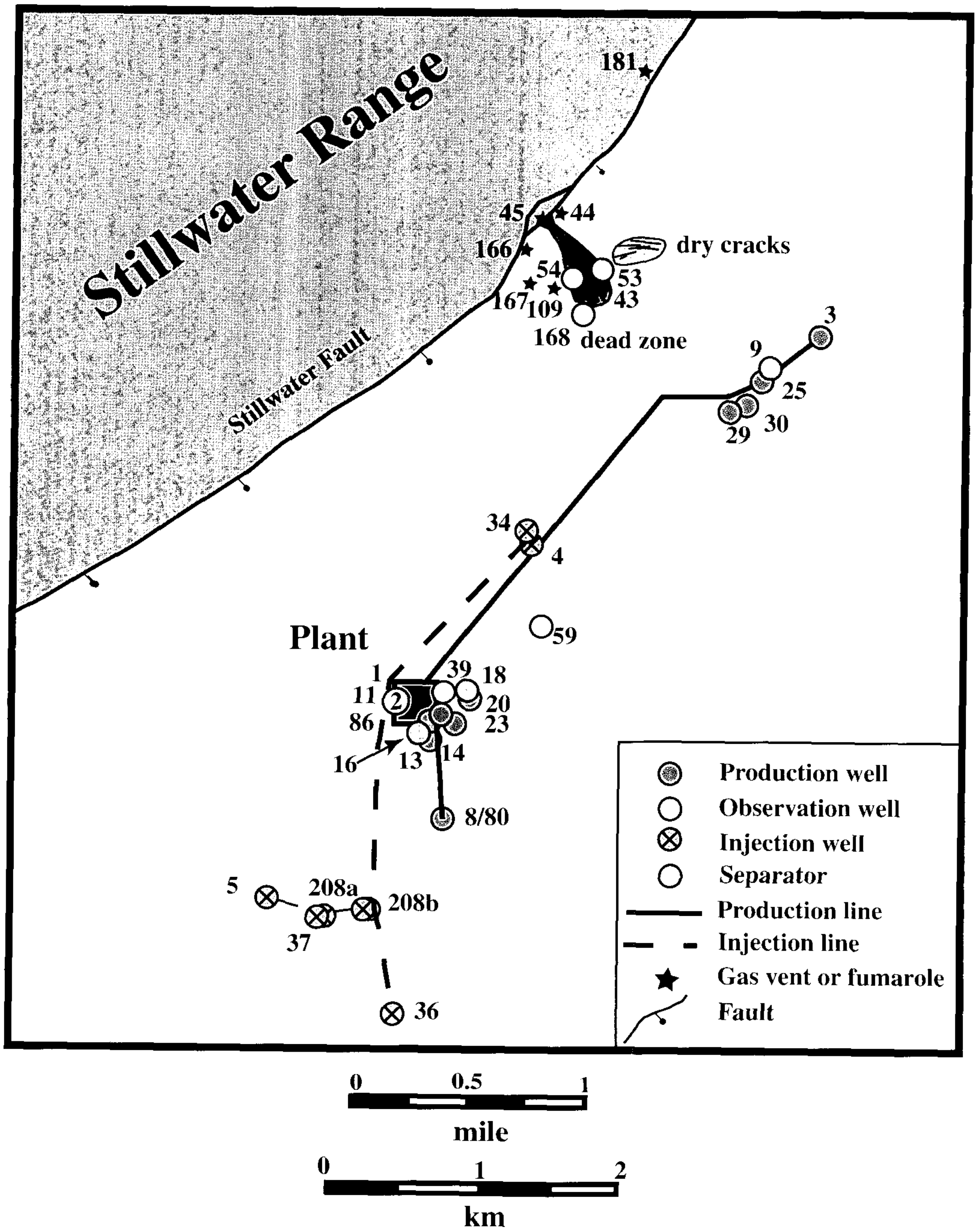

Figure 2. Map of west central Dixie Valley in the vicinity of the geothermal power plant showing locations of production, injection, shallow observation, and water supply wells, the locations of fumaroles along the Stillwater fault zone, and the location of the "dead" zone (Bergfeld et al. 2001). North is straight up on this figure.

Silica samples of initially hot or supersaturated fluids (such as those from production and injection wells, from power plant fluids, from other geothermal wells, and from hot springs) were obtained by pipetting 5 ml of fresh sample into 60 ml plastic vials containing 30 ml of deionized, silica-free water. Silica from cold features was determined on the filtered, acidified samples described above.

Additional Water Samples: Additional samples were collected for other kinds of analyses but were not collected at each sampling point or for all projects described above. For sulfide analysis, 5 ml raw water sample was pipeted into a 15 ml plastic bottle containing 5 ml of sulfide antioxidant buffer solution. Gold samples were collected by filling a 125-ml prewashed glass bottle with filtered water and adding 2 ml of aqua regia (a 3:1 mixture of trace-metal-grade HCl and HNO_3). Samples for carbon-13 analysis of dissolved inorganic carbon were collected by filling a 125- to 250-ml glass bottle with raw water and adding a saturated solution (in most cases10 ml) of $SrCl_2$ in NH_4OH.

Gases: Gas samples were obtained at fumaroles, gas vents, gaseous springs and gas-rich wells with funnels, pipes, tubing, and fittings as necessary. Gases were collected in 300-ml double-port, caustic-gas bottles as described by Trujillo et al. (1987), Fahlquist and Janik (1992), and Goff and McMurtry (2000). Caustic-gas bottles are prepared in the laboratory before sampling by adding roughly 100 ml of 4N NaOH solution (bicarbonate purged) to the bottle and pumping the remaining head space of the bottle to vacuum. Samples collected in caustic bottles can be used for bulk gas analysis and analysis of $\delta^{13}C\text{-}CO_2$, $\delta^{13}C\text{-}CH_4$, and other isotopic constituents.

Scales, Rocks, and Hot Springs Deposits: Samples of test bed scales were provided by J. Moore (EG&G). Samples of production and injection well scales were donated by S. Johnson (Oxbow Power Co.). Samples of representative volcanic, plutonic, metamorphic, and sedimentary rocks from the Dixie Valley region were identified using geologic and paleomagnetic maps and reports (Speed 1976; Hudson 1988; Hudson and Geissman 1984, 1991; Plank et al. 1999). These samples were analyzed for various isotopes using standard methods by several contract laboratories. Samples of hot spring deposits from the "dead" travertine in Cottonwood Canyon and the Lower Ranch sinter-travertine in northeastern Dixie Valley were collected for U-series dating methods. All scale and rock samples were collected in cloth or plastic bags for later chemical and isotopic analysis.

ANALYTICAL METHODS, RESULTS, AND CALCULATIONS

Waters: Major and trace element chemical analyses of waters were determined by D. Counce at Los Alamos National Laboratory using methods listed in Table 3 (Janik et al. 1999; Goff et al. 2001). Results of the analyses are given in Tables 4 and 5. Total aluminum was determined by inductively coupled plasma (ICP) spectroscopy on the acidified sample described above. Ionized aluminum was determined on methyl isobutyl ketone (MIBK) extracts described above using graphite furnace atomic adsorption (GFAA) spectroscopy. The aluminum results can be compared on Table 6. Isotope analyses of $\delta D\text{-}H_2O$, $\delta^{18}O\text{-}H_2O$, $\delta^{13}C\text{-}HCO_3$, and $\delta^{18}O\text{-}SO_4$ were determined by standard methods at various laboratories listed in Table 7. Tritium measurements were obtained primarily from the University of Miami. All isotope results on water samples are reported in Table 7.

Gases: Bulk gas analyses (Table 8) were obtained from either the U.S. Geological Survey by C. J. Janik or the EES-6 geochemistry lab at Los Alamos National Laboratory by D. Counce using gas methods listed in Table 3. Carbon-13 analyses of CO_2 were determined using standard methods at a variety of laboratories as listed in Table 8. Trace metals analyses of the caustic solutions from selected gas samples are listed in Table 9. These analyses used procedures for liquid samples listed in Table 3, and the results are adjusted for the density of the caustic solution.

Chemical Geothermometers: Results for the sulfate oxygen isotope geothermometer are listed in Table 7. Note that this geothermometer has many limitations due to brine flash, reequilibration, evaporation, and mixing of different fluids. Gas geothermometers that are used to estimate subsurface geothermal reservoir temperatures are listed for all gas samples in Table 9. Reconstructed chemical compositions of flashed brines are given in Table 10. Geothermometer calculations of the reconstructed brines are shown in Table 11. Geothermometer calculations of thermal and mineral springs and wells are listed in Table 12. All calculations use standard geothermometers that are referenced at the bottom of the various tables. Calculations were performed on a personal computer using the code of Urbani (1986).

Scales: About 0.25 g of dried scale and test-bed precipitates were mixed with a cocktail consisting of 2.0 ml HNO_3, 3.5 ml HCl, and 1.5 ml HF, heated in a microwave oven for about 10 minutes, and the resulting solution adjusted to 50 ml with deionized water. Analyses of selected metals by methods described in Table 2 appear in Table 13. This method extracts easily soluble metallic minerals and colloid particles from the scales without dissolving all the rock fragments, sand grains, and silt that may be in some samples.

Rocks: Rock samples were cleaned of debris and sent to contract laboratories for isotopic analyses as listed in Table 14. Rubidium and strontium concentrations were analyzed at LANL for a group of strontium isotope samples collected in 1998. The rubidium and strontium concentrations for strontium isotope samples collected for an earlier project were analyzed at the University of New Mexico (UNM).

Hot Spring Deposits: Two areas of hot-spring deposits were examined in detail and sampled for U-series radiometric dating: the Cottonwood Canyon travertine and the Lower Ranch mixed travertine and sinter. Samples were cleaned, crushed, and hand picked to obtain 5 to 20 g of pure carbonate and silica (opal and chalcedony). Samples were further processed in highly purified acids and analyzed by mass spectrometry according to procedures described in Edwards et al. (1997) and Pickett and Murrell (1997).

ACKNOWLEDGMENTS

Collection of the various samples and publication of this report was made possible by M. Reed and J. Renner of the U.S. Department of Energy, Office of Geothermal Technologies. C. J. Janik was also funded by the U.S. Geological Survey Volcano Hazards Program. Grants from the Geological Society of America supported some of the field work for D. Bergfeld. Stu Johnson and Dick Benoit (Oxbow Power Co.) provided valuable information and lots of muscle at the Dixie Valley geothermal system. Jerry Kelly (DJ Ranch) gave us free access to the Lower Ranch hot springs. J. Brinkerhoff cheerfully allowed us to sample his wells in northern Dixie Valley. The manuscript was reviewed by J. Heikoop (LANL), and Mable Amador provided the final editing.

REFERENCES

Barnes, R.B., 1975, The determination of specific forms of aluminum in natural water. Chemical Geology, v. 15, p. 177–191.

Bergfeld, D., 2001, Geothermal systems and CO_2 degassing: The Geysers–Clear Lake, and Dixie Valley regions of California and Nevada. Ph.D. thesis, University of New Mexico, Albuquerque, 123 pp.

Bergfeld, D., Goff, F.E., and Janik, C.J., 2001, Elevated carbon dioxide flux at the Dixie Valley geothermal field, Nevada; relations between surface phenomena and the geothermal reservoir, Chemical Geology, v. 177, p. 43–66.

Bergfeld, D., Goff, F.E., and Janik, C.J., Johnson, S., 1998, CO_2 flux measurements across portions of the Dixie Valley geothermal system, Nevada. Geothermal Resources Council Transactions, v. 22, p. 107–111.

Bruton, C., Counce, D., Bergfeld, D., Goff, F., Johnson, S., Moore, J., and Nimz, G., 1997, Preliminary investigation of scale formation and fluid chemistry at the Dixie Valley geothermal field, Nevada. Geothermal Resources Council Transactions, v. 21, p. 157–164.

Caine, J., Evans, J., and Forster, C.B., 1996, Fault zone architecture and permeability structure. Geology, v. 24, p. 1025–1028.

D'Amore, F., and Panichi, C., 1980, Evaluation of deep temperatures of hydrothermal systems by a new gas geothermometer. Geochimica Cosmochimica Acta, v. 44, p. 549–556.

Edwards, R.L., Cheng, H., Murrell, M.T., and Goldstein, S.J., 1997, Protactinium-231 dating of carbonates by thermal ionization mass spectrometry: Implications for quaternary climate change. Science, v. 276, p. 782–786.

Fahlquist, L., and Janik, C.J., 1992, Procedures for collecting and analyzing gas samples from geothermal systems. U.S. Geological Survey, Open-File Report 92–211, 19 pp.

Fouillac, C., and Michard, G., 1981, Sodium-lithium ratios in water applied to geothermometry of geothermal reservoirs. Geothermics, v. 10, p. 55–70.

Fournier, R.O., 1981, Application of water geochemistry to geothermal exploration and reservoir engineering, in (Rybach, L., and Muffler, L.J.P., eds.) Geothermal Systems, Principals and Case Histories. Wiley, NY, p. 109–143.

Fournier, R.O., and Potter, R.W., 1979, Magnesium correction to the Na-K-Ca chemical geothermometer. Geochimica Cosmochimica Acta, v. 43, p. 1543–1550.

Fournier, R.O., and Truesdell, A.H., 1973, An empirical Na-K-Ca geothermometer for natural waters. Geochimica Cosmochimica Acta, v. 37, p. 1255–1275.

Gallup, D.L., 1998, Aluminum silicate scale formation and inhibition (2): Scale solubilities and laboratory and field inhibition tests. Geothermics, v. 27, p. 485–501.

Giggenbach, W.F., 1986, Graphical techniques for the evaluation of water/rock equilibration conditions by use of Na, K, Mg, and Ca contents of discharge waters. Proceedings 8th N.Z. Geothermal Workshop, Auckland, N.Z., University of Auckland, p. 37–43.

Giggenbach, W.F., 1992, Chemical techniques in geothermal exploration. UNITAR/UNDP, Rome, Italy, p. 119–144.

Goff, F., and Janik, C.J., 2000, Geothermal Systems, in (H. Sigurdsson, ed.) Encyclopedia of Volcanoes. Academic Press, San Diego, p. 817–834.

Goff, F., and McMurtry, G.M., 2000, Tritium and stable isotopes of magmatic waters. Journal of Volcanology and Geothermal Research, v. 97, p. 347–396.

Goff, F., Hulen, J., Adams, A., Trujillo, P., Counce, D., and Evans, W.C., 1994, Geothermal characteristics of some oil field waters in the Great Basin, Nevada, in (Schalla, R.A., and Johnson, E.H., eds.) Oil Fields of the Great Basin. Nevada Petroleum Society, Reno, Nevada, p. 93–106.

Goff. F., Janik, C.J., Bergfeld, D., Counce, D., Bruton, C., and Nimz, G., 1998, Geothermal chemistry/exploration investigations at Dixie Valley, Nevada. U.S. Department of Energy, Geothermal Program Review, Berkeley, California, 7 pp.

Goff, F., Bergfeld, D., Janik, C.J., Counce, D., and Stimac, J.A., 2001, Geochemical data on waters, gases, rocks, and sediments from The Geysers-Clear Lake region, California (1991-2000). Los Alamos National Laboratory Report LA-13882-MS, 40 pp.

Goguel, R., 1976, Thermal water transport of some major rock constituents at Wairakei. New Zealand Journal of Science, v. 19, p. 359–368.

Goguel, R., 1988, Ultratrace metal analysis of New Zealand geothermal waters by ICP-MS. Proceedings of the New Zealand Trace elements Group Conference, 30 Nov - 2 Dec, 1988, Lincoln College, Canterbury, NZ, p. 263–270.

Honjas, W., Pullammanappillil, S.K., Lettis, W., Plank, G.L., Louie, J., and Schweichert, R., 1997, Predicting subsurface structure within the Dixie Valley geothermal field, Dixie Valley, Nevada, using a non-linear optimization scheme. Geothermal Resources Council Bulletin, February, pp. 45–52.

Hudson, M.R., 1988, Paleomagnetic and structural evidence bearing on the tectonic history of a region surrounding Dixie Valley, west-central Nevada. Ph.D. dissertation, Colorado School of Mines, Golden, Colorado, 352 pp.

Hudson, M.R., and Geissman, J.Wm., 1984, Preliminary paleomagnetic data from the Jurassic Humboldt Lopolith, west-central Nevada: Evidence for thrust belt rotation in the Fencemaker allochthon. Geophysical Research Letters, v. 1., p. 828–831.

Hudson, M.R., and Geissman, J.W., 1991, Paleomagnetic evidence for the age and extent of middle Tertiary counterclockwise rotation, Dixie Valley region, west central Nevada. Journal of Geophysical Research, v. 96, p. 3979–4006.

Hulen, J. B., Goff, F., Bereskin, S. R., and Bortz, L. C., 1994, Geology and geothermal origin of Grant Canyon and Bacon Flat oil fields, Railroad Valley, Nevada: American Association of Petroleum Geologists Bulletin, v. 78, p. 596–623.

Janik, C.J., Goff, F., Sorey, M., Rytuba, J., Counce, D., Colvard, E., Huebner, M., White, L.D., and Foster, A., 1999, Physical, chemical, and isotopic data for samples from the Anderson Springs area, Lake County, California, 1998-1999. U.S. Geological Survey Open-File Report 99-585, 27 pp.

Kennedy, B.M., Janik, C., Benoit, D., and Shuster, D., 1999, Natural geochemical tracers for injectate fluids at Dixie Valley. Proceedings, 24th Workshop on Geothermal Reservoir Engineering, Stanford University Report SGP-TR-162, Stanford, California, p. 108–115.

Kharaka, Y. and Mariner, R., 1989, Chemical geothermometers and their application to formation waters from sedimentary basins, in (Naeser, N., and McCulloh, T., eds.) Thermal History of Sedimentary Basins: Methods and Case Histories. Springer-Verlag, Berlin, p. 99–177.

Lutz, S., Moore, J., and Benoit, D., 1997, Geologic framework of Jurassic reservoir rocks in the Dixie Valley geothermal field, Nevada: Implications from hydrothermal alteration and stratigraphy. Proceedings, 22nd Workshop on Geothermal Reservoir Engineering, Stanford University Report SGP-TR-155, Stanford, California, p. 131–139.

McKenzie, W.F., and Truesdell, A.H., 1977, Geothermal reservoir temperatures estimated from the oxygen isotope compositions of dissolved sulfate and water from hot springs and shallow drillholes. Geothermics, v. 5, p. 51–61.

Nimz, G., Janik, C., Goff, F., Dunlap, C., Huebner, M., Counce, D., and Johnson, S., 1999, Regional hydrology of the Dixie Valley geothermal field, Nevada: preliminary interpretations of chemical and isotopic data. Geothermal Resources Council Transactions, v. 23, p. 333–338.

Norman, D., and Bernhardt, C., 1981, Assessment of geothermal reservoirs by analysis of gases in thermal waters. Final Technical Report, New Mexico Energy Institute, New Mexico State University, Las Cruces, 130 pp.

Picket, D.A., and Murrell, M.T., 1997, Observations of ^{231}Pa/ ^{235}U disequilibrium in volcanic rocks. Earth and Planetary Science Letters, v. 148, p. 259–271.

Plank, G., Schweickert, R., Benoit, D., and Simmons, A., 1999, Influence of fault surface geometry on the location of the Dixie Valley geothermal area, Dixie Valley, Nevada. Proceedings, 24th Workshop on Geothermal Reservoir Engineering, Stanford University Report SGP-TR-162, Stanford, California, 8 pp.

Speed, R.C., 1976, Geologic map of the Humboldt Lopolith. Geological Society of America Map Chart Series MC-14, 1:81050 scale, 1 sheet.

Stamates, M., 2001, Evaluation of injection effects on the Dixie Valley, Nevada, geothermal reservoir through the use of geochemical data. M.S. thesis, University of Nevada, Reno, 198 pp.

Trujillo, P., Counce, D., Grigsby, C., Goff, F., and Shevenell, L., 1987, Chemical analysis and sampling techniques for geothermal fluids and gases at the Fenton Hill laboratory. Los Alamos National Laboratory, Report LA-11006-MS, 84 pp.

Urbani, F., 1986, GTHERM, a spreadsheet and graphic setup for geothermal exploration. Unpublished report, Los Alamos National Laboratory, 103 pp.

Waibel, A.F., 1987, An overview of the geology and secondary mineralogy of the high temperature geothermal system in Dixie Valley, Nevada. Geothermal Resources Council Transactions, v. 11, p. 479–486.

Werner, C., Janik, C.J., Goff, F., Counce, D., Johnson, L., Siebe, C., Delgado, H., Williams, S.N., and Fischer, T.P., 1997, Geochemistry of summit fumarole vapors and flanking thermal/mineral waters at Popocatépetl Volcano, Mexico. Los Alamos National Laboratory, Report LA-13289-MS, 33 pp.

Williams, C., Sass, J., and Grubb, F., 1997, Thermal signature of subsurface fluid flow in the Dixie Valley geothermal field, Nevada. Proceedings, 22nd Workshop on Geothermal Reservoir Engineering, Stanford University Report SGP-TR-155, Stanford, California, Jan. 27–29, 8 pp.

Table 1: Sample Types, Locations, Elevations, and Surface Rocks of Fluid Samples Collected for the Dixie Valley Geothermal Project, Nevada.

Name or Description	Map[a] Number	Map Figure	Latitude (±25 m)	Longitude (±25 m)	Elevation (±3 m)	USGS 1:100,000 Metric Quadrangle	Surface Rocks	Comments
Production Wells								
27-33 Well	25	2	39.9869	117.8307	1050	Edwards Creek Valley	Alluvium	Bottoms in quartzite/granodiorite
28-33 Well	30	2	39.9852	117.8318	1057	Edwards Creek Valley	Alluvium	Bottoms in quartzite/granodiorite
37-33 Well	29	2	39.9861	117.8312	1055	Edwards Creek Valley	Alluvium	Added in July 1997; quartzite/granodiorite
45-33 Well Archived	3	2	39.9897	117.8260	1051	Edwards Creek Valley	Alluvium	Bottoms in quartzite/granodiorite
63-7 Well	86	2	39.9650	117.8580	1059	Edwards Creek Valley	Alluvium	Bottoms in gabbro/quartzite/granodiorite
73-7 Well	11	2	39.9655	117.8576	1059	Edwards Creek Valley	Alluvium	Bottoms in gabbro/quartzite/granodiorite
73B-7 Well	23	2	39.9652	117.8555	1058	Edwards Creek Valley	Alluvium	Added in 1995; gabbro/quartzite/granodiorite
74-7 Well	14	2	39.9637	117.8580	1059	Edwards Creek Valley	Alluvium	Bottoms in gabbro/quartzite/granodiorite
76-7 Well (V104 Separator)	8	2	39.9590	117.8570	1055	Edwards Creek Valley	Alluvium	Bottoms in gabbro/quartzite/granodiorite
76A-7 Well (V104 Separator)	80	2	39.9590	117.8570	1055	Edwards Creek Valley	Alluvium	Redrilled in July 1993 from 7,498'
82A-7 Well	20	2	39.9675	117.8548	1056	Edwards Creek Valley	Alluvium	Bottoms in gabbro/quartzite/granodiorite
84-7 Well	13	2	39.9639	117.8582	1059	Edwards Creek Valley	Alluvium	Bottoms in gabbro/quartzite/granodiorite
V101 Separator	9	2	39.9869	117.8307	1046	Edwards Creek Valley	Alluvium	27-33, 28-33, and 37-33 wells
V102 + V103 Separator	16	2	39.9639	117.8582	1055	Edwards Creek Valley	Alluvium	63-7, 73-7, 74-7, and 84-7 wells
V105 Separator	18	2	39.9663	117.8537	1063	Edwards Creek Valley	Alluvium	73B-7 and 82A-7 wells
Injection Well/Power Plant Fluids								
25-5 Injection Well	34	2	39.9774	117.8498	1052	Edwards Creek Valley	Alluvium	
32-18 Injection Well	37	2	39.9534	117.8629	1057	Edwards Creek Valley	Alluvium	
41-18 Injection Well	208a	2	39.9535	117.8632	1055	Edwards Creek Valley	Alluvium	
45-5 Injection Well	4	2	39.9771	117.8494	1052	Edwards Creek Valley	Alluvium	
52-18 Injection Well	208b	2	39.9534	117.8629	1049	Edwards Creek Valley	Alluvium	
65-18 Injection Well	36	2	39.9469	117.8609	1048	Edwards Creek Valley	Alluvium	
Lamb 1 Injection Well	5	2	39.9542	117.8713	1061	Edwards Creek Valley	Alluvium	Aka SWL-1 well
Power Plant Fluids, Miscellaneous	2	2	39.9668	117.8562	1058	Edwards Creek Valley	Alluvium	
Other Geothermal and On-Site Water Wells								
Domestic Well	1	2	39.9658	117.8556	1052	Edwards Creek Valley	Alluvium/Alluvial Fan	Water supply well
Goerenger Well	39	2	39.9693	117.8591	1050	Edwards Creek Valley	Alluvium	Water supply well
27-32 Well (Dick's Well)	54	2	39.9862	117.8484	1064	Edwards Creek Valley	Alluvial Fan	Quartizte @ 122 m
32-6 Well	123	1	39.9984	117.8463	1115	Edwards Creek Valley	Alluvial Fan	Observation well
38-32 Well	168	2	39.9843	117.8470	1055	Edwards Creek Valley	Alluvial Fan	Observation well
45-W-5 Well	59	2	39.9702	117.8582	1052	Edwards Creek Valley	Alluvium	Observation well
45-14 Well	102	1	39.8659	118.0049	1040	Carson Sink	Alluvium	Bedrock contact @ 1830 m
46-32 Well (Stu's Well)	53	2	39.9881	117.8434	1061	Edwards Creek Valley	Alluvial Fan	Quartzite @ 87 m
62-21 Well	111	1	39.9328	117.8198	1050	Edwards Creek Valley	Alluvium	Penetrates tuff, gabbro, shale
66-21 Well	67	1	39.9311	117.9284	1040	Edwards Creek Valley	Alluvium/Alluvial Fan	Bottoms in Humboldt Lopolith
97-2 Well	122	1	39.9821	117.8406	1055	Edwards Creek Valley	Alluvial Fan	Monitor well; bottoms in alluvium
Dixie Jack Gradient Well #1	near 122	1	39.9884	117.8427	1058	Edwards Creek Valley	Alluvial Fan	In vicinity of 97-2 well

Table 1: Continued

Name or Description	Map[a] Number	Map Figure	Latitude (±25 m)	Longitude (±25 m)	Elevation (±3 m)	USGS 1:100,000 Metric Quadrangle	Surface Rocks	Comments
Dixie Jack Gradient Well #4	near 122	1	39.9852	117.8463	1057	Edwards Creek Valley	Alluvial Fan	In vicinity of 97-2 well
Dixie Jack Gradient Well #7	near 122	1	39.9874	117.8484	1063	Edwards Creek Valley	Alluvial Fan	In vicinity of 97-2 well
Background Springs								
Basalt Spring	178	1	39.5985	117.8814	2250	Edwards Creek Valley	Basalt	
Big Horn Spring	68	1	39.9081	117.9865	1045	Edwards Creek Valley	Alluvium near Gabbro	
Dago Spring	64	1	40.2137	117.8277	1505	Fish Creek Mts	Alluvium	
Dead Travertine Spring, Upper	56	1	39.9879	117.8929	1465	Edwards Creek Valley	Gabbro/Quartzite	Northeast margin, travertine deposit
Dead Travertine Spring, Road Seep	210	1	39.9457	117.8972	1290	Edwards Creek Valley	Gabbro/Quartzite	Along main road
Dixie Hot Spring	69	1	39.8004	118.0592	1040	Carson Sink	Alluvium	Hottest spring near main road
Edward Creek Spring	50	1	39.6819	117.6444	1555	Edwards Creek Valley	Alluvium/Alluvial Fan	
Fault Line Spring	60	1	40.0317	117.6297	1140	Fish Creek Mts	Alluvium/Alluvial Fan	
Horse Creek Spring	72	1	39.5238	118.0138	1560	Carson Sink	Welded Tuff	
Horse Heaven Spring	52	1	39.8348	117.7220	1400	Edwards Creek Valley	Alluvium/Welded Tuff	
Hyder Hot Spring	48	1	40.0035	117.7169	1080	Fish Creek Mts	Alluvium	Spring at summit of deposit
Jersey Hot Spring	128	1	40.1782	117.4958	1355	Fish Creek Mts	Alluvial Fan	
Kitten Spring	66	1	40.0550	117.9159	1730	Fish Creek Mts	Basalt	
Kyle Spring	63	1	40.1736	117.7842	1600	Fish Creek Mts	Quartzite	
Lofthouse Spring	169	1	39.7337	117.8312	1460	Edwards Creek Valley	Alluvium	
Lower Ranch, Main Hot Spring	61	1	40.0335	117.5981	1240	Fish Creek Mts	Alluvial Fan/Limestone	Northern-most and hottest spring
Lower Ranch, Upper Warm Spring	211	1	40.0355	117.6026	1250	Fish Creek Mts	Alluvial Fan/Limestone	On summit of deposit
McCoy Hot Spring	62	1	40.0795	117.6036	1135	Fish Creek Mts	Alluvium/Alluvial Fan	Near cattle guard
Mustang Spring	65	1	40.0879	117.8774	1560	Fish Creek Mts	Volcanic sandstone	
Not-So-OK Spring	170	1	39.7192	117.8143	1690	Edwards Creek Valley	Quartzite/Argillite	
Old Man Main Spring	51	1	39.8000	117.6660	1500	Edwards Creek Valley	Welded Tuff	South canyon wall
Old Man, Upper Spring	51	1	39.7962	117.6822	1560	Edwards Creek Valley	Alluvium	0.5 km upstream of main spring
Pine Spring	177	1	39.6069	117.8586	2260	Edwards Creek Valley	Welded Tuff/Basalt	
Sou Hot Springs, Trav. Cone	46	1	40.0888	117.7240	1140	Fish Creek Mts	Alluvial Fan/Tuff	Aka Seven Devils Springs
Sou Hot Springs	47	1	40.0890	117.7240	1140	Fish Creek Mts	Alluvial Fan/Tuff	Hottest spring, constant gas emission
Spring in Spring Canyon	131	1	40.1664	117.6701	1195	Fish Creek Mts	Lake Beds/Mafic Volc.	
Stu's Seep	106	1	39.9450	117.9318	1200	Edwards Creek Valley	Fractured Gabbro	
Upper Cherry Spring	179	1	39.5815	117.9439	2345	Edwards Creek Valley	Welded Tuff	
Upper Jersey Seep	129	1	40.1779	117.4891	1380	Fish Creek Mts	Travertine/Alluvium	
War Canyon Spring	176	1	39.5747	117.8551	1950	Edwards Creek Valley	Silicified Welded Tuff	
Wild Rose Spring	132	1	40.2952	117.7308	1580	Fish Creek Mts	Quartzite/Metavolcanics	
Background Wells								
Bernice Well	172	1	39.7706	117.8092	1340	Edwards Creek Valley	Alluvium	At building foundation
Bolivia Artesian Well	57	1	39.9977	117.9157	1480	Edwards Creek Valley	Gabbro/Limestone	Iron hydroxide; flows into creek
Brinkerhoff Well	116	1	40.0849	117.6790	1120	Fish Creek Mts	Alluvium	Agricultrual well

Table 1: Continued

Name or Description	Map[a] Number	Map Figure	Latitude (±25 m)	Longitude (±25 m)	Elevation (±3 m)	USGS 1:100,000 Metric Quadrangle	Surface Rocks	Comments
Hole in the Wall #2 Well	49	1	39.8888	117.5562	1345	Edwards Creek Valley	Alluvium near Tuff	Abandoned wind mill
Flowing well @ AA Tank	70	1	39.7041	118.0592	1040	Carson Sink	Alluvium	In Dixie Valley Settlement
Shaw Well	71	1	39.6812	118.0503	1048	Carson Sink	Alluvium	In Dixie Valley Settlement
Unnamed Irrigation Well	115	1	40.0986	117.6450	1125	Fish Creek Mts	Alluvium	Agricultrual well
Background Streams and Rain								
Bernice Creek	173	1	39.7672	117.7897	1450	Edwards Creek Valley	Quartzite/Argillite	At Antimony King Mine
Bucher Creek	130	1	40.1792	117.4913	1375	Fish Creek Mts	Alluvial Fan	
Cedar Canyon Wash	127	1	40.1355	117.4791	1480	Fish Creek Mts	Lake Beds/Welded Tuff	
Cottonwood Creek, Lower	110	1	39.9763	117.8808	1189	Edwards Creek Valley	Gabbro/Quartzite	
Cottonwood Creek, Middle	58	1	39.9922	117.9128	1420	Edwards Creek Valley	Gabbro/Limestone	
Dixie Salt Lake	213	1	39.8542	118.0000	1030	Carson Sink	Alluvium	
Home Station Wash	126	1	40.1268	117.5117	1240	Fish Creek Mts	Welded Tuff	
Hoyt Creek	174	1	39.7817	117.7897	1435	Edwards Creek Valley	Argillite/Shale	
Mt. Augusta Creek	180	1	39.5679	117.9229	2350	Edwards Creek Valley	Welded Tuff	
Not-So-OK Creek	171	1	39.7101	117.8119	1700	Edwards Creek Valley	Argillite	
Rain, Lizard Well Tank	125	1	39.9352	117.7189	1140	Edwards Creek Valley	Alluvium/Alluvial Fan	
Unnamed Creek by Stu's Seep	107	1	39.9456	117.9317	1200	Edwards Creek Valley	Fractured Gabbro	Below waterfall
Unnamed Stream (east of 121)	119	1	39.8996	117.9953	1065	Edwards Creek Valley	Welded Tuff/Gabbro	
White Rock Canyon	121	1	39.8982	118.0180	1200	Carson Sink	Welded Tuff/Gabbro	
Fumaroles								
Calcite Fumarole, Senator area	109	2	39.9924	117.8537	1152	Edwards Creek Valley	Faulted Quartzite	Coarse calcite crystals; some sulfur
Crack 4 Fumarole near Stu's Well	43	2	39.9872	117.8432	1050	Edwards Creek Valley	Alluvial Fan	Recent ground crack; some alteration
Figure 8 Fumarole NE of Senator[b]	181	2	40.0025	117.8424	1143	Fish Creek Mts	Faulted Limestone and Fan	Weak vent; minor alteration
Lonely Fumarole SW of Senator	167	2	39.9915	117.8549	1134	Edwards Creek Valley	Faulted Alluvial Fan	Some sulfur
Range Front Fumarole, Senator area	45	2	39.9947	117.8539	1158	Edwards Creek Valley	Faulted Quartzite	Much sulfur
Senator Fumarole	44	2	39.9945	117.8520	1158	Edwards Creek Valley	Faulted Quartzite and Fan	Main vent; much sulfur
South Bench Fumarole, Senator area	166	2	39.9940	117.8546	1220	Edwards Creek Valley	Faulted Quartzite	Much sulfur
Unnamed Fumarole #1	105	1	39.9541	117.9172	1120	Edwards Creek Valley	Faulted Gabbro	Weak vent; 0.6 km NE of Stu's Seep
Unnamed Fumarole #2	212	1	39.9552	117.9159	1130	Edwards Creek Valley	Faulted Alluvial Fan	Weak vent; 1 km NE of Stu's Seep

[a] Locations are shown on Figures 1 and 2.

[b] Two samples listed on succeeding tables were mistakenly labeled 181; DV98-181 (Figure 8 Fumarole) and DV99-181 (Goerenger Well). Figure 8 Fumarole uses map number 181.

Table 2: Field Parameters for Various Geothermal and Regional Waters in the Dixie Valley Region, Nevada.

Sample No.	Name or Description	Date	Sampling Temp. (˚C)	Sampling Press. (psig)	Steam Fraction (y)	pH^a (field)	Alkalinity (ppm)	Conduc. (micromhos)	Eh (mV)	Eh Temp. (˚C)	Comments
Production Well Brines											
DIXE102-W	V102 + V103 Separator	10/02/95	---	---	0.153	---	---	---	---	---	Sample provided by L. Shevenell, Univ. Nevada-Reno
DV96-8	76-7 Well	10/25/96	163	110.0	0.184	9.00	137	2800	-75	18.7	Brine flow = about 520,000 lb/h; BHT = 249°C
DV96-9	V101 Separator	10/25/96	166	158.0	0.159	8.92	185	2800	-148	31.1	Brine flow = 1,280,000 lb/h
DV97-11	73-7 Well	10/29/97	---	85.4	0.158	8.98	178	2600	-298	15	Total flow = about 450,000 lb/h
DV97-13	84-7 Well	10/29/97	---	85.5	0.159	9.01	200	2600	-309	16.5	Total flow = about 200,000 lb/h; from 2500 m
DV97-14	74-7 Well	10/29/97	---	83.8	0.163	8.84	236	2700	-300	18.4	Total flow = about 650,000 lb/h
DV97-16	V102 + V103 Separator	10/29/97	---	82.2	0.161	8.77	184	2800	-274	27.7	Brine flow = 1,212,000 lb/h
DV97-18	V105 Separator	10/29/97	---	108.0	0.151	8.68	172	3300	-250	34	Brine flow = 1,312,000 lb/h
DV97-20	82A-7 Well	10/29/97	---	85.0	0.159	9.00	186	2400	-286	17	Total flow = about 600,000 lb/h
DV97-23	73B-7 Well	10/30/97	---	86.0	0.160	9.10	186	2900	-218	20	
DV97-25	27-33 Well	10/30/97	---	97.0	0.157	8.77	222	2300	-282	19.8	Gas in line; poor separation
DV97-26	V101 Separator	10/30/97	---	148.0	0.164	8.82	188	2600	-328	17.7	
DV97-29	37-33 Well	10/30/97	---	96.6	0.159	8.77	200	2600	-215	34.6	New well as of July 1997
DV97-30	28-33 Well	10/30/97	---	101.6	0.156	8.84	182	2500	-272	33.4	
DV98-73	V101 Separator	04/28/98	160	97.0	0.157	8.47	192	2900	-331	56	
DV98-75	27-33 Well	04/28/98	---	104.0	0.155	8.49	173	2600	-319	30	
DV98-77	37-33 Well	04/28/98	165	99.6	0.156	8.39	166	2800	-311	48	
DV98-79	28-33 Well	04/28/98	168	100.0	0.157	8.82	180	2300	-313	24	
DV98-80	76A-7 Well	04/28/98	---	88.5	0.157	8.66	160	2700	-308	31.2	
DV98-82	V102 + V103 Separator	04/28/98	---	87.3	0.150	8.53	146	2900	-310	30	
DV98-84	74-7 Well	04/28/98	---	89.8	0.158	8.63	160	2400	-311	26.2	
DV98-86	63-7 Well	04/28/98	---	88.8	0.154	8.62	150	2500	-280	23.9	
DV98-88	73-7 Well	04/29/98	---	90.5	0.154	8.63	158	2900	-303	25	
DV98-90	82A-7 Well	04/29/98	---	90.6	0.153	8.85	170	2600	-285	24.2	
DV98-92	V105 Separator	04/29/98	---	86.5	0.150	8.74	165	2800	-295	36	
DV98-95	73B-7 Well	04/29/98	174	92.5	0.152	8.73	156	2300	-296	31.1	
DV98-133	27-33 Well	10/20/98	---	94.0	---	8.57	---	---	---	---	Backflow from separator; BHT = 243°C
DV98-135	27-33 Well	10/20/98	---	52.0	0.184	8.77	---	---	---	---	Off line
DV98-138	V101 Separator	10/21/98	---	151.2	0.160	8.78	---	---	---	---	
DV98-140	37-33 Well	10/21/98	---	90.0	0.162	8.82	194	---	---	---	
DV98-141	28-33 Well	10/21/98	---	108.0	0.162	8.84	190	---	---	---	BHT = 246°C
DV98-145	76A-7 Well	10/22/98	---	112.0	0.158	8.50	192	---	---	---	
DV98-147	63-7 Well	10/22/98	---	87.2	0.155	8.60	192	---	---	---	BHT = 241°C
DV98-148	V102 + V103 Separator	10/22/98	166	---	0.164	8.58	174	---	---	---	
DV98-150	74-7 Well	10/22/98	---	---	0.160	8.71	170	---	---	---	BHT = 244°C
DV98-152	73-7 Well	10/22/98	---	93.0	0.154	8.53	168	---	---	---	
DV98-154	73B-7 Well	10/22/98	---	96.0	0.154	8.89	160	---	---	---	
DV98-156	82A-7 Well	10/23/98		---	0.154	8.85	190	---	---	---	BHT = 241°C
DV98-159	V105 Separator	10/23/98	143?	110.5	0.146	8.79	198	---	---	---	
DV99-182	76A-7 Well	05/04/99	---	92.0 psi WH	0.152	9.27	155	---	-70	21.7	
DV99-184	74-7 Well	05/04/99	---	85.5	0.160	9.55	162	---	-170	19.4	
DV99-186	V102 + V103 Separator	05/04/99	---	83.5 psi	0.137	9.12	159	---	-228	56.6	
DV99-188	63-7 Well	05/04/99	---	90.0	0.152	9.44	168	---	-178	18.9	
DV99-190	73-7 Well	05/04/99	---	88.0	0.154	9.21	141	---	-172	39.4	
DV99-194	V105 Separator	05/05/99	---	83.8 psi	0.138	8.74	138	---	387?	62.4	
DV99-196	82A-7 Well	05/05/99	---	87.8	0.152	8.86	148	---	-151	56.3	

Table 2: Continued

Sample No.	Name or Description	Date	Sampling Temp. (°C)	Sampling Press. (psig)	Steam Fraction (y)	pH^a (field)	Alkalinity (ppm)	Conduc. (micromhos)	Eh (mV)	Eh Temp. (°C)	Comments
DV99-197	73B-7 Well	05/05/99	---	80.5	0.159	9.48	150	---	-190	30.7	
DV99-199	37-33 Well	05/05/99	---	93.7	0.160	9.21	207	---	-437	43.1	
DV99-200	28-33 Well	05/05/99	---	97.0	0.159	8.98	193	---	-413	59.7	
DV99-204	V101 Separator	05/05/99	---	92.5	0.159	9.04	198	---	-422	42.6	
DV74782786-brine 2	74-7 Well Archived	08/27/86	---	---	0.199	---	---	---	---	---	Archived brine sample analyzed by LANL
DV76781986-brine 4	76-7 Well Archived	08/19/86	---	---	0.187	---	---	---	---	---	Archived brine sample analyzed by LANL
DV453382186-brine 6	45-33 Well Archived	08/21/86	---	---	0.165	---	---	---	---	---	Archived brine sample analyzed by LANL
DV73782886-brine 8	73-7 Well Archived	08/28/86	---	---	0.198	---	---	---	---	---	Archived brine sample analyzed by LANL
DV321882686-brine 10	32-18 Well Archived	08/26/86	---	---	---	---	---	---	---	---	Archived brine sample analyzed by LANL
DV651882686-brine 12	65-18 Well Archived	08/26/86	---	---	---	---	---	---	---	---	Archived brine sample analyzed by LANL
No number	28-33 Well Archived	09/23/93	---	---	0.158	---	---	---	---	---	Warm aquifer ~1,200' from liner hanger
Production Well Condensates											
DIXE102-S	V102 + V103 Separator	10/02/95	---	---	---	---	---	---	---	---	Sample provided by L. Shevenell, Univ. Nevada-Reno
DV96-7	76-7 Well	10/25/96	163	110	---	6.68	45	---	-17.8	61.6	Steam flow = 115,000 lb/h
DV96-10	V101 Separator	10/25/96	166	158	---	---	---	---	---	---	Steam flow = 250,000 lb/h
DV97-12	73-7 Well	10/29/97	---	85.4	---	---	---	---	---	---	Brine carry over in sample
DV97-15	74-7 Well	10/29/97	---	83.8	---	---	---	---	---	---	
DV97-17	V102 + V103 Separator	10/29/97	---	80.2	---	---	---	---	---	---	Steam flow = 230,000 lb/h
DV97-19	V105 Separator	10/29/97	---	81.3	---	---	---	---	---	---	Steam flow = 227,000 lb/h
DV97-21	82A-7 Well	10/29/97	---	84.7	---	---	---	---	---	---	
DV97-22	73B-7 Well	10/29/97	---	84	---	---	---	---	---	---	
DV97-24	V101 Separator	10/30/97	---	90.6	---	---	---	---	---	---	
DV97-27	27-33 Well	10/30/97	---	97	---	---	---	---	---	---	
DV97-28	37-33 Well	10/30/97	---	96.6	---	---	---	---	---	---	New well as of July 1997
DV97-31	28-33 Well	10/30/97	167.2	---	---	---	---	---	---	---	From mini-sep @ wellhead
DV98-74	V101 Separator	04/28/98	160	104	---	---	---	---	---	---	
DV98-76	27-33 Well	04/28/98	---	104	---	---	---	---	---	---	
DV98-78	37-33 Well	04/28/98	---	99.5	---	---	---	---	---	---	
DV98-81	76A-7 Well	04/28/98	---	88.5	---	---	---	---	---	---	
DV98-83	V102 + V103 Separator	04/28/98	---	87.25	---	---	---	---	---	---	
DV98-85	74-7 Well	04/28/98	---	88.7	---	---	---	---	---	---	
DV98-87	63-7 Well	04/28/98	---	88.8	---	---	---	---	---	---	
DV98-89	73-7 Well	04/29/98	---	90.5	---	---	---	---	---	---	Brine carry over in sample
DV98-91	82A-7 Well	04/29/98	---	89.8	---	---	---	---	---	---	Brine carry over in sample
DV98-93	V105 Separator	04/29/98	---	86.5	---	---	---	---	---	---	
DV98-94	73B-7 Well	04/29/98	174	90.5	---	---	---	---	---	---	
DV98-101	28-33 Well	04/30/98	168	99.5	---	---	---	---	---	---	
DV98-136	27-33 Well	10/20/98	---	94	---	---	---	---	---	---	Off line
DV98-137	V101 Separator	10/21/98	---	83	---	---	---	---	---	---	
DV98-139	37-33 Well	10/21/98	---	89.1	---	---	---	---	---	---	
DV98-142	28-33 Well	10/21/98	---	89.2	---	---	---	---	---	---	
DV98-144	76A-7 Well	10/22/98	---	83.3	---	---	---	---	---	---	
DV98-146	V102 + V103 Separator	10/22/98	---	82.7	---	---	---	---	---	---	
DV98-149	63-7 Well	10/22/98	---	87.2	---	---	---	---	---	---	BHT = 241°C
DV98-151	74-7 Well	10/22/98	---	85.4	---	---	---	---	---	---	
DV98-153	73-7 Well	10/22/98	---	87.5	---	---	---	---	---	---	Brine carry over in sample

Table 2: Continued

Sample No.	**Name or Description**	**Date**	**Sampling Temp. (°C)**	**Sampling Press. (psig)**	**Steam Fraction (y)**	**pH[a] (field)**	**Alkalinity (ppm)**	**Conduc. (micromhos)**	**Eh (mV)**	**Eh Temp. (°C)**	**Comments**
DV98-155	73B-7 Well	10/22/98	---	87.4	---	---	---	---	---	---	Brine carry over in sample
DV98-157	82A-7 Well	10/23/98	---	86.5	---	---	---	---	---	---	Brine carry over in sample
DV98-158	V105 Separator	10/23/98	163?	84.5	---	---	---	---	---	---	
DV99-183	76A-7 Well	05/04/99	---	---	---	---	---	---	---	---	
DV99-185	74-7 Well	05/04/99	---	---	---	---	---	---	---	---	Brine carry over in sample
DV99-187	V102 + V103 Separator	05/04/99	---	---	---	---	---	---	---	---	
DV99-189	63-7 Well	05/04/99	---	87.3	---	---	---	---	---	---	
DV99-191	73-7 Well	05/04/99	---	88	---	---	---	---	---	---	Brine carry over in sample
DV99-192	73B-7 Well	05/04/99	---	87	---	---	---	---	---	---	Brine carry over in sample
DV99-193	V105 Separator	05/05/99	---	---	---	---	---	---	---	---	
DV99-195	82A-7 Well	05/05/99	---	86.5	---	---	---	---	---	---	Brine carry over in sample
DV99-201	28-33 Well	05/05/99	---	96.7	---	---	---	---	---	---	
DV99-202	37-33 Well	05/05/99	---	96	---	---	---	---	---	---	
DV99-203	V101 Separator	05/05/99	---	90	---	---	---	---	---	---	
DV74782786-cond 1	74-7 Well Archived	08/27/86	---	---	---	---	---	---	---	---	Archived condensate sample analyzed by LANL
DV76781986-cond 3	76-7 Well Archived	08/19/86	---	---	---	---	---	---	---	---	Archived condensate sample analyzed by LANL
DV453382886-cond 5	45-33 Well Archived	08/28/86	---	---	---	---	---	---	---	---	Archived condensate sample analyzed by LANL
DV73782886-cond 7	73-7 Well Archived	08/28/86	---	---	---	---	---	---	---	---	Archived condensate sample analyzed by LANL
DV321882686-cond 9	32-18 Well Archived	08/26/86	---	---	---	---	---	---	---	---	Archived condensate sample analyzed by LANL
DV651882686-cond 11	65-18 Well Archived	08/26/86	---	---	---	---	---	---	---	---	Archived condensate sample analyzed by LANL
Injection Well/Power Plant Fluids											
DV96-2	Condensate from plant	10/24/96	41.8	---	---	6.28	7	300	363	37.9	Mix of condensate, raw steam, minor NaOH
DV96-3	LP brine @ plant	10/24/96	110	---	---	9.31	184	2700	-135	29.3	Low-pressure spent brine
DV96-4	45-5 Injection Well	10/24/96	107	10.5	---	8.77	180	---	-145	66	Spent brine + condensed steam; rate = 4,500 gpm
DV96-5	Lamb 1 Injection Well	10/24/96	107	14	---	8.99	184	---	-120	46.5	Pure spent brine; rate = 475 gpm
DV96-6	65-18 Injection Well	10/24/96	>60	---	---	8.67	198	2800	-145	55	Pure spent brine
DV97-32	Condensate from plant	10/31/97	40	---	---	---	---	---	---	---	From reinjection line
DV97-33	LP brine @ plant	10/31/97	107.2	38	---	9	204	3100	-267	35	From reinjection line
DV97-34	25-5 + 45-5 injectate	10/31/97	104.4	80	---	9.14	186	2700	-160	25.7	Brine + cond, well mixed
DV97-35	25-5 + 45-5 injectate	10/31/97	99.7	9	---	8.93	164	3100	-246	43.9	Line by N injection wells 25-5 & 45-5
DV97-36	65-18 Injection Well	10/31/97	108	27	---	8.95	196	3200	-185	45	Pure spent brine
DV97-37	32-18 Injection Well	10/31/97	102	---	---	9.07	210	3000	-225	35.8	
DV97-40	LP brine @ plant	10/31/97	---	100	---	8.97	178	3100	-245	40.1	
DV97-41	Condensate from plant	10/31/97	27.8	---	---	---	---	---	---	---	At cooling tower
DV97-42	High press. brine @ plant	10/31/97	---	89.4	---	8.86	195	2300	-172	25.3	North line above LP separators
DV98-97	Condensate from plant	04/29/98	41.0	---	---	6.29	---	---	---	---	From "hot well" line; sent to 65-18 injector
DV98-98	LP brine @ plant	04/29/98	110	94	---	9.07	166	2400	-307	35.7	Flow rate = 9,000 gpm
DV98-143	25-5 Injection Well	10/21/98	---	13.2	---	8.88(6.1)	190	---	---	---	LP brine
DV98-161	Condensate from plant	10/23/98	40.4	---	---	5.5	---	---	---	---	From "hot well" line
DV98-162	LP Brine @ Plant	10/23/98	100	100	---	9.29(27.2)	216	---	---	---	
DV98-163	65-18 Injection Well	10/23/98	>30	---	---	7.20	182	---	---	---	Injection Manifold Total fluid
DV99-198	65-18 Injection Well	05/05/99	---	---	---	7.4	174	---	181	31.4	
DV99-205	25-5 + 45-5 Injectate	05/06/99	---	12 psi WH	---	9.31(25.2)	214	---	341	39.9	
DV99-206	LP Brine @ Plant	05/06/99	---	---	---	9.32(27.9)	170	---	-89	48	
DV99-207	Condensate from plant	05/06/99	---	---	---	6.67	37	---	52	38.6	From "hot well" line
DV99-208	52-18 + 41-18 Injectate	05/06/99	---	---	---	9.08(15.0)	166	---	-108	51.4	

Table 2: Continued

Sample No.	Name or Description	Date	Sampling Temp. (°C)	Sampling Press. (psig)	Steam Fraction (y)	pH[a] (field)	Alkalinity (ppm)	Conduc. (micromhos)	Eh (mV)	Eh Temp. (°C)	Comments
Other Geothermal and On-Site Water Wells											
DV96-1	Domestic Well	10/24/96	34.2	---	---	---	---	---	---	---	
DV97-38	Domestic Well	10/31/97	29.2	---	---	7.46	244	1100	91.5	26.9	
DV97-39	Goerenger Well	10/31/97	27.8	---	---	7.13	312	1600	91.7	27.8	Depth = 73 m; cased to 67 m
DV97-53	46-32 Well	11/05/97	155	23	---	---	---	---	---	---	Depth = 101 m; static press. = 45 psig
DV97-54	27-32 Well	11/05/97	144	55	---	---	---	---	---	---	Depth = 296 m; static press. = 80 psig
DV97-55	27-32 Well	11/05/97	166	55	0.054	5	---	---	---	---	Producing fractures @ 148 m depth
DV97-59	45-W-5 Well	11/05/97	26.4	---	---	7.5	---	---	---	---	Depth = 6.9 m
DV97-67	66-21 Well	11/07/97	55.5	---	---	5.5	---	---	---	---	Artesian flow = 7 l/min; depth = 2,988 m
DV98-96	Goerenger Well	04/29/98	28.3	---	---	6.95	300	1500	249	27	Flow = 965 gpm, pumped; depth = 73 m
DV98-99	27-32 Well	04/29/98	---	47	---	---	---	---	---	---	Static press. = 62 psig
DV98-100	46-32 Well	04/29/98	---	10	---	---	---	---	---	---	Static press. = 13 psig
DV98-102	45-14 Well	04/30/98	123.5	---	---	---	---	---	---	---	Depth = 2440 m; condensate sampled w/ minisep.
DV98-103	45-14 Well	04/30/98	125	---	---	6.95	---	2350	---	---	Brine sampled w/ minisep.
DV98-104	66-21 Well	04/30/98	57.4	---	---	5.65	---	---	---	---	Sporadic artesian flow = 4 l/min
DV98-111	62-21 Well	05/01/98	75.5	---	---	6.85	436	2600	180	40	Depth = 3810 m; BHT = 190°C; flow = 36 gpm
DV98-122	97-2 Well	05/05/98	19.7	---	---	7.65	---	---	---	---	Depth = 61 m; no flow
DV98-123	32-6 Well	05/06/98	32	---	---	---	---	---	---	---	Depth = 152 m; flow 0 to 150 gpm
Dixie Jack #1	Gradient Well DJ #1	05/17/98	49	---	---	---	---	---	---	---	From 76 m depth during drilling and circulation
Dixie Jack #4	Gradient Well DJ #4	05/20/98	77	---	---	---	---	---	---	---	Artesian flow = 7 gpm @ 67 m depth
Dixie Jack #7	Gradient Well DJ #7	05/14/98	55	---	---	---	---	---	---	---	From 53 m depth during drilling; steam @ 61 m
DV98-160	Goerenger Well	10/23/98	26.7	90	---	7.64	296	---	---	---	Flow = 620 gpm pumped
DV98-168	38-32 Well	10/26/98	87.7	---	---	---	---	---	---	---	Depth to water = 9.1 m
DV98-175[b]	62-21 Well	10/28/98	11.5	---	---	6.0	---	---	---	---	Production @ 2,440 to 2,900 m; from gabbro
DV99-181[c]	Goerenger Well	05/04/99	27.7	68 psi	---	7.33	280	---	460	27.7	
Background Springs											
DV97-46	Sou Hot Spring	11/03/97	57.0	---	---	7.2	---	---	---	---	Pool in large travertine cone; no observed flow
DV97-47	Sou Hot Spring	11/03/97	72.6	---	---	7.0	---	---	---	---	Hottest spring with gas; flow = 4 l/min
DV97-48	Hyder Hot Spring	11/03/97	76.7	---	---	6.3	---	---	---	---	Summit of deposit; flow = 8 l/min (120 l/min total)
DV97-50	Edward Creek Spring	11/04/97	13.7	---	---	6.5	---	---	---	---	From broken corral; flow = 1 l/min
DV 97-51a	Old Man Spring, Upper	11/04/97	---	---	---	---	---	---	---	---	Isotope sample only; seep
DV 97-51b	Old Man Main Spring	11/04/97	10.8	---	---	6.5	---	---	---	---	Flow = 0.5 l/min
DV97-52	Horse Heaven Spring	11/04/97	13.2	---	---	6.0	---	---	---	---	Flow = 0.5 l/min
DV97-56	Dead Travertine Spring	11/05/97	17.4	---	---	6.5	---	---	---	---	Seep
DV97-60	Fault Line Spring	11/06/97	28.8	---	---	7.0	---	---	---	---	Flow = at least 2 l/min
DV97-61	Lower Ranch Hot Spring	11/06/97	40.8	---	---	7.0	---	---	---	---	Northern-most hottest spring; flow ≥120 l/min
DV97-62	McCoy Hot Spring	11/06/97	46.2	---	---	7.0	---	---	---	---	Flow ≥50 l/min
DV97-63	Kyle Spring	11/06/97	19.8	---	---	7.5	---	---	---	---	Flow = 30 l/min
DV97-64	Dago Spring	11/06/97	13.8	---	---	6.8	---	---	---	---	Flow = 1 l/min
DV97-65	Mustang Spring	11/06/97	14.2	---	---	6.5	---	---	---	---	Flow = 25 l/min
DV97-66	Kitten Spring	11/06/97	16.4	---	---	6.5	---	---	---	---	Flow = 5 l/min
DV97-68	Big Horn Spring	11/07/97	20.5	---	---	6.8	---	---	---	---	Flow = 1 l/min
DV97-69	Dixie Hot Spring	11/07/97	81.6	---	---	7.2	---	---	---	---	Hottest spring near road; flow = 10 l/min
DV97-72	Horse Creek Spring	11/07/97	14.4	---	---	6.2	---	---	---	---	Flow = 1 l/min
DV98-106	Stu's Seep	04/30/98	17.2	---	---	7.0	---	---	---	---	Seep
DV98-112	Hyder Hot Spring	04/30/98	75.3	---	---	6.44	---	---	---	---	Summit of deposit; flow ≥40 l/min

Table 2: Continued

Sample No.	Name or Description	Date	Sampling Temp. (°C)	Sampling Press. (psig)	Steam Fraction (y)	pH[a] (field)	Alkalinity (ppm)	Conduc. (micromhos)	Eh (mV)	Eh Temp. (°C)	Comments
DV98-113	Lower Ranch Hot Spring	05/04/98	40.4	---	---	7.05	---	---	---	---	Northern-most hottest spring; flow = 100 l/min
DV98-114	McCoy Hot Spring	05/04/98	46.0	---	---	7.05	---	---	---	---	Flow not measured
DV98-117	Sou Hot Spring	05/04/98	72.0	---	---	6.46	---	---	---	---	Hottest spring with gas; flow = 4 l/min
DV98-118	Big Horn Spring	05/04/98	18.1	---	---	7.35	---	---	---	---	Seep
DV98-120	Dixie Hot Spring	05/05/98	83.5	---	---	8.14	---	---	---	---	Hottest spring near road; flow = 10 l/min
DV98-128	Jersey Hot Spring	05/05/98	59.0	---	---	7.0	---	---	---	---	Flow = 200 l/min
DV98-129	Upper Jersey Seep	05/06/98	17.5	---	---	7.0	---	---	---	---	Seep
DV98-131	Spring in Spring Canyon	05/06/98	14.0	---	---	7.0	---	---	---	---	Flow = 1 l/min
DV98-132	Wild Rose Spring	05/07/98	8.0	---	---	6.5	---	---	---	---	Flow = 20 l/min
DV98-169	Lofthouse Spring	05/07/98	14.8	---	---	6.5	---	---	---	---	Flow = 8 l/min
DV98-170	Not-So-OK Spring	10/27/98	10.0	---	---	6.5	---	---	---	---	Flow = 4 l/min
DV98-176	War Canyon Spring	10/27/98	11.2	---	---	6.5	---	---	---	---	Flow = 1 l/min
DV98-177	Pine Spring	10/28/98	8.6	---	---	6.8	---	---	---	---	Flow = 20 l/min
DV98-178	Basalt Spring	10/28/98	8.4	---	---	6.5	---	---	---	---	Flow = 2 l/min
DV98-179	Upper Cherry Spring	10/28/98	7.4	---	---	6.5	---	---	---	---	Flow = 4 l/min
DV99-209	Dead Travertine Spring	05/07/99	19.2	---	---	6.7	---	---	---	---	Seep
DV99-210	Dead Travertine, road seep	05/08/99	19-22	---	---	7.5	---	---	---	---	Seep
DV99-211	Lower Ranch, upper spring	05/09/99	39.4	---	---	6.8	---	---	---	---	Flow = 10 l/min
Background Wells											
DV97-49	Hole in the Wall #2 Well	11/04/97	13.7	---	---	6.0	---	---	---	---	Unused well at abandoned wind mill
DV97-57	Bolivia Artesian Well	11/05/97	28.8	---	---	7.0	---	---	---	---	Flow = 40 l/min
DV97-70	Flowing well @ AA Tank	11/07/97	16.7	---	---	6.2	---	---	---	---	Flow = 5 l/min
DV97-71	Shaw Well	11/07/97	19.2	---	---	7.0	---	---	---	---	Flow >60 l/min
DV98-115	Irrigation Well	05/04/98	17.8	---	---	7.36	---	---	---	---	Flow ≤100 gpm pumped
DV98-116	Brinkerhoff Well	05/04/98	16.8	---	---	7.29	---	---	---	---	Pumped; flow unknown
DV98-172	Bernice Well	10/27/98	16.5	---	---	6.8	---	---	---	---	Unused well at building foundation
Background Streams and Rain											
DV97-58	Cottonwood Creek	11/05/97	14.0	---	---	7.0	---	---	---	---	Flow moderated but not measured
DV98-107	Unnamed Ck by Stu's Seep	04/30/98	16.2	---	---	8.0	---	---	---	---	Below waterfall; flow moderate but not measured
DV98-110	Cottonwood Creek	05/01/98	20.2	---	---	8.0	---	---	---	---	Flow large but not measured
DV98-119	Unnamed Stream	05/05/98	23.4	---	---	8.50	---	---	---	---	Flow roughly 200 l/min
DV98-121	White Rock Canyon	05/05/98	14.3	---	---	8.80	---	---	---	---	Flow roughly 300 l/min
DV98-125	Rain, Lizard Well Tank	05/06/98	15.0	---	---	---	---	---	---	---	
DV98-126	Home Station Wash	05/06/98	19.6	---	---	6.2	---	---	---	---	Flow roughly 2400 l/min (just rained)
DV98-127	Cedar Canyon Wash	05/06/98	18.6	---	---	6.5	---	---	---	---	Flow roughly 1600 l/min (just rained)
DV98-130	Bucher Creek	05/06/98	15.0	---	---	---	---	---	---	---	Flow roughly 200 l/min
DV98-171	Not-So-OK Creek	10/27/98	10.0	---	---	6.8	---	---	---	---	Flow roughly 120 l/min
DV98-173	Bernice Creek	10/27/98	13.4	---	---	7.2	---	---	---	---	At Antimony King Mine; flow roughly 120 l/min
DV98-174	Hoyt Creek	10/27/98	12.8	---	---	8.5	---	---	---	---	Flow = 20 l/min
DV98-180	Mt. Augusta Creek	10/28/98	8.0	---	---	6.5	---	---	---	---	Flow roughly 100 l/min
DV99-213	Dixie Salt Lake	05/10/99	19.2	---	---	8.2	---	---	---	---	Near Dixie Hot Spring; salty precipitates

[a] Two significant figures means pH was measured with paper; three significant figures means pH was measured with meter; number in parantheses gives hydroxide concentration in ppm (if measured).

[b] This temperature was obtained during nonflowing conditions; see DV98-111.

[c] Two samples were mistakenly labeled 181; DV98-181 (Figure 8 Fumarole) and DV99-181 (Goerenger Well).

Table 3: Analytical Methods Used for Water and Gas Analyses. Detection Limits (DLs) are in ppm unless noted.[a]

Methods For Waters						
Analyte	Method	DL	Method	DL	Method	DL
Ag	GFAA	0.0005	ICP-AES	0.002		
Al	GFAA	0.002	ICP-AES	0.01		
Alkalinity	Calculation					
As	Hydride-AA	0.0002	GFAA	0.002	ICP-AES	0.05
Au	GFAA	0.002	ICP-AES	0.02		
B	ICP-AES	0.002				
Ba	ICP-AES	0.002				
Be	ICP-AES	0.002				
Br	IC	0.005				
Ca	ICP-AES	0.002				
Cd	GFAA	0.0002	ICP-AES	0.005		
Cl	IC	0.01				
Co	GFAA	0.002	ICP-AES	0.01		
$CO_3/HCO_3/OH$	Titration	0.5				
Conductivity	Electrode	0.5				
Cr	GFAA	0.002	ICP-AES	0.01		
Cs	GFAA	0.002	AA	0.02		
Cu	GFAA	0.002	ICP-AES	0.01		
Eh	Electrode (in field)					
F	IC	0.01	Electrode	0.01		
Hg	CVAA	0.00005				
I	IC	0.01				
K	AA	0.01	ICP-AES	0.2		
Li	ICP-AES	0.005				
Mg	ICP-AES	0.002				
Mn	ICP-AES	0.002				
Mo	GFAA	0.002	ICP-AES	0.02		
Na	AA	0.01	ICP-AES	0.05		
NH_4	Electrode	0.02				
Ni	GFAA	0.002	ICP-AES	0.01		
NO_2	IC	0.01				
NO_3	IC	0.01				
Pb	GFAA	0.002	ICP-AES	0.05		
pH	Electrode	0.01				
PO_4	IC	0.02				
Rb	GFAA	0.002	AA	0.01		
S	Electrode	0.02	IC	0.01		
S_2O_3	IC	0.01				
Sb	Hydride AA	0.0002	GFAA	0.002	ICP-AES	0.05
Se	Hydride AA	0.0002	GFAA	0.002	ICP-AES	0.1
Si	ICP-AES	0.02				
SO_3	IC	0.01				
SO_4	IC	0.02				
Sr	ICP-AES	0.005				
TDS	Calculation					
Ti	ICP-AES	0.002				
Tl	GFAA	0.002				
V	ICP-AES	0.002				
Zn	ICP-AES	0.005				

Methods for gases		
Analyte	Method	DL
Ar	GC	0.01%
As	Hydride AA	0.002
Br	IC	0.2
C_2H_6	GC	0.01%
CH_4	GC	0.01%
Cl	IC	1
CO	GC	0.01%
CO_2	Titration	5
F	IC	0.1
H_2	GC	0.01%
H_2S	ISE	0.02
He	GC	0.01%
Hg	CVAA	0.0002
N_2	GC	0.01%
NH_3	ISE	0.05
O_2	GC	0.01%
S	IC	1

[a] Methods used: AA = Atomic Adsorption Spectroscopy; CVAA = Cold Vapor AA; GFAA = Graphite Furnace AA; GC = Gas Chromatograpl
IC = Ion Chromatography; ICP-AES = Inductively Coupled Plasma-Atomic Emission Spectroscopy; ISE = Ion Selective Electrode

Table 4: Major Element Chemistry for Various Geothermal and Regional Fluids, Dixie Valley Region, Nevada (values in ppm unless otherwise noted).

Sample	Name or Description	Date	pH (lab)	SiO_2	SiO_2[a] Method	Na	K	Li	Ca	Mg	Sr	F	Cl	Br
Brines														
DIXE102-W	V102 + V103 Separator	10/02/95	9.45	638	archived	462	71.8	2.29	7.92	0.04	0.40	17.6	495	0.49
DV96-8	76-7 Well	10/25/96	9.09	599	TD	474	69.5	2.29	8.53	0.026	0.43	13.4	524	0.44
DV96-9	V101 Separator	10/25/96	9.19	599	TD	407	64.0	2.03	8.03	0.007	0.37	15.5	438	0.32
DV97-11	73-7 Well	10/29/97	9.07	580	FD	508	74.4	2.45	8.96	0.02	0.45	14.3	594	0.65
DV97-13	84-7 Well	10/29/97	9.04	580	FD	496	70.8	2.46	9.66	0.01	0.46	13.5	558	0.61
DV97-14	74-7 Well	10/29/97	9.06	586	FD	500	72.2	2.43	9.20	<0.01	0.49	13.5	584	0.66
DV97-16	V102 + V103 Separator	10/29/97	9.04	586	FD	500	77.2	2.48	9.02	<0.01	0.48	13.9	580	0.66
DV97-18	V105 Separator	10/29/97	9.04	595	FD	502	73.5	2.29	9.53	0.02	0.46	14.3	574	0.72
DV97-20	82A-7 Well	10/29/97	9.05	556	FD	495	72.6	2.22	9.63	<0.01	0.47	14.5	575	0.73
DV97-23	73B-7 Well	10/30/97	9.07	569	FD	499	76.4	2.34	9.09	<0.01	0.45	13.7	571	0.64
DV97-25	27-33 Well	10/30/97	9.03	627	FD	423	66.8	2.22	7.69	<0.01	0.32	14.7	443	0.56
DV97-26	V101 Separator	10/30/97	9.10	627	FD	439	68.8	2.27	7.95	<0.01	0.34	15.4	463	0.55
DV97-29	37-33 Well	10/30/97	9.16	621	FD	431	68.8	2.26	7.20	0.02	0.32	16.1	475	0.41
DV97-30	28-33 Well	10/30/97	9.13	642	FD	429	70.1	2.24	7.40	0.02	0.34	15.4	470	0.61
DV98-73	V101 Separator	04/28/98	9.10	591	FD	448	70.5	2.40	7.41	0.05	0.33	17.2	449	0.43
DV98-75	27-33 Well	04/28/98	8.99	571	FD	430	60.2	2.27	6.97	<0.01	0.33	15.8	421	0.25
DV98-77	37-33 Well	04/28/98	9.03	554	FD	429	66.7	2.21	7.19	<0.01	0.34	17.4	444	0.27
DV98-79	28-33 Well	04/28/98	9.01	550	FD	447	67.8	2.28	7.50	<0.01	0.34	16.6	446	0.39
DV98-80	76A-7 Well	04/28/98	8.96	541	FD	498	75.6	2.58	8.56	0.01	0.42	14.1	556	<0.02
DV98-82	V102 + V103 Separator	04/28/98	8.94	518	FD	498	77.1	2.42	8.81	0.01	0.46	14.7	567	0.49
DV98-84	74-7 Well	04/28/98	8.99	531	FD	491	75.2	2.53	8.65	0.02	0.49	14.6	564	0.56
DV98-86	63-7 Well	04/28/98	8.97	516	FD	510	77.0	2.43	8.73	<0.01	0.46	15.1	560	0.41
DV98-88	73-7 Well	04/29/98	8.98	518	FD	498	76.8	2.40	8.44	0.02	0.46	14.7	547	0.37
DV98-90	82A-7 Well	04/29/98	8.97	520	FD	501	76.1	2.22	8.95	<0.01	0.42	15.6	561	0.41
DV98-92	V105 Separator	04/29/98	8.96	526	FD	496	75.9	2.32	8.65	<0.01	0.44	15.8	572	0.63
DV98-95	73B-7 Well	04/29/98	8.95	511	FD	500	74.2	2.27	8.43	<0.01	0.44	15.7	561	0.54
DV98-133	27-33 Well	10/20/98	9.22	529	FD	381	61.8	2.11	4.85	<0.01	0.24	14.4	405	0.28
DV98-135	27-33 Well	10/20/98	9.64	582	FD	467	60.0	2.61	9.46	<0.01	0.51	18.0	496	0.40
DV98-138	V101 Separator	10/21/98	9.35	546	FD	409	63.8	2.11	7.18	<0.01	0.35	15.6	436	0.40
DV98-140	37-33 Well	10/21/98	9.35	526	FD	398	66.3	2.02	6.08	0.21	0.26	15.4	432	0.37
DV98-141	28-33 Well	10/21/98	9.38	531	FD	412	65.5	2.03	7.21	0.03	0.34	15.6	441	0.40
DV98-145	76A-7 Well	10/22/98	9.29	499	FD	479	70.8	2.26	8.23	0.01	0.44	13.7	541	0.44
DV98-147	63-7 Well	10/22/98	9.32	501	FD	496	71.9	2.21	8.87	<0.01	0.45	14.6	565	0.55

Table 4: Continued

Sample	Name or Description	Date	pH (lab)	SiO_2	SiO_2[a] Method	Na	K	Li	Ca	Mg	Sr	F	Cl	Br
DV98-148	V102 + V103 Separator	10/22/98	9.31	514	FD	485	72.3	2.24	9.18	0.17	0.46	14.0	560	0.53
DV98-150	74-7 Well	10/22/98	9.30	518	FD	486	74.1	2.38	8.90	0.04	0.048	13.8	554	0.42
DV98-152	73-7 Well	10/22/98	9.32	509	FD	476	73.7	2.14	8.81	0.02	0.46	14.7	567	0.46
DV98-154	73B-7 Well	10/22/98	9.28	514	FD	485	72.0	2.15	7.75	0.01	0.42	14.2	560	0.59
DV98-156	82A-7 Well	10/23/98	9.30	514	FD	473	69.3	2.10	8.87	0.04	0.46	14.7	557	0.55
DV98-159	V105 Separator	10/23/98	9.30	507	FD	480	69.4	2.14	9.39	0.34	0.48	14.4	560	0.59
DV99-182	76A-7 Well	05/04/99	9.02	524	FA	508	73.7	2.51	8.52	0.24	0.43	14.0	576	0.64
DV99-184	74-7 Well	05/04/99	9.00	522	FA	482	74.3	2.32	8.65	0.33	0.46	15.1	592	0.47
DV99-186	V102 + V103 Separator	05/04/99	9.01	522	FA	496	72.7	2.33	8.47	<0.01	0.46	15.2	594	0.59
DV99-188	63-7 Well	05/04/99	9.01	516	FA	504	73.6	2.26	8.48	<0.01	0.45	15.5	604	0.49
DV99-190	73-7 Well	05/04/99	9.01	518	FA	508	74.6	2.21	8.79	<0.01	0.45	15.5	624	0.64
DV99-194	V105 Separator	05/05/99	8.98	514	FA	514	74.4	2.23	9.51	<0.01	0.47	15.9	620	0.58
DV99-196	82A-7 Well	05/05/99	9.01	503	FA	518	72.2	2.25	8.89	<0.01	0.47	16.0	623	0.58
DV99-197	73B-7 Well	05/05/99	9.00	520	FA	516	74.4	2.22	8.78	<0.01	0.47	15.9	624	0.44
DV99-199	37-33 Well	05/05/99	9.05	563	FA	433	65.7	2.23	6.66	0.12	0.31	16.0	475	0.38
DV99-200	28-33 Well	05/05/99	9.10	561	FA	432	66.2	2.24	6.68	0.02	0.32	16.3	483	0.50
DV99-204	V101 Separator	05/05/99	9.05	576	FA	428	68.4	2.39	7.35	<0.01	0.31	16.4	481	0.34
DV74782786-brine 2	74-7 Well Archived	08/27/86	9.13	574	archived	413	61.5	2.82	1.11	<0.01	0.16	11.3	396	0.40
DV76781986-brine 4	76-7 Well Archived	08/19/86	9.16	563	archived	403	54.2	2.79	1.53	<0.01	0.17	10.1	402	0.31
DV453382186-brine 6	45-33 Well Archived	08/21/86	9.12	589	archived	370	59.2	2.63	1.27	0.04	0.13	14.9	320	0.30
DV73782886-brine 8	73-7 Well Archived	08/28/86	9.01	548	archived	380	59.2	2.55	1.24	<0.01	0.15	10.6	363	0.39
DV321882686-brine 10	32-18 Well Archived	08/26/86	8.70	484	archived	406	43.3	2.65	2.07	<0.01	0.23	8.36	428	0.37
DV651882686-brine 12	65-18 Well Archived	08/26/86	8.85	417	archived	440	40.7	2.09	1.16	<0.01	0.21	7.17	404	0.37
No number	28-33 Well Archived	09/23/93	7.58	101	archived	228	6.13	0.35	15.6	2.08	1.33	4.28	70.1	0.19
<u>Condensates</u>														
DIXE102-S	V102 + V103 Separator	10/02/95	5.85	2.7	archived	2.74	---	---	---	---	---	0.07	3.1	<0.02
DV96-7	76-7 Well	10/25/96	5.98	4.6	T	1.05	1.03	<0.01	0.15	<0.01	<0.01	0.03	0.26	<0.02
DV96-10	V101 Separator	10/25/96	5.98	4.2	T	0.96	1.33	<0.01	0.22	0.01	<0.01	0.01	0.13	<0.02
DV97-12	73-7 Well	10/29/97	5.29	---	---	194	28.6	---	---	---	---	6	242	0.32
DV97-15	74-7 Well	10/29/97	4.93	---	---	6.77	3.21	---	---	---	---	0.14	7.26	<0.02
DV97-17	V102 + V103 Separator	10/29/97	4.99	---	---	0.74	1.38	---	---	---	---	<0.01	<0.02	<0.02
DV97-19	V105 Separator	10/29/97	5.24	---	---	0.16	0.14	---	---	---	---	<0.01	0.31	<0.02
DV97-21	82A-7 Well	10/29/97	5.20	---	---	19.1	5.43	---	---	---	---	0.52	20	<0.02

Table 4: Continued

Sample	Name or Description	Date	pH (lab)	SiO$_2$	SiO$_2$^{a} Method	Na	K	Li	Ca	Mg	Sr	F	Cl	Br
DV97-22	73B-7 Well	10/29/97	5.73	---	---	234	37.2	---	---	---	---	6.37	281	0.3
DV97-24	V101 Separator	10/30/97	4.96	---	---	0.28	0.48	---	---	---	---	0.05	<0.02	<0.02
DV97-27	27-33 Well	10/30/97	5.37	---	---	1.51	0.8	---	---	---	---	0.06	0.87	<0.02
DV97-28	37-33 Well	10/30/97	5.35	---	---	0.07	0.05	---	---	---	---	<0.01	<0.02	<0.02
DV97-31	28-33 Well	10/30/97	5.12	---	---	6.39	1.94	---	---	---	---	0.12	3.69	<0.02
DV98-74	V101 Separator	04/28/98	5.34	2.2	T	0.64	0.75	<0.01	0.13	<0.01	---	0.03	0.07	<0.02
DV98-76	27-33 Well	04/28/98	5.66	4.8	T	0.35	0.29	<0.01	0.10	<0.01	---	0.01	0.09	<0.02
DV98-78	37-33 Well	04/28/98	5.54	5.1	T	0.57	0.34	0.01	1.07	0.06	---	0.02	0.21	<0.02
DV98-81	76A-7 Well	04/28/98	5.60	0.8	T	0.08	0.16	<0.01	0.05	<0.01	---	<0.01	<0.02	<0.02
DV98-83	V102 + V103 Separator	04/28/98	5.87	0.5	T	0.93	0.73	<0.01	0.14	0.02	---	<0.01	0.20	<0.02
DV98-85	74-7 Well	04/28/98	5.58	15.1	T	13.2	2.23	0.05	0.13	<0.01	---	0.35	15.7	<0.02
DV98-87	63-7 Well	04/28/98	5.63	1.8	T	0.30	0.13	<0.01	0.17	<0.01	---	<0.01	0.10	<0.02
DV98-89	73-7 Well	04/29/98	6.03	342	T	344	51.5	1.63	5.04	0.01	---	10.2	388	0.30
DV98-91	82A-7 Well	04/29/98	5.94	244	T	246	34.5	1.09	4.13	<0.01	---	7.48	281	0.23
DV98-93	V105 Separator	04/29/98	5.70	0.6	T	0.29	0.26	<0.01	0.05	<0.01	---	<0.01	0.03	<0.02
DV98-94	73B-7 Well	04/29/98	5.85	1.0	T	0.93	0.33	<0.01	0.09	<0.01	---	0.05	0.45	<0.02
DV98-101	28-33 Well	04/30/98	5.78	1.2	T	0.85	0.33	<0.01	0.06	0.01	---	0.03	0.45	<0.02
DV98-136	27-33 Well	10/20/98	5.96	0.7	T	0.86	0.51	<0.01	0.12	0.02	---	0.02	0.50	<0.02
DV98-137	V101 Separator	10/21/98	5.93	0.3	T	0.06	0.07	<0.01	0.05	<0.01	---	<0.01	<0.02	<0.02
DV98-139	37-33 Well	10/21/98	5.75	0.6	T	0.45	0.47	<0.01	0.04	<0.01	---	<0.01	0.04	<0.02
DV98-142	28-33 Well	10/21/98	5.69	2.2	T	1.06	0.50	<0.01	1.14	0.07	---	0.03	0.62	<0.02
DV98-144	76A-7 Well	10/22/98	6.14	<0.05	T	0.79	0.73	<0.01	0.08	<0.01	---	<0.01	0.03	<0.02
DV98-146	V102 + V103 Separator	10/22/98	6.33	<0.05	T	0.08	0.07	<0.01	0.08	0.01	---	<0.01	0.02	<0.02
DV98-149	63-7 Well	10/22/98	5.50	0.5	T	0.03	<0.01	<0.01	0.09	<0.01	---	<0.01	0.03	<0.02
DV98-151	74-7 Well	10/22/98	5.71	15.3	T	13.4	2.18	0.06	0.26	0.01	---	0.40	14.9	<0.02
DV98-153	73-7 Well	10/22/98	5.90	81.5	T	86.9	12.5	0.37	1.47	0.31	---	2.65	105	0.09
DV98-155	73B-7 Well	10/22/98	6.15	248	T	239	33.2	0.99	3.65	0.03	---	7.31	287	0.24
DV98-157	82A-7 Well	10/23/98	5.67	80.5	T	83.4	12.1	0.35	1.24	0.03	---	2.48	90.9	0.07
DV98-158	V105 Separator	10/23/98	5.79	0.4	T	0.29	0.24	<0.01	0.05	<0.01	---	<0.01	0.03	<0.02
DV99-183	76A-7 Well	05/04/99	6.66	3.36	T	0.2	0.38	<0.01	0.11	0.05	---	0.01	0.08	<0.01
DV99-185	74-7 Well	05/04/99	6.24	56.3	T	54.8	7.94	0.26	0.84	<0.01	---	1.46	58	0.04
DV99-187	V102 + V103 Separator	05/04/99	6.52	2.95	T	1.25	2.14	<0.01	0.08	<0.01	---	<0.01	0.02	<0.01
DV99-189	63-7 Well	05/04/99	6.59	2.63	T	0.33	0.51	<0.01	0.02	<0.01	---	<0.01	0.16	<0.01
DV99-191	73-7 Well	05/04/99	6.53	114	T	117	17.3	0.51	1.49	<0.01	---	3.29	132	0.1

Table 4: Continued

Sample	Name or Description	Date	pH (lab)	SiO_2	SiO_2[a] Method	Na	K	Li	Ca	Mg	Sr	F	Cl	Br
DV99-192	73B-7 Well	05/04/99	6.60	166	T	164	22.5	0.74	1.80	<0.01	---	5.42	181	0.13
DV99-193	V105 Separator	05/05/99	5.95	2.40	T	0.79	1.79	<0.01	0.08	<0.01	---	0.01	0.03	<0.01
DV99-195	82A-7 Well	05/05/99	6.59	159	T	158	19.3	0.68	2.91	<0.01	---	4.82	175	0.13
DV99-201	28-33 Well	05/05/99	6.16	6.16	T	2.77	2.36	<0.01	0.12	<0.01	---	0.02	0.91	<0.01
DV99-202	37-33 Well	05/05/99	5.67	2.14	T	0.6	0.29	<0.01	0.27	<0.01	---	<0.01	0.43	<0.01
DV99-203	V101 Separator	05/05/99	6.50	1.95	T	0.16	0.14	<0.01	0.02	<0.01	---	<0.01	0.17	<0.01
DV74782786-cond 1	74-7 Well Archived	08/27/86	7.13	3.77	archived	3.79	0.01	0.03	0.94	<0.01	---	<0.01	0.04	<0.01
DV76781986-cond 3	76-7 Well Archived	08/19/86	6.97	5.39	archived	3.79	0.02	<0.01	0.33	<0.01	---	<0.01	0.2	<0.01
DV453382886-cond 5	45-33 Well Archived	08/28/86	7.00	5.11	archived	3.82	0.03	<0.01	0.38	<0.01	---	<0.01	0.15	<0.01
DV73782886-cond 7	73-7 Well Archived	08/28/86	6.78	5.09	archived	4	0.02	<0.01	0.36	<0.01	---	<0.01	0.44	<0.01
DV321882686-cond 9	32-18 Well Archived	08/26/86	6.82	5.29	archived	3.94	0.02	<0.01	0.38	<0.01	---	<0.01	0.13	<0.01
DV651882686-cond 11	65-18 Well Archived	08/26/86	7.03	3.21	archived	3.78	<0.01	<0.01	0.67	<0.01	---	<0.01	0.04	<0.01
Injection Well/Power Plant Fluids														
DV96-2	Condensate from plant	10/24/96	6.63	1.7	FA	0.65	0.11	<0.01	1.3	0.12	0.01	0.01	0.42	<0.02
DV96-3	LP Brine @ Plant	10/24/96	9.61	644	TD	493	73.4	2.61	8.74	0.027	0.41	17.8	519	0.409
DV96-4	45-5 Injection Well	10/24/96	9.54	601	TD	470	72.0	2.50	8.38	0.023	0.41	15.0	518	0.368
DV96-5	Lamb 1 Injection Well	10/24/96	9.59	618	TD	506	74.6	2.52	9.55	0.014	0.46	16.2	549	0.442
DV96-6	65-18 Injection Well	10/24/96	9.58	629	TD	506	75.2	2.57	8.68	0.009	0.45	16.1	556	0.451
DV97-32	Condensate from plant	10/31/97	6.22	---	---	56.4	7.83	---	---	---	---	1.46	62.2	0.06
DV97-33	LP Brine	10/31/97	9.49	655	FD	483	72.6	2.62	8.85	<0.01	0.46	16.1	579	0.58
DV97-34	25-5 + 45-5 Injectate	10/31/97	9.40	574	FD	434	66.4	2.24	7.76	0.03	0.39	14.4	515	0.54
DV97-35	25-5 + 45-5 Injectate	10/31/97	9.42	561	FD	450	67.6	2.29	7.93	0.03	0.39	14.4	511	0.47
DV97-36	65-18 Injection Well	10/31/97	9.50	629	FD	497	74.0	2.61	8.65	0.01	0.45	16.6	590	0.53
DV97-37	32-18 Injection Well	10/31/97	9.49	597	FD	499	76.8	2.53	8.95	<0.01	0.47	16.3	588	0.54
DV97-40	LP Brine @ Plant	10/31/97	9.49	642	FD	465	72.5	2.66	9.03	0.03	0.46	15.6	571	0.58
DV97-41	Condensate from plant	10/31/97	6.66	---	---	56.1	7.78	---	---	---	---	1.48	63.1	<0.02
DV97-42	High P Brine @ plant	10/31/97	9.09	593	FD	432	70.0	2.28	7.25	0.03	0.34	15.4	464	0.49
DV98-97	Condensate from plant	04/29/98	6.95	1.1	T	1.17	0.20	<0.01	0.65	0.15	---	0.04	0.70	<0.02
DV98-98	LP Brine @ Plant	04/29/98	9.38	597	FD	536	79.9	2.61	9.69	0.17	0.46	18.0	589	0.55
DV98-143	25-5 Injection Well	10/21/98	9.72	561	FD	508	74.5	2.33	9.03	0.01	0.45	16.4	576	0.52
DV98-161	Condensate from plant	10/23/98	7.16	25.7	FA	33.3	4.54	0.15	2.56	1.20	0.059	0.89	33.0	0.02
DV98-162	LP Brine @ Plant	10/23/98	9.74	599	FD	510	75.8	2.46	9.63	0.12	0.47	16.2	573	0.41
DV98-163	65-18 Injection Well	10/23/98	8.04	43.2	FD	134	12.3	0.48	28.7	23.5	0.61	1.02	146	0.09

Table 4: Continued

Sample	Name or Description	Date	pH (lab)	SiO_2	SiO_2[a] Method	Na	K	Li	Ca	Mg	Sr	F	Cl	Br
DV99-198	65-18 Injection Well	05/05/99	8.01	38.5	FA	151	12.8	0.57	32.7	27.5	0.71	0.61	166	0.12
DV99-205	25-5 + 45-5 Injectate	05/06/99	9.43	603	FA	539	80.5	2.63	9.08	<0.01	0.45	17.9	631	0.78
DV99-206	LP Brine @ Plant	05/06/99	9.44	603	FA	528	79.7	2.55	8.70	<0.01	0.46	17.2	634	0.63
DV99-207	Condensate from plant	05/06/99	7.36	2.78	FA	1.06	0.33	<0.01	0.12	<0.01	0.004	<0.01	0.45	<0.02
DV99-208	52-18 + 41-18 Injectate	05/06/99	9.41	595	FA	529	78.5	2.60	8.80	<0.01	0.44	17.0	621	0.63
<u>Other Geothermal and On-Site Water Wells</u>														
DV96-1	Domestic Well	10/24/96		74.3	FA	143	15.4	0.43	61.6	32.0	1.63	0.78	105	0.12
DV97-38	Domestic Well	10/31/97	7.82	77.0	FA	136	16.3	0.42	58.7	28.8	1.66	0.76	109	0.15
DV97-39	Goerenger Well	10/31/97	7.70	62.1	FA	228	20.4	0.9	50.3	37.5	1.06	1.21	222	0.26
DV97-53	46-32 Well	11/05/97	5.93	3.9	T	4.17	2.26	0.02	0.83	0.04	0.13	0.09	2.64	<0.02
DV97-54	27-32 Well	11/05/97	6.22	3.0	T	0.31	0.19	0.01	0.18	0.01	0.003	<0.02	0.27	<0.02
DV97-55	27-32 Well	11/05/97	6.29	58.2	FA	95.5	13.1	0.7	5.56	0.03	0.21	5.44	87.6	0.06
DV97-59	45-W-5 Well	11/05/97	7.75	22.5	FA	204	8.53	0.68	4.85	3.02	0.19	1.95	201	0.23
DV97-67	66-21 Well	11/07/97	6.97	321	FA	935	86.6	4.57	41.2	0.41	2.48	2.68	1476	1.32
DV98-96	Goerenger Well	04/29/98	7.88	61.4	FA	254	22.1	0.92	52.3	42.5	1.11	1.29	218	0.21
DV98-99	27-32 Well	04/29/98	5.81	61.2	T	88.0	11.6	0.48	5.91	0.91	---	4.00	84.8	0.05
DV98-100	46-32 Well	04/29/98	5.72	0.8	T	0.69	0.74	0.01	0.30	0.06	---	<0.01	0.24	<0.02
DV98-102	45-14 Well	04/30/98	5.71	19.8	T	31.0	2.83	0.07	1.93	0.02	---	0.58	36.0	<0.02
DV98-103	45-14 Well	04/30/98	7.23	285	FD	432	41.4	1.06	23.0	0.04	1.10	7.92	481	0.49
DV98-104	66-21 Well	04/30/98	6.51	325	FD	876	86.9	4.89	40.0	0.35	2.61	3.06	1440	1.05
DV98-111	62-21 Well	05/01/98	7.84	172	FD	513	17.1	0.49	6.10	0.41	0.48	6.60	79.6	0.15
DV98-122	97-2 Well	05/05/98	7.96	55.2	FA	383	35.3	1.45	52.6	47.5	1.10	3.73	325	0.25
DV98-123	32-6 Well	05/06/98	8.15	2.5	FA	179	6.83	0.07	28.1	64.1	0.31	1.55	189	0.20
Dixie Jack #1	Gradient Well DJ #1	05/17/98	7.93	43.2	FA	410	25.9	1.65	37.8	5.30	0.38	7.55	316	0.26
Dixie Jack #4	Gradient Well DJ #4	05/20/98	7.45	119	FA	281	24.7	1.17	12.2	0.57	0.34	20.4	282	0.21
Dixie Jack #7	Gradient Well DJ #7	05/14/98	7.13	5.0	FA	19.9	2.12	0.09	4.21	0.18	0.10	0.72	6.20	<0.02
DV98-160	Goerenger Well	10/23/98	8.18	59.7	FD	231	20.6	0.80	52.2	43.8	1.17	1.18	252	0.21
DV98-168	38-32 Well	10/26/98	8.22	166	FA	234	25.2	0.98	14.4	1.08	0.47	15.9	161	0.14
DV98-175	62-21 Well	10/28/98	7.86	162	FA	488	16.5	0.42	12.1	1.04	0.61	5.89	77.3	0.11
DV99-181	Goerenger Well	05/04/99	7.89	61.2	FA	266	21.1	0.93	56.6	47.8	1.24	1.46	296	0.26

Table 4: Continued

Sample	Name or Description	Date	pH (lab)	SiO$_2$	SiO$_2$[a] Method	Na	K	Li	Ca	Mg	Sr	F	Cl	Br
Background Springs														
DV97-46	Sou Hot Spring	11/03/97	7.98	64.2	FA	166	29.3	0.75	107	21.0	12.5	4.95	79.0	0.07
DV97-47	Sou Hot Spring	11/03/97	7.75	62.7	FA	162	28.2	0.72	112	20.9	12.4	4.72	77.1	0.09
DV97-48	Hyder Hot Spring	11/03/97	7.96	60.3	FA	325	20.5	1.71	42.1	10.1	1.23	7.38	46.6	0.07
DV97-50	Edward Creek Spring	11/04/97	7.83	87.5	FA	50.7	7.61	0.16	33.3	1.65	0.14	2.18	26.4	0.05
DV 97-51b	Old Man Spring	11/04/97	8.07	44.9	FA	228	7.78	0.08	32.4	1.38	0.27	0.74	130	0.33
DV97-52	Horse Heaven Spring	11/04/97	7.91	44.1	FA	152	7.53	0.04	36.2	4.36	0.44	0.58	141	0.21
DV97-56	Dead Travertine Spring	11/05/97	7.93	27.8	FA	325	48.5	2.03	201	79.4	2.62	2.34	527	0.64
DV97-60	Fault Line Spring	11/06/97	8.01	41.5	FA	162	11.9	0.36	67	18.5	1.51	2.62	32.1	<0.02
DV97-61	Lower Ranch Hot Spring	11/06/97	8.07	40.7	FA	141	11.4	0.28	37.5	13.2	0.73	3.09	29.9	<0.02
DV97-62	McCoy Hot Spring	11/06/97	8.00	35.7	FA	185	9.05	0.16	78.6	30.0	2.35	1.47	228	0.31
DV97-63	Kyle Spring	11/06/97	8.18	17.1	FA	84.7	2.32	0.02	90.5	41.4	1.20	0.59	189	0.29
DV97-64	Dago Spring	11/06/97	8.06	38.3	FA	186	1.96	0.05	105	29.3	0.93	1.31	253	0.35
DV97-65	Mustang Spring	11/06/97	8.13	29.5	FA	262	1.43	0.06	105	76.4	2.21	0.9	311	0.49
DV97-66	Kitten Spring	11/06/97	7.64	43.7	FA	50.6	3.89	<0.01	95.6	35.4	0.55	0.1	202	0.25
DV97-68	Big Horn Spring	11/07/97	7.88	36.4	FA	427	4.52	0.06	87.2	47.4	1.80	0.74	707	0.92
DV97-69	Dixie Hot Spring	11/07/97	8.00	105	FA	194	4.94	0.42	11	0.12	0.068	11.1	161	0.28
DV97-72	Horse Creek Spring	11/07/97	7.38	26.8	FA	16	0.98	<0.01	12.4	2.01	0.11	0.15	7.95	<0.02
DV98-106	Stu's Seep	04/30/98	8.00	18.9	FA	284	7.40	0.07	33.3	47.2	1.17	0.58	257	0.16
DV98-112	Hyder Hot Spring	04/30/98	7.73	57.6	FA	357	20.5	1.59	42.8	10.1	1.22	7.84	45.4	0.07
DV98-113	Lower Ranch Hot Spring	05/04/98	7.89	36.0	FA	157	11.4	0.28	38.6	13.3	0.71	3.26	27.8	<0.02
DV98-114	McCoy Hot Spring	05/04/98	7.83	32.3	FA	206	9.12	0.18	79.4	30.4	2.26	1.52	219	0.26
DV98-117	Sou Hot Spring	05/04/98	7.56	58.6	FA	174	28.7	<0.01	106	20.7	12.6	5.28	74.6	0.11
DV98-118	Big Horn Spring	05/04/98	7.83	33.8	FA	802	6.83	0.08	131	69.5	2.73	0.36	1359	1.18
DV98-120	Dixie Hot Spring	05/05/98	8.36	107	FA	211	4.91	0.42	10.7	0.22	0.086	12.6	162	0.23
DV98-128	Jersey Hot Spring	05/05/98	7.41	134	FA	188	17.5	1.13	23.1	3.12	0.57	9.27	37.8	0.04
DV98-129	Upper Jersey Seep	05/06/98	8.17	109	FA	261	26.4	1.50	23.7	2.84	0.52	10.5	48.6	0.07
DV98-131	Spring in Spring Canyon	05/06/98	7.80	52.2	FA	380	11.4	0.12	88.6	59.6	1.31	0.94	418	0.54
DV98-132	Wild Rose Spring	05/07/98	7.75	35.7	FA	176	5.96	0.04	97.0	30.4	0.92	1.01	135	0.13
DV98-169	Lofthouse Spring	05/07/98	7.99	20.8	FA	40.5	1.36	<0.01	58.7	15.6	0.67	0.30	43.2	0.07
DV98-170	Not-So-OK Spring	10/27/98	8.17	18.7	FA	33.5	3.32	<0.01	56.2	13.9	0.58	0.30	30.6	<0.02
DV98-176	War Canyon Spring	10/27/98	8.28	16.8	FA	32.5	0.61	0.05	42.1	1.61	0.62	0.17	30.1	0.04
DV98-177	Pine Spring	10/28/98	8.04	30.8	FA	31.8	3.20	<0.01	28.3	14.9	0.14	0.22	29.0	0.04
DV98-178	Basalt Spring	10/28/98	7.95	31.0	FA	18.0	2.22	<0.01	22.2	12.6	0.24	0.07	20.8	0.03

Table 4: Continued

Sample	Name or Description	Date	pH (lab)	SiO_2	SiO_2[a] Method	Na	K	Li	Ca	Mg	Sr	F	Cl	Br
DV98-179	Upper Cherry Spring	10/28/98	7.85	21.4	FA	24.4	1.59	<0.01	23.9	5.44	0.25	0.07	22.1	<0.02
DV99-209	Dead Travertine Spring	05/07/99	7.72	27.2	FA	331	48.9	2.05	200	76	2.51	2.46	551	0.49
DV99-210	Road seep, Dead Travertine	05/08/99	7.96	31.7	FA	370	56.4	2.28	158	90.4	2.92	2.72	630	0.51
DV99-211	Upper Spg, Lower Ranch	05/09/99	8.07	38.3	FA	149	12.1	0.27	40.3	13.3	0.68	3.06	27.8	0.05
Background Wells														
DV97-49	Hole in the Wall #2 Well	11/04/97	7.93	8.8	FA	77.7	7.61	0.03	30.4	5.62	0.33	0.49	69.6	0.14
DV97-57	Bolivia Artesian Well	11/05/97	8.08	26.1	FA	146	4.02	0.16	99.2	66.8	2.97	0.30	289	0.43
DV97-70	Flowing well @ AA Tank	11/07/97	7.89	61.8	FA	60.3	4.11	0.05	24.2	1.48	0.19	5.43	21.2	0.08
DV97-71	Shaw Well	11/07/97	7.92	65.3	FA	68.3	3.15	0.06	14.8	0.74	0.11	7.21	19.7	<0.02
DV98-115	Irrigation Well	05/04/98	7.87	47.5	FA	221	12.6	0.53	62.3	35.1	1.44	1.87	72.4	0.10
DV98-116	Brinkerhoff Well	05/04/98	7.78	36.0	FA	236	6.94	0.31	191	48.7	1.42	0.57	469	0.56
DV98-172	Bernice Well	10/27/98	8.35	3.0	FA	94.2	2.13	0.02	31.7	55.3	0.31	0.14	80.7	0.13
Background Streams/Rain														
DV97-58	Cottonwood Creek	11/05/97	8.12	34.5	FA	147	3.17	0.04	66.2	46.3	0.97	0.31	216	0.32
DV98-107	Unnamed Crk, Stu's Seep	04/30/98	8.42	21.1	FA	307	9.72	0.07	48.5	52.5	1.25	0.51	322	0.22
DV98-110	Cottonwood Creek	05/01/98	8.03	38.3	FA	155	6.40	0.08	89.4	40.7	0.82	0.41	191	0.15
DV98-119	Unnamed Stream	05/05/98	8.20	20.1	FA	262	3.40	0.04	61.6	49.1	0.90	0.43	306	0.24
DV98-121	White Rock Canyon	05/05/98	8.44	16.8	FA	112	2.44	0.01	52.3	28.8	0.70	0.34	96.2	0.06
DV98-125	Rain, Lizard Well Tank	05/06/98	7.03	7.8	FA	15.0	3.47	0.01	14.9	1.75	0.19	0.21	9.12	<0.02
DV98-126	Home Station Wash	05/06/98	7.47	33.0	FA	38.3	2.72	0.01	18.1	3.88	0.15	0.39	23.2	<0.02
DV98-127	Cedar Canyon Wash	05/06/98	7.52	35.3	FA	46.8	3.63	0.02	26.3	4.66	0.24	0.43	27.2	<0.02
DV98-130	Bucher Creek	05/06/98	7.90	31.2	FA	42.3	3.33	0.01	29.7	6.82	0.26	0.39	24.5	<0.02
DV98-171	Not-So-OK Creek	10/27/98	8.28	18.6	FA	34.0	1.53	<0.01	52.7	12.6	0.54	0.24	30.1	<0.02
DV98-173	Bernice Creek	10/27/98	8.43	21.2	FA	129	3.65	0.05	62.4	78.2	0.83	0.32	128	0.16
DV98-174	Hoyt Creek	10/27/98	8.72	17.1	FA	403	4.23	0.09	64.3	181	1.86	0.35	449	0.52
DV98-180	Mt. Augusta Creek	10/28/98	7.72	19.0	FA	14.3	1.71	<0.01	12.2	2.49	0.13	0.11	8.36	<0.02
DV99-213	Dixie Salt Lake	05/10/99	7.95	88.4	FA	4400	102	3.65	463	132	20.4	10.9	5310	5.51
Fumarole Condensates														
DV97-43	Crack 4 Fumarole	11/03/97	---	---	---	1.12	0.08	<0.01	0.39	0.05	---	<0.01	0.24	<0.04
DV97-44	Senator Fumarole	11/03/97	---	---	---	4.3	1.24	<0.01	4.01	0.79	---	0.06	2.90	<0.04
DV98-108	Senator Fumarole	05/01/98	7.11	1.8	T	0.23	0.06	<0.01	0.04	0.06	---	<0.01	0.44	<0.02

Table 4: Continued

Sample	Name or Description	Date	pH (lab)	SiO_2	SiO_2[a] Method	Na	K	Li	Ca	Mg	Sr	F	Cl	Br
DV98-109	Calcite Fumarole	05/01/98	6.56	1.6	T	0.26	0.12	<0.01	0.16	0.03	---	<0.01	0.18	<0.02
DV98-164	Senator Fumarole	10/24/98	6.72	5.5	T	6.25	<0.01	<0.01	0.32	0.08	---	<0.01	9.41	<0.02
DV98-165	Calcite Fumarole	10/25/98	7.05	3.7	T	0.17	<0.01	<0.01	0.25	0.01	---	<0.01	0.11	<0.02
DV98-166	South Bench Fumarole	10/26/98	3.13	2.5	T	0.11	<0.01	<0.01	0.14	0.03	---	<0.01	<0.02	<0.02

[a] Sample collection and analysis for silica varied; FA = filtered acidified, FD = filtered and diluted with deionized water, T = total (unacidified), TD = total diluted with deionized water.

[b] Bicarbonate and carbonate were analyzed in the field by pH titration on fresh samples.

[c] Bicarbonate and carbonate were analyzed in the labortory by pH titration on filtered, unacidified or raw, untreated samples. The values shown in bold type were not corrected for excess silica.

Table 4: continued

Sample	$HCO_3(F)^b$	$CO_3(F)^b$	$HCO_3(L)^c$	$CO_3(L)^c$	SO_4	B	TDS	Alkalinity	Conductivity (micromhos)
Brines									
DIXE102-W	---	---	**0**	**76.3**	225	9.35	2025	---	---
DV96-8	---	---	**32.8**	**87.8**	201	11.6	2026	173	2550
DV96-9	89.1	67.2	**18.2**	**93.2**	196	9.92	1855	170	2280
DV97-11	61	76.8	7.8	49.2	207	11.5	2078	161	2550
DV97-13	110	66	16.4	53.7	206	11.7	2042	172	2540
DV97-14	0	139	15	55.8	204	11.8	2076	183	2590
DV97-16	102	60	16.3	52.5	203	11.7	2072	168	2590
DV97-18	83	62.4	17.1	49	213	11.8	2084	162	2600
DV97-20	26.8	98.4	11.7	46.4	212	11.7	2028	164	2600
DV97-23	31.7	96	3.7	49.4	212	11.7	2040	159	2620
DV97-25	100	84	43.7	50.5	183	9.16	1907	188	2180
DV97-26	107	60	15.1	51.4	197	9.53	1930	173	2260
DV97-29	87.8	76.8	11	57.7	191	9.51	1918	172	2240
DV97-30	115	52.8	9.5	56.4	199	9.47	1938	169	2240
DV98-73	171	31.2	21.1	54.1	196	9.51	1334	177	2270
DV98-75	150	30.0	40.7	56.3	183	9.03	1282	188	2170
DV98-77	173	14.4	18.7	55.1	197	9.19	1303	174	2250
DV98-79	73.2	72.0	18.9	47.2	199	9.38	1329	171	2270
DV98-80	117	38.4	15.4	49.2	204	11.9	1494	169	2610
DV98-82	120	28.8	10.1	46.5	211	11.7	1502	156	2640
DV98-84	117	38.4	10.5	44.3	209	11.3	1494	163	2620
DV98-86	70.8	55.2	5.6	44.7	214	12.0	1505	153	2620
DV98-88	80.5	55.2	4.0	41.8	210	11.5	1473	150	2610
DV98-90	80.5	62.4	9.8	46.4	219	11.9	1509	156	2620
DV98-92	89.1	55.2	7.7	42.4	218	11.6	1510	153	2620
DV98-95	56.1	66.0	6.4	40.9	216	11.4	1496	153	2630
DV98-133	---	---	57.1	55.9	181	9.00	1713	190	2120
DV98-135	---	---	0	65.6	225	10.9	1947	224	2560
DV98-138	---	---	21.0	58.7	198	9.50	1777	180	2240
DV98-140	105	64.8	27.4	57.8	197	9.53	1749	181	2230
DV98-141	75.6	76.8	17.7	58.3	199	9.73	1770	178	2250
DV98-145	112	60.0	19.7	58.6	210	12.2	1923	173	2560
DV98-147	48.8	91.2	3.6	50.8	219	11.7	1953	150	2630

Table 4: Continued

Sample	**HCO$_3$(F)^b**	**CO$_3$(F)^b**	**HCO$_3$(L)^c**	**CO$_3$(L)^c**	**SO$_4$**	**B**	**TDS**	**Alkalinity**	**Conductivity (micromhos)**
DV98-148	85.4	62.4	7.4	53.6	215	11.8	1953	157	2610
DV98-150	90.3	57.6	10.4	56.1	212	11.9	1957	164	2570
DV98-152	107	48.0	2.8	50.9	214	11.8	1940	149	2600
DV98-154	78.1	57.6	6.6	54.0	218	11.9	1955	154	2590
DV98-156	56.1	86.4	13.1	54.3	222	11.8	1950	158	2600
DV98-159	26.8	106	8.6	54.0	218	12.0	1945	155	2600
DV99-182	87.4	50	17.1	53.1	229	11.7	2027	167	2550
DV99-184	57.3	69	8.2	48.5	231	11.5	2005	158	2590
DV99-186	15	88	3.7	48.9	235	11.5	2018	152	2590
DV99-188	28.1	87	0.8	46.1	239	11.5	2029	148	2630
DV99-190	86.6	42	0	40.2	236	11.8	2049	140	2660
DV99-194	76.9	45	3.7	45.2	243	12.0	2063	147	2650
DV99-196	91.1	44	2.8	47.4	243	11.8	2057	152	2660
DV99-197	40.7	70	0.6	46.2	243	12.0	2072	145	2650
DV99-199	110	70	27.1	55.7	207	9.34	1871	183	2230
DV99-200	85	74	19	57.2	213	9.6	1876	178	2270
DV99-204	83	78	22.2	57.6	211	9.69	1889	180	2230
DV74782786-brine 2	---	---	109	80.3	159	9.24	1822	309	2070
DV76781986-brine 4	---	---	90	79.2	158	9.42	1779	286	2040
DV453382186-brine 6	---	---	126	79.9	149	7.99	1726	311	1859
DV73782886-brine 8	---	---	131	68.6	150	8.72	1729	291	1953
DV321882686-brine 10	---	---	140	42	150	9.44	1721	223	2040
DV651882686-brine 12	---	---	221	57	162	9.18	1766	334	2180
No number	---	---	140	0	273	2.25	846	127	1162
<u>Condensates</u>									
DIXE102-S	---	---	**34.9**	**0**	3.35	0.12	---	---	---
DV96-7	54.9	0	**51**	**0**	1.26	0.16	78.2	41.8	114
DV96-10	---	---	**42**	**0**	1.96	0.13	64.1	34.4	97.7
DV97-12	---	---	**101**	**0**	88.5	4.9	---	83	---
DV97-15	---	---	**59.3**	**0**	2.74	0.28	---	49	---
DV97-17	---	---	**57.8**	**0**	5.19	0.16	---	47	---
DV97-19	---	---	**47**	**0**	0.87	0.12	---	39	---
DV97-21	---	---	**54.9**	**0**	8.89	0.54	---	45	---

Table 4: Continued

Sample	HCO$_3$(F)^b	CO$_3$(F)^b	HCO$_3$(L)^c	CO$_3$(L)^c	SO$_4$	B	TDS	Alkalinity	Conductivity (micromhos)
DV97-22	---	---	**121**	**0**	105	6.35	---	99	---
DV97-24	---	---	**45.8**	**0**	0.28	0.16	---	38	---
DV97-27	---	---	**48.3**	**0**	2.50	0.16	---	40	---
DV97-28	---	---	**46.1**	**0**	0.49	0.09	---	38	---
DV97-31	---	---	**54.3**	**0**	7.32	0.44	---	45	---
DV98-74	---	---	**42.0**	**0**	5.60	0.22	61.9	34.4	96.3
DV98-76	---	---	**46.1**	**0**	2.86	0.24	64.2	37.8	99.0
DV98-78	---	---	**29.4**	**0**	14.2	0.31	58.6	24.1	107
DV98-81	---	---	**47.2**	**0**	2.72	0.26	64.2	38.7	102
DV98-83	---	---	**48.5**	**0**	3.86	0.22	68.3	39.8	104
DV98-85	---	---	**51.9**	**0**	7.42	0.55	107	42.5	176
DV98-87	---	---	**49.9**	**0**	2.57	0.21	56.1	40.9	105
DV98-89	---	---	**142**	**0**	138	7.80	1096	116	1870
DV98-91	---	---	**120**	**0**	108	5.71	818	98.4	1380
DV98-93	---	---	**45.0**	**0**	2.92	0.22	64.3	36.9	101
DV98-94	---	---	**49.1**	**0**	2.51	0.17	68.6	40.2	103
DV98-101	---	---	**43.4**	**0**	2.54	0.16	60.4	35.6	93.1
DV98-136	---	---	**39.5**	**0**	2.58	0.05	58.1	32.4	97.9
DV98-137	---	---	**37.6**	**0**	2.66	0.08	41.6	30.8	90.2
DV98-139	---	---	**45.7**	**0**	1.02	0.03	61.4	37.5	94.0
DV98-142	---	---	**49.6**	**0**	1.25	0.07	69.5	40.7	104
DV98-144	---	---	**48.6**	**0**	1.48	0.10	65.3	39.8	102
DV98-146	---	---	**47.9**	**0**	3.41	0.10	65.5	39.3	102
DV98-149	---	---	**44.1**	**0**	7.33	0.09	67.8	36.1	107
DV98-151	---	---	**55.1**	**0**	6.20	0.42	123	45.2	176
DV98-153	---	---	**73.6**	**0**	42.3	2.21	424	60.3	608
DV98-155	---	---	**114**	**0**	112	5.81	1062	93.4	1426
DV98-157	---	---	**70.1**	**0**	38.0	2.03	393	57.5	545
DV98-158	---	---	**45.5**	**0**	2.34	0.14	62.9	37.3	97.0
DV99-183	---	---	**44**	**0**	2.55	0.13	65.8	36.1	96.6
DV99-185	---	---	**60**	**0**	24.9	1.39	280	---	---
DV99-187	---	---	**46.9**	**0**	2.45	0.15	69.8	38.4	94.4
DV99-189	---	---	**44.6**	**0**	2.96	0.10	67.7	36.6	97.3
DV99-191	---	---	**76.6**	**0**	51.3	2.96	532	62.8	711

Table 4: Continued

Sample	HCO$_3$(F)^b	CO$_3$(F)^b	HCO$_3$(L)^c	CO$_3$(L)^c	SO$_4$	B	TDS	Alkalinity	Conductivity (micromhos)
DV99-192	---	---	**85.3**	**0**	77.9	4.19	724	69.9	960
DV99-193	---	---	**44.8**	**0**	5.65	0.16	71.3	36.7	98.1
DV99-195	---	---	**83.5**	**0**	74.5	3.95	696	68.4	926
DV99-201	---	---	**37.7**	**0**	4.11	0.18	66.2	30.9	98.1
DV99-202	---	---	**18.8**	**0**	20.0	0.11	55.4	15.4	106
DV99-203	---	---	**35**	**0**	2.35	0.13	53.3	28.7	88.4
DV74782786-cond 1	---	---	**53.6**	**0**	4.7	0.043	80.0	43.9	108
DV76781986-cond 3	---	---	**58.9**	**0**	2.01	0.057	84.5	48.3	109
DV453382886-cond 5	---	---	**20**	**0**	28.1	0.057	69.5	16.4	118
DV73782886-cond 7	---	---	**52.8**	**0**	4.87	0.052	80.5	43.3	105
DV321882686-cond 9	---	---	**63.3**	**0**	9.52	0.071	99.8	51.9	136
DV651882686-cond 11	---	---	**66.2**	**0**	3.1	0.054	92.7	54.3	121
Injection Well/Power Plant Fluids									
DV96-2	8.5	0	**7.5**	**0**	26.4	0.24	109	6.1	176
DV96-3	0	73.2	**0**	**58**	228	11.5	2078	186	2580
DV96-4	31.7	92.4	**0**	**57.7**	213	11.4	2005	175	2510
DV96-5	0	104	**0**	**62.6**	224	12.6	2067	190	2690
DV96-6	39	99.6	**0**	**59.9**	226	12.5	2119	192	2700
DV97-32	---	---	**9.7**	**0**	49.9	1.5	---	8	
DV97-33	0	91.2	0	19.6	217	12	2093	188	2690
DV97-34	0	84	0	18.3	196	10.7	1868	161	2370
DV97-35	19.5	88.8	0	18.7	198	10.6	1870	162	2380
DV97-36	68.3	84	0	20.1	222	12.1	2095	191	2720
DV97-37	0	122	0	20.5	222	12.0	2066	188	2700
DV97-40	0	98.4	0	19	219	11.9	2053	188	2700
DV97-41	---	---	**<0.8**	**0**	51.4	1.51	---	0	---
DV97-42	37.8	98.4	18.3	55.5	193	9.43	1887	173	2220
DV98-97	---	---	**16.2**	**0**	21.5	0.36	90.4	13.3	168
DV98-98	17.1	91.2	0	14.5	228	11.9	1571	182	2750
DV98-143	0	103	0	22.0	229	12.6	2026	184	2720
DV98-161	---	---	**16.4**	**0**	47.8	0.96	211	13.4	340
DV98-162	0	81.6	0	21.7	230	12.2	2068	185	2720
DV98-163	222	0	**202**	**0**	117	1.88	734	166	1044

Table 4: Continued

Sample	HCO$_3$(F)^b	CO$_3$(F)^b	HCO$_3$(L)^c	CO$_3$(L)^c	SO$_4$	B	TDS	Alkalinity	Conductivity (micromhos)
DV99-198	212	0	197	14.8	124	1.93	784	192	1122
DV99-205	0	84	0	17.1	252	12.6	2182	181	2740
DV99-206	0	52.8	0	17.2	252	12.7	2173	181	2750
DV99-207	45.1	0	24.3	0	12.9	0.28	74.4	22	121
DV99-208	0	73.2	0	18.1	250	12.3	2149	177	2730
Other Geothermal and On-Site Water Wells									
DV96-1	293	0	**305**	**0**	194	1.46	937	---	---
DV97-38	298	0	297	0	191	1.65	921	249	1150
DV97-39	381	0	388	0	174	2.65	1190	318	1605
DV97-53	---	---	**53**	**0**	3.17	0.077	88.0	43.4	122
DV97-54	---	---	**59.6**	**0**	1.53	0.053	87.6	48.9	127
DV97-55	---	---	**59.8**	**0**	77.8	2.25	420	49	608
DV97-59	---	---	**226**	**0**	28.5	1.63	715	185	1039
DV97-67	---	---	**193**	**0**	84.7	5.79	3167	158	4850
DV98-96	366	0	**340**	**20.3**	177	2.71	1134	313	1705
DV98-99	---	---	**65.1**	**0**	54.2	2.03	329	53.4	557
DV98-100	---	---	**45.0**	**0**	2.91	0.14	63.8	36.9	99.3
DV98-102	---	---	**54.1**	**0**	16.9	0.51	159	44.3	282
DV98-103	---	---	89.5	0	195	6.77	1322	101	2250
DV98-104	---	---	162	0	80.2	5.78	2747	158	4890
DV98-111	532	0	688	0	219	5.52	1873	836	2150
DV98-122	---	---	**666**	**0**	161	6.66	1689	546	2300
DV98-123	---	---	**98.2**	**6.9**	334	1.26	910	92.0	1447
Dixie Jack #1	---	---	**430**	**0**	240	7.08	1527	352	2140
Dixie Jack #4	---	---	**131**	**0**	135	8.10	1020	107	1522
Dixie Jack #7	---	---	**39.7**	**0**	11.5	1.21	92.4	32.5	121
DV98-160	361	0	**338**	**19.8**	182	2.77	1207	310	1680
DV98-168	---	---	**243**	**19.2**	88.1	7.25	982	231	1227
DV98-175	---	---	**1016**	**0**	219	5.48	2011	833	2080
DV99-181	342	0	320	20.2	204	2.81	1303	292	1728

Table 4: Continued

Sample	HCO$_3$(F)^b	CO$_3$(F)^b	HCO$_3$(L)^c	CO$_3$(L)^c	SO$_4$	B	TDS	Alkalinity	Conductivity (micromhos)
Background Springs									
DV97-46	---	---	**278**	**16.5**	385	1.46	1169	255	1423
DV97-47	---	---	**315**	**0**	379	1.39	1179	258	1412
DV97-48	---	---	**817**	**31.3**	119	4.24	1490	722	1598
DV97-50	---	---	**139**	**0**	58.7	0.31	409	114	434
DV 97-51b	---	---	**185**	**9.9**	228	0.65	870	168	1250
DV97-52	---	---	**193**	**0**	113	0.59	695	158	957
DV97-56	---	---	**419**	**28.9**	422	1.21	2088	392	3010
DV97-60	---	---	**496**	**26**	133	1.4	994	450	1125
DV97-61	---	---	**408**	**20.7**	68.4	1.05	777	369	879
DV97-62	---	---	**292**	**15.4**	199	0.83	1079	265	1491
DV97-63	---	---	**219**	**14.6**	142	0.22	804	204	1177
DV97-64	---	---	**292**	**20.1**	179	0.97	1108	273	1589
DV97-65	---	---	**394**	**26.5**	333	1.05	1544	367	2130
DV97-66	---	---	**132**	**0**	123	0.45	693	108	1021
DV97-68	---	---	**221**	**0**	181	0.84	1716	181	2850
DV97-69	---	---	**93.5**	**0**	139	0.96	723	76.6	1011
DV97-72	---	---	**68.8**	**0**	8.05	0.09	144	56.4	152
DV98-106	---	---	**326**	**18.9**	213	1.63	1196	299	1774
DV98-112	---	---	666	0	118	4.01	1508	735	1596
DV98-113	---	---	**453**	**0**	66.2	1.03	773	371	887
DV98-114	---	---	**326**	**0**	186	0.84	1061	267	1496
DV98-117	---	---	282	0	363	1.31	1106	261	1427
DV98-118	---	---	**213**	**0**	243	1.08	2830	175	4920
DV98-120	---	---	57.2	8.9	121	0.95	608	76.4	1006
DV98-128	---	---	267	0	103	1.36	755	302	923
DV98-129	---	---	**471**	**24.2**	147	1.79	1019	426	1254
DV98-131	---	---	**432**	**0**	328	0.97	1722	354	2470
DV98-132	---	---	**376**	**0**	192	0.90	1016	308	1357
DV98-169	---	---	**210**	**0**	67.7	0.25	459	172	579
DV98-170	---	---	**203**	**0**	62.9	0.17	423	166	523
DV98-176	---	---	**131**	**0**	31.7	0.15	290	107	366
DV98-177	---	---	**164**	**0**	28.1	0.17	331	134	396
DV98-178	---	---	**117**	**0**	20.5	0.07	246	95.9	292

Table 4: Continued

Sample	HCO_3(F)^b	CO_3(F)^b	HCO_3(L)^c	CO_3(L)^c	SO_4	B	TDS	Alkalinity	Conductivity (micromhos)
DV98-179	---	---	**95.9**	**0**	21.9	0.10	222	78.6	280
DV99-209	---	---	407	0	451	1.42	2101	376	2770
DV99-210	---	---	315	20.8	515	1.46	2199	310	3120
DV99-211	---	---	395	18.8	67.4	1.10	768	378	792
Background Wells									
DV97-49	---	---	**116**	**0**	82.2	0.35	400	95.1	596
DV97-57	---	---	**244**	**17**	221	0.42	1118	228	1640
DV97-70	---	---	**105**	**0**	67.1	0.37	352	86.1	414
DV97-71	---	---	**92**	**0**	64.2	0.32	336	75.4	397
DV98-115	---	---	**648**	**0**	136	2.16	1201	531	1367
DV98-116	---	---	**277**	**0**	245	1.06	1514	227	2300
DV98-172	---	---	**282**	**15.1**	138	0.24	704	256	940
Background Streams/Rain									
DV97-58	---	---	**274**	**18**	148	0.78	956	255	1374
DV98-107	---	---	257	22.9	222	1.95	1349	340	1975
DV98-110	---	---	**264**	**17.3**	153	0.74	920	245	1301
DV98-119	---	---	**219**	**15.4**	241	1.12	1165	205	1795
DV98-121	---	---	**264**	**21.3**	82.7	0.55	661	252	886
DV98-125	---	---	**61.3**	**0**	16.4	0.23	124	50.2	173
DV98-126	---	---	**97.6**	**0**	22.6	0.19	208	80.0	284
DV98-127	---	---	**99.4**	**0**	62.0	0.19	272	81.5	384
DV98-130	---	---	**144**	**0**	32.0	0.27	284	118	371
DV98-171	---	---	**171**	**7.1**	62.9	0.15	391	152	495
DV98-173	---	---	**365**	**23.6**	223	0.32	1036	339	1348
DV98-174	---	---	**409**	**44.5**	756	0.84	2332	409	3180
DV98-180	---	---	**61.1**	**0**	8.71	0.06	129	50.1	149
DV99-213	---	---	314	54.6	3445	38.2	14390	415	20200
Fumarole Condensates									
DV97-43	---	---	---	---	0.91	0.07	---	---	---
DV97-44	---	---	---	---	37.8	0.11	---	---	---
DV98-108	---	---	**75.4**	**0**	1.62	0.04	99.5	61.8	151

Table 4: Continued

Sample	HCO_3(F)^b	CO_3(F)^b	HCO_3(L)^c	CO_3(L)^c	SO_4	B	TDS	Alkalinity	Conductivity (micromhos)
DV98-109	---	---	**195**	**0**	3.09	<0.02	257	160	387
DV98-164	---	---	**62.2**	**0**	3.61	<0.01	109	51.0	169
DV98-165	---	---	**188**	**0**	2.51	<0.01	251	154	---
DV98-166	---	---	**0**	**0**	33.1	<0.01	36.2	0	---

Table 5: Trace Element Chemistry for Various Geothermal and Regional Fluids, Dixie Valley Region, Nevada (values in ppm).

Sample	Name or Description	Date	Ag	Al (Total)	As	Au	Ba	Be	Cd	Co	Cr	Cs	Cu	Fe	Hg
Brines															
DIXE102-W	V102 + V103 Separator	10/02/95	---	1.41	0.46	---	---	---	---	---	---	0.58	---	0.02	---
DV96-8	76-7 Well	10/25/96	<0.001	1.12	0.51	---	0.07	0.002	<0.002	<0.002	<0.002	0.56	0.016	0.02	<0.0002
DV96-9	V101 Separator	10/25/96	<0.001	1.54	0.47	---	0.01	0.002	<0.002	<0.002	<0.002	0.6	0.009	<0.01	<0.0002
DV97-11	73-7 Well	10/29/97	<0.001	1.04	0.65	<0.002	0.078	0.002	<0.001	<0.002	<0.002	0.56	<0.002	0.04	<0.0001
DV97-13	84-7 Well	10/29/97	<0.001	1.12	0.52	<0.002	0.077	0.002	<0.001	<0.002	<0.002	0.56	<0.002	0.02	<0.0001
DV97-14	74-7 Well	10/29/97	<0.001	1.13	0.65	<0.002	0.073	0.002	<0.001	<0.002	<0.002	0.6	<0.002	0.01	<0.0001
DV97-16	V102 + V103 Separator	10/29/97	<0.001	1.12	0.65	<0.002	0.074	0.002	<0.001	<0.002	<0.002	0.53	<0.002	<0.01	<0.0001
DV97-18	V105 Separator	10/29/97	<0.001	1.05	0.54	<0.002	0.077	0.002	<0.001	<0.002	<0.002	0.62	0.003	0.01	<0.0001
DV97-20	82A-7 Well	10/29/97	<0.001	1.02	0.49	<0.002	0.078	0.002	<0.001	<0.002	<0.002	0.59	<0.002	0.02	<0.0001
DV97-23	73B-7 Well	10/30/97	<0.001	1.08	0.54	<0.002	0.079	0.002	<0.001	<0.002	<0.002	0.6	0.002	<0.01	<0.0001
DV97-25	27-33 Well	10/30/97	<0.001	1.44	0.27	<0.002	0.01	0.002	<0.001	<0.002	<0.002	0.48	<0.002	<0.01	<0.0001
DV97-26	V101 Separator	10/30/97	<0.001	1.47	0.37	<0.002	0.011	0.002	<0.001	<0.002	<0.002	0.5	0.004	0.01	0.0001
DV97-29	37-33 Well	10/30/97	<0.001	0.99	0.19	<0.002	0.007	0.002	<0.001	<0.002	<0.002	0.53	<0.002	0.02	0.107
DV97-30	28-33 Well	10/30/97	<0.001	1.27	0.25	<0.002	0.008	0.002	<0.001	<0.002	<0.002	0.54	<0.002	0.02	0.0001
DV98-73	V101 Separator	04/28/98	<0.001	1.34	0.49	---	0.010	ppm	<0.001	<0.002	<0.002	0.54	<0.002	<0.01	0.00012
DV98-75	27-33 Well	04/28/98	<0.001	1.29	0.35	---	0.010	---	<0.001	<0.002	<0.002	0.45	<0.002	0.01	0.00007
DV98-77	37-33 Well	04/28/98	<0.001	1.42	0.59	<0.0001	0.010	---	<0.001	<0.002	<0.002	0.49	<0.002	<0.01	0.00061
DV98-79	28-33 Well	04/28/98	<0.001	1.39	0.34	---	0.010	---	<0.001	<0.002	<0.002	0.46	<0.002	<0.01	<0.00005
DV98-80	76A-7 Well	04/28/98	<0.001	1.04	0.73	<0.0001	0.069	0.002	<0.001	<0.002	<0.002	0.50	<0.002	<0.01	0.00034
DV98-82	V102 + V103 Separator	04/28/98	<0.001	1.08	0.82	---	0.071	---	<0.001	<0.002	<0.002	0.54	<0.002	<0.01	0.00022
DV98-84	74-7 Well	04/28/98	<0.001	1.09	0.74	<0.0001	0.071	---	<0.001	<0.002	<0.002	0.59	<0.002	<0.01	<0.00005
DV98-86	63-7 Well	04/28/98	<0.001	1.03	0.72	---	0.074	---	<0.001	<0.002	<0.002	0.61	<0.002	<0.01	0.00019
DV98-88	73-7 Well	04/29/98	<0.001	1.04	0.70	0.0004	0.076	---	<0.001	<0.002	<0.002	0.56	<0.002	<0.01	0.00088
DV98-90	82A-7 Well	04/29/98	<0.001	1.01	0.72	---	0.081	---	<0.001	<0.002	<0.002	0.61	<0.002	<0.01	0.00007
DV98-92	V105 Separator	04/29/98	<0.001	1.01	0.80	---	0.080	---	<0.001	<0.002	<0.002	0.55	<0.002	<0.01	<0.00005
DV98-95	73B-7 Well	04/29/98	<0.001	0.97	0.69	<0.0001	0.085	---	<0.001	<0.002	<0.002	0.56	<0.002	<0.01	0.00028
DV98-133	27-33 Well	10/20/98	<0.001	1.31	0.30	---	0.012	<0.002	<0.001	<0.002	<0.002	0.51	<0.002	0.02	0.0003
DV98-135	27-33 Well	10/20/98	<0.001	0.39	0.79	---	0.021	0.003	<0.001	<0.002	<0.002	0.36	<0.002	<0.01	0.0010
DV98-138	V101 Separator	10/21/98	<0.001	1.32	0.35	---	0.012	---	<0.001	<0.002	<0.002	0.51	<0.002	<0.01	0.0013
DV98-140	37-33 Well	10/21/98	<0.001	1.04	0.30	---	0.005	---	<0.001	<0.002	<0.002	0.66	<0.002	<0.01	0.0021
DV98-141	28-33 Well	10/21/98	<0.001	1.36	0.28	---	0.010	<0.002	<0.001	<0.002	<0.002	0.48	<0.002	0.02	0.0001
DV98-145	76A-7 Well	10/22/98	<0.001	1.00	1.01	---	0.077	---	<0.001	<0.002	<0.002	0.53	<0.002	0.01	0.0001
DV98-147	63-7 Well	10/22/98	<0.001	1.02	0.95	---	0.069	---	<0.001	<0.002	<0.002	0.47	<0.002	<0.01	<0.0001
DV98-148	V102 + V103 Separator	10/22/98	<0.001	1.01	1.01	---	0.071	0.002	<0.001	<0.002	<0.002	0.42	<0.002	<0.01	0.0002
DV98-150	74-7 Well	10/22/98	<0.001	1.02	0.86	---	0.071	---	<0.001	<0.002	<0.002	0.48	<0.002	<0.01	<0.0001
DV98-152	73-7 Well	10/22/98	<0.001	1.02	0.95	---	0.079	---	<0.001	<0.002	<0.002	0.35	<0.002	<0.01	0.0004
DV98-154	73B-7 Well	10/22/98	<0.001	0.81	1.03	---	0.071	---	<0.001	<0.002	<0.002	0.50	<0.002	<0.01	0.0001
DV98-156	82A-7 Well	10/23/98	<0.001	0.90	0.81	---	0.068	---	<0.001	<0.002	<0.002	0.48	<0.002	0.01	<0.0001
DV98-159	V105 Separator	10/23/98	<0.001	0.99	0.80	---	0.079	---	<0.001	<0.002	<0.002	0.43	<0.002	<0.01	0.0004
DV99-182	76A-7 Well	05/04/99	<0.001	0.89	0.81	---	0.074	0.002	<0.001	<0.002	<0.002	0.93	<0.002	<0.01	<0.0001

Table 5: Continued

Sample	Name or Description	Date	Ag	Al (Total)	As	Au	Ba	Be	Cd	Co	Cr	Cs	Cu	Fe	Hg
DV99-184	74-7 Well	05/04/99	<0.001	0.97	0.73	---	0.068	0.002	<0.001	<0.002	<0.002	0.97	<0.002	<0.01	<0.0001
DV99-186	V102 + V103 Separator	05/04/99	<0.001	0.97	0.8	---	0.067	<0.002	<0.001	<0.002	<0.002	0.84	<0.002	<0.01	<0.0001
DV99-188	63-7 Well	05/04/99	<0.001	0.98	0.82	---	0.077	0.002	<0.001	<0.002	<0.002	0.9	<0.002	<0.01	<0.0001
DV99-190	73-7 Well	05/04/99	<0.001	1.0	0.83	---	0.074	0.002	<0.001	<0.002	<0.002	0.78	<0.002	<0.01	<0.0001
DV99-194	V105 Separator	05/05/99	<0.001	0.95	0.7	---	0.075	0.002	<0.001	<0.002	<0.002	0.94	<0.002	<0.01	0.0001
DV99-196	82A-7 Well	05/05/99	<0.001	0.86	0.78	---	0.079	0.002	<0.001	<0.002	<0.002	0.81	<0.002	<0.01	<0.0001
DV99-197	73B-7 Well	05/05/99	<0.001	0.96	0.75	---	0.078	0.002	<0.001	<0.002	<0.002	0.8	<0.002	<0.01	<0.0001
DV99-199	37-33 Well	05/05/99	<0.001	1.37	0.48	---	0.011	0.002	<0.001	<0.002	<0.002	0.67	<0.002	<0.01	<0.0001
DV99-200	28-33 Well	05/05/99	<0.001	1.37	0.49	---	0.011	0.002	<0.001	<0.002	<0.002	0.69	<0.002	<0.01	0.0001
DV99-204	V101 Separator	05/05/99	<0.001	1.3	0.43	---	0.01	0.002	<0.001	<0.002	<0.002	0.73	<0.002	<0.01	0.0001
DV74782786-brine	74-7 Well Archived	08/27/86	<0.001	1.1	0.81	---	0.046	0.002	<0.001	<0.002	<0.002	0.68	<0.002	0.01	<0.0001
DV76781986-brine	76-7 Well Archived	08/19/86	<0.001	1.19	0.86	---	0.05	0.002	<0.001	<0.002	<0.002	0.71	<0.002	<0.01	0.0003
DV453382186-brir	45-33 Well Archived	08/21/86	<0.001	1.52	0.68	---	0.019	0.003	<0.001	<0.002	<0.002	0.66	<0.002	0.04	0.0003
DV73782886-brine	73-7 Well Archived	08/28/86	<0.001	0.99	0.79	---	0.024	0.002	<0.001	<0.002	<0.002	0.68	<0.002	0.04	0.0006
DV321882686-brir	32-18 Well Archived	08/26/86	<0.001	0.75	0.75	---	0.047	0.002	<0.001	<0.002	<0.002	0.85	<0.002	0.02	0.0005
DV651882686-brir	65-18 Well Archived	08/26/86	<0.001	0.69	0.95	---	0.053	0.002	<0.001	<0.002	<0.002	0.77	<0.002	0.02	<0.0001
No number	28-33 Well Archived	09/23/93	<0.001	0.88	0.2	---	0.03	<0.002	<0.001	<0.002	<0.002	0.08	0.019	0.82	0.0009
Condensates															
DIXE102-S	V102 + V103 Separator	10/02/95	---	---	---	---	---	---	---	---	---	---	---	0.11	---
DV96-7	76-7 Well	10/25/96	<0.001	<0.01	0.0037	---	<0.01	<0.002	<0.002	<0.002	<0.002	0.055	0.025	1.02	0.0023
DV96-10	V101 Separator	10/25/96	<0.001	<0.01	0.0061	---	<0.01	<0.002	<0.002	<0.002	<0.002	0.06	0.12	0.25	0.103
DV97-12	73-7 Well	10/29/97	---	---	0.42	---	---	---	---	---	---	---	---	---	0.039
DV97-15	74-7 Well	10/29/97	---	---	0.023	---	---	---	---	---	---	---	---	---	0.011
DV97-17	V102 + V103 Separator	10/29/97	---	---	<0.0002	---	---	---	---	---	---	---	---	---	0.028
DV97-19	V105 Separator	10/29/97	---	---	0.0017	---	---	---	---	---	---	---	---	---	0.013
DV97-21	82A-7 Well	10/29/97	---	---	0.047	---	---	---	---	---	---	---	---	---	0.016
DV97-22	73B-7 Well	10/29/97	---	---	0.54	---	---	---	---	---	---	---	---	---	0.012
DV97-24	V101 Separator	10/30/97	---	---	0.0021	---	---	---	---	---	---	---	---	---	0.0054
DV97-27	27-33 Well	10/30/97	---	---	0.0046	---	---	---	---	---	---	---	---	---	0.022
DV97-28	37-33 Well	10/30/97	---	---	<0.0002	---	---	---	---	---	---	---	---	---	0.02
DV97-31	28-33 Well	10/30/97	---	---	0.0075	---	---	---	---	---	---	---	---	---	0.035
DV98-74	V101 Separator	04/28/98	---	---	0.0045	---	---	0.002	---	---	---	---	---	---	0.0090
DV98-76	27-33 Well	04/28/98	---	---	0.0046	---	---	0.002	---	---	---	---	---	---	0.0028
DV98-78	37-33 Well	04/28/98	---	---	0.0072	---	---	0.002	---	---	---	---	---	---	0.083
DV98-81	76A-7 Well	04/28/98	---	---	0.0028	---	---	0.002	---	---	---	---	---	---	0.0098
DV98-83	V102 + V103 Separator	04/28/98	---	---	0.0019	---	---	0.002	---	---	---	---	---	---	0.040
DV98-85	74-7 Well	04/28/98	---	---	0.040	---	---	0.002	---	---	---	---	---	---	0.0106
DV98-87	63-7 Well	04/28/98	---	---	0.0023	---	---	0.002	---	---	---	---	---	---	0.0105
DV98-89	73-7 Well	04/29/98	---	---	0.52	---	---	0.002	---	---	---	---	---	---	0.0094
DV98-91	82A-7 Well	04/29/98	---	---	0.39	---	---	0.002	---	---	---	---	---	---	0.019

Table 5: Continued

Sample	Name or Description	Date	Ag	Al (Total)	As	Au	Ba	Be	Cd	Co	Cr	Cs	Cu	Fe	Hg
DV98-93	V105 Separator	04/29/98	---	---	0.0036	---	---	0.002	---	---	---	---	---	---	0.015
DV98-94	73B-7 Well	04/29/98	---	---	0.0049	---	---	---	---	---	---	---	---	---	0.0037
DV98-101	28-33 Well	04/30/98	---	---	0.0024	---	---	---	---	---	---	---	---	---	0.0039
DV98-136	27-33 Well	10/20/98	---	---	0.0020	---	---	<0.002	---	---	---	---	---	---	0.0250
DV98-137	V101 Separator	10/21/98	---	---	0.0009	---	---	---	---	---	---	---	---	---	0.0156
DV98-139	37-33 Well	10/21/98	---	---	0.0011	---	---	0.002	---	---	---	---	---	---	0.0024
DV98-142	28-33 Well	10/21/98	---	---	0.0092	---	---	0.002	---	---	---	---	---	---	0.0180
DV98-144	76A-7 Well	10/22/98	---	---	0.0010	---	---	0.002	---	---	---	---	---	---	0.0162
DV98-146	V102 + V103 Separator	10/22/98	---	---	<0.0002	---	---	0.002	---	---	---	---	---	---	0.0218
DV98-149	63-7 Well	10/22/98	---	---	0.0004	---	---	0.002	---	---	---	---	---	---	0.0268
DV98-151	74-7 Well	10/22/98	---	---	0.027	---	---	0.002	---	---	---	---	---	---	0.0170
DV98-153	73-7 Well	10/22/98	---	---	0.22	---	---	<0.002	---	---	---	---	---	---	0.0350
DV98-155	73B-7 Well	10/22/98	---	---	0.57	---	---	<0.002	---	---	---	---	---	---	0.0175
DV98-157	82A-7 Well	10/23/98	---	---	0.21	---	---	<0.002	---	---	---	---	---	---	0.0368
DV98-158	V105 Separator	10/23/98	---	---	0.0057	---	---	---	---	---	---	---	---	---	0.0223
DV99-183	76A-7 Well	05/04/99	---	---	0.0019	---	---	---	---	---	---	---	---	---	0.0073
DV99-185	74-7 Well	05/04/99	---	---	0.1	---	---	---	---	---	---	---	---	---	0.0092
DV99-187	V102 + V103 Separator	05/04/99	---	---	0.002	---	---	---	---	---	---	---	---	---	0.0056
DV99-189	63-7 Well	05/04/99	---	---	0.0023	---	---	---	---	---	---	---	---	---	0.0079
DV99-191	73-7 Well	05/04/99	---	---	0.25	---	---	---	---	---	---	---	---	---	0.0072
DV99-192	73B-7 Well	05/04/99	---	---	0.4	---	---	---	---	---	---	---	---	---	0.010
DV99-193	V105 Separator	05/05/99	---	---	<0.0002	---	---	---	---	---	---	---	---	---	0.0024
DV99-195	82A-7 Well	05/05/99	---	---	0.38	---	---	---	---	---	---	---	---	---	0.0101
DV99-201	28-33 Well	05/05/99	---	---	0.0024	---	---	---	---	---	---	---	---	---	0.0031
DV99-202	37-33 Well	05/05/99	---	---	<0.0002	---	---	---	---	---	---	---	---	---	0.0047
DV99-203	V101 Separator	05/05/99	---	---	<0.0002	---	---	---	---	---	---	---	---	---	0.0077
DV74782786-cond	74-7 Well Archived	08/27/86	---	---	<0.0002	---	---	---	---	---	---	---	---	---	0.0004
DV76781986-cond	76-7 Well Archived	08/19/86	---	---	<0.0002	---	---	---	---	---	---	---	---	---	0.001
DV453382886-con	45-33 Well Archived	08/28/86	---	---	<0.0002	---	---	---	---	---	---	---	---	---	0.001
DV73782886-cond	73-7 Well Archived	08/28/86	---	---	0.0006	---	---	---	---	---	---	---	---	---	0.0005
DV321882686-con	32-18 Well Archived	08/26/86	---	---	<0.0002	---	---	---	---	---	---	---	---	---	0.0016
DV651882686-con	65-18 Well Archived	08/26/86	---	---	<0.0002	---	---	---	---	---	---	---	---	---	0.0015
Injection Well/Power Plant Fluids															
DV96-2	Condensate from plant	10/24/96	<0.001	0.14	0.0024	---	<0.01	<0.002	<0.002	<0.002	<0.002	<0.002	0.005	0.06	<0.0002
DV96-3	LP Brine @ Plant	10/24/96	<0.001	1.27	0.74	---	0.04	0.002	<0.002	<0.002	0.013	0.53	<0.002	0.05	<0.0002
DV96-4	45-5 Injection Well	10/24/96	<0.001	1.21	0.86	---	0.05	0.002	<0.002	<0.002	<0.002	0.52	<0.002	0.08	<0.0002
DV96-5	Lamb 1 Injection Well	10/24/96	<0.001	1.39	0.82	---	0.06	0.002	<0.002	<0.002	<0.002	0.61	<0.002	<0.01	<0.0002
DV96-6	65-18 Injection Well	10/24/96	<0.001	1.35	1.44	---	0.06	0.002	<0.002	<0.002	<0.002	0.59	<0.002	0.02	<0.0002
DV97-32	Condensate from plant	10/31/97	---	---	0.098	---	---	---	---	---	---	---	---	---	0.0004
DV97-33	LP Brine	10/31/97	<0.001	1.36	0.93	<0.002	0.056	0.002	<0.001	<0.002	0.003	0.86	0.013	<0.01	0.0002

Table 5: Continued

Sample	Name or Description	Date	Ag	Al (Total)	As	Au	Ba	Be	Cd	Co	Cr	Cs	Cu	Fe	Hg
DV97-34	25-5 + 45-5 Injectate	10/31/97	<0.001	1.14	0.79	<0.002	0.047	0.002	<0.001	<0.002	<0.002	0.68	<0.002	0.02	<0.0001
DV97-35	25-5 + 45-5 Injectate	10/31/97	<0.001	1.14	0.93	---	0.048	0.002	<0.001	<0.002	<0.002	0.71	<0.002	0.02	<0.0001
DV97-36	65-18 Injection Well	10/31/97	<0.001	1.32	1.03	<0.002	0.052	0.002	<0.001	<0.002	0.003	0.8	<0.002	0.01	0.0003
DV97-37	32-18 Injection Well	10/31/97	<0.001	1.34	1.03	<0.002	0.059	0.002	<0.001	<0.002	0.007	0.91	<0.002	0.02	<0.0001
DV97-40	LP Brine @ Plant	10/31/97	<0.001	1.36	1.03	<0.002	0.058	0.002	<0.001	<0.002	<0.002	0.75	<0.002	0.02	<0.0001
DV97-41	Condensate from plant	10/31/97	---	---	0.098	---	---	---	---	---	---	---	---	---	0.0001
DV97-42	High P Brine @ plant	10/31/97	<0.001	1.38	1.38	<0.002	0.01	0.002	<0.001	<0.002	<0.002	0.74	0.002	0.05	0.0001
DV98-97	Condensate from plant	04/29/98	---	---	0.0043	---	---	<0.002	---	---	---	---	---	---	0.00008
DV98-98	LP Brine @ Plant	04/29/98	<0.001	1.22	0.92	---	0.059	---	<0.001	<0.002	<0.002	0.59	<0.002	<0.01	0.00022
DV98-143	25-5 Injection Well	10/21/98	<0.001	1.19	1.06	---	0.060	---	<0.001	<0.002	<0.002	0.54	<0.002	<0.01	0.0001
DV98-161	Condensate from plant	10/23/98	<0.001	0.07	0.060	---	0.006	<0.002	<0.001	<0.002	<0.002	0.016	<0.002	0.07	0.0003
DV98-162	LP Brine @ Plant	10/23/98	<0.001	1.22	1.02	---	0.063	<0.002	<0.001	<0.002	<0.002	0.51	<0.002	<0.01	0.0003
DV98-163	65-18 Injection Well	10/23/98	<0.001	<0.02	0.034	---	0.026	0.002	<0.001	<0.002	<0.002	0.005	<0.002	0.43	0.0002
DV99-198	65-18 Injection Well	05/05/99	<0.001	<0.02	0.0095	---	0.024	<0.002	<0.001	<0.002	<0.002	0.041	<0.002	0.04	0.0001
DV99-205	25-5 + 45-5 Injectate	05/06/99	<0.001	1.19	0.97	---	0.055	0.002	<0.001	<0.002	<0.002	0.83	<0.002	<0.01	<0.0001
DV99-206	LP Brine @ Plant	05/06/99	<0.001	1.26	0.9	---	0.059	0.002	<0.001	<0.002	<0.002	0.86	<0.002	<0.01	0.0001
DV99-207	Condensate from plant	05/06/99	<0.001	0.04	0.0041	---	<0.002	<0.002	<0.001	<0.002	<0.002	0.011	<0.002	0.08	<0.0001
DV99-208	52-18 + 41-18 Injectate	05/06/99	<0.001	1.32	0.98	---	0.058	0.002	<0.001	<0.002	<0.002	0.87	<0.002	<0.01	0.0001
Other Geothermal and On-Site Water Wells															
DV96-1	Domestic Well	10/24/96	<0.001	0.2	0.052		0.04	<0.002	<0.002	<0.002	<0.002	0.084	0.008	1.18	<0.0002
DV97-38	Domestic Well	10/31/97	<0.001	0.1	0.053	<0.002	0.044	<0.002	<0.001	<0.002	<0.002	0.12	<0.002	0.88	0.0002
DV97-39	Goerenger Well	10/31/97	<0.001	0.18	0.013	<0.002	0.038	<0.002	<0.001	<0.002	<0.002	0.063	0.004	0.7	0.0016
DV97-53	46-32 Well	11/05/97	<0.001	0.03	0.008	<0.002	0.005	<0.002	<0.0002	<0.002	<0.002	0.15	<0.002	0.17	0.125
DV97-54	27-32 Well	11/05/97	<0.001	0.04	0.007	<0.002	<0.002	<0.002	0.0002	<0.002	0.002	0.035	0.006	0.2	0.159
DV97-55	27-32 Well	11/05/97	<0.001	0.13	0.31	<0.002	0.016	<0.002	0.0002	<0.002	<0.002	0.15	0.008	0.14	0.013
DV97-59	45-W-5 Well	11/05/97	<0.001	0.03	0.002	---	0.014	<0.002	<0.0002	<0.002	<0.002	0.034	<0.002	0.08	0.0003
DV97-67	66-21 Well	11/07/97	<0.001	0.05	0.23	<0.002	0.33	<0.002	<0.0002	<0.002	<0.002	0.6	<0.002	6.33	0.0004
DV98-96	Goerenger Well	04/29/98	<0.001	<0.02	0.015	---	0.041	<0.002	<0.001	<0.002	<0.002	0.040	<0.002	0.07	0.00025
DV98-99	27-32 Well	04/29/98	---	---	0.34	<0.0001	---	0.002	---	---	---	---	---	---	0.085
DV98-100	46-32 Well	04/29/98	---	---	0.0029	<0.0001	---	---	---	---	---	---	---	---	0.038
DV98-102	45-14 Well	04/30/98	---	---	0.10	---	---	---	---	---	---	---	---	---	0.076
DV98-103	45-14 Well	04/30/98	<0.001	0.23	0.32	---	0.055	---	<0.001	<0.002	<0.002	0.32	<0.002	0.07	0.00053
DV98-104	66-21 Well	04/30/98	<0.001	<0.02	0.14	---	0.34	<0.002	<0.001	<0.002	<0.002	0.52	<0.002	5.85	0.00012
DV98-111	62-21 Well	05/01/98	<0.001	0.09	0.56	<0.0001	0.12	<0.002	<0.001	<0.002	<0.002	0.11	<0.002	0.24	0.00090
DV98-122	97-2 Well	05/05/98	<0.001	<0.02	0.023	---	0.065	<0.002	<0.001	<0.002	0.003	<0.002	0.002	0.31	0.00031
DV98-123	32-6 Well	05/06/98	<0.001	0.04	0.0024	---	0.014	<0.002	<0.001	<0.002	<0.002	<0.002	<0.002	<0.01	0.00014
Dixie Jack #1	Gradient Well DJ #1	05/17/98	<0.001	<0.02	0.043	<0.001	0.049	<0.002	<0.001	<0.002	<0.002	0.09	<0.002	0.03	0.00046
Dixie Jack #4	Gradient Well DJ #4	05/20/98	<0.001	0.07	0.074	<0.001	0.043	<0.002	<0.001	<0.002	0.002	0.28	0.002	0.08	0.00021
Dixie Jack #7	Gradient Well DJ #7	05/14/98	<0.001	0.03	0.003	<0.001	0.003	<0.002	<0.001	<0.002	<0.002	0.009	<0.002	0.02	0.00021
DV98-160	Goerenger Well	10/23/98	<0.001	<0.02	0.014	---	0.039	0.002	<0.001	<0.002	<0.002	0.022	<0.002	0.07	0.0001

Table 5: Continued

Sample	Name or Description	Date	Ag	Al (Total)	As	Au	Ba	Be	Cd	Co	Cr	Cs	Cu	Fe	Hg
DV98-168	38-32 Well	10/26/98	<0.001	<0.02	0.13	---	0.062	---	<0.001	<0.002	<0.002	0.28	0.002	0.34	0.0010
DV98-175	62-21 Well	10/28/98	<0.001	<0.02	0.30	---	0.13	<0.002	<0.001	<0.002	<0.002	0.10	<0.002	4.34	0.0001
DV99-181	Goerenger Well	05/04/99	<0.001	<0.02	0.012		0.041	<0.002	<0.001	<0.002	<0.002	0.093	<0.002	0.05	0.0003
Background Springs															
DV97-46	Sou Hot Spring	11/03/97	<0.001	<0.01	0.012	<0.002	0.068	<0.002	<0.0002	<0.002	0.002	0.17	<0.002	0.01	0.0004
DV97-47	Sou Hot Spring	11/03/97	<0.001	<0.01	0.012	<0.002	0.066	<0.002	0.0003	<0.002	<0.002	0.12	0.022	0.27	0.0001
DV97-48	Hyder Hot Spring	11/03/97	<0.001	0.02	0.033	<0.002	0.15	<0.002	0.0011	<0.002	<0.002	0.35	<0.002	0.04	0.0005
DV97-50	Edward Creek Spring	11/04/97	<0.001	0.02	0.023	---	0.004	<0.002	<0.0002	<0.002	0.005	<0.002	<0.002	0.03	<0.0001
DV 97-51b	Old Man Spring	11/04/97	<0.001	0.02	0.017	<0.002	0.02	<0.002	<0.0002	<0.002	<0.002	<0.002	<0.002	0.02	<0.0001
DV97-52	Horse Heaven Spring	11/04/97	<0.001	<0.01	0.018	---	0.035	<0.002	<0.0002	<0.002	<0.002	<0.002	<0.002	0.04	0.0003
DV97-56	Dead Travertine Spring	11/05/97	<0.001	<0.01	<0.001	<0.002	0.028	<0.002	<0.0002	<0.002	0.009	0.18	0.002	<0.01	0.0002
DV97-60	Fault Line Spring	11/06/97	<0.001	<0.01	0.005	<0.002	0.053	<0.002	<0.0002	<0.002	<0.002	0.047	0.002	<0.01	<0.0001
DV97-61	Lower Ranch Hot Spring	11/06/97	<0.001	<0.01	0.008	<0.002	0.11	<0.002	<0.0002	<0.002	<0.002	0.046	0.003	<0.01	0.0002
DV97-62	McCoy Hot Spring	11/06/97	<0.001	<0.01	0.011	<0.002	0.072	<0.002	<0.0002	<0.002	<0.002	0.014	<0.002	<0.01	0.0003
DV97-63	Kyle Spring	11/06/97	<0.001	0.01	0.003	---	0.049	<0.002	<0.0002	<0.002	<0.002	<0.002	<0.002	0.28	0.0001
DV97-64	Dago Spring	11/06/97	<0.001	<0.01	0.004	---	0.058	<0.002	<0.0002	<0.002	<0.002	<0.002	<0.002	0.03	<0.0001
DV97-65	Mustang Spring	11/06/97	<0.001	<0.01	<0.001	<0.002	0.028	<0.002	<0.0002	<0.002	<0.002	0.047	<0.002	<0.01	<0.0001
DV97-66	Kitten Spring	11/06/97	<0.001	<0.01	<0.001	<0.002	0.008	<0.002	<0.0002	<0.002	0.004	<0.002	<0.002	<0.01	<0.0001
DV97-68	Big Horn Spring	11/07/97	<0.001	0.03	0.041	<0.002	0.075	<0.002	<0.0002	<0.002	0.004	<0.002	<0.002	0.03	<0.0001
DV97-69	Dixie Hot Spring	11/07/97	<0.001	0.03	0.004	<0.002	0.012	<0.002	<0.0002	<0.002	<0.002	0.12	<0.002	<0.01	<0.0001
DV97-72	Horse Creek Spring	11/07/97	<0.001	0.02	<0.001	<0.002	0.019	<0.002	<0.0002	<0.002	<0.002	<0.002	<0.002	0.09	<0.0001
DV98-106	Stu's Seep	04/30/98	<0.001	<0.02	0.010	---	0.028	0.002	<0.001	<0.002	<0.002	<0.002	<0.002	<0.01	0.0015
DV98-112	Hyder Hot Spring	04/30/98	<0.001	<0.02	0.027	---	0.15	<0.002	<0.001	<0.002	<0.002	0.25	<0.002	0.07	0.00019
DV98-113	Lower Ranch Hot Spring	05/04/98	<0.001	<0.02	0.0072	---	0.12	<0.002	<0.001	<0.002	<0.002	0.039	0.003	<0.01	0.00007
DV98-114	McCoy Hot Spring	05/04/98	<0.001	<0.02	0.011	---	0.062	<0.002	<0.001	<0.002	<0.002	0.009	0.003	<0.01	0.00030
DV98-117	Sou Hot Spring	05/04/98	<0.001	<0.02	0.0090	---	0.060	<0.002	<0.001	<0.002	<0.002	0.11	0.002	0.21	0.00031
DV98-118	Big Horn Spring	05/04/98	<0.001	<0.02	0.032	---	0.088	<0.002	<0.001	<0.002	0.004	<0.002	0.003	<0.01	0.00015
DV98-120	Dixie Hot Spring	05/05/98	<0.001	0.13	0.0013	---	0.011	<0.002	<0.001	<0.002	<0.002	0.10	0.003	0.09	<0.00005
DV98-128	Jersey Hot Spring	05/05/98	<0.001	0.04	0.011	---	0.10	<0.002	<0.001	<0.002	<0.002	0.24	<0.002	0.01	0.00016
DV98-129	Upper Jersey Seep	05/06/98	<0.001	0.09	0.042	---	0.014	<0.002	<0.001	<0.002	<0.002	0.15	0.002	0.05	0.00006
DV98-131	Spring in Spring Canyon	05/06/98	<0.001	<0.02	0.013	---	0.023	<0.002	<0.001	<0.002	<0.002	<0.002	<0.002	<0.01	0.00015
DV98-132	Wild Rose Spring	05/07/98	<0.001	<0.02	0.18	---	0.021	<0.002	<0.001	<0.002	<0.002	<0.002	<0.002	<0.01	0.00008
DV98-169	Lofthouse Spring	05/07/98	<0.001	<0.02	0.0078	---	0.058	<0.002	<0.001	<0.002	<0.002	0.005	<0.002	<0.01	0.0001
DV98-170	Not-So-OK Spring	10/27/98	<0.001	<0.02	0.0079	---	0.030	<0.002	<0.001	<0.002	<0.002	<0.002	0.002	<0.01	0.0001
DV98-176	War Canyon Spring	10/27/98	<0.001	<0.02	0.0034	---	0.005	<0.002	<0.001	<0.002	<0.002	0.003	<0.002	0.02	0.0001
DV98-177	Pine Spring	10/28/98	<0.001	<0.02	0.0029	---	0.012	<0.002	<0.001	<0.002	<0.002	<0.002	0.002	<0.01	0.0001
DV98-178	Basalt Spring	10/28/98	<0.001	<0.02	0.0012	---	0.015	<0.002	<0.001	<0.002	<0.002	<0.002	<0.002	<0.01	0.0002
DV98-179	Upper Cherry Spring	10/28/98	<0.001	<0.02	<0.0002	---	0.045	<0.002	<0.001	<0.002	<0.002	<0.002	<0.002	<0.01	0.0001
DV99-209	Dead Travertine Spring	05/07/99	<0.001	<0.02	<0.0002	---	0.023	<0.002	<0.001	<0.002	<0.002	0.2	<0.002	<0.01	0.0002
DV99-210	Dead Travertine, Road Seep	05/08/99	<0.001	<0.02	0.0042	---	0.047	<0.002	<0.001	<0.002	<0.002	0.21	0.005	0.36	0.0004
DV99-211	Upper Spring, Lower Ranch	05/09/99	<0.001	<0.02	0.0072	---	0.1	<0.002	<0.001	<0.002	<0.002	0.055	<0.002	<0.01	0.0002

Table 5: Continued

Sample	Name or Description	Date	Ag	Al (Total)	As	Au	Ba	Be	Cd	Co	Cr	Cs	Cu	Fe	Hg
Background Wells															
DV97-49	Hole in the Wall #2 Well	11/04/97	<0.001	0.01	<0.001	---	0.022	<0.002	0.0003	<0.002	<0.002	<0.002	0.01	<0.01	0.0002
DV97-57	Bolivia Artesian Well	11/05/97	<0.001	<0.01	0.027	<0.002	0.036	<0.002	<0.0002	<0.002	0.002	0.021	0.003	0.43	0.0003
DV97-70	Flowing well @ AA Tank	11/07/97	<0.001	<0.01	0.022	<0.002	0.012	<0.002	<0.0002	<0.002	0.003	<0.002	<0.002	<0.01	<0.0001
DV97-71	Shaw Well	11/07/97	<0.001	0.04	0.029	<0.002	0.014	<0.002	<0.0002	<0.002	0.004	<0.002	<0.002	<0.01	<0.0001
DV98-115	Irrigation Well	05/04/98	<0.001	<0.02	0.0067	---	0.054	<0.002	<0.001	<0.002	0.002	0.025	0.004	<0.01	0.00008
DV98-116	Brinkerhoff Well	05/04/98	<0.001	<0.02	0.0052	---	0.080	<0.002	<0.001	<0.002	0.003	<0.002	0.004	0.01	0.00010
DV98-172	Bernice Well	10/27/98	<0.001	<0.02	0.0008	---	0.002	<0.002	<0.001	<0.002	<0.002	<0.002	<0.002	0.43	0.0002
Background Streams/Rain															
DV97-58	Cottonwood Creek	11/05/97	<0.001	<0.01	0.004	---	0.036	<0.002	<0.0002	<0.002	<0.002	<0.002	<0.002	<0.01	<0.0001
DV98-107	Unnamed Ck by Stu's Seep	04/30/98	<0.001	<0.02	0.010	---	0.11	<0.002	<0.001	<0.002	<0.002	<0.002	0.003	0.01	0.00035
DV98-110	Cottonwood Creek	05/01/98	<0.001	0.19	0.023	---	0.044	---	<0.001	<0.002	0.003	<0.002	<0.002	0.18	0.00024
DV98-119	Unnamed Stream	05/05/98	<0.001	0.31	0.0048	---	0.038	<0.002	<0.001	<0.002	<0.002	<0.002	0.005	0.35	0.00007
DV98-121	White Rock Canyon	05/05/98	<0.001	<0.02	0.0050	---	0.038	<0.002	<0.001	<0.002	<0.002	<0.002	0.003	0.02	<0.00005
DV98-125	Rain, Lizard Well Tank	05/06/98	<0.001	<0.02	0.0043	---	0.004	<0.002	<0.001	<0.002	0.005	0.003	0.018	0.75	<0.00005
DV98-126	Home Station Wash	05/06/98	<0.001	0.28	0.0044	---	0.021	<0.002	<0.001	<0.002	<0.002	<0.002	0.004	0.25	0.00006
DV98-127	Cedar Canyon Wash	05/06/98	<0.001	0.52	0.0010	---	0.023	<0.002	<0.001	<0.002	<0.002	<0.002	0.003	0.38	0.00005
DV98-130	Bucher Creek	05/06/98	<0.001	0.02	0.0020	---	0.044	<0.002	<0.001	<0.002	<0.002	<0.002	<0.002	0.03	<0.00005
DV98-171	Not-So-OK Creek	10/27/98	<0.001	<0.02	0.0026	---	0.029	<0.002	<0.001	<0.002	<0.002	<0.002	<0.002	<0.01	0.0001
DV98-173	Bernice Creek	10/27/98	<0.001	<0.02	0.0065	---	0.029	<0.002	<0.001	<0.002	<0.002	<0.002	<0.002	<0.01	0.0003
DV98-174	Hoyt Creek	10/27/98	<0.001	<0.02	0.025	---	0.030	<0.002	<0.001	<0.002	<0.002	<0.002	<0.002	<0.01	0.0001
DV98-180	Mt. Augusta Creek	10/28/98	<0.001	<0.02	0.0030	---	0.029	<0.002	<0.001	<0.002	<0.002	<0.002	<0.002	<0.01	0.0001
DV99-213	Dixie Salt Lake	05/10/99	<0.001	<0.02	0.18	---	0.03	<0.002	<0.001	<0.002	<0.002	<0.01	<0.002	0.05	0.0004
Fumarole Condensates															
DV97-43	Crack 4 Fumarole	11/03/97	---	0.08	<0.001	---	---	<0.002	---	---	---	---	---	0.02	0.009
DV97-44	Senator Fumarole	11/03/97	<0.001	3.15	0.003	---	---	<0.002	<0.0002	<0.002	0.006	<0.002	<0.002	1.85	0.056
DV98-108	Senator Fumarole	05/01/98	---	---	<0.0002	---	---	<0.002	---	---	---	---	---	---	0.0026
DV98-164	Calcite Fumarole	05/01/98	---	---	0.014	---	---	<0.002	---	---	---	---	---	---	0.0100
DV98-109	Senator Fumarole	10/24/98	---	---	0.0023	---	---	---	---	---	---	---	---	---	0.0040
DV98-165	Calcite Fumarole	10/25/98	---	---	0.0066	---	---	---	---	---	---	---	---	---	0.0104
DV98-166	South Bench Fumarole	10/26/98	---	---	0.0093	---	---	---	---	---	---	---	---	---	0.0008

Table 5: Continued

Sample	I	Mn	Mo	NH_4	Ni	NO_2	NO_3	Pb	PO_4	Rb	S	Sb	Se	S_2O_3	SO_3	Ti	Tl	V	Zn
Brines																			
DIXE102-W	---	<0.01	---	1.46	---	<0.05	<0.05	---	<0.1	0.71	---	---	---	---	0.97	---	---	---	---
DV96-8	0.043	<0.002	0.04	2.13	<0.002	<0.04	0.19	<0.002	<0.1	0.53	0.6	0.088	<0.0001	1.38	0.11	<0.002	---	0.013	<0.01
DV96-9	0.03	<0.002	0.06	1.84	<0.002	<0.04	<0.04	<0.002	<0.1	0.55	1.84	0.069	<0.0001	2.3	0.43	<0.002	---	0.009	<0.01
DV97-11	0.058	<0.002	0.1	1.88	<0.002	<0.05	<0.05	0.002	<0.1	0.61	11.3	0.0082	<0.001	2.3	0.33	<0.002	<0.005	0.011	<0.01
DV97-13	0.051	<0.002	0.08	1.82	<0.002	<0.05	<0.05	0.002	<0.1	0.69	14.3	0.0013	<0.001	2.87	0.43	<0.002	<0.005	0.012	0.01
DV97-14	0.057	<0.002	0.11	1.86	<0.002	<0.05	<0.05	0.002	<0.1	0.64	12.2	0.0069	<0.001	2.51	0.65	<0.002	<0.005	0.009	<0.01
DV97-16	0.055	<0.002	0.12	1.81	0.033	<0.05	<0.05	0.002	<0.1	0.61	10.8	0.0046	<0.001	2.53	0.22	<0.002	<0.005	0.011	<0.01
DV97-18	0.049	<0.002	0.09	1.67	<0.002	<0.05	<0.05	<0.002	<0.1	0.61	13.2	0.0005	<0.001	2.69	0.36	<0.002	<0.005	0.011	<0.01
DV97-20	0.054	<0.002	0.07	1.62	<0.002	<0.05	<0.05	0.002	<0.1	0.64	12.5	0.0092	<0.001	2.75	0.24	<0.002	<0.005	0.011	<0.01
DV97-23	0.055	<0.002	0.07	1.76	<0.002	<0.05	<0.05	0.002	<0.1	0.62	13.9	0.0036	<0.001	2.79	0.23	<0.002	<0.005	0.011	0.02
DV97-25	0.033	<0.002	0.023	1.79	<0.002	<0.05	<0.05	0.002	<0.1	0.57	25.7	0.011	<0.001	4.07	0.93	<0.002	<0.005	0.009	<0.01
DV97-26	0.032	<0.002	0.015	1.67	<0.002	<0.05	<0.05	0.002	<0.1	0.61	23.2	0.02	<0.001	3.68	0.71	<0.002	<0.005	0.011	<0.01
DV97-29	0.04	<0.002	0.023	1.64	<0.002	<0.05	<0.05	<0.002	<0.1	0.58	18.9	0.005	<0.001	3.61	0.63	<0.002	<0.005	0.011	<0.01
DV97-30	0.036	<0.002	0.026	1.63	<0.002	<0.05	<0.05	0.002	<0.1	0.61	17.5	0.0086	<0.001	3.74	0.94	<0.002	<0.005	0.01	<0.01
DV98-73	0.02	<0.002	0.06	1.51	<0.002	<0.05	<0.05	<0.002	<0.1	0.62	0.33	---	---	3.79	0.60	<0.002	---	0.009	<0.01
DV98-75	0.02	<0.002	0.03	1.54	<0.002	<0.05	<0.05	<0.002	<0.1	0.55	1.17	---	---	4.73	0.42	<0.002	---	0.007	<0.01
DV98-77	0.02	<0.002	0.05	1.51	<0.002	<0.05	<0.05	<0.002	<0.1	0.57	1.29	---	---	3.52	0.25	<0.002	---	0.009	<0.01
DV98-79	0.03	<0.002	0.05	1.49	<0.002	<0.05	<0.05	<0.002	<0.1	0.62	1.49	---	---	7.14	0.26	<0.002	---	0.008	<0.01
DV98-80	0.03	<0.002	0.05	1.56	<0.002	<0.05	<0.05	<0.002	<0.1	0.62	0.25	---	---	2.31	<0.05	<0.002	---	0.011	<0.01
DV98-82	0.03	<0.002	0.05	1.68	<0.002	<0.05	<0.05	<0.002	<0.1	0.58	0.33	---	---	2.27	<0.05	<0.002	---	0.009	<0.01
DV98-84	0.03	<0.002	0.06	1.97	<0.002	<0.05	<0.05	<0.002	<0.1	0.60	0.40	---	---	2.36	<0.05	<0.002	---	0.008	<0.01
DV98-86	0.03	<0.002	0.04	1.98	<0.002	<0.05	<0.05	<0.002	<0.1	0.62	0.20	---	---	2.35	<0.05	<0.002	---	0.010	<0.01
DV98-88	0.03	<0.002	0.08	2.15	<0.002	<0.05	<0.05	<0.002	<0.1	0.62	0.32	---	---	3.71	<0.05	<0.002	---	0.008	<0.01
DV98-90	0.03	<0.002	0.06	1.69	<0.002	<0.05	<0.05	<0.002	<0.1	0.62	0.61	---	---	3.68	<0.05	<0.002	---	0.009	<0.01
DV98-92	0.03	<0.002	0.07	1.83	<0.002	<0.05	<0.05	<0.002	<0.1	0.60	0.46	---	---	2.57	<0.05	<0.002	---	0.009	<0.01
DV98-95	0.03	<0.002	0.03	1.63	<0.002	<0.05	<0.05	<0.002	<0.1	0.55	0.25	---	---	2.88	<0.05	<0.002	---	0.008	<0.01
DV98-133	0.03	<0.002	0.039	1.94	<0.002	<0.05	0.17	<0.002	<0.1	0.56	2.51	---	---	4.02	<0.1	<0.002	---	0.011	<0.01
DV98-135	0.04	<0.002	0.068	1.20	<0.002	<0.05	0.45	0.002	<0.1	0.47	1.44	---	---	2.60	<0.1	<0.002	---	0.011	<0.01
DV98-138	0.03	<0.002	0.056	1.99	<0.002	<0.05	<0.05	<0.002	<0.1	0.53	1.83	---	---	3.50	<0.1	<0.002	---	0.008	<0.01
DV98-140	0.03	<0.002	0.049	1.60	<0.002	<0.05	<0.05	<0.002	<0.1	0.63	2.47	---	---	3.7	<0.1	<0.002	---	0.008	<0.01
DV98-141	0.03	<0.002	0.032	1.58	<0.002	<0.05	<0.05	0.002	<0.1	0.57	1.99	---	---	3.85	<0.1	<0.002	---	0.008	<0.01
DV98-145	0.04	0.003	0.048	1.81	<0.002	<0.05	0.12	<0.002	<0.1	0.56	0.63	---	---	2.38	<0.1	<0.002	---	0.010	<0.01
DV98-147	0.04	<0.002	0.052	1.88	<0.002	<0.05	<0.05	<0.002	<0.1	0.57	0.66	---	---	2.22	<0.1	<0.002	---	0.010	<0.01
DV98-148	0.05	<0.002	0.086	1.89	<0.002	<0.05	<0.05	<0.002	<0.1	0.57	0.42	---	---	2.50	<0.1	<0.002	---	0.010	<0.01
DV98-150	0.04	<0.002	0.079	1.89	<0.002	<0.05	<0.05	<0.002	<0.1	0.58	1.08	---	---	2.41	<0.1	<0.002	---	0.010	<0.01
DV98-152	0.05	<0.002	0.095	2.18	<0.002	<0.05	<0.05	<0.002	<0.1	0.57	0.75	---	---	2.31	<0.1	<0.002	---	0.011	<0.01
DV98-154	0.04	<0.002	0.072	2.37	<0.002	<0.05	<0.05	<0.002	<0.1	0.58	0.73	---	---	2.08	<0.1	<0.002	---	0.009	0.03
DV98-156	0.04	<0.002	0.091	1.70	<0.002	<0.05	<0.05	<0.002	<0.1	0.57	1.13	---	---	2.98	<0.1	<0.001	---	0.009	<0.01
DV98-159	0.04	<0.002	0.094	1.88	<0.002	<0.05	<0.05	<0.002	<0.1	0.56	0.89	---	---	2.87	<0.1	<0.002	---	0.012	<0.01
DV99-182	0.04	<0.002	0.05	1.78	<0.002	<0.05	<0.05	<0.002	<0.1	0.59	0.37	---	---	1.74	<0.1	<0.002	---	0.013	<0.01

Table 5: Continued

Sample	I	Mn	Mo	NH_4	Ni	NO_2	NO_3	Pb	PO_4	Rb	S	Sb	Se	S_2O_3	SO_3	Ti	Tl	V	Zn
DV99-184	0.04	<0.002	0.06	1.84	<0.002	<0.05	<0.05	<0.002	<0.1	0.63	0.37	---	---	2.06	<0.1	<0.002	---	0.011	<0.01
DV99-186	0.04	<0.002	0.06	1.7	<0.002	<0.05	<0.05	<0.002	<0.1	0.57	0.37	---	---	1.98	<0.1	<0.002	---	0.011	<0.01
DV99-188	0.04	<0.002	0.07	1.9	<0.002	<0.05	<0.05	<0.002	<0.1	0.65	0.37	---	---	1.41	<0.1	<0.002	---	0.01	<0.01
DV99-190	0.04	<0.002	0.09	1.93	<0.002	<0.05	<0.05	<0.002	<0.1	0.62	0.37	---	---	2.11	<0.1	<0.002	---	0.012	<0.01
DV99-194	0.04	<0.002	0.05	2.05	<0.002	<0.05	<0.05	<0.002	<0.1	0.63	0.37	---	---	2.3	<0.1	<0.002	---	0.013	<0.01
DV99-196	0.04	<0.002	0.08	1.74	<0.002	<0.05	<0.05	<0.002	<0.1	0.62	0.37	---	---	2.66	<0.1	<0.002	---	0.011	<0.01
DV99-197	0.04	<0.002	0.06	1.92	<0.002	<0.05	<0.05	<0.002	<0.1	0.63	0.37	---	---	2.63	<0.1	<0.002	---	0.012	<0.01
DV99-199	0.02	<0.002	0.06	1.66	<0.002	<0.05	<0.05	<0.002	<0.1	0.61	0.37	---	---	3.91	<0.1	<0.002	---	0.009	<0.01
DV99-200	0.02	<0.002	0.06	1.66	<0.002	<0.05	<0.05	<0.002	<0.1	0.62	0.37	---	---	3.74	<0.1	<0.002	---	0.01	<0.01
DV99-204	0.02	0.002	0.06	1.75	<0.002	<0.05	<0.05	<0.002	<0.1	0.65	0.37	---	---	3.74	<0.1	<0.002	---	0.01	<0.01
DV74782786-brine 2	0.03	<0.002	0.04	1.28	<0.002	<0.05	<0.05	<0.002	<0.1	0.6	---	---	---	<0.01	<0.1	<0.002	---	0.008	<0.01
DV76781986-brine 4	0.03	<0.002	0.03	1.42	<0.002	<0.05	<0.05	<0.002	<0.1	0.52	---	---	---	0.18	<0.1	<0.002	---	0.007	<0.01
DV453382186-brine 6	0.03	<0.002	0.04	1.39	<0.002	<0.05	<0.05	<0.002	<0.1	0.59	---	---	---	0.96	<0.1	<0.002	---	0.007	<0.01
DV73782886-brine 8	0.03	0.002	0.04	1.6	<0.002	<0.05	<0.05	<0.002	<0.1	0.56	---	---	---	0.13	<0.1	<0.002	---	0.008	<0.01
DV321882686-brine 10	0.05	0.004	0.05	1.92	<0.002	<0.05	<0.05	<0.002	<0.1	0.38	---	---	---	0.05	<0.1	<0.002	---	0.003	<0.01
DV651882686-brine 12	0.04	0.003	0.04	1.63	<0.002	<0.05	<0.05	<0.002	<0.1	0.31	---	---	---	0.08	<0.1	<0.002	---	0.008	<0.01
No number	0.15	0.047	0.02	0.1	<0.002	<0.05	<0.05	<0.002	<0.1	0.035	---	---	---	<0.01	<0.1	0.019	---	0.003	<0.01
Condensates																			
DIXE102-S	---	---	---	11.4	---	<0.02	<0.02	---	<0.05	---	---	---	---	---	0.37	---	---	---	---
DV96-7	<0.005	0.016	<0.01	14.6	3.75	<0.02	<0.02	0.002	<0.05	0.03	---	0.0011	<0.0001	3.67	<0.05	<0.002	---	<0.002	0.07
DV96-10	<0.005	0.003	<0.01	12.7	<0.002	<0.02	<0.02	0.11	<0.05	0.026	---	0.0012	<0.0001	3.53	<0.05	<0.002	---	<0.002	0.48
DV97-12	---	---	---	11.6	---	<0.02	<0.02	---	<0.05	---	---	---	---	---	0.17	---	---	---	---
DV97-15	---	---	---	12.3	---	<0.02	<0.02	---	<0.05	---	---	---	---	---	0.2	---	---	---	---
DV97-17	---	---	---	13.3	---	<0.02	<0.02	---	<0.05	---	---	---	---	---	<0.05	---	---	---	---
DV97-19	---	---	---	13.5	---	<0.02	<0.02	---	<0.05	---	---	---	---	---	<0.05	---	---	---	---
DV97-21	---	---	---	10.8	---	<0.02	<0.02	---	<0.05	---	---	---	---	---	0.11	---	---	---	---
DV97-22	---	---	---	9.51	---	<0.02	<0.02	---	0.63	---	---	---	---	---	<0.05	---	---	---	---
DV97-24	---	---	---	12.8	---	<0.02	<0.02	---	<0.05	---	---	---	---	---	0.37	---	---	---	---
DV97-27	---	---	---	14.22	---	<0.02	<0.02	---	<0.05	---	---	---	---	---	0.35	---	---	---	---
DV97-28	---	---	---	13.9	---	<0.05	<0.05	---	<0.1	---	---	---	---	---	<0.05	---	---	---	---
DV97-31	---	---	---	13.1	---	<0.02	<0.02	---	<0.05	---	---	---	---	---	<0.05	---	---	---	---
DV98-74	---	---	---	12.3	---	<0.02	<0.02	---	<0.05	---	---	---	---	---	0.09	---	---	---	---
DV98-76	---	---	---	13.4	---	<0.02	<0.02	---	<0.05	---	---	---	---	---	0.81	---	---	---	---
DV98-78	---	---	---	12.3	---	<0.02	<0.02	---	<0.05	---	---	---	---	---	<0.05	---	---	---	---
DV98-81	---	---	---	13.8	---	<0.02	<0.02	---	<0.05	---	---	---	---	---	<0.05	---	---	---	---
DV98-83	---	---	---	13.6	---	<0.02	<0.02	---	<0.05	---	---	---	---	---	<0.05	---	---	---	---
DV98-85	---	---	---	15.7	---	<0.02	<0.02	---	<0.05	---	---	---	---	---	<0.05	---	---	---	---
DV98-87	---	---	---	1.99	---	<0.02	<0.02	---	<0.05	---	---	---	---	---	0.70	---	---	---	---
DV98-89	---	---	---	7.21	---	<0.02	<0.02	---	<0.05	---	---	---	---	---	<0.05	---	---	---	---
DV98-91	---	---	---	9.32	---	<0.02	<0.02	---	<0.05	---	---	---	---	---	0.20	---	---	---	---

Table 5: Continued

Sample	I	Mn	Mo	NH_4	Ni	NO_2	NO_3	Pb	PO_4	Rb	S	Sb	Se	S_2O_3	SO_3	Ti	Tl	V	Zn
DV98-93	---	---	---	15.5	---	<0.02	<0.02	---	<0.05	---	---	---	---	---	<0.05	---	---	---	---
DV98-94	---	---	---	14.2	---	<0.02	<0.02	---	<0.05	---	---	---	---	---	0.78	---	---	---	---
DV98-101	---	---	---	12.0	---	<0.02	0.03	---	<0.05	---	---	---	---	---	0.52	---	---	---	---
DV98-136	---	---	---	13.0	---	<0.02	<0.02	---	<0.05	---	---	---	---	---	0.19	---	---	---	---
DV98-137	---	---	---	0.65	---	<0.02	<0.02	---	<0.05	---	---	---	---	---	0.14	---	---	---	---
DV98-139	---	---	---	13.1	---	<0.02	<0.02	---	<0.05	---	---	---	---	---	0.06	---	---	---	---
DV98-142	---	---	---	12.8	---	<0.02	<0.02	---	0.07	---	---	---	---	---	0.08	---	---	---	---
DV98-144	---	---	---	13.5	---	<0.02	0.02	---	<0.05	---	---	---	---	---	<0.02	---	---	---	---
DV98-146	---	---	---	13.9	---	<0.02	<0.02	---	<0.05	---	---	---	---	---	<0.02	---	---	---	---
DV98-149	---	---	---	15.6	---	<0.02	<0.02	---	<0.05	---	---	---	---	---	<0.02	---	---	---	---
DV98-151	---	---	---	14.9	---	<0.02	0.04	---	<0.05	---	---	---	---	---	0.06	---	---	---	---
DV98-153	---	---	---	15.0	---	<0.02	<0.02	---	<0.05	---	---	---	---	---	<0.02	---	---	---	---
DV98-155	---	---	---	10.3	---	<0.02	<0.02	---	<0.05	---	---	---	---	---	<0.02	---	---	---	---
DV98-157	---	---	---	11.3	---	<0.02	<0.02	---	<0.05	---	---	---	---	---	0.07	---	---	---	---
DV98-158	---	---	---	13.9	---	<0.02	<0.02	---	<0.05	---	---	---	---	---	0.03	---	---	---	---
DV99-183	---	---	---	14.9	---	<0.01	<0.01	---	<0.02	---	---	---	---	---	<0.02	---	---	---	---
DV99-185	---	---	---	13.9	---	<0.01	<0.01	---	<0.02	---	---	---	---	---	<0.02	---	---	---	---
DV99-187	---	---	---	13.9	---	<0.01	<0.01	---	<0.02	---	---	---	---	---	<0.02	---	---	---	---
DV99-189	---	---	---	16.2	---	<0.01	<0.01	---	<0.02	---	---	---	---	---	0.18	---	---	---	---
DV99-191	---	---	---	15	---	<0.01	<0.01	---	<0.02	---	---	---	---	---	<0.02	---	---	---	---
DV99-192	---	---	---	14	---	<0.01	<0.01	---	<0.02	---	---	---	---	---	<0.02	---	---	---	---
DV99-193	---	---	---	15.6	---	<0.01	0.02	---	<0.02	---	---	---	---	---	<0.02	---	---	---	---
DV99-195	---	---	---	14.2	---	<0.01	<0.01	---	<0.02	---	---	---	---	---	<0.02	---	---	---	---
DV99-201	---	---	---	11.5	---	<0.01	<0.01	---	<0.02	---	---	---	---	---	0.33	---	---	---	---
DV99-202	---	---	---	12.8	---	<0.01	<0.01	---	<0.02	---	---	---	---	---	<0.02	---	---	---	---
DV99-203	---	---	---	13.4	---	<0.01	<0.01	---	<0.02	---	---	---	---	---	<0.02	---	---	---	---
DV74782786-cond 1	---	---	---	13	---	<0.01	<0.01	---	<0.02	---	---	---	---	---	<0.02	---	---	---	---
DV76781986-cond 3	---	---	---	13.8	---	<0.01	<0.01	---	<0.02	---	---	---	---	---	<0.02	---	---	---	---
DV453382886-cond 5	---	---	---	11.9	---	<0.01	<0.01	---	<0.02	---	---	---	---	---	<0.02	---	---	---	---
DV73782886-cond 7	---	---	---	12.8	---	<0.01	<0.01	---	<0.02	---	---	---	---	---	<0.02	---	---	---	---
DV321882686-cond 9	---	---	---	17.2	---	<0.01	<0.01	---	<0.02	---	---	---	---	---	<0.02	---	---	---	---
DV651882686-cond 11	---	---	---	15.6	---	<0.01	<0.01	---	<0.02	---	---	---	---	---	<0.02	---	---	---	---
Injection Well/Power Plant Fluids																			
DV96-2	<0.005	0.012	0.02	26.3	<0.002	0.03	43.5	<0.002	<0.05	<0.002	0.04	<0.0001	0.0003	<0.01	<0.05	<0.002	---	<0.002	<0.01
DV96-3	0.04	0.004	0.08	1.02	0.004	<0.04	0.15	<0.002	<0.1	0.58	0.91	0.02	<0.0001	1.45	0.21	<0.002	---	0.013	0.01
DV96-4	0.034	0.004	0.06	2.9	<0.002	<0.04	4.01	<0.002	<0.1	0.57	0.53	0.12	<0.0001	1.11	0.22	<0.002	---	0.012	<0.01
DV96-5	0.043	<0.002	0.06	0.95	<0.002	<0.04	0.08	<0.002	<0.1	0.61	0.78	0.094	<0.0001	0.9	0.35	<0.002	---	0.012	<0.01
DV96-6	0.053	0.003	0.07	0.91	<0.002	<0.04	0.11	<0.002	<0.1	0.61	0.71	0.015	<0.0001	0.76	0.31	<0.002	---	0.012	<0.01
DV97-32	---	---	---	19.1	---	<0.02	57.4	---	<0.05	---	---	---	---	---	<0.05	---	---	---	---
DV97-33	0.056	<0.002	0.059	0.82	<0.002	<0.05	<0.05	0.002	<0.1	0.73	8.91	0.046	<0.001	1.76	0.27	<0.002	<0.005	0.012	<0.01

Table 5: Continued

Sample	I	Mn	Mo	NH_4	Ni	NO_2	NO_3	Pb	PO_4	Rb	S	Sb	Se	S_2O_3	SO_3	Ti	Tl	V	Zn
DV97-34	0.044	<0.002	0.07	3.22	<0.002	<0.05	7.08	0.002	<0.1	0.55	5.44	0.0084	<0.001	0.84	<0.05	<0.002	<0.005	0.01	<0.01
DV97-35	0.039	<0.002	0.06	3.23	<0.002	<0.05	7.35	0.002	<0.1	0.62	5.64	0.0081	<0.001	0.06	<0.05	<0.002	<0.005	0.01	0.02
DV97-36	0.051	<0.002	0.07	0.76	<0.002	<0.05	<0.05	0.002	<0.1	0.72	6.78	0.15	<0.001	<0.01	0.26	<0.002	<0.005	0.014	0.02
DV97-37	0.052	<0.002	0.08	0.81	<0.002	<0.05	<0.05	0.002	<0.1	0.72	6.4	0.022	<0.001	<0.01	0.39	<0.002	<0.005	0.013	<0.01
DV97-40	0.055	<0.002	0.1	0.73	<0.002	<0.05	<0.05	0.002	<0.1	0.74	7.8	0.026	<0.001	1.62	0.42	<0.002	<0.005	0.011	<0.01
DV97-41	---	---	---	19.6	---	<0.02	60.1	---	<0.05	---	---	---	---	---	<0.05	---	---	---	---
DV97-42	0.034	<0.002	0.041	1.51	<0.002	<0.05	<0.05	0.002	<0.1	0.61	19.9	0.055	<0.001	0.25	0.49	<0.002	<0.005	0.013	<0.01
DV98-97	---	---	---	19.1	---	0.03	30.3	---	<0.05	---	---	---	---	---	<0.05	---	---	---	---
DV98-98	0.04	<0.002	0.06	0.94	<0.002	<0.05	0.12	<0.002	<0.1	0.66	0.18	---	---	1.58	<0.05	<0.002	---	0.012	<0.01
DV98-143	0.04	<0.002	0.068	1.02	<0.002	<0.05	<0.05	<0.002	<0.1	0.59	0.28	---	---	1.55	<0.1	<0.002	---	0.009	<0.01
DV98-161	<0.01	0.008	<0.002	15.8	<0.002	10.2	18.0	0.002	<0.05	0.047	0.01	---	---	<0.01	<0.02	<0.002	---	<0.002	<0.01
DV98-162	0.05	<0.002	0.074	0.99	<0.002	<0.05	<0.05	<0.002	<0.1	0.63	0.15	---	---	1.25	<0.1	<0.002	---	0.012	<0.01
DV98-163	0.01	0.14	0.015	7.59	<0.002	5.35	9.24	<0.002	<0.1	0.076	<0.01	---	---	<0.01	<0.1	<0.002	---	0.006	0.03
DV99-198	0.02	0.16	0.006	7.88	<0.002	1.48	6.17	<0.002	<0.02	0.081	0.37	---	---	<0.01	<0.02	<0.002	---	0.012	0.03
DV99-205	0.05	<0.002	0.1	0.81	<0.002	<0.05	<0.05	<0.002	<0.1	0.062	0.37	---	---	1.57	<0.1	<0.002	---	0.013	<0.01
DV99-206	0.04	<0.002	0.09	0.81	<0.002	<0.05	0.07	<0.002	<0.1	0.69	0.37	---	---	1.59	<0.1	<0.002	---	0.012	<0.01
DV99-207	<0.01	<0.002	<0.002	16.5	<0.002	<0.01	15.2	<0.002	<0.02	0.006	0.37	---	---	<0.01	<0.02	<0.002	---	<0.002	<0.01
DV99-208	0.05	<0.002	0.1	0.89	<0.002	<0.05	0.29	<0.002	<0.1	0.66	0.37	---	---	1.43	<0.1	<0.002	---	0.014	<0.01
<u>Other Geothermal and On-Site Water Wells</u>																			
DV96-1	0.027	0.259	0.03	0.17	<0.002	<0.02	0.09	<0.002	<0.1	0.085	0.21	0.0002	<0.0001	<0.01	<0.1	<0.002		<0.002	0.01
DV97-38	0.029	0.22	0.021	0.23	<0.002	<0.02	<0.02	<0.002	<0.05	0.09	---	<0.0002	<0.001	<0.01	<0.05	<0.002	<0.005	<0.002	<0.01
DV97-39	0.037	0.28	0.01	0.56	<0.002	<0.02	<0.02	<0.002	<0.05	0.11	---	<0.0002	<0.001	<0.01	<0.05	0.009	<0.005	0.019	<0.01
DV97-53	<0.005	0.006	0.002	13.1	<0.002	<0.02	0.05	<0.002	<0.05	0.057	---	0.003	<0.001	3.68	0.31	0.002	---	<0.002	<0.01
DV97-54	0.008	0.009	0.006	18.6	0.011	<0.02	<0.02	<0.002	<0.05	0.008	---	0.012	<0.001	3.35	<0.05	0.003	---	<0.002	<0.01
DV97-55	<0.005	0.015	0.31	9.96	<0.002	<0.02	0.54	<0.002	<0.05	0.11	---	0.012	<0.001	1.77	<0.05	<0.002	---	<0.002	<0.01
DV97-59	0.052	0.017	0.005	3.43	<0.002	8.65	0.14	<0.002	<0.05	0.03	---	<0.001	<0.001	<0.01	<0.05	<0.002	---	<0.002	<0.01
DV97-67	0.033	0.13	<0.002	2.06	<0.002	<0.1	<0.05	<0.002	<0.1	0.91	---	<0.001	<0.001	1.57	<0.1	<0.002	---	<0.002	0.01
DV98-96	0.04	0.27	<0.01	0.53	<0.002	<0.02	0.14	---	<0.05	0.092	---	---	---	<0.01	<0.05	<0.002	---	0.018	<0.01
DV98-99	---	---	---	11.3	---	<0.02	<0.02	---	<0.05	---	---	---	---	---	<0.05	---	---	---	---
DV98-100	---	---	---	12.9	---	0.03	0.08	---	<0.05	---	---	---	---	---	0.66	---	---	---	---
DV98-102	---	---	---	14.7	---	<0.02	<0.02	---	<0.05	---	---	---	---	---	<0.05	---	---	---	---
DV98-103	0.03	0.017	<0.01	2.31	<0.002	<0.05	<0.05	<0.002	<0.1	0.28	1.05	---	---	5.16	<0.05	<0.002	---	<0.002	<0.01
DV98-104	0.03	0.12	<0.01	2.08	<0.002	<0.05	<0.05	<0.002	<0.1	0.80	0.87	---	---	2.25	<0.05	<0.002	---	<0.002	<0.01
DV98-111	0.02	0.007	0.01	2.02	<0.002	<0.05	<0.05	---	<0.1	0.065	0.03	---	---	0.84	<0.05	<0.002	---	<0.002	<0.01
DV98-122	<0.01	0.38	0.02	0.76	<0.002	<0.05	0.62	<0.002	2.43	0.090	---	---	---	<0.01	<0.05	<0.002	---	0.025	0.02
DV98-123	<0.01	0.44	<0.01	0.04	<0.002	<0.02	0.03	<0.002	<0.05	0.007	---	---	---	<0.01	<0.05	<0.002	---	<0.002	<0.01
Dixie Jack #1	0.03	0.14	0.045	1.04	0.003	<0.1	0.53	0.003	<0.05	0.09	---	---	---	<0.01	<0.05	<0.002	<0.002	0.009	<0.01
Dixie Jack #4	0.03	0.009	0.009	1.83	<0.002	<0.1	0.25	0.004	1.56	0.19	---	---	---	<0.01	<0.05	<0.002	<0.002	0.003	0.01
Dixie Jack #7	0.01	0.002	0.008	0.44	<0.002	0.05	0.86	<0.002	<0.05	0.011	---	---	---	<0.01	<0.05	<0.002	<0.002	<0.002	<0.01
DV98-160	0.03	0.27	0.025	0.48	<0.002	<0.02	0.35	<0.002	<0.05	0.11	<0.01	---	---	<0.01	<0.05	<0.002	---	0.021	<0.01

Table 5: Continued

Sample	I	Mn	Mo	NH_4	Ni	NO_2	NO_3	Pb	PO_4	Rb	S	Sb	Se	S_2O_3	SO_3	Ti	Tl	V	Zn
DV98-168	0.04	0.093	0.004	2.08	<0.002	<0.05	<0.05	<0.002	<0.1	0.20	---	---	---	1.60	<0.1	<0.002	---	<0.002	0.02
DV98-175	0.02	0.035	<0.002	1.95	<0.002	<0.05	<0.05	0.002	<0.1	0.051	---	---	---	<0.01	<0.1	<0.002	---	<0.002	<0.01
DV99-181	0.03	0.26	0.015	0.52	<0.002	1.77	0.19	<0.002	<0.1	0.13	0.37	---	---	<0.01	<0.1	<0.002	---	0.021	<0.01
<u>Background Springs</u>																			
DV97-46	0.012	0.045	<0.002	0.11	<0.002	<0.02	2.32	0.002	<0.05	0.13	---	0.012	<0.001	<0.01	<0.05	<0.002	---	0.002	0.14
DV97-47	0.007	0.05	<0.002	0.69	<0.002	0.6	<0.02	0.002	<0.05	0.12	---	0.014	<0.001	<0.01	<0.05	<0.002	---	<0.002	0.32
DV97-48	0.012	0.016	<0.002	1.98	<0.002	0.21	<0.02	<0.002	<0.05	0.17	---	0.021	<0.001	<0.01	<0.05	<0.002	---	<0.002	<0.01
DV97-50	<0.005	0.007	0.004	0.1	<0.002	<0.02	0.72	<0.002	<0.05	0.002	---	0.001	<0.001	<0.01	<0.05	<0.002	---	0.015	<0.01
DV 97-51b	<0.005	0.002	0.009	0.05	<0.002	<0.02	<0.02	<0.002	<0.05	0.024	---	0.002	<0.001	<0.01	<0.05	<0.002	---	0.004	0.01
DV97-52	<0.005	0.006	0.007	0.05	0.025	<0.02	1.77	<0.002	0.11	0.013	---	<0.001	<0.001	<0.01	<0.05	<0.002	---	0.012	0.01
DV97-56	<0.005	<0.002	0.004	0.08	<0.002	<0.05	<0.05	<0.002	<0.1	0.43	---	<0.001	<0.001	<0.01	<0.1	<0.002	---	0.002	<0.01
DV97-60	<0.005	0.002	<0.002	0.05	<0.002	<0.02	<0.02	<0.002	<0.05	0.057	---	<0.001	<0.001	<0.01	<0.05	<0.002	---	0.006	<0.01
DV97-61	<0.005	<0.002	<0.002	0.05	<0.002	<0.02	0.48	<0.002	<0.05	0.058	---	0.001	<0.001	<0.01	<0.05	0.028	---	0.006	<0.01
DV97-62	<0.005	<0.002	0.007	0.05	<0.002	<0.05	0.34	<0.002	<0.05	0.035	---	0.001	<0.001	<0.01	<0.05	0.018	---	0.003	<0.01
DV97-63	<0.005	0.007	0.003	0.25	<0.002	<0.05	<0.02	<0.002	<0.05	0.006	---	<0.001	<0.001	<0.01	<0.05	0.015	---	<0.002	<0.01
DV97-64	<0.005	<0.002	0.01	0.18	<0.002	<0.05	<0.02	<0.002	<0.05	<0.002	---	<0.001	<0.001	<0.01	<0.05	<0.002	---	0.009	<0.01
DV97-65	<0.005	<0.002	0.007	0.18	<0.002	<0.05	<0.02	<0.002	<0.05	<0.002	---	0.005	<0.001	<0.01	<0.05	<0.002	---	0.002	<0.01
DV97-66	<0.005	<0.002	<0.002	0.21	<0.002	<0.05	5.38	<0.002	<0.05	0.009	---	0.005	<0.001	<0.01	<0.05	<0.002	---	0.006	<0.01
DV97-68	<0.005	0.003	<0.002	0.14	<0.002	<0.1	<0.05	<0.002	<0.1	0.004	---	0.002	<0.001	<0.01	<0.1	0.006	---	0.018	<0.01
DV97-69	0.013	0.006	<0.002	0.2	<0.002	<0.05	0.07	<0.002	<0.05	0.048	---	0.001	<0.001	1.2	<0.05	<0.002	---	<0.002	<0.01
DV97-72	<0.005	<0.002	<0.002	0.16	<0.002	<0.02	<0.02	<0.002	<0.05	<0.002	---	<0.001	<0.001	<0.01	<0.05	<0.002	---	<0.002	<0.01
DV98-106	<0.01	<0.002	<0.01	<0.02	<0.002	<0.02	6.05	---	<0.05	0.006	---	---	---	<0.01	<0.05	<0.002	---	0.011	<0.01
DV98-112	<0.01	0.015	<0.01	1.97	<0.002	<0.02	<0.02	---	<0.05	0.16	---	---	---	<0.01	<0.05	<0.002	---	<0.002	<0.01
DV98-113	<0.01	<0.002	<0.01	0.02	<0.002	<0.02	0.38	---	<0.05	0.048	---	---	---	<0.01	<0.05	<0.002	---	0.004	<0.01
DV98-114	<0.01	<0.002	<0.01	<0.02	<0.002	<0.02	0.20	---	<0.05	0.030	---	---	---	<0.01	<0.05	<0.002	---	0.004	<0.01
DV98-117	<0.01	0.041	<0.01	0.51	<0.002	<0.02	0.11	---	<0.05	0.12	---	---	---	<0.01	<0.05	<0.002	---	<0.002	<0.01
DV98-118	<0.01	0.004	<0.01	<0.02	<0.002	<0.05	<0.05	<0.002	<0.1	0.006	---	---	---	<0.01	<0.05	<0.002	---	0.010	<0.01
DV98-120	<0.01	0.009	0.03	0.21	<0.002	<0.02	<0.02	<0.002	<0.05	0.056	---	---	---	1.32	0.13	0.004	---	<0.002	<0.01
DV98-128	<0.01	0.12	<0.01	1.55	<0.002	<0.02	<0.02	<0.002	<0.05	0.27	---	---	---	<0.01	<0.05	<0.002	---	<0.002	<0.01
DV98-129	<0.01	0.017	<0.01	0.04	<0.002	<0.02	<0.02	<0.002	<0.05	0.22	---	---	---	<0.01	<0.05	0.003	---	0.003	0.01
DV98-131	<0.01	0.002	0.04	<0.02	<0.002	<0.05	0.13	<0.002	<0.1	0.005	---	---	---	<0.01	<0.05	<0.002	---	0.039	<0.01
DV98-132	<0.01	<0.002	0.03	<0.02	<0.002	<0.02	<0.02	<0.002	<0.05	<0.002	---	---	---	<0.01	<0.05	<0.002	---	0.015	<0.01
DV98-169	<0.01	<0.002	<0.002	0.05	<0.002	<0.02	<0.02	<0.002	<0.05	<0.002	---	---	---	<0.01	<0.05	<0.002	---	0.003	<0.01
DV98-170	<0.01	<0.002	<0.002	0.03	<0.002	<0.02	<0.02	0.003	0.15	<0.002	---	---	---	<0.01	<0.05	<0.002	---	0.004	<0.01
DV98-176	<0.01	<0.002	<0.002	0.03	<0.002	<0.02	2.38	<0.002	<0.05	0.002	---	---	---	<0.01	<0.05	<0.002	---	<0.002	<0.01
DV98-177	<0.01	<0.002	<0.002	<0.02	<0.002	<0.02	<0.02	<0.002	0.24	0.006	---	---	---	<0.01	<0.05	<0.002	---	0.005	<0.01
DV98-178	<0.01	<0.002	<0.002	<0.02	<0.002	<0.02	1.53	<0.002	<0.05	0.004	---	---	---	<0.01	<0.05	<0.002	---	0.009	<0.01
DV98-179	<0.01	<0.002	<0.002	0.02	<0.002	<0.02	4.78	<0.002	<0.05	<0.002	---	---	---	<0.01	<0.05	<0.002	---	0.005	<0.01
DV99-209	<0.01	0.002	0.03	0.08	<0.002	<0.05	<0.01	0.002	<0.02	0.45	---	---	---	<0.01	<0.05	<0.002		<0.002	0.01
DV99-210	<0.01	0.22	<0.002	0.07	<0.002	<0.05	<0.01	0.003	<0.02	0.56	---	---	---	<0.01	<0.05	0.013		0.006	<0.01
DV99-211	<0.01	<0.002	<0.002	<0.02	<0.002	<0.01	0.04	<0.002	<0.02	0.06	---	---	---	<0.01	<0.02	<0.002		0.006	<0.01

Table 5: Continued

Sample	I	Mn	Mo	NH_4	Ni	NO_2	NO_3	Pb	PO_4	Rb	S	Sb	Se	S_2O_3	SO_3	Ti	Tl	V	Zn
Background Wells																			
DV97-49	0.023	0.03	<0.002	0.09	<0.002	<0.02	0.05	<0.002	<0.05	0.019	---	<0.001	<0.001	<0.01	<0.05	<0.002	---	<0.002	0.23
DV97-57	<0.005	0.007	<0.002	0.11	<0.002	<0.05	<0.02	<0.002	<0.05	0.026	---	0.002	<0.001	<0.01	<0.05	<0.002	---	<0.002	<0.01
DV97-70	<0.005	<0.002	0.023	0.06	<0.002	<0.02	0.81	<0.002	<0.05	0.002	---	0.001	<0.001	<0.01	<0.05	<0.002	---	0.02	<0.01
DV97-71	<0.005	<0.002	0.018	0.04	<0.002	<0.02	0.31	0.004	<0.05	0.002	---	<0.001	<0.001	<0.01	<0.05	<0.002	---	0.015	<0.01
DV98-115	<0.01	<0.002	<0.01	<0.02	<0.002	<0.02	7.27	---	<0.05	0.055	---	---	---	<0.01	<0.05	<0.002	---	0.013	0.01
DV98-116	<0.01	<0.002	0.02	<0.02	<0.002	<0.05	36.0	---	<0.1	0.005	---	---	---	<0.01	<0.05	<0.002	---	0.007	0.10
DV98-172	<0.01	0.34	<0.002	0.06	<0.002	<0.02	<0.02	<0.002	<0.05	<0.002	---	---	---	<0.01	<0.05	<0.002	---	<0.002	<0.01
Background Streams/Rain																			
DV97-58	<0.005	<0.002	0.005	0.31	<0.002	<0.05	<0.02	<0.002	<0.05	0.005	---	<0.001	<0.001	<0.01	<0.05	<0.002	---	0.005	<0.01
DV98-107	<0.01	<0.002	0.02	<0.02	<0.002	<0.02	0.78	---	<0.05	0.005	---	---	---	<0.01	<0.05	<0.002	---	0.009	<0.01
DV98-110	<0.01	0.002	0.02	<0.02	<0.002	<0.02	<0.02	---	<0.05	0.005	---	---	---	<0.01	<0.05	0.004	---	0.009	<0.01
DV98-119	<0.01	0.012	<0.01	<0.02	<0.002	<0.02	3.30	<0.002	<0.05	0.004	---	---	---	<0.01	<0.05	0.011	---	<0.002	<0.01
DV98-121	<0.01	0.003	0.02	<0.02	<0.002	<0.02	<0.02	<0.002	<0.05	0.002	---	---	---	<0.01	<0.05	<0.002	---	0.004	<0.01
DV98-125	<0.01	<0.002	0.04	0.22	<0.002	<0.02	<0.02	<0.002	<0.05	0.011	---	---	---	<0.01	<0.05	<0.002	---	<0.002	0.05
DV98-126	<0.01	0.019	0.02	0.04	<0.002	<0.02	<0.02	<0.002	<0.05	0.004	---	---	---	<0.01	<0.05	0.012	---	0.002	<0.01
DV98-127	<0.01	0.007	0.02	0.02	<0.002	<0.02	<0.02	<0.002	0.18	0.005	---	---	---	<0.01	<0.05	0.021	---	<0.002	<0.01
DV98-130	<0.01	0.003	<0.01	<0.02	<0.002	<0.02	<0.02	<0.002	<0.05	0.004	---	---	---	<0.01	<0.05	<0.002	---	<0.002	<0.01
DV98-171	<0.01	<0.002	<0.002	0.02	<0.002	<0.02	<0.02	<0.002	<0.05	<0.002	---	---	---	<0.01	<0.05	<0.002	---	0.002	<0.01
DV98-173	<0.01	0.002	0.003	<0.02	<0.002	<0.02	<0.02	<0.002	<0.05	0.003	---	---	---	<0.01	<0.05	<0.002	---	0.004	<0.01
DV98-174	<0.01	<0.002	<0.002	<0.02	<0.002	<0.05	<0.05	0.002	<0.1	0.002	---	---	---	<0.01	<0.1	<0.002	---	0.003	<0.01
DV98-180	<0.01	<0.002	<0.002	0.02	<0.002	<0.02	0.68	<0.002	0.12	<0.002	---	---	---	<0.01	<0.05	<0.002	---	0.006	<0.01
DV99-213	0.19	0.022	0.003	0.16	<0.002	<0.5	<0.5	0.003	<1	0.035	---	---	---	<0.01	<1	<0.002	---	0.006	0.01
Fumarole Condensates																			
DV97-43	---	0.045	---	---	---	0.02	<0.04	---	<0.05	---	---	---	---	---	<0.05	---	---	<0.002	<0.01
DV97-44	---	0.031	<0.002	---	0.002	0.03	0.48	<0.002	<0.05	0.01	---	---	---	---	<0.05	---	---	0.01	0.1
DV98-108	---	---	---	21.5	---	<0.02	<0.02	---	<0.05	---	---	---	---	---	0.11	---	---	---	---
DV98-164	---	---	---	21.1	---	<0.02	0.06	---	<0.05	---	---	---	---	---	<0.02	---	---	---	---
DV98-109	---	---	---	58.1	---	<0.02	<0.02	---	<0.05	---	---	---	---	---	<0.05	---	---	---	---
DV98-165	---	---	---	56.0	---	<0.02	0.02	---	<0.05	---	---	---	---	---	<0.02	---	---	---	---
DV98-166	---	---	---	0.17	---	<0.02	0.06	---	<0.05	---	---	---	---	---	<0.02	---	---	---	---

Table 6: Analytical Results From Various Aluminum Samples And Extractions (All values in ppm).

Sample	Name or Description	Date	Total Al[a] (0.45 micron)	Ionized Al[b] (0.2 micron)	Ionized Al[b] (0.45 micron)	Ionized Al[c] (unfiltered)
Brines						
DIXE102-W	V102 + V103 Separator	10/02/95	1.41	---	---	---
DV96-8	76-7 Well	10/25/96	1.12	0.050	0.059	---
DV96-9	V101 Separator	10/25/96	1.54	0.101	0.0088	---
DV97-11	73-7 Well	10/29/97	1.04	0.063	---	---
DV97-13	84-7 Well	10/29/97	1.12	0.063	---	---
DV97-14	74-7 Well	10/29/97	1.13	0.082	---	---
DV97-16	V102 + V103 Separator	10/29/97	1.12	0.100	---	---
DV97-18	V105 Separator	10/29/97	1.05	0.126	---	---
DV97-20	82A-7 Well	10/29/97	1.02	0.043	---	---
DV97-23	73B-7 Well	10/30/97	1.08	0.049	---	---
DV97-25	27-33 Well	10/30/97	1.44	0.043	---	---
DV97-26	V101 Separator	10/30/97	1.47	0.055	---	---
DV97-29	37-33 Well	10/30/97	0.99	0.024	---	---
DV97-30	28-33 Well	10/30/97	1.27	0.060	---	---
DV98-73	V101 Separator	04/28/98	1.34	0.022	---	---
DV98-75	27-33 Well	04/28/98	1.29	0.028	---	---
DV98-77	37-33 Well	04/28/98	1.42	0.022	---	---
DV98-79	28-33 Well	04/28/98	1.39	0.032	---	---
DV98-80	76A-7 Well	04/28/98	1.04	0.035	---	---
DV98-82	V102 + V103 Separator	04/28/98	1.08	0.027	---	---
DV98-84	74-7 Well	04/28/98	1.09	0.039	---	---
DV98-86	63-7 Well	04/28/98	1.03	0.022	---	---
DV98-88	73-7 Well	04/29/98	1.04	0.057	---	---
DV98-90	82A-7 Well	04/29/98	1.01	0.054	---	---
DV98-92	V105 Separator	04/29/98	1.01	0.036	---	---
DV98-95	73B-7 Well	04/29/98	0.97	0.042	---	---
DV98-133	27-33 Well	10/20/98	1.31	0.032	---	---
DV98-135	27-33 Well	10/20/98	0.39	0.001	---	---
DV98-138	V101 Separator	10/21/98	1.32	0.041	---	---
DV98-140	37-33 Well	10/21/98	1.04	0.051	---	---
DV98-141	28-33 Well	10/21/98	1.36	0.044	---	---
DV98-145	76A-7 Well	10/22/98	1.00	0.022	---	---
DV98-147	63-7 Well	10/22/98	1.02	0.025	---	---
DV98-148	V102 + V103 Separator	10/22/98	1.01	0.038	---	---
DV98-150	74-7 Well	10/22/98	1.02	0.029	---	---
DV98-152	73-7 Well	10/22/98	1.02	0.026	---	---
DV98-154	73B-7 Well	10/22/98	0.81	0.037	---	---
DV98-156	82A-7 Well	10/23/98	0.90	0.061	---	---
DV98-159	V105 Separator	10/23/98	0.99	0.043	---	---
DV99-182	76A-7 Well	05/04/99	0.89	---	---	0.283
DV99-184	74-7 Well	05/04/99	0.97	---	---	0.233
DV99-186	V102 + V103 Separator	05/04/99	0.97	---	---	---
DV99-188	63-7 Well	05/04/99	0.98	---	---	0.33
DV99-190	73-7 Well	05/04/99	1.00	---	---	0.25
DV99-194	V105 Separator	05/05/99	0.95	---	---	0.261
DV99-196	82A-7 Well	05/05/99	0.86	---	---	0.29
DV99-197	73B-7 Well	05/05/99	0.96	---	---	0.242
DV99-199	37-33 Well	05/05/99	1.37	---	---	0.25

Table 6: Continued

Sample	Name or Description	Date	Total Al[a] (0.45 micron)	Ionized Al[b] (0.2 micron)	Ionized Al[b] (0.45 micron)	Ionized Al[c] (unfiltered)
DV99-200	28-33 Well	05/05/99	1.37	---	---	0.20
DV99-204	V101 Separator	05/05/99	1.30	---	---	0.33
DV74782786-brine 2	74-7 Well Archived	08/27/86	1.10	---	---	---
DV76781986-brine 4	76-7 Well Archived	08/19/86	1.19	---	---	---
DV453382186-brine 6	45-33 Well Archived	08/21/86	1.52	---	---	---
DV73782886-brine 8	73-7 Well Archived	08/28/86	0.99	---	---	---
DV321882686-brine 10	32-18 Well Archived	08/26/86	0.75	---	---	---
DV651882686-brine 12	65-18 Well Archived	08/26/86	0.69	---	---	---
No number	28-33 Well Archived	09/23/93	0.88	---	---	---
Injection Well/Power Plant Fluids						
DV96-2	Condensate from plant	10/24/96	0.14	0.0096	0.0106	---
DV96-3	LP Brine @ Plant	10/24/96	1.27	0.025	0.011	---
DV96-4	45-5 Injection Well	10/24/96	1.21	0.0079	0.0087	---
DV96-5	Lamb 1 Injection Well	10/24/96	1.39	0.0004	0.0004	---
DV96-6	65-18 Injection Well	10/24/96	1.35	0.0004	0.0014	---
DV97-33	LP Brine	10/31/97	1.36	0.04	---	---
DV97-34	25-5 + 45-5 Injectate	10/31/97	1.14	0.045	---	---
DV97-35	25-5 + 45-5 Injectate	10/31/97	1.14	0.103	---	---
DV97-36	65-18 Injection Well	10/31/97	1.32	0.0021	---	---
DV97-37	32-18 Injection Well	10/31/97	1.34	0.0036	---	---
DV97-40	LP Brine @ Plant	10/31/97	1.36	0.0081	---	---
DV97-42	High P Brine @ plant	10/31/97	1.38	0.038	---	---
DV98-98	LP Brine @ Plant	04/29/98	1.22	0.024	---	---
DV98-143	25-5 Injection Well	10/21/98	1.19	0.023	---	---
DV98-161	Condensate from plant	10/23/98	0.07	---	---	---
DV98-162	LP Brine @ Plant	10/23/98	1.22	0.040	---	---
DV98-163	65-18 Injection Well	10/23/98	<0.02	0.009	0.036	---
DV99-198	65-18 Injection Well	05/05/99	<0.02	---	---	0.001
DV99-205	25-5 + 45-5 Injectate	05/06/99	1.19	---	---	0.549
DV99-206	LP Brine @ Plant	05/06/99	1.26	---	---	0.774
DV99-207	Condensate from plant	05/06/99	0.04	---	---	0.004
DV99-208	52-18 + 41-18 Injectate	05/06/99	1.32	---	---	0.319
Other Geothermal and On-Site Water Wells						
DV96-1	Domestic Well	10/24/96	0.20	0.0026	---	---
DV97-38	Domestic Well	10/31/97	0.10	0.0028	---	---
DV97-39	Goerenger Well	10/31/97	0.18	0.022	---	---
DV97-53	46-32 Well	11/05/97	0.03	---	---	---
DV97-54	27-32 Well	11/05/97	0.04	---	---	---
DV97-55	27-32 Well	11/05/97	0.13	---	---	---
DV97-59	45-W-5 Well	11/05/97	0.03	---	---	---
DV97-67	66-21 Well	11/07/97	0.05	---	---	---
DV98-96	Goerenger Well	04/29/98	<0.02	0.0002	---	---
DV98-103	45-14 Well	04/30/98	0.23	---	---	---
DV98-104	66-21 Well	04/30/98	<0.02	---	---	---
DV98-111	62-21 Well	05/01/98	0.09	0.074	---	---
DV98-122	97-2 Well	05/05/98	<0.02	---	---	---
DV98-123	32-6 Well	05/06/98	0.04	---	---	---

Table 6: Continued

Sample	Name or Description	Date	Total Al[a] (0.45 micron)	Ionized Al[b] (0.2 micron)	Ionized Al[b] (0.45 micron)	Ionized Al[c] (unfiltered)
Dixie Jack #1	Gradient Well DJ #1	05/17/98	<0.02	---	---	---
Dixie Jack #4	Gradient Well DJ #4	05/20/98	0.07	---	---	---
Dixie Jack #7	Gradient Well DJ #7	05/14/98	0.03	---	---	---
DV98-160	Goerenger Well	10/23/98	<0.02	0.001	---	---
DV98-168	38-32 Well	10/26/98	<0.02	---	---	---
DV98-175	62-21 Well	10/28/98	<0.02	---	---	---
DV99-181	Goerenger Well	05/04/99	<0.02	---	---	0.004

[a] Analyses by ICP on filtered samples acidified with spectrographcially pure HNO_3 (see Table 3).

[b] Analyses by GFAA on filtered samples using MIBK extraction method of Barnes (1975).

[c] Analyses by GFAA on filtered samples using MIBK extraction method of Barnes (1975). Data were corrected using a "spike" procedure with duplicate unfiltered samples in which 1 ppm Al is added to a sample and the other is corrected.

Table 7: Miscellaneous Isotope Data for Various Geothermal and Regional Fluids from the Dixie Valley Region, Nevada.[a]

Sample	Name or Description	Date	^3H[b] (TU)	δD (USGS) (per mil)	$\delta^{18}O$ (USGS) (per mil)	δD (WM) (per mil)	$\delta^{18}O$ (WM) (per mil)	$\delta^{13}C-HCO_3^-$ (per mil)	$\delta^{18}O-SO_4^{2-}$[c] (per mil)	$\delta^{18}O$ (Total Fluid) (per mil)	$\delta^{18}O$ ($SO_4^{2-}-H_2O$)[d] (°C)
Brines											
DV96-8	76-7 Well	10/25/96	0.07	---	---	-124	-14.2	-8.0	---	---	---
DV96-8b	76-7 Well	10/25/96	0.07	---	---	-119	-14.0	---	---	---	---
DV96-9	V101 Separator	10/25/96	0.12	---	---	-123	-14.3	-8.0	---	---	---
DV96-9b	V101 Separator	10/25/96	---	---	---	-123	-14.3	---	---	---	---
DV97-11	73-7 Well	10/29/97	---	-126	-13.21	-113	-13.9	-7.36	-7.94	-13.51	271
DV97-13	84-7 Well	10/29/97	---	-128	-13.37	-118	-14.0	-8.23	-8.34	---	---
DV97-14	74-7 Well	10/29/97	---	-126	-13.40	-118	-14.0	-7.74	-8.04	-13.97	261
DV97-16	V102 + V103 Separator	10/29/97	---	-126	-13.21	-123	-14.0	-7.66	-8.56	---	---
DV97-18	V105 Separator	10/29/97	**-0.07**	-125	-13.21	-122	-13.9	-8.66	-8.29	---	---
DV97-20	82A-7 Well	10/29/97	---	-127	-13.24	-123	-14.0	-7.39	-8.46	-13.29	293
DV97-23	73B-7 Well	10/30/97	0.38	-125	-13.14	-125	-13.9	-8.06	-7.96	-13.52	271
DV97-25	27-33 Well	10/30/97	0.38	-128	-13.96	-125	-14.7	-7.85	-9.05	-14.40	277
DV97-26	V101 Separator	10/30/97	0.10	-129	-13.72	-124	-14.5	-7.23	-8.86	---	---
DV97-29	37-33 Well	10/30/97	0.48	-129	-13.79	-124	-14.5	-7.35	-9.01	-14.24	281
DV97-30	28-33 Well	10/30/97	---	-126	-13.75	-124	-14.5	-6.91	-9.21	-14.17	289
DV98-73	V101 Separator	04/28/98	---	-126	-13.80	---	---	-7.02	---	-14.24	---
DV98-75	27-33 Well	04/28/98	---	-126	-13.89	---	---	-7.28	---	-14.33	---
DV98-77	37-33 Well	04/28/98	---	-127	-13.76	---	---	-7.05	-9.07	-14.19	284
DV98-79	28-33 Well	04/28/98	---	-127	-13.75	---	---	-7.60	-8.89	---	---
DV98-80	76A-7 Well	04/28/98	---	-125	-13.33	---	---	-6.85	-8.45	-13.82	277
DV98-82	V102 + V103 Separator	04/28/98	---	-124	-13.21	---	---	-6.72	---	-13.63	---
DV98-84	74-7 Well	04/28/98	---	-125	-13.27	---	---	-6.60	-8.49	-13.74	278
DV98-86	63-7 Well	04/28/98	0.48	-125	-13.10	---	---	-7.64	-8.07	-13.55	273
DV98-88	73-7 Well	04/29/98	---	-125	-13.11	---	---	-7.67	---	-13.19	---
DV98-90	82A-7 Well	04/29/98	---	-125	-13.24	---	---	-8.58	-8.32	-13.44	284
DV98-92	V105 Separator	04/29/98	---	-124	-13.12	---	---	-6.58	---	-13.55	---
DV98-95	73B-7 Well	04/29/98	---	-126	-13.17	---	---	-7.95	-8.16	-13.60	275
DV98-133	27-33 Well	10/20/98	---	-129	-14.01	---	---	-7.28	---	---	---
DV98-135	27-33 Well	10/20/98	0.04	-127	-13.81	---	---	-6.26	-9.48	---	---
DV98-138	V101 Separator	10/21/98	---	-127	-13.71	---	---	-7.17	---	---	---
DV98-140	37-33 Well	10/21/98	0.08	-127	-13.76	---	---	-6.98	-8.69	---	---
DV98-141	28-33 Well	10/21/98	---	-127	-13.69	---	---	-7.24	-9.05	---	---
DV98-145	76A-7 Well	10/22/98	0.11	-126	-13.27	---	---	-7.26	-8.55	---	---
DV98-147	63-7 Well	10/22/98	0.33	-124	-12.97	---	---	-7.48	-8.51	---	---
DV98-148	V102 + V103 Separator	10/22/98	---	-125	-13.09	---	---	-7.38	---	---	---
DV98-150	74-7 Well	10/22/98	---	-126	-13.23	---	---	-8.78	-8.44	---	---
DV98-152	73-7 Well	10/22/98	---	-125	-12.96	---	---	-8.21	-8.60	---	---
DV98-154	73B-7 Well	10/22/98	---	-126	-13.14	---	---	-7.52	-7.88	---	---
DV98-156	82A-7 Well	10/23/98	---	-125	-13.14	---	---	-7.09	-7.75	---	---
DV98-159	V105 Separator	10/23/98	---	-125	-13.07	---	---	-7.37	---	---	---
DV99-182	76A-7 Well	05/04/99	---	-125	-13.21	---	---	-8.02	---	---	---

Table 7: Continued

Sample	Name or Description	Date	$^3H^b$ (TU)	δD (USGS) (per mil)	$\delta^{18}O$ (USGS) (per mil)	δD (WM) (per mil)	$\delta^{18}O$ (WM) (per mil)	$\delta^{13}C-HCO_3^-$ (per mil)	$\delta^{18}O-SO_4^{2-c}$ (per mil)	$\delta^{18}O$ (Total Fluid) (per mil)	$\delta^{18}O$ ($SO_4^{2-}-H_2O$)^d (°C)
DV99-184	74-7 Well	05/04/99	---	-126	-13.08	---	---	-6.87	-8.28	---	---
DV99-186	V102 + V103 Separator	05/04/99	---	-125	-13.10	---	---	-6.88	-7.82	---	---
DV99-188	63-7 Well	05/04/99	---	-125	-12.96	---	---	-8.01	---	---	---
DV99-190	73-7 Well	05/04/99	---	-124	-12.89	---	---	---	---	---	---
DV99-194	V105 Separator	05/05/99	---	-124	-13.04	---	---	-8.66	-8.08	---	---
DV99-196	82A-7 Well	05/05/99	---	-125	-13.07	---	---	-6.54	---	---	---
DV99-197	73B-7 Well	05/05/99	---	-124	-12.97	---	---	-7.13	-8.25	---	---
DV99-199	37-33 Well	05/05/99	---	-126	-13.80	---	---	-6.86	-9.00	---	---
DV99-200	28-33 Well	05/05/99	---	-127	-13.71	---	---	-6.67	---	---	---
DV99-204	V101 Separator	05/05/99	---	-128	-13.71	---	---	-6.97	-8.80	---	---
DV74782786-brine 2	74-7 Well Archived	08/27/86	---	-130	-14.11	---	---	---	**-8.31**	-14.76	**247**
DV76781986-brine 4	76-7 Well Archived	08/19/86	---	-130	-14.09	---	---	---	**-8.50**	-14.71	**254**
DV453382186-brine 6	45-33 Well Archived	08/21/86	---	-131	-14.44	---	---	---	---	-14.96	---
DV73782886-brine 8	73-7 Well Archived	08/28/86	---	-129	-14.20	---	---	---	**-8.27**	-14.91	**243**
DV321882686-brine 10	32-18 Well Archived	08/26/86	---	-130	-14.07	---	---	---	---	-14.51	---
DV651882686-brine 12	65-18 Well Archived	08/26/86	---	-131	-14.11	---	---	---	---	-14.64	---
No number	28-33 Well Archived	09/23/93	---	-133	-16.46	---	---	---	---	---	---
Mean brine temp., °C	Sulfate-oxygen geothermometer	n = 3	---	---	---	---	---	---	---	---	**248 ± 5**
Condensates											
DV96-7	76-7 Well	10/25/96	---	---	---	-130	-16.9	---	---	---	---
DV96-7b	76-7 Well	10/25/96	---	---	---	-130	-16.9	---	---	---	---
DV96-10	V101 Separator	10/25/96	---	---	---	-127	-17.1	---	---	---	---
DV96-10b	V101 Separator	10/25/96	---	---	---	-131	-17.2	-5.70	---	---	---
DV97-12	73-7 Well	10/29/97	---	-130	-15.11	-117	-15.5	---	---	---	---
DV97-15	74-7 Well	10/29/97	---	-133	-15.79	-134	-16.7	---	---	---	---
DV97-17	V102 + V103 Separator	10/29/97	---	-133	-16.18	-127	-16.9	---	---	---	---
DV97-19	V105 Separator	10/29/97	---	-133	-16.13	-114	-11.2	---	---	---	---
DV97-21	82A-7 Well	10/29/97	---	-126	-13.58	-127	-16.2	---	---	---	---
DV97-22	73B-7 Well	10/29/97	---	-132	-15.46	-130	-17.2	---	---	---	---
DV97-24	V101 Separator	10/30/97	---	-135	-16.47	-128	-17.3	---	---	---	---
DV97-27	27-33 Well	10/30/97	---	-135	-16.77	-130	-17.4	---	---	---	---
DV97-28	37-33 Well	10/30/97	---	-134	-16.58	-132	-17.3	---	---	---	---
DV97-31	28-33 Well	10/30/97	---	-134	-16.40	-129	-17	---	---	---	---
DV98-74	V101 Separator	04/28/98	---	-133	-16.60	---	---	---	---	---	---
DV98-76	27-33 Well	04/28/98	---	-134	-16.76	---	---	---	---	---	---
DV98-78	37-33 Well	04/28/98	---	-131	-16.53	---	---	---	---	---	---
DV98-81	76A-7 Well	04/28/98	---	-132	-16.18	---	---	---	---	---	---
DV98-83	V102 + V103 Separator	04/28/98	---	-131	-16.03	---	---	---	---	---	---
DV98-85	74-7 Well	04/28/98	---	-133	-16.24	---	---	---	---	---	---
DV98-87	63-7 Well	04/28/98	---	-132	-16.02	---	---	---	---	---	---
DV98-89	73-7 Well	04/29/98	---	-125	-13.64	---	---	---	---	---	---

Table 7: Continued

Sample	Name or Description	Date	$^3H^b$ (TU)	δD (USGS) (per mil)	$\delta^{18}O$ (USGS) (per mil)	δD (WM) (per mil)	$\delta^{18}O$ (WM) (per mil)	$\delta^{13}C-HCO_3^-$ (per mil)	$\delta^{18}O-SO_4^{2-}$ (per mil)	$\delta^{18}O$ (Total Fluid) (per mil)	$\delta^{18}O\ (SO_4^{2-}-H_2O)^d$ (°C)
DV98-91	82A-7 Well	04/29/98	---	-128	-14.57	---	---	---	---	---	---
DV98-93	V105 Separator	04/29/98	---	-133	-15.97	---	---	---	---	---	---
DV98-94	73B-7 Well	04/29/98	---	-131	-15.99	---	---	---	---	---	---
DV98-101	28-33 Well	04/30/98	---	-133	-16.50	---	---	---	---	---	---
DV98-134	27-33 Well	10/20/98	---	-135	-16.90	---	---	---	---	---	---
DV98-136	27-33 Well	10/20/98	---	-137	-17.10	---	---	---	---	---	---
DV98-137	V101 Separator	10/21/98	---	-134	-16.58	---	---	---	---	---	---
DV98-139	37-33 Well	10/21/98	---	-134	-16.69	---	---	---	---	---	---
DV98-142	28-33 Well	10/21/98	---	-134	-16.60	---	---	---	---	---	---
DV98-144	76A-7 Well	10/22/98	---	-133	-16.20	---	---	---	---	---	---
DV98-146	V102 + V103 Separator	10/22/98	---	-132	-15.97	---	---	---	---	---	---
DV98-149	63-7 Well	10/22/98	---	-132	-15.89	---	---	---	---	---	---
DV98-151	74-7 Well	10/22/98	---	-133	-16.06	---	---	---	---	---	---
DV98-153	73-7 Well	10/22/98	---	-129	-15.26	---	---	---	---	---	---
DV98-155	73B-7 Well	10/22/98	---	-133	-15.74	---	---	---	---	---	---
DV98-157	82A-7 Well	10/23/98	---	-133	-15.83	---	---	---	---	---	---
DV98-158	V105 Separator	10/23/98	---	-132	-15.91	---	---	---	---	---	---
DV99-183	76A-7 Well	05/04/99	---	-133	-16.10	---	---	---	---	---	---
DV99-185	74-7 Well	05/04/99	---	-131	-15.69	---	---	---	---	---	---
DV99-187	V102 + V103 Separator	05/04/99	---	-132	-16.04	---	---	---	---	---	---
DV99-189	63-7 Well	05/04/99	---	-131	-15.93	---	---	---	---	---	---
DV99-191	73-7 Well	05/04/99	---	-130	-15.12	---	---	---	---	---	---
DV99-192	73B-7 Well	05/04/99	---	-127	-14.47	---	---	---	---	---	---
DV99-193	V105 Separator	05/05/99	---	-131	-15.86	---	---	---	---	---	---
DV99-195	82A-7 Well	05/05/99	---	-131	-15.66	---	---	---	---	---	---
DV99-201	28-33 Well	05/05/99	---	-133	-16.46	---	---	---	---	---	---
DV99-202	37-33 Well	05/05/99	---	-134	-16.59	---	---	---	---	---	---
DV99-203	V101 Separator	05/05/99	---	-134	-16.57	---	---	---	---	---	---
DV74782786-cond 1	74-7 Well Archived	08/27/86	---	-140	-17.39	---	---	---	---	---	---
DV76781986-cond 3	76-7 Well Archived	08/19/86	---	-141	-17.42	---	---	---	---	---	---
DV453382886-cond 5	45-33 Well Archived	08/28/86	---	-139	-17.56	---	---	---	---	---	---
DV73782886-cond 7	73-7 Well Archived	08/28/86	---	-141	-17.5	---	---	---	---	---	---
DV321882686-cond 9	32-18 Well Archived	08/26/86	---	-139	-17.3	---	---	---	---	---	---
DV651882686-cond 11	65-18 Well Archived	08/26/86	---	-142	-17.5	---	---	---	---	---	---
Injection Well/Power Plant Fluids											
DV96-2	Condensate from plant	10/24/96	0.35	---	---	-98	-10.7	---	---	---	---
DV96-3	LP Brine @ Plant	10/24/96	0.17	---	---	-119	-13.8	-5.80	---	---	---
DV96-4	45-5 Injection Well	10/24/96	0.19	---	---	-118	-13.5	---	---	---	---
DV96-5	Lamb 1 Injection Well	10/24/96	---	---	---	-122	-13.7	---	---	---	---
DV96-6	65-18 Injection Well	10/24/96	---	---	---	-121	-13.7	---	---	---	---
DV97-32	Condensate from plant	10/31/97	---	-95	-9.0	-94	-9.7	---	---	---	---
DV97-33	LP Brine @ Plant	10/31/97	---	-124	-13.0	-120	-13.8	-4.70	-8.80	---	*314*

Table 7: Continued

Sample	Name or Description	Date	$^3H^b$ (TU)	δD (USGS) (per mil)	$\delta^{18}O$ (USGS) (per mil)	δD (WM) (per mil)	$\delta^{18}O$ (WM) (per mil)	$\delta^{13}C-HCO_3^-$ (per mil)	$\delta^{18}O-SO_4^{2-}$ (per mil)	$\delta^{18}O$ (Total Fluid) (per mil)	$\delta^{18}O$ $(SO_4^{2-}-H_2O)^d$ (°C)
DV97-34	25-5 + 45-5 Injectate	10/31/97	0.06	-120	-12.5	-116	-13.1	-8.20	-8.62	---	*326*
DV97-35	25-5 + 45-5 Injectate	10/31/97	---	-121	-12.4	---	---	-4.50	-8.80	---	*337*
DV97-36	65-18 Injection Well	10/31/97	---	-126	-13.0	---	---	-5.18	-9.26	---	*331*
DV97-37	32-18 Injection Well	10/31/97	---	-126	-13.0	---	---	-6.12	-9.22	---	*330*
DV97-40	LP Brine @ Plant	10/31/97	**-0.03**	-127	-12.9	---	---	-3.86	-8.62	---	*311*
DV97-41	*Condensate from plant*	10/31/97	---	-89	-8.5	---	---	---	---	---	---
DV97-42	High P Brine @ plant	10/31/97	---	-129	-13.8	---	---	-7.29	-9.02	---	*295*
DV98-97	Condensate from plant	04/29/98	---	-91	-8.5	---	---	---	---	---	---
DV98-98	LP Brine @ Plant	04/29/98	---	-124	-13.0	---	---	-5.99	---	---	---
DV98-143	25-5 Injection Well	10/21/98	---	-124	-13.0	---	---	-5.62	---	---	---
DV98-161	Condensate from plant	10/23/98	0.79	-95	-8.8	---	---	---	---	---	---
DV98-162	LP Brine @ Plant	10/23/98	---	-123	-12.9	---	---	-6.22	-8.11	---	*294*
DV98-163	65-18 Injection Well	10/23/98	0.62	-110	-12.1	---	---	-5.25	+1.22	---	*133*
DV99-198	65-18 Injection Well	05/05/99	---	-112	-12.7	---	---	-5.16	---	---	---
DV99-205	25-5 + 45-5 Injectate	05/06/99	**-0.10**	-123	-12.9	---	---	-4.99	-8.13	---	*295*
DV99-206	LP Brine @ Plant	05/06/99	---	-123	-12.8	---	---	-4.22	-8.05	---	*296*
DV99-207	Condensate from plant	05/06/99	1.08	-95	-8.9	---	---	---	---	---	---
DV99-208	52-18 + 41-18 Injectate	05/06/99	---	-123	-12.9	---	---	-2.47	-8.26	---	*299*
Other Geothermal and On-Site Water Wells											
DV96-1	Domestic Well	10/24/96	0.11	---	---	-122	-16.7	-6.40	---	---	---
DV97-38	Domestic Well	10/31/97	---	-125	-15.7	---	---	-5.70	+7.67	---	50
DV97-39	Goerenger Well	10/31/97	0.18	-127	-15.4	-121	-16	-5.49	+2.66	---	87
DV97-53	46-32 Well	11/05/97	---	-161	-22.3	---	---	---	---	---	---
DV97-54	27-32 Well	11/05/97	---	-134	-16.1	---	---	---	---	---	---
DV97-55	27-32 Well	11/05/97	0.41	-126	-14.1	---	---	-6.79	-9.02	-14.20	285
DV97-59	45-W-5 Well	11/05/97	---	-114	-12.7	---	---	---	---	---	---
DV97-67	66-21 Well	11/07/97	---	-124	-14.4	---	---	-6.12	-6.20	---	209
DV98-96	Goerenger Well	04/29/98	---	-127	-15.4	---	---	-5.26	+2.91	---	84
DV98-99	27-32 Well	04/29/98	---	-133	-16.0	---	---	---	---	---	---
DV98-100	46-32 Well	04/29/98	---	-148	-19.2	---	---	---	---	---	---
DV98-102	45-14 Well	04/30/98	---	-141	-18.4	---	---	---	---	---	---
DV98-103	45-14 Well	04/30/98	---	-128	-14.8	---	---	-6.58	-7.82	---	235
DV98-104	66-21 Well	04/30/98	---	-126	-14.5	---	---	-5.45	-6.21	---	207
DV98-111	62-21 Well	05/01/98	0.83	-135	-15.6	---	---	-4.41	-2.38	---	133
DV98-122	97-2 Well	05/05/98	---	-132	-15.0	---	---	---	---	---	---
DV98-123	32-6 Well	05/06/98	---	-120	-14.6	---	---	-8.07	+1.59	---	103
DV98-160	Goerenger Well	10/23/98	0.42	-128	-15.4	---	---	-5.28	---	---	---
DV98-168	38-32 Well	10/26/98	---	-134	-15.7	---	---	---	---	---	---
DV98-175	62-21 Well	10/28/98	---	-135	-15.6	---	---	---	---	---	---
DV99-181	Goerenger Well	05/04/99	---	-127	-15.3	---	---	-5.40	---	---	---

Table 7: Continued

Sample	Name or Description	Date	$^3H^b$ (TU)	δD (USGS) (per mil)	$\delta^{18}O$ (USGS) (per mil)	δD (WM) (per mil)	$\delta^{18}O$ (WM) (per mil)	$\delta^{13}C$-HCO_3^- (per mil)	$\delta^{18}O$-SO_4^{2-} (per mil)	$\delta^{18}O$ (Total Fluid) (per mil)	$\delta^{18}O$ (SO_4^{2-}-H_2O)^d (°C)
Background Springs											
DV97-46	Sou Hot Spring	11/03/97	---	-129	-15.7	---	---	-1.23	-9.62	---	*257*
DV97-47	Sou Hot Spring	11/03/97	**-0.02**	-131	-16.0	---	---	-3.35	+10.48	---	33
DV97-48	Hyder Hot Spring	11/03/97	0.12	-135	-15.6	---	---	-3.87	+4.88	---	68
DV97-50	Edward Creek Spring	11/04/97	0.05	-122	-15.4	---	---	---	---	---	---
DV97-51a	Upper Old Man's Spr.	11/04/97	---	-112	-14.3	---	---	---	---	---	---
DV97-51b	Old Man Spring	11/04/97	0.09	-132	-16.8	---	---	-10.46	---	---	---
DV97-52	Horse Heaven Spring	11/04/97	---	-123	-15.4	---	---	-10.59	---	---	---
DV97-56	Dead Travertine Spring, Upper	11/05/97	---	-123	-14.9	---	---	-3.07	---	---	---
DV97-60	Fault Line Spring	11/06/97	0.02	-132	-16.4	---	---	-3.64	+3.46	---	73
DV97-61	Lower Ranch Hot Spring	11/06/97	0.07	-131	-16.4	---	---	-3.31	+1.63	---	87
DV97-62	McCoy Hot Spring	11/06/97	---	-130	-16.1	---	---	-3.96	+3.55	---	74
DV97-63	Kyle Spring	11/06/97	0.04	-122	-15.7	---	---	-6.46	---	---	---
DV97-64	Dago Spring	11/06/97	---	-120	-14.9	---	---	---	---	---	---
DV97-65	Mustang Spring	11/06/97	9.2	-116	-14.3	---	---	-9.54	---	---	---
DV97-66	Kitten Spring	11/06/97	0.11	-119	-15.2	---	---	-11.11	---	---	---
DV97-68	Big Horn Spring	11/07/97	---	-117	-14.7	---	---	-7.64	---	---	---
DV97-69	Dixie Hot Spring	11/07/97	0.16	-128	-16.1	---	---	-6.93	-2.87	---	133
DV97-72	Horse Creek Spring	11/07/97	10.2	-119	-15.5	---	---	-16.09	---	---	---
DV98-106	Stu's Seep	04/30/98	---	-111	-13.4	---	---	---	---	---	---
DV98-112	Hyder Hot Spring	04/30/98	---	-134	-15.5	---	---	-3.12	---	---	---
DV98-113	Lower Ranch Hot Spring	05/04/98	---	-130	-16.4	---	---	-2.93	-0.52	---	105
DV98-114	McCoy Hot Spring	05/04/98	---	-128	-16.2	---	---	-3.68	---	---	---
DV98-117	Sou Hot Spring	05/04/98	---	-129	-16.0	---	---	-2.60	+10.08	---	35
DV98-118	Big Horn Spring	05/04/98	---	-117	-14.7	---	---	-7.52	+7.52	---	57
DV98-120	Dixie Hot Spring	05/05/98	---	-127	-16.0	---	---	-6.67	---	---	---
DV98-128	Jersey Hot Spring	05/05/98	1.1	-128	-15.9	---	---	-3.51	-6.15	---	181
DV98-129	Upper Jersey Seep	05/06/98	---	-126	-15.5	---	---	---	---	---	---
DV98-131	Spring in Spring Canyon	05/06/98	---	-123	-15.8	---	---	-9.52	---	---	---
DV98-132	Wild Rose Spring	05/07/98	4.46	-118	-14.6	---	---	-11.98	+0.29	---	---
DV98-169	Lofthouse Spring	05/07/98	---	-114	-14.8	---	---	-11.41	---	---	---
DV98-170	Not-So-OK Spring	10/27/98	9.2	-113	-14.8	---	---	-11.95	---	---	---
DV98-176	War Canyon Spring	10/27/98	3.45	-126	-16.3	---	---	-12.99	---	---	---
DV98-177	Pine Spring	10/28/98	6.73	-119	-15.4	---	---	-13.46	---	---	---
DV98-178	Basalt Spring	10/28/98	---	-122	-16.0	---	---	-13.01	---	---	---
DV98-179	Upper Cherry Spring	10/28/98	---	-119	-15.6	---	---	-12.72	---	---	---
DV99-209	Dead Travertine Spring, Upper	05/07/99	---	-122	-15.0	---	---	-2.37	---	---	---
DV99-210	Dead Travertine Spring, Road	05/08/99	---	-117	-13.8	---	---	-3.34	---	---	---
DV99-211	Upper Spring, Lower Ranch	05/09/99	---	-130	-16.6	---	---	-3.69	---	---	---

Table 7: Continued

Sample	Name or Description	Date	$^3H^b$ (TU)	δD (USGS) (per mil)	$\delta^{18}O$ (USGS) (per mil)	δD (WM) (per mil)	$\delta^{18}O$ (WM) (per mil)	$\delta^{13}C-HCO_3^-$ (per mil)	$\delta^{18}O-SO_4^{2-}$ (per mil)	$\delta^{18}O$ (Total Fluid) (per mil)	$\delta^{18}O$ $(SO_4^{2-}-H_2O)^d$ (°C)
Background Wells											
DV97-49	Hole in the Wall #2 Well	11/04/97	0.46	-121	-15.3	---	---	-6.09	---	---	---
DV97-57	Bolivia Artesian Well	11/05/97	0.10	-121	-14.8	---	---	-8.96	+2.84	---	90
DV97-70	Flowing well @ AA Tank	11/07/97	---	-129	-16.6	---	---	-8.93	---	---	---
DV97-71	Shaw Well	11/07/97	**-0.04**	-134	-16.6	---	---	-9.47	---	---	---
DV98-115	Irrigation Well	05/04/98	0.75	-132	-15.9	---	---	-2.41	+0.75	---	---
DV98-116	Brinkerhoff Well	05/04/98	---	-128	-15.9	---	---	-4.41	---	---	---
DV98-172	Bernice Well	10/27/98	---	-112	-13.9	---	---	-9.22	---	---	---
Background Streams/Rain											
DV97-58	Cottonwood Creek	11/05/97	---	-118	-14.6	---	---	-9.95	---	---	---
DV98-107	Unnamed Ck by Stu's Seep	04/30/98	---	-109	-12.8	---	---	---	---	---	---
DV98-110	Cottonwood Creek	05/01/98	---	-115	-14.6	---	---	---	---	---	---
DV98-119	Unnamed Stream	05/05/98	---	-110	-13.7	---	---	-4.43	+3.94	---	---
DV98-121	White Rock Canyon	05/05/98	11.3	-109	-14.2	---	---	-7.19	---	---	---
DV98-125	Rain, Lizard Well Tank	05/06/98	11.2	-64	-8.0	---	---	---	---	---	---
DV98-126	Home Station Wash	05/06/98	---	-115	-15.2	---	---	-6.86	---	---	---
DV98-127	Cedar Canyon Wash	05/06/98	10.4	-111	-14.6	---	---	-6.50	---	---	---
DV98-130	Bucher Creek	05/06/98	---	-113	-14.9	---	---	---	---	---	---
DV98-171	Not-So-OK Creek	10/27/98	---	-115	-14.8	---	---	---	---	---	---
DV98-173	Bernice Creek	10/27/98	---	-112	-13.8	---	---	-8.41	---	---	---
DV98-174	Hoyt Creek	10/27/98	---	-110	-13.2	---	---	-5.99	---	---	---
DV98-180	Mt. Augusta Creek	10/28/98	---	-120	-15.8	---	---	-9.30	---	---	---
DV99-213	Dixie Salt Lake	05/10/99	---	-92	-7.8	---	---	1.67	---	---	---
Fumaroles											
DV97-43	Crack 4 Fumarole	11/03/97	---	-155	-20.1	---	---	---	---	---	---
DV97-44	Senator Fumarole	11/03/97	---	-137	-17.5	---	---	---	---	---	---
DV98-105	Unnamed Fumarole	04/30/98	---	-162	-21.9	---	---	---	---	---	---
DV98-108	Senator Fumarole	05/01/98	---	-145	-19.1	---	---	---	---	---	---
DV98-109	Calcite Fumarole	05/01/98	---	-161	-21.4	---	---	---	---	---	---
DV98-124	Crack 4 Fumarole	05/06/98	---	-160	-21.4	---	---	---	---	---	---
DV98-165	Calcite Fumarole	10/25/98	---	-167	-21.9	---	---	---	---	---	---
DV98-166	South Bench Fumarole	10/26/98	---	-166	-22.9	---	---	---	---	---	---

[a] Tritium analyzed by University of Miami (error = ±10%), stable isotopes of water analyzed by T. Coplan, USGS, Reston, Virginia (error = ±1 per mil deuterium and ±0.15 per mil oxygen-18) and Western Michigan University (error = ±1 per mil deuterium and ±0.25 per mil oxygen-18); carbon-13 analyses performed by Geochron Laboratories, Cambridge, Massachusetts (error = ±0.2 per mil); oxygen-18 in sulfate analyses by USGS (error = ±0.15 per mil).

[b] Negative values shown in bold should be considered to be 0.00 TU for any calculations.

[c] Values in bold are averages of 1997 and 1998 analyses for the same well to perform the sulfate-oxygen isotope geothermometer calculations.

[d] Sulfate oxygen isotope geothermometer of McKenzie and Truesdell (1977). Estimated reservoir temperatures of 1997 and 1998 brine samples are too high because the oxygen-18 value of unflashed reservoir water has increased due to production (Kennedy et al, 1999). Temperatures estimated from 1986 archived samples (bold) are most representative of the pre-production resevoir temperature and isotope composition. Temperatures in italics are probably not reliable due to reequilibration, evaporation, or mixing of different waters.

Table 8: Gas Geochemistry and Geothermometer Calculations for Various Geothermal and Regional Fluids, Dixie Valley Region, Nevada (values in mol% dry gas unless otherwise noted).

Sample	Name or Description	Date	Laboratory	Sampling Temp. (°C)	Steam Fraction (y)	Steam/Gas (molar)	H_2O (mol%, wet)	CO_2	H_2S	H_2	CH_4	C_2H_6	N_2	NH_3	O_2	Ar
Production and On-Site Wells																
DIXE102G	V102 + V103 Separator	10/02/95	LANL	---	0.153	1021	99.9	96.6	2.260	0.0000	0.003	0	0.159	0.909	0.0364	0.0022
DV96-7a	76-7 Well	10/25/96	LANL	163	0.184	604	99.8	97.5	0.560	0.0125	0.459	0.01790	0.802	0.687	0.0300	0.0134
DV96-7b	76-7 Well	10/25/96	LANL	163	---	703	99.9	96.9	0.633	0.0140	0.563	0.02086	1.011	0.830	0.0491	0.0173
DV96-7c	76-7 Well	10/25/96	LANL	163	---	496	99.8	96.6	0.563	0.0195	0.823	0.03027	1.272	0.626	0.0228	0.0325
DV96-10a	V101 Separator	10/25/96	LANL	160	0.159	512	99.8	96.6	1.147	0.0290	0.414	0.00901	1.318	0.619	0.0340	0.0252
DV96-10b	V101 Separator	10/25/96	LANL	160	---	1438	99.9	96.4	0.775	0.0164	0.225	0.00473	0.757	1.792	0.0201	0.0302
Average 1996 Geothermometer (n = 5)																
DV97-12 (2)	73-7 Well	10/29/97	USGS	---	0.158	816	99.9	93.9	1.976	0.0390	0.941	---	2.049	1.024	0.0038	0.0392
DV97-15	74-7 Well	10/29/97	LANL	---	0.163	542	99.8	96.8	0.739	0.0152	0.572	0.01879	0.966	0.408	0.0168	0.0542
DV97-15 (2)	74-7 Well	10/29/97	USGS	---	---	551	99.8	94.8	1.095	0.0238	1.039	---	2.058	0.879	0.0031	0.0401
DV97-17	V102 + V103 Separator	10/29/97	LANL	---	0.161	476	99.8	96.6	0.765	0.0122	0.634	0.02021	1.257	0.651	0.0082	0.0231
DV97-17	V102 + V103 Separator	10/29/97	USGS	---	---	487	99.8	95.6	0.683	0.0208	0.979	---	1.931	0.748	0.0000	0.0340
DV97-19	V105 Separator	10/29/97	USGS	---	0.151	545	99.8	95.7	0.816	0.0231	0.838	---	1.918	0.693	0.0022	0.0382
DV97-21 (1)	82A-7 Well	10/29/97	USGS	---	0.159	540	99.8	93.9	1.093	0.0177	0.802	---	3.64	0.535	0.0000	0.0579
DV97-22	73B-7 Well	10/29/97	USGS	---	0.160	626	99.8	91.2	1.145	0.0322	0.739	---	6.00	0.811	0.0000	0.0866
DV97-24	V101 Separator	10/30/97	USGS	---	0.164	476	99.8	93.6	1.026	0.0206	0.519	---	4.11	0.627	0.0000	0.0650
DV97-27	27-33 Well	10/30/97	USGS	---	0.157	376	99.7	95.2	0.929	0.0310	1.028	---	2.22	0.531	0.0230	0.0447
DV97-28	37-33 Well	10/30/97	USGS	---	0.159	448	99.8	94.5	1.200	0.0252	0.590	---	3.06	0.560	0.0014	0.0554
DV97-31	28-33 Well	10/30/97	USGS	---	0.156	214	99.5	44.8	0.981	0.0123	0.192	---	43.1	0.233	10.1	0.5582
Average 1997 Geothermometer (n = 11)																
DV98-74	V101 Separator	04/28/98	LANL	160	0.157	499	99.8	96.7	1.194	0.0160	0.458	0.00880	1.467	0.109	0.0064	0.0298
DV98-74	V101 Separator	04/28/98	USGS	---	---	441	99.8	95.0	1.188	0.0259	0.676	---	2.17	0.851	0.0000	0.0432
DV98-76	27-33 Well	04/28/98	USGS	---	0.155	369	99.7	95.1	1.068	0.0253	1.007	---	2.01	0.703	0.0000	0.0414
DV98-78	37-33 Well	04/28/98	USGS	---	0.156	435	99.8	95.2	1.207	0.0332	0.610	---	2.21	0.726	0.0000	0.0427
DV98-81	76A-7 Well	04/28/98	LANL	---	0.157	433	99.8	96.1	0.609	0.0140	1.050	0.03780	1.555	0.112	0.0065	0.0275
DV98-81	76A-7 Well	04/28/98	USGS	---	---	450	99.8	95.5	0.635	0.0173	1.248	---	1.690	0.839	0.0000	0.0331
DV98-83	V102 + V103 Separator	04/28/98	USGS	---	0.150	523	99.8	95.3	0.795	0.0212	1.041	---	1.796	0.970	0.0039	0.0350
DV98-85	74-7 Well	04/28/98	USGS	---	0.158	464	99.8	95.5	0.753	0.0235	1.103	---	1.782	0.742	0.0047	0.0353
DV98-87	63-7 Well	04/28/98	USGS	---	0.154	518	99.8	95.5	0.685	0.0343	0.959	---	1.746	1.001	0.0043	0.0336
DV98-93	V105 Separator	04/29/98	USGS	---	0.150	573	99.8	95.2	0.912	0.0210	0.864	---	1.860	1.056	0.0129	0.0369
DV98-94	73B-7 Well	04/29/98	USGS	---	0.152	567	99.8	95.2	1.081	0.0827	0.826	---	1.781	0.980	0.0000	0.0356
DV98-137	V101 Separator	10/21/98	LANL	---	0.160	453	99.8	96.0	1.167	0.0180	0.543	0.01240	1.630	0.516	0.0056	0.0309
DV98-139	37-33 Well	10/21/98	LANL	---	0.162	357	99.7	96.0	1.203	0.0309	0.581	0.01383	1.690	0.526	0.0059	0.0309
DV98-142	28-33 Well	10/21/98	LANL	---	---	423	99.8	96.0	0.966	0.0640	0.406	0.00620	1.766	0.602	0.0240	0.0300
DV98-144	76A-7 Well	10/22/98	LANL	---	0.158	462	99.8	95.8	0.643	0.0162	1.090	0.04098	1.603	0.669	0.0031	0.0295
DV98-146	V102 + V103 Separator	10/22/98	LANL	---	0.164	515	99.8	96.5	0.742	0.0118	0.584	0.01994	1.115	0.761	0.0078	0.0210
DV98-149	63-7 Well	10/22/98	LANL	---	---	462	99.8	94.5	0.517	0.0150	0.572	0.01830	1.230	0.826	0.0140	0.0210
DV98-153	73-7 Well	10/22/98	LANL	---	---	505	99.8	91.8	0.868	0.0260	0.457	0.01420	0.892	0.968	0.0180	0.0150
DV98-157	82A-7 Well	10/23/98	LANL	---	0.154	623	99.8	91.7	1.183	0.0164	0.749	0.02149	1.467	0.656	0.0051	0.0409
Average 1998 Geothermometer (n = 19)																
DV99-183	76A-7 Well	05/04/99	LANL	---	0.152	438	99.8	96.3	0.604	0.0110	0.914	0.0314	1.208	0.557	0.0029	0.0227
DV99-185	74-7 Well	05/04/99	LANL	---	0.160	383	99.7	96.6	0.544	0.0115	0.554	0.0198	0.898	0.471	0.0027	0.0169
DV99-187	V102 + V103 Separator	05/04/99	LANL	---	0.137	629	99.8	95.8	0.694	0.0118	0.860	0.0305	1.600	0.788	0.0243	0.0297
DV99-189	63-7 Well	05/04/99	LANL	---	0.152	459	99.8	97.1	0.494	0.0205	0.574	0.0197	1.070	0.620	0.0257	0.0195

Table 8: Continued

Sample	Name or Description	Date	Laboratory	Sampling Temp. (°C)	Steam Fraction (y)	Steam/Gas (molar)	H_2O (mol%, wet)	CO_2	H_2S	H_2	CH_4	C_2H_6	N_2	NH_3	O_2	Ar
DV99-193	V105 Separator	05/05/99	LANL	---	---	536	99.8	95.8	0.817	0.0180	0.724	0.0224	1.419	1.004	0.0140	0.0240
DV99-203	V101 Separator	05/05/99	LANL	---	---	400	99.7	96.2	0.916	0.0150	0.466	0.0087	1.535	0.735	0.0120	0.0270
DV99-191	73-7 Well	05/04/99	LANL	---	0.154	471	99.8	94.7	0.825	0.0143	0.300	0.0102	0.611	0.646	0.0194	0.0109
DV99-192	73B-7 Well	05/04/99	LANL	---	0.159	812	99.9	86.9	1.714	0.0333	0.544	0.0167	1.097	0.700	0.0171	0.0363
DV99-195	82A-7 Well	05/05/99	LANL	---	0.152	475	99.8	93.4	1.128	0.0091	0.426	0.0127	0.825	0.418	0.0058	0.0269
DV99-201	28-33 Well	05/05/99	LANL	---	0.159	257	99.6	97.8	0.596	0.0268	0.253	0.0044	0.909	0.311	0.0072	0.0231
DV99-202	37-33 Well	05/05/99	LANL	---	0.160	229	99.6	97.2	0.597	0.0258	0.407	0.0093	1.250	0.302	0.0164	0.0263
Average 1999 Geothermometer (n = 11)																
Other Geothermal Wells																
DV97-53	46-32 Well	11/05/97	LANL	155	---	27.7	96.5	97.8	0.357	1.454	0.085	0.00109	0.229	0.046	0.0024	0.0060
DV97-53	46-32 Well	11/05/97	USGS	155	---	21.0	95.5	97.4	0.333	1.866	0.102	---	0.285	0.038	0.0000	0.0076
DV97-54	27-32 Well	11/05/97	USGS	144	0.054	454	99.8	97.1	0.378	0.2884	0.264	---	1.171	0.782	0.0349	0.0263
DV98-99	27-32 Well	04/29/98	USGS	---	---	588	99.8	95.9	1.452	0.5163	0.247	---	0.819	0.981	0.0000	0.0197
DV98-102	45-14 Well	04/30/98	USGS	123.5	---	47.0	97.9	67.8	1.181	0.5455	2.11	---	26.1	0.079	1.72	0.4685
DV98-111	62-21 Well	04/30/98	USGS	75.5	---	---	---	77.1	0.0035	0.1769	1.92	0.0153	20.1	---	0.298	0.3610
Hot Springs																
DV98-112	Hyder Hot Spring	04/30/98	LANL	75.3	---	2.51	71.5	94.6	<0.004	<0.0006	0.536	0.00052	4.24	<0.0006	0.2462	0.1252
DV98-117	Sou Hot Spring	05/04/98	LANL	72.0	---	1.76	63.8	52.0	<0.02	<0.005	0.801	<0.005	46.1	<0.003	0.5132	0.8394
Fumaroles, Senator Fumarole and Dead Zone Areas																
DV97-43	Crack 4 Fumarole	11/03/97	USGS	97.6	---	225	99.6	94.4	0.754	1.231	0.111	---	3.15	0.112	0.180	0.0725
DV97-44	Senator Fumarole	11/03/97	LANL	97.3	---	412	99.8	91.8	1.274	0.1753	0.125	0.00053	4.08	1.501	0.8473	0.0810
DV97-44	Senator Fumarole	11/03/97	USGS	97.3	---	420	99.8	88.8	1.883	0.2310	0.144	---	5.39	2.389	1.138	0.121
DV97-45	Range Front Fumarole	11/03/97	USGS	97.3	---	357	99.7	92.3	1.931	0.2230	0.147	---	5.25	0.014	0.0000	0.119
DV98-108	Senator Fumarole	05/01/98	USGS	97.1	---	345	99.7	96.6	0.579	0.3005	0.204	---	1.406	0.888	0.0000	0.0335
DV98-108	Senator Fumarole	05/01/98	LANL	97.1	---	289	99.7	96.5	0.515	0.3361	0.234	0.00173	1.824	0.139	0.0339	0.0393
DV98-109	Calcite Fumarole	05/01/98	USGS	95.8	---	258	99.6	96.0	0.739	0.6738	0.102	---	0.862	1.595	0.0007	0.0214
DV98-124	Crack 4 Fumarole	05/06/98	USGS	97.6	---	119	98.8	90.9	0.406	1.1680	0.165	---	6.771	0.00746	0.4518	0.0969
DV98-164	Senator Fumarole	10/24/98	LANL	96.5	---	471	99.8	91.0	0.574	0.1591	0.192	0.00292	5.42	1.023	1.4601	0.112
DV98-164	Senator Fumarole	10/24/98	USGS	96.5	---	---	---	88.6	0.0084	0.2461	0.224	0.0038	8.01	---	2.796	0.159
DV98-165	Calcite Fumarole	10/25/98	LANL	97.0	---	265	99.6	94.0	0.718	0.4084	0.104	0.00137	2.69	1.428	0.2025	0.0515
DV98-166	South Bench Fumarole	10/26/98	LANL	97.4	---	407	99.8	92.1	1.035	0.2251	0.209	0.00262	5.21	0.017	0.8531	0.104
DV98-167	Lonely Fumarole	10/26/98	LANL	96.4	---	29.7	96.7	97.2	0.417	0.5530	0.136	0.00215	1.62	<0.0004	0.0546	0.0270
DV98-181[d]	Figure 8 Fumarole	10/29/98	LANL	97.4	---	3.19	76.1	31.1	0.069	0.0895	<0.007	<0.007	53.6	0.012	14.7	0.647
Average Geothermometer (n = 12)																
Fumaroles, Southwest of Cottonwood Canyon Near Inactive Sinter Deposits																
DV98-105	Unnamed Fumarole #1	04/30/98	LANL	99.5	---	16.4	94.2	33.5	<0.004	0.0263	0.132	<0.007	52.4	0.004	13.1	0.639
DV99-212	Unnamed Fumarole #2	05/10/99	LANL	96.9	---	26.9	96.4	32.2	0.104	<0.006	0.000	<0.006	49.1	0.019	12.6	0.519

[a] CO_2-H_2S-H_2-CH_4 geothermometer equations of D'Amore and Panichi (1980).

[b] CO_2-CH_4 geothermometer equation of Norman and Bernhardt (1981).

[c] H_2-Ar geothermometer equation of Giggenbach (1992); parentheses mean value is ignored for averaging.

[d] Two samples were mistakenly labeled 181; DV98-181 (Figure 8 Fumarole) and DV99-181 (Goerenger Well).

Table 8: Continued

Sample	**He**	**Cl** **(as HCl)**	**F** **(as HF)**	**As**	**Hg**	**Total**	**δ^{13}C-CO_2** **(per mil)**	**Lab for ^{13}C**	**T D-P[a]** **(°C)**	**T CO_2-CH_4[b]** **(°C)**	**T H_2/Ar[c]** **(°C)**	**Comments**
Production and On-Site Wells												
DIXE102G	0	0	---	---	---	100.0	---	---	---	---	---	
DV96-7a	0.00584	0.0	---	---	---	100.0	-5.3	Geochron	182	174	173	
DV96-7b	0.00219	0.0	---	---	---	100.0	-4.8	Geochron	184	167	168	
DV96-7c	0.00307	0.0	---	---	---	100.0	---	---	188	153	160	
DV96-10a	0.00331	0.0	---	---	---	100.0	-4.8	Geochron	211	178	179	
DV96-10b	0.00226	0.0	---	---	---	100.0	-4.5	Geochron	197	200	156	
Average 1996 Geothermometer (n = 5)									**192**	**174**	**167**	
DV97-12 (2)	0.00215	---	---	---	---	100.0	-5.1	USGS	219	147	175	
DV97-15	0.00261	0.319	0.113	5.30E-04	4.18E-05	100.0	---	---	188	166	136	
DV97-15 (2)	0.00219	---	---	---	---	100.0	-4.8	USGS	198	144	159	
DV97-17	0.00196	<0.03	<0.04	6.94E-05	7.94E-05	100.0	---	---	182	162	155	
DV97-17	0.00219	---	---	---	---	100.0	-4.8	USGS	190	146	160	
DV97-19	0.00216	---	---	---	---	100.0	-4.8	USGS	196	152	160	
DV97-21 (1)	0.00209	---	---	---	---	100.0	-4.7	USGS	194	153	139	H_2S analysis may be suspect
DV97-22	0.00182	---	---	---	---	100.0	-5.0	USGS	210	155	145	High N_2 indicates air contamination?
DV97-24	0.00198	---	---	---	---	100.0	-4.5	USGS	200	168	140	Corrected for air contamination
DV97-27	0.00244	---	---	---	---	100.0	-4.7	USGS	203	144	164	
DV97-28	0.00235	---	---	---	---	100.0	-4.5	USGS	205	164	151	
DV97-31	0.00000	---	---	---	---	99.9	-4.8	USGS	*110*	*178*	*59*	Miniseparator; air contamination
Average 1997 Geothermometer (n = 11)									**199**	**155**	**153**	
DV98-74	0.00220	0.0445	<0.02	1.04E-04	4.53E-05	100.0	---	---	196	174	156	
DV98-74	0.00260	---	---	---	---	100.0	-4.7	USGS	205	159	159	
DV98-76	0.00222	---	---	---	---	100.0	-4.4	USGS	200	145	160	
DV98-78	0.00241	---	---	---	---	100.0	-4.6	USGS	212	163	167	
DV98-81	0.00270	0.0330	0.441	2.58E-05	2.59E-05	100.0	---	---	179	144	155	
DV98-81	0.00253	---	---	---	---	100.0	-5.0	USGS	183	137	155	
DV98-83	0.00234	---	---	---	---	100.0	-4.9	USGS	192	144	160	
DV98-85	0.00225	---	---	---	---	100.0	-5.2	USGS	193	142	163	
DV98-87	0.00217	---	---	---	---	100.0	-5.0	USGS	202	147	176	
DV98-93	0.00215	---	---	---	---	100.0	-5.0	USGS	195	150	158	
DV98-94	0.00209	---	---	---	---	100.0	-4.9	USGS	231	152	201	
DV98-137	0.00271	0.0227	<0.02	4.24E-05	3.94E-05	100.0	---	---	197	168	159	
DV98-139	0.00258	0.0134	<0.02	7.09E-05	4.51E-05	100.0	---	---	210	165	175	
DV98-142	<0.0002	0.1370	<0.3	1.52E-04	8.01E-05	100.0	---	---	229	178	203	
DV98-144	0.00279	0.0642	0.039	4.71E-05	8.40E-05	100.0	---	---	183	142	157	
DV98-146	0.00212	0.224	<0.02	2.69E-03	4.03E-05	100.0	---	---	182	165	158	
DV98-149	0.00110	0.211	2.060	1.06E-04	2.19E-04	100.0	---	---	184	165	169	
DV98-153	0.00110	2.520	2.440	2.17E-03	9.33E-05	100.0	---	---	205	172	196	
DV98-157	0.00416	3.78	0.410	2.17E-05	1.52E-04	100.0	---	---	194	154	147	
Average 1998 Geothermometer (n = 19)							---	---	**199**	**156**	**167**	
DV99-183	0.0018	0.269	0.0827	1.01E-05	3.85E-05	100.0	---	---	175	149	153	
DV99-185	0.0017	0.860	0.0403	6.71E-04	1.08E-04	100.0	---	---	178	167	163	
DV99-187	0.0023	0.0999	0.0245	6.75E-05	8.98E-05	100.0	---	---	179	151	147	
DV99-189	0.0016	0.0508	0.0293	2.12E-05	5.81E-05	100.0	---	---	190	166	177	

Table 8: Continued

Sample	He	Cl	F	As	Hg	Total	$\delta^{13}C$-CO_2	Lab for ^{13}C	T D-P[a]	T CO_2-CH_4[b]	T H_2/Ar[c]	Comments
		(as HCl)	(as HF)				(per mil)		(°C)	(°C)	(°C)	
DV99-193	0.0020	0.1929	<0.4	1.85E-04	5.09E-05	100.0	---	---	191	157	170	
DV99-203	0.0021	0.0677	<0.3	1.01E-04	5.75E-05	100.0	---	---	191	173	161	
DV99-191	0.0008	2.77	0.0898	2.46E-03	9.17E-05	100.0	---	---	193	188	183	
DV99-192	0.0021	8.56	0.342	8.47E-03	8.36E-05	100.0	---	---	220	164	172	
DV99-195	0.0014	3.50	0.213	3.36E-03	1.41E-04	100.0	---	---	184	175	142	
DV99-201	0.0014	0.0932	0.0000	1.13E-05	4.66E-05	100.0	---	---	204	196	180	
DV99-202	0.0017	0.0757	0.0748	9.03E-06	5.99E-05	100.0	---	---	200	178	174	
Average 1999 Geothermometer (n = 11)									**191**	**169**	**166**	
Other Geothermal Wells												
DV97-53	<0.0002	<0.002	<0.003	2.09E-05	3.45E-04	100.0	---	---	241	235	342	Well fluid is mostly vapor
DV97-53	0.00009	---	---	---	---	100.1	-4.54	USGS	245	229	342	Well fluid is mostly vapor
DV97-54	0.00063	---	---	---	---	100.0	-4.85	USGS	192	194	248	Miniseparator
DV98-99	0.00067	---	---	---	---	100.0	-5.16	USGS	223	196	274	
DV98-102	0.01194	---	---	---	---	100.0	-6.48	USGS	155	106	180	Miniseparator; air contamination
DV98-111	0.01850	---	---	---	---	100.0	---	---	128	114	157	Evacuated bottle; W.C. Evans analyst
Hot Springs												
DV98-112	0.00464	0.0044	0.243	1.43E-05	2.26E-06	100.0	---	---	87	167	13	Summit of deposit
DV98-117	0.03357	0.0130	0.0368	3.57E-05	6.67E-06	100.4	---	---	63	131	19	Hottest spring with gas
Fumaroles, Senator Fumarole and Dead Zone Areas												
DV97-43	0.00021	---	---	---	---	100.0	-4.4	USGS	245	224	261	
DV97-44	0.00106	<0.03	0.0822	7.31E-05	4.29E-03	100.0	---	---	201	219	198	
DV97-44	0.00071	---	---	---	---	100.0	-5.4	USGS	213	213	195	
DV97-45	0.00071	---	---	---	---	100.0	-5.3	---	211	213	194	
DV98-108	0.00092	---	---	---	---	100.0	-5.3	USGS	200	203	242	
DV98-108	0.00124	0.0164	0.388	5.02E-05	3.51E-04	100.0	---	---	200	198	240	
DV98-109	0.00029	---	---	---	---	100.0	-3.6	USGS	229	228	280	
DV98-124	0.00067	---	---	---	---	100.0	-5.12	USGS	233	209	257	
DV98-164	<0.0008	0.0958	<0.02	5.39E-05	3.02E-04	100.0	---	---	187	203	186	
DV98-164	0.0018	---	---	---	---	100.0	---	---	152	197	193	Evacuated bottle; W.C. Evans analyst
DV98-165	0.00069	0.0316	0.395	2.74E-05	1.52E-04	100.0	---	---	216	227	238	
DV98-166	0.00131	0.0328	0.221	1.44E-05	1.52E-05	100.0	---	---	201	201	198	
DV98-167	0.00096	0.0027	0.006	4.49E-06	4.13E-06	100.0	---	---	213	218	267	
DV98-181[d]	<0.007	0.0419	<0.02	5.86E-05	1.61E-06	100.2	---	---	175	355	115	
Average Geothermometer (n = 12)									**205**	**222**	**219**	
Fumaroles, Southwest of Cottonwood Canyon Near Inactive Sinter Deposits												
DV98-105	<0.007	0.0331	0.650	9.57E-05	6.50E-07	100.5	---	---	88	181	78	
DV99-212	<0.006	0.0386	5.04?	1.40E-04	9.2E--06	99.67	---	---	112	---	---	

Table 9: Trace Metal Analyses of Selected Dixie Valley Region Gas Samples (Values are in ppm unless otherwise noted).[a]

Sample	Name or Description	Ag	As	Au	Cu	Hg	Pb	Sb	Se	Zn	Density (g/cm^3)
Production Wells											
DV97-12(2)	73-7 Well	<0.01	0.205	<0.01	0.02	0.012	0.07	0.027	<0.0002	0.23	1.0719
DV97-15(2)	74-7 Well	<0.01	0.111	<0.01	0.02	0.010	<0.02	0.010	<0.0002	0.23	1.0783
DV97-17	V102 + V103 Separator	<0.01	0.020	<0.01	0.38	0.0039	<0.02	0.0038	<0.0002	0.21	1.0748
DV97-19	V105 Separator	0.050	0.007	<0.01	0.21	0.011	<0.02	0.0061	<0.0002	0.24	1.0758
DV97-21(1)	82A-7 Well	<0.01	0.084	<0.01	0.04	0.020	<0.02	0.0087	<0.0002	0.18	1.0436
DV97-21(2)	82A-7 Well	<0.01	0.215	<0.01	0.02	0.020	<0.02	0.032	<0.0002	0.15	1.0681
DV97-22	73B-7 Well	<0.01	0.079	<0.01	<0.01	0.012	<0.02	0.018	<0.0002	0.17	1.0820
DV97-24	V101 Separator	<0.01	0.008	<0.01	0.24	0.0035	<0.02	0.0094	0.0005	0.27	1.0660
DV97-27	27-33 Well	<0.01	0.008	<0.01	0.03	0.0056	<0.02	0.0062	<0.0002	0.21	1.0888
DV97-28	37-33 Well	<0.01	0.007	<0.01	<0.01	0.0070	<0.02	0.0064	0.0003	0.18	1.0942
DV97-31	28-33 Well	<0.01	0.078	<0.01	0.13	0.013	0.16	0.11	0.0007	0.61	1.1151
Other Geothermal Wells											
DV97-53	46-32 Well	<0.01	0.014	<0.01	0.02	0.56	<0.02	0.0084	<0.0002	0.24	1.1247
DV97-54	27-32 well	<0.01	0.010	<0.01	0.03	0.067	<0.02	0.010	<0.0002	0.16	1.0815
DV98-102	45-14 Well	<0.01	0.037	<0.01	0.03	0.20	<0.02	0.012	0.0005	0.02	1.1245
Fumaroles											
DV97-43	Crack 4 Fumarole	<0.01	0.008	<0.01	<0.01	0.11	<0.02	0.0076	<0.0002	0.17	1.0871
DV97-44	Senator Fumarole	<0.01	0.004	<0.01	0.02	0.18	<0.02	0.0062	0.0004	0.29	1.0778
DV97-45	Range Front Fumarole	<0.01	0.009	<0.01	<0.01	0.054	<0.02	0.0065	0.0005	0.24	1.0830
DV98-108	Senator Fumarole	<0.01	0.009	<0.01	<0.01	0.021	<0.02	0.0075	<0.0002	0.18	1.0844
DV98-109	Calcite Fumarole	<0.01	0.014	<0.01	0.02	0.028	0.03	0.023	<0.0002	0.18	1.0821
DV98-124	Crack 4 Fumarole	<0.01	0.009	<0.01	<0.01	0.023	<0.02	0.0090	<0.0002	0.06	1.1160

[a] Analyses performed on caustic solutions obtained from USGS samples (Table 8). Values are corrected for density and background (blank sample).

Table 10: Reconstructed Reservoir Compositions Used For Geothermometry Calculations (Values in ppm except where otherwise noted).[a]

Sample	Location	Date	y value	Brine Analyses							Reconstructed Reservoir Compositions						
				Cl	SiO_2	Ca	Mg[b]	Na	K	Li	Cl	SiO_2	Ca	Mg	Na	K	Li
DIXE102-W	V102 + V103 Separator	10/02/95	0.153	495	638.0	7.92	0.04	462	71.8	2.29	419.3	540.4	6.71	0.034	391.3	60.8	1.94
DV96-8	76-7 Well	10/25/96	0.184	524	599.0	8.53	0.026	474	69.5	2.29	427.6	488.8	6.96	0.021	386.8	56.7	1.87
DV96-9	V101 Separator	10/25/96	0.159	438	599.0	8.03	0.007	407	64	2.03	368.4	503.8	6.75	0.006	342.3	53.8	1.71
DV97-11	V101 Separator	10/29/97	0.158	594	580.0	8.96	0.02	508	74.4	2.45	500.1	488.4	7.54	0.017	427.7	62.6	2.06
DV97-13	84-7 Well	10/29/97	0.159	558	580.0	9.66	0.01	496	70.8	2.46	469.3	487.8	8.12	0.008	417.1	59.5	2.07
DV97-14	74-7 Well	10/29/97	0.163	584	586.0	9.2	**0.01**	500	72.2	2.43	488.8	490.5	7.70	0.008	418.5	60.4	2.03
DV97-16	V102 + V103 Separator	10/29/97	0.161	580	586.0	9.02	**0.01**	500	77.2	2.48	486.6	491.7	7.57	0.008	419.5	64.8	2.08
DV97-18	V105 Separator	10/29/97	0.151	574	595.0	9.53	0.02	502	73.5	2.29	487.3	505.2	8.09	0.017	426.2	62.4	1.94
DV97-20	82A-7 Well	10/29/97	0.159	575	556.0	9.63	**0.01**	495	72.6	2.22	483.6	467.6	8.10	0.008	416.3	61.1	1.87
DV97-23	73B-7 Well	10/30/97	0.160	571	569.0	9.09	**0.01**	499	76.4	2.34	479.6	478.0	7.64	0.008	419.2	64.2	1.97
DV97-25	27-33 Well	10/30/97	0.157	443	627.0	7.69	**0.01**	423	66.8	2.22	373.4	528.6	6.48	0.008	356.6	56.3	1.87
DV97-26	V101 Separator	10/30/97	0.164	463	627.0	7.95	**0.01**	439	68.8	2.27	387.1	524.2	6.65	0.008	367.0	57.5	1.90
DV97-29	37-33 Well	10/30/97	0.159	475	621.0	7.2	0.02	431	68.8	2.26	399.5	522.3	6.06	0.017	362.5	57.9	1.90
DV97-30	28-33 Well	10/30/97	0.156	470	642.0	7.4	0.02	429	70.1	2.24	396.7	541.8	6.25	0.017	362.1	59.2	1.89
DV98-73	V101 Separator	04/28/98	0.157	449	590.6	7.41	0.05	448	70.5	2.40	378.5	497.9	6.25	0.042	377.8	59.4	2.02
DV98-75	27-33 Well	04/28/98	0.155	421	571.4	6.97	**0.01**	430	60.2	2.27	355.7	482.8	5.89	0.008	363.4	50.9	1.92
DV98-77	37-33 Well	04/28/98	0.156	444	554.3	7.19	**0.01**	429	66.7	2.21	374.7	467.8	6.07	0.008	362.1	56.3	1.87
DV98-79	28-33 Well	04/28/98	0.157	446	550.0	7.50	**0.01**	447	67.8	2.28	376.0	463.6	6.32	0.008	376.4	57.2	1.92
DV98-80	76A-7 Well	04/28/98	0.157	556	541.4	8.56	0.01	498	75.6	2.58	468.7	456.4	7.22	0.008	419.8	63.7	2.17
DV98-82	V102 + V103 Separator	04/28/98	0.150	567	517.9	8.81	0.01	498	77.1	2.42	482.0	440.2	7.49	0.009	423.3	65.5	2.06
DV98-84	74-7 Well	04/28/98	0.158	564	530.7	8.65	0.02	491	75.2	2.53	474.9	446.9	7.28	0.017	413.7	63.3	2.13
DV98-86	63-7 Well	04/28/98	0.154	560	515.7	8.73	**0.01**	510	77.0	2.43	473.8	436.3	7.39	0.008	431.1	65.1	2.06
DV98-88	73-7 Well	04/29/98	0.154	547	517.9	8.44	0.02	498	76.8	2.40	462.8	438.1	7.14	0.017	421.3	65.0	2.03
DV98-90	82A-7 Well	04/29/98	0.153	561	520.0	8.95	**0.01**	501	76.1	2.22	475.2	440.5	7.58	0.008	424.6	64.5	1.88
DV98-92	V105 Separator	04/29/98	0.150	572	526.4	8.65	**0.01**	496	75.9	2.32	486.2	447.5	7.35	0.009	421.9	64.5	1.97
DV98-95	73B-7 Well	04/29/98	0.152	561	511.5	8.43	**0.01**	500	74.2	2.27	475.7	433.7	7.15	0.008	423.7	62.9	1.92
DV98-135	27-33 Well	10/20/98	0.184	496	582.1	9.46	**0.01**	467	60.0	2.61	404.7	475.0	7.72	0.008	381.1	49.0	2.13
DV98-138	V101 Separator	10/21/98	0.160	436	545.7	7.18	**0.01**	409	63.8	2.11	366.2	458.4	6.03	0.008	343.6	53.6	1.77
DV98-140	37-33 Well	10/21/98	0.162	432	526.4	6.08	0.21	398	66.3	2.02	362.0	441.2	5.10	0.176	333.5	55.6	1.69
DV98-141	28-33 Well	10/21/98	0.162	441	530.7	7.21	0.03	412	65.5	2.03	369.6	444.7	6.04	0.025	345.3	54.9	1.70
DV98-145	76A-7 Well	10/22/98	0.158	541	498.6	8.23	0.01	479	70.8	2.26	455.5	419.8	6.93	0.008	403.3	59.6	1.90
DV98-147	63-7 Well	10/22/98	0.155	565	500.8	8.87	0.01	496	71.9	2.21	477.4	423.1	7.50	0.008	419.1	60.8	1.87
DV98-148	V102 + V103 Separator	10/22/98	0.164	560	513.6	9.18	0.17	485	72.3	2.24	468.2	429.4	7.67	0.142	405.5	60.4	1.87
DV98-150	74-7 Well	10/22/98	0.160	554	517.9	8.90	0.04	486	74.1	2.38	465.4	435.0	7.48	0.034	408.2	62.2	2.00
DV98-152	73-7 Well	10/22/98	0.154	567	509.3	8.81	0.02	476	73.7	2.14	479.7	430.9	7.45	0.017	402.7	62.4	1.81
DV98-154	73B-7 Well	10/22/98	0.154	560	513.6	7.75	0.01	485	72.0	2.15	473.8	434.5	6.56	0.008	410.3	60.9	1.82
DV98-156	82A-7 Well	10/23/98	0.154	557	513.6	8.87	0.04	473	69.3	2.10	471.2	434.5	7.50	0.034	400.2	58.6	1.78
DV98-159	V105 Separator	10/23/98	0.146	560	507.2	9.39	0.34	480	69.4	2.14	478.2	433.1	8.02	0.290	409.9	59.3	1.83
DV99-182	76A-7 Well	05/04/99	0.152	576	524	8.52	0.24	508	73.7	2.51	488.4	444.6	7.22	0.204	430.8	62.5	2.13
DV99-184	74-7 Well	05/04/99	0.160	592	522	8.65	0.33	482	74.3	2.32	497.3	438.6	7.27	0.277	404.9	62.4	1.95
DV99-186	V102 + V103 Separator	05/04/99	0.137	594	522	8.47	**0.01**	496	72.7	2.33	512.6	450.6	7.31	0.009	428.0	62.7	2.01

Table 10: Continued

Sample	Location	Date	y value	Brine Analyses							Reconstructed Reservoir Compositions						
				Cl	SiO_2	Ca	Mg[b]	Na	K	Li	Cl	SiO_2	Ca	Mg	Na	K	Li
DV99-188	63-7 Well	05/04/99	0.152	604	516	8.48	**0.01**	504	73.6	2.26	512.2	437.3	7.19	0.008	427.4	62.4	1.92
DV99-190	73-7 Well	05/04/99	0.154	624	518	8.79	**0.01**	508	74.6	2.21	527.9	438.1	7.44	0.008	429.8	63.1	1.87
DV99-194	V105 Separator	05/05/99	0.138	620	514	9.51	**0.01**	514	74.4	2.23	534.4	442.7	8.20	0.009	443.1	64.1	1.92
DV99-196	82A-7 Well	05/05/99	0.152	623	503	8.89	**0.01**	518	72.2	2.25	528.3	426.5	7.54	0.008	439.3	61.2	1.91
DV99-197	73B-7 Well	05/05/99	0.159	624	520	8.78	**0.01**	516	74.4	2.22	524.8	437.3	7.38	0.008	434.0	62.6	1.87
DV99-199	37-33 Well	05/05/99	0.160	475	563	6.66	0.12	433	65.7	2.23	399.0	472.8	5.59	0.101	363.7	55.2	1.87
DV99-200	28-33 Well	05/05/99	0.159	483	561	6.68	0.02	432	66.2	2.24	406.2	471.5	5.62	0.017	363.3	55.7	1.88
DV99-204	V101 Separator	05/05/99	0.159	481	576	7.35	**0.01**	428	68.4	2.39	404.5	484.1	6.18	0.008	359.9	57.5	2.01
DV99-204	V101 Separator	05/05/99	0.159	481	576	7.35	**0.01**	428	68.4	2.39	404.5	484.1	6.18	0.008	359.9	57.5	2.01
DV74782786-brine 2	74-7 Well Archived	08/27/86	0.199	396	574	1.11	**0.01**	413	61.5	2.82	317.2	459.4	0.89	0.008	330.8	49.3	2.26
DV76781986-brine 4	76-7 Well Archived	08/19/86	0.187	402	563	1.53	**0.01**	403	54.2	2.79	326.8	457.6	1.24	0.008	327.6	44.1	2.27
DV453382186-brine 6	45-33 Well Archived	08/21/86	0.165	320	589	1.27	0.04	370	59.2	2.63	267.2	491.4	1.06	0.033	309.0	49.4	2.20
DV73782886-brine 8	73-7 Well Archived	08/28/86	0.198	363	548	1.24	**0.01**	380	59.2	2.55	291.1	439.4	0.99	0.008	304.8	47.5	2.05
No number	28-33 Well Archived	09/23/93	0.158	70.1	101	15.6	2.08	228	6.13	0.35	59.0	84.9	13.14	1.751	192.0	5.2	0.29
DV97-55	27-32 Well	11/05/97	0.054	87.6	58.2	5.56	0.03	95.5	13.1	0.7	82.9	55.1	5.26	0.028	90.3	12.4	0.66
DV98-99[c]	27-32 Well	04/29/98	0.054	84.8	61.2	5.91	0.91	88.0	11.6	0.48	80.2	57.9	5.59	0.861	83.2	11.0	0.45

[a] The reconstructed composition is calculated as C(r) =(1-y) * C(b), where C(b) = analyte concentration in the brine, C(r) = reconstructed analyte composition, and y = the steam fraction.

[b] Mg values shown in bold are "less than" values that are assumed to be 0.01 ppm for the calculations.

[c] The y value for DV98-99 uses the 1997 value.

Table 11: Chemical Geothermometry of Geothermal Production Fluids (Corrected for steam flash, Table 10; all values in °C).[a]

Sample	Name or description	Date	tCH	tQC	tNK(f)	tNL(d)	tL(d)	tML[b]	tKM[b]	<------- Na-K-Ca------>		<------ Na-K-Ca Mg correction ----->		
										t(beta1/3)[c]	t(beta4/3)[c]	R[b]	t(beta1/3)[c]	t(beta4/3)[c]
DV74782786-brine 2	74-7 Well Archived	08/27/86	235	245	254	221	185	**308**	**248**	252	348	**0.050**	252	348
DV76781986-brine 4	76-7 Well Archived	08/19/86	235	244	244	222	185	**308**	**241**	241	316	**0.056**	241	316
DV453382186-brine 6	45-33 Well Archived	08/21/86	243	251	261	225	184	256	212	254	335	0.208	254	335
DV73782886-brine 8	73-7 Well Archived	08/28/86	230	241	258	219	181	**301**	**246**	252	334	**0.052**	252	334
Average August 1986			***236***	***245***	***254***	***222***	***184***	***293***	***237***	***250***			***250***	
No number	28-33 Well Archived	09/23/93	100	128	125	101	115	84	72	123	94	15.466	99	94
DIXE102-W	V102 + V103 Separator	10/02/95	254	260	258	189	179	248	222	235	255	0.147	235	255
DV96-8	76-7 Well	10/25/96	242	250	252	186	178	260	230	231	248	0.097	231	248
DV96-9	V101 Separator	10/25/96	246	253	259	189	174	299	261	233	243	0.028	233	243
Average October 1996			***244***	***252***	***256***	***188***	***176***	***279***	***245***	***232***			***232***	
DV97-11	73-7 Well	10/29/97	242	250	252	186	181	275	241	232	253	0.070	232	253
DV97-13	84-7 Well	10/29/97	242	250	250	189	182	300	257	229	246	0.036	229	246
DV97-14	74-7 Well	10/29/97	243	251	251	187	181	**299**	**258**	230	249	**0.036**	230	249
DV97-16	V102 + V103 Separator	10/29/97	243	251	257	189	182	**300**	**261**	235	255	**0.034**	235	255
DV97-18	V105 Separator	10/29/97	246	253	252	181	179	270	240	231	250	0.070	231	250
DV97-20	82A-7 Well	10/29/97	237	246	252	180	178	**292**	**258**	231	247	**0.035**	231	247
DV97-23	73B-7 Well	10/30/97	240	248	256	184	180	**296**	**261**	234	254	**0.034**	234	254
DV97-25	27-33 Well	10/30/97	251	257	260	194	178	**292**	**253**	235	249	**0.039**	235	249
DV97-26	V101 Separator	10/30/97	250	257	259	193	178	**294**	**255**	235	250	**0.038**	235	250
DV97-29	37-33 Well	10/30/97	250	256	261	194	178	269	237	237	254	0.078	237	254
DV97-30	28-33 Well	10/30/97	254	260	263	194	178	269	238	238	254	0.076	238	254
Average October 1997			***245***	***253***	***256***	***188***	***179***	***287***	***251***	***233***			***233***	
DV98-73	V101 Separator	04/28/98	244	252	259	196	181	244	215	236	256	0.189	236	256
DV98-75	27-33 Well	04/28/98	241	249	248	195	179	**294**	**248**	228	246	**0.044**	228	246
DV98-77	37-33 Well	04/28/98	237	246	258	192	177	**292**	**253**	235	252	**0.040**	235	252
DV98-79	28-33 Well	04/28/98	236	246	256	192	179	**294**	**254**	234	252	**0.039**	234	252
DV98-80	76A-7 Well	04/28/98	235	244	256	193	184	303	260	235	256	0.035	235	256
DV98-82	V102 + V103 Separator	04/28/98	231	241	258	187	181	299	262	236	257	0.034	236	257
DV98-84	74-7 Well	04/28/98	232	242	256	192	183	277	241	235	255	0.070	235	255
DV98-86	63-7 Well	04/28/98	230	240	255	185	181	**299**	**261**	235	258	**0.034**	235	258
DV98-88	73-7 Well	04/29/98	230	241	257	186	181	273	242	236	258	0.069	236	258
DV98-90	82A-7 Well	04/29/98	231	241	256	179	178	**292**	**261**	234	255	**0.034**	234	255
DV98-92	V105 Separator	04/29/98	232	242	256	183	180	**296**	**261**	235	257	**0.035**	235	257
DV98-95	73B-7 Well	04/29/98	229	240	253	181	179	**294**	**259**	233	256	**0.035**	233	256
Average April 1998			***234***	***244***	***256***	***188***	***180***	***288***	***252***	***234***			***234***	
DV98-135	27-33 Well	10/20/98	239	248	239	200	183	**303**	**247**	221	232	**0.041**	221	232
DV98-138	V101 Separator	10/21/98	235	244	258	193	176	**288**	**251**	234	248	**0.041**	234	248
DV98-140	37-33 Well	10/21/98	231	241	265	191	174	194	181	240	258	0.857	240	258
DV98-141	28-33 Well	10/21/98	232	242	260	188	174	249	224	235	249	0.121	235	249

Table 11: Continued

Sample	Name or description	Date	tCH	tQC	tNK(f)	tNL(d)	tL(d)	tML[b]	tKM[b]	<------- Na-K-Ca------>		<------ Na-K-Ca Mg correction ----->		
										t(beta1/3)[c]	t(beta4/3)[c]	R[b]	t(beta1/3)[c]	t(beta4/3)[c]
DV98-145	76A-7 Well	10/22/98	226	237	253	184	178	293	257	232	253	0.037	232	253
DV98-147	63-7 Well	10/22/98	226	237	251	179	178	**292**	**258**	231	251	**0.036**	231	251
DV98-148	V102 + V103 Separator	10/22/98	228	239	254	182	178	205	189	232	249	0.603	228	246
DV98-150	74-7 Well	10/22/98	229	240	256	188	180	250	223	234	252	0.140	234	252
DV98-152	73-7 Well	10/22/98	228	239	258	180	176	266	240	235	252	0.071	235	252
DV98-154	73B-7 Well	10/22/98	229	240	253	179	177	290	258	234	257	0.037	234	257
DV98-156	82A-7 Well	10/23/98	229	240	252	179	176	242	220	231	247	0.148	231	247
DV98-159	V105 Separator	10/23/98	229	240	251	179	177	186	174	230	245	1.231	230	245
Average October 1998			***230***	***241***	***254***	***185***	***177***	***255***	***227***	***232***			***232***	
DV99-182	76A-7 Well	05/04/99	232	242	251	189	183	202	183	232	256	0.847	232	256
DV99-184	74-7 Well	05/04/99	230	241	257	186	179	190	177	235	254	1.151	235	254
DV99-186	V102 + V103 Separator	05/04/99	233	243	252	184	180	**297**	**259**	232	255	**0.036**	232	255
DV99-188	63-7 Well	05/04/99	230	240	252	180	179	**294**	**259**	232	255	**0.036**	232	255
DV99-190	73-7 Well	05/04/99	230	241	252	177	178	**292**	**260**	232	255	**0.035**	232	255
DV99-194	V105 Separator	05/05/99	231	241	251	177	179	**293**	**260**	231	252	**0.035**	231	252
DV99-196	82A-7 Well	05/05/99	227	238	247	177	178	**293**	**258**	229	252	**0.036**	229	252
DV99-197	73B-7 Well	05/05/99	230	240	250	176	178	**292**	**259**	232	255	**0.035**	232	255
DV99-199	37-33 Well	05/05/99	238	247	256	192	178	214	193	234	255	0.488	234	255
DV99-200	28-33 Well	05/05/99	238	247	257	193	178	268	235	235	255	0.081	235	255
DV99-204	V101 Separator	05/05/99	241	249	261	200	180	**298**	**255**	236	253	**0.039**	236	253
Average May 1999			***233***	***243***	***253***	***185***	***179***	***267***	***236***	***233***			***233***	
DV97-55	27-32 Monitoring Well	11/05/97	76	106	246	228	140	193	158	199	144	0.401	199	144
DV98-99	27-32 Monitoring Well	04/29/98	79	109	242	198	128	108	100	195	135	11.233	135	116
Average 27-32 Well			***78***	***108***	***244***	***213***	***134***	***151***	***129***	***197***			***167***	

[a] Calculations use the following geothermometers: tCH, tQC, and tNK(f) = the chalcedony, quartz (conductive) and Na/K equations of Fournier (1981); tNL(d) = the Na/Li (dilute) equation of Fouillac and Michard (1981); tL(d) and tML = the Li (dilute) and Mg/Li equations of Kharaka and Mariner (1989); tKM = the K/Mg equation of Giggenbach (1986); Na-K-Ca refers to the equations of Fournier and Truesdell, 1973 (see their paper for an explanation of the "beta" factor); Na-K-Ca Mg correction refers to the equations of Fournier and Potter, 1979 ("cool" means <70°C).

[b] Values in bold use assumed concentrations of 0.01 ppm Mg to perform the calculation (see Table 10).

[c] The underlined value is the preferred temperature according to the rules of the geothermometer.

Table 12: Chemical Geothermometry of Background Thermal/Mineral Springs and Wells.[a]

Sample	Name or Description	Date	Sampling Temp (°C)	tCH	tQC	tNK(f)	tNL(d)	tL(d)	tML	tKM	<------- Na-K-Ca------>		<---- Na-K-Ca Mg correction ---->		
											t(beta1/3)[b]	t(beta4/3)[b]	R	t(beta1/3)[b]	t(beta4/3)[b]
Springs															
DV97-46	Sou Hot Spring	11/03/97	57.0	85	114	271	180	145	75	84	196	104	22	83	80
DV97-47	Sou Hot Spring	11/03/97	72.6	83	113	270	179	143	74	83	195	102	21	86	82
DV98-117[c]	Sou Hot Spring[c]	05/04/98	72.0	80	109	264	**-29**	**37**	**-14**	84	193	104	22	83	80
DV97-48	Hyder Hot Spring	11/03/97	76.7	81	111	180	194	174	112	84	161	124	24	71	71
DV98-112	Hyder Hot Spring	04/30/98	75.3	79	109	174	179	171	109	84	158	125	24	72	72
DV97-56	Dead Travertine Spring, upper seep	11/05/97	17.4	44	76	254	211	181	85	80	194	116	37	39	43
DV99-210	Dead Travertine Spring, road seep	05/07/99	19-22	50	82	256	210	185	86	82	200	131	44	25	27
DV97-60	Fault Line Spring	11/06/97	28.8	62	93	192	125	121	57	64	154	83	29	55	68
DV97-61	Lower Ranch Hot Spring	11/06/97	40.8	62	92	199	117	114	55	67	161	93	33	45	56
DV98-113	Lower Ranch Hot Spring	05/04/98	40.4	56	87	191	110	114	55	67	157	94	33	46	56
DV99-211	Lower Ranch, upper spring	05/08/99	39.4	59	90	200	111	113	54	68	161	95	32	48	58
DV97-62	McCoy Hot Spring	11/06/97	46.2	55	87	163	69	98	33	53	136	72	37	39	57
DV98-114	McCoy Hot Spring	05/04/98	46.0	51	82	156	70	102	35	53	133	73	37	39	56
DV97-63	Kyle Spring	11/06/97	19.8	25	58	126	14	50	-8	24	101	26	43	37	26
DV97-68	Big Horn Spring	11/07/97	20.5	56	88	79	-4	74	9	35	87	58	47	36	58
DV98-118	Big Horn Spring	05/05/98	18.1	53	84	69	-14	81	11	39	84	68	46	37	68
DV97-69	Dixie Hot Spring	11/07/97	81.6	113	140	122	123	126	141	106	123	97	1	123	97
DV98-120	Dixie Hot Spring	05/05/98	83.5	114	141	117	117	126	130	97	120	98	3	120	98
DV98-128	Jersey Hot Spring	05/05/98	59.0	129	154	211	208	159	117	96	177	126	14	115	105
Wells															
DV96-1	Domestic Well	10/24/96	34.2	93	121	223	147	127	55	64	171	93	43	26	39
DV97-38	Domestic Well	10/24/96	29.2	95	123	233	149	126	56	66	177	95	41	29	40
DV97-39	Goerenger Well	10/31/97	27.8	83	112	208	169	151	72	69	172	114	50	Cool	Cool
DV98-160	Goerenger Well	10/23/98	26.7	81	110	207	158	147	67	67	171	113	54	Cool	Cool
DV98-96	Goerenger Well	04/29/98	28.3	82	112	205	161	151	71	69	172	117	52	Cool	Cool
DV99-181	Goerenger Well	05/04/99	27.7	82	111	198	159	152	70	67	167	114	54	Cool	Cool
DV97-57	Bolivia Artesian Well	11/05/97	28.8	42	74	127	81	98	25	30	107	42	52	Cool	42
DV97-59	45-W-5 Well	11/05/97	26.4	36	68	152	155	141	101	78	151	141	35	42	42
DV97-67	66-21 Well	11/07/97	55.5	199	215	210	188	215	225	182	202	216	1	200	215
DV98-104	66-21 Well	04/30/98	57.4	200	216	216	200	219	233	185	205	216	1	202	214
DV98-111	62-21 Well	04/30/98	75.5	147	170	138	74	131	124	124	153	184	4	151	171
DV98-122	97-2 Well	05/05/98	19.7	77	106	210	165	168	82	79	182	143	53	Cool	Cool
DV98-123	32-6 Well	05/06/98	32	-33	0	146	33	78	9	40	132	85	77	Cool	Cool
DV98-168	38-32 Well	10/26/98	87.7	144	168	223	174	154	131	121	194	161	6	167	148
DJ-1	Dixie Jack Gradient Well #1	05/17/98	49	64	95	181	170	173	121	99	166	140	15	108	103
DJ-4	Dixie Jack Gradient Well #4	05/20/98	77	121	147	206	173	160	151	131	187	168	4	178	164
DJ-7	Dixie Jack Gradient Well #7	05/14/98	55	-15	18	222	181	84	82	78	160	65	5	151	65

[a] Calculations use the geothermometers described on the bottom of Table 11.

[b] The underlined value is the preferred temperature according to the rules of the geothermometer.

[c] This sample assumes 0.01 ppm lithium to perform the geothermometer calculations shown in bold.

Table 13: Chemical Analyses of Scales and Precipitates from Dixie Valley Production Wells, Pipelines, and Test Beds.[a]

Sample	Name or description	Date	Al_2O_3 wt %	CaO wt %	CO_2 wt %	Fe_2O_3 wt %	Na_2O wt %	MgO wt %	MnO wt %	K_2O wt %	P_2O_5 wt %	SiO_2 wt %	TiO_2 wt %
Test bed scale	Inlet	1996	7.47	4.07	---	4.64	1.19	2.88	0.172	1.53	0.035	62.10	---
Test bed scale	Aged	1996	6.60	3.50	---	3.29	1.06	4.75	0.197	1.38	0.031	61.56	---
Test bed scale	Exit	1996	3.84	3.64	---	5.82	1.08	10.82	0.091	1.02	0.033	60.52	---
DS97-Pig, white	DS97-Pig, white part of scale	Oct-97	11.2	4.43	0.39	0.06	---	0.04	0.005	---	---	70.7	0.003
DS97-DV-32 white	DS97-DV-32 brine, white part of scale	Oct-97	10.8	3.29	0.12	0.03	---	0.02	0.010	---	---	71.0	0.003
DS97-DV-32 grey	DS97-DV-32 brine, grey part of scale	Oct-97	10.4	3.31	0.42	0.12	---	0.12	0.010	---	---	70.7	0.004
DS97-DV97-32/33	DS97-DV97-32/33, white part of scale	Oct-97	5.83	21.0	13.2	0.31	---	0.90	0.051	---	---	51.0	0.13
DS97-DV97-37	DS97-DV97-37 fines, total sample	Oct-97	5.43	26.0	7.86	1.50	---	0.65	0.078	---	---	50.9	0.07
DS97-76A7 white	DS97-76A7, white part of scale	Nov-97	0.05	55.9	35.5	0.01	---	0.06	0.028	---	---	0.22	0.001
DS97-76A7 grey	DS97-76A7, grey part of scale	Nov-97	3.79	16.7	20.6	5.20	---	15.4	0.68	---	---	34.4	0.01

Sample	Name or Description	Date	Ag ppm	Au ppm	Al ppm	As ppm	Ba ppm	Ca ppm	Cu ppm	Fe ppm	Hg ppm	K ppm	Li ppm
Test bed scale	Inlet	1996	---	---	---	181	---	---	101	---	---	---	18.5
Test bed scale	Aged	1996	---	---	---	185	---	---	77	---	---	---	18.3
Test bed scale	Exit	1996	---	---	---	172	---	---	50	---	---	---	170
DS97-Pig, white	DS97-Pig, white part of scale	Oct-97	4.96	0.125	59030	2.6	720	31640	---	399	0.040	20260	---
DS97-DV-32 white	DS97-DV-32 brine, white part of scale	Oct-97	1.58	0.093	57070	1.9	1510	23510	---	211	0.068	23510	---
DS97-DV-32 grey	DS97-DV-32 brine, grey part of scale	Oct-97	29.0	1.64	55070	5.0	1705	23690	---	847	0.068	24480	---
DS97-DV97-32/33	DS97-DV97-32/33, white part of scale	Oct-97	2.00	0.225	30850	1.8	294	150000	---	2180	<0.04	9760	---
DS97-DV97-37	DS97-DV97-37 fines, total sample	Oct-97	5.79	0.087	28730	13.8	689	185700	---	10470	0.178	11480	---
DS97-76A7 white	DS97-76A7, white part of scale	Nov-97	<0.3	<0.05	278	1.9	634	399400	---	77.3	<0.05	420	---
DS97-76A7 grey	DS97-76A7, grey part of scale	Nov-97	17.2	1.97	20080	2.1	358	119300	---	36370	<0.3	2480	---

[a] Data for the test-bed scale was previously published in Bruton et al. (1997).

Table 13: Continued

Sample	Cl wt %	F wt %	S wt %	TIC wt %	TOC wt %
Test bed scale	0.113	0.033	0.136	0.083	0.272
Test bed scale	0.058	0.067	0.130	0.065	0.172
Test bed scale	0.121	0.183	0.109	0.282	0.180
DS97-Pig, white	---	---	---	---	---
DS97-DV-32 white	---	---	---	---	---
DS97-DV-32 grey	---	---	---	---	---
DS97-DV97-32/33	---	---	---	---	---
DS97-DV97-37	---	---	---	---	---
DS97-76A7 white	---	---	---	---	---
DS97-76A7 grey	---	---	---	---	---

Sample	Mg ppm	Mn ppm	Mo ppm	Na ppm	Ni ppm	Si ppm	Sr ppm	Ti ppm	TIC ppm
Test bed scale	---	---	4.0	---	20.5	---	1180	---	---
Test bed scale	---	---	6.1	---	9.4	---	2070	---	---
Test bed scale	---	---	<4	---	32.3	---	7	---	---
DS97-Pig, white	250	38.7	---	8020	---	330400	2920	19.8	1060
DS97-DV-32 white	144	74.6	---	9300	---	332000	1940	18.1	333
DS97-DV-32 grey	743	74.3	---	9810	---	330400	1950	24.8	1160
DS97-DV97-32/33	5460	394	---	5410	---	238200	1570	801	36000
DS97-DV97-37	3900	608	---	5150	---	238100	939	421	21440
DS97-76A7 white	344	214	---	151	---	1050	8440	7.6	96900
DS97-76A7 grey	92840	5300	---	5670	---	160600	2980	73.9	56060

Table 14: Miscellaneous Isotope Data for Vein and Rock Samples, Dixie Valley Region, Nevada.[a]

Sample[b]	Name or Description	Location	Age	$\delta^{13}C$ (PDB) (per mil)	$\delta^{18}O$ (SMOW) (per mil)	$\delta^{34}S$ (CDT) (per mil)	Rb (ppm)	Sr (ppm)	$^{87/86}Sr$	Laboratory
Samples from Dixie Valley region [c]										
F97-22	Marine limestone, post Star Peak strata	Augusta Mts, 2 km SE of well DV97-49	U. Triassic	1.37	16.6	---	---	---	---	USGS
F98-8	Calcite vein in graphitic argillite	Stillwater fault zone NW of Senator Fumarole	Quaternary	-3.9	-2.9	---	---	---	---	UNM
F98-9	Gypsum in quartzite fault gouge beneath gabbro	Stillwater fault zone NW of Senator Fumarole	Holocene?	---	---	0.2	---	---	---	GC
F98-10	Graphitic marble, Stillwater Range	About 0.4 km NW of Senator Fumarole	Jurassic	1.3	15.8	---	<1	352	0.707926	UNM/LANL
F98-12	Calcite-quartz veins in altered quartzite, Stillwater Range	About 0.25 km NW of Senator Fumarole	Quaternary	-4.3	-5.3	---	---	---	---	UNM
F98-13	Calcite vein in gabbro	Stillwater fault zone SW of Senator Fumarole	Quaternary	-4.0	-6.3	---	---	---	---	UNM
F98-14	Calcite crystals in fault gouge,	Stillwater fault zone SW of Senator Fumarole	Quaternary	-3.9	-5.1	---	---	---	---	UNM
F98-15	Sulphur from Range Front Fumarole	Stillwater fault zone W of Senator Fumarole	1998	---	---	4.6	---	---	---	GC
F98-16	Pyrite in quartzite breccia	Stillwater fault zone W of Senator Fumarole	Quaternary	---	---	6.0	---	---	---	GC
F98-17	Sulphur from Senator Fumarole	From main vent	1998	---	---	2.6	---	---	---	GC
F98-18	Coarse-grained diorite (part of Humboldt Lopolith?)	Augusta Mts, Hole in the Wall, N edge of creek	Jurassic	---	---	---	56.8	472	0.704710	UNM/LANL
F98-19	Welded tuff, overlies diorite	Augusta Mts, Hole in the Wall, N edge of creek	Oligocene	---	---	---	105	34.3	0.710082	UNM/LANL
F98-20	Welded tuff, underlies pyroclastic fall and lacustrine beds	Augusta Range, Cedar Canyon (spg DV98-127)	Oligocene	---	---	---	127	72.6	0.708330	UNM/LANL
F98-40	Meta-argillite, occurs near quartzite, Bernice Formation	Clan Alpine Range, Lofthouse Canyon (spg DV98-170)	U. Triassic	---	---	---	85.2	60.1	0.720839	UNM/LANL
F98-44	Calcareous argillite, Hoyt Canyon Formation	Clan Alpine Range, Hoyt Canyon (crk DV98-174)	U. Triassic	---	---	---	32.2	2075	0.708686	UNM/LANL
F98-45	Quartzite, overlies argillite, Hoyt Canyon Formation	Clan Alpine Range, Hoyt Canyon (crk DV98-174)	U. Triassic	---	---	---	25.3	49.1	0.718175	UNM/LANL
F98-48	Medium-grained diorite, underlies quartzite, lmst, and tuff	Clan Alpine Range, 16 km NW of Shoshone Pass	Jurassic	---	---	---	8.1	254	0.705198	UNM/LANL
F98-49	Marine limestone, underlies welded tuff	Clan Alpine Range, 10 km NW of Shoshone Pass	U. Triassic	---	---	---	<1	281	0.708007	UNM/LANL
F98-50	Welded tuff, slightly altered and silicified	Clan Alpine Range, War Canyon (near spg DV98-176)	Oligocene	---	---	---	7.8	166	0.706148	UNM/LANL
F98-52	Sheared marine limestone, Star Peak Group	Stillwater fault zone at Figure 8 Fumarole	M. Triassic	---	---	---	35.9	275	0.707749	UNM/LANL
F98-54	Gabbro-diorite, underies thrust fault and quartzite	Stillwater Range, Cottonwood Canyon, W of travertine	Jurassic	---	---	---	---	---	0.705409	UNM/LANL
Samples from North Central Nevada [d]										
F92-42	Marine dolomite, Nevada Group	Sulphur Springs Range, east of Pine Valley	Devonian	---	---	---	5.0	385	0.708658	UNM
F92-43	Vinini Group chert	Sulphur Springs Range, east of Pine Valley	Ordovician	---	---	---	0.56	6.96	0.715335	UNM
F92-44	Vinini Group shale	Sulphur Springs Range, east of Pine Valley	Ordovician	---	---	---	4.0	53.3	0.714235	UNM
F92-45	Travertine deposit at Buffy Hot Spring	Sulphur Springs Range, east of Pine Valley	Holocene	---	---	---	11.4	86.8	0.712022	UNM
F92-46	Troy Canyon muscovite granite	Grant Range, east of Railroad Valley	Cretaceous	---	---	---	100.3	475	0.714216	UNM
F92-48	Troy Canyon ignimbrite	Grant Range, east of Railroad Valley	Oligocene	---	---	---	294	132	0.711504	UNM
F92-49	Goodwyn Canyon Dolomite	Grant Range, east of Railroad Valley	Ordovician	---	---	---	4.7	551	0.711282	UNM
F92-50	Chainman Shale	Grant Range, east of Railroad Valley	Mississippian	---	---	---	86	178	0.717174	UNM
F92-51	Guilmette Limestone	Grant Range, east of Railroad Valley	Devonian	---	---	---	0.77	22.8	0.709684	UNM
F92-52	Joana Limestone	Grant Range, east of Railroad Valley	Mississippian	---	---	---	0.55	194	0.708406	UNM
F92-53	Chainman Shale	Pancake Range, west of Railroad Valley	Mississippian	---	---	---	78.1	242	0.716672	UNM
F92-54	Pancake Range ignimbrite	Pancake Range, west of Railroad Valley	Oligocene	---	---	---	128	340	0.712557	UNM
F92-55	Stone Cabin ignimbrite	Pancake Range, west of Railroad Valley	Oligocene	---	---	---	129	372	0.712320	UNM
F92-56	Horse Heaven ignimbrite	Pancake Range, west of Railroad Valley	Oligocene	---	---	---	261	340	0.710694	UNM
F92-57	Sheep Pass Formation, organic-rich lacustrine beds	Grant Range, east of Railroad Valley	Eocene	---	---	---	1.81	969	0.708174	UNM

[a] Stable isotope analyses were performed at Geochron Laboratories, Cambridge, Massachusetts. Strontium isotope analyses were obtained from the University of New Mexico, Albuquerque, New Mexico.

[b] Collection years for all samples are in the sample number, i.e., F97-22 was collected in 1997.

[c] Many samples were identified using the geologic map of Speed (1976) and the report of Lutz et al (1997).

[d] This group of samples was collected for an earlier geothermal project but data were unpublished (Goff et al., 1994 and Hulen et al., 1994).

Table 15: Uranium-Thorium and Uranium-Protactinium Dates on Two Samples of Old Spring Deposits, Dixie Valley, Nevada

Sample No.	F99-50b[a]	F99-61[b]
Material	Travertine Vein	Sinter Layer
Location	Cottonwood Canyon	Lower Ranch
Weight (g)	1.6666	0.9924
Th (ppm)	0.00443	0.04653
(+/-, %)	0.36	0.85
U (ppm)	0.71	0.04
(+/-, %)	0.25	0.31
Th/U	0.0062	1.1691
(+/-, %)	0.44	0.91
$^{234}U/^{238}U$	1.598	1.245
$^{230}Th/^{234}U$ Age (ka)	**182 ± 4**	**54 ± 4**
$^{231}Pa/^{235}U$	0.967	0.565
(+/-, %)	0.74	1.05
$^{231}Pa/^{235}U$ Age (ka)	**161 ± 15**	**39 ± 2**
Initial $^{234}U/^{238}U$	1.842	1.344

[a] Honey-colored calcite vein cutting altered gabbro, base of spring deposit near seep sample DV97-56.

[b] Sinter separate from layered silica and carbonate, base of northwestern edge of deposit, about 0.3 km from hot spring DV97-61.

APPENDIX 8

SUMMARY OF THERMAL DATA IN THE DIXIE VALLEY REGION

Summary of thermal regime data for surface and blind hydrothermal sites in the Dixie Valley Geothermal District, Nevada. The data is derived from Goff et al. (2002), which is presented in Appendix 7 of this report; Dixon et al. (2003); and Lutz et al. (2003). This table is after Blackwell et al. (2005)-Table 2.3.1. Referenced sites can be found on maps presented by Goff et al. (2002) and Shevenell and Garside (2005). Bolded data represent significant values as identified by Blackwell et al. (2005).

Surface Site	**Features**	**Temp. Max.**	**Flow Rate**	**pH**	**Cl**	**Fluid**	**Geothermometers (°C)**		**Deposits**	**Comments**	**Deposits**
		(°C)	**(l/min)**		**(ppm)**	**°C**	**Gas**	**^{18}O-SO$_4$**			**Age (ka)**
Hot Spring											
Dixie Meadows	20 hot springs and seeps	84	200	8.0 - 8.4	162	≤120	No Gas	133?	None	End of hydrothermal plume?	
Hyder	2 principal springs	77	≤120	7.7 - 8.0	47	80	87	68	Travertine		
Jersey	1 large spring	59	200	7.4	38	≤120	No Gas	181?	Travertine	Extinct deposits to east	
Lower Ranch	5 hot springs; some seeps	41	400	7.9 - 8.1	30	60	No Gas	87 - 105?	Travertine	Minor sinter at base of deposit	39 - 54[a]
McCoy	1 large spring	46	≥50	7.8 - 8.0	228	60	No Gas	74	None		
Sou	7 or more hot springs and pools	73	200	7.5 - 8.0	77	≤85	63	35	Travertine		
Mineral Springs											
Big Horn	Several seeps	20	≤1	7.8 - 7.9	≤1360	≤60	No Gas	57	None	Evaporated salts in muck	
Dead Travertine	Several small springs and seeps	22	≤5	7.7 - 8.0	≤630	≤40	No Gas	nd	Travertine	Very large, complex deposit	19 - 180
Fumarole Clusters											
Unnamed	3 weak vents	98	nd	nd	nd	nd	≥100	nd	Sinter	Minor Travertine	0.4 - 4.3[b]
Senator	10 large to weak vents	98	nd	nd	nd	nd	≤270	nd	None	Sulfur and other sublimates	
Blind Thermal Aquifers or Reservoirs											
Bolivia Well	Artesian well	29	40	8.1	290	≤45	No Gas	90?	Fe-Oxides	Thermal gradient well	
DF 45-14	Artesian 2-phase well	125	nd	7.2	481	200	**≥100**[c]	235	None	Geothermal wildcat	**10.7**[d]
DF 62-21	Artesian well	76	140	7.8	80	≤150	No Gas	133	None	Geothermal wildcat	
DF 66-21	Artesian well	57	≤7	6.5 - 7.0	1476	210	No Gas	209	None	Geothermal wildcat	
Dixie Production Zone	Many 2-phase wells	250	na	8.0 - 9.0	550	≤255	**≤199**[e]	**248**[f]	None	Section 7, 18, and 33 wells	

[a] Age of interbedded siliceous material at base of NW part of deposit; U-Th and U-Pr disequilibrium dates from Goff et al., 2002, Table 14.

[b] Range of ^{14}C and U/Th disequilibrium dates.

[c] Gas geothermometers affected by severe air contamination.

[d] Date is on sinter fragments at the Dixie Comstock Mine (Lutz et al., 2003).

[e] Gases collected from production wells in late 1990s have been stripped of non-condensable components during flashing and power production; thus, the value shown is too low.

[f] Value given is based on data obtained from archived samples. Present samples yield estimates that are too high due to steam loss during power production.

APPENDIX 9

WELL LITHOLOGY DATA

Table of Contents

Suneco (Sun) Dixie Valley Wells' Lithologic Summary

The following summary is based on Sunoco data provided by Al Waibel of Columbia Geocience with the approval of Terra-Gen Power.

The wells included in the dataset are:

Sun Wells (S.W.L. 1, 2, 2B, 3), other production wells (52-18, 65-18, 85-7), injection well 45-5, and dry well 62-21 (located near surface center of the valley).

The lithology has been summary and categorized into the eight geologic formations identified below.

LEGEND FOR GENERALIZED FORMATIONS

Fm	Description
Tsed	Basin-fill sediments and lowermost tuffaceous sediments/tuffs
Tmb	Miocene basalt
Tma	Miocene lake sediments
Tvs	Oligocene silicic volcanics
Kgr	Cretaceous granodiorite
Jvh	Jurassic mafic extrusive rocks (Humboldt igneous comples: upper)
Jgh	Jurassic mafic intrusive rocks (Humboldt igneous complex: lower)
Tr	Triassic meta-sediments

Well ID	T.D.		Rock Type Interval				Rock Type Thickness	Inferred Fm	Description
	feet	meters	start (ft)	end (ft)	start (m)	end (m)	(m)		
S.W.L. #1	7255	2211	5500	5550	1676	1692	15	Tsed	Basin fill sediments and silicic tuffs
			5550	7255	1692	2211	520	Tmb	Miocene basalt and mixed volc seds
S.W.L. #2	8900	2713	6400	7400	1951	2256	305	Tmb	Miocene basalt
									Fault: mylontic zone (7400')
			7400	7980	2256	2432	177	Kgr	granodiorite
			7980	8070	2432	2460	27		Fault Zone (well established)
			8070	8900	2460	2713	253	Kgr	granodiorite
S.W.L. #2B	8588	2618	5600	6220	1707	1896	189	Tsed	Volc. derived seds, lithic crystal tuffs
			6220	8050	1896	2454	558	Tmb	Miocene basalt: heavily fractured zones
			8050	8380	2454	2554	101	Tma	Miocene lake sediments
			8380	8588	2554	2618	63	Kgr	granodiorite
S.W.L. #3	9126	2782		6620		2018	2018	Tsed	tuffaceous sediments
			6620	7840	2018	2390	372	Tmb	Miocene basalt
			7840	8230	2390	2509	119	Tma	Miocene lake sediments
			8230	8450	2509	2576	67	Tvs	Oligocene silicic volcanics
			8450	8740	2576	2664	88	Jvh	Jz Humboldt igneous complex (upper)
			8740	8880	2664	2707	43		FAULT ZONE: mylonite
			8880	9126	2707	2782	75	Kgr	granodiorite

Well ID	T.D.		Rock Type Interval				Rock Type Thickness	Inferred Fm	Description
	feet	meters	start (ft)	end (ft)	start (m)	end (m)	(m)		
U.S.A. 52-18	9816	2992	5540	6340	1689	1932	244	Tsed	Basin fill sediments
			6340	7485	1932	2281	349	Tvs	Oligocene volcanic sequence (upper)
			7485	8210	2281	2502	221		Eocene sedimentary sequence
			8210	8640	2502	2633	131	Jvh	mixed meta-volc/sed. (Humboldt ?)
			8640	9750	2633	2972	338	Jvh	Jz lower volc. seq. (Jz-K)(Humboldt)
			9750	9816	2972	2992	20	Jgh	Jz intrusives (Humboldt igneous com.)
U.S.A. 45-5	8261	2518	2500	3800	762	1158	396	Tsed	Basin fill sediments
			3800	4460	1158	1359	201	Tsed	tuffaceous sediment and silicic tuffs
			4460	5330	1359	1625	265	Tvs	Tuff
			5330	6100	1625	1859	235	Jvh	Basalt
			5950	6170	1814	1881	67		Fault Zone (mylonitized)
			6100	?	1859	?		Tr	Carbonaceous shales
U.S.A. 62-21	12500	3810	5000	7030	1524	2143	619	Tsed	Basin fill sediments
			7030	8450	2143	2576	433	Jgh	Hornfels sediments and meta-gabbro
			8450	8460	2576	2579	3		Fault or shear zone
			8460	9730	2579	2966	387	Jgh	Meta-seds(argill. siltstone),meta-gabbro
			9730	10280	2966	3133	168	Tr	Meta-seds (argill dolomite to dolo LS)
			10280	12500	3133	3810	677	Tr	Argillaceous Shale
U.S.A. 65-18	9305	2836	3700	5250	1128	1600	472	Tsed	Basin fill sediments
			5250	5740	1600	1750	149	Tsed	Tuffaceous sediments
			5740	7300	1750	2225	475	Tmb	Basalt
			7300	7650	2225	2332	107		Intercalated micro-gabbro/vol.-clastics
			7650	8135	2332	2480	148	Tma	Siltstone and shale
			8135	8220	2480	2505	26		Mylonitized Fault Zone
			8220	9270	2505	2825	320	Jvh	Basalt
			9270	9305	2825	2836	11		Fault Zone(mylonite/microbrecc bslt)
U.S.A. 84-7	8142	2482	5500	5970	1676	1820	143	Tsed	Basin fill sediments
			5970	6770	1820	2063	244	Tsed	Tuff and overlying tuffaceous sediment
			6770	7400	2063	2256	192	Tmb	Mafic Lava
			7440		2268				Fault? Loss of circulation
			7470	7710	2277	2350	73	Tma	Argillaceous Shale
			7710		2350				Fault
			7710	8130	2350	2478	128	Trs	Meta-arnaceous sediments
			8142		2482				Fault? Loss of circulation

Nevada Bureau of Mines and Geology (NBMG) Lithology Summary for Dixie Valley Wells

LEGEND FOR GENERALIZED FORMATIONS

Fm	Description
Tsed	Basin-fill sediments and lowermost tuffaceous sediments and tuffs
Tmb	Miocene basalt flows
Tma	Miocene lake sediments
Tvs	Oligocene silicic volcanics (tuffs, volcaniclastics, underlying sediments
Kgr	Cretaceous granodiorite (intrusive)
Jhg	Jurassic mafic rocks (Humboldt igneous group)
Jbrq	Jurassic sediments (Boyer Ranch quartzite)
Trs	Triassic meta-sediments

Well	Total Depth		Rock Type Interval				Lithology	Inferred Fm	Correlation to Sunoco Logs
	ft	m	start (ft)	end (ft)	start (m)	end (m)			Yes/No
65-18	9466	2885	0	5250	0	1600	Sand/gravel/clays	Tsed	Yes
			5250	5750	1600	1753	Tuffaceous sediments	Tsed	
			5750	7660	1753	2335	Mafic volcanics	Tmb	
			7660	8230	2335	2509	Siltstone/shales	Tma	
			8230	9466	2509	2885	Metavolcanics	Jhg	
62-21	12500	3810	0	900	0	274	Tuffaceous sediments	Tsed	No
			900	3500	274	1067	Jurassic oceanic crust	Jhg	
			3500		1067		Triassic marine sediments	Trs	
82-5	9942	3030	0	5450	0	1661	Alluvium	Tsed	N/A
			5450	5500	1661	1676	Tuff	Tsed	
			5500	5630	1676	1716	Siltstone	Tsed	
			5630	6040	1716	1841	Sandstone/conglomerate	Tsed	
			6040	7510	1841	2289	Andesite	Tmb	
			7510	8060	2289	2457	Tuff	Tvs	
			8060	8150	2457	2484	Siltstone		
			8150	8200	2484	2499	Tuff	Tvs	
			8200	9250	2499	2819	Sandstone/siltstone		
			9250	9450	2819	2880	Tuff	Tvs	
			9450	9500	2880	2896	Diorite	Tvs or Jhg	
			9500	9570	2896	2917	Sandstone/siltstone		
			9570	9690	2917	2954	Meta-ultramafic	Jhg	
			9690	9942	2954	3030	Granite	Kgr	

Well	Total Depth		Rock Type Interval				Lithology	Inferred Fm	Correlation to Sunoco Logs
	ft	m	start (ft)	end (ft)	start (m)	end (m)			Yes/No
28-33	9507	2898	0	5740	0	1750		Tsed	N/A
			5740	6080	1750	1853	Tuff	Tsed	
			6080	6120	1853	1865	Basalt	Tmb	
			6120	6310	1865	1923	Tuff		
			6310	7300	1923	2225	Basalt	Tmb	
			7300	8650	2225	2637	Tuff	Tvs	
			8650	9060	2637	2761	Albitite	Jhg	
			9060	9507	2761	2898	Quartzite	Jbrq	
52-18	9860	3005	0	4775	0	1455	Alluvium	Tsed	No
			4775	5020	1455	1530	Basalt	Tmb	
			5020	5330	1530	1625	Volcanic sediments	Tma/Tvs	
			5330	5700	1625	1737	Rhyolite	Tvs	
			5700	5850	1737	1783	Granite	Tvs	
			5850	7300	1783	2225	Meta-igneous complex	Jhg	
			7300	7380	2225	2249	Diabase basalt	Jhg	
			7380	7515	2249	2291	Granite	Kgr	
			7515	7670	2291	2338	Diabase	Jhg	
			7670	8040	2338	2451	Granite	Kgr	
			8040	8265	2451	2519	Basalt intrusive	Jhg	
			8265	9860	2519	3005	Granite??	Kgr	
76-7	7926	2416	0	6140	0	1871	Valley fill	Tsed	N/A
			6140	7120	1871	2170	Tuffaceous sediments	Tsed	
			7120	7926	2170	2416	Basalt	Tmb	
82-7	9838	2999	0	5690	0	1734	Alluvium	Tsed	N/A
			5690	5810	1734	1771	Lithic Tuff	Tsed	
			5810	6030	1771	1838	Alluvium	Tsed	
			6030	6600	1838	2012	Lithic Tuff	Tsed	
			6600	7620	2012	2323	Basalt	Tmb	
			7620	7640	2323	2329	Siltstone	Tma	
			7640	7760	2329	2365	Tuff	Tvs	
			7760	7800	2365	2377	Albitite	Jhg	
			7800	7900	2377	2408	Fault gouge		
			7900	9838	2408	2999	Albitite	Jhg	

Well	Total Depth		Rock Type Interval				Lithology	Inferred Fm	Correlation to Sunoco Logs
	ft	m	start (ft)	end (ft)	start (m)	end (m)			Yes/No
84-7	8139	2481	0	6000	0	1829	Valley Fill	Tsed	Yes
			6000	6785	1829	2068	Tuff and Tuffaceous sed.	Tsed	
			6785	7450	2068	2271	Andesite and basalt lava	Tmb	
			7450	7700	2271	2347	Shale	Tma	
			7700	8139	2347	2481	Metasediments and hornfels	Trs	
73-7	8890	2710	0	6120	0	1865	alluvium	Tsed	N/A
			6120	7120	1865	2170	Tuff and tuffaceous sed.	Tsed	
			7120	7590	2170	2313	Basalt	Tmb	
			7590	8433	2313	2570	Miocene sediments	Tma	
			8433	8668	2570	2642	Silicic tuff	Tvs	
			8668	8890	2642	2710	Humboldt Lopolith	Jhg	
SWL-2B	8901	2713	0	4000	0	1219	Sand, gravel	Tsed	Yes
			4000	5150	1219	1570	Volcaniclastic sediments	Tsed	
			5150	5500	1570	1676	Basal conglomerate	Tsed	
			5500		1676		Volc. flows, volcanic sed	Tmb?	
32-18	7461	2274	0	3480	0	1061	Alluvium	Tsed	N/A
			3480	5950	1061	1814	Valley fill conglomerate	Tsed	
			5950	6570	1814	2003	Tuffaceous sediments	Tsed	
			6570	7461	2003	2274	Basalt	Tmb	
76-28	10419	3176	0	5440	0	1658	Alluvium	Tsed	N/A
			5440	5500	1658	1676	Basalt	Tmb	
			5500	5820	1676	1774	Sandstone/conglomerate		
			5820	5920	1774	1804	Mylonite	FZ	
			5920	6100	1804	1859	Microdiorite/granodiorite	Kgr	
			6100	6940	1859	2115	Microdiorite	Kgr	
			6940	8070	2115	2460	Siltstone/sandstone		
			8070	9390	2460	2862	Argillite/shale/carbonate	Trs	
			9390	9780	2862	2981	Metasediments	Trs	
			9780	10419	2981	3176	Diorite	Kgr or Trs	
45-5	9118	2779	0	4390	0	1338	Alluvium	Tsed	Yes
			4390	5330	1338	1625	Tuffaceous sediments	Tsed	
			5330	6500	1625	1981	Tertiary basalt	Tmb	
			6500	7130	1981	2173	Miocene sediments	Tma	No
			7130	9118	2173	2779	Granite	Kgr	

Well	Total Depth		Rock Type Interval				Lithology	Inferred Fm	Correlation to Sunoco Logs
	ft	m	start (ft)	end (ft)	start (m)	end (m)			Yes/No
45-14	9022	2750	0	700	0	213	Alluvium	Tsed	N/A
			700	840	213	256	Tuff/andesite	Tsed	
			840	1100	256	335	Alluvium	Tsed	
			1100	1410	335	430	Tuff/siltstone	Tsed	
			1410	1650	430	503	Andesite	Tvs	
			1650	1860	503	567	Tuff	Tvs	
			1860	2180	567	664	Andesite/basalt	Tvs	
			2180	2500	664	762	Tuff	Tvs	
			2500	3740	762	1140	Siltstone		
			3740		1140		Shale/siltstone/gabroic dikes	Trs	
74(85)-7	8890	2710	0	3490	0	1064			N/A
			3490	4960	1064	1512	Alluvium	Tsed	
			4960	5210	1512	1588	Tuff	Tsed	
			5210	6380	1588	1945	Volcanic breccia		
			6380	6560	1945	1999	Mudstone	Tsed	
			6560	7110	1999	2167	Tuff	Tsed	
			7110	7410	2167	2259	Basalt	Tmb	
			7410	7610	2259	2320	Volcanic sediments	Tmb	
			7610	8300	2320	2530	Siltstone/sandstone	Tma	
			8300	8500	2530	2591	Volcaniclastics	Jhg	
			8500	8550	2591	2606	Metabasalt	Jhg	
			8550	8700	2606	2652	Metavolcaniclastics	Jhg	
			8700	8890	2652	2710	Anorthosite	Jhg	

APPENDIX 10

PROJECT AREA WELLFIELD LITHOLOGY WELLFIELD DATA GENERALIZED INTO SIX STRATIGRAPHIC UNITS

Wellfield Lithology 6-Layer Model

The table presents the stratigraphic divisions as defined by depth from surface(in meters).

Wells	Generalized Formations					
	Tbf	Tmb	Tvs	Kgr	Jz ign.	Jz-Tr meta-seds.
65-18	0-1753	1753-2335	2335-2509		2509-2885	
32-18	0-2003	2003-2274				
52-18	0-1932		1932-2502		2502-2992	
SWL-3	0-2018	2018-2390	2390-2576	2707-2782	2576-2664	
SWL-2	0-1951	1951-2256		2256-2713		
SWL-2B	0-1896	1896-2454	2454-2554	2554-2618		
SWL-1	0-1692	1692-2211				
62-21	0-2143				2143-2966	2966-3810
45-14	0-335		335-792			792-2774
66-21	0-1250		1250-1585	1585-2455		2455-2889
38-32	0-450				777-1006	450-777[1]; 1113-1168
76-28	0-1658	1658-1676	1676-1774	2981-3176	1774-2115	2115-2981
82-5	0-1841	1841-2289	2289-2917	2954-3030	2917-2954	
45-5	0-1625	1625-1981	1981-2173	2173-2779		
28-33	0-1853	1853-2225	2225-2637		2637-2761	2761-2898[1]
37-33	0-1759	1759-2158	2158-2524	2718-2758	2524-2646	2646-2718[1]
45-33	0-2737				2737-2926	2926-3124[1]
76-7	0-2170	2170-2416				
82-7	0-2012	2012-2323	2323-2365		2365-2999	
84-7	0-2068	2068-2347	2347-2481			
73-7	0-2170	2170-2313	2313-2642		2642-2710	
74-7	0-2167	2167-2320	2320-2530		2530-2710	

[1] Jurassic Boyer Ranch Quartzite footnoted because of its significance relative to EGS favorability (

Legend

Tbf:	Basin-fill sediments including the lowermost tuffaceous sediments
Tmb:	Miocene basalt
Tvs:	Oligocene silicic volcanics including the overlying Miocene lacustrine section and underlying sediments
Kgr:	Cretaceous granodiorite
Jz ign.:	Jurassic mafic igneous rocks (Humboldt igneous complex)
Jz-Tr meta-seds.:	Triassic meta-sediments and Jurassic Boyer Ranch quartzite

APPENDIX 11

TEMPERATURE GRADIENT HOLE (TGH) AND WELL TEMPERATURE DATA

Temperature Gradient Hole (TGH) and well temperature data derived from the SMU geothermal database and Blackwell et al. (2005)

Well	Depth	Temperature
	meters	°C
65-18	228.6	35.0
	2555.1	218.3
62-21	0.0	16.0
	3025.0	175.0
	3657.6	184.0
82-5	2842.0	223.4
25-5	1873.9	205.3
	1894.3	206.1
45-33	304.8	33.9
	2295.1	188.3
	3018.0	251.2
52-18	228.6	34.4
	2928.5	233.3
76-7	2261.6	204.4
27-33	228.6	36.7
	2762.1	245.6
63-7	30.5	76.7
	2721.9	200.6
	2902.0	243.0
82-7	2998.6	212.8
84-7	198.1	37.8
	2529.8	246.7
SWL-2	228.6	37.8
	2414.0	210.6
SWL-3	182.9	23.9
	2484.1	215.6
SWL-1	228.6	37.8
	2164.1	222.2
32-18	228.6	38.3
	2144.3	208.9
	2274.1	228.9
66-21	228.6	62.2
	2825.5	217.2
	2973.0	218.0
36-14	3050.0	285.0
	3551.0	283.7
76-28	152.4	57.2
	2350.0	162.0
	3169.0	175.0
45-5	225.6	61.1
	2438.4	212.2
45-14	2750.0	196.0

TGH	Depth	Temperature
	meters	°C
H-2	457.0	51.2
SR1-A	455.0	96.2
H-1	457.0	97.0
SR-2A	434.3	91.5
SR-3	457.2	92.4
SR-4	457.2	55.5
DD-9	438.9	84.4
H-1	457.2	97.3
H-2	457.2	51.2
DV-401	616.0	58.9
EDV-1	430.0	63.0
EDV-2	304.0	54.4
EDV-3	433.0	61.1
SR-3	0.0	23.9
	396.2	87.8
	457.0	91.2
74-7	228.6	46.1
	2704.0	249.6
82-5	2600.0	226.0
38-32	1100.0	201.0
53-15	1200.0	150.0
62-23	2900.0	250.0
62A-23	3475.0	267.0

APPENDIX 12

DIXIE VALLEY WELLFIELD CROSS-SECTIONS WITH ASSUMPTIONS

Table of Contents

Dixie Valley Baseline Conceptual Geothermal Model

Wellfield Cross-Sections

Introduction

Nine cross-sections have been constructed through the Dixie Valley wellfield (Figure 1). Six of the nine cross-sections, specifically A-A' through F-F', were quantitatively analyzed using various geostatistical methods, while all the sections were used for qualitative analysis, creation of the baseline conceptual model, and application for EGS favorability mapping. Information within the cross-sections utilize well data as the main control points including the known lithology and thermal data. Other factors taken into account were the surface geology, gravity and magnetic surveys (to infer depth to the basement, basin profile, and intrabasin faults), and seismic profiles (to infer faulting, depth of basin sediments, and depth to prominent reflectors). The Smith and Blackwell (2001) structure map (Figure 2) provided a template for inferring significant intrabasin faults and a Dixie Valley geophysical basement configuration model was used to constrain the depth of basin-filling sediments (Figure 3). Generic cross-sections provided by Blackwell were weighed heavily into these sections (see main body of text and Figures 4a and 4b). Detailed cross-sectional figures from Gabe Plank's work at the University of Nevada Reno held by the Great Basin Geothermal Center were also incorporated (2002 Dixie Valley Geothermal workshop).

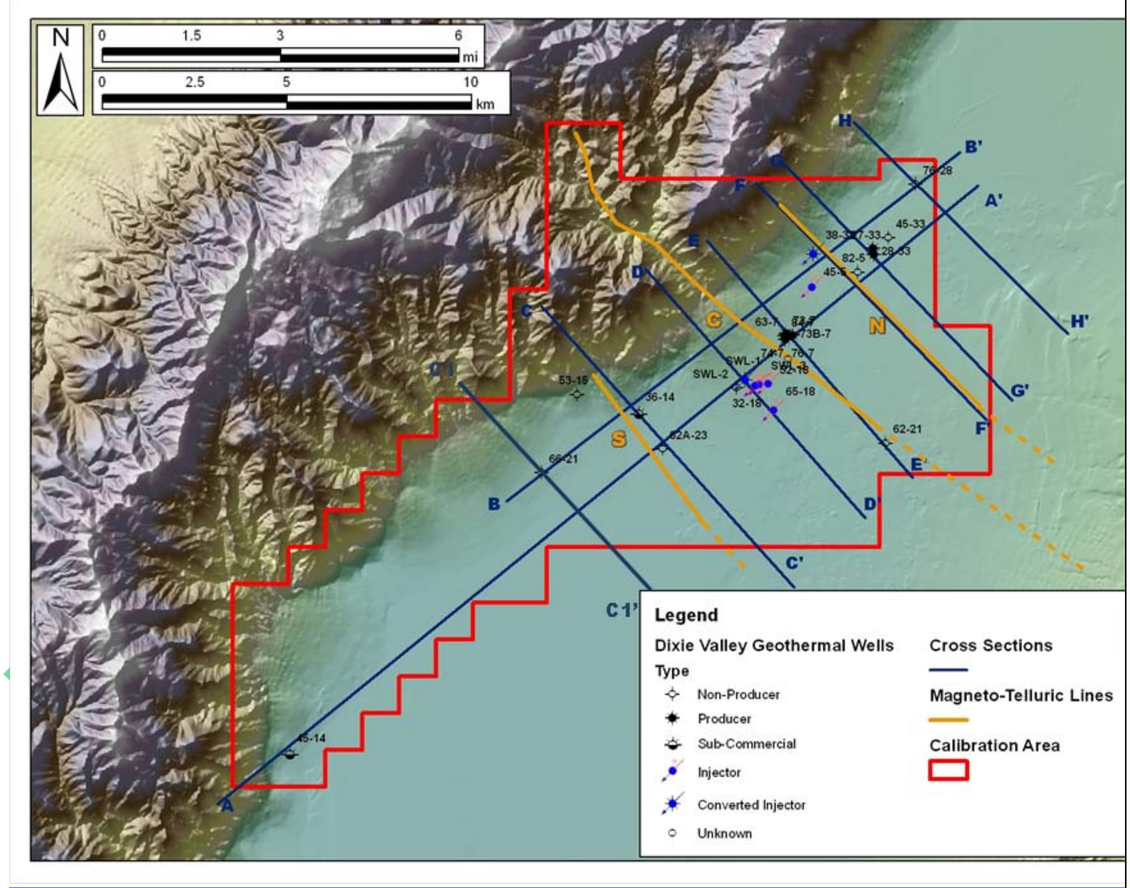

Figure 1. Index map for Dixie Valley with the nine cross-section line locations used in this report. Map produced by Matthew Clyne using GIS.

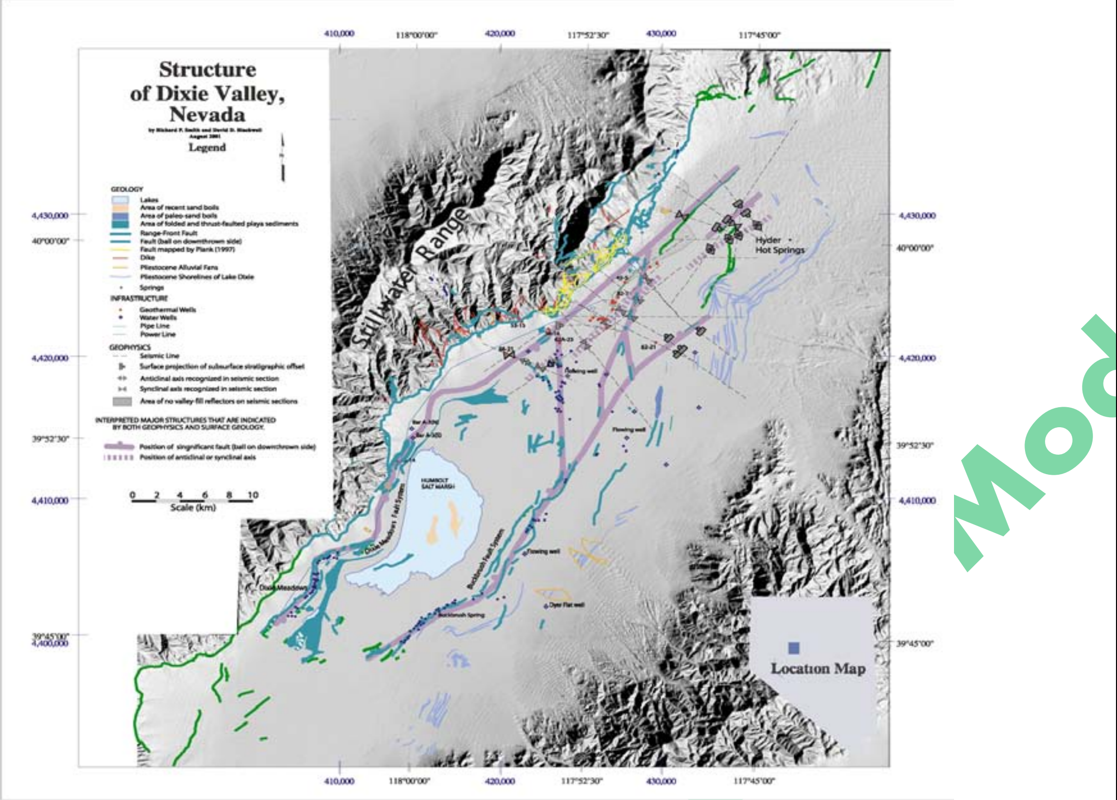

Figure 2. Structure of Dixie Valley from Smith and Blackwell (2001); thick purple lines indicate the positions of intepreted major intrabasin faults based on geophysical data and surface geology.

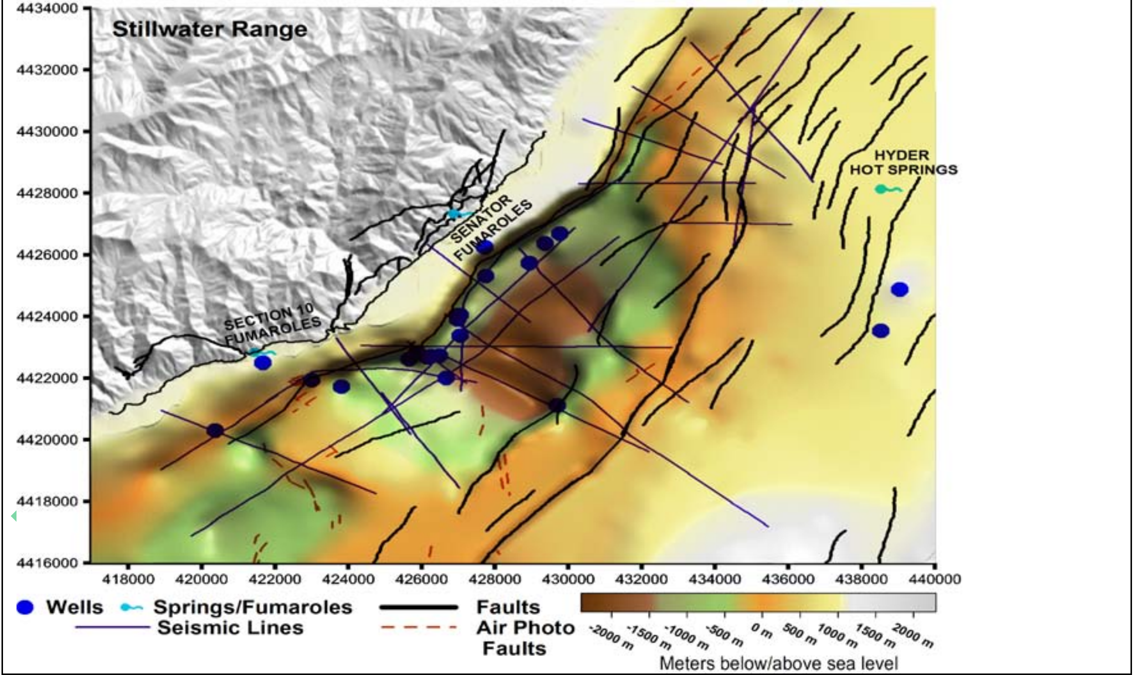

Figure 3. Dixie Valley basement configuration with valley fill removed based on seismic and well data using fault lines to limit contours; from Blackwell et al. (2005).

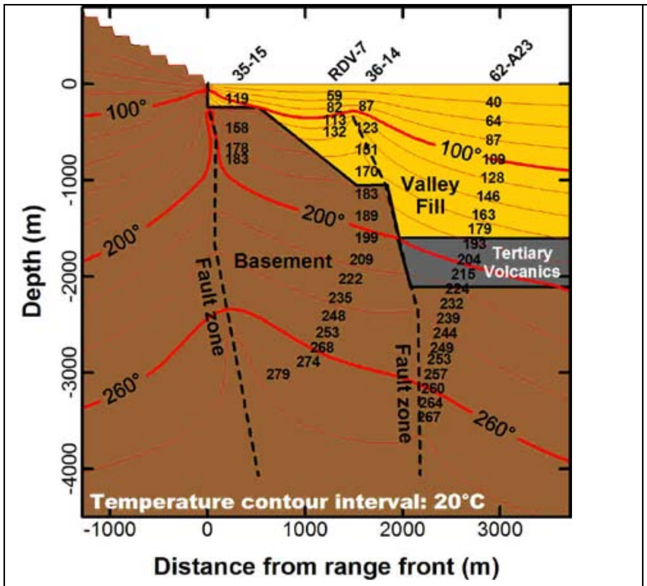

Figure 4A. Thermal model for the DVPP area based on temperature matching in the deep wells (Blackwell et al., 2000).

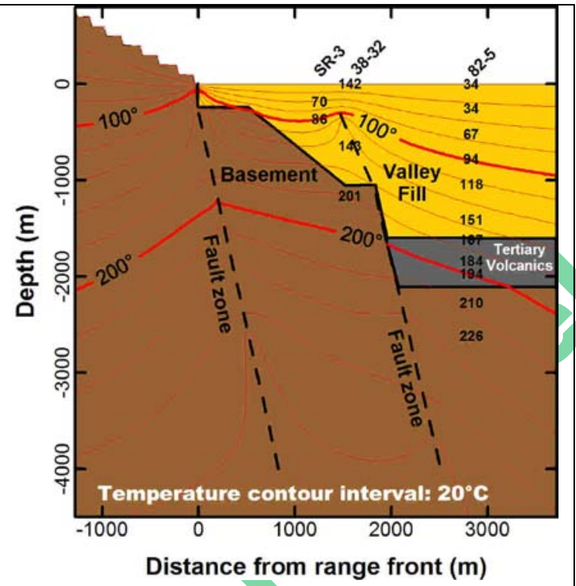

Figure 4B. Thermal model for the DVPF in section 32/33 based on temperature matching in the deep wells (Blackwell et al., 2000).

Well elevation, total depth, and lithology were extracted from public domain geothermal well databases, proprietary logs provided by Al Waibel with the permission of Terra-Gen Corporation, University of Nevada Reno, and well data provided directly from Terra-Gen Corporation. Thermal data was extracted mostly from the SMU online geothermal database. Well temperature data was obtained from temperature-depth profiles provided in Blackwell et al. (2005). See appendix 10 for a generalized description of the available subsurface well lithology subdivided into six stratigraphic units as described in the main body of this report. The depths and intervals in this table represent the depths and formation thicknesses used in the cross-sections.

Primary Assumptions

- The cross sections have no vertical exaggeration and use a meter scale.
- The grid system overlain on the sections are composed of 500m by 500m cells used for qualitative and quantitative analysis.
- The intersection points of the six main wellfield cross sections are labeled at the surface.
- The sections have been divided into six stratigraphic units to be comparable to Blackwell's geologic model presented in the main body of the text:
    - Tbf: basin-filling sediments and lowermost tuffaceous sediments;
    - Tmb: Miocene basalt;
    - Tv or Tvs: Oligocene silicic volcanics, volcaniclastic and lacustrine sediments;
    - Jz igneous section: Jurassic mafic igneous rocks;
    - Jz-Tr section: Jurassic and Triassic meta-sediments; and
    - Kgr: Cretaceous granodiorite (crystalline basement).
- While the Jz Boyer Ranch quartzite has been incorporated into the Tr-Jz meta-sediments stratigraphic unit, it has proven difficult to lump these units. Where the quartzite could not be included in this unit, it has been divided out and labeled Jbr.

- The topographic profile was inferred from well elevations and topographic maps.
- The axis of a syncline within the basin-fill sediments is from seismic data with the approximate location taken from Smith and Blackwell's (2001) structure map.
- If there was no data or structural control on the range-front/piedmont faults, a 75° SE dip was assumed. All of the intra-basin faults are assumed to have a steep dip, while the N-trending geophysical-inferred faults identified in the valley are shown as vertical structures.
- Crystalline basement (Kgr) is assumed to underlie the entire area at some depth in an idealized model (see Figures 2 and 3 within the main report). Idealized contacts with question marks infer where this contact is. At times this contact represents the Dixie Valley fault and/or the piedmont fault, both of which comprise the Dixie Valley fault zone (DVFZ).

Section A-A'

- Well 62-A23 has no lithology data available, so the contact of the Tertiary volcanics was taken from Blackwell's generic thermal model (Figure 4A) where the depth interval is approximately 1.6-2.1 km.
- A basement high was imaged in the seismic data north of 62-A23.
- The piedmont fault is oblique to the cross section line and the offset is unknown.
- The N-trending segment of the range-bounding fault that intersects the cross section near 45-14 must have a steep to near-vertical dip as the structure was not encountered by 45-14. In addition the NE-trending segment of the range-bounding fault at this location (near Dixie Meadows) and to the south have shallow interpreted dips of ~35° SE at Dixie Meadows and 25-30° SE ~ 10 km south of Dixie Meadows based on seismic studies. It is unknown how this interpreted low angle segment connects with the overall steep nature of the fault zone near the producing field.
- The range-bounding fault encountered in this cross section likely inherits an early NS oriented normal fault that has been re-activated in the current extensional phase. This fault segment appears to have an apparent strike-slip sensed motion.
- Similar strike to seismic line 101/8: used to infer basement depth between wells.
- A significant NS oriented fault near well 62-A23 could not be projected at depth as the dip and offset is unknown. This orientation would likely have a strike-slip component in the current stress regime and laterally offsets a syncline axis within the basin-fill sediments.
- The stratigraphy between 45-14 and 62-A23 is unknown and largely inferred.

Section B-B'

- Cross section images the stranded block between the range-bounding and piedmont fault.
- The section runs parallel to these structures and crosses the piedmont fault at a low angle. The exact offset at this intersection is interpreted with an assumed steep apparent dip.
- Within section 33: temperature extracted from 45-33 while the lithology used is from 28-33.
- Basement depth between wells inferred using seismic lines SRC-1, SRC-1N, and 9.
- Well 36-14 did not intersect the Tertiary volcanics but instead encountered basement at ~1 km.
- The range-bounding fault at some depth should be intersected by this section line as shown.

- The stratigraphy of 66-21 is known while 36-14 is inferred from Blackwell's idealized cross-sections.

Section C1-C1'

- Assumes multiple faults comprise the DVFZ in the area SW of the DVPP.
- Dextral strike-slip component on north-trending fault (Blackwell and Smith, 2001).
- Depth of basin-fill derived from geophysical data (Figure 3).
- NW-dipping antithetic faults in the valley imaged by seismic and magnetic data.

Section C-C'

- Wells 36-14 and 62-A23 are deviated towards the range-front at an unknown angle.
- Easternmost antithetic fault imaged by seismic and magnetic data.
- Intrabasin faults (from Smith and Blackwell's 2001 map and shown in Figure 2) are projected within the section and shown as vertical structures as the dip directions are not largely constrained.
- Lithology and thermal data inferred from Blackwell's thermal cross-section (Figure 4A).
- Cross section runs at a slight angle to seismic line 10/105.
- N-trending intrabasin fault is interpreted to be truncated by the piedmont fault near 62-23.

Section D-D'

- Sunoco mud logs provide evidence for a fault zone at 2.25km and 2.43-2.46 km in SWL-2.
- Antithetic fault derived from Plank's cross section and fault zones encountered by drilling.
- Surface intrabasin faults derived from Smith and Blackwell's 2001 map (Figure 2).
- Major intrabasin fault near 62-21 is derived from seismic and geophysics.

Section E-E'

- Basement inferred from seismic line 6.
- Section extends through the deepest part of basin (early NS oriented graben).
- Antithetic fault in producing zone: fault zone logged in section 7 wells.

Section F-F'

- 38-32: stranded shallow block between main strands of the DVFZ.
- 38-32: brecciated fault zone at a depth of ~1006-1113 meters assumed to be main range front (Johnson and Hulen, 2002) is interpreted as a more north-striking subsidiary strand of the DVFZ.
- 82-5: bottom of well intersects piedmont fault and the footwall block consisting of Kgr.
- 45-5: This well lies off of the cross section plane so the stratigraphy was not used.
- Major intrabasin fault (from Figure 2) intersects the cross section near the piedmont fault.
- Inferences from seismic line SRC-3 and 102.

Section G-G'

- Jurassic rocks thin (pinch-out) north of the producing field as evidenced by well data, geologic mapping of the Fencemaker and Boyer Thrusts (labeled BT on cross-section), reduced magnetic signature, general map of the Jurassic Lopolith by Wallace and Whitney (1985).

- The schematic of the Jurassic mafic rocks and the Boyer Ranch quartzite in the block between the range-front and piedmont fault is interpretive, but consistent with the lithology from 38-32.

- Producing wells 37-33 and 28-33 intersect the fractured Jurassic rocks in the hanging wall block of the piedmont fault.

- Inferences from seismic reflection line SRC-3 for basement depth in valley.

- Westward dipping faulting bounding the eastern segment of Dixie Valley is derived from the magnetic-gradient and seismic inferred faults (Figure 3).

Section H-H'

- Major displacement along the piedmont fault is distributed along several faults as evidenced by the surface faulting, geophysical-inferred faulting, and proprietary seismic reflection data provided by Terra-Gen Corp.

- Well 76-28 is a dry, relatively cold well, that doesn't intersect the major piedmont fault.

- Inferences for basement depth and intra-valley faulting derived from proprietary seismic reflection data provided by Terra-Gen Corp.

- Miocene basalt (Tmb) nearly pinches at this point north of the DVPF, as evidenced by lithology found in 76-28.

- The approximate position of the Fencemaker Thrust (FT) is labeled on the section.

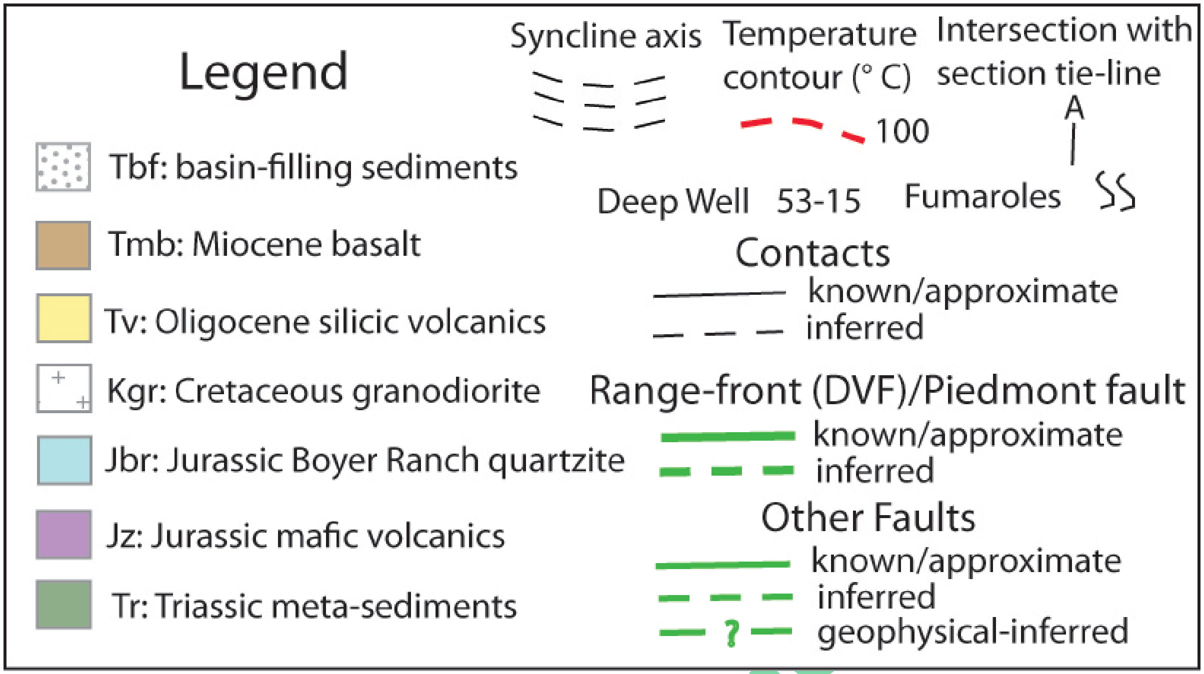
Legend
Tbf: basin-filling sediments
Tmb: Miocene basalt
Tv: Oligocene silicic volcanics
Kgr: Cretaceous granodiorite
Jbr: Jurassic Boyer Ranch quartzite
Jz: Jurassic mafic volcanics
Tr: Triassic meta-sediments
Syncline axis
Temperature contour (° C)
100
Intersection with section tie-line
A
Deep Well 53-15
Fumaroles
Contacts
known/approximate
inferred
Range-front (DVF)/Piedmont fault
known/approximate
inferred
Other Faults
known/approximate
inferred
?
geophysical-inferred

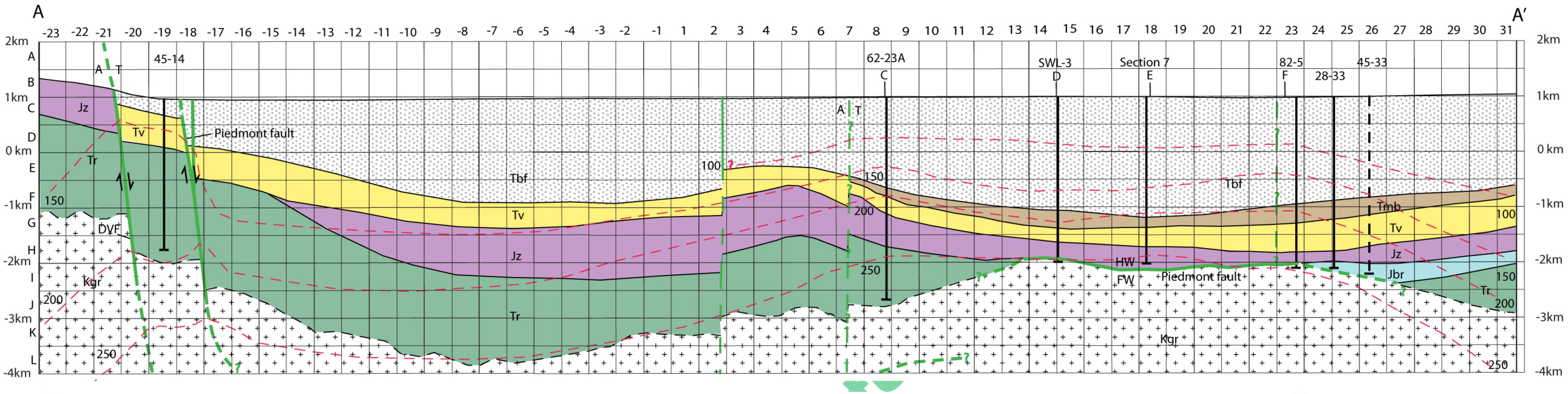
A
A′
2km
1km
0 km
-1km
-2km
-3km
-4km
A B C D E F G H I J K L
-23 -22 -21 -20 -19 -18 -17 -16 -15 -14 -13 -12 -11 -10 -9 -8 -7 -6 -5 -4 -3 -2 -1 1 2 3 4 5 6 7 8 9 10 11 12 13 14 15 16 17 18 19 20 21 22 23 24 25 26 27 28 29 30 31
45-14
62-23A
C
SWL-3
D
Section 7
E
82-5
F
28-33
45-33
A T
Jz
Tv
Tr
Piedmont fault
Tbf
Tmb
Jbr
DVF
Kgr
HW
FW
100
150
200
250

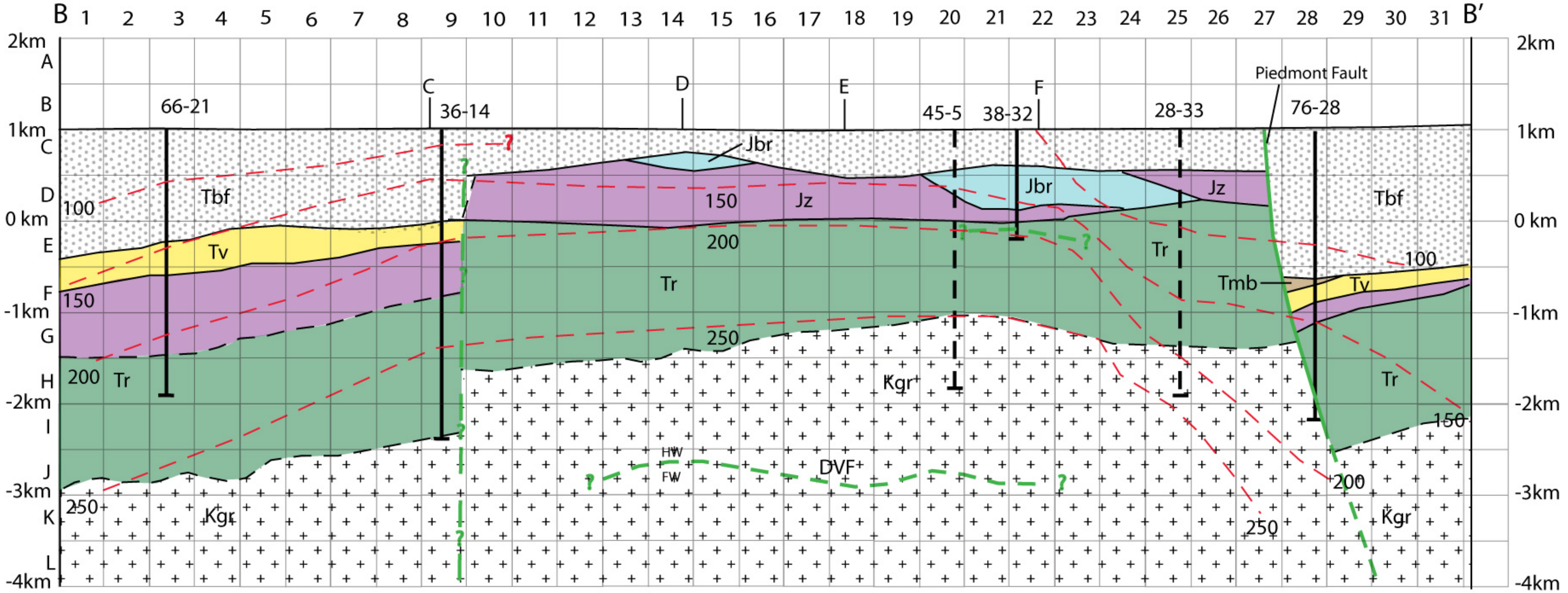
B
B′
1 2 3 4 5 6 7 8 9 10 11 12 13 14 15 16 17 18 19 20 21 22 23 24 25 26 27 28 29 30 31
2km
1km
0 km
-1km
-2km
-3km
-4km
A B C D E F G H I J K L
66-21
C
36-14
D
E
45-5
38-32
F
28-33
Piedmont Fault
76-28
Jbr
Jz
Tbf
Tv
Tr
Tmb
Kgr
DVF
HW
FW
100
150
200
250

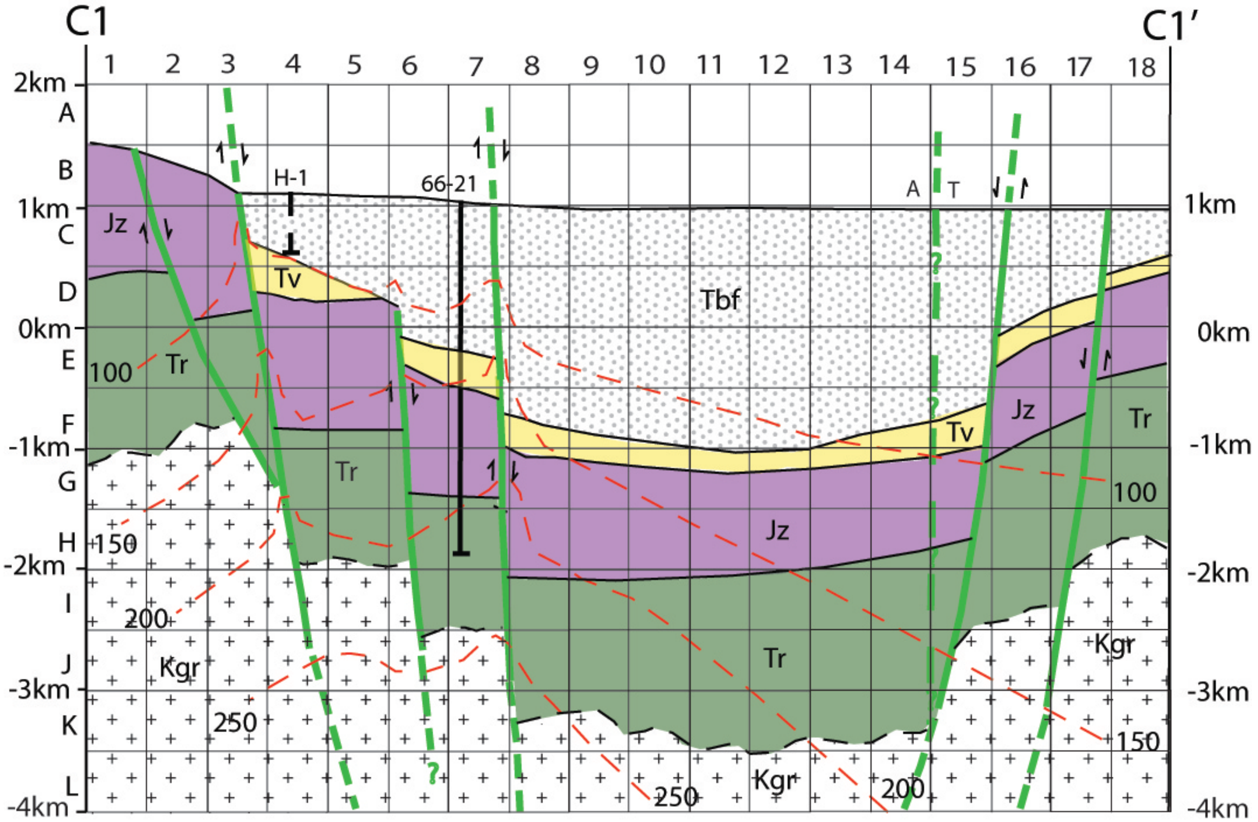
C1
C1′
1 2 3 4 5 6 7 8 9 10 11 12 13 14 15 16 17 18
2km
A
B
1km
C
D
0km
E
F
-1km
G
H
-2km
I
J
-3km
K
L
-4km
H-1
66-21
A
T
Jz
Tv
Tbf
Tr
Kgr
100
150
200
250
?

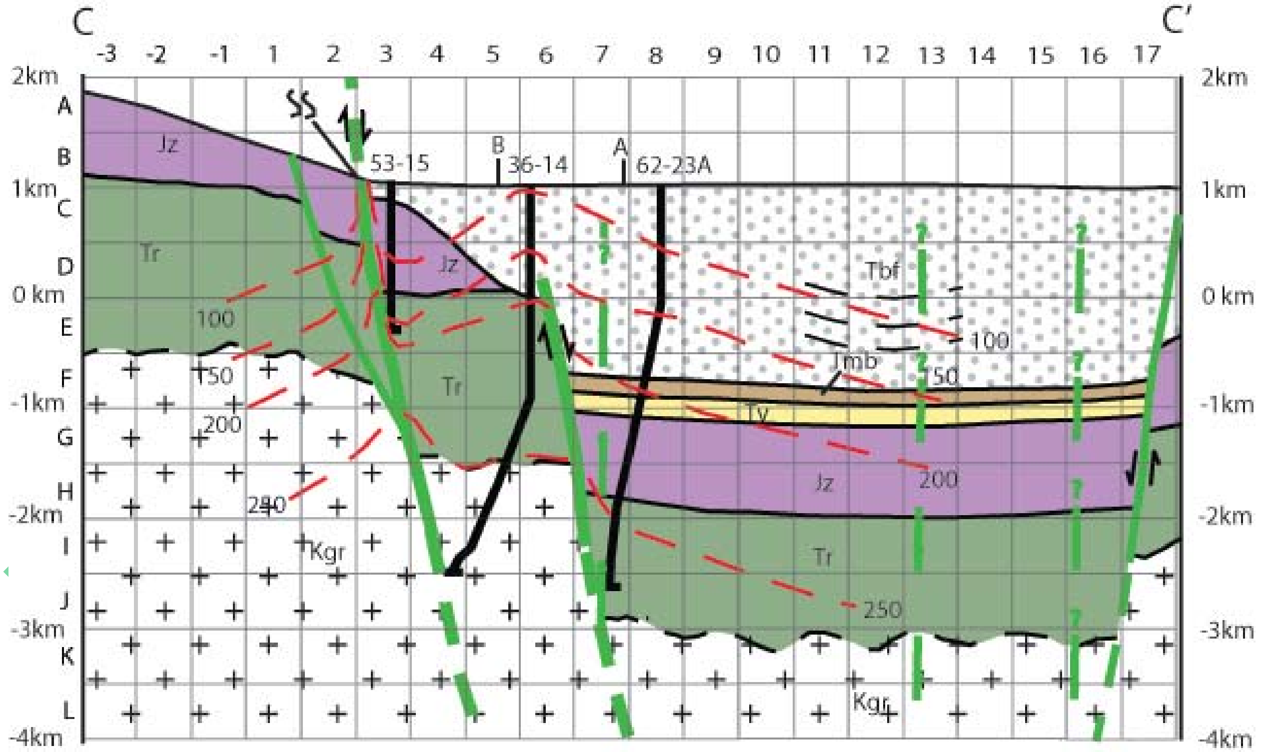
C
C′
-3 -2 -1 1 2 3 4 5 6 7 8 9 10 11 12 13 14 15 16 17
2km
A
B
1km
C
D
0 km
E
F
-1km
G
H
-2km
I
J
-3km
K
L
-4km
SS
53-15
B
36-14
A
62-23A
Jz
Tr
Tbf
Tmb
Tv
Kgr
100
150
200
250
?

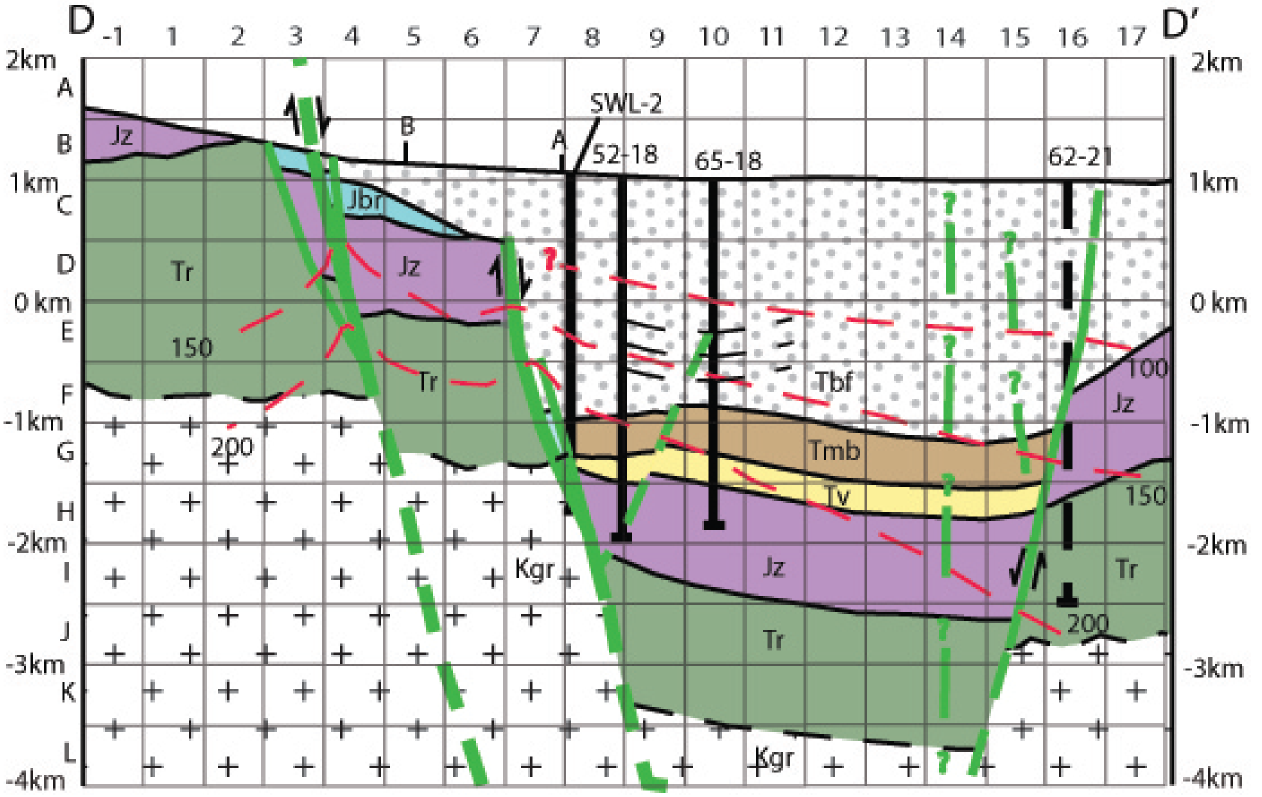
D
D′
-1
1
2
3
4
5
6
7
8
9
10
11
12
13
14
15
16
17
2km
1km
0 km
-1km
-2km
-3km
-4km
A
B
C
D
E
F
G
H
I
J
K
L
Jz
Jbr
Tr
150
200
Kgr
B
A
SWL-2
52-18
65-18
62-21
?
Tbf
Tmb
Tv
100
150
200

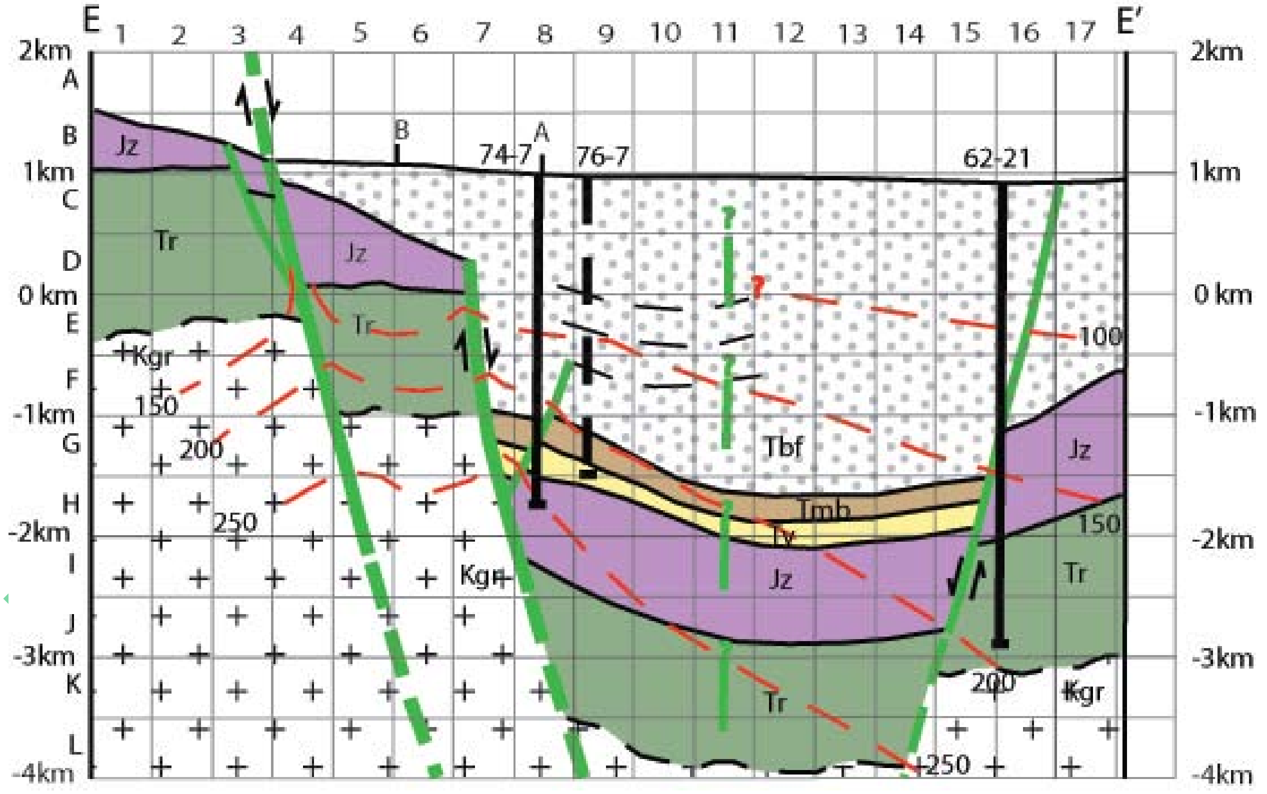
E
E′
1
2
3
4
5
6
7
8
9
10
11
12
13
14
15
16
17
2km
1km
0 km
-1km
-2km
-3km
-4km
A
B
C
D
E
F
G
H
I
J
K
L
Jz
Tr
Kgr
150
200
250
B
A
74-7
76-7
62-21
?
Tbf
Tmb
Tv
100
150
200
250

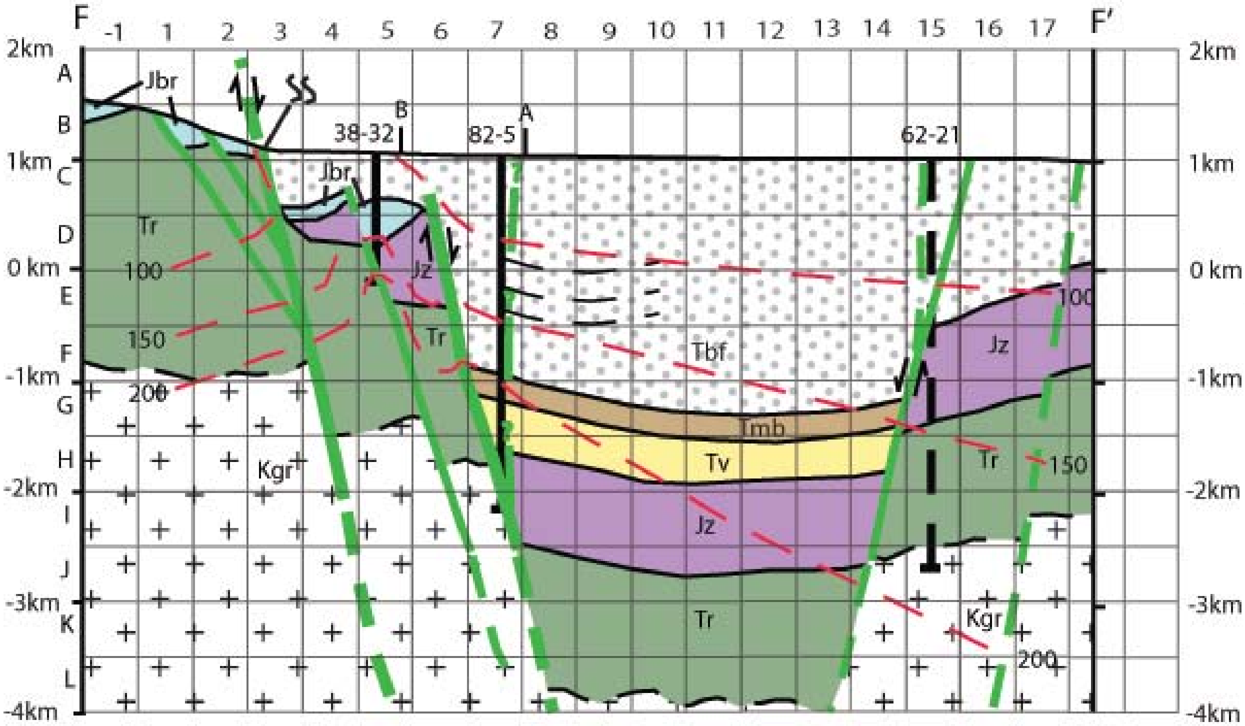
F
F′
-1 1 2 3 4 5 6 7 8 9 10 11 12 13 14 15 16 17
2km
1km
0 km
-1km
-2km
-3km
-4km
A
B
C
D
E
F
G
H
I
J
K
L
Jbr
SS
38-32
B
82-5
A
62-21
Tr
Jz
Tbf
Tmb
Tv
Kgr
100
150
200

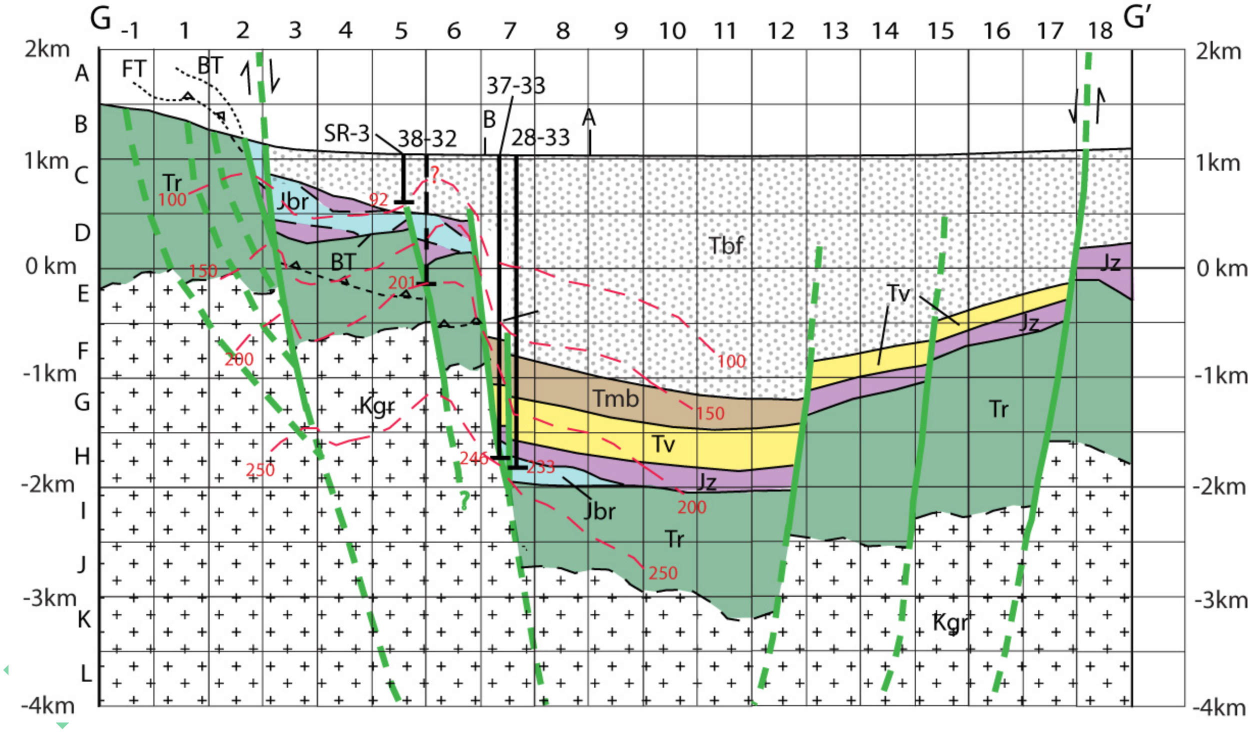
G
G′
-1 1 2 3 4 5 6 7 8 9 10 11 12 13 14 15 16 17 18
2km
1km
0 km
-1km
-2km
-3km
-4km
A
B
C
D
E
F
G
H
I
J
K
L
FT
BT
SR-3
38-32
37-33
B
28-33
A
Tr
Jbr
BT
Kgr
Tbf
Tmb
Tv
Jz
?
92
100
150
200
201
246
233
250

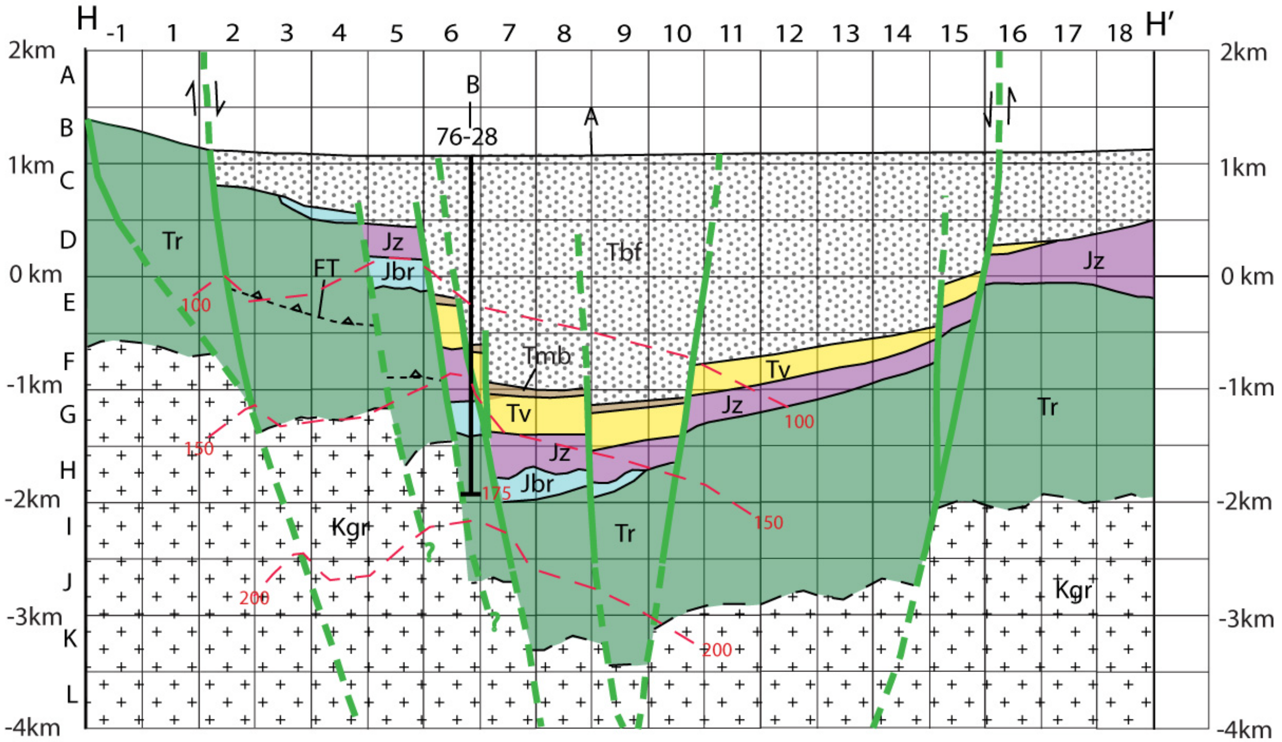
H
H′
-1
1
2
3
4
5
6
7
8
9
10
11
12
13
14
15
16
17
18
2km
1km
0 km
-1km
-2km
-3km
-4km
A
B
C
D
E
F
G
H
I
J
K
L
B
76-28
A
Tr
FT
Jz
Jbr
Tbf
Tmb
Tv
Jz
Jbr
Tv
Jz
Tr
Jz
Tr
Kgr
Kgr
100
100
150
150
175
200
200
?
?

APPENDIX 13

COULOMB 3.1 RE-INTERPRETED STRESS MODELING
IN DIXIE VALLEY, NEVADA

Table of Contents

List of Figures

List of Tables

Modeling fault-induced stress and strain near Dixie Valley Geothermal Field, NV

Authors: Maisie Nichols and Trenton Cladouhos, AltaRock Energy Inc.

Background

The Dixie Valley Geothermal Field (DVGF) sits within Dixie Valley, Nevada (Figure 1) located in the western Great Basin region of the extensional Basin and Range Province. The valley is bounded by normal faults that have produced several large earthquakes over the past ~3000 years, including the 2-2.5 ka "Gap" Earthquake along the Stillwater Gap Segment (SGS) of the Dixie Valley Fault (DVF), the 1915 Pleasant Valley Earthquake along the Pleasant Valley Fault (PVF), and 1954 Dixie Valley Earthquake along the southern section of the DVF. These earthquakes influence the stress and strain distribution throughout the region surrounding the DVGF.

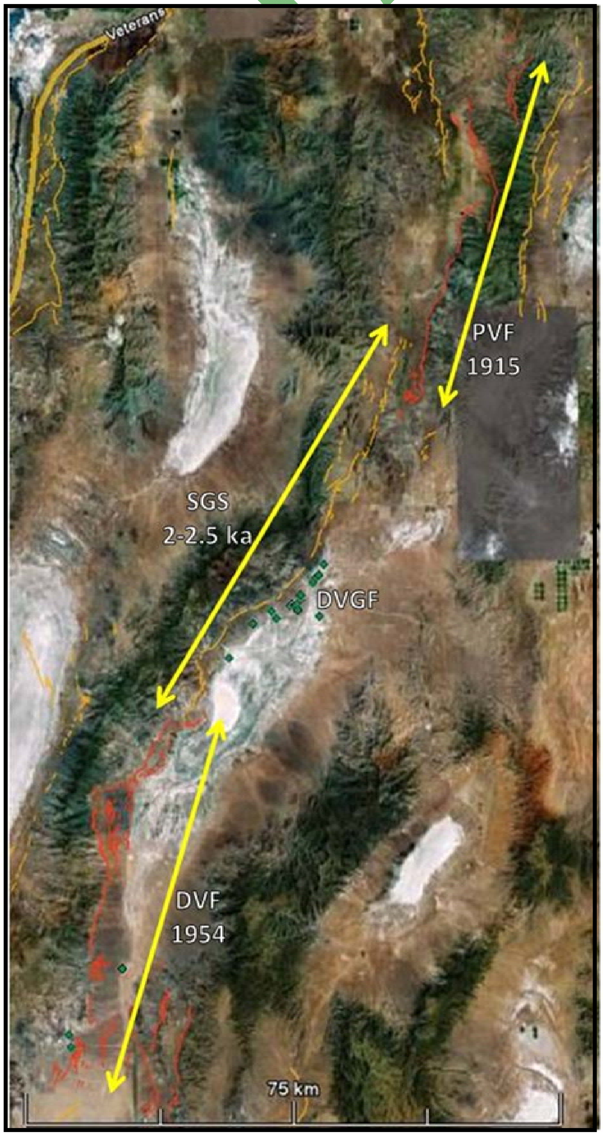

Figure 1 – Map of Dixie Valley region showing approximate location of DVGF (green dots are deep wells within DVGF) in relation to the PVF, SGS, and DVF fault traces (red and orange lines) provided by the USGS Quaternary Fault and Fold Database (QFFDB); see text for definition of the acronyms.

Coulomb 3.1

A numerical code called Coulomb 3.1 can calculate strain and Coulomb Stress Change (CSC) on a receiver fault (RF) due to slip on a source fault (SF) (Lin and Stein, 2004; Toda et al., 2005) in order to determine whether failure along the RF is promoted or inhibited. The first step in using this code is to create an input file containing the spatial boundaries and grid parameters of your model, as well as the appropriate fault parameters (including the starting and ending coordinates, top and bottom depths, dip, slip magnitude and direction) for both the seismogenic SFs and the passive RFs.

Coulomb assumes that a RF (with a specified strike, dip, and rake) exists within each grid cell, and then calculates and plots the strain or CSC value (as resolved onto the RF) at that location. As a result, the location of the RF given in input file does not influence the calculations, but is only used to display the fault on the map/cross section at a particular location of interest.

***Scenario 1** – Reproducing Model from Wesnousky et al. (2003)*

Wesnousky et al. (2003) modeled stress changes on a portion of the SGS as a result of slip on nearby Holocene faults. They represented the DVF as 2 sections and the SGS as 3 sections, but did not include the 1915 event. No evidence exists for a range-front scarp along the SGS section near DVGF, and therefore they suggested this central SGS section *did not rupture* during the "Gap" earthquake. Figure 2A illustrates the calculated change in CSC resolved onto the central SGS fault section (RF) due to slip on the DVF and the 2 other SGS segments (SFs). We use the slip amounts reported in Wesnounsky et al. (2003), and estimate the fault trace lengths and strikes using their Coulomb figure (Figure 2A). SF dips were not reported, so we assign them the same dip used for the RF (50°SE). Fault bottom depths were also not reported, so we assign a fault top and bottom depth of 0 km and 15 km, respectively, based the presence of surface ruptures and the observation that the seismogenic zone over most of the Basin and Range Province extends down to a depth of ~15 km (Smith, 1978). The input parameters used to create our reproduction (Figure 2B) of their figure are given in Table 1.

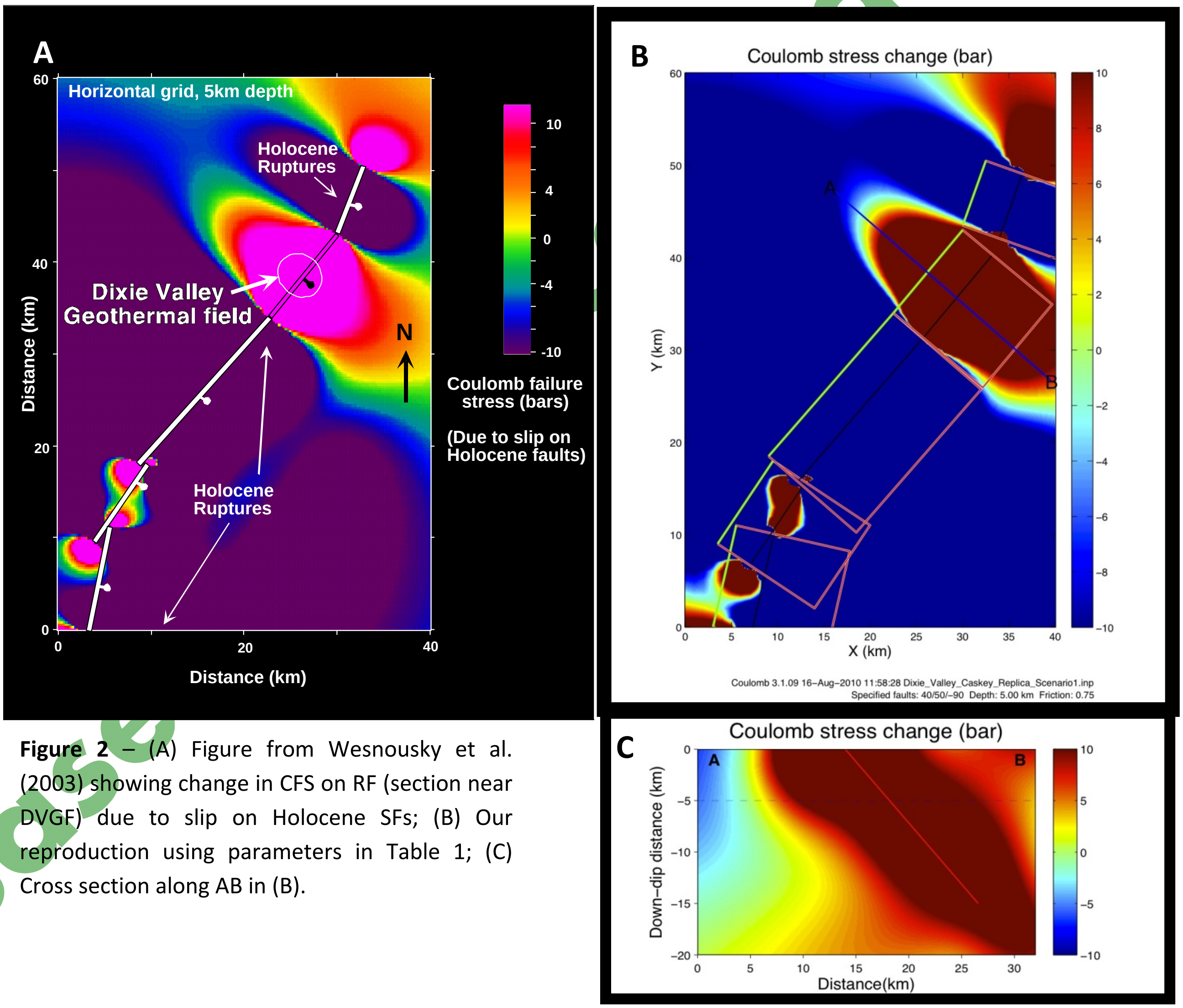

Figure 2 – (A) Figure from Wesnousky et al. (2003) showing change in CFS on RF (section near DVGF) due to slip on Holocene SFs; (B) Our reproduction using parameters in Table 1; (C) Cross section along AB in (B).

Table 1 – Input fault parameters for Scenario 1.

Fault	Segment (SF or RF)	Start x (km)	Start y (km)	End x (km)	End y (km)	Slip (m)	Dip (° SE)	Top (km)	Bottom (km)
SGS	North section (SF)	30	43.5	32.5	50.5	1.96	50	0	15
SGS	Middle section (RF)	22.5	34	30	43	0	50	0	15
SGS	South section (SF)	9	18.5	22.5	34	3.92	50	0	15
DVF	North section (SF)	3.5	9	9.5	18	2.21	50	0	15
DVF	South section (SF)	3	0	5.5	11	1.56	50	0	15

Scenario 1 Discussion

Assuming the middle SGS fault segment (RF) did not rupture 2-2.5 ka, figure 2 illustrates that failure (normal faulting) is promoted on the RF by slip resulting from Holocene ruptures, along with all other faults/cracks with the same orientation (strike, dip, rake) that fall within a region of positive CSC.

Hickman et al. (1998; 2000) suggest that the necessary conditions for high reservoir permeability are that both the local state of stress and orientation of the fault zone be such that the fault is critically stressed for frictional failure (i.e., Sh_{min} is both low and perpendicular to fault). This conclusion is based on stress orientations and magnitudes measured from well-bores (Hickman et al., 1998; 2000; see Table 2) that indicate the fault zone near producing wells of DVGF (73B-7 and 74-7) is critically stressed for normal failure, while the zone near non-producing wells (66-21 and 45-14) is not critically stressed for failure. This is consistent with CSC shown in Figure 2 because productive and non-productive wells fall within zones of positive (failure promoted) and negative (failure inhibited) CSC, respectively (Figure 3).

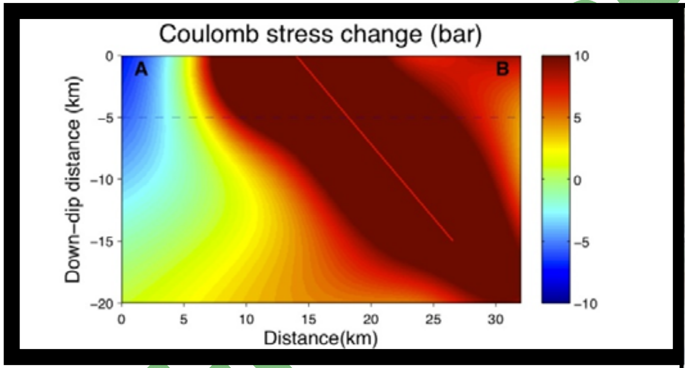

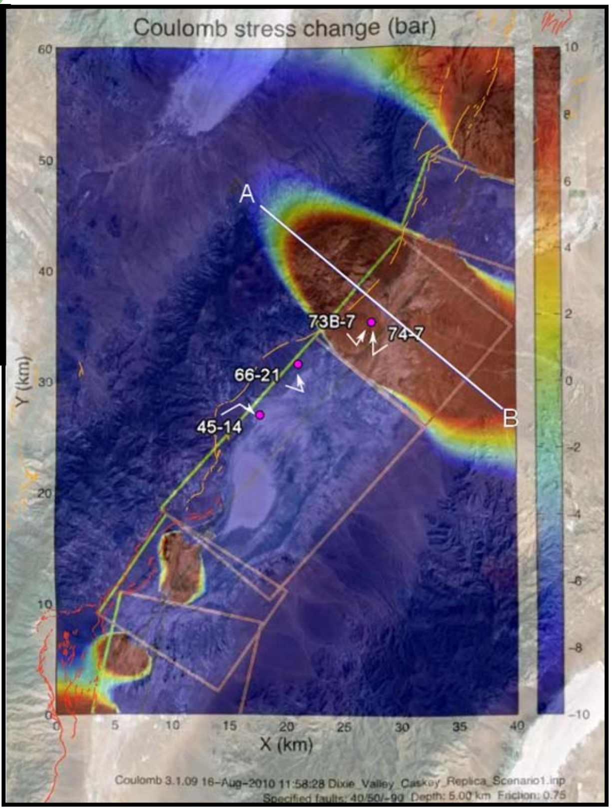

Figure 3 – Overlay of Figure 2B on Google Earth image showing QFFDB fault traces and locations of wells (green dots) mentioned above. Note that wells 74-7 and 73B-7 are close enough to one another (~220 meters) that their locations overlap on a map of this scale.

Table 2 – Information from deep wells penetrating the fault zone at 2-3 km depth. Red and blue indicate critically stressed and not critically stressed well sites (Hickman et al., 1998; 2000).

Well	Sh_{min}	Sh_{min}/Sv	Productive	Interpretation	Scenario 1
73B-7	N57W±10	0.45-0.62 @ 0.4-2.5 km	Y	SFZ optimally oriented and Shmin low (**critically stressed**)	Consistent with well data
74-7	N52W	not reported	Y	SFZ optimally oriented and Shmin low (**critically stressed**)	Consistent with well data
66-21	N20W±20	0.55-0.64 @ 1.9–2.2 km	N	SFZ optimally oriented BUT Shmin high (**not critically stressed**)	Consistent with well data
45-14	N41W±12	0.55-0.64 @ 1.9–2.2 km	N	Shmin low BUT SFZ not optimally oriented (**not critically stressed**)	Consistent with well data

***Scenario 2** – AltaRock Model*

As opposed to Scenario 1, Blackwell et al. (2005) postulated that the whole SGS *did rupture* in the "Gap" earthquake, and suggested that the scarp may have been confined to the range block near the DVGF, i.e. the lack of scarps is not significant. In addition to the main range-front fault, Dixie Valley also contains many piedmont and intrabasin faults of varying orientations. These structures are important to consider because several faults intersect or closely interact with each other in the area of the producing reservoir (Smith et al., 2001), and it has been suggested that none of the production wells in the geothermal field (located 2-3 km into the valley) produce from the exposed main strand of the DVF, but from blind valley (piedmont) segments (Blackwell et al., 2005). For Scenario 2, we represent the DVF as 1 section, the SGS as 3 sections (although not the same sections as Scenario 1), and unlike Scenario 1, we also include the PVF as 1 section. For the three large earthquakes previously discussed, several slightly varying fault orientations and slip magnitudes are suggested from multiple sources (e.g., Blackwell et al., in prep; Caskey et al., 1996; Caskey and Wesnousky, 1997; Smith et al., 2001; Caskey and Wesnousky, 2002; Caskey and Ramelli, 2004; UGSG Quaternary Fault and Fold Database (QFFDB)). The input values (Table 3) used to produce the model for Scenario 2 are based on the following information:

- *1915 Pleasant Valley Earthquake along PVF*
    - Max vertical/horizontal displacements are **5.8m/2m**, respectively (Wallace, 1980; 1984)
    - Dip varies from **47-65° NW** (QFFDB)

- *2-2.5 ka "Gap" Earthquake along SGS*
    - Max vertical displacement of **5m** (Caskey and Ramelli, 2004)
    - Dips to the SE, but no angle reported by QFFDB; Blackwell et al. (in prep) suggests dips **70-80° SE** down to at least 3km

- *1954 Dixie Valley Earthquake along DVF*
    - Max vertical displacement of **2.8m** (Caskey et al., 1996)
    - Dip varies from **30-80° SE** (QFFDB)

According to stress orientations and magnitudes presented by Hickman et al. (1998, 2000), the dominant population of permeable fractures within the fault zone near the DVGF is subparallel to the main fault, striking roughly NE and dipping 40-75 degrees SE, with a conjugate set striking roughly the same direction but dipping NW. Field observations suggest that roughly N-S oriented normal faults are also present (T. Cladouhos, personal communication, 2010) and may play a role within the DVGF. To be consistent with these observations, we explore three different types of RFs: (a) synthetic normal fault subparallel to SGS dipping 70°E, (b) antithetic normal fault subparallel to SGS dipping 70°W, and (c) normal fault oriented roughly N-S dipping 70°W. For each RF, we present figures showing the CSC and dilatational strain in both map and cross-sectional view (Figures 4-6). Please note that all dilatational strain figures are identical (because they are based on same slip amounts on the same SFs), but we chose to include them all in order to display the location of an example RF within the dilatational strain field.

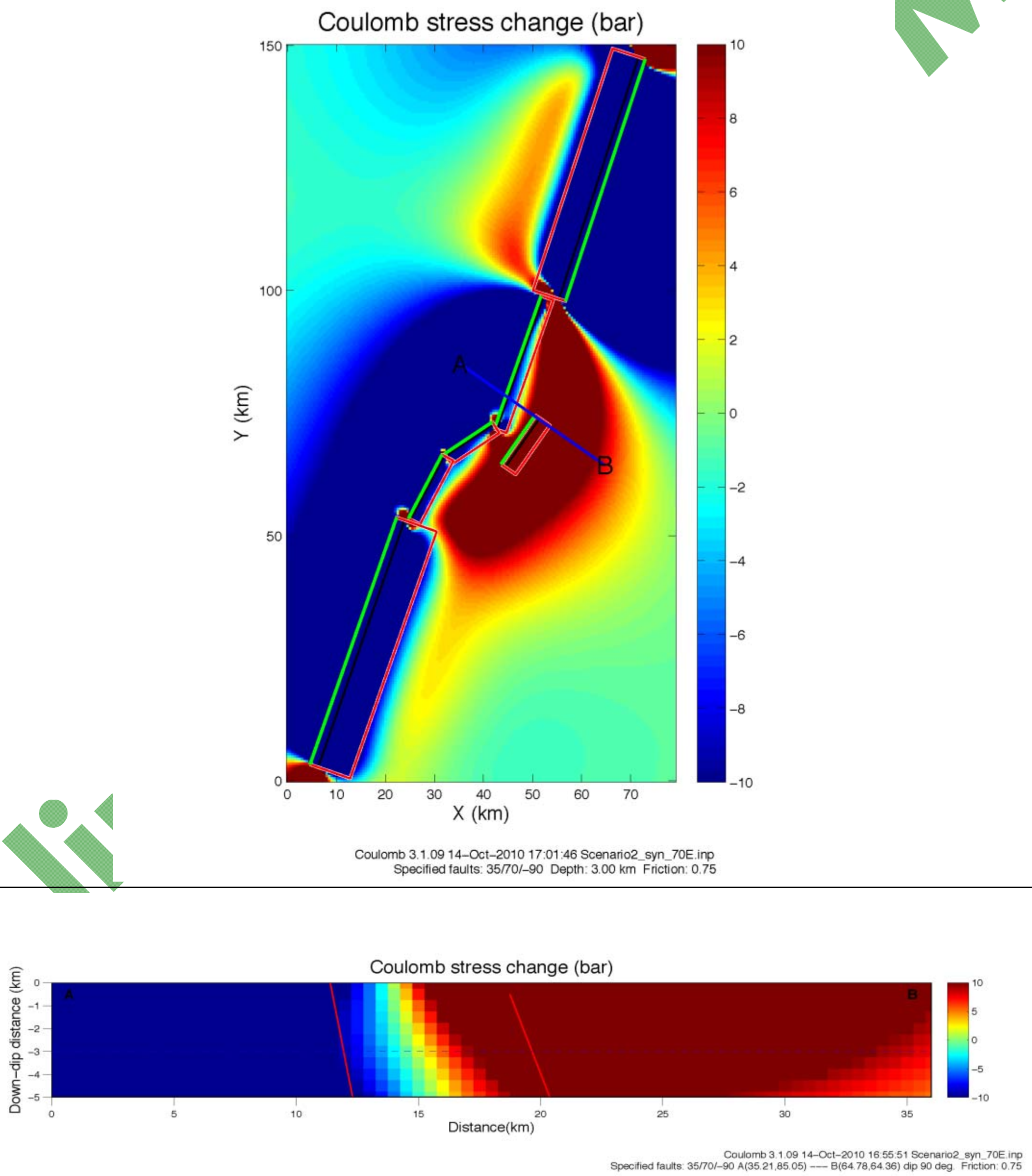

Figure 4(a) – CSC map (top) and cross-section (bottom) of Scenario 2(a) showing CSC resolved onto synthetic RF dipping 70°E due to slip on SFs.

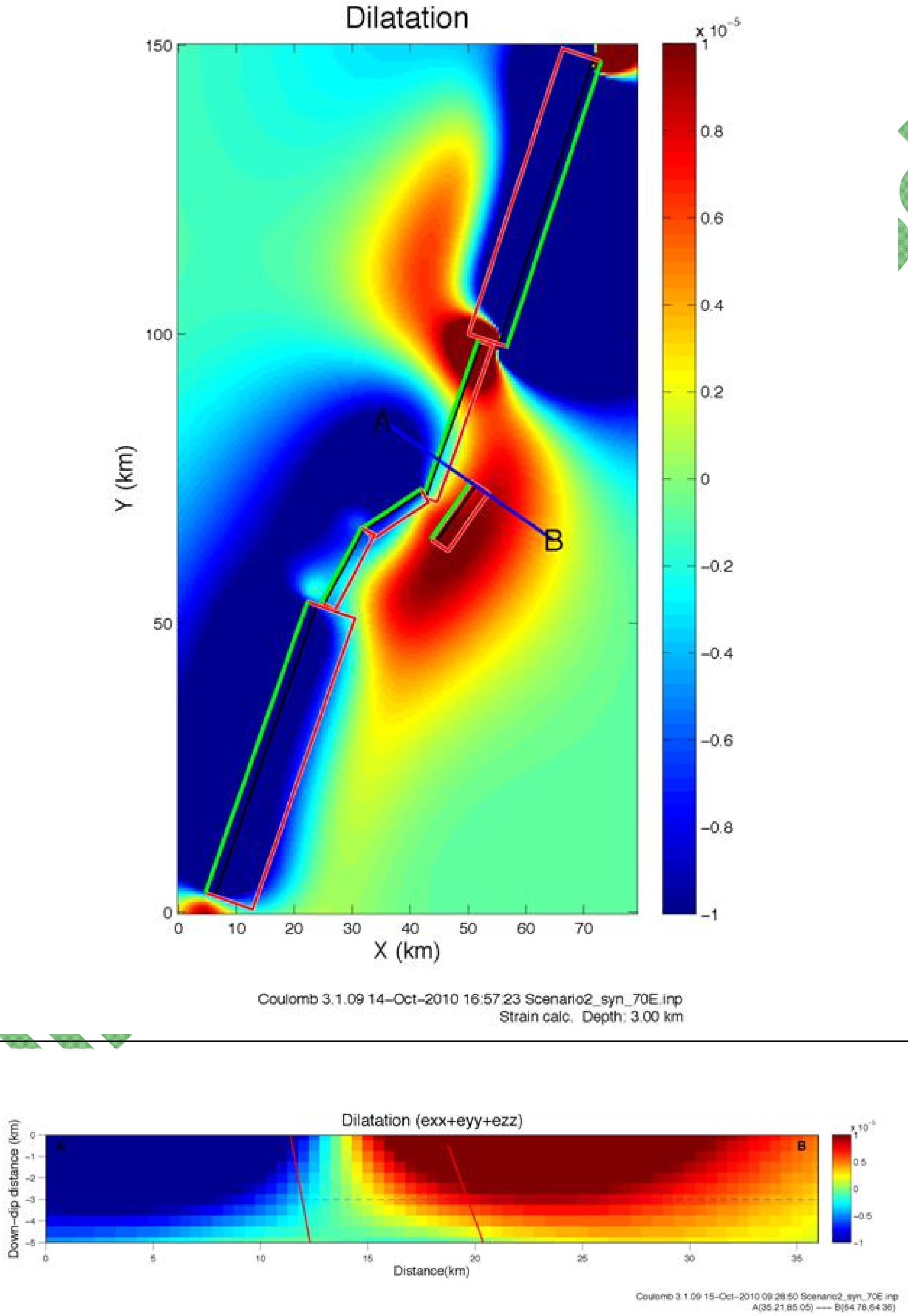

Figure 4(b) – Map (top) and cross-section (bottom) of Scenario 2(a) showing dilatation resolved onto synthetic RF dipping 70°E due to slip on SFs.

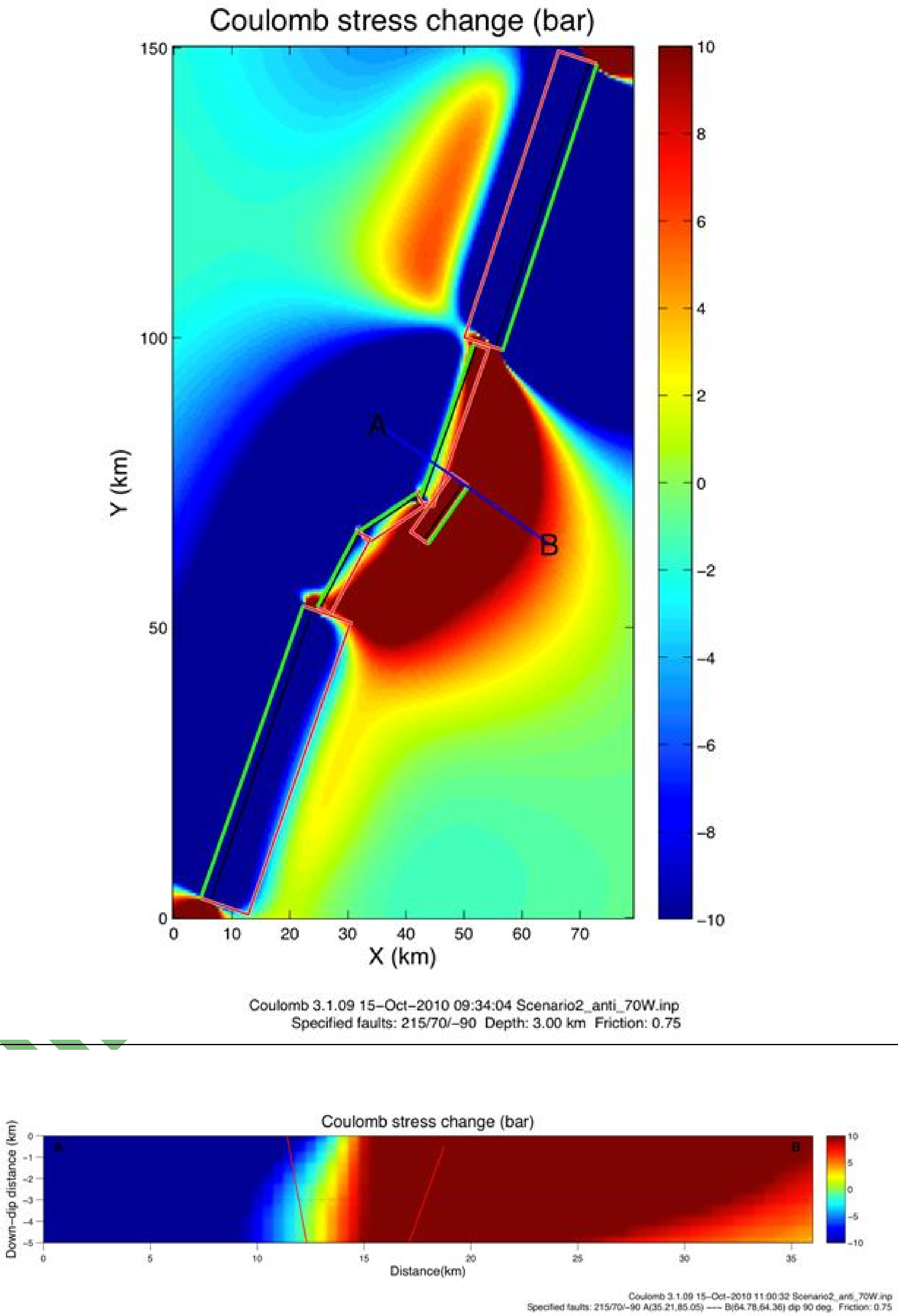

Figure 5(a) – Map (top) and cross-section (bottom) of Scenario 2(b) showing CSC resolved onto antithetic RF dipping 70^{o}W due to slip on SFs.

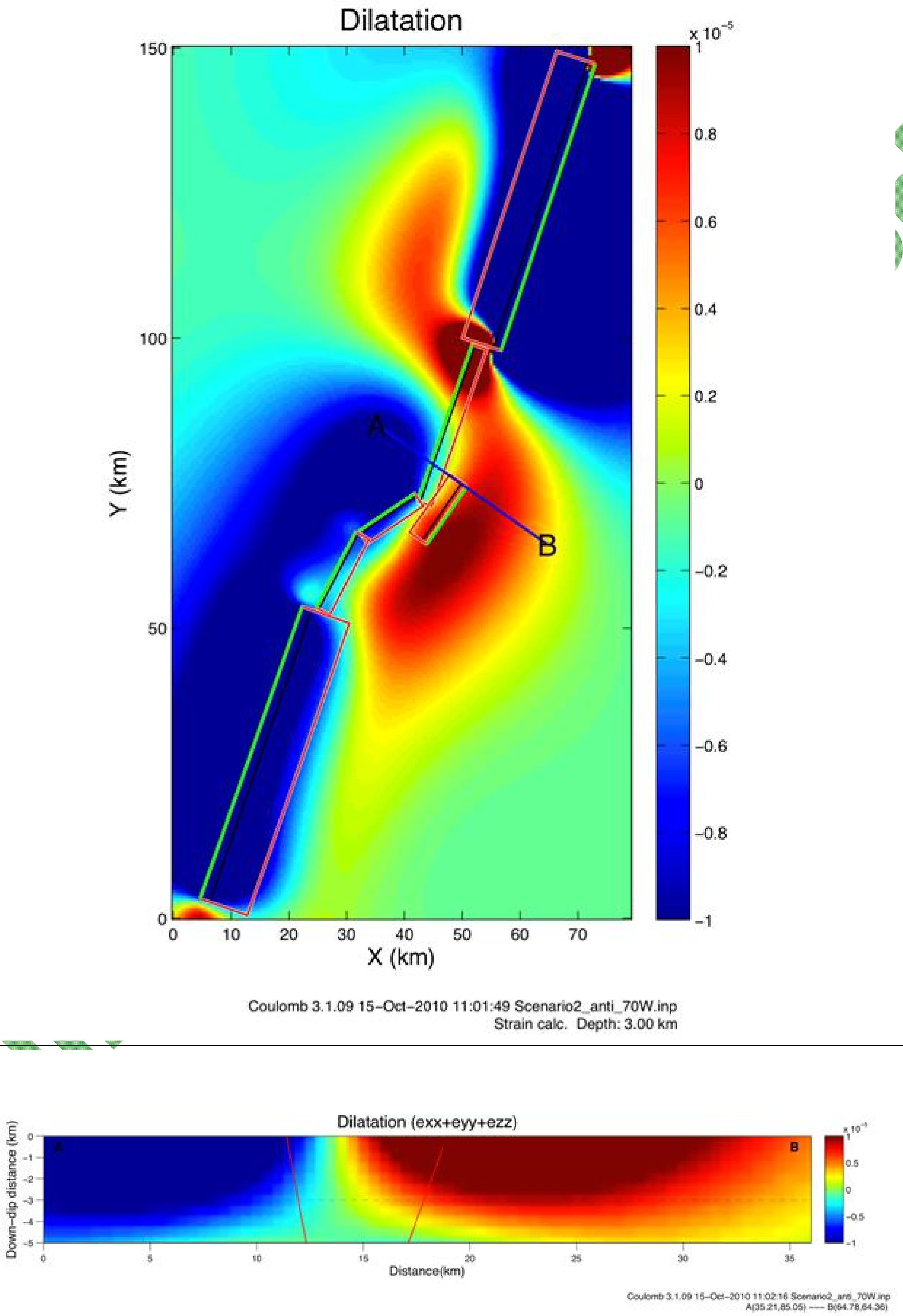

Figure 5(b) – Map (top) and cross-section (bottom) of Scenario 2(b) showing dilatation resolved onto antithetic RF dipping 70°W due to slip on SFs.

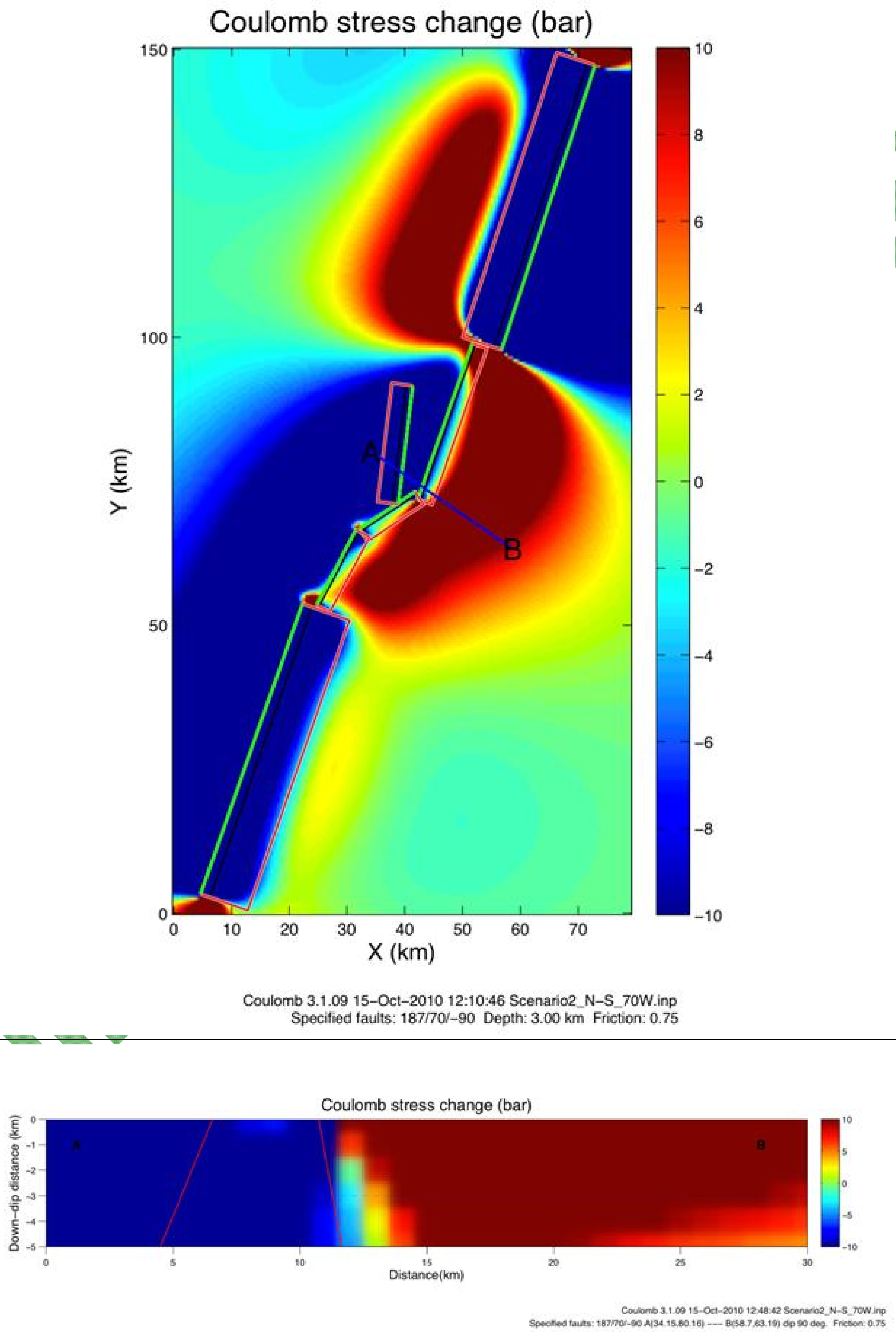

Figure 6(a) – Map (top) and cross-section (bottom) of Scenario 2(c) showing CSC resolved onto N-S oriented RF dipping 70°W due to slip on SFs.

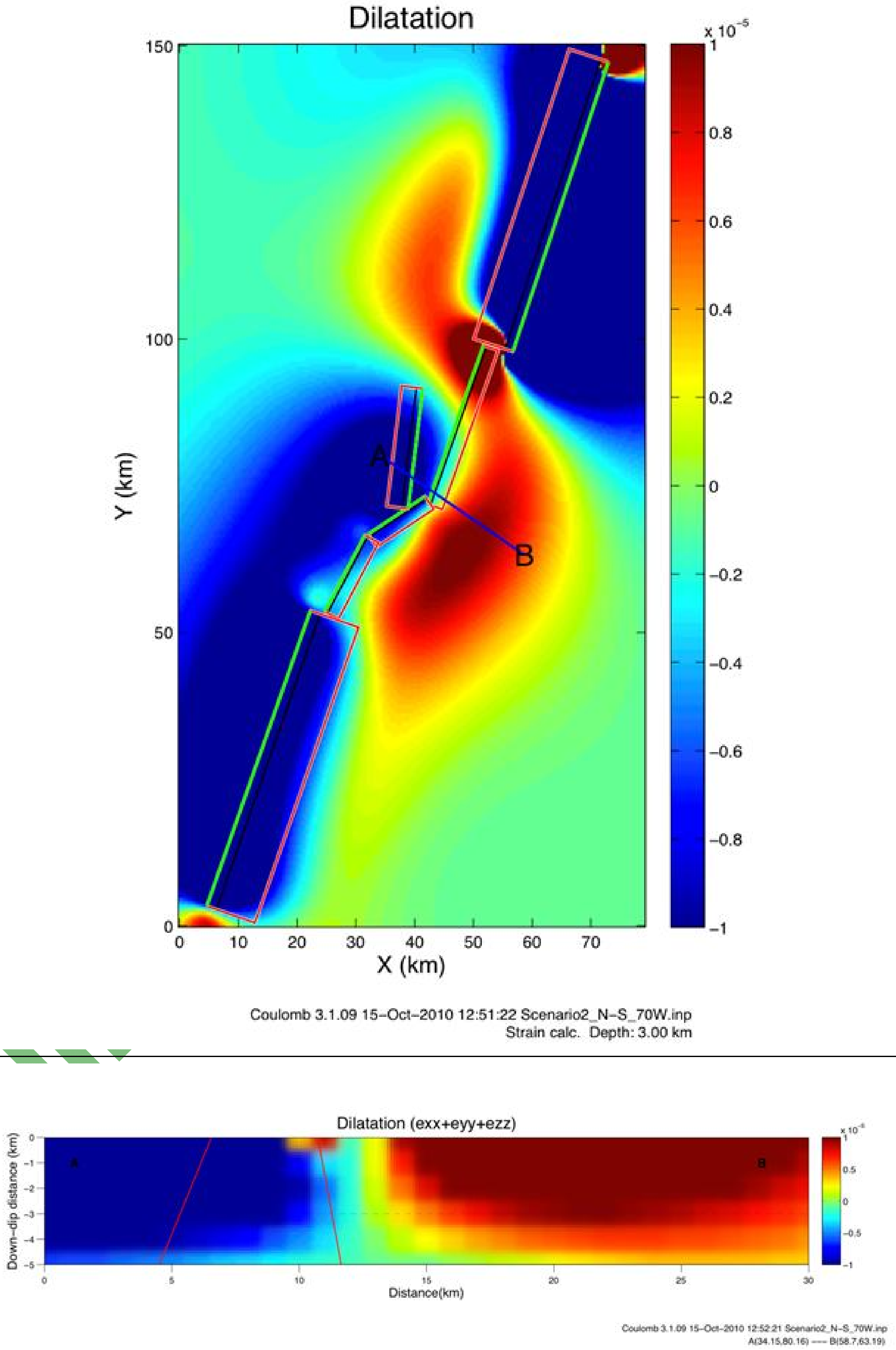

Coulomb 3.1.09 15−Oct−2010 12:51:22 Scenario2_N−S_70W.inp
Strain calc. Depth: 3.00 km

Coulomb 3.1.09 15−Oct−2010 12:52:21 Scenario2_N−S_70W.inp
A(34.15,80.16) --- B(58.7,63.19)

Figure 6(b) – Map (top) and cross-section (bottom) of Scenario 2(b) showing dilatation resolved onto N-S oriented RF dipping 70^{o}W due to slip on SFs.

Table 3 – Input fault parameters for Scenario 2. We estimate the trace lengths and strikes (start and end points) of the PVF, DVF, and SGS using Google Earth surface traces provided by the QFFDB. As in Scenario 1, we assume a fault top and bottom depth of 0km and 15km, respectively, for the SF.

Fault (SF or RF)	Start x (km)	Start y (km)	End x (km)	End y (km)	Slip (m)	Dip (^{o})	Top (km)	Bottom (km)
1915 PVF (SF)	72.96	147.22	56.71	97.85	5/2 (V/H)	65 W	0	15
2-2.5 ka SGS-North (SF)	42.205	71.843	51.716	98.94	3	80 E	0	15
2-2.5 ka SGS-Middle (SF)	32.066	66.729	41.756	73.189	3	80 E	0	15
2-2.5 ka SGS-South (SF)	24.708	53.539	31.528	66.549	3	80 E	0	15
1954 DVF (SF)	4.63	3.34	22.28	53.71	2	60 E	0	15
(a) synthetic fault (RF)	43.7	64.49	50.7	74.49	0	70 E	0	10
(b) antithetic fault (RF)	50.7	74.49	43.7	64.49	0	70 W	0	10
(c) N-S fault (RF)	41.398	91.583	38.885	71.036	0	70 W	0	10

Scenario 2 Discussion

Assuming that the whole SGS fault segment ruptured 2-2.5 ka (in addition to the 1954 DVF and 1915 PVF ruptures), these figures illustrate that the region near the DVGF lies within a zone of positive CSC and dilatation, and therefore we suggest that slip resulting from these Holocene ruptures promotes normal faulting on all three types of RFs.

As previously mentioned, the fault zone near producing wells of DVGF (73B-7 and 74-7) is critically stressed for normal failure, while the zone near non-producing wells (66-21 and 45-14) is not critically stressed for failure (Hickman et al., 1998; 2000). Figure 7 illustrates that for synthetic RFs dipping 70^{o}E (representative of the dominant set of permeable fractures), the distribution of CSC and dilatational strain is consistent with this observation where productive wells locate within zones of positive CSC (failure is promoted) and dilatation (fault is unclamped), and non-productive wells fall within regions of negative CSC (failure is inhibited) and compression (fault is clamped). Again, the dilatational strain distribution is identical for all three RFs and so we only include it within Figure 7. Figure 8 illustrates that for both antithetic and roughly N-S trending RFs dipping 70^{o}W (representative of the conjugate set of permeable fractures and the N-S oriented faults observed in the field, respectively), the distribution of CSC is also consistent with this observation where productive wells locate within zones of positive CSC (failure is promoted), but is inconsistent where non-productive wells locate within zones of slightly positive CSC. It is worth noting that although a positive CSC value acts to promote failure, the magnitude of CSC is smaller at non-producing wells than producing wells. It may be that productivity at 66-21 and 45-15 is more strongly *inhibited* by compression than *enhanced* by positive CSC (Figure 7). It is worth noting that our modeled fault locations do not coincide exactly with the actual fault locations, and because non-productive wells locate very closely to the transition from positive to negative CSC, this slight difference in fault location could result in non-productive wells plotting within the zone of slightly positive CSC when they are actually located within a zone of negative CSC.

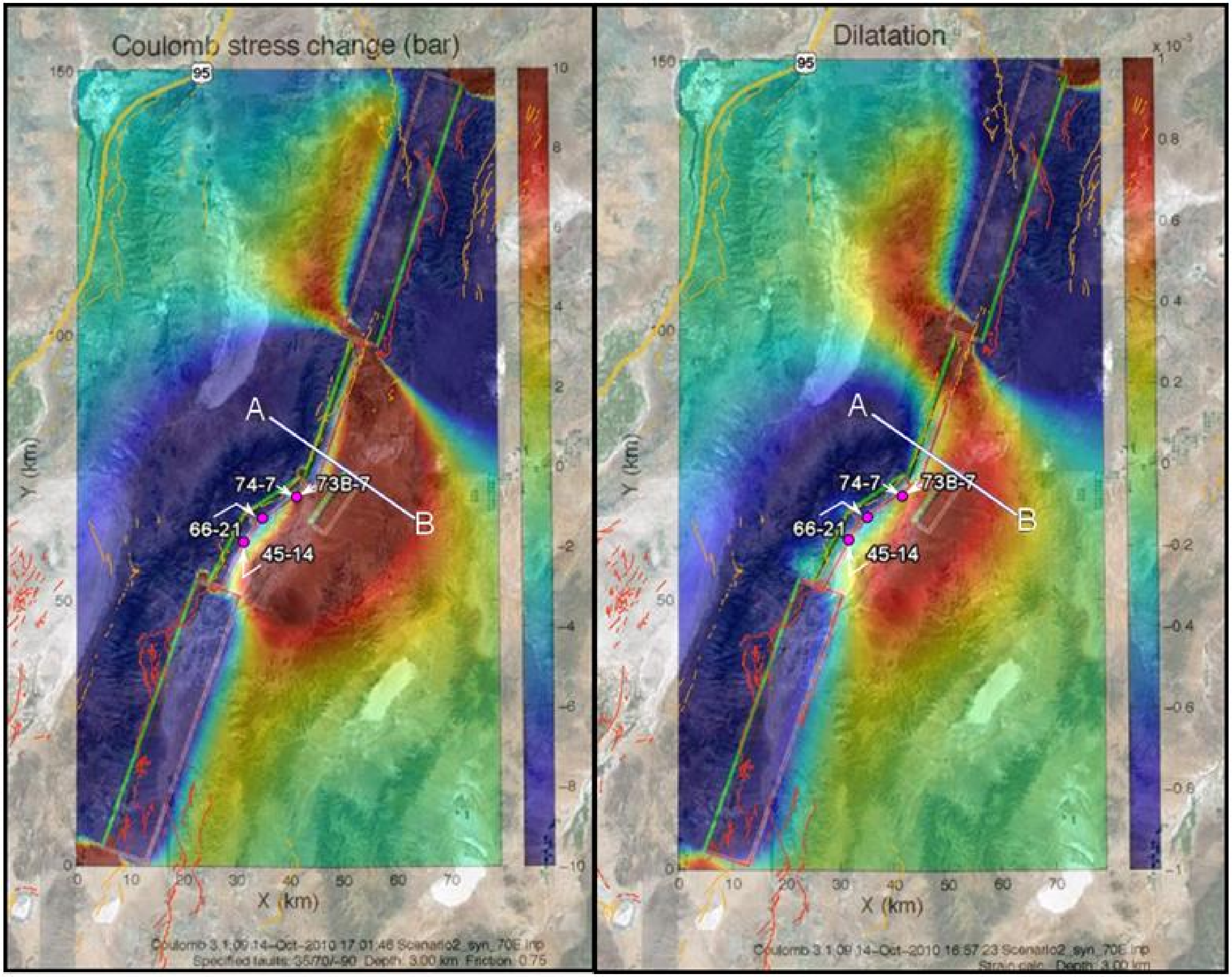

Figure 7 – Overlay of CSC (left) and dilatation (right) maps from Figure 4(a) and (b) on Google Earth image showing QFFDB fault traces and locations of deep wells (magenta dots) mentioned above. Note that wells 74-7 and 73B-7 are close enough to one another (~220 meters) that their locations overlap on a map of this scale.

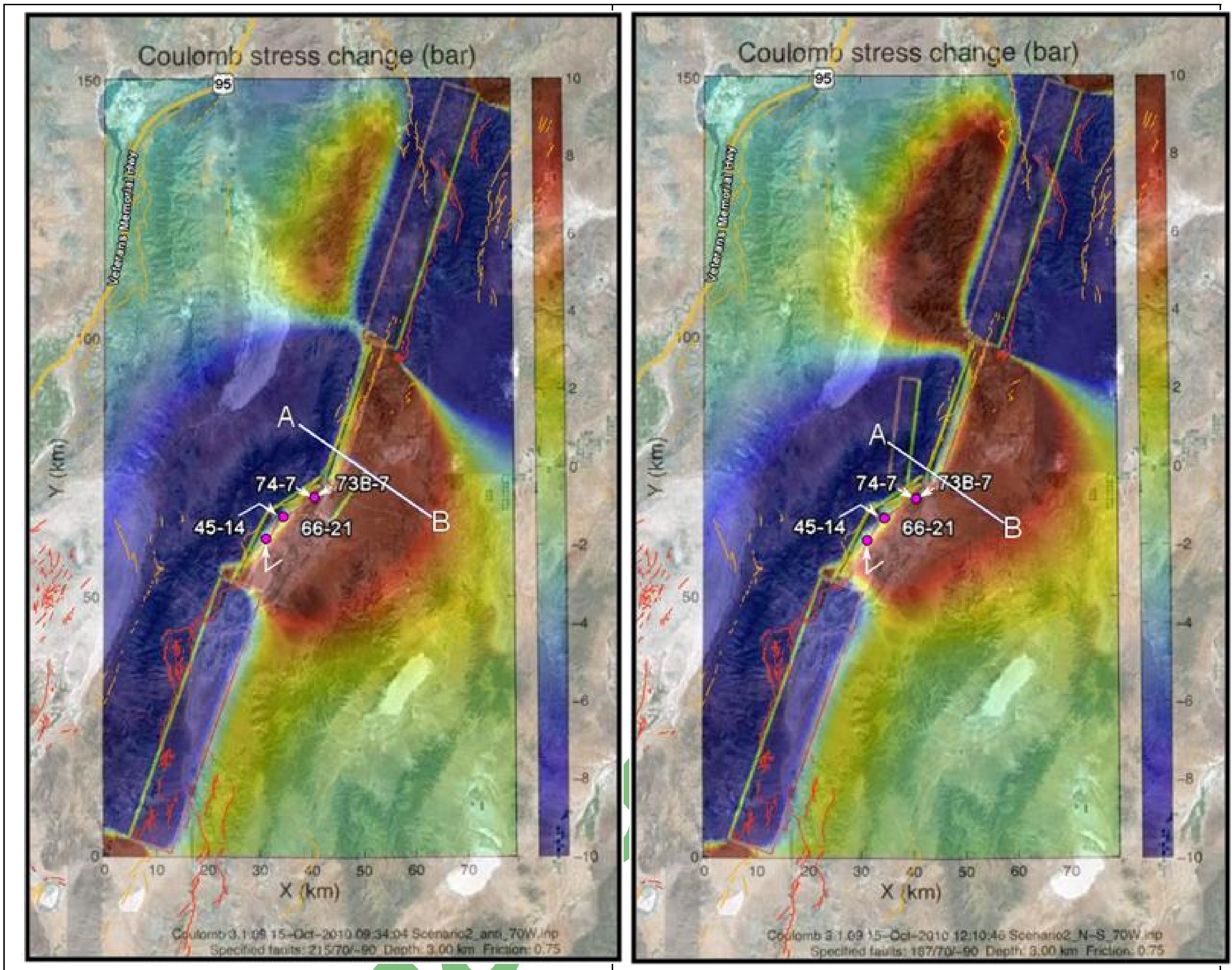

Figure 8 – Overlay of CSC maps from Figure 5(a) and Figure 6(a) on Google Earth image showing QFFDB fault traces and locations of deep wells (magenta dots) mentioned above. Note that wells 74-7 and 73B-7 are close enough to one another (~220 meters) that their locations overlap on a map of this scale.

Table 4 – Information from deep wells penetrating the fault zone at 2-3 km depth. Red and blue indicate critically stressed and not critically stressed well sites (Hickman et al., 1998; 2000).

Well	**Sh_{min}**	**Sh_{min}/Sv**	**Productive**	**Interpretation**	**Scenario 2**
73B-7	N57W±10	0.45-0.62 @ 0.4-2.5 km	Y	SFZ optimally oriented and Shmin low (**critically stressed**)	Consistent with well data
74-7	N52W	not reported	Y	SFZ optimally oriented and Shmin low (**critically stressed**)	Consistent with well data
66-21	N20W±20	0.55-0.64 @ 1.9–2.2 km	N	SFZ optimally oriented BUT Shmin high (**not critically stressed**)	Consistent with well data
45-14	N41W±12	0.55-0.64 @ 1.9–2.2 km	N	Shmin low BUT SFZ not optimally oriented (**not critically stressed**)	Consistent with well data

References

Blackwell, D.D., and R. P. Smith, Eds., with contributions from S. Bergman, D. Blackwell, F. Goff, M. Kennedy, J. McKenna, M. Richards, R. Smith, A. Waibel, and P. Wannamaker, 2005. DRAFT Description, Synthesis, and Interpretation of the Thermal Regime, Geology, Geochemistry and Geophysics of the Dixie Valley, Nevada Geothermal System, 191 pp, in review.

Caskey, S.J., Wesnousky, S.G., Zhang, P., and Slemmons, D.B., 1996. Surface faulting of the 1954 Fairview Peak (Ms 7.2) and Dixie Valley (Ms 6.8) earthquakes, central Nevada, Bull. Seismol. Soc. Am., 86, 761-787.

Caskey, S.J. and Wesnousky, S.G., 1997. Static stress changes and earthquake triggering during the 1954 Fairview Peak and Dixie Valley earthquakes, Central Nevada. Bull. Seismol. Soc. Am. 87, 521-527.

Caskey, S.J., and Wesnousky, S.G, 2002. Neotectonics of the Dixie Valley geothermal field and models for late Holocene static stress redistributions. Presentation to Dixie Valley Geothermal Workshop, June 12-13, Reno, Nevada, *http://www.unr.edu/geothermal/oldermeetings.htm*

Caskey, S.J., and Ramelli, A.R., 2004. Tectonic displacement and far-field isostatic flexure from pluvial lake shorelines, Dixie Valley, Nevada, Journal of Geodynamics, 38-2, 131-145.

Hickman, S., Zoback, M., and Benoit, D., 1998. Tectonic Controls on reservoir Permeability in the Dixie Valley, Nevada geothermal field: Proceedings, Twenty-Third Annual Workshop, January 27-28, Geothermal Reservoir Engineering, Stanford Geothermal Program, Stanford, California, 6 p.

Hickman, S. H., Zoback, M. D., Barton, C. A., Benoit, R., Svitek, J. and Summers, R., 2000. Stress and permeability heterogeneity within the Dixie Valley geothermal reservoir: Recent results from well 82-5, Proceedings, 25th Workshop on Geothermal Reservoir Engineering, Stanford University, Stanford, California, January 24-26, SGP-TR-165, p.256-265.

Lin, J. and R.S. Stein (2004), Stress triggering in thrust and subduction earthquakes, and stress interaction between the southern San Andreas and nearby thrust and strike-slip faults, J. Geophys. Res., 109, B02303, doi:10.1029/2003JB002607.

Smith, R.B., 1978. Seismicity, crustal structure, and intraplate tectonics of the interior of the western Cordillera. In: R.B. Smith and G.P. Eaton (Editors), Cenozoic Tectonics and Regional Geophysics of the Western Cordillera. Geol. Soc. Am. Mem., 152: 111-144.

Smith, R.P., Wisian, K.W., and Blackwell, D.D., 2001. Geologic and Geophysical evidence for intra-basin and footwall faulting at Dixie Valley, Nevada, GRC Transactions, 25, 323-326.

Toda, S., R. S. Stein, K. Richards-Dinger and S. Bozkurt, 2005. Forecasting the evolution of seismicity in southern California: Animations built on earthquake stress transfer, J. Geophys. Res., B05S16, doi:10.1029/2004JB003415.

USGS Quaternary Fault and Fold Database of the United States. Fault data updated 20 October 2009. *http://earthquake.usgs.gov/hazards/qfaults/*

Wesnousky, S., Caskey, S.J., and Bell, J.W, 2003. Recency of Faulting and Neotectonic Framework in the Dixie Valley Geothermal Field and Other Geothermal Fields of the Basin and Range, Final Technical Report, University of Nevada, Reno, 26 pp., *http://earthquake.usgs.gov/research/external/reports/08HQGR0027.pdf*

APPENDIX 14

DIXIE VAELLEY WELLFIELD CROSS-SECTIONAL CORRELATIONS BETWEEN VARIOUS DATA SETS: SUMMARY TABLE

Correlation between Various Cross-Sectional Data-Sets in the Dixie Valley Wellfield, see Plate 1. Cells highlighted orange indicate a lack of a correlation.

Section	***Geology Correlation with***					***Gravity/Magnetic inferred Lithology Correlation with***				***Temperature Correlation with***	
	Magneto-tellurics (MT)	***Seismic Reflection Profile***	***Gravity/Magnetics Model***	***Temperature***	***Vp***	***MT***	***Seismic Reflection Profile***	***Temperature***	***Vp***	***MT***	***Vp***
Section C	Array S	Line 102 not available	Section C	Section C	Section C	Array S	Line 102 not available	Section C	Section C	Array S	Section C
	Major geologic structures coincide with resistivity breaks		Inferred gravity/magnetic structures bound Jurassic rocks (Jg)		No correlations found				No correlations found		No correlations found
	Range-front and piedmont fault tightly bound bodies of high resistivity in their footwall blocks		Inferred gravity/magnetic structures comprising the DVFZ closely resemble geologic structures	Upward bend in isotherms (convective flow) correlate with the range-front and piedmont fault				Gap in magnetic Jurassic rocks (Jg) coincide with major thermal-upwelling zones		Shallow, localized high resistivity anomaly found to correlate with an intra-range structure suggesting thermal alteration	
	Shallow resistivity below Stillwater Range coincides with fumarole activity and infers hydrothermal alteration at shallow depth		Absence of Jg coincides with Section 10 fumaroles and suggests demagnetization in the DVFZ			Shallow low resistivity below Stillwater Range coincides with discontinuity in Jg					
	Infers steeply dipping structures in the DVFZ (~75-80°)		Infers steeply dipping structures in the DVFZ(~85°)			Infers steeply dipping structures in the DVFZ(~85°)					
	Wide very low resistivity (in the valley) interpreted as an alteration zone lies within N-S trending structural block		Termination of magnetic Jz rocks (Jg) and associated bounded structure directly coincide with the occurrence of a major north-trending structure			Magnetic Jurassic rocks (Jg) do not extend through alteration zone identified by the vertical-trending low resistivity structure					
			Basin-fill deeper than expected from geologic section								
Section D	No associated MT Array	Line 9/104	Section D	Section D	Section D	No associated MT array	Line 9/104	Section D	Section D	No MT array	Section D
		Seismic inferred piedmont fault coincides with geologic section	Major structural offset occurs in same position as piedmont fault and intra-range structure correlates with surface fault	Upward bend in isotherms (convective flow) correlate with the range-front and piedmont fault	No correlations found		Major piedmont fault identified in the same location by both data-sets	Thicker magnetic section found in the main injection zone suggest a hydrothermal alteration component	No correlations found		No correlations found
		Interpreted reflectors for volcanics are thicker than expressed in geologic sections	Missing magnetic rocks (Jg) in the valley coincides with a North-trending geologic structure				Basalt reflector and associated volcanics section not found				
			Occurrence of magnetic rocks (Jg) in the vicinity of the main injection zone is much thicker than Jurassic rocks encountered in the wells								
			Major range-bounding structure occurs ~ 1km rangeward than expected range-front fault from geologic section								

Section	Geology Correlation with					Gravity/Magnetic inferred Lithology Correlation with				Temperature Correlation with	
	Magneto-tellurics (MT)	Seismic Reflection Profile	Gravity/Magnetics Model	Temperature	Vp Seismic	Magneto-tellurics (MT)	Seismic Reflection Profile	Temperature	Vp Seismic	MT	Vp Seismic
Section E	Array C	Line 6	Section E	Section E	Section E	Array C	Line 6	Section E	Section D	Array C	Section E
	Low resistivity structure dipping ~70°SE lying NW of DVF infers a previously active structure within range that coincides with surface geology	Occurrence of side reflector (steep structure break) coincides with piedmont fault	No major structural discontinuity occurs at range-front fault	Upward bend in isotherms (convective flow) correlate with the range-front and piedmont fault	No correlations found	Jg unit is not continuous through low resistivity zone in valley	Major piedmont fault identified in the same location by both data-sets	Missing magnetic rocks (Jg) in the DVFZ suggest alteration	No correlations found	Higher resistivity in the shallow subsurface near the range-front fault suggest thermal alteration	No correlations found
	Higher resistivity block coincides with producing zone (Section 7 production wells)	Basalt (Tmb) is truncated by piedmont fault and major intrabasin fault near 62-21	Implies a broad zone of intermittent step-faulting bounds the eastern edge of the valley coinciding with geologic interpretations and geophysical surverys	Thermal Isotherms "fall off" in the area of 62-21 away from the DVFZ		Higher resistivity block near section 7 wells correlates with thick fault-bounded Jg section		Missing magnetic rocks (Jg) in the valley near 62-21 coincide with a non-thermal bearing west-dipping fault			
	North-trending structure tightly bounds higher resistivity to NE		No major intra-range faults identified by the Gravity-Magnetic Model								
	Resistivity above ~50 ohm-m infers basement rocks and coincides with geology										
	Moderately dipping (~60-65°) zone of higher resistivity below Cottonwood Canyon (CC) infers a more shallow dip for range-front fault										
	Very high resistivity block (~5600 ohm-m) occurs beneath central Stillwater Range and doesn't coincide with granodiorite (Kgr) within footwall of piedmont fault										
Section F	Array N	Line 102	Section F	Section F	Section F	Array N	Line 102	Section F	Section F	Array N	Section F
	Higher Resistivity beneath Stillwater Range and within DVFZ corresponds to basement rocks		Thick occurrence of Jg beneath the Stillwater Range does not coincide with surface geology indicating Triassic meta-seds	Upward bend in isotherms (convective flow) correlate with the range-front and piedmont fault	No correlations found	Gap in Jg beneath valley directly coincides with low resistivity zone	Major piedmont fault identified in the same location by both data-sets	Missing magnetic rocks (Jg) in the DVFZ suggest alteration	No correlations found		
	Sharp resistivity change occurs across piedmont fault	Interpreted side reflection in agreement with occurrence of piedmont fault	Multiple faults (at least three) comprising the DVFZ agree with geologic section	Area of shallow high geothermal gradients and increased temperature occur in the Senator Fumaroles and 38-32 area as expected				Missing magnetic rocks in valley does not coincide with any major N-trending structures		Very low resistivity structure found at surface coincides with surface and alluvium alteration near Senator Fumaroles	
	Shallow low resistivity occurs at Senator Fumaroles										
	Very low resistivity in the upper 0.5km subsurface near 38-32 concides with a zone of alteration at the surface (Senator fan) and encountered in 38-32					Shallow very low resistivity zone near well 38-32 coincides with a discontinuous Jg unit within the DVFZ					
	Prominent fault within the zone of step-faulting that bounds the eastern edge of the valley coincides with a sharp resistivity break										

APPENDIX 15

GENERAL GEOSCIENCE DATA PARAMETERS

Table of Contents

List of Tables

Table 15-1. Description of General Parameters for the Geoscience Data Sets

Geoscience Discipline	Task Leader	Raw Baseline Data	Data Source	Modeled Baseline Parameter
Gravity and Magnetics	Bob Karlin	Gravity and Density	Complete Bouguer anomaly gravity data PACES gravity data	Combined Gravity-Magnetic Modeling to infer Lithology
		Magnetics	HELIMAG aeromagnetic total field anomaly data Graugh (2002)	
		Horizontal Gradients	Blackwell et al. 2005	
Seismic	Ileana Tibuleac	Velocity Modeling	OPTIM interpreted velocity models General crustal-scale tomography	P-wave velocity S-wave velocity Attenuation Rho (density)
		Reflection Profiles	Available seismic profiles and interpreted lines	
Thermal	Dave Blackwell[1]	Temperature (°C)	surface measurements, temperature gradient holes and deep wells	Modeled Wellfield Temperatures
		Thermal Gradients	temperature-depth profiles	Conductive Model
		Heat Flow	Blackwell and SMU Thermal Modeling	Convective Model
		Thermal Conductivity		
Magnetotellurics (MT)	Phil Wannamaker	Resistivity	contiguous bi-pole deployments across three dense profiles (Arrays S, C and N) Wannamaker et al. 2006; 2007	Resistivity
Geo-chemistry	Mack Kennedy	Si, Cl and Total Bicarbonate (ppm) Bicarbonate-Cl (ratio) F[$_4$He] (ppm) Helium R/Ra CO$_2$ Geothermometry	surface (fumaroles, springs, shallow wells) and wells at depth (production fluids, etc.); compiled in Goff et al. 2002	None
Lithology	Trenton Cladouhos[2]	Lithology (surface and wells)	Geologic Maps and available well logs	Lithology Type Assigned Parameters:

Table 15-1. Description of General Parameters for the Geoscience Data Sets

Geoscience Discipline	Task Leader	Raw Baseline Data	Data Source	Modeled Baseline Parameter
				Density, Strength, Internal Friction
Stress	Trenton Cladouhos[3]	Coulomb Failure Stress	Stress Modeling: Caskey et al. 2000	Coulomb Stress Change Dilatation Fault Orientation Fracture Intensity Zones of Compression/Dilation
		Fault orientation/slip	Faulting Databases	
		Borehole stress data	Hickman et al. 1998; 2000	

[1] Supported by Mahesh Thakur of SMU

[2] Supported by Owen Callahan and Jon Sainsbury from AltaRock Inc.

[3] Supported by Maisie Nichols of AltaRock Inc.

Table 15-2. List of detailed Geoscience Parameters from the Dixie Valley baseline data set and associated applicability and resolution

Parameter	Type	Source	Description	Unit	Used in Statistical Analysis	Data Applicability	Resolution
LithDen	Assigned	Lithology	Density	g/cm^3	Y	N/A	N/A
LithStrength			Strength	Mpa	N		
LithInterFric			Internal Friction	N/A			
Rock Type	Measured/Modeled		Lithology Type	N/A	Y	at surface and at depth within wellfield	0.5 km
FracInten	Calculated	Stress	Fracture Intensity	m/m^2	Y	entire project area	0.5 km
VertStress			Vertical Stress	bars		entire project area	unknown
CSC	Modeled		Coulomb Stress Change	bars		wellfield only	
Dilatation			Dilational Strain	N/A			
Temperature	Measured/Modeled	Thermal	Temperature	° C	Y	Wellfield only	0.5 km
Vp	Modeled	Seismic	P-wave velocity	km/s	Y	Proximal to seismic reflection lines	0.5km
Vs			S-wave velocity	km/s			>10 km
Rho			Density	g/cm^3	N		
Qp			P-wave attenuation	-			
Qs			S-wave attenuation	-			
Resistivity	Modeled	MT	MT derived resistivity	ohm-m	Y	wellfield only	0.5 km
Si	Measured	Geochemistry	Silica	ppm	N	wellfield and other springs within project area	unknown
Cl			Chloride	ppm			
BiCarb			Total BiCarbonate	ppm			
BiCarb-Cl			BiCarb/Chloride	N/A			
F[$_4$He]			Fractionation of ^{4}He				
R/Ra			He^3/He^4 ratio	N/A			
Grav_Mag	Modeled	Gravity-Magnetics	Gravity-Magnetics inferred Lithology	N/A	Y	within wellfield	0.5 km

Other Potential Parameters							
Fault/Fracture Azimuth	Modeled	Geology-Stress	Favorable/Unfavorable Fault Orientations	degrees	N	entire project area	unknown
Compression-Dilation Zones	Modeled	Stress	Expected localized stress zones	N/A	N	major structural intersections	0.5 km
Gravity	Measured/Modeled	Gravity-Magnetics	gravity measurements	gals	N	entire project area	unknown
			density	g/cm^3			
Magnetics			magnetic susceptibility	emu/cm^3			
Horizontal Gradients			area of largest gradients infer major faulting	N/A		only at surface	
CO_2	Measured	Geochemistry	CO_2 Flux	g/m^2d	N	major structural intersections	<<500m

Table 15-3. Geologic and Thermal Cross-Sections Data Sources[3,4]

Type	Source	Inference	Baseline Conceptual Model Report	
			Figure Reference	Section/Appendix Reference
Surface Geology	Speed (1976) Map	geology and faulting in the Stillwater Range		Appendix 1
	GIS-referenced Dixie Valley Map	occurrence of stratigraphic units and major faults	51	Section 7.3
Well Data	Blackwell et. al. (2005)	available temperature and lithology at depth	40A, 42, 43, 46, Table 3	Section 6; Appendix 9, 10 and 11.
	Lithology logs[1] from Al Waibel[2]			
	SMU[5] & NBMG[6] databases			
Gravity / Magnetic Surveys	Blackwell et. al. (2005)	Horizontal gradients infer areas of intrabasinal faulting	8, 9, 10, 11 and 13	Section 3.1,3.2
		Location of piedmont structure		
Seismic Reflection Profiles	Blackwell et. al. (2005)	infer faulting and depth to prominent reflectors along interpreted profiles	17a	Section 3.5.3
DV Structure Map	Smith and Blackwell (2001)	Intra-basin structures	14	Section 3.2
DV Basement Configuration	Blackwell et. al. (2005)	Intra-basin structures, depth to basement	18	Section 3.5
		depth of basin-fill from drilling and seismic reflection profiles		
Cross-sections	Johnson and Hulen (2002)	northern producing field	47	Section 6.4
	Blackwell et. al. (2005)	conceptual geologic cross-sections		
	Blackwell et. al. (2005)	conceptual thermal sections	45A, 45B	Section 6.3
	Plank (2002)	Structure of the producing wellfield		

Table 15-3. Geologic and Thermal Cross-Sections Data Sources^{3,4}

Type	Source	Inference	Baseline Conceptual Model Report	
			Figure Reference	Section/Appendix Reference

Note. Structural Map from Waibel (2011) and unpublished structure maps (Figures 49A-C) produced by Jon Sainsbury of AltaRock Inc. were not used to construct the cross-sections

[1] Lithology Logs for selected Dixie Valley Wells were provided by Al Waibel with the permission of Terra-Gen Power.

[2] Geothermal consultant and member of Project Peer Review committee

[3] A detailed description of all the assumptions used in the cross-sections can be found in Appendix 12.

[4] A total of eight cross-sections through the Dixie Valley Geothermal Wellfield area can be found in Appendix 12.

[5] Southern Methodist University

[5] Nevada Bureau of Mines and Geology

Table 15-4. Lithology Parameters

Major Recognized Lithologic Units

Lithcode	**Description**
Air	There is almost two kilometers of relief in the project area, so all cells above the surface are given the designation "air".
Q-Tbf	This represents all Tertiary to Quaternary valley-fill sediments above the Miocene Basalt (Tmb).
Tmb	Overlying the Mesozoic section are Tertiary volcanics, with the Miocene basalt being the thickest single unit in the Stillwater Range and under the valley. Therefore, the Tmb is considered the dominant mechanical unit in these locations. Further east in the Clan Alpine Range, the Oligocene tuffs are far thicker and may dominate there.
Kgr	Cretaceous and possibly early Tertiary granodiorite which outcrops at edges of ranges (west and east side of Stillwater Range, west side of Clan Alpine). Granite is reached in some boreholes below the valley-fill within the footwall block of encountered faults.
Jz	The Jurassic Aulacogen includes a variety of keratophyric intrusive rocks, mafic extrusives and some marine sediments such as the Boyer Ranch Quartzite. From a mechanical standpoint these are grouped into a single, strong unit.
Tr	Triassic sediments are varied, consisting of mostly meta-sediments including shales, limestones and phylites and considered to be the autochthon into which the Jurassic rocks were thrust into and over. A Paleozoic section is not included as it only occurs in NE corner of Project Area.

Lithology Dependent Assigned Parameters

LithCode	density	strength	internal friction	EGS Favorability (0-1)
Air	0	0	0	0
Q-Tbf	1.3	1	0.5	0
Tmb	2.5	100	0.7	0.6
Jz	2.6	400	0.8	0.7
Tr	2.4	30	0.6	0.4
Kgr	2.5	230	1.4	0.8

Notes:

LithCode represent the abbreviation for the lithologic unit that encompasses the majority of a given cell.

Density values are estimated from standard samples. TAMU results will allow for more precise measures.

Strength is uniaxial compressive strength (Mpa) for standard samples.

EGS Favorability of Rock is qualitatively assigned based on field excursion by Cladouhos and Callahan.

-- Other qualitative parameters considered include fracturing, rock strength, and variability of a litho-unit.

Other parameters

Value	Data Quality	Description
0	no lithology	no data
0.3	Soft	Geologic educated guesses, usually shown with question marks on geologic cross sections
0.5	Semi-soft	Determined from geologic cross sections, geologic inference, and stratigraphic column thickness
0.8	Medium Hard	includes seismic data, and projection from cells within 1 km.
1	Hard	Hard data includes surface outcrops, and well data. In a 500x500 m grid, this is not considered achievable due to variability of lithology in the grid block

Note: Generally the uncertainty is considered to vary smoothly and gradually. So that if one cell is Medium Hard (0.8), then the adjacent cells, which obtains information from the Medium hard cell would be 0.7.

Table 15-5. Well Statistics Parameters

This sheet explains all the parameters in reference to Dixie Valley wells. A data file with all the available well data including hard data (well logs, temperature profiles, geochemistry) and modeled data (Gravity, Magnetics, Seismic, MT) in reference to well location was compiled for use in a geostatistical analysis (see Appendix 16b). The geoscience data was gridded along depth slices every 0.5km starting at the surface, around 1km above sea level (asl) and ending at -3km asl. The trust (confidence) of the data is included where applicable, highlighted light orange, and used for the geostatistical analysis and EGS Favorability Mapping.

🟥	Trust (Confidence) Value for the derived data in that specific cell (depth) ranging from 1 to 5.

Trust Value	Description
5	Hard Data (measured in wells)
4	Strongly Inferred Data, within 0.5km of hard data
3	Weakly Inferred Data, within 1km of hard data
2	Interpolated/Extrapolated Data, more than 1km from hard data point
1	No Data available

1. **Well:** The well name is as indicated and in reference to section number.
2. **Type:** Wells were divided into the following classes; Injector, Producer, Sub-Commercial, and Other. Other was used if the well type was unknown.
3. **Location:** X and Y are the coordinates of the well at the surface in latitude and longitude. Z is the elevation in meters at the surface (KB).
4. **Depth:** Well were divided into depth intervals from 1km asl (surface of Dixie Valley) to -3km asl in 0.5km increments.
5. **Lithology:** Well Lithology as reported in the literature, well logs, etc. that occurs at the identified horizontal slice (km above sea level). The following table divides the lithology into seven stratigraphic units.

Unit	Description
Tbf	Basin-filling sediments including lowermost tuffaceous sediments.
Tmb	Miocene basalt, aka Table Mountain Basalt.
Tv	Oligocene silicic volcanics, overlying lacustrine sediments, and underlying volcaniclastics.
Jbr	Jurassic Boyer Ranch quartzite
Jz	Jurassic Humboldt Igneous group
Tr	Triassic metasediments
Kgr	Cretaceous granodiorite

6. **Temperature: Measured** temperature in degrees Celsius extracted from the literature and Temp-Depth profiles (Blackwell et al., 2005).
7. **Modeled Temp:** Temperature in degree Celsius derived from the modeled temperature along the cross-sections.
8. **Vp-seismic:** P-wave velocity (km/sec) modeled at the University of Nevada Reno and derived from previous velocity modeling.
9. **MT:** Resistivity in ohm-m derived from Magneto-telluric data along three wellfield arrays (N,C,S).

*note. The MT data along Array C in the location of the Section 7 producing wells was applied to all the wells in this section.

10. **Grav_Mag:** Modeled Combined Gravity-Magnetic inferred lithology units

Unit	Description	Density (g/cm^3)	Magnetics (emu/cm^3)
Tbf	Basin-fill	2.445	-
Ja	Jurassic arenite	2.56	-
Jv	Jurassic volcanics (rhyolite)	2.47	-
Jg	Magnetized Jurassic mafic rocks	2.876	0.004
Tr/Kgr	Tr meta-seds and basement	2.88	-

11. **Stress Parameters:** stress parameters derived from an AltaRock Energy Inc. generated stress model of Dixie Valley using Coulomb 3.1 (see Appendix 13). ***CSC*** (Coulomb Stress Change) on a given fault/fracture due to slip constraints on a number of source faults. Positive CSC infers failure is promoted, while negative CSC values infer failure is inhibited. ***Dilation:*** expected dilatation on fault/fracture due to CSC and model constraints. Positive values infer fault is open (unclamped), while negative values (compression) infer fault is closed (clamped).
12. **VertStress:** Vertical Stress (bars) calculated based on the depth and density of overlying rocks.
13. **Productive (Hydrothermal):** 1 infers the referenced cell (depth) is capable of geothermal injection, production (permeable), or sub-commercial. 0 infers the cell (depth) is not hydrothermal.
14. **Faults Present:** Fault zones identified in the well logs (1 = fault present at the corresponding depth interval).

Table 15-6. Seismic Parameters

The baseline seismic parameters are derived from a University of Nevada Reno generated model that integrated the OPTIM velocity modeling results along the seismic reflection profiles with other regional studies and general crustal-scale tomography. Values were provided for pre-determined 500m by 500m cells up to a 5km depth within the Wellfield Calibration area and along key wellfield cross-sections lines. A "trust" factor was also included to give the SME opinion on the confidence in the model with a particular cell.

The seismic model includes 5 parameters:

1. Vp = P-wave velocity in km/s
2. Vs=S-wave velocity in km/s
3. Density (RHO) in g/cm2
4. P-wave Qp attenuation factor
5. S-wave Qs attenuation factor

"Trust" factor: Confidence of the Baseline Data

The trust factor is 0.9 for the models with highest resolution (Optim reflection lines) and 0.01 for the general models. Regional models are given a "trust" factor from 0.2 to 0.5.

Model derivation description

1. The models in Appendix 2, Tables 3 and 4 were used to create an integrated model for the study area.

2. We used algorithms written in Matlab. A set of depths of interest were chosen for all models. Each model was stored into a Matlab structure. Each structure includes the model reference, the model area (which is a square oriented North-South, East-West), and the parameter model.

3. The parameter model matrix consists of seven columns: depth, P velocity in km/s, S velocity in km/s, density (g/cm3), P and S attenuation factors Qp and Qs and a "trust" factor, described below. "No information" is marked by the parameter value set to -99.

4. The "trust" factor ranges from 0 to 1 and is, for example, set by the analyst up to 0.9 for the Optim reflection/refraction lines and is set to 0.01 for general and non-local models. Using the "trust" parameter, seismic lines and local data are given higher weights than the general model weights.

5. A "slack" factor for each model represents a chosen extension of the model area in all directions. The larger is the "slack" parameter, the smoother is the model. Because of their 25-50 km resolution, the UNR models have a 0.01 trust value.

How is a model at one location (lat, lon) extracted?

The user inputs the point coordinates and the code estimates a model for that point, with parameter value variations as a function of depth. To estimate the parameter values (for example Vp) at each point in space and at each depth, the program finds all the models which include the respective point. Next, it collects all the Vp values, together with their "trust" values at each depth. The resulting P-velocity at the respective point and depth is a "trust" parameter weighted mean, after the "-99" (no data) estimates are discarded. Sixty-four independent models and the UNR model are currently used for the integrated model, including all the information in the study area collected so far. Each parameter value is independently estimated, none of the parameter values are derived using an equation from the other parameter values.

Resolution

For the 0.5 km grid exercise,Vp has low-enough resolution precisely along the Optim lines, if the "slack" parameter is 0.005 (~0.5 km). The slack parameter, however, for the current "smoothed" models is 0.03 degrees. That means the "method" error is ~ 0.03 deg, which is actually larger than the grid size. The reason the "slack" was empirically chosen 0.03 is to extend the Optim models to points in the vicinity and to avoid as much as possible having to use, due to lack of data, an unrealistic parameter value (belonging to a world-wide model). All the lines and the slices have been calculated using this code. Outside the lines, Vp has ~ 25 km resolution. Vs has ~ 25-50 km resolution, and so do all the other variables.

Seismic Parameter	Description
Vp	derived from Optim model (Anonymous, 1998) reflection lines (highest resolution of around 0.5 km)
Rho	calculated from general earth model, regional studies (Abbott and Karlin) and independent of measured rock densities
Vs	uses a determined ratio factor of 1.6 for relationship with Vp, general earth model (low res.)
Qp, Qs	based on general relationships (very low resolution)

Table 15-7. Joint Gravity and Magnetics Modeling

Summary

The complete Bouguer anomaly gravity data, PACES gravity data and the HELIMAG aeromagnetic total field anomaly data were jointly modeled in along five lines labeled A-A' to F-F' in the geothermal area to create a 2 ½ D geophysical model consistent with the surface geology and well data. Lines C-C' through F-F' are perpendicular to the strike of the Stillwater Range and the Dixie Valley range-bounding fault. Lines A-A' and B-B' are parallel to the range. It was not possible to model the magnetics of the range- parallel line B-B' because of 3-D effects due to the extensive Jurassic section exposed in the southeastern part of the range.

Method

Gravity modeling was done using the GM-Sys module of the Oasis Montaj program from Geosoft Inc. Measured gravity models of unknown shape were forward modeled by trial and error adjustment of density and polygon vertices. Once the fit was considered close, XZ positions were optimized using inverse methods. The objective was to minimize the RMS error between observed and computed values. A fit was considered acceptable if the misfit F was less than 1% (F=100*RMS error/profile gravity data range). As described in the GM-Sys manual, 2-D models may be visualized as a number of tabular prisms with their axes perpendicular to the profile; blocks and surfaces are presumed to extend to infinity in the strike direction. 2¾-D modeling, as implemented in GM-SYS, allows the prisms to be truncated at some distance in the plus and minus strike directions (± Y). It also allows the strike direction to be skewed relative to the profile azimuth. The methods used to calculate the gravity and magnetic model response are based on the methods of Talwani et al., 1959, and Talwani and Heirtzler, 1964, and make use of the algorithms described in Won and Bevis, 1987. Two-and-a-half dimensional calculations are based on Rasmussen and Pedersen, 1979. The GM-SYS inversion routine utilizes a Marqardt inversion algorithm to linearize and invert the calculations (Marqardt, 1963). Gravity and magnetics models are non-unique, i.e., several model families can be created to match the data. It is up to the interpreter to assess whether the model(s) are geologically reasonable.

Model Parameters and Constraints

Basin-fill Density

1. Density contrasts, not absolute values are what control the gravity signature
2. Available well lithologies that defined the known basin depth were used to test densities for the basin-fill
3. The final basin fill density of 2.445 gm/cc was selected based on fitting the model to the observed basin fill depth in well 62-21 on line E-E'. Independent fits of lines D-D' and F-F' show basin fill depth are consistent with other wells in the area.
4. In some of the lines, it was necessary to introduce a surficial (<100 m) low density layer of D ~1.5-1.8 gm/cc to account for very short wavelength gravity variations. Likely representing the vadose zone or alternatively, lake and playa sediments.

Bedrock Density

1. Determined by modeling the outcropping bedrock on the eastern flank of the Stillwater Range which include Jurassic gabbros, Jurassic volcanics, and Triassic sediments.
2. A density of D=2.876 gm/cc. was found to provide the optimal fit to the slope of the CBA, and this value, which is typical of mafic volcanic rock was adopted for the rest of the lines.
3. A slightly reduced density of 2.4 to 2.5 gm/cc was proven necessary to model some near surface rocks in the Stillwater Range that are classified as rhyolites or mixed clay/limestone/arenites.

Regional Trend

1. Effects of removing a slight NW/SE regional trend was tested on the gravity models
2. The net effect was to slightly deepen the basins, but no significant changes were observed to the locations of the basin walls or the positions of postulated faulting.

Magnetization

1. Models with magnetizations of M=0.003 to M= 0.005 emu/cc yielded acceptable fits.
2. Positively magnetized units were assumed in the modeling due to the signature of rocks in the Stillwater Range that required positively magnetized bodies, prominent subsurface anomalies (positive highs) implying buried normally magnetized bodies, and the dominant positive magnetic field during the Jurassic.
3. Ambient field directions of inclination = 64° and declination = 0 were used in the modeling.
4. Susceptibility rather than remanence controls the magnetization.
5. A value of M=0.004 emu/cc was found to be optimal in modeling the magnetic signature of the Jurassic volcanics in all of the profiles.
6. The magnetic anomaly data can be successfully modeled with a single magnetic Jurassic mafic rock unit. The magnetic modeling is very sensitive to the shape and location of the individual blocks as well as the interaction between blocks.

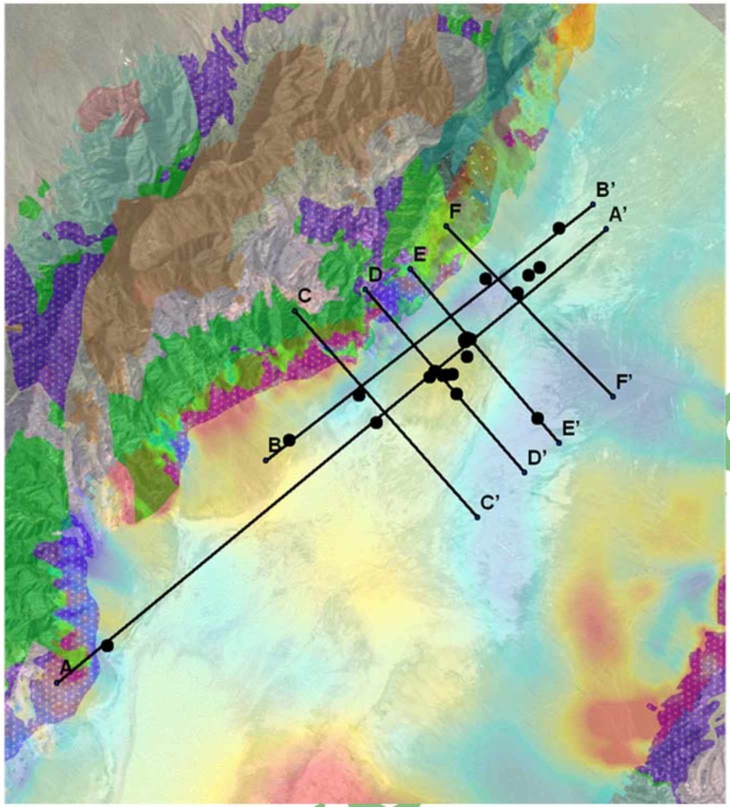

Location of modeled lines A-A' through F-F'' superimposed on the HELIMAG total magnetic field anomaly, the state geologic map and a satellite terrain map. Black dot are locations of geothermal wells. Purple and deep red colors are Jurassic gabbroic rocks (Jg), green colors area are Jurassic mafic volcanics (Jvb), and brown colors are Cenozoic volcanics, mostly basalts. Modeled Lines E and F are shown below.

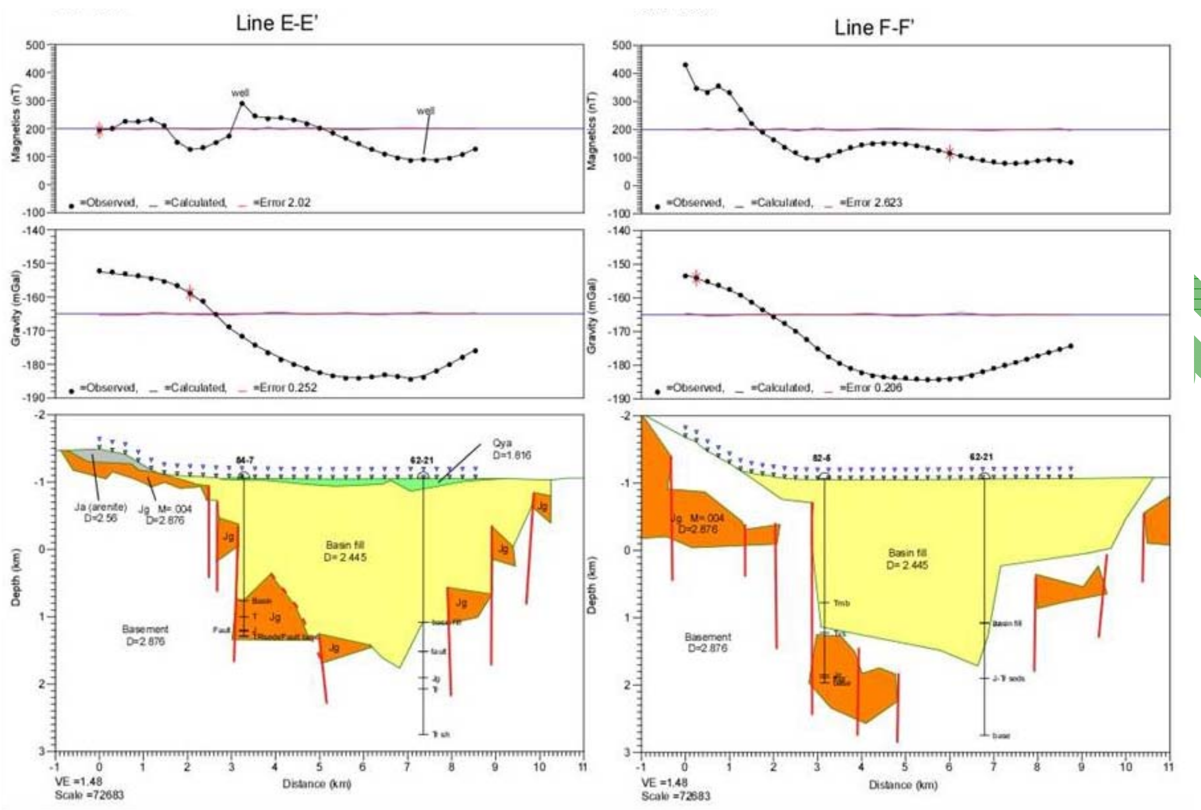

Joint gravity and magnetic model of lines E-E' and F-F'. Fits of gravity and magnetic profiles are <1%. Postulated faults are shown in red. Surfaces are basin fill (yellow, D=2.445 gm/cc); Jurassic mafic volcanics (orange, D=2.876 gm/cc, M=0.004 emu/cc); basement (white, D=2.876 gm/cc, M=0 emu/cc); lower density arenites or rhyolites (grey, D=~2.5 gm/cc, M=0 emu/cc).

Table 15-8. Magnetotellurics (MT) Modeling

A new generation MT-array system has been applied to three profiles over the Dixie Valley thermal area (see figure below). This study described in Wannamaker et al. (2007) is defined as state-of-the-art MT array measurements in contiguous bipole deployments across the Dixie Valley thermal area that have been integrated with regional MT transect data and other evidence. The modeling techniques can resolve the resistivity along the 2-D profiles at depth. Three profiles (N, C, and S) extend through the geothermal system, correlate geographically with the wellfield cross-sections and were used to quantitatively and quantitatively compare with the other geoscience data. The purpose of the MT survey in Dixie Valley was to (1) resolve the complex structural setting, (2) delineate fault zones which have experience fluid flux as indicated by low resistivity, (3) infer ultimate heat and fluid sources for the thermal area, and (4) investigate the capability of well-sampled electrical data for resolving subsurface structure.

Parameters

1. Contiguous bipole deployments across three arrays (N, C, and S).
2. Inversion techniques allow for higher resolution and account for 3-D effects.
3. Stand-alone MT soundings at one or both ends for local background control
4. Additional five-channel MT soundings to the SE end of each profile for improved aperture.
5. Array C integrated with regional transect data has a resolution to 10km (depth)

Array N

1. Derived from 60 array MT sites taken with contiguous E-field bipoles
2. Three stand-alone MT sites at the SE end.
3. Resolution to 4km depth
4. Extends through the northern producing area, 38-32 and Senator Fumaroles.

Array S

1. Dense MT array line plus three stand-alone MT sites to the SE.
2. Resolution to 4km depth
3. Extends through the hot and dry wells in the DVPP

Array C

1. 120 dense MT array measurements and 13 appended wideband MT sounding
2. Integrated with regional transect data
3. Resolution to 10km depth
4. Extends through the main producing area and 62-21 in the valley

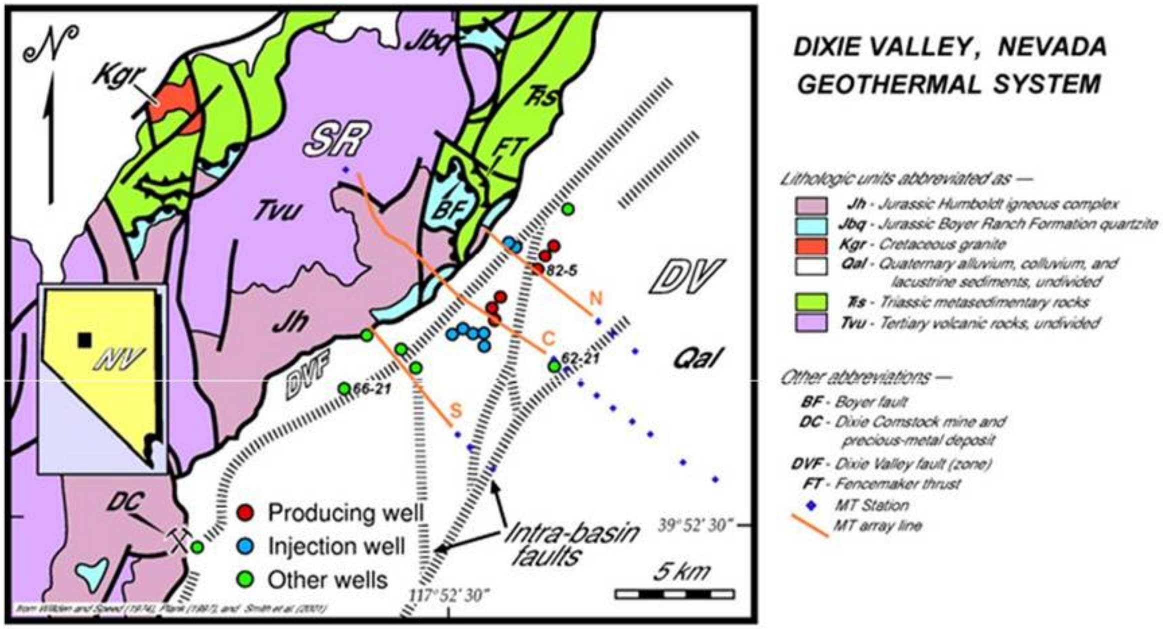

from Willden and Speed (1974), Plank (1997), and Smith et al (2001)

Simplified geologic map of the Dixie Valley (DV)-Stillwater Range (SR) area surrounding the Dixie Valley thermal field. Orange-brown lines are the MT profiles lines (see text) Lines are labeled N (north), C (central), and S (southern). Blue diamonds are five-channel MT stations added to extend profiles across the valley. Original figure courtesy of Jeff Hulen.

Table 15-9. Thermal Modeling

Thermal Models are shown as 50°C isocontours included on the major cross-sections (Appendix 12). A detailed description of assumptions used within the thermal cross-sections can also be found in Appendix 12. Using the thermal cross-sections and well data, an AltaRock thermal model was generated in the Wellfield Calibration Area in order the construct the EGS Favorability Maps. This model was derived from the well data, thermal cross-sections, and interpolations between the cross-sectional data.

Parameters

1. Modeled in degrees Celsius with 50°C contours from 100°C to 250°C
2. Used temperature measurements in available wells, temperature gradient holes (TGH) and fumaroles
3. Extracted temperature in incremental depths from T-D curves
4. General convective trend and extrapolated thermal conditions away from the wells were based on unpublished conceptual geothermal sections from Blackwell.
5. Assumes the range-bounding and piedmont faults are the main thermal-bearing structures in the DVFZ.
6. No temperature data beneath the Stillwater Range
7. Temperatures within Dixie Valley away from the DVFZ are poorly constrained

Cross-Sections

The table below shows the thermal data available per cross-section.

Section	Orientation	Fumarole	TGH	Well[1]
A-A'	SW-NE			**45-14**, **62-23A**, SWL-3, 74-7, **82-5**, **45-33**
B-B'	SW-NE			**66-21**, **36-14**, 45-5, **38-32**, **45-33**, **76-28**
C-C'	NW-SE	X	H-1	53-15, **36-14**, **62-23A**
D-D'	NW-SE			SWL-2, **52-18**, 65-18
E-E'	NW-SE			74-7, 76-7, **62-21**[2]
F-F'	NW-SE	X		**38-32**, 45-5, **82-5**
G-G'	NW-SE		SR-3	38-32, 37-33, 28-33
H-H'	NW-SE			**76-28**

1. Bolded wells have a T-D curve extracted from Blackwell et. al. (2005).
2. 62-21 was used to constrain temperatures in Dixie Valley for D-D' and F-F'.

Gridded Mapview Model

The expected temperature of the Wellfield Calibration Area at 12 different depths (1.5km to -4km above sea level at 0.5km increments) was modeled based on the available well data (hard measurements), thermal modeling along cross-sections (inferred) and interpolated temperatures between the modeled section lines. The thermal data was coded based on the type of data. Areas of elevated temperatures occur along the range-front fault at depth (36-14) and along the piedmont structure, consistent with recent interpretations of the thermal regime. The major constraint to the model is the lack of actual temperature measurements away from the wellfield and the reliance on inferred and interpolated data. Regardless, the Wellfield Calibration Area is the only portion of the EGS Study Area where any thermal data at depth is available.

Temperature-Depth Curves

1. T-D curves available for the following wells: 52-18, 62-21, 45-14, 66-21, 62-23A, 36-14, 76-28, 38-32, 82-5 and 45-33.
2. T-D curves represent equilibrium conditions except in 36-14, 66-21 and 45-14.
3. 66-21 and 45-14 have weak artesian flow.
4. 36-14 data below 2600m were derived from Horner-type extrapolations at a series of different BH depths, while at shallower depths the curve is based on more suspect extrapolations, as the upper portion of well was quite far from thermal equilibrium.

Table 15-10. Coulomb Stress Modeling

Overview

Coulomb 3.1 can calculate strain and Coulomb Stress Change (CSC) on a receiver fault (RF) due to the differing slip on a number of source faults (SF) in order to determine whether failure on the RF is promoted or inhibited. The program assigns the RF a specified strike, dip and rake and assumes that the RF exists within each grid cell. Coulomb then calculates and plots the strain or CSC value at that location. A first test, referred to as Scenario 1, reproduced the model from Wesnousky et. al. (2003) that broke up the slip into three sections based on Holocene ruptures namely, slip along the Dixie Valley Fault (1954), slip along the Pleasant Valley Fault (1915) and the lack any slip within the Stillwater Seismic Gap. This model assumes only a single range-bounding fault with a moderate dip (see figure 7 of main report).

Modeled Parameters

Coulomb Stress Change (CSC): The expected change in stress (+/-) on a receiver fault (3 options) in a given cell due to slip constraints on a number of pre-determined source faults.

Dilatation: The expected dilatational strain on a receiver fault (3 options) in a given cell due to slip constraints on a number of predetermined source faults.

Scenario 1

This first scenario replicated the stress analysis from Caskey et al. (2000) study using the same slip constraints.

Scenario 2

This second scenario builds on the replicated model (Scenario 1) and assumes that the whole Stillwater Seismic Gap (SSG) did rupture in the "Gap" earthquake. It also takes into account other significant structures such as piedmont faults, north-trending faults and other intrabasin structures. The Dixie Valley Fault (DVF) is still one section as is the Pleasant Valley Fault (PVF), while the SSG is broken up into three sections with different orientations and slip constraints. The three explored types of receiver faults (RF) are (a) a synthetic normal fault subparallel to SGS dipping 70oE, (b) antithetic normal fault subparallel to SGS dipping 70oW, and (c) normal fault oriented roughly N-S dipping 70°W.

Slip Parameters

- 1915 Pleasant Valley Earthquake along PVF
    - Max vertical/horizontal displacements are **5.8m/2m**, respectively (Wallace, 1980; 1984)
    - Dip varies from **47-65^{o} NW** (QFFDB)
- 2-2.5 ka “Gap” Earthquake along SGS
    - Max vertical displacement of 5m (Caskey and Ramelli, 2004)
    - Dips to the SE, but no angle reported by QFFDB; Blackwell et al. (2005) suggest dips 70-80° SE down to at least 3km
- *1954 Dixie Valley Earthquake along DVF*
    - Max vertical displacement of **2.8m** (Caskey et al., 1996)
    - Dip varies from **30-80^{o} SE** (QFFDB)

Summary of Model

A program called Coulomb 3.1 (http://earthquake.usgs.gov/research/modeling/coulomb/) was used to calculate strain and stress changes on receiver faults caused by slip on source faults in the region surrounding the Dixie Valley Geothermal Field (DVGF). Source faults of interest in DV include the 2-2.5 ka Stillwater Seismic Gap (modeled here as 3 segments), the 1915 Pleasant Valley Fault, and the 1954 Dixie Valley Fault.

Receiver faults of interest are normal faults synthetic to the SSG (Syn_70E), antithetic to the SGS (Anti_70W), and oriented roughly N-S (N-S_70W). Coulomb 3.1 resolves the strain and stress changes caused by slip on the source faults onto a specified receiver fault in each grid cell. For each of the 3 receiver faults, we have 2 output files ("strain_xx.cou" & "dcff_xx.cou") at 11 depth slices (from 0.0 - 5.0 km, w/0.5 km spacing), for a total of 66 output files (Excel-compatible). Depths are given within the filenames, i.e. "strain_3.5.cou" contains strain values at 3.5 km depth. Note that our depth datum is roughly the average elevation of surface faults in Dixie Valley, or ~1100 m (+/- 100 m).

Model Boundaries and Grid Parameters

Model boundaries:

min. lat = 39.3300000
max. lat = 40.6800000
min. lon = -118.3300000
max. lon = -117.4000000
zero lat = 39.3300000
zero lon = -118.3300000
(ORIGIN = zero lat, zero lon)

Grid Parameters (in km):

Start-x = 0.0000000
Start-y = 0.0000000
Finish-x = 79.2114774
Finish-y = 150.1131510
x-increment = 0.5000000
y-increment = 0.5000000

Output Data Files

Strain Output

1	2	3	4	5	6	7	8	9	10
x	y	z	exx	eyy	ezz	eyz	exz	exy	dilatation

1. The first 3 columns are the x, y, and z coordinates of the gridpoint (km from origin).
2. The next 3 are the principal strain values (extension is +).
3. The next 3 are the shear strain values (right-lateral is +).
4. The last column is the dilatational strain value (dilatation is +).

Coulomb Stress Change (CSC) Output

The dcff_xx.cou files "dcff" stands for change in Coulomb Failure Function $\Delta\sigma f = \Delta ts + \mu'\Delta\sigma n$, where: $\Delta\sigma f$ = change in Coulomb failure stress; Δts = change in shear stress; μ' = effective coefficient of friction on fault; and $\Delta\sigma n$ = change in normal stress) contain 6 columns:

1	2	3	4	5	6
x (km)	y (km)	Z (km)	Coulomb (bar)	Shear (bar)	Normal (bar)

1. The first 3 columns above are the x, y, and z coordinates of the gridpoint (km from origin).
2. The last 3 columns above are the Coulomb failure stress change (+ promotes failure), shear stress change (right-lateral is +), and normal stress change (unclamping fault is +)

Table 15-11. Geochemistry

Geochemical data was provided by Mack Kennedy of Lawrence Berkeley National Laboratory (LBNL) and derived mostly from the comprehensive geochemistry database within Goff et al. (2002). The data was provided along the gridded cross-sections A through F where the occurrence of deep wells, temperature gradient holes, fumaroles, and springs coincided with the cross-section lines. The data was placed in a 500m by 500m cell and depths were estimated based on SME. Only parameters that were considered potential geothermal indicators were provided. These parameters are listed below. Due to the limited data and point source nature, this data was analyzed, included in the baseline database, but was not used in the formulation of EGS Favorability Maps.

Parameters	Description
Si	Silica (ppm)
Cl	Chloride (ppm)
Bi-Carb-Cl	Ratio of Bicarbonate to Chloride
F[^{4}He]	Fractionation of Helium (ppm)
R/Ra	Ratio of ^{3}He/^{4}He

Example of gridded geochemical data for silica (ppm) along Cross-Section B-B"

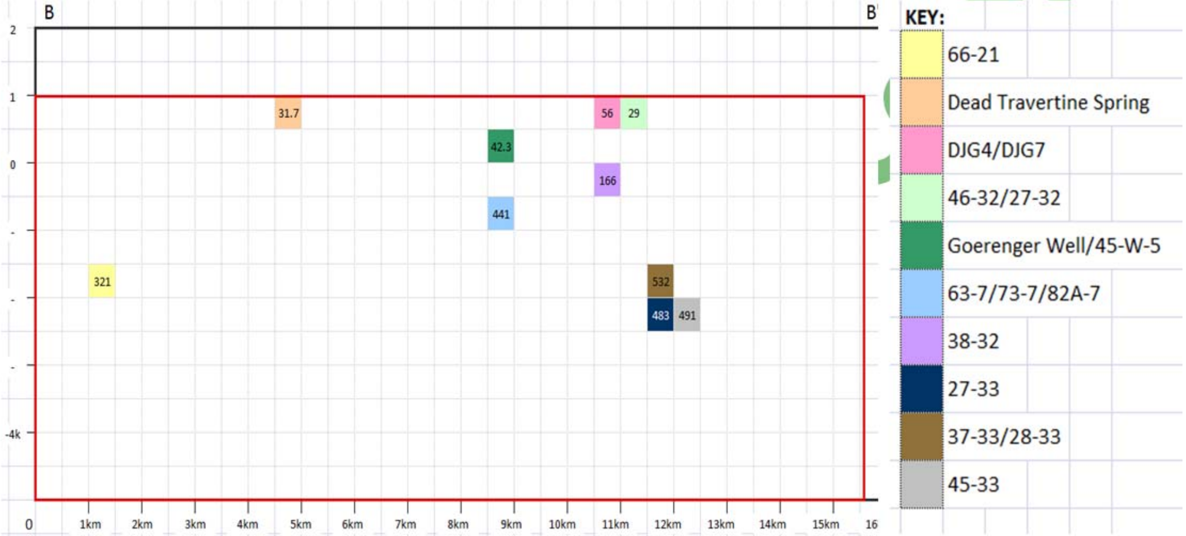

APPENDIX 16a

SECTION DATA FOR GEOSTATISTICAL ANALYSIS

Table of Contents

List of Tables

1. INTRODUCTION

The data shown in this appendix has been organized for the geostatistical analysis. It includes all the available cross-sectional data which is measured (hard data from well logs), modeled, and inferred as well as trust values identified by the individual subject matter experts (see Section 1.4 of the main body of the report). The data is organized by cross-section name (C, D, E, and F) and the data shown corresponds to 500m by 500m cells within the sections . The average elevation of each cell occurs as the midpoint, from 1.25km above sea level (asl) to a depth of -3.75 km asl, in 0.5km increments. The individual parameters included in the data set and a brief description are presented below (Table 16a-1) and in Section 2 of this appendix. The assigned trust value (TV) for applicable data, or the confidence/reliability of a specific data point based on the proximity to a hard data point or limitation of the geophysical model is used for the geostatistical analyses and paired EGS Favorability-Trust Maps. A summary of the trust values can be found in Table 16a-2.

Table 16a-1. Parameters included in the cross-sectional data set. Column Number and Column Identifier correspond to the number and column heading for the data presented.

Column ID No.	Column Identifier	Description of the Data
1	Cross-Section	Refers to the specific wellfield cross-section (CC, DD, EE, and FF) that the data is derived.
2	Domain	The cross-sections have been divided into three geographic/geologic domain and within Dixie Valley (**Valley**).
3	Location	X and Z are the lateral and vertical coordinates of a specified 500m by 500m cell numbered along the cross-section, respectively; Elevation refers to the average (mid-point) elevation of the referenced cell in km asl.
4	Lithology	Subsurface formations identified in the cross-sections and associated trust value as identified by the Geology Task Leader. All geologic formations in the area were divided into seven stratigraphic units. Table 3 (below) provides a summary description of each of the formations encountered.
5	EGS Fav[1]	*EGS-Fav* refers to a pre-determined Engineered Geothermal System (EGS) favorability value for each of the seven stratigraphic formations. The assigned lithologic parameters are outlined in Table 4 (below).
6	Friction[1]	Value of Internal Friction (unitless) for the specified rock type.
7	Certainty[1]	The certainty or confidence in the model predicting the correct rock type. This was defined early in the modeling procedure and differs slightly from the trust values (see Appendix 15, Table 15-4).
8	Density[1]	Density value (g/cc) as estimated from standard samples.
9	Strength[1]	Strength is uniaxial compressive strength in Mpa for standard samples.
10	Stress Parameters: FracIntens	*FracIntens* refers to a calculated parameter Fracture Intensity which depends on the number of faults present in a given cell, divided by the cell area, and does not include an associated trust value. This parameter was determined by the Geology Task Leader.
11	Stress Parameters: VertStress	*VertStress* refers to the calculated parameter Vertical Stress. This value was calculated based on the depth and density of overlying rocks and includes a trust value, given a neutral value of 2.5. Modeled data and trust value as determined by the Geology Task Leader.

Table 16a-1. Parameters included in the cross-sectional data set. Column Number and Column Identifier correspond to the number and column heading for the data presented.

Column ID No.	Column Identifier	Description of the Data
12	Coulomb Stress Parameters	Modeled coulomb stress change (CSC), dilatation and the associated trust value for the stress parameters as determined by the Geology Task Leader. The data was given a neutral trust value of 2.5.
13	Temperature	Modeled temperature (° Celsius) along the major wellfield cross-sections (see Plates 1 and 2) and trust value (Table A) as identified by the AltaRock-generated thermal model.
14	Seismic Parameters	*Vp* refers to a modeled primary-wave velocity value (km/sec), while *Vs* refers to shear-wave velocity (km/sec). The trust value (Table 3) pertains to both parameters as identified by the seismic task leader.
15	Gravity-Magnetics Lithology	Subsurface formations as determined by the joint gravity and magnetic modeling along the wellfield cross-sections and their associated trust values as determined by the gravity and magnetics Task Leader. Table 5 (below) provides a summary of the lithology units identified by the combined Gravity and Magnetics.
16	Resistivity (MT)	Modeled magnetotellurics (MT) as resistivity (ohm-m) and trust value as identified by the MT Task Leader.

[1] **Columns** nos. 5-9 refer to Assigned Parameters relating to Lithology derived from the Geology Task Leader. See Table 4 (below) for values in reference to lithology type.

2. Cross-sectional Data Summary and Legend

The data shown in Section 3 was developed as a data repository for the statistical anlysis of all the available cross-sectional data modeled along the wellfield cross-sections C-C', D-D', E-E', and F-F'. The data includes hard data (well logs) directly measured from wells that lie along the cross-sections, calculated parameters (vertical stress, lithology-dependent, etc.) and modeled data. Modeled data was either extracted from the vicinity of the cross-section lines (MT, seismic) or modeled along the indicated cross-sections (Grav-Mag, Stress). The trust (confidence) of the data is included where applicable, and used for the geostatisical analysis and EGS Favorability Mapping. Provided below is a description of the various geoscience parameters in Section 3.

Trust Value (TV): Conveys the confidence and/or reliability of derived data within a specific cell on a scale of 1-5, based on the proximity to a hard data point and/or limits of the geophysical modeling.

Table 16a-2. Description of Trust Value (1-5) assigned to the various data

Trust Value	Description
5	Hard Data (measured in wells)
4	Strongly Inferred Data, within 0.5km of hard data
3	Weakly Inferred Data, within 1km of hard data
2	Interpolated/Extrapolated Data, more than 1km from hard data point
1	No Data available

1. **Cross-Section**: Refers to the cross-section (CC, DD, EE, FF)
2. **Location**: refers to the location of the specified cell (500m by 500m) in the cross-section

Domain	The wellfield cross-sections have been divided into three geographic/geologic domains: Stillwater Range (**SR**), Dixie Valley Fault Zone (**DVFZ**), and Dixie Valley (**Valley**).
X	"X" (lateral) coordinate of the specified cell numbered along the cross-section
Z	"Z" (vertical) coordinate of the specified cell numbered along the cross-section
Elevation	Average elevation (km above sea level) or mid-point of a cell from 1.25 (cell from 1.0 to 1.5) to -3.75 (cell from -3.5 to -4.0).

3. **Lithology**: The lithology unit that encompasses the majority of the specified cell. See table that divides the lithology into seven stratigraphic units.

Table 16a-3. Summary Description of the seven major lithologic formations

Unit	Description
Q (QTbf)	Basin-filling sediments including lowermost tuffaceous sediments.
Tmb	Miocene basalt, aka Table Mountain Basalt.
Tv	Oligocene silicic volcanics, overlying lacustrine sediments, and underlying volcaniclastics.
Jbr	Jurassic Boyer Ranch quartzite
Jz	Jurassic Humboldt Igneous group
Tr	Triassic metasediments
Kgr	Cretaceous granodiorite

4. **Assigned Parameters-Lithology**: The following parameters were assigned to their respective lithologic unit.

EGS Fav	Engineered Geothermal System (EGS) Favorability Value (0-1), assigned qualitatively based on a field excursion.
Friction	Assigned value of Internal Friction of the rock.
Certainity	A qualitative measure of the certainity of the data point with regards to lithology (0-1).
Density	Density values (g/cc) are estimated from standard samples.
Strength	Strength is uniaxial compressive strength in Mpa for standard samples.

Table 16a-4. Assigned Lithlogy Parameters

label	density	strength	internal friction	EGS Fav.
Air	0	0	0	0
Tbf	1.3	1	0.5	0
Tmb	2.5	100	0.7	0.6
Jz	2.6	400	0.8	0.7
Tr	2.4	30	0.6	0.4
Kgr	2.5	230	1.4	0.8
Tv	2.4	75	0.7	0.4
Jbr	2.5	200	0.6	0.8

5. **Calculated Stress Parameters**: The following qualitative parameters were considered with relation to stress conditions.

FracIntens	Fracture Intensity: based on the cumulative fault length/cell area.
VertStress	Vertical Stress: lithostatic stress (bars) at the center of the cell base on depth and density of rock above.

6. **Coulomb Stress Parameters**: Stress Parameters derived from a ARE generated stress Model (2010) of Dixie Valley using Coulomb 3.1.

CSC	Coulomb Stress Change on a given fault/fracture due to slip constraints on a number of source faults. Positive CSC infers failure is promoted, while negative CSC values infers failure is inhibited.
Dilatation	Expected dilatation on fault/fracture due to the modeled CSC and model constraints. Positive values infer fault is open (unclamped), while negative values infer fault is closed (clamped).

7. **Modeled Temperature**: Average temperature (°C) within a specified cell derived from the modeled temperature along the cross-sections.
8. **Seismic Parameters**: Seismic parameters modeled at UNR were extracted from OPTIM reflection data, associated velocity modeling and general crustal models.

VP	P-wave velocity (km/sec)
VS	S-wave velocity (km/sec)

9. **Gravity-Magnetic inferred Lithology**: Lithology inferred by the combined gravity-magnetics model using the surface gravity (gm/cc) and magnetic (emu/cc) measurements.

Table 16a-5. Summary of Lithologic Units identified by the combined Gravity and Magnetics Modeling

Unit	Description	Density	Magnetics
Tbf	Basin-fill	2.445	-
Ja	Jurassic arenite	2.56	-
Jv	Jurassic volcanics (rhyolite)	2.47	-
Jg	Magnetized Jurassic mafic rocks	2.876	0.004
Tr/Kgr	Tr meta-seds and basement	2.88	-

10. **MT**: **Resistivity** in ohm-m derived from Magneto-telluric data along three wellfield arrays (N,C,S), see Wannamaker et al. (2007).

Table 16a-6. MT arrays inferred along the Cross-Sections

Array	Cross-Section
N	F-F'
C	D-D' and E-E'
S	C-C'

3. Dixie Valley Cross-Sectional Data

1	2	3			4		5	6	7	8	9	10	11		12			13		14			15		16	
Cross-Section	Do-main	Location			Lithology		Assigned Parameters: Lithology					Stress Parameters			Coulomb Stress Parameters			Temperature		Seismic Parameters			Gravity-Magnetics		MT (Resistivity)	
		X	Z	Ele-vation	Fm	TV	EGS-Fav	Frict-ion	Certain-ty	Densi-ty	Strength	Frac-Intens	Vert-Stress	TV	CSC	Dilatation	TV	° C	TV	Vp	Vs	TV	Lithology	TV	ohm-m	TV
CC	SR	1	3	-3.75	Kgr	1	0.8	1.4	0.3	2.5	230	0	146.51	2.5	-19.55	-4.48E-06	2.5			5.26	3.51	1.03	Tr/Kgr	4		
CC	SR	1	4	-3.25	Kgr	1	0.8	1.4	0.3	2.5	230	0	134.26	2.5	-19.67	-6.26E-06	2.5			5.23	3.50	1.07	Tr/Kgr	4		
CC	SR	1	5	-2.75	Kgr	1	0.8	1.4	0.4	2.5	230	0	122.01	2.5	-19.95	-8.06E-06	2.5			5.20	3.49	1.11	Tr/Kgr	4		
CC	SR	1	6	-2.25	Kgr	1	0.8	1.4	0.4	2.5	230	0	109.76	2.5	-20.41	-9.89E-06	2.5			5.16	3.48	1.15	Tr/Kgr	4		
CC	SR	1	7	-1.75	Kgr	1	0.8	1.4	0.4	2.5	230	0	97.51	2.5	-21.09	-0.0000118	2.5			4.67	3.44	1.17	Tr/Kgr	4		
CC	SR	1	8	-1.25	Kgr	1	0.8	1.4	0.4	2.5	230	0	85.26	2.5	-22.04	-0.0000138	2.5			4.67	3.31	0.94	Tr/Kgr	4		
CC	SR	1	9	-0.75	Kgr	2	0.8	1.4	0.5	2.5	230	0	73.01	2.5	-23.31	-0.0000158	2.5			5.13	3.15	0.70	Tr/Kgr	5		
CC	SR	1	10	-0.25	Tr	3	0.4	0.6	0.6	2.4	30	0	60.76	2.5	-24.96	-0.000018	2.5			5.10	2.99	0.70	Tr/Kgr	5		
CC	SR	1	11	0.25	Tr	4	0.4	0.6	0.7	2.4	30	0	49	2.5	-27.06	-0.0000204	2.5			4.23	2.68	0.83	Tr/Kgr	5		
CC	SR	1	12	0.75	Tr	4	0.4	0.6	0.7	2.4	30	0	37.24	2.5	-29.68	-0.0000228	2.5			2.79	1.66	0.96	Tr/Kgr	5		
CC	SR	1	13	1.25	Jz	5	0.7	0.8	0.8	2.6	400	0	25.48	2.5	-32.90	-0.0000255	2.5						Jg	5		
CC	SR	2	3	-3.75	Kgr	1	0.8	1.4	0.4	2.5	230	0	133.77	2.5	-19.12	-4.44E-06	2.5			5.26	3.51	0.96	Tr/Kgr	4		
CC	SR	2	4	-3.25	Kgr	1	0.8	1.4	0.4	2.5	230	0	121.52	2.5	-19.00	-0.0000061	2.5			5.23	3.50	1.00	Tr/Kgr	4		
CC	SR	2	5	-2.75	Kgr	1	0.8	1.4	0.4	2.5	230	0	109.27	2.5	-19.02	-7.79E-06	2.5			5.20	3.49	1.04	Tr/Kgr	4		
CC	SR	2	6	-2.25	Kgr	1	0.8	1.4	0.5	2.5	230	0	97.02	2.5	-19.20	-9.51E-06	2.5			5.16	3.48	1.08	Tr/Kgr	4		
CC	SR	2	7	-1.75	Kgr	1	0.8	1.4	0.5	2.5	230	0	84.77	2.5	-19.58	-0.0000113	2.5			4.74	3.44	1.17	Tr/Kgr	4		
CC	SR	2	8	-1.25	Kgr	1	0.8	1.4	0.5	2.5	230	0	72.52	2.5	-20.20	-0.0000132	2.5			4.73	3.31	1.12	Tr/Kgr	4		
CC	SR	2	9	-0.75	Kgr	2	0.8	1.4	0.5	2.5	230	0	60.27	2.5	-21.11	-0.0000152	2.5			5.12	3.15	1.08	Tr/Kgr	5		
CC	SR	2	10	-0.25	Tr	3	0.4	0.6	0.6	2.4	30	0	48.02	2.5	-22.37	-0.0000173	2.5			5.03	2.99	1.17	Tr/Kgr	5		
CC	SR	2	11	0.25	Tr	4	0.4	0.6	0.7	2.4	30	0	36.26	2.5	-24.04	-0.0000195	2.5			4.03	2.68	1.36	Tr/Kgr	5		
CC	SR	2	12	0.75	Tr	4	0.4	0.6	0.8	2.4	30	0	24.5	2.5	-26.21	-0.0000219	2.5			2.66	1.66	1.55	Tr/Kgr	5		
CC	SR	2	13	1.25	Jz	5	0.7	0.8	0.8	2.6	400	0	12.74	2.5	-28.98	-0.0000244	2.5						Jg	5		
CC	SR	3	3	-3.75	Kgr	1	0.8	1.4	0.5	2.5	230	0	133.77	2.5	-18.47	-4.41E-06	2.5	275	1	5.26	3.51	0.96	Tr/Kgr	4		
CC	SR	3	4	-3.25	Kgr	1	0.8	1.4	0.5	2.5	230	0	121.52	2.5	-18.11	-5.93E-06	2.5	265	1	5.23	3.50	1.00	Tr/Kgr	4		
CC	SR	3	5	-2.75	Kgr	1	0.8	1.4	0.5	2.5	230	0	109.27	2.5	-17.88	-7.48E-06	2.5	250	1	5.20	3.49	1.04	Tr/Kgr	4		
CC	SR	3	6	-2.25	Kgr	1	0.8	1.4	0.5	2.5	230	0	97.02	2.5	-17.78	-9.06E-06	2.5	250	1	5.16	3.48	1.08	Tr/Kgr	4		
CC	SR	3	7	-1.75	Kgr	1	0.8	1.4	0.6	2.5	230	0	84.77	2.5	-17.84	-0.0000107	2.5	225	2	4.74	3.44	1.17	Tr/Kgr	4		
CC	SR	3	8	-1.25	Kgr	1	0.8	1.4	0.6	2.5	230	0	72.52	2.5	-18.09	-0.0000125	2.5	200	2	4.73	3.31	1.12	Tr/Kgr	4		
CC	SR	3	9	-0.75	Kgr	2	0.8	1.4	0.6	2.5	230	0	60.27	2.5	-18.58	-0.0000143	2.5	150	3	5.12	3.15	1.08	Tr/Kgr	5		
CC	SR	3	10	-0.25	Tr	3	0.4	0.6	0.6	2.4	30	0	48.02	2.5	-19.37	-0.0000163	2.5	125	3	5.03	2.99	1.17	Tr/Kgr	5		
CC	SR	3	11	0.25	Tr	4	0.4	0.6	0.7	2.4	30	0	36.26	2.5	-20.52	-0.0000184	2.5	100	3	4.03	2.68	1.36	Tr/Kgr	5		
CC	SR	3	12	0.75	Tr	4	0.4	0.6	0.8	2.4	30	0	24.5	2.5	-22.12	-0.0000206	2.5	50	3	2.66	1.66	1.55	Tr/Kgr	5		
CC	SR	3	13	1.25	Jz	5	0.7	0.8	0.9	2.6	400	0	12.74	2.5	-24.26	-0.000023	2.5	50	3				Jg	5		
CC	SR	4	3	-3.75	Kgr	1	0.8	1.4	0.6	2.5	230	0	133.77	2.5	-17.58	-4.41E-06	2.5	275	1	5.17	3.51	1.39	Tr/Kgr	4		
CC	SR	4	4	-3.25	Kgr	1	0.8	1.4	0.6	2.5	230	0	121.52	2.5	-17.01	-5.75E-06	2.5	275	1	5.10	3.50	1.48	Tr/Kgr	4		
CC	SR	4	5	-2.75	Kgr	1	0.8	1.4	0.6	2.5	230	0	109.27	2.5	-16.53	-7.12E-06	2.5	260	1	5.03	3.49	1.57	Tr/Kgr	4	4000	4
CC	SR	4	6	-2.25	Kgr	1	0.8	1.4	0.6	2.5	230	0	97.02	2.5	-16.14	-8.54E-06	2.5	250	1	4.95	3.48	1.66	Tr/Kgr	4	3000	4
CC	SR	4	7	-1.75	Kgr	1	0.8	1.4	0.6	2.5	230	0	84.77	2.5	-15.88	-0.00001	2.5	250	2	4.70	3.44	1.77	Tr/Kgr	4	2000	4
CC	SR	4	8	-1.25	Kgr	1	0.8	1.4	0.7	2.5	230	0	72.52	2.5	-15.76	-0.0000116	2.5	225	2	4.68	3.31	1.76	Tr/Kgr	4	1000	4
CC	SR	4	9	-0.75	Kgr	2	0.8	1.4	0.7	2.5	230	0	60.27	2.5	-15.81	-0.0000133	2.5	175	3	4.88	3.15	1.76	Tr/Kgr	5	500	5
CC	SR	4	10	-0.25	Tr	3	0.4	0.6	0.7	2.4	30	0	48.02	2.5	-16.08	-0.0000151	2.5	125	3	4.85	2.99	1.84	Tr/Kgr	5	200	5
CC	SR	4	11	0.25	Tr	4	0.4	0.6	0.7	2.4	30	0	36.26	2.5	-16.63	-0.000017	2.5	100	4	4.03	2.68	2.07	Tr/Kgr	5	80	5
CC	SR	4	12	0.75	Tr	4	0.4	0.6	0.8	2.4	30	0	24.5	2.5	-17.55	-0.0000191	2.5	50	4	2.68	1.66	2.29	Tr/Kgr	5	100	5
CC	SR	4	13	1.25	Jz	5	0.7	0.8	0.9	2.6	400	0.1	12.74	2.5	-18.94	-0.0000212	2.5	50	4				Tr/Kgr	5		

Dixie Valley Cross-Sectional Data (continued)

1	2	3			4		5	6	7	8	9	10	11		12			13		14			15		16	
Cross-Section	Do-main	Location			Lithology		Assigned Parameters: Lithology					Stress Parameters			Coulomb Stress Parameters			Temperature		Seismic Parameters			Gravity-Magnetics		MT (Resistivity)	
		X	Z	Ele-vation	Fm	TV	EGS-Fav	Frict-ion	Certain-ty	Densi-ty	Strength	Frac-Intens	Vert-Stress	TV	CSC	Dilatation	TV	° C	TV	Vp	Vs	TV	Lithology	TV	ohm-m	TV
CC	SR	5	3	-3.75	Kgr	1	0.8	1.4	0.6	2.5	230	0	122.01	2.5	-16.44	-4.41E-06	2.5	275	2	5.17	3.51	1.39	Tr/Kgr	4		
CC	SR	5	4	-3.25	Kgr	1	0.8	1.4	0.7	2.5	230	0	109.76	2.5	-15.67	-5.55E-06	2.5	275	2	5.10	3.50	1.48	Tr/Kgr	4		
CC	SR	5	5	-2.75	Kgr	1	0.8	1.4	0.7	2.5	230	0	97.51	2.5	-14.97	-6.71E-06	2.5	260	2	5.03	3.49	1.57	Tr/Kgr	4	4000	4
CC	SR	5	6	-2.25	Kgr	1	0.8	1.4	0.7	2.5	230	0	85.26	2.5	-14.33	-7.93E-06	2.5	250	3	4.95	3.48	1.66	Tr/Kgr	4	4000	4
CC	SR	5	7	-1.75	Kgr	1	0.8	1.4	0.7	2.5	230	0	73.01	2.5	-13.76	-9.21E-06	2.5	250	3	4.70	3.44	1.77	Tr/Kgr	4	3000	4
CC	SR	5	8	-1.25	Kgr	2	0.8	1.4	0.7	2.5	230	0	60.76	2.5	-13.27	-0.0000106	2.5	225	4	4.68	3.31	1.76	Tr/Kgr	4	2000	4
CC	SR	5	9	-0.75	Kgr	2	0.8	1.4	0.8	2.5	230	0	48.51	2.5	-12.88	-0.0000121	2.5	200	4	4.88	3.15	1.76	Tr/Kgr	5	1000	5
CC	DVFZ	5	10	-0.25	Tr	3	0.4	0.6	0.8	2.4	30	0.2	36.26	2.5	-12.63	-0.0000136	2.5	150	4	4.85	2.99	1.84	Tr/Kgr	5	300	5
CC	DVFZ	5	11	0.25	Tr	3	0.4	0.6	0.8	2.4	30	0.2	24.5	2.5	-12.56	-0.0000153	2.5	125	4	4.03	2.68	2.07	Tr/Kgr	5	100	5
CC	DVFZ	5	12	0.75	Jz	4	0.7	0.8	0.8	2.6	400	0.2	12.74	2.5	-12.75	-0.0000171	2.5	100	4	2.68	1.66	2.29	Jg	5	200	5
CC	DVFZ	5	13	1.25			0	0	0.9	0	0	0	0	2.5	-13.29	-0.0000191	2.5	0								
CC	SR	6	3	-3.75	Kgr	1	0.8	1.4	0.6	2.5	230	0	122.5	2.5	-15.02	-4.41E-06	2.5	300	2	5.17	3.51	1.31	Tr/Kgr	4		
CC	SR	6	4	-3.25	Kgr	1	0.8	1.4	0.7	2.5	230	0	110.25	2.5	-14.11	-5.32E-06	2.5	275	2	5.10	3.50	1.39	Tr/Kgr	4		
CC	SR	6	5	-2.75	Kgr	1	0.8	1.4	0.8	2.5	230	0	98	2.5	-13.22	-6.25E-06	2.5	275	2	5.02	3.49	1.48	Tr/Kgr	4	3000	4
CC	SR	6	6	-2.25	Kgr	2	0.8	1.4	0.8	2.5	230	0	85.75	2.5	-12.36	-7.23E-06	2.5	260	3	4.95	3.48	1.56	Tr/Kgr	4	3000	4
CC	SR	6	7	-1.75	Kgr	2	0.8	1.4	0.8	2.5	230	0	73.5	2.5	-11.52	-8.28E-06	2.5	250	3	4.70	3.44	1.70	Tr/Kgr	4	3000	4
CC	SR	6	8	-1.25	Kgr	3	0.8	1.4	0.7	2.5	230	0.3	61.25	2.5	-10.70	-9.41E-06	2.5	250	4	4.67	3.31	1.78	Tr/Kgr	4	2000	4
CC	DVFZ	6	9	-0.75	Tr	3	0.4	0.6	0.8	2.4	30	0.4	49	2.5	-9.91	-0.0000106	2.5	225	4	4.85	3.15	1.87	Tr/Kgr	5	1000	5
CC	DVFZ	6	10	-0.25	Tr	4	0.4	0.6	0.9	2.4	30	0.3	37.24	2.5	-9.17	-0.0000119	2.5	200	5	4.82	2.99	2.02	Tr/Kgr	5	800	5
CC	DVFZ	6	11	0.25	Jz	4	0.7	0.8	0.9	2.6	400	0.2	25.48	2.5	-8.50	-0.0000134	2.5	150	5	4.04	2.68	2.30	Tr/Kgr	5	250	5
CC	DVFZ	6	12	0.75	Jz	5	0.7	0.8	0.9	2.6	400	0.2	12.74	2.5	-7.96	-0.0000149	2.5	100	5	2.78	1.66	2.54	Jg	5	50	5
CC		6	13	1.25			0	0	0.9	0	0	0.1	0	2.5	-7.62	-0.0000165	2.5	0								
CC	DVFZ	7	3	-3.75	Kgr	1	0.8	1.4	0.6	2.5	230	0.1	115.64	2.5	-13.34	-4.41E-06	2.5	300	3	5.17	3.51	1.23	Tr/Kgr	4		
CC	DVFZ	7	4	-3.25	Kgr	1	0.8	1.4	0.7	2.5	230	0.2	103.39	2.5	-12.32	-5.06E-06	2.5	290	4	5.10	3.50	1.32	Tr/Kgr	4		
CC	DVFZ	7	5	-2.75	Kgr	1	0.8	1.4	0.8	2.5	230	0.2	91.14	2.5	-11.31	-5.74E-06	2.5	280	4	5.03	3.49	1.40	Tr/Kgr	4	1500	4
CC	DVFZ	7	6	-2.25	Kgr	2	0.8	1.4	0.9	2.5	230	0.2	78.89	2.5	-10.28	-6.46E-06	2.5	260	4	4.95	3.48	1.48	Tr/Kgr	4	1000	4
CC	DVFZ	7	7	-1.75	Kgr	2	0.8	1.4	0.8	2.5	230	0.2	66.64	2.5	-9.23	-7.24E-06	2.5	250	4	4.72	3.44	1.64	Tr/Kgr	4	1000	4
CC	DVFZ	7	8	-1.25	Tr	3	0.4	0.6	0.8	2.4	30	0.1	54.39	2.5	-8.14	-8.09E-06	2.5	250	4	4.70	3.31	1.78	Tr/Kgr	4	1000	4
CC	DVFZ	7	9	-0.75	Tr	3	0.4	0.6	0.8	2.4	30	0	42.63	2.5	-7.00	-9.01E-06	2.5	200	4	4.87	3.15	1.93	Tr/Kgr	5	1000	5
CC	DVFZ	7	10	-0.25	Tr	4	0.4	0.6	0.8	2.4	30	0	30.87	2.5	-5.83	-0.00001	2.5	175	4	4.85	2.99	2.15	Tr/Kgr	5	200	5
CC	DVFZ	7	11	0.25	Jz	4	0.7	0.8	0.8	2.6	400	0	19.11	2.5	-4.62	-0.0000111	2.5	125	4	4.05	2.68	2.48	Tr/Kgr	5	50	5
CC	DVFZ	7	12	0.75	Q	5	0	0.5	0.9	1.3	1	0	6.37	2.5	-3.41	-0.0000123	2.5	100	4	2.78	1.66	2.73	Tr/Kgr	5	7	5
CC		7	13	1.25			0	0	1	0	0	0	0	2.5	-2.24	-0.0000135	2.5	0								
CC	DVFZ	8	3	-3.75	Kgr	1	0.8	1.4	0.7	2.5	230	0.1	109.27	2.5	-11.43	-0.0000044	2.5	300	4	5.18	3.51	1.17	Tr/Kgr	4		
CC	DVFZ	8	4	-3.25	Kgr	1	0.8	1.4	0.7	2.5	230	0	97.02	2.5	-10.36	-4.77E-06	2.5	290	5	5.11	3.50	1.25	Tr/Kgr	4		
CC	DVFZ	8	5	-2.75	Kgr	2	0.8	1.4	0.8	2.5	230	0	84.77	2.5	-9.26	-5.17E-06	2.5	275	5	5.03	3.49	1.33	Tr/Kgr	4	800	4
CC	DVFZ	8	6	-2.25	Kgr	2	0.8	1.4	0.9	2.5	230	0	72.52	2.5	-8.12	-5.61E-06	2.5	250	5	4.96	3.48	1.41	Tr/Kgr	4	200	4
CC	DVFZ	8	7	-1.75	Kgr	3	0.8	1.4	0.9	2.5	230	0	60.27	2.5	-6.92	-0.0000061	2.5	250	4	4.74	3.44	1.59	Tr/Kgr	4	200	4
CC	DVFZ	8	8	-1.25	Tr	3	0.4	0.6	0.9	2.4	30	0	48.02	2.5	-5.63	-6.64E-06	2.5	225	4	4.72	3.31	1.78	Jg	4	200	4
CC	DVFZ	8	9	-0.75	Tr	4	0.4	0.6	0.8	2.4	30	0	36.26	2.5	-4.24	-7.25E-06	2.5	225	4	4.89	3.15	1.99	Tr/Kgr	5	200	5
CC	DVFZ	8	10	-0.25	Tr	4	0.4	0.6	0.8	2.4	30	0	24.5	2.5	-2.72	-7.91E-06	2.5	200	4	4.87	2.99	2.26	Tr/Kgr	5	50	5
CC	DVFZ	8	11	0.25	Q	4	0	0.5	0.8	1.3	1	0	12.74	2.5	-1.07	-8.64E-06	2.5	150	4	4.04	2.68	2.63	Tr/Kgr	5	15	5
CC	DVFZ	8	12	0.75	Q	5	0	0.5	0.9	1.3	1	0	6.37	2.5	0.72	-9.42E-06	2.5	125	4	2.71	1.66	2.89	Tbf	5	5	5
CC		8	13	1.25			0	0	1	0	0	0	0	2.5	2.62	-0.0000103	2.5	0								

Dixie Valley Cross-Sectional Data (continued)

1	2	3			4		5	6	7	8	9	10	11		12			13		14			15		16	
Cross-Section	Domain	Location			Lithology		Assigned Parameters: Lithology					Stress Parameters			Coulomb Stress Parameters			Temperature		Seismic Parameters			Gravity-Magnetics		MT (Resistivity)	
		X	Z	Ele-vation	Fm	TV	EGS-Fav	Friction	Certainty	Density	Strength	Frac-Intens	Vert-Stress	TV	CSC	Dilatation	TV	° C	TV	Vp	Vs	TV	Lithology	TV	ohm-m	TV
CC	DVFZ	9	3	-3.75	Kgr	1	0.8	1.4	0.7	2.5	230	0	109.27	2.5	-9.32	-4.37E-06	2.5	300	3	5.17	3.51	1.07	Tr/Kgr	4		
CC	DVFZ	9	4	-3.25	Kgr	1	0.8	1.4	0.8	2.5	230	0	97.02	2.5	-8.25	-4.45E-06	2.5	290	3	5.10	3.50	1.15	Tr/Kgr	4		
CC	DVFZ	9	5	-2.75	Kgr	2	0.8	1.4	0.8	2.5	230	0	84.77	2.5	-7.13	-4.56E-06	2.5	275	4	5.02	3.49	1.22	Tr/Kgr	4	200	4
CC	DVFZ	9	6	-2.25	Kgr	2	0.8	1.4	0.8	2.5	230	0	72.52	2.5	-5.94	-4.71E-06	2.5	260	4	4.94	3.48	1.29	Tr/Kgr	4	100	4
CC	DVFZ	9	7	-1.75	Kgr	3	0.8	1.4	0.8	2.5	230	0	60.27	2.5	-4.65	-4.89E-06	2.5	250	4	4.70	3.44	1.60	Tr/Kgr	4	100	4
CC	DVFZ	9	8	-1.25	Tr	3	0.4	0.6	0.9	2.4	30	0.1	48.02	2.5	-3.24	-5.12E-06	2.5	225	4	4.62	3.31	1.95	Jg	4	100	4
CC	DVFZ	9	9	-0.75	Tr	4	0.4	0.6	0.9	2.4	30	0.2	36.26	2.5	-1.66	-5.38E-06	2.5	225	5	4.74	3.15	2.20	Tr/Kgr	5	100	5
CC	DVFZ	9	10	-0.25	Tr	4	0.4	0.6	0.9	2.4	30	0.2	24.5	2.5	0.10	-5.68E-06	2.5	200	5	4.72	2.99	2.49	Tr/Kgr	5	20	5
CC	DVFZ	9	11	0.25	Q	5	0	0.5	0.9	1.3	1	0.1	12.74	2.5	2.09	-6.02E-06	2.5	150	5	4.00	2.68	2.88	Tbf	5	5	5
CC	DVFZ	9	12	0.75	Q	5	0	0.5	0.9	1.3	1	0	6.37	2.5	4.33	-6.39E-06	2.5	125	5	2.73	1.66	3.14	Tbf	5	2	5
CC		9	13	1.25			0	0	1	0	0	0	0	2.5	6.82	-6.78E-06	2.5	0								
CC	DVFZ	10	3	-3.75	Kgr	1	0.8	1.4	0.7	2.5	230	0.2	105.35	2.5	-7.10	-4.31E-06	2.5	290	4	5.16	3.48	0.92	Tr/Kgr	4		
CC	DVFZ	10	4	-3.25	Kgr	1	0.8	1.4	0.8	2.5	230	0.2	93.1	2.5	-6.08	-0.0000041	2.5	275	5	5.08	3.48	0.99	Tr/Kgr	4		
CC	DVFZ	10	5	-2.75	Kgr	2	0.8	1.4	0.9	2.5	230	0.4	80.85	2.5	-4.98	-3.91E-06	2.5	270	5	5.01	3.47	1.05	Tr/Kgr	4	100	4
CC	DVFZ	10	6	-2.25	Tr	2	0.4	0.6	0.9	2.4	30	0.4	68.6	2.5	-3.78	-3.76E-06	2.5	260	4	4.92	3.46	1.11	Tr/Kgr	4	80	4
CC	DVFZ	10	7	-1.75	Jz	3	0.7	0.8	0.9	2.6	400	0.4	56.84	2.5	-2.46	-3.64E-06	2.5	250	4	4.69	3.43	1.37	Tr/Kgr	4	80	4
CC	DVFZ	10	8	-1.25	Jz	3	0.7	0.8	0.8	2.6	400	0.3	44.1	2.5	-0.98	-3.54E-06	2.5	225	4	4.61	3.32	1.66	Jg	4	80	4
CC	DVFZ	10	9	-0.75	Tmb	4	0.6	0.7	0.8	2.5	100	0.2	31.36	2.5	0.70	-3.46E-06	2.5	200	4	4.72	3.18	1.86	Tbf	5	30	5
CC	DVFZ	10	10	-0.25	Q	4	0	0.5	0.8	1.3	1	0.2	19.11	2.5	2.63	-3.39E-06	2.5	175	4	4.69	3.05	2.11	Tbf	5	10	5
CC	DVFZ	10	11	0.25	Q	4	0	0.5	0.8	1.3	1	0.2	12.74	2.5	4.84	-3.33E-06	2.5	125	4	3.96	2.68	2.64	Tbf	5	2	5
CC	DVFZ	10	12	0.75	Q	5	0	0.5	0.9	1.3	1	0.1	6.37	2.5	7.40	-3.27E-06	2.5	100	4	2.68	1.66	3.15	Tbf	5	2	5
CC		10	13	1.25			0	0	1	0	0	0	0	2.5	10.34	-3.21E-06	2.5	0								
CC	Valley	11	3	-3.75	Kgr	1	0.8	1.4	0.7	2.5	230	0	98.98	2.5	-4.84	-4.23E-06	2.5	285	4	5.14	3.48	0.84	Tr/Kgr	4		
CC	Valley	11	4	-3.25	Kgr	1	0.8	1.4	0.8	2.5	230	0	86.73	2.5	-3.89	-3.72E-06	2.5	275	4	5.06	3.48	0.90	Tr/Kgr	4		
CC	Valley	11	5	-2.75	Tr	2	0.4	0.6	0.8	2.4	30	0	74.48	2.5	-2.85	-3.25E-06	2.5	260	4	4.98	3.47	0.96	Tr/Kgr	4	50	4
CC	Valley	11	6	-2.25	Tr	2	0.4	0.6	0.8	2.4	30	0	62.72	2.5	-1.68	-0.0000028	2.5	250	5	4.90	3.46	1.02	Tr/Kgr	4	20	4
CC	Valley	11	7	-1.75	Jz	3	0.7	0.8	0.8	2.6	400	0	50.96	2.5	-0.37	-2.37E-06	2.5	225	5	4.64	3.43	1.34	Tr/Kgr	4	20	4
CC	Valley	11	8	-1.25	Jz	3	0.7	0.8	0.9	2.6	400	0	38.22	2.5	1.13	-1.95E-06	2.5	225	5	4.51	3.32	1.68	Jg	4	20	4
CC	Valley	11	9	-0.75	Q	4	0	0.5	0.9	1.3	1	0	25.48	2.5	2.86	-1.53E-06	2.5	200	5	4.59	3.18	1.85	Tbf	5	20	5
CC	Valley	11	10	-0.25	Q	4	0	0.5	0.9	1.3	1	0	19.11	2.5	4.87	-0.0000011	2.5	150	5	4.56	3.05	2.07	Tbf	5	8	5
CC	Valley	11	11	0.25	Q	5	0	0.5	0.9	1.3	1	0	12.74	2.5	7.23	-6.49E-07	2.5	125	5	3.94	2.68	2.71	Tbf	5	1	5
CC	Valley	11	12	0.75	Q	5	0	0.5	0.9	1.3	1	0	6.37	2.5	9.99	-1.75E-07	2.5	100	5	2.71	1.66	3.37	Tbf	5	2	5
CC		11	13	1.25			0	0	1	0	0	0	0	2.5	13.24	3.36E-07	2.5	0								
CC	Valley	12	3	-3.75	Kgr	1	0.8	1.4	0.7	2.5	230	0	98.98	2.5	-2.62	-0.0000041	2.5	275	4	5.16	3.48	0.78	Tr/Kgr	4		
CC	Valley	12	4	-3.25	Kgr	1	0.8	1.4	0.7	2.5	230	0	86.73	2.5	-1.76	-3.32E-06	2.5	260	4	5.08	3.48	0.84	Tr/Kgr	4		
CC	Valley	12	5	-2.75	Tr	1	0.4	0.6	0.7	2.4	30	0	74.48	2.5	-0.79	-2.57E-06	2.5	250	4	5.00	3.47	0.89	Tr/Kgr	4	20	4
CC	Valley	12	6	-2.25	Tr	1	0.4	0.6	0.7	2.4	30	0	62.72	2.5	0.33	-1.84E-06	2.5	250	4	4.91	3.46	0.95	Tr/Kgr	4	10	4
CC	Valley	12	7	-1.75	Jz	1	0.7	0.8	0.8	2.6	400	0	50.96	2.5	1.61	-1.12E-06	2.5	225	4	4.68	3.43	1.27	Tr/Kgr	4	10	4
CC	Valley	12	8	-1.25	Jz	2	0.7	0.8	0.8	2.6	400	0	38.22	2.5	3.09	-3.89E-07	2.5	200	4	4.57	3.32	1.66	Jg	4	10	4
CC	Valley	12	9	-0.75	Q	3	0	0.5	0.8	1.3	1	0	25.48	2.5	4.83	3.59E-07	2.5	175	4	4.66	3.18	1.90	Tbf	5	10	5
CC	Valley	12	10	-0.25	Q	4	0	0.5	0.8	1.3	1	0	19.11	2.5	6.88	1.14E-06	2.5	150	4	4.63	3.05	2.17	Tbf	5	5	5
CC	Valley	12	11	0.25	Q	4	0	0.5	0.8	1.3	1	0	12.74	2.5	9.32	1.96E-06	2.5	100	4	3.98	2.68	2.87	Tbf	5	1	5
CC	Valley	12	12	0.75	Q	5	0	0.5	0.9	1.3	1	0	6.37	2.5	12.21	2.83E-06	2.5	50	4	2.72	1.66	3.54	Tbf	5	2	5
CC		12	13	1.25			0	0	1	0	0	0	0	2.5	15.64	3.77E-06	2.5	0								

Dixie Valley Cross-Sectional Data (continued)

1	2	3			4		5	6	7	8	9	10	11		12			13		14			15		16	
Cross-Section	Do-main	Location			Lithology		Assigned Parameters: Lithology					Stress Parameters			Coulomb Stress Parameters			Temperature		Seismic Parameters			Gravity-Magnetics		MT (Resistivity)	
		X	Z	Ele-vation	Fm	TV	EGS-Fav	Frict-ion	Certain-ty	Densi-ty	Strength	Frac-Intens	Vert-Stress	TV	CSC	Dilatation	TV	° C	TV	Vp	Vs	TV	Lithology	TV	ohm-m	TV
CC	Valley	13	3	-3.75	Kgr	1	0.8	1.4	0.6	2.5	230	0	98.98	2.5	-0.51	-3.94E-06	2.5	275	3	5.15	3.48	0.72	Tr/Kgr	4		
CC	Valley	13	4	-3.25	Kgr	1	0.8	1.4	0.6	2.5	230	0	86.73	2.5	0.26	-2.89E-06	2.5	260	3	5.07	3.48	0.77	Tr/Kgr	4		
CC	Valley	13	5	-2.75	Tr	1	0.4	0.6	0.6	2.4	30	0	74.48	2.5	1.16	-1.88E-06	2.5	250	3	4.99	3.47	0.82	Tr/Kgr	4	10	4
CC	Valley	13	6	-2.25	Tr	1	0.4	0.6	0.7	2.4	30	0	62.72	2.5	2.22	-8.9E-07	2.5	225	4	4.90	3.46	0.88	Tr/Kgr	4	7	4
CC	Valley	13	7	-1.75	Jz	1	0.7	0.8	0.7	2.6	400	0	50.96	2.5	3.47	1.06E-07	2.5	225	4	4.68	3.43	1.29	Tr/Kgr	4	8	4
CC	Valley	13	8	-1.25	Jz	2	0.7	0.8	0.7	2.6	400	0	38.22	2.5	4.93	1.12E-06	2.5	200	4	4.56	3.32	1.76	Jg	4	8	4
CC	Valley	13	9	-0.75	Q	3	0	0.5	0.8	1.3	1	0	25.48	2.5	6.66	2.17E-06	2.5	175	4	4.61	3.18	1.98	Tbf	5	8	5
CC	Valley	13	10	-0.25	Q	4	0	0.5	0.8	1.3	1	0	19.11	2.5	8.72	3.27E-06	2.5	125	4	4.56	3.05	2.21	Tbf	5	3	5
CC	Valley	13	11	0.25	Q	4	0	0.5	0.8	1.3	1	0	12.74	2.5	11.19	4.43E-06	2.5	100	4	3.93	2.68	2.97	Tbf	5	1	5
CC	Valley	13	12	0.75	Q	5	0	0.5	0.9	1.3	1	0	6.37	2.5	14.15	5.68E-06	2.5	50	4	2.69	1.66	3.70	Tbf	5	2	5
CC		13	13	1.25			0	0	1	0	0	0	0	2.5	17.69	7.01E-06	2.5	0								
CC	Valley	14	3	-3.75	Kgr	1	0.8	1.4	0.5	2.5	230	0	98.98	2.5	1.43	-3.73E-06	2.5	260	3	5.14	3.48	0.70	Tr/Kgr	4		
CC	Valley	14	4	-3.25	Kgr	1	0.8	1.4	0.5	2.5	230	0	86.73	2.5	2.13	-2.45E-06	2.5	250	3	5.05	3.48	0.76	Tr/Kgr	4		
CC	Valley	14	5	-2.75	Tr	1	0.4	0.6	0.6	2.4	30	0	74.48	2.5	2.97	-0.0000012	2.5	250	3	4.97	3.47	0.81	Tr/Kgr	4	8	4
CC	Valley	14	6	-2.25	Tr	1	0.4	0.6	0.6	2.4	30	0	62.72	2.5	3.99	3.37E-08	2.5	225	3	4.88	3.46	0.86	Tr/Kgr	4	5	4
CC	Valley	14	7	-1.75	Jz	1	0.7	0.8	0.6	2.6	400	0	50.96	2.5	5.20	1.28E-06	2.5	225	3	4.67	3.43	1.26	Tr/Kgr	4	5	4
CC	Valley	14	8	-1.25	Jz	2	0.7	0.8	0.7	2.6	400	0	38.22	2.5	6.64	2.56E-06	2.5	200	3	4.55	3.32	1.72	Jg	4	5	4
CC	Valley	14	9	-0.75	Q	3	0	0.5	0.8	1.3	1	0	25.48	2.5	8.37	3.88E-06	2.5	150	3	4.59	3.18	1.93	Tbf	5	5	5
CC	Valley	14	10	-0.25	Q	4	0	0.5	0.8	1.3	1	0	19.11	2.5	10.44	5.27E-06	2.5	125	3	4.54	3.05	2.15	Tbf	5	2	5
CC	Valley	14	11	0.25	Q	4	0	0.5	0.8	1.3	1	0	12.74	2.5	12.92	6.74E-06	2.5	100	3	3.92	2.68	2.91	Tbf	5	1	5
CC	Valley	14	12	0.75	Q	5	0	0.5	0.9	1.3	1	0	6.37	2.5	15.91	8.32E-06	2.5	50	3	2.67	1.66	3.68	Tbf	5	3	5
CC		14	13	1.25			0	0	1	0	0	0	0	2.5	19.52	0.00001	2.5	0								
CC	Valley	15	3	-3.75	Kgr	1	0.8	1.4	0.4	2.5	230	0	98.98	2.5	3.16	-3.48E-06	2.5	260	2	5.10	3.48	0.70	Tr/Kgr	4		
CC	Valley	15	4	-3.25	Kgr	1	0.8	1.4	0.5	2.5	230	0	86.73	2.5	3.82	-1.99E-06	2.5	250	2	5.01	3.48	0.75	Tr/Kgr	4		
CC	Valley	15	5	-2.75	Tr	1	0.4	0.6	0.5	2.4	30	0	74.48	2.5	4.63	-5.3E-07	2.5	250	2	4.92	3.47	0.80	Tr/Kgr	4	5	4
CC	Valley	15	6	-2.25	Tr	1	0.4	0.6	0.5	2.4	30	0	62.72	2.5	5.62	9.23E-07	2.5	225	3	4.83	3.46	0.85	Tr/Kgr	4	5	4
CC	Valley	15	7	-1.75	Jz	1	0.7	0.8	0.6	2.6	400	0	50.96	2.5	6.81	2.39E-06	2.5	225	3	4.58	3.43	1.36	Tr/Kgr	4	5	4
CC	Valley	15	8	-1.25	Jz	2	0.7	0.8	0.7	2.6	400	0	38.22	2.5	8.25	0.0000039	2.5	175	3	4.40	3.32	1.88	Jg	4	5	4
CC	Valley	15	9	-0.75	Q	3	0	0.5	0.8	1.3	1	0	25.48	2.5	9.98	5.47E-06	2.5	150	3	4.39	3.18	2.01	Tbf	5	5	5
CC	Valley	15	10	-0.25	Q	4	0	0.5	0.8	1.3	1	0	19.11	2.5	12.05	7.12E-06	2.5	100	3	4.28	3.05	2.12	Tbf	5	1	5
CC	Valley	15	11	0.25	Q	4	0	0.5	0.8	1.3	1	0	12.74	2.5	14.55	8.86E-06	2.5	50	3	3.69	2.68	2.81	Tbf	5	1	5
CC	Valley	15	12	0.75	Q	5	0	0.5	0.9	1.3	1	0	6.37	2.5	17.57	0.0000107	2.5	50	3	2.56	1.66	3.63	Tbf	5	3	5
CC		15	13	1.25			0	0	1	0	0	0	0	2.5	21.20	0.0000127	2.5	0								
CC	Valley	16	3	-3.75	Kgr	1	0.8	1.4	0.4	2.5	230	0.2	98.98	2.5	4.68	-3.18E-06	2.5	250	2	5.09	3.49	0.78	Tr/Kgr	4		
CC	Valley	16	4	-3.25	Kgr	1	0.8	1.4	0.4	2.5	230	0.2	86.73	2.5	5.32	-1.51E-06	2.5	250	2	5.01	3.49	0.83	Tr/Kgr	4		
CC	Valley	16	5	-2.75	Tr	1	0.4	0.6	0.4	2.4	30	0.2	74.48	2.5	6.12	1.31E-07	2.5	225	2	4.92	3.48	0.89	Tr/Kgr	4	5	4
CC	Valley	16	6	-2.25	Tr	1	0.4	0.6	0.5	2.4	30	0.2	62.72	2.5	7.11	1.77E-06	2.5	225	2	4.83	3.47	0.94	Tr/Kgr	4	5	4
CC	Valley	16	7	-1.75	Jz	1	0.7	0.8	0.6	2.6	400	0.2	50.96	2.5	8.30	3.44E-06	2.5	200	2	4.56	3.43	1.37	Tr/Kgr	4	5	4
CC	Valley	16	8	-1.25	Jz	2	0.7	0.8	0.7	2.6	400	0.2	38.22	2.5	9.75	5.15E-06	2.5	175	2	4.38	3.30	1.82	Jg	4	5	4
CC	Valley	16	9	-0.75	Q	3	0	0.5	0.8	1.3	1	0.2	25.48	2.5	11.49	6.93E-06	2.5	150	2	4.39	3.14	1.96	Tbf	5	5	5
CC	Valley	16	10	-0.25	Q	4	0	0.5	0.8	1.3	1	0.2	19.11	2.5	13.58	8.79E-06	2.5	100	2	4.30	2.98	2.10	Tbf	5	2	5
CC	Valley	16	11	0.25	Q	4	0	0.5	0.8	1.3	1	0.2	12.74	2.5	16.11	0.0000108	2.5	50	2	3.71	2.68	2.75	Tbf	5	2	5
CC	Valley	16	12	0.75	Q	5	0	0.5	0.9	1.3	1	0.1	6.37	2.5	19.14	0.0000129	2.5	50	2	2.58	1.66	3.55	Tbf	5	5	5
CC		16	13	1.25			0	0	1	0	0	0	0	2.5	22.79	1.516E-05	2.5	0								

Dixie Valley Cross-Sectional Data (continued)

1	2	3			4		5	6	7	8	9	10	11		12			13		14			15		16	
Cross-Section	Do-main	Location			Lithology		Assigned Parameters: Lithology					Stress Parameters			Coulomb Stress Parameters			Temperature		Seismic Parameters			Gravity-Magnetics		MT (Resistivity)	
		X	Z	Ele-vation	Fm	TV	EGS-Fav	Frict-ion	Certain-ty	Densi-ty	Strength	Frac-Intens	Vert-Stress	TV	CSC	Dilatation	TV	° C	TV	Vp	Vs	TV	Lithology	TV	ohm-m	TV
CC	Valley	17	3	-3.75	Kgr	1	0.8	1.4	0.3	2.5	230	0	98.98	2.5	5.96	-2.84E-06	2.5	250	1	5.08	3.49	0.81	Tr/Kgr	4		
CC	Valley	17	4	-3.25	Kgr	1	0.8	1.4	0.3	2.5	230	0	86.73	2.5	6.62	-1.02E-06	2.5	250	1	5.00	3.49	0.87	Tr/Kgr	4		
CC	Valley	17	5	-2.75	Tr	1	0.4	0.6	0.4	2.4	30	0	74.48	2.5	7.45	7.74E-07	2.5	225	2	4.91	3.48	0.93	Tr/Kgr	4	5	4
CC	Valley	17	6	-2.25	Tr	1	0.4	0.6	0.5	2.4	30	0	62.72	2.5	8.45	2.58E-06	2.5	225	2	4.81	3.47	0.98	Tr/Kgr	4	7	4
CC	Valley	17	7	-1.75	Jz	1	0.7	0.8	0.6	2.6	400	0	50.96	2.5	9.67	4.41E-06	2.5	200	2	4.53	3.43	1.40	Tr/Kgr	4	7	4
CC	Valley	17	8	-1.25	Jz	2	0.7	0.8	0.7	2.6	400	0	38.22	2.5	11.14	6.29E-06	2.5	150	2	4.31	3.30	1.79	Tbf	4	8	4
CC	Valley	17	9	-0.75	Q	3	0	0.5	0.8	1.3	1	0	25.48	2.5	12.91	8.24E-06	2.5	125	2	4.28	3.14	1.84	Tbf	5	5	5
CC	Valley	17	10	-0.25	Q	4	0	0.5	0.8	1.3	1	0	19.11	2.5	15.04	0.0000103	2.5	100	2	4.17	2.98	1.92	Tbf	5	3	5
CC	Valley	17	11	0.25	Q	4	0	0.5	0.8	1.3	1	0	12.74	2.5	17.58	0.0000125	2.5	50	2	3.64	2.68	2.61	Tbf	5	2	5
CC	Valley	17	12	0.75	Q	5	0	0.5	0.9	1.3	1	0	6.37	2.5	20.64	0.0000148	2.5	50	2	2.57	1.66	3.46	Tbf	5	10	5
CC		17	13	1.25			0	0	1	0	0	0	0	2.5	24.30	0.0000173	2.5	0								
CC	Valley	18	3	-3.75	Kgr	1	0.8	1.4	0.2	2.5	230	0	98.98	2.5	7.03	-2.46E-06	2.5	250	1	5.11	3.49	0.59	Tr/Kgr	4		
CC	Valley	18	4	-3.25	Kgr	1	0.8	1.4	0.3	2.5	230	0	86.73	2.5	7.74	-5.24E-07	2.5	250	1	5.04	3.49	0.62	Tr/Kgr	4		
CC	Valley	18	5	-2.75	Tr	1	0.4	0.6	0.4	2.4	30	0	74.48	2.5	8.61	0.0000014	2.5	225	1	4.97	3.48	0.66	Tr/Kgr	4	8	4
CC	Valley	18	6	-2.25	Tr	1	0.4	0.6	0.5	2.4	30	0	62.72	2.5	9.65	3.33E-06	2.5	225	1	4.89	3.47	0.69	Tr/Kgr	4	8	4
CC	Valley	18	7	-1.75	Jz	1	0.7	0.8	0.6	2.6	400	0	50.96	2.5	10.92	0.0000053	2.5	175	1	4.53	3.43	1.05	Tr/Kgr	4	8	4
CC	Valley	18	8	-1.25	Jz	2	0.7	0.8	0.7	2.6	400	0	38.22	2.5	12.43	7.32E-06	2.5	150	1	4.26	3.30	1.39	Tbf	4	8	4
CC	Valley	18	9	-0.75	Q	3	0	0.5	0.8	1.3	1	0	25.48	2.5	14.24	9.42E-06	2.5	125	1	4.28	3.14	1.45	Tbf	5	8	5
CC	Valley	18	10	-0.25	Q	4	0	0.5	0.8	1.3	1	0	19.11	2.5	16.40	1.163E-05	2.5	100	1	4.15	2.98	1.54	Tbf	5	3	5
CC	Valley	18	11	0.25	Q	4	0	0.5	0.8	1.3	1	0	12.74	2.5	18.98	0.000014	2.5	50	1	3.64	2.68	2.31	Tbf	5	2	5
CC	Valley	18	12	0.75	Q	5	0	0.5	0.9	1.3	1	0	6.37	2.5	22.05	0.0000164	2.5	50	1	2.58	1.66	3.29	Tbf	5	10	5
CC		18	13	1.25			0	0	1	0	0	0	0	2.5	25.71	0.0000191	2.5	0								
CC	Valley	19	3	-3.75	Kgr	1	0.8	1.4	0.2	2.5	230	0.4	98.98	2.5	7.90	-2.05E-06	2.5	250	1	4.98	3.49	0.24	Tr/Kgr	4		
CC	Valley	19	4	-3.25	Kgr	1	0.8	1.4	0.3	2.5	230	0.4	86.73	2.5	8.68	-2.17E-08	2.5	225	1	4.86	3.49	0.26	Tr/Kgr	4		
CC	Valley	19	5	-2.75	Tr	1	0.4	0.6	0.4	2.4	30	0.3	74.48	2.5	9.61	0.000002	2.5	225	1	4.73	3.48	0.28	Tr/Kgr	4	10	4
CC	Valley	19	6	-2.25	Tr	1	0.4	0.6	0.5	2.4	30	0.2	62.72	2.5	10.72	4.03E-06	2.5	200	1	4.60	3.47	0.30	Tr/Kgr	4	10	4
CC	Valley	19	7	-1.75	Jz	1	0.7	0.8	0.6	2.6	400	0.2	50.96	2.5	12.04	6.11E-06	2.5	150	1	4.40	3.43	0.71	Tr/Kgr	4	10	4
CC	Valley	19	8	-1.25	Jz	2	0.7	0.8	0.7	2.6	400	0.2	38.22	2.5	13.60	8.24E-06	2.5	125	1	4.22	3.30	1.18	Tbf	4	10	4
CC	Valley	19	9	-0.75	Q	3	0	0.5	0.8	1.3	1	0.2	25.48	2.5	15.46	0.0000105	2.5	100	1	4.15	3.14	1.33	Tbf	5	10	5
CC	Valley	19	10	-0.25	Q	4	0	0.5	0.8	1.3	1	0.2	19.11	2.5	17.66	0.0000128	2.5	50	1	4.02	2.98	1.43	Tbf	5	5	5
CC	Valley	19	11	0.25	Q	4	0	0.5	0.8	1.3	1	0.2	12.74	2.5	20.27	0.0000152	2.5	50	1	3.57	2.68	2.25	Tbf	5	3	5
CC	Valley	19	12	0.75	Q	5	0	0.5	0.9	1.3	1	0.1	6.37	2.5	23.36	0.0000179	2.5	50	1	2.59	1.66	3.21	Tbf	5	10	5
CC		19	13	1.25			0	0	1	0	0	0	0	2.5	27.01	0.0000206	2.5	0								
CC	Valley	20	3	-3.75	Kgr	1	0.8	1.4	0.2	2.5	230	0	104.86	2.5	8.58	-1.61E-06	2.5	225	1	5.03	3.49	0.22	Tr/Kgr	4		
CC	Valley	20	4	-3.25	Kgr	1	0.8	1.4	0.3	2.5	230	0	92.61	2.5	9.45	4.8E-07	2.5	225	1	4.90	3.49	0.23	Tr/Kgr	4		
CC	Valley	20	5	-2.75	Kgr	1	0.8	1.4	0.4	2.5	230	0.1	80.36	2.5	10.46	2.57E-06	2.5	225	1	4.78	3.48	0.25	Tr/Kgr	4	20	4
CC	Valley	20	6	-2.25	Tr	1	0.4	0.6	0.5	2.4	30	0.2	68.11	2.5	11.64	4.68E-06	2.5	200	1	4.65	3.47	0.27	Tr/Kgr	4	25	4
CC	Valley	20	7	-1.75	Tr	1	0.4	0.6	0.6	2.4	30	0.2	56.35	2.5	13.03	6.84E-06	2.5	150	1	4.43	3.43	0.59	Tr/Kgr	4	25	4
CC	Valley	20	8	-1.25	Jz	2	0.7	0.8	0.7	2.6	400	0.2	44.59	2.5	14.65	9.06E-06	2.5	125	1	4.22	3.30	0.96	Tbf	4	25	4
CC	Valley	20	9	-0.75	Jz	3	0.7	0.8	0.7	2.6	400	0.2	31.85	2.5	16.57	0.0000114	2.5	100	1	4.12	3.14	1.06	Tbf	5	20	5
CC	Valley	20	10	-0.25	Q	4	0	0.5	0.8	1.3	1	0.2	19.11	2.5	18.81	0.0000138	2.5	50	1	3.95	2.98	1.11	Tbf	5	7	5
CC	Valley	20	11	0.25	Q	4	0	0.5	0.8	1.3	1	0.2	12.74	2.5	21.44	0.0000163	2.5	50	1	3.57	2.68	1.94	Tbf	5	3	5
CC	Valley	20	12	0.75	Q	5	0	0.5	0.9	1.3	1	0.1	6.37	2.5	24.54	0.000019	2.5	50	1	2.63	1.66	2.95	Tbf	5	15	5
CC		20	13	1.25			0	0	1	0	0	0	0	2.5	28.17	0.0000219	2.5	0								

Dixie Valley Cross-Sectional Data (continued)

1	2	3			4		5	6	7	8	9	10	11		12			13		14			15		16	
Cross-Section	Domain	Location			Lithology		Assigned Parameters: Lithology					Stress Parameters			Coulomb Stress Parameters			Temperature		Seismic Parameters			Gravity-Magnetics		MT (Resistivity)	
		X	Z	Ele-vation	Fm	TV	EGS-Fav	Friction	Certainty	Density	Strength	Frac-Intens	Vert-Stress	TV	CSC	Dilatation	TV	° C	TV	Vp	Vs	TV	Lithology	TV	ohm-m	TV
DD	SR	1	3	-3.75	Kgr	1	0.8	1.4	0.2	2.5	230	0	134	2.5	-21.01	-4.47E-06	2.5			4.98	3.51	0.48	Tr/Kgr	4	3000	3
DD	SR	1	4	-3.25	Kgr	1	0.8	1.4	0.2	2.5	230	0	122	2.5	-20.62	-6.31E-06	2.5			4.86	3.50	0.52	Tr/Kgr	4	3000	3
DD	SR	1	5	-2.75	Kgr	1	0.8	1.4	0.2	2.5	230	0	109	2.5	-20.34	-8.21E-06	2.5			4.73	3.49	0.56	Tr/Kgr	4	1200	3
DD	SR	1	6	-2.25	Kgr	1	0.8	1.4	0.2	2.5	230	0	97	2.5	-20.23	-0.0000102	2.5			4.61	3.48	0.60	Tr/Kgr	4	1000	3
DD	SR	1	7	-1.75	Kgr	1	0.8	1.4	0.3	2.5	230	0	85	2.5	-20.32	-0.0000124	2.5			4.61	3.44	0.78	Tr/Kgr	4	1100	3
DD	SR	1	8	-1.25	Kgr	1	0.8	1.4	0.4	2.5	230	0	73	2.5	-20.73	-0.0000147	2.5			4.70	3.31	1.09	Tr/Kgr	4	900	3
DD	SR	1	9	-0.75	Kgr	2	0.8	1.4	0.5	2.5	230	0	60	2.5	-21.55	-0.0000173	2.5			4.75	3.15	1.43	Tr/Kgr	5	600	3
DD	SR	1	10	-0.25	Tr	3	0.4	0.6	0.6	2.4	30	0	48	2.5	-22.96	-0.0000202	2.5			4.77	2.99	1.76	Tr/Kgr	5	250	3
DD	SR	1	11	0.25	Tr	4	0.4	0.6	0.7	2.4	30	0	36	2.5	-25.12	-0.0000232	2.5			4.15	2.68	2.23	Tr/Kgr	5	80	3
DD	SR	1	12	0.75	Tr	4	0.4	0.6	0.8	2.4	30	0	25	2.5	-28.23	-0.0000266	2.5			2.89	1.66	2.54	Jg	5	50	3
DD	SR	1	13	1.25	Jz	5	0.7	0.8	0.9	2.6	400	0	13	2.5	-32.45	-0.0000301	2.5						Jg	5		
DD	SR	2	3	-3.75	Kgr	1	0.8	1.4	0.3	2.5	230	0	133.28	2.5	-20.61	-0.0000043	2.5	260	1	4.96	3.51	0.47	Tr/Kgr	4	1000	3
DD	SR	2	4	-3.25	Kgr	1	0.8	1.4	0.3	2.5	230	0	121.03	2.5	-19.91	-5.95E-06	2.5	250	1	4.84	3.50	0.51	Tr/Kgr	4	800	3
DD	SR	2	5	-2.75	Kgr	1	0.8	1.4	0.3	2.5	230	0	108.78	2.5	-19.29	-7.66E-06	2.5	250	1	4.71	3.49	0.55	Tr/Kgr	4	200	3
DD	SR	2	6	-2.25	Kgr	1	0.8	1.4	0.3	2.5	230	0	96.53	2.5	-18.74	-9.48E-06	2.5	200	1	4.58	3.48	0.59	Tr/Kgr	4	120	3
DD	SR	2	7	-1.75	Kgr	1	0.8	1.4	0.3	2.5	230	0	84.28	2.5	-18.30	-0.0000114	2.5	200	1	4.50	3.44	0.92	Tr/Kgr	4	175	3
DD	SR	2	8	-1.25	Kgr	1	0.8	1.4	0.4	2.5	230	0	72.03	2.5	-18.03	-0.0000136	2.5	200	1	4.49	3.31	1.38	Tr/Kgr	4	200	3
DD	SR	2	9	-0.75	Tr	2	0.4	0.6	0.5	2.4	30	0	59.78	2.5	-18.02	-0.000016	2.5	175	1	4.52	3.15	1.69	Tr/Kgr	5	350	3
DD	SR	2	10	-0.25	Tr	3	0.4	0.6	0.6	2.4	30	0	48.02	2.5	-18.39	-0.0000186	2.5	150	1	4.52	2.99	1.99	Tr/Kgr	5	200	3
DD	SR	2	11	0.25	Tr	4	0.4	0.6	0.7	2.4	30	0	36.26	2.5	-19.34	-0.0000215	2.5	100	1	3.95	2.68	2.44	Tr/Kgr	5	50	3
DD	SR	2	12	0.75	Tr	4	0.4	0.6	0.8	2.4	30	0	24.5	2.5	-21.08	-0.0000247	2.5	50	1	2.78	1.66	2.73	Tr/Kgr	5	90	3
DD	SR	2	13	1.25	Jz	5	0.7	0.8	0.9	2.6	400	0	12.74	2.5	-23.88	-0.0000281	2.5	50	1				Tr/Kgr	5		
DD	SR	3	3	-3.75	Kgr	1	0.8	1.4	0.4	2.5	230	0	132.3	2.5	-19.81	-4.11E-06	2.5	270	1	5.09	3.51	0.66	Tr/Kgr	4	500	3
DD	SR	3	4	-3.25	Kgr	1	0.8	1.4	0.4	2.5	230	0	120.05	2.5	-18.82	-5.53E-06	2.5	265	1	4.98	3.50	0.72	Tr/Kgr	4	250	3
DD	SR	3	5	-2.75	Kgr	1	0.8	1.4	0.4	2.5	230	0	107.8	2.5	-17.83	-7.01E-06	2.5	250	1	4.87	3.49	0.78	Tr/Kgr	4	150	3
DD	SR	3	6	-2.25	Kgr	1	0.8	1.4	0.4	2.5	230	0	95.55	2.5	-16.84	-8.58E-06	2.5	225	1	4.76	3.48	0.84	Tr/Kgr	4	100	3
DD	SR	3	7	-1.75	Kgr	1	0.8	1.4	0.4	2.5	230	0	83.3	2.5	-15.83	-0.0000103	2.5	200	1	4.65	3.44	1.14	Tr/Kgr	4	150	3
DD	SR	3	8	-1.25	Kgr	1	0.8	1.4	0.4	2.5	230	0	71.05	2.5	-14.83	-0.0000122	2.5	200	1	4.59	3.31	1.53	Tr/Kgr	4	200	3
DD	SR	3	9	-0.75	Tr	2	0.4	0.6	0.5	2.4	30	0	58.8	2.5	-13.85	-0.0000143	2.5	200	1	4.59	3.15	1.80	Tr/Kgr	5	400	3
DD	SR	3	10	-0.25	Tr	3	0.4	0.6	0.6	2.4	30	0	47.04	2.5	-12.96	-0.0000166	2.5	175	1	4.58	2.99	2.06	Jg	5	250	3
DD	SR	3	11	0.25	Tr	4	0.4	0.6	0.7	2.4	30	0	35.28	2.5	-12.31	-0.0000192	2.5	125	1	3.94	2.68	2.51	Jg	5	125	3
DD	SR	3	12	0.75	Tr	4	0.4	0.6	0.8	2.4	30	0	23.52	2.5	-12.11	-0.000022	2.5	100	1	2.70	1.66	2.93	Tr/Kgr	5	350	3
DD	SR	3	13	1.25	Tr	5	0.4	0.6	0.9	2.4	30	0	11.76	2.5	-12.68	-0.0000251	2.5	50	1				Tr/Kgr	5		
DD	SR	4	3	-3.75	Kgr	1	0.8	1.4	0.5	2.5	230	0	133.77	2.5	-18.45	-0.0000039	2.5			5.14	3.51	0.99	Tr/Kgr	4	145	3
DD	SR	4	4	-3.25	Kgr	1	0.8	1.4	0.5	2.5	230	0	121.52	2.5	-17.17	-5.06E-06	2.5	275	1	5.07	3.50	1.05	Tr/Kgr	4	90	3
DD	SR	4	5	-2.75	Kgr	1	0.8	1.4	0.5	2.5	230	0	109.27	2.5	-15.84	-6.26E-06	2.5	265	1	4.99	3.49	1.12	Tr/Kgr	4	100	3
DD	SR	4	6	-2.25	Kgr	1	0.8	1.4	0.5	2.5	230	0	97.02	2.5	-14.43	-7.54E-06	2.5	250	1	4.90	3.48	1.19	Tr/Kgr	4	130	3
DD	SR	4	7	-1.75	Kgr	1	0.8	1.4	0.5	2.5	230	0	84.77	2.5	-12.89	-8.93E-06	2.5	225	2	4.66	3.44	1.46	Tr/Kgr	4	185	3
DD	SR	4	8	-1.25	Kgr	1	0.8	1.4	0.5	2.5	230	0	72.52	2.5	-11.17	-0.0000105	2.5	200	2	4.58	3.31	1.75	Tr/Kgr	4	450	3
DD	SR	4	9	-0.75	Tr	2	0.4	0.6	0.5	2.4	30	0	60.27	2.5	-9.24	-0.0000122	2.5	200	2	4.69	3.15	1.95	Tr/Kgr	5	650	3
DD	SR	4	10	-0.25	Tr	3	0.4	0.6	0.6	2.4	30	0	48.51	2.5	-7.06	-0.000014	2.5	200	2	4.68	2.99	2.23	Jg	5	325	3
DD	DVFZ	4	11	0.25	Tr	4	0.4	0.6	0.7	2.4	30	0.2	36.75	2.5	-4.67	-0.0000161	2.5	150	2	3.98	2.68	2.74	Jg	5	150	3
DD	DVFZ	4	12	0.75	Jz	4	0.7	0.8	0.8	2.6	400	0.3	24.99	2.5	-2.20	-0.0000185	2.5	100	2	2.69	1.66	3.21	Tr/Kgr	5	14	3
DD	DVFZ	4	13	1.25	Jbr	5	0.8	0.6	0.9	2.5	200	0.2	12.25	2.5	0.04	-0.000021	2.5	0								

Dixie Valley Cross-Sectional Data (continued)

1	2	3			4		5	6	7	8	9	10	11		12			13		14			15		16	
Cross-Section	Do-main	Location			Lithology		Assigned Parameters: Lithology					Stress Parameters			Coulomb Stress Parameters			Temperature		Seismic Parameters			Gravity-Magnetics		MT (Resistivity)	
		X	Z	Ele-vation	Fm	TV	EGS-Fav	Frict-ion	Certain-ty	Densi-ty	Strength	Frac-Intens	Vert-Stress	TV	CSC	Dilatation	TV	° C	TV	Vp	Vs	TV	Lithology	TV	ohm-m	TV
DD	SR	5	3	-3.75	Kgr	1	0.8	1.4	0.5	2.5	230	0	122.01	2.5	-16.38	-3.68E-06	2.5	275	1	5.14	3.51	0.83	Tr/Kgr	4	150	3
DD	SR	5	4	-3.25	Kgr	2	0.8	1.4	0.6	2.5	230	0	109.76	2.5	-14.85	-4.54E-06	2.5	275	1	5.06	3.50	0.89	Tr/Kgr	4	90	3
DD	SR	5	5	-2.75	Kgr	2	0.8	1.4	0.6	2.5	230	0	97.51	2.5	-13.23	-5.44E-06	2.5	265	1	4.98	3.49	0.95	Tr/Kgr	4	130	3
DD	SR	5	6	-2.25	Kgr	3	0.8	1.4	0.6	2.5	230	0	85.26	2.5	-11.47	-6.38E-06	2.5	250	2	4.89	3.48	1.01	Tr/Kgr	4	185	3
DD	SR	5	7	-1.75	Kgr	3	0.8	1.4	0.6	2.5	230	0	73.01	2.5	-9.50	-7.39E-06	2.5	240	2	4.65	3.44	1.44	Tr/Kgr	4	220	3
DD	SR	5	8	-1.25	Kgr	3	0.8	1.4	0.6	2.5	230	0.1	60.76	2.5	-7.23	-8.49E-06	2.5	225	2	4.53	3.31	1.96	Tr/Kgr	4	800	3
DD	DVFZ	5	9	-0.75	Tr	3	0.4	0.6	0.6	2.4	30	0.2	48.51	2.5	-4.54	-9.68E-06	2.5	200	2	4.61	3.15	2.26	Tr/Kgr	5	400	3
DD	DVFZ	5	10	-0.25	Tr	4	0.4	0.6	0.6	2.4	30	0.4	36.75	2.5	-1.31	-0.000011	2.5	175	2	4.58	2.99	2.57	Jg	5	125	3
DD	DVFZ	5	11	0.25	Jz	4	0.7	0.8	0.7	2.6	400	0.3	24.99	2.5	2.58	-0.0000124	2.5	125	2	4.00	2.68	3.11	Jg	5	15	3
DD	DVFZ	5	12	0.75	Jbr	5	0.8	0.6	0.8	2.5	200	0.3	12.25	2.5	7.14	-0.0000141	2.5	50	2	2.76	1.66	3.58	Tr/Kgr	5	8	3
DD		5	13	1.25			0	0	0.9	0	0	0.1	0	2.5	12.17	-0.0000159	2.5	0								
DD	DVFZ	6	3	-3.75	Kgr	1	0.8	1.4	0.5	2.5	230	0	115.64	2.5	-13.54	-3.45E-06	2.5	280	1	5.14	3.51	0.83	Tr/Kgr	4	150	3
DD	DVFZ	6	4	-3.25	Kgr	2	0.8	1.4	0.6	2.5	230	0.1	103.39	2.5	-11.83	-0.000004	2.5	280	2	5.06	3.50	0.89	Tr/Kgr	4	100	3
DD	DVFZ	6	5	-2.75	Kgr	2	0.8	1.4	0.7	2.5	230	0.2	91.14	2.5	-10.02	-4.55E-06	2.5	275	2	4.98	3.49	0.95	Tr/Kgr	4	165	3
DD	DVFZ	6	6	-2.25	Kgr	3	0.8	1.4	0.7	2.5	230	0.2	78.89	2.5	-8.04	-5.13E-06	2.5	265	3	4.89	3.48	1.01	Tr/Kgr	4	250	3
DD	DVFZ	6	7	-1.75	Kgr	3	0.8	1.4	0.7	2.5	230	0.2	66.64	2.5	-5.82	-5.72E-06	2.5	250	3	4.65	3.44	1.44	Tr/Kgr	4	300	3
DD	DVFZ	6	8	-1.25	Tr	3	0.4	0.6	0.7	2.4	30	0.2	54.39	2.5	-3.25	-6.34E-06	2.5	225	3	4.53	3.31	1.96	Tr/Kgr	4	450	3
DD	DVFZ	6	9	-0.75	Tr	3	0.4	0.6	0.7	2.4	30	0	42.63	2.5	-0.16	-6.98E-06	2.5	200	3	4.61	3.15	2.26	Tr/Kgr	5	135	3
DD	DVFZ	6	10	-0.25	Tr	4	0.4	0.6	0.7	2.4	30	0	30.87	2.5	3.64	-7.64E-06	2.5	150	3	4.58	2.99	2.57	Jg	5	20	3
DD	DVFZ	6	11	0.25	Jz	4	0.7	0.8	0.7	2.6	400	0	19.11	2.5	8.40	-8.35E-06	2.5	125	3	4.00	2.68	3.11	Tr/Kgr	5	15	3
DD	DVFZ	6	12	0.75	Q	5	0	0.5	0.8	1.3	1	0	6.37	2.5	14.28	-9.13E-06	2.5	50	3	2.76	1.66	3.58	Tr/Kgr	5	6	3
DD		6	13	1.25			0	0	0.9	0	0	0	0	2.5	21.29	-0.0000101	2.5	0								
DD	DVFZ	7	3	-3.75	Kgr	2	0.8	1.4	0.5	2.5	230	0.2	115.64	2.5	-10.09	-3.21E-06	2.5	280	1	5.14	3.51	0.76	Tr/Kgr	4	135	3
DD	DVFZ	7	4	-3.25	Kgr	3	0.8	1.4	0.6	2.5	230	0.2	103.39	2.5	-8.32	-3.43E-06	2.5	275	2	5.06	3.50	0.82	Tr/Kgr	4	140	3
DD	DVFZ	7	5	-2.75	Kgr	3	0.8	1.4	0.7	2.5	230	0.1	91.14	2.5	-6.44	-3.64E-06	2.5	260	2	4.97	3.49	0.87	Tr/Kgr	4	200	3
DD	DVFZ	7	6	-2.25	Kgr	4	0.8	1.4	0.8	2.5	230	0	78.89	2.5	-4.41	-3.83E-06	2.5	250	3	4.89	3.48	0.93	Tr/Kgr	4	230	3
DD	DVFZ	7	7	-1.75	Kgr	4	0.8	1.4	0.8	2.5	230	0	66.64	2.5	-2.15	-0.000004	2.5	200	3	4.65	3.44	1.42	Tr/Kgr	4	250	3
DD	DVFZ	7	8	-1.25	Tr	4	0.4	0.6	0.8	2.4	30	0	54.39	2.5	0.44	-4.13E-06	2.5	200	3	4.52	3.31	2.03	Tr/Kgr	4	220	3
DD	DVFZ	7	9	-0.75	Tr	4	0.4	0.6	0.8	2.4	30	0	42.63	2.5	3.54	-4.21E-06	2.5	200	3	4.57	3.15	2.37	Tr/Kgr	5	18	3
DD	DVFZ	7	10	-0.25	Tr	4	0.4	0.6	0.8	2.4	30	0.1	30.87	2.5	7.36	-4.21E-06	2.5	150	3	4.51	2.99	2.70	Jg	5	10	3
DD	DVFZ	7	11	0.25	Jz	4	0.7	0.8	0.8	2.6	400	0.2	19.11	2.5	12.20	-4.15E-06	2.5	100	3	3.91	2.68	3.24	Tr/Kgr	5	8	3
DD	DVFZ	7	12	0.75	Q	5	0	0.5	0.8	1.3	1	0.1	6.37	2.5	18.33	-4.08E-06	2.5	50	3	2.72	1.66	3.73	Tbf	5	8	3
DD		7	13	1.25			0	0	0.9	0	0	0	0	2.5	25.97	-4.11E-06	2.5	0								
DD	DVFZ	8	3	-3.75	Kgr	2	0.8	1.4	0.5	2.5	230	0	98.49	2.5	-6.37	-2.97E-06	2.5	280	2	5.13	3.51	0.73	Tr/Kgr	4	125	3
DD	DVFZ	8	4	-3.25	Kgr	3	0.8	1.4	0.6	2.5	230	0	86.24	2.5	-4.65	-2.86E-06	2.5	275	3	5.05	3.50	0.78	Tr/Kgr	4	150	3
DD	DVFZ	8	5	-2.75	Kgr	3	0.8	1.4	0.7	2.5	230	0	73.99	2.5	-2.85	-2.72E-06	2.5	260	3	4.96	3.49	0.84	Tr/Kgr	4	250	3
DD	DVFZ	8	6	-2.25	Kgr	4	0.8	1.4	0.8	2.5	230	0	61.74	2.5	-0.92	-2.55E-06	2.5	250	4	4.87	3.48	0.89	Tr/Kgr	4	250	3
DD	DVFZ	8	7	-1.75	Kgr	4	0.8	1.4	0.9	2.5	230	0.1	49.49	2.5	1.19	-2.31E-06	2.5	225	4	4.63	3.44	1.42	Tr/Kgr	4	210	3
DD	DVFZ	8	8	-1.25	Tr	4	0.4	0.6	0.9	2.4	30	0.3	37.24	2.5	3.58	-1.97E-06	2.5	225	4	4.47	3.31	2.06	Tr/Kgr	4	110	3
DD	DVFZ	8	9	-0.75	Q	4	0	0.5	0.9	1.3	1	0.4	25.48	2.5	6.38	-1.52E-06	2.5	200	4	4.51	3.15	2.38	Tr/Kgr	5	12	3
DD	DVFZ	8	10	-0.25	Q	4	0	0.5	0.9	1.3	1	0.2	19.11	2.5	9.80	-9.19E-07	2.5	150	4	4.44	2.99	2.68	Jg	5	8	3
DD	DVFZ	8	11	0.25	Q	4	0	0.5	0.9	1.3	1	0	12.74	2.5	14.09	-1.81E-07	2.5	100	4	3.86	2.68	3.26	Tr/Kgr	5	7	3
DD	DVFZ	8	12	0.75	Q	5	0	0.5	0.9	1.3	1	0	6.37	2.5	19.58	6.43E-07	2.5	50	4	2.71	1.66	3.78	Tbf	5	10	3
DD		8	13	1.25			0	0	0.9	0	0	0	0	2.5	26.57	1.44E-06	2.5	0								

Dixie Valley Cross-Sectional Data (continued)

1	2	3			4		5	6	7	8	9	10	11		12			13		14			15		16	
Cross-Section	Do-main	Location			Lithology		Assigned Parameters: Lithology					Stress Parameters			Coulomb Stress Parameters			Temperature		Seismic Parameters			Gravity-Magnetics		MT (Resistivity)	
		X	Z	Ele-vation	Fm	TV	EGS-Fav	Frict-ion	Certain-ty	Densi-ty	Strength	Frac-Intens	Vert-Stress	TV	CSC	Dilatation	TV	° C	TV	Vp	Vs	TV	Lithology	TV	ohm-m	TV
DD	DVFZ	9	3	-3.75	Kgr	3	0.8	1.4	0.5	2.5	230	0	99.47	2.5	-2.77	-2.73E-06	2.5	280	2	5.20	3.51	0.94	Tr/Kgr	4	100	3
DD	DVFZ	9	4	-3.25	Kgr	4	0.8	1.4	0.6	2.5	230	0.1	87.22	2.5	-1.22	-0.0000023	2.5	275	3	5.12	3.50	1.02	Tr/Kgr	4	110	3
DD	DVFZ	9	5	-2.75	Kgr	4	0.8	1.4	0.7	2.5	230	0.2	74.97	2.5	0.40	-1.84E-06	2.5	250	3	5.04	3.49	1.10	Tr/Kgr	4	165	3
DD	DVFZ	9	6	-2.25	Kgr	5	0.8	1.4	0.8	2.5	230	0.3	62.72	2.5	2.11	-1.31E-06	2.5	250	4	4.95	3.48	1.17	Tr/Kgr	4	175	3
DD	DVFZ	9	7	-1.75	Jz	5	0.7	0.8	0.9	2.6	400	0.3	50.47	2.5	3.97	-6.96E-07	2.5	225	4	4.72	3.44	1.72	Tr/Kgr	4	165	3
DD	DVFZ	9	8	-1.25	Tmb	5	0.6	0.7	0.9	2.5	100	0.1	37.73	2.5	6.04	4.8E-08	2.5	200	5	4.55	3.29	2.39	Tr/Kgr	4	75	3
DD	DVFZ	9	9	-0.75	Q	5	0	0.5	0.9	1.3	1	0	25.48	2.5	8.41	9.55E-07	2.5	175	4	4.55	3.12	2.70	Jg	5	10	3
DD	Valley	9	10	-0.25	Q	5	0	0.5	0.9	1.3	1	0	19.11	2.5	11.24	2.05E-06	2.5	125	4	4.38	2.94	2.96	Jg	5	7	3
DD	Valley	9	11	0.25	Q	5	0	0.5	0.9	1.3	1	0	12.74	2.5	14.72	3.33E-06	2.5	100	4	3.78	2.68	3.47	Tbf	5	6	3
DD	Valley	9	12	0.75	Q	5	0	0.5	0.9	1.3	1	0	6.37	2.5	19.14	4.75E-06	2.5	50	4	2.67	1.66	3.92	Tbf	5	4	3
DD		9	13	1.25			0	0	1	0	0	0	0	2.5	24.82	6.21E-06	2.5	0								
DD	DVFZ	10	3	-3.75	Kgr	3	0.8	1.4	0.5	2.5	230	0.2	98	2.5	0.37	-0.0000025	2.5	275	3	5.19	3.51	0.92	Tr/Kgr	4	90	3
DD	DVFZ	10	4	-3.25	Tr	4	0.4	0.6	0.6	2.4	30	0.1	85.75	2.5	1.70	-1.77E-06	2.5	265	4	5.11	3.50	1.00	Tr/Kgr	4	85	3
DD	DVFZ	10	5	-2.75	Tr	4	0.4	0.6	0.7	2.4	30	0	73.99	2.5	3.08	-0.000001	2.5	250	4	5.02	3.49	1.07	Tr/Kgr	4	110	3
DD	DVFZ	10	6	-2.25	Tr	5	0.4	0.6	0.8	2.4	30	0	62.23	2.5	4.55	-1.6E-07	2.5	245	5	4.94	3.48	1.15	Tr/Kgr	4	90	3
DD	DVFZ	10	7	-1.75	Jz	5	0.7	0.8	0.9	2.6	400	0.1	50.47	2.5	6.14	7.87E-07	2.5	225	5	4.71	3.44	1.69	Tr/Kgr	4	75	3
DD	DVFZ	10	8	-1.25	Tmb	5	0.6	0.7	0.9	2.5	100	0.2	37.73	2.5	7.88	1.88E-06	2.5	200	5	4.55	3.29	2.34	Jg	4	65	3
DD	DVFZ	10	9	-0.75	Q	5	0	0.5	0.9	1.3	1	0.1	25.48	2.5	9.84	3.15E-06	2.5	150	5	4.54	3.12	2.64	Tbf	5	7	3
DD	Valley	10	10	-0.25	Q	5	0	0.5	0.9	1.3	1	0	19.11	2.5	12.12	4.63E-06	2.5	125	5	4.37	2.94	2.89	Tbf	5	5	3
DD	Valley	10	11	0.25	Q	5	0	0.5	0.9	1.3	1	0	12.74	2.5	14.87	6.31E-06	2.5	100	5	3.77	2.68	3.40	Tbf	5	5	3
DD	Valley	10	12	0.75	Q	5	0	0.5	0.9	1.3	1	0	6.37	2.5	18.26	8.16E-06	2.5	50	5	2.66	1.66	3.89	Tbf	5	5	3
DD		10	13	1.25			0	0	1	0	0	0	0	2.5	22.57	0.0000101	2.5	0								
DD	Valley	11	3	-3.75	Kgr	4	0.8	1.4	0.5	2.5	230	0	98.98	2.5	2.93	-2.26E-06	2.5	270	3	5.18	3.51	0.89	Tr/Kgr	4	85	2
DD	Valley	11	4	-3.25	Tr	4	0.4	0.6	0.6	2.4	30	0	86.73	2.5	4.02	-1.26E-06	2.5	260	4	5.10	3.50	0.96	Tr/Kgr	4	50	2
DD	Valley	11	5	-2.75	Tr	5	0.4	0.6	0.7	2.4	30	0	74.97	2.5	5.19	-2.22E-07	2.5	250	4	5.01	3.49	1.04	Tr/Kgr	4	65	2
DD	Valley	11	6	-2.25	Jz	5	0.7	0.8	0.8	2.6	400	0	63.21	2.5	6.43	8.95E-07	2.5	225	5	4.92	3.48	1.11	Tr/Kgr	4	75	2
DD	Valley	11	7	-1.75	Jz	5	0.7	0.8	0.9	2.6	400	0	50.47	2.5	7.79	2.12E-06	2.5	200	4	4.70	3.44	1.63	Tr/Kgr	4	65	2
DD	Valley	11	8	-1.25	Tmb	5	0.6	0.7	0.9	2.5	100	0	37.73	2.5	9.27	0.0000035	2.5	175	4	4.54	3.29	2.28	Tr/Kgr	4	20	2
DD	Valley	11	9	-0.75	Q	5	0	0.5	0.9	1.3	1	0.1	25.48	2.5	10.94	5.05E-06	2.5	150	3	4.54	3.12	2.60	Tbf	5	4	2
DD	Valley	11	10	-0.25	Q	5	0	0.5	0.9	1.3	1	0.1	19.11	2.5	12.84	6.81E-06	2.5	100	4	4.35	2.94	2.86	Tbf	5	3	2
DD	Valley	11	11	0.25	Q	5	0	0.5	0.9	1.3	1	0	12.74	2.5	15.05	8.78E-06	2.5	50	4	3.71	2.68	3.37	Tbf	5	5	2
DD	Valley	11	12	0.75	Q	5	0	0.5	0.9	1.3	1	0	6.37	2.5	17.71	0.0000109	2.5	50	5	2.62	1.66	3.89	Tbf	5	15	2
DD		11	13	1.25			0	0	1	0	0	0	0	2.5	21.01	0.0000132	2.5	0								
DD	Valley	12	3	-3.75	Kgr	2	0.8	1.4	0.5	2.5	230	0	98.98	2.5	4.93	-2.02E-06	2.5	260	3	5.15	3.51	0.71	Tr/Kgr	4	60	2
DD	Valley	12	4	-3.25	Tr	3	0.4	0.6	0.6	2.4	30	0	86.73	2.5	5.82	-7.83E-07	2.5	250	4	5.05	3.50	0.77	Tr/Kgr	4	32	2
DD	Valley	12	5	-2.75	Tr	3	0.4	0.6	0.7	2.4	30	0	74.97	2.5	6.81	4.97E-07	2.5	225	4	4.95	3.49	0.84	Tr/Kgr	4	22	2
DD	Valley	12	6	-2.25	Jz	4	0.7	0.8	0.8	2.6	400	0	63.21	2.5	7.89	1.85E-06	2.5	225	4	4.85	3.48	0.91	Tr/Kgr	4	15	2
DD	Valley	12	7	-1.75	Jz	4	0.7	0.8	0.8	2.6	400	0	50.47	2.5	9.09	3.31E-06	2.5	200	4	4.66	3.44	1.46	Tr/Kgr	4	10	2
DD	Valley	12	8	-1.25	Tmb	4	0.6	0.7	0.8	2.5	100	0	37.73	2.5	10.42	4.92E-06	2.5	175	4	4.50	3.29	2.21	Tr/Kgr	4	8	2
DD	Valley	12	9	-0.75	Q	4	0	0.5	0.8	1.3	1	0	25.48	2.5	11.91	6.69E-06	2.5	150	4	4.45	3.12	2.59	Tbf	5	5	2
DD	Valley	12	10	-0.25	Q	4	0	0.5	0.8	1.3	1	0	19.11	2.5	13.60	8.66E-06	2.5	100	4	4.27	2.94	2.87	Tbf	5	2	2
DD	Valley	12	11	0.25	Q	4	0	0.5	0.8	1.3	1	0	12.74	2.5	15.54	0.0000108	2.5	50	4	3.68	2.68	3.39	Tbf	5	2	2
DD	Valley	12	12	0.75	Q	5	0	0.5	0.9	1.3	1	0	6.37	2.5	17.79	0.0000132	2.5	50	4	2.63	1.66	3.91	Tbf	5	11	2
DD		12	13	1.25			0	0	1	0	0	0	0	2.5	20.50	0.0000156	2.5	0								

Dixie Valley Cross-Sectional Data (continued)

1	2	3			4		5	6	7	8	9	10	11		12			13		14			15		16	
Cross-Section	Do-main	Location			Lithology		Assigned Parameters: Lithology					Stress Parameters			Coulomb Stress Parameters			Temperature		Seismic Parameters			Gravity-Magnetics		MT (Resistivity)	
		X	Z	Ele-vation	Fm	TV	EGS-Fav	Frict-ion	Certain-ty	Densi-ty	Strength	Frac-Intens	Vert-Stress	TV	CSC	Dilatation	TV	° C	TV	Vp	Vs	TV	Lithology	TV	ohm-m	TV
DD	Valley	13	3	-3.75	Kgr	2	0.8	1.4	0.5	2.5	230	0	98.98	2.5	6.45	-1.77E-06	2.5	250	2	5.07	3.49	0.69	Tr/Kgr	4	10	2
DD	Valley	13	4	-3.25	Tr	3	0.4	0.6	0.6	2.4	30	0	86.73	2.5	7.21	-3.27E-07	2.5	250	3	4.96	3.49	0.75	Tr/Kgr	4	10	2
DD	Valley	13	5	-2.75	Tr	3	0.4	0.6	0.7	2.4	30	0	74.97	2.5	8.08	1.16E-06	2.5	225	3	4.85	3.48	0.82	Tr/Kgr	4	10	2
DD	Valley	13	6	-2.25	Jz	4	0.7	0.8	0.7	2.6	400	0	63.21	2.5	9.07	2.71E-06	2.5	200	3	4.74	3.47	0.88	Tr/Kgr	4	9	2
DD	Valley	13	7	-1.75	Jz	4	0.7	0.8	0.7	2.6	400	0	50.47	2.5	10.19	4.37E-06	2.5	175	3	4.58	3.43	1.43	Tr/Kgr	4	8	2
DD	Valley	13	8	-1.25	Tmb	4	0.6	0.7	0.7	2.5	100	0	37.73	2.5	11.45	6.15E-06	2.5	150	3	4.45	3.30	2.15	Tbf	4	7	2
DD	Valley	13	9	-0.75	Q	4	0	0.5	0.8	1.3	1	0	25.48	2.5	12.89	0.0000081	2.5	125	3	4.40	3.14	2.53	Tbf	5	5	2
DD	Valley	13	10	-0.25	Q	4	0	0.5	0.8	1.3	1	0	19.11	2.5	14.51	0.0000102	2.5	100	3	4.22	2.98	2.80	Tbf	5	3	2
DD	Valley	13	11	0.25	Q	4	0	0.5	0.8	1.3	1	0	12.74	2.5	16.35	0.0000125	2.5	50	3	3.65	2.68	3.35	Tbf	5	2	2
DD	Valley	13	12	0.75	Q	5	0	0.5	0.9	1.3	1	0	6.37	2.5	18.45	0.000015	2.5	50	4	2.62	1.66	3.91	Tbf	5	9	2
DD		13	13	1.25			0	0	1	0	0	0	0	2.5	20.92	0.0000176	2.5	0								
DD	Valley	14	3	-3.75	Kgr	1	0.8	1.4	0.6	2.5	230	0	98	2.5	7.62	-1.51E-06	2.5	250	2	5.07	3.49	0.55	Tr/Kgr	4	10	2
DD	Valley	14	4	-3.25	Tr	1	0.4	0.6	0.6	2.4	30	0	85.75	2.5	8.32	1.1E-07	2.5	250	3	4.96	3.49	0.60	Tr/Kgr	4	10	2
DD	Valley	14	5	-2.75	Tr	1	0.4	0.6	0.6	2.4	30	0	73.99	2.5	9.13	1.77E-06	2.5	225	3	4.85	3.48	0.65	Tr/Kgr	4	9	2
DD	Valley	14	6	-2.25	Jz	1	0.7	0.8	0.6	2.6	400	0	62.23	2.5	10.09	3.49E-06	2.5	200	3	4.74	3.47	0.71	Tr/Kgr	4	8	2
DD	Valley	14	7	-1.75	Tv	1	0.4	0.7	0.6	2.4	75	0	49.49	2.5	11.19	0.0000053	2.5	175	3	4.56	3.43	1.27	Tr/Kgr	4	7	2
DD	Valley	14	8	-1.25	Tmb	2	0.6	0.7	0.7	2.5	100	0	37.73	2.5	12.45	7.23E-06	2.5	150	3	4.41	3.30	2.04	Tbf	4	6	2
DD	Valley	14	9	-0.75	Q	3	0	0.5	0.8	1.3	1	0	25.48	2.5	13.90	0.0000093	2.5	125	3	4.35	3.14	2.42	Tbf	5	5	2
DD	Valley	14	10	-0.25	Q	4	0	0.5	0.8	1.3	1	0	19.11	2.5	15.54	0.0000115	2.5	100	3	4.16	2.98	2.69	Tbf	5	4	2
DD	Valley	14	11	0.25	Q	4	0	0.5	0.8	1.3	1	0	12.74	2.5	17.41	1.395E-05	2.5	50	3	3.57	2.68	3.27	Tbf	5	2	2
DD	Valley	14	12	0.75	Q	5	0	0.5	0.9	1.3	1	0	6.37	2.5	19.54	0.0000165	2.5	50	3	2.58	1.66	3.86	Tbf	5	10	2
DD		14	13	1.25			0	0	1	0	0	0	0	2.5	21.99	0.0000193	2.5	0								
DD	Valley	15	3	-3.75	Kgr	1	0.8	1.4	0.6	2.5	230	0.4	98	2.5	8.54	-1.24E-06	2.5	250	1	5.01	3.49	0.47	Tr/Kgr	4	10	2
DD	Valley	15	4	-3.25	Tr	1	0.4	0.6	0.7	2.4	30	0	85.75	2.5	9.22	5.33E-07	2.5	225	2	4.90	3.49	0.52	Tr/Kgr	4	10	2
DD	Valley	15	5	-2.75	Tr	1	0.4	0.6	0.7	2.4	30	0.4	73.99	2.5	10.03	2.33E-06	2.5	200	2	4.78	3.48	0.56	Tr/Kgr	4	8	2
DD	Valley	15	6	-2.25	Jz	1	0.7	0.8	0.7	2.6	400	0	62.23	2.5	11.00	4.18E-06	2.5	200	2	4.66	3.47	0.60	Tr/Kgr	4	8	2
DD	Valley	15	7	-1.75	Tv	1	0.4	0.7	0.7	2.4	75	0.4	49.49	2.5	12.12	6.12E-06	2.5	175	2	4.50	3.43	1.19	Tr/Kgr	4	7	2
DD	Valley	15	8	-1.25	Tmb	2	0.6	0.7	0.7	2.5	100	0	37.73	2.5	13.43	8.17E-06	2.5	150	2	4.37	3.30	1.98	Tbf	4	5	2
DD	Valley	15	9	-0.75	Q	3	0	0.5	0.8	1.3	1	0.4	25.48	2.5	14.94	0.0000103	2.5	125	2	4.32	3.14	2.36	Tbf	5	3	2
DD	Valley	15	10	-0.25	Q	4	0	0.5	0.8	1.3	1	0	19.11	2.5	16.66	0.0000127	2.5	100	2	4.15	2.98	2.62	Tbf	5	2	2
DD	Valley	15	11	0.25	Q	4	0	0.5	0.8	1.3	1	0.4	12.74	2.5	18.62	0.0000152	2.5	50	2	3.57	2.68	3.21	Tbf	5	2	2
DD	Valley	15	12	0.75	Q	5	0	0.5	0.9	1.3	1	0	6.37	2.5	20.85	0.0000178	2.5	50	2	2.56	1.66	3.82	Tbf	5	12	2
DD		15	13	1.25			0	0	1	0	0	0.4	0	2.5	23.41	2.065E-05	2.5	0								
DD	Valley	16	3	-3.75	Kgr	1	0.8	1.4	0.6	2.5	230	0	99.47	2.5	9.26	-9.38E-07	2.5	240	1	4.92	3.49	0.39	Tr/Kgr	4	10	2
DD	Valley	16	4	-3.25	Kgr	1	0.8	1.4	0.7	2.5	230	0.2	87.22	2.5	9.97	9.44E-07	2.5	225	2	4.79	3.49	0.42	Tr/Kgr	4	13	2
DD	Valley	16	5	-2.75	Tr	1	0.4	0.6	0.8	2.4	30	0.2	74.97	2.5	10.82	2.85E-06	2.5	200	2	4.67	3.48	0.46	Tr/Kgr	4	12	2
DD	Valley	16	6	-2.25	Jz	2	0.7	0.8	0.8	2.6	400	0.2	63.21	2.5	11.83	4.81E-06	2.5	175	2	4.54	3.47	0.49	Tr/Kgr	4	9	2
DD	Valley	16	7	-1.75	Jz	2	0.7	0.8	0.8	2.6	400	0.3	50.47	2.5	13.02	6.85E-06	2.5	175	2	4.41	3.43	1.08	Tr/Kgr	4	9	2
DD	Valley	16	8	-1.25	Tmb	2	0.6	0.7	0.8	2.5	100	0.2	37.73	2.5	14.39	8.99E-06	2.5	150	2	4.34	3.30	1.86	Tr/Kgr	4	8	2
DD	Valley	16	9	-0.75	Q	3	0	0.5	0.8	1.3	1	0.2	25.48	2.5	15.98	0.0000113	2.5	125	2	4.30	3.14	2.23	Tbf	5	6	2
DD	Valley	16	10	-0.25	Q	4	0	0.5	0.8	1.3	1	0.2	19.11	2.5	17.81	0.0000137	2.5	100	2	4.10	2.98	2.49	Tbf	5	5	2
DD	Valley	16	11	0.25	Q	4	0	0.5	0.8	1.3	1	0.2	12.74	2.5	19.88	0.0000162	2.5	50	2	3.52	2.68	3.09	Tbf	5	4	2
DD	Valley	16	12	0.75	Q	5	0	0.5	0.9	1.3	1	0	6.37	2.5	22.25	1.892E-05	2.5	50	2	2.55	1.66	3.75	Tbf	5	14	2
DD		16	13	1.25			0	0	1	0	0	0	0	2.5	24.96	0.0000218	2.5	0								

Dixie Valley Cross-Sectional Data (continued)

1	2	3			4		5	6	7	8	9	10	11		12			13		14			15		16	
Cross-Section	Domain	Location			Lithology		Assigned Parameters: Lithology					Stress Parameters			Coulomb Stress Parameters			Temperature		Seismic Parameters			Gravity-Magnetics		MT (Resistivity)	
		X	Z	Ele-vation	Fm	TV	EGS-Fav	Friction	Certainty	Density	Strength	Frac-Intens	Vert-Stress	TV	CSC	Dilatation	TV	° C	TV	Vp	Vs	TV	Lithology	TV	ohm-m	TV
DD	Valley	17	3	-3.75	Kgr	1	0.8	1.4	0.6	2.5	230	0	104.37	2.5	9.83	-6.22E-07	2.5	235	1	4.92	3.49	0.39	Tr/Kgr	4	18	2
DD	Valley	17	4	-3.25	Kgr	1	0.8	1.4	0.7	2.5	230	0	92.12	2.5	10.61	1.35E-06	2.5	225	1	4.79	3.49	0.42	Tr/Kgr	4	25	2
DD	Valley	17	5	-2.75	Tr	1	0.4	0.6	0.8	2.4	30	0	79.87	2.5	11.52	3.34E-06	2.5	200	1	4.67	3.48	0.46	Tr/Kgr	4	25	2
DD	Valley	17	6	-2.25	Tr	2	0.4	0.6	0.9	2.4	30	0	68.11	2.5	12.59	5.38E-06	2.5	175	1	4.54	3.47	0.49	Tr/Kgr	4	35	2
DD	Valley	17	7	-1.75	Tr	2	0.4	0.6	0.9	2.4	30	0.1	56.35	2.5	13.85	0.0000075	2.5	175	1	4.41	3.43	1.08	Jg	4	35	2
DD	Valley	17	8	-1.25	Jz	2	0.7	0.8	0.9	2.6	400	0.2	44.59	2.5	15.31	9.71E-06	2.5	150	1	4.34	3.30	1.86	Jg	4	25	2
DD	Valley	17	9	-0.75	Jz	3	0.7	0.8	0.9	2.6	400	0.2	31.85	2.5	16.99	0.000012	2.5	125	1	4.30	3.14	2.23	Tbf	5	15	2
DD	Valley	17	10	-0.25	Q	4	0	0.5	0.9	1.3	1	0.2	19.11	2.5	18.92	0.0000145	2.5	100	1	4.10	2.98	2.49	Tbf	5	8	2
DD	Valley	17	11	0.25	Q	4	0	0.5	0.9	1.3	1	0.2	12.74	2.5	21.11	1.708E-05	2.5	50	1	3.52	2.68	3.09	Tbf	5	3	2
DD	Valley	17	12	0.75	Q	5	0	0.5	0.9	1.3	1	0.2	6.37	2.5	23.61	0.0000198	2.5	50	1	2.55	1.66	3.75	Tbf	5	7	2
DD		17	13	1.25			0	0	1	0	0	0	0	2.5	26.47	0.0000228	2.5	0								
DD	Valley	18	3	-3.75	Kgr	1	0.8	1.4	0.6	2.5	230	0	104.37	2.5	10.28	-2.89E-07	2.5	225	1	4.86	3.49	0.39	Tr/Kgr	4		
DD	Valley	18	4	-3.25	Kgr	1	0.8	1.4	0.7	2.5	230	0	92.12	2.5	11.13	1.74E-06	2.5	200	1	4.73	3.49	0.43	Tr/Kgr	4		
DD	Valley	18	5	-2.75	Tr	1	0.4	0.6	0.8	2.4	30	0	79.87	2.5	12.13	0.0000038	2.5	200	1	4.59	3.48	0.47	Tr/Kgr	4		
DD	Valley	18	6	-2.25	Tr	1	0.4	0.6	0.8	2.4	30	0	68.11	2.5	13.28	0.0000059	2.5	175	1	4.46	3.47	0.50	Jg	4		
DD	Valley	18	7	-1.75	Tr	1	0.4	0.6	0.8	2.4	30	0	56.35	2.5	14.62	8.07E-06	2.5	175	1	4.31	3.43	1.13	Jg	4		
DD	Valley	18	8	-1.25	Jz	2	0.7	0.8	0.8	2.6	400	0	44.59	2.5	16.16	0.0000103	2.5	150	1	4.17	3.30	1.83	Jg	4		
DD	Valley	18	9	-0.75	Jz	3	0.7	0.8	0.8	2.6	400	0	31.85	2.5	17.93	0.0000127	2.5	125	1	4.07	3.14	2.00	Tr/Kgr	5		
DD	Valley	18	10	-0.25	Q	4	0	0.5	0.8	1.3	1	0	19.11	2.5	19.96	1.518E-05	2.5	100	1	3.90	2.98	2.10	Tbf	5		
DD	Valley	18	11	0.25	Q	4	0	0.5	0.8	1.3	1	0	12.74	2.5	22.26	0.0000178	2.5	50	1	3.46	2.68	2.75	Tbf	5		
DD	Valley	18	12	0.75	Q	5	0	0.5	0.9	1.3	1	0	6.37	2.5	24.87	2.059E-05	2.5	50	1	2.54	1.66	3.52	Tbf	5		
DD		18	13	1.25			0	0	1	0	0	0	0	2.5	27.85	0.0000235	2.5	0								
EE	SR	1	3	-3.75	Kgr	1	0.8	1.4	0.3	2.5	230	0	133.77	2.5	-26.45	-4.03E-06	2.5	250	1	5.58	3.50	0.15			3000	3
EE	SR	1	4	-3.25	Kgr	1	0.8	1.4	0.3	2.5	230	0	121.52	2.5	-26.47	-5.88E-06	2.5	250	1	5.50	3.50	0.16			3000	3
EE	SR	1	5	-2.75	Kgr	1	0.8	1.4	0.3	2.5	230	0	109.27	2.5	-26.60	-7.87E-06	2.5	225	1	5.42	3.49	0.17	Tr/Kgr	4	1200	3
EE	SR	1	6	-2.25	Kgr	1	0.8	1.4	0.3	2.5	230	0	97.02	2.5	-26.86	-0.0000101	2.5	200	1	5.34	3.48	0.18	Tr/Kgr	4	1000	3
EE	SR	1	7	-1.75	Kgr	1	0.8	1.4	0.3	2.5	230	0	84.77	2.5	-27.33	-0.0000127	2.5	175	1	5.23	3.45	0.29	Tr/Kgr	4	1100	3
EE	SR	1	8	-1.25	Kgr	1	0.8	1.4	0.3	2.5	230	0	72.52	2.5	-28.20	-0.0000157	2.5	150	1	5.12	3.33	0.51	Tr/Kgr	4	900	3
EE	SR	1	9	-0.75	Kgr	2	0.8	1.4	0.3	2.5	230	0	60.27	2.5	-29.85	-0.0000195	2.5	125	1	5.07	3.20	0.74	Tr/Kgr	5	600	3
EE	SR	1	10	-0.25	Tr	3	0.4	0.6	0.5	2.4	30	0	48.02	2.5	-33.07	-0.0000242	2.5	100	1	5.03	3.07	0.98	Tr/Kgr	5	250	3
EE	SR	1	11	0.25	Tr	4	0.4	0.6	0.6	2.4	30	0	36.26	2.5	-39.19	-0.0000301	2.5	50	1	4.63	2.68	1.52	Tr/Kgr	5	80	3
EE	SR	1	12	0.75	Tr	4	0.4	0.6	0.7	2.4	30	0	24.5	2.5	-49.99	-0.000037	2.5	50	1	3.26	1.66	1.96	Tr/Kgr	5	50	3
EE	SR	1	13	1.25	Jz	5	0.7	0.8	0.9	2.6	400	0	12.74	2.5	-66.75	-0.0000447	2.5	50	1				Jg	5		
EE	SR	2	3	-3.75	Kgr	1	0.8	1.4	0.3	2.5	230	0	133.77	2.5	-29.17	-3.77E-06	2.5	275	1	5.33	3.50	0.21			1000	3
EE	SR	2	4	-3.25	Kgr	1	0.8	1.4	0.3	2.5	230	0	121.52	2.5	-29.02	-5.39E-06	2.5	250	1	5.23	3.50	0.22			800	3
EE	SR	2	5	-2.75	Kgr	1	0.8	1.4	0.3	2.5	230	0	109.27	2.5	-28.86	-7.14E-06	2.5	250	1	5.14	3.49	0.24			200	3
EE	SR	2	6	-2.25	Kgr	1	0.8	1.4	0.3	2.5	230	0	97.02	2.5	-28.66	-9.12E-06	2.5	225	1	5.04	3.48	0.26	Tr/Kgr	4	120	3
EE	SR	2	7	-1.75	Kgr	1	0.8	1.4	0.3	2.5	230	0	84.77	2.5	-28.40	-0.0000114	2.5	200	1	4.85	3.45	0.57	Tr/Kgr	4	175	3
EE	SR	2	8	-1.25	Kgr	1	0.8	1.4	0.3	2.5	230	0	72.52	2.5	-28.09	-0.0000143	2.5	175	1	4.72	3.33	1.07	Tr/Kgr	4	200	3
EE	SR	2	9	-0.75	Kgr	2	0.8	1.4	0.3	2.5	230	0	60.27	2.5	-27.88	-0.0000178	2.5	150	1	4.73	3.20	1.46	Tr/Kgr	4	350	3
EE	SR	2	10	-0.25	Tr	3	0.4	0.6	0.5	2.4	30	0	48.02	2.5	-28.23	-0.0000225	2.5	125	1	4.66	3.07	1.82	Tr/Kgr	5	200	3
EE	SR	2	11	0.25	Tr	4	0.4	0.6	0.6	2.4	30	0	36.26	2.5	-30.22	-0.0000285	2.5	100	1	4.10	2.68	2.44	Tr/Kgr	5	50	3
EE	SR	2	12	0.75	Tr	4	0.4	0.6	0.7	2.4	30	0	24.5	2.5	-35.89	-0.0000359	2.5	50	1	2.94	1.66	2.89	Tr/Kgr	5	90	3
EE	SR	2	13	1.25	Jz	5	0.7	0.8	0.9	2.6	400	0	12.74	2.5	-47.77	-0.0000444	2.5	50	1				Jg	5		

Dixie Valley Cross-Sectional Data (continued)

1	2	3			4		5	6	7	8	9	10	11		12			13		14			15		16	
Cross-Section	Do-main	Location			Lithology		Assigned Parameters: Lithology					Stress Parameters			Coulomb Stress Parameters			Temperature		Seismic Parameters			Gravity-Magnetics		MT (Resistivity)	
		X	Z	Ele-vation	Fm	TV	EGS-Fav	Frict-ion	Certain-ty	Densi-ty	Strength	Frac-Intens	Vert-Stress	TV	CSC	Dilatation	TV	° C	TV	Vp	Vs	TV	Lithology	TV	ohm-m	TV
EE	SR	3	3	-3.75	Kgr	1	0.8	1.4	0.3	2.5	230	0	133.77	2.5	-31.66	-3.48E-06	2.5	285	1	5.03	3.51	0.45			500	3
EE	SR	3	4	-3.25	Kgr	1	0.8	1.4	0.3	2.5	230	0	121.52	2.5	-31.05	-4.82E-06	2.5	275	1	4.91	3.50	0.49			250	3
EE	SR	3	5	-2.75	Kgr	1	0.8	1.4	0.3	2.5	230	0	109.27	2.5	-30.27	-6.27E-06	2.5	250	1	4.79	3.49	0.53	Tr/Kgr	4	150	3
EE	SR	3	6	-2.25	Kgr	1	0.8	1.4	0.3	2.5	230	0	97.02	2.5	-29.24	-7.92E-06	2.5	250	2	4.67	3.48	0.57	Tr/Kgr	4	100	3
EE	SR	3	7	-1.75	Kgr	1	0.8	1.4	0.3	2.5	230	0	84.77	2.5	-27.82	-9.85E-06	2.5	225	2	4.63	3.44	0.94	Tr/Kgr	4	150	3
EE	SR	3	8	-1.25	Kgr	1	0.8	1.4	0.3	2.5	230	0	72.52	2.5	-25.85	-0.0000122	2.5	200	2	4.67	3.31	1.55	Tr/Kgr	4	200	3
EE	SR	3	9	-0.75	Kgr	2	0.8	1.4	0.3	2.5	230	0	60.27	2.5	-23.08	-0.0000153	2.5	175	2	4.71	3.15	2.05	Tr/Kgr	5	400	3
EE	SR	3	10	-0.25	Tr	3	0.4	0.6	0.5	2.4	30	0	48.02	2.5	-19.27	-0.0000192	2.5	125	2	4.65	2.99	2.49	Tr/Kgr	5	250	3
EE	SR	3	11	0.25	Tr	4	0.4	0.6	0.6	2.4	30	0	36.26	2.5	-14.29	-0.0000244	2.5	100	2	4.04	2.68	2.96	Tr/Kgr	5	125	3
EE	DVFZ	3	12	0.75	Tr	4	0.4	0.6	0.7	2.4	30	0.2	24.5	2.5	-8.75	-0.0000311	2.5	100	2	2.83	1.66	3.23	Tr/Kgr	5	350	3
EE	DVFZ	3	13	1.25	Jz	5	0.7	0.8	0.9	2.6	400	0.1	12.74	2.5	-5.05	-0.0000389	2.5	0					Jg	5		
EE	SR	4	3	-3.75	Kgr	1	0.8	1.4	0.3	2.5	230	0	122.99	2.5	-31.66	-3.16E-06	2.5	300	2	5.20	3.51	0.85			145	3
EE	SR	4	4	-3.25	Kgr	1	0.8	1.4	0.3	2.5	230	0	110.74	2.5	-30.04	-4.18E-06	2.5	285	2	5.10	3.50	0.93			90	3
EE	SR	4	5	-2.75	Kgr	1	0.8	1.4	0.3	2.5	230	0	98.49	2.5	-28.09	-5.28E-06	2.5	275	3	5.01	3.49	1.00	Tr/Kgr	4	100	3
EE	SR	4	6	-2.25	Kgr	1	0.8	1.4	0.3	2.5	230	0	86.24	2.5	-25.70	-6.51E-06	2.5	260	3	4.91	3.48	1.08	Tr/Kgr	4	130	3
EE	SR	4	7	-1.75	Kgr	1	0.8	1.4	0.3	2.5	230	0	73.99	2.5	-22.69	-7.93E-06	2.5	250	3	4.73	3.44	1.70	Tr/Kgr	4	185	3
EE	SR	4	8	-1.25	Kgr	2	0.8	1.4	0.3	2.5	230	0	61.74	2.5	-18.78	-9.63E-06	2.5	225	3	4.60	3.29	2.51	Tr/Kgr	4	450	3
EE	SR	4	9	-0.75	Kgr	3	0.8	1.4	0.5	2.5	230	0	49.49	2.5	-13.43	-0.0000117	2.5	200	3	4.55	3.12	2.92	Tr/Kgr	5	650	3
EE	DVFZ	4	10	-0.25	Tr	4	0.4	0.6	0.5	2.4	30	0.2	37.24	2.5	-5.66	-0.0000143	2.5	150	3	4.36	2.94	3.24	Tr/Kgr	5	325	3
EE	DVFZ	4	11	0.25	Jz	4	0.7	0.8	0.7	2.6	400	0.4	25.48	2.5	6.37	-0.0000175	2.5	125	3	3.75	2.68	3.51	Tr/Kgr	5	150	3
EE	DVFZ	4	12	0.75	Jz	5	0.7	0.8	0.9	2.6	400	0.2	12.74	2.5	25.21	-0.0000213	2.5	100	3	2.68	1.66	3.65	Tr/Kgr	5	14	3
EE		4	13	1.25			0	0	1	0	0	0	0	2.5	51.78	-0.0000259	2.5	0								
EE	DVFZ	5	3	-3.75	Kgr	1	0.8	1.4	0.3	2.5	230	0	116.62	2.5	-26.13	-2.82E-06	2.5	300	2	5.21	3.51	0.97			150	3
EE	DVFZ	5	4	-3.25	Kgr	1	0.8	1.4	0.3	2.5	230	0	104.37	2.5	-23.08	-0.0000035	2.5	290	2	5.11	3.50	1.07			90	3
EE	DVFZ	5	5	-2.75	Kgr	1	0.8	1.4	0.3	2.5	230	0	92.12	2.5	-19.64	-0.0000042	2.5	280	2	5.02	3.49	1.16	Tr/Kgr	4	130	3
EE	DVFZ	5	6	-2.25	Kgr	1	0.8	1.4	0.3	2.5	230	0	79.87	2.5	-15.75	-4.96E-06	2.5	275	3	4.92	3.48	1.25	Tr/Kgr	4	185	3
EE	DVFZ	5	7	-1.75	Kgr	1	0.8	1.4	0.3	2.5	230	0.2	67.62	2.5	-11.25	-5.78E-06	2.5	250	3	4.75	3.44	1.86	Tr/Kgr	4	220	3
EE	DVFZ	5	8	-1.25	Tr	2	0.4	0.6	0.4	2.4	30	0.2	55.37	2.5	-5.88	-6.66E-06	2.5	225	3	4.61	3.29	2.64	Tr/Kgr	4	800	3
EE	DVFZ	5	9	-0.75	Tr	3	0.4	0.6	0.5	2.4	30	0.2	43.61	2.5	0.89	-7.54E-06	2.5	200	3	4.55	3.12	3.02	Tr/Kgr	5	400	3
EE	DVFZ	5	10	-0.25	Jz	4	0.7	0.8	0.6	2.6	400	0	31.85	2.5	10.22	-8.25E-06	2.5	150	3	4.38	2.94	3.31	Tr/Kgr	5	125	3
EE	DVFZ	5	11	0.25	Jz	4	0.7	0.8	0.7	2.6	400	0	19.11	2.5	24.74	-8.44E-06	2.5	125	3	3.76	2.68	3.58	Tr/Kgr	5	15	3
EE	DVFZ	5	12	0.75	Q	5	0	0.5	1	1.3	1	0	6.37	2.5	49.43	-7.78E-06	2.5	50	3	2.65	1.66	3.77	Tr/Kgr	5	8	3
EE		5	13	1.25			0	0	1	0	0	0	0	2.5	90.10	-0.0000068	2.5	0								
EE	DVFZ	6	3	-3.75	Kgr	1	0.8	1.4	0.3	2.5	230	0	116.62	2.5	-14.51	-2.48E-06	2.5	300	3	5.21	3.51	1.19			150	3
EE	DVFZ	6	4	-3.25	Kgr	1	0.8	1.4	0.3	2.5	230	0.2	104.37	2.5	-10.40	-2.79E-06	2.5	290	3	5.13	3.50	1.29			100	3
EE	DVFZ	6	5	-2.75	Kgr	1	0.8	1.4	0.3	2.5	230	0.2	92.12	2.5	-6.06	-3.09E-06	2.5	280	3	5.05	3.49	1.39	Tr/Kgr	4	165	3
EE	DVFZ	6	6	-2.25	Kgr	1	0.8	1.4	0.3	2.5	230	0.2	79.87	2.5	-1.44	-3.36E-06	2.5	270	4	4.96	3.48	1.49	Tr/Kgr	4	250	3
EE	DVFZ	6	7	-1.75	Kgr	1	0.8	1.4	0.3	2.5	230	0	67.62	2.5	3.50	-3.56E-06	2.5	250	4	4.75	3.44	2.04	Tr/Kgr	4	300	3
EE	DVFZ	6	8	-1.25	Tr	2	0.4	0.6	0.4	2.4	30	0	55.37	2.5	8.91	-0.0000036	2.5	225	3	4.61	3.29	2.70	Tr/Kgr	4	450	3
EE	DVFZ	6	9	-0.75	Tr	3	0.4	0.6	0.7	2.4	30	0	43.61	2.5	15.07	-3.27E-06	2.5	200	3	4.60	3.12	3.04	Tr/Kgr	5	135	3
EE	DVFZ	6	10	-0.25	Jz	4	0.7	0.8	0.7	2.6	400	0	31.85	2.5	22.63	-2.15E-06	2.5	150	3	4.41	2.94	3.33	Tr/Kgr	5	20	3
EE	DVFZ	6	11	0.25	Jz	4	0.7	0.8	0.7	2.6	400	0.2	19.11	2.5	33.30	4.77E-07	2.5	125	3	3.74	2.68	3.62	Jg	5	15	3
EE	DVFZ	6	12	0.75	Q	5	0	0.5	1	1.3	1	0	6.37	2.5	51.03	5.28E-06	2.5	100	4	2.63	1.66	3.86	Tbf	5	6	3
EE		6	13	1.25			0	0	1	0	0	0	0	2.5	82.50	0.0000116	2.5	0								

Dixie Valley Cross-Sectional Data (continued)

1	2	3			4		5	6	7	8	9	10	11		12			13		14			15		16	
Cross-Section	Do-main	Location			Lithology		Assigned Parameters: Lithology					Stress Parameters			Coulomb Stress Parameters			Temperature		Seismic Parameters			Gravity-Magnetics		MT (Resistivity)	
		X	Z	Ele-vation	Fm	TV	EGS-Fav	Frict-ion	Certain-ty	Densi-ty	Strength	Frac-Intens	Vert-Stress	TV	CSC	Dilatation	TV	° C	TV	Vp	Vs	TV	Lithology	TV	ohm-m	TV
EE	DVFZ	7	3	-3.75	Kgr	1	0.8	1.4	0.4	2.5	230	0	98.98	2.5	-1.02	-2.15E-06	2.5	300	3	5.20	3.51	0.98			135	3
EE	DVFZ	7	4	-3.25	Kgr	1	0.8	1.4	0.4	2.5	230	0	86.73	2.5	2.98	-0.0000021	2.5	290	4	5.10	3.50	1.08			140	3
EE	DVFZ	7	5	-2.75	Kgr	1	0.8	1.4	0.5	2.5	230	0	74.48	2.5	6.98	-0.000002	2.5	280	4	5.00	3.49	1.17	Tr/Kgr	4	200	3
EE	DVFZ	7	6	-2.25	Kgr	1	0.8	1.4	0.6	2.5	230	0	62.23	2.5	10.97	-0.0000018	2.5	275	4	4.91	3.48	1.26	Tr/Kgr	4	230	3
EE	DVFZ	7	7	-1.75	Kgr	1	0.8	1.4	0.7	2.5	230	0.24	49.98	2.5	14.95	-1.43E-06	2.5	250	4	4.73	3.44	1.86	Tr/Kgr	4	250	3
EE	DVFZ	7	8	-1.25	Kgr	2	0.8	1.4	0.5	2.5	230	0.2	37.73	2.5	18.92	-7.38E-07	2.5	225	4	4.57	3.29	2.65	Jg	4	220	3
EE	DVFZ	7	9	-0.75	Q	3	0	0.5	0.8	1.3	1	0.2	25.48	2.5	22.89	5.47E-07	2.5	200	4	4.52	3.12	3.05	Jg	5	18	3
EE	DVFZ	7	10	-0.25	Q	4	0	0.5	0.8	1.3	1	0.2	19.11	2.5	26.96	2.93E-06	2.5	150	4	4.32	2.94	3.34	Tbf	5	10	3
EE	DVFZ	7	11	0.25	Q	4	0	0.5	0.8	1.3	1	0	12.74	2.5	31.46	7.14E-06	2.5	125	4	3.71	2.68	3.68	Tbf	5	8	3
EE	Valley	7	12	0.75	Q	5	0	0.5	1	1.3	1	0	6.37	2.5	37.56	1.378E-05	2.5	100	4	2.65	1.66	3.95	Tbf	5	8	3
EE		7	13	1.25			0	0	1	0	0	0	0	2.5	48.33	2.219E-05	2.5	0								
EE	DVFZ	8	3	-3.75	Kgr	4	0.8	1.4	0.4	2.5	230	0	99.47	2.5	8.77	-1.83E-06	2.5	300	3	5.15	3.51	0.98			125	4
EE	DVFZ	8	4	-3.25	Kgr	4	0.8	1.4	0.5	2.5	230	0.2	87.22	2.5	11.69	-1.44E-06	2.5	285	4	5.05	3.50	1.08			150	4
EE	DVFZ	8	5	-2.75	Tr	5	0.4	0.6	0.6	2.4	30	0.2	74.97	2.5	14.46	-9.64E-07	2.5	275	4	4.94	3.49	1.17	Tr/Kgr	4	250	4
EE	DVFZ	8	6	-2.25	Jz	5	0.7	0.8	0.7	2.6	400	0.2	63.21	2.5	17.06	-3.5E-07	2.5	250	5	4.84	3.48	1.26	Tr/Kgr	4	250	4
EE	DVFZ	8	7	-1.75	Jz	5	0.7	0.8	0.8	2.6	400	0	50.47	2.5	19.49	4.96E-07	2.5	250	5	4.68	3.44	1.86	Tr/Kgr	4	210	4
EE	DVFZ	8	8	-1.25	Tmb	5	0.6	0.7	0.7	2.5	100	0.2	37.73	2.5	21.68	1.73E-06	2.5	225	4	4.53	3.29	2.65	Jg	4	110	4
EE	DVFZ	8	9	-0.75	Q	5	0	0.5	1	1.3	1	0.2	25.48	2.5	23.56	3.62E-06	2.5	200	4	4.48	3.12	3.05	Jg	5	12	5
EE	Valley	8	10	-0.25	Q	5	0	0.5	1	1.3	1	0	19.11	2.5	24.92	6.58E-06	2.5	150	4	4.27	2.94	3.34	Tbf	5	8	5
EE	Valley	8	11	0.25	Q	5	0	0.5	1	1.3	1	0	12.74	2.5	25.44	0.0000111	2.5	125	4	3.66	2.68	3.68	Tbf	5	7	5
EE	Valley	8	12	0.75	Q	5	0	0.5	1	1.3	1	0	6.37	2.5	24.66	1.754E-05	2.5	50	5	2.62	1.66	3.95	Tbf	5	10	5
EE		8	13	1.25			0	0	1	0	0	0	0	2.5	22.63	0.0000253	2.5	0								
EE	Valley	9	3	-3.75	Kgr	4	0.8	1.4	0.4	2.5	230	0	98.98	2.5	13.06	-1.54E-06	2.5	295	4	5.15	3.51	0.68			100	4
EE	Valley	9	4	-3.25	Tr	4	0.4	0.6	0.4	2.4	30	0	86.73	2.5	14.79	-8.33E-07	2.5	275	4	5.04	3.50	0.74			110	4
EE	Valley	9	5	-2.75	Tr	5	0.4	0.6	0.5	2.4	30	0	74.97	2.5	16.37	-2.69E-08	2.5	250	5	4.94	3.49	0.80	Tr/Kgr	4	165	4
EE	Valley	9	6	-2.25	Jz	5	0.7	0.8	0.6	2.6	400	0	63.21	2.5	17.82	9.37E-07	2.5	250	5	4.84	3.48	0.87	Tr/Kgr	4	175	4
EE	Valley	9	7	-1.75	Jz	5	0.7	0.8	0.7	2.6	400	0	50.47	2.5	19.11	2.15E-06	2.5	225	4	4.64	3.44	1.50	Tr/Kgr	4	165	4
EE	Valley	9	8	-1.25	Tmb	5	0.6	0.7	0.7	2.5	100	0	37.73	2.5	20.22	3.75E-06	2.5	200	4	4.48	3.29	2.36	Jg	4	75	4
EE	Valley	9	9	-0.75	Q	5	0	0.5	0.8	1.3	1	0	25.48	2.5	21.02	5.95E-06	2.5	175	4	4.42	3.12	2.80	Jg	5	10	5
EE	Valley	9	10	-0.25	Q	5	0	0.5	0.8	1.3	1	0	19.11	2.5	21.29	9.02E-06	2.5	150	4	4.22	2.94	3.11	Tbf	5	7	5
EE	Valley	9	11	0.25	Q	5	0	0.5	0.8	1.3	1	0	12.74	2.5	20.54	0.0000133	2.5	125	4	3.64	2.68	3.54	Tbf	5	6	5
EE	Valley	9	12	0.75	Q	5	0	0.5	1	1.3	1	0	6.37	2.5	17.93	0.0000187	2.5	50	4	2.62	1.66	3.89	Tbf	5	4	5
EE		9	13	1.25			0	0	1	0	0	0	0	2.5	12.54	0.0000251	2.5	0			-99.00					
EE	Valley	10	3	-3.75	Tr	1	0.4	0.6	0.3	2.4	30	0	93.1	2.5	13.72	-1.27E-06	2.5	280	4	5.15	3.51	0.67			90	4
EE	Valley	10	4	-3.25	Tr	1	0.4	0.6	0.3	2.4	30	0	81.34	2.5	14.66	-2.83E-07	2.5	275	4	5.04	3.50	0.73			85	4
EE	Valley	10	5	-2.75	Jz	1	0.7	0.8	0.3	2.6	400	0	69.58	2.5	15.55	8.06E-07	2.5	250	4	4.94	3.49	0.79	Tr/Kgr	4	110	4
EE	Valley	10	6	-2.25	Jz	1	0.7	0.8	0.3	2.6	400	0	56.84	2.5	16.40	2.05E-06	2.5	225	4	4.84	3.48	0.85	Tr/Kgr	4	90	4
EE	Valley	10	7	-1.75	Tmb	1	0.6	0.7	0.7	2.5	100	0	44.1	2.5	17.21	3.54E-06	2.5	200	3	4.64	3.44	1.47	Tr/Kgr	4	75	4
EE	Valley	10	8	-1.25	Q	2	0	0.5	0.7	1.3	1	0	31.85	2.5	17.94	5.37E-06	2.5	175	3	4.48	3.29	2.30	Tbf	4	65	4
EE	Valley	10	9	-0.75	Q	3	0	0.5	0.8	1.3	1	0	25.48	2.5	18.50	0.0000077	2.5	150	3	4.42	3.12	2.73	Tbf	5	7	5
EE	Valley	10	10	-0.25	Q	4	0	0.5	0.8	1.3	1	0	19.11	2.5	18.69	1.069E-05	2.5	125	3	4.22	2.94	3.03	Tbf	5	5	5
EE	Valley	10	11	0.25	Q	4	0	0.5	0.8	1.3	1	0	12.74	2.5	18.07	1.447E-05	2.5	100	3	3.64	2.68	3.51	Tbf	5	5	5
EE	Valley	10	12	0.75	Q	5	0	0.5	1	1.3	1	0	6.37	2.5	15.92	1.905E-05	2.5	50	4	2.63	1.66	3.91	Tbf	5	5	5
EE		10	13	1.25			0	0	1	0	0	0	0	2.5	11.35	2.421E-05	2.5	0								

Dixie Valley Cross-Sectional Data (continued)

1	2	3			4		5	6	7	8	9	10	11		12			13		14			15		16	
Cross-Section	Do-main	Location			Lithology		Assigned Parameters: Lithology					Stress Parameters			Coulomb Stress Parameters			Temperature		Seismic Parameters			Gravity-Magnetics		MT (Resistivity)	
		X	Z	Ele-vation	Fm	TV	EGS-Fav	Frict-ion	Certain-ty	Densi-ty	Strength	Frac-Intens	Vert-Stress	TV	CSC	Dilatation	TV	° C	TV	Vp	Vs	TV	Lithology	TV	ohm-m	TV
EE	Valley	11	3	-3.75	Tr	1	0.4	0.6	0.3	2.4	30	0.2	93.1	2.5	13.01	-1.02E-06	2.5	275	3	5.14	3.51	0.65			85	4
EE	Valley	11	4	-3.25	Tr	1	0.4	0.6	0.3	2.4	30	0.2	81.34	2.5	13.59	2.12E-07	2.5	250	3	5.04	3.50	0.72			50	4
EE	Valley	11	5	-2.75	Jz	1	0.7	0.8	0.3	2.6	400	0.2	69.58	2.5	14.21	1.54E-06	2.5	225	4	4.94	3.49	0.78	Tr/Kgr	4	65	4
EE	Valley	11	6	-2.25	Jz	1	0.7	0.8	0.3	2.6	400	0.2	56.84	2.5	14.87	3.01E-06	2.5	225	4	4.84	3.48	0.84	Tr/Kgr	4	75	4
EE	Valley	11	7	-1.75	Tmb	1	0.6	0.7	0.7	2.5	100	0.2	44.1	2.5	15.58	0.0000047	2.5	200	3	4.64	3.44	1.44	Tr/Kgr	4	65	4
EE	Valley	11	8	-1.25	Q	2	0	0.5	0.7	1.3	1	0.2	31.85	2.5	16.32	6.68E-06	2.5	175	3	4.48	3.29	2.25	Jg	4	20	4
EE	Valley	11	9	-0.75	Q	3	0	0.5	0.8	1.3	1	0.2	25.48	2.5	17.02	9.05E-06	2.5	150	3	4.43	3.12	2.68	Tbf	5	4	5
EE	Valley	11	10	-0.25	Q	4	0	0.5	0.8	1.3	1	0.2	19.11	2.5	17.51	0.0000119	2.5	125	3	4.20	2.94	2.98	Tbf	5	3	5
EE	Valley	11	11	0.25	Q	4	0	0.5	0.8	1.3	1	0.2	12.74	2.5	17.47	0.0000153	2.5	100	3	3.61	2.68	3.49	Tbf	5	5	5
EE	Valley	11	12	0.75	Q	5	0	0.5	1	1.3	1	0.2	6.37	2.5	16.38	0.0000192	2.5	50	3	2.60	1.66	3.93	Tbf	5	15	5
EE		11	13	1.25			0	0	1	0	0	0	0	2.5	13.61	0.0000236	2.5	0								
EE	Valley	12	3	-3.75	Tr	1	0.4	0.6	0.3	2.4	30	0	93.1	2.5	12.18	-7.82E-07	2.5	250	3	5.13	3.51	0.65			60	4
EE	Valley	12	4	-3.25	Tr	1	0.4	0.6	0.3	2.4	30	0	81.34	2.5	12.65	6.58E-07	2.5	250	3	5.02	3.50	0.71			32	4
EE	Valley	12	5	-2.75	Jz	1	0.7	0.8	0.3	2.6	400	0	69.58	2.5	13.21	2.18E-06	2.5	225	3	4.92	3.49	0.78	Tr/Kgr	4	22	4
EE	Valley	12	6	-2.25	Jz	1	0.7	0.8	0.3	2.6	400	0	56.84	2.5	13.88	3.83E-06	2.5	225	3	4.81	3.48	0.84	Tr/Kgr	4	15	4
EE	Valley	12	7	-1.75	Tmb	1	0.6	0.7	0.7	2.5	100	0	44.1	2.5	14.67	5.67E-06	2.5	200	3	4.62	3.44	1.43	Tr/Kgr	4	10	4
EE	Valley	12	8	-1.25	Q	2	0	0.5	0.7	1.3	1	0	31.85	2.5	15.56	7.74E-06	2.5	175	3	4.46	3.29	2.21	Tbf	4	8	4
EE	Valley	12	9	-0.75	Q	3	0	0.5	0.8	1.3	1	0	25.48	2.5	16.51	0.0000101	2.5	150	3	4.40	3.12	2.61	Tbf	5	5	5
EE	Valley	12	10	-0.25	Q	4	0	0.5	0.8	1.3	1	0	19.11	2.5	17.39	1.287E-05	2.5	125	3	4.16	2.94	2.89	Tbf	5	2	5
EE	Valley	12	11	0.25	Q	4	0	0.5	0.8	1.3	1	0	12.74	2.5	17.97	0.000016	2.5	100	3	3.59	2.68	3.40	Tbf	5	2	5
EE	Valley	12	12	0.75	Q	5	0	0.5	1	1.3	1	0	6.37	2.5	17.91	0.0000195	2.5	50	3	2.61	1.66	3.89	Tbf	5	11	5
EE		12	13	1.25			0	0	1	0	0	0	0	2.5	16.81	0.0000233	2.5	0								
EE	Valley	13	3	-3.75	Tr	1	0.4	0.6	0.3	2.4	30	0	93.1	2.5	11.63	-5.45E-07	2.5	250	2	5.11	3.51	0.64			10	4
EE	Valley	13	4	-3.25	Tr	1	0.4	0.6	0.3	2.4	30	0	81.34	2.5	12.11	1.07E-06	2.5	225	2	5.01	3.50	0.70			10	4
EE	Valley	13	5	-2.75	Jz	1	0.7	0.8	0.3	2.6	400	0	69.58	2.5	12.72	2.75E-06	2.5	225	3	4.90	3.49	0.76	Tr/Kgr	4	10	4
EE	Valley	13	6	-2.25	Jz	1	0.7	0.8	0.3	2.6	400	0	56.84	2.5	13.48	4.54E-06	2.5	200	3	4.80	3.48	0.82	Tr/Kgr	4	9	4
EE	Valley	13	7	-1.75	Tmb	1	0.6	0.7	0.7	2.5	100	0	44.1	2.5	14.40	6.49E-06	2.5	175	3	4.61	3.44	1.40	Tr/Kgr	4	8	4
EE	Valley	13	8	-1.25	Q	2	0	0.5	0.7	1.3	1	0	31.85	2.5	15.47	8.63E-06	2.5	150	3	4.45	3.29	2.16	Tbf	4	7	4
EE	Valley	13	9	-0.75	Q	3	0	0.5	0.8	1.3	1	0	25.48	2.5	16.67	1.102E-05	2.5	125	3	4.39	3.12	2.55	Tbf	5	5	5
EE	Valley	13	10	-0.25	Q	4	0	0.5	0.8	1.3	1	0	19.11	2.5	17.90	0.0000137	2.5	100	3	4.15	2.94	2.82	Tbf	5	3	5
EE	Valley	13	11	0.25	Q	4	0	0.5	0.8	1.3	1	0	12.74	2.5	19.01	0.0000166	2.5	50	3	3.58	2.68	3.34	Tbf	5	2	5
EE	Valley	13	12	0.75	Q	5	0	0.5	1	1.3	1	0	6.37	2.5	19.80	0.0000199	2.5	50	3	2.60	1.66	3.88	Tbf	5	9	5
EE		13	13	1.25			0	0	1	0	0	0	0	2.5	20.00	0.0000234	2.5	0								
EE	Valley	14	3	-3.75	Tr	1	0.4	0.6	0.3	2.4	30	0.2	93.1	2.5	11.38	-3.04E-07	2.5	250	3	5.15	3.49	0.66			10	4
EE	Valley	14	4	-3.25	Tr	1	0.4	0.6	0.3	2.4	30	0.2	81.34	2.5	11.92	1.44E-06	2.5	225	3	5.04	3.49	0.72			10	4
EE	Valley	14	5	-2.75	Jz	1	0.7	0.8	0.3	2.6	400	0	69.58	2.5	12.62	3.25E-06	2.5	200	4	4.94	3.48	0.79	Tr/Kgr	4	9	4
EE	Valley	14	6	-2.25	Jz	1	0.7	0.8	0.3	2.6	400	0	56.84	2.5	13.50	5.16E-06	2.5	200	4	4.84	3.47	0.85	Tr/Kgr	4	8	4
EE	Valley	14	7	-1.75	Tmb	1	0.6	0.7	0.7	2.5	100	0	44.1	2.5	14.56	7.19E-06	2.5	175	4	4.65	3.43	1.40	Tr/Kgr	4	7	4
EE	Valley	14	8	-1.25	Q	2	0	0.5	0.7	1.3	1	0	31.85	2.5	15.80	9.39E-06	2.5	150	4	4.49	3.30	2.15	Tbf	4	6	4
EE	Valley	14	9	-0.75	Q	3	0	0.5	0.8	1.3	1	0	25.48	2.5	17.21	0.0000118	2.5	125	4	4.43	3.14	2.54	Tbf	5	5	5
EE	Valley	14	10	-0.25	Q	4	0	0.5	0.8	1.3	1	0	19.11	2.5	18.74	0.0000144	2.5	100	4	4.18	2.98	2.80	Tbf	5	4	5
EE	Valley	14	11	0.25	Q	4	0	0.5	0.8	1.3	1	0	12.74	2.5	20.27	0.0000172	2.5	50	4	3.59	2.68	3.33	Tbf	5	2	5
EE	Valley	14	12	0.75	Q	5	0	0.5	1	1.3	1	0	6.37	2.5	21.70	0.0000203	2.5	50	4	2.61	1.66	3.85	Tbf	5	10	5
EE		14	13	1.25			0	0	1	0	0	0	0	2.5	22.86	2.362E-05	2.5	0								

Dixie Valley Cross-Sectional Data (continued)

1	2	3			4		5	6	7	8	9	10	11		12			13		14			15		16	
Cross-Section	Do-main	Location			Lithology		Assigned Parameters: Lithology					Stress Parameters			Coulomb Stress Parameters			Temperature		Seismic Parameters			Gravity-Magnetics		MT (Resistivity)	
		X	Z	Ele-vation	Fm	TV	EGS-Fav	Frict-ion	Certain-ty	Densi-ty	Strength	Frac-Intens	Vert-Stress	TV	CSC	Dilatation	TV	° C	TV	Vp	Vs	TV	Lithology	TV	ohm-m	TV
EE	Valley	15	3	-3.75	Kgr	1	0.8	1.4	0.3	2.5	230	0	93.1	2.5	11.34	-5.3E-08	2.5	225	3	5.10	3.47	0.56			10	4
EE	Valley	15	4	-3.25	Kgr	1	0.8	1.4	0.3	2.5	230	0	80.85	2.5	11.98	0.0000018	2.5	225	3	4.99	3.46	0.61			10	4
EE	Valley	15	5	-2.75	Tr	1	0.4	0.6	0.3	2.4	30	0.2	68.6	2.5	12.79	3.71E-06	2.5	200	4	4.88	3.45	0.66	Tr/Kgr	4	8	4
EE	Valley	15	6	-2.25	Jz	1	0.7	0.8	0.3	2.6	400	0.2	56.84	2.5	13.78	0.0000057	2.5	175	4	4.77	3.45	0.72	Tr/Kgr	4	8	4
EE	Valley	15	7	-1.75	Tmb	1	0.6	0.7	0.7	2.5	100	0.2	44.1	2.5	14.97	0.0000078	2.5	175	4	4.59	3.42	1.26	Tr/Kgr	4	7	4
EE	Valley	15	8	-1.25	Q	2	0	0.5	0.7	1.3	1	0.2	31.85	2.5	16.36	1.004E-05	2.5	150	4	4.43	3.31	2.00	Tr/Kgr	4	5	4
EE	Valley	15	9	-0.75	Q	3	0	0.5	0.8	1.3	1	0	25.48	2.5	17.95	1.244E-05	2.5	125	4	4.37	3.18	2.38	Tbf	5	3	5
EE	Valley	15	10	-0.25	Q	4	0	0.5	0.8	1.3	1	0	19.11	2.5	19.70	0.000015	2.5	100	4	4.07	3.04	2.62	Tbf	5	2	5
EE	Valley	15	11	0.25	Q	4	0	0.5	0.8	1.3	1	0	12.74	2.5	21.57	0.0000178	2.5	50	4	3.45	2.68	3.19	Tbf	5	2	5
EE	Valley	15	12	0.75	Q	5	0	0.5	1	1.3	1	0	6.37	2.5	23.46	0.0000208	2.5	50	4	2.52	1.66	3.78	Tbf	5	12	5
EE		15	13	1.25			0	0	1	0	0	0	0	2.5	25.31	0.000024	2.5	0								
EE	Valley	16	3	-3.75	Kgr	4	0.8	1.4	0.3	2.5	230	0	98.98	2.5	11.43	2.11E-07	2.5	225	4	5.09	3.47	0.59			10	4
EE	Valley	16	4	-3.25	Kgr	4	0.8	1.4	0.3	2.5	230	0	86.73	2.5	12.17	2.15E-06	2.5	200	4	4.98	3.46	0.65			13	4
EE	Valley	16	5	-2.75	Tr	5	0.4	0.6	0.3	2.4	30	0	74.48	2.5	13.09	4.13E-06	2.5	175	5	4.88	3.45	0.70	Tr/Kgr	4	12	4
EE	Valley	16	6	-2.25	Tr	5	0.4	0.6	0.3	2.4	30	0	62.72	2.5	14.19	6.18E-06	2.5	175	5	4.77	3.45	0.76	Tr/Kgr	4	9	4
EE	Valley	16	7	-1.75	Jz	5	0.7	0.8	0.3	2.6	400	0	50.96	2.5	15.50	8.33E-06	2.5	150	5	4.59	3.42	1.30	Tr/Kgr	4	9	4
EE	Valley	16	8	-1.25	Jz	5	0.7	0.8	0.5	2.6	400	0	38.22	2.5	17.02	0.0000106	2.5	125	5	4.45	3.31	2.04	Tr/Kgr	4	8	4
EE	Valley	16	9	-0.75	Q	5	0	0.5	0.8	1.3	1	0.2	25.48	2.5	18.75	0.000013	2.5	125	5	4.38	3.18	2.44	Tbf	5	6	5
EE	Valley	16	10	-0.25	Q	5	0	0.5	0.8	1.3	1	0.2	19.11	2.5	20.68	0.0000156	2.5	100	5	4.05	3.04	2.69	Tbf	5	5	5
EE	Valley	16	11	0.25	Q	5	0	0.5	0.8	1.3	1	0.2	12.74	2.5	22.79	0.0000183	2.5	50	5	3.34	2.68	3.16	Tbf	5	4	5
EE	Valley	16	12	0.75	Q	5	0	0.5	1	1.3	1	0.2	6.37	2.5	25.02	2.123E-05	2.5	50	5	2.43	1.66	3.66	Tbf	5	14	5
EE		16	13	1.25			0	0	1	0	0	0	0	2.5	27.36	0.0000243	2.5	0							0	
EE	Valley	17	3	-3.75	Kgr		0.8	1.4	0.3	2.5	230	0	104.37	2.5	11.56	4.88E-07	2.5	200	4	5.05	3.47	0.51			18	4
EE	Valley	17	4	-3.25	Kgr	4	0.8	1.4	0.3	2.5	230	0	92.12	2.5	12.42	2.48E-06	2.5	200	4	4.93	3.46	0.56			25	4
EE	Valley	17	5	-2.75	Tr	4	0.4	0.6	0.3	2.4	30	0	79.87	2.5	13.44	4.52E-06	2.5	175	4	4.82	3.45	0.61	Tr/Kgr	4	25	4
EE	Valley	17	6	-2.25	Tr	4	0.4	0.6	0.3	2.4	30	0	68.11	2.5	14.65	6.61E-06	2.5	175	4	4.70	3.45	0.66	Tr/Kgr	4	35	4
EE	Valley	17	7	-1.75	Tr	4	0.4	0.6	0.3	2.4	30	0	56.35	2.5	16.06	0.0000088	2.5	150	4	4.54	3.42	1.26	Tr/Kgr	4	35	4
EE	Valley	17	8	-1.25	Jz	4	0.7	0.8	0.5	2.6	400	0	44.59	2.5	17.69	0.0000111	2.5	125	4	4.41	3.31	2.09	Tr/Kgr	4	25	4
EE	Valley	17	9	-0.75	Jz	4	0.7	0.8	0.5	2.6	400	0	31.85	2.5	19.53	0.0000135	2.5	125	4	4.35	3.18	2.52	Jg	5	15	5
EE	Valley	17	10	-0.25	Q	4	0	0.5	0.8	1.3	1	0	19.11	2.5	21.60	0.000016	2.5	100	4	4.04	3.04	2.77	Tbf	5	8	5
EE	Valley	17	11	0.25	Q	4	0	0.5	0.8	1.3	1	0	12.74	2.5	23.88	0.0000187	2.5	50	4	3.30	2.68	3.18	Tbf	5	3	5
EE	Valley	17	12	0.75	Q	5	0	0.5	1	1.3	1	0	6.37	2.5	26.36	0.0000216	2.5	50	4	2.38	1.66	3.56	Tbf	5	7	5
EE		17	13	1.25			0	0	1	0	0	0	0	2.5	29.02	0.0000247	2.5	0								
FF	SR	1	3	-3.75	Kgr	1	0.8	1.4	0.2	2.5	230	0	132.3	2.5	-13.74	-0.0000033	2.5	250	1	5.36	3.51	1.02	Tr/Kgr	4		
FF	SR	1	4	-3.25	Kgr	1	0.8	1.4	0.3	2.5	230	0	120.05	2.5	-13.52	-5.18E-06	2.5	250	1	5.28	3.50	1.11	Tr/Kgr	4		
FF	SR	1	5	-2.75	Kgr	1	0.8	1.4	0.4	2.5	230	0	107.8	2.5	-13.54	-7.17E-06	2.5	225	1	5.19	3.49	1.20	Tr/Kgr	4		
FF	SR	1	6	-2.25	Kgr	1	0.8	1.4	0.4	2.5	230	0	95.55	2.5	-13.87	-9.36E-06	2.5	200	1	5.11	3.48	1.30	Tr/Kgr	4		
FF	SR	1	7	-1.75	Kgr	1	0.8	1.4	0.4	2.5	230	0	83.3	2.5	-14.65	-0.0000118	2.5	200	1	5.06	3.44	1.45	Tr/Kgr	4		
FF	SR	1	8	-1.25	Kgr	1	0.8	1.4	0.4	2.5	230	0	71.05	2.5	-16.06	-0.0000147	2.5	200	1	5.04	3.31	1.65	Tr/Kgr	4		
FF	SR	1	9	-0.75	Tr	2	0.4	0.6	0.5	2.4	30	0	58.8	2.5	-18.38	-0.0000183	2.5	150	1	5.00	3.15	1.84	Tr/Kgr	5		
FF	SR	1	10	-0.25	Tr	3	0.4	0.6	0.6	2.4	30	0	47.04	2.5	-21.88	-0.0000227	2.5	125	2	4.69	2.99	1.96	Tr/Kgr	5		
FF	SR	1	11	0.25	Tr	4	0.4	0.6	0.7	2.4	30	0	35.28	2.5	-26.57	-0.0000282	2.5	100	2	4.02	2.68	2.26	Tr/Kgr	5		
FF	SR	1	12	0.75	Tr	4	0.4	0.6	0.8	2.4	30	0	23.52	2.5	-31.25	-0.0000352	2.5	50	2	2.86	1.66	2.53	Tr/Kgr	5		
FF	SR	1	13	1.25	Tr	5	0.4	0.6	0.9	2.4	30	0	11.76	2.5	-31.83	-0.0000432	2.5	50	2				Tr/Kgr	5		

Dixie Valley Cross-Sectional Data (continued)

1	2	3			4		5	6	7	8	9	10	11		12			13		14			15		16	
Cross-Section	Do-main	Location			Lithology		Assigned Parameters: Lithology					Stress Parameters			Coulomb Stress Parameters			Temperature		Seismic Parameters			Gravity-Magnetics		MT (Resistivity)	
		X	Z	Ele-vation	Fm	TV	EGS-Fav	Frict-ion	Certain-ty	Densi-ty	Strength	Frac-Intens	Vert-Stress	TV	CSC	Dilatation	TV	° C	TV	Vp	Vs	TV	Lithology	TV	ohm-m	TV
FF	SR	2	3	-3.75	Kgr	1	0.8	1.4	0.3	2.5	230	0	132.3	2.5	-10.62	-3.06E-06	2.5	250	1	5.35	3.51	1.21	Tr/Kgr	4		
FF	SR	2	4	-3.25	Kgr	1	0.8	1.4	0.3	2.5	230	0	120.05	2.5	-10.22	-4.74E-06	2.5	250	1	5.27	3.50	1.32	Tr/Kgr	4		
FF	SR	2	5	-2.75	Kgr	1	0.8	1.4	0.4	2.5	230	0	107.8	2.5	-10.05	-6.55E-06	2.5	225	1	5.18	3.49	1.44	Tr/Kgr	4	3500	4
FF	SR	2	6	-2.25	Kgr	1	0.8	1.4	0.5	2.5	230	0	95.55	2.5	-10.19	-8.55E-06	2.5	225	1	5.10	3.48	1.55	Tr/Kgr	4	3500	4
FF	SR	2	7	-1.75	Kgr	2	0.8	1.4	0.5	2.5	230	0	83.3	2.5	-10.78	-0.0000109	2.5	200	1	5.05	3.44	1.70	Tr/Kgr	4	3500	4
FF	SR	2	8	-1.25	Kgr	2	0.8	1.4	0.5	2.5	230	0	71.05	2.5	-12.07	-0.0000137	2.5	200	2	5.03	3.31	1.89	Tr/Kgr	4	3000	4
FF	SR	2	9	-0.75	Tr	3	0.4	0.6	0.5	2.4	30	0	58.8	2.5	-14.51	-0.0000173	2.5	150	2	5.00	3.15	2.06	Tr/Kgr	5	3000	5
FF	SR	2	10	-0.25	Tr	3	0.4	0.6	0.6	2.4	30	0	47.04	2.5	-18.74	-0.000022	2.5	125	3	4.72	2.99	2.18	Tr/Kgr	5	1500	5
FF	SR	2	11	0.25	Tr	4	0.4	0.6	0.7	2.4	30	0	35.28	2.5	-25.22	-0.0000287	2.5	100	3	4.05	2.68	2.47	Tr/Kgr	5	500	5
FF	SR	2	12	0.75	Tr	4	0.4	0.6	0.8	2.4	30	0	23.52	2.5	-31.96	-0.0000385	2.5	50	3	2.88	1.66	2.73	Tr/Kgr	5	100	5
FF	SR	2	13	1.25	Tr	5	0.4	0.6	0.9	2.4	30	0.2	11.76	2.5	-25.92	-0.000052	2.5	50	3				Tr/Kgr	5		
FF	SR	3	3	-3.75	Kgr	1	0.8	1.4	0.4	2.5	230	0	120.54	2.5	-3.71	-0.0000028	2.5	260	1	5.33	3.51	1.44	Tr/Kgr	4		
FF	SR	3	4	-3.25	Kgr	1	0.8	1.4	0.4	2.5	230	0	108.29	2.5	-2.66	-4.25E-06	2.5	250	1	5.24	3.50	1.57	Tr/Kgr	4		
FF	SR	3	5	-2.75	Kgr	2	0.8	1.4	0.4	2.5	230	0	96.04	2.5	-1.73	-5.82E-06	2.5	240	1	5.16	3.49	1.71	Tr/Kgr	4	2000	4
FF	SR	3	6	-2.25	Kgr	2	0.8	1.4	0.5	2.5	230	0	83.79	2.5	-0.95	-7.59E-06	2.5	225	1	5.07	3.48	1.85	Tr/Kgr	4	2000	4
FF	SR	3	7	-1.75	Kgr	3	0.8	1.4	0.6	2.5	230	0	71.54	2.5	-0.43	-9.69E-06	2.5	200	1	5.01	3.44	2.02	Tr/Kgr	4	2000	4
FF	SR	3	8	-1.25	Kgr	3	0.8	1.4	0.6	2.5	230	0	59.29	2.5	-0.43	-0.0000123	2.5	200	2	4.98	3.31	2.22	Tr/Kgr	4	2500	4
FF	SR	3	9	-0.75	Tr	3	0.4	0.6	0.6	2.4	30	0	47.04	2.5	-1.53	-0.0000158	2.5	175	2	4.94	3.15	2.41	Tr/Kgr	5	3000	5
FF	SR	3	10	-0.25	Tr	4	0.4	0.6	0.6	2.4	30	0	35.28	2.5	-5.05	-0.0000207	2.5	125	3	4.62	2.99	2.55	Tr/Kgr	5	2000	5
FF	SR	3	11	0.25	Tr	4	0.4	0.6	0.7	2.4	30	0	23.52	2.5	-13.39	-0.0000281	2.5	100	3	3.95	2.68	2.87	Jg	5	1000	5
FF	DVFZ	3	12	0.75	Tr	5	0.4	0.6	0.8	2.4	30	0.3	11.76	2.5	-26.63	-0.0000415	2.5	50	3	2.79	1.66	3.13	Tr/Kgr	5	80	5
FF		3	13	1.25			0	0	0.9	0	0	0.1	0	2.5	22.47	-0.0000792	2.5	0								
FF	SR	4	3	-3.75	Kgr	1	0.8	1.4	0.5	2.5	230	0	120.54	2.5	18.85	-2.52E-06	2.5	265	1	5.23	3.51	1.43	Tr/Kgr	4		
FF	SR	4	4	-3.25	Kgr	1	0.8	1.4	0.5	2.5	230	0	108.29	2.5	24.82	-0.0000037	2.5	260	1	5.14	3.50	1.56	Tr/Kgr	4		
FF	SR	4	5	-2.75	Kgr	2	0.8	1.4	0.5	2.5	230	0	96.04	2.5	32.73	-4.99E-06	2.5	250	1	5.04	3.49	1.70	Tr/Kgr	4	1000	4
FF	SR	4	6	-2.25	Kgr	2	0.8	1.4	0.5	2.5	230	0	83.79	2.5	43.90	-6.46E-06	2.5	225	2	4.95	3.48	1.83	Tr/Kgr	4	1000	4
FF	SR	4	7	-1.75	Kgr	3	0.8	1.4	0.6	2.5	230	0	71.54	2.5	60.86	-8.24E-06	2.5	225	2	4.86	3.44	2.07	Tr/Kgr	4	1000	4
FF	SR	4	8	-1.25	Kgr	3	0.8	1.4	0.7	2.5	230	0	59.29	2.5	89.30	-0.0000105	2.5	200	3	4.77	3.31	2.40	Tr/Kgr	4	1200	4
FF	SR	4	9	-0.75	Tr	3	0.4	0.6	0.7	2.4	30	0	47.04	2.5	144.97	-0.0000138	2.5	200	3	4.70	3.15	2.65	Tr/Kgr	5	2000	5
FF	DVFZ	4	10	-0.25	Tr	4	0.4	0.6	0.7	2.4	30	0	35.28	2.5	290.69	-0.0000186	2.5	150	4	4.43	2.99	2.82	Tr/Kgr	5	1500	5
FF	DVFZ	4	11	0.25	Tr	4	0.4	0.6	0.7	2.4	30	0.2	23.52	2.5	1093.44	-0.000026	2.5	125	4	3.84	2.68	3.14	Tr/Kgr	5	1000	5
FF	DVFZ	4	12	0.75	Tr	5	0.4	0.6	0.8	2.4	30	0.5	11.76	2.5	644.50	-0.0000359	2.5	100	4	2.75	1.66	3.39	Tr/Kgr	5	80	5
FF		4	13	1.25			0	0	0.9	0	0	0.1	0	2.5	279.95	0.0000997	2.5	0								
FF	SR	5	3	-3.75	Kgr	2	0.8	1.4	0.6	2.5	230	0	115.64	2.5	193.37	-2.22E-06	2.5	275	1	5.23	3.51	1.37	Tr/Kgr	4		
FF	SR	5	4	-3.25	Kgr	2	0.8	1.4	0.6	2.5	230	0	103.39	2.5	319.11	-3.11E-06	2.5	265	1	5.14	3.50	1.50	Tr/Kgr	4		
FF	DVFZ	5	5	-2.75	Kgr	3	0.8	1.4	0.6	2.5	230	0	91.14	2.5	563.65	-4.07E-06	2.5	260	1	5.04	3.49	1.63	Tr/Kgr	4	600	4
FF	DVFZ	5	6	-2.25	Kgr	3	0.8	1.4	0.6	2.5	230	0	78.89	2.5	764.72	-5.18E-06	2.5	250	2	4.95	3.48	1.76	Tr/Kgr	4	800	4
FF	DVFZ	5	7	-1.75	Kgr	4	0.8	1.4	0.6	2.5	230	0	66.64	2.5	394.19	-6.55E-06	2.5	225	2	4.85	3.44	2.03	Tr/Kgr	4	800	4
FF	DVFZ	5	8	-1.25	Kgr	4	0.8	1.4	0.7	2.5	230	0	54.39	2.5	91.27	-8.39E-06	2.5	225	3	4.77	3.31	2.44	Tr/Kgr	4	800	4
FF	DVFZ	5	9	-0.75	Tr	4	0.4	0.6	0.8	2.4	30	0	42.14	2.5	-22.44	-0.0000111	2.5	200	3	4.68	3.15	2.75	Tr/Kgr	5	1000	5
FF	DVFZ	5	10	-0.25	Tr	4	0.4	0.6	0.8	2.4	30	0	30.38	2.5	-69.14	-0.0000156	2.5	150	4	4.40	2.99	2.91	Tr/Kgr	5	1000	5
FF	DVFZ	5	11	0.25	Jbr	4	0.6	0.8	0.8	2.5	200	0.2	18.62	2.5	-95.48	-0.0000238	2.5	125	4	3.84	2.68	3.21	Tr/Kgr	5	400	5
FF	DVFZ	5	12	0.75	Q	5	0	0.5	0.8	1.3	1	0	6.37	2.5	-123.17	-0.0000391	2.5	125	4	2.77	1.66	3.46	Tbf	5	60	5
FF		5	13	1.25			0	0	0.9	0	0	0	0	2.5	-143.49	-0.0000567	2.5	0								

Dixie Valley Cross-Sectional Data (continued)

1	2	3			4		5	6	7	8	9	10	11		12			13		14			15		16	
Cross-Section	Do-main	Location			Lithology		Assigned Parameters: Lithology					Stress Parameters			Coulomb Stress Parameters			Temperature		Seismic Parameters			Gravity-Magnetics		MT (Resistivity)	
		X	Z	Ele-vation	Fm	TV	EGS-Fav	Frict-ion	Certain-ty	Densi-ty	Strength	Frac-Intens	Vert-Stress	TV	CSC	Dilatation	TV	° C	TV	Vp	Vs	TV	Lithology	TV	ohm-m	TV
FF	DVFZ	6	3	-3.75	Kgr	2	0.8	1.4	0.6	2.5	230	0	117.11	2.5	99.46	-1.92E-06	2.5	280	1	5.23	3.51	1.32	Tr/Kgr	4		
FF	DVFZ	6	4	-3.25	Kgr	2	0.8	1.4	0.7	2.5	230	0	104.86	2.5	18.17	-2.49E-06	2.5	275	2	5.14	3.50	1.45	Tr/Kgr	4		
FF	DVFZ	6	5	-2.75	Kgr	3	0.8	1.4	0.7	2.5	230	0	92.61	2.5	-32.41	-0.0000031	2.5	265	2	5.04	3.49	1.57	Tr/Kgr	4	400	4
FF	DVFZ	6	6	-2.25	Kgr	3	0.8	1.4	0.7	2.5	230	0	80.36	2.5	-66.88	-0.0000038	2.5	250	3	4.95	3.48	1.70	Tr/Kgr	4	500	4
FF	DVFZ	6	7	-1.75	Kgr	4	0.8	1.4	0.7	2.5	230	0	68.11	2.5	-93.25	-4.68E-06	2.5	225	3	4.86	3.44	1.97	Tr/Kgr	4	450	4
FF	DVFZ	6	8	-1.25	Kgr	4	0.8	1.4	0.7	2.5	230	0	55.86	2.5	-115.08	-5.91E-06	2.5	225	4	4.78	3.31	2.41	Tr/Kgr	4	500	4
FF	DVFZ	6	9	-0.75	Tr	5	0.4	0.6	0.8	2.4	30	0.3	43.61	2.5	-133.01	-7.84E-06	2.5	200	4	4.69	3.15	2.74	Tr/Kgr	5	300	5
FF	DVFZ	6	10	-0.25	Jz	5	0.7	0.8	0.9	2.6	400	0.3	31.85	2.5	-145.25	-0.0000114	2.5	200	5	4.44	2.99	2.94	Tr/Kgr	5	300	5
FF	DVFZ	6	11	0.25	Jbr	5	0.6	0.8	0.9	2.5	200	0.1	19.11	2.5	-146.62	-0.0000197	2.5	150	5	3.86	2.68	3.27	Tr/Kgr	5	200	5
FF	DVFZ	6	12	0.75	Q	5	0	0.5	0.9	1.3	1	0	6.37	2.5	-127.42	-0.0000449	2.5	125	5	2.77	1.66	3.51	Tbf	5	10	5
FF		6	13	1.25			0	0	1	0	0	0	0	2.5	-123.01	-0.0001159	2.5	0								
FF	DVFZ	7	3	-3.75	Kgr	2	0.8	1.4	0.6	2.5	230	0	110.25	2.5	-121.75	-1.62E-06	2.5	275	1	5.22	3.51	1.13	Tr/Kgr	4		
FF	DVFZ	7	4	-3.25	Kgr	2	0.8	1.4	0.7	2.5	230	0	98	2.5	-161.87	-1.85E-06	2.5	260	2	5.13	3.50	1.24	Tr/Kgr	4		
FF	DVFZ	7	5	-2.75	Kgr	3	0.8	1.4	0.8	2.5	230	0	85.75	2.5	-200.88	-0.0000021	2.5	250	2	5.03	3.49	1.35	Tr/Kgr	4	100	4
FF	DVFZ	7	6	-2.25	Kgr	3	0.8	1.4	0.8	2.5	230	0.2	73.5	2.5	-230.93	-2.38E-06	2.5	225	3	4.94	3.48	1.45	Tr/Kgr	4	200	4
FF	DVFZ	7	7	-1.75	Kgr	4	0.8	1.4	0.8	2.5	230	0.2	61.25	2.5	-243.39	-2.74E-06	2.5	225	3	4.82	3.44	1.84	Jg	4	400	4
FF	DVFZ	7	8	-1.25	Tr	4	0.4	0.6	0.8	2.4	30	0.3	49	2.5	-235.50	-3.28E-06	2.5	200	4	4.73	3.31	2.45	Jg	4	200	4
FF	DVFZ	7	9	-0.75	Tr	4	0.4	0.6	0.8	2.4	30	0.3	37.24	2.5	-211.91	-4.21E-06	2.5	175	4	4.67	3.15	2.90	Jg	5	100	5
FF	DVFZ	7	10	-0.25	Jz	4	0.7	0.8	0.8	2.6	400	0.2	25.48	2.5	-178.79	-6.14E-06	2.5	150	4	4.38	2.99	3.21	Tbf	5	80	5
FF	DVFZ	7	11	0.25	Q	4	0	0.5	0.8	1.3	1	0.2	12.74	2.5	-135.94	-0.0000111	2.5	125	4	3.71	2.68	3.53	Tbf	5	10	5
FF	DVFZ	7	12	0.75	Q	5	0	0.5	0.9	1.3	1	0.1	6.37	2.5	-62.45	-0.0000268	2.5	100	4	2.67	1.66	3.73	Tbf	5	8	5
FF		7	13	1.25			0	0	1	0	0	0	0	2.5	151.65	-0.0000709	2.5	0								
FF	DVFZ	8	3	-3.75	Kgr	3	0.8	1.4	0.6	2.5	230	0.2	98.98	2.5	-395.94	-1.33E-06	2.5	280	4	5.22	3.51	1.18	Tr/Kgr	4		
FF	DVFZ	8	4	-3.25	Kgr	4	0.8	1.4	0.7	2.5	230	0.2	86.73	2.5	-290.37	-1.23E-06	2.5	275	4	5.12	3.50	1.29	Tr/Kgr	4		
FF	DVFZ	8	5	-2.75	Kgr	4	0.8	1.4	0.8	2.5	230	0.2	74.48	2.5	-212.06	-1.11E-06	2.5	250	4	5.03	3.49	1.40	Tr/Kgr	4	80	4
FF	DVFZ	8	6	-2.25	Kgr	5	0.8	1.4	0.9	2.5	230	0.3	62.23	2.5	-159.64	-9.78E-07	2.5	200	5	4.93	3.48	1.51	Tr/Kgr	4	100	4
FF	DVFZ	8	7	-1.75	Jz	5	0.7	0.8	0.9	2.6	400	0.4	49.98	2.5	-124.01	-8.33E-07	2.5	200	5	4.82	3.44	1.92	Jg	4	200	4
FF	DVFZ	8	8	-1.25	Tv	5	0.4	0.7	0.9	2.4	75	0.4	37.24	2.5	-98.29	-6.97E-07	2.5	200	5	4.73	3.29	2.55	Tbf	4	100	4
FF	DVFZ	8	9	-0.75	Q	5	0	0.5	0.9	1.3	1	0.2	25.48	2.5	-77.76	-6.25E-07	2.5	175	5	4.67	3.12	3.02	Tbf	5	80	5
FF	Valley	8	10	-0.25	Q	5	0	0.5	0.9	1.3	1	0.2	19.11	2.5	-58.26	-7.88E-07	2.5	125	5	4.38	2.94	3.34	Tbf	5	50	5
FF	Valley	8	11	0.25	Q	5	0	0.5	0.9	1.3	1	0.2	12.74	2.5	-33.58	-0.0000017	2.5	100	5	3.71	2.68	3.60	Tbf	5	10	5
FF	Valley	8	12	0.75	Q	5	0	0.5	0.9	1.3	1	0.2	6.37	2.5	11.93	-4.69E-06	2.5	50	5	2.67	1.66	3.73	Tbf	5	7	5
FF		8	13	1.25			0	0	1	0	0	0	0	2.5	124.13	-0.0000114	2.5	0								
FF	DVFZ	9	3	-3.75	Kgr	3	0.8	1.4	0.6	2.5	230	0.2	98.98	2.5	-48.58	-1.06E-06	2.5	275	4	5.20	3.51	1.09	Tr/Kgr	4		
FF	DVFZ	9	4	-3.25	Tr	4	0.4	0.6	0.7	2.4	30	0.2	86.73	2.5	-42.70	-6.41E-07	2.5	265	4	5.10	3.50	1.19	Tr/Kgr	4		
FF	DVFZ	9	5	-2.75	Tr	4	0.4	0.6	0.8	2.4	30	0.1	74.97	2.5	-37.76	-1.81E-07	2.5	245	4	5.00	3.49	1.29	Tr/Kgr	4	80	4
FF	DVFZ	9	6	-2.25	Jz	4	0.7	0.8	0.8	2.6	400	0	63.21	2.5	-33.32	3.37E-07	2.5	235	4	4.91	3.48	1.40	Tr/Kgr	4	100	4
FF	Valley	9	7	-1.75	Jz	4	0.7	0.8	0.8	2.6	400	0	50.47	2.5	-28.97	9.35E-07	2.5	225	4	4.74	3.44	1.98	Tr/Kgr	4	80	4
FF	Valley	9	8	-1.25	Tmb	4	0.6	0.7	0.8	2.5	100	0	37.73	2.5	-24.23	1.64E-06	2.5	200	4	4.59	3.29	2.76	Tbf	4	80	4
FF	Valley	9	9	-0.75	Q	4	0	0.5	0.8	1.3	1	0	25.48	2.5	-18.36	2.51E-06	2.5	150	4	4.51	3.12	3.18	Tbf	5	15	5
FF	Valley	9	10	-0.25	Q	4	0	0.5	0.8	1.3	1	0	19.11	2.5	-9.96	3.58E-06	2.5	125	4	4.24	2.94	3.47	Tbf	5	10	5
FF	Valley	9	11	0.25	Q	4	0	0.5	0.8	1.3	1	0	12.74	2.5	3.86	4.92E-06	2.5	100	4	3.62	2.68	3.70	Tbf	5	1	5
FF	Valley	9	12	0.75	Q	5	0	0.5	0.9	1.3	1	0	6.37	2.5	29.24	6.56E-06	2.5	50	4	2.62	1.66	3.82	Tbf	5	10	5
FF		9	13	1.25			0	0	1	0	0	0	0	2.5	77.05	8.46E-06	2.5	0								

Dixie Valley Cross-Sectional Data (continued)

1	2	3			4		5	6	7	8	9	10	11		12			13		14			15		16	
Cross-Section	Do-main	Location			Lithology		Assigned Parameters: Lithology					Stress Parameters			Coulomb Stress Parameters			Temperature		Seismic Parameters			Gravity-Magnetics		MT (Resistivity)	
		X	Z	Ele-vation	Fm	TV	EGS-Fav	Frict-ion	Certain-ty	Densi-ty	Strength	Frac-Intens	Vert-Stress	TV	CSC	Dilatation	TV	° C	TV	Vp	Vs	TV	Lithology	TV	ohm-m	TV
FF	Valley	10	3	-3.75	Tr	2	0.4	0.6	0.6	2.4	30	0	97.51	2.5	-8.04	-7.99E-07	2.5	260	3	5.21	3.49	1.03	Tr/Kgr	4		
FF	Valley	10	4	-3.25	Tr	3	0.4	0.6	0.7	2.4	30	0	85.75	2.5	-8.53	-9.07E-08	2.5	250	3	5.11	3.49	1.12	Tr/Kgr	4		
FF	Valley	10	5	-2.75	Tr	3	0.4	0.6	0.7	2.4	30	0	73.99	2.5	-8.39	6.77E-07	2.5	225	3	5.01	3.48	1.22	Tr/Kgr	4	15	4
FF	Valley	10	6	-2.25	Jz	4	0.7	0.8	0.7	2.6	400	0	62.23	2.5	-7.63	1.53E-06	2.5	225	4	4.92	3.47	1.32	Tr/Kgr	4	20	4
FF	Valley	10	7	-1.75	Tv	4	0.4	0.7	0.7	2.4	75	0	49.49	2.5	-6.17	0.0000025	2.5	200	4	4.75	3.43	1.89	Tr/Kgr	4	20	4
FF	Valley	10	8	-1.25	Tmb	4	0.6	0.7	0.7	2.5	100	0	37.73	2.5	-3.77	3.65E-06	2.5	175	4	4.61	3.30	2.66	Tbf	4	10	4
FF	Valley	10	9	-0.75	Q	4	0	0.5	0.8	1.3	1	0	25.48	2.5	0.03	5.04E-06	2.5	150	4	4.54	3.14	3.10	Tbf	5	5	5
FF	Valley	10	10	-0.25	Q	4	0	0.5	0.8	1.3	1	0	19.11	2.5	6.05	6.79E-06	2.5	125	4	4.23	2.98	3.39	Tbf	5	1	5
FF	Valley	10	11	0.25	Q	4	0	0.5	0.8	1.3	1	0	12.74	2.5	15.73	0.000009	2.5	100	4	3.57	2.68	3.67	Tbf	5	1	5
FF	Valley	10	12	0.75	Q	5	0	0.5	0.9	1.3	1	0	6.37	2.5	31.21	0.0000118	2.5	50	4	2.57	1.66	3.84	Tbf	5	10	5
FF		10	13	1.25			0	0	1	0	0	0	0	2.5	54.72	0.0000151	2.5	0								
FF	Valley	11	3	-3.75	Tr	1	0.4	0.6	0.6	2.4	30	0	91.63	2.5	0.13	-5.59E-07	2.5	250	3	5.20	3.49	1.05	Tr/Kgr	4		
FF	Valley	11	4	-3.25	Tr	1	0.4	0.6	0.6	2.4	30	0	79.87	2.5	-0.12	4.12E-07	2.5	200	3	5.11	3.49	1.15	Tr/Kgr	4		
FF	Valley	11	5	-2.75	Tr	1	0.4	0.6	0.6	2.4	30	0	68.11	2.5	0.09	1.45E-06	2.5	200	3	5.01	3.48	1.25	Tr/Kgr	4	8	4
FF	Valley	11	6	-2.25	Jz	1	0.7	0.8	0.6	2.6	400	0	56.35	2.5	0.83	2.58E-06	2.5	200	3	4.91	3.47	1.35	Tr/Kgr	4	10	4
FF	Valley	11	7	-1.75	Tv	1	0.4	0.7	0.6	2.4	75	0	43.61	2.5	2.21	3.85E-06	2.5	200	3	4.75	3.43	1.92	Tr/Kgr	4	10	4
FF	Valley	11	8	-1.25	Q	2	0	0.5	0.7	1.3	1	0	31.85	2.5	4.43	5.31E-06	2.5	175	3	4.60	3.30	2.69	Tbf	4	3	4
FF	Valley	11	9	-0.75	Q	3	0	0.5	0.8	1.3	1	0	25.48	2.5	7.83	7.03E-06	2.5	150	3	4.53	3.14	3.11	Tbf	5	2	5
FF	Valley	11	10	-0.25	Q	4	0	0.5	0.8	1.3	1	0	19.11	2.5	12.91	0.0000091	2.5	125	3	4.20	2.98	3.39	Tbf	5	2	5
FF	Valley	11	11	0.25	Q	4	0	0.5	0.8	1.3	1	0	12.74	2.5	20.32	0.0000116	2.5	100	3	3.52	2.68	3.65	Tbf	5	1	5
FF	Valley	11	12	0.75	Q	5	0	0.5	0.9	1.3	1	0	6.37	2.5	30.73	0.0000146	2.5	50	3	2.54	1.66	3.82	Tbf	5	8	5
FF		11	13	1.25			0	0	1	0	0	0	0	2.5	44.41	0.000018	2.5	0								
FF	Valley	12	3	-3.75	Tr	1	0.4	0.6	0.5	2.4	30	0	92.61	2.5	3.42	-3.33E-07	2.5	250	2	5.20	3.49	1.05	Tr/Kgr	4		
FF	Valley	12	4	-3.25	Tr	1	0.4	0.6	0.5	2.4	30	0	80.85	2.5	3.56	8.68E-07	2.5	200	2	5.11	3.49	1.15	Tr/Kgr	4		
FF	Valley	12	5	-2.75	Jz	1	0.7	0.8	0.5	2.6	400	0	69.09	2.5	4.08	2.13E-06	2.5	200	2	5.01	3.48	1.25	Tr/Kgr	4	7	4
FF	Valley	12	6	-2.25	Jz	1	0.7	0.8	0.5	2.6	400	0	56.35	2.5	5.06	0.0000035	2.5	200	3	4.91	3.47	1.35	Tr/Kgr	4	4	4
FF	Valley	12	7	-1.75	Tv	1	0.4	0.7	0.6	2.4	75	0	43.61	2.5	6.61	0.000005	2.5	175	3	4.75	3.43	1.92	Tr/Kgr	4	4	4
FF	Valley	12	8	-1.25	Q	2	0	0.5	0.7	1.3	1	0	31.85	2.5	8.89	6.68E-06	2.5	175	3	4.60	3.30	2.69	Tbf	4	2	4
FF	Valley	12	9	-0.75	Q	3	0	0.5	0.8	1.3	1	0	25.48	2.5	12.12	0.0000086	2.5	150	3	4.53	3.14	3.11	Tbf	5	2	5
FF	Valley	12	10	-0.25	Q	4	0	0.5	0.8	1.3	1	0	19.11	2.5	16.60	1.082E-05	2.5	125	3	4.20	2.98	3.39	Tbf	5	3	5
FF	Valley	12	11	0.25	Q	4	0	0.5	0.8	1.3	1	0	12.74	2.5	22.60	0.0000134	2.5	100	3	3.52	2.68	3.65	Tbf	5	1	5
FF	Valley	12	12	0.75	Q	5	0	0.5	0.9	1.3	1	0	6.37	2.5	30.28	0.0000163	2.5	50	3	2.54	1.66	3.82	Tbf	5	10	5
FF		12	13	1.25			0	0	1	0	0	0	0	2.5	39.52	0.0000196	2.5	0								
FF	Valley	13	3	-3.75	Tr	1	0.4	0.6	0.6	2.4	30	0	91.63	2.5	5.46	-1.14E-07	2.5	200	2	5.20	3.49	1.04	Tr/Kgr	4		
FF	Valley	13	4	-3.25	Tr	1	0.4	0.6	0.6	2.4	30	0	79.87	2.5	5.88	1.28E-06	2.5	200	2	5.11	3.49	1.14	Tr/Kgr	4		
FF	Valley	13	5	-2.75	Tr	1	0.4	0.6	0.6	2.4	30	0	68.11	2.5	6.64	2.74E-06	2.5	200	2	5.01	3.48	1.24	Tr/Kgr	4	5	4
FF	Valley	13	6	-2.25	Jz	1	0.7	0.8	0.6	2.6	400	0	56.35	2.5	7.82	4.29E-06	2.5	200	2	4.91	3.47	1.33	Tr/Kgr	4	3	4
FF	Valley	13	7	-1.75	Tv	1	0.4	0.7	0.6	2.4	75	0	43.61	2.5	9.51	5.96E-06	2.5	175	2	4.74	3.43	1.87	Tr/Kgr	4	3	4
FF	Valley	13	8	-1.25	Q	2	0	0.5	0.7	1.3	1	0	31.85	2.5	11.83	0.0000078	2.5	150	2	4.59	3.30	2.60	Tbf	4	2	4
FF	Valley	13	9	-0.75	Q	3	0	0.5	0.8	1.3	1	0	25.48	2.5	14.93	9.85E-06	2.5	125	2	4.50	3.14	3.00	Tbf	5	2	5
FF	Valley	13	10	-0.25	Q	4	0	0.5	0.8	1.3	1	0	19.11	2.5	18.97	1.215E-05	2.5	125	2	4.11	2.98	3.24	Tbf	5	3	5
FF	Valley	13	11	0.25	Q	4	0	0.5	0.8	1.3	1	0	12.74	2.5	24.05	1.472E-05	2.5	100	2	3.41	2.68	3.50	Tbf	5	1	5
FF	Valley	13	12	0.75	Q	5	0	0.5	0.9	1.3	1	0	6.37	2.5	30.20	0.0000176	2.5	50	2	2.49	1.66	3.69	Tbf	5	10	5
FF		13	13	1.25			0	0	1	0	0	0	0	2.5	37.24	0.0000207	2.5	0								

Dixie Valley Cross-Sectional Data (continued)

1	2	3			4		5	6	7	8	9	10	11		12			13		14			15		16	
Cross-Section	Do-main	Location			Lithology		Assigned Parameters: Lithology					Stress Parameters			Coulomb Stress Parameters			Temperature		Seismic Parameters			Gravity-Magnetics		MT (Resistivity)	
		X	Z	Ele-vation	Fm	TV	EGS-Fav	Frict-ion	Certain-ty	Densi-ty	Strength	Frac-Intens	Vert-Stress	TV	CSC	Dilatation	TV	° C	TV	Vp	Vs	TV	Lithology	TV	ohm-m	TV
FF	Valley	14	3	-3.75	Tr	1	0.4	0.6	0.7	2.4	30	0.2	91.63	2.5	7.03	1.04E-07	2.5	200	1	5.14	3.49	0.88	Tr/Kgr	4		
FF	Valley	14	4	-3.25	Tr	1	0.4	0.6	0.7	2.4	30	0.1	79.87	2.5	7.64	1.66E-06	2.5	200	1	5.04	3.49	0.96	Tr/Kgr	4		
FF	Valley	14	5	-2.75	Tr	1	0.4	0.6	0.7	2.4	30	0	68.11	2.5	8.57	3.28E-06	2.5	200	1	4.94	3.48	1.04	Tr/Kgr	4	10	4
FF	Valley	14	7	-1.75	Tv	1	0.4	0.7	0.7	2.4	75	0	43.61	2.5	11.67	6.78E-06	2.5	175	2	4.68	3.43	1.60	Tr/Kgr	4	5	4
FF	Valley	14	7	-1.75	Tv	1	0.4	0.7	0.7	2.4	75	0	43.61	2.5	11.67	6.78E-06	2.5	175	2	4.68	3.43	1.60	Tr/Kgr	4	5	4
FF	Valley	14	8	-1.25	Q	2	0	0.5	0.7	1.3	1	0	31.85	2.5	14.00	8.74E-06	2.5	150	2	4.54	3.30	2.28	Tr/Kgr	4	3	4
FF	Valley	14	9	-0.75	Q	3	0	0.5	0.8	1.3	1	0	25.48	2.5	16.98	0.0000109	2.5	125	2	4.47	3.14	2.70	Tbf	5	3	5
FF	Valley	14	10	-0.25	Q	4	0	0.5	0.8	1.3	1	0	19.11	2.5	20.69	0.0000132	2.5	125	2	4.12	2.98	2.98	Tbf	5	3	5
FF	Valley	14	11	0.25	Q	4	0	0.5	0.8	1.3	1	0	12.74	2.5	25.18	0.0000158	2.5	50	2	3.39	2.68	3.29	Tbf	5	1	5
FF	Valley	14	12	0.75	Q	5	0	0.5	0.9	1.3	1	0	6.37	2.5	30.42	0.0000186	2.5	50	2	2.47	1.66	3.51	Tbf	5	10	5
FF		14	13	1.25			0	0	1	0	0	0	0	2.5	36.29	0.0000216	2.5	0								
FF	Valley	15	3	-3.75	Kgr	1	0.8	1.4	0.7	2.5	230	0	98	2.5	8.32	3.25E-07	2.5	200	1	5.09	3.49	0.60	Tr/Kgr	4		
FF	Valley	15	4	-3.25	Kgr	1	0.8	1.4	0.8	2.5	230	0.1	85.75	2.5	9.08	2.02E-06	2.5	200	1	4.98	3.49	0.66	Tr/Kgr	4		
FF	Valley	15	5	-2.75	Kgr	1	0.8	1.4	0.8	2.5	230	0.2	73.5	2.5	10.14	3.75E-06	2.5	200	1	4.87	3.48	0.71	Tr/Kgr	4	20	4
FF	Valley	15	6	-2.25	Tr	1	0.4	0.6	0.8	2.4	30	0.2	61.25	2.5	11.56	5.57E-06	2.5	175	1	4.76	3.47	0.77	Tr/Kgr	4	20	4
FF	Valley	15	7	-1.75	Tv	1	0.4	0.7	0.8	2.4	75	0.2	49.49	2.5	13.39	7.48E-06	2.5	175	1	4.63	3.43	1.19	Tr/Kgr	4	10	4
FF	Valley	15	8	-1.25	Tmb	2	0.6	0.7	0.8	2.5	100	0.2	37.73	2.5	15.72	9.52E-06	2.5	150	1	4.54	3.30	1.89	Tr/Kgr	4	6	4
FF	Valley	15	9	-0.75	Q	3	0	0.5	0.8	1.3	1	0	25.48	2.5	18.58	0.0000117	2.5	125	1	4.52	3.14	2.43	Tr/Kgr	5	5	5
FF	Valley	15	10	-0.25	Q	4	0	0.5	0.8	1.3	1	0	19.11	2.5	22.05	1.409E-05	2.5	100	1	4.15	2.98	2.80	Tbf	5	5	5
FF	Valley	15	11	0.25	Q	4	0	0.5	0.8	1.3	1	0	12.74	2.5	26.13	0.0000167	2.5	50	1	3.35	2.68	3.15	Tbf	5	2	5
FF	Valley	15	12	0.75	Q	5	0	0.5	0.9	1.3	1	0	6.37	2.5	30.81	0.0000194	2.5	50	1	2.44	1.66	3.35	Tbf	5	10	5
FF		15	13	1.25			0	0	1	0	0	0	0	2.5	36.00	0.0000224	2.5	0								
FF	Valley	16	3	-3.75	Kgr	1	0.8	1.4	0.7	2.5	230	0	104.86	2.5	9.39	5.56E-07	2.5	200	1	5.09	3.49	0.61	Tr/Kgr	4		
FF	Valley	16	4	-3.25	Kgr	1	0.8	1.4	0.8	2.5	230	0	92.61	2.5	10.27	2.35E-06	2.5	200	1	4.98	3.49	0.67	Tr/Kgr	4		
FF	Valley	16	5	-2.75	Kgr	1	0.8	1.4	0.9	2.5	230	0	80.36	2.5	11.44	4.18E-06	2.5	175	1	4.87	3.48	0.73	Tr/Kgr	4	40	4
FF	Valley	16	6	-2.25	Tr	1	0.4	0.6	0.9	2.4	30	0	68.11	2.5	12.93	6.08E-06	2.5	175	1	4.76	3.47	0.78	Tr/Kgr	4	40	4
FF	Valley	16	7	-1.75	Tr	1	0.4	0.6	0.9	2.4	30	0	56.35	2.5	14.80	8.08E-06	2.5	250	1	4.63	3.43	1.20	Tr/Kgr	4	40	4
FF	Valley	16	8	-1.25	Jz	2	0.7	0.8	0.9	2.6	400	0.1	44.59	2.5	17.10	1.018E-05	2.5	150	1	4.53	3.30	1.88	Tr/Kgr	4	10	4
FF	Valley	16	9	-0.75	Jz	3	0.7	0.8	0.9	2.6	400	0.3	31.85	2.5	19.88	1.242E-05	2.5	125	1	4.51	3.14	2.38	Tr/Kgr	5	10	5
FF	Valley	16	10	-0.25	Q	4	0	0.5	0.9	1.3	1	0.4	19.11	2.5	23.16	0.0000148	2.5	100	1	4.14	2.98	2.72	Jg	5	8	5
FF	Valley	16	11	0.25	Q	4	0	0.5	0.9	1.3	1	0.4	12.74	2.5	26.96	0.0000174	2.5	50	1	3.38	2.68	3.07	Tbf	5	2	5
FF	Valley	16	12	0.75	Q	5	0	0.5	0.9	1.3	1	0.3	6.37	2.5	31.27	0.0000201	2.5	50	1	2.46	1.66	3.27	Tbf	5	8	5
FF		16	13	1.25			0	0	1	0	0	0	0	2.5	36.05	0.0000231	2.5	0								
FF	Valley	17	3	-3.75	Kgr	1	0.8	1.4	0.7	2.5	230	0.2	103.88	2.5	10.27	7.96E-07	2.5	200	1	5.09	3.49	0.61	Tr/Kgr	4		
FF	Valley	17	4	-3.25	Kgr	1	0.8	1.4	0.8	2.5	230	0.2	91.63	2.5	11.26	2.67E-06	2.5	200	1	4.98	3.49	0.67	Tr/Kgr	4		
FF	Valley	17	5	-2.75	Kgr	1	0.8	1.4	0.8	2.5	230	0.1	79.38	2.5	12.51	4.57E-06	2.5	175	1	4.87	3.48	0.73	Tr/Kgr	4	80	4
FF	Valley	17	6	-2.25	Tr	1	0.4	0.6	0.8	2.4	30	0	67.13	2.5	14.06	6.54E-06	2.5	175	1	4.76	3.47	0.78	Tr/Kgr	4	80	4
FF	Valley	17	7	-1.75	Tr	1	0.4	0.6	0.8	2.4	30	0	55.37	2.5	15.96	8.59E-06	2.5	150	1	4.63	3.43	1.21	Tr/Kgr	4	60	4
FF	Valley	17	8	-1.25	Tr	2	0.4	0.6	0.8	2.4	30	0	43.61	2.5	18.24	0.0000107	2.5	125	1	4.54	3.30	1.90	Tr/Kgr	4	50	4
FF	Valley	17	9	-0.75	Jz	3	0.7	0.8	0.8	2.6	400	0	31.85	2.5	20.94	0.000013	2.5	125	1	4.52	3.14	2.42	Tr/Kgr	5	40	5
FF	Valley	17	10	-0.25	Q	4	0	0.5	0.8	1.3	1	0	19.11	2.5	24.08	0.0000154	2.5	100	1	4.13	2.98	2.77	Tr/Kgr	5	10	5
FF	Valley	17	11	0.25	Q	4	0	0.5	0.8	1.3	1	0	12.74	2.5	27.68	0.000018	2.5	50	1	3.26	2.68	3.10	Tbf	5	2	5
FF	Valley	17	12	0.75	Q	5	0	0.5	0.9	1.3	1	0.2	6.37	2.5	31.73	0.0000207	2.5	50	1	2.35	1.66	3.28	Tbf	5	12	5
FF		17	13	1.25			0	0	1	0	0	0	0	2.5	36.22	0.0000236	2.5	0								

Dixie Valley Cross-Sectional Data (continued)

1	2	3			4		5	6	7	8	9	10	11		12			13		14			15		16	
Cross-Section	Do-main	Location			Lithology		Assigned Parameters: Lithology					Stress Parameters			Coulomb Stress Parameters			Temperature		Seismic Parameters			Gravity-Magnetics		MT (Resistivity)	
		X	Z	Ele-vation	Fm	TV	EGS-Fav	Frict-ion	Certain-ty	Densi-ty	Strength	Frac-Intens	Vert-Stress	TV	CSC	Dilatation	TV	° C	TV	Vp	Vs	TV	Lithology	TV	ohm-m	TV
FF	Valley	18	3	-3.75	Kgr	1	0.8	1.4	0.7	2.5	230	0	110.74	2.5	10.97	1.05E-06	2.5	200	1	5.11	3.49	0.63	Tr/Kgr	4		
FF	Valley	18	4	-3.25	Kgr	1	0.8	1.4	0.7	2.5	230	0	98.49	2.5	12.06	2.97E-06	2.5	175	1	5.00	3.49	0.69	Tr/Kgr	4		
FF	Valley	18	5	-2.75	Kgr	1	0.8	1.4	0.7	2.5	230	0.1	86.24	2.5	13.39	4.92E-06	2.5	175	1	4.89	3.48	0.75	Tr/Kgr	4	80	4
FF	Valley	18	6	-2.25	Kgr	1	0.8	1.4	0.7	2.5	230	0.2	73.99	2.5	14.99	6.94E-06	2.5	175	1	4.78	3.47	0.80	Tr/Kgr	4	90	4
FF	Valley	18	7	-1.75	Tr	1	0.4	0.6	0.7	2.4	30	0.2	61.74	2.5	16.91	9.02E-06	2.5	150	1	4.65	3.43	1.23	Tr/Kgr	4	80	4
FF	Valley	18	8	-1.25	Tr	2	0.4	0.6	0.7	2.4	30	0.2	49.98	2.5	19.17	0.0000112	2.5	125	1	4.56	3.30	1.92	Tr/Kgr	4	80	4
FF	Valley	18	9	-0.75	Jz	3	0.7	0.8	0.7	2.6	400	0.2	38.22	2.5	21.80	0.0000135	2.5	125	1	4.54	3.14	2.42	Tr/Kgr	5	80	5
FF	Valley	18	10	-0.25	Jz	4	0.7	0.8	0.7	2.6	400	0.2	25.48	2.5	24.83	0.0000159	2.5	100	1	4.12	2.98	2.74	Tr/Kgr	5	30	5
FF	Valley	18	11	0.25	Q	4	0	0.5	0.8	1.3	1	0.1	12.74	2.5	28.27	0.0000184	2.5	50	1	3.17	2.68	3.04	Tbf	5	3	5
FF	Valley	18	12	0.75	Q	5	0	0.5	0.9	1.3	1	0	6.37	2.5	32.12	2.115E-05	2.5	50	1	2.26	1.66	3.19	Tbf	5	15	5
FF		18	13	1.25			0	0	1	0	0	0	0	2.5	36.40	2.402E-05	2.5	0								

APPENDIX 16b

WELL DATA FOR GEOSTATISTICAL ANALYSIS

Table of Contents

List of Tables

1. INTRODUCTION

The data presented has been organized for the geostatistical analysis (Section 3) and used to directly compare measured data from wells with inferred/modeled data in the well vicinity. This includes all the available well data which is measured (hard data from well logs), modeled, and inferred along with trust values identified by the individual subject matter experts (see Section 1.4 of the main body of the report). The data set is organized in the following fashion by well name and data is shown that corresponds to differing depth intervals from the surface (1km above sea level) to a depth of -3km above sea level, in 0.5km increments. A description of the individual parameters included in the data set is given in Table 16b-1. The trust value legend is presented in Table 16b-2 and is identified as “TV” in Section 3. In addition to the geostatistical analyses, the Trust data is also used in paired EGS Favorability-Trust Maps (Section 8 of the report). Table 16b-3 presents the stratigraphy used in this analysis. Table 16b-4 presents a description of the five lithologic units identified by the combined gravity and magnetics parameters.

Table 16b-1. Parameters included in the well data set. Column Number and Column Identifier correspond to the number and column heading for the data presented.

Column Number	Column Identifier	Description of the Data
1	Well	Well ID Number and corresponding section.
2	Type	Current use/type of the well: producer, injector, sub-commercial, other (when the well type was not available to this study). Well Type was identified from the public domain characterization, limited private sector data provided by Terra-Gen Corp, and personal communication from Dr. David Blackwell, 2011.
3	Location	X, Y coordinates in latitude and longitude, respectively; Z coordinate is the elevation of the well pad in meters above sea level.
4	Depth	Well data has been subdivided into 500m horizontal intervals from 1km above sea level (asl) to -3km asl. The data corresponds to the average value at the indicated depth.
5	Lithology	Subsurface formations identified in the well (well logs, Nevada Bureau of Mines and Geology (NBMG) online geothermal database, Blackwell et al. 2005, published literature) and associated trust value as identified by the Geology Task Leader. Table 16b-2 provides a summary description of each of the formations encountered.
6	Measured Temperature	Measured temperature (°C) in well (online geothermal databases including Southern Methodist University and NBMG, Blackwell et al. (2005) and proprietary data provided by Terra-Gen Corp.) and trust value as identified by the Thermal Task Leader.
7	Modeled Temperature	Modeled temperature (°C) in a well as extracted from the wellfield cross-sections (Plates 1 and 2) and trust value (Table 16b-2) as identified by the Blackwell et al. (2005) and AltaRock-generated thermal model.
8	Vp (P-wave velocity)	Modeled primary-velocity value (km/sec) and P-wave velocity (Vp) trust value (Table 16b-2) as identified by the Seismic Task Leader.
9	Resistivity (MT)	Modeled Magneto-tellurics (MT) as resistivity (ohm-m) and trust value as identified by the MT Task Leader.

Table 16b-1. Parameters included in the well data set. Column Number and Column Identifier correspond to the number and column heading for the data presented.

Column Number	Column Identifier	Description of the Data
10	Lithology (Grav-Mag)	Subsurface formations as determined by the joint gravity and magnetic modeling and their associated trust values as determined by the Gravity and Magnetics Task Leader. Table 3 provides a summary of the lithology units identified by the joint gravity and magnetics modeling.
11	Stress Parameters	Modeled coulomb stress change (CSC), dilatation and the associated trust value for the stress parameters as determined by the Geology Task Leader. The data was given a neutral trust value of 2.5.
12	Vertical Stress	Modeled data and trust value as determined by the Geology Task Leader. This value was calculated based on the depth and density of overlying rocks. The data was given a neutral trust value of 2.5.
13	Productive (Hydrothermal)	Measured data presented as a 0 or a 1 for non-hydrothermally productive or productive, respectively (D. Blackwell, pers. comm., 2010; Reed, 2009; Blackwell et al. 2005). A "1" infers that the indicated depth is capable of geothermal injection, production (permeable), or is sub-commercial. A "0" indicates no hydrothermal component.
14	Fault Present	Fault Zones identified in the well logs and occurring as measured data, as determined by AltaRock Energy Inc. project geologists.
15	EGS	Cells (depths) that would be expected to potentially favorable for an Engineered Geothermal System, including selected depths from low permeability hot wells, and wells that are not part of the producing system.

2. Well Data Summary and Legend

The data shown in Section 3 was created to analyze the statistics of all the available well data including hard data (well logs) directly measured from wells, as well as inferred and modeled data with respect to well location. The trust (confidence) of the data is included where applicable, and used for the geostatisical analysis and EGS Favorability Mapping. Provided below is a description of the various geoscience parameters in Section 3.

Trust Value (TV): Conveys the confidence and/or reliability of derived data within a specific cell on a scale of 1-5, based on the proximity to a hard data point and/or limits of the geophysical modeling. Some data sets are labeled with a neutral value (2.5) if no trust values can be assigned to the model.

Table 16b-2. Description of Trust Value (TV) assigned to the various data

Trust Value	Description
5	Hard Data (measured in wells)
4	Strongly Inferred Data, within 0.5km of hard data
3	Weakly Inferred Data, within 1km of hard data
2	Interpolated/Extrapolated Data, more than 1km from hard data point
1	No Data available

1. **Well**: The well name is as indicated and in reference to section number.
2. **Type**: Wells were divided into the following classes; Injector, Producer, Sub-Commercial, and Other. Other was used if the well type was unknown.
3. **Location**: X and Y are the coordinates of the well at the surface in latitude and longitude. Z is the elevation in meters at the surface (KB).
4. **Depth**: Well were divided into depth intervals from 1km asl (surface of Dixie Valley) to -3km asl in 0.5km increments.
5. **Lithology**: Well Lithology as reported in the literature, well logs, etc. that occurs at the identified horizontal slice (km above sea level).

The following table divides the lithology into seven stratigraphic units.

Table 16b-3. Summary Description of the seven major lithologic formations

Unit	Description
Tbf	Basin-filling sediments including lowermost tuffaceous sediments.
Tmb	Miocene basalt, aka Table Mountain Basalt.
Tv	Oligocene silicic volcanics, overlying lacustrine sediments, and underlying
Jbr	Jurassic Boyer Ranch quartzite
Jz	Jurassic Humboldt Igneous group
Tr	Triassic metasediments
Kgr	Cretaceous granodiorite

6. **Temp.**: Measured temperature in degrees Celsius extracted from the literature and Temp-Depth profiles (Blackwell et al., 2005).
7. **Modeled Temp**: Temperature in degree Celsius derived from the modeled temperature along the cross-sections.
8. **Vp-seismic**: P-wave velocity (km/sec) modeled at the University of Nevada Reno and derived from previous velocity modeling.
9. **MT**: Resistivity in ohm-m derived from Magneto-telluric data along three wellfield arrays (N,C,S).

*note. The MT data along Array C in the location of the Section 7 producing wells was applied to all the wells in this section.

10. **Grav_Mag**: Modeled Combined Gravity-Magnetic inferred lithology units

Table 16b-4. Summary of Lithologic Units identified by the combined Gravity and Magnetics Modeling

Unit	Description	Density (g/cm^3)	Magnetics (emu/cm^3)
Tbf	Basin-fill	2.445	-
Ja	Jurassic arenite	2.56	-
Jv	Jurassic volcanics (rhyolite)	2.47	-
Jg	Magnetized Jurassic mafic rocks	2.876	0.004
Tr/Kgr	Tr meta-seds and basement	2.88	-

11. **Stress Parameters**: stress parameters derived from a ARE generated Stress Model of Dixie Valley (2010) using Coulomb 3.1.

CSC: Coulomb Stress Change on a given fault/fracture due to slip constraints on a number of source faults.

Positive CSC infers failure is promoted, while negative CSC values infers failure is inhibited.

Dilation: expected dilatation on fault/fracture due to CSC and model constraints.

Positive values infer fault is open (unclamped), while negative values (compression) infer fault is closed (clamped).

12. **VertStress**: Vertical Stress (bars) calculated based on the depth and density of overlying rocks.
13. **Productive (Hydrothermal)**: 1 infers the referenced cell (depth) is capable of geothermal injection, production (permeable), or sub-commercial. 0
14. **Faults Present**: Fault zones identified in the well logs (1 = fault present at the corresponding depth interval).
15. **EGS**: Cells identified with a 1 indicate conditions that are expected to be potentially favorable for an Engineered Geothermal System. This includes selected depth intervals of low permeability wells and wells that are not part of the producing hydrothermal system. The EGS determination was not limited to a favorable rock type and temperature exclusively, but more an overall SME evaluation.

3. Dixie Valley Well Data Sheet

1	2	3			4	5		6		7		8		9		10		11			12		13	14	15
Well	Type	Location			Depth	Lithology		Temp.		ModeledTemp		Vp-seismic		MT-Resistivity		Grav_Mag		Stress Parameters			Vertical Stress		Productive (Hydrothermal)	Fault Present	EGS
		X	Y	Z (m)	km	Fm.	TV	° C	TV	° C	TV	km/s	TV	ohm-m	TV	Unit	TV	CSC	Dilatation	TV	Bars	TV			
65-18	Injector	39.947	117.861	1048	1	Tbf	5					2.01	4.01	15	2	Tbf	5	21.01	1.317E-05	2.5	6.37	2.5	0		
					0.5	Tbf	5	35	5	35	5	3.24	3.775	60	2	Tbf	5	17.71	1.092E-05	2.5	12.74	2.5	0		
					0	Tbf	5			100	4	4.19	2.965	1	2	Tbf	5	15.05	8.779E-06	2.5	19.11	2.5	0		
					-0.5	Tbf	5			150	4	4.51	2.755	2	2	Tbf	5	12.84	6.815E-06	2.5	25.48	2.5	0		
					-1	Tmb	5			175	4	4.57	2.435	8	2	Tr/Kgr	5	10.94	5.055E-06	2.5	37.73	2.5	1		
					-1.5	Jz	5	218.3	5	200	5	4.52	2.12	20	2	Jg	4	9.27	3.498E-06	2.5	50.47	2.5	1	1	
					-2					225	4	4.88	1.145	60	2	Tr/Kgr	4				62.23	2.5	0	1	
					-2.5					225	4					Tr/Kgr	4				73.99	2.5	0		
					-3					250	3					Tr/Kgr	4				85.75	2.5	0		
32-18	Injector	39.953	117.862	1057	1	Tbf	5					2.03	3.965	20	2	Tbf	3	24.82	6.206E-06	2.5	6.37	2.5	0		
					0.5	Tbf	5			60	4	3.31	3.865	3	2	Tbf	3	19.14	4.754E-06	2.5	12.74	2.5	0		
					0	Tbf	5			110	4	4.25	3.065	2	2	Tbf	3	14.72	3.334E-06	2.5	19.11	2.5	0		
					-0.5	Tbf	5			160	4	4.52	2.855	8	2	Tbf	3	11.24	2.051E-06	2.5	25.48	2.5	0		
					-1	Tmb	5			200	4	4.58	2.545	20	2	Jg	3	8.41	9.551E-07	2.5	37.24	2.5	1		
					-1.5					218	4	4.53	2.235	50	2	Tr/Kgr	3	6.04	4.799E-08	2.5	49.49	2.5	0		
					-2					225	4	4.91	1.21	100	2	Tr/Kgr	3				61.74	2.5	0		
					-2.5					225	4	5	1.135			Tr/Kgr	3				73.99	2.5	0		
					-3					250	4					Tr/Kgr	3				86.24	2.5	0		
52-18	Injector	39.953	117.861	1054	1	Tbf	5					2.02	3.965	20	3	Tbf	5	24.82	6.206E-06	2.5	6.37	2.5	0		
					0.5	Tbf	5	60	5	60	5	3.3	3.865	3	3	Tbf	5	19.14	4.754E-06	2.5	12.74	2.5	0		
					0	Tbf	5	110	5	110	5	4.25	3.065	2	3	Tbf	5	14.72	3.334E-06	2.5	19.11	2.5	0		
					-0.5	Tbf	5	160	5	160	5	4.51	2.855	8	3	Tbf	5	11.24	2.051E-06	2.5	25.48	2.5	0		
					-1	Tv	5	200	5	200	5	4.57	2.545	20	3	Jg	5	8.41	9.551E-07	2.5	37.24	2.5	1		
					-1.5	Jz	5	230	5	218	5	4.52	2.235	50	3	Tr/Kgr	4	6.04	4.799E-08	2.5	49.49	2.5	1		
					-2	Jz	5	233	5	225	5	4.9	1.21	100	3	Tr/Kgr	4				61.74	2.5	0		
					-2.5					225	4	5	1.14			Tr/Kgr	4				73.99	2.5	0		
					-3					250	4					Tr/Kgr	4				86.24	2.5	0		
SWL-3	Injector	39.953	117.864	1057	1	Tbf	5					2.03	3.965	20	3	Tbf	3	24.82	6.206E-06	2.5	6.37	2.5	0		
					0.5	Tbf	5			60	4	3.31	3.865	10	3	Tbf	3	19.14	4.754E-06	2.5	12.74	2.5	0		
					0	Tbf	5			110	4	4.25	3.065	7	3	Jg	3	14.72	3.334E-06	2.5	19.11	2.5	0		
					-0.5	Tbf	5			160	4	4.52	2.855	8	3	Jg	3	11.24	2.051E-06	2.5	25.48	2.5	0		
					-1	Tmb	5			200	4	4.58	2.545	30	3	Tr/Kgr	3	8.41	9.551E-07	2.5	37.73	2.5	1		
					-1.5	Tv	5	215	5	218	4	4.53	2.235	200	3	Tr/Kgr	3	6.04	4.799E-08	2.5	50.47	2.5	0	1	
					-2	Kgr	5			225	4	4.91	1.21	250	3	Tr/Kgr	3				62.72	2.5	0		
					-2.5					225	4	5	1.135			Tr/Kgr	3				74.97	2.5	0		
					-3					250	4					Tr/Kgr	3				87.22	2.5	0		
SWL-2	Injector	39.952	117.871	1058	1	Tbf	5			99	3	2.04	3.845	20	2	Tbf	5	24.82	6.206E-06	2.5	6.37	2.5	0		
					0.5	Tbf	5			100	3	3.33	3.72	10	2	Tbf	5	19.14	4.754E-06	2.5	12.74	2.5	0		
					0	Tbf	5			110	3	4.31	2.8	7	2	Jg	5	14.72	3.334E-06	2.5	19.11	2.5	0		
					-0.5	Tbf	5			150	3	4.51	2.56	8	2	Jg	5	11.24	2.051E-06	2.5	25.48	2.5	0		
					-1	Tmb	5			175	3	4.55	2.2	30	2	Tr/Kgr	5	8.41	9.551E-07	2.5	37.24	2.5	1		1
					-1.5	Kgr	5	210	5	200	3	4.48	1.915	200	2	Tr/Kgr	4	6.04	4.799E-08	2.5	49.49	2.5	0	1	1
					-2					225	3	4.87	0.92	250	2	Tr/Kgr	4				61.74	2.5	0		
					-2.5					250	3					Tr/Kgr	4				73.99	2.5	0		
					-3					250	3					Tr/Kgr	4				86.24	2.5	0		

Dixie Valley Well Data (continued)

1	2	3			4	5		6		7		8		9		10		11			12		13	14	15
Well	Type	Location			Depth	Lithology		Temp.		ModeledTemp		Vp-seismic		MT-Resistivity		Grav_Mag		Stress Parameters			Vertical Stress		Productive (Hydrothermal)	Fault Present	EGS
		X	Y	Z (m)	km	Fm.	TV	° C	TV	° C	TV	km/s	TV	ohm-m	TV	Unit	TV	CSC	Dilatation	TV	Bars	TV			
SWL-2B	Injector	39.952	117.871	1058	1	Tbf	5			99	1	2.04	3.845	20	2	Tbf	5	24.82	6.206E-06	2.5	6.37	2.5	0		
					0.5	Tbf	5			100	3	3.33	3.72	10	2	Tbf	5	19.14	4.754E-06	2.5	12.74	2.5	0		
					0	Tbf	5			110	3	4.31	2.8	7	2	Jg	5	14.72	3.334E-06	2.5	19.11	2.5	0		
					-0.5	Tbf	5			150	3	4.51	2.56	8	2	Jg	5	11.24	2.051E-06	2.5	25.48	2.5	0		
					-1	Tmb	5			175	3	4.55	2.2	30	2	Tr/Kgr	5	8.41	9.551E-07	2.5	37.24	2.5	1		1
					-1.5	Tv	5			200	3	4.48	1.915	200	2	Tr/Kgr	4	6.04	4.799E-08	2.5	49.49	2.5	0		
					-2					225	3	4.87	0.92	250	2	Tr/Kgr	4				61.74	2.5	0		
					-2.5					250	3					Tr/Kgr	4				73.99	2.5	0		
					-3					250	3					Tr/Kgr	4				86.24	2.5	0		
41-18	Injector	39.954	117.863	1055	1	Tbf	5					2.03	3.965	20	2	Tbf	5	24.82	6.206E-06	2.5	6.37	2.5	0		
					0.5					60	4	3.31	3.865	10	2	Tbf	5	19.14	4.754E-06	2.5	12.74	2.5	0		
					0					110	4	4.25	3.065	7	2	Jg	5	14.72	3.334E-06	2.5	19.11	2.5	0		
					-0.5					160	4	4.52	2.855	8	2	Jg	5	11.24	2.051E-06	2.5	25.48	2.5	0		
					-1					200	4	4.58	2.545	30	2	Tr/Kgr	5	8.41	9.551E-07	2.5	37.24	2.5	0		
					-1.5					218	4	4.53	2.235	200	2	Tr/Kgr	4	6.04	4.799E-08	2.5	49.49	2.5	0		
					-2					225	4	4.91	1.21	250	2	Tr/Kgr	4				61.74	2.5	0		
					-2.5					225	4	5	1.135			Tr/Kgr	4				73.99	2.5	0		
					-3					250	4					Tr/Kgr	4				86.24	2.5	0		
SWL-1	Injector	39.954	117.869	1061	1	Tbf	5			99	1	2.04	3.845	20	2	Tbf	5	26.44	7.105E-06	2.5	6.37	2.5	0		
					0.5	Tbf	5			125	4	3.33	3.72	10	2	Tbf	5	20.35	5.403E-06	2.5	12.74	2.5	0		
					0	Tbf	5			150	4	4.31	2.8	7	2	Jg	5	15.71	3.753E-06	2.5	19.11	2.5	0		
					-0.5	Tbf	5			200	4	4.51	2.56	8	2	Jg	5	12.10	2.294E-06	2.5	25.48	2.5	0		
					-1	Tmb	5	222	5	222	5	4.55	2.2	30	2	Tr/Kgr	5	9.20	1.083E-06	2.5	37.24	2.5	1		
					-1.5					225	4	4.48	1.915	200	2	Tr/Kgr	4	6.75	1.127E-07	2.5	49.49	2.5	0		
					-2					250	4	4.87	0.92	250	2	Tr/Kgr	4				61.74	2.5	0		
					-2.5					250	4					Tr/Kgr	4				73.99	2.5	0		
					-3					275	4					Tr/Kgr	4				86.24	2.5	0		
62-21	Other	39.939	117.823	1050	1	Tbf	5	16	5	16	5	1.93	3.76	10	5	Tbf	5	27.36	2.433E-05	2.5	6.37	2.5	0		
					0.5	Tbf	5	50	5	50	5	2.92	3.55	6	5	Tbf	5	25.02	2.123E-05	2.5	12.74	2.5	0		
					0	Tbf	5	85	5	85	5	3.76	2.77	2	5	Tbf	5	22.79	1.831E-05	2.5	19.11	2.5	0		
					-0.5	Tbf	5	115	5	115	5	4.35	2.6	3	5	Tbf	5	20.68	1.557E-05	2.5	25.48	2.5	0		
					-1	Tbf	5	140	5	140	5	4.42	2.275	6	5	Tbf	5	18.75	1.301E-05	2.5	38.22	2.5	0		
					-1.5	Jz	5	155	5	155	5	4.47	1.805	7	4	Tr/Kgr	4	17.02	1.06E-05	2.5	50.96	2.5	0	1	
					-2	Tr	5	175	5	175	5	4.71	0.785	8	4	Tr/Kgr	4	15.50	8.332E-06	2.5	62.72	2.5	0		
					-2.5	Tr	5	184	5	184	5	4.82	0.73	9	4	Tr/Kgr	4	14.19	6.184E-06	2.5	74.48	2.5	0		
					-3					225	4	4.93	0.675	10	4	Tr/Kgr	4				86.73	2.5	0		
45-14	Sub-Comm.	39.862	118.011	1039	1	Tbf	5	100	5	100	5	3.06	0.075			Tbf	5	-17.61	-5.76E-06	2.5	6.37	2.5	0		
					0.5	Tv	5	145	5	145	5	4.11	0.075			Tr/Kgr	5	-16.52	-5.3E-06	2.5	18.13	2.5	0		
					0	Tr	5	170	5	170	5	4.9	0.065			Tr/Kgr	5	-15.74	-4.89E-06	2.5	29.89	2.5	0		
					-0.5	Tr	5	180	5	180	5	5.23	0.065			Tr/Kgr	5	-15.22	-4.53E-06	2.5	41.65	2.5	0		
					-1	Tr	5	190	5	190	5	5.56	0.065			Tr/Kgr	5	-14.92	-4.21E-06	2.5	53.41	2.5	0		
					-1.5	Tr	5	196	5	196	5	5.85	0.065			Tr/Kgr	4	-14.83	-3.91E-06	2.5	65.17	2.5	0		1
					-2					225	4	5.93	0.065			Tr/Kgr	4				77	2.5	0		
					-2.5					225	4					Tr/Kgr	4				90	2.5	0		
					-3					250	3					Tr/Kgr	4				102	2.5	0		

Dixie Valley Well Data (continued)

1	2	3			4	5		6		7		8		9		10		11			12		13	14	15
Well	Type	Location			Depth	Lithology		Temp.		ModeledTemp		Vp-seismic		MT-Resistivity		Grav_Mag		Stress Parameters			Vertical Stress		Productive (Hydrothermal)	Fault Present	EGS
		X	Y	Z (m)	km	Fm.	TV	° C	TV	° C	TV	km/s	TV	ohm-m	TV	Unit	TV	CSC	Dilatation	TV	Bars	TV			
66-21	Other	39.931	117.932	1052	1	Tbf	5					1.95	0.05			Tbf	5	-9.94	-1.68E-05	2.5	6.37	2.5	0		
					0.5	Tbf	5	90	5	90	5	3.07	0.05			Tr/Kgr	5	-11.03	-1.41E-05	2.5	12.74	2.5	0		
					0	Tbf	5	130	5	130	5	4.72	0.05			Tr/Kgr	5	-11.09	-1.18E-05	2.5	24.5	2.5	0		
					-0.5	Tv	5	160	5	160	5	4.92	0.05			Tr/Kgr	5	-11.00	-9.9E-06	2.5	36.75	2.5	0		1
					-1	Jz	5	185	5	185	5	4.99	0.05			Tr/Kgr	5	-11.17	-8.46E-06	2.5	49	2.5	0		1
					-1.5	Tr	5	210	5	210	5	4.48	0.05			Tr/Kgr	4	-11.67	-7.4E-06	2.5	60.76	2.5	0		1
					-2	Tr	5	218	5	218	5	5.14	0.05			Tr/Kgr	4				73.01	2.5	0		
					-2.5	Tr	5			250	4					Tr/Kgr	4				85.26	2.5	0		
					-3					250	4					Tr/Kgr	4				97.51	2.5	0		
62-23A	Other	39.937	117.894	1036	1	Tbf	5					2.08	3.46	6	5	Tbf	5	13.24	3.36E-07	2.5	6.37	2.5	0		
					0.5	Tbf	5	80	5	80	5	3.35	3.27	1	5	Tbf	5	9.99	-1.75E-07	2.5	12.74	2.5	0		
					0	Tbf	5	125	5	125	5	4.53	2.155	6	5	Tbf	5	7.23	-6.49E-07	2.5	19.11	2.5	0		
					-0.5	Tbf	5	175	5	175	5	4.59	1.975	15	5	Tbf	5	4.87	-1.1E-06	2.5	30.87	2.5	0		
					-1	Tv	4	215	5	215	5	4.6	1.73	25	5	Tbf	5	2.86	-1.53E-06	2.5	43.61	2.5	0		1
					-1.5	Jz	4	240	5	240	5	4.43	1.625	60	4	Jg	4	-0.98	-3.54E-06	2.5	55.37	2.5	0		1
					-2	Tr	3	255	5	255	5	4.88	1.145	100	4	Tr/Kgr	4	-2.46	-3.64E-06	2.5	67.13	2.5	0		1
					-2.5	Tr	3	267	5	267	5	4.97	1.08			Tr/Kgr	4	-3.78	-3.76E-06	2.5	78.89	2.5	0		
					-3					275	4	5.05	1.015			Tr/Kgr	4				91.14	2.5	0		
36-14	Sub-Comm.	39.946	117.901	1043	1	Tbf	5					2.16	3.14	6	5	Tbf	5	6.82	-6.78E-06	2.5	6.37	2.5	0		
					0.5	Tbf	5	150	5	150	5	3.3	3.14	6	5	Tr/Kgr	5	4.33	-6.39E-06	2.5	12.74	2.5	0		
					0	Tbf	4	190	5	190	5	4.69	2.615	20	5	Tr/Kgr	5	2.09	-6.02E-06	2.5	24.5	2.5	0		
					-0.5	Tr	4	215	5	215	5	4.74	2.365	60	5	Tr/Kgr	5	0.10	-5.68E-06	2.5	36.26	2.5	0		
					-1	Tr	3	235	5	235	5	4.74	2.03	150	5	Tr/Kgr	5	-4.24	-7.25E-06	2.5	48.02	2.5	0		
					-1.5	Tr	3	250	5	250	5	4.56	1.725	250	4	Tr/Kgr	4	-5.63	-6.64E-06	2.5	60.27	2.5	0		1
					-2	Kgr	2	270	5	270	5	4.92	1.45	600	4	Tr/Kgr	4	-8.07	-6.67E-06	2.5	72.52	2.5	0		1
					-2.5	Kgr	2	285	5	285	5	4.99	1.44			Tr/Kgr	4				84.77	2.5	0	1	1
					-3					285	4	5.07	1.355			Tr/Kgr	4				97.02	2.5	0		
53-15	Other	-	-	-	1	Tbf	5					2.27	2.535	3	3			4.33	-1.65E-05	2.5	12.74	2.5	0		
					0.5	Jz	5	130	5	130	5	3.29	2.535	60	3			2.09	-1.49E-05	2.5	25.48	2.5	0		
					0	Jz	4	150	5	150	5	4.79	2.07	350	3			0.10	-1.34E-05	2.5	37.24	2.5	0		
					-0.5	Tr	4			180	4	4.85	1.97								49	2.5	0		
					-1					203	4										61.25	2.5	0		
					-1.5					225	3										73.5	2.5	0		
					-2					225	3										85.75	2.5	0		
					-2.5					280	3										98	2.5	0		
					-3					280	3										110.25	2.5	0		
76-28	Other	40.002	117.814	1051	1	Tbf	5					1.98	0.05					-17.28	1.597E-06	2.5	6.37	2.5	0		
					0.5	Tbf	5	30	5	30	5	3.42	0.05					-11.96	1.135E-06	2.5	12.74	2.5	0		
					0	Tbf	5	50	5	50	5	4.22	0.05					-9.20	6.717E-07	2.5	19.11	2.5	0		
					-0.5	Tbf	5	65	5	65	5	4.79	0.05					-8.02	2.648E-07	2.5	30.87	2.5	0		
					-1	Jz	5	80	5	80	5	4.86	0.05					-7.72	-6.69E-08	2.5	42.63	2.5	0	1	
					-1.5	Tr	5			150	4	4.89	0.05					-7.88	-3.29E-07	2.5	54.39	2.5	0		
					-2	Kgr	5	175	5	175	5	4.9	0.05					-8.28	-5.37E-07	2.5	66.64	2.5	0		1
					-2.5					175	4	5	0.05								78.89	2.5	0		
					-3					200	4										91.14	2.5	0		

Dixie Valley Well Data (continued)

1	2	3			4	5		6		7		8		9		10		11			12		13	14	15
Well	Type	Location			Depth	Lithology		Temp.		ModeledTemp		Vp-seismic		MT-Resistivity		Grav_Mag		Stress Parameters			Vertical Stress		Productive (Hydrothermal)	Fault Present	EGS
		X	Y	Z (m)	km	Fm.	TV	° C	TV	° C	TV	km/s	TV	ohm-m	TV	Unit	TV	CSC	Dilatation	TV	Bars	TV			
38-32	Injector	39.984	117.847	1055	1	Tbf	5					2.04	3.515	2	5	Tbf	5	-123.01	-0.000116	2.5	6.37	2.5	0		
					0.5	Jbr	5	145	5	145	5	3.49	3.505	60	5	Tr/Kgr	5	-127.42	-4.49E-05	2.5	18.62	2.5	1	1	
					0	Tr	5	170	5	170	5	4.23	3.025	200	5	Tr/Kgr	5	-146.62	-1.97E-05	2.5	30.38	2.5	0		
					-0.5			201	5	201	5	4.65	2.86	400	5	Tr/Kgr	5				42.63	2.5	0		
					-1					200	4										54.88	2.5	0		
					-1.5					225	4										67.13	2.5	0		
					-2					250	3										79.38	2.5	0		
					-2.5					250	3										91.63	2.5	0		
					-3					250	3										103.88	2.5	0		
27-32	Injector	39.986	117.849	1062	1	Tbf	5					2.04	3.515	2	5	Tbf	5	-123.01	-0.000116	2.5	6.37	2.5	0		
					0.5	Jbr	5			145	4	3.49	3.505	60	5	Tr/Kgr	5	-127.42	-4.49E-05	2.5	18.62	2.5	1		
					0	Tr	5			170	4	4.23	3.025	200	5	Tr/Kgr	5	-146.62	-1.97E-05	2.5	30.38	2.5	0		
					-0.5					201	3	4.65	2.86	400	5	Tr/Kgr	5				42.63	2.5	0		
					-1					200	3										54.88	2.5	0		
					-1.5																	2.5	0		
					-2																	2.5	0		
					-2.5																	2.5	0		
					-3																	2.5	0		
82-5	Injector	39.981	117.832	1050	1	Tbf	5					2.03	3.73	20	5	Tbf	5	124.13	-1.14E-05	2.5	6.37	2.5	0		
					0.5	Tbf	5	65	5	65	5	3.31	3.72	6	5	Tbf	5	11.93	-4.69E-06	2.5	12.74	2.5	0		
					0	Tbf	5	115	5	115	5	4.12	3.47	20	5	Tbf	5	-33.58	-1.7E-06	2.5	19.11	2.5	0		
					-0.5	Tbf	5	155	5	155	5	4.64	3.21	50	5	Jg	5	-58.26	-7.88E-07	2.5	25.48	2.5	0		
					-1	Tmb	5	195	5	195	5	4.71	2.825	100	5	Jg	5	-77.76	-6.25E-07	2.5	37.73	2.5	0		1
					-1.5	Tv	5	226	5	226	5	4.76	2.27	200	4	Jg	4	-98.29	-6.97E-07	2.5	49.49	2.5	0		1
					-2	Kgr	5			225	4	4.89	1.565	200	4	Jg	4	-124.01	-8.33E-07	2.5	61.74	2.5	0	1	1
					-2.5	Kgr	4			250	4	4.98	1.455			Tr/Kgr	4				73.99	2.5	0		1
					-3					250	4					Tr/Kgr	4				86.24	2.5	0		
45-5	Injector	39.977	117.849	1052	1	Tbf	5	60	5	60	5	2.06	3.89					204.00	3.916E-05	2.5	6.37	2.5	0		
					0.5	Tbf	5			108	4	3.36	3.8					100.25	1.088E-05	2.5	19.11	2.5	0		
					0	Tbf	5			150	4	4.22	3.53					63.29	-1.63E-06	2.5	30.87	2.5	0		
					-0.5	Tbf	5			183	4	4.61	3.285					42.50	-4.92E-06	2.5	42.63	2.5	0		
					-1	Tv	5			217	4	4.68	2.945					26.56	-5.31E-06	2.5	54.88	2.5	1	1	
					-1.5	Kgr	5	212	5	225	5	4.71	2.47					13.03	-4.92E-06	2.5	67.13	2.5	0		
					-2	Kgr	5			250	4	4.88	1.35								79.38	2.5	0		
					-2.5					250	4										91.63	2.5	0		
					-3					250	4										103.88	2.5	0		
27-33	Producer	39.987	117.831	1050	1	Tbf	5			0	1	1.97	3.695	20	3	Tbf	3	42.13	1.395E-06	2.5	6.37	2.5	0		
					0.5	Tbf	4			85	4	3.33	3.685	6	3	Tbf	3	18.72	2.09E-06	2.5	12.74	2.5	0		
					0	Tbf	4			103	4	4.03	3.04	20	3	Tbf	3	3.13	2.403E-06	2.5	19.11	2.5	0		
					-0.5	Tbf	4			138	4	4.61	2.84	50	3	Tbf	3	-7.20	2.342E-06	2.5	25.48	2.5	0		
					-1	Tmb	4			168	4	4.71	2.52	100	3	Tbf	3	-14.27	2.023E-06	2.5	37.73	2.5	0		
					-1.5	Tv	4	245	5	225	4	4.78	2.045	200	3	Jg	3	-19.43	1.57E-06	2.5	49.49	2.5	1		
					-2	Jbr	4			235	4	4.9	1.43	200	3	Tr/Kgr	3	-23.50	1.065E-06	2.5	61.74	2.5	0		
					-2.5					250	3	4.99	1.33			Tr/Kgr	3				73.99	2.5	0		
					-3					256	3										86.24	2.5	0		

Dixie Valley Well Data (continued)

1	2	3			4	5		6		7		8		9		10		11			12		13	14	15
Well	Type	Location			Depth	Lithology		Temp.		ModeledTemp		Vp-seismic		MT-Resistivity		Grav_Mag		Stress Parameters			Vertical Stress		Productive (Hydrothermal)	Fault Present	EGS
		X	Y	Z (m)	km	Fm.	TV	° C	TV	° C	TV	km/s	TV	ohm-m	TV	Unit	TV	CSC	Dilatation	TV	Bars	TV			
28-33	Producer	39.985	117.832	1057	1	Tbf	5			0	1	1.97	3.695	20	3	Tbf	3	42.13	1.395E-06	2.5	6.37	2.5	0		
					0.5	Tbf	5			85	4	3.33	3.685	6	3	Tbf	3	18.72	2.09E-06	2.5	12.74	2.5	0		
					0	Tbf	5			103	4	4.03	3.04	20	3	Tbf	3	3.13	2.403E-06	2.5	19.11	2.5	0		
					-0.5	Tbf	5			138	4	4.61	2.84	50	3	Tbf	3	-7.20	2.342E-06	2.5	25.48	2.5	0		
					-1	Tmb	5			168	4	4.71	2.52	100	3	Tbf	3	-14.27	2.023E-06	2.5	37.73	2.5	0		
					-1.5	Tv	5			225	4	4.78	2.045	200	3	Jg	3	-19.43	1.57E-06	2.5	49.49	2.5	0		
					-2	Jbr	4			235	4	4.9	1.43	200	3	Tr/Kgr	3	-23.50	1.065E-06	2.5	61.74	2.5	1		
					-2.5					250	3	4.99	1.33			Tr/Kgr	3				73.99	2.5	0		
					-3					256	3										86.24	2.5	0		
37-33	Producer	39.986	117.831	1055	1	Tbf	5			0	1	1.97	3.695			Tbf	3	42.13	1.395E-06	2.5	6.37	2.5	0		
					0.5	Tbf	5			92	4	3.33	3.685			Tbf	3	18.72	2.09E-06	2.5	12.74	2.5	0		
					0	Tbf	5			100	4	4.03	3.04			Tbf	3	3.13	2.403E-06	2.5	19.11	2.5	0		
					-0.5	Tbf	5			137	4	4.61	2.84			Tbf	3	-7.20	2.342E-06	2.5	25.48	2.5	0		
					-1	Tmb	5			159	4	4.71	2.52			Tbf	3	-14.27	2.023E-06	2.5	37.73	2.5	0		
					-1.5	Jz	5			206	4	4.78	2.045			Jg	3	-19.43	1.57E-06	2.5	49.49	2.5	1	1	
					-2	Kgr	5	246	5	225	4	4.9	1.43			Tr/Kgr	3	-23.50	1.065E-06	2.5	61.74	2.5	0		
					-2.5	Kgr	4			231	3	4.99	1.33			Tr/Kgr	3				73.99	2.5	0		
					-3					256	3										86.24	2.5	0		
45-33	Producer	39.989	117.823	1050	1	Tbf	5			0	1	2	3.395			Tbf	3	26.92	3.522E-06	2.5	6.37	2.5	0		
					0.5	Tbf	5	65	5	65	5	3.43	3.38			Tbf	3	14.09	3.489E-06	2.5	12.74	2.5	0		
					0	Tbf	5	100	5	100	5	4.11	2.635			Tbf	3	4.52	3.292E-06	2.5	19.11	2.5	0		
					-0.5	Tbf	5	135	5	135	5	4.6	2.555			Tbf	3	-2.46	2.931E-06	2.5	25.48	2.5	0		
					-1	Tbf	5	170	5	170	5	4.72	2.41			Tbf	3	-7.57	2.45E-06	2.5	37.24	2.5	0		
					-1.5	Tbf	5	215	5	215	5	4.8	2.065			Jg	3	-11.42	1.904E-06	2.5	49.98	2.5	0		
					-2	Jbr	5	251	5	251	5	4.9	1.715			Tr/Kgr	3	-14.44	1.335E-06	2.5	62.23	2.5	1		1
					-2.5							4.99	1.59			Tr/Kgr	3				74.48	2.5	0		
					-3																86.73	2.5	0		
76A-7	Producer	39.959	117.857	1055	1	Tbf	5			99	3	2.02	3.945	4	5	Tbf	3	12.54	2.51E-05	2.5	6.37	2.5	0		
					0.5	Tbf	4			125	3	3.23	3.84	6	5	Tbf	3	17.93	1.873E-05	2.5	12.74	2.5	0		
					0	Tbf	4			150	3	4.05	3.24	7	5	Tbf	3	20.54	1.325E-05	2.5	19.11	2.5	0		
					-0.5	Tbf	4			175	3	4.39	2.985	10	5	Tbf	3	21.29	9.025E-06	2.5	25.48	2.5	0		
					-1	Tbf	4			204	3	4.45	2.605	75	5	Jg	3	21.02	5.952E-06	2.5	37.73	2.5	0		
					-1.5	Tmb	4			225	3	4.5	2.105	165	4	Tr/Kgr	3	20.22	3.752E-06	2.5	50.47	2.5	1		
					-2					250	3	4.79	0.9	175	4	Tr/Kgr	3				63.21	2.5	0		
					-2.5					250	3			165	4	Tr/Kgr	3				74.97	2.5	0		
					-3					250	3			110	4	Tr/Kgr	3				86.73	2.5	0		
76-7	Producer	39.959	117.857	1055	1	Tbf	5			99	3	2.02	3.945	4	5	Tbf	3				6.37	2.5	0		
					0.5	Tbf	5			125	3	3.23	3.84	6	5	Tbf	3				12.74	2.5	0		
					0	Tbf	5			150	4	4.05	3.24	7	5	Tbf	3				19.11	2.5	0		
					-0.5	Tbf	5			175	4	4.39	2.985	10	5	Tbf	3				25.48	2.5	0		
					-1	Tbf	5	204	5	204	5	4.45	2.605	75	5	Jg	3				37.73	2.5	0		
					-1.5	Tmb	5			225	4	4.5	2.105	165	4	Tr/Kgr	3				50.47	2.5	1		1
					-2					250	4	4.79	0.9	175	4	Tr/Kgr	3				63.21	2.5	0		
					-2.5					250	3			165	4	Tr/Kgr	3				74.97	2.5	0		
					-3					250	3			110	4	Tr/Kgr	3				86.73	2.5	0		

Dixie Valley Well Data (continued)

1	2	3			4	5		6		7		8		9		10		11			12		13	14	15
Well	Type	Location			Depth	Lithology		Temp.		ModeledTemp		Vp-seismic		MT-Resistivity		Grav_Mag		Stress Parameters			Vertical Stress		Productive (Hydrothermal)	Fault Present	EGS
		X	Y	Z (m)	km	Fm.	TV	° C	TV	° C	TV	km/s	TV	ohm-m	TV	Unit	TV	CSC	Dilatation	TV	Bars	TV			
82A-7	Producer	39.968	117.855	1056	1	Tbf	5			100	3	2.01	3.995	6	5	Tbf	5	22.63	2.533E-05	2.5	6.37	2.5	0		
					0.5	Tbf	4			125	3	3.22	3.895	6	5	Tbf	5	24.66	1.754E-05	2.5	12.74	2.5	0		
					0	Tbf	4			150	3	4.08	3.455	20	5	Tbf	5	25.44	1.111E-05	2.5	19.11	2.5	0		
					-0.5	Tbf	4			200	3	4.41	3.22	60	5	Tbf	5	24.92	6.576E-06	2.5	25.48	2.5	0		
					-1	Tmb	4			225	3	4.48	2.875	300	5	Jg	5	23.56	3.62E-06	2.5	37.73	2.5	0		
					-1.5	Jz	4			250	3	4.53	2.415	300	4	Tr/Kgr	4	21.68	1.73E-06	2.5	50.47	2.5	1		
					-2					250	3	4.79	1.31	300	4	Tr/Kgr	4				63.21	2.5	0		
					-2.5					275	3			200	4	Tr/Kgr	4				74.97	2.5	0		
					-3					275	3			200	4	Tr/Kgr	4				86.73	2.5	0		
82-7	Producer	39.968	117.855	1056	1	Tbf	5			100	3	2.01	3.995	6	5	Tbf	5	22.63	2.533E-05	2.5	6.37	2.5	0		
					0.5	Tbf	5			125	3	3.22	3.895	6	5	Tbf	5	24.66	1.754E-05	2.5	12.74	2.5	0		
					0	Tbf	5			150	3	4.08	3.455	20	5	Tbf	5	25.44	1.111E-05	2.5	19.11	2.5	0		
					-0.5	Tbf	5			200	3	4.41	3.22	60	5	Tbf	5	24.92	6.576E-06	2.5	25.48	2.5	0		
					-1	Tmb	5			225	4	4.48	2.875	300	5	Jg	5	23.56	3.62E-06	2.5	37.73	2.5	0		
					-1.5	Jz	5			250	4	4.53	2.415	300	4	Tr/Kgr	4	21.68	1.73E-06	2.5	50.47	2.5	1		1
					-2			212	5	250	5	4.79	1.31	300	4	Tr/Kgr	4				63.21	2.5	1		1
					-2.5					275	4			200	4	Tr/Kgr	4				74.97	2.5	0		
					-3					275	4			200	4	Tr/Kgr	4				86.73	2.5	0		
84-7	Producer	39.964	117.858	1059	1	Tbf	5			100	3	2.01	3.995	6	5	Tbf	5	22.63	2.533E-05	2.5	6.37	2.5	0		
					0.5	Tbf	5			125	3	3.22	3.895	6	5	Tbf	5	24.66	1.754E-05	2.5	12.74	2.5	0		
					0	Tbf	5			150	3	4.08	3.455	20	5	Tbf	5	25.44	1.111E-05	2.5	19.11	2.5	0		
					-0.5	Tbf	5			200	4	4.41	3.22	60	5	Tbf	5	24.92	6.576E-06	2.5	25.48	2.5	0		
					-1	Tmb	5			225	4	4.48	2.875	300	5	Jg	5	23.56	3.62E-06	2.5	37.73	2.5	1		1
					-1.5	Tv	5	247	5	250	5	4.53	2.415	300	4	Tr/Kgr	4	21.68	1.73E-06	2.5	50.47	2.5	0	1	1
					-2					250	4	4.79	1.31	300	4	Tr/Kgr	4				63.21	2.5	0		
					-2.5					275	4			200	4	Tr/Kgr	4				74.97	2.5	0		
					-3					275	3			200	4	Tr/Kgr	4				86.73	2.5	0		
73-7	Producer	39.966	117.858	1059	1	Tbf	5			100	3	2.01	3.995	6	5	Tbf	5	22.63	2.533E-05	2.5	6.37	2.5	0		
					0.5	Tbf	5			125	3	3.22	3.895	6	5	Tbf	5	24.66	1.754E-05	2.5	12.74	2.5	0		
					0	Tbf	5			150	3	4.08	3.455	20	5	Tbf	5	25.44	1.111E-05	2.5	19.11	2.5	0		
					-0.5	Tbf	5			200	3	4.41	3.22	60	5	Tbf	5	24.92	6.576E-06	2.5	25.48	2.5	0		
					-1	Tmb	5			225	3	4.48	2.875	300	5	Jg	5	23.56	3.62E-06	2.5	37.73	2.5	0		
					-1.5	Jz	5			250	3	4.53	2.415	300	4	Tr/Kgr	4	21.68	1.73E-06	2.5	50.47	2.5	1		
					-2					250	3	4.79	1.31	300	4	Tr/Kgr	4				63.21	2.5	0		
					-2.5					275	3			200	4	Tr/Kgr	4				74.97	2.5	0		
					-3					275	3			200	4	Tr/Kgr	4				86.73	2.5	0		
73B-7	Producer	39.965	117.853	1056	1	Tbf	5			100	3	2.01	3.995	6	5	Tbf	5	22.63	2.533E-05	2.5	6.37	2.5	0		
					0.5	Tbf	4			125	3	3.22	3.895	6	5	Tbf	5	24.66	1.754E-05	2.5	12.74	2.5	0		
					0	Tbf	4			150	3	4.08	3.455	20	5	Tbf	5	25.44	1.111E-05	2.5	19.11	2.5	0		
					-0.5	Tbf	4			200	3	4.41	3.22	60	5	Tbf	5	24.92	6.576E-06	2.5	25.48	2.5	0		
					-1	Tmb	4			225	3	4.48	2.875	300	5	Jg	5	23.56	3.62E-06	2.5	37.73	2.5	0		
					-1.5	Jz	4			250	3	4.53	2.415	300	4	Tr/Kgr	4	21.68	1.73E-06	2.5	50.47	2.5	1		
					-2					250	3	4.79	1.31	300	4	Tr/Kgr	4				63.21	2.5	0		
					-2.5					275	3			200	4	Tr/Kgr	4				74.97	2.5	0		
					-3					275	3			200	4	Tr/Kgr	4				86.73	2.5	0		

Dixie Valley Well Data (continued)

1	2	3			4	5		6		7		8		9		10		11			12		13	14	15
Well	Type	Location			Depth	Lithology		Temp.		ModeledTemp		Vp-seismic		MT-Resistivity		Grav_Mag		Stress Parameters			Vertical Stress		Productive (Hydrothermal)	Fault Present	EGS
		X	Y	Z (m)	km	Fm.	TV	° C	TV	° C	TV	km/s	TV	ohm-m	TV	Unit	TV	CSC	Dilatation	TV	Bars	TV			
63-7	Producer	39.965	117.855	1059	1	Tbf	5			100	3	2.01	3.995	6	5	Tbf	5	22.63	2.533E-05	2.5	6.37	2.5	0		
					0.5	Tbf	4			125	3	3.22	3.895	6	5	Tbf	5	24.66	1.754E-05	2.5	12.74	2.5	0		
					0	Tbf	4			150	3	4.1	3.455	20	5	Tbf	5	25.44	1.111E-05	2.5	19.11	2.5	0		
					-0.5	Tbf	4			200	4	4.44	3.22	60	5	Tbf	5	24.92	6.576E-06	2.5	25.48	2.5	0		
					-1	Tbf	4			225	4	4.51	2.875	300	5	Jg	5	23.56	3.62E-06	2.5	37.73	2.5	0		
					-1.5	Jz	4	240	5	240	5	4.56	2.415	300	4	Tr/Kgr	4	21.68	1.73E-06	2.5	50.47	2.5	1		
					-2			243	5	249	5	4.79	1.31	300	4	Tr/Kgr	4				63.21	2.5	1		
					-2.5					250	4			200	4	Tr/Kgr	4				74.97	2.5	0		
					-3					250	4			200	4	Tr/Kgr	4				86.73	2.5	0		
74-7	Producer	39.964	117.858	1059	1	Tbf	5			100	3	2.01	3.995	6	5	Tbf	5	22.63	2.533E-05	2.5	6.37	2.5	0		
					0.5	Tbf	5			125	3	3.22	3.895	6	5	Tbf	5	24.66	1.754E-05	2.5	12.74	2.5	0		
					0	Tbf	5			150	3	4.1	3.455	20	5	Tbf	5	25.44	1.111E-05	2.5	19.11	2.5	0		
					-0.5	Tbf	5			200	3	4.44	3.22	60	5	Tbf	5	24.92	6.576E-06	2.5	25.48	2.5	0		
					-1	Tbf	5			225	4	4.51	2.875	300	5	Jg	5	23.56	3.62E-06	2.5	37.73	2.5	0		
					-1.5	Jz	5			240	4	4.56	2.415	300	4	Tr/Kgr	4	21.68	1.73E-06	2.5	50.47	2.5	1		
					-2			249	5	249	5	4.79	1.31	300	4	Tr/Kgr	4				63.21	2.5	0		
					-2.5					250	4			200	4	Tr/Kgr	4				74.97	2.5	0		
					-3					250	4			200	4	Tr/Kgr	4				86.73	2.5	0		

APPENDIX 17

CORRELATION AND CHI-SQUARE TEST GEOSTATISTICAL ANALYSES RESULTS

Table of Contents

List of Figures

List of Tables

1. Introduction

This appendix describes the results of the correlation analyses and the Chi-square test conducted. The correlation analysis consisted of:

a. global linear correlations between selected geoscience parameters along the section lines and the combined section data;

b. multivariate linear correlations by lithology per section and combined sections; and

c. domain analysis by geographic/geologic sub-element along the sections (i.e., Stillwater Range, DVFZ, and valley).

2. Global Linear Correlation Results

The first step in the geostatistical analysis was to determine which parameters to analyze and these are:

- Fracture Intensity (FracInten)
- Lithologic Density (LithDen)
- Vertical Stress (VertStress)
- Coulomb Stress Change (CSC)
- Dilatation
- Temperature
- P-wave velocity (Vp)
- Resistivity (MT)

The listed geoscience parameters were selected based on (1) preliminary analyses indicating that other geoscience parameters were not significant, (2) SME input, (3) poor parameter resolution, and/or (4) no known potential for inferring EGS. LithDen, an assigned density value for each of the major stratigraphic units, was the parameter used to translate lithology, a categorical data set, into a numerical data set. Appendix 15-Table 15-2 presents the data type for each of these parameters (e.g., measured, modeled, etc.) along the individual section lines presented in Plate 1.

For statistical purposes having such varied data types is non-ideal. However, we treat these data as if each dataset is independent and can be used for geostatistical analysis. This is based on the concept that whatever parameter uncertainty exists can be considered a measurement error, and is, at least from a practical standpoint, unbiased.

The association of selected geoscience parameters was evaluated using a correlation analysis which identified the correlation coefficient, a statistic that summarizes the linear relationship between two variables. The square of the correlation coefficient indicates the "goodness" of the regression line fit to the data (r^2-value). Note that a positive correlation between two factors does not necessarily reflect a causal relationship for there may be another factor (or factors) in play. Taylor (1990) reported that "Correlation coefficients should…indicate whether an investigation should be taken to look for causal relationships or other matters to understand the data." However, such investigation is beyond the scope of this study. Further efforts were undertaken to also qualitatively analyze the spread of the data and the number of data points to see if the reflected r^2 values are valid (see Tables 17.1 through 17.4).

Sectional Data Analysis

The global linear correlations were conducted on the individual cross-section data sets C-C' through F-F' (Plate 1) and the combined sections. This discussion describes the results of three types of analyses (1) bivariate, (2) multivariate, and (3) domain. These analyses produce a correlation coefficient which describes the correlation between the variables being evaluated. The results of this analysis are divided into two broad categories (1) non-correlated parameters is where the correlation coefficient is less than 0.7400 and (2) correlated parameters where the correlation coefficient is greater than 0.7400. A correlation coefficient of 0.7400 equates to a r-squared value of 0.55 which for the purposes of this study is not negligible. Figure 16-1 presents the results of this analysis for the combined section data set and is representative of the analysis conducted for each individual section. Table 17.1 summarizes the results of this analysis.

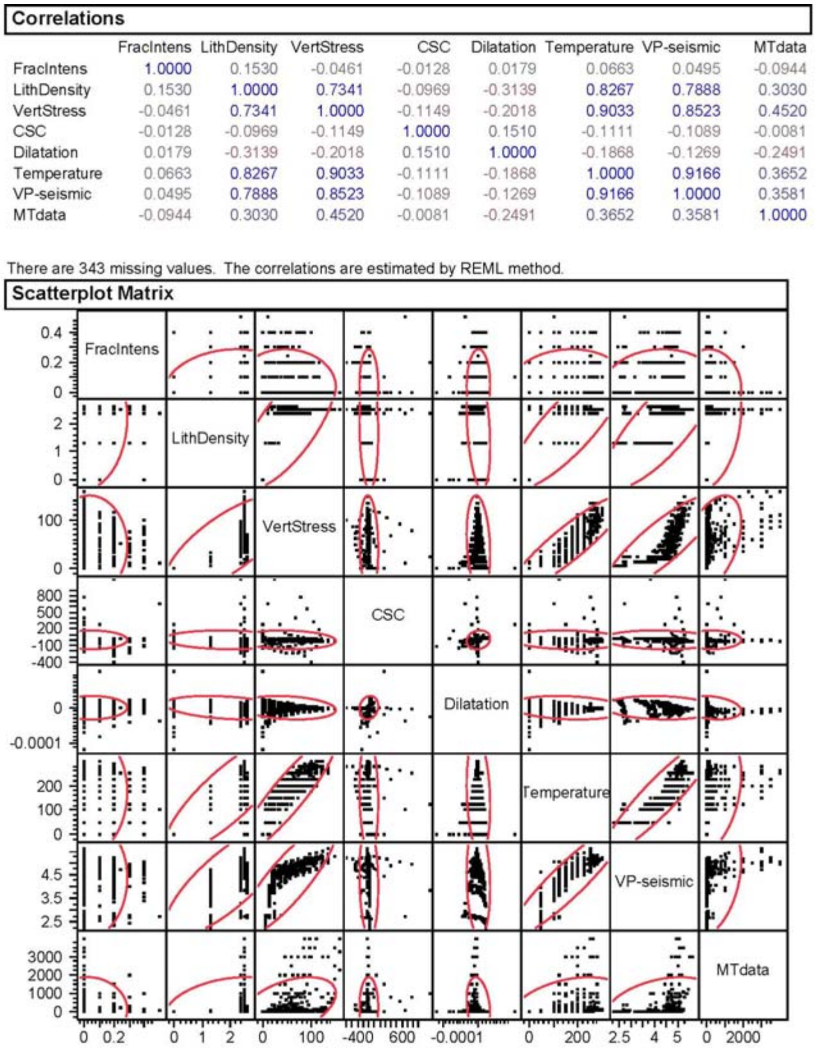

Correlations

	FracIntens	LithDensity	VertStress	CSC	Dilatation	Temperature	VP-seismic	MTdata
FracIntens	1.0000	0.1530	-0.0461	-0.0128	0.0179	0.0663	0.0495	-0.0944
LithDensity	0.1530	1.0000	0.7341	-0.0969	-0.3139	0.8267	0.7888	0.3030
VertStress	-0.0461	0.7341	1.0000	-0.1149	-0.2018	0.9033	0.8523	0.4520
CSC	-0.0128	-0.0969	-0.1149	1.0000	0.1510	-0.1111	-0.1089	-0.0081
Dilatation	0.0179	-0.3139	-0.2018	0.1510	1.0000	-0.1868	-0.1269	-0.2491
Temperature	0.0663	0.8267	0.9033	-0.1111	-0.1868	1.0000	0.9166	0.3652
VP-seismic	0.0495	0.7888	0.8523	-0.1089	-0.1269	0.9166	1.0000	0.3581
MTdata	-0.0944	0.3030	0.4520	-0.0081	-0.2491	0.3652	0.3581	1.0000

There are 343 missing values. The correlations are estimated by REML method.

Scatterplot Matrix

Figure 17.1. Correlation Matrix for the Combined Section Data (C-C', D-D', E-E' and F-F' in Plate 1). Correlation Coefficients between parameters are shown in upper table. The scatterplot matrix graphically shows the relationship between the coupled parameters. The red ellipse per scatterplot shows the grouping data points used in the correlation coefficient determination.

2.1 BIVARIATE ANALYSIS

The selected geoscience parameters which are correlated are:

1. LithDen (Appendix 15-Table 15.4) with:
    (a) VertStress along sections D-D’ and F-F’ but the scatterplots for these data are not well-behaved (Table 17.1) ; and
    (b) Temperature and Vp along all sections and the combined sections but the scatterplots for these data are not well-behaved (Table 17.1).
2. VertStress (Appendix 15-Table 15.4) with:
    (a) Temperature and Vp along all section lines and the combined sections, except that scatterplots for sections D-D’ and E-E’ are not well-behaved.
3. CSC (Appendix 15-Table 15.10) with:

    (a) dilatation along sections C-C’ and D-D’ but the scatterplot for section D-D’ is not well-behaved.

4. Temperature (Appendix 15-Table 15.9) with:
    (a) Vp across all sections and the combined sections.

2.2 MULTIVARIATE ANALYSIS

The aforementioned global linear correlation per section and for all combined sections examined any correlation among the selected geoscience parameters on an entire cross-section basis. As a result, the varying geologic formations and varying geologic environments (e.g., Stillwater Range and valley) were not considered. This section and the next, presented below, evaluate these factors.

Table 17.2 summarizes the results of global linear correlations by the major identified formations (Q-Tbf, Tmb, Kgr, Jz, and Tr; see Section 2.1.1 in the main report for a formation description). As in the aforementioned analysis, correlation coefficients <0.7400 (r-squared values <0.55) are not considered significant. Geoscience parameter correlations per lithologic formation follow.

Quaternary-Tertiary Basin Fill (QTbf)

1. VertStress-Temperature show no correlation along C-C’ but is correlated along all other sections and the combined sections. However, the scatterplot for the combined sections is not well-behaved.
2. VertStress-Vp is correlated along all sections and the combined sections.
3. CSC-Dilatation is correlated along sections C-C’ and F-F’ only.
4. CSC-Temperature is **negatively correlated** along sections C-C’ and D-D’.
5. CSC-Vp is correlated only along section D-D’ but the scatter plot is not well-behaved.
6. Temperature-Vp is correlated only along sections D-D’ through F-F’.

Tertiary Miocene Basalt (Tmb)

1. FracInten-CSC is correlated along section F-F’ but the scatter plot is not well-behaved.
2. FracInten-Dilatation is correlated along section F-F’ but the scatter plot is not well-behaved.
3. FracInten-Temperature is **negatively correlated** along section F-F’ but the scatter plot is not well-behaved.
4. FracInten-Vp is **negatively correlated** along section F-F’ but the scatter plot is not well-behaved.
5. VertStress-CSC is **negatively correlated** along section E-E’.
6. CSC-Dilatation is correlated along sections D-D’ and F-F’ but **negatively correlated** along E-E’. However, the scatterplot for section F-F’ is not well-behaved.
7. CSC-Temperature is correlated along section E-E’ and **negatively correlated** along sections D-D’ and F-F’ whose scatterplot is not well-behaved.
8. CSC-Vp is **negatively correlated** along sections D-D’ and E-E’.
9. CSC-Resistivity (MT) is **negatively correlated** along sections D-D’ through F-F’ whose scatterplot is not well-behaved.
10. Dilatation-Temperature is **negative correlated** along D-D’ through F-F’ and the combined sections. However, the scatterplot for section F-F’ is not well-behaved.
11. Dilatation-Vp is **negatively correlated** along sections D-D’ and F-F’ but the scatterplot for F-F’ is not well-behaved.

12. Temperature-Vp is correlated along section D-D’.
13. Temperature-Resistivity (MT) is correlated along sections D-D’ through F-F’ and the combined sections. However, the scatterplot for section F-F’ is not well-behaved.

Cretaceous Granite (Kgr)

1. VertStress-Vp is correlated along sections E-E’ and F-F’.
2. CSC-Dilatation is correlated along sections C-C’ and D-D’.
3. CSC-Resistivity (MT) is **negatively correlated** along section C-C’.
4. Temperature-Vp is correlated along section D-D’.

Jurassic Humboldt Igneous Complex (Jz)

1. VertStress-Temperature Is correlated long all sections and the combined sections. However, the scatterplot for section C-C’ is not well-behaved.
2. VertStress-Vp Is correlated long all sections and the combined sections. However, the scatterplot for section C-C’ is not well-behaved.
3. CSC-Dilatation is correlated along sections C-C’ through F-F’ but not correlated along the combined sections.
4. CSC-Vp is correlated along sections C-C’ and D-D’ but the scatterplot for C-C’ is not well-behaved. However, the scatterplot for section C-C’ is not well-behaved.
5. CSC-Resistivity (MT) is **negatively correlated** along section C-C’.
6. Dilatation-Vp is correlated along sections C-C’ and D-D’, and the combined sections. However, the scatterplot for section C-C’ is not well-behaved.
7. Temperature-Vp is correlated along sections CC-C’ through E-E’ and the combined sections.

Triassic Meta-Sediments (Tr)

1. VertStress-CSC-is correlated along section E-E’.
2. VertStress-Dilatation is correlated along all sections and the combined sections.
3. VertStress-Temperature is correlated along all sections and the combined sections.
4. VertStress-Vp is correlated along sections D-D’ through F-F’ and the combined sections.
5. CSC-Dilatation is correlated along sections C-C’ through E-E’.
6. CSC-Temperature is correlated along section E-E’.
7. Dilatation-Temperature is correlated along sections C-C’ and E-E’, and the combined sections but **negatively correlated** along section F-F’. The scatterplot for the combined sections is not well-behaved.
8. Dilatation-Vp is correlated along sections E-E’ and F-F’.
9. Temperature-Vp is correlated along all sections and in the combined sections.

Table 17.2 and 17.3 presents the aforementioned data in a format designed to show the geoscience parameters correlations with respect to lithology. Lithologic units are described in Section 2.1.1 in the main report. The following correlations are noted:

1. FracInten-CSC is correlated only along section F-F’ for the Tmb.
2. FracInten-Dilatation is correlated only along section F-F’ for the Tmb.
3. FracInten-Temperature is **negatively correlated** only along section F-F’ for the Tmb.
4. FracInten-Vp is **negatively correlated** only along section F-F’ for the Tmb.

5. VertStress-CSC is **negatively correlated** along section E-E’ for the Tmb and Tr.
6. VertStress-Temperature is correlated across all sections and the combined sections for the QT (except section C-C’), Jz, and Tr.
7. VertStress-Vp is correlated across all sections and the combined sections for the QT, Kgr, Jz, and Tr (except for section C-C’).
8. CSC-Dilatation is correlated along sections C-C’ and F-F’ for the QT, D-D’ and F-F’ for the Tmb and **negatively correlated** along section E-E’ for the Tmb, along sections C-C’ and D-D’ for the Kgr, across sections C-C’ through F-F’ in the Jz, and across C-C’ through E-E’ for the Tr.
9. CSC-Temperature is **negatively correlated** along sections C-C’ and D-D’ for the QT, is **negatively correlated** along sections C-C’ and F-F’ and correlated along section E-E’ for the Tmb, and correlated along section F-F’ for the Tr.
10. CSC-Vp is **negatively correlated** along section D-D’ for the QT, **negatively correlated** along section D-D’ and E-E’ for the Tmb, correlated along section C-C’ and D-D’ for the Jz, and **negatively correlated** along sections D-D’ and E-E’ for the Tr.
11. CSC-Resistivity is **negatively correlated** along F-F’ for the Jz.
12. Dilatation-Temperature is **negatively correlated** along sections D-D’ through F-F’ and the combined section for the Tmb, and correlated along sections C-C’, E-E’ and the combined section for Tr and **negatively correlated** along section F-F’ for the Tr..
13. Dilatation-Vp is **negatively correlated** along sections D-D’ and F-F’ for the Tmb, correlated along sections C-C’, D-D’ and the combined sections in the Jz, and correlated along E-E’ and F-F’ for the Tr.
14. Temperature-Vp is correlated along sections D-D’ through F-F’ for the QT, along section D-D’ for the Tmb, and Kgr, along sections C-C’ through E-E’ and the combined sections for the Jz, and across all sections in the Tr.

The causal relationships for the correlated and negatively correlated data are beyond the scope of this investigation. It is noteworthy, however, that the bulk of the negative correlations occur in the Tmb.

Table 17.1. Linear correlation analysis between selected geoscience parameters along the indicated four cross-section lines (Figure 48B in main report) and the combined data sets from all four section lines. Only correlation coefficients of 0.7400 (r-square value of 0.55) or greater are shown. A "0" indicates a correlation less than 0.7400. A gray-shaded cell indicates self-correlation. Blue shaded values indicate limited data points, a limited data distribution, too large a data spread, and/or too many outliers. A green-shaded cell indicates a repeated parameter couple.

Cross-Section	Geoscience Parameter							
	FracInten[1]	LithDen[2]	VertStress[3]	CSC[4]	Dilatation[5]	Temperature	Vp[6]	MT[7]
FracInten								
No correlation coefficients >0.7400 were found (except for the parameter self-correlation) in cross-section data C-C' through F-F' or the combined cross-section data; see text for an explanation.								
LithDen								
C-C'	0		0	0	0	0.842	0.7567	0
D-D'	0		0.7577	0	0	0.8383	0.7849	0
E-E'	0		0	0	0	0.7985	0.7610	0
F-F'	0		0.7577	0	0	0.8513	0.8470	0
Combined	0		0			0.8267	0.7888	
VertStress								
C-C'	0	0		0	0	0.898	0.8292	0
D-D'	0	0.7570		0	0	0.9388	0.8473	0
E-E'	0	0		0	0	0.8982	0.8856	0
F-F'	0	0.7577		0	0	0.8924	0.8480	0
Combined	0	0		0	0	0.9085	0.8599	0
CSC								
C-C'	0	0	0		0.9067	0	0	0
D-D'	0	0	0		0.8319	0	0	0
E-E'	0	0	0		0	0	0	0
F-F'	0	0	0		0	0	0	0
Combined	0	0	0		0	0	0	0
Dilatation								
No meaningful correlations found or are repeated parameters couples from above.								
Temperature								
C-C'	0			0	0		0.9039	0
D-D'	0			0	0		0.9287	0
E-E'	0			0	0		0.9039	0
F-F'	0			0	0		0.9271	0
Combined	0			0	0		0.9107	0
Vp and MT								
No meaningful correlation or are repeated parameter couples from above.								

[1] Fracture Intensity

[2] Lithologic Density

[3] Vertical Stress

[4] Coulomb Stress Change

[5] Dilatation

[6] P-wave velocity

[7] Resistivity

1.3 GEOLOGIC DOMAIN ANALYSIS

The selected geoscience parameters gridded along the sections identified above were analyzed on a domain basis within the Calibration Area. That is, it was recognized that the global correlation analysis described above integrated the correlation between selected geoscience parameters along the entire cross-section analyzed. Some of the data (i.e. MT resistivity sections) shows a qualitative difference within domains present in the sections. The geologic domain analysis focuses the correlation analysis on three geologic domains within each cross-section and the overall Calibration Area, i.e., the Stillwater Range, the DVFZ, and the Valley. Table 17.3 summarizes the results of the Geologic Domain Analysis and the following correlation coefficients were found to be significant (>0.7400) per domain:

Stillwater Range

1. VertStress - Dilatation;
2. VertStress – Temperature;
3. VertStress-Vp;
4. Dilatation-Temperature;
5. Dilatation – Vp; and
6. Temperature – Vp.

Dixie Valley Fault Zone

1. VertStress-Temperature;
2. VertStress –Vp; and
3. Temperature-Vp.

Valley

1. LithDen-VertStress;
2. LithDen –Temperature but the scatterplot for this correlation is not well-behaved;
3. VertStress-Temperature;
4. VertStress –Vp;
5. CSC – Dilatation;
6. Dilatation-Temperature which is **negatively correlated;**
7. Dilatation **-**Vp, which is **negatively correlated**; and
8. Temperature-Vp

Table 17.2. Summary of correlation coefficients for multivariate analysis with lithologies per individual cross-section (Figure 48B in the main report) and combined sections. Only correlation coefficients of 0.7400 (r-squared value of 0.55) are presented. A "0" indicates a correlation coefficient less than 0.7400. Stipple pattern indicates limited data points, a limited data distribution, too large data spread, and/or too many outliers. Negative correlations are presented in red font.

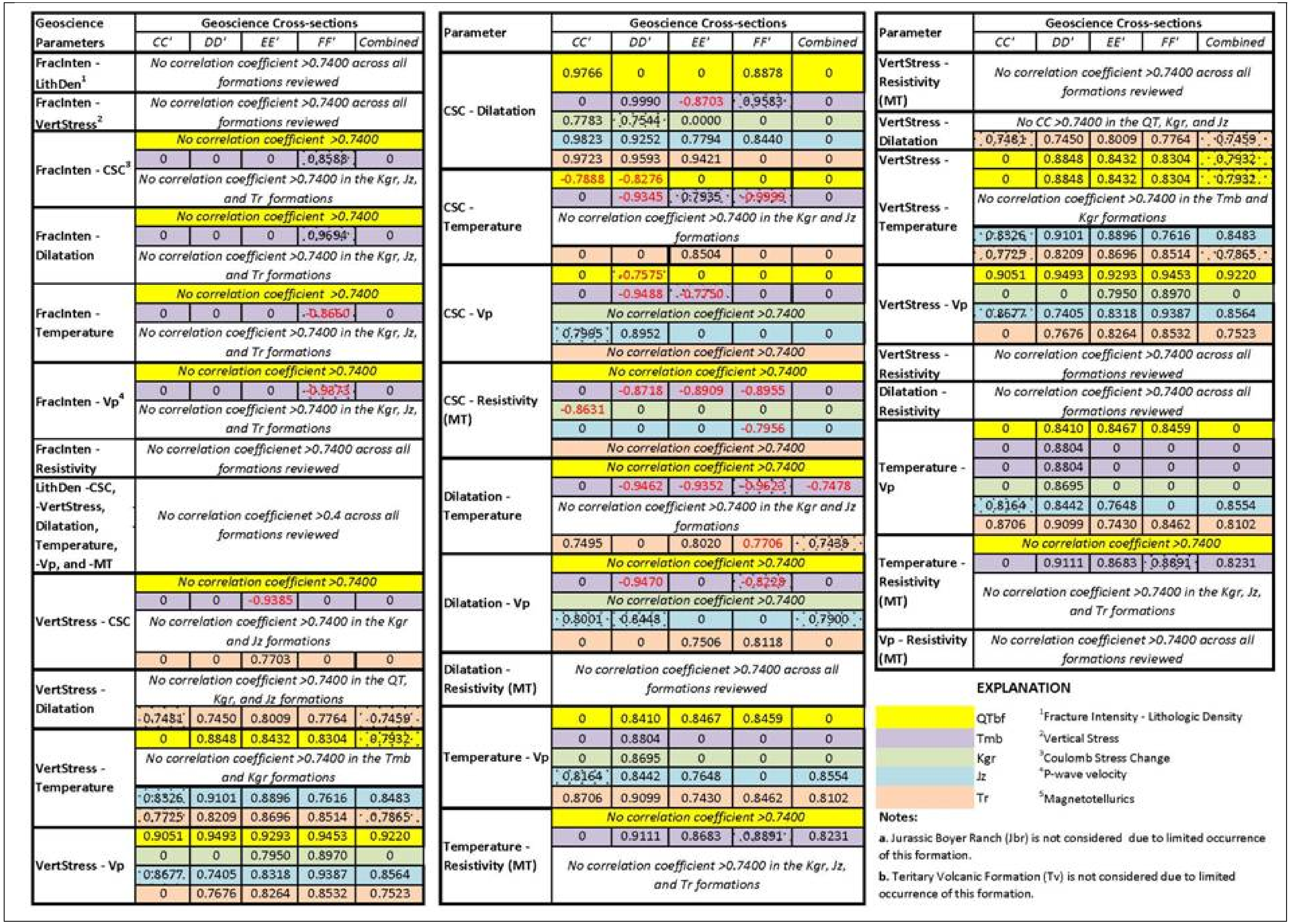

Geoscience Parameters	Geoscience Cross-sections				
	CC'	*DD'*	*EE'*	*FF'*	*Combined*
FracInten - LithDen[1]	*No correlation coefficient >0.7400 across all formations reviewed*				
FracInten - VertStress[2]	*No correlation coefficient >0.7400 across all formations reviewed*				
FracInten - CSC[3]	*No correlation coefficient >0.7400*				
	0	0	0	0.8588	0
	No correlation coefficient >0.7400 in the Kgr, Jz, and Tr formations				
FracInten - Dilatation	*No correlation coefficient >0.7400*				
	0	0	0	0.9694	0
	No correlation coefficient >0.7400 in the Kgr, Jz, and Tr formations				
FracInten - Temperature	*No correlation coefficient >0.7400*				
	0	0	0	-0.8660	0
	No correlation coefficient >0.7400 in the Kgr, Jz, and Tr formations				
FracInten - Vp[4]	*No correlation coefficient >0.7400*				
	0	0	0	-0.9873	0
	No correlation coefficient >0.7400 in the Kgr, Jz, and Tr formations				
FracInten - Resistivity	*No correlation coefficienet >0.7400 across all formations reviewed*				
LithDen -CSC, -VertStress, Dilatation, Temperature, -Vp, and -MT	*No correlation coefficienet >0.4 across all formations reviewed*				
VertStress - CSC	*No correlation coefficient >0.7400*				
	0	0	-0.9385	0	0
	No correlation coefficient >0.7400 in the Kgr and Jz formations				
	0	0	0.7703	0	0
VertStress - Dilatation	*No correlation coefficient >0.7400 in the QT, Kgr, and Jz formations*				
	0.7481	0.7450	0.8009	0.7764	0.7459
VertStress - Temperature	0	0.8848	0.8432	0.8304	0.7932
	No correlation coefficient >0.7400 in the Tmb and Kgr formations				
	0.8326	0.9101	0.8896	0.7616	0.8483
	0.7725	0.8209	0.8696	0.8514	0.7865
VertStress - Vp	0.9051	0.9493	0.9293	0.9453	0.9220
	0	0	0.7950	0.8970	0
	0.8677	0.7405	0.8318	0.9387	0.8564
	0	0.7676	0.8264	0.8532	0.7523

Parameter	Geoscience Cross-sections				
	CC'	*DD'*	*EE'*	*FF'*	*Combined*
CSC - Dilatation	0.9766	0	0	0.8878	0
	0	0.9990	-0.8703	0.9583	0
	0.7783	0.7544	0.0000	0	0
	0.9823	0.9252	0.7794	0.8440	0
	0.9723	0.9593	0.9421	0	0
CSC - Temperature	-0.7888	-0.8276	0	0	0
	0	-0.9345	0.7935	-0.9999	0
	No correlation coefficient >0.7400 in the Kgr and Jz formations				
	0	0	0.8504	0	0
CSC - Vp	0	-0.7575	0	0	0
	0	-0.9488	-0.7750	0	0
	No correlation coefficient >0.7400				
	0.7995	0.8952	0	0	0
	No correlation coefficient >0.7400				
CSC - Resistivity (MT)	*No correlation coefficient >0.7400*				
	0	-0.8718	-0.8909	-0.8955	0
	-0.8631	0	0	0	0
	0	0	0	-0.7956	0
	No correlation coefficient >0.7400				
Dilatation - Temperature	*No correlation coefficient >0.7400*				
	0	-0.9462	-0.9352	-0.9623	-0.7478
	No correlation coefficient >0.7400 in the Kgr and Jz formations				
	0.7495	0	0.8020	0.7706	0.7488
Dilatation - Vp	*No correlation coefficient >0.7400*				
	0	-0.9470	0	-0.8228	0
	No correlation coefficient >0.7400				
	0.8001	0.6448	0	0	0.7900
	0	0	0.7506	0.8118	0
Dilatation - Resistivity (MT)	*No correlation coefficienet >0.7400 across all formations reviewed*				
Temperature - Vp	0	0.8410	0.8467	0.8459	0
	0	0.8804	0	0	0
	0	0.8695	0	0	0
	0.8164	0.8442	0.7648	0	0.8554
	0.8706	0.9099	0.7430	0.8462	0.8102
Temperature - Resistivity (MT)	*No correlation coefficient >0.7400*				
	0	0.9111	0.8683	0.8891	0.8231
	No correlation coefficient >0.7400 in the Kgr, Jz, and Tr formations				

Parameter	Geoscience Cross-sections				
	CC'	*DD'*	*EE'*	*FF'*	*Combined*
VertStress - Resistivity (MT)	*No correlation coefficient >0.7400 across all formations reviewed*				
VertStress - Dilatation	*No CC >0.7400 in the QT, Kgr, and Jz*				
	0.7461	0.7450	0.8009	0.7764	0.7459
VertStress -	0	0.8848	0.8432	0.8304	0.7932
	0	0.8848	0.8432	0.8304	0.7932
VertStress - Temperature	*No correlation coefficient >0.7400 in the Tmb and Kgr formations*				
	0.8326	0.9101	0.8896	0.7616	0.8483
	0.7729	0.8209	0.8696	0.8514	0.7865
VertStress - Vp	0.9051	0.9493	0.9293	0.9453	0.9220
	0	0	0.7950	0.8970	0
	0.8677	0.7405	0.8318	0.9387	0.8564
	0	0.7676	0.8264	0.8532	0.7523
VertStress - Resistivity	*No correlation coefficient >0.7400 across all formations reviewed*				
Dilatation - Resistivity	*No correlation coefficient >0.7400 across all formations reviewed*				
Temperature - Vp	0	0.8410	0.8467	0.8459	0
	0	0.8804	0	0	0
	0	0.8804	0	0	0
	0	0.8695	0	0	0
	0.8164	0.8442	0.7648	0	0.8554
	0.8706	0.9099	0.7430	0.8462	0.8102
Temperature - Resistivity (MT)	*No correlation coefficient >0.7400*				
	0	0.9111	0.8683	0.8691	0.8231
	No correlation coefficient >0.7400 in the Kgr, Jz, and Tr formations				
Vp - Resistivity (MT)	*No correlation coefficienet >0.7400 across all formations reviewed*				

EXPLANATION

🟨	QTbf	[1]Fracture Intensity - Lithologic Density
🟪	Tmb	[2]Vertical Stress
🟩	Kgr	[3]Coulomb Stress Change
🟦	Jz	[4]P-wave velocity
🟧	Tr	[5]Magnetotellurics

Notes:

a. Jurassic Boyer Ranch (Jbr) is not considered due to limited occurrence of this formation.

b. Teritary Volcanic Formation (Tv) is not considered due to limited occurrence of this formation.

Table 17.3. Selected geoscience parameter multivariate correlation coefficient analysis by lithology and geologic cross-sections. A "X" represents a correlation coefficient >0.7400. A blank indicates a correlation coefficient <0.7400. A black "X" indicates a positive correlation coefficient and a red "X" indicates a negative coefficient. Blue shaded values indicate limited data points, a limited data distribution, too large a data spread, and/or too many outliers. The data used to construct this table is presented in Table 17.2.

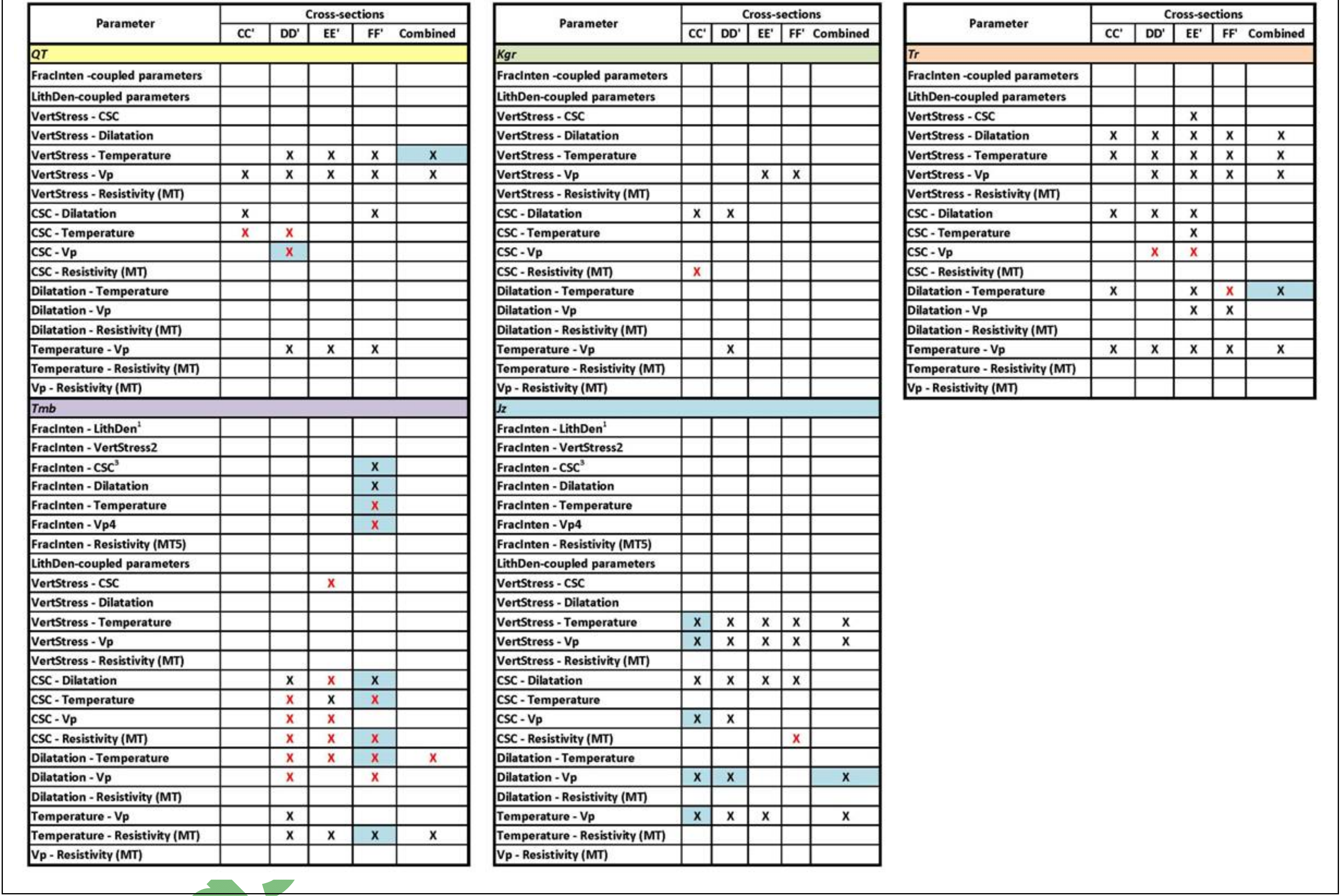

Parameter	Cross-sections				
	CC'	DD'	EE'	FF'	Combined
QT					
FracInten -coupled parameters					
LithDen-coupled parameters					
VertStress - CSC					
VertStress - Dilatation					
VertStress - Temperature		X	X	X	X
VertStress - Vp	X	X	X	X	X
VertStress - Resistivity (MT)					
CSC - Dilatation	X			X	
CSC - Temperature	X	X			
CSC - Vp		X			
CSC - Resistivity (MT)					
Dilatation - Temperature					
Dilatation - Vp					
Dilatation - Resistivity (MT)					
Temperature - Vp		X	X	X	
Temperature - Resistivity (MT)					
Vp - Resistivity (MT)					
Tmb					
FracInten - LithDen^1					
FracInten - VertStress2					
FracInten - CSC^3				X	
FracInten - Dilatation				X	
FracInten - Temperature				X	
FracInten - Vp4				X	
FracInten - Resistivity (MT5)					
LithDen-coupled parameters					
VertStress - CSC			X		
VertStress - Dilatation					
VertStress - Temperature					
VertStress - Vp					
VertStress - Resistivity (MT)					
CSC - Dilatation		X	X	X	
CSC - Temperature		X	X	X	
CSC - Vp		X	X		
CSC - Resistivity (MT)		X	X	X	
Dilatation - Temperature		X	X	X	X
Dilatation - Vp		X		X	
Dilatation - Resistivity (MT)					
Temperature - Vp		X			
Temperature - Resistivity (MT)		X	X	X	X
Vp - Resistivity (MT)					

Parameter	Cross-sections				
	CC'	DD'	EE'	FF'	Combined
Kgr					
FracInten -coupled parameters					
LithDen-coupled parameters					
VertStress - CSC					
VertStress - Dilatation					
VertStress - Temperature					
VertStress - Vp			X	X	
VertStress - Resistivity (MT)					
CSC - Dilatation	X	X			
CSC - Temperature					
CSC - Vp					
CSC - Resistivity (MT)	X				
Dilatation - Temperature					
Dilatation - Vp					
Dilatation - Resistivity (MT)					
Temperature - Vp		X			
Temperature - Resistivity (MT)					
Vp - Resistivity (MT)					
Jz					
FracInten - LithDen^1					
FracInten - VertStress2					
FracInten - CSC^3					
FracInten - Dilatation					
FracInten - Temperature					
FracInten - Vp4					
FracInten - Resistivity (MT5)					
LithDen-coupled parameters					
VertStress - CSC					
VertStress - Dilatation					
VertStress - Temperature	X	X	X	X	X
VertStress - Vp	X	X	X	X	X
VertStress - Resistivity (MT)					
CSC - Dilatation	X	X	X	X	
CSC - Temperature					
CSC - Vp	X	X			
CSC - Resistivity (MT)				X	
Dilatation - Temperature					
Dilatation - Vp	X	X			X
Dilatation - Resistivity (MT)					
Temperature - Vp	X	X	X		X
Temperature - Resistivity (MT)					
Vp - Resistivity (MT)					

Parameter	Cross-sections				
	CC'	DD'	EE'	FF'	Combined
Tr					
FracInten -coupled parameters					
LithDen-coupled parameters					
VertStress - CSC			X		
VertStress - Dilatation	X	X	X	X	X
VertStress - Temperature	X	X	X	X	X
VertStress - Vp		X	X	X	X
VertStress - Resistivity (MT)					
CSC - Dilatation	X	X	X		
CSC - Temperature			X		
CSC - Vp		X	X		
CSC - Resistivity (MT)					
Dilatation - Temperature	X		X	X	X
Dilatation - Vp			X	X	
Dilatation - Resistivity (MT)					
Temperature - Vp	X	X	X	X	X
Temperature - Resistivity (MT)					
Vp - Resistivity (MT)					

Table 17.4. Summary of results of a geologic domain analysis in the Calibration Area (see Figure 48B in the main report). Three domains shown: Stillwater Range (SR), Dixie Valley Fault Zone (DVFZ), and valley. Only correlation coefficients >0.7400 are shown. A "0" indicates a correlation coefficient <0.7400. Negatively correlated values are indicated in red and a minus sign. Green shaded values indicate limited data points, a limited data distribution, too large a data spread, and/or too many outliers.

Geoscience Parameters	**SR**	**DVFZ**	**Valley**
FracInten[1] with all geoscience	0	0	0
LithDen[2] - VertStress[3]	0	0	**0.8025**
LithDen - CSC[4]	0	0	0
LithDen - Dilatation	0	0	0
LithDen - Temperature	0	0	**0.7824**
LIthDen - Vp[5]	0	0	0
LIthDen - Resistivity (MT[6])	0	0	0
VertStress - CSC	0	0	0
VertStress - Dilatation	**0.8555**	0	0
VertStress - Temperature	**0.9148**	**0.9102**	**0.8998**
VertStress - Vp	**0.7805**	**0.8069**	**0.8326**
VertStress - Resistivity (MT)	0	0	0
CSC - Dilatation	0	0	**0.7259**
CSC - Temperature	0	0	0
CSC - Vp	0	0	0
CSC - Resistivity (MT)	0	0	0
Dilatation - Temperature	**0.9166**	0	**-0.8798**
Dilatation - Vp	**0.7918**	0	**-0.8045**
Dilatation - MT	0	0	0
Temperature - Vp	**0.7979**	**0.9128**	**0.8948**
Temperature - Resistivity (MT)	0	0	0
Vp - Resistivity (MT)	0	0	0

Notes:

[1] Fracture Intensity
[2] Lithologic Density
[3] Vertical Stress
[4] Coulomb Stress Change
[5] P-wave velocity
[6] Magnetotelluric resistivity

3. Chi-Squared Test

A Chi-Square test was conducted on the correspondence between the gravity/magnetic geologic model and the generalized geology model presented in Plate 1. Figure 17.2 presents the result of this analysis. A high degree of correlation was found between the two models. The Chi-Squared statistic indicates that the degree of correspondence observed is unlikely if both models were independent. The 11 measures of association also suggest a reasonable agreement between the two models. The Gravity/Magnetic Task Leader, Dr. Karlin (Section 1.3 in the main report) provides a discussion of his approach in conducting the joint gravity/magnetic modeling gravity and has reported that he conducted his modeling efforts independent of the generalized geology modeling (Plate 1), with the exception of modeling the surface geology and using 62-21 for a constraint on the depth to the basin-fill. Based on his analysis, it is reported herein that the geology and the gravity/magnetic model were developed independently. This correspondence of the models allows for the use of the Gravity-Magnetic inferred Lithology model as a complimentary data-set to the Geologic sections for inferring the lithology type to be used for EGS Favorability Mapping.

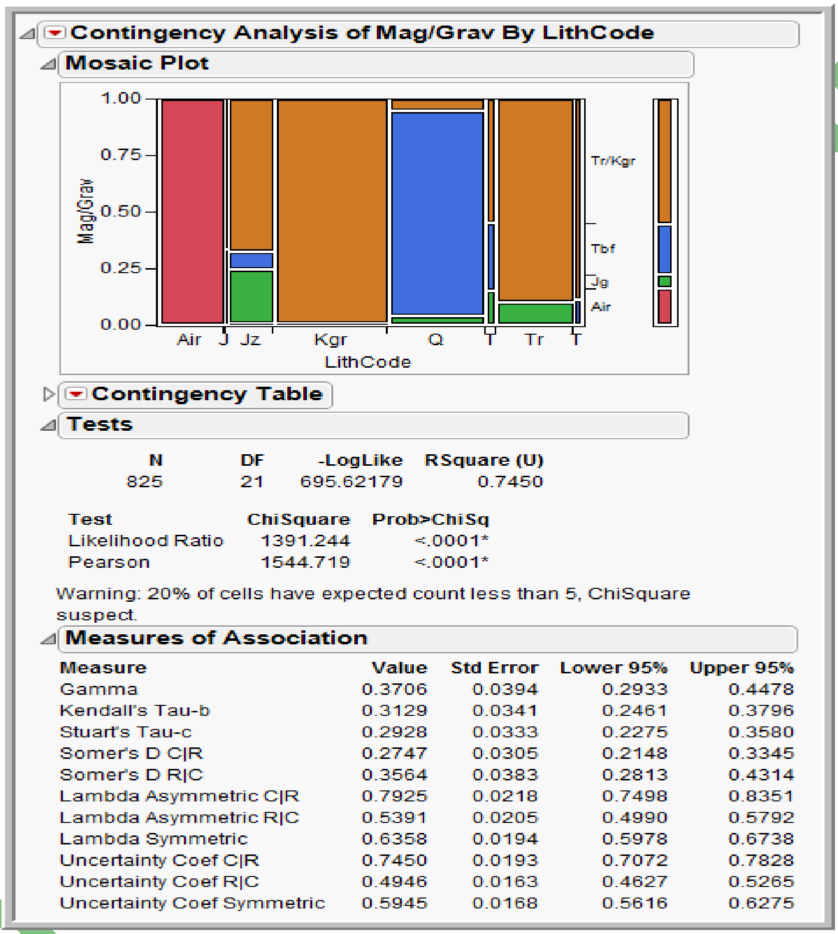

N	DF	-LogLike	RSquare (U)
825	21	695.62179	0.7450

Test	ChiSquare	Prob>ChiSq
Likelihood Ratio	1391.244	<.0001*
Pearson	1544.719	<.0001*

Warning: 20% of cells have expected count less than 5, ChiSquare suspect.

Measures of Association

Measure	Value	Std Error	Lower 95%	Upper 95%
Gamma	0.3706	0.0394	0.2933	0.4478
Kendall's Tau-b	0.3129	0.0341	0.2461	0.3796
Stuart's Tau-c	0.2928	0.0333	0.2275	0.3580
Somer's D C|R	0.2747	0.0305	0.2148	0.3345
Somer's D R|C	0.3564	0.0383	0.2813	0.4314
Lambda Asymmetric C|R	0.7925	0.0218	0.7498	0.8351
Lambda Asymmetric R|C	0.5391	0.0205	0.4990	0.5792
Lambda Symmetric	0.6358	0.0194	0.5978	0.6738
Uncertainty Coef C|R	0.7450	0.0193	0.7072	0.7828
Uncertainty Coef R|C	0.4946	0.0163	0.4627	0.5265
Uncertainty Coef Symmetric	0.5945	0.0168	0.5616	0.6275

Figure 17.2. Chi-Square Test for the Geologic Model vs. the Gravity-Magnetic inferred Lithology Model for data along the four key cross-sections (C-C', D-D', E-E' and F-F'). The R-square value for combined sections is 0.7450 while the values for the individual sections are 0.8033, 0.7166, 0.7749 and 0.8006 respectively. The geologic units correlate with the Gravity-Magnetic units as follows: Jz corresponds with Jg, Kgr and Tr corresponds with Tr/Kgr, and Q corresponds with Tbf. Air is in respect to values above the surface.

APPENDIX 18

P-WAVE VELOCITY AND TEMPERATURE RELATIONSHIP: EFFECT OF DEPTH, CONDUCTIVE VS. CONVECTIVE DOMAINS, AND LITHOLOGY TYPe

Table of Contents

[1] *Selected well data removes data occurring the surface and wells with a low seismic trust in reference to the baseline seismic model.*

Vp-T Relationship: Respect to Depth

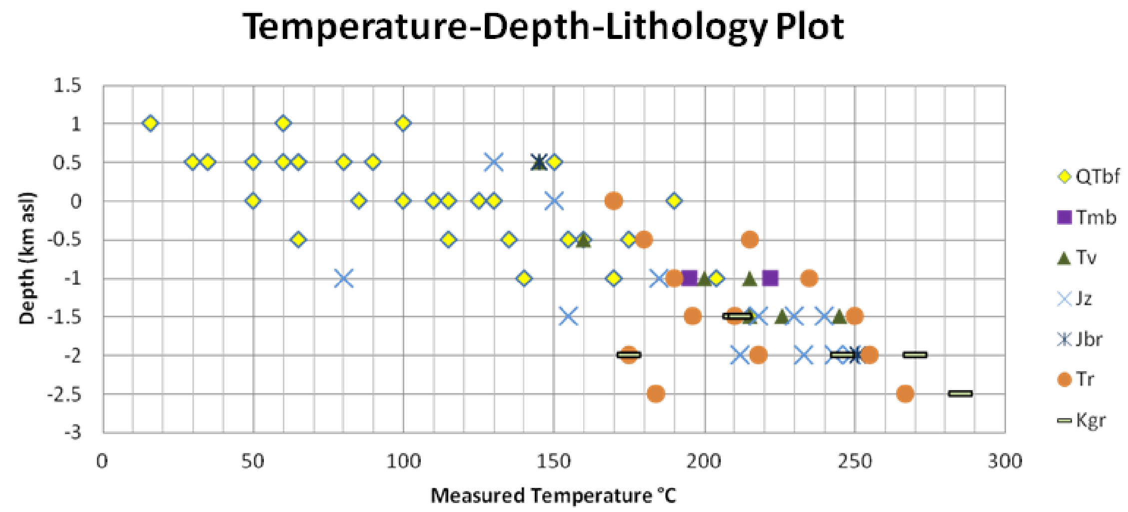

A

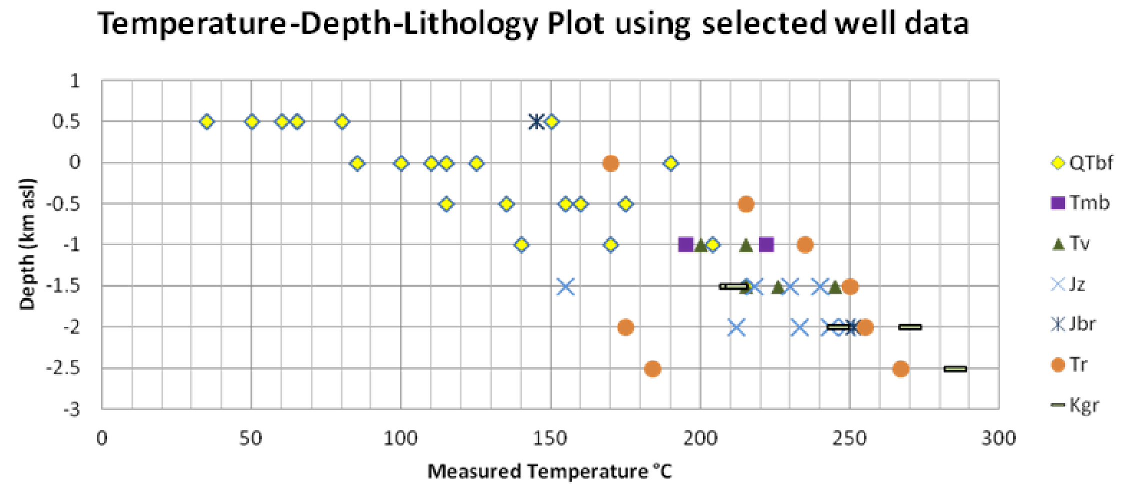

B

Figure 1. Temperature-Depth-Lithology plots using the well data. **(A)** Includes all data. **(B)** Excludes surface values (at 1km-asl) and wells with low seismic trust values (53-15, 66-21, 76-28, and 45-14), where the Vp data extracted in the vicinity of the well is considered unreliable by the seismic task leader. The lithology encountered in the Dixie Valley wells is divided into seven geologic units: basin-filling sediments (QTbf), Miocene basalt (Tmb), Oligocene silicic volcanics (Tv), Jurassic mafic rocks (Jz), Jurassic Boyer Ranch quartzite (Jbr), Triassic meta-sediments (Tr), and Cretaceous granodiorite (Kgr). Basin-filling sediments (QTbf) occur at shallower depths (1.0 to -1.0 km-asl) while basement rock (Tmb, Tv, Jz, Jbr, Tr and Kgr) occur at deeper depths (mostly -1.0 to -2.5km-asl).

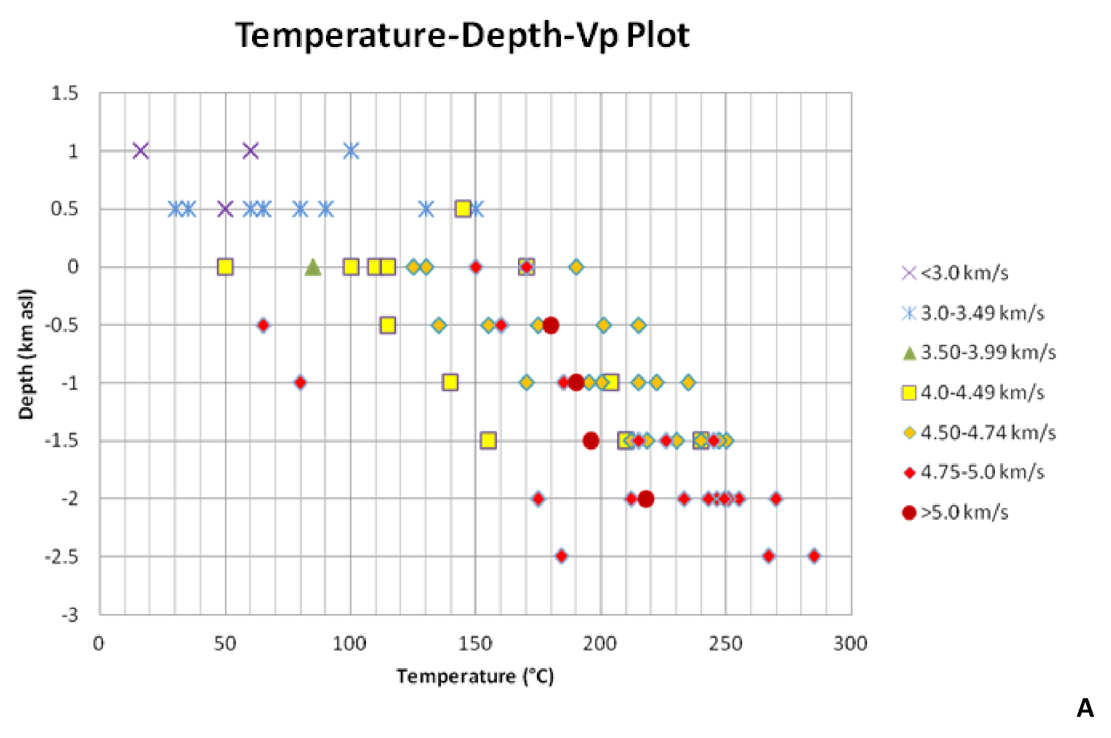

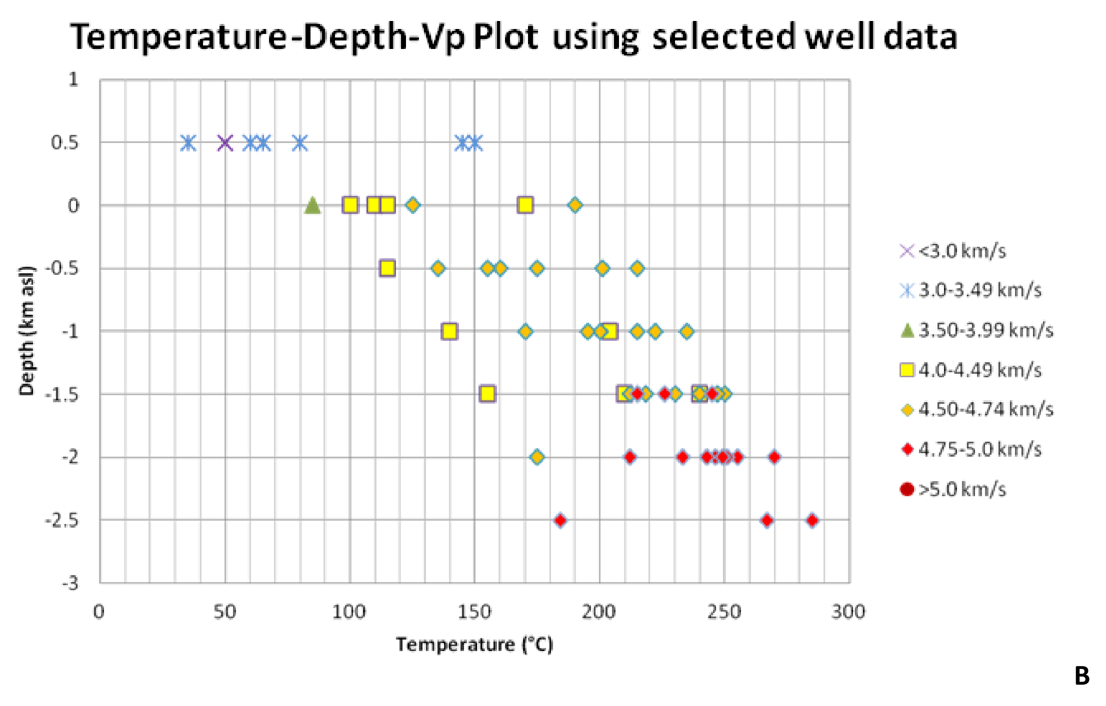

Figure 2. Temperature-Depth-Vp plots using well data. **(A)** Includes all data. **(B)** Excludes surface data and wells with low seismic trust values (53-15, 66-21, 76-28, and 45-14).

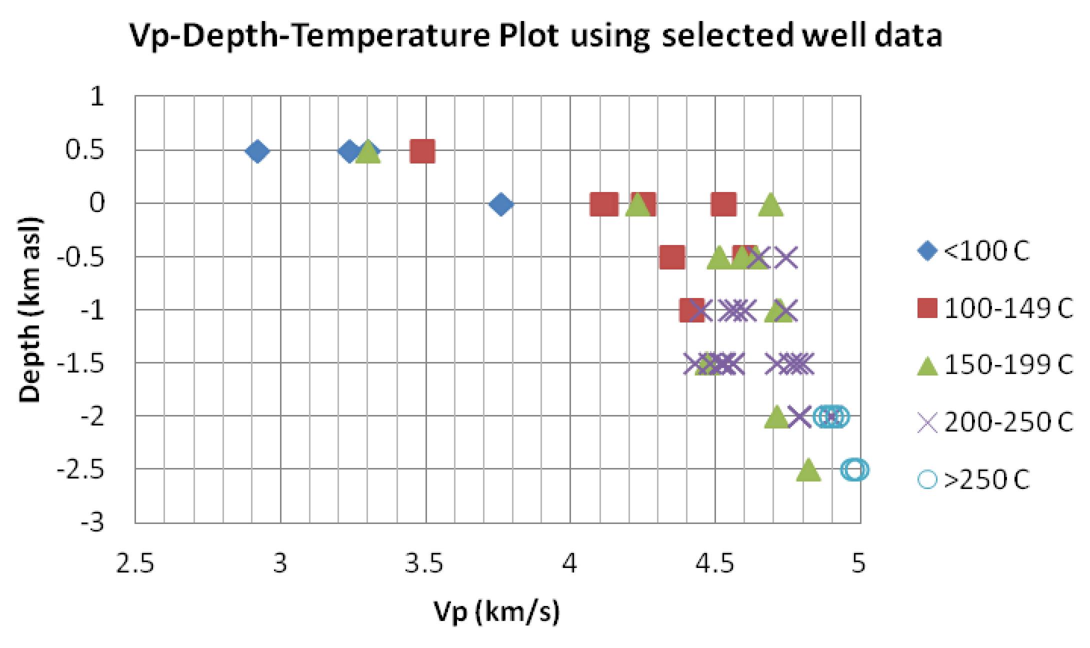

Figure 3. Vp-depth plot with respect to temperature using well data. The plot removes data occurring at the surface and wells with low seismic trust values (53-15, 66-21, 76-28, and 45-14).

Vp-T Relationship: Conductive vs. Convective Domains

The relationship between Vp, Depth and Lithology Type, and Temperature is assessed when comparing the various wells to a known conductive well, 62-21. The well being compared is shown above each of the successive plots.

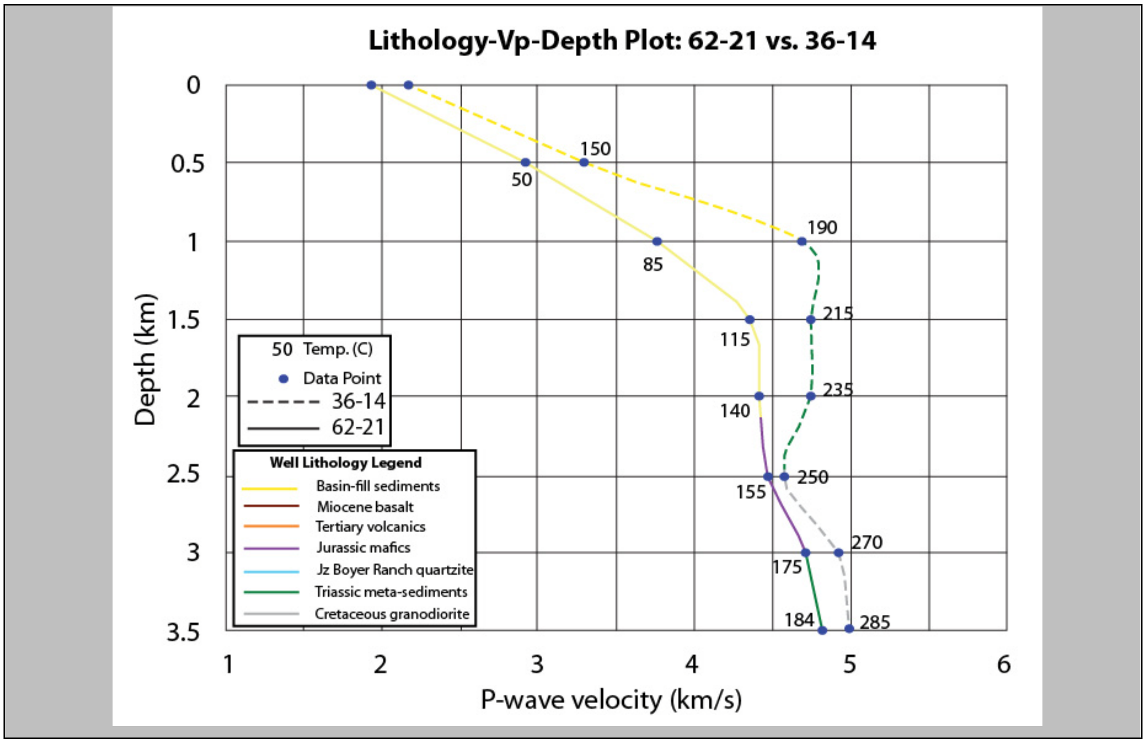

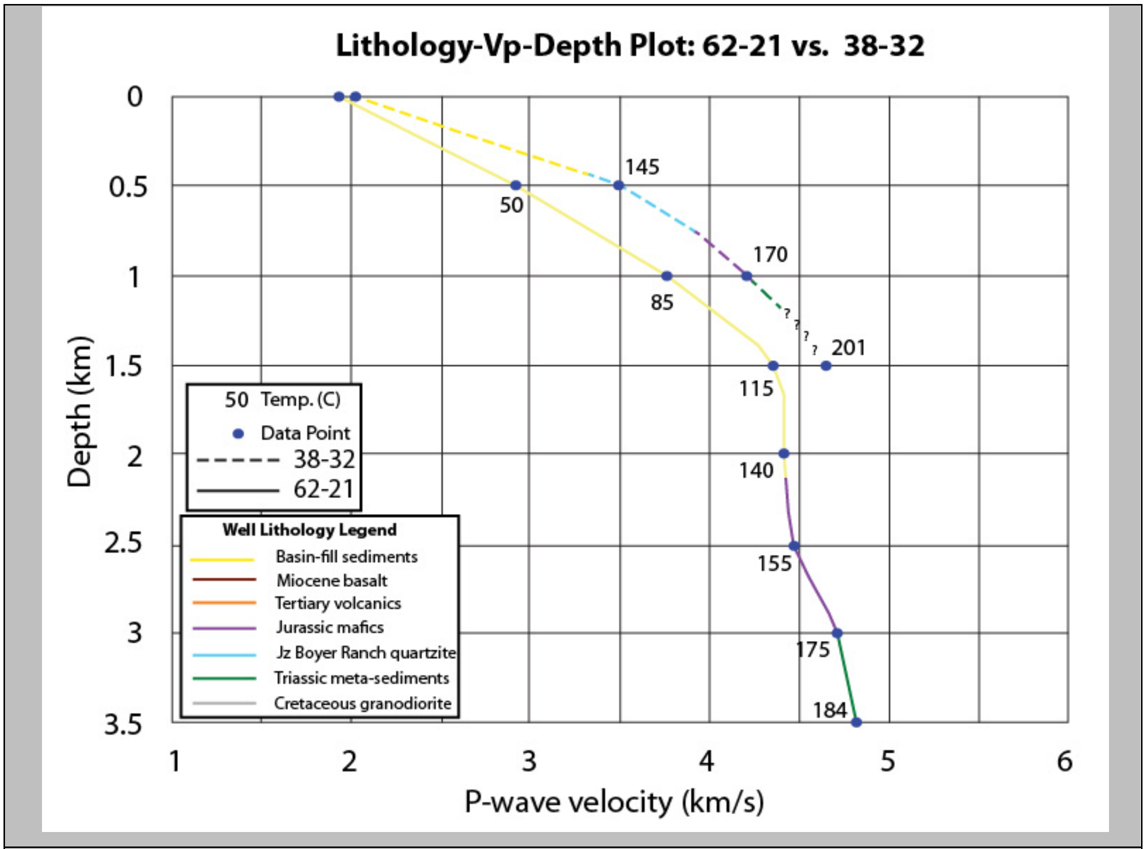
Lithology-Vp-Depth Plot: 62-21 vs. 38-32
Depth (km)
0
0.5
1
1.5
2
2.5
3
3.5
P-wave velocity (km/s)
1
2
3
4
5
6
145
50
170
85
?
?
?
?
201
115
140
155
175
184
50 Temp. (C)
● Data Point
38-32
62-21
Well Lithology Legend
Basin-fill sediments
Miocene basalt
Tertiary volcanics
Jurassic mafics
Jz Boyer Ranch quartzite
Triassic meta-sediments
Cretaceous granodiorite

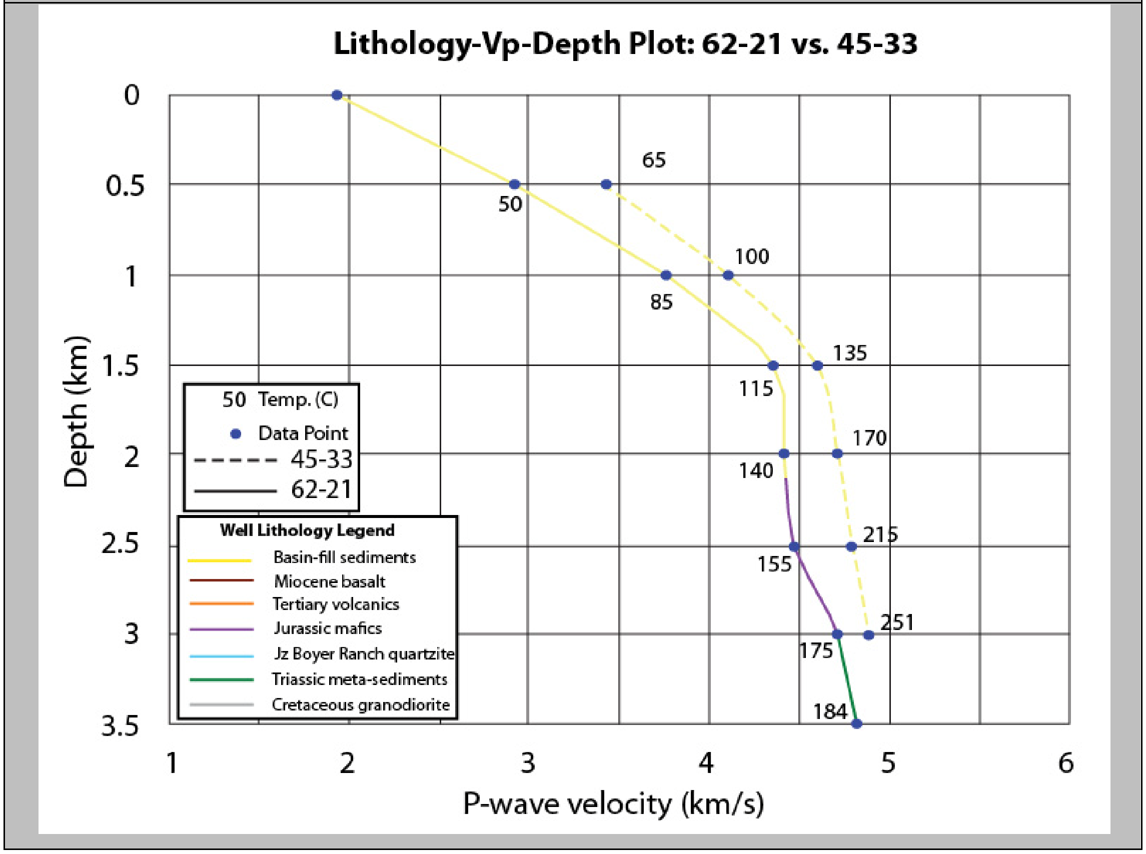
Lithology-Vp-Depth Plot: 62-21 vs. 45-33
Depth (km)
0
0.5
1
1.5
2
2.5
3
3.5
P-wave velocity (km/s)
1
2
3
4
5
6
65
50
100
85
135
115
170
140
215
155
251
175
184
50 Temp. (C)
● Data Point
45-33
62-21
Well Lithology Legend
Basin-fill sediments
Miocene basalt
Tertiary volcanics
Jurassic mafics
Jz Boyer Ranch quartzite
Triassic meta-sediments
Cretaceous granodiorite

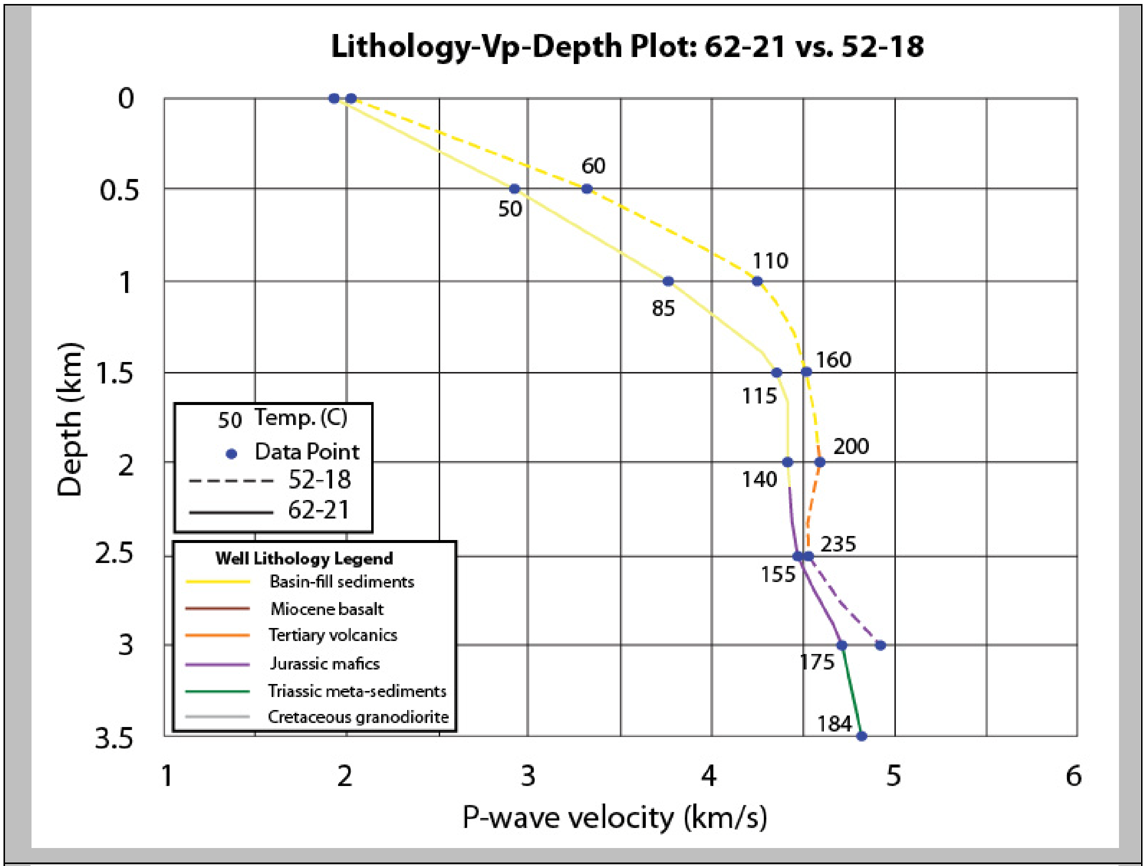

Lithology-Vp-Depth Plot: 62-21 vs. 52-18

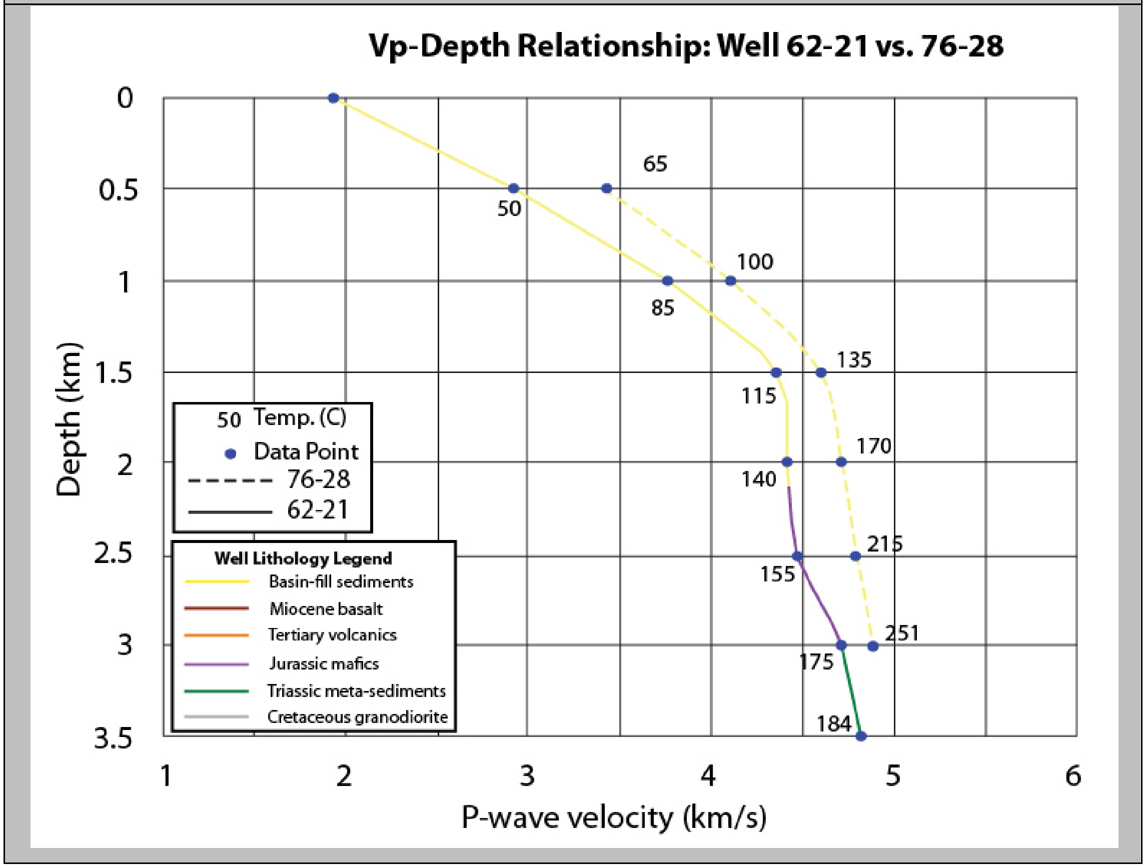

Vp-Depth Relationship: Well 62-21 vs. 76-28

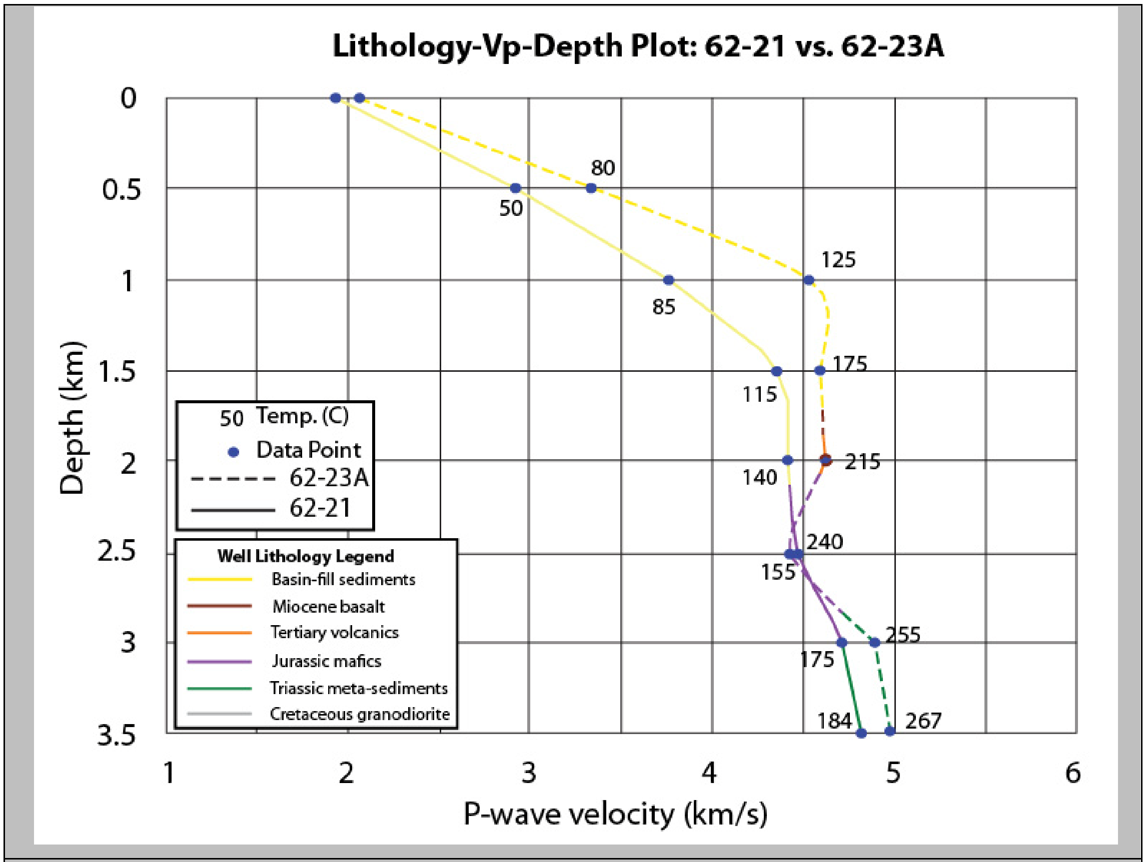
Lithology-Vp-Depth Plot: 62-21 vs. 62-23A
Depth (km)
0
0.5
1
1.5
2
2.5
3
3.5
P-wave velocity (km/s)
1
2
3
4
5
6
80
50
125
85
175
115
215
140
240
155
255
175
184
267
50 Temp. (C)
● Data Point
62-23A
62-21
Well Lithology Legend
Basin-fill sediments
Miocene basalt
Tertiary volcanics
Jurassic mafics
Triassic meta-sediments
Cretaceous granodiorite

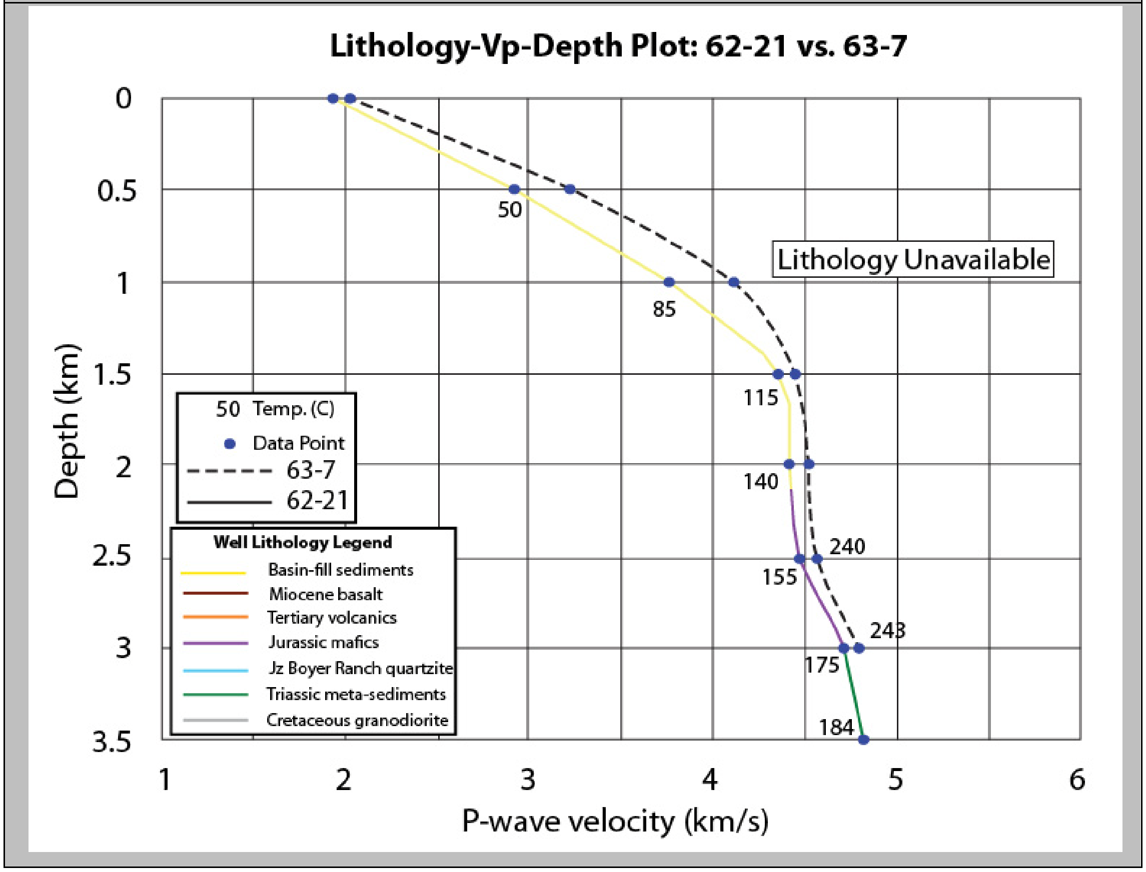
Lithology-Vp-Depth Plot: 62-21 vs. 63-7
Depth (km)
0
0.5
1
1.5
2
2.5
3
3.5
P-wave velocity (km/s)
1
2
3
4
5
6
50
Lithology Unavailable
85
115
140
240
155
243
175
184
50 Temp. (C)
● Data Point
63-7
62-21
Well Lithology Legend
Basin-fill sediments
Miocene basalt
Tertiary volcanics
Jurassic mafics
Jz Boyer Ranch quartzite
Triassic meta-sediments
Cretaceous granodiorite

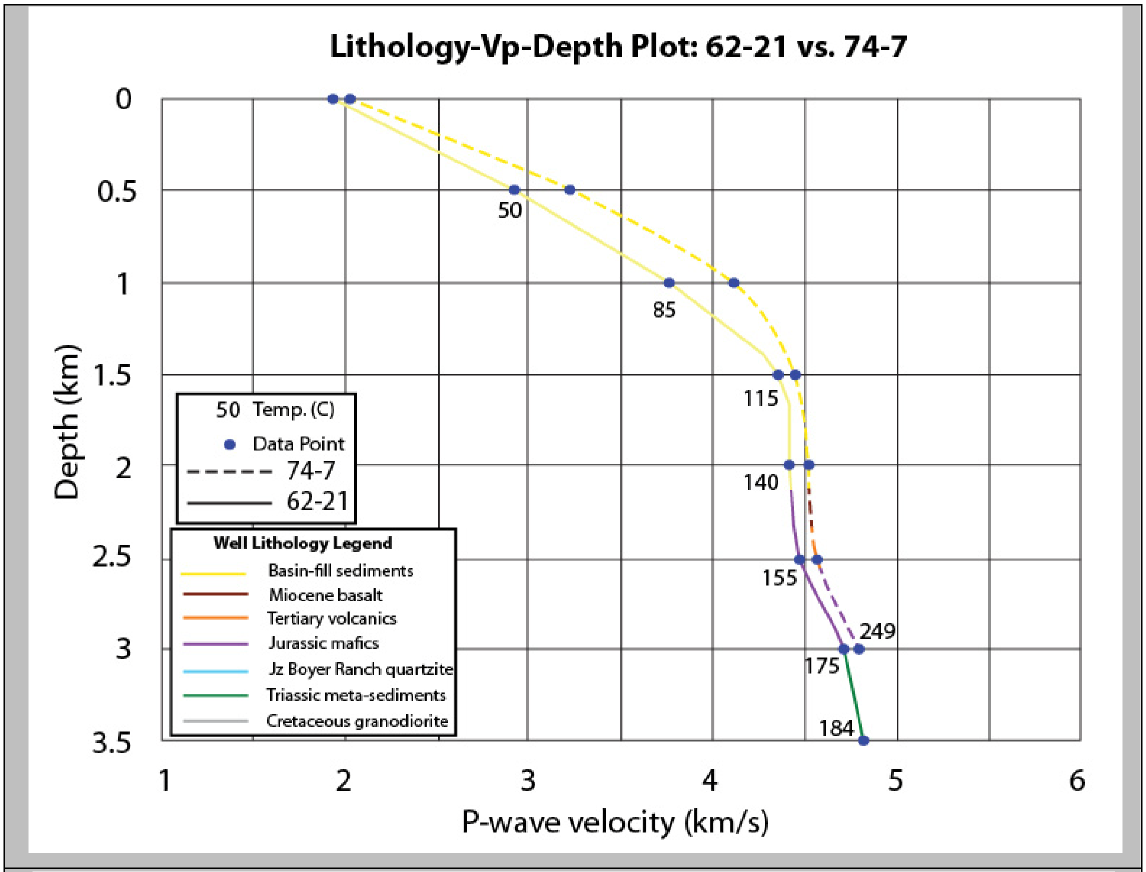
Lithology-Vp-Depth Plot: 62-21 vs. 74-7
Depth (km)
0
0.5
1
1.5
2
2.5
3
3.5
P-wave velocity (km/s)
1
2
3
4
5
6
50
85
115
140
155
249
175
184
50 Temp. (C)
Data Point
74-7
62-21
Well Lithology Legend
Basin-fill sediments
Miocene basalt
Tertiary volcanics
Jurassic mafics
Jz Boyer Ranch quartzite
Triassic meta-sediments
Cretaceous granodiorite

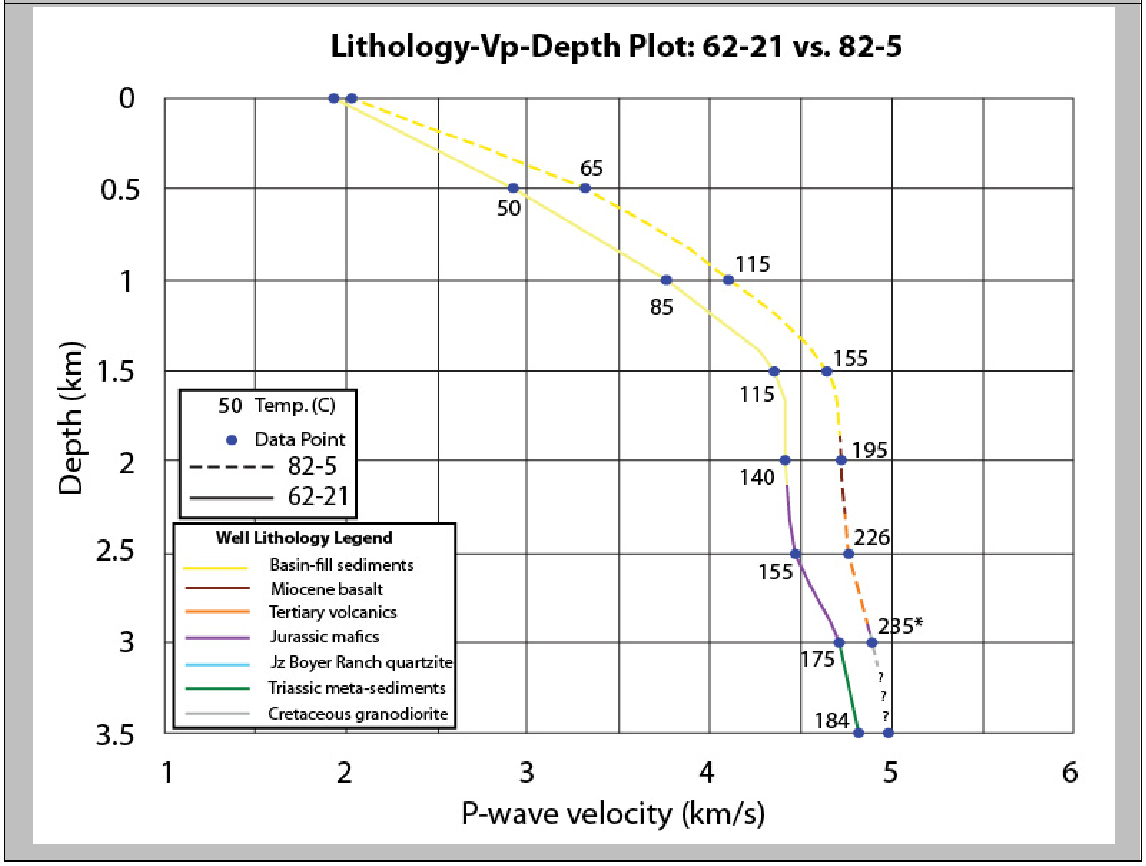
Lithology-Vp-Depth Plot: 62-21 vs. 82-5
Depth (km)
0
0.5
1
1.5
2
2.5
3
3.5
P-wave velocity (km/s)
1
2
3
4
5
6
65
50
115
85
155
115
195
140
226
155
235*
175
?
?
?
184
50 Temp. (C)
Data Point
82-5
62-21
Well Lithology Legend
Basin-fill sediments
Miocene basalt
Tertiary volcanics
Jurassic mafics
Jz Boyer Ranch quartzite
Triassic meta-sediments
Cretaceous granodiorite

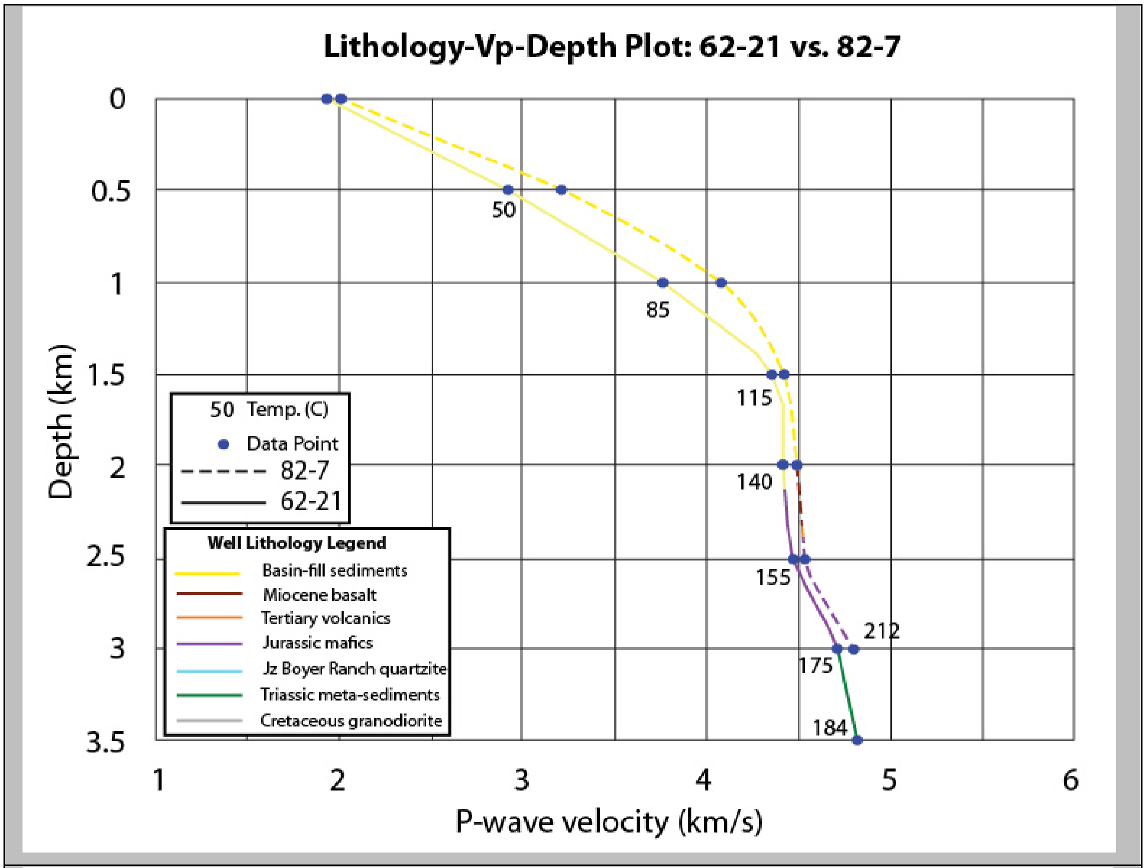
Lithology-Vp-Depth Plot: 62-21 vs. 82-7
Depth (km)
0
0.5
1
1.5
2
2.5
3
3.5
P-wave velocity (km/s)
1
2
3
4
5
6
50
85
115
140
155
212
175
184
50 Temp. (C)
Data Point
82-7
62-21
Well Lithology Legend
Basin-fill sediments
Miocene basalt
Tertiary volcanics
Jurassic mafics
Jz Boyer Ranch quartzite
Triassic meta-sediments
Cretaceous granodiorite

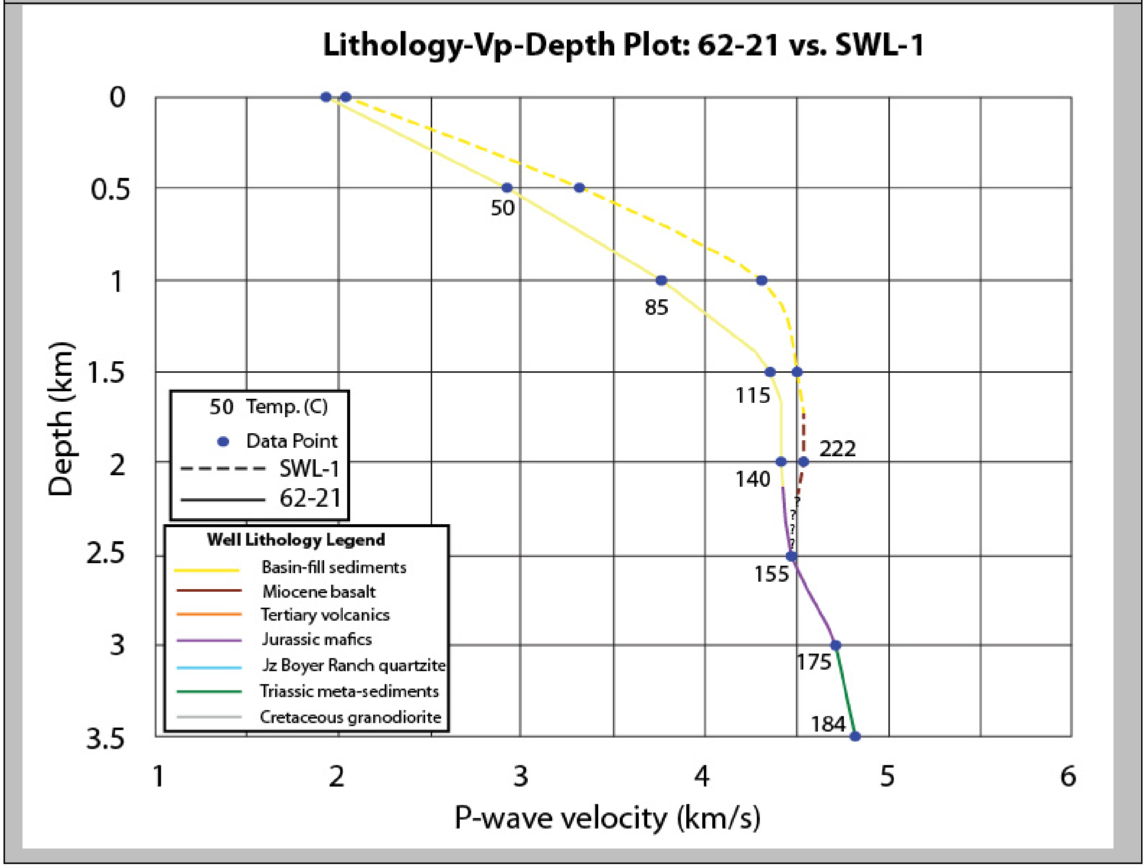
Lithology-Vp-Depth Plot: 62-21 vs. SWL-1
Depth (km)
0
0.5
1
1.5
2
2.5
3
3.5
P-wave velocity (km/s)
1
2
3
4
5
6
50
85
115
222
140
?
?
?
155
175
184
50 Temp. (C)
Data Point
SWL-1
62-21
Well Lithology Legend
Basin-fill sediments
Miocene basalt
Tertiary volcanics
Jurassic mafics
Jz Boyer Ranch quartzite
Triassic meta-sediments
Cretaceous granodiorite

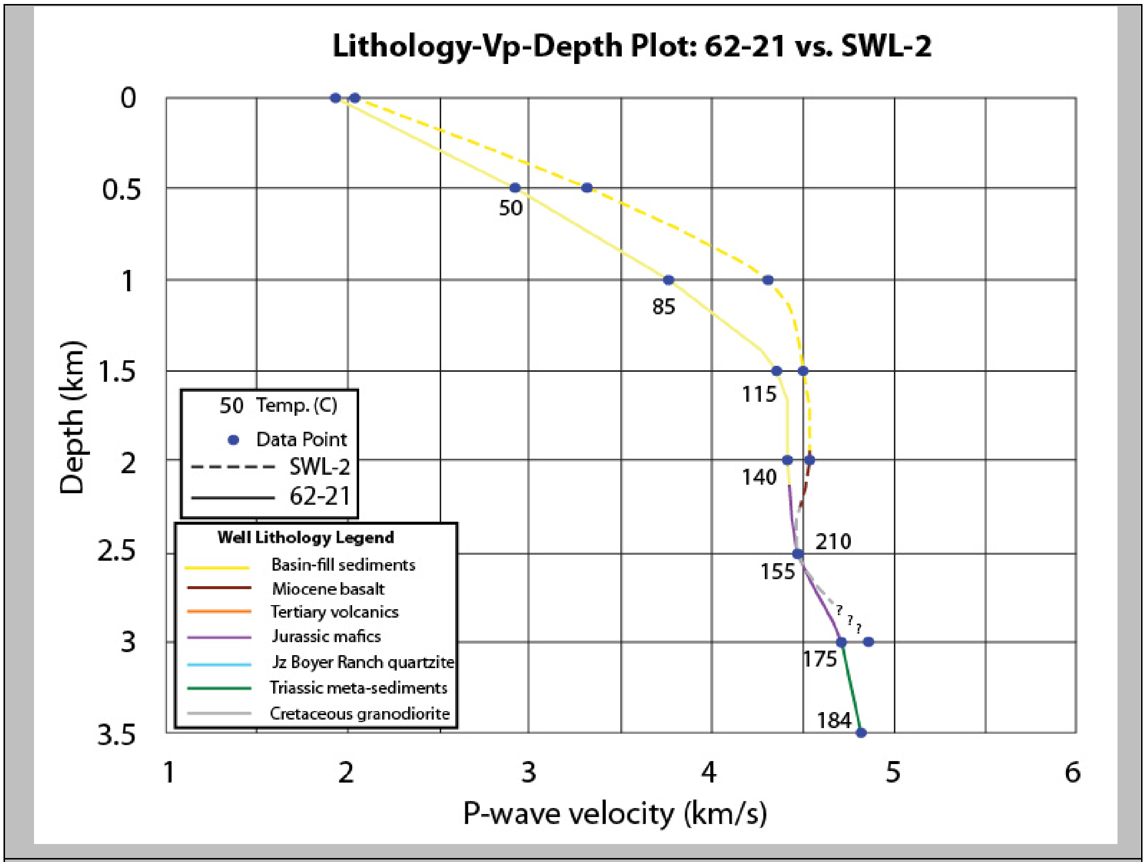
Lithology-Vp-Depth Plot: 62-21 vs. SWL-2
Depth (km)
0
0.5
1
1.5
2
2.5
3
3.5
P-wave velocity (km/s)
1
2
3
4
5
6
50
85
115
140
210
155
? ? ?
175
184
50 Temp. (C)
● Data Point
SWL-2
62-21
Well Lithology Legend
Basin-fill sediments
Miocene basalt
Tertiary volcanics
Jurassic mafics
Jz Boyer Ranch quartzite
Triassic meta-sediments
Cretaceous granodiorite

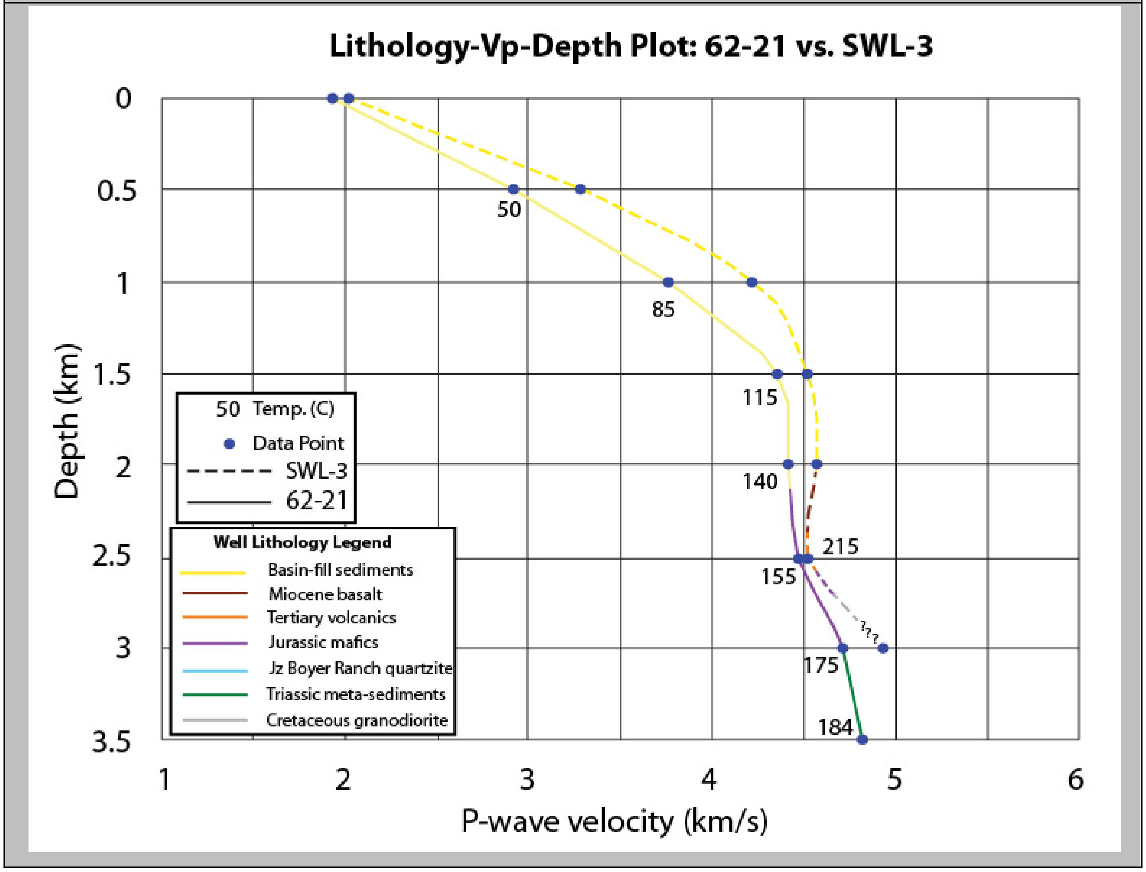
Lithology-Vp-Depth Plot: 62-21 vs. SWL-3
Depth (km)
0
0.5
1
1.5
2
2.5
3
3.5
P-wave velocity (km/s)
1
2
3
4
5
6
50
85
115
140
215
155
? ? ?
175
184
50 Temp. (C)
● Data Point
SWL-3
62-21
Well Lithology Legend
Basin-fill sediments
Miocene basalt
Tertiary volcanics
Jurassic mafics
Jz Boyer Ranch quartzite
Triassic meta-sediments
Cretaceous granodiorite

Vp-T Relationship: Divided into the major geologic formations

The relationship between Vp, Depth, and Temperature is assessed with respect to the six major geologic formations. Data is labeled by temperature and coded for well name.

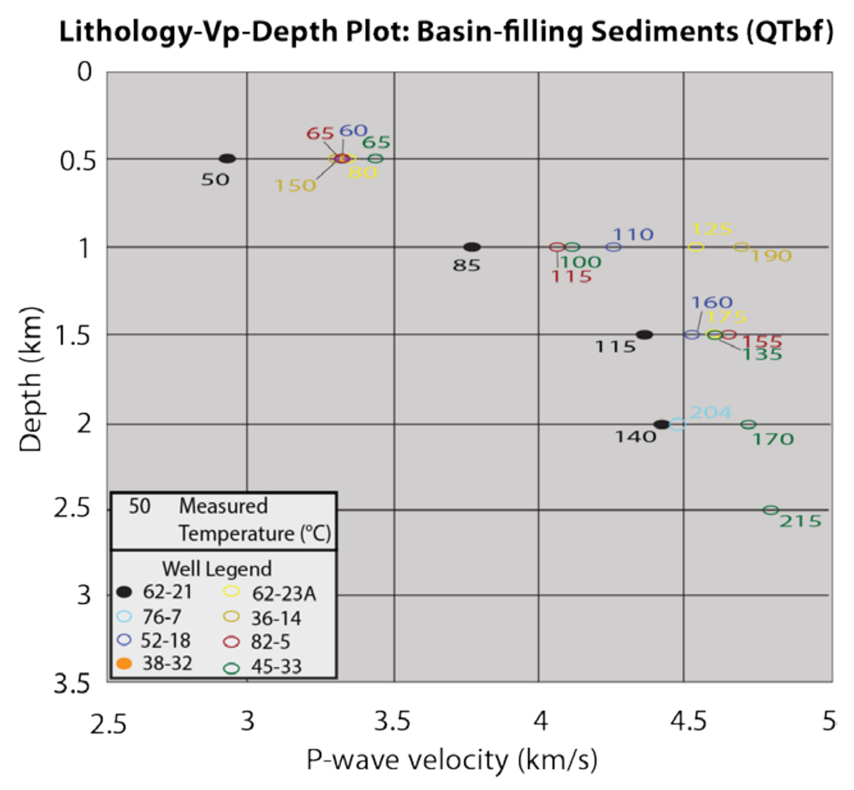
Lithology-Vp-Depth Plot: Basin-filling Sediments (QTbf)

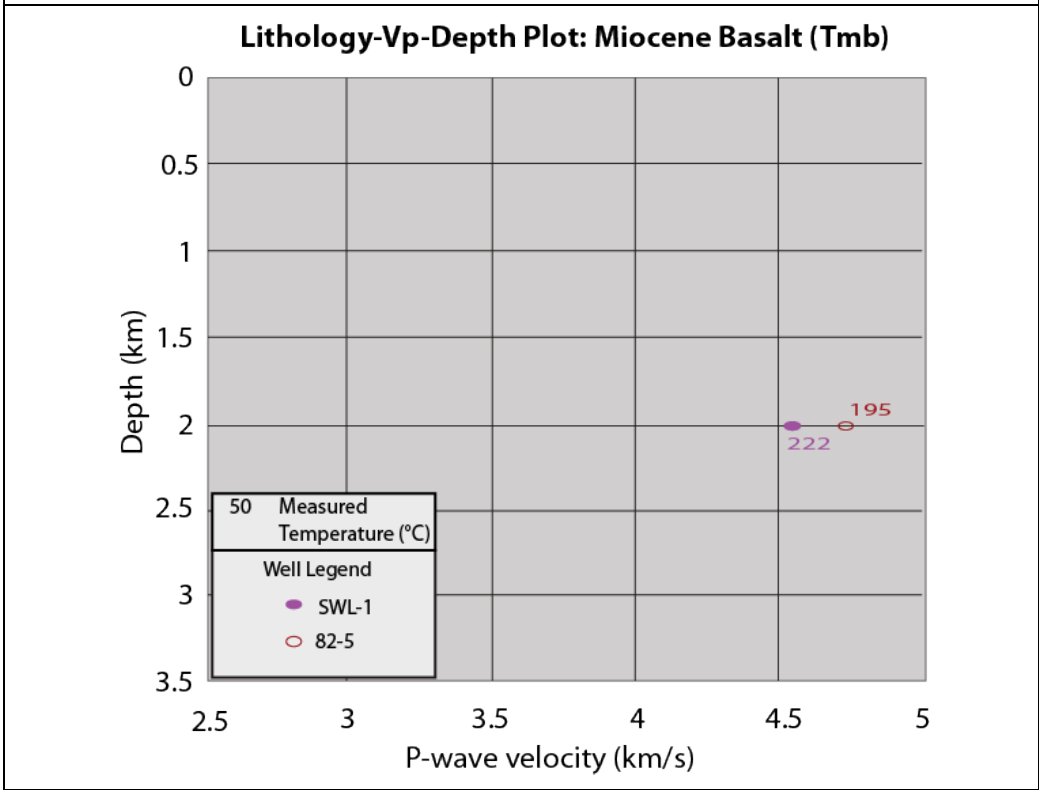
Lithology-Vp-Depth Plot: Miocene Basalt (Tmb)

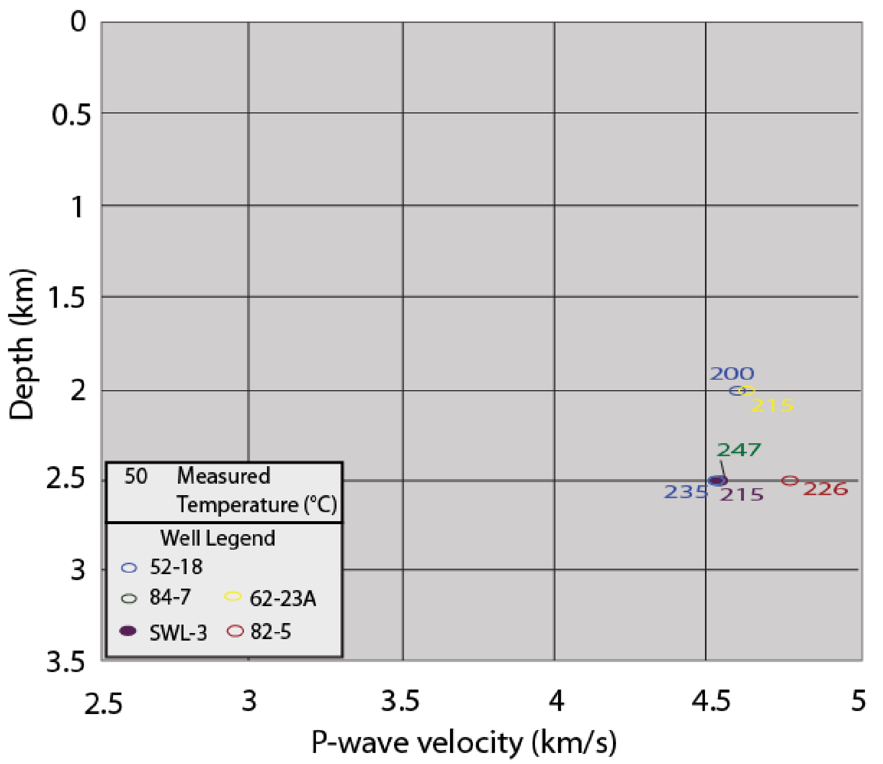

Lithology-Vp-Depth Plot: Oligocene Silicic Volcanics (Tv)

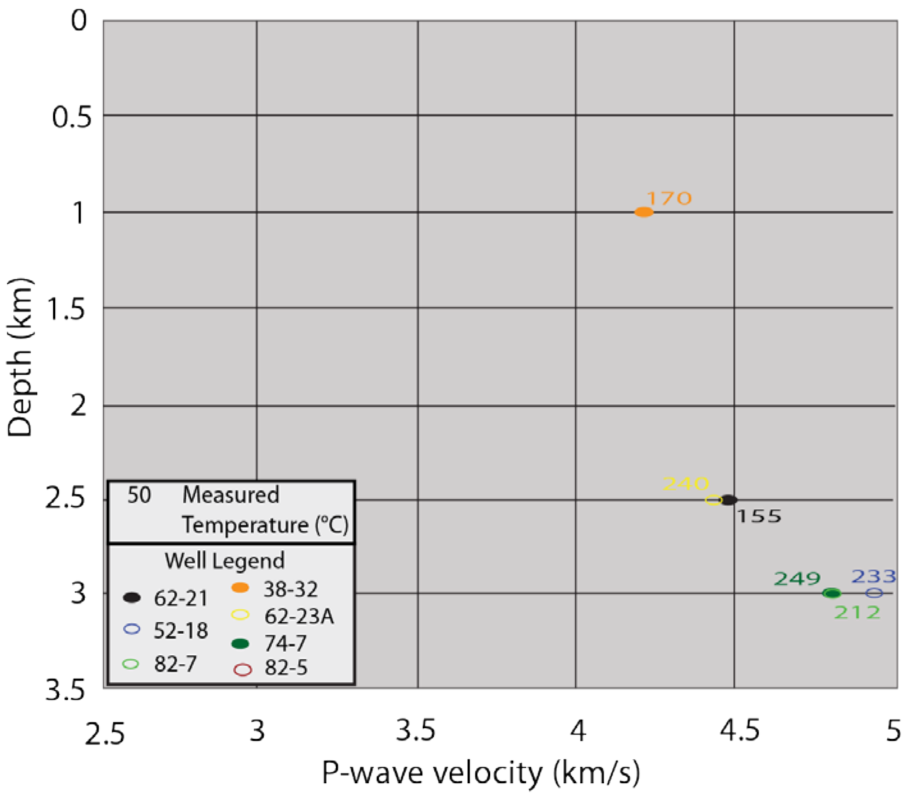

Lithology-Vp-Depth Plot: Jurassic Mafic Volcanics (Jz)

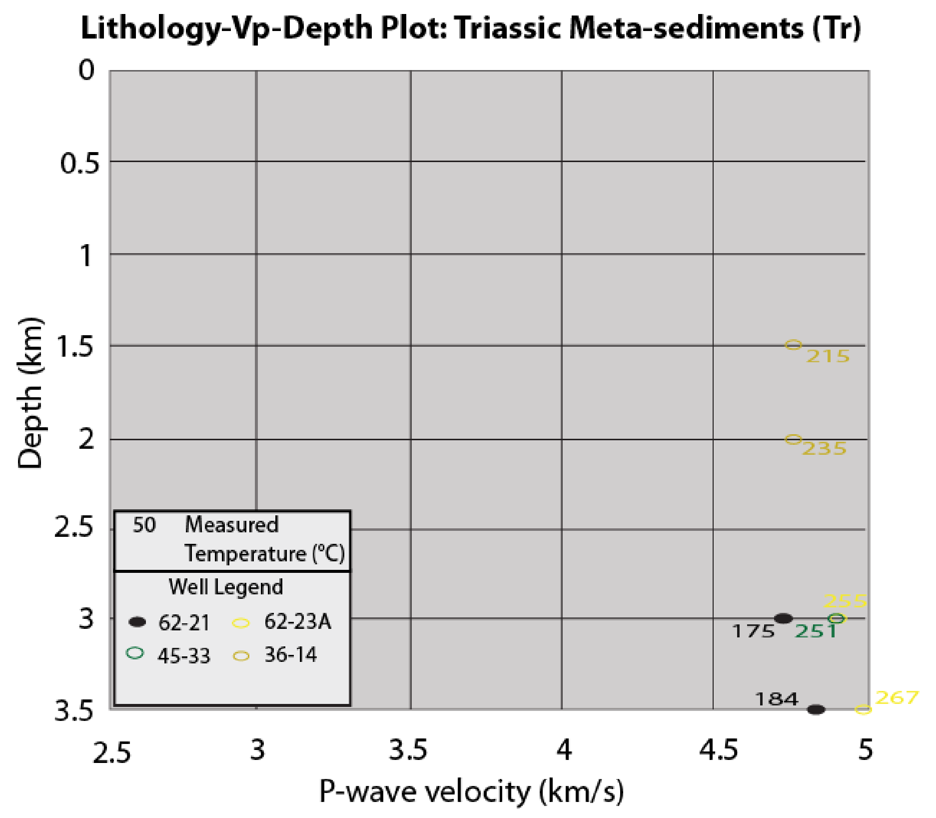

Lithology-Vp-Depth Plot: Triassic Meta-sediments (Tr)

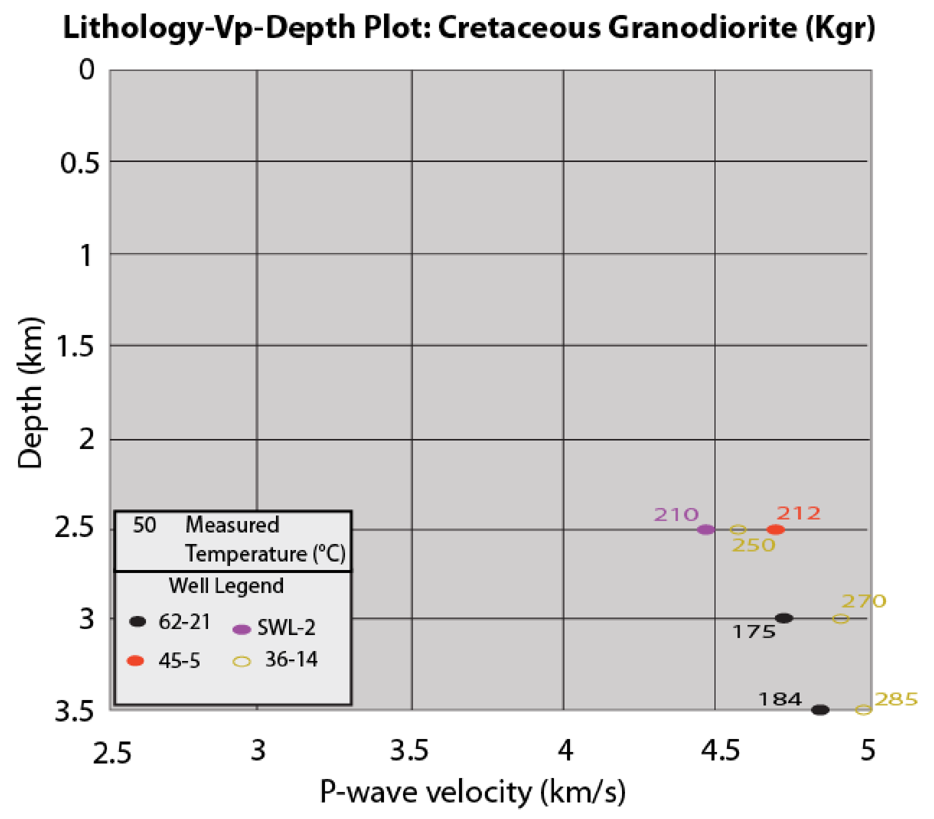

Lithology-Vp-Depth Plot: Cretaceous Granodiorite (Kgr)

APPENDIX 19

CLASSIFICATION AND REGRESSION TREE (CART) ANALYSIS

Table of Contents

List of Figures

List of Tables

Table 1. Preliminary Summary of CART Analyses Conducted

Description of Analysis Conducted	**Data Type**	**Selected Geoscience Parameters Considered (X) and Used (X) in the Data Splitting Process**								**r^2 - value**	**Summary**
		T^a	*Vp*	*Resist. (MT)*	*CSC*	*Dilat-ation*	*Fault Presence*	*Vertical Stress[f]*	*Lith-ology[bc]*		
Predicting Temperature	section	---	**X**	---	---	**X**	---	**X**	**X**	**0.91**	
Predicting Temperature		---	**X**	**X**	**---**	---	---	---	**X**	**0.8**	
Predicting Lithology[d]		X	**X**	**X**	**X**	**X**	---	X	---	**0.82**	
Predicting Lithology[d]		**X**	**X**	**X**	**X**	**X**	---	---	**---**	**0.54**	Removing VertStress dropped R^2 value by 34%
Predicting Productive (hydrothermal) Wells for the productive and non-productive well data set	well	X	**X**	**X**	**X**	X	X	**X**	**X**	**0.66**	
		X	**X**	**X**	**X**	**X**	X	**X**	---	**0.52**	R^2-value dropped 21% when Lithology was removed and Dilatation was considered
		---	**X**	**X**	---	---	X	---	**X**	**0.62**	Vp, MT and Lithology accounts for 94% of the 0.66 r^2-value above
		X	**X**	**X**	---	---	X	---	**X**	**0.54**	
Predicting Temperature	well	---	**X**	---	---	---	---	---	---	**0.62**	
Predicting Temperature[e]		---	**X**	---	---	---	---	---	---	**0.75**	R^2-valued increased by ~21%
Predicting Temperature[e]		---	**X**	**X**	---	---	---	---	**X**	**0.75**	Adding Resistivity (MT) and Lithology does not change R^2-value relative to using Vp alone
Predicting Temperature[e]		---	**X**	**X**	---	---	---	---	---	**0.78**	Highest R^2 value using Vp and Resistivity (MT)

[a] Temperature; [b] Lithologic Density is a parameter that is directly related to the various lithology identified in this investigation; [c] Gravity-magnetic data was found to be highly correlated to lithology and as such is not shown as a separate parameter; [d] Fracture Intensity was also considered in some of these analysis but not used; [e] Uses all data except wells with a low seismic trust (i.e., 66-21, 45-14, 76-28); [f] Vertical Stress

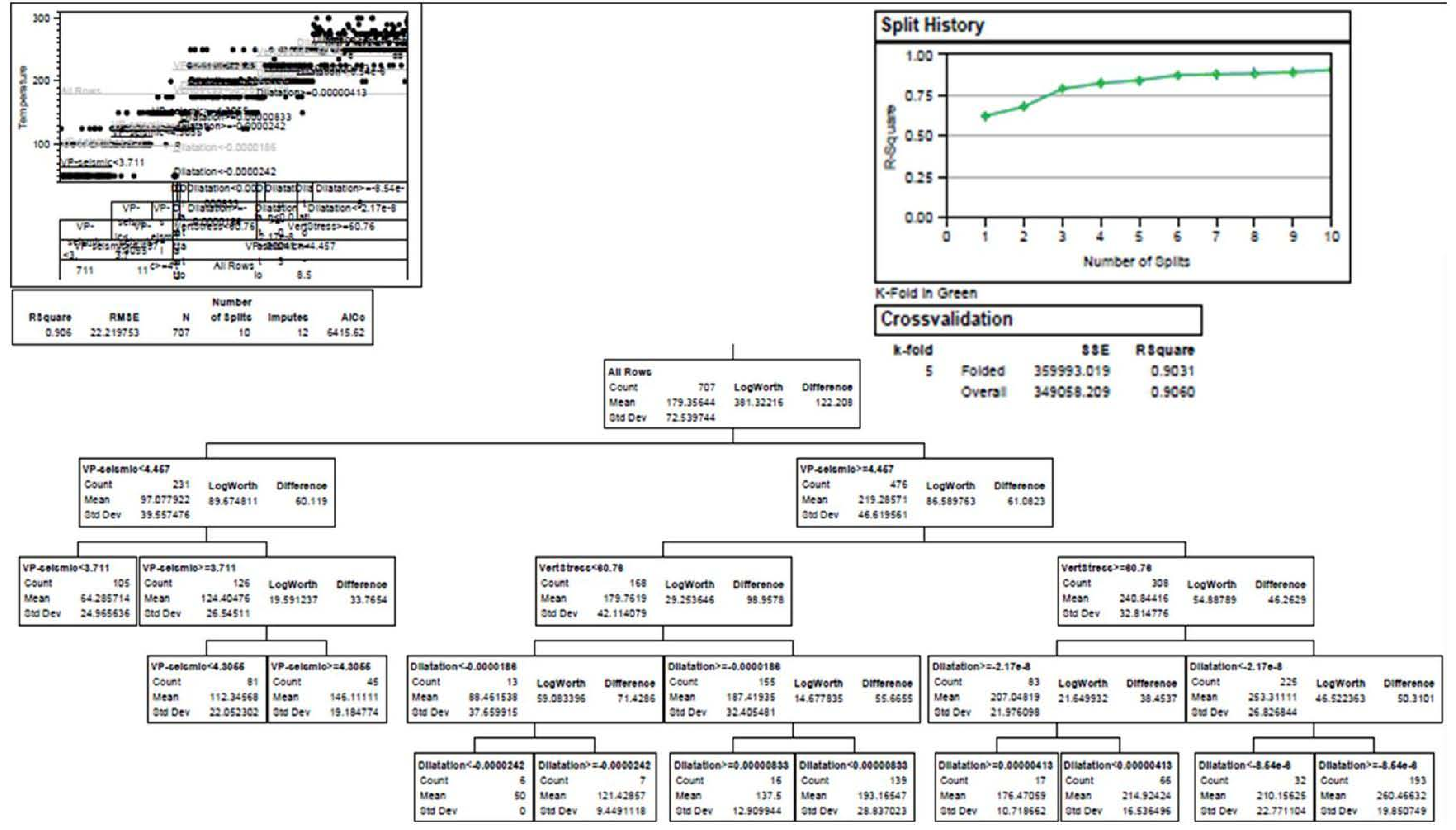

RSquare	RMSE	N	Number of Splits	Imputes	AICc
0.906	22.219753	707	10	12	6415.62

Crossvalidation

k-fold		SSE	RSquare
5	Folded	359993.019	0.9031
	Overall	349058.209	0.9060

Figure 1. CART Analysis with Section Data for predicting temperature using all parameters. The analysis split on Vp, VertStress, and Dilatation with an r^2 value of 0.91. See Table 1, row 1.

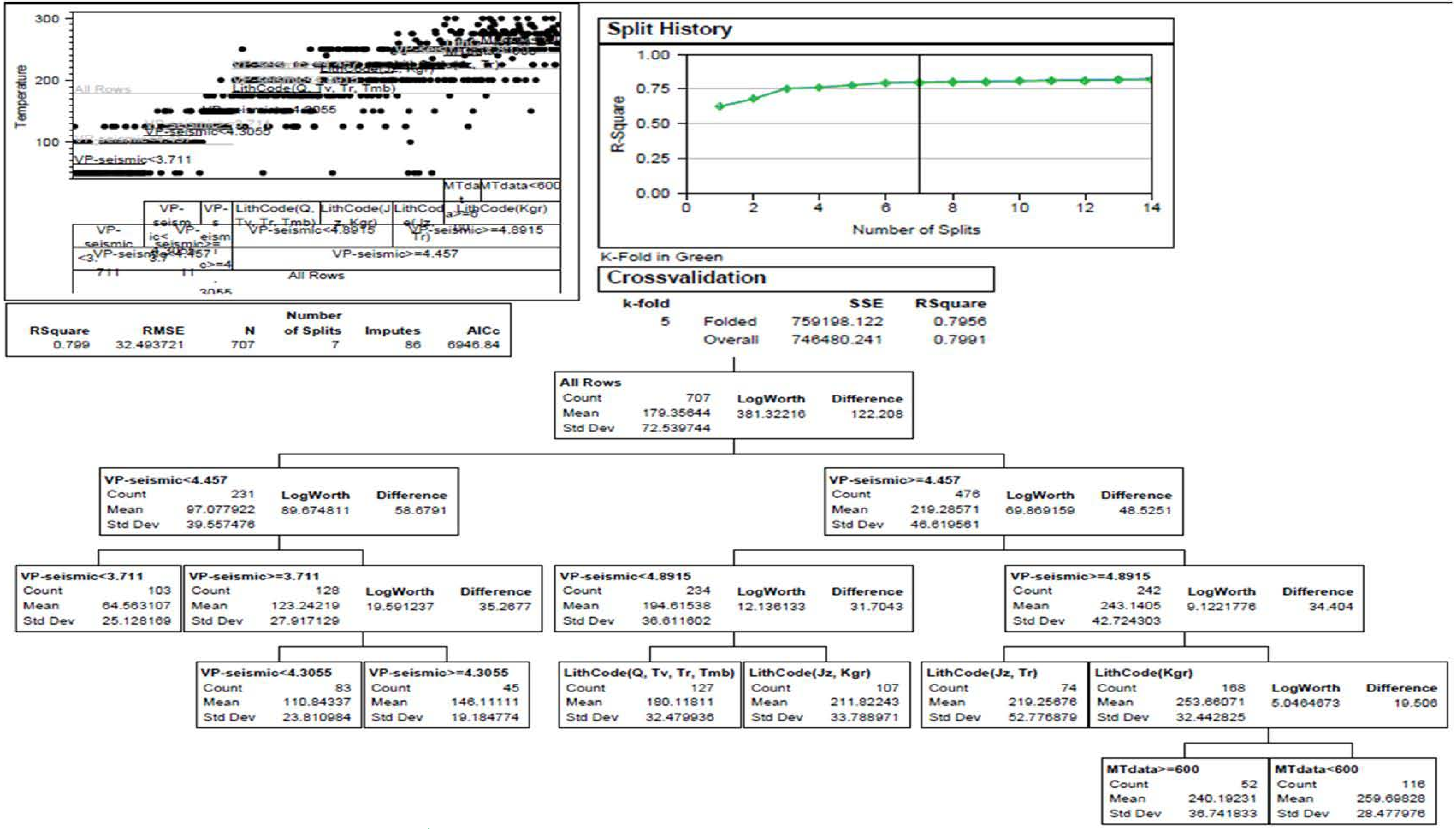

RSquare	RMSE	N	Number of Splits	Imputes	AICc
0.799	32.493721	707	7	86	6946.84

Crossvalidation

k-fold		SSE	RSquare
5	Folded	759198.122	0.7956
	Overall	746480.241	0.7991

All Rows

		LogWorth	Difference
Count	707	381.32216	122.208
Mean	179.35644		
Std Dev	72.539744		

VP-seismic<4.457

		LogWorth	Difference
Count	231	89.674811	58.6791
Mean	97.077922		
Std Dev	39.557476		

VP-seismic>=4.457

		LogWorth	Difference
Count	476	69.869159	48.5251
Mean	219.28571		
Std Dev	46.619561		

VP-seismic<3.711

Count	103
Mean	64.563107
Std Dev	25.128169

VP-seismic>=3.711

		LogWorth	Difference
Count	128	19.591237	35.2677
Mean	123.24219		
Std Dev	27.917129		

VP-seismic<4.8915

		LogWorth	Difference
Count	234	12.136133	31.7043
Mean	194.61538		
Std Dev	36.611602		

VP-seismic>=4.8915

		LogWorth	Difference
Count	242	9.1221776	34.404
Mean	243.1405		
Std Dev	42.724303		

VP-seismic<4.3055

Count	83
Mean	110.84337
Std Dev	23.810984

VP-seismic>=4.3055

Count	45
Mean	146.11111
Std Dev	19.184774

LithCode(Q, Tv, Tr, Tmb)

Count	127
Mean	180.11811
Std Dev	32.479936

LithCode(Jz, Kgr)

Count	107
Mean	211.82243
Std Dev	33.788971

LithCode(Jz, Tr)

Count	74
Mean	219.25676
Std Dev	52.776879

LithCode(Kgr)

		LogWorth	Difference
Count	168	5.0464673	19.506
Mean	253.66071		
Std Dev	32.442825		

MTdata>=600

Count	52
Mean	240.19231
Std Dev	36.741833

MTdata<600

Count	116
Mean	259.69828
Std Dev	28.477976

Figure 2. CART Analysis with section data predicting temperature using Vp, MT and lithology; $R^2 = 0.80$. See Table 1, row 2.

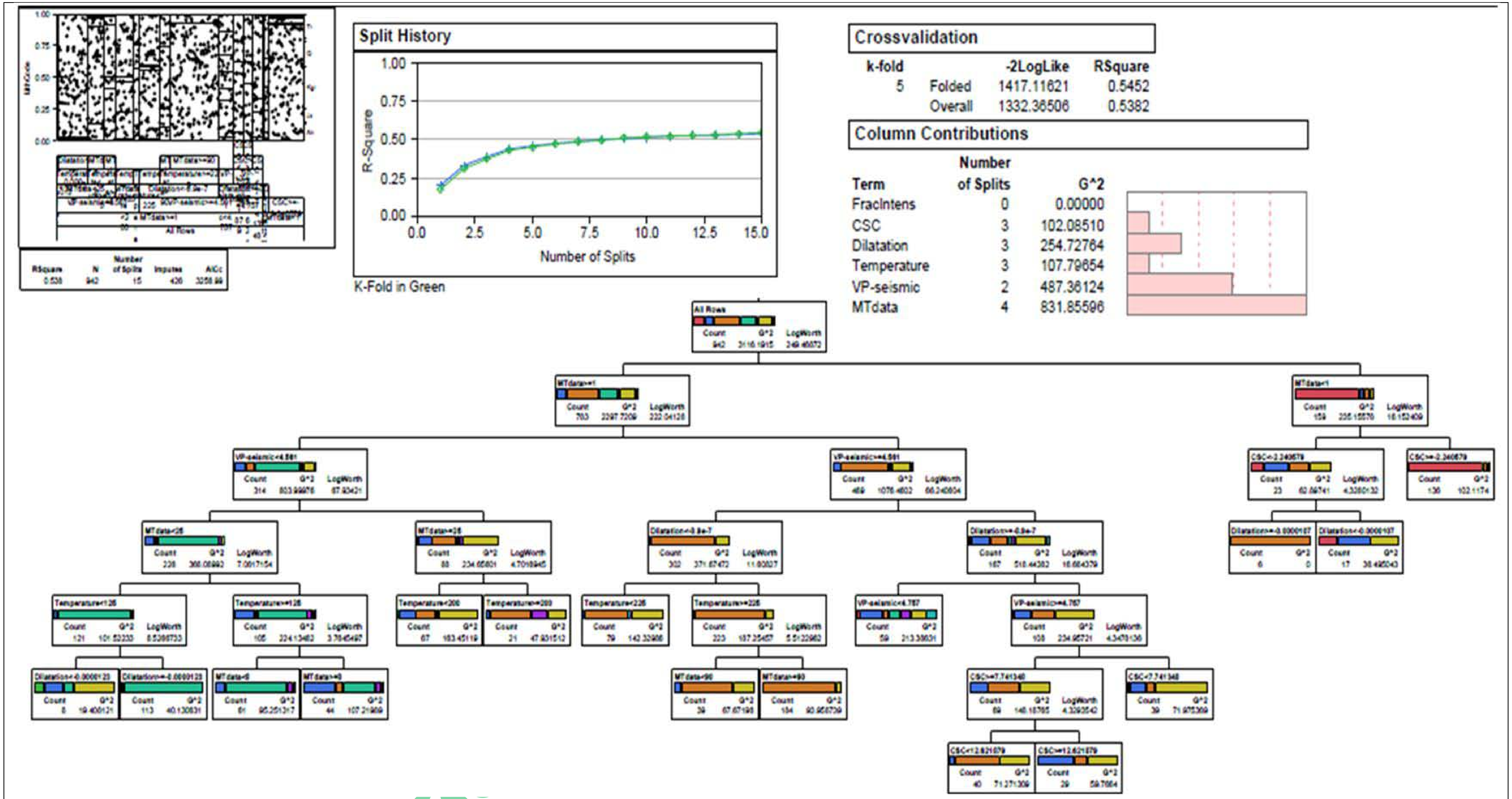

RSquare	N	Number of Splits	Imputes	AICc
0.538	942	15	426	3258.99

Crossvalidation

k-fold		-2LogLike	RSquare
5	Folded	1417.11621	0.5452
	Overall	1332.36506	0.5382

Column Contributions

Term	Number of Splits	G^2
FracIntens	0	0.00000
CSC	3	102.08510
Dilatation	3	254.72764
Temperature	3	107.79654
VP-seismic	2	487.36124
MTdata	4	831.85596

Figure 3. CART Analysis with Section Data for predicting Lithology using all parameters except VertStress; r^2 = 0.54. See Table 1, row 4.

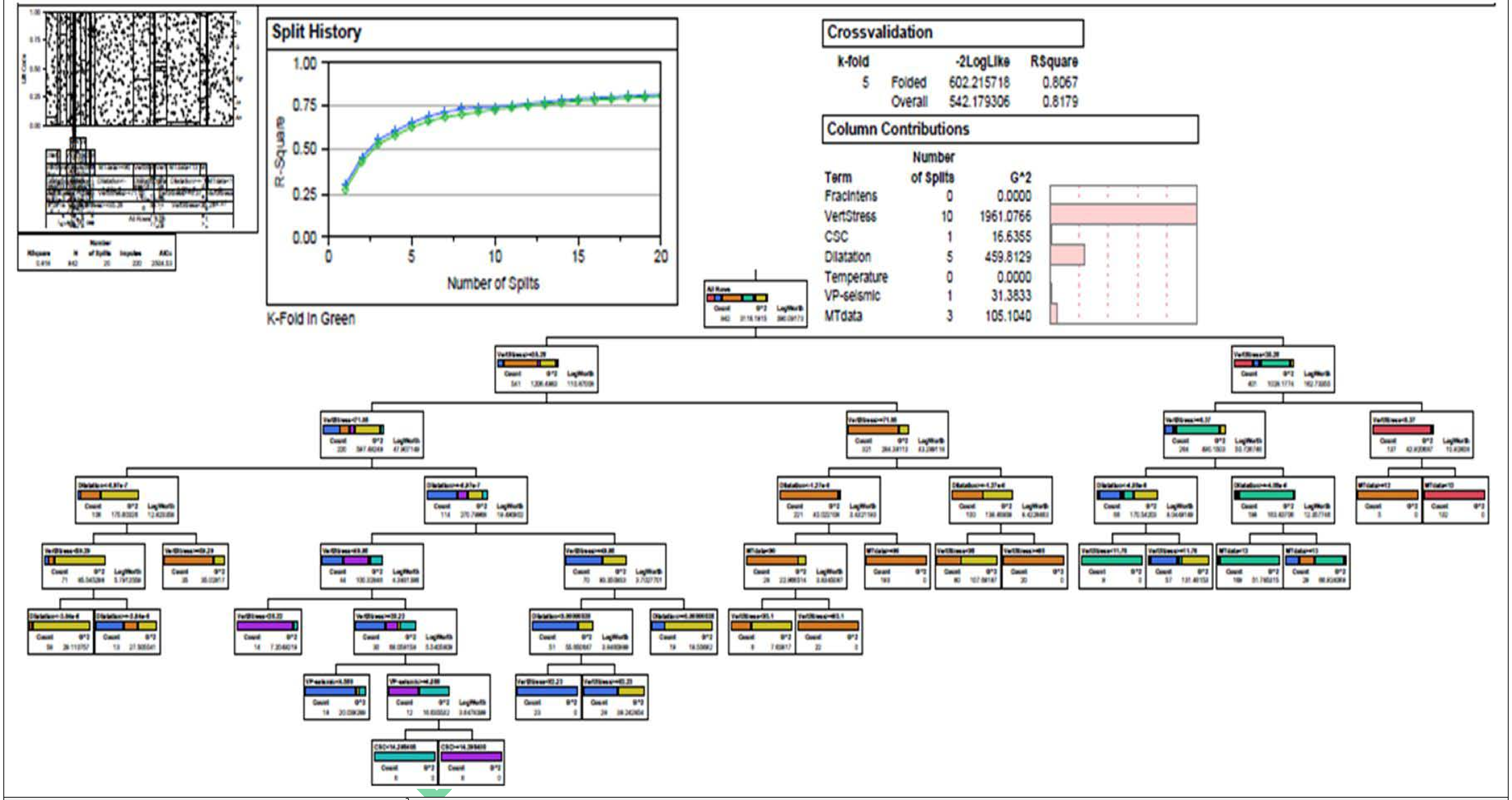

Crossvalidation

k-fold		-2LogLike	RSquare
5	Folded	602.215718	0.8067
	Overall	542.179306	0.8179

Column Contributions

Term	Number of Splits	G^2
FracIntens	0	0.0000
VertStress	10	1961.0766
CSC	1	16.6355
Dilatation	5	459.8129
Temperature	0	0.0000
VP-seismic	1	31.3833
MTdata	3	105.1040

Figure 4. CART Analysis for predicting Lithology using all parameters; r^2 = 0.82. The analysis split on mostly on the parameter Vertical Stress with other contributions from CSC, Dilatation, Vp and MT. See Table 1, row 3.

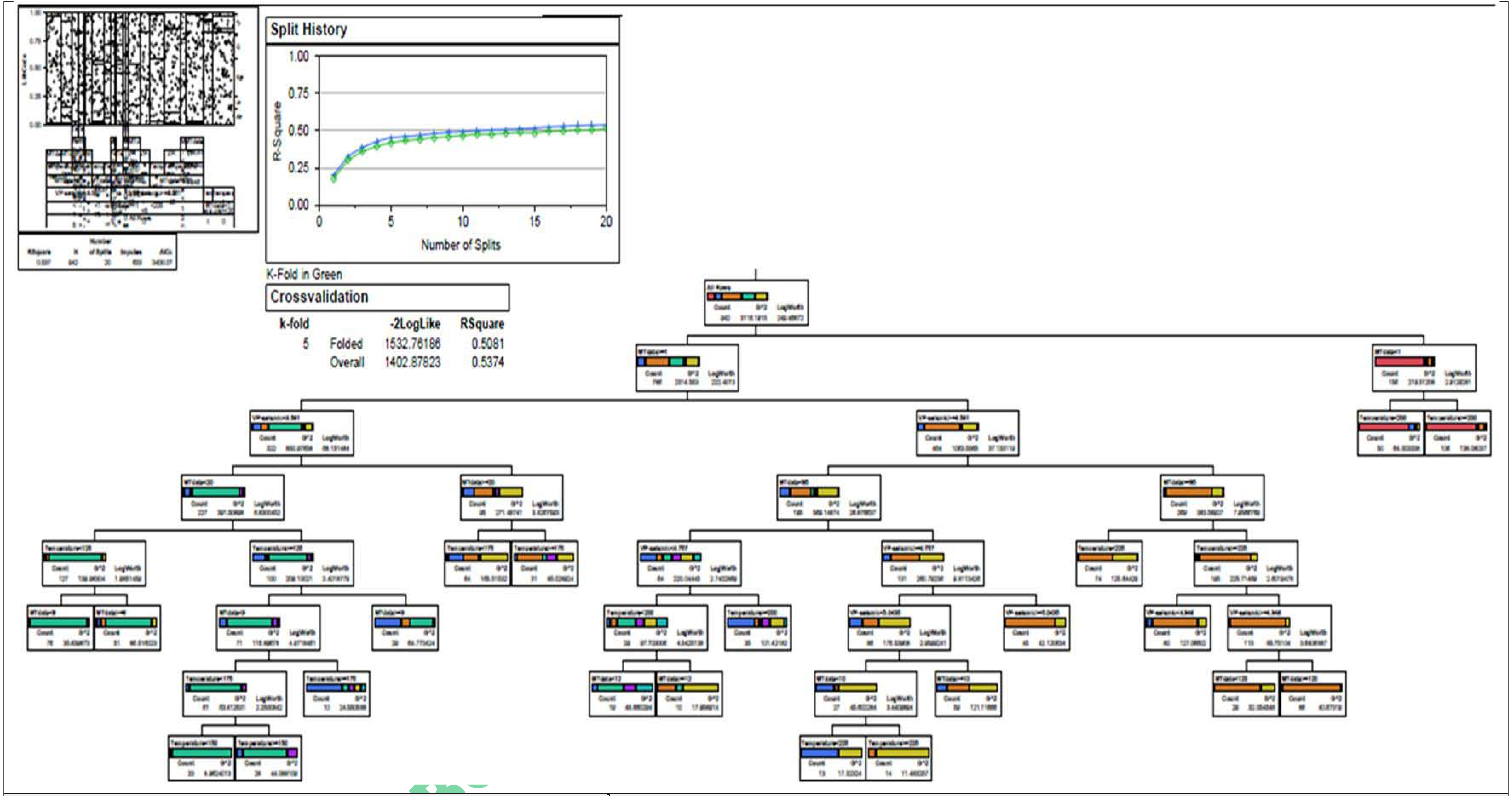

Crossvalidation

k-fold		-2LogLike	RSquare
5	Folded	1532.76186	0.5081
	Overall	1402.87823	0.5374

Figure 5. CART Analysis with Section Data for predicting Lithology using MT, Vp and Temperature. The r^2 value is 0.537.

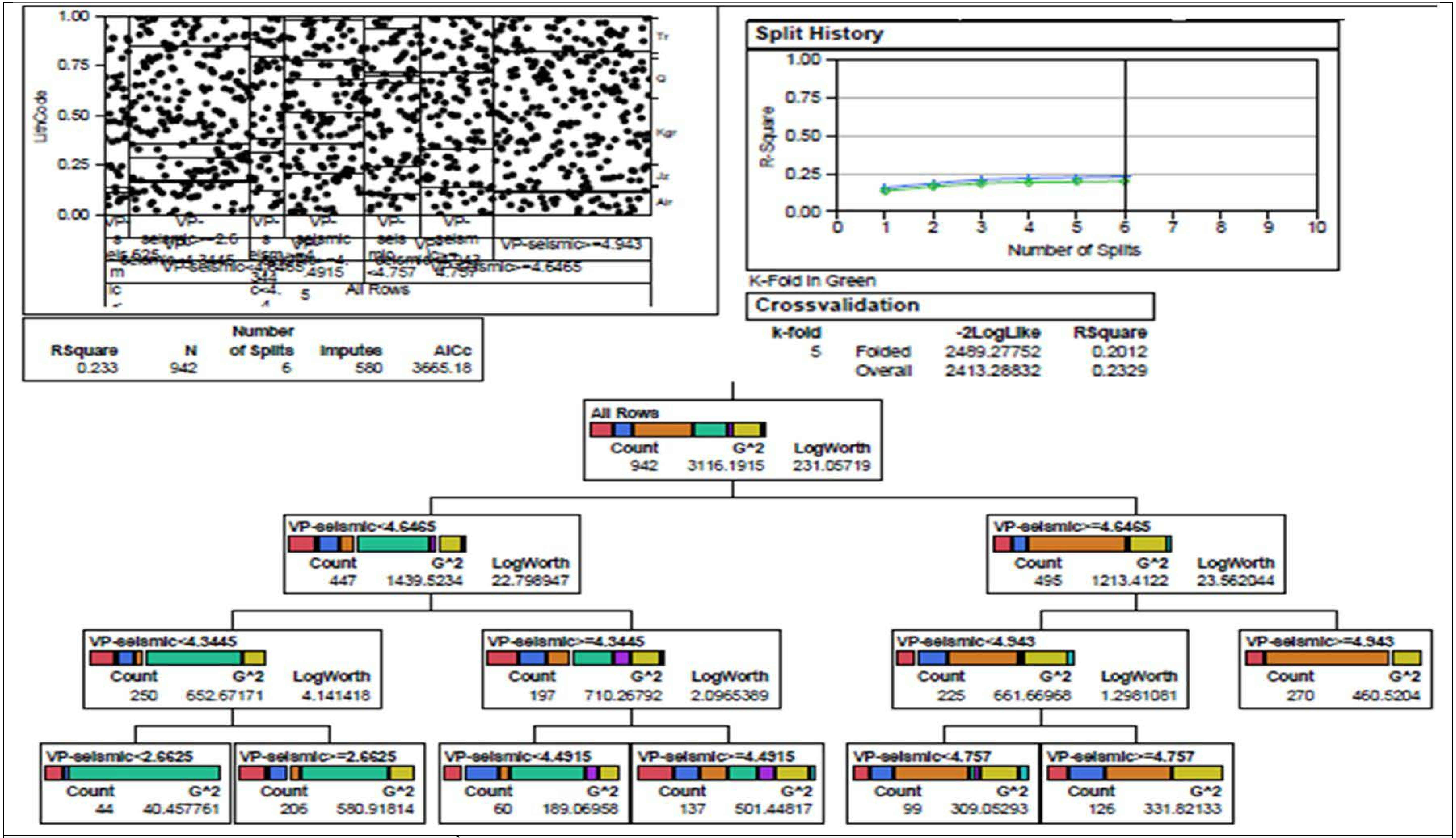

RSquare	N	Number of Splits	Imputes	AICc
0.233	942	6	580	3665.18

Crossvalidation

k-fold		-2LogLike	RSquare
5	Folded	2489.27752	0.2012
	Overall	2413.28832	0.2329

Figure 6. CART Analysis with Section Data predicting Lithology using Vp. The low r^2 value (0.23) infers that Temperature cannot be predicted from Vp using the section data.

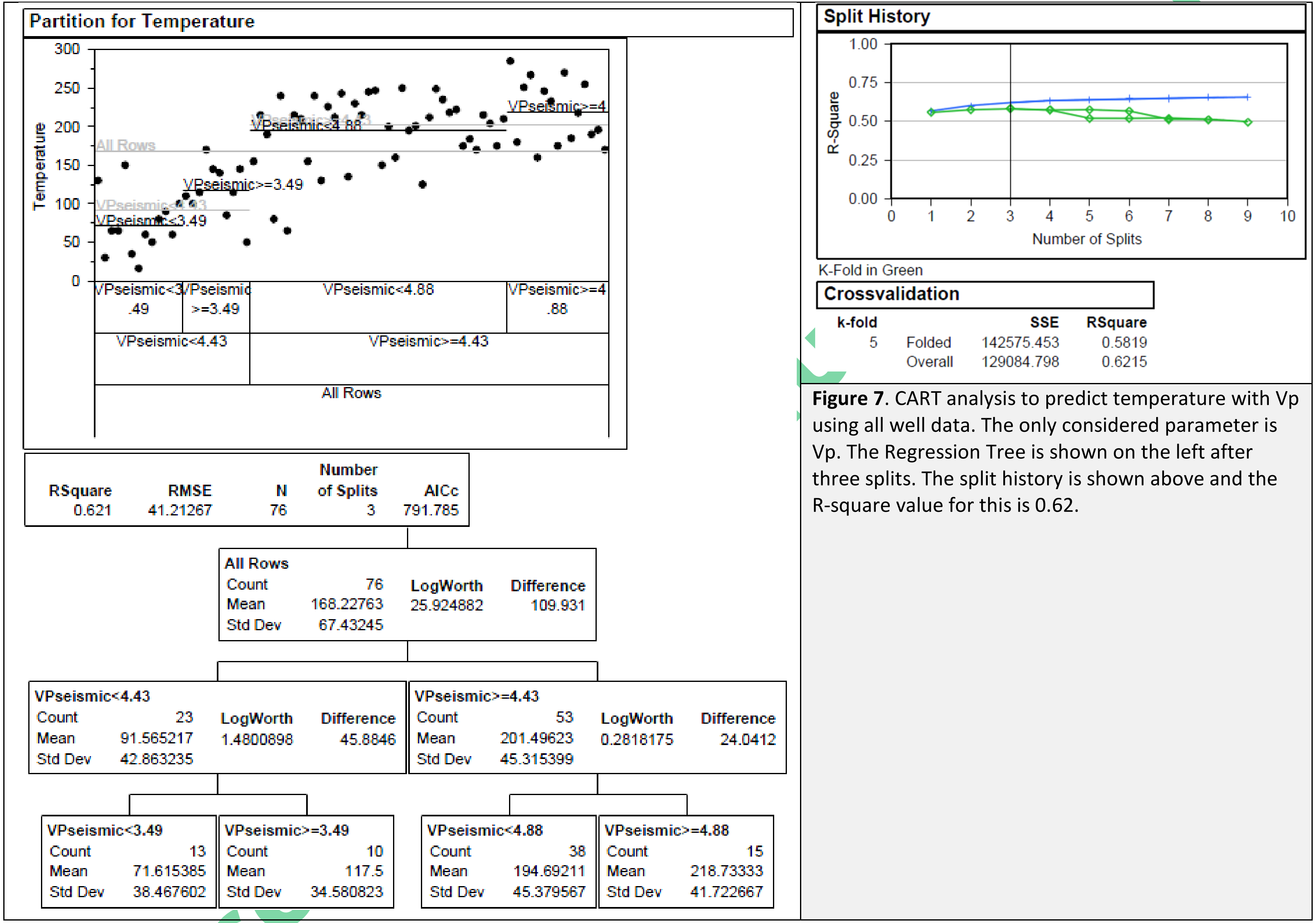

RSquare	RMSE	N	Number of Splits	AICc
0.621	41.21267	76	3	791.785

All Rows

		LogWorth	Difference
Count	76	25.924882	109.931
Mean	168.22763		
Std Dev	67.43245		

VPseismic<4.43

		LogWorth	Difference
Count	23	1.4800898	45.8846
Mean	91.565217		
Std Dev	42.863235		

VPseismic>=4.43

		LogWorth	Difference
Count	53	0.2818175	24.0412
Mean	201.49623		
Std Dev	45.315399		

VPseismic<3.49

Count	13
Mean	71.615385
Std Dev	38.467602

VPseismic>=3.49

Count	10
Mean	117.5
Std Dev	34.580823

VPseismic<4.88

Count	38
Mean	194.69211
Std Dev	45.379567

VPseismic>=4.88

Count	15
Mean	218.73333
Std Dev	41.722667

Crossvalidation

k-fold		SSE	RSquare
5	Folded	142575.453	0.5819
	Overall	129084.798	0.6215

Figure 7. CART analysis to predict temperature with Vp using all well data. The only considered parameter is Vp. The Regression Tree is shown on the left after three splits. The split history is shown above and the R-square value for this is 0.62.

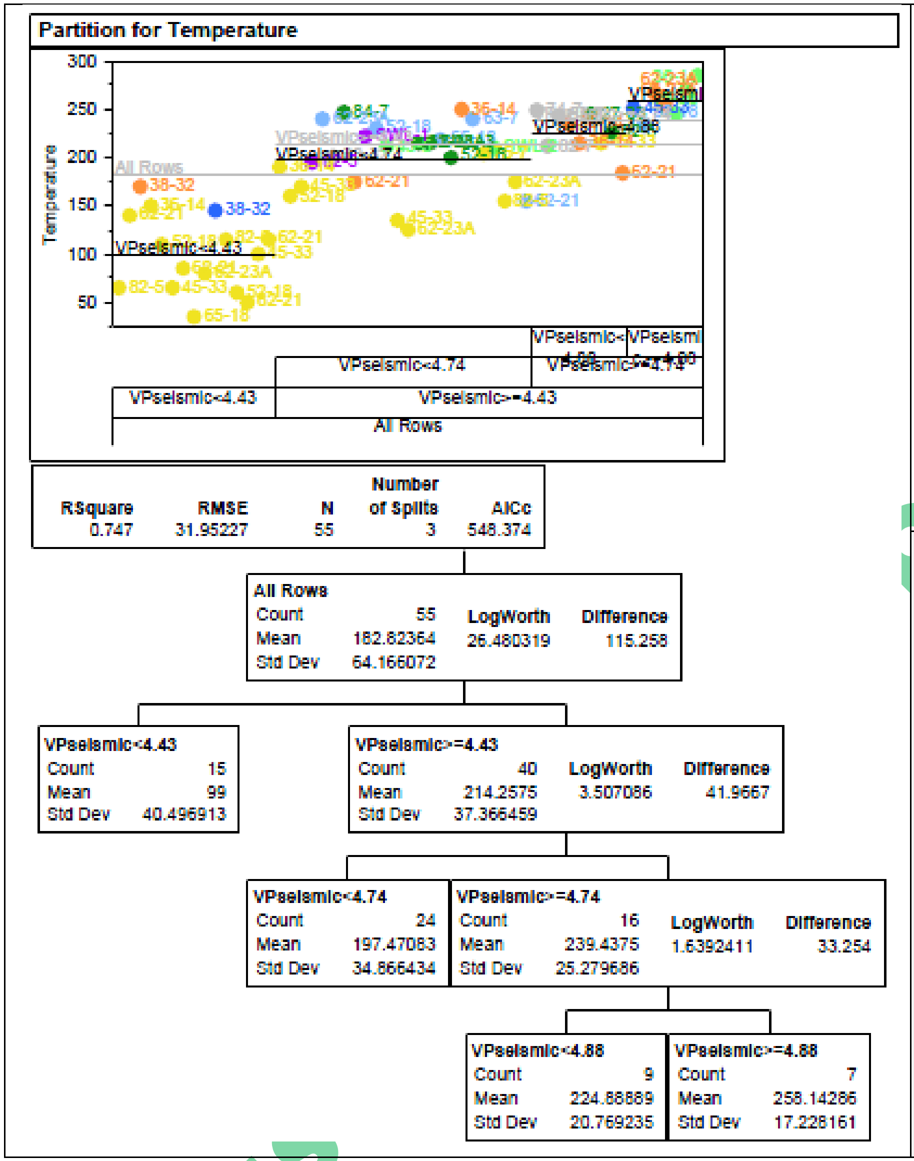

RSquare	RMSE	N	Number of Splits	AICc
0.747	31.95227	55	3	548.374

All Rows

		LogWorth	Difference
Count	55		
Mean	182.62364	26.480319	115.258
Std Dev	64.166072		

VPseismic<4.43

Count	15
Mean	99
Std Dev	40.496913

VPseismic>=4.43

		LogWorth	Difference
Count	40		
Mean	214.2575	3.507086	41.9667
Std Dev	37.366459		

VPseismic<4.74

Count	24
Mean	197.47083
Std Dev	34.866434

VPseismic>=4.74

		LogWorth	Difference
Count	16		
Mean	239.4375	1.6392411	33.254
Std Dev	25.279686		

VPseismic<4.88

Count	9
Mean	224.88889
Std Dev	20.769235

VPseismic>=4.88

Count	7
Mean	258.14286
Std Dev	17.228161

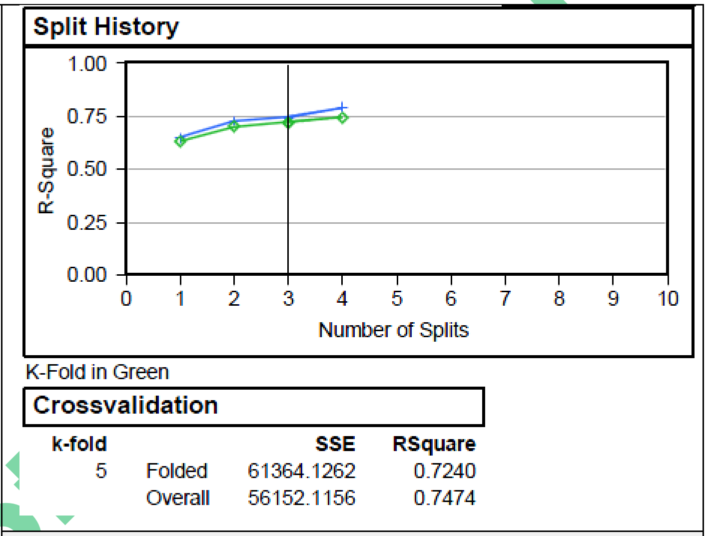

Crossvalidation

k-fold		SSE	RSquare
5	Folded	61364.1262	0.7240
	Overall	56152.1156	0.7474

Figure 8. CART analysis to predict temperature with Vp using all well data excluding selected wells (66-21, 76-28 and 45-14) with a low seismic trust. The Regression Tree is shown on the left after three splits. The split history is shown above and the R-square value is 0.75 .

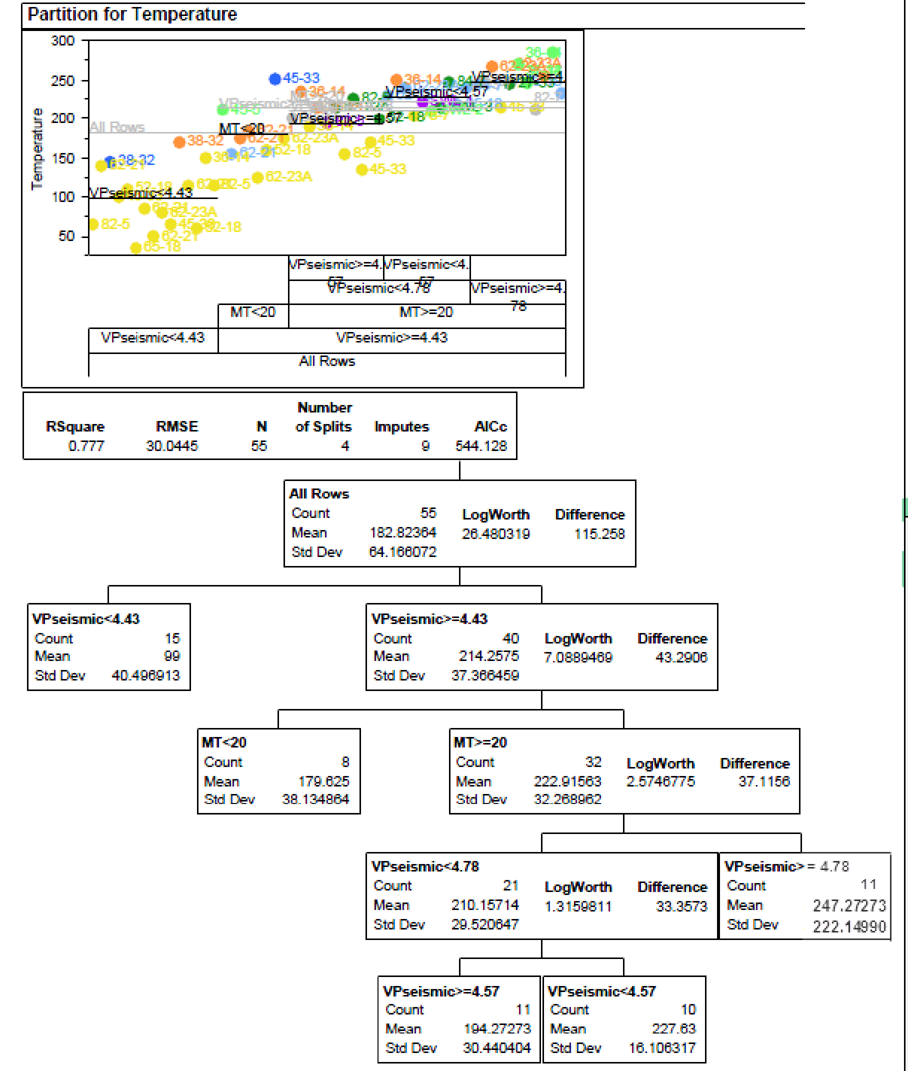

```
RSquare    RMSE     N   Number      Imputes   AICc
                        of Splits
  0.777   30.0445   55      4          9     544.128
```

```
All Rows
Count        55    LogWorth    Difference
Mean  182.82364    26.480319      115.258
Std Dev 64.166072

VPseismic<4.43              VPseismic>=4.43
Count        15             Count        40    LogWorth    Difference
Mean         99             Mean   214.2575    7.0889469      43.2906
Std Dev 40.496913           Std Dev 37.366459

MT<20                       MT>=20
Count         8             Count        32    LogWorth    Difference
Mean    179.625             Mean  222.91563    2.5746775      37.1156
Std Dev 38.134864           Std Dev 32.268962

VPseismic<4.78                                   VPseismic>= 4.78
Count        21    LogWorth    Difference        Count        11
Mean  210.15714    1.3159811      33.3573        Mean  247.27273
Std Dev 29.520647                                Std Dev 222.14990

VPseismic>=4.57             VPseismic<4.57
Count        11             Count        10
Mean  194.27273             Mean     227.63
Std Dev 30.440404           Std Dev 16.106317
```

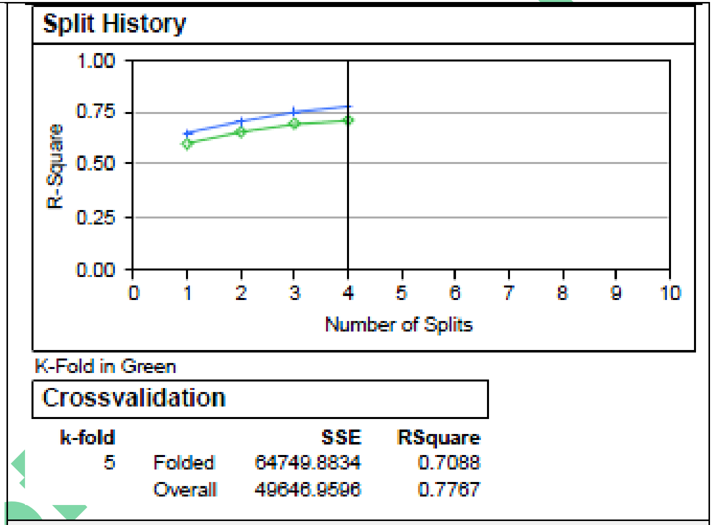

```
Crossvalidation
k-fold              SSE      RSquare
    5   Folded   64749.8834   0.7088
        Overall  49646.9596   0.7767
```

Figure 9. CART analysis to predict temperature using Vp, and Resistivity (MT), and all well data excluding selected wells (66-21, 76-28 and 45-14) with a low seismic trust. The Regression Tree is shown on the left after four splits. The split history is shown above and the R-square value is 0.77.

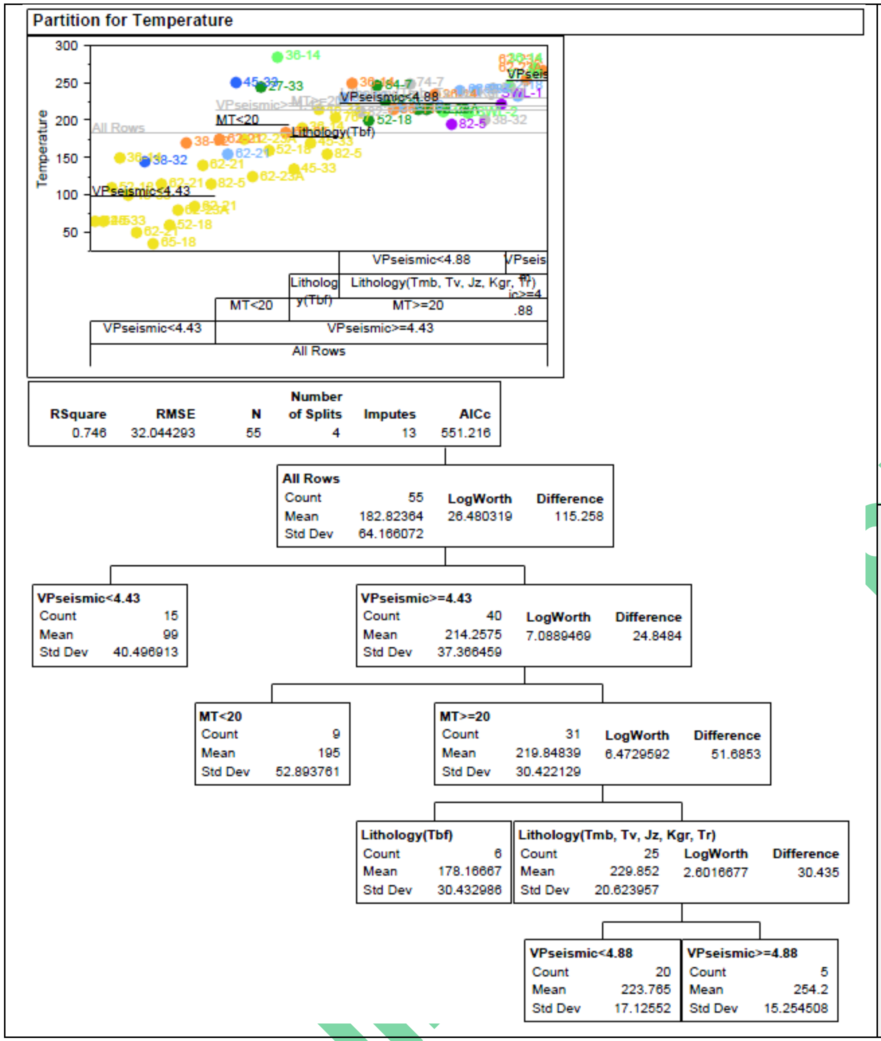

RSquare	RMSE	N	Number of Splits	Imputes	AICc
0.746	32.044293	55	4	13	551.216

All Rows

		LogWorth	Difference
Count	55		
Mean	182.82364	26.480319	115.258
Std Dev	64.166072		

VPseismic<4.43

Count	15
Mean	99
Std Dev	40.496913

VPseismic>=4.43

		LogWorth	Difference
Count	40		
Mean	214.2575	7.0889469	24.8484
Std Dev	37.366459		

MT<20

Count	9
Mean	195
Std Dev	52.893761

MT>=20

		LogWorth	Difference
Count	31		
Mean	219.84839	6.4729592	51.6853
Std Dev	30.422129		

Lithology(Tbf)

Count	6
Mean	178.16667
Std Dev	30.432986

Lithology(Tmb, Tv, Jz, Kgr, Tr)

		LogWorth	Difference
Count	25		
Mean	229.852	2.6016677	30.435
Std Dev	20.623957		

VPseismic<4.88

Count	20
Mean	223.765
Std Dev	17.12552

VPseismic>=4.88

Count	5
Mean	254.2
Std Dev	15.254508

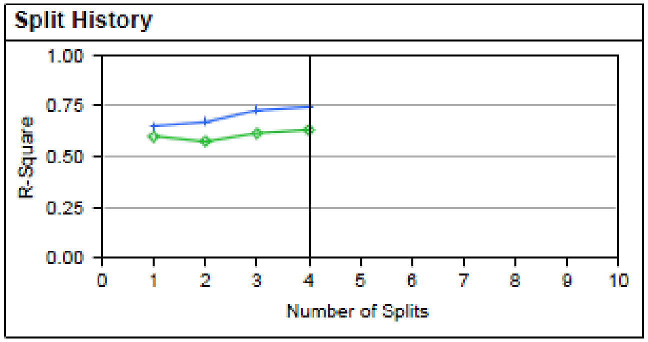

K-Fold in Green

Crossvalidation

k-fold		SSE	RSquare
5	Folded	81532.2118	0.6333
	Overall	56476.0188	0.7460

Figure 10. CART analysis to predict temperature with Vp, Resistivity (MT), Lithology and all well data excluding selected wells (66-21, 76-28 and 45-14) with a low seismic trust. The Regression Tree is shown on the left after four splits. The split history is shown above and the R-square value is 0.75.

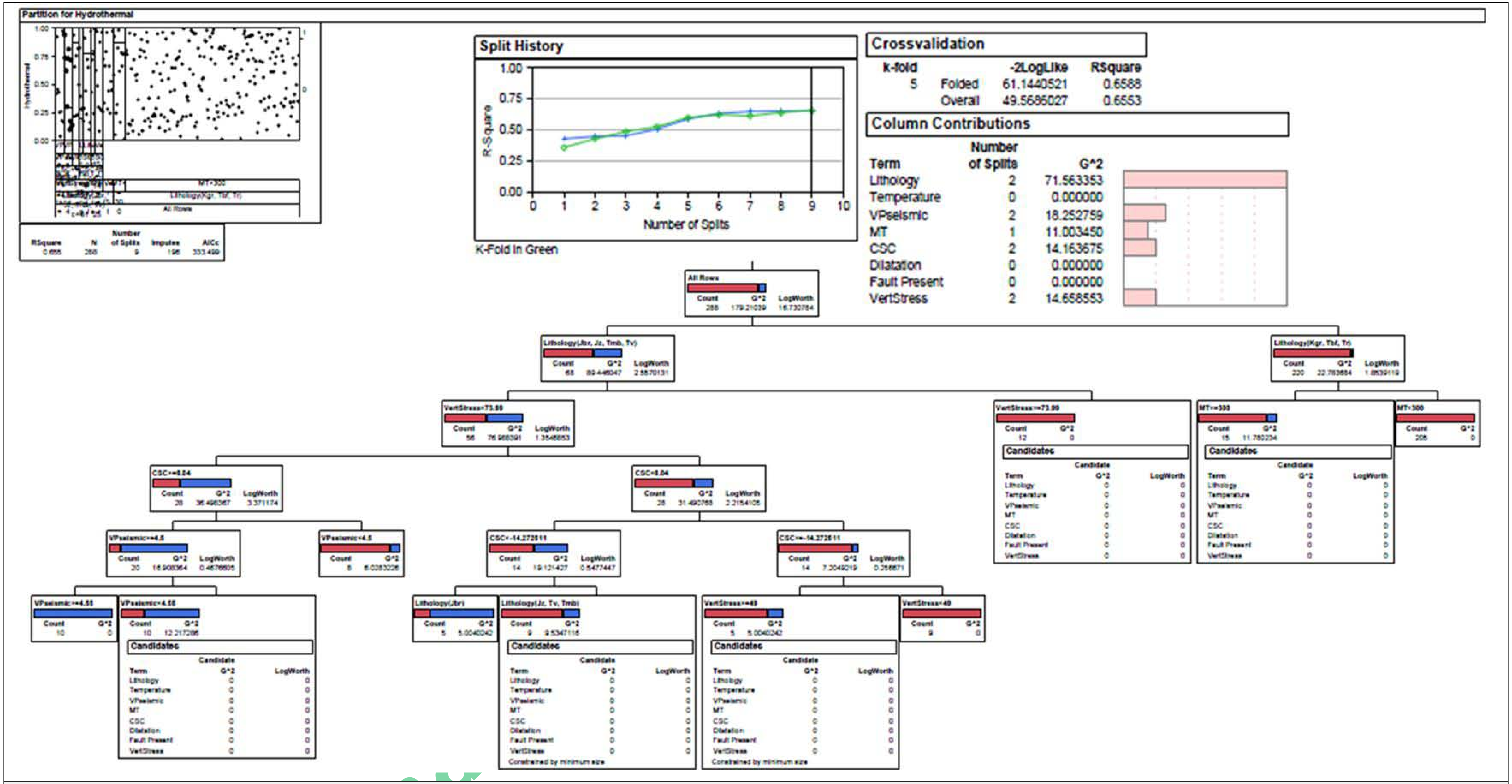

RSquare	N	Number of Splits	Imputes	AICc
0.655	268	9	198	333.499

Crossvalidation

k-fold		-2LogLike	RSquare
5	Folded	61.1440521	0.6588
	Overall	49.5686027	0.6553

Column Contributions

Term	Number of Splits	G^2
Lithology	2	71.563353
Temperature	0	0.000000
VPseismic	2	18.252759
MT	1	11.003450
CSC	2	14.163675
Dilatation	0	0.000000
Fault Present	0	0.000000
VertStress	2	14.658553

Figure 11. CART Analysis for the prediction of productivity (hydrothermal) using all the available well data and the following parameters: Lithology, Temperature, Vp, VertStress, Resistivity (MT), CSC, Dilatation, and Presence of a Fault. Note in the column contributions that the parameters "Temperature" and "Fault Present" were not used. The R=square value is 0.66.

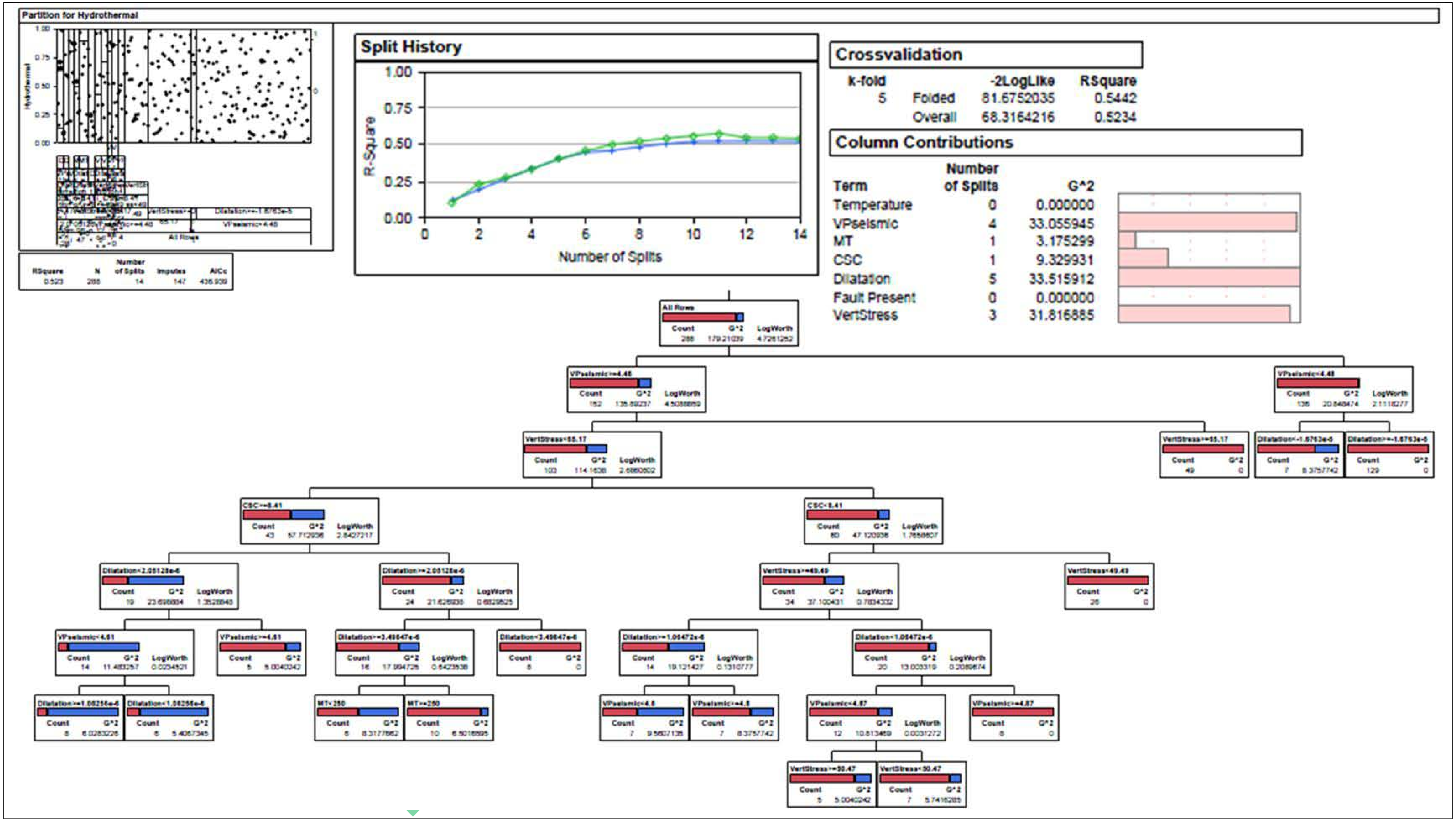

RSquare	N	Number of Splits	Imputes	AICc
0.523	288	14	147	436.939

Crossvalidation

k-fold		-2LogLike	RSquare
5	Folded	81.6752035	0.5442
	Overall	68.3164216	0.5234

Column Contributions

Term	Number of Splits	G^2
Temperature	0	0.000000
VPseismic	4	33.055945
MT	1	3.175299
CSC	1	9.329931
Dilatation	5	33.515912
Fault Present	0	0.000000
VertStress	3	31.816885

Figure 12. CART Analysis for the prediction of productivity (hydrothermal) using all the available well data and the following parameters: Temperature, Vp, VertStress, Resistivity (MT), CSC, Dilatation, and Presence of a Fault. The parameters are the same as the previous figure except lithology has been removed. Note in the column contributions that the parameter "Temperature" was not used. The R-square value is 0.52.

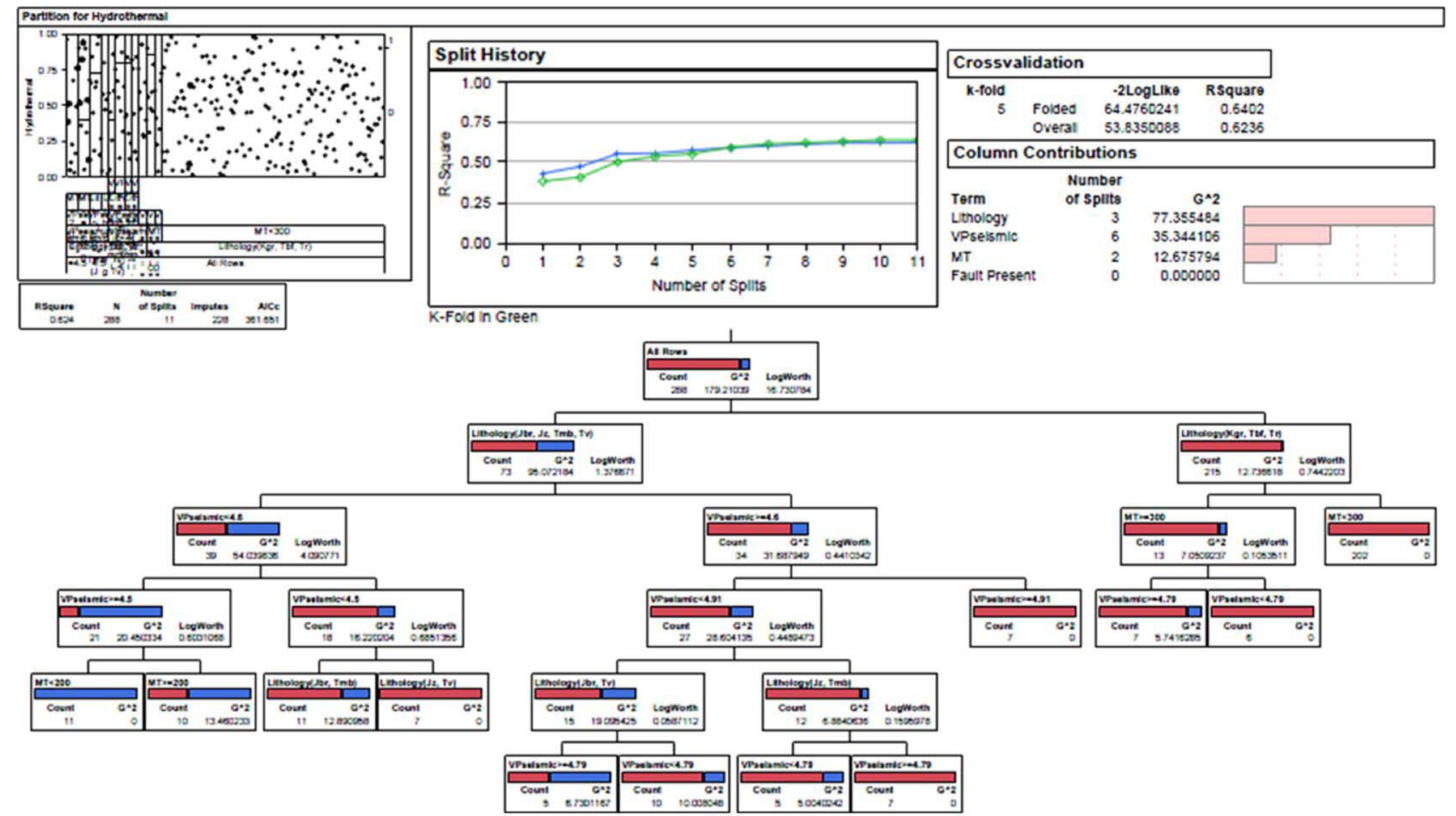

RSquare	N	Number of Splits	Imputes	AICc
0.624	288	11	228	361.651

Crossvalidation

k-fold		-2LogLike	RSquare
5	Folded	64.4760241	0.6402
	Overall	53.8350088	0.6236

Column Contributions

Term	Number of Splits	G^2
Lithology	3	77.355484
VPseismic	6	35.344106
MT	2	12.675794
Fault Present	0	0.000000

Figure 13. CART Analysis for the prediction of productivity (hydrothermal) using all the available well data and the following parameters: Lithology, Vp, Resistivity (MT) and Presence of a Fault. Note in the column contributions that the parameter "Fault Present" was not used. The R-square value is 0.62 which infers that productivity can be predicted based on lithology, Vp and Resistivity (MT).

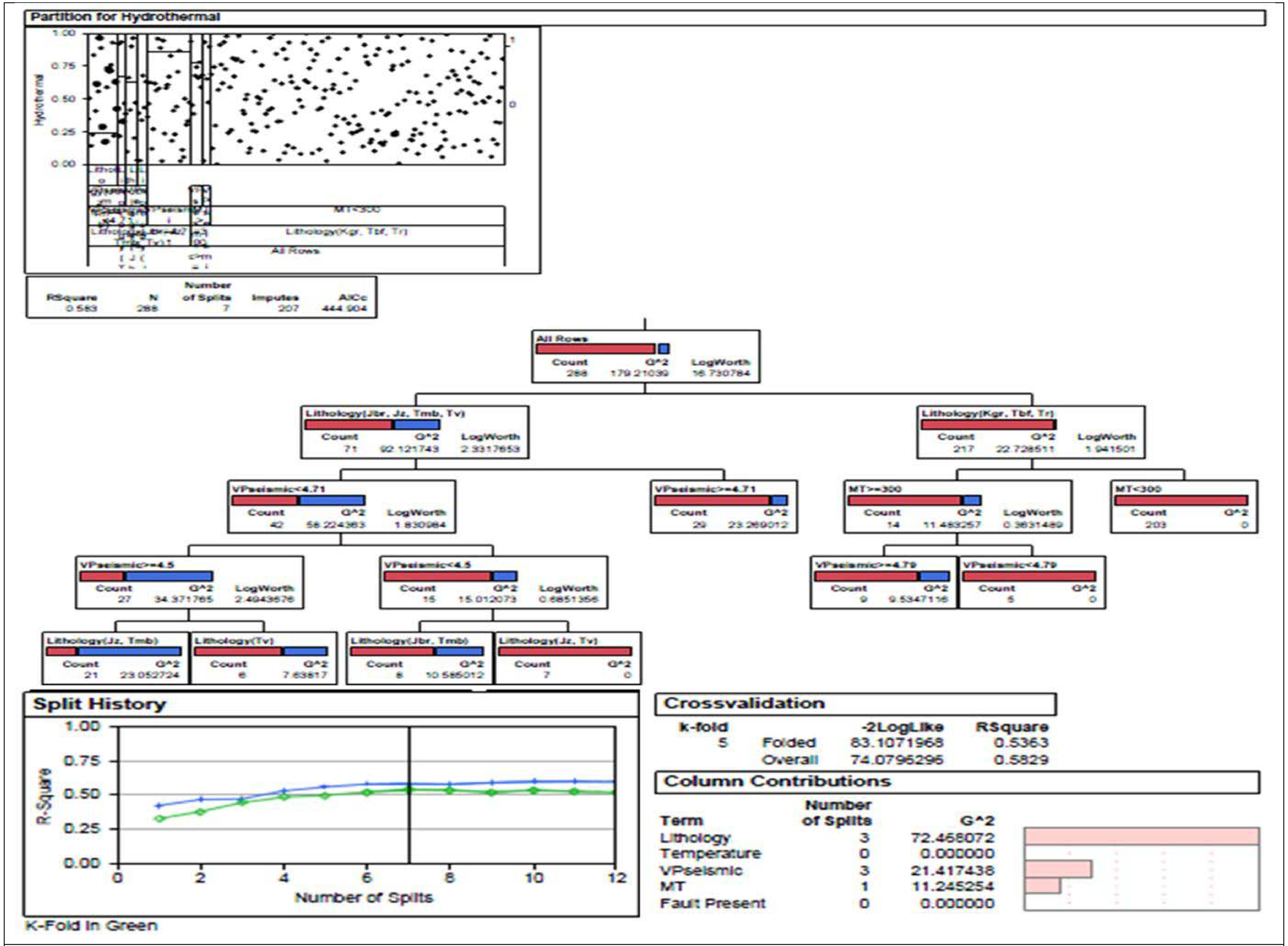

RSquare	N	Number of Splits	Imputes	AICc
0.583	288	7	207	444.904

Crossvalidation

k-fold		-2LogLike	RSquare
5	Folded	83.1071968	0.5363
	Overall	74.0796295	0.5829

Column Contributions

Term	Number of Splits	G^2
Lithology	3	72.468072
Temperature	0	0.000000
VPseismic	3	21.417438
MT	1	11.245254
Fault Present	0	0.000000

Figure 14. CART Analysis for the prediction of productivity (hydrothermal) using all the available well data and the following parameters: Lithology, Temperature, Vp, Resistivity (MT) and Presence of a Fault. Note in the column contributions that Temperature and Fault Present were not used. The R-square value is 0.54.

APPENDIX 20a

CLASSIFICATION AND REGRESSION TREE (CART) SENSITIVITY ANALYSIS
PREDICTING TEMPERATURE USING SECTION AND WELL DATA

Table of Contents

List of Tables

1. INTRODUCTION

This analysis was performed to understand the predictive powers and relationships between seven key geoscience parameters using Classification and Regression Tree Analysis (CART, see Section 7 of the main report). This statistical method used JMP Pro 9.0, part of the SAS Predictive Analytics Suite.

The following series of tables document the CART sensitivity analysis exploring all possibilities of the indicated parameters (Table 20a.1) for predicting temperature using section and well data. Each parameter (response variable) is systematically removed from the analysis starting with one variable removed and ending with six out of the seven variables removed, Tables 20a.2 to 20a.7 for the section data and theTables 20a.8 to 20a.13 for the well data. Parameters considered in the analysis are labeled in light purple, while if. parameter was used, the cell also has a X. The parameter that the analysis first splits on contains a red X. Parameters that have been removed from the analysis are blank (highlighted white).

The R^2 value corresponds to the accuracy of CART to predict temperature along the key cross-sections (Section Data) according to the divisions of the data used. The range of R^2 values results are from 0.175 to 0.918 in the following tables, with all values over 0.75 bolded. A color scheme (green-yellow-orange-red) distinguishes the relative range of R^2 values per individual analysis, with red representing high values, and green representing low values. The # of splits was recorded as each analysis was terminated due to the split history curve "leveling out" and the R^2 value not increasing substantially as the analysis continued to split on the remaining data. The analysis was also terminated if the cross-validation curve (a seperate automatic analysis performed with a sub-set of the remaining data) was not in agreement with the expressed R^2 value.

Table 20a.1. Geoscience parameters considered in the CART sensitivity analysis

Parameter	Description
Lith	Lithology, specifically referring to a lithologic unit
Vp	Seismic parameter: P-wave velocity
Resistivity	Magneto-telluric data
CSC	Coulomb Stress Change derived from modeled stress data
Dilatation	Dilatation derived from modeled stress data
VertStress	Vertical Stress: calculated parameter
Grav_Mag	Combined Gravity and Magnetic inferred Lithologic Unit
Temp	Temperature derived from thermal models

Table 20a.2. CART Sensitivity Analysis for Prediction of Temperature Using Section Data and Removing One Variable for Each Case Analyzed. The Base Case Is where No Variable Is Removed.

▨ Variable Considered

□ Variable Removed

Predictor	**Response Variables** (X Used, **X** First Split)							R^2 Value	Splits
Temp.	Vp	Resistivity	CSC	Dilatation	VertStress	Grav_Mag	Lithology		
Case 1: All Variables Considered with each parameter systematically removed									
---		X		X	X	X	X	**0.871**	6
---	X	X	X	X	X	X		**0.918**	7
---		X			X		X	**0.855**	5
---	X	X				X		0.677	5
---		X	X		X	X	X	0.729	6
---		X			X	X	X	**0.855**	6
---					X	X	X	**0.855**	6
---		X			X	X	X	**0.853**	6

Table 20a.3. CART Sensitivity Analysis for Prediction of Temperature Using Section Data and Removing Two Variables for Each Case Analyzed.

▨ Variable Considered
☐ Variable Removed
▧ Base Case

Predictor	Response Variables (X Used, **X** First Split)							R^2 Value	Splits
Temp.	Vp	Resistivity	CSC	Dilatation	VertStress	Grav_Mag	Lithology		
Case 1. All Variables excluding Lithology + one variable									
---	X	X	X	X	**X**	X		**0.918**	7
---		X		X	**X**			**0.891**	5
---	**X**	X				X		**0.806**	6
---		X			**X**	X		**0.849**	5
---		X			**X**	X		**0.853**	5
---				X	**X**	X		**0.877**	7
---		X		X	**X**	X		**0.870**	6
Case 2. All Variables excluding Gravity and Magnetic inferred Lithology (Grav_Mag) + one variable									
---		X			**X**		X	**0.855**	5
---		X		X	**X**			**0.891**	5
---	**X**	X		X				**0.794**	7
---		X	X		**X**		X	0.727	5
---		X		X	**X**		X	**0.875**	6
---				X	**X**		X	**0.876**	6
---		X		X	**X**		X	**0.876**	6
Case 3. All Variables excluding Vertical Stress (VertStress) + one variable									
---	**X**	X				X		0.677	5
---	**X**	X				X		**0.806**	6
---	**X**	X		X				**0.794**	7
---	**X**	X				X		**0.774**	6
---	**X**	X				X	X	0.747	8
---	**X**					X	X	0.388	7
---		**X**	X	X			X	**0.810**	8
Case 4. All Variables excluding Dilatation + one variable									
---		X	X		**X**	X	X	0.729	6
---		X			**X**	X		**0.849**	5
---		X	X		**X**		X	0.727	5
---	**X**	X				X		**0.774**	6
---		X			**X**	X	X	**0.850**	6
---					**X**	X	X	**0.854**	6
---		X	X		**X**		X	0.729	5
Case 5. All Variables excluding Coulomb Stress Change (CSC) + one variable									
---		X			**X**	X	X	**0.855**	6
---		X			**X**	X		**0.853**	5
---		X		X	**X**		X	**0.875**	6
---	**X**	X				X	X	0.747	8
---		X			**X**	X	X	**0.850**	6
---				X	**X**	X	X	**0.870**	7

Table 20a.3. CART Sensitivity Analysis for Prediction of Temperature Using Section Data and Removing Two Variables for Each Case Analyzed.

Variable Considered
Variable Removed
Base Case

Predictor	**Response Variables** (X Used, **X** First Split)							R^2 Value	Splits
Temp.	Vp	Resistivity	CSC	Dilatation	VertStress	Grav_Mag	Lithology		
---		X			X	X	X	**0.852**	6
Case 6. All Variables excluding Resistivity + one variable									
---					X	X	X	**0.855**	6
---				X	X	X		**0.877**	7
---				X	X		X	**0.876**	6
---	X					X	X	0.388	7
---					X	X	X	**0.854**	6
---				X	X	X	X	**0.870**	7
---				X	X	X	X	**0.871**	7
Case 7. All Variables excluding P-wave velocity (Vp) + one variable									
---		X			X	X	X	**0.853**	6
---		X		X	X	X		**0.870**	6
---		X		X	X		X	**0.876**	6
---		X	X	X			X	**0.810**	8
---		X	X		X		X	0.729	5
---		X			X	X	X	**0.852**	6
---				X	X	X	X	**0.871**	7

Table 20a.4. CART Sensitivity Analysis for Prediction of Temperature Using Section Data and Removing Three Variables for Each Case Analyzed.

▨ Variable Considered

☐ Variable Removed

Predictor	**Response Variables** (X Used, **X** First Split)							R^2 Value	Splits
Temp.	Vp	Resistivity	CSC	Dilatation	VertStress	Grav_Mag	Lithology		
Case 1. Removal of Lithology plus two variables									
---	X	X	▨	▨				0.748	5
---	X	X	▨		X			**0.887**	5
---	▨	X		X	X			**0.894**	5
---	X		▨	X	X			**0.907**	5
---		X	▨	▨	X			**0.872**	3
---	X	X	▨			X		0.717	5
---	X	X		▨		X		**0.769**	6
---	X		▨	X		X		0.519	6
---		X	▨	X		X		0.646	5
---	▨	X			X	X		**0.850**	5
---	▨		▨		X	X		**0.854**	5
---		X	▨		X	X		**0.855**	5
---	▨			X	X	X		**0.878**	7
---		X		▨	X	X		**0.853**	5
---			▨	▨	X	X		**0.856**	5
Case 2. Removal of Gravity and Magnetic inferred Lithology (Grav_Mag) plus two variables									
---	X	X	▨	▨				0.748	5
---	X	X	▨		X			**0.887**	5
---	▨	X		X	X			**0.894**	5
---	X		▨	X	X			**0.907**	5
---		X	▨	▨	X			**0.872**	3
---	X	X	▨				X	**0.760**	6
---	X	X		X			▨	**0.792**	6
---	X		▨	▨			X	0.341	6
---		X	▨	X			X	0.710	6
---	▨	X			X		X	**0.857**	5
---	▨		▨		X		X	**0.860**	5
---		X	▨		X		X	**0.859**	5
---	▨			X	X		X	**0.874**	6
---		X		▨	X		X	**0.858**	5
---			▨	X	X		X	**0.878**	6

Table 20a.4. CART Sensitivity Analysis for Prediction of Temperature Using Section Data and Removing Three Variables for Each Case Analyzed.

▨ Variable Considered

☐ Variable Removed

Predictor	**Response Variables** (X Used, **X** First Split)							R^2 Value	Splits
Temp.	Vp	Resistivity	CSC	Dilatation	VertStress	Grav_Mag	Lithology		
Case 3. Removal of Vertical Stress (VertStress) plus two variables									
---	X	X						0.748	5
---	X	X				X		0.717	5
---	X	X				X		**0.769**	6
---	X			X		X		0.519	6
---		X		X		X		0.646	5
---	X	X					X	**0.760**	6
---	X	X		X				**0.792**	6
---	X						X	0.341	6
---		X		X			X	0.710	6
---	X	X				X		0.726	5
---	X					X	X	0.316	5
---		X	X				X	0.686	6
---	X					X	X	0.296	5
---		X		X			X	**0.770**	8
---				X		X	X	0.599	7
Case 4. Removal of Dilatation plus two variables									
---	X	X			X			**0.887**	5
---	X	X				X		0.717	5
---		X			X	X		**0.850**	5
---					X	X		**0.854**	5
---		X			X	X		**0.855**	5
---	X	X					X	**0.760**	6
---		X			X		X	**0.857**	5
---					X		X	**0.860**	5
---		X			X		X	**0.859**	5
---	X	X				X		0.726	5
---	X					X	X	0.316	5
---		X	X				X	0.686	6
---					X	X	X	**0.856**	6
---		X			X	X	X	**0.847**	6
---					X	X	X	**0.851**	6
Case 5. Removal of Coulomb Stress Change (CSC) plus two variables									
---		X		X	X			**0.894**	5
---	X	X				X		**0.769**	6
---		X			X	X		**0.850**	5
---				X	X	X		**0.878**	7

Table 20a.4. CART Sensitivity Analysis for Prediction of Temperature Using Section Data and Removing Three Variables for Each Case Analyzed. The Base Case R2 Value Is 0.871 (Table 20a.2).

▨	Variable Considered
☐	Variable Removed

Predictor	**Response Variables** (X Used, **X** First Split)							R^2 Value	Splits
Temp.	Vp	Resistivity	CSC	Dilatation	VertStress	Grav_Mag	LIthology		
---		X			X	X		**0.853**	5
---	X	X		X				**0.792**	6
---		X			X		X	**0.857**	5
---				X	X		X	**0.874**	6
---		X			X		X	**0.858**	5
---	X	X				X		0.726	5
---	X					X	X	0.296	5
---		X		X			X	**0.770**	8
---					X	X	X	**0.856**	6
---		X			X	X	X	**0.847**	6
---					X	X	X	**0.853**	6
Case 6. Removal of Resisitivity plus two variables									
---	X			X	X			**0.907**	5
---	X			X		X		0.519	6
---					X	X		**0.854**	5
---				X	X	X		**0.878**	7
---					X	X		**0.856**	5
---	X						X	0.341	6
---					X		X	**0.860**	5
---				X	X		X	**0.874**	6
---				X	X		X	**0.878**	6
---	X					X	X	0.316	5
---	X					X	X	0.296	5
---				X		X	X	0.599	7
---					X	X	X	**0.856**	6
---					X	X	X	**0.851**	6
---					X	X	X	**0.853**	6
Case 7. Removal of P-wave velocity (Vp) plus two variables									
---		X			X			**0.872**	3
---		X		X		X		0.646	5
---		X			X	X		**0.855**	5
---		X			X	X		**0.853**	5
---					X	X		**0.856**	5
---		X		X			X	0.710	6
---		X			X		X	**0.859**	5
---		X			X		X	**0.858**	5
---				X	X		X	**0.878**	6
---		X	X				X	0.686	6
---		X		X			X	**0.770**	8
---				X		X	X	0.599	7
---		X			X	X	X	**0.847**	6
---					X	X	X	**0.851**	6
---					X	X	X	**0.853**	6

Table 20a.5. CART Sensitivity Analysis for Prediction of Temperature Using Section Data and Removing Four Variables for Each Case Analyzed.

▨ Variable Considered

☐ Variable Removed

Predictor	Response Variables (X Used, **X** First Split)							R² Value	Splits
Temp.	Vp	Resistivity	CSC	Dilatation	VertStress	Grav_Mag	Lithology		
Case 1. Removal of Lithology plus three other variables									
---	**X**	X	▨					**0.794**	5
---	**X**	X		X				**0.848**	7
---	**X**		X	X				0.651	8
---		**X**	X	X				0.748	6
---	▨	X			**X**			**0.876**	4
---	X		▨		**X**			**0.898**	5
---		X	▨		**X**			**0.871**	3
---	▨			X	**X**			**0.892**	4
---		X		X	**X**			**0.893**	5
---			▨	X	**X**			**0.892**	4
---	**X**	X				X		**0.765**	6
---	**X**		▨			X		0.399	5
---		**X**	X			X		0.655	6
---	**X**			X		X		0.530	6
---		**X**		X		X		0.665	5
---			▨	**X**		X		0.704	5
---	X				**X**	X		**0.863**	6
---		X			**X**	X		0.735	4
---			▨		**X**	X		**0.853**	5
---				▨	**X**	X		**0.852**	5
Case 2. Removal of Grav_Mag plus three other variables									
---	**X**	X	▨					**0.794**	5
---	**X**	X		X				**0.848**	7
---	**X**		X	X				0.651	8
---		**X**	X	X				0.748	6
---	▨	X			**X**			**0.876**	4
---	X		▨		**X**			**0.898**	5
---		X	▨		**X**			**0.871**	3
---	▨			X	**X**			**0.892**	4
---		X		X	**X**			**0.893**	5
---			▨	X	**X**			**0.892**	4
---	**X**	X					▨	0.735	3
---	**X**		▨				X	0.286	3
---		X	X				**X**	**0.828**	5
---	**X**			X			X	**0.885**	6
---		**X**		X			X	**0.757**	8
---			X	**X**			X	0.634	8
---	X				**X**		X	**0.881**	7
---		X			**X**		X	**0.857**	5
---			▨		**X**		X	**0.858**	5

Table 20a.5. CART Sensitivity Analysis for Prediction of Temperature Using Section Data and Removing Four Variables for Each Case Analyzed.

▨ Variable Considered

☐ Variable Removed

Predictor	Response Variables (X Used, **X** First Split)							R² Value	Splits
Temp.	Vp	Resistivity	CSC	Dilatation	VertStress	Grav_Mag	Lithology		
---					**X**		X	**0.862**	5
Case 3. Removal of Vertical Stress plus three other variables									
---	**X**	X						**0.794**	5
---	**X**	X		X				**0.848**	7
---	**X**		X	X				0.651	8
---		**X**	X	X				0.748	6
---	**X**	X				X		**0.765**	6
---	**X**					X		0.399	5
---		**X**	X			X		0.655	6
---	**X**			X		X		0.530	6
---		**X**		X		X		0.665	5
---				**X**		X		0.704	5
	X	X						0.735	3
---	**X**						X	0.286	3
---		X	X				**X**	**0.828**	5
---	**X**			X			X	**0.885**	6
---		**X**		X			X	**0.757**	8
---			X	**X**			X	0.634	8
---	**X**					X	X	0.290	4
---		**X**					X	0.670	7
---			X			**X**	X	0.629	9
---				**X**		X	X	0.603	7
Case 4. Removal of Dilatation plus three other variables									
---	**X**	X						**0.794**	5
---		X			**X**			**0.876**	4
---	X				**X**			**0.898**	5
---		X			**X**			**0.871**	3
---	**X**	X				X		**0.765**	6
---	**X**					X		0.399	5
---		**X**	X			X		0.655	6
---	X				**X**	X		**0.863**	6
---		X			**X**	X		0.735	4
---					**X**	X		**0.853**	5
	X	X						0.735	3
---	**X**						X	0.286	3
---		X	X				**X**	**0.828**	5
---	X				**X**		X	**0.881**	7
---		X			**X**		X	**0.857**	5
---					**X**		X	**0.858**	5
---	**X**					X	X	0.290	4

Table 20a.5. CART Sensitivity Analysis for Prediction of Temperature Using Section Data and Removing Four Variables for Each Case Analyzed.

▨ Variable Considered

☐ Variable Removed

Predictor	Response Variables (X Used, **X** First Split)							R^2 Value	Splits
Temp.	Vp	Resistivity	CSC	Dilatation	VertStress	Grav_Mag	Lithology		
---		**X**					X	0.670	7
---			X			**X**	X	0.629	9
---					**X**	X	X	**0.860**	7
Case 5. Removal of CSC and three other variables									
---	**X**	X		X				**0.848**	7
---		X			**X**			**0.876**	4
---				X	**X**			**0.892**	4
---		X		X	**X**			**0.893**	5
---	**X**	X				X		**0.765**	6
---	**X**			X		X		0.530	6
---		**X**		X		X		0.665	5
---	X				**X**	X		**0.863**	6
---		X			**X**	X		0.735	4
---					**X**	X		**0.852**	5
---	**X**	X						**0.735**	3
---	**X**			X			X	**0.885**	6
---		**X**		X			X	**0.757**	8
---	X				**X**		X	**0.881**	7
---		X			**X**		X	**0.857**	5
---					**X**		X	**0.862**	5
---	**X**					X	X	0.290	4
---		**X**					X	0.670	7
---				**X**		X	X	0.603	7
---					**X**	X	X	**0.860**	7
Case 6. Removal of Resistivity plus three other variables									
---	**X**		X	X				0.651	8
---	X				**X**			**0.898**	5
---				X	**X**			**0.892**	4
---				X	**X**			**0.892**	4
---	**X**					X		0.399	5
---	**X**			X		X		0.530	6
---				**X**		X		0.704	5
---	X				**X**	X		**0.863**	6
---					**X**	X		**0.853**	5
---					**X**	X		**0.852**	5
---	**X**						X	0.286	3
---	**X**			X			X	**0.885**	6
---			X	**X**			X	0.634	8
---	X				**X**		X	**0.881**	7
---					**X**		X	**0.858**	5

Table 20a.5. CART Sensitivity Analysis for Prediction of Temperature Using Section Data and Removing Four Variables for Each Case Analyzed.

▨ Variable Considered

□ Variable Removed

Predictor	Response Variables (X Used, **X** First Split)							R^2 Value	Splits
Temp.	Vp	Resistivity	CSC	Dilatation	VertStress	Grav_Mag	Lithology		
---					X		X	**0.862**	5
---	X					X	X	0.290	4
---			X			X	X	0.629	9
---				X		X	X	0.603	7
---					X	X	X	**0.860**	7
Case 7. Removal of Vp plus three other variables									
---		X	X	X				0.748	6
---		X			X			**0.871**	3
---		X		X	X			**0.893**	5
---				X	X			**0.892**	4
---		X	X			X		0.655	6
---		X		X		X		0.665	5
---				X		X		0.704	5
---		X			X	X		0.735	4
---					X	X		**0.853**	5
---					X	X		**0.852**	5
---		X	X				X	**0.828**	5
---		X		X			X	**0.757**	8
---			X	X			X	0.634	8
---		X			X		X	**0.857**	5
---					X		X	**0.858**	5
---					X		X	**0.862**	5
---		X					X	0.670	7
---			X			X	X	0.629	9
---				X		X	X	0.603	7
---					X	X	X	**0.860**	7

Table 20a.6. CART Sensitivity Analysis for Prediction of Temperature Using Section Data and Removing Five Variables for Each Case Analyzed.

▨ Variable Considered

☐ Variable Removed

Predictor	Response Variables (X Used, **X** First Split)							R^2 Value	Splits
Temp.	Vp	Resistivity	CSC	Dilatation	VertStress	Grav_Mag	Lithology		
Case 1. Removal of Lithology plus four other variables									
---	X	X						**0.775**	6
---	X		X					0.577	8
---		X	X					0.642	7
---	X			X				0.639	7
---		X		X				0.682	5
---				X				0.684	4
---	X				X			**0.901**	5
---		X			X			**0.872**	3
---					X			**0.885**	4
---				X	X			**0.892**	4
---	X					X		0.310	4
---		X				X		0.588	6
---			X			X		0.501	4
---				X		X		0.684	4
---					X	X		**0.856**	5
Case 2. Removal of Grav_Mag plus four other variables									
---	X	X						**0.775**	6
---	X		X					0.577	8
---		X	X					0.642	7
---	X			X				0.639	7
---		X		X				0.682	5
---				X				0.684	4
---	X				X			**0.901**	5
---		X			X			**0.872**	3
---					X			**0.885**	4
---				X	X			**0.892**	4
---	X						X	0.386	6
---		X					X	0.571	5
---			X				X	0.540	7
---				X				0.684	4
---					X		X	**0.870**	6
Case 3. Removal of Vertical Stress plus four other variables									
---	X	X						**0.775**	6
---	X		X					0.577	8
---		X	X					0.642	7
---	X			X				0.639	7
---		X		X				0.682	5
---				X				0.684	4
---	X					X		0.310	4
---		X				X		0.588	6
---			X			X		0.501	4
---				X		X		0.684	4
---	X						X	0.386	6
---		X					X	0.571	5
---			X				X	0.540	7
---				X				0.684	4

Table 20a.6. CART Sensitivity Analysis for Prediction of Temperature Using Section Data and Removing Five Variables for Each Case Analyzed.

▨ Variable Considered
☐ Variable Removed

Predictor	**Response Variables** (X Used, **X** First Split)							R^2 Value	Splits
Temp.	Vp	Resistivity	CSC	Dilatation	VertStress	Grav_Mag	Lithology		
---						X	X	0.230	6
Case 4. Removal of Dilatation plus four other variables									
---	X	X						**0.775**	6
---	X		X					0.577	8
---		X	X					0.642	7
---	X				X			**0.901**	5
---		X			X			**0.872**	3
---					X			**0.885**	4
---	X					X		0.310	4
---		X				X		0.588	6
---			X			X		0.501	
---					X	X		**0.856**	5
---	X						X	0.386	6
---		X					X	0.571	5
---			X				X	0.540	7
---					X		X	**0.870**	6
---						X	X	0.230	6
Case 5. Removal of CSC plus four other variables									
---	X	X						**0.775**	6
---	X			X				0.639	7
---		X		X				0.682	5
---	X				X			**0.901**	5
---		X			X			**0.872**	3
---				X	X			**0.892**	4
---	X					X		0.310	4
---		X				X		0.588	6
---				X		X		0.684	4
---					X	X		**0.856**	5
---	X						X	0.386	6
---		X					X	0.571	5
---				X				0.684	4
---					X		X	**0.870**	6
---						X	X	0.230	6
Case 6. Removal of Resistivity plus four other variables									
---	X		X					0.577	8
---	X			X				0.639	7
---				X				0.684	4
---	X				X			0.310	4
---					X			**0.885**	4
---				X	X			**0.892**	4
---	X					X		0.310	4
---			X			X		0.501	4
---				X		X		0.684	4
---					X	X		**0.856**	5

Table 20a.6. CART Sensitivity Analysis for Prediction of Temperature Using Section Data and Removing Five Variables for Each Case Analyzed.

▨ Variable Considered

□ Variable Removed

Predictor	**Response Variables** (X Used, **X** First Split)							R^2 Value	Splits
Temp.	Vp	Resistivity	CSC	Dilatation	VertStress	Grav_Mag	Lithology		
---	X						X	0.386	6
---			X				X	0.540	7
---				X				0.684	4
---					X		X	**0.870**	6
Case 7. Removal of P-wave velocity (Vp) plus four other variables									
---		X	X					0.642	7
---		X		X				0.682	5
---				X				0.684	4
---		X			X			**0.872**	3
---					X			**0.885**	4
---				X	X			**0.892**	4
---		X				X		0.588	6
---			X			X		0.501	4
---				X		X		0.533	4
---					X	X		**0.856**	5
---		X					X	0.588	6
---			X				X	0.540	7
---				X				0.684	4
---					X		X	**0.870**	6
---						X	X	0.230	6

Table20a.7. CART Sensitivity Analysis for Prediction of Temperature Using Section Data and Removing Six Variables for Each Case Analyzed.

▨ Variable Considered

☐ Variable Removed

Predictor	**Response Variables** (X Used, **X** First Split)							R^2 Value	Splits
Temp.	Vp	Resistivity	CSC	Dilatation	VertStress	Grav_Mag	Lithology		
Case 1. Removal of six variables systematically									
---							X	0.244	3
---						X		0.175	2
---					X			**0.874**	3
---				X				0.684	4
---			X					0.479	3
---		X						0.502	4
---	X							0.359	5

Table 20a.8. CART Sensitivity Analysis for Prediction of Temperature Using Well Data and Removing One Variable for Each Case Analyzed. The Base Case, where no variable is removed, Has a R^2 Value of 0.822.

▨ Variable Considered

☐ Variable Removed

Predictor	**Response Variables** (X Used, **X** First Split)							R^2 Value	Splits
Temp.	Vp	Resistivity	CSC	Dilatation	VertStress	Grav_Mag	Lithology		
Case 1: All Variables Considered with each parameter systematically removed									
---		X		X	**X**			**0.822**	6
---		X		X	**X**		☐	**0.830**	6
---		X		X	**X**	☐		**0.808**	6
---	**X**	X	X	X	☐		X	**0.750**	7
---		X		☐	**X**			**0.769**	5
---		X	☐	X	**X**			**0.828**	7
---		☐		X	**X**			**0.824**	6
---	☐	X		X	**X**		X	**0.841**	7

Table20a.9. CART Sensitivity Analysis for Prediction of Temperature Using Well Data and Removing Two Variables for Each Case Analyzed.

▨ Variable Considered

☐ Variable Removed

🟧 Baseline Case

Predictor	**Response Variables** (X Used, X First Split)							R^2 Value	Splits
Temp.	Vp	Resistivity	CSC	Dilatation	VertStress	Grav_Mag	Lithology		
Case 1. All Variables excluding Lithology + one variable									
		X		X	X			**0.830**	6
		X		X	X			**0.831**	6
	X	X	X	X		X		**0.767**	7
		X			X			**0.774**	4
		X		X	X			**0.822**	6
				X	X			**0.816**	6
		X		X	X			**0.831**	6
Case 2. All Variables excluding Gravity and Magnetic inferred Lithology (Grav_Mag) + one variable									
		X		X	X			**0.808**	6
		X		X	X			**0.831**	6
	X	X		X			X	0.748	5
					X			0.749	3
		X		X	X			**0.808**	6
				X	X			**0.803**	5
		X		X	X			**0.802**	5
Case 3. All Variables excluding Vertical Stress (VertStress) + one variable									
	X	X	X	X			X	**0.750**	7
	X	X	X	X		X		**0.767**	7
	X	X		X			X	0.748	5
	X	X	X				X	0.714	5
	X	X		X			X	0.747	5
	X			X			X	0.730	4
		X	X	X			X	0.717	7
Case 4. All Variables excluding Dilatation + one variable									
		X			X			**0.769**	5
		X			X			**0.774**	4
					X			0.749	3
	X	X	X				X	0.714	5
		X			X			**0.775**	4
					X			**0.766**	4
		X			X			**0.774**	4
Case 5. All Variables excluding Coulomb Stress Change (CSC) + one variable									
		X		X	X			**0.828**	7
		X		X	X			**0.822**	6
		X		X	X			**0.808**	6
	X	X		X			X	0.747	5
		X			X			**0.775**	4
				X	X			**0.780**	4
		X			X			**0.824**	6

Table20a.9. CART Sensitivity Analysis for Prediction of Temperature Using Well Data and Removing Two Variables for Each Case Analyzed.

▨	Variable Considered
☐	Variable Removed
🟧	Baseline Case

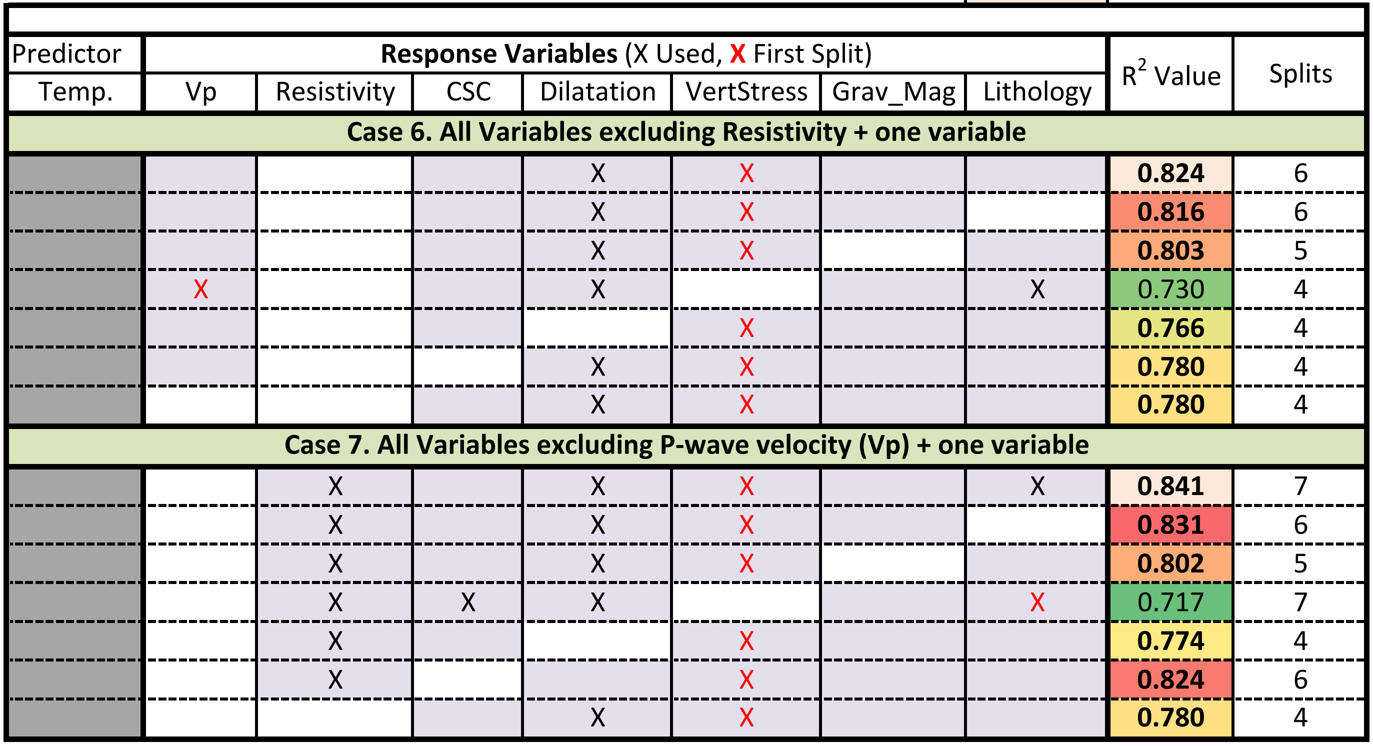

Predictor	**Response Variables** (X Used, **X** First Split)								
Temp.	Vp	Resistivity	CSC	Dilatation	VertStress	Grav_Mag	Lithology	R^2 Value	Splits
Case 6. All Variables excluding Resistivity + one variable									
				X	**X**			**0.824**	6
				X	**X**			**0.816**	6
				X	**X**			**0.803**	5
	X			X			X	0.730	4
					X			**0.766**	4
				X	**X**			**0.780**	4
				X	**X**			**0.780**	4
Case 7. All Variables excluding P-wave velocity (Vp) + one variable									
		X		X	**X**		X	**0.841**	7
		X		X	**X**			**0.831**	6
		X		X	**X**			**0.802**	5
		X	X	X			**X**	0.717	7
		X			**X**			**0.774**	4
		X			**X**			**0.824**	6
				X	**X**			**0.780**	4

Table 20a.10. CART Sensitivity Analysis for Prediction of Temperature Using Well Data and Removing Three Variables for Each Case Analyzed.

▨ Variable Considered

□ Variable Removed

Predictor Temperatu	Response Variables (X Used, **X** First Split)							R^2 Value	Splits
	Vp	Resistivity	CSC	Dilatation	VertStress	Grav_Mag	Lithology		
Case 1. Removal of Lithology plus two variables									
---	X	X		X				0.733	5
---		X			X			**0.756**	4
---		X		X	X			**0.810**	6
---				X	X			**0.780**	4
---		X		X	X			**0.822**	6
---	X	X	X			X		0.682	7
---	X	X		X				0.738	6
---	X		X	X		X		**0.775**	7
---		X	X	X		X		0.661	7
---		X			X			**0.765**	4
---					X			0.749	3
---		X			X			**0.787**	5
---				X	X			**0.822**	6
---		X		X	X			**0.813**	6
				X	X			**0.780**	4
Case 2. Removal of Gravity and Magnetic inferred Lithology (Grav_Mag) plus two variables									
---	X	X		X				0.733	5
---		X			X			**0.756**	4
---		X		X	X			**0.810**	6
---				X	X			**0.780**	4
---		X		X	X			**0.822**	6
---	X	X	X				X	0.705	4
---	X	X		X			X	0.717	5
---	X			X			X	0.730	4
---		X	X	X			X	0.548	4
---		X			X			**0.780**	4
---					X			0.749	3
---		X			X			**0.788**	5
---				X	X			**0.780**	4
---		X			X			**0.778**	4
Case 3. Removal of Vertical Stress (VertStress) plus two variables									
---	X	X		X				0.733	5
---	X	X	X			X		0.682	7
---	X	X		X				0.738	6
---	X		X	X		X		**0.775**	7
---		X	X	X		X		0.661	7
---	X	X	X				X	0.705	4
---	X	X		X			X	0.717	5
---	X			X			X	0.730	4

Table 20a.10. CART Sensitivity Analysis for Prediction of Temperature Using Well Data and Removing Three Variables for Each Case Analyzed. The Base Case, where no variable is removed, Has a R2 Value of 0.822.

▨	Variable Considered
☐	Variable Removed

Predictor	**Response Variables** (X Used, **X** First Split)							R^2 Value	Splits
Temp.	Vp	Resistivity	CSC	Dilat	VertStress	Grav_Mag	Lithology		
---		X	X	X			**X**	0.548	4
---	**X**	X					X	0.724	6
---	**X**		X				X	0.686	4
---			X			X	**X**	0.501	3
---	**X**			X			X	0.730	4
---		X		X		X	**X**	0.641	5
---			X	X		X	**X**	0.651	6
Case 4. Removal of Dilatation plus two variables									
---		X			**X**			**0.756**	4
---	**X**	X	X			X		0.682	7
---		X			**X**			**0.765**	4
---					**X**			0.749	3
---		X			**X**			**0.787**	5
---	**X**	X	X				X	0.705	4
---		X			**X**			**0.780**	4
---					**X**			0.749	3
---		X			**X**			**0.788**	5
---	**X**	X					X	0.724	6
---	**X**		X				X	0.686	4
---			X			X	**X**	0.501	3
---					**X**			0.749	3
---								**0.773**	4
---					**X**			0.749	3
Case 5. Removal of Coulomb Stress Change (CSC) plus two variables									
---		X		X	**X**			**0.810**	6
---	**X**	X		X				0.738	6
---		X			**X**			**0.765**	4
---				X	**X**			**0.822**	6
---		X		X	**X**			**0.813**	6
---	**X**	X		X			X	0.717	5
---		X			**X**			**0.780**	4
---				X	**X**			**0.780**	4
---		X			**X**			**0.778**	4
---	**X**	X					X	0.724	6
---	**X**			X			X	0.730	4
---		X		X		X	**X**	0.641	5
---					**X**			0.749	3
---								**0.773**	4
Case 6. Removal of Resisitivity plus two variables									
---				X	**X**			**0.780**	4
---	**X**		X	X		X		**0.775**	7
---					**X**			0.749	3
---				X	**X**			**0.822**	6

Table 2a.10. CART Sensitivity Analysis for Prediction of Temperature Using Well Data and Removing Three Variables for Each Case Analyzed.

▨ Variable Considered

□ Variable Removed

Predictor	Response Variables (X Used, **X** First Split)							R^2 Value	Splits
Temperatu	Vp	Resistivity	CSC	Dilatation	VertStress	Grav_Mag	Lithology		
---				X	**X**			**0.780**	4
---	**X**			X			X	0.730	4
---					**X**			0.749	3
---				X	**X**			**0.780**	4
---				X	**X**			**0.780**	4
---	**X**		X				X	0.686	4
---	**X**			X			X	0.730	4
---			X	X		X	**X**	0.651	6
---					**X**			0.749	3
---					**X**			0.749	3
---				X	**X**			**0.780**	4
Case 7. Removal of P-wave velocity (Vp) plus two variables									
---		X		X	**X**			**0.822**	6
---		X	X	X		**X**		0.661	7
---		X			**X**			**0.787**	5
---		X		X	**X**			**0.813**	6
---				X	**X**			**0.780**	4
---		X	X	X			**X**	0.548	4
---		X			**X**			**0.788**	5
---		X			**X**			**0.778**	4
---				X	**X**			**0.780**	4
---			X			X	**X**	0.501	3
---		X		X		X	**X**	0.641	5
---			X	X		X	**X**	0.651	6
---								**0.773**	4
---					**X**			0.749	3
---				X	**X**			**0.780**	4

Table20a.11. CART Sensitivity Analysis for Prediction of Temperature Using Well Data and Removing Four Variables for Each Case Analyzed.

Variable Considered

Variable Removed

Predictor	**Response Variables** (X Used, **X** First Split)							R^2 Value	Splits
Temp.	Vp	Resistivity	CSC	Dilatation	VertStress	Grav_Mag	Lithology		
Case 1. Removal of Lithology plus three other variables									
---	**X**	X	X					0.672	5
---	**X**	X		X				0.663	4
---	**X**		X	X				0.703	6
---		**X**	X	X				0.541	5
---		X			**X**			**0.765**	4
---					**X**			0.749	3
---		X			**X**			**0.763**	4
---				X	**X**			**0.803**	5
---				X	**X**			**0.805**	6
---				X	**X**			**0.803**	5
---	**X**	X						0.646	3
---	**X**		X			X		0.643	5
---		X	X			**X**		0.477	6
---	**X**			X		X		0.672	4
---		X		X		**X**		0.478	5
---			X	X		**X**		0.513	6
---					**X**			0.749	3
---		X			**X**			**0.800**	6
---					**X**			0.749	3
---				X	**X**			**0.803**	5
Case 2. Removal of Grav_Mag plus three other variables									
---	**X**	X	X					0.672	5
---	**X**	X		X				0.663	4
---	**X**		X	X				0.703	6
---		**X**	X	X				0.541	5
---		X			**X**			**0.765**	4
---					**X**			0.749	3
---		X			**X**			**0.763**	4
---				X	**X**			**0.803**	5
---				X	**X**			**0.805**	6
---				X	**X**			**0.803**	5
---	**X**	X					X	0.723	5
---	**X**		X				X	0.720	5
---		X					**X**	0.511	4
---	**X**			X			X	0.730	4
---		X		X			**X**	0.581	4
---			X	X			**X**	0.677	8
---					**X**			0.749	3
---					**X**			0.749	3
---					**X**		X	**0.785**	5

Table20a.11. CART Sensitivity Analysis for Prediction of Temperature Using Well Data and Removing Four Variables for Each Case Analyzed.

▨ Variable Considered

☐ Variable Removed

Predictor	**Response Variables** (X Used, **X** First Split)							R^2 Value	Splits
Temp.	Vp	Resistivity	CSC	Dilatation	VertStress	Grav_Mag	Lithology		
---				X	X			**0.780**	4
Case 3. Removal of Vertical Stress plus three other variables									
---	X	X	X					0.672	5
---	X	X		X				0.663	4
---	X		X	X				0.703	6
---		X	X	X				0.541	5
---	X	X						0.646	3
---	X		X			X		0.643	5
---		X	X			X		0.477	6
---	X			X		X		0.672	4
---		X		X		X		0.478	5
---			X	X		X		0.513	6
	X	X					X	0.723	5
---	X		X				X	0.720	5
---		X					X	0.511	4
---	X			X			X	0.730	4
---		X		X			X	0.581	4
---			X	X			X	0.677	8
---	X						X	0.696	6
---		X				X	X	0.603	4
---			X			X	X	0.599	7
---				X			X	0.646	7
Case 4. Removal of Dilatation plus three other variables									
---	X	X	X					0.672	5
---		X			X			**0.765**	4
---					X			0.749	3
---		X			X			**0.763**	4
---	X	X						0.646	3
---	X		X			X		0.643	5
---		X	X			X		0.477	6
---					X			0.749	3
---		X			X			**0.800**	6
---					X			0.749	3
	X	X					X	0.723	5
---	X		X				X	0.720	5
---		X					X	0.511	4
---					X			0.749	3
---					X			0.749	3
---					X		X	**0.785**	5
---	X						X	0.696	6
---		X				X	X	0.603	4

Table20a.11. CART Sensitivity Analysis for Prediction of Temperature Using Well Data and Removing Four Variables for Each Case Analyzed.

▨ Variable Considered

☐ Variable Removed

Predictor	**Response Variables** (X Used, **X** First Split)							R^2 Value	Splits
Temp.	Vp	Resistivity	CSC	Dilatation	VertStress	Grav_Mag	Lithology		
Case 5.Removal of CSC plus three other variables									
---			X			X	X	0.599	7
---					X			0.749	3
---	X	X		X				0.663	4
---		X			X			**0.765**	4
---				X	X			**0.803**	5
---				X	X			**0.805**	6
---	X	X						0.646	3
---	X			X		X		0.672	4
---		X		X		X		0.478	5
---					X			0.749	3
---		X			X			**0.800**	6
---				X	X			**0.803**	5
---	X	X					X	0.723	5
---	X			X			X	0.730	4
---		X		X			X	0.581	4
---					X			0.749	3
---					X			0.749	3
---				X	X			**0.780**	4
---	X						X	0.696	6
---		X				X	X	0.603	4
---				X			X	0.646	7
---					X			0.749	3
Case 6. Removal of Resistivity plus three other variables									
---	X		X	X				0.703	6
---					X			0.749	3
---				X	X			**0.803**	5
---				X	X			**0.803**	5
---	X		X			X		0.643	5
---	X			X		X		0.672	4
---			X	X		X		0.513	6
---					X			0.749	3
---					X			0.749	3
---				X	X			**0.803**	5
---	X		X				X	0.720	5
---	X			X			X	0.730	4
---			X	X			X	0.677	8
---					X			0.749	3
---					X		X	**0.785**	5
---				X	X			**0.780**	4
---	X						X	0.696	6

Table20a.11. CART Sensitivity Analysis for Prediction of Temperature Using Well Data and Removing Four Variables for Each Case Analyzed.

▨ Variable Considered

☐ Variable Removed

Predictor	Response Variables (X Used, X First Split)							R^2 Value	Splits
Temp.	Vp	Resistivity	CSC	Dilatation	VertStress	Grav_Mag	Lithology		
---			X			X	X	0.599	7
---				X			X	0.646	7
---					X			0.749	3
Case 7. Removal of Vp plus three other variables									
---		X	X	X				0.541	5
---		X			X			0.763	4
---				X	X			**0.805**	6
---				X	X			**0.803**	5
---		X	X			X		0.477	6
---		X		X		X		0.478	5
---			X	X		X		0.513	6
---		X			X			**0.800**	6
---					X			0.749	3
---				X	X			**0.803**	5
---		X					X	0.511	4
---		X		X			X	0.581	4
---			X	X			X	0.677	8
---					X			0.749	3
---					X		X	**0.785**	5
---				X	X			**0.780**	4
---		X				X	X	0.603	4
---			X			X	X	0.599	7
---				X			X	0.646	7
---					X			0.749	3

Table 20a.12. CART Sensitivity Analysis for Prediction of Temperature Using Well Data and Removing Five Variables for Each Case Analyzed.

▨ Variable Considered

☐ Variable Removed

Predictor	**Response Variables** (X Used, **X** First Split)							R^2 Value	Splits
Temp.	Vp	Resistivity	CSC	Dilatation	VertStress	Grav_Mag	Lithology		
Case 1. Removal of Lithology plus four other variables									
---	**X**	X						0.625	3
---	**X**		X					0.677	5
---		**X**	X					0.323	4
---	**X**			X				0.667	4
---		**X**		X				0.256	5
---			X	**X**				0.295	5
---	▨				**X**			0.749	3
---		X			**X**			**0.769**	5
---			▨		**X**			0.749	3
---				X	**X**			**0.803**	5
---	**X**					X		0.632	3
---		X				**X**		0.488	3
---			X			**X**		0.482	5
---				X		**X**		0.424	3
---					**X**	X		0.749	3
Case 2. Removal of Grav_Mag plus four other variables									
---	**X**	X						0.625	3
---	**X**		X					0.677	5
---		**X**	X					0.323	4
---	**X**			X				0.667	4
---		**X**		X				0.256	5
---			X	**X**				0.295	5
---	▨				**X**			0.749	3
---		X			**X**			**0.769**	5
---			▨		**X**			0.749	3
---				X	**X**			**0.803**	5
---	**X**						X	0.680	4
---		X					**X**	0.492	3
---			X				**X**	0.587	5
---				X			**X**	0.546	3
---					**X**		▨	0.749	3
Case 3. Removal of Vertical Stress plus four other variables									
---	**X**	X						0.625	3
---	**X**		X					0.677	5
---		**X**	X					0.323	4
---	**X**			X				0.667	4
---		**X**		X				0.256	5
---			X	**X**				0.295	5

Table 20a.12. CART Sensitivity Analysis for Prediction of Temperature Using Well Data and Removing Five Variables for Each Case Analyzed.

▨ Variable Considered

☐ Variable Removed

Predictor	Response Variables (X Used, **X** First Split)							R^2 Value	Splits
Temp.	Vp	Resistivity	CSC	Dilatation	VertStress	Grav_Mag	Lithology		
---	X					X		0.632	3
---		X				X		0.488	3
---			X			X		0.482	5
---				X		X		0.424	3
---	X						X	0.680	4
---		X					X	0.492	3
			X				X	0.587	5
---				X			X	0.546	3
---						X	X	0.586	5
Case 4. Removal of Dilatation plus four other variables									
---	X	X						0.625	3
---	X		X					0.677	5
---		X	X					0.323	4
---	▨				X			0.749	3
---		X			X			**0.769**	5
---			▨		X			0.749	3
---	X					X		0.632	3
---		X				X		0.488	3
---			X			X		0.482	5
---					X	X		0.749	3
---	X						X	0.680	4
---		X					X	0.492	3
---			X				X	0.587	5
---					X		▨	0.749	3
---						X	X	0.586	5
Case 5. Removal of CSC plus four other variables									
---	X	X						0.625	3
	X			X				0.667	4
---		X		X				0.256	5
---	▨				X			0.749	3
---		X			X			**0.769**	5
---				X	X			**0.803**	5
---	X					X		0.632	3
---		X				X		0.488	3
---				X		X		0.424	3
---					X	X		0.749	3
---	X						X	0.680	4
---		X					X	0.492	3
---				X			X	0.546	3
---					X		▨	0.749	3

Table 20a.12. CART Sensitivity Analysis for Prediction of Temperature Using Well Data and Removing Five Variables for Each Case Analyzed.

▨ Variable Considered

☐ Variable Removed

Predictor	Response Variables (X Used, **X** First Split)							R^2 Value	Splits
Temp.	Vp	Resistivity	CSC	Dilatation	VertStress	Grav_Mag	Lithology		
Case 6. Removal of Resistivity plus four other variables									
---	X		X					0.677	5
---	X			X				0.667	4
---			X	X				0.295	5
---					X			0.749	3
---					X			0.749	3
---				X	X			**0.803**	5
---	X					X		0.632	3
---			X			X		0.482	5
---				X		X		0.424	3
---					X	X		0.749	3
---	X						X	0.680	4
---			X				X	0.587	5
---				X			X	0.546	3
---					X			0.749	3
---						X	X	0.586	5
Case 7. Removal of Vp plus four other variables									
---		X	X					0.323	4
---		X		X				0.256	5
---			X	X				0.295	5
---		X			X			**0.769**	5
---					X			0.749	3
---				X	X			**0.803**	5
---		X				X		0.488	3
---			X			X		0.482	5
				X		X		0.424	3
---					X	X		0.749	3
---		X					X	0.492	3
---			X				X	0.587	5
---				X			X	0.546	3
---					X			0.749	3
---						X	X	0.586	5

Table 2a.13. CART Sensitivity Analysis for Prediction of Temperature Using Well Data and Removing Six Variables for Each Case Analyzed.

▨ Variable Considered

☐ Variable Removed

Predictor	**Response Variables** (X Used, **X** First Split)							R^2 Value	Splits
Temp.	Vp	Resistivity	CSC	Dilatation	VertStress	Grav_Mag	Lithology		
Case 1. Removal of six variables systematically									
---							X	0.516	3
---						X		0.437	2
---					X			0.749	3
---				X				0.287	3
---			X					0.192	3
---		X						0.253	2
---	X							0.621	3

APPENDIX 20b

CLASSIFICATION AND REGRESSION TREE (CART) SENSITIVITY ANALYSIS
PREDICTING LITHOLOGY USING SECTION AND WELL DATA

Table of Contents

List of Tables

1. INTRODUCTION

This analysis was performed to understand the predictive powers and relationships between seven key geoscience parameters using Classification and Regression Tree Analysis (CART, see Section 7 of the main report). This statistical method used JMP Pro 9.0, part of the SAS Predictive Analytics Suite.

The following series of tables document the CART sensitivity analysis exploring all possibilities of the indicated parameters (Table 20a.1) for predicting lithology type using section and well data. Each parameter (response variable) is systematically removed from the analysis starting with one variable removed and ending with six out of the seven variables removed, Tables 20a.2 to 20a.7 for the section data and theTables 20a.8 to 20a13 for the well data. Parameters considered in the analysis are labeled in light purple, while if. parameter was used, the cell also has a X. The parameter that the analysis first splits on contains a red X. Parameters that have been removed from the analysis are blank (highlighted white).

The R^2 value corresponds to the accuracy of CART to predict lithology type along the key cross-sections (Section Data) and by wells (Well Data) according to the divisions of the data used. All values over **0.6** are bolded. A color scheme (green-yellow-orange-red) distinguishes the relative range of R^2 values per individual analysis, with red representing high values, and green representing low values. The # of splits was recorded as each analysis was terminated due to the split history curve "leveling out" and the R^2 value not increasing substantially as the analysis continued to split on the remaining data. The analysis was also terminated if the cross-validation curve (a seperate automatic analysis performed with a sub-set of the remaining data) was not in agreement with the expressed R^2 value.

Table 20a.1. Geoscience parameters considered in the CART sensitivity analysis

Parameter	Description
Lith	Lithology, specifically referring to a lithologic unit
Vp	Seismic parameter: P-wave velocity
Resistivity	Magneto-telluric data
CSC	Coulomb Stress Change derived from modeled stress data
Dilatation	Dilatation derived from modeled stress data
VertStress	Vertical Stress: calculated parameter
Grav_Mag	Combined Gravity and Magnetic inferred Lithologic Unit
Temp	Temperature derived from thermal models

Table 20b.2. CART Sensitivity Analysis for Prediction of Lithology Using Section Data and Removing One Variable for Each Case Analyzed. The Base Case Is where No Variable is Removed.

▨ Variable Considered

□ Variable Removed

Predictor	**Response Variables** (**X** Used, **X** First Split)							R^2 Value	Splits
Lith.	Vp	Resistivity	CSC	Dilatation	VertStress	Grav_Mag	Temp		
Case 1: All Variables Considered with each parameter systematically removed									
---				X	X			**0.631**	6
---				X	X		□	**0.627**	6
---				X	X	□		**0.655**	7
---	X	X		X	□	X		0.438	6
---		X		□	X	X		0.613	7
---			□	X	X			**0.647**	7
---		□		X	X			**0.627**	6
---	□			X	X			0.632	6

Table 20b.3. CART Sensitivity Analysis for Prediction of Lithology Using Section Data and Removing Two Variables for Each Case Analyzed.

▨ Variable Considered
□ Variable Removed
🟧 Baseline Case

Predictor	Response Variables (X Used, **X** First Split)							R^2 Value	Splits
Lithology	Vp	Resistivity	CSC	Dilatation	VertStress	Grav_Mag	Temp		
Case 1. All Variables excluding Temperature (Temp) + one variable									
				X	**X**			**0.627**	6
				X	**X**			**0.628**	6
	X	X		X		X		0.443	6
		X			**X**	X		0.594	6
				X	**X**			**0.630**	6
				X	**X**			**0.628**	6
				X	**X**			**0.631**	6
Case 2. All Variables excluding Gravity and Magnetic inferred Lithology (Grav_Mag) + one variable									
				X	**X**			**0.655**	7
				X	**X**			**0.628**	6
	X	X		X			X	0.453	8
		X			**X**			0.541	5
				X	**X**			**0.634**	6
				X	**X**			**0.652**	7
				X	**X**			**0.634**	6
Case 3. All Variables excluding Vertical Stress (VertStress) + one variable									
	X	X		X		X		0.438	6
	X	X		X		X		0.413	4
	X	X		X			X	0.453	8
	X	X				X		0.384	4
	X	X		X		X	X	0.449	6
	X			X		X		0.420	4
		X		X		**X**	X	0.401	6
Case 4. All Variables excluding Dilatation + one variable									
		X			**X**	X		**0.613**	7
		X			**X**	X		0.594	6
		X			**X**			0.541	5
	X	X				X		0.384	4
		X			**X**	X		0.590	6
					X	X		0.559	5
		X			**X**	X		0.592	6
Case 5. All Variables excluding Coulomb Stress Change (CSC) + one variable									
				X	**X**			**0.647**	7
				X	**X**			**0.630**	6
				X	**X**			**0.634**	6
	X	X		X		X	X	0.449	6
		X			**X**	X		0.590	6
				X	**X**			**0.651**	7
				X	**X**			**0.630**	6

Table 20b.3. CART Sensitivity Analysis for Prediction of Lithology Using Section Data and Removing Two Variables for Each Case Analyzed. The Base Case Is where only One Variable Is Removed.

▨ Variable Considered
☐ Variable Removed
🟧 Baseline Case

Predictor	**Response Variables** (X Used, X First Split)							R^2 Value	Splits
Lithology	Vp	Resistivity	CSC	Dilatation	VertStress	Grav_Mag	Temp		
Case 6. All Variables excluding Resistivity + one variable									
	▨		▨	X	X	▨	▨	**0.627**	6
	▨		▨	X	X	▨		**0.628**	6
	▨		▨	X	X		▨	**0.652**	7
	X		▨	X		X	▨	0.420	4
	▨		▨		X	X	▨	0.559	5
	▨			X	X	▨	▨	**0.651**	7
			▨	X	X	▨	▨	**0.653**	7
Case 7. All Variables excluding P-wave velocity (Vp) + one variable									
		▨	▨	X	X	▨	▨	**0.632**	6
		▨	▨	X	X	▨		**0.631**	6
		▨	▨	X	X		▨	**0.634**	6
		X	▨	X		X	X	0.401	6
		X	▨		X	X	▨	0.592	6
		▨		X	X	▨	▨	**0.630**	6
			▨	X	X	▨	▨	**0.653**	7

Table 20b.4 CART Sensitivity Analysis for Prediction of Lithology Using Section Data and Removing Three Variables for Each Case Analyzed. The Base Case Is where Three Variables Are Removed

▨ Variable Considered

☐ Variable Removed

Predictor	**Response Variables** (X Used, **X** First Split)							R^2 Value	Splits
Lithology	Vp	Resistivity	CSC	Dilat	VertStress	Grav_Mag	Temp		
Case 1. Removal of Temperature (Temp) plus two variables									
---	X	X	X	X				0.384	5
---		X	X		X			**0.604**	8
---		X		X	X			**0.665**	8
---				X	X			**0.664**	8
---				X	X			**0.663**	8
---	X	X				X		0.403	5
---	X	X		X		X		0.433	6
---	X			X		X		0.368	6
---		X		X		X		0.376	6
---		X			X	X		**0.635**	8
---			X		X	X		**0.621**	8
---		X			X	X		**0.636**	8
---				X	X			**0.662**	8
---		X		X	X			**0.663**	8
---				X	X			**0.664**	8
Case 2. Removal of Gravity and Magnetic inferred Lithology (Grav_Mag) plus two variables									
---	X	X	X	X				0.384	5
---		X	X		X			**0.604**	8
---		X		X	X			**0.665**	8
---				X	X			**0.664**	8
---				X	X			**0.663**	8
---	X	X					X	0.365	4
---	X	X		X				0.383	4
---	X			X				0.407	6
---		X		X			X	0.408	7
---		X			X			**0.611**	8
---			X		X			0.578	7
---		X	X		X			**0.615**	8
---				X	X			**0.653**	7
---				X	X			**0.629**	6
---				X	X			**0.654**	7
Case 3. Removal of Vertical Stress (VertStress) plus two variables									
---	X	X	X	X				0.384	5
---	X	X				X		0.403	5
---	X	X		X		X		0.433	6
---	X			X		X		0.368	6
---		X		X		X		0.376	6
---	X	X					X	0.365	4
---	X	X		X				0.383	4

Table 20b.4 CART Sensitivity Analysis for Prediction of Lithology Using Section Data and Removing Three Variables for Each Case Analyzed. The Base Case Is where Three Variables Are Removed

▨ Variable Considered

☐ Variable Removed

Predictor	**Response Variables** (X Used, **X** First Split)							R^2 Value	Splits
Lithology	Vp	Resistivity	CSC	Dilat	VertStress	Grav_Mag	Temp		
---	**X**			X				0.407	6
---		X		**X**			X	0.408	7
---	**X**	X				X	X	0.423	7
---	**X**		X			X		0.385	4
---		X				**X**	X	0.367	5
---	**X**			X		X		0.416	4
---		X		**X**		X	X	0.388	5
---				**X**		X	X	0.393	5
Case 4. Removal of Dilatation plus two variables									
---		X	X		**X**			**0.604**	8
---	**X**	X				X		0.403	5
---		X			**X**	X		**0.635**	8
---			X		**X**	X		**0.621**	8
---		X			**X**	X		**0.636**	8
---	**X**	X					X	0.365	4
---		X			**X**			**0.611**	8
---			X		**X**			0.578	7
---		X	X		**X**			**0.615**	8
---	**X**	X				X	X	0.423	7
---	**X**		X			X		0.385	4
---		X				**X**	X	0.367	5
---					**X**	X		0.555	5
---		X			**X**	X		0.553	4
---					**X**	X		0.523	4
Case 5. Removal of Coulomb Stress Change (CSC) plus two variables									
---		X		X	**X**			**0.665**	8
---	**X**	X		X		X		0.433	6
---		X			**X**	X		**0.635**	8
---				X	**X**			**0.662**	8
---		X		X	**X**			**0.663**	8
---	**X**	X		X				0.383	4
---		X			**X**			**0.611**	8
---				X	**X**			**0.653**	7
---				X	**X**			**0.629**	6
---	**X**	X				X	X	0.423	7
---	**X**			X		X		0.416	4
---		X		**X**		X	X	0.388	5
---					**X**	X		0.555	5
---		X			**X**	X		0.553	4
---				X	**X**			**0.654**	7
Case 6. Removal of Resisitivity plus two variables									
---				X	**X**			**0.664**	8
---	X			**X**		X		0.368	6

Table 20b.4 CART Sensitivity Analysis for Prediction of Lithology Using Section Data and Removing Three Variables for Each Case Analyzed. The Base Case Is where Three Variables Are Removed

▨ Variable Considered

☐ Variable Removed

Predictor	**Response Variables** (X Used, **X** First Split)							R^2 Value	Splits
Lithology	Vp	Resistivity	CSC	Dilat	VertStress	Grav_Mag	Temp		
---	▨		X		**X**	X		**0.621**	8
---	▨			X	**X**	▨		**0.662**	8
---			▨	X	**X**	▨		**0.664**	8
---	**X**		▨	X			▨	0.407	6
---	▨		X		**X**		▨	0.578	7
---	▨			X	**X**		▨	**0.653**	7
---			▨	X	**X**		▨	**0.654**	7
---	**X**		X			X	▨	0.385	4
---	**X**			X		X	▨	0.416	4
---			▨	**X**		X	X	0.393	5
---	▨				**X**	X	▨	0.555	5
---			▨		**X**	X	▨	0.523	4
---				X	**X**	▨	▨	**0.654**	7
Case 7. Removal of P-wave velocity (Vp) plus two variables									
---		▨	▨	X	**X**			**0.663**	8
---		X	▨	**X**		X		0.376	6
---		X	▨		**X**	X		**0.636**	8
---		X		X	**X**	▨		**0.663**	8
---			▨	X	**X**	▨		**0.664**	8
---		X	▨	**X**			X	0.408	7
---		X	X		**X**		▨	**0.615**	8
---		▨		X	**X**		▨	**0.629**	6
---			▨	X	**X**		▨	**0.654**	7
---		X	▨			**X**	X	0.367	5
---		X		**X**		X	X	0.388	5
---			▨	**X**		X	X	0.393	5
---		X			**X**	X	▨	0.553	4
---			▨		**X**	X	▨	0.523	4
---				X	**X**	▨	▨	**0.654**	7

Table 20b.5. CART Sensitivity Analysis for Prediction of Lithology Using Section Data and Removing Four Variables for Each Case Analyzed.

▨ Variable Considered

☐ Variable Removed

Predictor	Response Variables (X Used, **X** First Split)							R^2 Value	Splits
Lithology	Vp	Resistivity	CSC	Dilat	VertStress	Grav_Mag	Temp		
Case 1. Removal of Temperature plus three other variables									
---	**X**	X	X					0.369	5
---	**X**	X		X				0.397	5
---	**X**		▨	X				0.391	5
---		X	X	**X**				0.318	5
---	▨	X			**X**			0.563	6
---	▨		X		**X**			0.558	6
---		X	▨		**X**			0.586	7
---	▨			X	**X**			**0.660**	8
---		▨		X	**X**			**0.653**	7
---			▨	X	**X**			**0.650**	7
---	**X**	X				X		0.406	5
---	**X**		X			X		0.406	5
---		X	X			**X**		0.334	4
---	**X**			X		X		0.421	4
---		X		**X**		X		0.384	7
---			X	**X**		X		0.413	7
---	X				**X**	X		0.588	7
---		X			**X**	X		**0.625**	8
---			X		**X**	X		**0.601**	7
---				X	**X**	▨		**0.653**	7
Case 2. Removal of Grav_Mag plus three other variables									
---	**X**	X	X					0.369	5
---	**X**	X		X				0.397	5
---	**X**		▨	X				0.391	5
---		X	X	**X**				0.318	5
---	▨	X			**X**			0.563	6
---	▨		X		**X**			0.558	6
---		X	▨		**X**			0.586	7
---	▨			X	**X**			**0.660**	8
---		▨		X	**X**			**0.653**	7
---			▨	X	**X**			**0.650**	7
---	**X**	X					X	0.382	5
---	**X**		X				X	0.344	5
---		X	X				**X**	0.333	4
---	**X**			X			X	0.412	6
---		X		**X**			X	0.396	6
---			X	**X**			X	0.402	7
---	▨				**X**		▨	0.484	4
---		X			**X**		▨	0.563	6
---			X		**X**		▨	0.577	7
---				X	**X**		▨	**0.654**	7

Table 20b.5. CART Sensitivity Analysis for Prediction of Lithology Using Section Data and Removing Four Variables for Each Case Analyzed.

▨ Variable Considered

☐ Variable Removed

Predictor	Response Variables (X Used, X First Split)							R^2 Value	Splits
Lithology	Vp	Resistivity	CSC	Dilat	VertStress	Grav_Mag	Temp		
Case 3. Removal of Vertical Stress plus three other variables									
---	X	X	X					0.369	5
---	X	X		X				0.397	5
---	X			X				0.391	5
---		X	X	X				0.318	5
---	X	X				X		0.406	5
---	X		X			X		0.406	5
---		X	X			X		0.334	4
---	X			X		X		0.421	4
---		X		X		X		0.384	7
---			X	X		X		0.413	7
---	X	X					X	0.382	5
---	X		X				X	0.344	5
---		X	X				X	0.333	4
---	X			X			X	0.412	6
---		X		X			X	0.396	6
---			X	X			X	0.402	7
---	X					X	X	0.375	5
---		X				X	X	0.371	6
---			X			X	X	0.384	6
---				X		X	X	0.409	6
Case 4. Removal of Dilatation plus three other variables									
---	X	X	X					0.369	5
---		X			X			0.563	6
---			X		X			0.558	6
---		X			X			0.586	7
---	X	X				X		0.406	5
---	X		X			X		0.406	5
---		X	X			X		0.334	4
---	X				X	X		0.588	7
---		X			X	X		**0.625**	8
---			X		X	X		**0.601**	7
	X	X					X	0.382	5
---	X		X				X	0.344	5
---		X	X				X	0.333	4
---					X			0.484	4
---		X			X			0.563	6
---			X		X			0.577	7
---	X					X	X	0.375	5
---		X				X	X	0.371	6

Table 20b.5. CART Sensitivity Analysis for Prediction of Lithology Using Section Data and Removing Four Variables for Each Case Analyzed.

▨ Variable Considered

☐ Variable Removed

Predictor	Response Variables (X Used, **X** First Split)							R^2 Value	Splits
Lithology	Vp	Resistivity	CSC	Dilat	VertStress	Grav_Mag	Temp		
---			X			**X**	X	0.384	6
---					**X**	X	▨	**0.606**	8
Case 5.Removal of CSC and three other variables									
---	**X**	X		X				0.397	5
---	▨	X			**X**			0.563	6
---	▨			X	**X**			**0.660**	8
---		▨		X	**X**			**0.653**	7
---	**X**	X				X		0.406	5
---	**X**			X		X		0.406	5
---		X		X		**X**		0.334	4
---	X				**X**	X		0.588	7
---		X			**X**	X		**0.625**	8
---				X	**X**	▨		**0.653**	7
---	**X**	X					X	0.382	5
---	**X**			X			X	0.412	6
---		X		**X**			X	0.396	6
---	▨				**X**		▨	0.484	4
---		X			**X**		▨	0.563	6
---				X	**X**		▨	**0.654**	7
---	**X**					X	X	0.375	5
---		X				**X**	X	0.371	6
---				**X**		X	X	0.409	6
---					**X**	X	▨	**0.606**	8
Case 6. Removal of Resistivity plus three other variables									
---	**X**		▨	X				0.391	5
---	▨		X		**X**			0.558	6
---	▨			X	**X**			**0.660**	8
---			▨	X	**X**			**0.650**	7
---	**X**		X			X		0.406	5
---	**X**			X		X		0.421	4
---			X	**X**		X		0.413	7
---	X				**X**	X		0.588	7
---			X		**X**	X		**0.601**	7
---				X	**X**	▨		**0.653**	7
---	**X**		X				X	0.344	5
---	**X**			X			X	0.412	6
---			X	**X**			X	0.402	7
---	▨				**X**		▨	0.484	4
---			X		**X**		▨	0.577	7
---				X	**X**		▨	**0.654**	7

Table 20b.5. CART Sensitivity Analysis for Prediction of Lithology Using Section Data and Removing Four Variables for Each Case Analyzed.

▨	Variable Considered
☐	Variable Removed

Predictor	**Response Variables** (X Used, **X** First Split)							R^2 Value	Splits
Lithology	Vp	Resistivity	CSC	Dilat	VertStress	Grav_Mag	Temp		
---	X					X	X	0.375	5
---			X			X	X	0.384	6
---				X		X	X	0.409	6
---					X	X		**0.606**	8
Case 7. Removal of Vp plus three other variables									
---		X	X	X				0.318	5
---		X			X			0.586	7
---				X	X			**0.653**	7
---				X	X			**0.650**	7
---		X	X			X		0.334	4
---		X		X		X		0.384	7
---			X	X		X		0.413	7
---		X			X	X		**0.625**	8
---			X		X	X		**0.601**	7
---				X	X			**0.653**	7
---		X	X				X	0.333	4
---		X		X			X	0.396	6
---			X	X			X	0.402	7
---		X			X			0.563	6
---			X		X			0.577	7
---				X	X			**0.654**	7
---		X				X	X	0.371	6
---			X			X	X	0.384	6
---				X		X	X	0.409	6
---					X	X		**0.606**	8

Table 20b.6. CART Sensitivity Analysis for Prediction of Lithology Using Section Data and Removing Five Variables for Each Case Analyzed.

▨ Variable Considered

☐ Variable Removed

Predictor	**Response Variables** (X Used, **X** First Split)							R^2 Value	Splits
Lithology	Vp	Resistivity	CSC	Dilat	VertStress	Grav_Mag	Temp		
Case 1. Removal of Temperature plus four other variables									
---	X	X						0.314	3
---	X		X					0.325	4
---		X	X					0.255	3
---	X			X				0.406	6
---		X		X				0.312	5
---			X	X				0.303	5
---	X				X			0.525	6
---		X			X			0.586	7
---			X		X			0.579	7
---				X	X			**0.656**	7
---	X					X		0.376	4
---		X				X		0.32	3
---			X			X		0.31	4
---				X		X		0.374	5
---					X	X		0.569	6
Case 2. Removal of Grav_Mag plus four other variables									
---	X	X						0.314	3
---	X		X					0.325	4
---		X	X					0.255	3
---	X			X				0.406	6
---		X		X				0.312	5
---			X	X				0.303	5
---	X				X			0.525	6
---		X			X			0.586	7
---			X		X			0.579	7
---				X	X			**0.656**	7
---	X						X	0.278	3
---		X					X	0.357	5
---			X				X	0.307	4
---				X			X	0.38	6
---					X			0.505	5
Case 3. Removal of Vertical Stress plus four other variables									
---	X	X						0.314	3
---	X		X					0.325	4
---		X	X					0.255	3
---	X			X				0.406	6
---		X		X				0.312	5
---			X	X				0.303	5
---	X					X		0.376	4
---		X				X		0.32	3
---			X			X		0.31	4
---				X		X		0.374	5
---	X						X	0.278	3
---		X					X	0.357	5
---			X				X	0.307	4

Table 20b.6. CART Sensitivity Analysis for Prediction of Lithology Using Section Data and Removing Five Variables for Each Case Analyzed.

▨ Variable Considered

☐ Variable Removed

Predictor	**Response Variables** (X Used, **X** First Split)							R^2 Value	Splits
Lithology	Vp	Resistivity	CSC	Dilat	VertStress	Grav_Mag	Temp		
---				**X**			X	0.38	6
---						**X**	X	0.344	4
Case 4. Removal of Dilatation plus four other variables									
---	**X**	X						0.314	3
---	**X**		X					0.325	4
---		**X**	X					0.255	3
---	X				**X**			0.525	6
---		X			**X**			0.586	7
---			X		**X**			0.579	7
---	**X**					X		0.376	4
---		X				**X**		0.32	3
---			X			**X**		0.31	4
---					**X**	X		0.569	6
---	**X**						X	0.278	3
---		X					**X**	0.357	5
---			X				**X**	0.307	4
---					**X**		▨	0.505	5
---						**X**	X	0.344	4
Case 5. Removal of CSC plus four other variables									
---	**X**	X						0.314	3
	X			X				0.406	6
---		X		**X**				0.312	5
---	X				**X**			0.525	6
---		X			**X**			0.586	7
---				X	**X**			**0.656**	7
---	**X**					X		0.376	4
---		X				**X**		0.32	3
---				**X**		X		0.374	5
---					**X**	X		0.569	6
---	**X**						X	0.278	3
---		X					**X**	0.357	5
---				**X**			X	0.38	6
---					**X**		▨	0.505	5
---						**X**	X	0.344	4
Case 6. Removal of Resistivity plus four other variables									
---	**X**		X					0.325	4
---	**X**			X				0.406	6
---			X	**X**				0.303	5
---	X				**X**			0.525	6
---			X		**X**			0.579	7
---				X	**X**			**0.656**	7
---	**X**					X		0.376	4
---			X			**X**		0.31	4

Table 20b.6. CART Sensitivity Analysis for Prediction of Lithology Using Section Data and Removing Five Variables for Each Case Analyzed.

▨	Variable Considered
☐	Variable Removed

Predictor	**Response Variables** (X Used, **X** First Split)							R² Value	Splits
Lithology	Vp	Resistivity	CSC	Dilat	VertStress	Grav_Mag	Temp		
---				**X**		X		0.374	5
---					**X**	X		0.569	6
---	**X**						X	0.278	3
---			X				**X**	0.307	4
---				**X**			X	0.38	6
---					**X**			0.505	5
---						**X**	X	0.344	4
Case 7. Removal of Vp plus four other variables									
---		**X**	X					0.255	3
---		X		**X**				0.312	5
---			X	**X**				0.303	5
---		X			**X**			0.586	7
---			X		**X**			0.579	7
---				X	**X**			**0.656**	7
---		X				**X**		0.32	3
---			X			**X**		0.31	4
				X		X		0.374	5
---					**X**	X		0.569	6
---		X					**X**	0.357	5
---			X				**X**	0.307	4
---				**X**			X	0.38	6
---					**X**			0.505	5
---						**X**	X	0.344	4

Table 20b.7. CART Sensitivity Analysis for Prediction of Lithology Using Section Data and Removing Six Variables for Each Case Analyzed.

▨ Variable Considered

☐ Variable Removed

Predictor	**Response Variables** (X Used, **X** First Split)							R^2 Value	Splits
Lithology	Vp	Resistivity	CSC	Dilat	VertStress	Grav_Mag	Temp		
Case 1. Removal of six variables systematically									
---							X	0.254	3
---						X		0.263	2
---					X			0.507	5
---				X				0.277	4
---			X					0.181	4
---		X						0.234	4
---	X							0.283	3

Table 20b.8. CART Sensitivity Analysis for Prediction of Lithology Using Well Data and Removing One Variable for Each Case Analyzed

▨ Variable Considered

☐ Variable Removed

Predictor	**Response Variables** (X Used, **X** First Split)							R^2 Value	Splits
Lithology	Vp	Resistivity	CSC	Dilat	VertStress	Grav_Mag	Temp		
Case 1: All Variables Considered with each parameter systematically removed									
---	X			X	X			**0.611**	6
---	X			X	X			**0.611**	6
---	X			X	X			**0.611**	6
---	X	X	X			X		0.521	7
---	X	X			X			0.593	6
---	X			X	X			**0.611**	6
---	X			X	X			**0.611**	6
---				X	X			0.577	5

Table 20b.9. CART Sensitivity Analysis for Prediction of Lithology Using Well Data and Removing Two Variables for Each Case Analyzed.

▨	Variable Considered
☐	Variable Removed
▨	Base Case

Predictor	**Response Variables** (X Used, **X** First Split)							R² Value	Splits
Lithology	Vp	Resistivity	CSC	Dilatation	VertStress	Grav_Mag	Temp		
Case 1. All Variables excluding Temperature + one variable									
	X			X	X			**0.611**	6
	X			X	X			**0.611**	6
	X	X				X		0.491	6
		X			X			0.562	5
	X			X	X			**0.611**	6
	X			X	X			**0.611**	6
				X	X			0.580	5
Case 2. All Variables excluding Grav_Mag + one variable									
	X			X	X			**0.611**	6
	X			X	X			**0.611**	6
	X		X	X			X	0.463	5
	X	X			X			0.593	6
	X			X	X			**0.611**	6
	X			X	X			**0.611**	6
				X	X			0.577	5
Case 3. All Variables excluding Vertical Stress + one variable									
	X	X	X			X		0.521	7
	X	X				X		0.491	6
	X		X	X			X	0.463	5
	X	X	X			X		0.529	7
	X	X		X		X		0.494	6
	X		X	X		X		0.481	6
		X	X			X	X	0.447	6
Case 4. All Variables excluding Dilatation + one variable									
	X	X			X			0.593	6
		X			X			0.562	5
	X	X			X			0.593	6
	X	X	X			X		0.529	7
	X	X			X			0.594	6
	X				X	X		**0.602**	6
		X			X			0.562	5
Case 5. All Variables excluding Coulomb Stress Change (CSC) + one variable									
	X			X	X			**0.611**	6
	X			X	X			**0.611**	6
	X			X	X			**0.611**	6
	X	X		X		X		0.494	6
	X	X			X			0.594	6
	X			X	X			**0.609**	6
				X	X			0.597	6

Table 20b.9. CART Sensitivity Analysis for Prediction of Lithology Using Well Data and Removing Two Variables for Each Case Analyzed.

▨ Variable Considered
☐ Variable Removed
▨ Base Case

Predictor	**Response Variables** (X Used, **X** First Split)							R^2 Value	Splits
Lithology	Vp	Resistivity	CSC	Dilatation	VertStress	Grav_Mag	Temp		
Case 6. All Variables excluding Resistivity + one variable									
	X			X	X			**0.611**	6
	X			X	X			**0.611**	6
	X			X	X			**0.611**	6
	X		X	X		X		0.481	6
	X				X	X		**0.602**	6
	X			X	X			**0.609**	6
				X	X			0.580	5
Case 7. All Variables excluding P-wave velocity (Vp) + one variable									
				X	X			0.577	5
				X	X			0.580	5
				X	X			0.577	5
		X	X			X	X	0.447	6
		X			X			0.562	5
				X	X			0.597	6
				X	X			0.580	5

Table 20b.10. CART Sensitivity Analysis for Prediction of Lithology Using Well Data and Removing Three Variables for Each Case Analyzed

▨ Variable Considered

☐ Variable Removed

Predictor	**Response Variables** (X Used, **X** First Split)							R^2 Value	Splits
Lithology	Vp	Resistivity	CSC	Dilatation	VertStress	Grav_Mag	Temp		
Case 1. Removal of Temperature plus two variables									
---	X	X	X	X				0.518	7
---	X	X			X			0.593	6
---	X			X	X			**0.611**	6
---	X			X	X			**0.611**	6
---				X	X			0.577	5
---	X	X				X		0.517	7
---	X	X		X		X		0.518	7
---	X		X			X		0.469	5
---		X	X			X		0.412	5
---	X	X			X			0.593	6
---	X				X	X		**0.621**	7
---		X			X			0.562	5
---	X			X	X			**0.611**	6
---				X	X			**0.613**	7
---				X	X			0.577	5
Case 2. Removal of Gravity and Magnetic inferred Lithology (Grav_Mag) plus two variables									
---	X	X	X	X				0.518	7
---	X	X			X			0.593	6
---	X			X	X			**0.611**	6
---	X			X	X			**0.611**	6
---				X	X			0.577	5
---	X		X				X	0.435	5
---	X	X		X			X	0.548	8
---	X		X	X			X	0.511	7
---		X	X	X			X	0.314	7
---	X	X			X			0.593	6
---	X		X		X			0.599	6
---		X			X			0.562	5
---	X			X	X			**0.644**	8
---				X	X			**0.618**	7
---			X	X	X			0.589	6
Case 3. Removal of Vertical Stress (VertStress) plus two variables									
---	X	X	X	X				0.518	7
---	X	X				X		0.517	7
---	X	X		X		X		0.518	7
---	X		X			X		0.469	5
---		X	X			X		0.412	5
---	X		X				X	0.435	5
---	X	X		X			X	0.548	8
---	X		X	X			X	0.511	7

Table 20b.10. CART Sensitivity Analysis for Prediction of Lithology Using Well Data and Removing Three Variables for Each Case Analyzed

▨ Variable Considered

☐ Variable Removed

Predictor	**Response Variables** (X Used, **X** First Split)							R^2 Value	Splits
Lithology	Vp	Resistivity	CSC	Dilatation	VertStress	Grav_Mag	Temp		
---		X	X	**X**			X	0.314	7
---	**X**	X				X		0.515	7
---	**X**		X			X		**0.600**	5
---		X	X			**X**	X	0.444	6
---	**X**			X		X		0.531	7
---		X		X		**X**	X	0.400	7
---			X	X		**X**		0.398	5
Case 4. Removal of Dilatation plus two variables									
---	X	X			**X**			0.593	6
---	**X**	X				X		0.517	7
---	X	X			**X**			0.593	6
---	X				**X**	X		**0.621**	7
---		X			**X**			0.562	5
---	**X**		X				X	0.435	5
---	X	X			**X**			0.593	6
---	X		X		**X**			0.599	6
---		X			**X**			0.562	5
---	**X**	X				X		0.515	7
---	**X**		X			X		**0.600**	5
---		X	X			**X**	X	0.444	6
---	X				**X**	X		**0.620**	7
---		X			**X**			0.562	5
---					**X**	X		0.570	5
Case 5. Removal of Coulomb Stress Change (CSC) plus two variables									
---	X			X	**X**			**0.611**	6
---	**X**	X		X		X		0.518	7
---	X	X			**X**			0.593	6
---	X			X	**X**			**0.611**	6
---				X	**X**			**0.613**	7
---	**X**	X		X			X	0.548	8
---	X	X			**X**			0.593	6
---	X			X	**X**			**0.611**	6
---				X	**X**			**0.618**	7
---	**X**	X				X		0.515	7
---	**X**			X		X		0.531	7
---		X		X		**X**	X	0.400	7
---	X				**X**	X		**0.620**	7
---		X			**X**			0.562	5
Case 6. Removal of Resisitivity plus two variables									
---	X			X	**X**			**0.611**	6
---	**X**		X			X		0.469	5
---	X				**X**	X		**0.621**	7
---	X			X	**X**			**0.611**	6
---				X	**X**			0.577	5

Table 20b.10. CART Sensitivity Analysis for Prediction of Lithology Using Well Data and Removing Three Variables for Each Case Analyzed

▨ Variable Considered

☐ Variable Removed

Predictor	**Response Variables** (X Used, **X** First Split)							R^2 Value	Splits
Lithology	Vp	Resistivity	CSC	Dilatation	VertStress	Grav_Mag	Temp		
---	X		X	X			X	0.511	7
---	X		X		X			0.599	6
---	X			X	X			**0.611**	6
---			X	X	X			0.589	6
---	X		X			X		**0.600**	5
---	X			X		X		0.531	7
---			X	X		X		0.398	5
---	X				X	X		**0.620**	7
---					X	X		0.570	5
---				X	X			**0.616**	7
Case 7. Removal of P-wave velocity (Vp) plus two variables									
---				X	X			0.577	5
---		X	X			X		0.412	5
---		X			X			0.562	5
---				X	X			**0.613**	7
---				X	X			0.577	5
---		X	X	X			X	0.314	7
---		X			X			0.562	5
---				X	X			**0.618**	7
---			X	X	X			0.589	6
---		X	X			X	X	0.444	6
---		X		X		X	X	0.400	7
---			X	X		X		0.398	5
---		X			X			0.562	5
---					X	X		0.570	5
---				X	X			**0.616**	7

Table 20b.11. CART Sensitivity Analysis for Prediction of Lithology Using Well Data and Removing Four Variables for Each Case Analyzed

▨	Variable Considered
☐	Variable Removed

Predictor	**Response Variables** (X Used, **X** First Split)							R^2 Value	Splits
Lithology	Vp	Resistivity	CSC	Dilatation	VertStress	Grav_Mag	Temp		
Case 1. Removal of Temperature plus three other variables									
---	**X**	X	X					0.475	7
---	**X**	X		X				0.542	8
---	**X**		X	X				0.522	7
---		X	X	**X**				0.341	7
---	X	X			**X**			**0.613**	7
---	X		X		**X**			0.599	6
---		X			**X**			0.562	5
---	X			X	**X**			**0.611**	6
---				X	**X**			**0.620**	7
---			X	X	**X**			0.597	7
---	**X**	X				X		0.518	7
---	**X**		X			X		0.550	9
---		X	X			**X**		0.422	5
---	**X**			X		X		0.514	7
---		X		X		**X**		0.376	6
---			X	X		**X**		0.472	8
---	X				X	**X**		**0.615**	7
---		X			**X**			0.562	5
---					**X**	X		0.584	6
---				X	**X**			0.597	6
Case 2. Removal of Grav_Mag plus three other variables									
---	**X**	X	X					0.475	7
---	**X**	X		X				0.542	8
---	**X**		X	X				0.522	7
---		X	X	**X**				0.341	7
---	X	X			**X**			**0.613**	7
---	X		X		**X**			0.599	6
---		X			**X**			0.562	5
---	X			X	**X**			**0.611**	6
---				X	**X**			**0.620**	7
---			X	X	**X**			0.597	7
---	**X**	X					X	0.398	4
---	**X**		X				X	0.448	6
---		**X**	X					0.276	6
---	**X**			X			X	0.549	8
---		X		**X**			X	0.294	7
---			X	**X**			X	0.341	9
---	X				**X**			0.570	5
---		X			**X**			0.562	5
---			X		**X**			0.567	5

Table 20b.11. CART Sensitivity Analysis for Prediction of Lithology Using Well Data and Removing Four Variables for Each Case Analyzed

▨ Variable Considered

☐ Variable Removed

Predictor	Response Variables (X Used, **X** First Split)							R^2 Value	Splits
Lithology	Vp	Resistivity	CSC	Dilatation	VertStress	Grav_Mag	Temp		
---				X	**X**			0.577	5
Case 3. Removal of Vertical Stress plus three other variables									
---	**X**	X	X					0.475	7
---	**X**	X		X				0.542	8
---	**X**		X	X				0.522	7
---		X	X	**X**				0.341	7
---	**X**	X				X		0.518	7
---	**X**		X			X		0.550	9
---		X	X			**X**		0.422	5
---	**X**			X		X		0.514	7
---		X		X		**X**		0.376	6
---			X	X		**X**		0.472	8
	X	X					X	0.398	4
---	**X**		X				X	0.448	6
---		**X**	X					0.276	6
---	**X**			X			X	0.549	8
---		X		**X**			X	0.294	7
---			X	**X**			X	0.341	9
---	**X**					X		0.530	8
---		X				**X**		0.336	4
---			X			**X**	X	0.442	7
---				X		**X**	X	0.445	7
Case 4. Removal of Dilatation plus three other variables									
---	**X**	X	X					0.475	7
---	X	X			**X**			**0.613**	7
---	X		X		**X**			0.599	6
---		X			**X**			0.562	5
---	**X**	X				X		0.518	7
---	**X**		X			X		0.550	9
---		X	X			**X**		0.422	5
---	X				X	**X**		**0.615**	7
---		X			**X**			0.562	5
---					**X**	X		0.584	6
	X	X					X	0.398	4
---	**X**		X				X	0.448	6
---		**X**	X					0.276	6
---	X				**X**			0.570	5
---		X			**X**			0.562	5
---			X		**X**			0.567	5
---	**X**					X		0.530	8
---		X				**X**		0.336	4

Table 20b.11. CART Sensitivity Analysis for Prediction of Lithology Using Well Data and Removing Four Variables for Each Case Analyzed

▨ Variable Considered

☐ Variable Removed

Predictor	**Response Variables** (X Used, **X** First Split)							R^2 Value	Splits
Lithology	Vp	Resistivity	CSC	Dilatation	VertStress	Grav_Mag	Temp		
---			X			**X**	X	0.442	7
---					**X**	X	▨	0.570	5
Case 5. Removal of CSC plus three other variables									
---	**X**	X		X				0.542	8
---	X	X			**X**			**0.613**	7
---	X			X	**X**			**0.611**	6
---		▨		X	**X**			**0.620**	7
---	**X**	X				X		0.518	7
---	**X**			X		X		0.514	7
---		X		X		**X**		0.376	6
---	X				X	**X**		**0.615**	7
---		X			**X**	▨		0.562	5
---				X	**X**	▨		0.597	6
---	X	X			**X**			**0.613**	7
---	**X**			X		X		0.514	7
---		X		X		**X**		0.376	6
---	X				X	**X**		**0.615**	7
---		X			**X**	▨		0.562	5
---				X	**X**	▨		0.597	6
---	**X**					X	▨	0.530	8
---		X				**X**	▨	0.336	4
---				X		**X**	X	0.445	7
---					**X**	X	▨	0.570	5
Case 6. Removal of Resistivity plus three other variables									
---	**X**		X	X				0.522	7
---	X		X		**X**			0.599	6
---	X			X	**X**			**0.611**	6
---			X	X	**X**			0.597	7
---	**X**		X			X		0.550	9
---	**X**			X		X		0.514	7
---			X	X		**X**		0.472	8
---	X				X	**X**		**0.615**	7
---			▨		**X**	X		0.584	6
---				X	**X**	▨		0.597	6
---	**X**		X			X		0.550	9
---	**X**			X		X		0.514	7
---			X	X		**X**		0.472	8
---	X				**X**		▨	0.570	5
---			X		**X**		▨	0.567	5
---				X	**X**		▨	0.577	5
---	**X**					X	▨	0.530	8

Table 20b.11. CART Sensitivity Analysis for Prediction of Lithology Using Well Data and Removing Four Variables for Each Case Analyzed

▨ Variable Considered

☐ Variable Removed

Predictor	**Response Variables** (X Used, **X** First Split)							R^2 Value	Splits
Lithology	Vp	Resistivity	CSC	Dilatation	VertStress	Grav_Mag	Temp		
---			X			X	X	0.442	7
---				X		X	X	0.445	7
---					X	X		0.570	5
Case 7. Removal of Vp plus three other variables									
---		X	X	X				0.341	7
---		X			X			0.562	5
---				X	X			**0.620**	7
---			X	X	X			0.597	7
---		X	X			X		0.422	5
---		X		X		X		0.376	6
---			X	X		X		0.472	8
---		X			X			0.562	5
---					X	X		0.584	6
---				X	X			0.597	6
---		X	X					0.276	6
---		X		X			X	0.294	7
---			X	X			X	0.341	9
---		X			X			0.562	5
---			X		X			0.567	5
---				X	X			0.577	5
---		X				X		0.336	4
---			X			X	X	0.442	7
---				X		X	X	0.445	7
---					X	X		0.570	5

Table 20b.12. CART Sensitivity Analysis for Prediction of Lithology Using Well Data and Removing Five Variables for Each Case Analyzed

▨ Variable Considered

☐ Variable Removed

Predictor	**Response Variables** (X Used, **X** First Split)							R^2 Value	Splits
Lithology	Vp	Resistivity	CSC	Dilatation	VertStress	Grav_Mag	Temp		
Case 1. Removal of Temperature plus four other variables									
---	X	X						0.415	6
---	X		X					0.518	8
---		X	X					0.310	7
---	X			X				0.550	8
---		X		X				0.305	5
---			X	X				0.366	8
---	X				X			0.583	6
---		X			X			0.562	5
---			X		X			0.567	5
---				X	X			**0.615**	7
---	X					X		0.532	8
---		X				X		0.340	5
---			X			X		0.463	8
---				X		X		0.418	7
---					X	X		**0.600**	7
Case 2. Removal of Grav_Mag plus four other variables									
---	X	X						0.415	6
---	X		X					0.518	8
---		X	X					0.310	7
---	X			X				0.550	8
---		X		X				0.305	5
---			X	X				0.366	8
---	X				X			0.583	6
---		X			X			0.562	5
---			X		X			0.567	5
---				X	X			**0.615**	7
---	X						X	0.352	4
---		X					X	0.174	4
---			X				X	0.133	3
---				X			X	0.266	5
---					X			0.552	5
Case 3. Removal of Vertical Stress plus four other variables									
---	X	X						0.415	6
---	X		X					0.518	8
---		X	X					0.310	7
---	X			X				0.550	8
---		X		X				0.305	5
---			X	X				0.366	8
---	X					X		0.532	8
---		X				X		0.340	5
---			X			X		0.463	8
---				X		X		0.418	7

Table 20b.12. CART Sensitivity Analysis for Prediction of Lithology Using Well Data and Removing Five Variables for Each Case Analyzed

▨ Variable Considered

☐ Variable Removed

Predictor	Response Variables (X Used, **X** First Split)							R^2 Value	Splits
Lithology	Vp	Resistivity	CSC	Dilatation	VertStress	Grav_Mag	Temp		
---	**X**						X	0.352	4
---		**X**					X	0.174	4
			X				X	0.133	3
---				**X**			X	0.266	5
---						**X**	X	0.309	3
Case 4. Removal of Dilatation plus four other variables									
---	**X**	X						0.415	6
---	**X**		X					0.518	8
---		**X**	X					0.310	7
---	X				**X**			0.583	6
---		X			**X**			0.562	5
---			X		**X**			0.567	5
---	**X**					X		0.532	8
---		X				**X**		0.340	5
---			X			**X**		0.463	8
---					**X**	X		**0.600**	7
---	**X**						X	0.352	4
---		**X**					X	0.174	4
---			**X**				X	0.133	3
---					**X**			0.552	5
---						**X**	X	0.309	3
Case 5. Removal of CSC plus four other variables									
---	**X**	X						0.415	6
	X			X				0.550	8
---		X		**X**				0.305	5
---	X				**X**			0.583	6
---		X			**X**			0.562	5
---				X	**X**			**0.615**	7
---	**X**					X		0.532	8
---		X				**X**		0.340	5
---				X		**X**		0.418	7
---					**X**	X		**0.600**	7
---	**X**						X	0.352	4
---		**X**					X	0.174	4
---				**X**			X	0.266	5
---					**X**			0.552	5
---						**X**	X	0.309	3
Case 6. Removal of Resistivity plus four other variables									
---	**X**		X					0.518	8
---	**X**			X				0.550	8
---			X	**X**				0.366	8
---	X				**X**			0.583	6
---			X		**X**			0.567	5

Table 20b.12. CART Sensitivity Analysis for Prediction of Lithology Using Well Data and Removing Five Variables for Each Case Analyzed

▨ Variable Considered

☐ Variable Removed

Predictor	**Response Variables** (X Used, **X** First Split)							R^2 Value	Splits
Lithology	Vp	Resistivity	CSC	Dilatation	VertStress	Grav_Mag	Temp		
---				X	**X**			**0.615**	7
---	**X**					X		0.532	8
---			X			**X**		0.463	8
---				X		**X**		0.418	7
---					**X**	X		**0.600**	7
---	**X**						X	0.352	4
---			**X**				X	0.133	3
---				**X**			X	0.266	5
---					**X**		▨	0.552	5
---						**X**	X	0.309	3
Case 7. Removal of Vp plus four other variables									
---		**X**	X					0.310	7
---		X		**X**				0.305	5
---			X	**X**				0.366	8
---		X			**X**			0.562	5
---			X		**X**			0.567	5
---				X	**X**			**0.615**	7
---		X				**X**		0.340	5
---			X			**X**		0.463	8
				X		**X**		0.418	7
---					**X**	X		**0.600**	7
---		**X**					X	0.174	4
---			**X**				X	0.133	3
---				**X**			X	0.266	5
---					**X**		▨	0.552	5
---						**X**	X	0.309	3

Table 20b13. CART Sensitivity Analysis for Prediction of Lithology Using Well Data and Removing Six Variables for Each Case Analyzed

▨ Variable Considered

☐ Variable Removed

Predictor	**Response Variables** (X Used, **X** First Split)							R^2 Value	Splits
Lithology	Vp	Resistivity	CSC	Dilatation	VertStress	Grav_Mag	Temp		
Case 1. Removal of six variables systematically									
---							X	0.089	4
---						X		0.284	2
---					X			0.552	5
---				X				0.279	5
---			X					0.254	6
---		X						0.204	5
---	X							0.408	5

APPENDIX 20c

CLASSIFICATION AND REGRESSION TREE (CART) SENSITIVITY ANALYSIS PREDICTING PRODUCTIVE VS. NON-PRODUCTIVE CELLS USING WELL DATA

Table of Contents

List of Tables

1. INTRODUCTION

This analysis was performed to understand the predictive powers and relationships between seven key geoscience parameters using CART. This statistical method was utilized using JMP Pro 9.0, part of the SAS Predictive Analytics Suite.

The following series of tables document the CART sensitivity analysis exploring all possibilities of the indicated parameters (Table 20c.1) for predicting the productive vs. non-productive nature of a given cell. Each parameter (response variable) is systematically removed from the analysis starting with one variable removed and ending with six out of the seven variables removed, presented in Tables 20c.2 to 20c.7. Parameters considered in the analysis are highlighted in light purple, while if the parameter was used in the analysis, the cell also has a X. The parameter that the analysis first splits on contains a red X. Parameters that have been removed from the analysis are blank (highlighted white).

The R^2 value corresponds to the accuracy of CART to predict productive vs. non-productive cells using the Well Data according to the divisions of the data used. The range of R^2 values results are from 0.055 to 0.665, while all values over **0.6** are bolded. A color scheme (green-yellow-orange-red) was implemented to distinguish the relative range of R^2 values per individual analysis, with red representing high values, and green representing low values. The # of splits was recorded as each analysis was terminated due to the split history curve "leveling out" and the R^2 value not increasing substantially as the analysis continued to split on the remaining data. The analysis was also terminated if the cross-validation curve (a separate automatic analysis performed with a sub-set of the remaining data) was not in agreement with the expressed R^2 value.

Table 20c.1 Geoscience Parameters Description Used in this Analysis.

Parameter	Description
Productive	Cells occurring as incremental depth slices (500m) of well are considered productive (hydrothermal) if they contain known injection or production zones or are considered sub-commercial at that depth. Non-productive cells include all other cells.
Lith	Lithology, specifically referring to a lithologic unit.
Vp	Seismic parameter: P-wave velocity
Resistivity	Magneto-telluric data
Dilatation	Dilatation derived from modeled stress data
VertStress	Vertical Stress: calculated parameter
Grav_Mag	Combined Gravity and Magnetic inferred Lithologic Unit
Temp	Temperature derived from AltaRock thermal models (see Plates 1 and 2)

Table 20c.2. CART Sensitivity Analysis for Prediction of Productive vs. Non-Productive Cells Using Well Data and Removing One Variable for Each Case Analyzed.

▨ Variable Considered

☐ Variable Removed

Predictor	**Response Variables** (X Used, **X** First Split)							R^2 Value	Splits
Productive	Vp	Resistivity	Lithology	Dilatation	VertStress	Grav_Mag	Temp		
Case 1: All Variables Considered with each parameter systematically removed									
---	X	X	X	X	X	X	X	**0.625**	6
---	X	X	X		X			**0.617**	6
---	X		X		X			0.589	5
---	X	X	X					0.528	4
---	X	X	X		X			0.561	6
---				X	X	X		0.447	5
---			X	X	X			0.527	4
---		X	X	X	X			0.524	5

Table 20c.3. CART Sensitivity Analysis for Prediction of Productive vs. Non-Productive Cells Using Well Data and Removing Two Variables for Each Case Analyzed. The Base Case has One Variable Removed.

Variable Considered
Variable Removed
Baseline Case

Predictor	**Response Variables** (X Used, **X** First Split)							R^2 Value	Splits
Productive	Vp	Resistivity	Lithology	Dilatation	VertStress	Grav_Mag	Temp		
Case 1. All Variables excluding Temperature (Temp) + one variable									
	X	X	X		X			**0.617**	6
	X	X	X		X			**0.647**	8
	X	X	X	X				**0.615**	6
	X	X	X		X	X		0.576	6
				X	X	X		0.442	4
	X		X		X			**0.663**	7
		X	X	X	X			0.574	6
Case 2. All Variables excluding Gravity and Magnetic inferred Lithology (Grav_Mag) + one variable									
	X		X		X			0.589	5
	X	X	X		X			**0.647**	8
		X	X	X				0.507	5
	X	X	X		X			**0.637**	8
	X			X	X			0.431	6
			X	X	X			0.534	4
		X	X	X	X			0.534	5
Case 3. All Variables excluding Vertical Stress (VertStress) + one variable									
	X	X	X					0.528	4
	X	X	X	X				**0.615**	6
		X	X	X				0.507	5
	X	X	X			X	X	0.540	6
	X	X		X		X		0.363	6
	X		X					0.583	4
		X	X	X		X		0.581	7
Case 4. All Variables excluding Dilatation + one variable									
	X	X	X		X			0.561	6
	X	X	X		X	X		0.576	6
	X	X	X		X			**0.637**	8
	X	X	X			X	X	0.540	6
	X	X			X	X		0.512	8
	X		X		X			**0.607**	5
		X	X		X			0.460	4
Case 5. All Variables excluding Lithology + one variable									
				X	X	X		0.447	5
				X	X	X		0.442	4
	X			X	X			0.431	6
	X	X		X		X		0.363	6
	X	X			X	X		0.512	8
	X			X	X	X		0.498	7

Table 20c.3. CART Sensitivity Analysis for Prediction of Productive vs. Non-Productive Cells Using Well Data and Removing Two Variables for Each Case Analyzed. The Base Case has One Variable Removed.

🟪 Variable Considered

⬜ Variable Removed

🟧 Baseline Case

Predictor	**Response Variables** (X Used, **X** First Split)							R^2 Value	Splits
Productive	Vp	Resistivity	Lithology	Dilatation	VertStress	Grav_Mag	Temp		
Case 6. All Variables excluding Resistivity + one variable									
			X	X	X			0.527	4
	X		**X**		X			**0.663**	7
			X	X	X			0.534	4
	X		**X**					0.583	4
	X		**X**		X			**0.607**	5
	X			X	X	**X**		0.498	7
			X	X	X	X		0.594	7
Case 7. All Variables excluding P-wave Velovity (Vp) + one variable									
		X	**X**	X	X			0.524	5
		X	**X**	X	X			0.574	6
		X	**X**	X	X			0.534	5
		X	**X**	X		X		0.581	7
		X	**X**		X			0.460	4
				X	X	**X**		0.458	5
			X	X	X	X		0.594	7

Table 20c.4. CART Sensitivity Analysis for Prediction of Productive vs. Non-Productive Cells Using Well Data and Removing Three Variables for Each Case Analyzed. The response variable (parameter) CSC was used instead of Lithology. This produced lower overall R^2 values and the determination that the parameter (CSC) is not useful in predicting productive vs. non-productive cells. The remaining analyses used lithology as a primary response variable, and did not consider CSC.

▨ Variable Considered

☐ Variable Removed

Predictor	**Response Variables** (X Used, **X** First Split)							R^2 Value	Splits
Productive	Vp	Resistivity	CSC	Dilatation	VertStress	Grav_Mag	Temp		
Case 1. Removal of Temperature (Temp) plus two variables									
---	**X**	X	X	X				0.384	5
---		X	X		**X**			**0.604**	8
---		X		X	**X**			**0.665**	8
---				X	**X**			**0.664**	8
---				X	**X**			**0.663**	8
---	**X**	X				X		0.403	5
---	**X**	X		X		X		0.433	6
---	X			**X**		X		0.368	6
---		X		**X**		X		0.376	6
---		X			**X**	X		**0.635**	8
---			X		**X**	X		**0.621**	8
---		X			**X**	X		**0.636**	8
---				X	**X**			**0.662**	8
---		X		X	**X**			**0.663**	8
---				X	**X**			**0.664**	8
Case 2. Removal of Gravity and Magnetic inferred Lithology (Grav_Mag) plus two variables									
---	**X**	X	X	X				0.384	5
---		X	X		**X**			**0.604**	8
---		X		X	**X**			**0.665**	8
---				X	**X**			**0.664**	8
---				X	**X**			**0.663**	8
---	**X**	X					X	0.365	4
---	**X**	X		X				0.383	4
---	**X**			X				0.407	6
---		X		**X**			X	0.408	7
---		X			**X**			**0.611**	8
---			X		**X**			0.578	7
---		X	X		**X**			**0.615**	8
---				X	**X**			**0.653**	7
---				X	**X**			**0.629**	6
---				X	**X**			**0.654**	7
Case 3. Removal of Vertical Stress (VertStress) plus two variables									
---	**X**	X	X	X				0.384	5
---	**X**	X				X		0.403	5
---	**X**	X		X		X		0.433	6

Table 20c.4. CART Sensitivity Analysis for Prediction of Productive vs. Non-Productive Cells Using Well Data and Removing Three Variables for Each Case Analyzed. The response variable (parameter) CSC was used instead of Lithology. This produced lower overall R^2 values and the determination that the parameter (CSC) is not useful in predicting productive vs. non-productive cells. The remaining analyses used lithology as a primary response variable, and did not consider CSC.

▨ Variable Considered

☐ Variable Removed

Predictor	**Response Variables** (X Used, **X** First Split)							R^2 Value	Splits
Productive	Vp	Resistivity	CSC	Dilatation	VertStress	Grav_Mag	Temp		
---	X			**X**		X		0.368	6
---		X		**X**		X		0.376	6
---	**X**	X					X	0.365	4
---	**X**	X		X				0.383	4
---	**X**			X				0.407	6
---		X		**X**			X	0.408	7
---	**X**	X				X	X	0.423	7
---	**X**		X			X		0.385	4
---		X				**X**	X	0.367	5
---	**X**			X		X		0.416	4
---		X		**X**		X	X	0.388	5
---				**X**		X	X	0.393	5
Case 4. Removal of Dilatation plus two variables									
---		X	X		**X**			**0.604**	8
---	**X**	X				X		0.403	5
---		X			**X**	X		**0.635**	8
---			X		**X**	X		**0.621**	8
---		X			**X**	X		**0.636**	8
---	**X**	X					X	0.365	4
---		X			**X**			**0.611**	8
---			X		**X**			0.578	7
---		X	X		**X**			**0.615**	8
---	**X**	X				X	X	0.423	7
---	**X**		X			X		0.385	4
---		X				**X**	X	0.367	5
---					**X**	X		0.555	5
---		X			**X**	X		0.553	4
---					**X**	X		0.523	4
Case 5. Removal of LIthology plus two variables									
---		X		X	**X**			**0.665**	8
---	**X**	X		X		X		0.433	6
---		X			**X**	X		**0.635**	8
---				X	**X**			**0.662**	8
---		X		X	**X**			**0.663**	8
---	**X**	X		X				0.383	4
---		X			**X**			**0.611**	8
---				X	**X**			**0.653**	7
---				X	**X**			**0.629**	6
---	**X**	X				X	X	0.423	7

Table 20c.4. CART Sensitivity Analysis for Prediction of Productive vs. Non-Productive Cells Using Well Data and Removing Three Variables for Each Case Analyzed. The response variable (parameter) CSC was used instead of Lithology. This produced lower overall R^2 values and the determination that the parameter (CSC) is not useful in predicting productive vs. non-productive cells. The remaining analyses used lithology as a primary response variable, and did not consider CSC.

Variable Considered

Variable Removed

Predictor	Response Variables (X Used, **X** First Split)							R^2 Value	Splits
Productive	Vp	Resistivity	CSC	Dilatation	VertStress	Grav_Mag	Temp		
---	X			X		X		0.416	4
---		X		X		X	X	0.388	5
---					X	X		0.555	5
---		X			X	X		0.553	4
---				X	X			**0.654**	7
Case 6. Removal of Resisitivity plus two variables									
---				X	X			**0.664**	8
---	X			X		X		0.368	6
---			X		X	X		**0.621**	8
---				X	X			**0.662**	8
---				X	X			**0.664**	8
---	X			X				0.407	6
---			X		X			0.578	7
---				X	X			**0.653**	7
---				X	X			**0.654**	7
---	X		X			X		0.385	4
---	X			X		X		0.416	4
---				X		X	X	0.393	5
---					X	X		0.555	5
---					X	X		0.523	4
---				X	X			**0.654**	7
Case 7. Removal of P-wave velocity (Vp) plus two variables									
---				X	X			**0.663**	8
---		X		X		X		0.376	6
---		X			X	X		**0.636**	8
---		X		X	X			**0.663**	8
---				X	X			**0.664**	8
---		X		X			X	0.408	7
---		X	X		X			**0.615**	8
---				X	X			**0.629**	6
---				X	X			**0.654**	7
---		X				X	X	0.367	5
---		X		X		X	X	0.388	5
---				X		X	X	0.393	5
---		X			X	X		0.553	4
---					X	X		0.523	4
---				X	X			**0.654**	7

Table20c.5. CART Sensitivity Analysis for Prediction of Productive vs. Non-Productive Cells Using Well Data and Removing Four Variables for Each Case Analyzed.

▨ Variable Considered

☐ Variable Removed

Predictor	**Response Variables** (X Used, **X** First Split)							R^2 Value	Splits
Productive	Vp	Resistivity	Lithology	Dilatation	VertStress	Grav_Mag	Temp		
Case 1. Removal of Temperature plus three other variables									
---	X	X	X					0.594	6
---	X	X		X				0.425	7
---	X		X	X				0.598	5
---		X	X	X				0.502	4
---	X	X			X			0.496	8
---	X		X		X			**0.648**	6
---		X	X		X			0.596	7
---	X			X	X			0.486	7
---				X	X			0.493	5
---			X	X	X			0.526	4
---	X					X		0.320	4
---	X		X					0.567	4
---		X	X					0.450	3
---	X			X		X		0.394	5
---				X		X		0.395	3
---			X	X		X		0.478	3
---	X				X	X		0.485	6
---		X			X	X		0.425	6
---			X		X	X		0.571	5
---				X	X	X		0.439	4
Case 2. Removal of Grav_Mag plus three other variables									
---	X	X	X					0.594	6
---	X	X		X				0.425	7
---	X		X	X				0.598	5
---		X	X	X				0.502	4
---	X	X			X			0.496	8
---	X		X		X			**0.648**	6
---		X	X		X			0.596	7
---	X			X	X			0.486	7
---				X	X			0.493	5
---			X	X	X			0.526	4
---	X	X						0.334	5
---	X		X					0.505	3
---		X	X				X	0.445	3
---	X			X			X	0.357	5
---		X		X				0.281	5
---			X	X			X	0.525	7
---	X				X			0.465	7
---		X			X			0.361	4
---			X		X		X	0.473	4
---				X	X			0.484	5

Table20C.5. CART Sensitivity Analysis for Prediction of Productive vs. Non-Productive Cells Using Well Data and Removing Four Variables for Each Case Analyzed

▨ Variable Considered

☐ Variable Removed

Predictor	Response Variables (X Used, **X** First Split)							R^2 Value	Splits
Productive	Vp	Resistivity	Lithology	Dilatation	VertStress	Grav_Mag	Temp		
Case 3. Removal of Vertical Stress plus three other variables									
---	X	X	X					0.594	6
---	X	X		X				0.425	7
---	X		X	X				0.598	5
---		X	X	X				0.502	4
---	X					X		0.320	4
---	X		X					0.567	4
---		X	X					0.450	3
---	X			X		X		0.394	5
---				X		X		0.395	3
---			X	X		X		0.478	3
	X	X						0.334	5
---	X		X					0.505	3
---		X	X				X	0.445	3
---	X			X			X	0.357	5
---		X		X				0.281	5
---			X	X			X	0.525	7
---	X					X		0.325	4
---		X				X		0.206	5
---			X			X	X	0.494	4
---				X		X		0.352	4
Case 4. Removal of Dilatation plus three other variables									
---	X	X	X					0.594	6
---	X	X			X			0.496	8
---	X		X		X			**0.648**	6
---		X	X		X			0.596	7
---	X					X		0.320	4
---	X		X					0.567	4
---		X	X					0.450	3
---	X				X	X		0.485	6
---		X			X	X		0.425	6
---			X		X	X		0.571	5
	X	X						0.334	5
---	X		X					0.505	3
---		X	X				X	0.445	3
---	X				X			0.465	7
---		X			X			0.361	4
---			X		X		X	0.473	4
---	X					X		0.325	4
---		X				X		0.206	5
---			X			X	X	0.494	4

Table20c.5. CART Sensitivity Analysis for Prediction of Productive vs. Non-Productive Cells Using Well Data and Removing Four Variables for Each Case Analyzed.

▨ Variable Considered

☐ Variable Removed

Predictor	**Response Variables** (X Used, **X** First Split)							R^2 Value	Splits
Productive	Vp	Resistivity	Lithology	Dilatation	VertStress	Grav_Mag	Temp		
---					X	**X**	X	0.437	6
Case 5. Removal of Lithology plus three other variables									
---	**X**	X		X				0.425	7
---	**X**	X			X			0.496	8
---	**X**			X	X			0.486	7
---				X	**X**			0.493	5
---	X					**X**		0.320	4
---	X			X		**X**		0.394	5
---				X		**X**		0.395	3
---	X				X	**X**		0.485	6
---		X			X	**X**		0.425	6
---				X	X	**X**		0.439	4
---	**X**	X						0.334	5
---	**X**			X			X	0.357	5
---		X		**X**				0.281	5
---	**X**				X			0.465	7
---		X			**X**			0.361	4
---				X	**X**			0.484	5
---	X					**X**		0.325	4
---		X				**X**		0.206	5
---				X		**X**		0.352	4
---					X	**X**	X	0.437	6
Case 6. Removal of Resistivity plus three other variables									
---	X		**X**	X				0.598	5
---	X		**X**		X			**0.648**	6
---	**X**			X	X			0.486	7
---			**X**	X	X			0.526	4
---	X		**X**					0.567	4
---	X			X		**X**		0.394	5
---			**X**	X		X		0.478	3
---	X				X	**X**		0.485	6
---			**X**		X	X		0.571	5
---				X	X	**X**		0.439	4
---	X		**X**					0.505	3
---	**X**			X			X	0.357	5
---			**X**	X			X	0.525	7
---	**X**				X			0.465	7
---			**X**		X		X	0.473	4
---				X	**X**			0.484	5
---	X					**X**		0.325	4
---			**X**			X	X	0.494	4

Table20c.5. CART Sensitivity Analysis for Prediction of Productive vs. Non-Productive Cells Using Well Data and Removing Four Variables for Each Case Analyzed.

▨	Variable Considered
☐	Variable Removed

Predictor	**Response Variables** (X Used, **X** First Split)							R^2 Value	Splits
Productive	Vp	Resistivity	Lithology	Dilatation	VertStress	Grav_Mag	Temp		
---				X		**X**		0.352	4
---					**X**	**X**	X	0.437	6
Case 7. Removal of Vp plus three other variables									
---		X	**X**	X				0.502	4
---		X	**X**		X			0.596	7
---				X	**X**			0.493	5
---			**X**	X	X			0.526	4
---		X	**X**					0.450	3
---				X		**X**		0.395	3
---			**X**	X		X		0.478	3
---		X			X	**X**		0.425	6
---			**X**		X	X		0.571	5
---				X	X	**X**		0.439	4
---		X	**X**				X	0.445	3
---		X		**X**				0.281	5
---			**X**	X			X	0.525	7
---		X			**X**			0.361	4
---			**X**		X		X	0.473	4
---				X	**X**			0.484	5
---		X				**X**		0.206	5
---			**X**			X	X	0.494	4
---				X		**X**		0.352	4
---					X	**X**	X	0.437	6

Table 20c.6. CART Sensitivity Analysis for Prediction of Productive vs. Non-Productive Cells Using Well Data and Removing Five Variables for Each Case Analyzed.

▨ Variable Considered

☐ Variable Removed

Predictor	**Response Variables** (X Used, **X** First Split)							R² Value	Splits
Productive	Vp	Resistivity	Lithology	Dilatation	VertStress	Grav_Mag	Temp		
Case 1. Removal of Temperature plus four other variables									
---	**X**	X						0.358	6
---	X		**X**					0.550	4
---		X	**X**					0.484	3
---	**X**			X				0.350	5
---		X		**X**				0.223	3
---			**X**	X				0.534	4
---	**X**				X			0.427	6
---		X			**X**			0.485	8
---			**X**		X			0.587	6
---				X	**X**			0.513	6
---	X					**X**		0.395	7
---		X				**X**		0.261	4
---			**X**			X		0.458	3
---				X		**X**		0.282	3
---					X	**X**		0.500	7
Case 2. Removal of Grav_Mag plus four other variables									
---	**X**	X						0.358	6
---	X		**X**					0.550	4
---		X	**X**					0.484	3
---	**X**			X				0.350	5
---		X		**X**				0.223	3
---			**X**	X				0.534	4
---	**X**				X			0.427	6
---		X			**X**			0.485	8
---			**X**		X			0.587	6
---				X	**X**			0.513	6
---	**X**						X	0.305	4
---		**X**						0.160	3
---			**X**				X	0.429	2
---				**X**			X	0.154	3
---					**X**		X	0.315	3
Case 3. Removal of Vertical Stress plus four other variables									
---	**X**	X						0.358	6
---	X		**X**					0.550	4
---		X	**X**					0.484	3
---	**X**			X				0.350	5
---		X		**X**				0.223	3
---			**X**	X				0.534	4
---	X					**X**		0.395	7

Table 20c.6. CART Sensitivity Analysis for Prediction of Productive vs. Non-Productive Cells Using Well Data and Removing Five Variables for Each Case Analyzed.

▨	Variable Considered
□	Variable Removed

Predictor	**Response Variables** (X Used, **X** First Split)							R^2 Value	Splits
Productive	Vp	Resistivity	Lithology	Dilatation	VertStress	Grav_Mag	Temp		
---		X				**X**		0.261	4
---			**X**			X		0.458	3
---				X		**X**		0.282	3
---	**X**						X	0.305	4
---		**X**						0.160	3
			X				X	0.429	2
---				**X**			X	0.154	3
---						**X**	X	0.167	2
Case 4. Removal of Dilatation plus four other variables									
---	**X**	X						0.358	6
---	X		**X**					0.550	4
---		X	**X**					0.484	3
---	**X**				X			0.427	6
---		X			**X**			0.485	8
---			**X**		X			0.587	6
---	X					**X**		0.395	7
---		X				**X**		0.261	4
---			**X**			X		0.458	3
---					X	**X**		0.500	7
---	**X**						X	0.305	4
---		**X**						0.160	3
---			**X**				X	0.429	2
---					**X**		X	0.315	3
---						**X**	X	0.167	2
Case 5. Removal of Lithology plus four other variables									
---	**X**	X						0.358	6
	X			X				0.350	5
---		X		**X**				0.223	3
---	**X**				X			0.427	6
---		X			**X**			0.485	8
---				X	**X**			0.513	6
---	X					**X**		0.395	7
---		X				**X**		0.261	4
---				X		**X**		0.282	3
---					X	**X**		0.500	7
---	**X**						X	0.305	4
---		**X**						0.160	3
---				**X**			X	0.154	3
---					**X**		X	0.315	3
---						**X**	X	0.167	2
Case 6. Removal of Resistivity plus four other variables									
---	X		**X**					0.550	4
---	**X**			X				0.350	5
---			**X**	X				0.534	4

Table 20c.6. CART Sensitivity Analysis for Prediction of Productive vs. Non-Productive Cells Using Well Data and Removing Five Variables for Each Case Analyzed.

▨ Variable Considered

☐ Variable Removed

Predictor	Response Variables (X Used, **X** First Split)							R^2 Value	Splits
Productive	Vp	Resistivity	Lithology	Dilatation	VertStress	Grav_Mag	Temp		
---	**X**				X			0.427	6
---			**X**		X			0.587	6
---				X	**X**			0.513	6
---	X					**X**		0.395	7
---			**X**			X		0.458	3
---				X		**X**		0.282	3
---					X	**X**		0.500	7
---	**X**						X	0.305	4
---			**X**				X	0.429	2
---				**X**			X	0.154	3
---					**X**		X	0.315	3
---						**X**	X	0.167	2
Case 7. Removal of Vp plus four other variables									
---		X	**X**					0.484	3
---		X		**X**				0.223	3
---			**X**	X				0.534	4
---		X			**X**			0.485	8
---			**X**		X			0.587	6
---				X	**X**			0.513	6
---		X				**X**		0.261	4
---			**X**			X		0.458	3
				X		**X**		0.282	3
---					X	**X**		0.500	7
---		**X**						0.160	3
---			**X**				X	0.429	2
---				**X**			X	0.154	3
---					**X**		X	0.315	3
---						**X**	X	0.167	2

Table 20c.7. CART Sensitivity Analysis for Prediction of Productive vs. Non-Productive Cells Using Well Data and Removing Six Variables for Each Case

🟪 Variable Considered
⬜ Variable Removed

Predictor	**Response Variables** (X Used, **X** First Split)							R² Value	Splits
Productive	Vp	Resistivity	Lithology	Dilatation	VertStress	Grav_Mag	Temp		
Case 1. Removal of six variables systematically									
---							X	0.055	2
---						X		0.156	2
---					X			0.389	4
---				X				0.282	3
---			X					0.457	4
---		X						0.156	4
---	X							0.29	4

APPENDIX 20d

CLASSIFICATION AND REGRESSION TREE (CART) SENSITIVITY ANALYSIS PREDICTING EXPECTED EGS FAVORABLE CELLS USING WELL DATA

Table of Contents

List of Tables

1. INTRODUCTION

This analysis was performed to understand the predictive powers and relationships between eight key geoscience parameters using CART. This statistical method was utilized using *RStudio*, a publically available user interface for performing various statistics. See www.rstudio.com for more information.

The following series of tables document the CART sensitivity analysis exploring all possibilities of the indicated parameters (Table 20d.1) for predicting expected EGS favorable cells. A total of eight parameters were used as explanatory variables and listed in the table below. The analysis explored every possible combination from eight variables considered to only one variable considered. The results are organized by the number of variables used in the analysis from eight to one, and are reported from the highest to lowest r^2-values (Tables 20d.2 to 20d.9). Selected analyses that are significant are bolded. The explanatory variables used in the analysis are listed in column 1. The number of variables used can be found in column 2. Whether the parameter vertical stress, considered a surrogate for depth that could be influencing the analysis, was used in the analysis is shown in column 3. The resulting r^2-value can be found in column 4.

Table 20d.1. Explanatory Variables used in the CART Sensitivity Analysis.

Notation	Parameter Description
MTemp	Temperature
VS	Vertical Stress
VPS	Seismic parameter: p-wave velocity
Lith	Lithology type
Fault	Presense of Absence of a Fault
MT	Resistivity derived from the Magnetotellurics
CSC	Modeled Stress parameter: Coulomb Stress Change
Dil	Modeled Stress parameter: Dilatational Strain

Table 20d.2. Results from CART Sensitivity Analysis for predicting EGS Favorable Cells with eight variables used out of eight considered.

Variables Used	# Variables Used	Vertical Stress Used	r^2-value
MTemp,VPS,CSC,MT,Dil,Fault,VS,Lith	8	X	0.708

Table 20d.3. Results from CART Sensitivity Analysis for predicting EGS Favorable Cells with seven variables used out of eight considered.

Variables Used	# Variables Used	Vertical Stress Used	r^2-value
MTemp,VPS,CSC,MT,Dil,Fault,VS	7	X	0.727
MTemp,VPS,CSC,MT,Dil,Fault,Lith	7		0.708
MTemp,VPS,CSC,MT,Dil,VS,Lith	7	X	0.708
MTemp,VPS,CSC,Dil,Fault,VS,Lith	7	X	0.708
MTemp,VPS,MT,Dil,Fault,VS,Lith	7	X	0.708
MTemp,CSC,MT,Dil,Fault,VS,Lith	7	X	0.708
VPS,CSC,MT,Dil,Fault,VS,Lith	7	X	0.661
MTemp,VPS,CSC,MT,Fault,VS,Lith	7	X	0.523

Table 20d.4. Results from CART Sensitivity Analysis for predicting EGS Favorable Cells with six variables used out of eight considered.

Variables Used	# Variables Used	Vertical Stress Used	r^2-value
MTemp,VPS,CSC,MT,Dil,Fault	6		0.769
MTemp,VPS,CSC,MT,Dil,VS	6	X	0.727
MTemp,VPS,CSC,Dil,Fault,VS	6	X	0.727
MTemp,VPS,MT,Dil,Fault,VS	6	X	0.727
MTemp,CSC,MT,Dil,Fault,VS	6	X	0.727
MTemp,VPS,CSC,MT,Dil,Lith	6		0.708
MTemp,VPS,CSC,Dil,Fault,Lith	6		0.708
MTemp,VPS,CSC,Dil,VS,Lith	6	X	0.708
MTemp,VPS,MT,Dil,Fault,Lith	6		0.708
MTemp,VPS,MT,Dil,VS,Lith	6	X	0.708
MTemp,VPS,Dil,Fault,VS,Lith	6	X	0.708
MTemp,CSC,MT,Dil,Fault,Lith	6	X	0.708
MTemp,CSC,MT,Dil,VS,Lith	6	X	0.708
MTemp,CSC,Dil,Fault,VS,Lith	6		0.708
MTemp,MT,Dil,Fault,VS,Lith	6	X	0.708
VPS,CSC,MT,Dil,Fault,Lith	6		0.708
VPS,CSC,MT,Dil,VS,Lith	6	X	0.661
VPS,CSC,Dil,Fault,VS,Lith	6	X	0.661
VPS,MT,Dil,Fault,VS,Lith	6	X	0.661
CSC,MT,Dil,Fault,VS,Lith	6	X	0.661
VPS,CSC,MT,Dil,Fault,VS	6	X	0.637
MTemp,VPS,CSC,MT,Fault,VS	6	X	0.578
MTemp,VPS,CSC,MT,VS,Lith	6	X	0.523
MTemp,VPS,CSC,Fault,VS,Lith	6	X	0.523
MTemp,CSC,MT,Fault,VS,Lith	6	X	0.523
VPS,CSC,MT,Fault,VS,Lith	6	X	0.511
MTemp,VPS,CSC,MT,Fault,Lith	6		0.504
MTemp,VPS,MT,Fault,VS,Lith	6	X	0.409

Table 20d.5. Results from CART Sensitivity Analysis for predicting EGS Favorable Cells with five variables used out of eight considered.

Variables Used	# Variables Used	Vertical Stress Used	r^2-value
MTemp,VPS,CSC,MT,Dil	5		0.769
MTemp,VPS,CSC,Dil,Fault	5		0.769
MTemp,VPS,CSC,Dil,VS	5	X	0.727
MTemp,VPS,MT,Dil,VS	5	X	0.727
MTemp,CSC,MT,Dil,VS	5	X	0.727
MTemp,CSC,Dil,Fault,VS	5	X	0.727
MTemp,MT,Dil,Fault,VS	5	X	0.727
MTemp,VPS,CSC,Dil,Lith	5		0.708
MTemp,VPS,MT,Dil,Lith	5		0.708
MTemp,VPS,Dil,Fault,Lith	5		0.708
MTemp,VPS,Dil,VS,Lith	5	X	0.708
MTemp,CSC,MT,Dil,Lith	5		0.708
MTemp,CSC,Dil,Fault,Lith	5		0.708
MTemp,CSC,Dil,VS,Lith	5	X	0.708
MTemp,MT,Dil,Fault,Lith	5		0.708
MTemp,MT,Dil,VS,Lith	5	X	0.708
MTemp,Dil,Fault,VS,Lith	5	X	0.708
VPS,CSC,MT,Dil,Lith	5		0.708
VPS,CSC,Dil,Fault,Lith	5		0.708
VPS,MT,Dil,Fault,Lith	5		0.708
CSC,MT,Dil,Fault,Lith	5		0.708
MTemp,CSC,MT,Dil,Fault	5		0.690
VPS,CSC,Dil,VS,Lith	5	X	0.661
VPS,MT,Dil,VS,Lith	5	X	0.661
VPS,Dil,Fault,VS,Lith	5	X	0.661
CSC,MT,Dil,VS,Lith	5	X	0.661
CSC,Dil,Fault,VS,Lith	5	X	0.661
MT,Dil,Fault,VS,Lith	5	X	0.661
VPS,CSC,MT,Dil,VS	5	X	0.637
VPS,CSC,Dil,Fault,VS	5	X	0.637
VPS,MT,Dil,Fault,VS	5	X	0.637
CSC,MT,Dil,Fault,VS	5	X	0.637
MTemp,VPS,CSC,MT,Fault	5		0.619
MTemp,VPS,MT,Dil,Fault	5		0.579
MTemp,VPS,CSC,Fault,VS	5	X	0.578
MTemp,CSC,MT,Fault,VS	5	X	0.578
VPS,CSC,MT,Dil,Fault	5		0.547
MTemp,VPS,CSC,VS,Lith	5	X	0.523
MTemp,CSC,MT,VS,Lith	5	X	0.523
MTemp,CSC,Fault,VS,Lith	5	X	0.523
MTemp,VPS,MT,Fault,VS	5	X	0.517
VPS,CSC,MT,VS,Lith	5	X	0.511

Table 20d.5. Results from CART Sensitivity Analysis for predicting EGS Favorable Cells with five variables used out of eight considered.

Variables Used	# Variables Used	Vertical Stress Used	r^2-value
VPS,CSC,Fault,VS,Lith	5	X	0.511
CSC,MT,Fault,VS,Lith	5	X	0.511
MTemp,VPS,CSC,MT,Lith	5		0.504
MTemp,VPS,CSC,Fault,Lith	5		0.504
MTemp,CSC,MT,Fault,Lith	5		0.504
VPS,CSC,MT,Fault,Lith	5		0.480
VPS,CSC,MT,Fault,VS	5	X	0.477
MTemp,VPS,MT,Fault,Lith	5		0.425
MTemp,VPS,MT,VS,Lith	5	X	0.409
MTemp,VPS,Fault,VS,Lith	5	X	0.409
MTemp,MT,Fault,VS,Lith	**5**	**X**	**0.409**
VPS,MT,Fault,VS,Lith	5	X	0.383

Table 20d.6. Results from CART Sensitivity Analysis for predicting EGS Favorable Cells with four variables used out of eight considered.

Variables Used	# Variables Used	Vertical Stress Used	r^2-value
MTemp,VPS,CSC,Dil	**4**		**0.769**
MTemp,VPS,Dil,VS	4	X	0.727
MTemp,CSC,Dil,VS	4	X	0.727
MTemp,MT,Dil,VS	4	X	0.727
MTemp,Dil,Fault,VS	4	X	0.727
MTemp,VPS,Dil,Fault,VS	4	X	0.727
MTemp,VPS,Dil,Lith	4		0.708
MTemp,CSC,Dil,Lith	4		0.708
MTemp,MT,Dil,Lith	4		0.708
MTemp,Dil,Fault,Lith	4		0.708
MTemp,Dil,VS,Lith	4	X	0.708
VPS,CSC,Dil,Lith	4		0.708
VPS,MT,Dil,Lith	4		0.708
VPS,Dil,Fault,Lith	4		0.708
CSC,MT,Dil,Lith	4		0.708
CSC,Dil,Fault,Lith	4		0.708
MT,Dil,Fault,Lith	4		0.708
MTemp,CSC,MT,Dil	4	X	0.690
CSC,MT,Dil,Fault	4		0.673
VPS,Dil,VS,Lith	4	X	0.661
CSC,Dil,VS,Lith	4	X	0.661
MT,Dil,VS,Lith	4	X	0.661
Dil,Fault,VS,Lith	4	X	0.661
MTemp,CSC,Dil,Fault	4		0.654
VPS,CSC,Dil,VS	4	X	0.637
VPS,MT,Dil,VS	4	X	0.637
VPS,Dil,Fault,VS	4	X	0.637
CSC,MT,Dil,VS	4	X	0.637
CSC,Dil,Fault,VS	4	X	0.637
MT,Dil,Fault,VS	4	X	0.637
MTemp,VPS,CSC,MT	4		0.619
MTemp,VPS,CSC,Fault	4		0.619
MTemp,VPS,Dil,Fault	4		0.611
MTemp,VPS,MT,Dil	4		0.579
MTemp,VPS,CSC,VS	4	X	0.578
MTemp,CSC,MT,VS	4	X	0.578
MTemp,CSC,Fault,VS	4	X	0.578
MTemp,VPS,CSC,MT,VS	4	X	0.578
MTemp,MT,Dil,Fault	4		0.562
VPS,CSC,MT,Dil	4		0.547
VPS,MT,Dil,Fault	4		0.547
MTemp,CSC,MT,Fault	4		0.541

Table 20d.6. Results from CART Sensitivity Analysis for predicting EGS Favorable Cells with four variables used out of eight considered.

Variables Used	# Variables Used	Vertical Stress Used	r^2-value
VPS,CSC,Dil,Fault	4		0.531
MTemp,CSC,VS,Lith	4	X	0.523
MTemp,VPS,MT,VS	4	X	0.517
VPS,CSC,VS,Lith	4	X	0.511
CSC,MT,VS,Lith	4	X	0.511
CSC,Fault,VS,Lith	4	X	0.511
MTemp,VPS,CSC,Lith	4		0.504
MTemp,CSC,MT,Lith	4		0.504
MTemp,CSC,Fault,Lith	4		0.504
VPS,CSC,MT,Lith	4		0.480
VPS,CSC,Fault,Lith	4		0.480
VPS,CSC,MT,VS	4	X	0.477
VPS,CSC,Fault,VS	4	X	0.477
MTemp,VPS,Fault,VS	4	X	0.469
VPS,MT,Fault,Lith	4		0.459
CSC,MT,Fault,Lith	4		0.451
VPS,CSC,MT,Fault	4		0.450
CSC,MT,Fault,VS	4	X	0.445
MTemp,MT,Fault,VS	4	X	0.435
MTemp,VPS,MT,Lith	4		0.425
MTemp,VPS,Fault,Lith	4		0.425
MTemp,MT,Fault,Lith	4		0.425
MTemp,VPS,VS,Lith	4	X	0.409
MTemp,MT,VS,Lith	4	X	0.409
MTemp,Fault,VS,Lith	4	X	0.409
VPS,MT,Fault,VS	4	X	0.409
MTemp,VPS,MT,Fault	4		0.391
VPS,MT,VS,Lith	4	X	0.383
VPS,Fault,VS,Lith	4	X	0.383
MT,Fault,VS,Lith	4	X	0.369

Table 20d.7. Results from CART Sensitivity Analysis for predicting EGS Favorable Cells with three variables used out of eight considered.

Variables Used	# Variables Used	Vertical Stress Used	r^2-value
MTemp,Dil,VS	**3**	**X**	**0.727**
MTemp,Dil,Lith	3		0.708
VPS,Dil,Lith	3		0.708
CSC,Dil,Lith	3		0.708
MT,Dil,Lith	3		0.708
Dil,Fault,Lith	3		0.708
CSC,MT,Dil	3		0.673
Dil,VS,Lith	3	X	0.661
MTemp,CSC,Dil	3		0.654
VPS,Dil,VS	3	X	0.637
CSC,Dil,VS	3	X	0.637
MT,Dil,VS	3	X	0.637
Dil,Fault,VS	3	X	0.637
MT,Dil,Fault	3		0.621
MTemp,VPS,CSC	3		0.619
MTemp,VPS,Dil	3		0.611
MTemp,Dil,Fault	3		0.611
MTemp,CSC,VS	3	X	0.578
MTemp,MT,Dil	3		0.562
VPS,MT,Dil	3		0.547
MTemp,CSC,MT	3		0.541
VPS,CSC,Dil	3		0.531
VPS,Dil,Fault	3		0.531
CSC,Dil,Fault	3		0.525
CSC,VS,Lith	3	X	0.511
MTemp,CSC,Fault	3		0.504
MTemp,CSC,Lith	3		0.504
VPS,CSC,Lith	3		0.48
VPS,CSC,VS	3	X	0.477
CSC,MT,Fault	3		0.47
MTemp,VPS,VS	3	X	0.469
VPS,MT,Lith	3		0.459
CSC,MT,Lith	3		0.451
VPS,CSC,MT	3		0.45
CSC,MT,VS	3	X	0.445
MTemp,MT,Fault	3		0.439
MTemp,MT,VS	3	X	0.435
CSC,Fault,Lith	3		0.435
CSC,Fault,VS	3	X	0.434
MTemp,VPS,Lith	3		0.425
MTemp,MT,Lith	3		0.425
MTemp,Fault,Lith	3		0.425

Table 20d.7. Results from CART Sensitivity Analysis for predicting EGS Favorable Cells with three variables used out of eight considered.

Variables Used	# Variables Used	Vertical Stress Used	r^2-value
VPS,Fault,Lith	3		0.422
VPS,CSC,Fault	3		0.422
MTemp,Fault,VS	3	X	0.414
MTemp,VS,Lith	3	X	0.409
VPS,MT,VS	3	X	0.409
MT,Fault,VS	3	X	0.409
MTemp,VPS,MT	3		0.391
VPS,VS,Lith	3	X	0.383
VPS,Fault,VS	3	X	0.377
MT,VS,Lith	3	X	0.369
VPS,MT,Fault	3		0.343
Fault,VS,Lith	3	X	0.34
MT,Fault,Lith	3		0.331
MTemp,VPS,Fault	3		0.311

Table 20d.8. Results from CART Sensitivity Analysis for predicting EGS Favorable Cells with two variables used out of eight considered.

Variables Used	# Variables Used	Vertical Stress Used	r^2-value
Dil,Lith	**2**		**0.708**
Dil,VS	2	X	0.637
MT,Dil	2		0.621
MTemp,Dil	2		0.611
VPS,Dil	2		0.531
CSC,Dil	2		0.525
MTemp,CSC	2		0.504
CSC,MT	2		0.47
MTemp,MT	2		0.439
CSC,Lith	2		0.435
CSC,VS	2	X	0.434
MTemp,Lith	2		0.425
VPS,Lith	2		0.422
VPS,CSC	2		0.422
MTemp,VS	2	X	0.414
MT,VS	2	X	0.409
Dil,Fault	2		0.398
VPS,VS	2	X	0.377
Fault,VS	2	X	0.349
CSC,Fault	**2**		**0.345**
VPS,MT	2		0.343
VS,Lith	2	X	0.34
MT,Lith	2		0.331
VPS,Fault	2		0.32
MTemp,VPS	2		0.311
Fault,Lith	2		0.303
MT,Fault	2		0.275
MTemp,Fault	2		0.187

Table 20d.9. Results from CART Sensitivity Analysis for predicting EGS Favorable Cells with one variables used out of eight considered.

Variables Used	# Variables Used	Vertical Stress Used	r^2-value
Dil	1		0.398
VS	1	X	0.349
CSC	1		0.345
VPS	1		0.32
Lith	1		0.303
MT	1		0.275
MTemp	1		0.187
Fault	1		0.026

APPENDIX 21

EGS FAVORABILITY AND DATA TRUST MAPPING, AVERGAE DATA AND EQUAL WEIGHTING

Table of Contents

Temp[1] (.32 w[5])	Fav Value[2]	Lith-ology[6] (.32 w)	Fav Value	Stress Sub-parameters (.34 w)							
				C/D [3] (.08 w)	Fav Value	Fault Orientation (.08 w)	Fav Value	Structure Present (.08 w)	Fav Value	CSC [4] (.08 w)	Fav Value
< 100	1	QTbf	1	Compression	4	30-60°	7	Stucture	7	< -22	2
100	1	Tmb	5	Dilation	7	Other	4	None	5	-22	3
125	2	Jz	7	Neither	5	Neither	5			-14	3
150	2	Tr	3							-6	4
175	4	Kgr	9							0	5
200	7	Tv	3							6	6
225	7	Jbr	8							14	7
250	8	Jznm	4							22	8
275	9									> 22	9
300	8										
325	7										
350	5										
> 374	3										

[1] Temperature in °C

[2] Favorability Value

[3] Zones of Compression/Dilation

[4] Coulomb Stress Change

[5] Favorability weights

[6] Lithology formations included the QTbf (Quaternary-Tertiary basin fill), Tmb (Miocene basalt), Jz (Jurassic mafic rocks), Kgr (Cretaceous granodiorite), Tv (Tertiary silicic volcanics), Jbr (Jurassic Boyer Ranch Fm), Jznm (Jurassic non-magnetic mafic rocks)

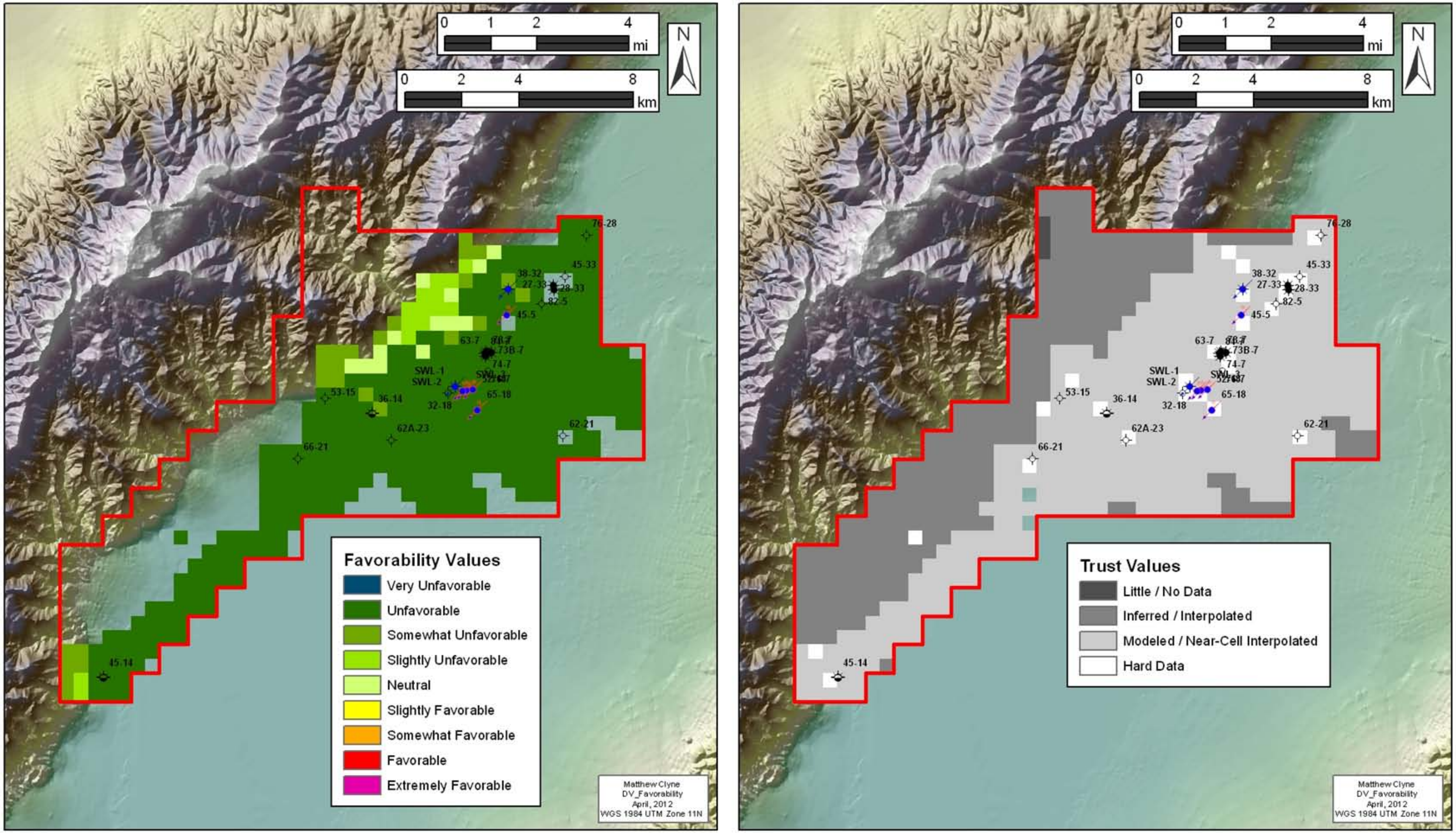

EGS Favorability-Trust Maps: Averaged Data with Equal Weighting
Depth: 1.0km Above Sea Level

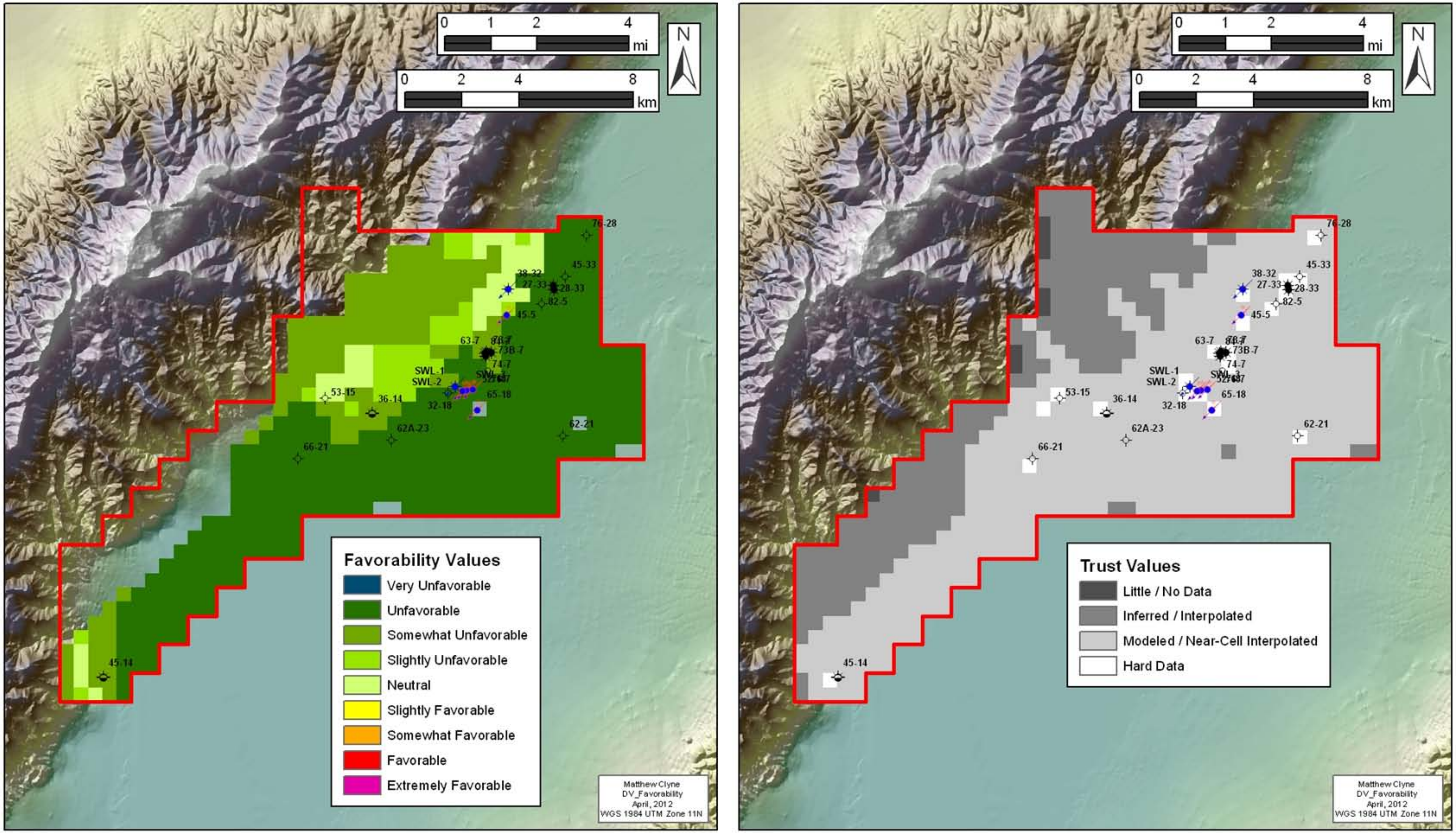

EGS Favorability-Trust Maps: Averaged Data with Equal Weighting
Depth: 0.5km Above Sea Level

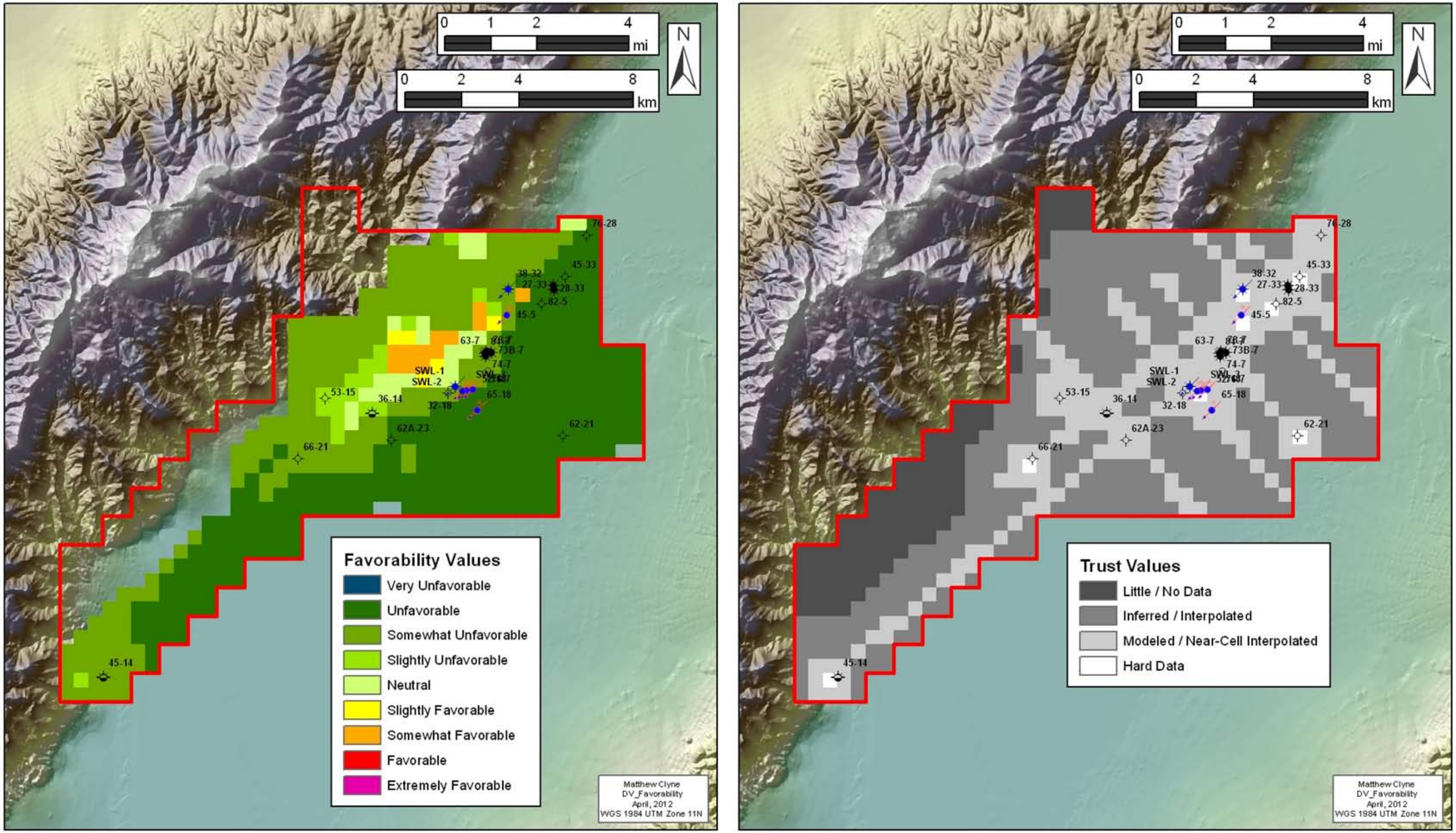

EGS Favorability-Trust Maps: Averaged Data with Equal Weighting
Depth: 0.0km At Sea Level

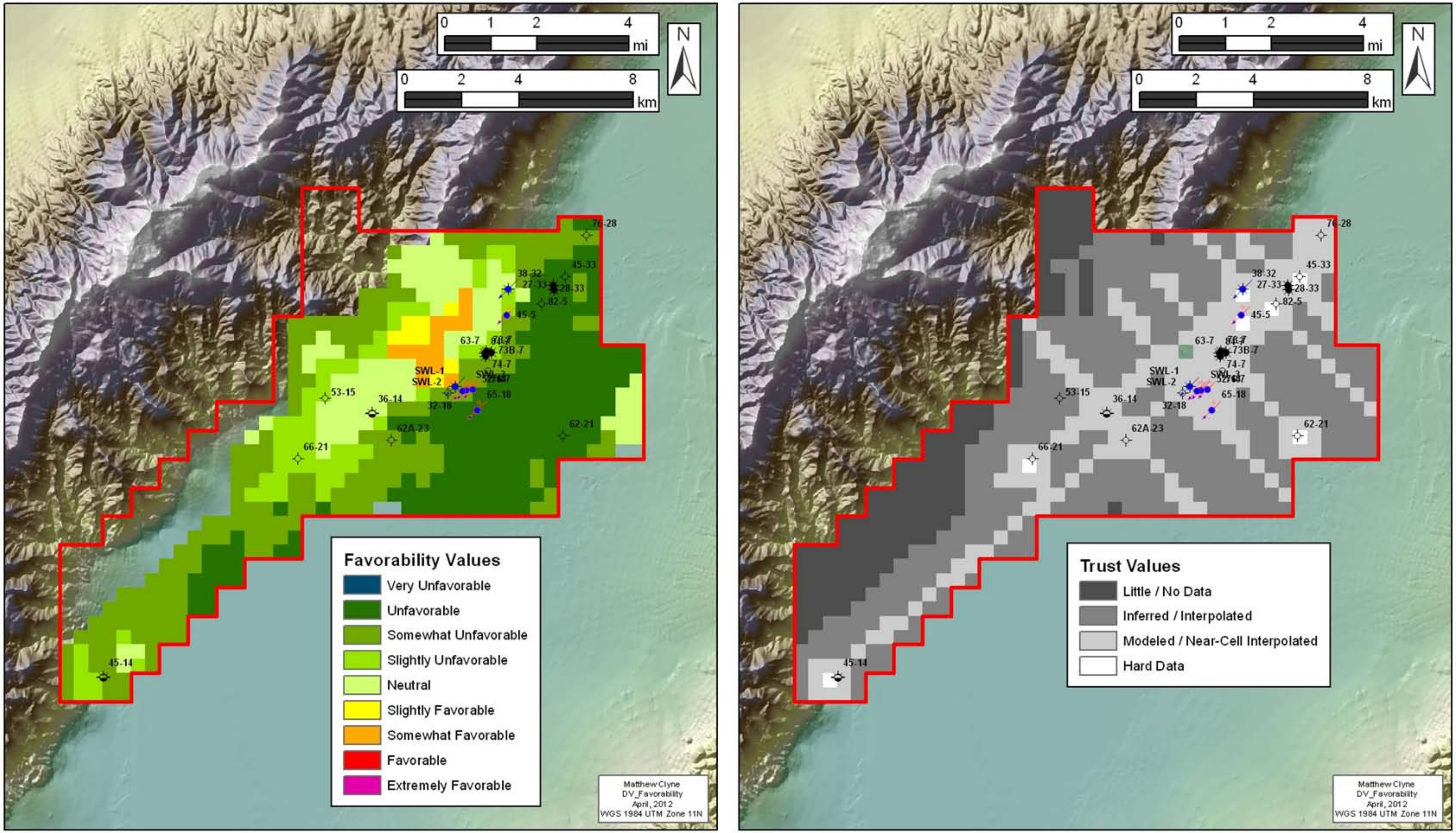

EGS Favorability-Trust Maps: Averaged Data with Equal Weighting
Depth: 0.5km Below Sea Level

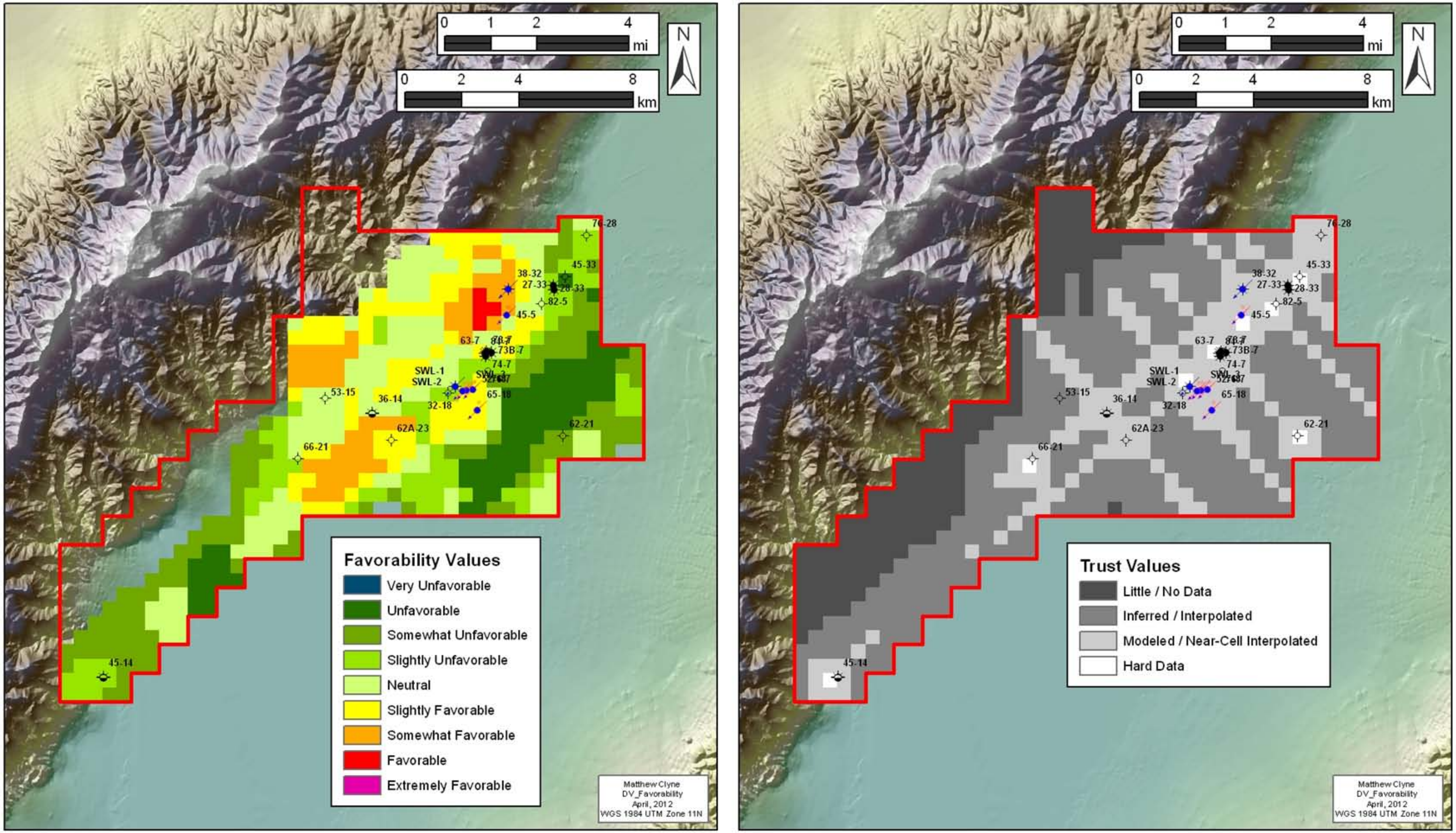

EGS Favorability-Trust Maps: Averaged Data with Equal Weighting
Depth: 1.0km Below Sea Level

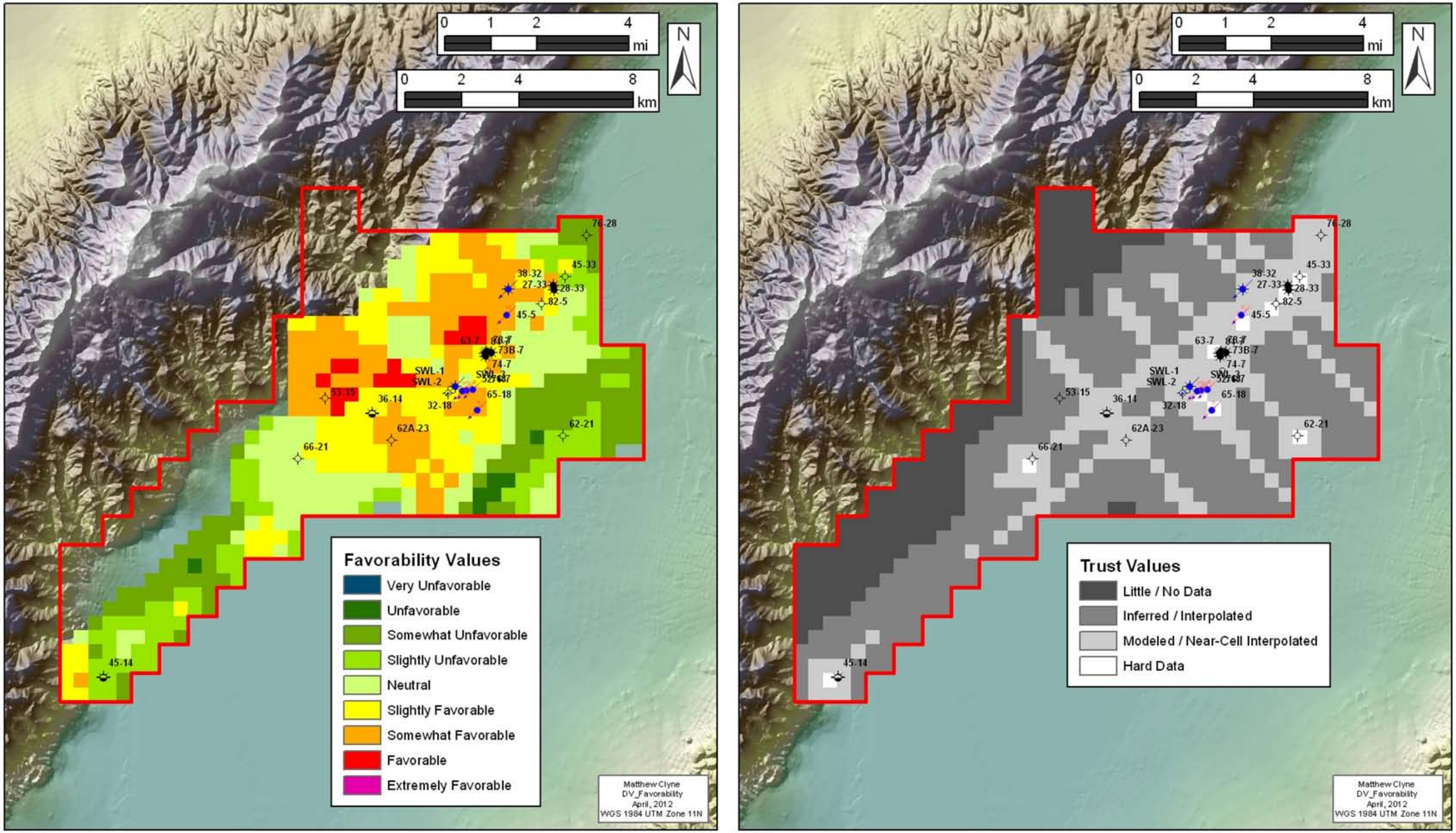

EGS Favorability-Trust Maps: Averaged Data with Equal Weighting
Depth: 1.5km Below Sea Level

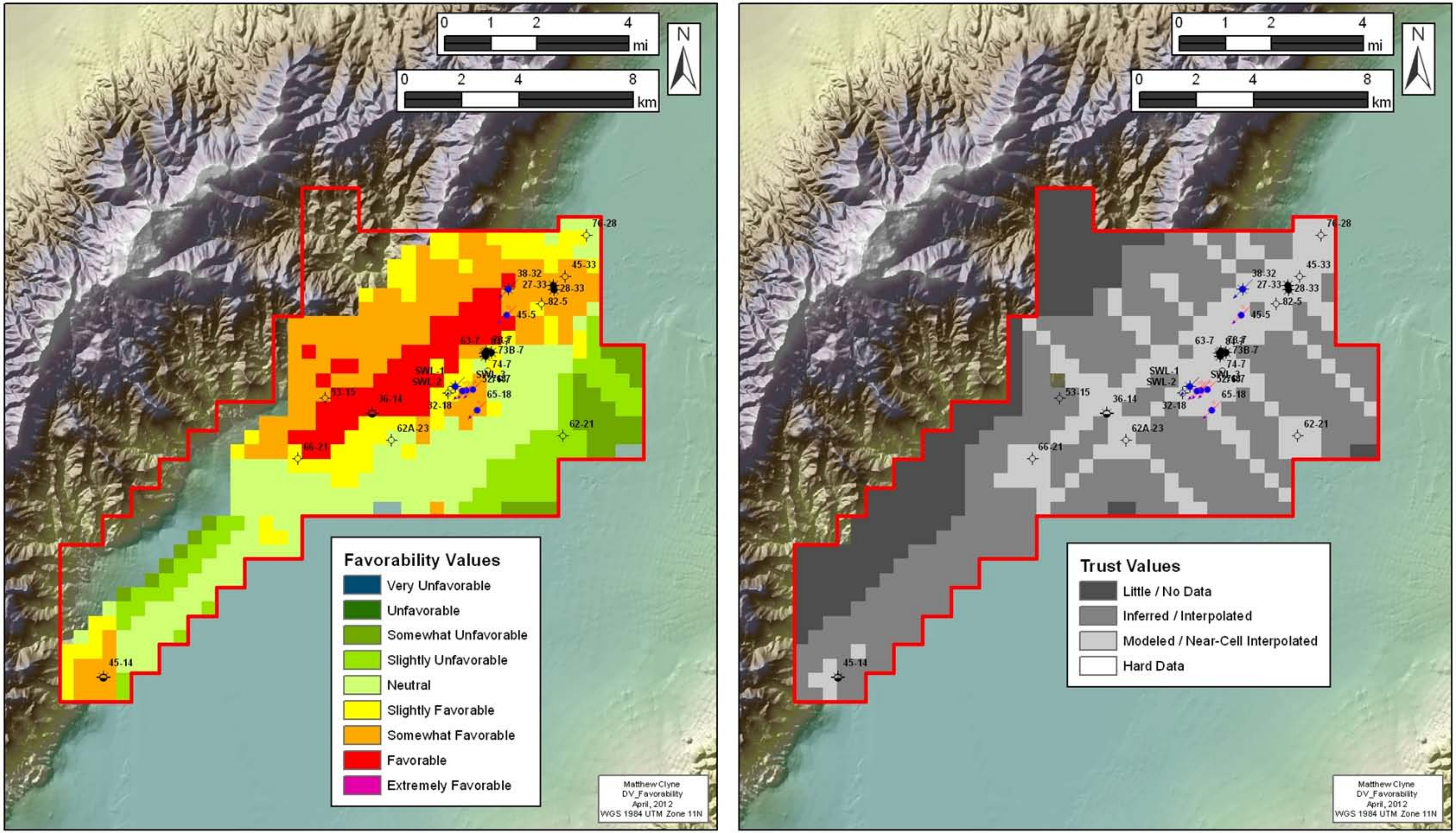

EGS Favorability-Trust Maps: Averaged Data with Equal Weighting
Depth: 2.0km Below Sea Level

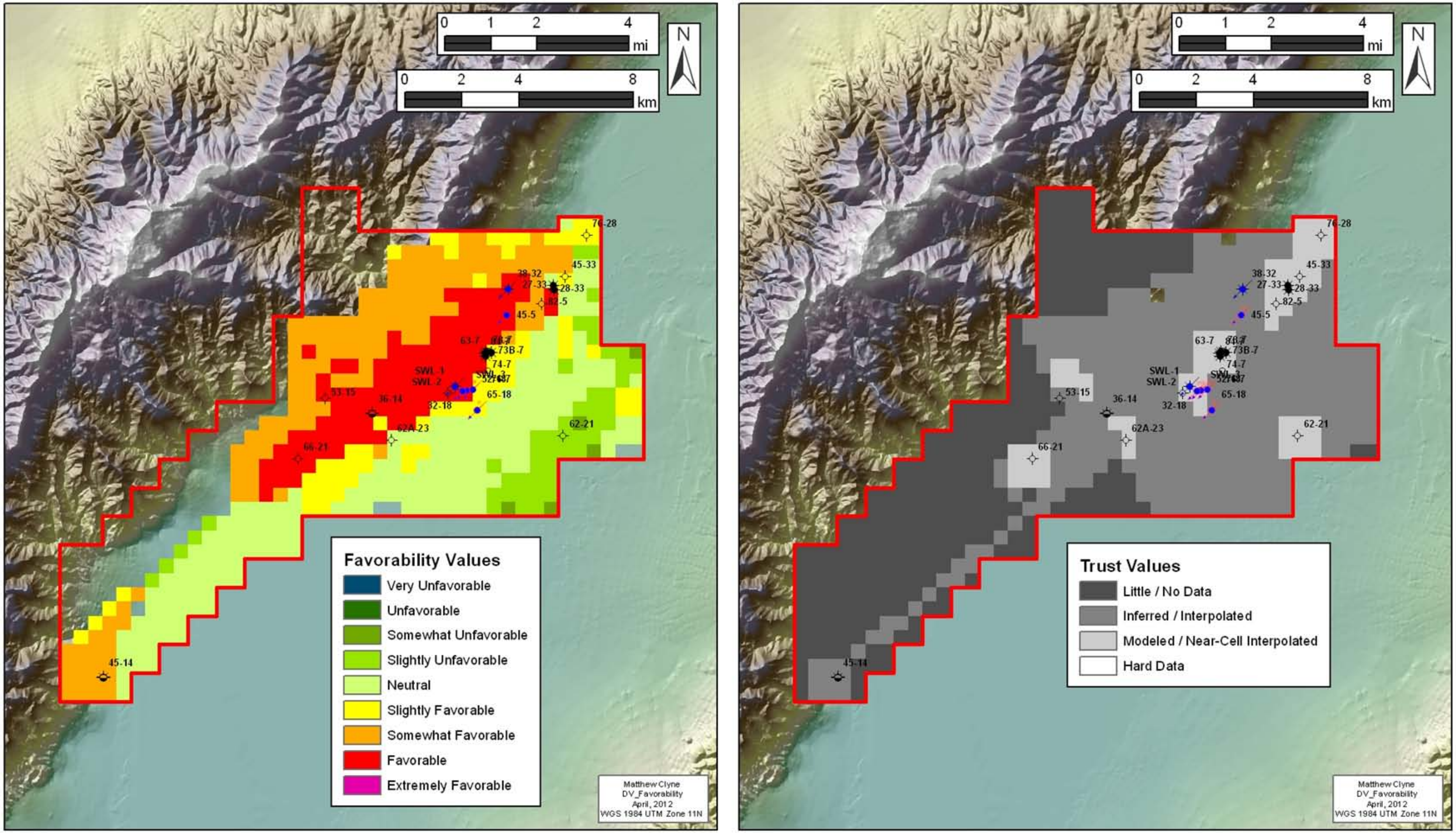

EGS Favorability-Trust Maps: Averaged Data with Equal Weighting
Depth: 2.5km Below Sea Level

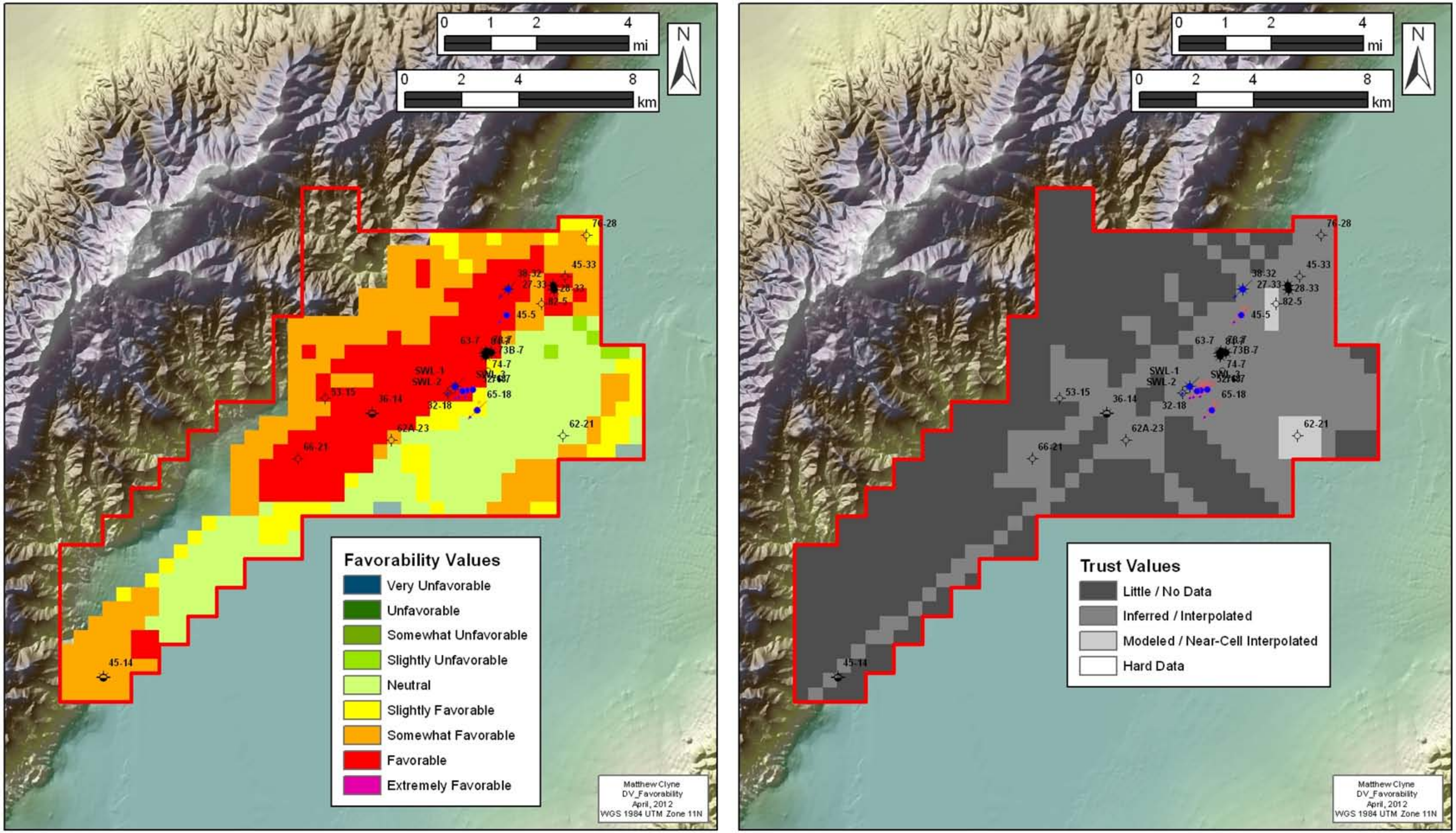

EGS Favorability-Trust Maps: Averaged Data with Equal Weighting
Depth: 3.0km Below Sea Level

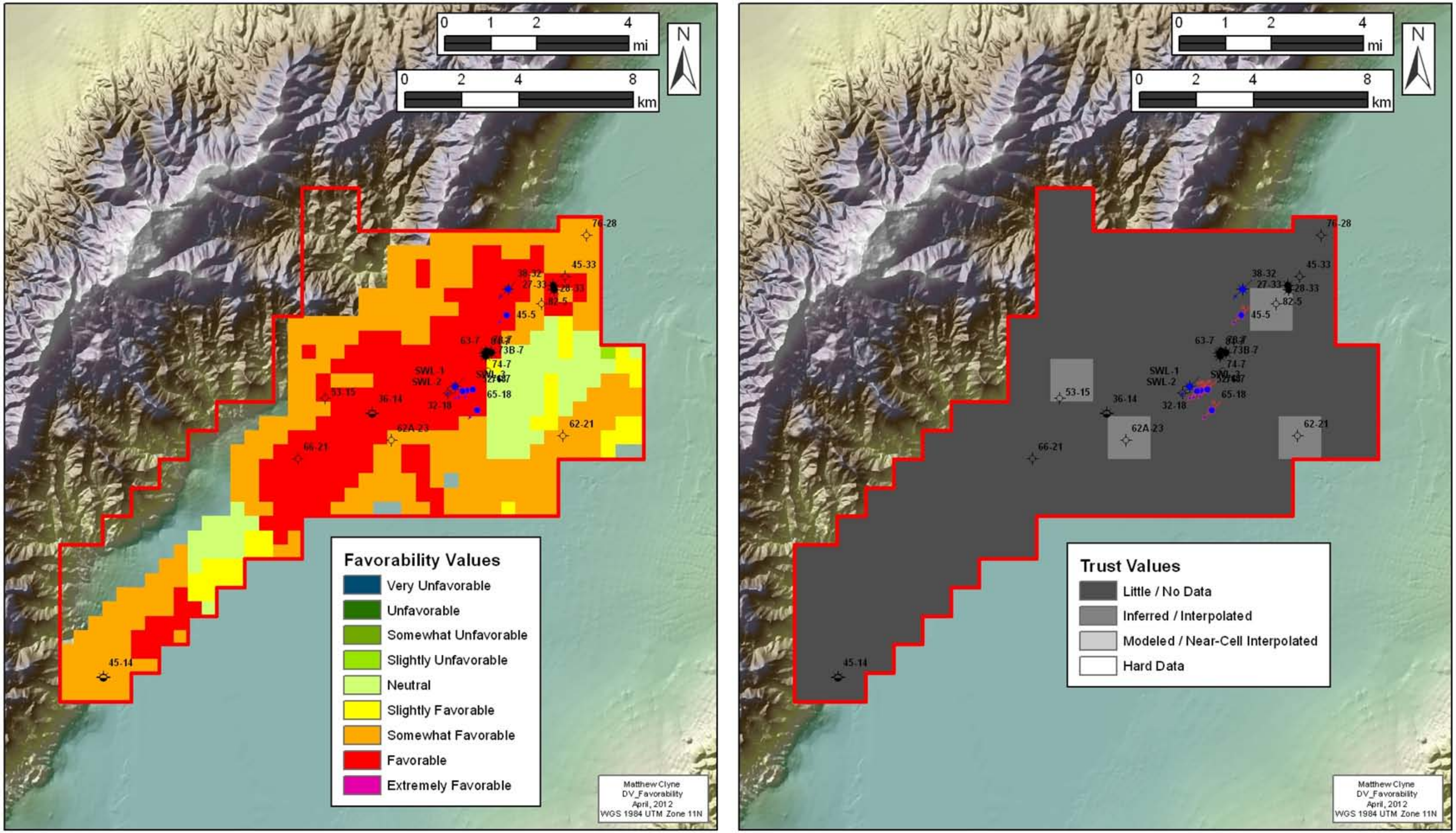

EGS Favorability-Trust Maps: Averaged Data with Equal Weighting
Depth: 3.5km Below Sea Level

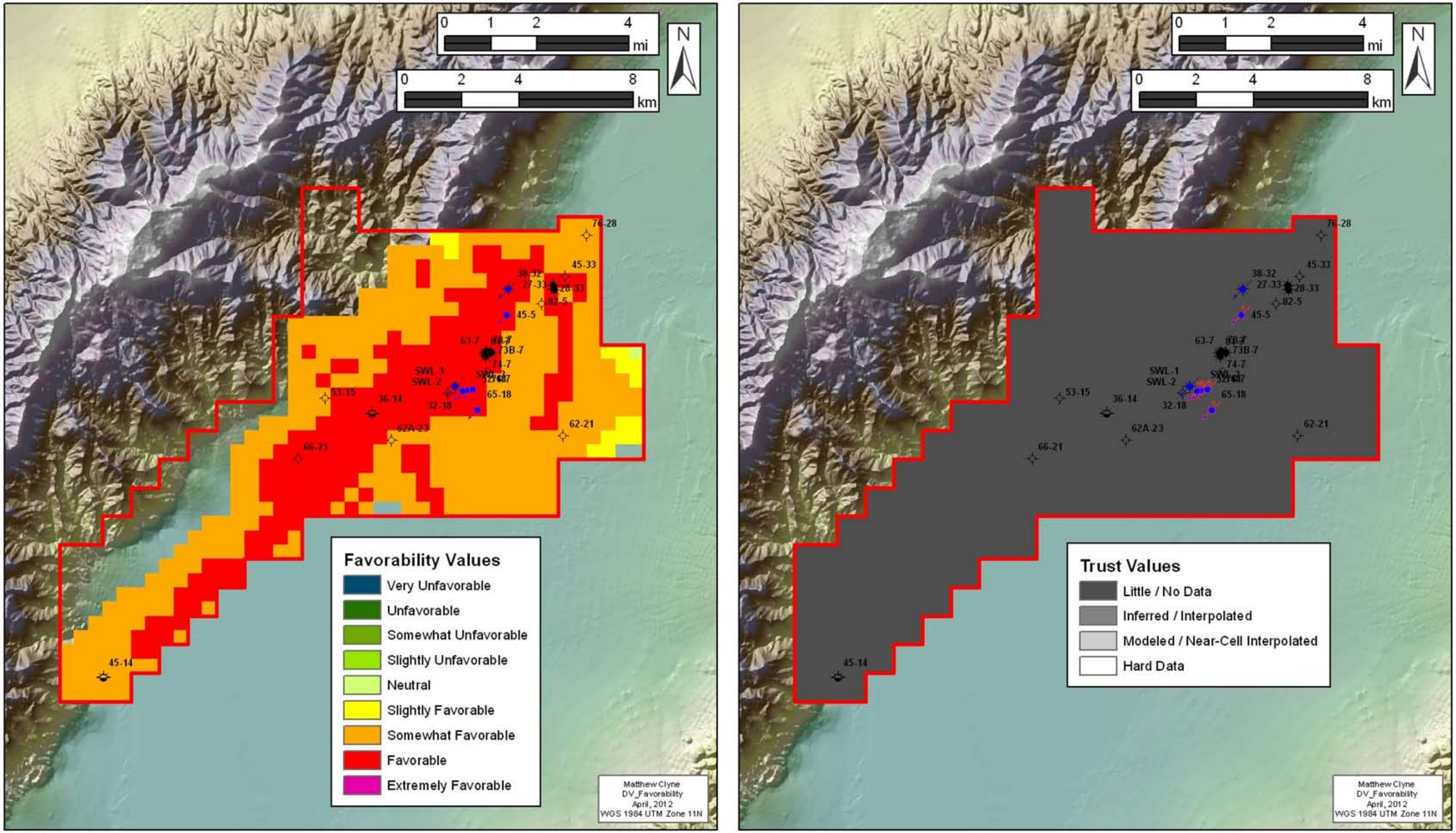

EGS Favorability-Trust Maps: Averaged Data with Equal Weighting
Depth: 4.0km Below Sea Level

Seismic Profile Key

SRC-3 — Interpretation by Okaya and Thompson (1985)
A: Valley-fill
B-Alluvial fan (piedmont block)
C: Basalt/volcanics
D: Basement
Dm: Supposed fault reflection

Line 102
LIne 6
Line 9/104
— Interpretation by Blackwell et al. 2005

Legend

▨ Tbf: basin-filling sediments
🟫 Tmb: Miocene basalt
🟨 Tv: Oligocene silicic volcanics
☐ Kgr: Cretaceous granodiorite
🟦 Jbr: Jurassic Boyer Ranch quartzite
🟪 Jz: Jurassic mafic volcanics
🟩 Tr: Triassic meta-sediments

Syncline axis
Temperature contour (° C) 100
Intersection with section tie-line A
Deep Well 53-15
Fumaroles

Contacts
known/approximate
inferred

Range-front (DVF)/Piedmont fault
known/approximate
inferred

Other Faults
known/approximate
inferred
geophysical-inferred

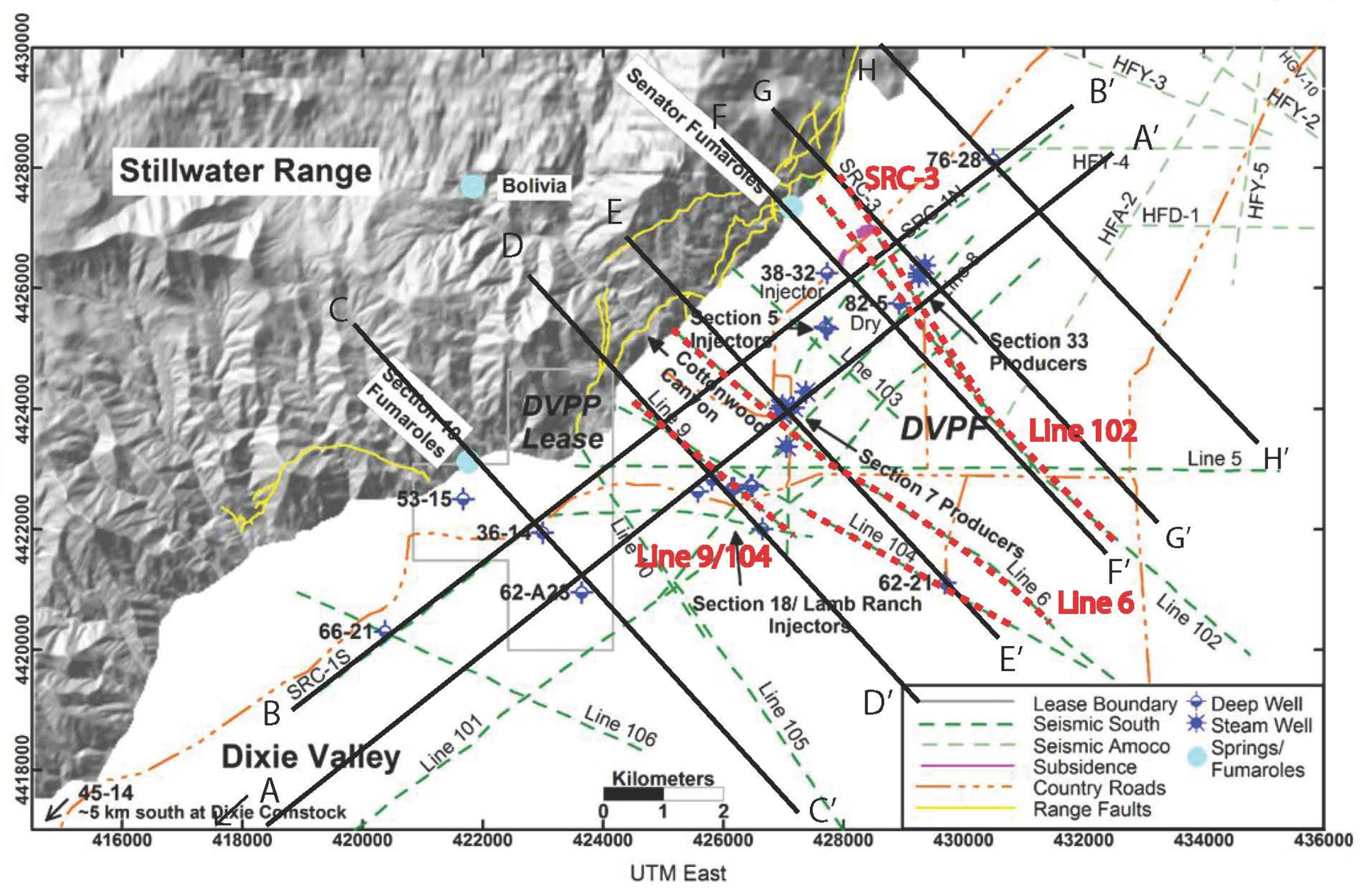

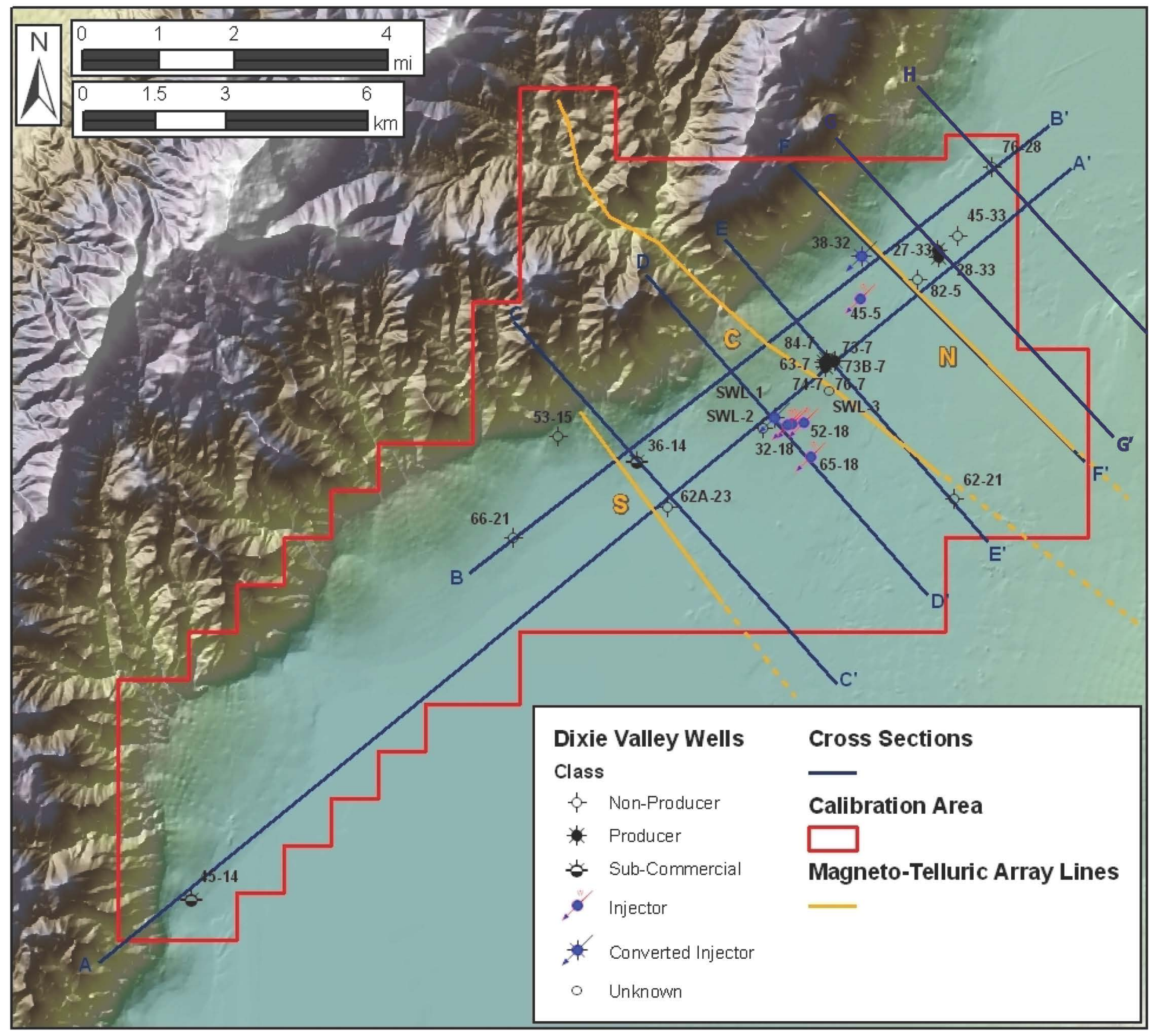

Legend
Thermal Iso-Contours
🟨 100-150°C
🟨 150-200°C
🟧 200-250°C
🟥 250+°C

Legend
Gravity/Magnetic Inferred Stratigraphic Units
🟩 Tls: Lake Sediments (D= 1.351)
🟨 Tbf: Basin-filling sediments (D=2.445)
🟧 Jg: Jz igneous group (D=2.876, M=0.004)
⬜ Jz: (Jv) rhyolite; (Ja)arenite [Jbrq]) (D=2.47; 2.56)
☐ Tr/Kgr: Basement; Tr meta-seds, K granodiorite (D=2.88)

Seismic Legend
P-Wave Velocity (km/s)
2.00
2.50
3.00
3.50
4.00
4.50
5.00
5.50
6.00

Plate 1. Correlation of Sections perpendicular to the Dixie Valley Fault Zone

Section	Geology	Seismic Reflection Profiles	Thermal	Gravity/Magnetics
B-B′	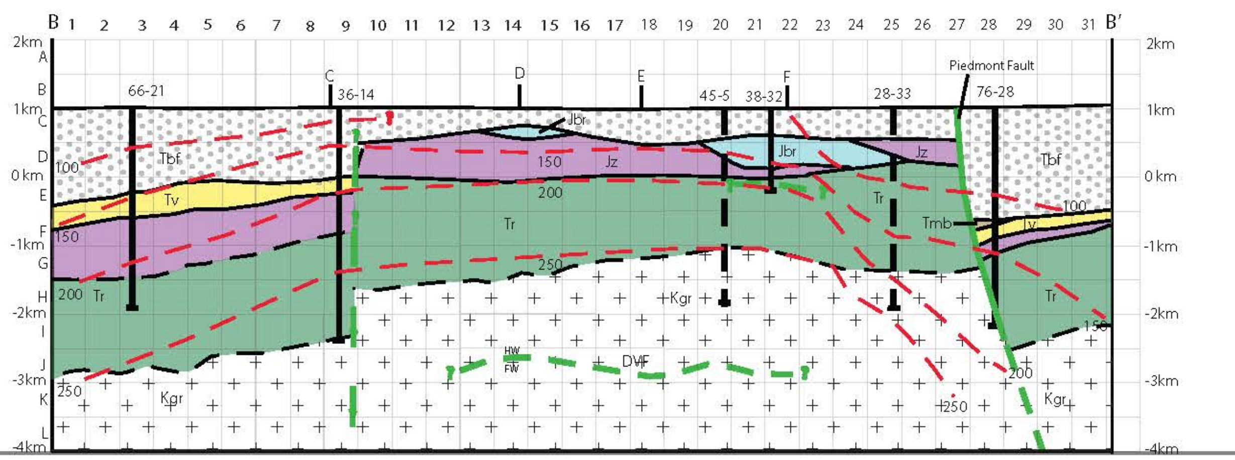	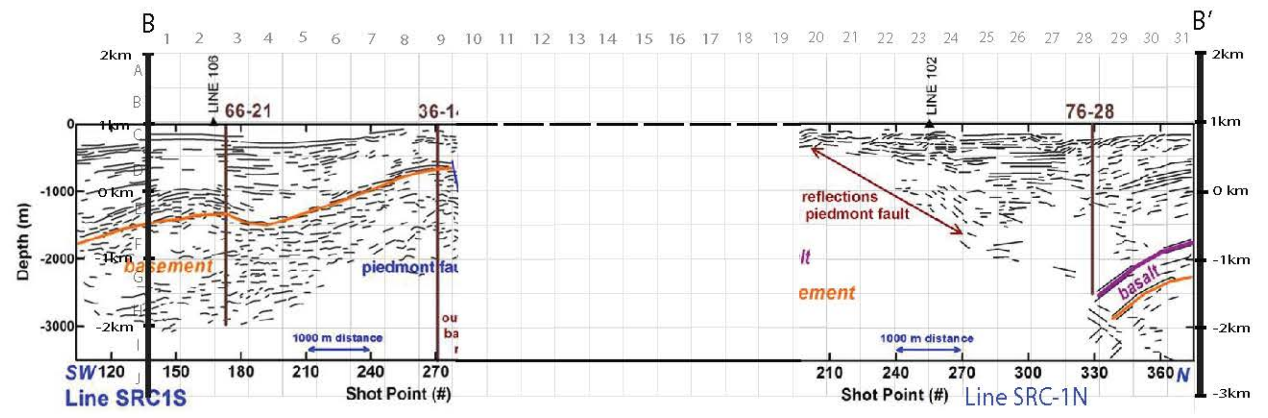	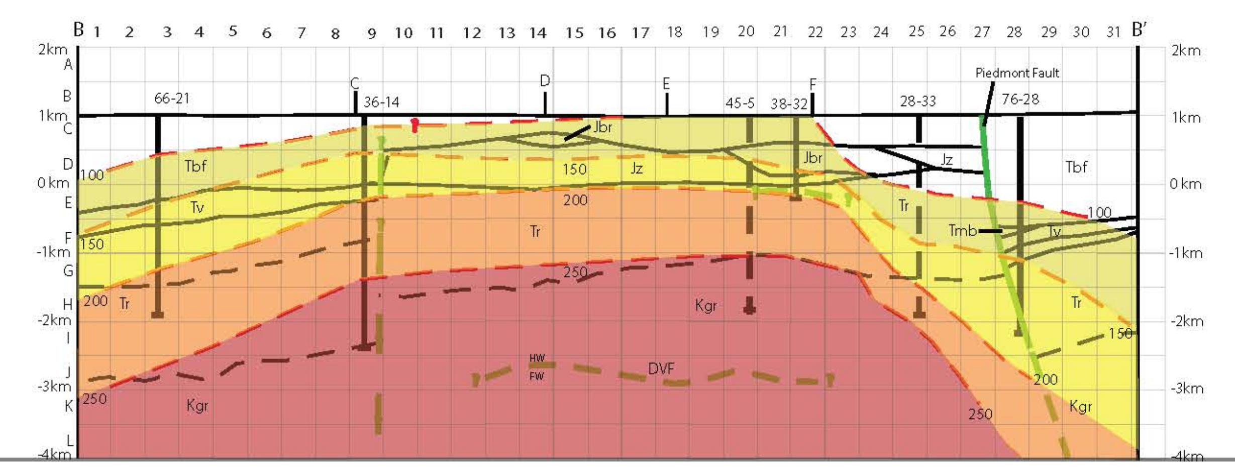	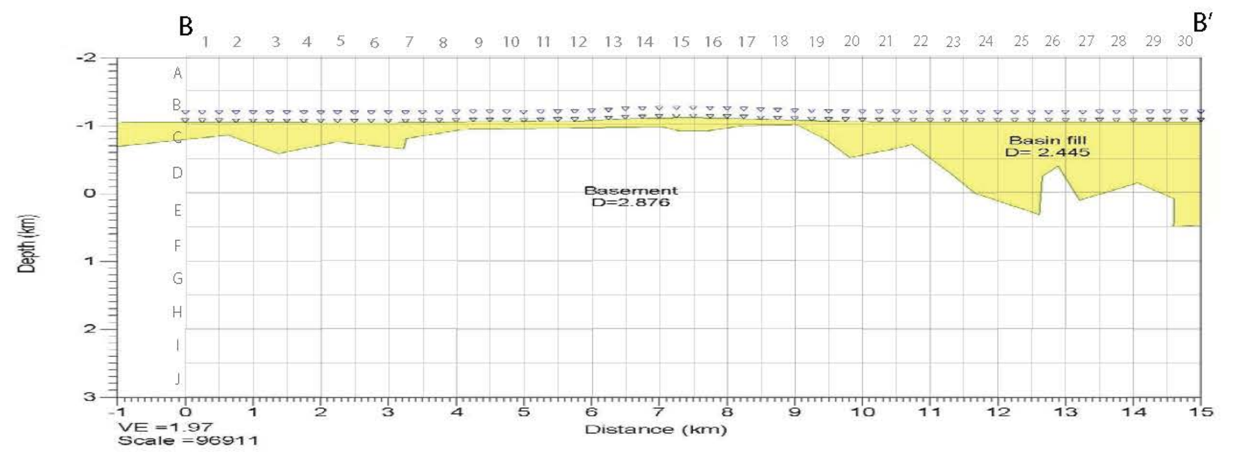
A-A′	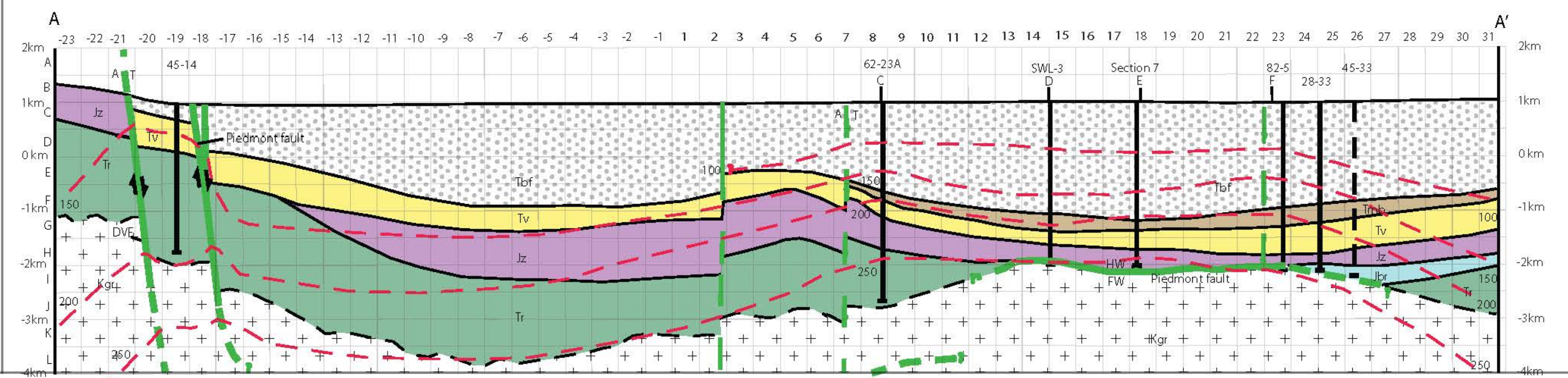	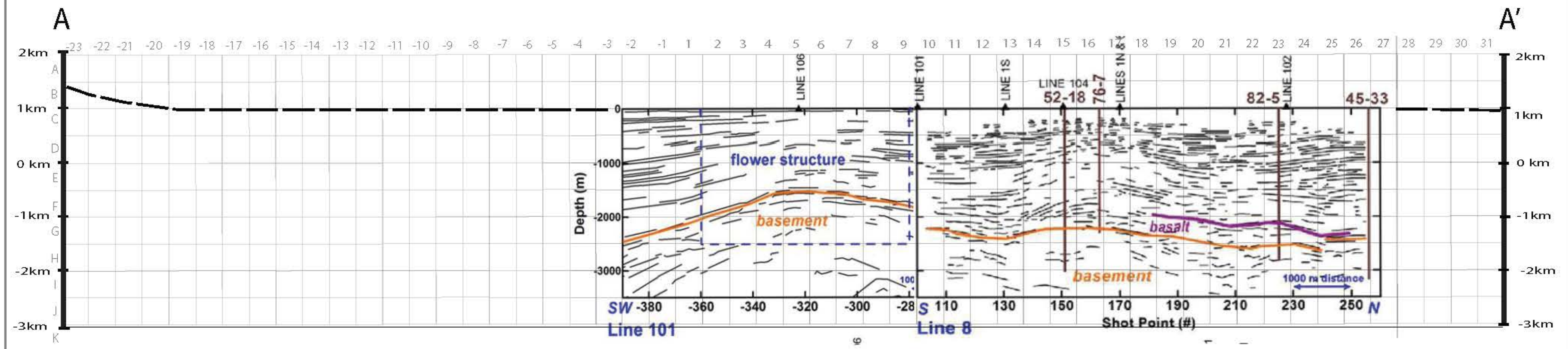	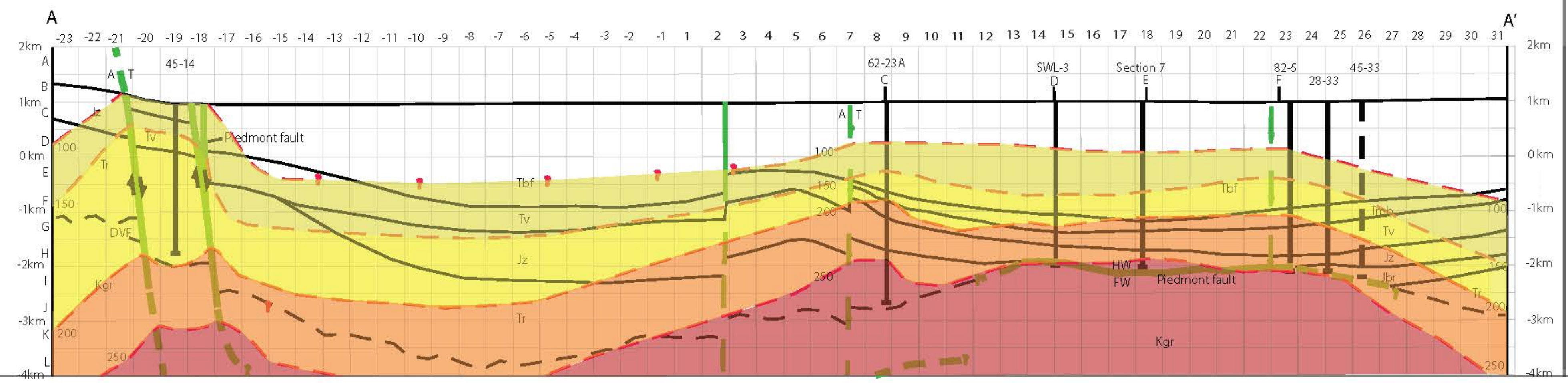	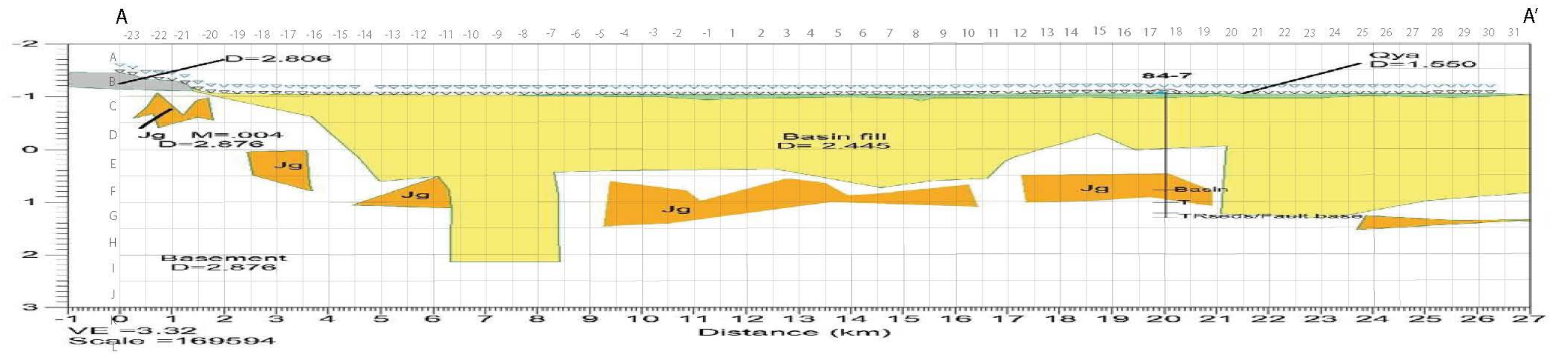

Legend

- ▨ Tbf: basin-filling sediments
- 🟫 Tmb: Miocene basalt
- 🟨 Tv: Oligocene silicic volcanics
- ▨ Kgr: Cretaceous granodiorite
- 🟦 Jbr: Jurassic Boyer Ranch quartzite
- 🟪 Jz: Jurassic mafic volcanics
- 🟩 Tr: Triassic meta-sediments

Syncline axis

Temperature contour (° C) 100

Intersection with section tie-line A

Deep Well 53-15

Fumaroles

Contacts
- known/approximate
- inferred

Range-front (DVF)/Piedmont fault
- known/approximate
- inferred

Other Faults
- known/approximate
- inferred
- geophysical-inferred

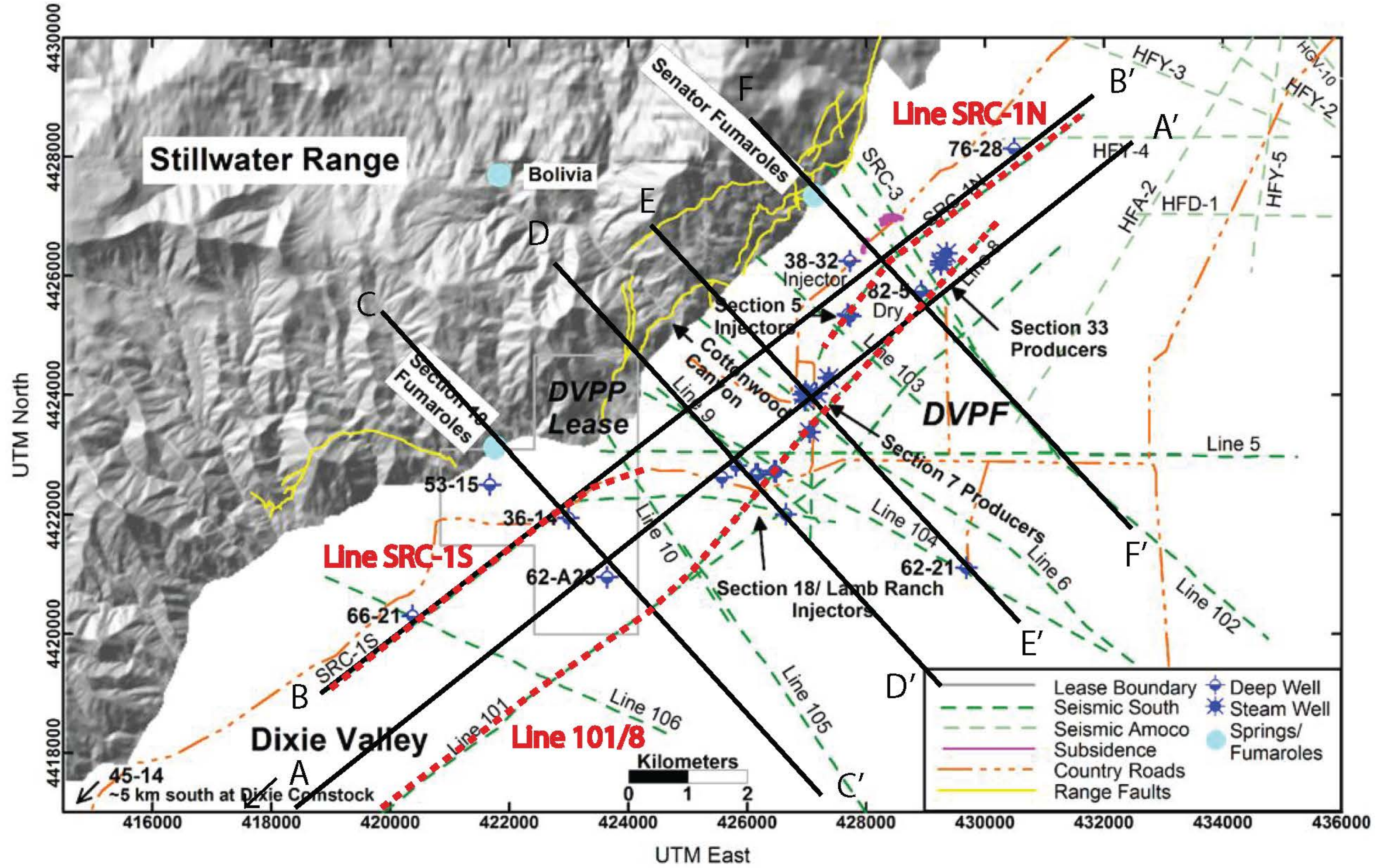

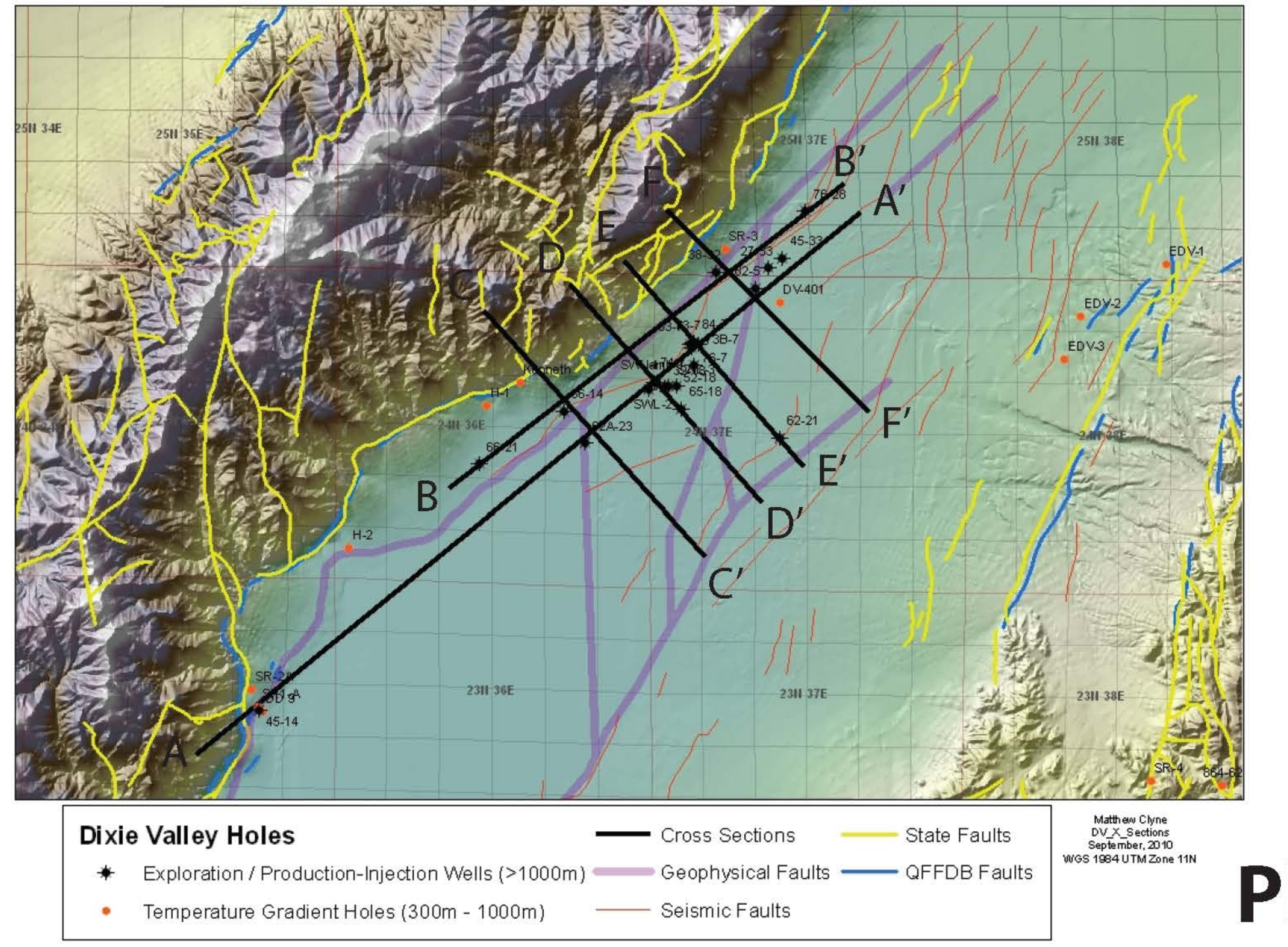

Legend

Thermal Iso-Contours

- 🟨 100-150ºC
- 🟨 150-200ºC
- 🟧 200-250ºC
- 🟥 250+ºC

Legend

Gravity/Magnetic Inferred Stratigraphic Units

- 🟩 Tls: Lake Sediments (D= 1.351)
- 🟨 Tbf: Basin-filling sediments (D=2.445)
- 🟧 Jg: Jz igneous group (D=2.876, M=0.004)
- ⬜ Jz: (Jv) rhyolite; (Ja)arenite [Jbrq]) (D=2.47; 2.56)
- ⬜ Tr/Kgr: Basement; Tr meta-seds, K granodiorite (D=2.88)

Plate 2. Correlation of Sections parallel to the Dixie Valley Fault Zone